航 空 航 天

CHINA AEROSPACE STUDIES INSTITUTE

In Their Own Words:

Hypersonic Vehicle Technology

Translations from Chinese source documents

The “In Their Own Words” series is dedicated to translations of Chinese documents in order to help non-Mandarin speaking audiences access and understand Chinese thinking. CASI would like to thank all of those involved in this effort.

In the “In Their Own Words” series, CASI and its collaborators aim to provide Chinese texts that illustrate thoughtful, clearly articulated, authoritative foreign perspectives on approaches to warfare at the strategic, operational, and tactical levels.

This translation and publication does not constitute approval by any U.S. Government organization of the contents, inferences, findings and conclusions contained therein. Publication is solely for the exchange and stimulation of ideas.

Printed in the United States of America
by the China Aerospace Studies Institute

To request additional copies, please direct inquiries to
Director, China Aerospace Studies Institute,
Air University, 55 Lemay Plaza, Montgomery, AL 36112

All photos licensed under the Creative Commons Attribution-Share Alike 4.0 International license, or under the Fair Use Doctrine under Section 107 of the Copyright Act for nonprofit educational and noncommercial use.
All other graphics created by or for China Aerospace Studies Institute

E-mail: Director@CASI-Research.ORG
Web: http://www.airuniversity.af.mil/CASI
https://twitter.com/CASI_Research @CASI_Research
https://www.facebook.com/CASI.Research.Org
https://www.linkedin.com/company/11049011

Disclaimer
The views expressed in this academic research paper are those of the authors and do not necessarily reflect the official policy or position of the U.S. Government or the Department of Defense. In accordance with Air Force Instruction 51-303, *Intellectual Property, Patents, Patent Related Matters, Trademarks and Copyrights*; this work is the property of the U.S. Government.

Limited Print and Electronic Distribution Rights
Reproduction and printing is subject to the Copyright Act of 1976 and applicable treaties of the United States. This document and trademark(s) contained herein are protected by law. This publication is provided for noncommercial use only. Unauthorized posting of this publication online is prohibited. Permission is given to duplicate this document for personal, academic, or governmental use only, as long as it is unaltered and complete however, it is requested that reproductions credit the author and China Aerospace Studies Institute (CASI). Permission is required from the China Aerospace Studies Institute to reproduce, or reuse in another form, any of its research documents for commercial use. For information on reprint and linking permissions, please contact the China Aerospace Studies Institute.

Cleared for Public Release; Distribution Unlimited.

CASI would like to acknowledge the work and effort of the team at BluePath Labs for their help with this translation. This translation was done through an automated translation engine. While we have tried to ensure that this is an accurate and readable translation, we expect there to be inconsistencies and errors. In addition, the page numbers of this translation correspond to the page numbers of the original (i.e., the page numbered page ten in this document has the content of the page numbered ten in the original).

China Aerospace Studies Institute

CASI's mission is to advance the understanding of the strategy, doctrine, operating concepts, capabilities, personnel, training and organization of China's aerospace forces and the civilian and commercial infrastructure that supports them.

CASI supports the Secretary, Chief of Staff of the Air Force, the Chief of Space Operations, and other senior Air and Space leaders. CASI provides expert research and analysis supporting decision and policy makers in the Department of Defense (DoD) and across the U.S. government. CASI can support the full range of units and organizations across the United States Air Force (USAF), U.S. Space Force (USSF), and the DoD. CASI accomplishes its mission through conducting the following activities:

- CASI primarily conducts open-source native-language research supporting its five main topic areas.
- CASI conducts conferences, workshops, roundtables, subject matter expert panels, and senior leader discussions to further its mission. CASI personnel attend such events, government, academic, and public, in support of its research and outreach efforts.
- CASI publishes research findings and papers, journal articles, monographs, and edited volumes for both public and government-only distribution as appropriate.
- CASI establishes and maintains institutional relationships with organizations and institutions in the PLA, the PRC writ large, and with partners and allies involved in the region.
- CASI maintains the ability to support senior leaders and policy decision makers across the full spectrum of topics and projects at all levels, related to Chinese aerospace.

CASI supports the U.S. Defense Department and the China research community writ-large by providing high quality, unclassified research on Chinese aerospace developments in the context of U.S. strategic imperatives in the Asia-Pacific region. Primarily focused on China's Military Air, Space, and Missile Forces, CASI capitalizes on publicly available native language resources to gain insights as to how the Chinese speak to and among one another on these topics.

Hypersonic Vehicle Technology

[高超声速飞行器技术]

{Gaochaoshengsu Feixing Jishu}

Cai Guobiao [蔡国飙] and Xu Dajun [徐大军], eds

Science Press [科学出版社]

Beijing

Introduction

This book systematically analyzes the key technologies of hypersonic vehicles, expounds the main research contents and research methods of each key technology, and summarizes the development process and main research results of hypersonic vehicle technology in foreign countries. The book is divided into two parts, with a total of 16 chapters, the first part (Chapters 1 to 8) expounds the key technologies of hypersonic vehicles, and the second part (Chapters 9 to 16) introduces the development of hypersonic vehicle technology in various countries, and gives research summaries and prospects.

This book can be used as a reference book for engineers and technicians engaged in related research in the field of hypersonic vehicles and reusable space launch vehicles, as well as teachers and students of related majors in colleges and universities.

Book-in-Publication Inventory (CIP) data

Hypersonic Vehicle Technology / Cai Guobiao, Xu Dajun, eds. — Beijing: Science Press, 2012. 1
ISBN 978-7-03-033062-8

I.① Gao (高)… II.① Cai (蔡)… ② Xu (徐)… III.① Hypersonic flight vehicles (高超声速飞行器) IV.① V47

CIP Data Verification (2011) No. 264958

Editor-in-charge: Tong Anqi / Proofreader: Wang Wanhong
Responsible Printing: Lü Chunmin / Cover Design: Cultivator Design Studio

Published by Science Press
No. 16, Genbei Street, East Huangcheng, Beijing, 100717
http://www.sciencep.com
Printed by China Scientific Printing House
Published by Science Press Distributed by Xinhua bookstores around the country
*
First edition, January 2012 Format: 787 x 1092 1/16
First printing in January 2012 Sheets: 30 1/4 Inserts: 4
Word Count: 700 000
Price: 100.00 RMB
(If there is a printing quality problem, our company is responsible for replacement)
Sales Tel: 010-62136131 Editorial Tel: 010-62137026 (BA08)
All rights reserved, infringement will be investigated
Report Tel: 010-64030229; 010-64034315; 13501151303

PREFACE

The pursuit of faster flight speeds is an important feature in the development of aircraft. The practical benefits that can be brought about by increased speed are obvious: the time required for the same transportation distance is greatly shortened; the side with the higher speed in information warfare has greater initiative and rapid reaction ability; increased speed enhances the combat effectiveness and attack capability of missile weapons; and increased speed gives the orbital vehicle the basic ability to get rid of the earth's gravity. The realization of a vehicle capable of hypersonic flight in the atmosphere has been a dream of mankind for a long time, and this dream is gradually becoming a reality.

Hypersonic vehicles refer to aircraft with a Mach number greater than 5, an air-breathing engine or its combination engine as the main power, and the ability to fly long distances in the atmosphere and transatmosphere, with application forms including hypersonic cruise missiles, hypersonic manned/unmanned aircraft, aerospace aircraft, and aerospace missiles.

As a combination of aviation and aerospace technology, hypersonic vehicle technology involves hypersonic aerodynamics, computational fluid dynamics, high-temperature aerothermodynamics, chemical dynamics, navigation and control, electronic information, material structure, process manufacturing, and other disciplines, and is a highly comprehensive combination of many advanced technologies, such as hypersonic propulsion, airframe/propulsion integrated design, supersonic combustion, thermal protection, heat-absorbing hydrocarbon fuel, hypersonic ground simulation, and flight testing. Hypersonic vehicles are the cutting-edge technology in the aerospace field today, and they are a hot field of research for aerospace powers. In recent years, many domestic research institutes, universities, and other research institutions have also carried out extensive research on hypersonic vehicle related technologies, and great research progress has been made. In addition to the considerable technical difficulty, hypersonic vehicles also have their own unique characteristics, such as the integrated design of fuselage and propulsion, and the high coupling of multiple disciplines, which make its research methods, methods, and technical approaches different from those of traditional aircraft development.

The purpose of compiling this book is to enable scientific researchers engaged in the research of hypersonic vehicle technology to have a comprehensive and macroscopic understanding of the hypersonic vehicle technology system from the perspective of the overall hypersonic vehicle and the height and breadth of the development process of foreign technologies, so that they can not be limited to their own professional division of labor in scientific research work but also take into account the internal requirements of other disciplines to better grasp the keys to the development of hypersonic vehicle technology. In light of the fact that there is no comprehensive introduction to hypersonic vehicle technology at home and abroad, another purpose of compiling this book is in the hope that it can become a primary text for scientific researchers engaged in the research of hypersonic vehicle technology, and a map towards the field of hypersonic vehicle technology. Therefore, this book provides a definition of some basic concepts, a description of basic parameters, and an introduction of basic methods related to key technologies in the corresponding chapters, so that readers can initially grasp some basic knowledge through the reading of this book, and can then further consult and read the corresponding references, and we believe that they can quickly enter the arena of hypersonic vehicle technology research.

The first part [of this book] systematically and comprehensively introduces several key technologies of hypersonic vehicles, including scramjet engine technology, combined propulsion systems technology, overall and integrated design technology, structural and thermal protection technology, navigation guidance and control technology, and wind tunnel test technology, etc. The second part undertakes a comprehensive summary of research processes in the field of hypersonic vehicle technology in the United States, Russia, France, Germany, Japan, Australia, the United Kingdom, India, and other countries. The compilation of this book refers to a large number of technical and academic literature at home and abroad and is marked in the corresponding position of the book as much as possible, but the size of the literature, the discipline, and professional leap is large, if there be omissions and deficiencies, we respectfully request the understanding of readers and the original authors. In addition, due to the limitation of the authors' professional field, it is difficult to digest and grasp the subject expertise and research progress in a relatively short period of time, so in the process of compilation, more reference was made to the review literature of the corresponding discipline, as well as the research review part of the domestic doctoral and master's dissertations, and the corresponding references of the quoted text were marked in the book and listed in the references of each chapter.

The compilation of this book has been supported by Tao Ping, member of the Science and Technology Committee of the General Armament Department of the People's Liberation Army, Zhao Tongkai, director of the New Technology Bureau of the Ministry of Electronic Information Infrastructure, Liu Zhiwei, deputy director, Zhu Wenfeng, researcher Wang Jue of the First Academy of Aerospace Science and Technology Group, and academicians Huang Ruisong, Wei Yiyin, Shi Xinxing, Tang Longsheng and Zhao Wensheng of the Third Academy of Aerospace Science and Industry Group, researcher Xie Haibo, and many other leading experts. we would like to express our heartfelt thanks for their interest, and strong support. We would like to express our gratitude to the peer experts from various research institutes and universities for their help. Professor Xu Xu and Professor Sun Bing of the Department of Propulsion, and Associate Professor Li Huifeng of the Department of Aerospace Navigation Guidance and Control, who have been engaged in the research of hypersonic vehicle technology in the School of Astronautics of our university for many years, have provided a lot of information materials for the compilation of this book, and we would like to express our sincere gratitude. Academician Zhuang Fenggan, a well-known aerodynamics expert, and Academician Liu Xingzhou, an expert in the power of flying missiles, have also been concerned about the progress of this book, but it is a great pity that this book was not published during their lifetimes.

Due to the limited professional level of the authors, there are inevitably deficiencies in the book, and we sincerely invite readers to criticize and advise, for which we are very grateful.

Cai Guobiao, Xu Dajun
December 2011

TABLE OF CONTENTS

PART I – HYPERSONIC VEHICLE TECHNOLOGY

CHAPTER 1: INTRODUCTION

1.1: Hypersonic vehicles

As one of the high-tech fields, aerospace technology is an important symbol of a country's scientific and technological strength and industrial base, and is also a powerful symbol of a country's political status and military strength. The competition between countries in the 21st century is a competition of comprehensive national strength, and all the major powers in the world have launched fierce competition in the field of aerospace in an effort to gain a place in this field, so as to establish their own political, military, and even economic status in the international arena. Looking back at the 100-year development of aerospace technology, the dream of human beings to "fly to the sky" has become a reality in the hands of countless scientists, engineers, and technicians. At the beginning of the 20th century, after the birth of the Wright brothers' "Aviator" aircraft, aviation technology developed inexorably, and at the same time, the theory of rocket power created by Tsiolkovsky and other space pioneers was also maturing, and mankind finally had the powerful power to break free from the gravitational pull of the earth.

The pursuit of higher the aircraft speeds is not the pursuit of imaginative scientists seeking the new and different, but rather an effort to attain the real benefits that can be brought about by an increase in speed. The increase in speed greatly shortens the time required for the same transportation distance; the side with the higher speed in air combat has greater initiative, and the increase in speed enhances the combat effectiveness and attack capability of missile weapons; and the increase in speed gives the orbital vehicle the basic ability to be rid of the earth's gravity. The realization of a vehicle capable of traveling at hypersonic speeds in the atmosphere has been a dream of mankind for a long time, and this dream is gradually becoming a reality.

Hypersonic vehicles refer to aircraft with a Mach number greater than 5, an air-breathing engine or its combination engine as their main power, which can fly long distances in the atmosphere and transatmosphere. Application forms include hypersonic cruise missiles, hypersonic manned/unmanned aircraft, aerospace aircraft and aerospace missiles.

As the combination of aviation and aerospace technology, hypersonic vehicle technology involves hypersonic aerodynamics, computational fluid dynamics, high-temperature aerothermodynamics, chemical dynamics, navigation and control, electronic information, material structure, process manufacturing and other disciplines, and is a highly comprehensive of many cutting-edge technologies such as hypersonic propulsion, airframe/propulsion integrated design, supersonic combustion, thermal protection, heat-absorbing hydrocarbon fuel, hypersonic ground simulation and flight test.

The development of hypersonic vehicle technology began with the concept of supersonic combustion proposed in the 1950s, which enabled the aircraft to fly in the atmosphere to obtain a faster power mode, that is, a scramjet engine (Scramjet)[1]. Theoretically, a hydrogen-fueled scramjet engine can operate up to Mach 12 to 16, and a hydrocarbon-fueled scramjet engine can work up to Mach 9 to 10 (Figure 1-1)[2]. The combination of scramjet engine technology, rocket engine, and turbojet engine technology constitutes a combination of various forms of engines, enabling the aircraft propelled by scramjet engine to work from low speed to high speed, which is more practical. The hypersonic air-breathing propulsion technology based on scramjet engines and their combined engines has greatly expanded the flight speed range of aircraft, so hypersonic vehicles have broad application prospects.

Although this idea has not yet been realized due to the technical difficulty of hypersonic vehicles, it is an inevitable development path from the perspective of the future development of human space technology, and its related key technologies are gradually maturing.

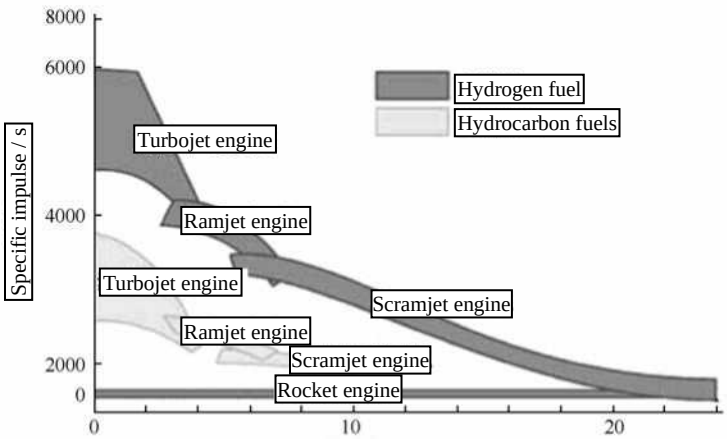

Figure 1-1: Mach number range of aircraft propelled by various engine types

Hypersonic vehicle technology has been slow to advance in the past half century, but in recent years has shown a trend of accelerated development, and the successful development of many flight tests in various countries marks the feasibility of scramjet as a hypersonic flight power mode on the one hand, and the technology of hypersonic vehicles is gradually maturing on the other hand.

Hypersonic vehicles will be at the forefront of aerospace technology development for a long time to come. In the short term (10 to 15 years), missile weapons that can be developed into a rapid response will greatly change the battlefield pattern and alter the balance of military forces. In the medium and long term, a reusable space launch vehicle, that is, an aerospace aircraft, can be developed, which can reduce the cost of entering space, so that mankind can use space more effectively and quickly, which is of great military and economic significance, and it can also allow for the application of hypersonic aircraft for military reconnaissance, if firepower was dropped, and can even be used in civil aviation, to shorten the time of travel and cargo transportation.

1.2: Research on the overall scheme of foreign hypersonic vehicles

The development of hypersonic vehicle technology is ultimately to realize the flight and application of hypersonic vehicles, so the overall scheme of these vehicles plays two roles in the whole research and development process, one is to describe the application prospects of the current subsystem technology research, and the other is to achieve the ultimate goal of technology development, which is the object to be studied after the integration of various technologies.

The concept of scramjet engine makes it possible for aircraft to achieve hypersonic flight in the atmosphere, but to achieve hypersonic aircraft, it is necessary to integrate other related technologies, some of which are common to other aircraft, and the other part of the technology is the same as scramjet technology, which is a key technology that needs to be solved by targeted technical research. From the beginning of the concept of a scramjet engine, research on the overall scheme of hypersonic vehicles began, and the research of the overall scheme plays a role in describing the application prospect of technology, defining the content of technical research, and developing traction technology in the whole process of hypersonic vehicle technology development.

A core element of the overall plan of the world's aerospace powers is national hypersonic vehicle application research and development, and this is the ultimate goal of their plans. The U.S.’s NASP (National Aerospace Program) and Germany’s Sanger program, are typically representative of the 1980s efforts that sought to realize the goal an aerospace aircraft, through a specific overall plan to lead and organize the development of various technical research.

In addition, the overall scheme research of the aircraft itself has some characteristics that are different from the research of individual technologies and subsystems, and it is an innovative process of developing the aircraft from scratch, so it has its corresponding research methods and research methods. Due to the harshness of the flight environment and the complexity of the system, hypersonic vehicles have different design requirements and design characteristics from other aircraft.

The following summarizes the research on the overall scheme of hypersonic vehicles carried out abroad from the three application forms of hypersonic vehicles, reusable space launch vehicles, hypersonic aircraft, and hypersonic cruise missiles.

1.2.1: Reusable space launch vehicles

Reusable space launch vehicle (RLV) is the development direction of the next generation of space transportation systems, in which a single-stage and two-stage orbit space launch vehicle, powered by an air-breathing combined propulsion system, is the most ideal form of solution, although there are technical difficulties greater than the complexity of the aircraft system. However, when formulating their RLV development plans, all countries take the realization of air-breathing reusable space launch vehicles as the ultimate development goal, and only by using the air-breathing power propulsion mode can we truly reflect on the many advantages of RLV and realize the goal of "fast, reliable and inexpensive access to space."

As early as 1965, NASA, together with Marquardt, Rocketdyne, and Lockheed, jointly carried out research on a space launch vehicle with a combination of air-breathing engine and rocket engine as power propulsion [3]. This work laid the foundation for research on air-breathing reusable space launch vehicles. In the 1980s, NASP in the United States and Sanger in Germany were two important national development programs in the development of reusable space launch vehicles, both of which aimed to realize air-breathing hypersonic flight with a scramjet engine as the core power source and be applied to aerospace transportation. The two planned vehicle programs have drawn an exciting blueprint for the development of space launch vehicles and have invested considerable efforts in research on some key technologies, laying the foundation for the development of hypersonic vehicle technology in the future. However, the NASP program and the Sanger program, due to the large technical span, failed to achieve their intended purpose. After the NASP program and the Sanger program, countries continue to develop hypersonic vehicle technology, downscale specific research programs, and aim to break through on key technologies. With the development of key technologies, in recent years, new overall conceptual design schemes of reusable space launch vehicles have been proposed to drive the further development direction of key technologies.

Table 1-1 and Figure 1-2 summarize the typical and representative air-breathing reusable space launch vehicle schemes proposed by the United States, Russia, Japan, and the European Space Agency (ESA) in recent years [4~25].

Table 1-1: Air-breathing reusable space launch vehicle schemes by country and region

Country	Name	Research institute	Task mode	Pneumatic shape	Propulsion system
United States	DF-space	NASA	HTHL TSTO	Lifting bodies	AceTR + DMRS + Aerospike
	ABLV-4/9	NASA	HTHL SSTO	Lifting bodies	AceTR + DMRS + Aerospike
	Trailblazer	NASA	VTHL TSTO	Wing cone assembly	RBCC
	Axisymmetric VTHL	Boeing/Aerojet/NASA	VTHL SSTO	Wing cone assembly	Aerojet Strutjet RBCC
	FASST	Boeing/NASA	HTHL TSTO	Wing-body fused with waverider	FSA + RBCC
	XCALIBUR	SpaceWorks **(**SEI)	VTHL TSTO	Wing cone assembly	RBCC
	Argus	SSDL	Magnetic levitation boost SSTO	Wing cone assembly	SERJ RBCC
	Hyperion	SSDL	HTHL SSTO	Wing half-cone	Lox/L2 Ejector Scramjet
	Stargazer	SSDL	HTHL TSTO	Wedge body + wing	Lox/L2 Ejector Scramjet
	Starsaber	SSDL	HTHL TSTO	Wing cone assembly	RBCC

Table 1-1: Continued

Country	Name	Research institute	Task mode	Pneumatic shape	Propulsion system
Russia	Tu-2000	Tupolev ASTC	HTHL SSTO	Lifting bodies	LACE/DMSCRJ
	MIGAKS	ME ARPC	HTHL TSTO	Wing-body	TFAB
Japan	JAXA-1	JAXA	HTHL TSTO	Wing-body	ATREX
	JAXA-2	JAXA	HTHL SSTO	Lifting bodies	RBCC
Europe	FSSC-12	ESA	HTHL TSTO	Wing-body combination / wing-body fusion	Turbojet Propulsion System

In recent years, NASA has made several plans to carry out the research of air-breathing reusable space launch vehicles, such as the Air-breathing Launch Vehicle (ABLV) program that aims to undertake conceptual system design research of air-breathing space launch vehicles, and the Advanced Space Transportation Program (ASTP) program, which has carried out the Integrated System Test of An Airbreathing Rocket Program (ISTAR) sub-program aimed at conducting flight tests of the RBCC propulsion system. Around 1996, the U.S.'s Boeing Company and NASA's Langley Research Center of carried out the design and research of dual-fuel (DF) air-breathing hypersonic vehicles and realized the single-stage orbit entry of the aircraft through the integration of hydrocarbon fuel and hydrogen fuel. In the ABLV program, NASA has designed and studied a variety of schemes, typical of which are ABLV-4 and ABLV-9. FASST is a similar research protocol conducted by Boeing and NASA. The above schemes all employ horizontal take-off and horizontal landing. NASA and some industrial research institutions have also proposed several vertical take-off and horizontal landing concepts, such as NASA's Trailblazer program, Boeing, Aerojet and NASA jointly developed the axisymmetric vertical take-off single-stage orbit aerospace aircraft conceptual design scheme, and Space Works Engineering (SEI). The company proposed a two-stage conceptual design scheme called XCALIBUR for vertical take-off and horizontal landing into orbit. The Aerospace Systems Design Laboratory (SSDL) of the Georgia Institute of Technology in the United States is an academic research institute developed in recent years to focus on the conceptual design of space vehicles. In recent years, this laboratory has also proposed a variety of conceptual design schemes for air-breathing reusable launch vehicles, such as Argus, Hyperion, Stargazer, Starsaber, etc., and has also developed some theories and methods of overall conceptual design.

At the end of the 20th century, Russia carried out research on two air-breathing reusable space launch vehicle schemes: the Tu-2000 scheme with a single stage into orbit and the MIGAKS with a two-stage orbit. In Russia's ORYOL-2-1 research program, design analysis and experimental studies of propulsion systems were carried out for both schemes. In recent years, Japan's JAXA has also carried out conceptual research on the concept of a two-stage orbital air-breathing space launch vehicle, and a large number of ground tests have been performed on the air-breathing turboramjet-ramjet-cycle (ATREX) engine used in its air-breathing engine, and the concept of a single-stage orbiting space shuttle using RBCC as a propulsion system has also been proposed. The Future European Space Transport Research Programme (FESTIP) is one of the largest research programs for reusable space launch vehicles in Europe in recent years. As many as 16 conceptual designs have been proposed in this research program, among which FSSC12 is a two-stage orbital breathing reusable space launch vehicle.

The shape design of foreign air-breathing reusable space launch vehicles is diverse. These designs can be broken down by four main shape types, namely lifting body, wing-body combination, axisymmetric cone, and wing-body fusion. The lifting body is the fuselage of the aircraft as the main lifting surface, and the tail is only used as the aerodynamic control surface, which is mainly used for single-stage and two-stage space launch vehicles for horizontal take-off and landing and horizontal landing, which is also the most typical air-breathing reusable space launch vehicle shape; the United States has undertaken a large number of ground wind tunnel tests with X-43A as its test vehicle, and successfully carried out flight tests. The wing-body assembly is basically the same as the layout of an aircraft, the fuselage is combined with the wing, and the engine is hoisted under the fuselage or on/under the wing, which is mainly used for two-stage space launch vehicles with horizontal take-off and horizontal landing capabilities.

The idea of an axisymmetric cone is to maximize the capture of incoming air in the intake tract and thus increase thrust, which is usually vertically launched due to the limited aerodynamic lift. To a large extent, the wing-body fusion is similar to the design concept of the waverider, which increases the lift by enclosing the high-pressure gas on the lower surface of the fuselage, but often the complete design of the waverider will make the effective volume of the aircraft too small, and the structure is difficult to realize, so it has no practical application value.

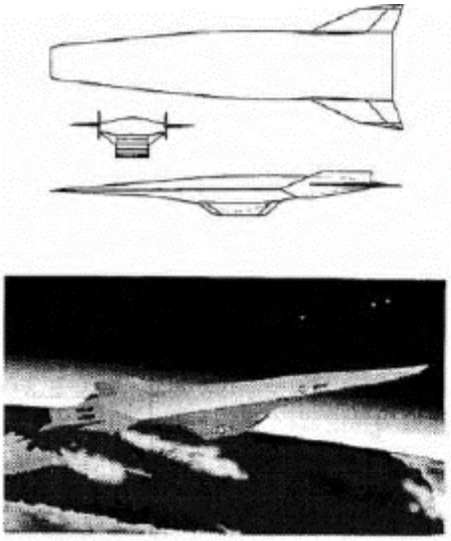

(a) The concept and scheme of the U.S. DF-9

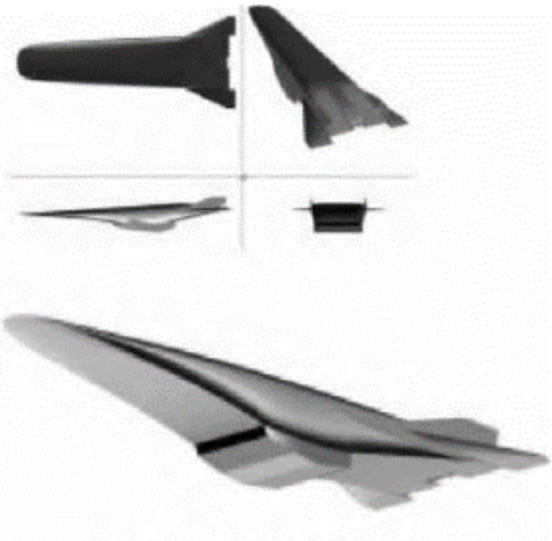

(b) American ABLV-4 conceptual design scheme

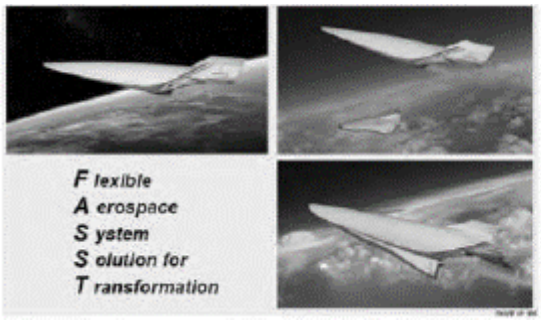

(c) Boeing conceptual design

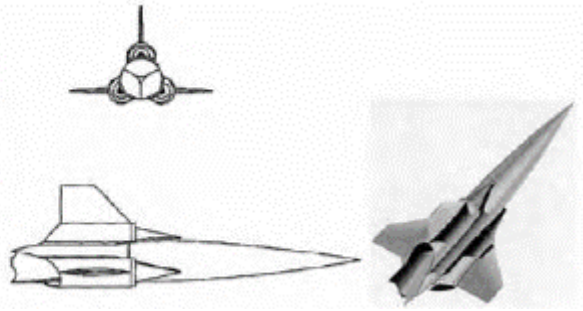

(d) Trailblazer conceptual design in the United States

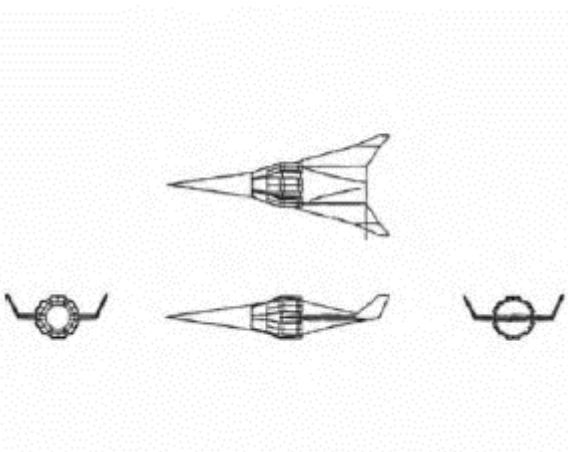

(e) U.S. asymmetric single-stage orbit entry conceptual design scheme

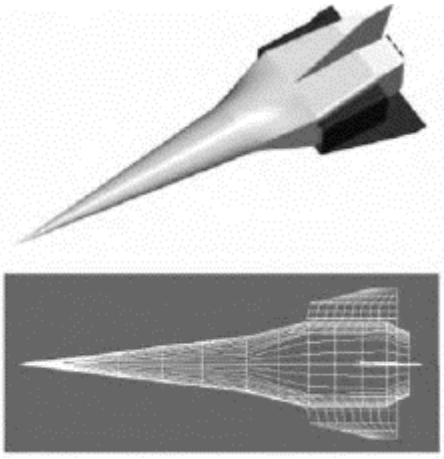

(f) U.S. XCALIBUR conceptual design

Figure 1-2: Conceptual design scheme of foreign reusable space launch vehicles

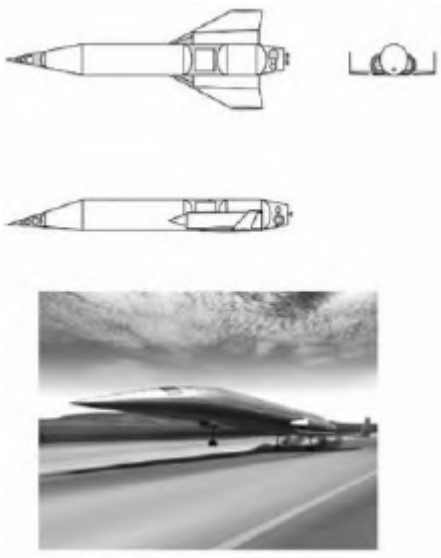

(g) U.S. Argus Conceptual Design Scheme

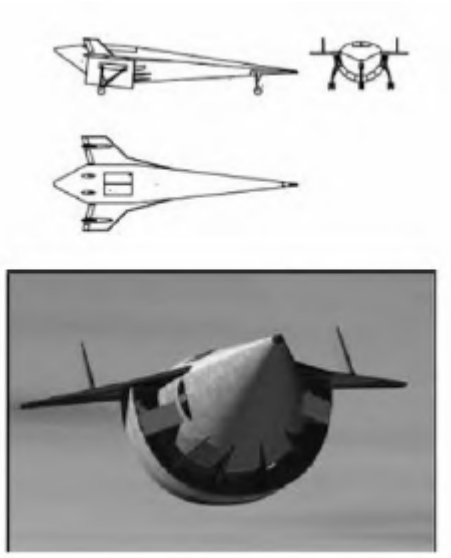

(h) U.S. Hyperion Conceptual Design Scheme

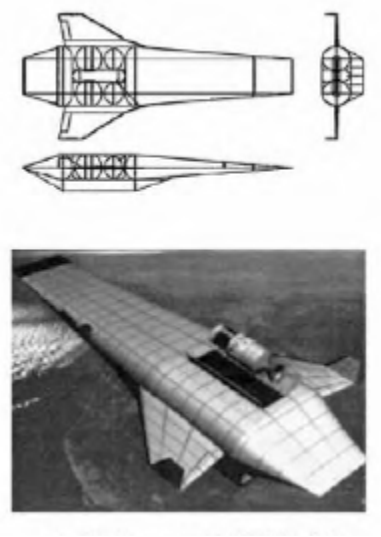

(i) U.S. Stargazer conceptual design scheme

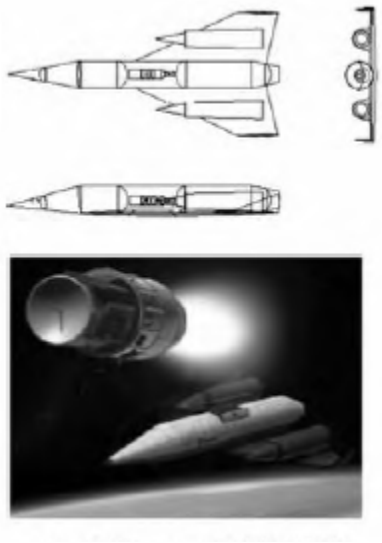

(j) Starsaber conceptual design scheme

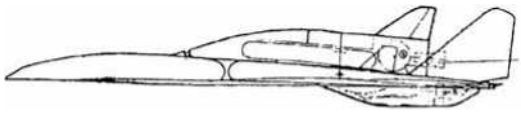

(k) Russian MIGAKS two-stage orbit entry concept design (l) Russian Tu-2000 single-stage orbit entry concept design

Figure 1-2: Conceptual design scheme of foreign reusable space launch vehicles (continued)

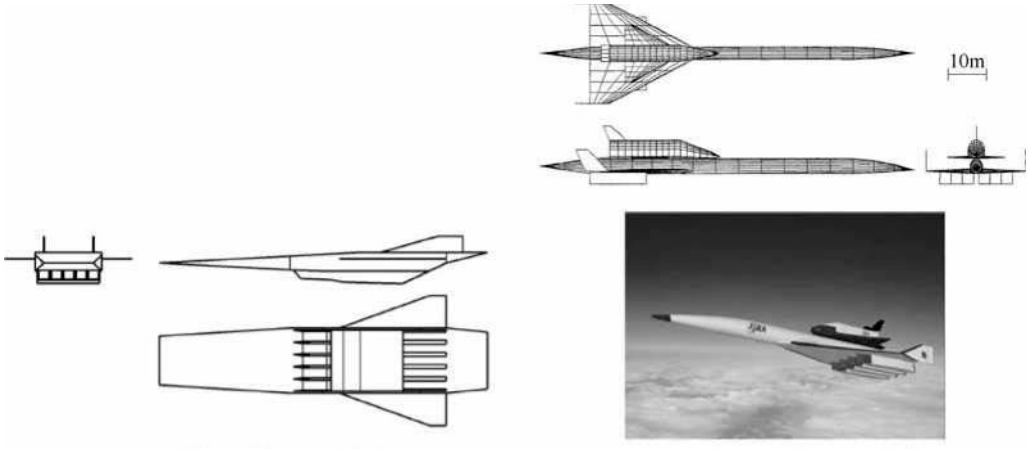

(m) Japanese single-stage orbital aerospace aircraft program (n) Japanese two-stage orbital aerospace aircraft program

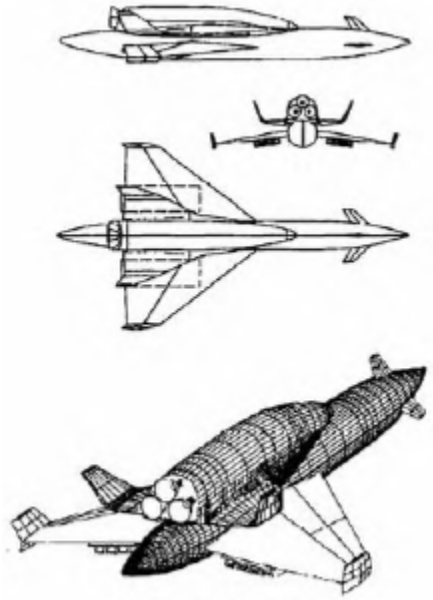

(o) European Aerospace 6 programme

Figure 1-2: Conceptual design scheme of foreign reusable space launch vehicles **(**continued**)**

Therefore, Boeing's FASST (Flexible Aerospace System Solution for Transformation) space launch vehicle adopts the shape design of wing-body fusion, which is a good compromise application form of waverider design. As shown in Figure 1-3, the shape scheme of the air-breathing aerospace aircraft is described in the form of a "matrix." The right side is two extreme design schemes, the left side is the traditional fuselage plus wing aircraft shape design, the engine is hung under the wing, has good cruising performance, so it is called the cruising shape; the right side is the axisymmetric conical design adopted for obtaining the maximum air capture flow, the maximum thrust that the breathing engine can provide is proportional to the air capture flow that can be captured, so this shape scheme has better acceleration performance, so it is called the acceleration shape. Considering the influence of the flight angle of attack of the aircraft on the engine performance and the required lift during reentry and return, the axisymmetric vertical take-off scheme cannot meet the needs of the air-breathing space launch vehicle. For the application of a single-stage space launch vehicle, the aerodynamic shape should take into account both acceleration performance and lift performance, so the lift-body configuration, wing-body fusion configuration, and semi-conical configuration are the main shape research objects.

For the application of the space launch vehicle as a two-stage orbit entry vehicle, the selection of the separation point is a crucial influencing factor, for the Mach number of the two-stage orbit separation of $Ma = 4$, the first stage can be regarded as a high-altitude and high-speed launch platform, and its shape can adopt the aircraft-like shape layout of the wing-body combination. However, for the higher separation Mach number, the acceleration role of the first stage is more important, so the influence of its shape on acceleration performance should be considered, and the principle of shape selection is similar to that of the single-stage orbit scheme.

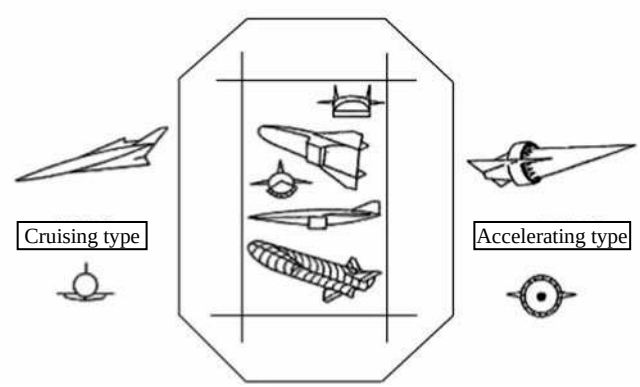

Figure 1-3: Aerospace aircraft design matrix

The propulsion system of air-breathing space launch vehicles can be divided into two categories: rocket-based combined cycle engines (RBCC) and turbine-based combined cycle engines (TBCC). The working Mach number of the RBCC combined cycle engine in the atmosphere can be from 0 to 15, and the rocket working mode can be used until the launch vehicle enters the space orbit, so the RBCC combined cycle engine has a large flight speed range adaptability and can be used for single-stage orbit space launch vehicle and the first stage of two-stage orbit space launch vehicle. The TBCC combined cycle engine, which adopts a turbojet engine below Mach number 4 or 4.5, and then adopts the ramjet/scramjet working mode, is usually used as the first-stage power propulsion system of a two-stage orbiting space launch vehicle, and can also be used as the propulsion system of a single-stage orbiting space launch vehicle if it is combined with a plug nozzle engine installed at the tail of the aircraft. RBCC can achieve four modes of work in a common flow channel, while TBCC needs to arrange the flow channel of two working modes of turbojet and ramjet, and there are great limitations in the internal layout of the aircraft, so another propulsion system scheme is that the first stage of the two-stage orbiting space launch vehicle adopts a turbojet engine, and the second stage can use a ramjet/scramjet engine, or a liquid rocket engine as the power propulsion system. A high Mach number turbojet engine is the key technology of TBCC, but also the technical basis of whether this power propulsion system is feasible, the focus of research is to expand the working range of the turbojet engine, one of the research ideas is to install a liquid injection system in the front of the compressor of the turbojet engine, so that the temperature of the air flow drops. The maximum working Mach number of this pre-cooled TBCC engine can reach 6. In 1986, Japan proposed the concept of an air-breathing turbojet expansion cycle engine (ATREX) and has completed a series of ground tests with satisfactory results, and the flight test program is underway.

Thermal protection systems are another key technology for reusable space launch vehicles. There are three main types of thermal protection systems for breathing reusable space carrier gas: active thermal protection systems, semi-active thermal protection systems, and passive thermal protection systems. In the active heat protection scheme, all or most of the heat is taken away by the working fluid or cooling flow (a small part may be reflected), so that it is blocked and cannot be transmitted to the secondary structure, three cooling methods can be used: sweat cooling, film cooling and convection cooling. In the passive heat protection scheme, heat is radiated or absorbed from the surface, and the working fluid (working fluid) is not required to remove the heat, and it can adopt three heat protection structures, which are heat sink structure, thermal structure and heat insulation structure.

The semi-active heat protection scheme is between the passive heat protection scheme and the active cooling scheme, most of the heat is carried away by the working fluid or air flow, and it can adopt two structural forms, in turn heat pipe structure and ablation structure. The structure and technology of the active heat protection system are more complex and technically difficult, while the passive heat protection scheme has a simple structure, reliable technology, and is easy to realize, so a large number of experimental studies have been carried out in various countries.

1.2.2: Hypersonic aircraft

In February 1986, U.S. President Ronald Reagan announced the "Orient Express," the space plane X-30, in his State of the Union address (Figure 1-4). In addition to its use as a new generation of space transportation, it also describes its promising application as a hypersonic aircraft, that is, at a cruising altitude of 30km, it can fly continuously for 12,000 km at 5 times the speed of sound, and it takes only 2 hours to cross the Pacific Ocean from New York, USA to Tokyo. But this assumption ended with the failure of the NASP program. The Aurora hypersonic aircraft (Figures 1-5) has maintained its mysterious appearance for many years, but the existence of the vehicle has been denied by US officials, and there are no relevant technical reports in the academic literature.

Figure 1-4: The “Orient Express” in the U.S. NASP plan

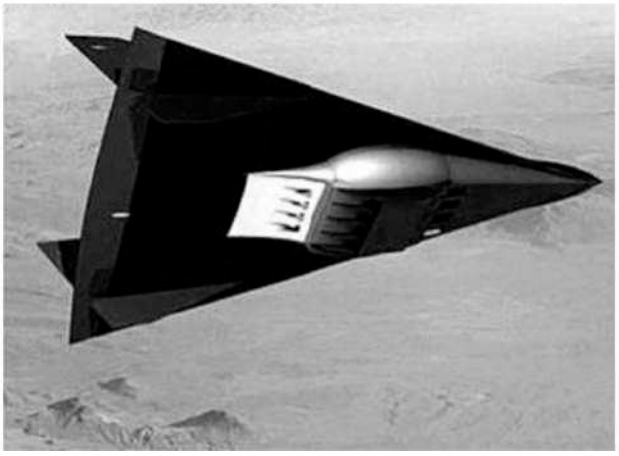

Figure 1-5: “Aurora” hypersonic aircraft

Whether it is the unrealized "Orient Express" or the mysterious "Aurora" hypersonic aircraft, from one side, it reflects a kind of military strike force that the U.S. military has been trying to develop, that is, "global arrival, global strike." In August 1996, in a research report submitted to the U.S. Air Force on the future (2025) combat system, the hypersonic weapon platform: S3 concept was proposed, that is, the Supersonic/Hypersonic Attack Aircraft (SHAAFT) and Standoff Hypersonic Missiles with Attack Capability (SHMAC) and Space Control with a Reusable Military Aircraft (SCREMAR) are all-in-one weapons platforms. The platform enables the U.S. Air Force to deliver a decisive blow to the enemy at the beginning of a war to deter the enemy's attempts to delay the war; when a procrastination war is unavoidable, to strike the enemy's time-critical targets with weapons at a reasonable cost to establish a defense zone advantage; and to enter space easily and flexibly. Among them, the SHMAC has the ability to quickly and accurately attack the target and will not be intercepted; the flight Mach number can reach 8 and can be launched in a variety of ways, such as hypersonic aircraft, low-speed conventional aircraft, maritime vertical launch systems, or from ground launch stands. With this missile, the United States can be guaranteed control in the theater; the Mach number of the SHAAFT flight can reach 12, thus ensuring that it can reach any point on the earth within 2 to 4 hours, and has the ability to reach and attack globally, and SCREMAR has the ability to enter space conveniently and flexibly.

The Mach 10 dual-fuel hypersonic cruise aircraft (Figure 1-6) is a detailed hypersonic aircraft design study carried out by Boeing and NASA. The aircraft scheme largely inherits the research results of the NASP program, using a lifting body configuration, a low-speed propulsion system using four Pratt & Whitney Ace-TR turbojet engines, a high-speed propulsion system of three P&W-developed ramjet/scramjet engines, and a low-speed and high-speed propulsion system flow channel integrated into the aircraft by way of upper and lower arrangement. A plug nozzle engine is installed at the tail of the aircraft, which can be used to increase thrust during maneuvering flight. Another scheme of propulsion system is the RBCC rocket-based combined cycle engine. Research on structural materials, thermal protection systems, and fuel supply systems was also carried out for the aircraft.

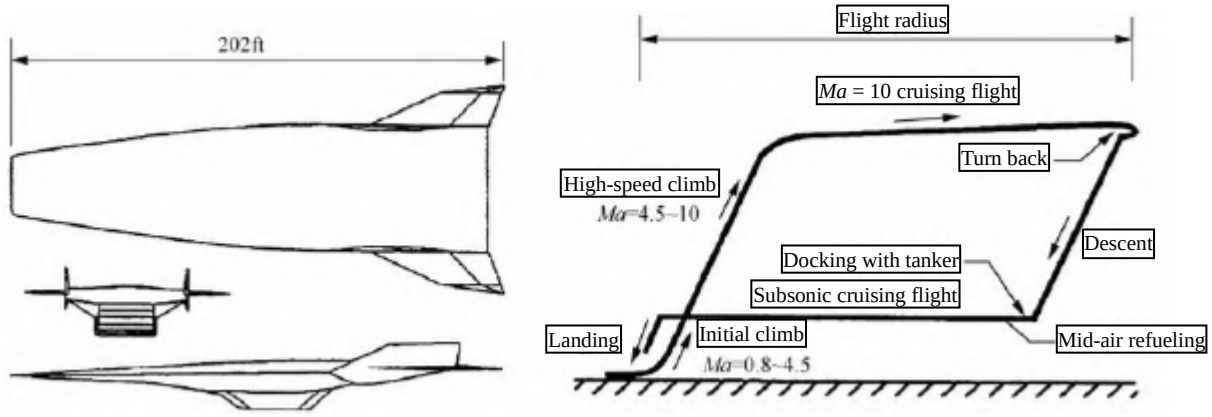

Figure 1-6: DF Hypersonic cruise aircraft and its flight trajectory

The U.S. military also proposed a design scheme for a hypersonic aircraft with a jumping flight trajectory (Figure 1-7), the flight trajectory changes periodically according to the climb-dive, climbing to the low-density atmosphere can reduce aerodynamic heating, and jumping and diving can save fuel, so it is compared with ballistic missile trajectory, iso-altitude hypersonic cruise flight trajectory, and iso-altitude subsonic cruise flight trajectory. It is believed that the periodic hypersonic flight trajectory has superior "global reach" capabilities and can improve the load performance of the aircraft.

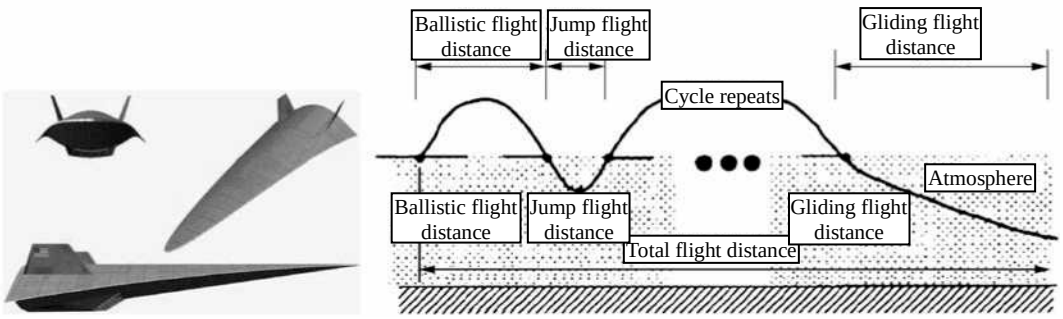

Figure 1-7: Hypersonic Angle jumping trajectory hypersonic aircraft

1.2.3: Hypersonic cruise missile

Since the end of the 20th century, the United States has launched a number of hypersonic cruise missile technology development programs to achieve its global combat goal of "strike time-critical," such as the ARRMD program and the HyFly program of the US Defense Advanced Research Projects Agency, and the HyStrike program of the U.S. Navy.

The HyFly program was launched in 2002 by the Defense Advanced Research Projects Agency (DARPA) in conjunction with the U.S. Navy to develop and test demonstration of a ramjet-powered cruise missile with Mach 6 or more. The main contractor for the HyFly missile is Boeing, and Aerojet manufactures its main engine. The HyFly missile is carried by the F-15E aircraft for air launch, after which it is accelerated by a solid rocket booster to the ignition working speed of the ramjet engine. The main engine of the HyFly is a dual-combustion ramjet engine (DCR), which is designed with two different complex intake tract systems that can work in the mode of a conventional ramjet engine with subsonic combustion or in the mode of a scramjet engine under a hypersonic vehicle. In addition, the engine uses a general hydrocarbon fuel, i.e., JP10, which is more convenient to use than cryogenic fuel (liquid hydrogen). The concept of DCR was developed by the Johns Hopkins University Applied Physics Laboratory. In May 2002, APL successfully tested the HyFly engine with a simulated flight Mach number of 6.5 and an altitude of 27,400m in the wind tunnel. To evaluate the flight of the fuselage at high speeds before real flight tests, a ground-launched unpowered HyFly scaled-size missile was carried out. The test was conducted by ATK and was boosted to Mach 6 at an altitude of 18,300 m by a two-stage Terrier-Orion sounding rocket. Subsequent tests were carried out in HyFly's sub-program FASTT (Free-Flying Atmospheric Scramjet Test Technology). FASTT achieved its planned objectives in December 2005 when the aircraft with a true DCR scaled engine was launched and flew for 15 seconds at 19,200m at 5,815 km/h (*Ma [Mach]* = ~5.5) in scramjet mode. Aerojet conducted ground trials of a full-scale DCR engine, simulating the ignition operation of the ramjet engine at *Ma* = 3 to 4 after the booster work was completed. The first HyFly free-flight test was conducted on January 26, 2005, with an F15E aircraft carrying an unpowered bomb body. The flight successfully tested separation from the carrier aircraft and basic guidance and control functions. In the second test on August 26, 2005, the Hy-Fly booster accelerated the vehicle to *Ma* = to 3, testing the ability of boost-boosting acceleration. Three more tests are scheduled to be completed by the end of 2007, culminating in the acceleration of the ramjet main engine of the test HyFly to *Ma* = 6 (Fig. 1-8).

Figure 1-8: Schematic diagram of the ship-launched HyFly hypersonic missile

In early 2003, the U.S. Air Force Research Laboratory (AFRL) launched a program called EFSEFD (Flight Demonstrator Program for Endothermic Fuel Scramjet Engines) to test the SED-WR (Scramjet Demonstrator – Waverider) flight demonstrator. The program continues the earlier DARPA research component of the ARRMD (Advanced Rapid Response Missile Demonstrator) program. In January 2004, AFRL selected Boeing and P&W, respectively, to manufacture the fuselage and engine for the SED-WR flight tester. In September 2005, the vehicle was officially designated X-51A (Figure 1-9).

Figure 1-9: Conceptual design of the X-51A

The X-51A will be launched from the air, powered by a hydrocarbon-fueled scramjet engine. The engine has been developed by P&W since 2000 in AFRL's HySET (Hypersonic Scramjet Technology) program, which is part of the U.S. Air Force's overall HyTech program. The prototype engine GDE-1 (Ground Demonstration Engine No. 1) has been tested on the ground in September 2002 and June 2003, simulating *Ma* = 4.5 and 6.5 flight speed. Initially, AFRL planned to test P&W's engines on NASA's X-43C vehicle, but this was canceled in March 2004.

The X-51A will be carried by B52 aircraft up to 10,700m and accelerated by the solid rocket-booster engine of the MGM-140 ATACMS missile (0.61m in diameter and about 2m in length) to a scramjet ignition starting speed of *Ma* = 4.5. The target velocity of the X-51A is in the *Ma* = 6 to 7 range. Since the HyFly uses an axisymmetric projectile, it is necessary to have a certain flight angle of attack in order to obtain a certain lift, but this will also deteriorate the working performance of the air intake. The X-51A adopts a lift-body configuration with the characteristics of a wave-riding body, with good angle of attack characteristics and a large lift-to-drag ratio, which is more suitable for use as a cruise aircraft. From a power point of view, the HyFly uses a dual-combustion scramjet engine, while the X-51A uses a dual-mode scramjet engine, and the former has a limited flight speed range, which can only reach a maximum of *Ma* = 6.5, the latter can reach *Ma* = 7, and the structure is also more suitable for high-speed flight, and the X-51A also has more advantages in terms of impulse. From relevant public reports, the length and mass of the X-51A cruising segment, as well as the total length and total mass of take-off, the length of the MGM-140 ATACMS missile solid booster is about 2m, and the mass is about 1,000kg. Taking into account the length and mass of the connector between the booster and the cruiser, the above parameters basically coincide. The flight range is 600nm, which is about 1,100km. The basic coefficients for X-51A are shown in Table 12.

Table 1-2: Basic parameters of the X-51A

Project	Cruise		Launch		Booster rockets
Length	14ft	4.267m	26ft	7.925m	Approx. 2m (0.61m diameter)
quality	1,400lbs	635kg	4,000lbs	1,814kg	About 1,000kg

Note: 1ft = 3.048×10^{-1}m, 1lb = 0.453592 kg, the same below.

The X-51A is powered by a scramjet engine developed in the HySET program and has already undergone ground tests. The minimum test Mach number was 4.5, so it is possible that the X-51A was accelerated by a solid booster rocket to *Ma* = 4.5 and then started a scramjet engine. The basic structure of the PDE and PTE engines for ground testing is two compression surfaces, a self-starting air intake, an isolation section with a small expansion angle, a combustion chamber, and a single-wall expansion nozzle, and the engine width is 6 inches (about 15.2 cm) due to the limitations of the ground test equipment. Since the X-51A is already listed as one of the X-series test vehicles, it is most likely to develop into a prototype of a hypersonic cruise missile.

1.3: The development process of foreign hypersonic vehicle technology [26~34]

1.3.1: A brief history of the development of foreign hypersonic vehicle technology

The development of hypersonic vehicle technology began with the research of supersonic combustion (scramjet) and scramjet engines. In the 1950s, research focused on the conceptual and basic problems of scramjet, verified the feasibility of combustion in supersonic flow, and analyzed the main technical obstacles to the realization of scramjet engine. In 1958, Ferri experimentally proved that stable combustion without strong shock wave could be achieved in a supersonic flow of *Ma* = 3, which set off a boom in supersonic combustion research, and the research on supersonic combustion mechanisms and the development of model engines were widely carried out.

In the 1960s and mid-1970s, the research on hydrogen-fueled scramjet engines, which focused on hypersonic test vehicles as the application background, was the first peak of the development of scramjet technology. In 1964, NASA began the Hypersonic Research Engine (HRE) program with axisymmetric structures, and from 1962 to 1978, the U.S. Navy funded the Applied Physics Laboratory at Hopkins University to develop the Scramjet Missile (SCRAM) program. The ESOPE research program was carried out in France. During this period, a large number of research results have been obtained in the ignition auxiliaries, accelerants, various nozzle structures, fuel injection methods, combustion chamber configurations and their interaction with the intake tract of scramjet engines.

From the mid-to-late 1970s to the mid-1980s, the research on intercontinental missiles powered by rocket engines occupied a large amount of technical resources and research funds, and the investment in research manpower and research funds was relatively small, and the research on air-breathing hypersonic vehicle technology during this period was relatively silent.

From the mid-to-late 1980s to the mid-1990s, a new round of research on hypersonic vehicle technology was set off by the National Aero-Space Plane (NASP) program of the United States, and at the same time, the Sänger research program (1988-1995) was carried out in Germany. However, in the process of implementing the above two plans, they encountered a series of technical, financial, and managerial difficulties, and were forced to discontinue one after another. At this time, after a long period of technology accumulation in Russia, CIAM began to carry out flight demonstration and verification tests of axisymmetric engines, and from 1991 to 1998, four tests were carried out, and a large number of valuable combustion data of bimodal scramjet engines were obtained.

Since the late 1990s, hypersonic vehicle technology has entered a period of comprehensive and rapid development, and many countries have carried out the development of model engines, especially the United States has entered the stage of engineering prototype development. NASA has carried out the hypersonic vehicle test program Hyper-X program, the Air Force has carried out the hypersonic technology HyTech program, and the Navy has implemented the hypersonic flight HyFly program. In March and November 2004, the X-43A, a test prototype of the Hyper-X program, successfully achieved a controlled flight with Mach numbers of 7 and 10, marking the official transition of hypersonic vehicle technology from the laboratory stage to the engineering development stage. France has launched the PREPHA program and the Promethee program, the purpose of which is to develop a dual-mode ramjet engine suitable for the use of liquid hydrocarbon fuel in the hypersonic range.

This kind of engine uses liquid kerosene as fuel and makes use of kerosene's high bulk density and excellent transportation and storage performance, which reduces the cost of logistics support and the cost of weapon systems, and makes the weapon have strategic and tactical mobility. The University of Queensland in Australia has launched the HyShot program, which aims to conduct research on supersonic combustion performance. India proposes the AVATAR program. Japan has also proposed the Hope-X program, which aims to develop a space-to-earth round-trip reusable launch vehicle.

1.3.2: Development trends of flight tests of foreign hypersonic vehicle technology [35]

Scramjet engine is the primary key technology of hypersonic aircraft, and the research in the field of hypersonic vehicle technology in all countries around the world is mainly focused on the development of scramjet engine. A large number of principle research, numerical simulation research and ground wind tunnel test research have been carried out, and a large number of research results have been obtained, which fully proves the feasibility of scramjet engine. However, in order to move towards practical application as a power plant for hypersonic vehicles, the flight test of the scramjet engine is an inevitable stage. In addition, the development of scramjet engines also needs the three means of numerical simulation, ground tests, flight tests to cooperate with each other to carry out research and development work, numerical simulation, and ground tests need flight tests to verify and test, and flight tests also need numerical simulation and ground tests to reduce test risk, cost, and analysis of phenomena, problems, in order to further improve.

Up to now, the world's major countries that carry out hypersonic vehicle technology research, including Russia, France, the United States, Australia, the United Kingdom, and Japan, have successively carried out flight test research on scramjet engines independently or in the form of international cooperation. The following is a brief summary of the flight tests that have been carried out abroad.

1. Russian Kholod flight tests

Russia was one of the first countries to carry out flight tests of scramjets, known as Project Khlod from 1991 to 1998 (Figures 1-10). The "Cold" program is carried out in cooperation with the Central Institute of Aviation Motors (CIAM) and the Central Research Institute of Aerohydrodynamics (TsAGI) of Russia. The test model was an axisymmetric subsonic/scramjet engine with liquid hydrogen fuel. The test vehicle uses the long-range medium-altitude surface-to-air missile system SA-5, which has been decommissioned, and has been modified to serve as a carrier for flight test models. On November 27, 1991, the first flight test was carried out at the shooting range near the Baikonur Space Center, during the flight time, the subsonic combustion/scramjet engine was programmed to complete two independent pre-programmed combustions, the first lasting nearly 20 seconds, starting at an altitude of 18 km at Ma = 3.5 and ending at an altitude of 28 km at $Ma = 6$; the second time, which lasted for nearly 10 seconds, from an altitude of 22 km, Ma = $4$5 starts at an altitude of 1 8km, Ma = 35 ends. Flight tests enabled the conversion of ramjet engines from subsonic combustion mode to supersonic combustion mode, an event of great significance in the field of modern engine technology.

In the subsequent Kholod program, Russia conducted two flight tests in 1992 and 1995, in cooperation with France, and two tests in 1997 and 1998, in cooperation with the United States. The purpose of the joint U.S.-Russian experimental research is: to verify the results of basic theoretical research; verification of the constructed mathematical model, software, and correction system; achieve supersonic combustion; calculate thrust; increase awareness of the complexity of flight tests; and to compare test equipment and test technology levels between the two countries. The Russian-American joint flight test obtained valuable flight data on subsonic combustion and supersonic combustion in the range of Ma = 3.5 to 6.45 and quite high dynamic pressure flight conditions, which provided valuable information for the design of the Hyper-X test vehicle in the United States.

Figure 1-10: Russian Kholod flight test system

2. Russian IGLA flight tests

Unlike Kholod, which is scheduled to conduct only supersonic combustion tests, the IGLA is a winged hypersonic test vehicle (Figs. 1-11). The flight test program is one of the most important Russian research projects in the field of hypersonic in recent years. The test vehicle adopts a lift body configuration, which is similar to the shape of the Buran space shuttle, with a head radius of 40 mm. Three scramjet engines are suspended under the fuselage of the test aircraft, and the model of the test ramjet engine is a two-dimensional dual-modal regenerative cooled scramjet engine, and the air intake duct and tail nozzle are located under the fuselage.

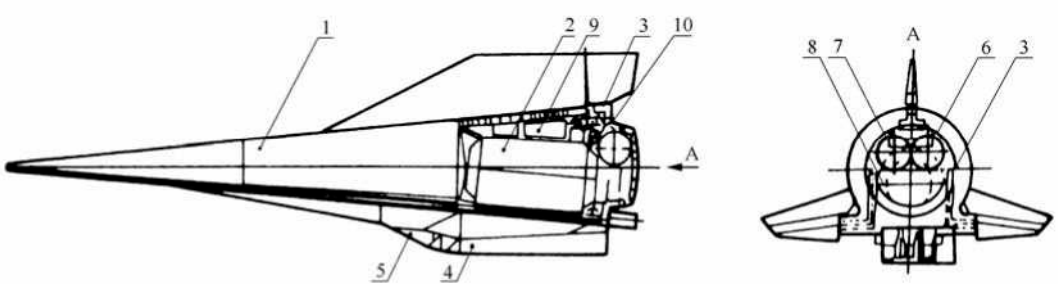

Figure 1-11: Russian IGLA test vehicle

1. Hypersonic test vehicle, 2. Liquid hydrogen fuel tank, 3. Rudder assembly, 4. Scramjet engine, 5. Tail; 6. Spherical ammonia cylinder, 7. Spherical helium cylinder, 8. Recovery umbrella bag, 9. Telemetry system equipment, 10. Pressurized feedback system

The planned course of flight tests was the installation of the IGLA test vehicle in the position of the warhead of the SS-19 missile; after being ready for launch, the SS-19 launch system was launched vertically; at an altitude of 80 km, it reaches a speed of 5,900 m/s. The IGLA test vehicle was separated from the SS-19 launch vehicle. Subsequently, the hypersonic test vehicle flew in the following four stages: in the first stage, the test vehicle separated from the SS-19 operator first reduced its altitude at a certain dive angle and turned into a taxiing state at a high altitude with high atmospheric density; in the second stage, adjust the attitude, roll, yaw and azimuth angle are zero, and maintain the cruising level flight state; in the third stage, the scramjet model test is carried out according to the given flight conditions; in the fourth stage, the scramjet engine is recovered and landed after combustion, and the test is completed. The entire test range was 6,000 to 8,000 km, and the flight speed was Ma = 12 to 14 when entering the third stage.

Scramjet ignition test at *Ma* = 10. Two flight tests were carried out in June 2001 and February 2004, but there were no detailed public reports. The project aims to develop a power system that can be used for hypersonic cruise missiles, and this power system can also be used for experimental research of military aircraft and space-to-earth shuttle systems.

3. American X-43A flight tests

The purpose of the X-43A Flight Demonstration Validation Flight Test is to collect flight test data to verify the performance and maneuverability of an integrated, hydrogen-fueled/dual-modal scramjet engine, and to demonstrate the flight of a controlled-powered and uncontrolled-powered hypersonic vehicle. The X-43A test vehicle is 3.66 meters long and 1.53 meters wide, with a flight Mach number of 7 to 10. The X-43A is boosted by a Pegasus rocket, dropped at 5.2 to 13 km, and then accelerated to test conditions with a booster rocket, and the booster is separated from the X-43A. After separation, in the powered flight test section, the scramjet engine works for 5 to 10 seconds, and performs hypersonic flight under its own power.

The X-43A uses a lift-body configuration with control surfaces at the rear of the fuselage, including a full-motion horizontal tail and dual vertical tails and rudder (Fig. 1-12). The shape design is based on the conceptual design of the aircraft with Mach 10 hypersonic cruise carried out in the United States in the late 1990s. In order to reduce drag, the leading edge of the aircraft is designed to be sharp, and the control surfaces are correspondingly thin. The lower part of the front fuselage is designed to provide an external compression slope for the scramjet intake, while the lower part of the rear fuselage is designed to provide a surface for further expansion of the nozzle. The upper surface of the fuselage has a gentle curvature, and the front section of the fuselage contains large chunks of ballast, so that the center of gravity of the aircraft is high enough to provide sufficient longitudinal stability. The fuselage truss and partitions of the aircraft are made of steel, titanium, aluminum, and other materials, and are covered with steel and aluminum skin. These materials are determined by the hardness requirements of the aircraft, while titanium is chosen for the tail compartment due to the need for thermal protection. For trim requirements, a solid tungsten wedge weighing about 392 kg was used in the front compartment. The X-43A body is thermally protected by a carbon-carbon leading edge (wrapped around a tungsten wedge to form a side strip), and the upper and lower surfaces are covered with reinforced alumina heat-resistant porcelain tiles.

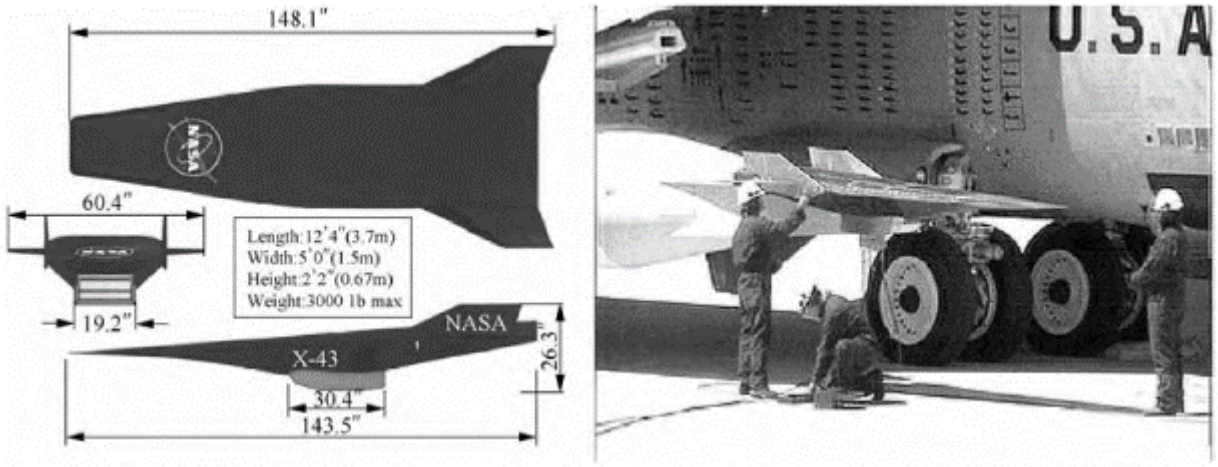

Figure 1-12: X-43A Hypersonic test vehicle

On June 2, 2001, the X-43A conducted its first flight tests, which failed due to a malfunction of the booster. After two years of analysis of the cause of the crash, the X-43 Accident Investigation Commission submitted an accident analysis report in July 2003 and resumed the follow-up flight tests of the X-43A. In March and November 2004, NASA conducted the second and third flight tests of the X-43A, and the tests were successful, with Mach numbers of 6.8 and 9.68 respectively, setting a record for humanity's highest speed of a vehicle in the atmosphere.

4. HyFly flight test in the United States

The scramjet engine of the X-43A test vehicle uses hydrogen fuel, and as an application of hypersonic cruise missile, the U.S. military hopes to use hydrocarbon fuel that is stable and easy to maintain, and can meet the requirements of a single fuel on the battlefield, that is, JP10 is used as the fuel for scramjet engine. Therefore, the Defense Advanced Research Projects Agency (DARPA) and the US Naval Research Office, launched the HyFly hypersonic demonstrator project. The contractors of the project include Boeing and ATK. The aim of the project is to develop key technologies for hypersonic cruise missiles that can be launched by surface ships, submarines, and aircraft.

The goal of the program is to use flight tests to validate a 1,100 km range hypersonic missile with a range of up to 1,100 km, powered by a liquid hydrocarbon-fueled scramjet engine, with a Mach number of 6, a cruise altitude of 27 km. The missile is powered by a dual-combustion scramjet engine (DCR), adopts an axisymmetric shape, has a body diameter of 0.5m, a second stage length of 4.3m, a first stage length of 5.8m, a launch mass of about 1,100kg, and can carry a 113kg warhead, mainly hitting moving targets and deep underground targets.

In January and August 2005, the HyFly test vehicle was tested by Boeing as an airborne version, but the purpose of the test was to verify the separation from the F-15E fighter-based aircraft and the ability of the booster to work (Figure 1-13). On 10 December 2005, the United States Navy conducted a ground-launched flight test at the flight test site in Wallops, United States. The flight test is also known as the Free-Flying Atmospheric Scramjet Test Technology (FASTT) program. The tests were successful, and the test vehicle was boosted by a two-stage Terrier-Orion solid rocket with a temperature of *Ma* = 55. The ignition work of scramjet engine is 15s, which is the world's first flight test of scramjet engine using hydrocarbon fuel. But the next few trials didn't go well. On September 25, 2007, HyFly conducted flight tests with the aim of demonstrating DCR ignition, fuel control, climb and acceleration to *Ma* = 5. In the flight test, after the booster was separated, the DCR was ignited, and due to a problem with the fuel supply system, the flight demonstrator only accelerated to *Ma* = 3.5, and the flight test failed. On January 16, 2008, HyFly conducted another flight test, which failed again due to a malfunction after the launch of the flight demonstrator.

The HyFly program's flight demonstrator is currently the closest to being engineered, and although flight tests have not been successful so far, the US military has not given up. In the course of the project, a number of key technologies such as the scramjet engine with dual combustion chambers, aircraft structure, and control system have been comprehensively verified, and a large number of test data have been accumulated.

Figure 1-13: The HyFly hypersonic test vehicle of the United States

5. American X-51A flight tests

The X-51A is mainly used to conduct flight tests of the endothermic hydrocarbon-fueled scramjet engine of the U.S. Air Force HyTech program, and at the same time to verify the feasibility of using this engine for long-term flight, with the following main objectives: (1) to collect ground and flight data of the actively cooled, autonomously controlled operation of the scramjet engine for understanding the physical phenomena mastered, and to develop and improve tools for the design of scramjet engines; (2) verify the feasibility of the scramjet engine of heat-absorbing fuel in flight state; (3) generate greater thrust to demonstrate the viability of a free-flying vehicle propelled by a scramjet engine; (4) to provide a technical basis for the development of long-range hypersonic cruise missiles with global rapid strikes, and then provide technical support for the US military to develop rapid and economic access to space.

The X-51A consists of two key components, the scramjet engine and the waverider vehicle (Fig. 1-14). In December 2004, the initial design review of the project was completed. The X-51A adopts a waverider design, with a maximum flight Mach number of 6, a maximum flight altitude of about 30km, a total length of 4.27m, a launch mass of about 1,700kg, a mass of about 670kg, and a power range of about 700km.

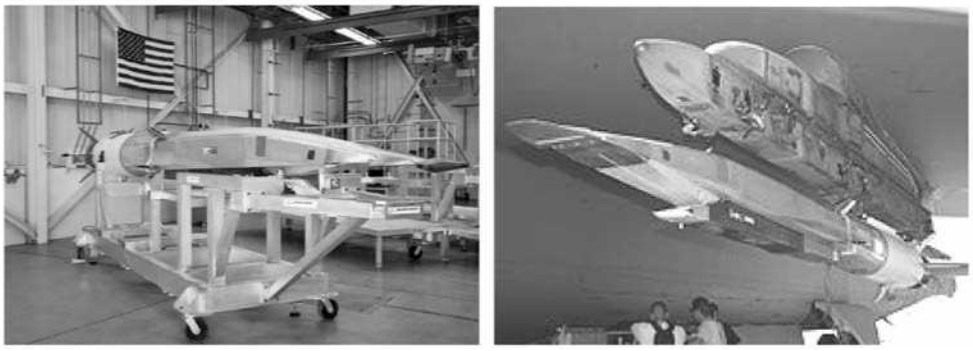

Figure 1-14: American X-51A hypersonic test vehicle

In the development of scramjet engines, Pratt & Whitney has successively developed performance test engines (PTE), ground demonstration and verification engines (GDE-1 and GDE-2), and SJX61 engines. The test objectives of the SJX61-1 (X-1) include demonstrating engine ignition, the X-51A closed-loop fuel system, the thermal and structural integrity of the engine and control hardware, and verifying the flow channel performance and operability required for the X-51A mission. The X2 engine is the flight engine of the X-51A, and a total of 8 ignition tests with Ma = 4.6 and 11 with Ma = 5 were conducted. The X2 test successfully demonstrated that the HyTech engine technology has a moderate level of risk and is capable of flight testing of the X-51A aircraft.

In terms of aerodynamic layout, a total of 15 rounds of improvement studies were carried out in 15 months from June 2004 to 2005, and for nine years, wind tunnel tests were carried out, and a flight aerodynamic database was obtained. In terms of structural thermal protection, the main body of the fuselage is made of conventional metal, the surface is covered with lightweight thermal protection foam and ceramic tiles, and the engine adopts active cooling.

On December 9, 2009, the first on-board flight test was completed, mainly to test the performance of the X-51A aircraft after being mounted on the B-52 bomber, as well as the performance of the aircraft's own telemetry device. The X-51A successfully conducted its first powered flight test on May 26, 2010, with a flight time of 200s and a flight Mach number of 5. Three tests of the same flight trajectory are planned for follow-up, and Boeing is proposing two additional flight tests for AFRL.

6. German SHEFEX flight test

Germany's Sharp Frontier Flight Test Project SHEFEX is a research and development project for reentry technology and hypersonic technology, which has been carried out by the German Aerospace Research Center (DLR) to conduct performance studies on a new type of re-entry vehicle composed of multiple planes with a sharp leading edge. SHEFEX used a new re-entry vehicle structure consisting of multiple planes with a sharp leading edge to test materials and structures, and compared the actual flight data collected with numerical simulations and ground test results to adjust and verify the validity of simulation tools and ground test results. The multi-planar structure of the head of the test vehicle in the project is particularly noteworthy and has become an important test platform for German reentry technology and hypersonic technology. The SHEFEX flight test program is a series of strategic plans that may eventually lead to hypersonic vehicles, platforms and technologies for space travel and microgravity research. At present, the flight test program mainly uses a modified sounding rocket engine system (which was used for microgravity research tests) to carry out high-efficiency flight tests in a short period of time.

On October 27, 2005, DLR successfully conducted the first flight test SHEFEX 1 of the pointed leading-edge shaped vehicle. SHEFEX 1 flew for 6s at a speed of 20 at $Ma = 20$ and obtained complete and valuable aerodynamic data. Following the success of the SHEFEX 1 flight test, preparations for the test of the SHEFEX 2 vehicle began (Figure 1-15).

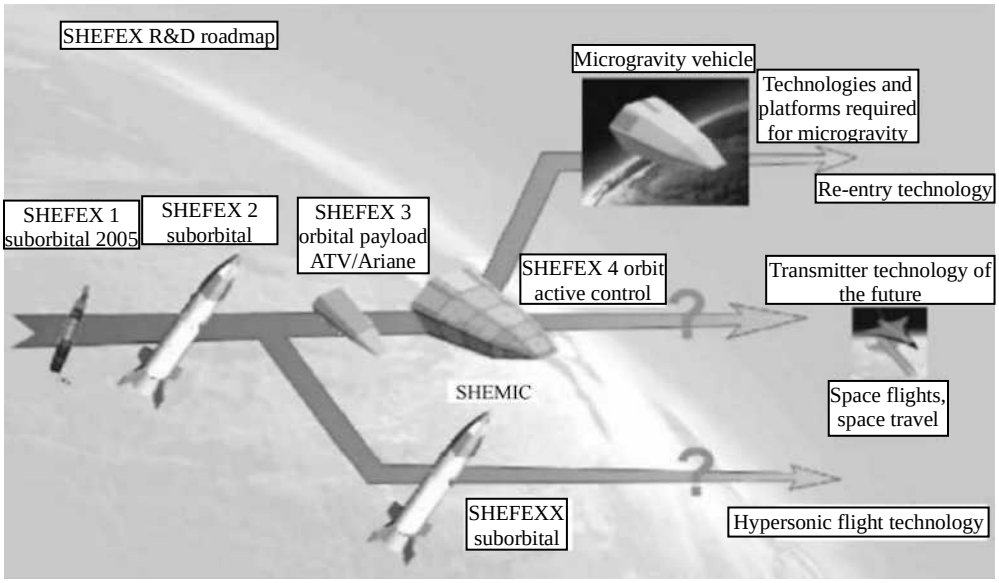

Figure 1-15: Strategic roadmap for the development of the SHEFEX flight test platform in Germany

7. Australian HyShot flight test

The HyShot program is an international cooperation program begun in the 1990s and is a successful example of international hypersonic technology cooperation. In this project, the sounding rocket has successfully carried out flight tests on a variety of hypersonic vehicle components (especially the propulsion system) developed by many countries, and obtained a large number of valuable test data, which plays an important role in promoting the research of hypersonic technology in the participating countries. The countries participating in the project are Australia, the United Kingdom, the United States, France, Germany, South Korea, and Japan.

The project is led by the University of Queensland in Australia, with participation and funding from the Australian DSTO, the Australian Department of Defence, the Australian Space Technology Command, the Australian Department of Industry, Scientific Resources, the Australian Space Research Institute, the Australian Research and Development Unit, the British QinetiQ Company, the British Defence Assessment and Research Agency, the United States NASA, the United States Air Force Scientific Research Office (AFOSR), the German Aerospace Center (DLR), National University of Korea, and the National Aerospace Laboratory (NAL) of Japan.

The program conducted a large number of ground tests, including sensor response time, structural integrity of individual components, vibration testing, shock testing, vacuum testing, and source code evaluation. The most important ground tests were the wind tunnel tests of the engines, conducted in the T4 shock wave wind tunnel at the Hypersonic Centre at the University of Queensland in Australia, which was upgraded in 2004 to simulate a flight of *Ma* = 10 at an altitude of 30 km. In order to ensure the success of the test (especially to ensure stability during re-entry), extensive aerodynamic tests were also carried out on the ground.

On October 30, 2001, the first launch test of HyShot was conducted at the Woomera Range in Australia, testing a two-dimensional combustion chamber engine designed by the University of Queensland, known as the HyShot-1. However, the experiment ended in failure. On July 30, 2002, the second launch test of HyShot was conducted at the Woomera range, using the HyShot-2 two-dimensional combustion chamber engine, and during the landing, the scramjet engine experienced a brief ignition combustion at a speed of *Ma* = 7.6. The trial was a success. Two more launch tests were conducted at the Woomera range on March 25 and 30, 2006, both of which were successful. On March 25, 2006, the HyShot-3 three-dimensional combustion chamber engine designed by the British company QinetiQ was launched, and on the 30th, the HyShot-4 engine developed by Japan was launched, with a mass of 100kg and an advanced fuel injector. Through the series of tests of HyShot, the technology of sounding rockets applied to hypersonic flight tests is becoming more and more mature. At the same time, with the progress of the project, the relevant facilities of the shooting range have been improved, and the level of data tracking, transmission, and processing has been greatly improved (Figure 1-16).

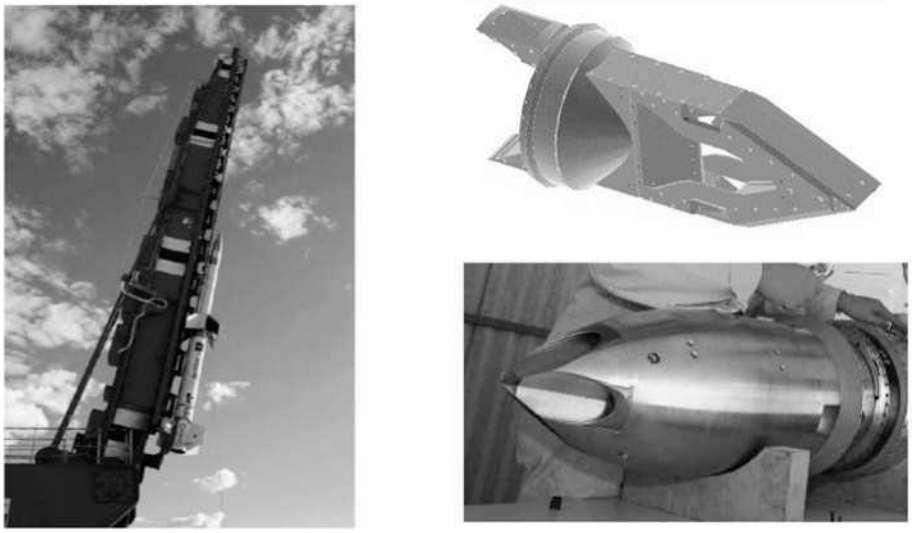

Figure 1-16: Australian HyShot flight test platform and various engine test models

8. HyCAUSE flight test conducted by the United States in cooperation with Australia

Hypersonic Collaborative Australia/United States Experiment (HyCAUSE) is a scramjet flight test project funded by DARPA, which was jointly carried out by researchers in the United States and Australia, beginning in April 2004. The program has developed a hypersonic vehicle scheme using an inward-turning inlet scramjet engine, which can be better integrated with the configuration of the wave-riding vehicle. The scramjet model (Fig. 1-17) was tested in the T4 wind tunnel of the University of Queensland in Australia and the LEN 1 wind tunnel of CUBRC in the United States, and the performance and operation ability of this type of hydrogen fuel engine under the condition of *Ma* = 10 were studied, covering a wide range of dynamic pressure to fuel equivalent ratios.

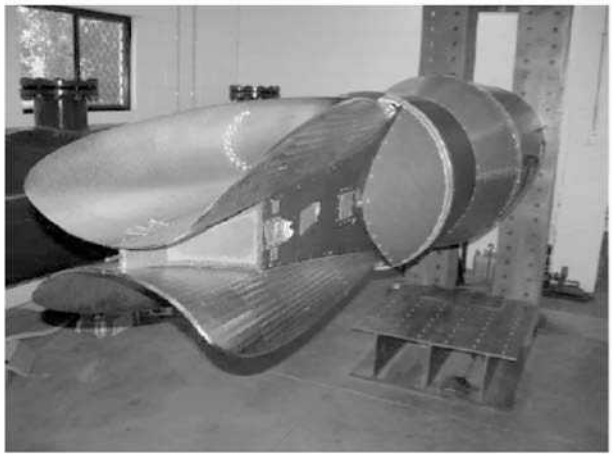

Figure 1-17: HyCAUSE flight test engine model

The flight test was carried out on June 15, 2007, and was propelled by a two-stage uncontrolled sounding rocket to fly on a ballistic trajectory, with a re-entry Mach number of 10 and a dynamic pressure of 500 to 1,600 psf (1 psf = 4.78486×10^{-5} MPa) to perform the test. However, due to the failure of the booster, the test did not achieve the expected results, and the data analysis after the test showed that the test engine went through the process of starting the intake tract, not starting and restarting, but the hydrogen fuel was not able to burn under the conditions of the inlet tract starting.

9. HIFiRE flight test conducted by the United States in cooperation with Australia

HIFiRE stands for Hypersonic International Flight Research and Experimentation, which is a collaboration between the U.S. Air Force Laboratory and the Australian Defence Science and Technology Organization. The aim of the program is to carry out basic research and verification of the key technologies needed to realize the next generation of hypersonic aerospace vehicle systems at a low cost, and the program will accelerate the development and maturity of component technologies through the testing of basic problems. Specific test objectives include: developing and validating computational models for hypersonic flow; ground test research on typical hypersonic flight environment; development of flight test equipment and measurement technology; development of hypersonic flight test and integrated payload design technology; flight tests of key technologies in a real hypersonic environment; develop methods for correcting numerical models, ground and flight test data; evaluation of hypersonic technologies and test methods.

The scope of the HIFiRE program includes 10 specific research and flight test areas, which will be conducted at the Woomera Proving Ground in Australia. These 10 aspects are aerodynamic propulsion integration technology, aerodynamics, aerodynamic heating, high-temperature materials and structures, thermal management technology, navigation technology, guidance technology, control technology, sensor technology, and weapon system component technology. The research work on these projects includes modeling, simulation, and ground testing, but the main is the study of mechanistic phenomena and component technologies through flight tests.

The flight conditions range from *Ma* = 5 to 12, and the flight trajectory includes ballistic trajectory and long-term atmospheric flight trajectory.

The HIFiRE project is a collection of flight tests, each of which is different. Each test vehicle will have a main test and a set of other tests, and it will fly up to 4 to 5 times. The first flight of HIFiRE was successfully completed on 7 May 2009 at the Bumera range. In March 2010, a second flight test was successfully carried out, with the flight test payload shown in Figure 1-18, which was led by the United States, and subsequent tests will also be led by the United States. The HIFiRE collaboration has been successful at several key junctures such as the design and assembly of hypersonic vehicles, the design of complex electronic devices, and flight systems. HIFiRE is a high-profile international collaboration that undoubtedly plays a very important role in the research and validation of future hypersonic technologies in the United States and Australia.

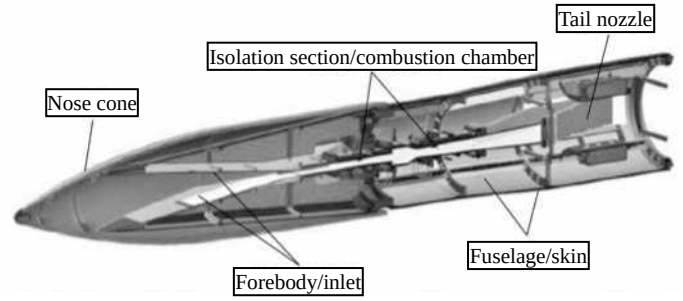

Figure 1-18: HIFiRE-2 flight test payload

1.3.3: Other hypersonic vehicle technology development programs

After the successful first flight of the X-51A, the U.S. Air Force has begun to work on the RIPTIDE rapid response missile program. This means that hypersonic technology will take the first step towards the application of weapons, and it is possible to transfer air-breathing hypersonic technology from laboratory research to practical application, but this concept is still in its infancy, and whether it can be realized depends on the results of subsequent flight tests of the X-51A waverider hypersonic vehicle. The successor model of the X-51A is the X-51A+, and if the X-51A+ project is approved, it will become a stepping-stone to the realization of the RIPTIDE hypersonic missile, which can evolve into a hypersonic missile for use with partial improvements to the X-51A+ while expanding the performance range. It is assumed that the RIPTIDE missile has a range of about 1,600km and has more typical combat characteristics. The program will include more system-level trials and possibly additional payloads.

The French MBDA and ONERA are leading a hypersonic scientific research program called LEA. The main objectives of the project are: to develop methods for studying hypersonic vehicle technology using ground tests and numerical simulations; development of the tools (experimental or numerical methods) required to implement the above methods; the method was validated through a series of flight tests. The LEA program was launched in January 2003 and originally planned to conduct six flight tests by 2012, with Mach numbers ranging from 4 to 8. The entire program was divided into four phases, with flight tests scheduled to be carried out from 2010 to 2012 to explore *Ma* = 4 to 8. The flight test program will allow for the validation of the ability of the methods used in the study to be applied to future aircraft development. The engine chosen for the test vehicle is a variable-geometry PIAF engine, but thermal regulation will also be used. Each flight will take place at a fixed Mach number, so the engine will remain in a fixed geometric position, which corresponds to the operating Mach number of the variable geometry engine. In the selection of fuel, the size of the fuel storage tank and the requirements of fuel ignition reliability were considered in a compromise, and the fuel form of methane and gas hydrogen combination was adopted, and stable ignition and controlled heat release along the combustion chamber will also be obtained by changing the H2/CH4 ratio during flight.

The LEA project has been launched since 2003, and the date and number of flight tests have been postponed several times. The ultimate goal of the project is to verify the performance of a dual-mode ramjet engine at *Ma* = 4 to 8. The flight test period is currently expected to be between 2013 and 2015 (Figure 1-19). Flight tests will take place at military launch sites in Russia, and the LEA vehicle will use boosters improved from the X-22 (AS-4) missile, which are supplied by the Rainbow Design Bureau, which is part of the Tactical Missile Group. The LEA aircraft will be mounted on the nose of the X-22 fuselage. After launch, the LEA vehicle will be accelerated from the booster to the conversion speed of the ramjet engine, with the aim of enabling the aircraft to fly freely for 20 to 30 seconds at an altitude of 30 to 40 km.

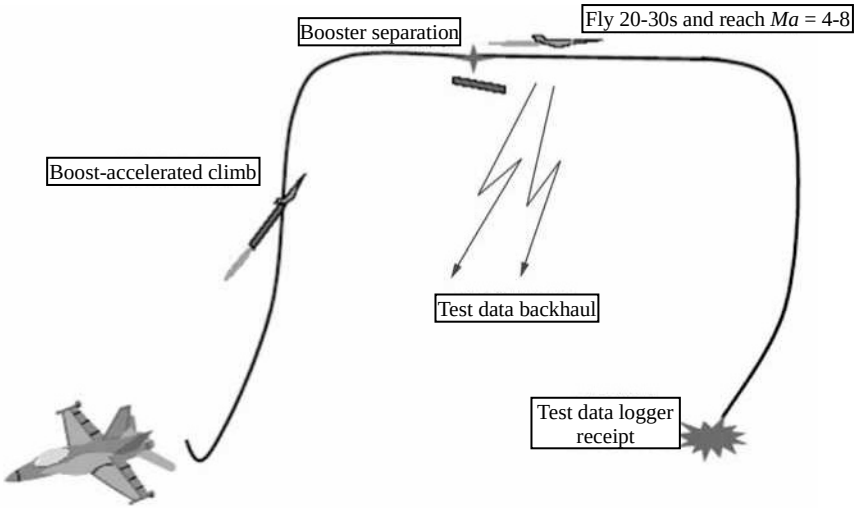

Figure 1-19: Flight test timing of the LEA flight test program

In the past 20 years, Japan has been actively conducting research in the field of hypersonic technology. Judging from the published literature reports, Japan has carried out a large number of theoretical and experimental studies on RBCC and TBCC in the context of aerospace aircraft application. From 1990 to 2003, TBCC's ATREX500 engine has been carried out 67 times, with a cumulative period of 3636 seconds of ignition test research and is currently preparing for flight tests of the engine. The engine, called the "S-engine," is a flight test scheme for balloon tethered lift-off to an altitude of 40 km (Fig. 1-20).

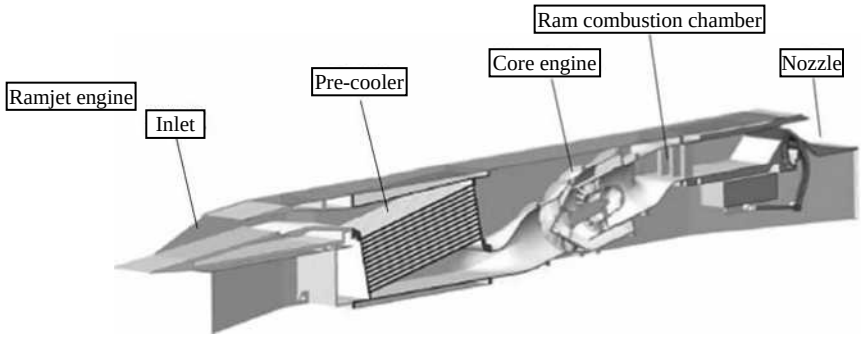

Figure 1-20: Japan's S-engine test vehicle

The SHYFE (Sustained Hypersonic Flight Experiment) program is a flight demonstration verification program for small hypersonic vehicles funded by the British Ministry of Defense and carried out by the British company QinetiQ. The test vehicle was in an axisymmetric head intake configuration (Fig. 1-21). The test vehicle was first boosted by a solid rocket to an altitude of 15 km, *Ma* = 4, and accelerated to an altitude of 32 km, *Ma* = 6, and a cruising flight of 300 km under the impetus of its own engine. The test vehicle is made of C/SiC material, which is passively heat-protected by radiation, and the purpose of the test is to test scramjet engines and thermal structural materials through low-cost flight tests.

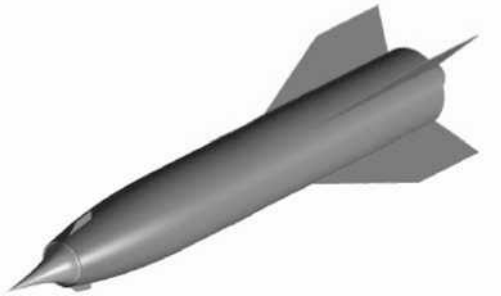

Figure 1-21: UK Sustained Hypersonic Flight Experiment (SHYFE**)** test vehicle

In recent years, the potential of hypersonic technology for the application of space and missiles has aroused great interest in India. In addition to its focus on the design and construction of launch vehicles and satellites, India has several hypersonic flight programs, including the Capsule Recovery Test (SRE), the Reusable Vehicle (RLV), the scramjet engine development, and the Hypersonic Technology Demonstrator Vehicle (HSTDV). Among them, the HSTDV project has attracted much attention. The aim of the project is to verify the performance of an aircraft propelled by a scramjet engine in autonomous mode. In addition to validating the design and performance of the scramjet, the HSTDV project will also validate aerodynamic performance, aerothermal design, materials and thermal protection techniques in high Mach number flight (Fig. 1-22). The HSDTV project includes the launch of an air-breathing hypersonic vehicle, called a cruise vehicle. The vehicle is launched to an altitude of 30 to 35 km by rocket booster, and then transferred to a single-modal scramjet engine fueled by kerosene to reach a speed of *Ma* = 6.5 and continue to fly for 20 seconds. The hypersonic technology demonstrator currently being built is 5.6m long and has a mass of 1,000kg, with a flat octagonal cross-section, a pair of short wings in the middle of the fuselage and a sloping vertical tail in the rear of the fuselage. The length of the intake duct is 3.7 m, and the cross-sectional shape is rectangular. The scramjet engine is located in the lower middle part of the fuselage (its development is also underway), and the tail part of the fuselage serves as part of the exhaust nozzle. Israel and the UK's Cranfield University have provided partial assistance to India's Hypersonic Technology Demonstrator program, which includes wind tunnel testing. There may be other countries, including Russia, which are also providing technical assistance to India.

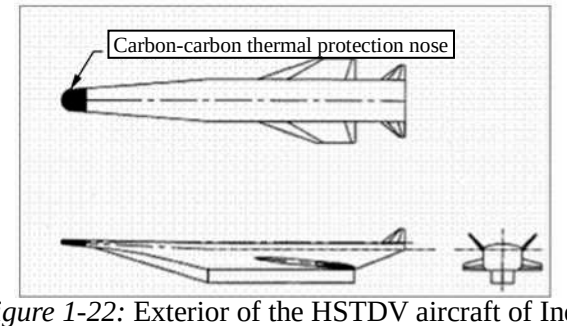

Figure 1-22: Exterior of the HSTDV aircraft of India

1.4: Main content of this book

The main contents of this book: the first part introduces the key technologies of hypersonic vehicles; the second part describes the development process of hypersonic vehicle technology in various countries and the main research results obtained.

In the introduction of Chapter 1, the definition of hypersonic vehicle is given, its application prospect is expounded on, and the development process of hypersonic vehicle technology and the development of flight tests are briefly described.

Based on the technical level and technology classification analysis of key technologies, Chapter 2 summarizes the key technologies of hypersonic vehicles, ranks the criticality of each key technology of hypersonic vehicles by using quantitative evaluation methods, and introduces the definition of technology maturity and system integration maturity adopted abroad, as well as the path of technology development.

Chapter 3 introduces the basic concepts and main research contents of scramjet engine technology, including the definition of supersonic combustion and its key technologies, the component technology and overall technology of scramjet engine.

Chapter 4 describes other types of combined cycle engines, such as rocket-based combined cycle engines, turbine-based combined cycle engines, and pre-cooled air turbine-based combined cycle engines, focusing on scramjet-based hypersonic combined cycle systems.

Chapter 5 introduces the overall and integrated design technology of hypersonic vehicles, including some basic knowledge of hypersonic aerodynamics, engineering calculation methods and numerical simulation techniques of hypersonic aerodynamics, and design methods of "waverider" aircraft. This paper focuses on the related issues of airframe and propulsion integration, such as the computing power system, the integrated design of the forebody air intake, the integrated design of the rear nozzle, the numerical calculation method of the integration of aeropropulsion, and the parametric geometric modeling method of the integrated shape of the aircraft. The analysis results of the integrated aerodynamic characteristics of hypersonic vehicles are also given. The chapter also addresses the integration of the scramjet engine with the aerodynamic shape of the "waverider," and the integration of the "circular cross-section" propulsion system with the fuselage of the hypersonic vehicle.

Chapter 6 introduces the thermal protection technology of hypersonic vehicles, including the thermal environment analysis of hypersonic vehicles, the definition of thermal corridors, and the calculation methods of hypersonic aerothermal engineering, and other basic concepts, expounds the typical thermal protection technologies and methods in the aerospace field, as well as the metal thermal protection system of reusable space vehicles, and also introduces the thermal protection system and structural components of air-breathing hypersonic vehicles.

Chapter 7 introduces the integrated navigation system of hypersonic vehicles, the dynamics modeling technology of hypersonic vehicles, the control and attitude measurement technology of hypersonic vehicles, the guidance and control technology of hypersonic vehicles, and the flight control technology of typical reusable space launch vehicles.

Chapter 8 introduces hypersonic wind tunnel technology, including the tasks and requirements of wind tunnel testing, the types of equipment and test forms of wind tunnels, and the situation of large-scale hypersonic wind tunnels abroad.

Chapters 9 to 15 of the second part introduce the development history and research results of the United States, Russia, France, Germany, Japan, Australia, the United Kingdom, and India in the field of hypersonic vehicle technology, and summarize the research structure of hypersonic technology in each country.

Finally, Chapter 16 provides a summary of the book and an outlook for the future development of hypersonic vehicle technology.

References

[1] Edward T Curran. Scramjet engines: The first forty years [J]. Journal of Propulsion and Power, 2001, 17 (6): 1138-1148.

[2] Paul J Waltrup. Upper bounds on the flight speed of hydrocarbon-fueled scramjet-powered vehicles [J]. Journal of Propulsion and Power, 1999, 17(6): 1199-1204.

[3] William J D Escher, Carl F Ehrlich Jr. An early TSTO fully reusable vehicle design used to calibrate stage 1 combined-cycle hypersonic propulsion systems [R]. AIAA 2001-01-5602, 2000.

[4] National Aeronautics and Space Administration. 2006 NASA strategic plan [EB/OL]. http://www.nasa.gov/pdf/142302main_2006_NASA_Strategic_Plan.pdf, 2006.

[5] Japan Aerospace Exploration Agency. JAXA Vision: JAXA 2025 [EB/OL]. http://www.jaxa.jp/about/vision_missions/long_term/jaxa_vision_e.pdf 2005-3-31.

[6] Frederick S Biliig. SCRAM - a supersonic combustion ramjet missile [R]. AIAA 93-2329, 1993.

[7] Mercier R A, Ronald TMF. Hypersonic technology (HyTech) program overview [R]. AIAA-98-1566, 1998.

[8] Laurent SERRE, Francois FALEMPIN. PROMETHEE: the French military hypersonic propulsion program status in 2002 [R]. AIAA 2002-5426, 2002.

[9] Michael E White, Walter R Price. Affordable hypersonic missiles for long-range precision strike [J]. Johns Hopkins APL Technical Digest, 1999, V20(3): 415-423.

[10] Moses P L, Bouchard K A, Vause RF, et al. An airbreathing launch vehicle design with turbine-based low-speed propulsion and dual mode scramjet high-speed propulsion [R]. AIAA- 99-4948, 1999.

[11] Lee F Scuderi, George F Orton. Mach 10 cruise/space access vehicle study [R]. AIAA-98-1584, 1998.

[12] Trefny C. An air-breathing launch vehicle concept for single-stag-to-orbit [R]. AIAA-99-2730, 1999.

[13] Joseph N Stemler, Thomas J Bogar, Daniel J Farrell, et al. Assessment of RBCC-powered VTHL SSTO Vehicles [R]. AIAA 99-4947, 1999.

[14] Bradford J E, Charania A, Olds J R, et al. Xcalibur: a Vertical Takeoff TSTO RLV Concept with a HEDM Upperstage and a Scram-Rocket Booster. [A], 53th International Astronautics Congress [C], IAC-02-S. 5. 02, 2002.

[15] Olds J R, Bellini P X. Argus, a Highly reusable SSTO rocket-based combined cycle launch vehicle with Maglifter Launch Assist [R]. AIAA 98-1557, 1998.

[16] Olds J, Bradford J, Charania A, et al. Hyperion: An SSTO vision vehicle concept utilizing rocket-based combined cycle propulsion [R]. AIAA 99-4944, 1999.

[17] Olds John R, Laura Ledsinger, John Bradford, et al. Stargazer: A TSTO bantam-x vehicle concept utilizing rocket-based combined-cycle propulsion [R]. AIAA 99-4888, 1999.

[18] Brad St Germain, John R Olds, Laura Ledsinger, et al. Starsaber: A small payload-class TSTO vehicle concept Utilizing Rocket-Based Combined Cycle Propulsion [R]. AIAA-2001-3516, 2001.

[19] Uwe Hueter, Charles R McClinton. NASA's advanced space transportation hypersonic program [R]. AIAA- 2002-5175, 2000.

[20] Dean Andreadis, Alan Drake, Joseph L Garrett, et al. Design considerations of ISTAR hydrocarbon fueled combustor operation in air augmented rocket, ramjet and scramjet modes [R]. AIAA-2002-1401, 2002.

[21] Marty Bradley, Kevin Bowcutt, James McComb, et al. Revolutionary turbine accelerator (RTA) two-stage-to- orbit (TSTO) vehicle study [R]. AIAA 2002-3902, 2002.

[22] Dulepov N P, Lanshin A I, Sokova OV, et al. Propulsion systems for TSTO airplane-accelerators of different types [R]. AIAA 2001-1914, 2001.

[23] Fujita K, Sawai S, Kobayashi H, et al. Precooled turbojet engine flight experiment using balloon-based operation vehicle [A]. 56th International Astronautics Congress [C], IAC-05-C4. 5. 01, 2005.

[24] Takeshi Kanda, Sadatake Tomioka, Shuichi Ueda, et al. Design of sub-scale rocket-ramjet combined cycle en-

gine model [A]. 56th International Astronautics Congress [C], IAC-05-C4. 5. 03, 2005.
[25] Grallent H. Synthesis of a FESTIP air-breathing TSTO space transportation system [R], AIAA-99-4884, 1999.
[26] Charles R McClinton, Vincent L Rausch, Luat T Nguyen. Preliminary X-43 flight test results [R]. IAC 04-V6- X43A 2, 2004.
[27] James L Hunt, John G Martin. Scramjet Propulsion [M]. Chapter 15 Rudiments and Methodology for Design and Analysis of Hypersonic Air-breathing Vehicles: 939-940, 2000.
[28] Tetsuya Sato, Hideyuki Taguchi, Hiroaki Kobayashi. Development study of precooled-cycle hypersonic turbojet engine for light demonstration [A]. 57th International Astronautics Congress [C], IAC-06-C4. 5. 02, 2006.
[29] Preston H Carter, Darryll J Pines, Lae von Eggers Rudd. Approximate Performance of Periodic Hypersonic Cruise Trajectories for Global Reach [R]. AIAA 98-1644, 1998.
[30] Michael S Holden. Studies of scramjet performance in the lens facilities [R]. AIAA 2000-3604, 2000.
[31] Boweutt Kevin G. Multidisciplinary optimization of airbreathing hypersonic vehicles considering aerodynamics, propulsion, control and mass property effects [A]. 14th International Symposium on Air Breathing Engines [C], ISABE 99-7089, 1999.
[32] Liu Tonglin, Russian Hypersonic Technology Flight Test Program [J]. Flying Missile, 2000, (4):23-30.
[33] Liu Tonglin. Analysis on the development of foreign hypersonic technology [J]. Flying Missile, 2002, (6): 30-40.
[34] Liu Tonglin. Development and prospect of hypersonic technology in the United States [J]. Aerospace Control, 2004, 22(4):36-41.
[35] Wei Yiyin, Liu Peng, Zhang Dongqing, et al. Analysis of the development of foreign hypersonic technology and flight tests [J]. Aeronautical Missile, 2010, (5): 2-9.

CHAPTER 2: BREAKDOWN OF KEY TECHNOLOGIES FOR HYPERSONIC VEHICLES

2.1: Breakdown of key technologies for hypersonic vehicles

The hypersonic vehicle is a new type of aircraft with scramjet engine as the core technology, which also has a certain inheritance continuity with the existing subsonic aircraft and supersonic vehicles, and still plays a certain role in the research and development, manufacturing, production and use of hypersonic vehicles, but at the same time, hypersonic vehicles are more significant because of their own unique characteristics and some new requirements for technology, and even some requirements for innovation, as well as new solutions to the new problems encountered. Through the decomposition of the key technologies of hypersonic vehicles, the technical composition of each system, the difficulty of the technology, and the priority in the development plan are clarified.

2.1.1: Technical level and technical classification

According to the development process of hypersonic vehicles from pre-research to model development, the key technologies involved in this book are divided into three levels, namely, the research design layer, the test verification layer, and the application development layer.

The research and design layer is the pre-basic research stage for hypersonic vehicle technology, which strives to achieve a breakthrough in its basic principles and solve the crucial technical basic problems in the subsequent development process.

The test verification layer is the stage of test verification research in combination with the upcoming or ongoing engineering model development to determine the feasibility of the component or overall design and explore the best design state.

The application development layer is to develop and manufacture engineering models for hypersonic vehicles, and continuously improve and modify them in practical applications to improve their performance and adapt to higher and more application requirements.

The division of the development level of hypersonic vehicle technology can more clearly clarify the priority of various technologies in the development plan and play a certain reference role in the arrangement of research plans.

According to the division of disciplines in China, the setting of aerospace industry departments and the actual use of operations, the technologies involved in the development of hypersonic vehicles can be divided into six categories: overall technology, propulsion technology, material technology and manufacturing process technology, flight control and control guidance and navigation technology, test verification technology, and flight demonstration verification technology.

The classification of technologies provides a clear scope and direction guidance for the further decomposition of key technologies of hypersonic vehicles, and the decomposition of key technologies from the entire research and development process is conducive to a comprehensive understanding of the technical components necessary to achieve the final development goals, so as to avoid the lag of some technology development and lead to the delay of the overall project development progress.

Figure 2-1 shows the interrelationship between the development level of hypersonic vehicle technology and the classification of key technologies.

At the research and design level, the focus is on the development of overall technology and propulsion technology. The breakthrough of propulsion technology is crucial for hypersonic vehicles powered by air-breathing propulsion systems, and the integration characteristics with the aircraft body are not encountered in the design and development of previous aircraft. The breakthrough in the principle and theory of propulsion system and overall integrated design plays a primary and decisive role in the further research of hypersonic vehicles.

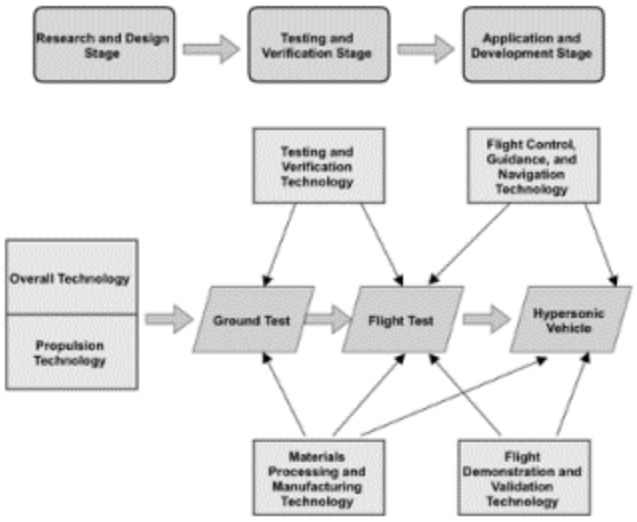

Figure 2-1: The interrelationship between the development level of hypersonic vehicle technology and the classification of key technologies

In the test verification layer, it is necessary to carry out the necessary ground test and the flight verification test of the aircraft, the ground test includes the combustion test of the engine, the free jet test in the hypersonic wind tunnel, etc., and the flight verification test of the aircraft, including the aerodynamic verification of the aircraft body, the working verification test of the engine, etc. These two aspects of the test involve experimental verification technology, and the manufacturing of component and model principle prototypes involves material technology and manufacturing technology. At the level of technology development, the feasibility of propulsion and overall technology is often actually verified, and the theoretical basic research should be re-conducted for incorrect and unsuitable designs, so there must be a certain process of repeated iterative interaction between these technologies and overall technology and propulsion technology.

In the application development layer, most of the key factors involved in hypersonic vehicles have been broken through, entering the development and development stage of engineering models, material technology and manufacturing technology are playing an increasingly important role, for hypersonic vehicles to have practical application value, flight control and control navigation technology will play an important role, for the actual use of hypersonic vehicles, the comprehensive flight demonstration and verification of the whole system will inevitably be put on the research agenda. At the same time, at this level of development, there may be some problems that were not considered in the design research stage before, and it is necessary to re-carry out some basic research work on theories and principles.

At present, in global terms, the United States is in a leading position in the development of hypersonic vehicle technology, in the past 40 years, a large number of theoretical design studies, as well as ground test research. In the 21st century, several flight tests of hypersonic test vehicles have been carried out since September 2005, including the establishment of the X-51A project, indicating that the United States is about to enter the application and development stage of hypersonic vehicle technology.

2.1.2: Key technology decomposition based on technology classification

1. Propulsion technology

For hypersonic vehicles, the breakthrough of scramjet engine is the key, and the combined propulsion system with scramjet engine as the core is also the focus of development. The development of hypersonic vehicles must emphasize the guiding ideology of "power first.” There are many problems that need to be solved in scramjet engines, first of all, the realization of supersonic combustion, and the numerical simulation of scramjet, etc., and secondly, the design and performance calculation of intake ducts and tail nozzles. In addition, the matching of the intake tract and the combustion chamber is also a very critical issue in the study, and the conversion of subsonic combustion and supersonic combustion working modes is also one of the technologies that need to be studied.

The technologies covered in the field of propulsion technology include: (1) scramjet engine technology, (2) combined propulsion system technology, (3) propulsion system control technology, (4) thermal structure and cooling technology of hyperpropulsion engine, and (5) endothermic hydrocarbon fuel technology.

The above technologies can also be further refined, such as scramjet engine technology can be further decomposed into air inlet technology, combustion chamber technology, tail nozzle technology, flow channel integration design technology, dual-modal conversion technology, dual-combustion chamber technology, etc. Combined propulsion system technologies include RBCC propulsion technology and TBCC propulsion technology. The MHD energy bypass technology based on magnetohydrodynamic power can be classified as propulsion system control technology.

2. Overall technology

The overall technology of the aircraft plays a leading role in the design, development and modification of the aircraft. From the proposal of the design concept, the preliminary design, and the detailed design, to the development of the project model, the overall technology is all involved, playing the role of guidance and command.

The overall technology of the aircraft includes not only the method research of its overall design, the optimization study of the design, but also the related technical categories as its foundation and support, mainly including aerodynamics and structure. For different aircraft uses, there are some general related technologies that have been upgraded to the overall technical requirements. For example, for military combat aircraft, stealth design is emphasized, etc. For hypersonic vehicles, the design of aerothermal and heat-resistant structures, as well as thermal protection systems and thermal management technologies have been raised to a level that must be considered in the conceptual design and preliminary design stages.

In addition, the integrated design idea required by hypersonic vehicles is also a revolutionary innovation and development that is different from traditional aircraft design. At the same time, the requirements of integrated design make multidisciplinary design optimization an indispensable design idea and method for the overall design of hypersonic vehicles.

The technologies covered in the overall technical field of hypersonic vehicles are: (1) shape design and aerodynamic numerical simulation technology; (2) integrated design technology; (3) multidisciplinary design optimization technology; (4) aerothermal numerical simulation technology; (5) structural design, thermal protection and thermal management technology; (6) flight simulation technology.

3. Materials/Processes/Manufacturing Technologies

The problem of aerodynamic heating of hypersonic vehicles has brought higher requirements for heat-proof materials to the aircraft, and how to use heat-proof materials and design heat-proof structures are new problems. In order to be able to increase the loading capacity, it is also necessary to develop lightweight materials under the condition of meeting the requirements for strength and heat resistance.

The technical aspects involved in this field include: (1) heat-proof and heat-insulating materials (such as C/C composite materials, C/SiC ceramic matrix composites, honeycomb sandwich composites, etc.), (2) heat-resistant coating materials (such as zirconia, etc.; (), 3) lightweight and high-strength materials (such as aluminum-lithium alloys, titanium alloys, etc.), ; (4) special-shaped structure design and molding technology; (5) component connection, welding and sealing technology.

4. Test verification technology

The test verification technology is the key to moving from theory to practical application, and the test of hypersonic vehicles mainly includes the test of supersonic combustion, the test of the free jet model engine, the aerodynamic force of the aircraft, the pneumatic hot wind tunnel test, etc., as well as the related test methods, data measurement and processing. The specific research aspects included in the test verification technology are: (1) direct-connected supersonic combustion chamber test technology; (2) free jet test technology of scramjet engine; (3) combined propulsion system test technology; (4) hypersonic wind tunnel technology;

(5) aerodynamic test technology of hypersonic aircraft, (6) aerothermal test technology of hypersonic aircraft, (7) thermal environment simulation and test technology of heat-proof structural materials.

5. Flight navigation guidance and control technology

In the process of high-speed flight, the navigation guidance and control of hypersonic vehicles will encounter some new technical difficulties, so they should be studied under new conditions.

The main research problems in this field are: (1) hypersonic vehicle pneumatic/propulsion integrated control technology; (2) hypersonic cruise vehicle navigation and control technology; (3) precision guidance and control technology for hypersonic long-range strike weapons.

6. Flight demonstration verification technology

Flight demonstration verification is an extremely important link in the development process of hypersonic aircraft, whether it is pre-research or model engineering research, it is necessary to test and develop the research work of each system through flight demonstration verification, which is the integration and test of the research work of various subsystems and sub-departments. At the same time, flight demonstration verification is also a landmark and milestone research work in the development of hypersonic vehicles.

The main research problems in this field are: (1) flight test risk assessment technology; (2) air launch technology; (3) ground launch technology; (4) hypersonic separation technology; (5) flight test telemetry technology.

On the one hand, the risk of flight test is reduced as much as possible through a large number of ground test research and simulation studies, and on the other hand, through the analysis and quantification of uncertainty factors in test research and numerical simulation research, the risk of flight test is evaluated, and the flight test is carried out only when there is the greatest certainty of test success.

For example, for hypersonic cruise missiles, precision guidance technology is crucial, but for hypersonic aircraft and aerospace aircraft, it is not required; similarly, for single-use hypersonic cruise missiles, in terms of thermal protection technology, there are obviously different technical requirements from hypersonic aircraft and aerospace aircraft.

2.2: The need for quantitative analysis in development strategy research

Hypersonic vehicles will be at the forefront of the development of aerospace technology for a long time to come, and all major aerospace powers are actively carrying out research work in this field. Because the research and development of hypersonic vehicles involves multidisciplinary and multi-system, it is a highly comprehensive system work, so all countries have deployed the research of hypersonic vehicle technology by formulating national development plans, such as the NASP program of the United States and the Sanger program of Germany in the 1980s. In September 2008, in order to strengthen its leading position in this field, the United States announced the establishment of three national hypersonic scientific research centers.

The development strategy is the soul of the development plan, which influences and determines the direction of the development plan, so the development strategy is a crucial work. The study of development strategy itself is an intricate work, or a system engineering, and it is impossible to rely solely on the subjective experience and intuitive thinking methods of the formulators, but must mainly use scientific methods and technical means, supplemented by empirical judgment and intuitive thinking to carry out strategic analysis and inference.

The word "strategy" is derived from military and originally referred to the method of directing the overall situation of war, that is, military strategy.

With the development of human society, the word "strategy" has been extended to the political, social, economic, and other fields, and the development of major aerospace projects pays more attention to the development of development strategy research, so as to form a plan and guidance or guidelines and policies with overall guiding significance in a certain period of time in the future. Therefore, establishing a scientific way of thinking is the foothold of the research and demonstration of the development strategy of weapons and equipment. "The so-called scientific way of thinking is to consciously integrate the intuitive way of thinking and the way of analytical thinking in the process of demonstration of development strategy, so as to achieve the purpose of comprehensive, systematic and accurate analysis of development strategy issues. The intuitive way of thinking here refers to those that subjectively analyze problems mainly by relying on the perceptual cognition and rational reasoning of the argumentator, while the analytical thinking style refers to those that rely mainly on various analytical methods and techniques to quantitatively analyze problems" [1].

Reference [1] points out that the advantage of intuitive thinking is that it can comprehensively deal with the intricate phenomena in the argument for development strategy, so as to give full play to the wisdom of the argumentators and put forward creative ideas. However, intuitive thinking is often limited by the arguer, and it is easy to be one-sided or misunderstand the problem. The advantage of the analytical way of thinking is to comprehensively analyze the situation of the system and its parts, as well as the interrelationship between the components of the system, according to scientific and technological methods, and to obtain the optimal combination of various elements. However, analytical thinking does not describe the conception and analysis of development strategies that are difficult to quantify, and it is difficult to make full use of subjective information and creative insights. The argument for development strategy often needs to use the function of intuitive thinking to generate new concepts through intuitive thinking from some information that is difficult to quantify and the vague feelings of the people involved. However, in the process of research and demonstration of development strategy, it is also necessary to use some quantitative calculation analysis results and a large number of rigorous logical reasoning to transform some qualitative analysis conclusions into quantitative analysis results, and to transform some image thinking into sequential thinking as much as possible. Therefore, one-sided emphasis on intuitive thinking, relying on qualitative analysis and subjective judgment, or blindly pursuing analytical thinking, relying on quantitative analysis and derivation of mathematical models, are not scientific ways of thinking for research and demonstration of development strategies. The scientific way of thinking is not only different from the analytical way of thinking, but also different from the intuitive way of thinking, but organically combines these two ways of thinking and flexibly applies them to the research and demonstration of development strategies.

In recent years, the Aerospace System Design Laboratory of the Georgia Institute of Technology in the United States has developed quantitative analysis methods for technology determination, selection and evaluation that can be applied to the formulation of aircraft development plans [2~4], making the formulation of research plans more scientific. The following chapter focuses on how to apply analytical thinking to transform some qualitative analysis into quantitative analysis in the process of hypersonic vehicle development strategy research, including quantitative analysis of key technologies of hypersonic vehicles, and analysis and research on the maturity of hypersonic vehicle technology. Through these quantitative and quantitative analysis studies, the results obtained can more strongly support the overall planning of the development path of key technologies of hypersonic vehicles.

2.3: Hypersonic vehicle technology criticality analysis

In Reference [5], the analytic hierarchy process was used to quantitatively rank the key technologies involved in hypersonic cruise missiles. The Analytic Hierarchy Process (AHP) was developed by the famous American operations researcher T. L. In the 1970s, Satty et al., proposed a multi-criteria decision-making method combining qualitative and quantitative analysis. This method provides hierarchies and quantifies the human thinking process, and uses mathematics to provide a quantitative basis for analysis, decision-making, forecasting or control. The characteristic of this method is that after in-depth analysis of the essence, influencing factors and internal relationships of complex decision-making problems, a hierarchical model is constructed, and then the thinking process of decision-making is mathematized by using less quantitative information, so as to provide a simple decision-making method for solving complex decision-making problems with multiple objectives, multiple criteria or no structural characteristics.

It is especially suitable for occasions where people's qualitative judgment plays an important role and it is difficult to directly and accurately measure the results of decision-making.

The analytic hierarchy process is mostly used in program decision-making and resource allocation, and its mathematical essence is to give a comprehensive ranking result for different target items according to different criteria. The analytic hierarchy process is broadly divided into six steps: identify the problem; establish a hierarchical structure, compare two pairs, establish a judgment matrix, and solve the weight vector; hierarchical single ranking and its consistency test, hierarchical total ranking and its consistency test, and considering the corresponding decision according to the analysis and calculation results.

In the analytic hierarchy process, in order to quantify the decision-making judgment and form a numerical judgment matrix, the judgment is often quantified according to a certain ratio scale. In this section, a scale of 1 to 9 was used, as shown in Table 2-1. In this table, C_{ij} represents the factor, and factor j is relative to the target important value, and the numerical judgment matrix $C = (C_{ij})_{nxn}$ is obtained by comparing n elements in pairs.

Table 2-1: Judgment matrix scale and its meaning

Serial number	Importance level	C_{ij} value
1	Both elements *i* and *j* are equally important	1
2	The *i* element is slightly more important than the *j* element	3
3	The *i* element is significantly more important than the *j element*	5
4	The *i* element is more strongly important than the *j* element	7
5	The *i* element is more important than the *j* element	9
6	The *i* element is slightly less important than the *j* element	1/3
7	The *i* element is significantly less important than the *j element*	1/5
8	It is not important that the *i* element is stronger than the *j element*	1/7
9	The *i* element is extremely unimportant than the *j* element	1/9

In general, the constructed numerical judgment matrix is in the following form:

B_k	C_1	C_2	$\cdots$	C_n
C_1	C_{11}	C_{12}	$\cdots$	C_{1n}
C_2	C_{21}	C_{22}	$\cdots$	C_{2n}
$\vdots$	$\vdots$	$\vdots$		$\vdots$
C_n	C_{n1}	C_{n2}	$\cdots$	C_{nn}

(2.1)

According to the decomposition of key technologies based on technology classification, a five-layer analytic hierarchy process model was constructed. The analytic hierarchy process is divided into two phases: first, the quantitative analysis of the six technical categories; secondly, the key technologies in each technology category are quantitatively analyzed. Each technology category is a collection of a number of key technologies, with a certain correlation and similarity, and at the same time there are certain obvious differences between the technology categories, some classifications are bound to only carry out research in the specific field of hypersonic technology, while some categories may be carried out in other fields, some results can be directly applied, and some are required to carry out new research. In addition, there is a certain degree of research sequence between the categories, some of which are the entry points for the start, and some of which are very important but can be slightly delayed. After the technology categories are hierarchically sorted, the hierarchical ranking analysis of each technology in each technology category is carried out. Figure 2-2 shows the analytic hierarchy process model for key technologies of hypersonic vehicles.

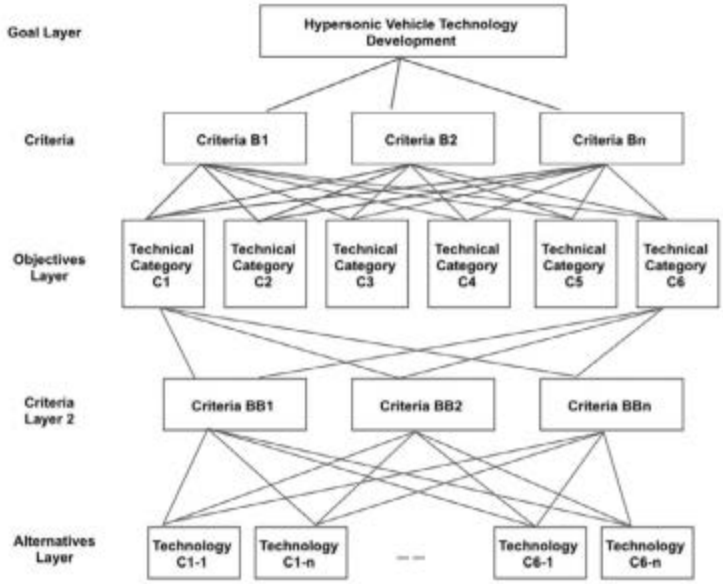

Figure 2-2: Analytic hierarchy process model for key technologies of hypersonic vehicles

Table 2-2 is based on the technical level and technical classification of key technologies in Section 1, and the classification of key technologies of hypersonic vehicles with reference to relevant foreign literature.

Table 2-2: Classification of key technologies of hypersonic vehicles

Code	Name	Code	Name
C1	Overall Integrated Design Technology	C1-1	External design and aerodynamic force numeric simulation technology
		C1-2	Integrated design technology
		C1-3	Interdisciplinary design optimization technology
		C1-4	Aerodynamic heating numeric simulation technology
		C1-5	Structural design thermal protection and heat management technology
		C1-6	Flight emulation technology
C2	Propulsion Technology	C2-1	Scramjet engine technology
		C2-2	Combined propulsion system technology
		C2-3	Propulsion system control technology
		C2-4	Hypersonic propulsion engine thermal structure and cooling technology
		C2-5	Endothermic hydrocarbon fuel technology
C3	Materials / Processing / Manufacturing Technology	C3-1	Heat-resistant and thermal insulation materials
		C3-2	Heat-resistant coating materials
		C3-3	Light(weight) high-strength materials
		C3-4	Atypical structural design and shaping technology
		C3-5	Component joining, welding and sealing technology

Table 2-2 Continued

Code	Name	Code	Name
C4	Testing and Verification Technology	C4-1	Direct-connected super-combustion chamber testing technology
		C4-2	Scramjet engine free jet testing technology
		C4-3	Combined propulsion systems testing technology
		C4-4	Hypersonic wind tunnel technology
		C4-5	Hypersonic aircraft aerodynamic force testing technology
		C4-6	Hypersonic vehicle aerodynamic heating testing technology
		C4-7	Heat-resistant structural materials thermal environment simulation and testing technology
C5	Flight Navigation, Guidance, and Control Technology	C5-1	Hypersonic vehicle aerodynamics / propulsion integrated control technology
		C5-2	Hypersonic cruise vehicle navigation and control technology
		C5-3	Hypersonic remote strike weapon precision guidance and control technology
C6	Flight Demonstration and Validation Technology	C6-1	Flight testing risk assessment technology
		C6-2	Aerial launch technology
		C6-3	Ground launch technology
		C6-4	Hypersonic separation technology
		C6-5	Flight testing telemetry technology

The quantitative evaluation criteria for the six technology categories are as follows:

B_1 - A type of technology unique to hypersonic vehicles.

B_2 - Categories of technologies that have intersections with other fields of technology (the greater the intersection, the less important).

B_3 - is the technical category at the beginning of hypersonic vehicles.

The judgment matrix A-B of criterion layer 1 for the target layer is:

A	B_1	B_2	B_3
B_1	1	5	1/3
B_2	1/5	1	1/7
B_3	3	7	1

(2.2)

For the convenience of calculation, the above matrix is denoted as A, abbreviated as (the same hereinafter):

$$A = \begin{bmatrix} 1 & 5 & 1/3 \\ 1/5 & 1 & 1/7 \\ 3 & 7 & 1 \end{bmatrix} \quad (2.3)$$

Write out the judgment matrix B_1 (relative to criterion B_1, the comparison between the various technology categories), B_2 (relative to criterion B_2, comparison between technology categories), *B3* (comparison between technology categories relative to guideline B_3) is:

$$\boldsymbol{B}_1 = \begin{bmatrix} 1 & 1/2 & 3 & 1 & 3 & 1 \\ 3 & 1 & 5 & 1 & 5 & 3 \\ 1/3 & 1/5 & 1 & 1/5 & 1 & 1/5 \\ 1 & 1 & 5 & 1 & 5 & 1 \\ 1/3 & 1/5 & 1 & 1/5 & 1 & 1/5 \\ 1 & 1/3 & 5 & 1 & 5 & 1 \end{bmatrix}$$

$$\boldsymbol{B}_2 = \begin{bmatrix} 1 & 1/3 & 7 & 1 & 5 & 3 \\ 3 & 1 & 7 & 1 & 7 & 1 \\ 1/7 & 1/7 & 1 & 1/5 & 1/3 & 1/5 \\ 1 & 1 & 5 & 1 & 5 & 1 \\ 1/5 & 1/7 & 3 & 1/5 & 1 & 1/5 \\ 1/3 & 1 & 5 & 1 & 5 & 1 \end{bmatrix} \qquad (2.4)$$

$$\boldsymbol{B}_3 = \begin{bmatrix} 1 & 1/3 & 7 & 3 & 5 & 7 \\ 3 & 1 & 7 & 3 & 7 & 7 \\ 1/7 & 1/7 & 1 & 1/3 & 1 & 1 \\ 1/3 & 1/3 & 3 & 1 & 5 & 3 \\ 1/5 & 1/7 & 1 & 1/5 & 1 & 1 \\ 1/7 & 1/7 & 1 & 1/3 & 1 & 1 \end{bmatrix}$$

The establishment of numerical judgment matrix makes judgment thinking mathematical, simplifies the analysis of problems, and makes it possible to quantify complex problems. In addition, this mathematical approach helps decision-makers check and maintain consistency in their judgmental thinking. It is very important to apply analytic hierarchy process and maintain consistency in critical thinking.

The so-called consistency of judgment thinking refers to the coordination between various judgments when judging the importance of indicators, so that there will be no contradictory results.

When the judgment matrix cannot guarantee complete consistency, the eigenroot of the corresponding judgment matrix will change, which can be used to test the consistency of the judgment by changing the eigenroot of the judgment matrix. In the analytic hierarchy process, the negative average value of the other eigenroots except the largest eigenroot of the judgment matrix is introduced as an index to measure the deviation consistency of the judgment matrix:

$$\mathrm{CI} = \frac{\lambda_{\max} - n}{n - 1} \qquad (2.5)$$

Check the consistency of decision-makers' judgment thinking.

Obviously, when the judgment matrix has full agreement, CI = 0. In addition, when the judgment matrix has satisfactory consistency, λ_{max} is slightly greater than n, and the other eigenroots are also close to zero. However, this statement is not rigorous enough, and a measure of "satisfaction consistency" must be given. Therefore, to measure whether different judgment matrices have satisfactory consistency, it is also necessary to introduce the average random consistency index RI value of the judgment matrix. For order 1 to 9 judgment matrices, the values of RI are listed in Table 23.

Table 2-3: Average Random Consistency Index RI of the Judgment Matrix

Tier 1	Tier 2	Tier 3	Tier 4	Tier 5	Tier 6	Tier 7	Tier 8	Tier 9
0.00	0.00	0.58	0.90	1.12	1.24	1.32	1.41	1.45

When the order is greater than 2, the ratio of the CI of the consistency index of the judgment matrix to the RI of the average random consistency index of the same order is called the random agreement ratio, which is the CR. When $CR = \frac{CI}{RI} < 0.10$, it is considered that the judgment matrix has satisfactory consistency, otherwise the judgment matrix needs to be adjusted to have satisfactory consistency.

For the judgment matrix A, the result is:

$$\boldsymbol{W} = \begin{bmatrix} 0.2789 \\ 0.0719 \\ 0.6491 \end{bmatrix}, \lambda_{max} = 3.0648, \mathrm{CI} = 0.0324, \mathrm{RI} = 0.58, \mathrm{CR} = 0.0559 \quad (2.6)$$

For the judgment matrix B_1, the result is:

$$\boldsymbol{W} = \begin{bmatrix} 0.1684 \\ 0.3232 \\ 0.0488 \\ 0.2241 \\ 0.0488 \\ 0.1866 \end{bmatrix}, \lambda_{max} = 6.2419, \mathrm{CI} = 0.0484, \mathrm{RI} = 1.2400, \mathrm{CR} = 0.0390 \quad (2.7)$$

For the judgment matrix B_2, the result is:

$$\boldsymbol{W} = \begin{bmatrix} 0.2294 \\ 0.2914 \\ 0.0323 \\ 0.2169 \\ 0.0493 \\ 0.1806 \end{bmatrix}, \lambda_{max} = 6.4526, \mathrm{CI} = 0.0905, \mathrm{RI} = 1.2400, \mathrm{CR} = 0.0730 \quad (2.8)$$

For the judgment matrix B3, the result is:

$$\boldsymbol{W} = \begin{bmatrix} 0.2805 \\ 0.4279 \\ 0.0488 \\ 0.1466 \\ 0.0474 \\ 0.0488 \end{bmatrix}, \lambda_{max} = 6.1986, \mathrm{CI} = 0.0397, \mathrm{RI} = 1.2400, \mathrm{CR} = 0.0320 \quad (2.9)$$

Table 2-4 shows the total ranking of the criticality of each technology category. The criticality from high to low is propulsion technology, overall technology, test verification technology, flight demonstration verification technology, flight navigation guidance and control technology, and material/process/manufacturing technology.

Table 2-4: Ranking of the criticality of each technology category

Level B / Level C	B_1	B_2	B_3	Overall order W $\sum_{j=1}^{3} b_j c_{ij} (i = 1,2,3)$
	0.2789	0.0719	0.6491	
C_1	0.1684	0.2294	0.2805	0.245 533
C_2	0.3232	0.2914	0.4279	0.388 842
C_3	0.0488	0.0323	0.0488	0.047 609
C_4	0.2241	0.2169	0.1466	0.173 255
C_5	0.0488	0.0493	0.0474	0.047 922
C_6	0.1866	0.1806	0.0488	0.096 704

The analytic hierarchy process is used for the key technologies in each technology category, and the same quantitative evaluation criteria for the key technologies are adopted as follows:

BB1 - Hypersonic vehicle unique technology; *BB2* - This technology is a development of hypersonic vehicles necessary and with great difficulty; *BB3* - Entry point technology for the development of hypersonic vehicle technology.

The judgment matrix of the evaluation criteria is:

$$\boldsymbol{AA} = \begin{bmatrix} 1 & 1/3 & 1/5 \\ 3 & 1 & 1/3 \\ 5 & 3 & 1 \end{bmatrix} \tag{2.10}$$

1. Propulsion technology:

$$\boldsymbol{BB}_1 = \begin{bmatrix} 1 & 1 & 3 & 5 & 3 \\ 1 & 1 & 3 & 5 & 3 \\ 1/3 & 1/3 & 1 & 1 & 1/3 \\ 1/5 & 1/5 & 1 & 1 & 1/3 \\ 1/3 & 1/3 & 3 & 3 & 1 \end{bmatrix}, \boldsymbol{BB}_2 = \begin{bmatrix} 1 & 3 & 1 & 1 & 5 \\ 1/3 & 1 & 1/3 & 1/3 & 3 \\ 1 & 3 & 1 & 1 & 3 \\ 1 & 3 & 1 & 1 & 3 \\ 1/5 & 1/3 & 1/3 & 1/3 & 1 \end{bmatrix},$$

$$\boldsymbol{BB}_3 = \begin{bmatrix} 1 & 3 & 5 & 5 & 5 \\ 1/3 & 1 & 1/3 & 1/3 & 1/3 \\ 1/5 & 3 & 1 & 1 & 1 \\ 1/5 & 3 & 1 & 1 & 3 \\ 1/5 & 3 & 1 & 1/3 & 1 \end{bmatrix} \tag{2.11}$$

For the judgment matrix AA, the result is:

$$\boldsymbol{W} = \begin{bmatrix} 0.1047 \\ 0.2582 \\ 0.6369 \end{bmatrix}, \lambda_{\max} = 3.0385, \mathrm{CI} = 0.0192, \mathrm{RI} = 0.58, \mathrm{CR} = 0.0331 \tag{2.12}$$

For the judgment matrix BB_1, the result is:

$$\boldsymbol{W}=\begin{bmatrix}0.3442\\0.3442\\0.0831\\0.0678\\0.1607\end{bmatrix},\ \lambda_{max}=5.1466,\ \mathrm{CI}=0.0366,\ \mathrm{RI}=1.1200,\ \mathrm{CR}=0.0327 \tag{2.13}$$

For the judgment matrix BB_2, the result is:

$$\boldsymbol{W}=\begin{bmatrix}0.2942\\0.1103\\0.2656\\0.2656\\0.0642\end{bmatrix},\ \lambda_{max}=5.1333,\ \mathrm{CI}=0.0333,\ \mathrm{RI}=1.1200,\ \mathrm{CR}=0.0298 \tag{2.14}$$

For the judgment matrix BB_3, the result is:

$$\boldsymbol{W}=\begin{bmatrix}0.4986\\0.2449\\0.0829\\0.1286\\0.0451\end{bmatrix},\ \lambda_{max}=5.2759,\ \mathrm{CI}=0.0690,\ \mathrm{RI}=1.1200,\ \mathrm{CR}=0.0616 \tag{2.15}$$

The criticality of each technology in the propulsion technology category from high to low is as follows: scramjet engine technology, combined propulsion system technology, thermal structure and cooling technology of high-level propulsion engine, propulsion system control technology, and heat-absorbing hydrocarbon fuel technology (Table 2-5).

Table 2-5: The total ranking of the criticality of each technology in the promotion technology category

Level BB / Level C_2	BB_1	BB_2	BB_3	Overall order W
	0.1047	0.2582	0.6369	$\sum_{j=1}^{3} b_j c_{ij}\ (i=1,2,3)$
$C_{2\text{-}1}$	0.3442	0.2942	0.4986	0.429 559
$C_{2\text{-}2}$	0.3442	0.1103	0.2449	0.220 494
$C_{2\text{-}3}$	0.0831	0.2656	0.0829	0.130 078
$C_{2\text{-}4}$	0.0678	0.2656	0.1286	0.157 582
$C_{2\text{-}5}$	0.1607	0.0642	0.0451	0.062 126

2. Overall technology

The key degree of each technology in the overall technology category from high to low is as follows**:** shape design and aerodynamic numerical simulation technology, integrated design technology, aerothermal numerical simulation technology**,** structural design thermal protection and thermal management technology**,** multidisciplinary design optimization technology, and flight simulation technology (Table 2-6).

Table 2-6: Ranking of the criticality of each technology in the overall technology category

Level BB / Level C_1	BB_1	BB_2	BB_3	Overall order W
	0.1047	0.2582	0.6369	$\sum_{j=1}^{3} b_j c_{ij} (i = 1,2,3)$
$C_{1\text{-}1}$	0.079 964 175	0.143 886	0.416 656	0.310 892
$C_{1\text{-}2}$	0.257 881 913	0.207 52	0.208 876	0.213 615
$C_{1\text{-}3}$	0.079 964 175	0.083 073	0.112 182	0.101 27
$C_{1\text{-}4}$	0.096 031 933	0.271 365	0.168 946	0.187 723
$C_{1\text{-}5}$	0.428 342 104	0.238 995	0.059 482	0.144 44
$C_{1\text{-}6}$	0.057 815 7	0.055 161	0.033 858	0.041 86

3. Test verification technology

The key degree of each technology in the test verification technology category from high to low is as follows: direct-connected scramjet test technology, scramjet engine free jet test technology, hypersonic vehicle aerodynamic test technology, combined propulsion system test technology, hypersonic vehicle aerothermal test technology, hypersonic wind tunnel technology, and thermal environment simulation and test technology of heat-proof structural materials (Table 2-7).

Table 2-7: The total ranking of the criticality of each technology in the test verification technology category

Level BB / Level C_4	BB_1	BB_2	BB_3	Overall order W
	0.1047	0.2582	0.6369	$\sum_{j=1}^{3} b_j c_{ij} (i = 1,2,3)$
$C_{4\text{-}1}$	0.234 464	0.077 043	0.393 743	0.295 216
$C_{4\text{-}2}$	0.234 464	0.197 559	0.209 925	0.209 259
$C_{4\text{-}3}$	0.234 464	0.197 559	0.060 472	0.114 073
$C_{4\text{-}4}$	0.045 371	0.248 628	0.049 263	0.100 322
$C_{4\text{-}5}$	0.085 001	0.071 621	0.153 371	0.125 074
$C_{4\text{-}6}$	0.116 344	0.155 263	0.096 836	0.113 945
$C_{4\text{-}7}$	0.049 891	0.052 327	0.036 389	0.041 911

4. Flight demonstration verification technology

The criticality of each technology in the flight demonstration verification technology category from high to low is as follows: hypersonic separation technology, flight test telemetry technology, flight test risk assessment technology, air launch technology, and ground launch technology (Table 2-8).

5. Flight navigation guidance and control technology

The criticality of flight navigation guidance and control technology is as follows: hypersonic vehicle aerodynamic/propulsion integrated control technology, hypersonic cruise vehicle navigation and control technology, and hypersonic long-range strike weapon precision guidance and control technology (Table 2-9).

Table 2-8: Ranking of the criticality of each technology in the flight demonstration verification technology category

Level BB / Level C_6	BB_1	BB_2	BB_3	Overall order W
	0.1047	0.2582	0.6369	$\sum_{j=1}^{3} b_j c_{ij} (i = 1,2,3)$
$C_{6\text{-}1}$	0.1111	0.2068	0.1142	0.137 745
$C_{6\text{-}2}$	0.1111	0.1070	0.1015	0.103 907
$C_{6\text{-}3}$	0.1111	0.0775	0.0917	0.090 027
$C_{6\text{-}4}$	0.5556	0.4427	0.5155	0.500 776
$C_{6\text{-}5}$	0.1111	0.1660	0.1772	0.167 345

Table 2-9: Ranking of the criticality of each technology in the category of flight navigation guidance and control technology

Level BB / Level C	BB_1	BB_2	BB_3	Overall order W
	0.1047	0.2582	0.6369	$\sum_{j=1}^{3} b_j c_{ij} (i = 1,2,3)$
$C_{5\text{-}1}$	0.730 64	0.669 42	0.730 64	0.714 689 52
$C_{5\text{-}2}$	0.188 39	0.242 64	0.188 39	0.202 361 92
$C_{5\text{-}3}$	0.080 96	0.087 95	0.080 96	0.082 748 56

6. Materials/Processes/Manufacturing Technologies

The criticality of each technology in the material/process/manufacturing technology category from high to low is as follows: heat-proof and heat-insulating materials, heat-resistant coating materials, component connection welding and sealing technology, lightweight and high-strength materials, and special-shaped structure design and molding technology (Table 2-10).

Table 2-10: Ranking of the criticality of each technology in the material/process/manufacturing technology category

Level BB / Level C_3	BB_1	BB_2	BB_3	Overall order W
	0.1047	0.2582	0.6369	$\sum_{j=1}^{3} b_j c_{ij} (i = 1,2,3)$
$C_{3\text{-}1}$	0.2000	0.4027	0.3426	0.343 111
$C_{3\text{-}2}$	0.2000	0.2595	0.2208	0.228 545
$C_{3\text{-}3}$	0.2000	0.1342	0.1423	0.146203
$C_{3\text{-}4}$	0.2000	0.0694	0.0736	0.085 736
$C_{3\text{-}5}$	0.2000	0.1342	0.2208	0.196 205

According to the product of the weight of the technology category group where the key technology is located and the weight in the group, the key technology is ranked as the key degree, the total ranking of each key technology is obtained, the criticality is normalized, and the classification of key technology level 1~9 is given, as shown in Table 2-11. Among them, the scramjet engine is in the position of the highest key technology, which is in line with the general understanding of the key technologies of hypersonic vehicles, and the hypersonic separation technology is in a relatively high position among various technologies, indicating that the application of analytic hierarchy process can analyze the key technology of hypersonic vehicle more comprehensively and scientifically, and can obtain a more global understanding of the development of hypersonic vehicle.

Table 2-11: Ranking of the criticality of key technologies of hypersonic vehicles

Code	Intensity of Category	Intensity of Technology within Category	Criticality	Name of Technology	Value
C_{2-1}	0.388 842	0.429 559	0.167 031	Scramjet engine technology	9
C_{2-2}	0.388 842	0.220 494	0.085 737	Combined propulsion system technology	5
C_{1-1}	0.245 533	0.310 892	0.076 334	External design and aerodynamic force numeric simulation technology	5
C_{2-4}	0.388 842	0.157 582	0.061275	Hypersonic propulsion engine thermal structure and cooling	4
C_{1-2}	0.245 533	0.213 615	0.052 450	Integrated design technology	3
C_{4-1}	0.173 255	0.295 216	0.051 148	Direct-connected super-combustion chamber testing technology	3
C_{2-3}	0.388 842	0.130 078	0.050 580	Propulsion system control technology	3
C_{6-4}	0.096 704	0.500 776	0.048 427	Hypersonic separation technology	3
C_{1-4}	0.245 533	0.187 723	0.046 092	Aerodynamic heating numeric simulation technology	3
C_{4-2}	0.173 255	0.209 259	0.036 255	Scramjet engine free jet testing technology	3
C_{1-5}	0.245 533	0.144 44	0.035 465	Structural design thermal protection and heat management technology	3
C_{5-1}	0.047 922	0.714 689	0.034 249	Hypersonic flight vehicle aerodynamics / propulsion integrated control technology	2
C_{1-3}	0.245 533	0.101 27	0.024 865	Interdisciplinary design optimization technology	2
C_{2-5}	0.388 842	0.062 126	0.024 157	Endothermic hydrocarbon fuel technology	2
C_{4-5}	0.173 255	0.125 074	0.021 670	Hypersonic aircraft aerodynamic testing technology	2
C_{4-3}	0.173 255	0.114 073	0.019 764	Combined propulsion systems testing technology	2
C_{4-6}	0.173 255	0.113 945	0.019 742	Hypersonic vehicle aerodynamic heating testing technology	2
C_{4-4}	0.173 255	0.100 322	0.017 381	Hypersonic wind tunnel technology	2
C_{3-1}	0.047 609	0.343 111	0.016 335	Heat-resistant and thermal insulation materials	2
C_{6-5}	0.096 704	0.167 345	0.016 183	Flight testing telemetry technology	2
C_{6-1}	0.096 704	0.137 745	0.013 320	Flight testing risk assessment technology	1
C_{3-2}	0.047 609	0.228 545	0.010 881	Heat-resistant coating materials	1
C_{1-6}	0.245 533	0.041 86	0.010 278	Flight emulation technology	1
C_{6-2}	0.096 704	0.103 907	0.010 048	Aerial launch technology	1
C_{5-2}	0.047 922	0.202 361	0.009 698	Hypersonic cruise vehicle navigation and control technology	1
C_{3-5}	0.047 609	0.196 205	0.009 341	Component joining, welding and sealing technology	1
C_{6-3}	0.096 704	0.090 027	0.008 706	Ground launch technology	1
C_{4-7}	0.173 255	0.041 911	0.007 261	Heat-resistant structural materials thermal environment simulation and testing technology	1
C_{3-3}	0.047 609	0.146 203	0.006 961	Light(weight) high-strength materials	1
C_{3-4}	0.047 609	0.085 736	0.004 082	Atypical structural design and shaping technology	1
C_{5-3}	0.047 922	0.082 748	0.003 965	Hypersonic remote strike weapon precision guidance and control technology	1

2.4: Hypersonic vehicle technology maturity analysis

2.4.1: Technology maturity analysis model

In the 1990s, NASA proposed the concept of technology readiness level (TRL). Technology maturity is a systematic and objective technology evaluation system that evaluates the maturity of a specific technology according to different development stages or key nodes and divides the technology maturity level into nine levels [7], as shown in Figure 2-3 and Table 2-12.

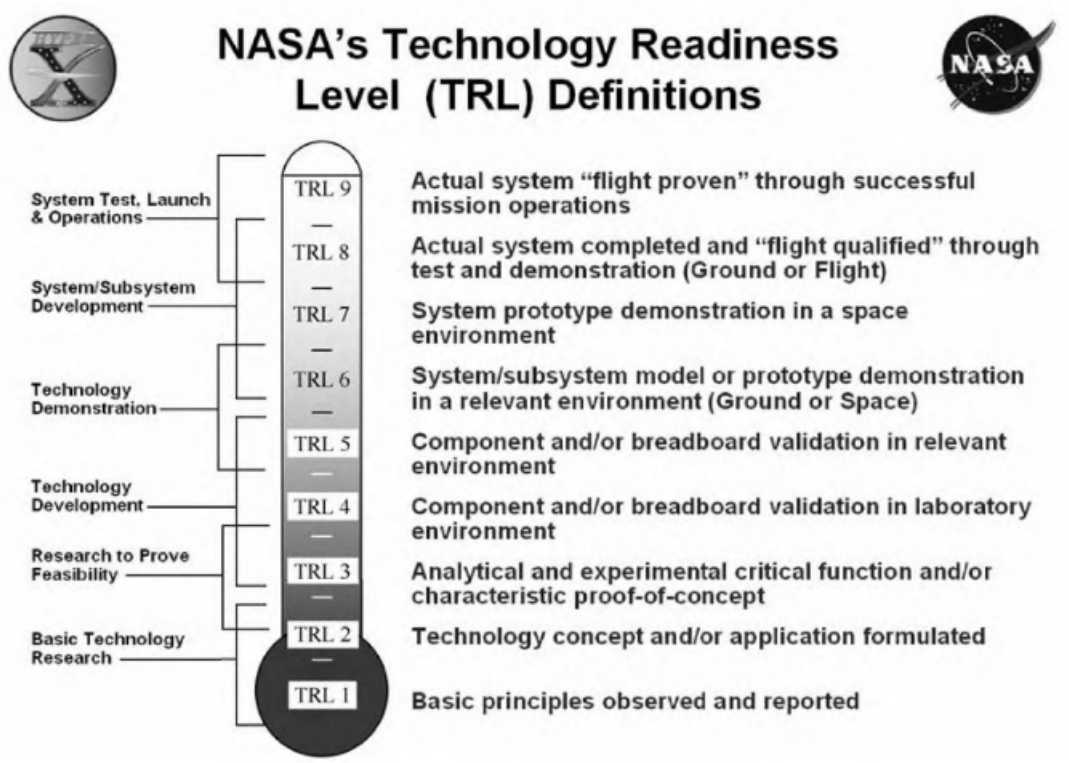

Figure 2-3: NASA's definition of technology maturity (see Table 2-12)

Table 2-12: Technology Maturity Level (TRL) Criteria

Level	Criterion
9	Real-world systems are flight tested through continuous use
8	Complete the development of real systems and obtain flight verification through test or demonstration
7	Prototypes of the system technology are validated in a real-world environment
6	A technical model or prototype of a system or subsystem is validated in the relevant environment
5	The part or breadboard is validated in the relevant environment
4	The part or breadboard is validated in the relevant laboratory environment
3	Critical functions or features are verified by analysis and testing
2	Form a technical solution or application method
1	Research and report on rationale

Note: If a technology that has been flight validated is applied to a new environment that has not been qualified, the technical maturity assessment of the technology should be reconducted.

Through this classification, the maturity level of the technology can be calibrated and compared across domains.

TRL is mainly for technology development, and when integrating technology into a system or platform, there is still a lot of comprehensive integration work to be done, which involves the maturity of technology comprehensive integration. To this end, NASA has proposed the concept of integration readiness level (IRL). The definition of IRL is shown in Table 2-13.

Table 2-13: Integrated Integration Maturity (IRL) Criteria

Level	Criterion
5	Manufacturing, launching and operation of practical systems
4	Prototype/Demonstration validated in a representative flight environment
3	The physical prototype of the system has been verified by the ground test environment
2	Complete the detailed design analysis of the system
1	Complete a conceptual system analysis

Based on the two indicators of TRL and IRL, the "Technology Maturity Analysis Model" is formed, which is used to determine and control the risk of a technology project by assessing the gap between the current maturity of a technology and the maturity required for application, as well as the risks and possibilities of reaching a certain technology maturity level. On the other hand, according to the maturity status of the technology, the gap between it and the application, the system integration of the aircraft, and the flight demonstration and verification needs of the technology, is used to guide the formulation of a phased technology development strategy.

In 2001, NASA and some units of the U.S. Air Force established the RLV Technology Flight Demonstration and Verification Research Group to study the needs, factors to be considered and feasible test plans for RLV technology flight demonstration and verification. As part of this study, a technology development and maturation model called a "phased development pathway" (PDA) was proposed [8].

The PDA model divides the technology development path into four stages: basic research and technology development stage, key technology demonstration and verification stage, aircraft system demonstration and verification stage, and mission vehicle development stage.

The PDA model uses two evaluation parameters: Technology Maturity (TRL) and Integrated Integration Maturity (IRL). TRL is used to judge the maturity of a single technology, and IRL is used to judge the overall maturity of a technology in a specific application system and the overall maturity of the entire system. Through the evaluation of these two technology maturity parameters, the development stage of the technology and the work content of the corresponding stage are determined to ensure that the relevant technologies and systems reach the required maturity level.

The analysis steps of the Technology Maturity Analysis Model are as follows:

(1) Definition of background scheme.

(2) Analyze the background scheme.

(3) Determine the maturity of the technologies that need to be developed.

(4) Judge the maturity of the comprehensive integration of related technologies and background aircraft.

(5) Determine the requirements of relevant technologies for flight demonstration verification.

(6) Carry out technology development planning according to the needs of technology maturity and demonstration verification.

When formulating the technology development plan, a technology maturity level below 4 will continue to be researched and developed in the laboratory, and then through ground or flight demonstration verification. For technologies with a technology maturity level of 4 to 5, a key technology demonstration and verification project should be conducted to increase the technology maturity level to 6. Flight validation screening criteria are used to determine which items need to be flight tested, based on whether flight testing is necessary to obtain a relevant or effective test environment in order to continue to advance the technology. For technologies with a technology maturity level higher than 6, they should be demonstrated and verified to increase the technology maturity to 8 and the comprehensive integration maturity to 4.

Here, again, the flight validation project screening criteria are used to determine which demonstration validations require flight testing. Repeat the above process until all flight technologies have reached technical maturity level 8 or above, and all aircraft concepts have reached integrated maturity level 4 or above, at which point the project can move to the development stage of practical aircraft.

2.4.2: Application analysis of technology maturity to reusable space launch vehicles

Table 2-14 shows NASA's division of the technical composition of the *Ma* = 15 air-breathing reusable space launch vehicle, as well as the assessment of the technical maturity of each technology. Through such a division, the technology required for the development of air-breathing reusable space launch vehicles is clarified, and the assessment of technology maturity is conducive to a more comprehensive and reasonable development plan of technology.

Table 2-14: *Ma* = 15 Air-breathing Reusable Space Launch Vehicle Technology Composition and Technology Maturity Analysis

1.0	Aircraft systems	5.0	Thermal protection system
1.01	Task requirements definition	5.01	Active cooling of the leading edge
1.02	Definition of aircraft system requirements	5.02	Actively cools the windward panel of the
1.03	Aircraft system analysis	5.03	Passively cools the leading edge
1.04	Aircraft operation analysis	5.04	Passively cooled fuselage leeward panels
2.0	Propulsion system - performance	5.05	Passively cooled body windward panels
2.01	Dual-modal scramjet engine	5.06	Passively cooled control surface panel
2.02	Low-speed propulsion system	6.0	Mechanical subsystems
2.03	Liquid oxygen replenishes scramjet engine	6.01	Fuel system
2.04	External combustion	6.02	Oxidizer system
2.05	External rocket systems	6.03	valves, pressure sensors, etc.
2.06	Integration of flow channels	6.04	Auxiliary power unit
3.0	Propulsion system - structure	6.05	Power source and control system
3.01	The combustion chamber actively cools the	6.06	Active-action control system
3.02	Active cooling structure of intake/tail nozzle	6.07	Hydraulic and high-pressure actuators
3.03	The leading edge of the active energy but	6.08	undercarriage
3.04	Thermal protection system	6.09	Aircraft thermal control system
3.05	High-temperature propellant pipelines	6.10	Hydrogen fuel pumps
3.06	Cryogenic propellant pipelines	6.11	Oxygen fuel pump
3.07	Main structure	7.0	Avionics & Electronic Systems
3.08	Sealing (static vs. dynamic)	7.01	Integrated avionics system
4.0	Airframe - structure	7.02	Integrated main engine control and monitoring
4.01	Fuselage shell with liquid hydrogen storage	7.03	GNC mission design
4.02	Liquid oxygen storage tank	7.04	Thermal management of electronic devices
4.03	Horizontal control surfaces	7.05	Power supply system
4.04	Vertical control surfaces	7.06	Powertrain management and control
4.05	Load compartment	7.07	Airborne data system
4.06	Landing gear compartment	7.08	Pneumatic actuation controller
4.07	Aileron	7.09	RLV sensor
4.08	Seal		

As can be seen from Table 2-14, the main technical difficulties of air-breathing reusable space launch vehicles are concentrated in three aspects: first, the comprehensive analysis of the system of this new type of vehicle; the second is the related technology of hypersonic propulsion system; the third is the relevant technology of structure and thermal protection under hypersonic flight conditions.

Technology maturity assessment is a complex undertaking that requires an objective and accurate assessment based on a fairly comprehensive and in-depth understanding of aerospace technology and related industrial sectors. In the development planning of hypersonic vehicle technology, it is necessary to introduce the concept of technology maturity to the development of project plans. In terms of the assessment of technology maturity, the assessment of the technical maturity of hypersonic vehicles that is more in line with China's national conditions should be given through the investigation of experts in various professional disciplines in China and the use of scientific analysis methods, and on this basis, the project plan and research task arrangement should be carried out in a targeted manner.

2.5: Hypersonic vehicle technology development path

The biggest feature that distinguishes hypersonic vehicles from other aircraft is a high degree of integration, which makes the aircraft fuselage and propulsion system use each other and are inseparable. Therefore, the hypersonic vehicle first decomposes the research object and research stage "from top to bottom," and then gradually integrates the research of various parts with the development of technology, and gradually forms a complete aircraft research object step by step. The complete aircraft designed from the overall scheme can be divided into four levels of research, as shown in Figure 2-4.

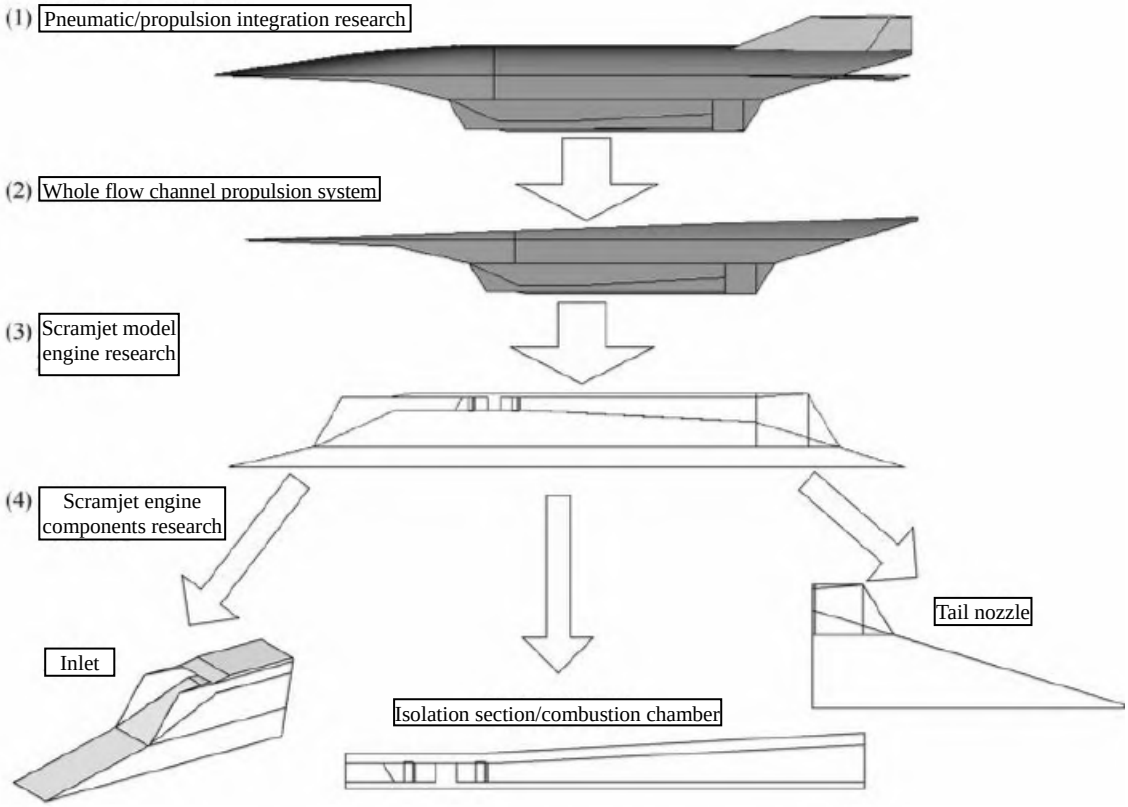

Figure 2-4: Four levels of study of a complete aircraft as an object of study

After the hypersonic vehicle is decomposed "from top to bottom," it gradually develops from the decomposed bottom-level components to the top-level vehicle. The United States has also gone through the above two stages in the development of hypersonic vehicle technology [8].

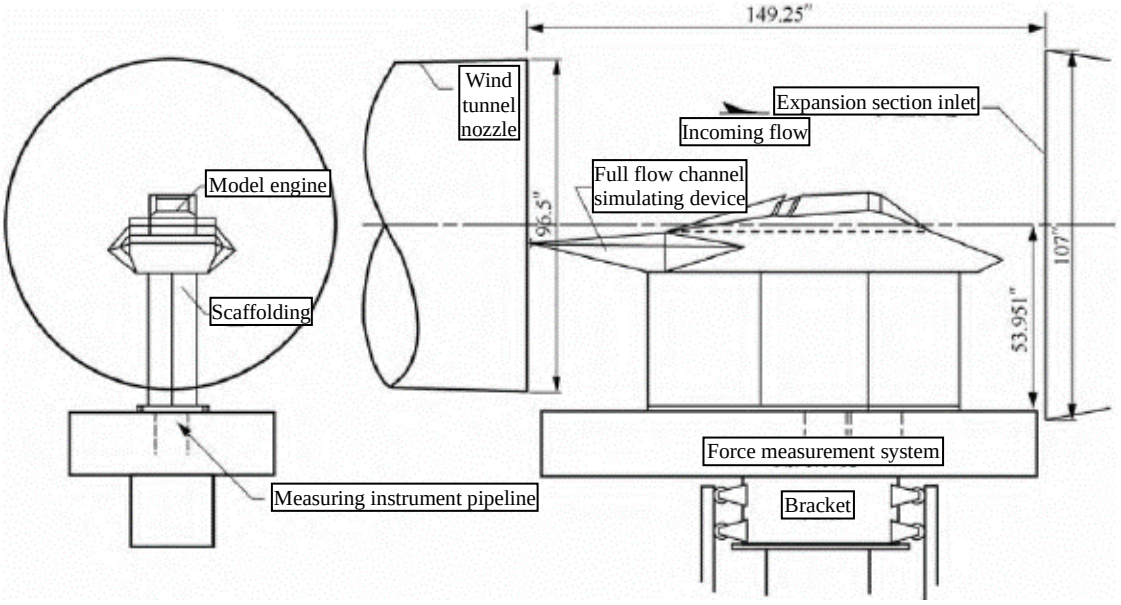

Front view Side view

(a) Hyper-X model engine

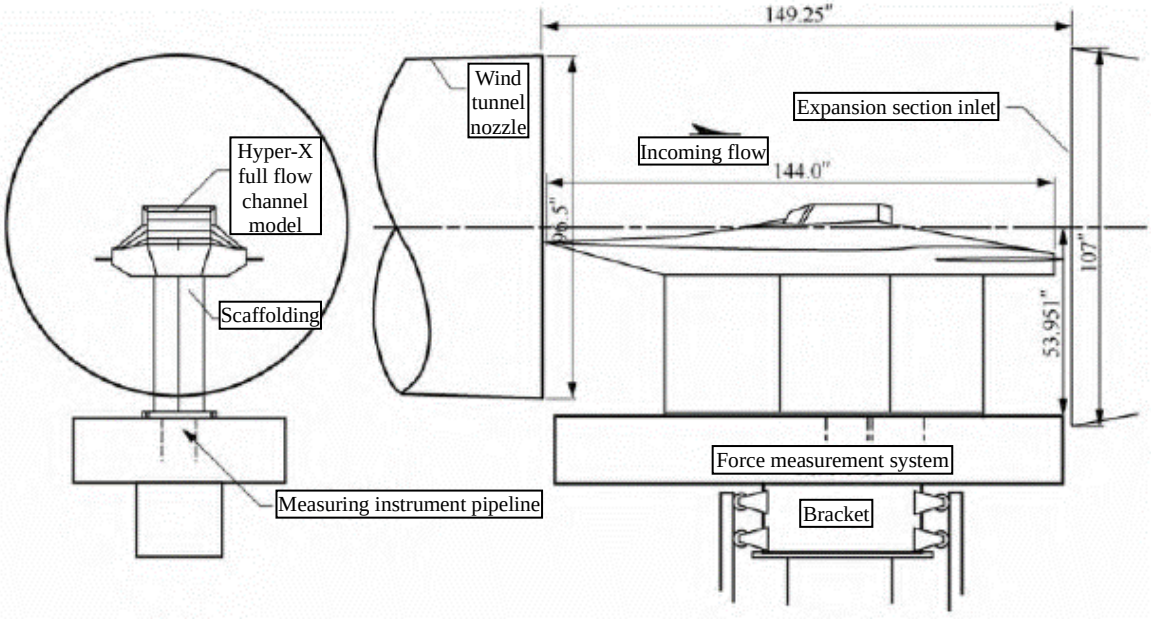

Front view Side view

(b) Hyper-X model engine and full flow channel wind tunnel test

Figure 2-5: The verification path of the fuselage propulsion integration test in the Hyper-X plan

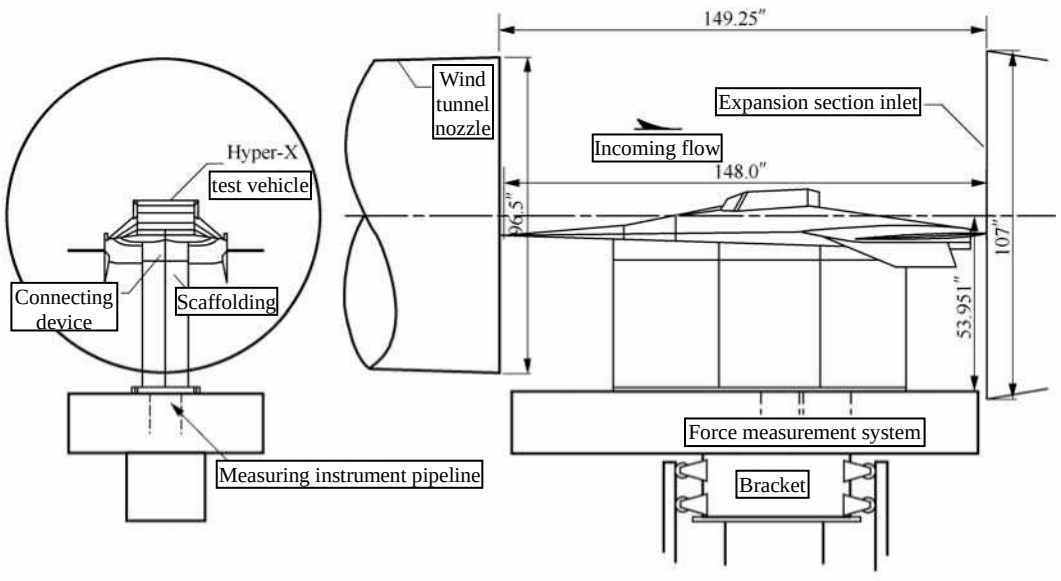

Front view Side view

(c) Wind tunnel test of the whole Hyper-X test vehicle

Figure 2-5: Verification path of fuselage propulsion integration test in the Hyper-X program (continued)

Taking the ground test of the X-43A aircraft as an example, the test study of the full flow channel propulsion system (Fig. 2-5(b)) and the test study of aerodynamic/propulsion integration (Fig. 2-5(c)) were carried out after the component and engine tests (Fig. 2-5(a)). The research object of the full flow channel propulsion system test research institute includes the flow channel of the entire propulsion system from the head to the tail of the aircraft, which can simulate and study the working conditions of the scramjet engine under the compression of its own forebody and the gas expansion of the rear body, under the test conditions, the scramjet engine is closer to the real working condition, and the measured thrust is the thrust of the scramjet engine actually acting on the aircraft; the experimental study of aerodynamic/propulsion integration is to take the complete aircraft as the research object, and the data measurement of the engine working state and the aerodynamic and propulsion characteristics of the integrated aircraft, which is the most comprehensive ground test before the flight test, and the obtained data combined with the flight simulation study is the most direct and beneficial support for the flight test.

The research on the components of the hypersonic vehicle must be decomposed based on the background of the overall aircraft scheme, and the component research has gradually developed into the free jet test of the model engine, the engine test of the full flow channel, and finally the wind tunnel test of the full integration of aerodynamics/propulsion of the whole aircraft. Figures 2-6 show the technical breakdown of the "top-down" hypersonic vehicle described earlier, the development path of the integration with the "bottom-up" technology, and the relationship between the two lines. At the same time, the two lines are interactive, and problems found at any stage of experimental research should be fed back to the overall design of the aircraft, and the research objects of components and subsystems should be redefined.

The flight demonstration and verification test of hypersonic vehicle is a necessary stage for hypersonic technology to move from laboratory and test bench to engineering application. The purpose of the flight demonstration verification includes verifying the design of the overall system, the method of verifying the overall design, verifying the design tools and simulation methods, conducting actual propulsion system tests and airframe/engine integration inspections, verifying stability and control characteristics, and obtaining flow and aerothermal data that cannot be obtained from ground tests. It can be seen that the flight demonstration test is a necessary means to test the correctness and feasibility of the theoretical analysis and calculation and the ground test results.

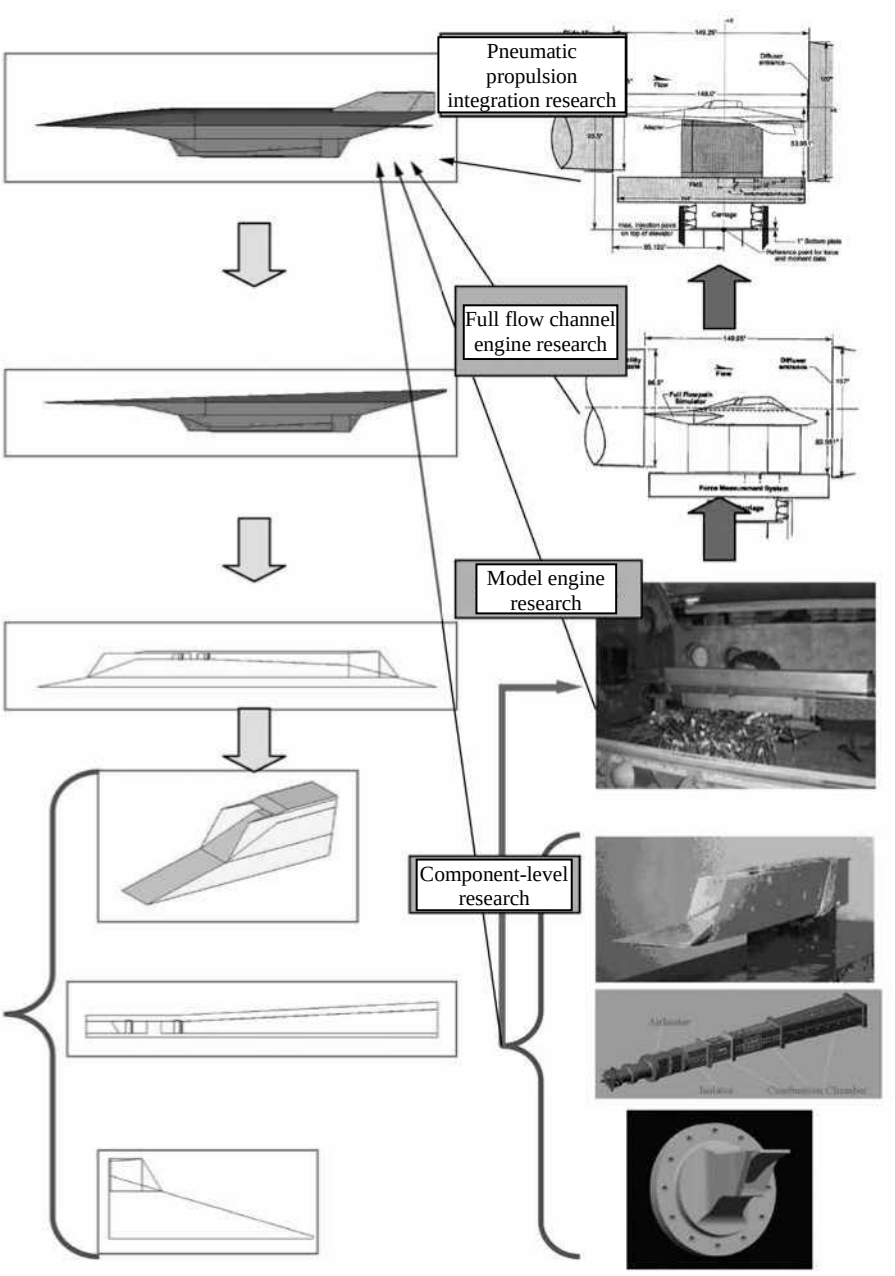

Figure 2-6: The technical development path of hypersonic vehicle technology decomposition and integration

For the program of flight demonstration verification test, it must be low cost and low risk, and the required information can be obtained within the flight envelope; according to the planned schedule, its technology must be available. The core key technologies of hypersonic vehicles include scramjet engine technology, aircraft aerodynamic shape, hypersonic vehicle control, thermal protection materials and thermal management technology, and fuselage/engine integration technology.

At present, hypersonic flight demonstration verification carried out abroad can be divided into two types: one is the flight demonstration verification of key technologies, such as the five flight tests of the scramjet engine in the “Cold” program carried out by Russia in the 1990s, the flight test of thermal protection materials in the SHEFEX program carried out by Germany, and the flight test of the S-Engine engine proposed by Japan; the other is the flight demonstration and verification of integrated comprehensive performance, such as the flight test of the X-43A and X-51A hypersonic test vehicles that have been successfully carried out by the United States, and the flight test of the Russian IGLA vehicle. The reason why the United States was able to participate in only one test of the scramjet engine in cooperation with Russia and immediately carry out the flight demonstration of the X-43A vehicle is mainly because it has inherited the technology accumulated in the NASP program for more than ten years, as well as a large number of ground wind tunnel tests, coupled with the thermal protection technology accumulated by the Space Shuttle, and the achievements of the flight control technology of multiple winged reentry vehicles, so that the flight test risk of the X-43A has been reduced to an acceptable range. Even so, the United States is still carrying out flight tests of some individual technologies through a variety of methods, such as HyCAUSE, HIFiRE program, etc.

From the feasibility and reliability analysis of the flight test program, the flight demonstration and verification of the integrated comprehensive performance involves many technical aspects, the test system is also more complex, the design, development and testing cycle of the flight demonstrator and the test system are also longer, and the cost and risk of the whole test are higher. The authors of this book believe that before conducting integrated comprehensive performance flight demonstration and verification, several individual key technology flight demonstrations should be conducted. At the same time, in order to reduce costs, it is not necessary to conduct flight demonstration verification tests for each key technology separately. Efforts should be made to carry out multiple tests in one flight, such as conducting thermal protection structure material tests simultaneously with the supersonic combustion ramjet engine flight test.

References

[1] Li Ming, Liu Peng. Demonstration method and application of weapon and equipment development system [M] Beijing: National Defense Industry Press, 2000.

[2] Michelle R Kirby. A methodology for technology identification, evaluation, and selection in conceptual and preliminary aircraft design [D]. PhD thesis, Georgia Institute of Technology, 2001.

[3] Michelle R Kirby, Dimitri N Mavris. An approach for the intelligent assessment of future technology portfolios [R]. AIAA 2002-0515, 2002.

[4] Dimitri N Mavris, Elena Garcia. Formulation of a method to assess capacity enhancing technologies [R]. AIAA 2003-2677, 2003.

[5] Journal of Beijing University of Aeronautics and Astronautics, 2010, 36(1): 110-113.

[6] Du Dong, Pang Qinghua, Modern comprehensive evaluation methods and case selection [M]. Beijing: Tsinghua University Press, 2005.

[7] Charles R McClinton, Vincent L Rausch, Robert J Shaw. X-43: Foundation for future hypersonic research [A]. 55th International Astronautical Congress [C], IAC 04-V8. 08, 2004.

[8] Paul L Moses, Vincent L Rausch, Luat T Nguyen, et al. NASA hypersonic flight demonstrators overview, status, and future plans [J]. Acta Astronautica, 2004, 55: 619-630.

CHAPTER 3: SCRAMJET TECHNOLOGY

3.1: Introduction

Scramjet engine technology is the core technology of hypersonic vehicle propulsion technology and even the entire hypersonic vehicle technology system. Scramjet and Ramjet belong to the same type of air-breathing jet engine, which is composed of an air intake, a combustion chamber and a tail nozzle, without rotating parts such as compressors and turbines, and the high-speed oncoming air flow through the intake tract decelerates and pressurizes, directly enters the combustion chamber and combusts with fuel, and produces high-temperature gas through the tail nozzle expansion and acceleration and discharge, thereby generating thrust.

When the inlet airflow velocity of the combustion chamber of the ramjet engine is subsonic, the combustion is mainly carried out in the subsonic airflow, this kind of engine is called the subsonic combustion ramjet engine, which has been widely used; when the inlet airflow velocity of the combustion chamber of the ramjet engine is supersonic speed, the combustion begins in the supersonic gas flow, this kind of engine is called scramjet engine, which is being widely studied. Subsonic combustion ramjet engines are generally used in aircraft with Mach numbers below 6, such as supersonic missiles and high-altitude reconnaissance aircraft. Scramjet engines are generally used in aircraft with Mach numbers higher than 6, such as hypersonic cruise missiles, hypersonic aircraft, and aerospace aircraft.

Scramjet engines are generally divided into dual mode ramjets and dual combustor ramjets. A dual-mode ramjet engine means that the combustion chamber of the engine works in the subsonic combustion state, supersonic combustion state or supersonic combustion/subsonic combustion/supersonic combustion state according to different incoming flow speeds. For this kind of engine, if its geometry is fixed, it can usually work across 4 flight Mach numbers, and the current research is more on the dual-modal ramjet engine with Ma_∞= 3 to 7 or 4 to 8, and the dual-modal ramjet engine can work in a wider range of Mach numbers if the geometry is adjustable, such as Ma_∞= 2~12. The main purpose of using dual cycle is to use the subsonic combustion ramjet engine to ignite the scramjet engine to solve the ignition and stable combustion problems of kerosene fuel. The dual-combustion chamber ramjet engine operates in a small Mach number range and can mainly be applied to hypersonic missiles with Ma = 6, such as the demonstration verification vehicle in the American HyFly program. The bimodal scramjet engine has a wide range of applications and has been widely studied, so this chapter focuses on the bimodal scramjet engine as the background.

Scramjet technology is the key to the development of hypersonic technology. It involves the frontier issues of aerodynamics, aerothermodynamics, computational fluid dynamics, combustion, materials science and other disciplines and their intersections, and is the integration of many high-tech such as supersonic combustion, endothermic hydrocarbon fuel, thermal protection, engine/aircraft airframe integration, ground simulation test and flight test. Both space operations and space transportation are of great significance in the future[1].

3.2: Supersonic combustion concept and key technology

3.2.1: Formulation and concept of supersonic combustion

Based on the Brayton thermal cycle analysis of isobaric combustion, Builder[2] proposed the concept of "optimal compression" for aspirated engines, pointing out that under certain compression and expansion efficiency, the air entering the engine has an optimal amount of compression, so that the engine efficiency is the highest. The higher the calorific value of the fuel and the efficiency of the process, the higher its optimal compression. Engines that are below or above this compression will be less efficient. According to this understanding, when the flight speed is low, it is not enough for all the kinetic energy of the inlet air to be pressurized, and further pressurization is required to achieve relatively high efficiency. Turbojet engines, for example, use a turbo to continue supercharging. When the flight exceeds a certain speed, the flow into the combustion chamber remains supersonic when the inlet air is compressed at an optimal compression. If the deceleration continues to increase the pressure to the point that it becomes subsonic, it will be difficult for the engine to generate thrust even if the temperature resistance allows, due to the huge total pressure loss and entropy increase.

As a result, only partial deceleration and pressurization were possible, and the combustion process had to be carried out in conditions of supersonic flow. Such a breathing engine, which operates in hypersonic conditions, is called a supersonic combustion ramjet. The term "supersonic combustion" is used here. So, in the case of an engine, supersonic combustion refers to combustion in supersonic flow (relative to the combustion chamber).

However, the phenomenon of supersonic combustion does not only appear in the engine, so it is necessary to clarify the concept of supersonic combustion in order to facilitate the understanding of the supersonic combustion phenomenon and the development of supersonic combustion engines. Literally, supersonic combustion can be understood as combustion in supersonic flow or combustion with a combustion rate of supersonic speed. According to the former, regardless of whether the combustion process is supersonic or subsonic, as long as the flow is supersonic is supersonic combustion. Corresponding to this understanding, subsonic combustion should refer to combustion in subsonic flow or even in a stationary medium. Obviously, this understanding does not highlight the physical essence of the combustion process. Because of the relativity of the motion, the flow velocity can vary depending on the reference. However, for the same physicochemical process, it should not vary due to the choice of coordinate system. The latter understanding takes into account the relativity of velocity and highlights the physical essence of the combustion process. The former understanding focuses on flow and combustion chambers and refers to the combustion phenomenon in a specific object, which has its own specific research content.

From the perspective of combustion, supersonic combustion should be the latter: the combustion process of incombustible material flowing into the combustion zone at supersonic speed relative to the combustion zone is supersonic combustion, or supersonic combustion means that the velocity of the combustion zone relative to the incombustible material exceeds the sound velocity of incombustible matter (referring to normal velocity). Thus, subsonic and supersonic combustion correspond to deflagration and detonation. The difference is that deflagration and detonation concepts are for wave combustion, while subsonic combustion and supersonic combustion contain not only wave combustion, but also regional combustion. According to this understanding, some of the knowledge accumulated in detonation studies can be used in supersonic combustion studies[3].

3.2.2: Key technologies for supersonic combustion

The key technologies for supersonic combustion are described below[4].

1. Gaseous fuel injection technology

For gaseous fuel jets, the main research objectives are to improve the penetration of the fuel, enhance the mixing between the jet and the main stream, and reduce the total pressure loss caused by the jet. The research contents include the shape of the nozzle hole, the injection angle, the dynamic pressure ratio of the jet to the main stream, the molecular weight of the jet substance, and the spatial distribution of the jet[5].

The basic flow field structure of a transverse jet in supersonic flow is shown in Figure 3-1. Biliig[6] performed extensive analyses of fuel jet penetration; Schetz[7] studied channel jets in supersonic flow; Gruber [8,9] studied different nozzle configurations using particle scattering techniques and accurately measured the pressure near the jet nozzle. These results show that the jet has strong three-dimensional characteristics due to the influence of the shear layer and the counterclockwise vortex pair.

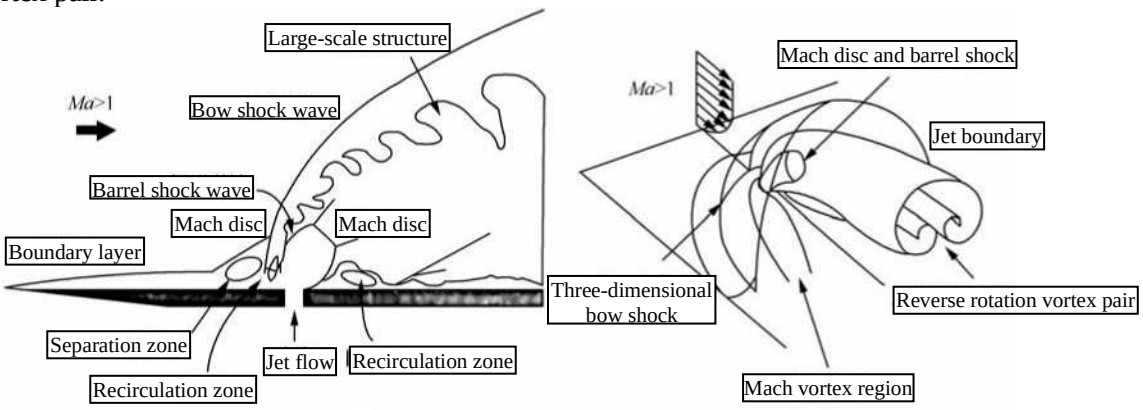

(a) The instantaneous structure of the flow field on the axial wearing surface at the center of the nozzle hole (b) Three-dimensional structure of the flow field

Figure 3-1: Basic flow field structure of a transverse jet in supersonic flow[5]

In terms of jet penetration enhancement, Glawe[10] compared the effects of different nozzle configurations on jet flow. The results show that a large part of the fuel can be directly entered into the main stream by the non-circular nozzle jet, especially when the jet is perpendicular to the main stream. Tam[11] conducted numerical simulation studies on vertical spraying of walls. The results show that the jet penetration of the circular hole is higher than that of the oval hole, but the elliptical hole spreads faster in the longitudinal direction than the circular hole. Although the calculated pressure is relatively close to the test results, the penetration of the fuel is somewhat different from the test results. Hsu[12] used Raman scattering to study the distribution of small-angle fuel jets along the cavity on the wall. The results show that the interaction between the fuel in the shear layer and the slope at the trailing edge of the cavity is the key factor affecting the fuel transport into the cavity, and the downstream counterpressure of the cavity has a great influence on the fuel distribution near the cavity.

In terms of fuel injection techniques, Mathur[13] studied the combustion flow field of the ethylene jet and analyzed the distribution of fuel near the cavity. The results show that the combustion area is more exothermic and the flame propagation velocity is fast, which indicates that the circular nozzle can provide sufficient penetration and mixing characteristics. Cox-Stouffer[14] studied the jet direction overlapping nozzle group, which uses the matching of jet pressure and incoming pressure to reduce the lateral expansion of the jet, so as to reduce the loss of jet volume, and this type of jet has the potential to enhance jet penetration. In addition, Mathur [15] conducted numerical simulations of this type of nozzle. The results show that this type of nozzle improves the penetration of the fuel jet but causes a strong total pressure loss and shock wave. Cox-Stouffer [16,17] conducted a numerical simulation study on the arrangement scheme between the nozzles of the aerodynamic ramp. Fuller [18] compared the mixing effects of different nozzle arrangements. The results show that the strong transverse vortex generated by the aerodynamic slope can achieve the mixing enhancement, and the reasonable arrangement of the distance between the nozzles can improve the penetration and reduce the total pressure loss. Eklund [19,20] studied the coupling between the pneumatic ramp nozzle and the cavity and compared the ethylene combustion with and without backpressure. The results show that the fuel exchange rate between the aerodynamic ramp injection fuel and the cavity is low, and the overall mixing efficiency is not high. Gruber [21] compared aero-ramp fuel injection with small-angle injection on the wall.

The results show that although the resistance of the pneumatic ramp is small, the mixing effect is not good. Donbar [22] analyzed the results using post-processing procedures such as FPERF, GASL-1D, and RJPA. The results show that the effect of complex aerodynamic slope injection is comparable to that of a single wall surface with small angle spraying, and its obvious advantages cannot be seen. In summary, there is no obvious difference in combustion performance between different fuel injection methods, so wall jets are widely used due to their simple structure.

In addition, Gruber [23] used scattering techniques to compare the differences between gas jets of different molecular masses. The results show that the molecular mass of the jet gas has little influence on the penetration of the jet, and the difference in the structure of the flow field is also small, but the process of the jet vortex is different due to the different compressibility of each substance. Tam [24] conducted a three-dimensional simulation study of air and helium with different compressed properties. The results showed that the air jet was under-expanded, causing stronger blockages, resulting in larger barrel shocks and Mach discs. As a result, the air mixing characteristics of the more compressible are stronger than those of helium.

2. Liquid fuel injection technology

Liquid hydrocarbon fuels are widely used in ramjet engines due to their high calorific value, small size, easy storage, safety, and low price. In scramjet engines, the air flow in the combustion chamber is supersonic before the ignition and subsonic in some areas after the ignition, so it is necessary to understand the fuel jet characteristics in both supersonic and subsonic flows. The research contents mainly include the liquid fuel jet crushing process, droplet atomization/evaporation process, fuel jet penetration, reduction of total jet pressure loss and mixing enhancement.

In supersonic flow, the liquid jet droplets exhibit a rapid crushing, atomizing, and mixing mechanism under the influence of shock waves. Tam [25] and Kush [26] studied the transverse jet of liquid in supersonic flow and gave a model for estimating the penetration of liquid transverse jet in supersonic flow.

Lin [27,28] studied the penetration of fuel jets in high-velocity streams. The results show that the liquid crushing process is extremely fast, and the droplet diameter of the pure liquid jet and the liquid jet after bubble atomization is about 10 μm. Sallam [29] studied the crushing process of a transverse jet of a liquid in a supersonic stream. The results show that compared with the transverse jet in the subsonic stream, the crushing process of the transverse jet droplets in the supersonic stream is accelerated, and the atomization mixing process is enhanced.

In subsonic flow, the penetration of the jet in the subsonic flow is greater than that in the supersonic flow under the same dynamic pressure ratio. Wu [30] used a schlieren instrument to study the jet crushing process, the process of liquid column turning into liquid beads, and the crushing distance of liquid column near the transverse jet nozzle in subsonic flow. The results show that the crushing process of the liquid column is similar to the secondary crushing process of a single droplet, and the liquid column gradually forms liquid beads due to the surface fragmentation due to the force deformation when the injection flow pressure ratio is high. Fuller [31] experimentally studied the angular liquid jet crushing process in subsonic flow. The results show that with the gradual decrease of the jet angle, the penetration of the liquid column gradually decreases, and the distance between the liquid column crushing area gradually increases, and the size of the liquid column is not controlled by the pneumatic crushing process but is similar to the turbulent jet in the stationary environment. Wu [32] used PDPA to study the downstream flow field structure of the liquid jet in subsonic flow, which showed the droplet size downstream of the jet, the velocity of the droplet along the flow direction, the spatial distribution of the liquid, the penetration of the jet, and the jet plume. The results show that with the increase of the jet pressure ratio, the jet penetration, plume width, plume equivalent ratio and plume area all increase gradually, and the large droplets are mainly distributed in the middle of the jet plume when the dynamic pressure ratio is small.

The mixing process of liquid jets can be enhanced by bubble atomization, which is widely used in scramjet engines. As shown in Figure 3-2, the liquid fuel crushing and mixing processes are enhanced after bubble atomization. Lefebvre [33-35], Sojka [36,37], and Lin [38-40] studied the liquid jet atomized by bubbles. The results show that bubble atomization has the advantages of large cross distribution area, small droplet diameter, high droplet velocity and regular jet plume distribution. Mathur [41] compared the liquid JP-7 with bubble atomization with JP-7 without bubble atomization. The results show that the stable combustion of JP-7 can only be achieved by bubble atomization at room temperature.

Lin [42] studied the mutual interference between the shock wave and the jet caused by the backpressure. The results show that when the shock wave exists near the upstream of the jet, the incoming flow decreases due to the increase of the thickness of the boundary layer, resulting in a longitudinal flow velocity and a significant increase in jet penetration. When the shock wave is farther upstream of the jet, the jet penetration decreases and is even higher when there is no backpressure.

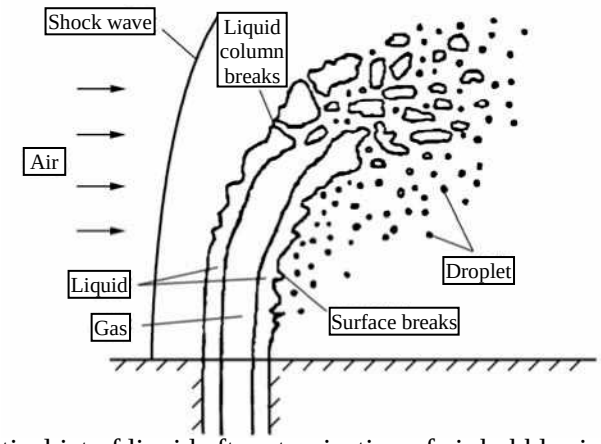

Figure 3-2: Vertical jet of liquid after atomization of air bubbles in supersonic flow

At present, the purpose of the research on liquid fuel jet technology is still to enhance the mixing of fuel and mainstream, improve the penetration of fuel jet and reduce the total pressure loss of incoming stream.

3. Hybrid enhancement technology

Due to the periodic oscillations generated by the perturbation excitation, the development of the shear layer is accelerated, and the mixing characteristics in the combustion chamber are enhanced. Based on this idea, various hybrid enhancement techniques of passive and active have been produced. The aforementioned pneumatic ramps, bubble atomization, and jet penetration enhancement are all examples of passive hybrid enhancement techniques. In addition, shock waves, cavities and support plates are also passive hybrid enhancement techniques. Active flow field control, acoustic excitation, and the introduction of pressure disturbance sources are examples of active hybrid enhancement techniques [43]. Bushnell [44] pointed out that the hybrid enhancement must weigh the balance between combustion efficiency and thrust performance, select the hybrid enhancement technology suitable for the characteristics of the engine, and make full use of pressure gradient, reflux, exothermic, turbulence, shock, and expansion waves to achieve the purpose of enhanced mixing.

Uwe [45] experimentally investigated the effect of slope shock wave on the free-shear layer of hydrogen flow to the jet in supersonic flow. The results show that the development of the shear layer accelerates sharply after the shock wave incident point, and the specific reasons need to be further analyzed. Nedungadi [46] studied the structural change of the flow field after the jet using the shock wave incident generated by the slope. The results show that the slope shock accelerates the development of jet vortex pairs and enhances the mixing of jet and mainstream. Obata [47] also obtained the results of shock-enhanced fuel mixing by about 10% through simulation studies. Kim [48] investigated the enhanced properties of shock waves on hydrogen supersonic combustion flames. The results show that the shock wave enhances the mixing of fuel and mainstream, expands the flame distribution range, and improves combustion efficiency.

Drummond [49] studied the enhancement of the mixing by the ramp shock wave in supersonic flow. The results show that the swept slope can produce a transverse large-scale vortex structure, and the strong density gradient caused by the shock wave leads to the flow vortex between the jet and the main stream, both of which enhance the mixing process of the fuel jet, but the increase of exothermic and Mach number reduces the turbulence in the supersonic flow and weakens the mixing process.

In conclusion**,** as shown in Figure 3-3, the positive shock wave sweeps through the vortex induction process in the presence of density gradient airflow, and the shock incident enhances the development rate of the jet shear layer vortex on the jet, and the shock incident expands the pre-jet separation region caused by the shock incident downstream of the jet expands, and the incident in the upstream of the jet can reduce the pre-jet separation zone [50]; shock waves enhance flame stabilization**,** and the three-dimensional results are extremely complex [51].

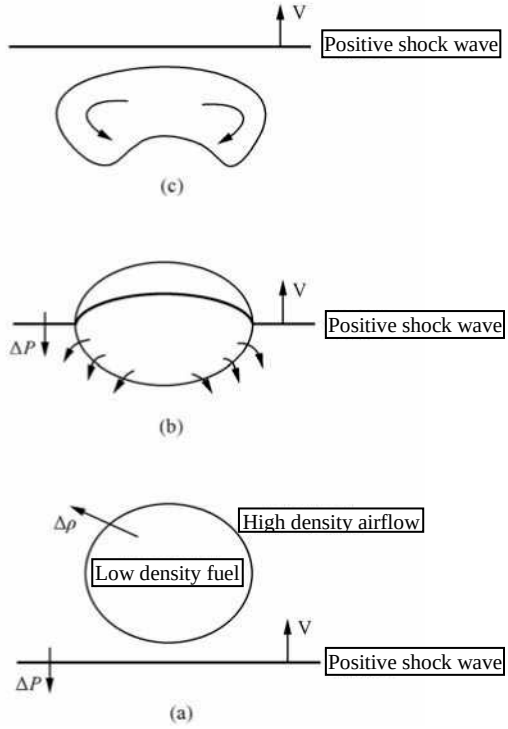

Figure 3-3: Vortex induction of a positive shock wave through a gas jet

4. Ignition technology

In the combustion chamber, when the total enthalpy of the incoming flow is high (the flight Mach number is greater than or equal to 7), the fuel can usually spontaneously combustion, and when the total enthalpy of the incoming flow is low, an additional ignition source is required. Additional ignition sources include pilot flames, plasma flares, support plates, spark plugs, throttle ignition devices, and gunpowder igniters, which enable fuel ignition by providing a high-static, low-flow, and activate-rich environment for combustible mixtures.

Pilot flame ignition is the production of a pilot flame by pre-injecting a reactive pilot fuel into the incoming stream, and then igniting the main fuel using the high temperature and activating molecule-rich environment created by the pilot flame. Commonly used pilot fuels include hydrogen, silane (SiH4), fluorine, and others [53].

The plasma torch ionizes gases (such as N2 and O2) through electrode discharge, making them plasma, and these plasma substances will directly generate or regenerate a large number of activated molecules through chemical reactions**,** which will promote fuel ignition**.** Harrison [54-56] found that the high concentration of flammable components generated by the plasma torch was the main reason for the combustion promotion, and the effect of ionized Ar on promoting combustion was not obvious**,** while ionized N2 did not only add ionization energy or heat energy. More importantly, it generates free radicals that can promote combustion, so the effect of promoting combustion is obvious.

Mader [52] found that the Ar-H2 torch is an effective igniter at temperatures below 800 K, while the Ar torch can only be used at temperatures above 890 K, and that increasing the flow of H2 in the plasma torch can increase the output energy of the torch.

The ignition of the support plate is to promote the ignition by using the shock wave of the leading edge of the support plate and the higher static temperature and static pressure obtained by the stagnation of the incoming flow. Masuya [57] found that the total temperature of the incoming flow is lower than that of the wall injection fuel, and that the fuel injected in the same direction as the incoming flow on the support plate is easy to ignite at a lower fuel flow, and the transverse injection fuel on the support plate can achieve ignition at a higher fuel flow.

Spark plugs are often used where high ignition energy is not required, such as inside cavities with combustible mixtures and low flow rates, while in high-velocity gas streams, it is difficult to successfully ignite directly in high-velocity gas streams because it is difficult for spark plugs to provide sufficient energy to activate fuel molecules in a short dwell time [58,59].

5. Flame propagation process

After the fuel is ignited near the ignition source in the supersonic flow, the flame propagation process shows strong turbulence characteristics due to the influence of the high-speed air flow, and the pulsating turbulent large-scale vortex may quickly propagate the flame to the main stream area, or it may quickly consume heat dissipation to quench the flame during the propagation process. Therefore, the key to achieving engine ignition is the turbulent flame propagation process in the supersonic gas stream. The main factors that affect the propagation of the flame are the airflow velocity and temperature, the degree of mixing of fuel and air, the degree of turbulence, the energy and duration of the ignition source, etc. Due to the rapid and complex process of flame propagation, there are few research results on this issue.

Yuan Shengxue [3] argues that the flame propagation mechanism of supersonic combustion is different from that of traditional subsonic combustion since the propagation of disturbances cannot exceed the local speed of sound. In supersonic combustion, the cause of combustion comes from the upstream of the combustion zone, that is, the fuel reaches the combustion conditions before the combustion zone, or the temperature rises, or free radicals or catalysts are injected, or the composition is changed to allow the exothermic chemical reaction to proceed. Mitani [60] conducted a numerical simulation of the initial ignition process of hydrogen in the combustion chamber. The results show that hydrogen first achieves spontaneous combustion in the high-temperature boundary layer downstream of the jet, and since the flame propagates at a speed of more than 1,300 m/s, he believes that it cannot be a propagation mechanism of a premixed flame, but an automatic ignition mechanism of an upstream fuel.

O'Byrne [61] studied the upstream propagation of downstream pressure disturbances during combustion. The results show that after the formation of downstream combustion exothermy, the high pressure of the combustion zone will compress the upstream supersonic flow, causing the upstream boundary layer separation, so that the flame region can propagate against the current, however, the results do not indicate whether the flame propagation is determined by exothermic or separation. In addition, the test results also show that the initial turbulent flame first occurs near the fuel nozzle under the conditions of 8 incoming Mach number, 1100K static temperature and 1 atm, but the flame is blown out before the downstream combustion wave is reversed to the upstream jet region. This suggests that flame stabilization and flame counter-current propagation must be coupled with the incoming compression effect caused by combustion exothermy when the fuel remains at the limit of spontaneous combustion. Sun Yingying [62] studied the effect of shock waves on the ignition of premixed airflow. The results show that the shock incident causes fuel ignition in an area with a suitable temperature and equivalent ratio, and the flame propagates downstream. The analysis shows that this is actually a process in which the ignition delay time is shortened by the shock wave, so as to realize the spontaneous combustion of the fuel induced by the shock wave incidence, and the diffusion and propagation of the burned high-temperature gas downstream.

6. Flame stabilization technology

The flow velocity in the combustion chamber of the scramjet engine reaches more than 500 m/s, and it changes with the change of the equivalent ratio, which puts forward higher requirements for the flame stabilization range and working stability of the flame stabilizer.

Designing a flame stabilizer with high combustion efficiency, wide stable flame boundary, low resistance and low loss has become one of the important aspects of supersonic combustion flow research and combustion chamber design.

One of the simplest methods of flame stabilization is the vertical injection of fuel into the wall [63,64]. The vertical jet in the supersonic gas flow will form a bow shock wave, which directly leads to the separation of the boundary layer of the wall upstream of the nozzle and forms a reflux zone, and part of the fuel enters the reflux zone and mixes and burns at low speed with the boundary layer gas flow to achieve the effect of stabilizing the flame. However, it has a small flame stabilization range and high requirements for fuel and incoming flow conditions. In addition, as mentioned earlier, jet bow shock waves tend to cause significant total pressure losses, especially at high flying Mach numbers, which limit the application of this flame stabilization method.

The support plate [65,66] integrates airflow compression and fuel injection, and is widely used. The most important feature of the incoming flow is the existence of a bottom reflux zone, which plays a role in flame stabilization to a certain extent, and the turbulence of the air flow increases due to the support plate, which helps to improve the propagation speed of the flame. However, there are also many shortcomings in the support plate: it is directly exposed to the high-speed air flow, and the resistance and total pressure loss are large; cooling and thermal protection are carried out with the help of advanced composite materials.

The reflux zone formed by the regression step [67,68] is also one of the most widely used flame stabilization methods in scramjet engines, and the reflux zone formed by it is generally much larger than that at the bottom of the support plate, so the flame stability range of the backward step is wider than that of the support plate, but its resistance is greater, and the separation flow will produce a strong shock wave when it is reattached to the downstream wall, and the total pressure loss cannot be underestimated.

The cavity flame stabilizer is structurally composed of a backward step and a forward step. The flow of air through the cavity creates a large reflux zone within the cavity, which enhances flame stabilization, and the reattachment point of the cavity separation flow is basically located near the trailing edge, resulting in a weaker shock wave and reduced total pressure loss. Several tests have shown that the cavity is an effective flame stabilizer for supersonic combustion, which is now widely adopted.

In addition to the above-mentioned major flame stabilizers, plasma jet flame stabilizers [69], cut and free reflux zone flame stabilization methods [70] have also received extensive attention.

3.3: Scramjet engine component technology

3.3.1: Intake tract

1. Research content and key issues of air intake

The hypersonic air inlet can be divided into three sub-components: the forebody compression surface (the compression section outside the air intake), the compression section in the air inlet and the isolation section. The function of the compression surface of the forebody is to provide a pre-compressed airflow with sufficient flow field quality and flow rate to meet the requirements for the inlet tract; the function of the compression section in the inlet tract is to further compress the airflow, so that the Mach number and pressure of the airflow meet the design index; the function of the isolation section is twofold, that is, one is to isolate the influence of the pressure fluctuation of the combustion chamber on the inlet tract, and the other is to form a pre-combustion shock system under the condition of high combustion chamber back pressure. The three sub-components are coupled and independent of each other, and the study of the intake tract can be a detailed study of the three sub-components or an integrated study of the entire intake system.

Whether it is for sub-components or for the entire inlet system, the study of the intake tract can be broken down into two parts: one is the design of the intake; the second is the evaluation of the performance of the inlet tract. The two are not only the content of the inlet tract research, but also the two processes that must be experienced in the development of the inlet tract. In the vast majority of inlet development, these two contents need to be repeated continuously, that is, preliminary design, performance evaluation, improved design, and performance evaluation...until the designed air intake reaches the design index. Therefore, the design and performance evaluation of the intake tract are often intertwined in the development process of the inlet duct.

According to Reference [71], "The design goal of a hypersonic air inlet is to design an inlet configuration that is as small in size and weight as possible, can provide efficient compression, produces only very low drag, has uniform flow at the combustion chamber inlet, and can maintain these properties over a wide range of Mach numbers." From this description, it can be seen that obtaining a perfect inlet configuration belongs to the category of inlet design, and how to evaluate whether the inlet meets the requirements belongs to the category of inlet performance evaluation.

The design of the inlet tract can be divided into the following three levels [72]:

(1) Scheme design of the air intake. The design of the inlet scheme is closely related to the overall scheme of the aircraft, and for the traditional design of the air-breathing aircraft, the layout of the inlet is often determined by the overall scheme. For example, an aircraft with a head-intake layout often needs to design an axisymmetric air intake, while an aircraft with a rear air intake layout (including fuselage belly air intake and fuselage side air intake) often needs to design a two-dimensional or three-dimensional compressed air intake. Since the design theory and method of hypersonic vehicle are in their infancy, the relationship between the design of the air inlet scheme and the overall design of the aircraft follows the traditional design theory and method of aircraft on the one hand, and gradually forms some inherent characteristics on the other hand.

(2) The configuration design of the air intake. Different from the design of the inlet scheme, the design of the inlet configuration refers to the study of the design method for a basic configuration. Under the premise that the overall scheme is basically determined, the selection of the inlet scheme has been basically determined, and how to design the inlet to meet the overall requirements is the research content of the configuration design. In particular, the parametric design of a specific configuration is most worthy of in-depth research in the design level of the inlet configuration.

(3) Improved design of the inlet duct. The development of the air inlet needs to go through the design and evaluation process of preliminary design, performance evaluation, improved design, and performance evaluation. After obtaining the basic configuration design scheme and obtaining the basic performance parameters, various technical means are adopted to improve the initial design problems to obtain a better performance of the inlet configuration, which is the research content of this design level. Both the "improved design" with human participation and the "optimal design" with the participation of computers developed in recent years belong to this level of research.

The performance evaluation of the inlet tract is also an important part of the inlet study, which mainly includes the selection of performance evaluation parameters, the variation of the performance of the inlet tract with the parameters, and the trade-off of various evaluation parameters. The establishment of an effective inlet performance evaluation system is an important goal of inlet performance evaluation. The evaluation of the performance of the intake tract can be broken down into the following two levels [72].

(1) Single performance evaluation. That is, through theoretical analysis, numerical calculation, or ground experiment, the physical phenomena existing in the intake tract are studied, the basic performance of the designed inlet is determined, and the variation law of the inlet performance with the configuration parameters of the inlet duct is given, so as to enhance the designer's understanding of the key factors affecting the performance of the inlet tract, and put forward the design basis for the improvement or optimization of the inlet tract.

(2) Comprehensive performance evaluation. The essence of this level of research is to comprehensively weigh various performance evaluation criteria, and often establish a reasonable comprehensive evaluation system in combination with the requirements of the overall design. For the evaluation of hypersonic air inlet performance, at least the propulsion performance of the engine, the aerodynamic performance of the aircraft, and thermal/structural performance should be comprehensively considered.

There are two key problems in the design of hypersonic air inlet [71]: first, aerodynamics, which involves problems such as inlet channel initiation, boundary layer separation, and uniformity of the inlet air flow field of the combustion chamber; the second is the mechanical aspect, including the sharp leading edge, variable geometry, wall cooling and other problems.

Reference [72] further summarizes some of the problems faced in the design of the inlet tract as follows:

(1) Inlet tract activation restriction. When the inlet tract contraction ratio is too large or inlet backpressure is too high, the inlet will fall into a non-activated state.

In this state, the intake air flow is sharply reduced, which will directly lead to a decrease in engine thrust and even stalling. Therefore, the minimum requirement for the inlet design is to be able to activate properly and ensure sufficient intake air flow. For a fixed geometry of the inlet and the same incoming flow conditions, the start-up can only be achieved under a certain shrinkage ratio, and once the inlet is actuated, the shrinkage ratio can be increased to a maximum value. The ratio of contraction corresponding to inlet tract actuation and the maximum ratio of contraction increase with the increase of Mach number. There are many factors that affect the initiation of the inlet tract, including the local Mach number, the shrinkage ratio of the inlet tract, the flow field structure, the thickness of the boundary layer, the Reynolds number, the ratio of wall temperature to free flow temperature, and the details of the initiation process. The starting performance of the inlet is the key parameter to evaluate the design of the inlet tract, and it occupies a very important position in the evaluation of the inlet tract, but due to the many influencing factors, it is difficult to find the law that can be widely applied to various inlet tracts, so this is the focus and difficulty of the inlet design.

(2) High temperature effect. For hypersonic atmospheric vehicles, due to the influence of compression effect and viscosity, when the Mach number is high, the total temperature of the incoming flow is high, and the inlet airflow will be excitation of vibrational energy, dissociation, ionization, etc., that is, the high-temperature gas effect. It is generally believed that at $Ma < 5$, the inlet airflow can be treated as an ideal gas; at $5 < Ma < 12$, the vibrational energy in the inlet boundary layer is excited and can no longer be treated as an ideal gas. This high-temperature effect must be taken into account in the design of high Mach number inlet ducts.

(3) Blunt leading edge effect. In order to meet the needs of aerodynamic heating, the leading edge of the hypersonic vehicle (including the leading edge of the head, the side edge of the air intake, and the leading edge of the hood) needs to be passivated. The hypersonic blunt leading edge will lead to the emergence of an entropy layer, which will affect the development and transition of the boundary layer and affect the performance of the inlet tract. In addition, the mutual interference between the head shock wave and the blunt leading edge of the inlet also has a significant effect on the local heat flux at the leading edge. Therefore, the blunt leading edge effect is an issue that needs to be carefully addressed in the in-depth study of the inlet airway.

(4) Sticky effect. Under hypersonic conditions, the boundary layer has a great impact on the performance of the inlet road: boundary layer separation will occur in the region with backpressure gradient, and the position and magnitude of the separation must be carefully analyzed in the design of the inlet configuration, and there are many uncertainties in the design of the air inlet configuration. The mechanical energy loss caused by the flowing boundary layer accounts for an important part of the mechanical energy loss of the hypersonic air intake, and how to balance the boundary layer loss with other related issues is an important part of the air inlet design.

The boundary layer transition has a great influence on the heat flow and friction resistance of the inlet forebody, and the turbulent boundary layer can inhibit the separation to a large extent, which is conducive to the operability of the inlet channel, but at the same time, it will lead to the increase of friction loss and heat protection burden. Accurate prediction or control of boundary layer transitions is important for detailed evaluation of inlet performance.

The control of the boundary layer is an important means to improve the performance of the inlet airway, and severe boundary layer separation can even affect the start-up performance of the inlet airway, so it is very important to control and inhibit the occurrence of boundary layer separation.

The main parameters to evaluate the aerodynamic/propulsion performance of the inlet tract are the external resistance of the inlet tract, the temperature-rise ratio, the number of self-starting Mach, the ability to withstand engine backpressure and the efficiency of the inlet tract, among which the efficiency parameters of the inlet tract are defined in various ways. Van Wie elaborated on the definitions of various inlet performance evaluation parameters in Reference [71] and analyzed the physical significance and applicability of these performance evaluation parameters. These parameters include total pressure recovery efficiency, kinetic energy efficiency, hydrostatic pressure efficiency, dimensionless entropy increase, entropy increase efficiency, process efficiency, and compression efficiency. Each of these parameters has its own advantages and disadvantages when used to evaluate the performance of the inlet tract, so it is not possible to use a single efficiency parameter to evaluate the performance of the inlet tract. However, to establish an effective inlet performance evaluation system, it is necessary to comprehensively consider the influence of various performance parameters, and also need to combine the application background of the inlet tract and the consideration of other disciplines, such as the design of the inlet structure, the layout of the aircraft, the design of the combustion chamber and other factors. Therefore, the overall design of the aircraft must be partially included in the design, and it is difficult to establish an effective performance evaluation system.

As a tool for inlet design and performance evaluation, the inlet flow field numerical analysis software plays a very important role. In order to accurately simulate the flow field of the inlet tract and predict various flow phenomena caused by viscous effects, the numerical calculation software of the flow field must have the ability to accurately simulate the turbulent boundary layer.

In order to realize the fast CFD calculation in the process of inlet design to meet the requirements of inlet design and selection, and to realize the integrated large-scale calculation of internal and external flow in the inlet channel to meet the requirements of integrated design, the flow field numerical calculation software needs to have the ability of large-scale parallel processing, and in order to reflect the high temperature effect under high Mach number conditions, the flow field numerical calculation software needs to have the ability to deal with non-equilibrium flow. All the above factors put forward high requirements for the numerical calculation software of the inlet flow field.

With the development of computer technology and optimization methods, many inlet designers use computer programs and optimization algorithms to optimize the design of the inlet tract. Therefore, the parametric design of the inlet tract and the study of the variation law of the inlet performance with parameters are important problems to be solved before the optimal design of the inlet tract.

2. Inlet performance evaluation parameters

The main parameters for evaluating the performance of the inlet design include the flow coefficient, the total pressure recovery coefficient, the drag coefficient, the lift coefficient, and the pressure rise [73].

1) Flow coefficient

The flow coefficient is defined φ as the ratio of the actual captured flow rate $\dot{m}_a$ of the inlet tract to the theoretical captured flow rate $\dot{m}_d$ calculated by the person in the windward area of the inlet under the same incoming flow conditions, i.e.:

$$\varphi = \frac{\dot{m}_a}{\dot{m}_d} = \frac{\dot{m}_a}{\rho_0 V_0 A_c} \tag{3.1}$$

For two-dimensional inlet tracts, capture flow $\dot{m}_a$ unit width captures flow. Due to variations in incoming flow conditions, the actual captured flow rate of the same inlet tract under different incoming flows does not coincide with the change in flow coefficient.

2) Total pressure recovery coefficient

When the inlet tract compresses high-velocity air, it is accompanied by the loss of functional energy of the airflow, and the total pressure recovery coefficient can be used. , it is defined as the ratio of the total pressure of the inlet outlet airflow to the total pressure of the free flow, i.e.:

$$\sigma = \frac{P_{t2}}{P_{t0}} \tag{3.2}$$

Where: P_t—total pressure;

Subscripts "0," "2" — free flow and inlet outlet cross-section parameters.

3) Drag coefficient and lift coefficient

For two-dimensional air intakes/forebodies, aerodynamic forces can be decomposed into drag and lift drag in a coordinate system.

For two-dimensional air intakes/forebodies, the aerodynamic force can be decomposed into drag F_{drag} and lift F_{lift} in the coordinate system. The drag coefficient C_d and the lift coefficient C_1 are defined respectively

$$C_d = \frac{F_{drag}}{qA_{ref}} \tag{3.3}$$

$$C_l = \frac{F_{lift}}{qA_{ref}} \tag{3.4}$$

where: $q = p_0 V_0^2/2$ ——dynamic pressure;

A_{ref}——Reference area, which can be taken as the windward area of the intake.

For integrated intake/forebodies, the lift-to-drag ratio R_{ld} can also be used as a performance evaluation parameter, i.e.

$$R_{ld} = \frac{C_l}{C_d} \tag{3.5}$$

4) Pressure-lift ratio

The pressure rise ratio R_p is defined as the ratio of the inlet outlet pressure P_2 to the free flow pressure P_0, i.e.:

$$R_p = \frac{P_2}{P_0} \tag{3.6}$$

Under the same incoming flow conditions, a higher pressure-rise ratio means that the outlet pressure is higher, which helps to prevent the inlet tract from moving due to the interference of combustion chamber backpressure on the inlet tract.

3. Two-dimensional supersonic air intake

The two-dimensional supersonic air inlet can be divided into three types: external pressure type, internal pressure type and mixed pressure type according to its imported compression form.

1) Externally pressure supersonic air intake

In principle, the supersonic compression process of the external pressure supersonic air inlet is carried out outside the inlet. According to the different wave system structure of the import, the external pressure supersonic air inlet can be divided into pitot tube air intake, two-wave system, three-wave system and multi-wave system air inlet and isentropic compression air intake.

2) Internal pressure supersonic air intake

An internal pressure supersonic airway is a tube that first contracts and then expands. In an ideal situation, the supersonic incoming stream flows directly into the inlet, slows down in the contraction section until the larynx reaches the speed of sound, and becomes subsonic in the expansion section, like an inverted Laval nozzle. The most important difficulties in the internal pressure supersonic airway are the problems with the initiation and the influence of the surface layer.

3) Mixed pressure supersonic air intake

The mixed-pressure supersonic inlet is compressed both externally and internally. This form is used to reduce the external resistance of the external pressure type, and at the same time alleviate the starting problem of the internal pressure type and the unfavorable influence of the surface layer.

The air flow at the inlet and outlet of the scramjet engine is supersonic, generally *Ma* = 1.5 to 4.0, the flow direction should be consistent with the axis of the supersonic combustion chamber, for this purpose, a mixed pressure inlet is usually used, and the starting problem should be solved in the design calculation.

When designing the mixed pressure inlet, the wave system is first designed to achieve the goal of minimizing the total pressure loss and wave resistance of the airflow. Here, it is assumed that the airflow is an ideal gas and has no viscosity, the inlet airflow has no angle of attack and yaw angle, the direction of the inlet and outlet airflow is parallel to the axis of the engine, and the design of the inlet channel adopts the shock wave sealing method. The advantage of this is that there is no overflow in the inlet tract when it is designed, and the inlet tract is the smallest in size and lightest in weight under the condition of meeting the inlet flow requirements; and because of the shock sealing, there is no additional drag in the intake tract, which reduces the resistance of the engine. However, when the Mach number is greater than the design Mach number in this form of air intake, the shock wave will hit the inner wall of the lip, producing reflected waves, affecting the normal flow of airflow in the air inlet tract and causing additional airflow loss.

1) Design of external pressure wave system

In the design of the wave system, it is necessary to consider not only the total pressure recovery of the external pressure wave system, but also the shock wave detachment problem of the internal pressure wave system, that is, the starting problem of the internal pressure part. Because the Mach number of the airflow after compression by the external pressure wave system is low, and the maximum reflex angle that can produce the appendage shock wave is small, when the flight Mach number range of the aircraft is large, the external pressure wave system should adopt the wave system structure that can consider two or more shock waves in the design state, so that the total pressure recovery can be improved, and the working Mach number range of the air inlet can be expanded.

Using the Oswatitsch optimal wave system theory, in order to obtain the maximum total pressure recovery value, the external pressure wave system can be designed with equal intensity, that is, the total pressure loss caused by the air flow passing through the shock wave is equal, i.e.:

$$Ma_1 \sin\beta_1 = Ma_2 \sin\beta_2 = \cdots = Ma_n \sin\beta_n = C \tag{3.7}$$

2) Internal pressure wave system design

For the design of the internal pressure zone, the Mach number of the inlet outlet and the starting problem in the non-design state are mainly considered. Since the direction of the inlet and outlet airflow is parallel, the total fold angle of the airflow in the internal pressure zone is equal to the total fold angle in the external pressure zone. However, after passing through the shock wave in the external pressure area, the Mach number and total pressure of the airflow in the internal pressure area are lower, and the flow capacity is relatively reduced. In order to obtain a high total pressure recovery and alleviate the starting problem in the non-designed state under the premise of satisfying the outlet Mach number, the wave system structure of two oblique shock waves can be considered. In the design state, the shock waves generated outside the body of the air inlet are intersected at the lips. The structure of the lip with a wedge angle and a straight lip inlet is shown in Figure 3-4 and Figure 3-5.

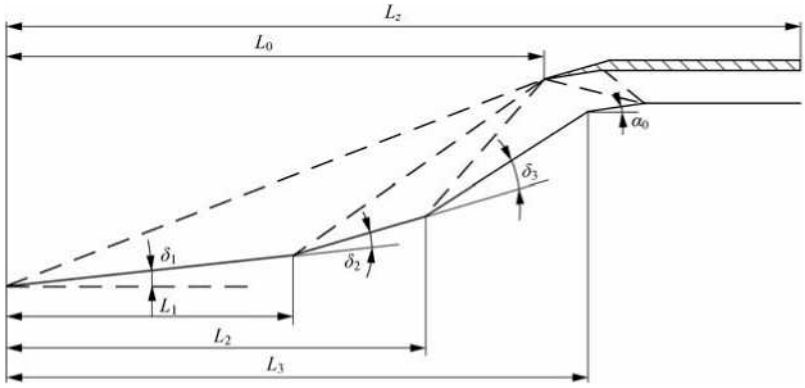

Figure 3-4: Mixed-pressure hypersonic two-dimensional airway structure with wedge angle at the lip

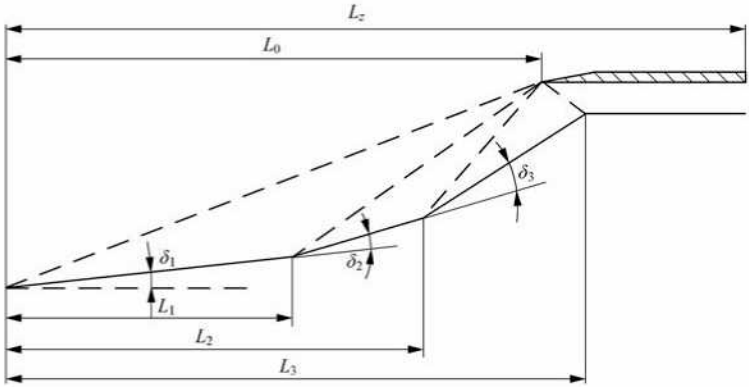

Figure 3-5: Mixed-pressure hypersonic airway structure with straight lips

3) Check the internal shrinkage ratio of the inlet tract

In the design of the air inlet, it is necessary to ensure that the air inlet can be started within the working range required by the design. The design of the scramjet intake must take into account the problem of starting at low Mach number flights, when the intake tract is overly constricted and its throat is congested, or when the backpressure increase caused by combustion exceeds the level that the intake and isolation sections can tolerate, the intake tract will remain in a state of immobilization. In order for the designed air inlet to be self-starting within the required flight range, it must be ensured that its internal shrinkage ratio is less than the allowable self-starting internal shrinkage ratio limit [74]. Within a certain range of flight Mach numbers, the empirical formula of the maximum contraction ratio of the following inlet tract [71] was used to preliminarily check the internal shrinkage ratio:

$$\frac{A_2}{A_{cr}} = \frac{1}{0.05 - \frac{0.52}{Ma_0} + \frac{3.65}{Ma_0^2}} \tag{3.8}$$

where: Ma_0——flight Mach number, $2.5 < Ma_0 < 10$;

A_2——Internal shrinkage starting cross-sectional area;

A_{cr}——Laryngeal area.

4. Three-dimensional side pressure intake

The side-pressure intake consists of two wedge-shaped swept side plates, a wedge plate, rear lip, and isometric isolation segment. The two sides of the plate are compression surfaces, which work together with the wedge plate to complete the compression of air flow. The structure is shown in Figure 3-6. In the sidewall compression intake, which consists of two erect wedge-shaped faces, further compression is carried out horizontally. The airflow in the sidewall compression intake is fully three-dimensional and is more difficult to analyze than axisymmetric or horizontal-wall compression intakes. Sidewall compression intakes can provide effective overflow and better inlet starting characteristics within a certain range of Mach numbers while maintaining the same shape and size, unlike horizontal wall compression intakes. Moreover, since further compression of the airflow in the inlet tract occurs mainly in the horizontal plane, the possibility of separation of the thick boundary layer entering the inlet tract due to shock-boundary layer interaction is reduced.

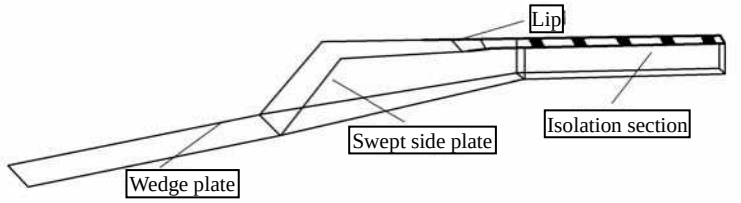

Figure 3-6: Schematic diagram of the three-dimensional side-pressure intake

The advantages of the three-dimensional side-pressure intake are very prominent, and the main advantages of it are described below.

1) Fixed geometric shape

Due to severe aerodynamic heating and prominent cooling problems, it is desirable that the inlet geometry is not adjustable, requiring a minimum infiltration surface area of the inlet tract. At present, the *Ma* = 3 to 6 inlet with good performance and the possibility of geometrical non-adjustment is the side pressure intake. From the perspective of aerodynamic layout, it is an internal contraction channel, but in front of its throat, there is a completely open overflow window, after the inlet is started, under the dual action of geometric overflow and pressure gradient overflow, the excess captured flow of low-ultrasonic Mach number can flow out automatically through the overflow window, resulting in the effect of automatic overflow with the change of Mach number, which basically solves the flow coordination problem of geometrically adjustable inlet airway. While there will be overflow resistance, it also provides an additional lift. Due to the fixed geometry, the heat-resistant design of the structure is relatively easy to implement. This is the outstanding advantage of this type of air intake.

2) Low sensitivity to the surface layer of incoming flow

Different from the two-dimensional inclined plate intake, the compression of the intake airflow is partly completed by a series of oblique shock waves between the two sides of the inclined plate, and the pressure gradient along the flow to the vicinity of the roof plate is not as serious as that of the binary inclined plate intake, so it is less sensitive to the attached surface layer on the lower surface of the front fuselage, which is conducive to alleviating the problem of insufficient flow during high Mach number flight.

3) The compression channel is short

Due to a series of compressions on the sidewalls, the compression channel can be shortened with the same number of shocks and pressure ratios. This reduces the weight of the structure and the cooling surface area.

4) Low Mach number starting and self-starting capability

Due to the rear of the lip, one side of the passage is open in front of the smallest section, creating an overflow window. The Mach number of the throat cross-section near the high Mach number design point is usually 2 to 3, so the throat area has a greater ability to pass through the low Mach number high dense flow, and the automatic adjustment function of the overflow window allows the inlet tract to be activated at a low ultrasonic Mach number. However, it is still a question to determine at what Mach number the inlet tract is activated. Ordinary wind tunnel tests can only study the "impulse" starting problem and "self-starting" ability of the inlet at one Mach number, and the former starting method is different from the starting of the inlet during actual flight. The inlet after starting may be re-activated by increased backpressure in the downstream combustion chamber or disturbed by other factors. Wind tunnel tests have shown that downstream disturbances disappear and this air inlet can restart on its own, i.e. with self-starting capability.

5) Small external resistance

The inlet and outlet momentum of the scramjet engine airflow is very large, and in order to get the maximum net thrust possible, it is desirable that the total drag of the entire engine should be small. Because the windward area of the inlet is consistent with the cross-sectional area of the engine, in addition to the overflow resistance, wave resistance and friction resistance of the inner channel, the external resistance of the inlet itself is small, and the engine can get a larger net thrust.

The structural characteristics of the above three-dimensional side pressure air inlet have good working performance and are very suitable for scramjet engines.

The main aerodynamic design parameters of the three-dimensional side-pressure air intake are described below.

1) The design of the sweep angle of the side panel

Three-dimensional side-pressure intakes are usually swept by side plates: first, to reduce the aerodynamic heat load on these edges; the second is to facilitate the airflow overflow of the leading edge of the fairing at low Mach numbers. The size of the sweep angle determines the overflow characteristics of the intake tract and, partly, the starting characteristics of the intake. If the sweep angle is too large, the component of the velocity along the flow velocity in the lateral plate intake normal may be as low as subsonic. In this way, the shock wave will be detached, and the lower limit of the Mach number will be increased so that the inlet tract can work properly, and the shock system will be established smoothly. If the sweep angle is too small and the downwash effect of the airflow after the first wave is not obvious, it is unlikely to produce an effective overflow in front of the intake lip and also affect the inlet starting performance. Currently, the range of the swept angle studied is 30° to 60°. Reference [75] shows that the 45° leading-edge swept structure has the best performance characteristics.

2) Selection of the compression angle of the side plate

The compression angle of the side plate is considered together with the sweep angle, and the side pressure inlet with a large sweep angle is large, and the effective compression angle perpendicular to the intake edge is larger under the same side plate wedge angle, so that the incoming Mach number of the shock wave possession is higher. Under a certain sweep angle, the size of the compression angle is related to the shock loss and the length of the side plate, and the compression angle is large, which can make the side plate shorter, but the shock wave becomes stronger, and the total pressure loss increases, and it is easy to produce the problem of separation of the attached surface layer; on the other hand, if a small compression angle is used, the shock wave loss is smaller, but the length of the inlet tract increases, which leads to an increase in the weight of the structure and the amount of coolant. After research and comparison, Langley Trexler believes that 6° is more appropriate, and the compression angle in the mouth is basically 6° in the published side-pressure airway data [76~78].

3) Air inlet aspect ratio

Under a certain inlet area, if the width is greater than the height, in order to achieve a certain shrinkage ratio, the inlet will become longer, and at the same time, the proportion of the laminar flow on the top surface and the side to the laryngeal cross-section will increase, and the ternary flow of the laryngeal area will increase when the large sweep angle is large;

If the width ratio is much smaller, under the same shrinkage ratio, the narrow inlet shortens the length of the inlet channel, and the starting Mach number of the inlet tract is increased under the same inlet area, and the uniformity of flow in the throat area is better than the former. NASA Langley Center and NAL Japan both opted for a design with a 0.8 aspect ratio. The MA194 dual-modal ramjet engine from Marquardt and the test air inlet model of the Russian CIAM used a 1.0 aspect ratio scheme.

4) Determination of the inlet tract contraction ratio CR

The contraction ratio of the lateral pressure intake is also an important parameter**,** and the geometric and pneumatic contraction ratios are usually used to indicate the degree of contraction of the intake, and in the absence of wedge plate compression, the geometric contraction ratio is equal to the pneumatic contraction ratio. The geometrical in-inlet shrinkage ratio is defined as the ratio of the inlet at the beginning of the sidewall to the area of the inlet outlet**,** i.e., CR = (D_i x H_i)/(D_0 x H_0), as shown in Figure 3-7. The shrinkage ratio is closely related to the starting performance of the inlet tract**,** which in turn is related to the lip position. In Reference [75], it was found that the inlet tract could be successfully activated in a wind tunnel with a shrinkage ratio of CR = 9 at a contraction ratio of CR = 9. Obviously, such a large shrinkage ratio is not possible at low Mach numbers, and at the same time, the three-dimensional intake tract with a higher shrinkage ratio causes a lot of engine drag. In the case of a geometrically non-adjustable inlet tract, the CR ratio should be based on the maximum allowable value at the starting Mach number. It is suggested that the shrinkage ratio CR of the inlet tract under study can be adjusted within a certain range**,** and the initial CR = 3 to 4 can be taken to ensure that the inlet tract with isolation section is successfully activated at *Ma* = 3.5.

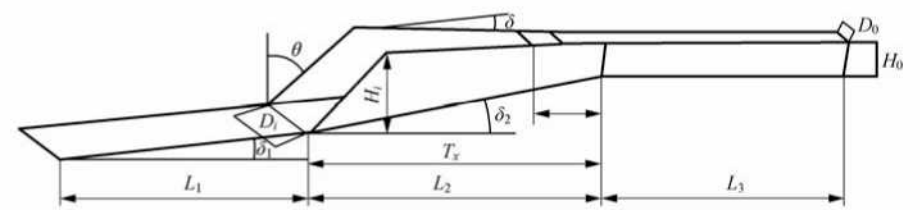

Figure 3-7: Aerodynamic design parameters of a three-dimensional side-pressure inlet tract

5) Fairing position

The fairing position is defined as the distance between the leading edge of the fairing and the inlet larynx as a percentage of the distance between the equal-section larynx and the leading edge of the sidewall, i.e., *Cx*/*Tx*, as shown in Figure 3-7. For the selected inlet tract, when the fairing is located at the beginning of the equal-section throat, the sidewall can be swept back by 0° to 30° without negatively affecting the inlet performance. A backswept leading edge causes the airflow to rotate towards the fairing plane. As a result, the subsequent grazing angle increases, the overflow increases and the mass capture decreases. For the same sweep angle, moving the leading edge of the fairing forward will improve the mass capture. Reference [75] shows that the 30° sweep angle and 0% fairing position and the 60° sweep angle and 50% fairing position do not significantly change the overall performance calculation.

5. Three-dimensional internal contraction of the inlet tract

The hypersonic three-dimensional retractable inlet is a form of airway that is distinct from typical hypersonic intakes (axisymmetric intake, binary intake, side-pressure intake). This scheme was used in the program of the SCRAM hypersonic missile, designed by Johns Hopkins University in the United States in the 1960s [79,80]. Since then, the three-dimensional inward shrink intake has not been developed for a considerable period of time due to the engineering advantages of the binary air intake. In recent years, with the deepening of research, foreign scholars generally believe that this type of air inlet has high overall performance [81,82], so this type of air inlet has attracted attention again. The design of the internal restriction inlet is reviewed in Reference [83]. The main three-dimensional inward retractable air inlets generated by the direct streamline tracing method are: Busemann air intake, modular wave-riding air intake, Funnel air intake, HYCAUSE air inlet and Jaw air intake.

1) Busemann intake

In 1942, Busemann proposed an internal contraction flow field. This flow field belongs to the category of conical flow, and the flow field parameters are equal everywhere on the isopolar line. Since there is only one terminal shock wave, and the rest of the pressure rise is achieved by isentropic compression, the Busemann flow field is the best internal shrinkage flow field to achieve the specified pressure rise. However, the disadvantages of directly using the Busemann flow field as the inlet channel are also obvious: first, the length of the Busemann flow field is quite long due to excessive isentropic compression, which cannot be used in engineering practice; second, the complete internal contraction makes it impossible for the inlet to start at all at low Mach numbers. The solutions to these two fatal drawbacks include replacing the reference Busemann flow field with a truncated Busemann flow field to generate a truncated Busemann inlet and using streamline tracing technology to take a portion of the Busemann flow field as the profile of the inlet channel to reduce the degree of internal compression and improve the inlet tract starting performance. Holder et al. [84,85] first applied this concept to hypersonic airway design in 1966, and since the 1960s, Billig et al. have carried out a lot of research work around this airway scheme [79,80]. In recent years, O'Brien, Jacobsen, Tam, and Billig et al. have conducted in-depth research on the engineering design, optimization methods, starting characteristics, and performance testing of Busemann inlet tracts [81,86,90]. Figure 3-8 shows the Busemann inlet tract reduction Mach number test performed by Jacobsen et al. in the *Ma* = 4 wind tunnel [81].

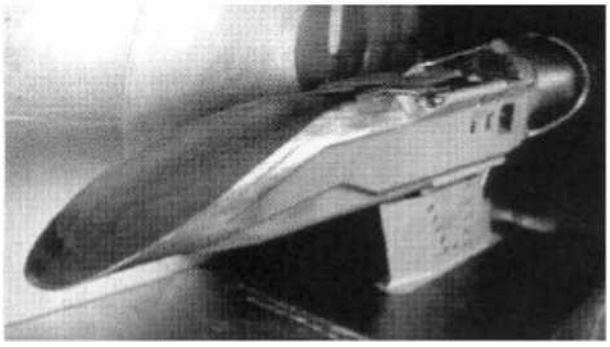

Figure 3-8: Busemann inlet tract reduction starting Mach number test

2) Modular waverider inlet[91]

Matthews and Jones et al. designed a wave-riding air intake scheme with a fan-inlet, multi-module layout (Fig. 3-9). The influence of factors such as the basic flow field of internal contraction (isobaric ratio and isointernal shrinkage angle design) and the number of modules on the wave-riding air inlet and the overall performance of the aircraft were studied. Based on the one-dimensional flow path analysis method and the corresponding mathematical model, the influence of the air inlet scheme on the overall performance of the aircraft was studied. The wind tunnel test of *Ma* = 7 was carried out to study the working characteristics of the inlet channel and the starting performance of the low Mach number under the condition of variable flow Reynolds number. The results show that viscosity plays an important role in the performance of the inlet channel, and the influence of factors such as incoming Reynolds number and wall heat flow on the inlet scheme must be fully considered in the design process. In addition, Matthews et al. believe that the main advantages of this type of air inlet may be reflected in its low Mach number starting capability, higher isolation section backpressure resistance and reduced frictional resistance of the inner channel.

3) Funnel intake

Kothari et al. [92] first proposed to design the waverider with an internally contracted elementary flow field, and obtained the shape of the aircraft as shown in Figure 3-10 [93,94]. To a large extent, this shape subverts people's traditional understanding of aircraft shape, it is actually a highly integrated design scheme of aircraft and air intake, which can also be regarded as a kind of funnel-type intractable air inlet scheme.

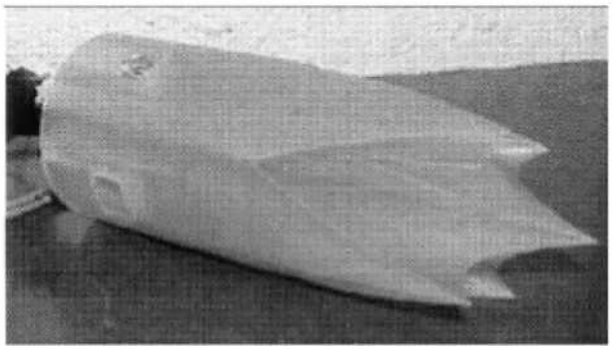

Figure 3-9: Modular wave-riding air inlet test model

Although this work is only at the conceptual design stage, Kothari clearly describes the close relationship between internal contraction flow, two-dimensional plane flow, and external inflection flow, establishes a relationship between the design of the outflow waverider and the design of the inflow inlet from a theoretical perspective, and expounds the theoretical starting point of the waveriding characteristics of the intractable inlet [92].

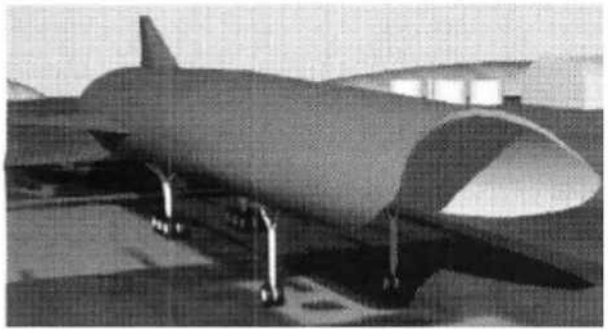

Figure 3-10: Conceptual diagram of the Funnel's internal retractable air intake

4) HYCAUSE intake tract

The HYCAUSE inlet also adopts a three-dimensional internal shrinkage configuration [95] as shown in Figure 3-11. The design method of the inlet is not based on the Busemann flow field, but on the basic flow field of an internal shrinking cone obtained by the numerical optimization method. The test mainly focuses on the low Mach starting capacity of this type of air inlet and the turbulent surface layer flow regime during the working process of the air intake. Preliminary studies have shown that during the flight, due to the failure of the sensor on the booster, the rocket shook in the hypersonic phase, and the airflow could not enter the intake as designed, and the combustion process was aborted, although the effective data acquisition process was only 2 seconds, the test completed the key verification of the first Mach number of 10 (downward dive process) in the three-dimensional in-shrink inlet intake, and the test data also proved that the HYCAUSE vehicle had achieved combustion in the descent phase [96] .

5) Jaw intake

Malo-Molina proposed a new three-dimensional hypersonic air intake, the Jaw air intake [92,97], as shown in Figure 3-12, and designed the Jaw air intake with a combustion chamber. In her research, Molina found that the key factor restricting the overall performance of the rectangular section inlet is the complex shock/adherent layer in the intake, and the shock/shock wave interferes with each other, so the main design idea of the Jaw inlet is to minimize these two complex flow phenomena in the intake.

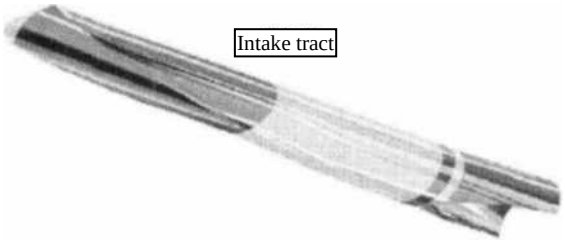

Figure 3-11: Conceptual diagram of the HYCAUSE inlet tract

This kind of inlet design method draws on the concept of three-dimensional inward contraction, and uses a two-dimensional complex surface to obtain the regular plane shock wave inside the intake, and through the comparison and analysis of the overall performance of the binary inlet with the same design parameters, the following quantitative conclusion is obtained: the three-dimensional inward shrinkage design can capture 20% more than the rectangular section inlet and the reduced wetting area reduces the friction of the Jaw intake, which can increase the thrust of the engine by 24.87%. In addition, the reasonable three-dimensional internal shrinkage inlet design can weaken the cross-reflection between the complex wave systems inside the inlet and reduce the flow loss, and similarly, due to the reduction of the wetting area, the thickness of the attached surface layer can be reduced, which can reduce the mutual interference between the shock wave and the attached surface layer, so as to avoid separation to a certain extent, and improve the overall aerodynamic performance of the air intake.

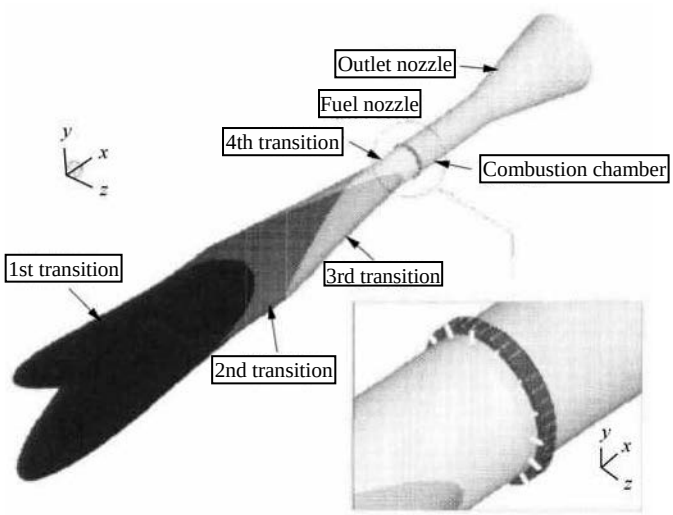

Figure 3-12: Jaw inlet flow field structure

The direct streamline tracking internal shrinkage inlet adopts the direct streamline tracking design of the basic flow field of the internal shrinkage cone, and its advantage is that the obtained air inlet surface can maintain the flow characteristics of the airflow at the same position in the original internal shrinkage flow field, and has the characteristics of reverse design; however, its main disadvantage is that the inlet shape of the inlet is determined solely by the basic flow field and the outlet of the inlet channel. Therefore, this type of air inlet cannot be integrated with complex shape aircraft and is usually used for multi-module projectile body layout or directly using the air inlet as the forebody of the aircraft.

3.3.2: Isolation Segment

1. The role of the isolation segment

The isolation section is an important part of a scramjet engine. It is usually a pipe of equal cross-section or with a slight expansion angle, located between the inlet tract and the combustion chamber, and has two important functions: one is to isolate (or minimize) the mutual interference between the inlet duct and the combustion chamber, which can support the higher backpressure in the combustion chamber to provide a wide and stable working range of the inlet tract; the other is to make the scramjet engine work in a dual-mode mode, that is, the scramjet engine can be converted between the subsonic combustion mode and the scramjet mode [98].

An isolation section is a pipe with an equal cross-section or a micro-expansion angle, and in the last few decades, people have mainly studied pipes with circular and rectangular sections. In fact, when Curran and Stull [99] proposed the concept of bimodality in 1964, it was realized that a pipe could be placed between the intake tract and the combustion chamber of a scramjet engine to complete the modal transition and they called this pipe an isolation section. The biggest feature of the flow field in the isolation section is that there is a mutual interference between the shock wave and the attached surface layer. In this article, the internal flow of the isolated section is analyzed, and on this basis, a length-to-height ratio estimation method for the isolated segment is given.

2. The shock wave interferes with each other with the surface layer

Over the past 50 years, many studies have been done on the interaction between shock waves and the adherent layer, including a large number of theoretical and experimental studies, which have shown that the interaction between the shock wave and the adherent layer is very important for the overall flow field. The mutual interference between the shock wave and the attached surface layer will occur in many flow fields, which are mainly divided into two categories: one is the so-called "outflow," such as wings, aircraft bodies and missile bodies; the other type is "inflow," such as the isolation section of a scramjet engine, a supersonic wind tunnel diffuser, a shock tube, a supersonic nozzle, etc. The interference between the shock wave and the adherent surface layer of the "outflow" is mainly affected by the shock wave front parameters and geometric configuration;" The interference between the "inflow" shock wave and the attached surface layer is not only affected by the shock wave front parameters and geometry configuration, but also by other parameters in the flow field, such as the backpressure at the outlet of the isolation section.

The first to observe the interference between the "inflow" shock wave and the episurface layer were Neumann and Lustwerk [100,101]. They observed this physical phenomenon in 1949 in a supersonic wind tunnel diffuser of their own design. In 1953, Lukasiewicz [102] also observed the interference between the shock wave and the adherent surface layer in a supersonic wind tunnel diffuser. He described the flow field of this phenomenon as "a few curved shock waves." Shapiro [103] also mentions this phenomenon in his book published in 1953. He described the flow field in Reference [100] as "a series of bifurcated positive shock waves." Since then, many researchers have started research in this area.

Figure 3-13 shows the mutual interference between the shock wave and the attached surface layer in the pipe of equal cross-section. Assuming the Mach number before the shock wave does not exceed 1.2, as shown in Figure 3-13(a), it is difficult for the shock wave to separate the surface layer, and it is difficult for the surface layer to affect the shock wave, and the shock wave is very similar to an inviscous positive shock wave. When the Mach number is 1.2 to 1.3, as shown in Figure 3-13(b), although the mutual interference between the shock wave and the surface layer is very weak, the surface layer has begun to separate, but the tendency of the surface layer to reattach is stronger, so when the shock wave moves forward, the surface layer will not separate, but will make the shock wave more and more oblique, which is the curve shock wave seen in Figure 3-13. When the Mach number continues to increase to 1.3 to 1.5, the tendency of the attachment layer to separate is greater than the tendency of reattachment, as shown in Figure 3-13(c), the root of the shock wave is bifurcated, which is called the bifurcation shock (or shock wave).

If the Mach number continues to increase to greater than 1.5, the shock wave and the surface layer interfere with each other very violently, and the surface layer will be separated in a wide range, and one or more bifurcated shock waves will appear in the flow field, as shown in Figure 3-13(d), such a series of bifurcated shock waves are called "shock strings" (or "shock chains").

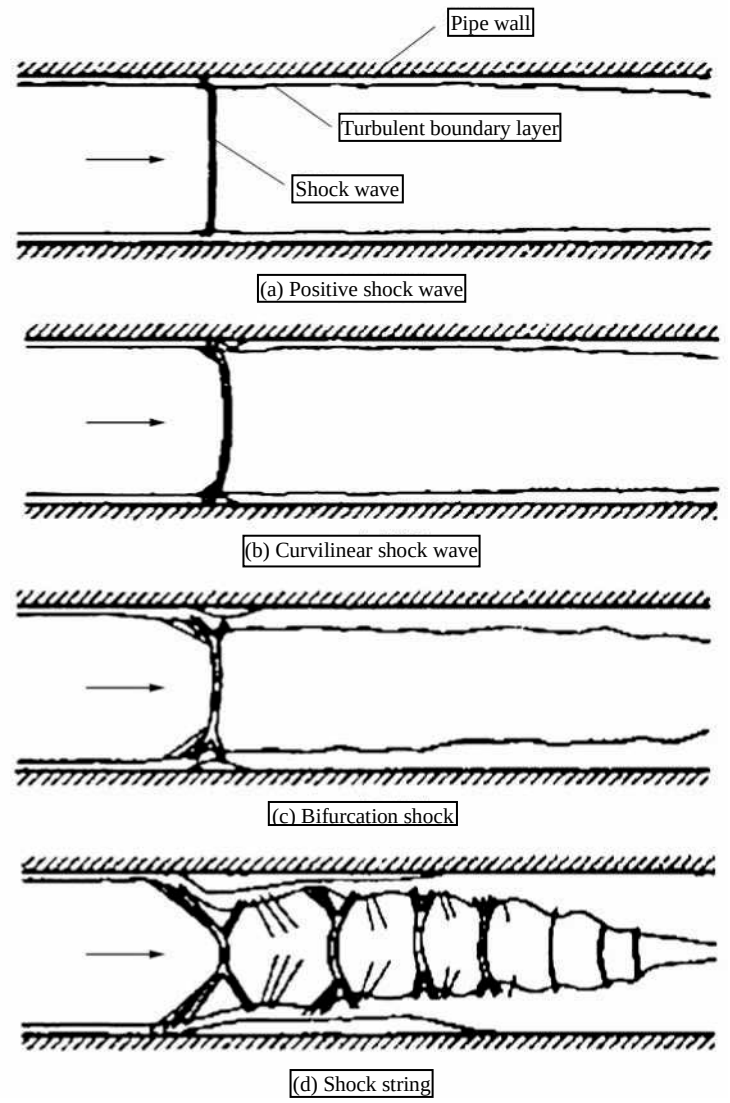

Figure 3-13: Schematic diagram of the mutual interference between shock waves and the attached surface layer in a pipe of equal cross-section

3. Formation process and morphological analysis of shock wave strings

A classic schlieren photograph of a shock string is shown in Figure 3-14 [104]. The cross-section of the pipe in Figure 3-14 is square, with an area of 32 mm X 32 mm, and the air flow flows from left to right, with the Mach number before the first shock wave being about 1.75 and the Reynolds number being 8.2×10^5. As can be seen from Figure 3-15, a wide range of separation has occurred in the surface layer, and the shock string in Figure 3-15 contains about 1. Dao shock. In particular, it is noted in Reference [104] that the airflow is not entirely subsonic after passing through the shock string, and that there are also some supersonic regions in which the airflow will eventually decelerate to subsonic, but its deceleration is not accomplished by the shock string.

The name "shock string" was first proposed by Billig [105] in 1988, and before that, researchers used many names, such as "multi-branch shock wave [106],” "shock wave system [107],” etc.

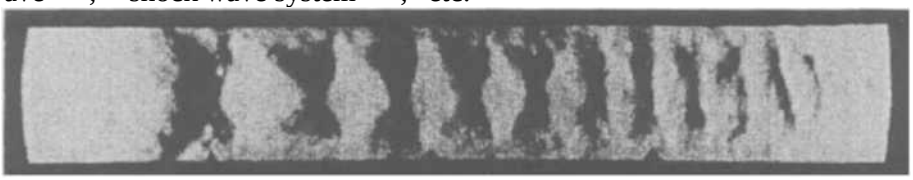

Figure 3-14: Schlieren diagram of a shock string

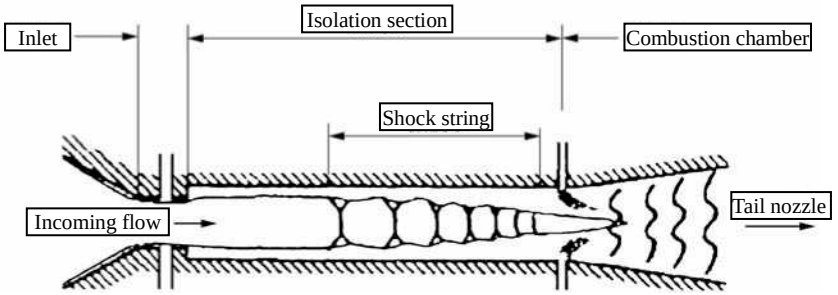

Figure 3-15: Schematic diagram of shock wave string in an isolated section

In the flow field of the isolated section, the shock wave and the attached surface layer interfere with each other, at this time, at the intersection of the shock wave and the attached surface layer, the wall surface layer is separated, causing the convergence of the main cross-section, so that the subsonic main stream in the central region after the initial positive shock wave accelerates to the speed of sound, and then the attached surface layer is re-attached, and the main supersonic expansion of the central area expands until the second wave is formed, so that the shock wave string is finally formed.

The following is a detailed explanation of how the shock wave and the surface layer interfere with each other to form a shock string.

(1) In the undisturbed area of the isolation section, the surface layer in front of the shock string gradually thickens, the static pressure gradually increases, and the Mach number gradually decreases.

(2) With the disturbance of the counterpressure propagating upstream along the attached surface layer, a compression wave is generated near the attached surface layer, thus forming a shock wave, and the pressure increases a lot after the shock wave, and the airflow in the core area is deflected to the center line at a certain angle.

(3) After the shock waves intersect the center line, they are compressed by each other and two shock waves are generated. These two shock waves are reflected to the wall and collide with the wall, and the flow in the core area becomes parallel to the wall, and the pressure at the wall rises sharply, and the attached surface layer is seriously separated, and a high-pressure platform is formed in the airflow separation area.

(4) After the impact point, the difference between the pressure in the airflow separation zone and the core zone causes the shock wave to form a sparse expansion wave in the Plante-Meyer reflection near the wall, and the airflow in the core area deviates from the center line at a certain angle.

(5) These expansion waves intersect and reflect at the center line and are still expansion waves, and the air flow in the core area is parallel to the center line.

(6) If the pressure in the airflow separation zone is lower than the pressure downstream, another compression wave will be formed in the attached surface layer.

The above (3) to (6) recurrence, that is, the repetition of the expansion wave and the shock wave, the shock wave string is formed.

The morphology of the shock string is mainly affected by the Mach number of the wavefront, the back pressure and the attached surface layer, and some literature also calls the influence of the attached surface layer "constraint,” which is generally expressed by the ratio of the thickness of the surface layer of the wavefront to the half-height of the pipe (if the pipe is a round pipe, it is expressed by the ratio of the thickness of the surface layer to the radius of the pipe).

Carroll and Dutton [108] used a series of schlieren photographs to illustrate the effect of the episurface layer on the morphology of the shock string, as shown in Figure 3-16.

In Figure 3-16, the direction of air flow is from left to right, the Mach number of the wavefront is 1.61, the Reynolds number is 3 x 10^7, the restriction condition δ_u/h indicates, the middle δ_u is the thickness of the surface layer of the wavefront**,** and the half-height of the rectangular pipe ***h*****,** from Figure 3-16(a).(f), the thickness of the surface layer is gradually increasing.

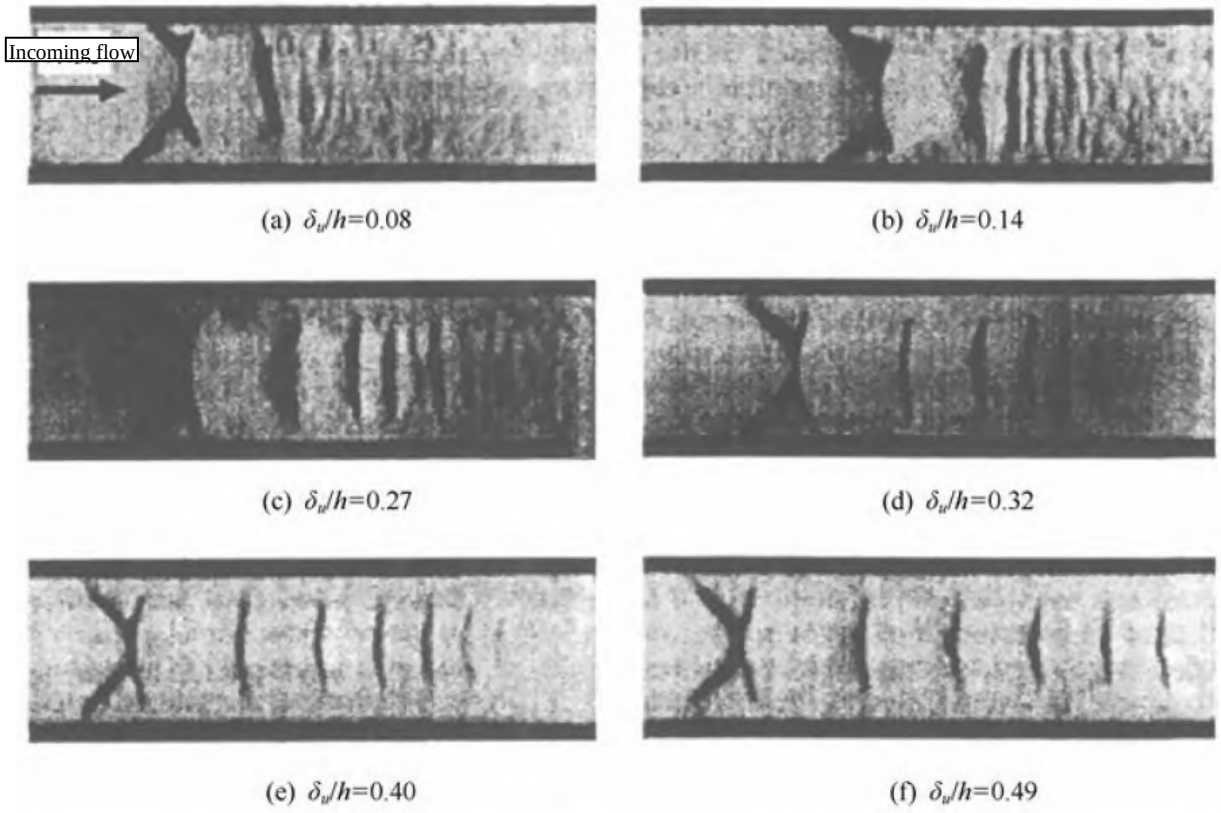

Figure 3-16: Shock string schlieren diagram of Reference [108]

As can be seen from Figures 3-16, the first shock wave in all diagrams has a bifurcation, but it is difficult to observe the subsequent shock waves. In addition, as the surface layer thickens, the bifurcation point approaches the center line, and the spacing between the shock wave increases. From Figure 3-16, it can be concluded that when the Mach number of the wavefront remains constant, the number of shocks and the distance between shocks and shocks increase as δ_u/h increases, and the length of the shock strings also increases. Similarly, if the adjoining surface layer remains constant, the number of shocks, the spacing between shocks, and the length of the shock strings will also increase when the Mach number of the incoming flow increases [109].

As can be seen from Figure 3-16, the interaction between the shock wave and the surface layer is not particularly violent, the bifurcation point of the first shock wave is close to the wall, and the subsequent shock wave is arranged along the center line, and such a shock wave string is called a "positive shock string." If the Mach number increases, the interaction between the shock wave and the surface layer will be more violent, and the bifurcation point of the first shock wave will move from the wall to the center line, and the intensity of the subsequent shock wave will become weaker, and such a shock wave string is called "oblique shock string." The biggest difference between the positive shock string and the oblique shock string is the different wall pressure distribution and the different Mach number after the wave. Generally speaking, the wall pressure distribution of oblique shock wave strings fluctuates, with the Mach number being less than 1 after strong oblique shock wave and Mach number being greater than 1 after weak oblique shock wave stringing. There is no fluctuation in the wall pressure of the positive shock string, and the Mach number after the wave is less than 1.

For oblique shock strings, the number of shocks and the interval between shocks and shocks are not significantly changed with the surface layer [108,109]. The positive shock string and the oblique shock string are mainly affected by the incoming Mach number. In general, when the incoming Mach number is greater than 1.8 to 2.2 [109~112], the oblique shock string will appear.

4. Estimation of the length of the isolation segment

It is difficult to calculate the length of the isolation segment, and it is generally estimated by a semi-empirical formula. The length of the isolation section has an important influence on the matching of the inlet tract and the combustion chamber. The isolation section should be long enough so that the entire shock string contained in it can match the pressure fluctuation of the combustion chamber, so as not to make the shock string move to the upstream air intake, causing the air intake tract not to move, but the isolation section is too long and increases the weight of the engine, so the relationship between the two needs to be coordinated. It is difficult to accurately calculate the length of the isolation segment, and it is generally estimated using a semi-empirical formula.

$$\frac{L}{H}=\frac{\sqrt{\frac{\theta}{H}}}{\sqrt[4]{Re_\theta}}\times\frac{\left[50\left(\frac{P_2}{P_1}-1\right)+170\left(\frac{P_2}{P_1}-1\right)^2\right]}{(Ma_1^2-1)} \tag{3.9}$$

Where: L —Shock string length;

Ma_1 — The Mach number of the inlet airflow in the isolation section;

Re_θ — Reynolds number in terms of the thickness of momentum;

H — Isolation section height;

θ — Momentum thickness of the attached surface layer when undisturbed;

P_1 — Hydrostatic pressure before shock wave;

P_2 — Static pressure of the air flow after shock wave.

(1) Obtained from the pneumatic relation

$$\frac{\theta}{L}=\frac{0.664}{\sqrt{Re_L}} \tag{3.10}$$

Where: L—axial length of flow tube;

Re_L—Reynolds number on the scale l.

(2) It is defined by the Reynolds number

$$Re_L=\frac{\rho VL}{\mu},\quad Re_\theta=\frac{\rho V\theta}{\mu},\quad Re_H=\frac{\rho VH}{\mu}$$

The following relationships exist:

$$\frac{Re_\theta}{Re_L}=\frac{\theta}{L},\quad \frac{Re_\theta}{Re_H}=\frac{\theta}{H},\quad \frac{Re_L}{Re_H}=\frac{L}{H} \tag{3.11}$$

(3) If the maximum pressure ratio of the shock string before and after the isolation section is less than the pressure ratio of a positive shock wave, the strength limit of the shock string in the isolation section is the intensity of a positive shock wave. Let the length of the isolation section *L be equal to the length of the shock string*, then substituting Equation (3.10) and Equation (3.11) into Equation (3.9) can be obtained:

$$1.1078\times\left(\frac{L}{H}\right)^{1/8}(Ma_1^2-1)Re_H^{3/8}=50\times\left(\frac{P_2}{P_1}-1\right)+170\times\left(\frac{P_2}{P_1}-1\right)^2 \tag{3.12}$$

(4) The pressure ratio relation before and after the positive shock wave can be obtained from the pneumatic relation formula:

$$\frac{P_2}{P_1}=\frac{2k}{k+1}Ma_1^2-\frac{k-1}{k+1} \tag{3.13}$$

(5) Substituting Equation (3.13) into the right end of Equation (3.12) and taking k = 1.4 to obtain:

$$\frac{L}{H}=\frac{\left[52.67+209(Ma_1^2-1)\right]^{8/7}}{Re_H^{3/7}} \tag{3.14}$$

where: L — length of the isolation section;

H — isolation section height;
Ma_1 — Mach number of inlet airflow;
Re_H — The Reynolds number of the length characterized by height.

(6) According to the theory of gas molecular motion, the relationship between the viscosity coefficient and temperature of the gas can be obtained, i.e.:

$$\mu = \mu_0 \left(\frac{T}{273}\right)^{1.5} \frac{273 + T_0}{T + T_0} \tag{3.15}$$

where $\mu_0 = 1.711 \times 10^{-5} N \cdot s/m^2$; $T_0 = 122K$, Re_H can be calculated using Equation (3.11) and Equation (3.15).

3.3.3: Combustion chamber

The combustion chamber is the core and key component of the scramjet engine, and the key technologies involved in supersonic combustion are embodied in the combustion chamber.

1. Fuel blending enhancement and flame stabilization technology

Among the many key technologies of supersonic combustion, the full mixing of fuel/air and stable combustion are important factors affecting the performance of scramjet engines [71]. Compared with a subsonic combustion ramjet, scramjet fuel mixing and combustion is much more difficult, mainly because: (1) the inlet flow of the combustion chamber is supersonic and the residence time of the gas flow in the combustion chamber is only on the order of milliseconds. Past experiments, theoretical analysis, and numerical simulations have shown that in the supersonic region, the mixing efficiency decreases rapidly with the increase of Mach number [113]. In a short stay time, it is difficult to complete the fuel injection, fully mix the fuel with the air, and burn. (2) The stability of the supersonic shear layer is strong, and the diffusivity of the shear layer is only 1/4 to 1/3 of that of the non-compressible shear layer under the same density ratio of the main stream and the shear layer. (3) Hydrocarbon fuels exist for a long ignition time [114] (in a typical supersonic combustion chamber, the pressure is 50 to 100 kPa, the temperature is 600 to 1000 K, and the ignition delay time of kerosene vapor is 5 to 10 ms), slow reaction speed, etc., there is also an evaporation and mixing process for liquid fuels, so it is difficult for hydrocarbon fuels to achieve ignition and flame stability, high efficiency and low loss combustion in a limited length combustion chamber using traditional fuel injection methods and flame stabilizers.

Some injection schemes cause significant total pressure losses to achieve flame stabilization, and some equipment adds complexity to the system design, such as the need for a corresponding active cooling system. In order to ensure efficient combustion in the combustion chamber with the shortest possible length, while ensuring low system complexity and low performance loss, it is necessary to design a good fuel injection device to quickly mix fuel and air on the one hand, and a high-performance flame stabilizer on the other hand.

In response to this problem, a lot of research work has been carried out in countries around the world, and many technologies, concepts and methods that can enhance fuel mixing and stable combustion have been studied, each with its own advantages and disadvantages. Among the many hybrid enhancement and flame stabilization concepts, leeward steps, ramps, slabs (rods), wall grooves and their combinations with each other are commonly considered configurations, and these methods are often used in the specific combustion chamber design according to the design requirements and operating conditions of the supersonic combustion chamber. The methods and measures adopted by researchers at home and abroad to enhance fuel/air mixing, solve ignition and flame stabilization are mainly as follows.

1) Fuel injection directly from the wall

The simplest way to inject fuel is to inject fuel horizontally from the wall (Fig. 3-1(a)), when the injected fuel and the supersonic main stream interact, a bow shock wave is formed, and the upstream surface layer separates, so that the surface layer and the fuel injected are mixed at subsonic speed upstream of the injection hole, and the flame propagation is stable. However, at high flight speeds, this jetting scheme causes a large loss of total pressure due to the formation of a three-dimensional bow shock wave.

If the injection method is used at a certain angle (e.g., 30° or 60°), the bow shock wave can be weakened, the total pressure loss during the injection can be reduced, and the axial momentum of the injection can provide part of the net thrust, but at the same time reduce the mixing effect of fuel and incoming air and the ability to stabilize the flame [114]. In recent years, some researchers have used the method of wall injection and shock wave interaction to enhance the mixing (Fig. 3-17), which has achieved certain results, but its disadvantage is that the total pressure loss is increased while enhancing the mixing.

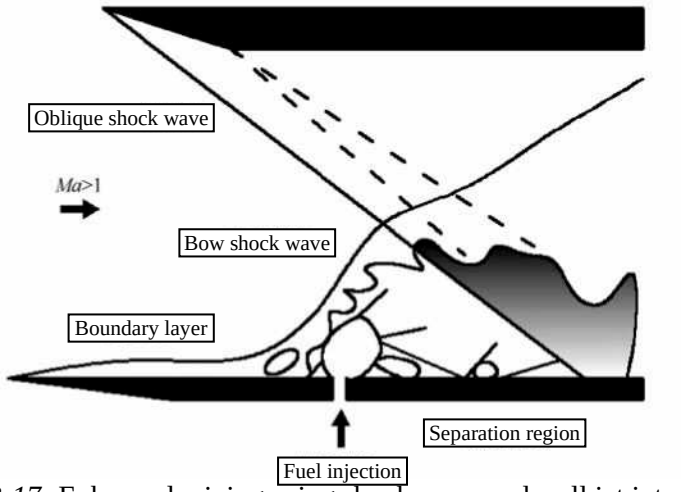

Figure 3-17: Enhanced mixing using shock wave and wall jet interaction

2) Leeward step or slope jetting

Another way to achieve flame stabilization is to use a leeward step, behind which a large return zone is formed, and the gas in the return zone becomes a continuous ignition source. Stable combustion can be achieved in this way, but the disadvantages are a large loss of total pressure and an increase in resistance due to the low pressure after the step. The use of a slope in the combustion chamber (Fig. 3-18) can disturb the incoming flow, generate shock waves, expansion waves, flow vortices and other phenomena in the flow field, enhance the flow direction vortex in the flow field, and achieve the purpose of enhancing mixing [115].

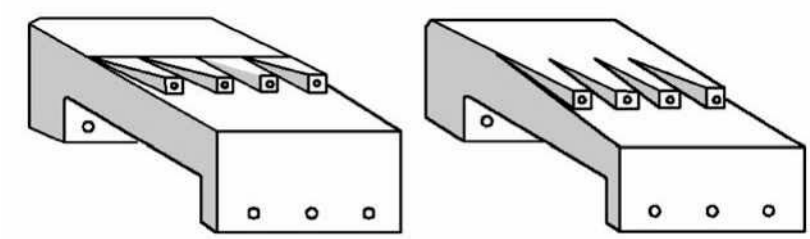

(a) Compression jet ramps (b) Expansive jet ramps

Figure 3-18: The injection ramp used in the combustion chamber

3) Plate or (or rod) jetting

Plate (or rod) injection is also a common method used in supersonic combustion chamber design (Figure 3-19). Experiments have shown that the mixing of fuel and incoming air and flame stabilization are better by using the support plate injection method, but the resistance and thermal load are increased [71]. Russia's CIAM (Russian Central Aeronautical Power Research Institute) and TSAGI have conducted a large number of tests on the two-dimensional two-modal ramjet engine model using (tubular and sheet) fuel initiators using direct-connected and free-jet test equipment, studied the influence of the type and position of the initiator on the combustion mode, and analyzed the main mechanism that determines reliable ignition.

ITAM in Russia experimentally studied the influence of the bottom nozzle configuration of the support plate ejector on the mixing performance and cooperated with CIAM to numerically simulate the corresponding flow field. The results show that the plate ejector with the same number of elliptical cross-section nozzles achieves the best mixing effect with the lowest total pressure loss [71]. The NAL (National Aerospace Laboratory of Japan) in Japan has conducted a large number of tests on a model of a dual-modal ramjet engine with a support plate injector configuration and has also studied the effect of support plates on combustion performance [116].

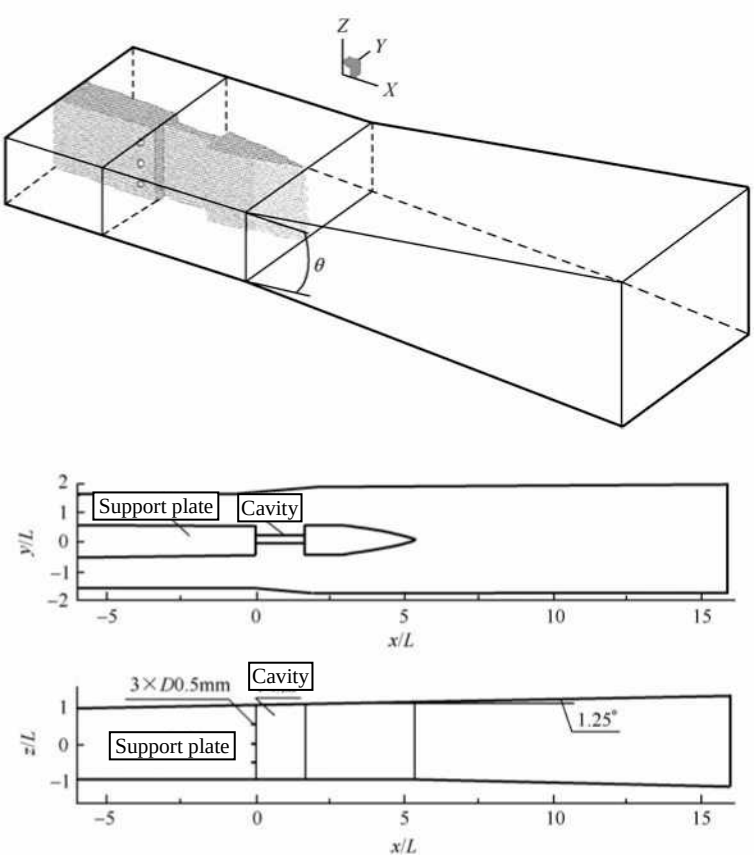

Figure 3-19: Combustion chamber and its support plate injected with support plates

In France's hydrocarbon-fueled hypersonic cruise missile program, researchers from the aerospace company Matra used an arrow-shaped full-height support plate fuel ejector in the combustion chamber of a dual-modal ramjet engine and conducted a large number of tests and numerical simulations on the combustion chamber [117]. The results show that the plate configuration ejector strengthens the fuel mixture, so that the fuel can achieve strong combustion in the combustion chamber.

Kanda et al. also conducted a large number of experiments on a model scramjet engine with a support plate injector configuration and studied the effect of the height of the support plate on the combustion performance [118]. Semenov [71] noted that a plate (or strut) type of fuel injection system in a large-size ram combustion chamber allows the fuel to be more evenly distributed in a high-speed gas stream, completing the mixing process over a short distance. However, in order to increase the penetration depth of the fuel, the plate (or pole) ejector will penetrate deep into the high-velocity gas stream, which inevitably brings the problem of heat protection for the ejector and increases the demand for materials.

In the combustion chamber of a full-size ramjet engine, the length of the combustion chamber will be increased in order to reach the core area if the fuel is injected only by the wall injection method of the combustion chamber. In large-scale ram combustion chambers, the plate type fuel ejector increases the penetration depth of the fuel in the high-velocity gas stream and allows the fuel to complete the mixing process over a short distance. The configuration of the support plate makes the local area of the combustion chamber produce vortex and reflux zone, which improves the fuel blending process, prolongs the residence time of the mixture, ensures the reaction time, and then improves the combustion efficiency. In addition, based on the consideration of structural strength, the use of support plate configuration is the development trend of hypersonic ramjet engine design. Therefore, the researchers have conducted extensive research on the influence of the plate configuration on the flow field structure, fuel mixing, and combustion stability of the combustion chamber, and have achieved a large number of guiding conclusions [71,113,119].

4) Adopt double combustion chamber

In 1977, Biliig et al. from the Applied Physics Laboratory of Hopkins University in the United States combined the advantages of supersonic and subsonic ramjet engines to propose the concept of a ramjet engine with two combustion chambers [120]. (DCR), the airflow of this engine is divided into two strands after passing through the inlet duct, and a small part of the airflow is reduced to subsonic speed through positive shock wave compression, and then enters the subsonic combustion chamber; the other part of the gas flow is compressed by the oblique shock wave and enters the supersonic combustion chamber at supersonic speed. Most of the fuel is added in the subsonic combustion chamber to form high-temperature oil-rich gas, which is accelerated to the speed of sound through the nozzle of the subsonic combustion chamber, and then sprayed into the supersonic gas flow of the supersonic combustion chamber to continue mixed combustion, and at the same time can ignite the mixture in the supersonic combustion chamber. When the Mach number is low, all the fuel is injected into the subsonic combustion chamber, and the over-combustion chamber is used as the after-combustion chamber, and after the flight Mach number increases, the gas flow into the subsonic combustion chamber decreases, and more airflow enters the super-combustion chamber from the outer air intake, at this time, the subsonic combustion chamber plays the role of guiding the flame, such as the dual-combustion chamber engine used in the HyFly program in the United States (Figure 3-20).

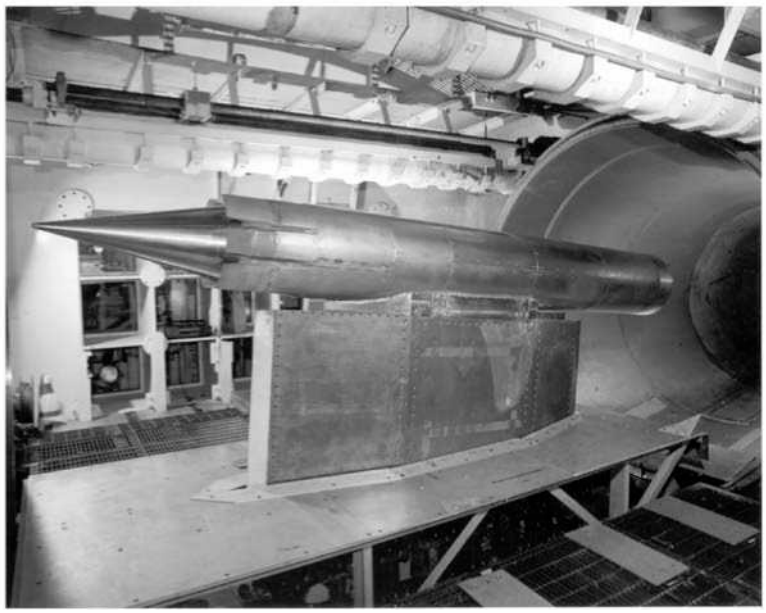

Figure 3-20: HyFly's planned dual-chamber engine

5) Add additives to hydrocarbon fuels

The use of highly reactive fuels as additives can effectively shorten the ignition delay of hydrocarbon fuels and the induction time of chemical reactions, which is advantageous for ignition, but to achieve stable combustion, the additives required reach 25% of the total fuel, which increases the volume and complexity of the aircraft (especially the fuel supply system), which leads to a decrease in the specific impulse of the engine [71].

6) Vanguard Flame

The use of fast-reacting fuels (such as H2, CIF3, SiH4, etc.) as a pioneer flame can provide hydrocarbon fuels with the high temperatures and free radicals necessary for faster combustion. Chang performed numerical simulations of hydrogen and SiH4 ignition of Jet-A (liquid hydrocarbon fuel) [71]. The results show that the ignition effect of SiH4 is very good, when the concentration of SiH4 in the ignition flame is 5% of oxygen, the flame of Jet-A is shortened to 20% of the original length, when the injection amount of SiH4 is increased to 10%, the flame of Jet-A is shortened to 5%, and the concentration of SiH4 is further increased to 20%, and the flame length is only 1% of the original length.

The use of a pioneer flame must be optimally combined with leeward steps, grooves, and nozzle settings to achieve good results [113]. Some Pioneer flame fuels contain toxic, spontaneously combustible or carcinogenic components such as fluorine, chlorine, boron, silicon, etc., which are logistically unacceptable. The use of a small amount of hydrogen (Φ = 0.01 to 0.03) as a pioneer flame for low-temperature ignition of hydrocarbon fuels has been widely used [71].

At present, the most studied is hydrogen-guided flames. Boughi studied the super-ignition flow field of liquid hydrocarbon fuel (toluene) ejected downstream of a hydrogen-guided flame [71], in which the hydrogen-guided flame was injected downstream on the leeward side of the leeward step, and toluene was injected vertically in the wake region of the rear step, with an incoming Mach number of 2.5 and a total temperature of 1000 K. The results show that the flow rate of liquid fuel for stable combustion is limited to a certain extent due to the cooling effect of the liquid fuel on the hydrogen-guided flame.

7) Preheat the fuel

Vinogradov et al. [71,121] preheated the methane fuel to 550 to 880 K under the incoming flow conditions of the imported Mach number of 2.0, the total temperature of 650 to 910 K, and the total pressure of 0.42 to 0.74 MPa, and used the combination of support plate and wall injection and spark plug ignition to achieve the ignition and flame stability of methane, and the equivalent oil-gas ratio of the injected fuel ranged from 0.6-0.85, and the combustion zone *Ma* = 0.5 to 0.6. Lin et al. [71] successfully achieved the ignition and stable combustion of kerosene JP-7 when the equivalent oil-gas ratio was 0.9 to 1.0 under the incoming flow conditions of Mach number of 1.8, total temperature of 555 to 1000 K, and total pressure of 0.186 MPa.

8) Forced ignition with a high-energy igniter

After the 1980s, a large number of countries have reported the use of plasma igniters in scramjet engines, and believe that plasma igniters can produce high temperature and hydrogen atoms, hydrogen atoms are the chain carriers in the process of chemical reactions, increasing the number of hydrogen atoms can accelerate the combustion chemical reaction rate, shorten the chemical reaction induction period. In addition, the use of high-energy spark plug forced ignition in scramjet engines with hydrogen and hydrocarbon fuels has also been widely used [115].

In conclusion, fuel-enhanced blending and stable combustion technology in limited space and residence time is one of the main problems faced in the research of scramjet combustion chambers.

2. Cavity flame stabilizer

Cavity flame stabilizer (also known as niche flame stabilizer in early domestic research) is a more commonly used flame stabilization technology. In 1993, the Central Aero-Engine-Engines Institute (CIAM) of Russia first announced the use of a recess as a flame stabilizer for scramjet engines [122,123]. In a series of ground and flight demonstration verifications, hydrogen and kerosene combustion tests have shown that the cavity flame has strong stability ability. Later, the U.S. Air Force began to study the integrated technology of fuel injection/ignition/flame stabilization/cooling based on the cavity, which proved that the cavity is a very effective flame stabilization device for supersonic combustion, which can greatly improve the combustion efficiency of fuel in supersonic flow. These research results prove the possibility of the application of cavity in supersonic combustion, which makes the cavity widely concerned in the field of scramjet engine research.

Reference [4] provides a comprehensive summary of the research on cavity stabilizers.

1) Research on the structure of concave cavity flow field

The cavities were classified according to the distance of the cavity shear layer development and the depth of the cavities, and the cavities with a length-to-depth ratio *of* $L/D < 10$ were open cavities and $L/D \geq 10$ were closed cavities. In addition, it is also said that the $7 \leq L/D \leq 10$ cavity is a transitional cavity. The biggest feature of the closed cavity is that the free shear layer of the cavity can hit the bottom wall of the cavity, and two stationary reflux zones are formed inside the cavity. However, the free shear layer of the open cavity cannot hit the bottom wall of the cavity, and there is a large reflux zone within the cavity. At present, scramjet engines mainly use open cavities as flame stabilizers. According to the function of the cavity, it is customary to call the cavity with a trailing edge angle of 90° as an acoustic cavity, and the cavity with a trailing edge angle of less than 90° as a flame-stabilized cavity. The structure of the cavity flow field in supersonic flow is basically similar, as shown in Figure 3-21, which mainly includes: (1) shock wave or expansion wave at the leading edge of the cavity (2) cavity-free shear layer; (3) shock wave at the trailing edge of the cavity; (4) expansion waves formed by airflow after shock waves. The leading edge wave system is determined according to the cavity structure, which is usually a shock wave for an open cavity and an expansion wave for a closed cavity.

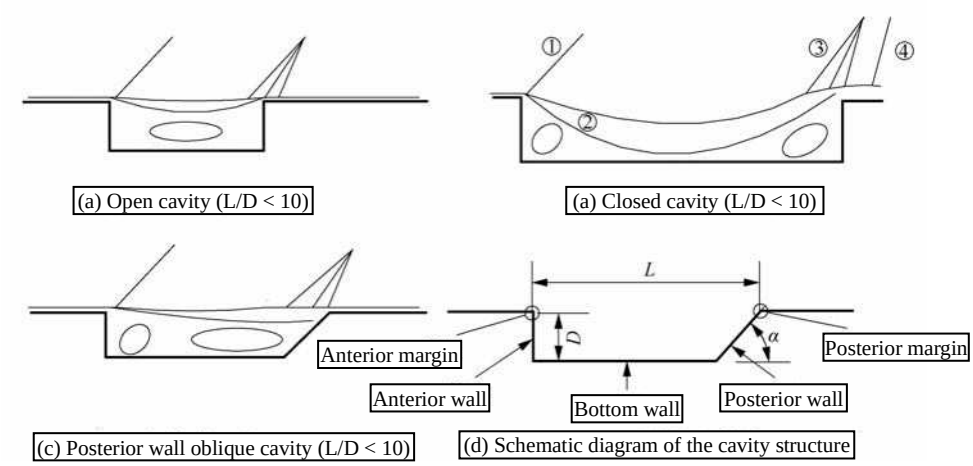

α—trailing edge angle; D—depth; L—Length

Fig. 3-21: Schematic diagram of the basic flow field and structure of the cavity [124]

2) Concave cavity mixing enhancement study

Burnes [125] used the outlet total pressure measurement method to study the influence of different cavity configurations on the mixing and took images of the flow field schlieren and combustion flame around the cavity in supersonic flow. By comparing the results with the results without the cavity, it can be seen that a part of the fuel injected upstream of the cavity enters the cavity, which inhibits or reduces the oscillation characteristics of the cavity. At the same time, the fuel is entrapped in a coherent structure formed at the front of the cavity, and the mixing is enhanced by periodic oscillations in the cavity. Yu et al. [126] pointed out that the enhanced cavity mixing mechanism caused by flow is related to the large coherent structure of the vortex generated by the cavity. Anand [127] investigated the effects of incoming Mach number and incoming boundary conditions on cavity enhancement mixing. The results show that the self-oscillation of the cavity can be used to enhance supersonic mixing. The downstream counterpressure of the cavity changes the Mach number of the upstream of the cavity, thereby changing the self-oscillation characteristics of the cavity, and the cavity can still maintain good oscillation characteristics in a wide range of Mach numbers, but the oscillation frequency of the cavity will change with the change of downstream counterpressure. Lee et al. [128] used numerical simulation to compare the fuel jet penetration, mixing rate, and total pressure loss under two types of backpressure. The results show that the cavity enhances the mixing of fuels and the total pressure loss of the flow field is small. Yu [129] measured the outlet flow field of the supersonic jet using the plane scattering technique, and compared the mixing enhancement characteristics of the channel-shaped acoustic cavity and the annular acoustic cavity for the supersonic jet at different temperatures.

The results show that the self-excited oscillation caused by the cavity affects the development of the supersonic hybrid shear layer and enhances the mixing rate of the fuel. Gruber [130] used a combination of schlieren and PLIF techniques to study the flame stability and mixing enhancement performance of cavities in supersonic cold and reacting flows. The results show that: (1) the fuel injected from the front of the cavity is greatly affected by the flow in the combustion chamber, while the fuel injected from the inside of the cavity is less affected by different flight Mach numbers and different flow states; (2) fuel injection from the back wall of the cavity can efficiently organize combustion in a wider range of fuel variation than that injected from other positions in the cavity, and is less affected by the ignition process; (3) when the fuel equivalent ratio inside the cavity is appropriate, the flame oscillation in the cavity is small, and the combustion is more stable; when the equivalent ratio deviates from this suitable range, the combustion oscillation and the spatial gradient of the flow field are larger; (4) the shock wave has a great influence on the mixing and combustion in the cavity. With the combustion of fuel in the cavity, the shear layer upstream of the cavity will be biased towards the main stream, and the mass exchange between the cavity and the main stream will be increased, thus enhancing the combustion.

3) Cavity stabilization flame study

The principle of using a cavity to stabilize the flame is that the fuel is injected in or upstream of the cavity groove, and the flow characteristics of the gas flow through the cavity enhance the mixing of fuel and gas flow; when ignition is carried out under external energy conditions, or when the main stream reaches the spontaneous combustion condition of the fuel, the fuel is burned and a large amount of heat is released, so that the cavity forms a high-temperature and low-speed reflux zone. This reflux zone helps in the chemical reaction that stabilizes the flame.

The cavity flame stabilizer for supersonic combustion was first designed by CIAM [122,131], and Russian scientists have demonstrated the effectiveness of the cavity in the combustion of scramjet engines, especially the success of test flight experiments, which facilitated in-depth research in this area. Niioka et al. [132] investigated flame stabilization between two plates (similar to a cavity). Hydrogen fuel is sprayed parallel from the front support plate between the two plates, that is, inside the cavity, and when the main Mach number is 1.5, the flame is stable, and its stability depends on the distance between the two plates. Morrison et al. [133] investigated the extinguishing range of the flame in the return zone where the fuel was injected directly into the cavity. The experimental results support the idea that a cavity flame stabilizer can be used in the design of combustion chambers where a general ramjet engine is combined with a scramjet engine. In Reference [134], it was studied that the mainstream Mach number is 3 to 5, the fuel is injected parallel from the upstream nozzle of the cavity, and the cavity of L = 25 and D = 18 can improve flame stability and combustion efficiency. Under the same conditions, the combustion efficiency decreases as the equivalent ratio increases.

Reference [135] is a comparative analysis of the flow path and evaluation of the design of an axisymmetric hydrogen-fueled scramjet engine in flight tests with Mach number 6.5. In the combustion chamber of the scramjet engine used, there are two cavities (20mm x 40mm and 30mm x 53mm) and a trailing edge step, and the fuel is injected into the downflow at an angle from the cavity and upstream of the step, and 60% of the injected fuel reacts in the cavity, indicating that the cavity enhances the mixing of fuel and gas flow; there is no need for spark plug ignition, the fuel ignites spontaneously in the cavity, and the flame can continue to be maintained; however, spontaneous combustion will not occur in the absence of a cavity. Owens et al. [136] studied flame stabilizers for kerosene combustion. The experimental conditions were a mainstream Mach number of 1.8, a stagnation temperature of 300 to 1,000 K, hydrogen as a guide flame was injected from the cavity, kerosene was injected at the leading edge of the cavity, and two flame stabilizers (a rear edge step, a cavity with a trailing edge inclination of 30°, and other deformations) were used. The results show that the stagnation temperature of the gas flow plays a great role in the stability of the flame by changing the local equivalent ratio. The use of a cavity (L/D = 2.8) creates a large reflux zone and thus a stable flame. Yu et al. [137] experimentally investigated the performance of the cavity in the supersonic reacting flow. Using equipment used to simulate the combustion of a bimodal scramjet engine, including an isolator section of equal cross-section and an expanded combustion chamber behind it, they analyzed the main stream Mach number of 2, the injection of fuel ethylene into the main stream at a 45° angle upstream of the cavity, several different L/D (0.5, 1, 2, 3, respectively) and inclined trailing edge structures (L/D = 5) flow field characteristics and flame stability of the cavity. The cavities with small ratios L/D (1, 2, 3) have good flame stabilization characteristics. The cavity with a large ratio (L/D = 5) shortens the flame length and has a large loss of pressure. Mathur et al. [138] combined fuel injection and flame stabilization in a direct-coupled supersonic combustion chamber device, L/D = 48. The flame stability characteristics of the cavity with a trailing edge inclination angle of 22° were studied.

Under the conditions of 4 to 5 Mach number and 47.88 kPa of dynamic pressure, a small amount of ethylene fuel is first injected inside the cavity as a guiding flame, and then fuel is injected upstream, without external auxiliary ignition equipment, and the fuel ignites by itself and continues to burn. The flame can continue to be maintained when the equivalent ratio of ethylene to air is 0.25 to 0.75, and the measured net thrust is 667 to 1,780 N, and the combustion efficiency is 80%; with the increase of the equivalent ratio, the net thrust increases, and after the equivalent ratio is greater than 0.6, the net thrust increase decreases due to the decrease of combustion efficiency.

As a flame stabilizer for supersonic combustion, the cavity has been tested and studied, and a large number of results have been obtained. However, there are still some problems that need to be solved urgently, such as how to determine the geometry of the cavity to make it have good flame stability characteristics and minimize the total pressure loss for certain mainstream conditions, which has not been considered in the current research. There is a lack of systematic research on the interaction between the mainstream conditions, the geometry of the cavity, the type of fuel and the injection mode, and the chemical reaction. Solving these problems is essential to optimize the cavity flame stabilization and maximize the performance of scramjet engines.

4) Study of the interaction between the jet and the cavity

The cavity flame stabilizer is mainly used to stabilize the flame and achieve efficient tissue combustion, which requires an in-depth study of the exchange process between the fuel and the cavity and the effect of fuel injection on the flow of the cavity. The main contents include the distribution of fuel injection upstream of the cavity along the cavity, the combustion performance of the fuel jet at different positions in the cavity and the influence of the cavity on the fuel distribution.

Hsu [12] used Raman scattering to quantitatively measure the fuel jet upstream of the cavity at an incoming Mach number of 2. The interaction between cavity configuration, fuel injection pressure, downstream counterpressure and fuel distribution and fuel transport mechanism was studied. The results show that for the wall fuel jet upstream of the cavity, the fuel distribution in the shear layer and the interaction between the shear layer and the trailing edge angle of the cavity are the main factors determining the fuel transport into the cavity. The backpressure-induced shock string leads to boundary layer separation, which has a great impact on the fuel distribution. Yu [137] investigated the flame stabilization and mixing enhancement properties of the cavity in the reacting stream. The results show that the cavity enhances the fuel exothermia, improves the temperature and pressure recovery at the combustion chamber outlet, and accelerates the mixing rate. Ben-Yakar [64,139] experimentally studied the hydrogen jet upstream of the cavity in a high-enthalpy supersonic flow simulating a flight with a Mach number of 10. The test used OH-PLIF and schlieren to obtain a continuous 8-frame image using a combination of high-speed photography capable of capturing 105 to 107 frames per second. The OH-PLIF image shows the distribution of the spontaneous combustion and combustion zone of hydrogen, and the high-speed schlieren image compares the transport characteristics, penetration and instability of the shock structure of the jet, and also observes the wave structure near the cavity with different aspect ratios and trailing edge angles. The results show that hydrogen and air combustion is a process controlled by mixing under high enthalpy flow conditions. O'Byrne, Ingo, et al. [140] used planar laser-induced hydroxyl fluorescence to study cavity-based fuel injection systems. Under the condition of Mach number of 11.5 simulated flight, the combustion characteristics of hydrogen and ethylene fuels at lean fuel equivalent ratio were compared. The results show that combustion usually occurs within the shear layer upstream of the cavity and not within the cavity reflux zone. Hydrogen is mainly diffusion combustion in the shear layer and downstream, and the jet penetration is linearly related to the jet pressure, and the shear layer produces periodic shedding vortices during the combustion process: ethylene has basically the same characteristics as hydrogen at low equivalent ratio, but the combustion is slightly stronger. Ding Meng [141] compared the combustion of injected fuel at different locations. The results show that the cavity shear layer will deviate from the cavity in the combustion flow field, resulting in the shear layer no longer adhering to the back wall of the cavity, so that part of the fuel injected upstream of the cavity enters the main stream with the shear layer, and part of it directly passes through the shear layer and enters the internal structure of the cavity for combustion.

5) Research on cavity resistance characteristics

The force experienced by the cavity is made up of piezoresistive and frictional resistance, and the piezoresistive resistance is much greater than the frictional resistance. As a result, cavity resistance is essentially caused by pressure differences.

In high-velocity airflow, there is a pressure difference between the front and rear walls of the cavity, so a certain thrust or drag is bound to occur [142].

Zhang [143] simulated the variation of the subsequent edge angle of the cavity resistance coefficient. The results show that the drag coefficient decreases with the decrease of the subsequent edge angles (90°, 67.5° and 45°) in supersonic cold flow. The simulation results of Gruber [144] show that the drag increases slightly with the increase of *L/D*. As the trailing edge angle decreases, the drag increases. Due to the influence of the computational model, Reference [143] and Reference [144] have reached opposite conclusions, and the specific reasons are unknown. Baurle [145] used two-dimensional numerical simulations to compare the drag characteristics of *L/D* = 3 and 7 cavities with trailing edge angles of 30°, 60°, and 90°. The results show that the drag coefficient of the long cavity is large, and the influence of the depth of the cavity on the drag coefficient is slightly smaller. Quinn [146] studied the injection of fuel into the cavity in a supersonic stream with an incoming Mach number of 2.0. The results show that the jet reduces the resistance of the cavity. Ding Meng [147] experimentally studied the cold flow resistance of a concave flame stabilizer with a depth of 10 mm, 15 mm, and 20 mm, an aspect ratio of 4 to 10 and a rear wall inclination angle of 18° to 60° in a supersonic flow with an incoming Mach number of 1.92, a static temperature of 509 K, and a static pressure of 86.6 kPa. The results show that the cold flow resistance of the cavity flame stabilizer is proportional to the cavity depth. It is also proportional to the cavity length-to-depth ratio; then the increase of the edge angle first decreases and then increases, and there should be an angle within 30° to 60° to minimize the cold flow resistance. At the same time, hydrogen was used as fuel and spark plug igniter was used to ignite, and the resistance characteristics of the cavity flame stabilizer at different injection positions and different equivalent ratios were compared under the combustion mode. The results show that the thermal test resistance of the cavity flame stabilizer is smaller than that of the cold flow resistance, and is greatly affected by the fuel injection mode, and the resistance of the cavity flame stabilizer decreases with the increase of the equivalent ratio, and finally shows a positive thrust.

6) Research on the application of multi-cavity in supersonic combustion

The cavity enhances both fuel mixing and flame stabilization. Therefore, in order to improve the fuel mixing characteristics in the combustion chamber, enhance the ignition and flame stabilization capabilities, and obtain higher combustion performance, researchers have actively explored the use of multi-acoustic cavities, multi-flame stabilization cavities, and the combination of acoustic cavities and flame stabilization cavities to improve the performance of combustion chambers. As shown in Figure 3-22, in a multi-cavity combustion chamber, the arrangement of the cavity can be roughly divided into two types: the cavity arranged on the same side of the combustion chamber is called the tandem cavity; the cavities arranged on different sides are called parallel cavities. Therefore, the study of multiple cavities is converted into the study of parallel and series of cavities.

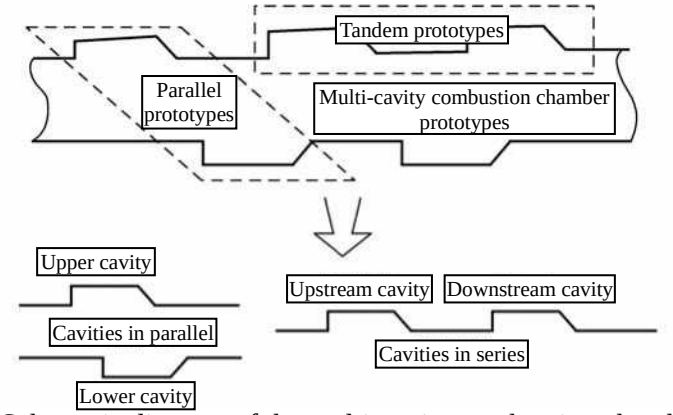

Figure 3-22: Schematic diagram of the multi-cavity combustion chamber model [142]

In terms of the flow field structure of the combined cavity, Yu [148] experimentally studied the flow field structure of the concave cavity in the supersonic combustion flow, took the flame image of the combustion area and the flow field schlieren image of the cavity, and compared the total pressure loss and schlieren image of the outlet of the supersonic pipe under the seven concave combination configurations, as well as the flame distribution perpendicular to the direction of the cavity.

The results show that the mixing and combustion of fuel are significantly enhanced by using the acoustic cavity in series with the flame stabilizing cavity in series. Zhang [149] studied the flow field characteristics of the two acoustic cavity series combinations of A (L/D = 1) and B (L/D = 3) in supersonic flows with incoming Mach numbers of 1.5, 2.5, and 3.5. Through the analysis of the time-averaged results and instability of the flow field, the following conclusions are obtained: when the B cavity is located before the A cavity, the flow of A cavity is a periodic turbulent boundary layer, and the oscillation frequency of A cavity is controlled by B cavity, and no longer appears as a single cavity longitudinal wave oscillation. When a B cavity is also installed in front of the B cavity, the rear B cavity is only affected by the unstable level of pressure and the frequency of the oscillation, but still shows its own shear wave oscillation characteristics. The distance between the two cavities changes the thickness of the incoming boundary layer but has little influence on the oscillation characteristics of the cavities themselves. Rho [150] carried out numerical simulations on Zhang's experimental results, and the calculated results are in good agreement with the experimental results, and the calculated results illustrate the periodic change process of the incoming flow boundary layer of the precavity to the posterior cavity. Taborda [151] experimentally investigated the effect of the series connection of two acoustic cavities on the active control of flow oscillation in a transonic flow with an incoming Mach number of 0.9. The results show that when active control is adopted, the concave series arrangement can produce low sound wave intensity, and the tandem arrangement of the two acoustic cavities has higher safety. Jeyakumar [152] studied the effect of acoustic cavity series combination on mixing in supersonic mixing pipes, and analyzed the mixing efficiency in the mixing pipes by measuring the total temperature distribution and total pressure loss in the mixing pipes. The results show that the mixing enhancement effect of the two acoustic cavities in series is the best. Holmes [153] investigated the thermal conductivity of the combined acoustic cavities in the fastening holes of rocket engine screws in a supersonic flow with an incoming Mach number of 4. The thermal conductivity of the cavity wall and the infrared images of each wall of the cavity were measured, and it was concluded that the thermal conductivity of the combination of the two tandem cavities was better than that of the combination of single cavity and tandem cavity, which may be related to the corner effect of the parallel arrangement of the tandem cavities.

In terms of mixing/combustion enhancement, Yu [154] studied the flow characteristics of the acoustic cavity and the flame stabilization cavity by measuring the mixing rate and total pressure loss, and pointed out that the acoustic cavity and flame stabilization cavity can be used for flame stabilization and mixing enhancement respectively, and suggested that the combination of the two can be applied to the engine to improve combustion performance. Situ Ming [155,156] studied the combustion of kerosene in a double-combustion chamber with gas-ignited acoustic cavities and flame-stabilized recesses arranged in series. The results show that the combined cavity enhances the combustion process. Chen Jianqiang [157] also conducted numerical simulation studies on the cold flow field in the double-cavity combined combustion chamber. The results show that the combination of the mixing cavity and the flame-stabilized cavity enhances the mixing characteristics of the flow field. CIAM has demonstrated through extensive research that the use of multi-flame stabilized cavities can achieve efficient combustion. In the flight verification engine, a flame stabilization method combining a tandem cavity and a rear-facing step is also used. Yu Gang [137] conducted a direct test on the combustion characteristics of kerosene after bubble atomization in the series arrangement of the acoustic cavity and the flame stabilization cavity, in which the Mach number of the incoming flow was 2.5, and the total pressure and total temperature of the incoming flow ranged from 1.0 to l.1 MPa and 1,700 to 1,900K, respectively. The results show that the combustion efficiency of hydrogen bubble atomization is high, and the combustion performance can be improved by using the acoustic cavity in series with the flame stabilization cavity or the two flame stabilization cavities in series. Adam Quick [158] experimentally studied the coupling between the upstream acoustic cavity and the downstream flame stabilization cavity using NO-PLIF convection field structure, in which the upstream cavity L/D is 1 and the downstream cavity L/D is 47, the trailing edge angle is 22.5°, and the incoming Mach number is 2. The results show that the upstream cavity can be used to control the mixing characteristics between the fuel jet and the main stream, which can improve engine performance by reducing the position requirements of fuel injection, that is, accelerating the diffusion of fuel to the entire engine interior. Li Dapeng [142] and Ding Meng [141] studied the flow process of kerosene combustion in a multi-cavity combustion chamber, showing that the multi-cavity configuration combustion chamber has high performance in terms of ignition, flame stability and net thrust. The multi-cavity technique mentioned in Reference [4] uses a combination of multiple flame-stabilized cavities to study supersonic combustion flow in the case of multi-cavity combination. The results show that: (1) the mechanism of parallel cavity enhancement ignition, flame stabilization and combustion is that the shock wave at the anterior/trailing edge of the cavity enhances fuel ignition, flame stabilization and combustion; the exothermic zone near the cavity compresses the supersonic incoming flow, which generates a complex pre-combustion shock system, which promotes the combustion of the fuel.

(2) The mechanism of the tandem cavity to enhance ignition, flame stabilization and combustion is such that the upstream cavity can prolong the fuel residence time, heat, blend and pre-ignite the fuel, and promote the fuel ignition; the high-temperature gas in the downstream cavity can continuously ignite and refuel the fuel heated and premixed by the upstream cavity, compress the upstream flow, and further promote the heating and pre-ignition of the fuel in the upstream cavity, thereby enhancing combustion.

3. Fuel injector for support plates

One of the key technologies of the supersonic combustion process of liquid hydrocarbon fuel, the fuel injection and mixing enhancement technology, is reflected in the design of the fuel injector, one of the components of the scramjet compulsion machine. Due to the constraints of combustion efficiency and engine performance, the key factors in the design of the fuel injector [159] are mainly to achieve rapid mixing and combustion, minimize total pressure loss, and make the outlet section of the combustion chamber flow as uniform as possible (to ensure that the nozzle can achieve an efficient expansion process), of which rapid mixing and combustion are the most important, as it will directly determine the length and weight of the combustion chamber. Due to the extremely short fuel retention time and the strong stability of the supersonic mixing layer (its expansion rate is only 1/3 of that of the non-compressible shear layer under the same density ratio), the mixing enhancement technology must be fully considered to achieve the purpose of rapid mixing.

Fuel injection technology can be divided into two broad categories: wall injection and plug-in injection. In the wall injection method, the vertical injection of the circular nozzle is the simplest form, which can provide faster near-field mixing and good fuel penetration ability, and the reflux zone generated by the jet can play a role in flame stabilization, but the jet produces a strong shock wave, the total pressure loss is large, and the heat load on the ground wall is also high, and the compressibility effect is not conducive to the production and shedding of vortices in the fuel/air mixed layer, which inhibits the coil suction mixing and slows down the mixing and combustion in the far field. In order to reduce the shock wave intensity and total pressure loss of vertical injection, small-angle injection can be used. The results show that the near-field mixing effect decreases with the decrease of angle, but the far-field and overall mixing effect basically do not change. Although the non-circular nozzles (oval, wedge, etc.) reduce the penetration of the fuel, they are better improved in terms of total pressure loss, wall heat load, development of the mixing layer, and overall mixing effect. In order to further enhance the mixing, the researchers designed the fuel injector and the combustion chamber wall into a special shape and enhanced the flow vorticity in the flow field through the phenomena such as shock waves, expansion waves, and flow vortices generated in the flow field, so as to achieve the purpose of mixing enhancement. As the vortex propagates downstream, it will trap the fuel and air, increasing the contact area between the fuel and the air, increasing the local concentration gradient, and thus enhancing the mixing. Because the side area of the swept slope is dilated, the airflow expands, the pressure difference with the front is larger, and the flow vortex is stronger, and the hybrid enhancement effect is better than that without sweep. Of course, the slope structure protrudes from the combustion chamber wall, which causes a large total pressure loss, and the heat load on the slope front is large. Cox [160] uses multiple rows of nozzles with different axial and transverse angles to form a nozzle array, forming a pneumatic ramp through the pneumatic action between the individual jets. The results show that the pneumatic slope is only slightly smaller than the swept slope in terms of penetration and plume area but is basically equivalent to the swept slope in terms of fuel lateral diffusion capacity, and greatly reduces the total pressure loss and local heat load. Wall cavity injection is a new type of fuel injection technology that has been proven to have good flame stability. Structurally, it consists of a backward step and a forward step, and the fuel can be injected into the combustion chamber through nozzles located on the bottom wall, front wall and upstream wall of the cavity; when the air flows through the cavity, a reflux zone will be formed in the cavity, which basically fills the entire cavity, so the reflux zone is larger, which undoubtedly increases the flame stabilization ability, and at the same time, the acoustic disturbance induced by the cavity and the large-scale coherent structure detached from the trailing edge of the cavity can enhance the mixing. The reattachment point of the cavity separation flow is basically located near the inflection point of the trailing edge, and the shock wave intensity is weak, and the total pressure loss is small. Among the plug-in injection methods, the most common is lateral and/or bottom injection of the support plate

Because the fuel injector of this mode is arranged in the middle of the main stream, it can directly inject the fuel into the main stream of supersonic incoming flow, can provide good fuel space distribution and mixing effect, especially when the combustion chamber flow channel is large, the wall injection is difficult to meet the requirements in the penetration of the fuel, and the advantages of the support plate injection are more prominent; the mixing is further enhanced, and the reflux zone formed at the bottom of the support plate can have a certain effect of stabilizing the flame, of course, the injection of the support plate usually produces a large total pressure and piezoresistance loss, and the high thermal load puts forward higher requirements for the material.

The fuel injection system that can be truly applied to scramjet engines must meet the requirements of resistance and total pressure loss is small enough, and at the same time, the injector must realize the rapid mixing of fuel and oxidizer at the macro scale, and allow the fuel to have enough residence time to realize the heating of the fuel itself, when there are enough reactants to complete the mixing at the macro scale, the large-scale turbulent structure will be further broken to promote the generation of the small-scale turbulent structure, thereby accelerating the mixing at the microscopic scale, and the rate of microscopic mixing must be consistent with the chemical reaction time. In addition, the injector must be able to control the pressure increase due to the release of heat.

In the mid-1970s, the Langley Research Center in the United States proposed an integrated body/engine configuration scheme with a rectangular cross-section, and compared the two-plate model engine (Nickel 3-Strut & Copper 3-Strut), the non-supported plate parameter engine (SLPE), and the stepped parameter engine (SSPE) [161]. A large number of ground tests were carried out, among which the concept of the support plate was proposed for the first time and its function was verified, and the integrated configuration and support plate were later widely adopted.

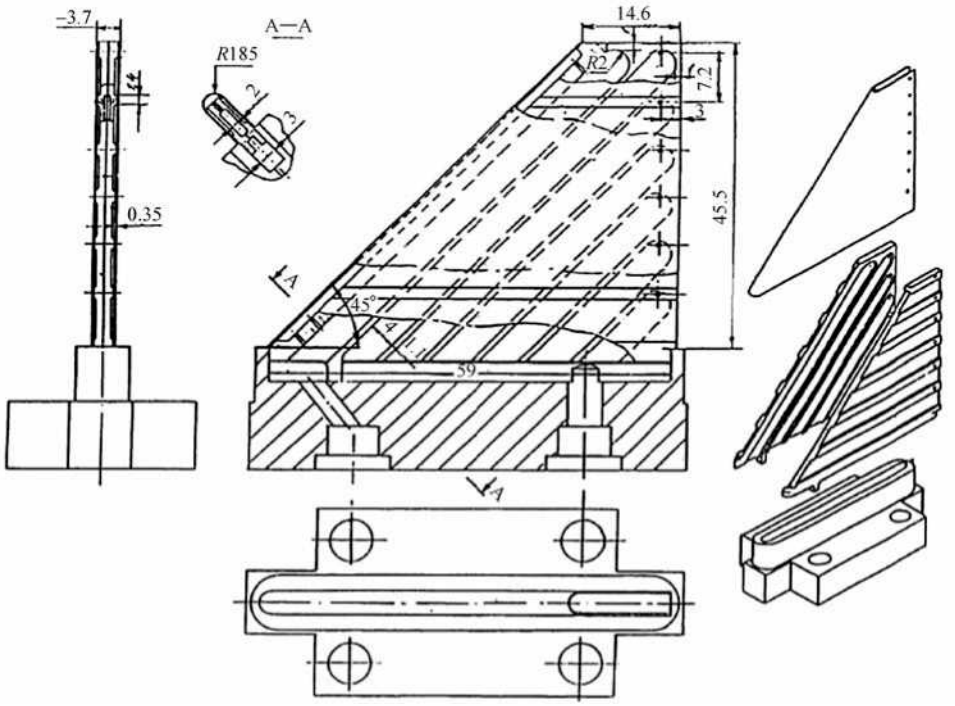

Figure 3-23: Support plate designed by Semenov et al

In the 1990s, Russia, Japan, and other countries also began to study the injection of support plates. Figure 3-23 is the support plate designed by Semenov et al. [162] in Russia, the structure of this support plate is to weld two metal plates together, and there is a groove on the inner surface of the metal plate as a flow channel for fuel, and the fuel absorbs the heat of the support plate itself when passing through the inside of the support plate, which plays a role in cooling the support plate. The experimental results show that this structure has a good cooling effect, and the use of this support plate injection fuel can enhance the mixing and improve the combustion efficiency. Vinogradov et al. [163] of CIAM also conducted an experimental study on support plate injection.

Figure 3-24 shows the combustion chamber and fuel injection of the experimental model engine. The engine combustion chamber is divided into two stages, is connected by steps, and has four places that can be injected with fuel as shown in Figure 3-24, I is the injection after the slope, II is the injection of the support plate, III is the injection of the wall surface, and IV is the injection after the step. The experimental results show that the combustion efficiency is the highest and the best mixing is when the fuel is injected with the support plate.

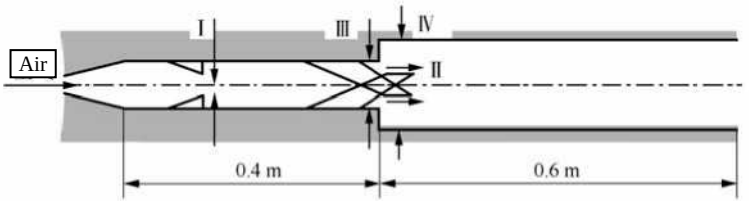

Figure 3-24: Schematic diagram of the combustion chamber and fuel injection of the experimental model engine of Vinogradov et al. [163]

Japan's research on support plates started in the 1990s, they have done a lot of research work on support plate spraying and have achieved certain results. Sadatake Tomioka et al. [164] carried out hydrogen fuel *Ma* = 2.5 combustion chamber experiments, as shown in Figure 3-25. The combustion chamber is divided into two stages: the first stage can inject fuel through the water-cooled support plate and the wall; the second stage is wall spraying. The experimental results show that the penetration and mixing of the fuel are poor and the combustion efficiency is low when only the wall is sprayed. Sunami et al. [165] designed a support plate with a staggered geometric structure at the tail as shown in Figure 3-26, carried out several experiments, and carried out numerical research, the numerical research results are consistent with the experimental results, and all of them show that the support plate can generate eddy currents well, and the large vortex is broken to form a small vortex to promote the mixing of fuel and air to form efficient supersonic combustion.

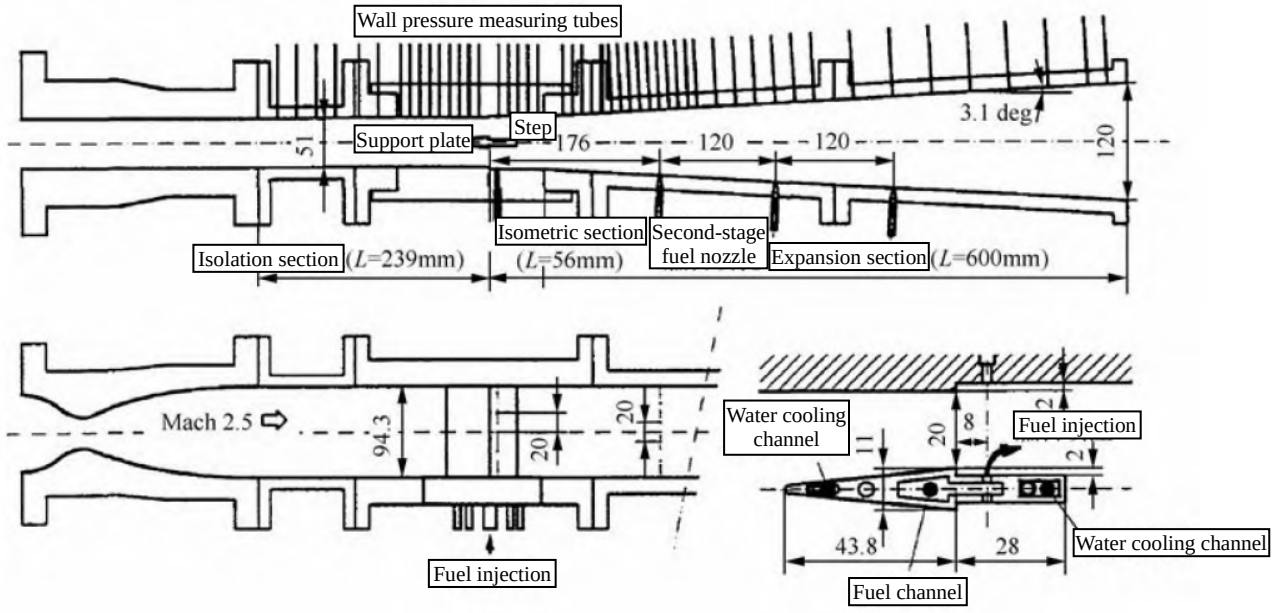

Figure 3-25: Schematic diagram of the injection of engine and support plate in the experimental model of Tomioka et al. [164]

In 1997, France conducted experiments with the hydrocarbon-fueled CHAMOIS scramjet model engine in a domestic research program called Aerospatiale Matra Missiles (AMM) [166], which used kerosene-cooled support plate injection fuel. Figure 3-27 shows the experimental model engine, and the injection method of the two plates of fuel is also studied in combination with the model engine itself. The experimental results show that spontaneous combustion can be achieved by injecting hydrogen from the bottom of the support plate, and can realize the ignition of liquid kerosene at a static temperature of 700 K.

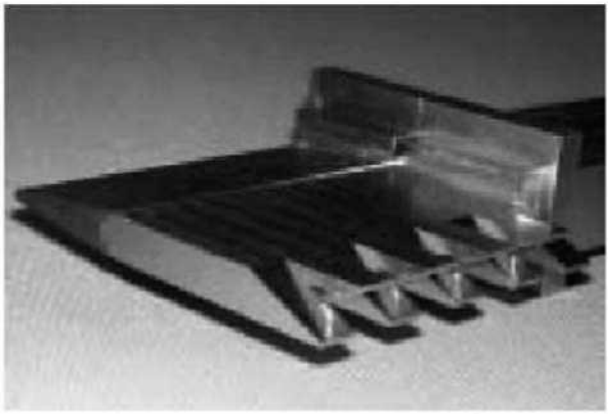

Figure 3-26: A support plate with a staggered geometry at the tail designed by Sunami et al. [165]

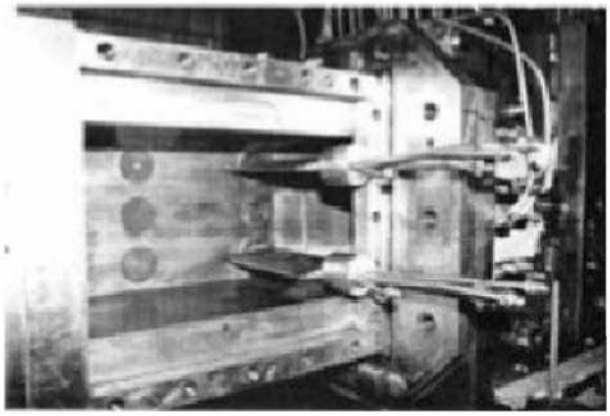

Figure 3-27: CHAMOIS scramjet engine with support plates [166]

Combustion chamber experiments with supported plates were also carried out at the University of Munich in Germany [167] (Fig. 3-28). They designed this support plate with a straight metal rod at the end. Studies have shown that this structure works well in flame stabilization.

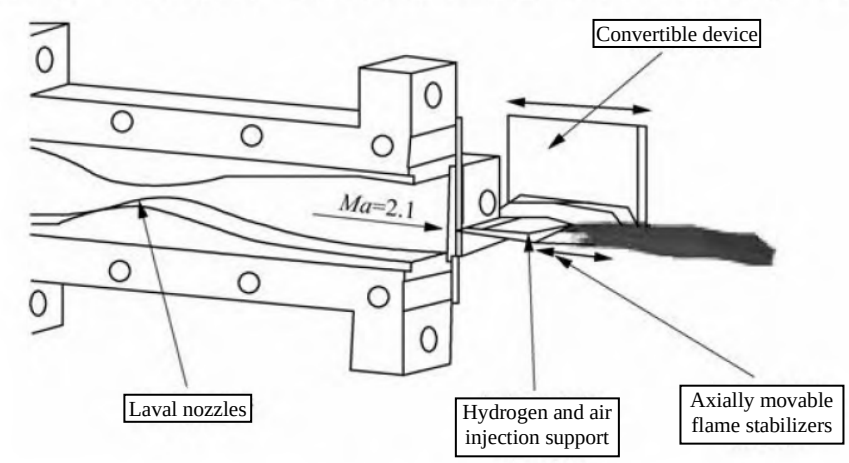

Figure 3-28: Supporting plate designed by the University of Munich [167]

In addition, the University of Stuttgart, Germany, compared the support plate with staggered geometry at the tail and the support plate without the staggered geometry at the tail [168]. The results show that the support plate with staggered geometry at the tail can better enhance the mixing. Australia has also done a lot of research work on support plate injection. Most of the experiments they completed in the T3 and T4 wind tunnels were fueled with support plates.

4. Combustion chamber surface design

Scramjet engines are often highly integrated with the airframe, which requires comprehensive consideration of the aerodynamic effects between the propulsion system and the aircraft, as well as the influence of the design and installation of the engine on the performance of the aircraft. In addition, the design of scramjet engines must also take into account complex issues such as structural thermal loads due to aerodynamic heating. Due to the complexity of the internal physical and chemical processes in the combustion chamber of scramjet engines, the profile design and analysis of scramjet combustion chambers are quite complex. Here, the basic design process and method are illustrated by taking the design of the combustion chamber of the scramjet model engine in Reference [169] as an example.

1) The geometric parameters of the passage in the combustion chamber are determined

The content of the combustion chamber profile design of scramjet engine is based on the requirements of the overall design of the aircraft, that is, the geometry of the supersonic combustion chamber is designed under the given engine geometric constraints and inlet conditions, and the main performance parameters of the scramjet engine are estimated in the design and non-design state.

Theoretically, it can be shown that there is a fully defined limit value Q_{max} [170] given the initial parameters of the air flow when heating in a pipe of equal cross-section. It is impossible to add more heat than Q_{max} to the airflow without decreasing the inlet Mach number, or without increasing the total inlet airflow temperature when the inlet Mach number is constant. In order to improve the heating ratio and improve the performance of scramjet engines, it is necessary to heat in the combustion chamber with an expanding cross-sectional area. Therefore, the model engine combustion chamber designed in Reference [169] is designed according to isostatic pressure, and the cross-sectional area of the combustion chamber gradually expands in order to add more heat to the combustion chamber and to prevent the pressure in the combustion chamber from gradually increasing with the heat released from combustion.

(1) Entrance size. The total design flow rate of the air heater is 7.88kg/s, according to the heater nozzle outlet conditions: P_{in} = 70,530Pa, T_{in} = 746.36K, R = 290.00J/(kg • K), V_{in} = 1,599.94m/s

The model engine inlet area can be obtained from the flow formula:

$$A_{in} = 0.015m^2$$

The size of the inlet is: 100mm x 150mm^2.

(2) Calculation of export area expansion ratio. Design Criteria: Isobaric combustion chambers. Given the inlet parameters of the combustion chamber in the design state, the combustion chamber outlet parameters can be calculated using a one-dimensional theory.

(1) Combustion chamber inlet parameters. Under the conditions of simulated flight altitude H = 25km and simulated flight Ma = 6, the airflow parameters entering the combustion chamber after passing through the shock wave string of the isolation section are

$$Ma_{in} = 2.0,\ P_{in} = 220.93kPa,\ T_{in} = 963.3K$$

(2) Combustion chamber outlet parameters

$$V_e = V_{in}\left\{\frac{1+f\frac{V_{fx}}{V_{in}}}{1+f} - \frac{C_f\frac{A_w}{A_{in}}}{2(1+f)}\right\} \tag{3.16}$$

$$T_e = \frac{T_{in}}{1+f}\left\{1+\frac{1}{C_p \cdot T_{in}}\left[\eta_b \cdot f \cdot H_u + f \cdot h_f + f \cdot C_p \cdot T_{ref} + \left(1+f\frac{V_f^2}{V_{in}^2}\right)\frac{V_{in}^2}{2}\right]\right\} - \frac{V_e^2}{2C_p} \tag{3.17}$$

$$\frac{A_e}{A_{in}} = (1+f)\frac{T_e}{T_{in}} \times \frac{V_{in}}{V_e} \tag{3.18}$$

where: *C-A/Am* — equivalent drag coefficient of the combustion chamber;

$h = C_p (T - T_{ref})$ —Static enthalpy

According to the above formula, it is assumed that the design state equivalent ratio is ER = O.8 and the combustion efficiency is $\eta_b = 0.7$, then

$V_e = 1106.9$m/s, *Te* = 1908K, $A_e/A_{in} = 2.224$

(3) The geometric parameters of the dimensions of each section of the combustion chamber. After determining the expansion ratio of the combustion chamber of the model engine, the determination of the expansion angle of each section is mainly based on the following considerations: (1) the total length of the model engine is about 2.2m; (2) due to the long delay time of kerosene ignition, the combustion chamber is designed into three stages with a gradually increasing expansion angle in order to make it easier to organize combustion. Among them, the first section of the combustion chamber is basically designed as an equal-section combustion chamber; the second segment is an expansion segment with a smaller angle; the third segment is an expansion segment with a larger angle. Figure 3-29 is a schematic diagram of the model engine structure, and the specific dimensions of each section are:

- The length of the isolinear combustion section is 300mm, and the full angle is expanded by 1.0°.
- The length of the first expansion section is 600mm, and the expansion angle is 4.0°.
- The length of the second expansion section is 1000mm, and the full angle of expansion is 5.5°.

The design method of the 8kg/s circular cross-section direct-coupled scramjet model engine is the same, and the specific dimensions of each section are:

- The length of the isolinear combustion section is 300mm, and the full angle is expanded by 1.0°.
- The length of the first expansion section is 600mm, and the full angle of expansion is 2.0°.
- The length of the second expansion section is 1000mm, and the full angle of expansion is 3.0°.

The specific dimensions of each section of the 2kg/s direct-connected scramjet model engine are:

- The length of the isolinear combustion section is 260mm, and the full angle of expansion is 1.0°.
- The length of the first expansion section is 500mm, and the full angle of expansion is 2.0°.
- The length of the second expansion section is 487mm, and the full angle of expansion is 3.0°.

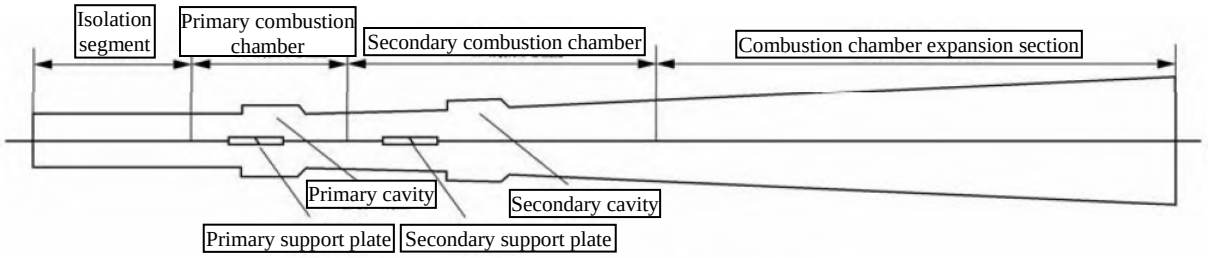

Figure 3-29: Schematic diagram of the model engine structure [169]

2) Design of cavity, spraying panel and support plate

The cavity, injection panel, and support plate are important components for flame stabilization and fuel injection in scramjet engines. In order to improve the flame stability performance of the cavity, the cavity and the fuel injection panel are generally integrated. The fuel injection position can be selected upstream of the cavity, at the bottom of the cavity, downstream of the cavity, or a combination of these different positions. The support plate acts as a component to improve fuel penetration and further compress the gas flow, while its leading edge shock also acts as an ignition.

In Reference [169], considering the long ignition delay time of kerosene, the two-stage symmetrical front and rear cavities are used in the bilateral expansion model engine, which are arranged in the first and second stages of the combustion chamber respectively as an integrated fuel injection/flame stabilization device. The single-sided expansion model engine arranges four-stage cavity windows at different positions at the top, and two-stage cavity windows at the bottom and the top are dislocated, which is convenient for studying the influence of different injection positions on combustion performance.

In order to study the fuel injection scheme, the model engine arranged a number of fuel nozzles with different apertures, which were arranged on the cavity step, the bottom surface of the cavity, and the side wall and trailing edge of the support plate.

(1) Cavity design. The structural parameters of the cavity are mainly the length-to-depth ratio and length of the cavity and the inclination angle of the back wall of the cavity. In Reference [169], the open cavity with an aspect ratio L/D = 4 to 8 was mainly selected in the research work. According to Baurle's research, the residence time of gases and fuels in the cavity is mainly determined by the depth of the cavity, and considering the long ignition delay time of kerosene, in order to increase the residence time of gases and fuels in the cavity, the depth of the cavity is relatively large.

(2) Injection panel design. There are two types of spraying panels: a fixed structure (Figure 3-31) and a combinable structure (Figure 3-31). The form of the fuel nozzle is all direct flow, and the nozzle hole is available in a variety of combinations. The large diameter of the nozzle hole upstream of the cavity is the main fuel injection location, from which most of the kerosene enters the combustion chamber; the nozzle at the bottom of the cavity consists of smaller diameter holes and serves primarily for flame stabilization. There are many combinations of injection methods and the number of nozzles: (1) main spray. The main nozzle injection method includes vertical injection, 60°, 45° angle inclined injection, etc. The diameter of the kerosene nozzle is 0.5 to 1.2 mm, and the number is 3 to 4. The diameter of the hydrogen nozzle is 1.0 to 4.0 mm, and the number of holes is 1 to 4. (2) secondary spray. The secondary nozzle hole is located at the bottom of the cavity, the aperture is 0.5 mm, and the injection mode is vertical spraying. In order to study the influence of different injection positions of fuel nozzles on the ignition characteristics and combustion performance of the model engine, multiple rows of nozzles are designed at the bottom of the cavity, with 2 to 8 in each row, and there are separate nozzles, which can be controlled separately, and any row or more of the nozzles can be selected during the test.

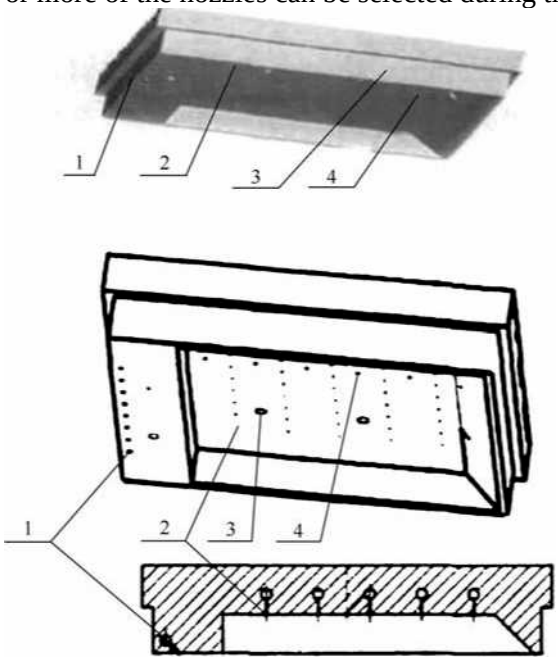

1. Main nozzle hole, 2. Secondary nozzle, 3. Temperature measuring hole, 4. Pressure measuring hole

Figure 3-30: Schematic diagram of the structure of the fixed structure spraying panel

(3) Support plate design. The scale of the scramjet model engine with 8kg/s flow rate is large, and the relative penetration depth of the fuel jet is not enough, so the relative penetration of the fuel jet must be increased with the help of support plates. The scramjet model engine with a flow rate of 2 kg/s is smaller, and the relative penetration depth of the fuel jet is larger, so it is not necessary to have a support plate to increase the relative penetration of the fuel jet. In addition, the support plate itself also has a compressive effect on the airflow, but if the local blockage caused by the support plate is too large, it may cause aerodynamic/thermal congestion of the airflow, and the shock wave resistance of the leading edge of the support plate is also relatively large.

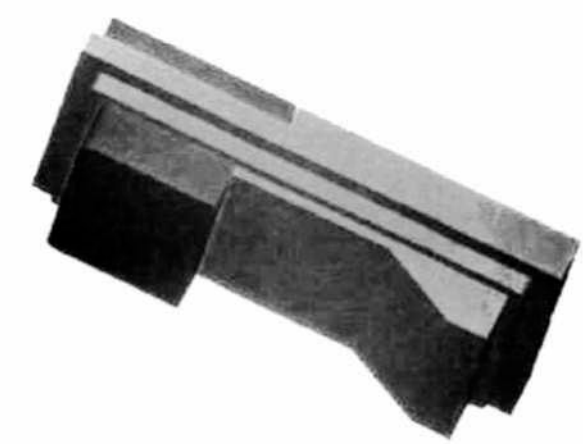

Figure 3-31: Schematic diagram of the structure of the spraying panel of the composite structure

In order to quantitatively study these issues, a variety of support plates were designed in Reference [169] to carry out related studies. The support plate is a detachable part. Figure 3-32(a) shows a support plate without a sweep angle, and Figure 3-32(b) shows a support plate with a 45° sweep angle. The structural parameters of the support plate include the sweep angle, height, width and length. According to the proportional relationship between the height of the support plate and the height of the combustion chamber, there are four types: 1/5 height, 1/3 height, half height and full height; there are three types of plate widths, 6 mm, 10 mm and 33 mm. In the first and second combustion chambers, there are two mounting positions of supporting plates. All plates are water-cooled and can be tested for long periods of time. The fuel injection position on the support plate is on both sides or at the bottom of the trailing edge, the diameter of the nozzle hole is 0.5 to 1 mm, and the number is 2 to 10 on each side.

(a) No sweep angle (b) 45° sweep angle

Figure 3-32: Schematic diagram of the structure of the support plate assembly

5. Combustion chamber performance evaluation index

The combustion chamber is an important part of a scramjet engine, located after the air intake, before the nozzle, and often includes an isolation section in experimental studies. In the combustion chamber, fuel is injected into the flow and violently burned to form gas, which expands in the nozzle to provide power to the aircraft. Therefore, the energy required for the movement of the aircraft is added by the combustion chamber, which is designed to have high combustion efficiency, low flow loss, and can provide large thrust itself. The commonly used parameters for evaluating the overall performance of the combustion chamber include thrust, internal thrust, specific impulse, combustion efficiency, and total pressure recovery coefficient at the outlet of the combustion chamber. The magnitude of thrust directly affects the acceleration performance of the aircraft, and the specific impulse has a better reference value when considering the endurance and economic ability. The combustion efficiency can reflect the completeness of the combustion process in the combustion chamber, but it cannot fully reflect the flow efficiency. The total pressure loss at the outlet of the combustion chamber reflects the amount of force with which the outlet air flow continues to function, but it may be inversely proportional to the combustion efficiency. Each performance parameter shows the performance of all aspects of the combustion chamber, and is interrelated and mutually influencing, and the overall performance of the combustion chamber cannot be measured by a single index.

In the direct test of the combustion chamber of a scramjet engine, the main parameters that can be directly and accurately measured are the bench thrust and the pressure on the upper wall of the combustion chamber. Due to the influence of the test conditions, the measured bench thrust gain does not fully reflect the thrust performance of the combustion chamber and cannot be equated with the thrust gain of the combustion chamber in the flight state. Combustion efficiency and total pressure recovery coefficient are difficult to obtain in experiments and can be obtained by theoretical and numerical means. The definitions of bench thrust gain, bench fuel specific impulse gain, combustion chamber hot internal thrust, combustion efficiency and combustion chamber total pressure recovery efficiency are introduced in detail, and the advantages and disadvantages of bench thrust gain and hot internal thrust of combustion chamber are compared when measuring the actual thrust performance of the combustion chamber.

1) Bench thrust gain

Based on the measured bench thrust F_{ped}, the bench thrust gain (referred to as thrust gain) $F_{ped,gain}$ during steady-state operation of the combustion chamber can be obtained, i.e.:

$$F_{ped,gain} = F_{ped,hot} - F_{ped,cold} \tag{3.19}$$

Where: $F_{ped,hot}$ — bench thrust measured when the combustion chamber is working at steady state (i.e., the combustion chamber is supplied with oil to stabilize the combustion state);

$F_{ped,cold}$ — the bench thrust measured only when the heater is operating at steady state (i.e., in the cold state of the combustion chamber without oil).

The measurement error of the bench thrust is small, and when the adjustment error of the heater working condition and the fuel flow rate of the combustion chamber is small, the thrust gain can measure the performance of the combustion chamber in the ground test more accurately. However, due to the limitations of the direct-connected test simulation conditions, it is difficult to accurately evaluate the thrust performance of the combustion chamber under flight conditions.

2) Bench fuel specific impulse gain

From the bench thrust gain $F_{comb,hot}$ and the fuel flow rate $\dot{m}_{fuel}$ the bench fuel specific impulse gain (referred to as fuel specific impulse gain) $I_{sp,fuel}$, can be calculated, i.e.:

$$I_{sp,fuel} = \frac{F_{comb,hot}}{\dot{m}_{fuel}} \tag{3.20}$$

3) Hot internal thrust of the combustion chamber

In the bench thrust exploded diagram of the direct-connected test shown in Figure 3-33, the measured bench thrust F_{peds} are mainly composed of the inner heater thrust F_{heater}, the combustion chamber thrust F_{comb}, and the initial bench force $F_{ped,initial}$ and the external wall aerodynamic resistance generated by the ambient pressure $F_{drag,out}$, etc., i.e.:

$$F_{ped} = F_{heater} + F_{comb} + F_{ped,initial} - F_{drag,out} \tag{3.21}$$

The test system starts to supply cooling water immediately after start-up and enters the heater working sequence after 2s. The initial force of the bench is the measured bench thrust when the heater cooling water is supplied in steady state, including the bench preload, the zero drift of the sensor measurement, and other systematic errors.

In the direct-connected test, the heater internal thrust F_{heater} for the heater steady-state operation of the gas acting on the inner wall surface of the heater, due to the heater and the combustion chamber docking surface of the static pressure matching, Equation (3.21) in the F_{heater} and $F_{drag,out}$ can be calculated as follows, respectively

In the direct-connection test, the F_{heater} internal thrust of the heater is the gas acting on the inner wall of the heater when the heater is working in a steady state.

The resultant force of the surface, since the heater and the combustion chamber are matched by the static pressure at the docking surface, the F_{heater} and $F_{drag,out}$ in Equation (3.21) can be calculated separately:

$$F_{heater} = q_m v_i \tag{3.22}$$

$$F_{drag,out} = P_a A_e \tag{3.23}$$

where: v_i — gas flow velocity at the outlet section i of the heater;

P_a — Ambient pressure;

A_e — The area of the combustion chamber outlet section e

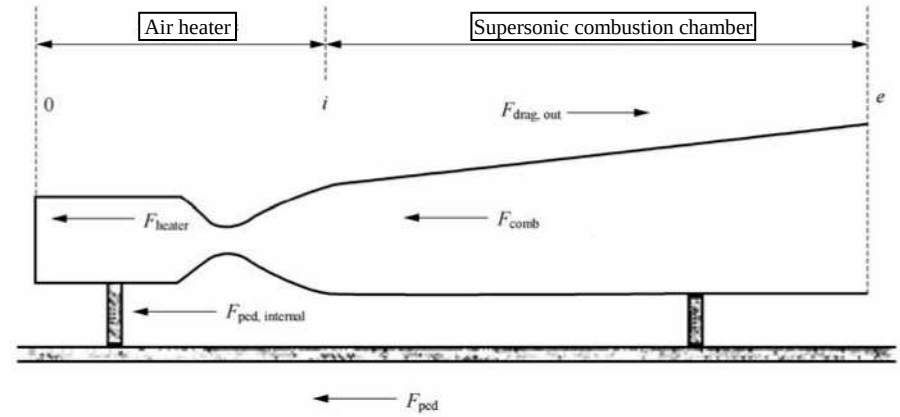

Figure 3-33: Exploded thrust of a direct-attached test bench

q_m — Working fluid flow, calculated from the flow rate of heater air, oxygen and alcohol measured by the test, i.e:

$$q_m = \dot{m}_{air} + \dot{m}_{oxygen} + \dot{m}_{alcohol} \tag{3.24}$$

Therefore, the thrust inside the combustion chamber can be calculated as:

$$F_{comb} = Restored - (q_{mvi} + F_{ped,early} - P_{aAe}) \tag{3.25}$$

The thrust inside the heater can be obtained by the thermal calculation method, and the thrust in the combustion chamber can be calculated from the above equation according to the measured bench thrust curve.

The cold and hot internal thrust of the combustion chamber can be calculated as follows:

$$F_{comb,cold} = F_{ped,cold} - (q_{mvi} + F_{ped,early} - P_{aAe}) \tag{3.26}$$

$$F_{comb,cold} = F_{ped,cold} - (q_{mvi} + F_{ped,early} - P_{aAe}) \tag{3.27}$$

The hot internal thrust of the combustion chamber can be further expressed by the bench thrust gain and the cold internal thrust of the combustion chamber, i.e:

$$\begin{aligned} F_{comb,hot} &= F_{ped,hot} - F_{ped,cold} + F_{comb,cold} \\ &= F_{ped,gain} + F_{comb,cold} \end{aligned} \tag{3.28}$$

Equation (3.28) shows that the thrust gain is actually the result of the hot internal thrust minus the cold internal thrust of the combustion chamber, while the hot internal thrust is calculated based on the unflowed water. The internal thrust in the cold state may be negative, which is manifested as the internal resistance in the cold state, and if the internal resistance in the cold state is too large, the internal thrust in the hot state may also be negative. In other words, even if a large bench thrust gain is measured, the combustion chamber may not be able to provide the actual operating force. Therefore, the hot internal thrust of the combustion chamber comprehensively reflects the internal flow and combustion efficiency of the engine, which is more suitable for evaluating the actual thrust performance of the combustion chamber under flight conditions.

However, the thermal calculation method cannot accurately obtain the actual internal thrust of the heater by the calculation of the hot internal thrust of the combustion chamber, as it includes influence of the initial force fluctuation of the bench in different tests, so the error of the hot internal thrust is large. Comparatively speaking, the error of thrust gain is smaller. Since the cold internal thrust is much smaller than the thrust gain, the large change in thrust gain basically reflects the change in the hot internal thrust. Therefore, the magnitude of the thrust gain can more accurately reflect the advantages and disadvantages of the thrust performance of the combustion chamber.

4) The recovery coefficient of the total pressure of the combustion chamber

The total pressure recovery efficiency η_{Pi} is defined as

$$\eta_{P_i} = \frac{P_{te}}{P_{ti}} \tag{3.29}$$

where: P_{ti} — The total pressure of the inlet flow of the combustion chamber;

P_{te} — The total pressure at the outlet of the combustion chamber.

The total pressure recovery efficiency reflects the ability of the combustion chamber outlet airflow to continue to do work. After the supersonic gas flow is burned in the combustion chamber, it also enters the tail nozzle to expand and do work, so the total pressure recovery efficiency is an indispensable consideration for evaluating the performance of the combustion chamber. But due to the total pressure of the combustion chamber outlet P_{te}. It is difficult to obtain in experiments, and it is ignored when studying combustion chamber performance purely by experiments and is measured only in terms of thrust and specific impulse gain. When the test is combined with simulation, the total pressure at the outlet of the combustion chamber can be obtained by simulating the combustion flow in the combustion chamber, so as to obtain the total pressure recovery efficiency.

5) Combustion efficiency

Combustion efficiency is defined as:

$$\eta_{\mathrm{f,burn}} = \frac{\dot{Q}_{\mathrm{f,burn}}}{\dot{Q}_{\mathrm{f}}} \tag{3.30}$$

Where: $\dot{Q}_{\mathrm{f,burn}}$ — the heat that needs to be released when the combustion product at the outlet of the combustion chamber is converted into the initial reactant at the same temperature and pressure

$\dot{Q}_{\mathrm{f}}$ — The energy released by the complete combustion of the fuel.

Due to the limitation of measuring equipment, it is still difficult to measure the composition of the gas at the outlet of the combustion chamber at this stage, and the combustion efficiency cannot be obtained by means of testing. The simulation method can obtain the gas flow components at the outlet of the combustion chamber, but due to the unclear mechanism of the crushing, atomization and mixing process of the fuel, the spray model and combustion model are inaccurate, and the results obtained are incorrect, which are only used as a reference.

The chemical kinetic model uses the turnkey reaction formula:

$$C_{12}H_{23} + 17.75O_2 \Leftrightarrow 12CO_2 + 11.5H_2O$$

Therefore, the combustion efficiency can be simplified to:

$$\eta_{\mathrm{f,burn}} = \frac{\dot{m}_{CO_2,\mathrm{out}}}{\dot{m}_{CO_2}} \tag{3.31}$$

Where: $\dot{m}_{CO_2,out}$ — the mass flow rate of the CO2 component at the outlet of the combustion chamber;

$\dot{m}_{CO_2}$ — the mass flow rate of CO2 resulting from the complete reaction of the fuel.

After the above analysis, it can be seen that the hot internal thrust of the combustion chamber is suitable for evaluating the actual thrust performance of the combustion chamber under flight conditions, but it is not easy to measure and the error is large. Relatively speaking, the thrust gain can be obtained directly by test means, and it can basically reflect the actual thrust performance of the combustion chamber. The specific impulse gain can also be obtained by experimental means; the combustion efficiency and total pressure recovery efficiency, which have important reference value, can be obtained by simulating the combustion flow in the combustion chamber. Therefore, it is reasonable to choose thrust gain, specific impulse gain, total pressure recovery coefficient and combustion efficiency as the overall performance evaluation indexes of the combustion chamber.

3.3.4: Tail nozzles

1. Tail nozzle profile design method

The main methods for the design of asymmetric large expansion ratio nozzle surface of hypersonic vehicles include maximum thrust theory, shortest length nozzle management theory and other design methods. Since the ideal nozzle with a uniform level of outlet airflow appears too long for the actual aircraft to cooperate with the thrust nozzle, it is based on the variational principle, Rao. The design method of the maximum thrust nozzle under a certain length and flow rate limit is proposed [171], which is also known as the Rao nozzle. The Rao nozzle outlet airflow has a certain angle with the axis. The shortest length nozzle design method [172] obtains the ideal nozzle with a uniform level of outlet airflow, but the length is still long, and it needs to be truncated when used as a thrust nozzle for aircraft. It is based on the disadvantage of the long ideal nozzle that truncated ideal contoured nozzles (TIC) [173] and compressed truncated ideal contoured nozzles (CTIC) have been proposed. The following is a brief review of the various nozzle design methods.

1) Eigenline method

The design of supersonic nozzles is mostly based on the theory of characteristic lines. An eigenline is defined as a curve along which a partial differential equation can be turned into a full differential equation. From a strictly mathematical point of view, the physical parameter is continuous across the characteristic line, but the derivative of the physical parameter can be discontinuous. In a supersonic flow field, Mach lines are the characteristic lines.

Now, applying the general theory of the feature line method, a numerical method for analyzing a constant two-dimensional, planar, and axisymmetric non-vortex supersonic flow field is given. Applying the eigenline theory, the flow governing equations can be transformed from partial differential equations to eigenline equations and compatibility equations. For specific equations, please refer to the relevant textbooks on aerodynamics. According to the basic feature line theory, the ideal isentropic two-dimensional symmetry and axisymmetric nozzle wall profiles can be obtained, and the outlet airflow level is generally mainly used for the design of wind tunnel nozzles [174].

2) Maximum thrust nozzle design method

Such a thrust nozzle is too large for a large chemical rocket engine nozzle due to the fact that the ideal nozzle with parallel and uniform outlet air flow is too long. Guderley and Hantsch were the first to propose a nozzle profile design theory that can generate maximum thrust under certain nozzle length and outlet back pressure, using the variational method [173]. Because the solution method used by Guderley and Hantsch was too complex, it was not until Rao simplified the method that it became widely used. In Russia, Shmyglevsky independently proposed this method of designing the maximum thrust nozzle, known as the Shmyglevsky nozzle. The thrust nozzle designed by this method proposed by Rao can greatly improve the performance of the conical nozzle, so it is widely used in rocket engines.

The Rao nozzle produces the maximum thrust under two constraints: one is for a given nozzle length; one is a certain nozzle mass flow. Mathematically, this is a constrained maximum value problem, and its solution can be obtained by applying the Lagrange multiplier method.

3) Short nozzle design method

The short nozzle is to compress the entire expansion section into an acute angle (sharp angle) of the larynx, so the shortest length of the nozzle is obtained, also known as the acute angle nozzle. Figure 3-34 and Figure 3-35 show the pneumatic profile of the wind tunnel nozzle for general wind tunnel nozzle and short spray management theory. The initial segment in Figure 3-34 is compressed into a sharp point of the throat in Figure 3-35 in the short nozzle design theory. There are two design theories of short nozzles [172]: one is the theory of straight sound velocity lines, that is, the laryngeal velocity lines are assumed to be straight; the other is the curvilinear velocity line theory, which assumes that the laryngeal velocity line is an arc. Four nozzle shapes can be obtained from the two theories, namely two axisymmetric nozzle shapes and two two-dimensional symmetrical nozzle shapes. The length of the two axisymmetric nozzles is shorter than that of the two two-dimensional symmetrical nozzles, and the two-dimensional symmetrical nozzles obtained by the linear sound velocity line theory are shorter than those obtained by the curved sound velocity line theory.

The element process of the short nozzle design theory is slightly different from the basic feature line theory mentioned above, and the inner point element process is illustrated as an example. For any inner point in the flow field, the airflow turning angle and airflow direction angle of the point are determined firstly, and then the Mach number of the point is calculated according to the Plante-Meyer relation, and then the flow parameters of the point are determined, and then the coordinates of the point are determined by the characteristic line equation. The basic short nozzle design method can only design two-dimensional symmetrical or axisymmetric nozzles. Goeing [174] of Germany proposed a method for designing a cluster of two-dimensional shortest length nozzles, corresponding to the same inlet and outlet conditions, and this method can obtain a series of different nozzle shapes, with the ratio of the length of the lower and upper walls of the nozzle from 0 to 1.

4) Truncate the ideal nozzle

As mentioned earlier, the ideal isentropic nozzle to obtain a uniform horizontal outlet airflow is very long, and even if the ideal shortest length nozzle obtained by applying the short spray management theory is still long, it is generally not suitable for thrust nozzles.

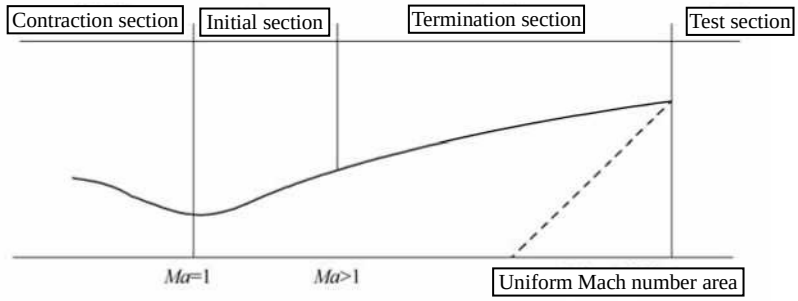

Figure 3-34: Pneumatic profile of a general wind tunnel nozzle

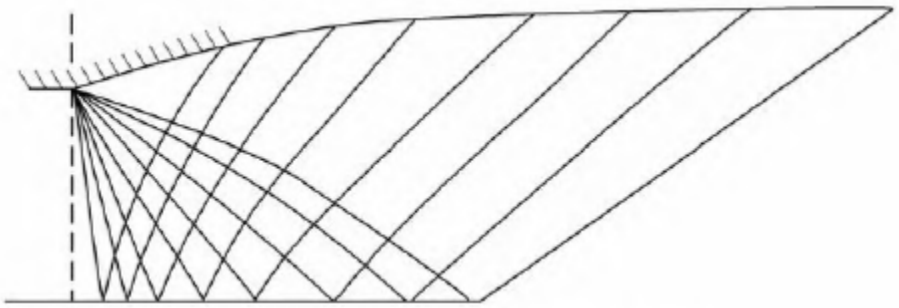

Figure 3-35: Pneumatic profile of nozzle in the management of short spray with straight sonic velocity

Because these nozzles have a long section of the wall and have a small slope and a small contribution to thrust, they are considered to be truncated. Figure 3-36 shows a schematic diagram of the truncated ideal nozzle for the short spray management theory. The K point in Figure 3-36 is the intersection point of the last feature line and the symmetry axis in the core area, and the flow parameters of this point reach the design state, which is also the end point of the lower wall of the asymmetrical ideal nozzle. In the two-dimensional case, the region behind the feature line *AK* is the simple wave region, a point *D* is found on the feature line *AK*, and according to the principle of wall extinction, a point *E* is found, and if the point *E* satisfies the required length limit, the iteration is stopped, and the truncated ideal nozzle that satisfies the given length limit is found. For the ideal nozzle obtained by using the Saul method to obtain the basic characteristic line theory of the laryngeal sound velocity line and the supersonic initial line, the same method can be used to truncate the ideal nozzle to obtain the truncated ideal nozzle that meets the length requirements.

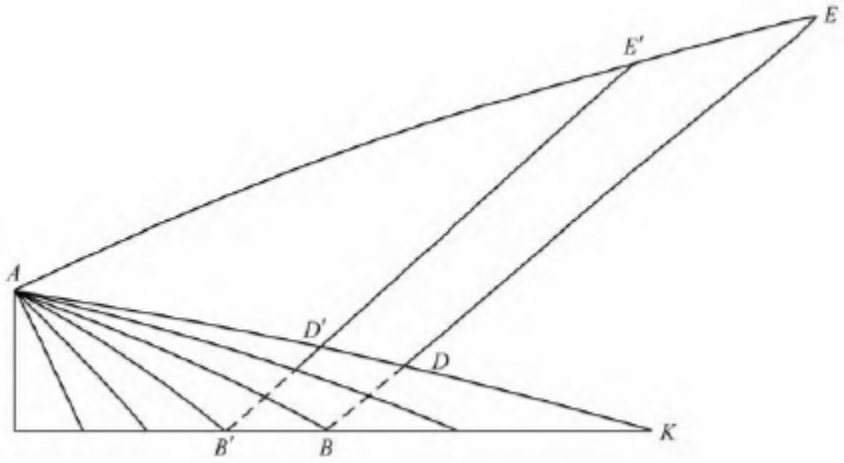

Figure 3-36: Schematic diagram of truncated ideal nozzle

5) Compression type truncated ideal nozzle

In 1966, Gogish proposed linear compression of truncated ideal nozzles to obtain shorter nozzles [173].

This design method is to obtain a nozzle profile that satisfies a given length by cutting off the ideal nozzle by axial compression, but this often brings discontinuities in the wall slope, which can generally be eliminated by a smooth connection between the initial expansion line and the compression profile by a quadratic equation. The resulting nozzle has a faster initial expansion than a truncated ideal nozzle, while the wall surface turns towards the axis at a faster rate. As a result, the right-row compression waves on the compression profile intersect to form a right-row oblique shock wave. If the shock wave is near the wall, the wall pressure increases, resulting in an increase in thrust. That is how Gogish thinks the compression-cut nozzle will produce better performance than the Rao nozzle. However, Hoffmann [174] has shown that this is not the case. Hoffman developed a design method for compression-type truncated nozzles. He found that the performance of the compression truncated nozzle was not as good as that of the Rao nozzle, but the difference was very small, so the compression truncated ideal nozzle was a good thrust nozzle.

2. Three-dimensional flow characteristics of the tail nozzle

The NASA Langley Research Center in the United States has carried out asymmetric afterbody nozzle test research on the rear body nozzle of aerospace aircraft in the NASP program [176~178]. References [179,180] compared the data presented in this experimental study to verify the adaptability of the software and the PNS algorithm for the calculation of the flow field of the two-dimensional asymmetric rear body nozzle.

In order to further study the three-dimensional effect of the afterbody nozzle flow field, a three-dimensional afterbody nozzle calculation model was constructed in Reference [181], and the numerical simulation of the coupling of the internal and external flow fields was carried out. As shown in Figure 3-37, the dimensions of the calculated object are consistent with the NASA test model, and in order to compare the flow field parameters, four observation positions are set along the expansion surface of the nozzle, corresponding to the 2.5 in[1], 4.5 in, 6.5 in, and 8.5 in Pitot measurement positions of the original test, and four lateral observation positions are set equidistant in the Z direction of the model, and the model structure considers whether there are two forms of side wall (fence).

The flow field calculation is coupled with the implicit solution of the three-dimensional N-S equation and the turbulence model adopts the RNG k-ε model. The calculated working conditions correspond to the 155th, 366th, 908th, and 382nd measurements in the literature [178], respectively, and the nozzle inlet condition: Ma = 1.78, T = 300.0K, P = 3,3350.0Pa, free flow conditions: Ma = 6.02, T = 200.0K, P = 1,541.9Pa. The internal and external gases of the rear body nozzle are ideal air, and the specific heat ratio is $\gamma = 1.4$. Figure 3-38 shows the symmetry of the flow field inside and outside the three-dimensional rear body nozzle and the typical cross-sectional pressure contour distribution. From the distribution of the pressure contours of the three cross-sections, it can be seen that the flow field inside and outside the rear body nozzle presents a significant three-dimensional effect, and the gas expands in all directions except for the solid wall. Figure 3-39 shows a comparison of the calculated results of the four observation positions with the Pitot pressure measurement test data. In the test, the pressure rake is placed on the central axis of the test model, corresponding to the position of Z = 0 mm in the 3D calculation. From Figure 3-39(a), it can be seen that in the position closer to the outlet of the inner nozzle, the two-dimensional calculation results as well as the three-dimensional calculation results at the Z position closer to the centerline are in good agreement with the Pitot measurement data, and only at the edge of the expansion surface of the model at the Z = 38.1 mm there is a certain deviation from the experimental data, which indicates that the structure of the flow field in this location is still closer to the two-dimensional, and that the inward flow is less influenced by the outward flow. With the backward movement of the X measurement position, it can be seen from Fig. 3-39(b) and (c) that the two 3D calculation curves leaning against the outer side deviate from the test data significantly more than those of the inner side and the 2D calculation curves, and when the X measurement position is moved back to the tail part of the model, the curves of the 3D calculation results are located on the two sides of the measurement data, which are significantly different from the 2D calculation results. This shows that the inflow at the tail of the model has completely deviated from the two-dimensional flow field structure due to the interference of the outflow, and the influence of the outflow on the flow field distribution here cannot be ignored.

[1] 1 in = 2.54 cm, same below.

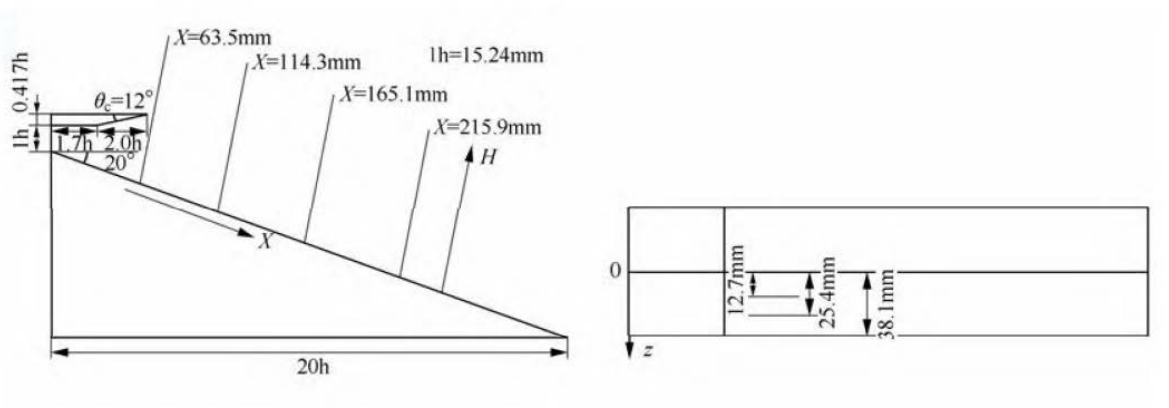

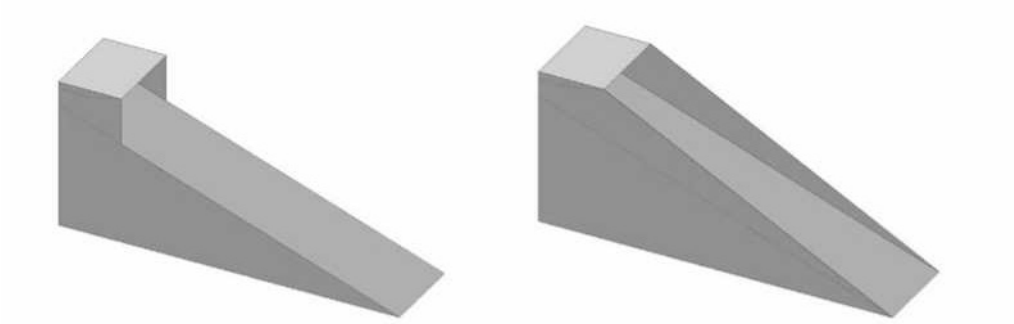

(a) No sidewalls (b) With side walls

Figure 3-37: Three-dimensional asymmetrical rear body nozzle size and configuration

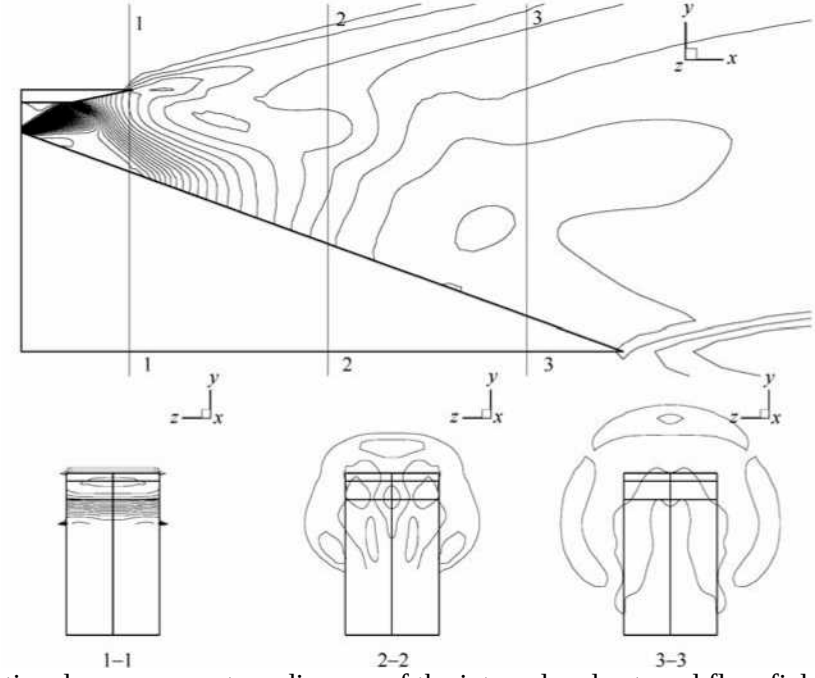

Figure 3-38: Cross-sectional pressure contour diagram of the internal and external flow field of the rear body nozzle

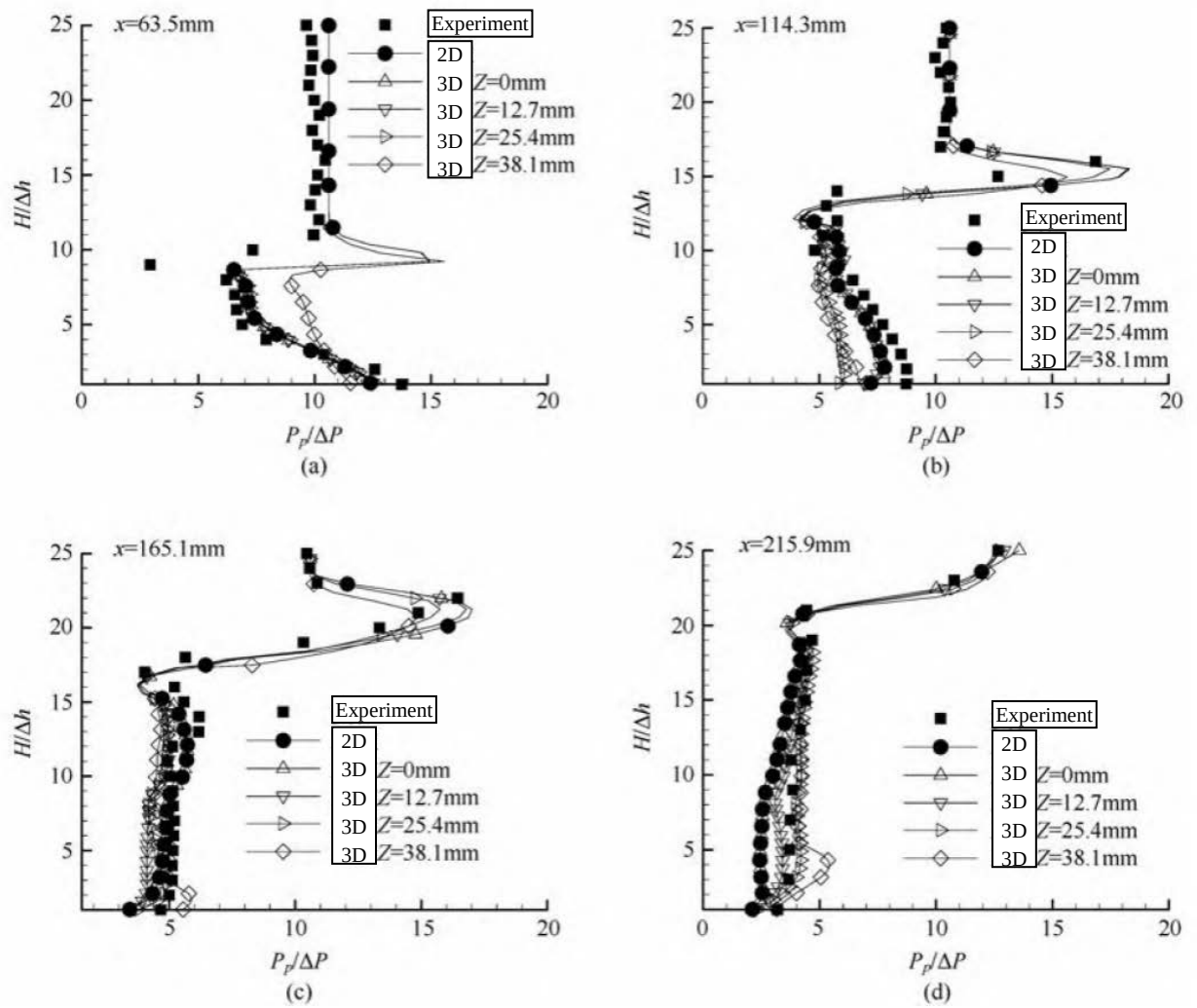

Figure 3-39: Pitot pressure comparison (Δh = 5.088mm, Δp = 6894.757Pa)

In order to further study the influence of the sidewall on the flow field and performance of the three-dimensional rear body nozzle, the flow field of the three-dimensional rear body nozzle model with side wall was calculated. Figure 3-40 shows the pressure distribution in the Z-direction of the model expansion surface at four observed locations. It can be seen that the flow field of the three-dimensional rear body nozzle without side wall is significantly affected by the outflow, while the flow field in the three-dimensional rear body nozzle with side wall still maintains good Z-direction uniformity.

The pressure contour distribution of the expansion surface of the three-dimensional rear nozzle (Fig. 3-41) shows that the gas without sidewall is disturbed by the outflow from the outlet of the inner nozzle, while the three-dimensional configuration with sidewall can still maintain the two-dimensional characteristics of the flow field in a large range. Based on the three-dimensional calculation model of the rear body nozzle without side wall, Table 3-1 shows the performance comparison of dimensionless rear body nozzles. If the three-dimensional nozzle configuration without sidewall is calculated by the two-dimensional calculation model, the thrust is 3.2% larger and the lift force is 22.6% larger, and the three-dimensional rear nozzle configuration with sidewall is 5.4% higher and the lift is increased by 34.8% than that without sidewall. It can be seen that the presence of sidewalls can significantly increase the performance of the three-dimensional rear body nozzle.

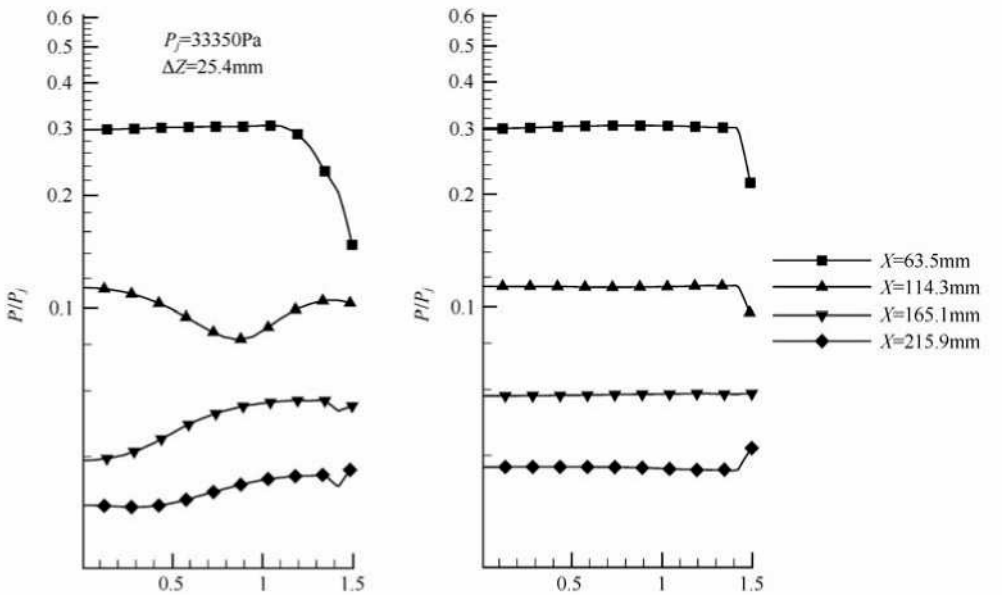

Figure 3-40: Comparison of Z-direction pressures at each position

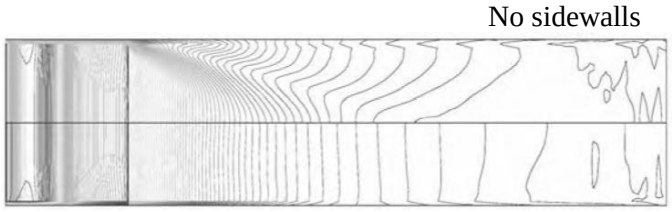

Figure 3-41: Comparison of sidewall isobars on the expansion surface of the rear body nozzle

Table 3-1: Comparison of 2D and 3D computing performance with and without sidewalls

Computational model	Dimensionless comparison		
	Thrust	Lift	Total force
Two-dimensional	1.032	1.226	1.064
Three-dimensional without sidewalls	1	1	1
Three-dimensional with sidewalls	1.054	1.348	1.104

3.4: Evaluation index of the total performance of scramjet engine

Based on the analysis of the working process and mechanism of the combustion chamber of the scramjet engine and the need to evaluate the performance of the model engine in ground tests, this section introduces the performance parameters used in the development of the scramjet engine to reveal the essential characteristics of each parameter and facilitate the selection of indicators suitable for evaluating the performance of the engine [182].

3.4.1: Combustion efficiency

The percentage of the actual combustion consumption of the same substance to the theoretical combustion consumption is the combustion efficiency. Like rocket engines, scramjet engines work to convert the chemical energy of fuel into thrust work of working fluid gases. Therefore, we are mainly concerned with that part of the chemical energy which is eventually converted into thrust work due to combustion. As far as the research purpose of the ground direct connection test is concerned, the compression performance and resistance characteristics of the forebody and air intake tract are not investigated, and the experimental research focuses on the working process and performance of the combustion chamber, and the combustion efficiency is generally determined by measuring the air flow components at the outlet of the engine.

3.4.2: Internal thrust

For the integrated body/engine configuration shown in Figure 3-42, the dotted line is the inner engine runner surface. Internal thrust refers to the net force of the inner wall surface of the engine in the direction of flight speed, which is equal to the pressure thrust generated by the pressure integration of the surface pressure of the inner runner of the engine minus the friction force on the surface of the inner runner.

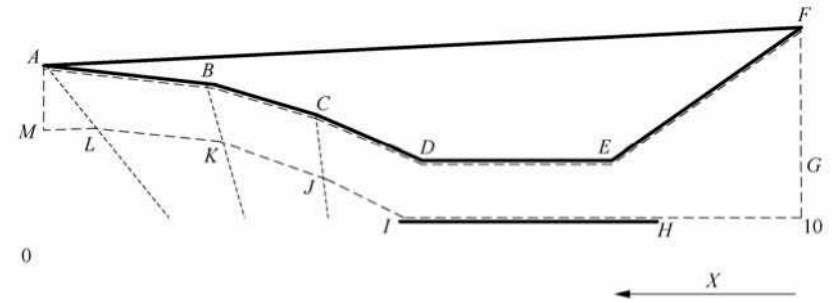

Figure 3-42: Runner surface in the engine

Take the control body as the area shown by the dashed line, that is, *A—B—C—D—E—F—G—H—I—J—K—L—M—A*, where *I—J—K—L—M* and *G—H* surfaces are not solid wall surfaces, which are called engine inlet flow pipes and tail nozzle flow pipes. Note that the dotted line in Figure 3-42 is close to the wall and does not coincide with the wall. The inlet of the control body is M-A, and the outlet is F-G. From the momentum theorem, it can be seen that the resultant force acting on the control body is equal to the rate of change of momentum as the air flow through the control body. Taking the direction of flight speed as positive, we get

$$\begin{aligned}\sum F =& -\int_{M-A} P\,\mathrm{d}A + \int_{A-B} P\,\mathrm{d}A + \int_{A-B} \tau_W\,\mathrm{d}A_W + \int_{B-C} P\,\mathrm{d}A + \int_{B-C} \tau_W\,\mathrm{d}A_W + \int_{C-D} P\,\mathrm{d}A \\ &+ \int_{C-D} \tau_W\,\mathrm{d}A_W + \int_{D-E} P\,\mathrm{d}A + \int_{D-E} \tau_W\,\mathrm{d}A_W - \int_{E-F} P\,\mathrm{d}A + \int_{E-F} \tau_W\,\mathrm{d}A_W + \int_{F-G} P\,\mathrm{d}A \\ &- \int_{G-H} P\,\mathrm{d}A + \int_{H-I} P\,\mathrm{d}A + \int_{H-I} \tau_W\,\mathrm{d}A - \int_{I-J} P\,\mathrm{d}A - \int_{J-K} P\,\mathrm{d}A - \int_{K-L} P\,\mathrm{d}A - \int_{L-M} P\,\mathrm{d}A\end{aligned} \tag{3.32}$$

The difference between the inlet and outlet momentum of the control body is $-\dot{m}_{10}V_{10}$ *-(-* $\dot{m}1V1$*)*, so there is

$$\Sigma F = -\dot{m}_{10}V_{10} + \dot{m}_0V_0 \tag{3.33}$$

The force acting on the inner wall surface is positive and magnitude is

$$F_{\text{int}} = -\int_{A-B} P\,\mathrm{d}A - \int_{A-B} \tau_W\,\mathrm{d}A_W - \int_{B-C} P\,\mathrm{d}A - \int_{B-C} \tau_W\,\mathrm{d}A_W - \int_{C-D} P\,\mathrm{d}A - \int_{C-D} \tau_W\,\mathrm{d}A_W$$
$$- \int_{D-E} P\,\mathrm{d}A - \int_{D-E} \tau_W\,\mathrm{d}A_W + \int_{E-F} P\,\mathrm{d}A - \int_{E-F} \tau_W\,\mathrm{d}A_W - \int_{H-I} P\,\mathrm{d}A - \int_{H-I} \tau_W\,\mathrm{d}A_W$$
$$= + \int_{\text{Inner wall surface}} P\mathrm{d}A - \int_{\text{Inner wall surface}} \tau_W\,\mathrm{d}A_W \tag{3.34}$$

And can get

$$-m_{10}V_{10} + m_0V_0 = -F_{\text{int}} - \int_{M-A} P\,\mathrm{d}A + \int_{F-G} P\,\mathrm{d}A - \int_{G-H} P\,\mathrm{d}A$$
$$- \int_{I-J} P\,\mathrm{d}A - \int_{J-K} P\,\mathrm{d}A - \int_{K-L} P\,\mathrm{d}A - \int_{L-M} P\,\mathrm{d}A \tag{3.35}$$

From the known

$$\int_{M-A} P\,\mathrm{d}A = P_0A_0 \tag{3.36}$$
$$\int_{F-G} P\,\mathrm{d}A = -P_{10}A_{10} \tag{3.37}$$

Then

$$F_{\text{int}} = \dot{m}_{10}V_{10} + P_{10}A_{10} - \dot{m}_0V_0 - P_0A_0 - \int_{G-H} P\,\mathrm{d}A$$
$$- \int_{I-J} P\,\mathrm{d}A - \int_{J-K} P\,\mathrm{d}A - \int_{K-L} P\,\mathrm{d}A - \int_{L-M} P\,\mathrm{d}A \tag{3.38}$$

and the impulse function

$$\phi = \dot{m}V + PA \tag{3.39}$$

Therefore

$$F_{\text{int}} = \phi_{10} - \phi_0 - \int_{G-H} P\,\mathrm{d}A - \int_{I-J-K-L-M} P\,\mathrm{d}A$$

= Control body inlet impulse difference – Tail nozzle flow pipe absolute resistance – Inlet flow pipe absolute resistance (3.40)

From the above equation, it can be seen that the projection of Fint in the x-axis direction is the internal thrust, which is expressed as the difference between the pressure of the inner wall of the engine and the friction resistance of the inner wall surface along the thrust direction, and can also be expressed as the difference between the impulse difference between the inlet and outlet of the control body and the absolute resistance of the flow pipe (inlet and tail nozzle).

3.4.3: Net thrust

Net thrust refers to the total thrust generated by the engine minus the total drag, which is a comprehensive indicator of the comprehensive performance of the engine intake, combustion chamber and tail nozzle of a hypersonic vehicle. For the integrated configuration of scramjet engine, the flight direction is also positive, and the resistance acting on the outside of the aircraft is negative, and the magnitude is:

$$F_{\text{ext}} = \int_{\text{Outside of (A-F)}} P\mathrm{d}A + \int_{\text{Outside of (A-F)}} \tau_W\,\mathrm{d}A + \int_{\text{Outside of (H-D)}} P\mathrm{d}A + \int_{\text{Outside of (H-D)}} \tau_W\,\mathrm{d}A \tag{3.41}$$

So, the net thrust of the engine is expressed as:

$$
\begin{aligned}
F_{\text{net}} &= F_{\text{int}} - F_{ext} \\
&= F_{\text{int}} - \Big(\underbrace{\int PdA}_{\text{Outside of (A-F)}} + \underbrace{\int PdA}_{\text{Outside of (A-F)}} \Big) - \Big(\underbrace{\int \tau_W dA}_{\text{Outside of (H-D)}} + \underbrace{\int \tau_W dA}_{\text{Outside of (H-D)}} \Big) \\
&= F_{\text{int}} - \underbrace{\int PdA}_{\text{Outside of (A-F+ H-D)}} - \underbrace{\int \tau_W dA}_{\text{Outside of (A-F+ H-}}
\end{aligned}
$$

= engine internal thrust - outer wall surface piezoresistive - outer wall surface friction

$$
= \phi_{10} - \phi_0 - \underbrace{\int P dA}_{\text{G-H}} - \underbrace{\int P dA}_{\text{I-J-K-L-M}} - \underbrace{\int P dA}_{\text{Outside of (A-F+ H-D)}} - \underbrace{\int \tau_W dA}_{\text{Outside of (A-F+ H-}}
$$

(3.42)

As can be seen from Equation (3.42), the net thrust is the integral of the thrust inside the engine minus the absolute pressure on the outer wall of the aircraft and the absolute friction on the outer wall. It is customary to express the static pressure as the reference pressure in the form of the outside atmospheric pressure P_0.

$$
\begin{aligned}
F_{net} &= \phi_{10} - \phi_0 - \int_{G-H} (P - P_0)\,dA - \int_{I-J-K-L-M} (P - P_0)\,dA - \underbrace{\int (P - P_0)\,dA}_{\text{Outside of (A-F+ H-D)}} \\
&\quad - \underbrace{\int P_0\,dA}_{\text{Outside of (G—H+ I—J—K—L—M+(A—F+ H—I)}} - \underbrace{\int \tau_W dA}_{\text{Outside of (A—F+ H—I)}} \\
&= \dot{m}_{10} V_{10} - \dot{m}_0 V_0 + \int_{F-G} P\,dA - \int_{M-A} P\,dA - \int_{G-H} (P - P_0)\,dA - \int_{I-J-K-L-M} (P - P_0)\,dA \\
&\quad - \underbrace{\int (P - P_0)\,dA}_{\text{Outside of (A-F+ H-D)}} - \underbrace{\int P_0\,dA}_{\text{Outside of (G—H+ I—J—K—L—M+(A—F+ H—}} - \underbrace{\int \tau_W dA}_{\text{Outside of (A-F+ H-D)}} \\
&= \dot{m}_{10} V_{10} - \dot{m}_0 V_0 + \int_{F-G} (P - P_0)\,dA - \int_{M-A} (P - P_0)\,dA - \int_{G-H} (P - P_0)\,dA \\
&\quad - \int_{I-J-K-L-M} (P - P_0)\,dA - \underbrace{\int (P - P_0)\,dA}_{\text{Outside of (A-F+ H-D)}} \\
&\quad - \underbrace{\int P_0\,dA}_{\text{Outside of (G—H+ I—J—K—L—M+(A—F+ H—}} - \underbrace{\int \tau_W dA}_{\text{Outside of (A-F+ H-D)}}
\end{aligned}
$$

Since A—*F*, *F*—*G*, *G*—*H*, *H*—*I*, the interfaces between I—*J*—*K*—*L*—M and N—A form a closed interface, and the integral of the external atmospheric pressure on these surfaces is zero, i.e.:

$$
\underbrace{\int P_0\,dA}_{\text{Outside of (G—H+ I—J—K—L—M+(A—F+ H—}} = 0 \qquad (3.44)
$$

At the same time, since L—*N is a free boundary, so*

$$
\int_{L-M} (P - P_0)\,dA = 0 \qquad (3.45)
$$

So the net thrust is expressed as

$$
\begin{aligned}
F_{\text{net}} &= \Big(\dot{m}_{10} V_{10} - \dot{m}_0 V_0 + \int_{F-G} (P - P_0)\,dA - \int_{M-A} (P - P_0)\,dA \Big) - \int_{G-H} (P - P_0)\,dA \\
&\quad - \int_{I-J-K-L} (P - P_0)\,dA - \underbrace{\int (P - P_0)\,dA}_{\text{Outside of (A-F+ H-D)}} - \underbrace{\int \tau_W dA}_{\text{Outside of (A-F+ H-D)}}
\end{aligned}
$$

$= F_{int}$ – Relative piezoresistance of the tail nozzle – Relative piezoresistance of the inlet tract – Relative piezoresistance of the outer wall surface – Friction of the outer wall surface

(3.46)

It should be noted that the relative values here are for the ambient atmospheric pressure P_0.

3.4.4: Thrust Gain

The difference in thrust of the model engine when the model engine injects fuel and cold flow is called the model engine thrust gain. When the simulated working conditions are the same, the external force of the engine cold test and the hot test is the same, so the engine thrust gain is mainly the engine cold, and the engine internal thrust difference during the hot test is:

$$F_{add} = F_{int\text{-}hot} - F_{int\text{-}cold} \tag{3.47}$$

3.4.5: Selection of Performance Indicators

For the ground test of a single-module scramjet engine, the internal flow and combustion process of the scramjet engine are mainly studied. Two types of indicators are widely used as the performance evaluation standard of scramjet engine: they are related to thrust gain and combustion efficiency respectively. Thrust gain can reflect the performance of engine combustion to produce thrust, but cannot comprehensively reflect the ability of the engine to provide thrust to the aircraft, it is possible that the engine thrust gain and cold state internal resistance are relatively large, but the internal thrust provided to the aircraft is relatively small; the combustion efficiency is not easy to calculate, it can only reflect the complete degree of the combustion process inside the engine, cannot reflect the flow efficiency, so high combustion efficiency does not mean that the engine is provided with large thrust. Therefore, it is necessary to find new operable engine performance indicators in order to comprehensively evaluate the engine flow combustion process.

The following principles should be followed to accurately evaluate the performance of a scramjet engine:

(1) The scramjet engine is very different from the traditional aero engine and ramjet engine, mainly because its internal flow and combustion process are closely coupled, and both have a great impact on the performance of the engine. Therefore, it is necessary to comprehensively evaluate the overall performance of the engine, based on the performance indicators that can comprehensively reflect the efficiency of the combustion and flow process, and not only focus on individual performance.

(2) The function of the engine is to provide thrust for acceleration and cruising for the aircraft, so the thrust performance should be taken as the main aspect of the overall performance evaluation of the engine.

(3) As far as possible, the quantity that can be directly measured is used for comparison, and if there is a part that must rely on calculation, the model and flow process should be relatively simple to calculate, so as to reduce the difficulty of calculation and increase the credibility of the calculation results.

The internal thrust is suitable for comprehensively evaluating the efficiency of the internal combustion and flow process of the engine, while for the flight test of the airframe/engine integration, the net thrust is suitable to measure the overall performance of the engine. The external configuration of the aircraft is not the focus of current research, so in order to independently evaluate the thrust performance of the engine during the current test process, it is appropriate to use the internal thrust as the evaluation index.

Internal thrust is an absolute quantity, and the flow and combustion efficiency of the scramjet engine are evaluated taking into account the size and flow rate of the scramjet engine. The internal thrust per unit air flow, the internal thrust per unit windward area, and the specific impulse of the internal thrust are given:

$$F_{\text{int}-m} = \frac{F_{\text{int}}}{\dot{m}} \tag{3.48}$$

$$F_{\text{int}-S} = \frac{F_{\text{int}}}{S} \tag{3.49}$$

$$I_S = \frac{F_{\text{int}}}{\dot{m}g} \tag{3.50}$$

3.5: Fuel technology for scramjet engines

Hypersonic vehicles have become a hot spot in the development of the aerospace field today and in the future, and the traditional heat insulation and heat protection methods can no longer meet the requirements, and the process of using the fuel to flow through the surface of the heating parts to take away the heat before entering the combustion chamber is the best solution, that is, the fuel itself is the most economical and efficient combustible coolant.

From the perspective of cooling capacity and calorific value per unit mass, liquid hydrogen is undoubtedly the most ideal coolant and propellant. Since the specific heat capacity of constant pressure and the latent heat of vaporization of liquid hydrogen are greater than those of hydrocarbon fuels, the total endothermic capacity of liquid hydrogen is much greater than that of hydrocarbon fuels. When liquid hydrogen is heated from liquid heat (20 K) to 1,000 K, its heat sink can reach 14.082 J/kg. In addition to its high cooling capacity, liquid hydrogen also has a high calorific value. With a calorific value of 123.187 J/kg per unit mass, liquid hydrogen is considered to be the preferred cryogenic fuel that meets both cooling and combustion requirements on the $Ma > 8$ aircraft. However, there are also some unavoidable problems with the use of liquid hydrogen fuel.

(1) Liquid hydrogen is a cryogenic liquid, its liquefaction temperature is very low (20K), and energy is required to liquefy hydrogen and keep it in a liquefied state. Theoretically, the energy required to liquefy H2 is about 11.8 J/kg, but in fact the energy required is much higher than the above theoretical value, so the preparation cost of liquid hydrogen fuel is high.

(2) The calorific value of combustion per unit mass of liquid hydrogen fuel is large, but due to its small density (p = 0.071g/cm^3), the calorific value of combustion per unit volume is very low, about 8,746 kJ/m^3. Therefore, the use of liquid hydrogen fuel requires a large amount of storage equipment, which increases the weight of the aircraft, reduces the payload of the aircraft, and increases the flight resistance when flying in the atmosphere. Because both ground equipment and the supply and storage system on the aircraft need to have a cryogenic device, it is inconvenient to carry, fill and operate.

(3) Liquid hydrogen is extremely volatile, flammable, and explosive. When the hydrogen in the air accounts for 18.3% to 59% (volume fraction), a slight friction, impact, static electricity, or spark will explode: it will cause combustion at 4% to 75%. As a result, there are logistical and security problems, both on the roadbed and on the aircraft, which also create great difficulties for military tactics.

(4) Liquid hydrogen is a low-temperature fuel, and the storage and transportation of cryogenic liquids have strict requirements for containers and pipeline materials, and preventing hydrogen embrittlement and leakage is another key problem that must be solved in the storage and use of liquid hydrogen.

Compared with liquid hydrogen, hydrocarbon fuels have obvious advantages of low cost, convenient storage and transportation, and high safety factor, but the cooling capacity of traditional jet fuel can only be limited to physical heat sink, its thermal stability and oxidation resistance are limited, and it is easy to undergo electrostatic reaction, so it can only be used at medium temperatures, and the heat sink cannot meet the cooling requirements of future hypersonic vehicles. In addition, if the traditional jet fuel is used at high temperatures, strong coking will occur, which will clog the fuel system of the engine, and cause the injector system to scale or corrode the material of the system, affecting the normal operation of the engine. As a result, conventional jet fuel is not suitable for cooling the high-temperature engines of high-Mach number aircraft.

Based on the above factors, the concept of high-density endothermic hydrocarbon fuel is proposed. In addition to its own physical heat sink, it can also use its chemical reaction under gas phase conditions to absorb heat (chemical heat sink), that is, it is cracked into small molecule products before entering the combustion chamber, and the cracking process absorbs heat, so that the cooling capacity is greatly enhanced, so as to meet the cooling requirements of hypersonic vehicles. What is even more superior is that when the volume of the engine fuel tank is limited, it can effectively increase the energy of the fuel carried by the missile and reduce the fuel consumption of the engine, so as to meet the requirements of the missile's high speed and long range; or reduce the volume of the engine fuel tank to make the missile miniaturized under the condition that the missile's speed and range remain unchanged, so as to improve the missile's mobility and penetration capability.

The research on endothermic hydrocarbon fuels mainly focuses on the endothermic mechanisms of catalytic dehydrogenation and high-temperature thermal cracking/catalytic cracking, and the research focuses on the selection and preparation of fuels, the screening and evaluation of catalysts, the determination of heat sediment, and the inhibition of coking.

In the 1970s and 1980s, the research of endothermic hydrocarbon fuels emerged worldwide, mainly focusing on the catalytic dehydrogenation of naphthenes. The advantages of catalytic dehydrogenation are that it has a high conversion rate at a lower temperature, a large heat absorption of the reaction, a single and stable product, and can produce a large amount of hydrogen, which is beneficial to combustion and catalysts; the disadvantages are that the Pt in the selected catalyst Pt-Al2O3 system is expensive, and the combustion performance of toluene is not good, and it is easy to coke in the combustion chamber. The dehydrogenation of methylcyclohexane (MCH) and decahydronaphthalene was a hot topic of research at that time and was often used as a model compound for dehydrogenation reactions. Methylcyclohexane can be counted as the first generation of endothermic hydrocarbon fuel in the United States, which can provide a heat sink of 2.72 MJ/kg, which can meet the flight of Ma = 4 to 6. However, after the 1980s, due to the shift of research focus, almost no breakthroughs occurred in catalytic dehydrogenation research. If you want to make achievements in this field, you must find cheap and high-performance catalysts and coking inhibitors.

In the 1990s, the research of endothermic hydrocarbon fuels shifted to thermal cracking and catalytic cracking. Compared with pyrolysis, catalytic cracking requires low reaction temperature, fast endothermic reaction rate, high selectivity, fast combustion rate and not easy coking, which is more favored by research institutions in various countries. So far, the cracking reaction is still the focus of research in the field of endothermic fuels developed by the US military, which includes petroleum distillation products containing hundreds of hydrocarbon molecules, such as JP-7 and JP-8 (a single fuel common to the Air Force and Army), and mixtures of pure substances or a few pure substances, such as JP10. The U.S. has conducted ground tests of catalytic cracking of liquid hydrocarbon fuels such as JP-7, JP-8+ 100, and JP-10. The results show that at 700°C, there is no obvious difference in the physical heat sink of JP-7 and JP-8+ 100, both are 2.06MJ/kg. The chemical heat sink of JP-7 is the highest (1.07 MJ/kg), and JP-8 + 100 followed by (0.82MJ/kg), JP-10 has the lowest heat sink value (0.54MJ/kg), the total heat sink provided by the three can meet the supersonic flight of Ma 4~6; although the main products of the cracking of the three are the same , but the product distribution is significantly different.

As a coolant, the first thing to consider is the thermal stability of endothermic fuel, that is, the degree to which solid deposits are formed on the surface of the fuel system and in the fuel body under the condition of being heated, and whether it can meet the requirements of normal flight. Measures to mitigate deposition include additives, fuel deoxygenation and surface treatment, with additives and fuel deoxidation being the most effective. The United States has two major concepts for improving the thermal stability of fuels at high temperatures: adding thermal stability additives (such as JP-8+ 100) and developing new fuels with high thermal stability (such as JP-900), both of which have achieved good results.

In order to improve fuel performance, additives are being researched in various countries, and a variety of fuel additives such as antioxidants, metal deactivators, corrosion inhibitors, antifreeze and other fuel additives have been developed. Prior to the advent of JP-8+ 100, JP-TS was the only in-service fuel that used a heat-stabilized additive (JFA-5, a special additive manufactured by DuPont), which is a highly refined kerosene product specifically for U-2 aircraft. JP8+ 100 was developed in 1995, and the newly developed military additives were added to JP-8, which improved the thermal stability by 38°C and the heat sink by 50% compared with JP-8.

JP900 developed in the 20th century is a new type of coal-based jet fuel, which can maintain long-term stability at a temperature of 900°F (482°C) and will not produce deposits to block valves, nozzles or carbon deposits on other parts, so it is called JP900. The high stability of JP900 benefits from its raw material: JP900 is a by-product of coal and petroleum, coal contains a large number of aromatic hydrocarbons, naphthenes and other cyclic hydrocarbons, which are converted into naphthenes after hydrogenation, naphthenes not only have high thermal stability, but also act as a stabilizer in the fuel, greatly inhibiting the decomposition of the fuel. Experiments show that JP900 not only has a high relative density (0.97) and volumetric energy value (41.14MJ/L), but also has good high temperature stability and high heat absorption capacity, which plays a positive role in promoting the development of advanced turbine engines for the fifth generation fighter. It has been reported that the United States is also developing heat sink JP fuel with an endothermic capacity of 10 to 15 times that of JP900, and in 2015 the United States will use synthetic heat-absorbing fuel [183~186].

3.6: Scramjet Ground Test Technology

In the development of scramjet engines, testing plays an extremely important role. Testing scramjet engines requires complex, complete sets of equipment, as no single machine can undertake a complete set of test plans. For example, a research device can perform tests at high Mach numbers, but only for small specimens, and for full-scale devices, it is limited by Mach numbers. Therefore, the overall scheme designer is required to carefully weigh and compromise the ability of ground testing and build test facilities of different types and scales in a planned manner. The size of a country's scramjet engine test scale, the strength of its capabilities, and the advanced means often determine the research level of the country's hypersonic vehicle technology.

Scramjet engine tests are divided into two categories: ground tests and flight tests. In the ground test, the main problems are solved in the working of engine components, the overall working characteristics of the engine, and the matching of the engine and the aircraft. Taking the United States as an example, in the research of scramjet engines, we have carried out experimental studies of PTE (Performance Test Engine) engines, GDE (Ground Demonstrator Engine) engines and SED (Single Engine Demonstrator) engines, and verified the key engine technologies in stages, and the engines studied are getting closer and closer to the actual single-module engines. After the ground tests are completed, the flight test verification of the engine can be carried out.

3.6.1: Ground test systems

The development of advanced ramjet engines is inseparable from ground test facilities. According to the different purposes of the test, the ground test facilities are mainly divided into two categories: direct-connected and free-jet.

The direct-coupled test system (Figure 3-43) is characterized by the fact that all the test gas supplied by the equipment enters the engine (test piece). This type of equipment is a relatively economical test equipment, but it is not possible to study the operating characteristics of the entire ramjet engine. The direct-connected test system is mainly used to solve the combustion problem of the engine combustion chamber.

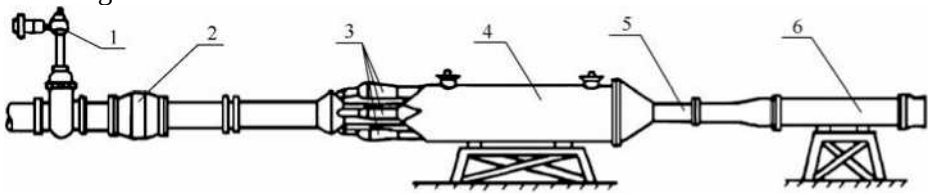

1. Electric valve**;** 2. Pressure regulator**;** 3. Heater, 4. Stabilization section, 5. Intake measurement section, 6. Test engine

Figure 3-43: Direct Coupled Test Bench

A free-jet testing system resembles a small wind tunnel system. During the test, the test piece (which can be the inlet of the engine, the engine or the combination of the engine and the aircraft) is placed into the supersonic jet flow field formed by the nozzle of the equipment, and the wave structure, inflow and even the outflow of the engine generated by the inlet can be partially simulated.

Free jet testing systems are generally more complex and larger than direct-coupled testing systems, because of the large vacuum chamber to mount the test specimens, and the test gas flow rate is also larger. Generally speaking, the free jet test needs to provide more than twice the gas flow rate of a direct-coupled test system of the same size, because nearly half of the gas overflows from the inlet tract of the engine, and the actual gas flow into the engine is only about 50%, or even less.

In addition, because the free jet test needs to simulate the real high-altitude working environment, a vacuum system is also required to dynamically discharge the gas discharged during the engine test to maintain the low air pressure during the test. The ejector is the most commonly used vacuum device.

Scramjet testing requires the simulation of high-altitude, high-speed flight conditions, and the test facility needs to provide a high-temperature, high-pressure (also known as high-enthalpy) test airflow. According to the distribution of atmospheric parameters, Figures 3-44 and 3-45 show the Mach number of different flights, the total temperature at flight altitude, the total pressure, the air flow per unit inlet area, the dynamic pressure, and the Reynolds number per unit length, respectively. It can be seen that with the increase of the flight Mach number, the total temperature and total pressure of the flow need to be simulated to continuously increase, and the dynamic pressure accounts for the vast majority of the total pressure. Dynamic pressure is an important parameter of aircraft design, lift, drag, thrust are proportional to the dynamic pressure, in order to reduce the design difficulty, the aircraft powered by scramjet engine generally chooses a flight trajectory close to the same dynamic pressure. As can also be seen from Figures 3-44 and 3-45, the air flow per unit intake area and the Reynolds number per unit length decrease rapidly as the flight height increases. The air flow rate that the test bench can provide is an indicator of its test capacity, and it is extremely difficult to provide a large flow rate of high-temperature test air. Therefore, it is very difficult to simulate the full-scale flight of large Mach numbers at low altitudes, and it is necessary to reduce the area of the air intake cross-section and adopt a scaled test model. This leads to a decrease in the simulated Reynolds number, which must be compensated for by effective means.

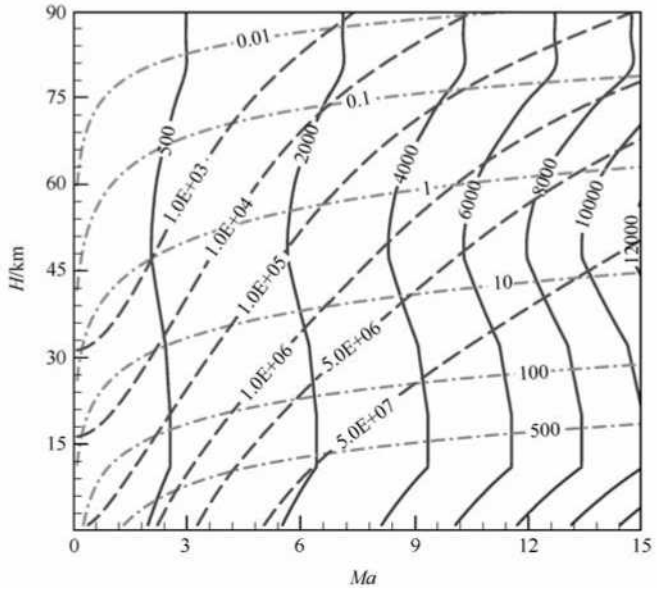

Figure 3-44: Total temperature (K) (———), total pressure (Pa) (– – –), flow per unit area [kg/(s • m2)] (-•-) under different flight conditions

Table 3-2 shows the total incoming temperature *(p*)* and total pressure *(T*)* required for the simulation test. For example, at 15 km with *Ma* = 4 (typical subsonic combustion mode) and 30 km with *Ma* = 6 (typical supersonic combustion mode), the test system must provide a high enthalpy gas flow with a total pressure of about 1.9 MPa and a total temperature of 910 to 1857 K. It is not difficult to provide a "high pressure" of 1.9 MPa for a general testing system, but for a high temperature of 1857 K, it is necessary to have special equipment, usually called a heater.

NASA has built a large number of test facilities in the course of many years of ramjet engine research, and the five facilities located in the Langley Center are the most well-known. Table 3-3 summarizes the main parameters.

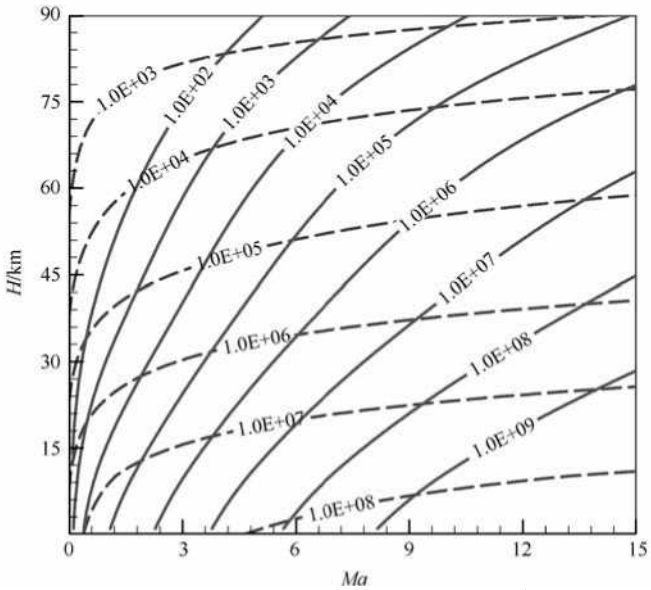

Figure 3-45: Dynamic pressure (Pa) (——), Reynolds number per unit (m^{-1}) (- - -) under different flight conditions

Table 3-2: Total incoming pressure and temperature [ρ^* (MPa) / T^* (K)] at different Mach numbers and altitudes

Flight altitude / km \ Flight Mach number	3	4	5	6
15	0. 445/606.8	1.839/910.1	6.408/1300.2	18.12/1776.9
20	0-203/606.8	0.840/910.1	2.925/1300.2	8.730/1776.9
25	0.094/620.2	0.387/930.3	1.349/1328.0	4.025/1816.3
30	0.044/634.2	0.182/951.3	0.633/1358.0	1.890/1857.3

Table 3-3: Ramjet engine test equipment at NASA Langley Center, USA

Equipment	Use	Heating method & temperature/K	Flight simulation Mach number	Nozzle outlet Mach number	Nozzle outlet size/in	Test section size /ft
Direct-attached test benches (DCSCTF)	Combustion chamber test	Hydrogen is burned to supplement oxygen 2100	4~7	2 2.7	1-52x3.46 1-50x6.69	
Combustion heating test bench (CHSTF)	Engine testing	Burn hydrogen to supplement oxygen 1700	3.5~5 4.6~6	3.5 4.7	ϕ 764 13.26x13.26	2.5x3.5x8 (W x H x L)
Arc heating test bench (AHSTF)	Engine testing	Arc heating 2900	4-7~5.5 6~8	4-7 6-0	11-17x11.17 10.89x10.89	ϕ 4x11(L)
8ft high-temperature wind tunnel (8'HT)	Engine testing	Hydrogen and oxygen are 2000	4 5 6.8	4-0 5-0 6-8	ϕ 96	ϕ 8x12(L)
Hypersonic pulse wind tunnel (HYPLUS)	Combustion chamber test	Shockwave tube 8500	12,14, 15,17	4-7,4.8 5-0,7.2	ϕ 6 ϕ 12	ϕ 4x34.5(L)

3.6.2: Direct Test

The direct-connected test, also known as the tubular test, is mainly used to test the combustion chamber of a ramjet engine. In the direct-connected test, the parameters that need to be simulated are such as flow, total temperature, total pressure, etc. The simulated flow rate needs to be consistent with the captured flow rate of the engine inlet tract, and the total temperature and total pressure must also be as consistent as possible. In engineering, the flow-limiting hose in the gas supply pipeline is often used to achieve this function.

The direct connection test of scramjet engine is divided into two categories: cold flow test and heat flow test. The cold flow test is to study the flow process in the combustion chamber, without injecting fuel, or injecting fuel but not ignition, only studying the blending, atomization (for liquid fuels), aerodynamic resistance of the combustion chamber, etc. The heat flow test is to study the ignition characteristics of the engine, as well as the combustion flow under different combustion chamber structures, different incoming flow conditions, different fuel types, and different fuel equivalent ratios.

Combustion chamber test of a kerosene-fueled direct-coupled scramjet engine. During the test, the air in the high-pressure gas tank is heated to a specified temperature by the heater, and the specified Mach number is reached through the Rafal nozzle into the supersonic combustion chamber, where fuel is injected at different positions in the combustion chamber to organize combustion (Figure 3-46). Since the combustion flow occurs inside the combustion chamber, it is not convenient to observe and measure directly, so the combustion flow will be analyzed by measuring the wall pressure of the combustion chamber and using the basic equation of aerodynamics.

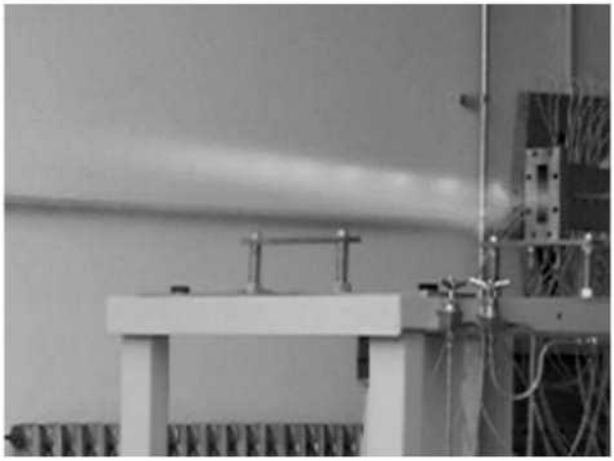

Figure 3-46: Direct-connected supersonic combustion test in progress

3.6.3: Free Jet Test

The free jet test is mainly used to carry out the overall test of scramjet engine, as well as the integrated test of engine and aircraft. If the Mach number and pressure of the air flow during the free jet test are the Mach number and pressure faced by the aircraft during flight, it is called a full free jet test, and if the Mach number and pressure simulated by the test cannot fully simulate the conditions of real flight, it is called a semi-free jet test. For example, when scramjet engine is tested, only the local Mach number and pressure at the inlet of the air inlet can be guaranteed, but the flight conditions of the entire engine cannot be simulated, which is called a semi-free jet test. For another example, when the integrated test of a hypersonic vehicle is carried out, the simulated state is the parameters after the shock wave of the aircraft forebody, which is smaller than the Mach number in real flight, which is also called a semi-free jet test. When the flight Mach number of the aircraft is very high, it is difficult to carry out the full free jet test: the length of the large Mach number nozzle is very long, and the uniformity of the air flow is difficult to guarantee.

The simulated total pressure is high, the test airflow flow is large, and it is difficult to ensure a certain high-altitude test environment, while the cost and difficulty of carrying out the semi-free jet test are lower.

The inlet performance verification test mainly investigates the performance of the inlet channel in the designed and non-designed states, including the flow coefficient of the inlet channel under different incoming angles of attack and sideslip angles, the total pressure recovery coefficient, the conditions of different incoming surface layers (laminar flow, turbulence), the thickness of the attached surface layer, and the influence of incoming flow distortion on the performance of the inlet airway, etc.

One of the main elements of the free-jet test is to test the intake tract and combustion chamber (and sometimes the nozzle) as a whole, or the integrated test of the engine and aircraft (Figure 3-47). The test contents include engine speed characteristics, altitude characteristics, air intake/combustion chamber matching characteristics, engine/aircraft integration characteristics, etc.

Figure 3-47: Free jet test of a scramjet engine

Free-jet testing requires a simulation of a high-altitude environment, and the higher the altitude of the aircraft, the more difficult the simulation becomes. The high-altitude environment needs a vacuum chamber and vacuum extraction facilities to achieve, because the gas generated in the test process is to be discharged dynamically, so dynamic vacuum facilities are required, and the ejector is the most widely used type of equipment at present. The ejector is a dynamic vacuum pump that dynamically discharges the exhaust gas generated by the test to ensure the low pressure required for the normal operation of the test. The larger the test exhaust volume and the higher the vacuum degree, the stronger the injection capacity of the injector is required.

There are two types of ejectors used in engineering: passive ejectors and active ejectors. The passive ejector refers to the test gas flow using its own energy to discharge the test exhaust gas into a relatively high ambient pressure. This type of ejector is often used in rocket engines for high-altitude simulation tests and can be launched to an altitude of more than 20km. The working principle of the active ejector is to introduce a high-energy ejection gas, mix it with the low-energy exhaust gas generated in the test, and discharge it into the external environment. The ejection gas is called the primary flow, and the test exhaust gas is called the secondary flow. There is no secondary flow in a passive ejector, or zero secondary flow ejector.

3.6.4: Test the effect of airflow parameters on engine performance

In scramjet engine testing, the most common method used is to burn heated air to obtain a high enthalpy flow that simulates high-speed flight. This method is relatively easy to implement, but the "polluting" gases produced by combustion can have a certain impact on the results of combustion chamber tests, mainly the effect of turbulence and the influence of gas composition.

1. The effects of turbulence

Turbulence has a great influence on the speed of flame propagation in the combustion chamber, which in turn affects the combustion stability boundary and combustion efficiency. Large-scale turbulence is easy to cause the combustion chamber to stall, while small-scale turbulence is beneficial to combustion, which increases the flame propagation speed and improves the combustion stability and combustion efficiency of the combustion chamber.

In the case of scramjet engines, the total temperature simulated in the test is very high, and in the case of combustion-heated test equipment, it is difficult to arrange a stabilization section like a test bench for a subsonic combustion ramjet engine to stabilize the air flow, so the degree of turbulence of the test air flow entering the engine is high. High turbulence can lead to incorrect transition simulations downstream, as well as strong turbulence-combustion interactions, compounding the already complex problem of supersonic combustion. The turbulence of the test device is an important indicator, and how to build a "quiet" hypersonic wind tunnel is a very important part of the experimental research.

2. Effect of gas composition

In addition to water vapor and carbon dioxide (depending on the type of heating fuel), the gases contained in the heater also include various active ingredients. The effect of the water vapor contained in the test gas on combustion is similar to the effect of humidity on combustion efficiency: water vapor causes the ignition to increase in delay and the combustion temperature to decrease. In addition, water vapor condenses as the gas expands and cools, especially when the total temperature of the gas stream is not high. The large amount of water vapor condensation will produce a sudden jump in condensation, resulting in a sudden change in the airflow parameters and affecting the reliability of the test data. The presence of carbon dioxide also lowers the combustion temperature and pressure level. The presence of active ingredients can significantly affect the ignition and combustion process of supersonic combustion, which needs to be taken seriously. It was once thought that the active ingredient in the heater had a very short lifetime and could not affect the combustion process in the combustion chamber. However, after careful research, it has been found that the heater active ingredient does affect the ignition delay and flame stability of the combustion chamber [187,188].

References

[1] Liu Xiaoyong. Scramjet engine technology [J]. Flying Missile, 2003, (2): 38-42

[2] Builder C H. On the thermodynamic spectrum of airbreathing propulsion [R]. AIAA Paper, 1964: 64-243.

[3] Yuan Shengxue. On supersonic combustion [J]. Science in China (Series A),1998, 28(8):735-741.

[4] Pan Yu. Study on combustion and flow process of scramjet engine multi-cavity combustion chamber [D]. Changsha: Graduate School of National University of Defense Technology, 2007

[5] Ben-Yakar A. Experimental investigation of mixing and ignition of transverse jets in supersonic crossflows [D]. PhD Dissertation, Stanford University, 2000.

[6] Billig F S, Orth R C, Lasky M. A unified analysis of gaseous jet penetration [J]. AIAA Journal, 1971, 9(6): 1048-1058.

[7] Schetz J A, Gilreath E H. Tangential slot injection in supersonic flow [J]. AIAA Journal, 1967, 5 (2):2149-2154.

[8] Gruber M R, Nejad A S, Chen T H, et al. Transverse injection from circular and elliptic nozzles into a supersonic crossflow [J]. Journal of Propulsion and Power, 2000, 16(3):449-457.

[9] Gruber M R, Goss L P. Surface pressure measurements in supersonic transverse injection flowfields [J]. Journal of Propulsion and Power, 1999, 15(5):633-641.

[10] Glawe D D, Samimy M, Nejad A S, et al. Effects of nozzle geometry on parallel injection into a supersonic flow [J]. Journal of Propulsion and Power, 1996, 12(6): 1159-1168.

[11] Tam C -J, Baurle R A, Gruber M R. Numerical study of jet injection into a supersonic crossflow [R]. AIAA 1999-2254, 1999.

[12] Hsu K -Y, Carter C, Crafton J, et al. Fuel distribution about a cavity flameholder in supersonic flow [R]. Came 2000-3585, 2000.

[13] Mathur T, Streby G D, Gruber M R, et al. Supersonic combustion experiments with a cavity-based fuel injector [R]. AIAA 1999-2102, 1999.
[14] Cox-Stouffer S K, Gruber M R, Bulman MJ. A streamlined pressure-matched fuel injector for scramjet application [R]. AIAA 2000-3707, 2000.
[15] Mathur T, Cox-Stouffer S K, Hsu K-Y, et al. Experimental assessment of a fuel injector for scramjet applications [R]. AIAA 2000-3703, 2000.
[16] Cox-Stouffer S K, Gruber M R. Effects of injector yaw on mixing characteristics of aerodynamic ramp injectors [R]. AIAA 1999-0086, 1999.
[17] Cox-Stouffer S K, Gruber M R. Further investigation of the effects of 'aerodynamic ramp' design upon mixing characteristics [R]. AIAA 1999-2238, 1999.
[18] Fuller R P, Wu P-K, Nejad A S, et al. Comparison of physical and aerodynamic ramps as fuel injectors in supersonic flow [J]. Journal of Propulsion and Power, 1998, 14(2):135-145.
[19] Eklund D R, Gruber M R. Study of a supersonic combustor employing an aerodynamic ramp pilot injector [R]. AIAA 1999-2249, 1999.
[20] Eklund D R, Baurle R A, Gruber M R. Numerical study of a scramjet combustor fueled by an aerodynamic ramp injector in Dual-Mode combustion [R]. AIAA 2001-0379, 2001.
[21] Gruber M R, Donbar J M, Jackson T A, et al. Performance of an aerodynamic ramp fuel injector in a scramjet combustor [R]. AIAA 2000-3708, 2000.
[22] Donbar J M, Powell O, Gruber M R, et al. Post-test analysis of flush-wall fuel injection experiments in a scramjet [R]. AIAA 2001-3197, 2001.
[23] Gruber M R, Nejad A S, Chen T H, et al. Compressibility effects in supersonic transverse injection flowfields [J]. Physics of Fluids, 1997, 9(5): 1148-1160.
[24] Chung-Fen Tam, Robert A. Baurle, Mark R. Gruber. Numerical study of jet injection into a supersonic crossflow [R]. AIAA 99-2254.
[25] Yates C L. Liquid injection into a supersonic stream. AFAPL-TR-71-97, Vol. 1, Aero Propulsion Laboratory, Wright-Patterson AFB, OH, 1972.
[26] Kush E A, Schetz J A. Liquid jet injection into a supersonic flow [J]. AIAA Journal, 1973, 11(9).
[27] Lin K -C, Kennedy P J, Jackson T A. Penetration heights of liquid jets in high-speed crossflows [R]. AIAA 2002-0873, 2002.
[28] Lin K -C, Kennedy P J, Jackson T A. Structures of waterjets in a Mach 1.94 supersonic crossflow [R]. AIAA 2004-0971, 2004.
[29] Sallam K A, Aalburg C, Faeth G M, et al. Breakup of aerated-liquid jets in supersonic crossflows [R]. AIAA 2004-0972, 2004.
[30] Wu P-K, Kirkendall K A, Fuller R P, et al. Breakup processes of liquid jets in subsonic crossflows [J]. Journal of Propulsion and Power, 1997, 13(1):64-73.
[31] Fuller R P, Wu P K, Kirkendall K A, et al. Effects of injection angle on the breakup processes of liquid jets in subsonic crossflows [R]. AIAA 1997-2966, 1997.
[32] Wu P K, Kirkendall K A, Fuller R P, et al. Spray structures of liquid jets atomized in subsonic crossflows [J]. Journal of Propulsion and Power, 1998, 13(2): 173-182.
[33] Lefebvre A H. Atomization and Sprays [M]. New York: Hemisphere, 1989.
[34] Lefebvre A H, Wang X F, Martin C A. Spray characteristics of aerated-liquid pressure atomizers [J]. Journal of Propulsion and Power, 1998, 4(4):293-298.
[35] Daniel A Cassidy, Jung-Ilchoi, Ming Tian. Numerical simulation of two-phase flow within an aerated liquid injector [R]. AIAA 2010-98, 2010.

[36] Santangelo PJ, Sojka P E. Focused-image holography as a dense-spray diagnostic [J]. Applied Optics, 1994, 33(19):4132-4136.
[37] Santangelo P J, Sojka P E. A holographic investigation of the near-nozzle structure of an effervescent atomizer-produced spray [J]. Atomization and Sprays, 1995(5).
[38] Lin K-C, Kirkendall K A, Kennedy P J, et al. Spray structures of aerated liquid fuel jets in supersonic crossflows [R]. AIAA, 1999, 2374.
[39] Lin K-C, Kennedy P J, Jackson T A. Spray structures of aerated-liquid jets in subsonic crossflows [R]. AIAA 2001-0330, 2001.
[40] Lin K-C, Kennedy P J, Jackson T A. Structures of aerated-liquid Jets in high-speed crossflows [R]. AIAA 2002-3178, 2002.
[41] Mathur T, Lin K -C, Kennedy PJ, et al. Liquid JP-7 combustion in a scramjet combustor [R]. AIAA 2000-3581, 2000.
[42] Lin K -C, Kennedy P J, Jackson T A. Structures of aerated liquid fuel jets interacting with a shock train in supersonic crossflows [C]. Eighth International Conference on Liquid Atomization and Spray Systems, July 2000, Pasadena CA.
[43] Su Yi, Li Dapeng, Liu Weidong. Hybrid Enhancement Technology of Scramjet Engine, Aeronautical Missile, 2006, (11): 41-46
[44] Bushnell D M. Hypervelocity scramjet mixing enhancement [J]. Journal of Propulsion, 1994, 11 (5):1088-1090.
[45] Uwe Brummund, Joachim R N. Interaction of a compressible shear layer with shock waves: An experimental study [R]. AIAA 97-0392, 1997.
[46] Nedungadi A, Lewis M J. A numerical study of fuel mixing enhancement using an oblique shock/vortex interaction [R]. AIAA 96-2920, 1996.
[47] Obata S, Hermanson J C, Numerical simulation of shock enhanced mixing in axisymmetric turbulent jets [R]. AIAA 2001-0149, 2001.
[48] Ji-Ho Kim, Jaeheon Sim, Jaehung Kim. Mixing enhancement of hydrogen diffusion flames in supersonic air using shock waves [R]. AIAA 99-2785, 1999.
[49] Drummond J P. Enhancement of mixing and reaction in high-speed combustor flowfields [R]. NASA-97-acac-pd, 1997.
[50] Oliger K M, Mo J D, Driver M A. Shock wave/flat plate boundary layer injection interactions [R]. AIAA 95-2481, 1995.
[51] Hwanil Huh, Jungyona Kim, Jam F D. Measured characteristics of flow and combustion in supersonic flame/ shock wave interaction [R]. AIAA 2001-3935, 2001.
[52] Mader B. Scramjet ignition technology [R]. ME 8362, April 30, 2002.
[53] A new scheme for studying kerosene super-ignition [J]. Fluid Mechanics Experiments and Measurements, 2001, 15(3):7-12.
[54] YU Gang, LI Jianguo, CHEN Lihong, et al. Study on supersonic ignition characteristics of kerosene-hydrogen dual fuel, Fluid Mechanics Experiment and Measurement, 2001, 14(1): 63-71.
[55] Harrison A J, Weinberg F J. Flame stabilization by plasma jets [C]. Proceedings of the Royal Society of London, 1971, 321(1544).
[56] Scott D. Gallimore. A study of plasma ignition enhancement for aeroramp injectors in supersonic combustion applications [D]. Virginia Polytechnic Institute and State University, 2001.
[57] Masuya G, Komuro T, Murakami A, et al. Ignition and combustion performance of combustors with fuel injection struts [J]. Journal of Propulsion and Power, 1995, 11 (2): 301-307.
[58] Yu Yong, Ding Meng, Liu Weidong, et al. Experimental study on supersonic combustion of kerosene [J]. Journal of National University of Defense Technology, 2004, 26 (1): 1-4.
[59] Ding Meng, Yu Yong, Liang Jianhan, et al. Experimental ignition technology of hydrocarbon fuel scramjet engine [J]. Propulsion Technology, 2004, 25(6)566-569.
[60] Tohru Mitani, Toshinori Kouchi. Flame structures and combustion efficiency computed for a Mach 6 scramjet engine [J]. Combustion and Flame, 2005, (142): 187-196.

[61] O'Byrne S, Doolan M, Olsen S, et al. Analysis of transient thermal choking process in a model scramjet engine [J] Journal of Propulsion and Power, 2000, 16(5): 808-814.
[62] SUN Yingying, HAN Zhaoyuan, SI Tuming. Ignition and combustion of supersonic premixed combustible gas flow [J]. Engineering Physics, 2002, 23(6):776-778.)
[63] Huber P W, Schexnayder C J, McClinton C R. Criteria for self-ignition of supersonic hydrogen-air mixtures [R]. NASA TP 1457, 1979.
[64] Ben-Yakar A, Hanson R K. Experimental investigation of flame-holding capability of a transverse hydrogen jet in supersonic cross-flow [C]. Proceeding of the 27th International Symposium on Combustion, 1998.
[65] Gouskov O V, Kopchenov V I. Investigation of ignition and flame stabilization behind the strut in supersonic flow [R]. AIAA 2002-5227, 2002.
[66] Brandstetter A, Denis S R, Kau H P, et al. Flame stabilization in supersonic combustion [R]. AIAA 2002-5224, 2002.
[67] Bussing TRA, Murman E M. Numerical investigation of 2-Dimensional H2-Air flame holding over ramps and rearward facing steps [R]. AIAA 85-1250, 1985.
[68] Donel N D, Thompson D S. A two-dimensional numerical simulation of shock-enhanced mixing in a rectangular scramjet flowfield with parallel hydrogen injection [R]. AIAA 91-0377, 1991.
[69] Northam G B, McClinton C R, Wagner T C, O'Brien W F. Development and evaluation of a plasma jet flameholder for scramjets. AIAA 84-1408, 1984.
[70] Sabel'nikov V A, Korontsvit Y P, Ivanyushkin A K, Ivanov V V. Experimental investigation of combustion stabilization in supersonic flow using free zone. AIAA 98-1515, 1998.
[71] Curran E T, Murthy S N B. Scramjet Propulsion, Progress in Astronautics and Aeronautics [M]. American Institute of Aeronautics and Astronautics, Inc., 2001.
[72] FAN Xiaoqiao. Design, calculation and experimental research of hypersonic air intake [D]. Changsha: National University of Defense Technology, 2006.
[73] WU Xianyu. Research on optimization of integrated flow channel design of scramjet engine [D]. Changsha: National University of Defense Technology, 2007.
[74] Song Wenyan, et al., Aerodynamic design of scramjet engine forebody/air inlet and isolation section [J], Journal of Northwestern Polytechnical University, 2004, 22(1):96-99.
[75] Holland S. D. Computational parametric study of sidewall compression scramjet inlet performance at Mach 10 [R]. NASA 0TM 4411, Feb., 1993.
[76] Fangrong Ye, Ziaul Huaue and Nelson Butuk. Effect of sidewall leading edge sweep direction on performance of a Hypersonic 3-D Inlet [R]. AIAA 2000-3600, 2000.
[77] Dr M A Goldfeld, Nestoulia R V. Numerical and experimental studies of 3D hypersonic inlet [R]. AIAA 200314, 2003.
[78] Cheng-Peng Wang, Kunyuan Zhang, Jianjun Yang. Analysis of lows in scramjet isolator combined with hypersonic inlet [R]. AIAA 2005-24, 2005.
[79] Billig F S. SCRAM-a supersonic combustion ramjet missile [R]. AIAA Paper, AIAA-1993-2329, 1993.
[80] van Wie D, Molder S. Applications of busemann inlet designs for light at hypersonic speeds [R]. AIAA-1992- 1210, 1992
[81] Jacobsen L S, Tam CJ, Robert B F. Starting and operation of a streamline-traced busemann inlet at Mach 4 [R]. AIAA-2006-4508, 2006.
[82] Michael K Smart, Carl A Trexler. Mach 4 performance of a fixed geometry hypersonic inlet with rectangular-to-elliptical shape transition [R]. AIAA-2003-0012, 2003.
[83] YOU Yancheng. Advances in Mechanics, 2009, 39(5):513-525.)
[84] Molder S. Internal, axisymmetric., conical flow [J]. AIAA Journal, 1967, 5(7): 1252-1255.
[85] Dsouza N, Molder S. Applicability of hypersonic small-disturbance theory and similitude to internal hypersonic conical Flows [J]. Journal of Spacecraft, 1970, 7(2): 149-154.
[86] O'Brien Timothy F, Colville J R. Analytical computation of leading edge truncation effects on inviscid busemann inlet performance [R]. AIAA-2007-0026, 2007.

[87] Billig F S, Jacobsen L S. Comparison of planar and axisymmetric flowpaths for hydrogen fueled space access vehicles [R]. AIAA-2003-4407, 2003.
[88] Billig F S, Kothari A P. Streamline tracing: technique for designing hypersonic vehicles [J]. Journal of Propulsion anal Power, 2000, 16(3): 465-471.
[89] Tam C J, Baurle R A. Inviscid CFD analysis of streamline traced hypersonic inlets at off-design conditions [R]. AIAA-2001-0675, 2001.
[90] Billig F S. Design and analysis of streamline traced hypersonic inlets [R]. AIAA-1999-4974, 1999.
[91] Matthews A, Jones T. Design and test of a modular waverider hypersonic intake [J]. Journal of Propulsion and power, 2006, 22(4): 913-920.
[92] Kothari A P, Tarpley C, Mclaughlin T A, et al. Hypersonic vehicle design using inward turning flow fields [R]. AIAA Paper, AIAA-1996-2552, 1996.
[93] Dissel A F, Kothari A P. Investigation of two-stage-to-orbit airbreathing launch-vehicle configurations [J]. Journal of Spacecraft and Rockets, 2006, 43(3): 568-574.
[94] Dissel A F, Kothari AP, Lewis M J. Comparison of horizontally and vertically launched airbreathing and rocket vehicles [J]. Journal of Spacecraft and Rockets, 2006, 43(1): 161-169.
[95] Walker S H, Rodgers F. Falcon hypersonic technology overview [R]. AIAA Paper, AIAA-2005-3253. 2005.
[96] Ye Lei, Han Xu. HyCAUSE Promotes Falcon Aircraft Air Inlet Research. Flight Missile, 2008(1): 4, 5.
[97] Malo F J, Gaitonde D V. Numerical investigation of an innovative inward turning inlet [R]. AIAA-2005-4871, 2005.
[98] Study on flow characteristics of isolation section of scramjet engine [D]. Xi’an: Northwestern Polytechnical University, 2005.
[99] Curran E T, Heiser W H, Pratt D T. Fluid phenomena in scramjet combustion systems [J]. Annu Rev Fluid Mech, 1996, 323-360.
[100] Neumann E P, Lustwerk F. Supersonic diffusers for wind tunnels [J]. J Appl Mech, 1949, 16(2): 195-202.
[101] Newman E P, Lustwerk F. High-efficiency supersonic diffusers [J]. J Aeronaut Sci, 1951, (18)6: 369-374.
[102] Lukasiewicz J. Diffusers for supersonic wind tunnels [J]. J Aeronaut Sci, 1953, 20(9): 617-626.
[103] Shapiro AH. The dynamics and thermodynamics of compressible fluid flow, vols [M]. 1 and 2. New York, Ronald Press, 1953: 135-139, 1153-1156.
[104] Ikui T, Matsuo K. Researches of supersonic flow with the shock wave as main subject [J]. J JSME, 1969: 1306-1312.
[105] Billig F S. Combustion processes in supersonic flow [J]. J Propulsion Power, 1988, 4(3): 209-216.
[106] Cohen C B, Valerino A S. Investigation of operating pressure ratio of a supersonic wind tunnel utilizing distributed boundary-layer suction in test section [R]. NACA Res Memo ESOH04, 1950.
[107] Faro IDV. Handbook of Supersonic Aerodynamics [M], Vol. 6. Sec. 17, Navweps Rep. 1964.
[108] B. F. Carroll, J. C. Dutton. Characteristics of multiple shock wave/turbulent boundary-layer interactions in rectangular ducts [J]. J Propulsion Power, 1990: 6(2): 186-193.
[109] Lin P, Rao GVR, O'Connor GM. Numerical analysis of normal shock train in a constant area isolator [R]. AIA. A Paper, 1991: 91-2162.
[110] Ikui T, Matsuo K, Nagai M. The mechanism of pseudo-shock waves [R]. Bull J5ME, 1974: 731-739.
[111] Hunter LGS Couch BD. A CFD study of precombustion shock-trains from Mach 3-6 [R]. AIAA Paper, 1990: 90-2220.
[112] Tamaki T, Tomita Y, Yamane R. A study of pseudo-shock, 2nd Report, X-type pseudo-shock [R]. Bull JSME, 1971: 807-817.
[113] John M. Seiner S. M. Dash and D. C Kenzakowski Historical Survey on Enhanced Mixing in Scramjet Engines [R]. Journal of Propulsion and Power, 1998, 4(4): 1273-1286.
[114] Adela Hen-Yakar and Ronald K. Hanson, cavity flame-holders for ignition and flame stabilization in scramjets:

An Overview [J]. Journal of Propulsion and Power January-February, 2001: 17(1): 869-877.
[115] Scott D. Gallimore. A study of plasma ignition enhancement for aeroramp injectors in supersonic combustion applications [D]. Ph. D Dissertation.
[116] T. O. Mohieldin and S. N. Tiwari, Numerical Study of 2D Dual-Mode Scramjet Combustion Part 1: Cold Flow Analysis [R]. AIAA Paper 2003-7036, 2003.
[117] ONERA, France Mixing Enhancement Techniques in a Scramjet [R]. AIAA1998-1517, 1998.
[118] Tomioka S, Kanda T, Mitani T, Shimura T, Chinzei N. Testing of a scramjet engine with a strut in M8 Flight Conditions [R]. AIAA 98-3134, 1998.
[119] William H. Heiser and David T. Pratt. Hypersonic Airbreathing Propulsion [M]. AIAA Education Series, 1993.
[120] Liu Ling, et al. Supersonic combustion and supersonic combustion ramjet engine [M]. Xi'an: Northwestern Polytechnical University Press, 1993.
[121] C. Segal, M. G. Owens and S. Tehranian flame holding configurations for kerosene combustion in a Mach 1.8 airflow [R]. AIAA97-2888, 1997.
[122] Roudakov A S, Schikhmann Y, Semenov V, et al. Fight testing of an axisymmetric scramjet, Russian recent advances [C]. International Astronautical Federation, IAF paper 93-S4.485, Oct., 1993.
[123] Vinagradov V, Kobigsky S A, Petrov MD. Experimental investigation of kerosene fuel combustion in supersonic flow [J]. Journal of propulsion and power, 1995, 11(1): 130-134.
[124] A D, Harding G C, Diskin G S. Supersonic pulsed injection [R]. AIAA 2001-0517, 2001.
[125] Burnes R, Parr T P, Wilson KJ, et al. Investigation of supersonic mixing control using cavities: effect of fuel injection location [R]. AIAA 2000-3618, 2000.
[126] Yu K H, Schadow K C. Role of large coherent structures in turbulent compressible mixing [J]. Exp. Thermal and Fluid Science, 1997, 14: 75-84.
[127] Anand Nenmen V, Yu K. Cavity-induced mixing enhancement in confined supersonic flows [R]. AIAA 2002-1010, 2002.
[128] Sang-Hyeon Lee, Yong-Jin Kim. Mixing augmentation of transverse injection in scramjet combustor [R]. AIAA 2000-0090, 2000.
[129] Yu K H, Schadow K C. Cavity-actuated supersonic mixing and combustion control [J]. Combustion and Flame, 1994, 99: 295-301.
[130] Gruber M R, Donbar J M, Carter C D. Mixing and combustion studies using cavity-based flameholders in a supersonic flow [J]. Journal of Propulsion and Power, 2004, 20(5): 769-778.
[131] Vinagradov V, Crachev V, Petrov M, et al. Experimental investigation of 2-D dual mode scramjet with hydrogen fuel at Mach 4-6 [R]. AIAA 90-5269, 1990.
[132] Niioka T, Terada K H, Kobavashi S, et al. Flame stabilization characteristics of a strut divided into two parts in supersonic airflow [J]. Journal of Propulsion and Power, 1995, 11 (1): 112-116.
[133] Morrison C Q, Campbell P L, Edelrnan R B, et al. Hydrocarbon fueled dual-mode ramjet/ scramjet concept evaluation [R]. JANNAF Propulsion and Joint Subcommittee Meeting, 1996.
[134] Ortweth P, Mather A, Vinogradov V, et al. Experimental and numerical investigation of hydrogen and ethylene combustion in a Mach 3-5 channel with a single injector [R]. AIAA 96-3245, 1996.
[135] McClinton C, Roudakov A, Semenov V, et al. Comparative low path analysis and design assessment of an axisymmetric hydrogen fueled scramjet flight test engine at a Mach number of 6.5 [R]. AIAA 96-4571, 1996.
[136] Owens M G, Tehranian S, Segal C. Flam-holding configurations for combustion in Mach 1.8 airflow [J]. Journal of Propulsion and Power, 1998, 14(4): 456-461.
[137] Yu K, Wlson K J, Schadow K C. Effect of lam-holding cavities on supersonic combustion performance [R]. AIAA 99-2638, 1999.
[138] Mathur T, Streby G, Gruber M, et al. Supersonic combustion experiment with a cavity-based fuel injector

[R] AIAA 99-2102, 1999.
[139] Ben-Yakar A**,** Hanson R K. Supersonic combustion of cross-flow jets and the influence of cavity flame-holders **[**R**]** AIAA 99-0484**,** 1999.
[140] O'Byrne S O**,** Stotz I, A J**,** Neely R R**,** et al. OH PLIF imaging of supersonic combustion using cavity injection **[**R**]**. AIAA 2005-3357**,** 2005.
[141] Research on flame stabilization technology of supersonic combustion based on cavity **[**D**]**. Changsha**:** Graduate School of National University of Defense Technology, 2005
[142] Study on the working process of kerosene dual-modal ramjet engine **[**D**]**. Changsha**:** Graduate School of National University of Defense Technology, 2006
[143] Zhang X**,** Rona A**,** Edwards J A. The effect of trailing edge geometry on cavity flow oscillation driven by a supersonic shear layer [J]. Aeronautical Journal, 1998, 102(1013): 129-136.
[144] Gruber M R, Baurle R A, Mathur T, et al. Fundamental studies of cavity-based flameholder concepts for supersonic combustor [R]. AIAA 99-2248, 1999.
[145] Baurle R A, Gruber M R. A study of recessed cavity flowfields for supersonic combustion applications [R]. AIAA 99-0938, 1999.
[146] Quinn J E, Cutler A D, Northam G B. Drag reduction of supersonic cavities via mass injection with applications to scramjet [R]. AIAA 97-0550, 1997.
[147] Ding Meng, Wang Zhenguo. Experimental study on resistance characteristics of concave flame stabilizer [J]. Acta Aeronautica Sinica, 2005.12(6):556-560.
[148] Yu K, Wilson K J, R A Smith, et al. Experimental investigation on dual-purpose cavity in supersonic reacting flows **[**R**]**. AIAA 98-0723**,** 1998.
[149] Zhang Xin, Edwards J A. Experimental investigation of supersonic flow over two cavities in tandem [J]. AIAA Journal, 1992, 30(5): 1182-1190.
[150] Rho O, Hwang S. Numerical simulation of supersonic over double cavity [R]. AIAA 94-2206, 1994.
[151] Taborda N, Bray D, Knowles K. Passive control of cavity resonances in tandem configurations [R]. AIAA 2001-2770.
[152] Jeyakumar S, Balachandran P. Experimental investigations on supersonic stream past axisymmetric cavities [R]. AIAA 2005-3553, 2005.
[153] Holmes S G, Landrum D B. Experimental investigation of the heat transfer to parallel tandem cavities [R]. AIAA950631, 1995.
[154] Yu K H, Wilson K J, Schadow K C. Effect of flame holding cavities on supersonic combustion performance [J]. Journal of Propulsion and Power, 2001, 17(6): 1287-1295.
[155] Stu M, Wang C, LuHP. Hot gas piloted energy for supersonic combustion of kerosene with dual-cavity [R]. AIAA 2001-0523, 2001.
[156] Stu M, Wang C, Zhuang F G, Investigation of supersonic combustion of kerosene jets with hot gas piloted energy and dual-cavity [R]. AIAA 2002-0804, 2002.
[157] Chen Jianqiang, Situ Ming. Numerical simulation of supersonic flow field in combustion chamber with double groove [J]. Chinese Journal of Aerodynamics, 2004, 22(4.)):395-398.
[158] Adam Quick, King P I, Gruber M R, Carter C D, et al. Upstream mixing cavity coupled with downstream flameholding cavity behavior in supersonic flow [R]. AIAA 2005-3709, 2005.
[159] Tishkoff J M, Drummond J P, Edwards T, et al. Future directions of supersonic combustion research: Air Force / NASA workshop on supersonic combustion [R]. AIAA Paper 97-1017. 1997.
[160] Cox S K, Schetz R P, Walters R W. Vortical interactions generated by an injector array to enhance mixing in supersonic flow [R]. AIAA Paper 94-0708. 1994.
[161] Rogers R C, Capriotti D P, Guy R W. Experimental supersonic combustion research at NASA Langley [R]. AIAA Paper 98-2506. 1998.
[162] Semenov V L. The possibility investigation of strut fuel feed system use in scramjet combustors on results of tests with hydrocarbon fuel [R]. AD A-332687**,** 1997.
[163] Viacheslav A Vinogradov**,** Yurii M Shikhman**,** Ruslan V Albegov**,** Georgi K Vedeshkin. About Possibility of

Effective Methane Combustion in High Speed Subsonic Airflow [R]. AIAA Paper 2003-6940-5206, 2003.
[164] Sadatake Tomioka, Atsuo Murakami, Kenji Kudo, et al. Combustion tests of a staged supersonic combustor with a strut [R]. AIAA Paper 98-3273, 1998.
[165] Masatoshi Kodera, Tetsuji Sunami, Frithjof Scheef. Numerical Study on The Supersonic Mixing Enhancement Using Streamwise Vortices [R]. AIAA Paper 2002-5117, 2002.
[166] Emmanuel Dufour, Marc Bouchez. Computational analysis of a kerosene-fueled scramjet [R]. AIAA Paper 2001-1817. 2001.
[167] Brandstetter A, Rocci Denis S, Kau H P, et al. Flame stabilization in supersonic combustion [R]. AIAA Paper 2002-5224. 2002.
[168] Kasaf P, Gerlinger P, Walther R, et al. Supersonic Combustion: Fundamental Investigations of Aerothermodynamic Key Problems [R]. AIAA Paper 2002-5119, 2002.
[169] Yu Yong. Theory and experimental study on the combustion process of scramjet engine [D]. Changsha: National University of Defense Technology, 2004.
[170] Zhu Yefu, Ma Kalan, Principles of Ramjet and Rocket Ramjet Engines, Liu Xingzhou, et al., trans. 1975.
[171] Rao GVR, Exhaust Nozzle Contour for Optimum Thrust [J], Jet Propulsion, 1958, 28: 377-382.
[172] Argrowb M. Comparison of minimum length nozzles [J], Journal of Fluids Engineering, 1988. 9: 283-288.
[173] Jan Ostlund. Flow processes in rocket engine nozzles with focus on flow separation and side-loads [D], Licentiate Thesis, Sweden, Royal Institute of Technology Department of Mechanics, 2002.
[174] Goeing M. Nozzle design optimization by method-of-characteristics [R]. AIAA-90-2024, 1990.
[175] Hoffman J D. Design of compressed truncated perfect nozzles [R], AIAA-85-1172, 1985.
[176] Cubbage Jame M, William J Monta. Parametric experimental investigation of a scramjet nozzle at Mach 6 with freon and argon or air used for exhaust simulation [R]. NASA TP-3048, 1991.
[177] Watanabe, Shigeya. A Scramjet Nozzle Experiment with Hypersonic External Flow [R]. AIAA-92-3289, 1992.
[178] William J Monta. Pitot survey of exhaust flow field of a 2-D scramjet nozzle at Mach 6 with air or freon and argon used for exhaust simulation [R]. NASA-TM-4361, 1992.
[179] LI Nian, ZHANG Xu, XU Jinglei. Numerical simulation and verification of two-dimensional asymmetric nozzle [J]. Journal of Aerodynamics, 2004, 19(6): 802-805.
[180] CHEN Bing, XU Xu, CAI Guobiao. Optimal design of single-wall expansion nozzle based on genetic algorithm and space propulsion method [J]. Acta Aeronautica Sinica, 2007, 28 (4): 827-832.
[181] Xu Dajun, Chen Bing, Cai Guobiao. Research on three-dimensional configuration design of rear body nozzle of hypersonic vehicle [J]. Journal of Aerodynamics, 2009, (2): 247-254.
[182] Wang Fang. Research on performance evaluation method of scramjet engine [D]. Changsha: National University of Defense Technology, 2005.
[183] Determination and influencing factors of heat sink of endothermic hydrocarbon fuel [D]. Tianjin: Tianjin University, 2004.
[184] Study on catalytic cracking and carbon deposition of n-alkanes under supercritical conditions [D]. Tianjin: Tianjin University, 2005.
[185] Wu Xiang. Application of fuzzy control in RBCC combustion structure [D]. Xi'an: Northwestern Polytechnical University, 2002.
[186] Research on proportional gas-liquid two-phase high-temperature fuel flow control valve [D]. Harbin: Harbin Institute of Technology, 2008.
[187] Pellett G L, Bruno C, Chinitz W. Review of air vitiation effects on scramjet ignition and flameholding combustion processes [R], AIAA 2002-3880, 2002.
[188] Mitani T. Ignition problems in scramjet testing [J], Combustion and Flame, 1995, 101: 347-349.

CHAPTER 4: COMBINED PROPULSION SYSTEM TECHNOLOGY FOR HYPERSONIC VEHICLES

The scramjet engine is the core key technology in the technology system of hypersonic vehicles, but because the scramjet engine needs to start and work at a high flight Mach number, it needs to be combined with other types of power systems to complete the flight mission within the larger flight envelope. Generally speaking, the lower limit of the starting operation of the scramjet engine is $Ma = 5$, and the dual-mode scramjet can be extended down to $Ma = 3$, then for the starting working point, other power units are required to promote the take-off and acceleration of the aircraft.

For a single-use hypersonic cruise missile, a solid rocket can be used as a booster, and the hypersonic cruise missile powered by a scramjet engine accelerates to the relay point, and then the booster is separated, and the scramjet engine starts to work to achieve hypersonic cruise flight. For multi-reusable space launch vehicles or hypersonic aircraft, it is necessary to arrange other power systems on the aircraft and form a combined propulsion system with scramjet engines to achieve powered flight within the full flight envelope. The choice of other power modes in the combined propulsion system is mainly to solve the power problem between take-off acceleration and relay point, and for single-stage orbit aircraft, it is also necessary to solve the power problem of flight after exiting the atmosphere.

At present, the ways to solve this problem can be divided into two categories: one is the rocket-based combined cycle engine propulsion system (RBCC) and the other is the turbine combined cycle engine propulsion system (TBCC). In addition to these two types of combined propulsion systems, there are also some slightly modified and improved options, such as pre-cooled TBCCs that extend the operating range of turbine engines, and liquid-air combined circulation propulsion systems that use oxygen in the air and store it for use after leaving the atmosphere [1]. In the following chapter, we will introduce some typical hypersonic vehicle combined propulsion systems.

4.1: Rocket-based combined cycle engine propulsion system (RBCC)

4.1.1: RBCC Basic Concepts and Working Principles [2,3]

The RBCC propulsion system combines a rocket engine and an air-breathing propulsion system to form an integrated propulsion system. The propulsion system integrates a rocket engine, a subsonic combustion ramjet and a scramjet engine, with four operating modes: the induction mode, the subsonic combustion ramjet mode, the scramjet mode and the pure rocket mode. By using oxygen from the air in part of the orbital ascent, an RBCC propulsion system-powered vehicle can achieve a higher average specific impulse. In addition, the RBCC propulsion system has a higher installed thrust-to-weight ratio relative to its competitor, the Turbine-Based Combined Cycle Engine (TBCC).

The RBCC propulsion system includes the launch mode, the subsonic combustion ramjet mode, the scramjet mode and the pure rocket mode. Here's how they work:

(1) Ejector jet mode, the main working range is $Ma = 0\sim3$. The rocket engine embedded in the runner works, through the induction and suction of its high-speed air flow, introduces the secondary air flow, and organizes the secondary combustion in the combustion chamber of the runner to improve the overall gas energy, and increases the thrust on the basis of the pure rocket to improve the specific impulse of the engine.

(2) Ramjet mode, the main working range is Ma = 3 to 6. The rocket engine is turned off, and the speed of the incoming air is used to ram, and subsonic combustion is organized in the combustion chamber in the sprue to realize the propulsion of the aircraft.

(3) Scramjet mode, the main working range is Ma = 6 ~ 8. Due to the further increase of flight speed, if the flow is reduced to subsonic speed and then combustion, the static temperature of the air flow in the combustion chamber will be very high, so that the dissociation of combustion products will reach an unbearable level, and the added fuel will not be able to heat the air flow. Therefore, it is the main way to effectively improve the combustion efficiency of the thruster by using the air inlet to properly compress the hypersonic incoming flow so that it can still maintain supersonic speed in the combustion chamber and directly organize supersonic combustion in the combustion chamber.

(4) Pure rocket mode, the main working range is Ma > 8. As the aircraft gradually flies out of the atmosphere, the amount of incoming air gradually decreases and tends to zero, at this time, the air intake channel is closed, the scramjet is ended, and the rocket engine is ignited again, and the rocket engine is used to send the aircraft into the predetermined orbit to complete the orbit entry task.

In the actual engineering design, some working modes can be subdivided, such as the rocket launch mode is divided into the ejector rocket mode and the air augmented rocket mode, and the scramjet engine mode is divided into scramjet mode and scramjet/rocket mode. In terms of the conversion Mach number of subsonic combustion mode and supersonic combustion mode, the above mentioned Ma = 4, 6, 8 are not absolute fixed values, depending on the design of the engine and flight trajectory, for example, in the literature, the scramjet engine can also work to Ma = 10 or 12, and then switch to the pure rocket mode.

Because the main propulsion stage of the rocket-based combined cycle engine is in the ramjet/scramjet working mode, especially the scramjet mode with high flight Mach number, the overall design of the rocket-based combined cycle engine is improved on the basis of the scramjet engine design. The specific details of this improvement are to place and increase the launch of the main rocket in the flow channel of the ramjet/scramjet engine, and the launch of the main rocket plays an important role in the rocket-based combined cycle engine: under subsonic flight conditions, the launch of the main rocket works to produce a supersonic primary stream, and a large amount of air in the external environment is introduced into the engine through the injection suction, and then the introduced air is used to organize secondary combustion to produce thrust enhancement; in ramjet/scramjet modes, the gradual shutdown of the main rocket can play the role of a flame stabilizer, and can also be used as a fuel injector. According to the geometry of the scramjet engine and the position of the main rocket in the engine, the RBCC can be structurally divided into the following four types.

(1) The axisymmetric configuration of the main rocket installed in the center of the engine. This configuration appeared mainly in the early days of RBCC engine research (Fig. 4-1), including experimental engines manufactured by Marquardt Corporation of the United States and NASA's Langley Research Center in the 1950s and 1960s. This type of engine is generally intended to be used as a stand-alone module in the form of a pod, otherwise it has too little space to install other components such as fuel tanks. However, the practical use of engines in this form is unlikely due to the fact that vehicles with pod-type engines have too much drag during hypersonic flight.

(2) The axisymmetric configuration of the main rocket mounted on the side wall of the engine. The most representative of this configuration is the GTX aircraft scheme developed by the NASA Galen Research Center in the United States, which attaches three engine modules around the main body of the aircraft and makes full use of the pre-compression function of the aircraft forebody. This configuration is compact and uses the least amount of material for the same volume, which allows for some reduction in structural mass (Fig. 4-2).

(3) The binary structure configuration of the main rocket installed in the center of the engine. The scramjet engine in the binary configuration not only makes use of the pre-compression function of the aircraft forebody, but also the forebody can also bring the necessary lift to the aircraft, so that the aircraft can take off horizontally. The engine of this configuration generally needs to be installed in the flow channel with a support plate, and the primary rocket is installed in the support plate.

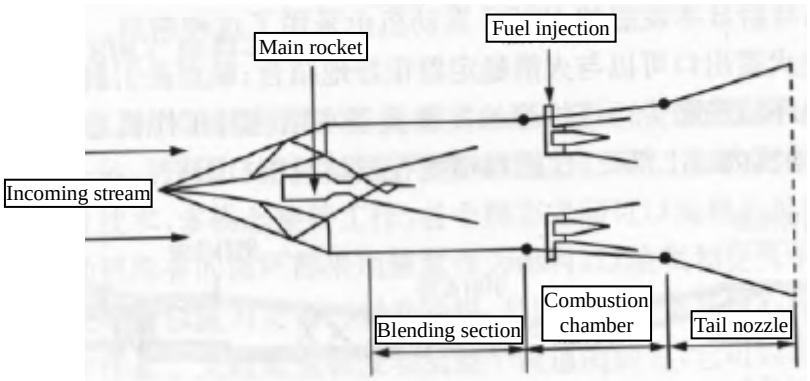

Figure 4-1: An RBCC engine in a classic axisymmetric configuration

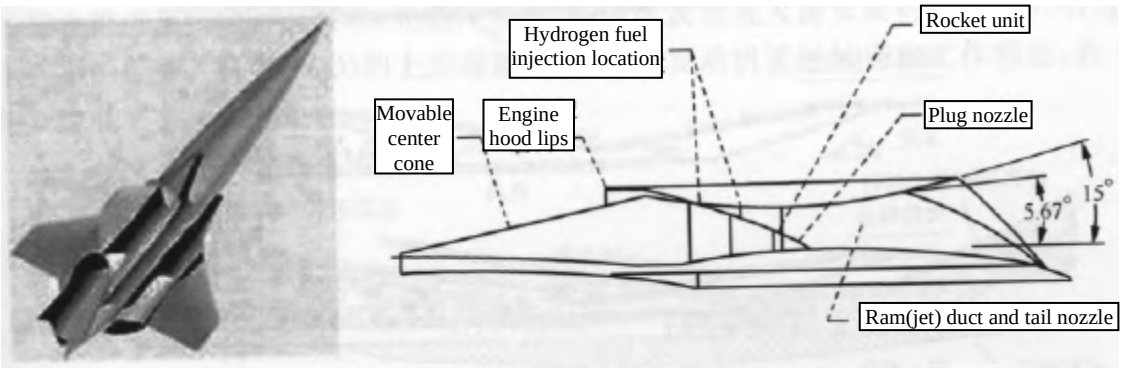

Figure 4-2: NASA's GTX vehicle and its launch mechanism

The engine was proposed and manufactured by the American company Aerojet [4], which was later planned for the X-43B with the ISTAR (Integrated System Test of an Airbreathing Rocket) engine. The advantage of this configuration is that the support plate can be used for a variety of functions, such as flame stabilizer, fuel nozzle, etc., but the disadvantage is that the support plate may bring greater resistance in the supersonic combustion mode (Figure 4-3).

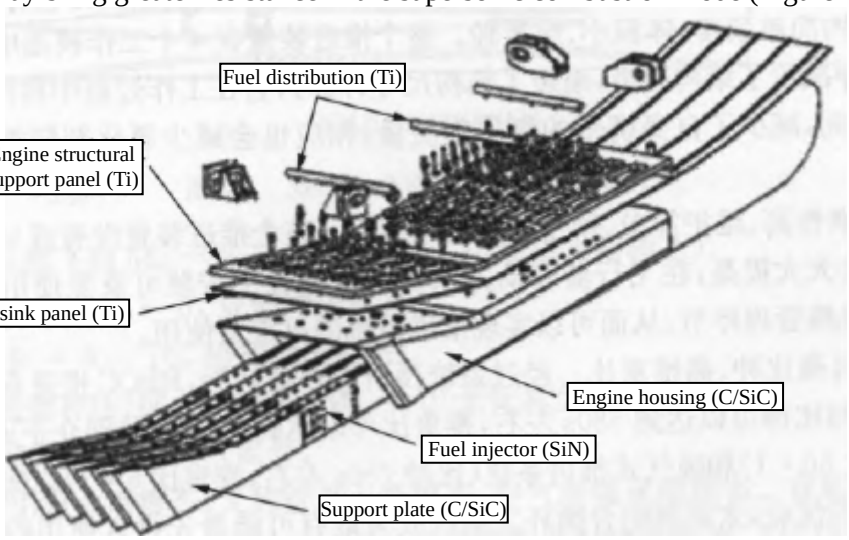

Figure 4-3: RBCC engine of a support rocket

(4) The binary structure configuration of the main rocket mounted on the side wall of the engine.

This configuration was first used in Boeing's A-5 engine, and was also used in the RBCC engine envisioned in Japan. The advantage of this configuration is that the flow channel is unobstructed, and the exit of the main rocket can be well combined with the rocket stabilizer; the disadvantage is that the performance loss of the main rocket is large, and the thermal environment of the engine sidewall is harsh. Figure 4-4 shows the basic structure and working mode of the engine of this configuration. The lead rocket is placed in the upper part inside the engine, and the secondary fuel nozzle is near the engine outlet.

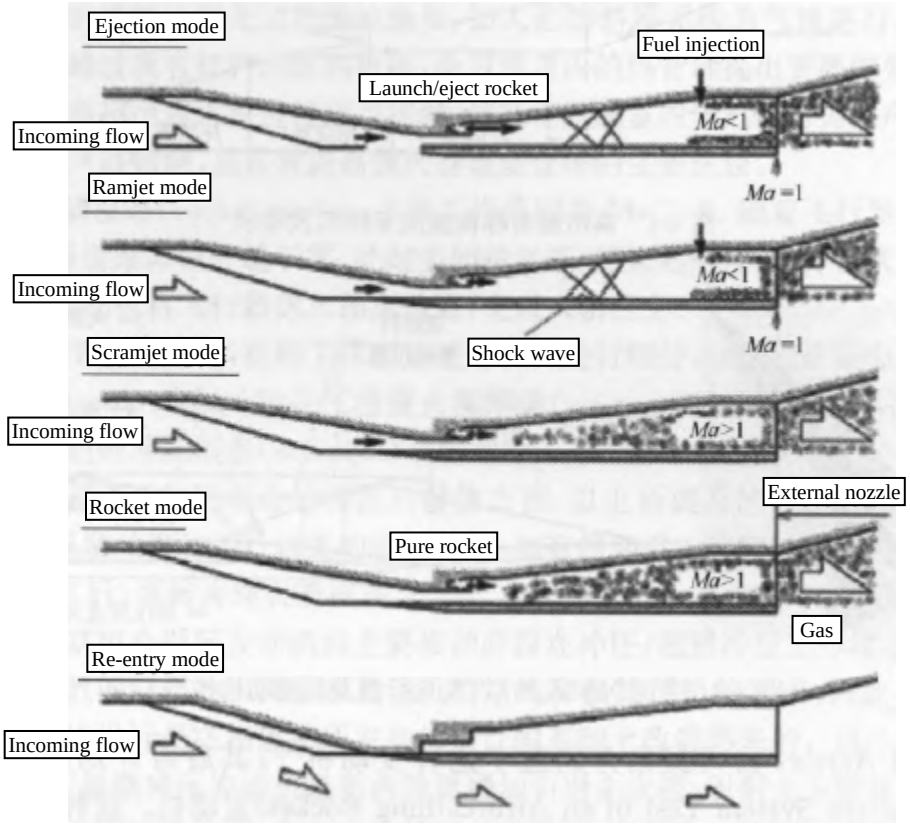

Figure 4-4: RBCC engine of the main rocket with sidewall leading

The reason that rocket-based combined cycle engine has attracted extensive research in various countries is that it has the following three advantages.

(1) Simple and compact structure, small size, and light weight. The entire propulsion unit uses only one flow channel in the four working modes, which reduces the structural mass and shortens the structural size; at the same time, it will use oxygen in the air as an oxidizer in the working process, which reduces the quality of the oxidant it carries, and correspondingly reduces the structural weight and size of the oxidant storage tank.

(2) High reliability, simple maintenance, easy to reuse. There are no or few moving parts in the entire propulsion unit, and the reliability is greatly improved; in the design process of aircraft and power system, the design is carried out according to the requirements of reusability, and the thermal management link is optimized, so that the reuse of the propulsion system can be realized.

(3) It has both high specific impulse and high thrust-to-weight ratio. After the system pre-research and evaluation, it is found that the average specific impulse of the RBCC propulsion system can reach about 580s and the thrust-to-weight ratio can reach 20:1 under typical flight trajectory, which is between the rocket (specific impulse about 430s, thrust-to-weight ratio of 60:1) and the air-breathing propulsion system (specific impulse of about 750s, thrust-to-weight ratio of 6:1).

Because of these advantages, the rocket-based combined cycle engine is the most likely to be the first to be put into service.

4.1.2: Structure and principle of RBCC initiated by support plate

Among the many RBCC structural configuration schemes, the support plate injection (strutjet) engine of Aerojet Company of the United States is the most attractive one, and its outstanding feature is the integrated structural design and modular design technology of engine air intake/secondary combustion chamber/nozzle, multi-modal succession, and smooth conversion between various modes.

Liquid hydrogen is used as fuel for all cycles of the plate-driven engine, and liquid oxygen and oxygen in the air are used as oxidizers. The reason why this new propulsion system is a support plate injection engine is that the support plate is its core component and plays an important role in the whole working process. The support plate is placed in front of the entire flow path of the engine, which can achieve a number of functions, such as the compression of incoming air, the isolation of the intake tract from the combustion chamber, the arrangement of the nozzle of the subsonic combustion ramjet / scramjet fuel, the installation of the pilot rocket, etc. Structurally speaking, the support plate injection engine is mainly composed of side plates, top plates, bottom plates, and support plates, as shown in Figure 4-5. The entire propulsion system is a close combination of pipeline rocket, subsonic combustion ramjet/scramjet and conventional rocket engine. For a typical single-stage to orbit (SSTO) ascent trajectory, the support plate priming engine goes through five working modes, each of which transitions smoothly between each other.

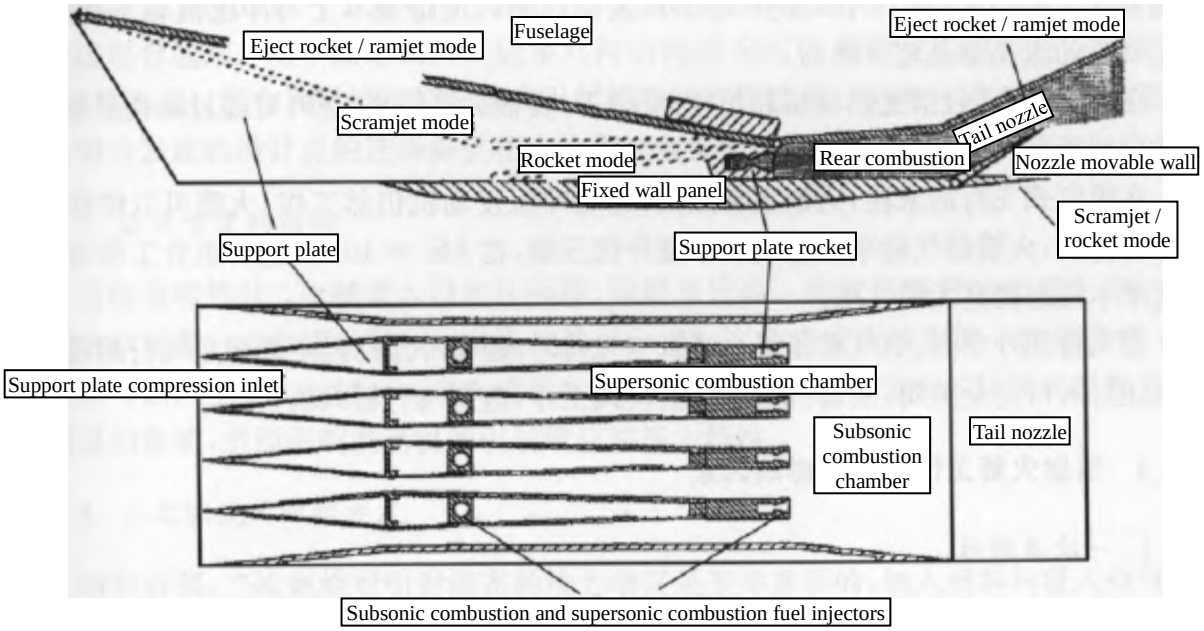

Figure 4-5: Aerojet's plate-driven engine

Mode 1: From take-off to *Ma* = 2.5, launch rocket mode (pipeline rocket mode).

Mode 2: *Ma* = 2.5 to 6, subsonic combustion ram mode.

Mode 3: *Ma* = 6 to 10, supersonic combustion mode.

Mode 4: Scramjet/pure rocket mode, *Ma* = 10 to low vacuum.

Mode 5: Pure rocket mode, outside the atmosphere.

Mode 1 is the induction rocket mode, also known as the pipeline rocket mode and the air enhancement rocket mode. In this mode, through the additional fuel injection and combustion tissue, it is possible to obtain higher thrust and specific impulse than a pure rocket, accelerating the vehicle to *Ma* = 2.5. The thrust enhancement of the launch rocket mode is about 10% at take-off and can reach 100% by the time the ramjet mode takes over. After the flight speed reaches the relay point, the subsonic combustion ram mode takes over. There are two combustion structures in the ejector-ram mode:

diffusion and afterburning (DAB) and simultaneous mixing and combustion (SMC). In the case of DAB, the chemical yield ratio of the primary rocket jet produced by the rocket is sufficiently mixed with the secondary stream and then the downstream jet fuel is combusted; in the case of the SMC, when the rich-burning rocket began to work, the chemical reaction took place simultaneously with the mixing, and no additional fuel was added. The study of the working process of the launch rocket mode is the focus of RBCC engine research.

During the transition to the subsonic combustion ramjet mode, the ramjet fuel nozzle begins to work. As the flight speed increases, the air captured in the intake tract increases, and the air and the injected fuel produce intense subsonic combustion. At this time, the support plate rocket stops working, and the pressure of the combustion chamber is adjusted by adjusting the tail plate (nozzle flap) of the nozzle, and the geometry of the engine is the same as that of the launch rocket.

When $Ma = 5$, if the incoming flow is reduced to subsonic velocity and then combustion, it is necessary to compress the incoming air more strongly by the shock wave in the inlet channel, resulting in a large increase in entropy, causing a serious loss of total pressure, and putting forward higher requirements for the cooling system in the overall flow channel. Therefore, the geometry of the inlet is changed, and only the inlet is used to properly compress the hypersonic incoming flow, so that it remains supersonic at the inlet of the combustion chamber, and the supersonic combustion is directly organized in the combustion chamber. In scramjet mode, except for the partial closure of the inlet, the inner flow channel of the engine is basically similar to that in the ramjet mode, and the flow of the entire engine is supersonic throughout.

In the ram mode (including subsonic combustion ram and scramjet), the support plate rocket stops working and can adapt to changes in the amount of captured air by adjusting the fuel flow.

At the end of the air-breathing flight, the rocket is re-ignited, the scramjet engine is still working, the rocket can improve the scramjet performance, the rocket gas gives an additional compression of the incoming air, and at $Ma = 10$, this combined operation can improve the performance by about 2 times compared to the single modality.

When flying into outer space, the aerodynamic pressure is very small or the vacuum is flying, the scramjet can no longer meet the power demand of the flight, at this time, the inlet is completely closed, and the engine works in pure rocket mode until the aircraft enters orbit [4~7].

4.1.3: Factors influencing the working performance of the launch rocket

1. Primary stream characteristics

The connotation of primary flow characteristics includes mass flow rate, outlet static pressure, outlet Mach number, injection angle and expansion state, and epitaxy includes the number and layout of primary nozzles. The primary flow is the power source that produces the initiation effect, and the gas generator as the initiator discharges the high-speed gas into the pipe (mixing chamber), and the induction and suction effect is caused by the pressure difference and viscous shear force, and the air is introduced from the inlet tract. Because of this, the primary flow parameters strongly influence the secondary flow. Under static conditions at sea level, the mass flow rate of the secondary stream is strongly dependent on the working state of the primary rocket, regardless of the size of the primary rocket. For the outlet pressure of the fixed primary nozzle, with the increase of the outlet Mach number, the mass flow rate of the secondary flow increases, the flow ratio decreases, the mixing effect becomes worse, and the thickness of the mixing layer decreases. For fixed outlet Mach number and static temperature, outlet pressure has little effect on the ejection performance. Studies have shown that there are two types of congestion in secondary flow, namely conventional surface congestion and Fabri congestion. When the flow is confined to a minimum area, a conventional congestion is generated, which is conceptually equivalent to the first critical point described above. In the support plate launch rocket, the channel area between the support plate and the wall surface is the smallest, and the conventional congestion occurs here. Since the jet angle and expansion state of the primary flow will produce the aerodynamic boundary, the secondary flow reaches a congestion state between the aerodynamic boundary and the wall, which is the Fabri congestion. In order to improve the working performance of the pilot rocket mode, it is necessary to adjust the primary flow parameters and reasonably use the congestion to achieve a high gas ejection amount.

A deeper understanding of the role of primary flow characteristics on secondary flow requires more in-depth theoretical and experimental research. Since the structure of the primary nozzle has an impact on the ejection effect, the weight and length of the engine, if the liquid two-component injection method is adopted, the combustion of the rocket jet itself becomes a matter of concern, and the reasonable design of the nozzle can make the mixing and combustion completed in the shortest possible time.

2. Geometry of integral injection combustion chamber

Different injection chamber geometries produce different induction effects, as does the thrust generated by the combined engine. Under the condition of static sea level and no secondary combustion, the mixed gas is in a state of expansion in the expanded induced combustion chamber, and the velocity is continuously reduced, and the static pressure of the whole channel is lower than the ambient atmospheric pressure. Despite the fact that this structure produced a good ejection, the thrust level of the engine as a whole was low. The conceptual analysis of the launch rocket showed that in the case of DAB, the adoption of a classic engine structure can produce better thrust performance. The importance of the boost ratio for the performance of the launch rocket is illustrated from two aspects. The consideration of the structure of the ejection combustion chamber should be based on two aspects: in terms of mechanism research, a variety of ejection combustion chamber structures can be designed according to the classical ejector theory, and sufficient theoretical and experimental research can be carried out; in terms of application, since the ejection mode is only a short working stage of the RBCC, the specific structure of the ejection combustion chamber should be combined with the flight trajectory of the combined engine. For RBCCs with fixed secondary combustion chamber geometry, the working performance of the injection mode is improved as much as possible by mixing and combustion structure according to the geometry of the engine design point. Of course, the study of the mechanism of the induction mode also provides a corresponding theoretical and experimental basis for the selection of the design point of the combined engine.

3. The structure of the rear body nozzle

When there is a shrink nozzle, the pressure at the inlet of the secondary nozzle is high, that is, the pressurization ratio is high. The momentum ratio [(exit momentum of the mixture, primary and secondary flow)/primary flow] is higher with a contracting nozzle, which means that under given primary flow conditions, the launch rocket can produce greater thrust. The addition of the secondary nozzle has a significant effect on the pressure and temperature distribution in the flow channel of the injection combustion chamber, which in turn affects the injection effect and thrust characteristics of the engine.

4. The organization of secondary combustion

The results show that secondary combustion is crucial for the thrust enhancement of the induced mode, and the combustion of fuel and inhaled air is the main source of thrust enhancement. The organization of secondary combustion affects the ejection effect, and ultimately affects the structural design and performance of the engine. There are two different views on the preference for fuel injection locations: post-diffusion combustion (DAB) and immediate hybrid combustion (SMC), as shown in Figure 4-6. In the case of DAB, the primary rocket jet and secondary stream generated by the gas generator at the yield ratio are fully mixed and burned in the downstream jet fuel; in the case of SMC, when the fuel-rich gas generator starts working, the chemical reaction occurs simultaneously with the mixing, and there is no secondary fuel injection.

DAB injects fuel and tissue combustion downstream, so it can be optionally heated at the peak of the pressure; the SMC is heated throughout the induction suction and mixing process, so heating may occur at lower effective pressures. At low speeds, the launch process of the launch rocket is a process with a low compression ratio, and the pressurization of the mixing chamber is relatively small, so there is a clear difference between the two working methods in terms of thermodynamic efficiency, and the efficiency of DAB is higher than that of SMC. As the flight speed increases, the secondary flow passes through the inlet tract to create a ramming effect, and the ram compression provides a higher compression ratio and a higher pressure in the mixing chamber, so that at high Mach numbers (Ma = 2 to 3), the difference in thermodynamic efficiency between the two modalities becomes smaller.

Structurally, SMC can lead to a short mixing chamber length, and since the rocket exhaust itself is combustible, fuel injection devices are no longer needed downstream, reducing the structural weight of the engine and the complexity of the system.

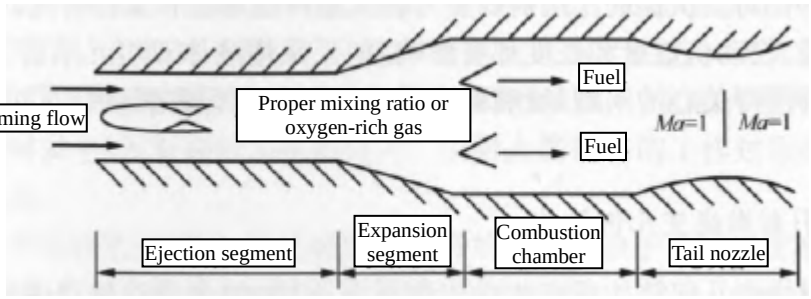

(a) Tandem injection combustion chamber (DAB structure)

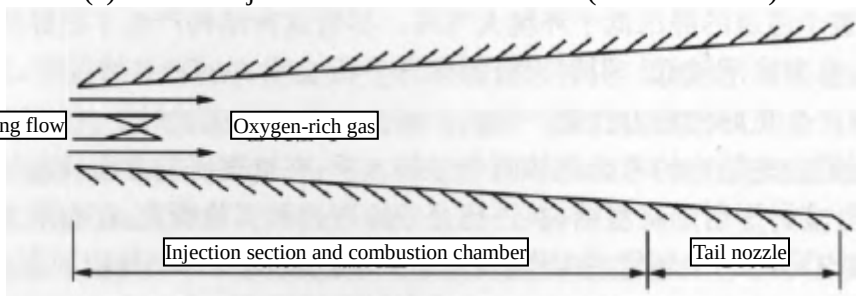

(b) Integral injection combustion chamber (SMC structure)

Figure 4-6: Combustion organization of the launch rocket

DAB is at a disadvantage in terms of engine length, increasing the length and weight of the engine, but the performance of the DAB engine is better, it has an advantage in the transition to the subsonic combustion/scramjet mode, and it avoids the negative thrust enhancement problem that SMC tends to have in the case of low Mach numbers.

DAB and SMC have their own advantages and disadvantages, and when designing the combustion organization, it is desirable to have a short length of the secondary combustion chamber and light structural weight, as well as high efficiency and thrust enhancement. Primary Jet Shielding (SPI) technology concentrates the advantages of DAB and SMC and is currently receiving widespread attention.

The SPI installs the fuel nozzle in the middle of the nozzle of the rocket, and the rocket is in a state of chemical yield ratio. After the fuel is ejected from the nozzle, it is surrounded by a rocket jet, which delays contact with the incoming stream, and this shielding delays the chemical reaction. On the left of Figure 4-7 is the outlet end face of the research model, the turbine nozzle injects fuel, the rocket nozzle discharges a primary stream, and the fuel is shielded by the primary stream after the fuel is ejected, and the fuel injection scheme is adopted by the support plate of Aerojet engine. Figure 4-8 shows a schematic diagram of the primary flow and the turbine nozzle exhaust interfering with and mixing with each other after the SPI method is adopted [8-10].

4.1.4: RBCC engine performance analysis model research

In the field of RBCC engine research, in addition to carrying out experimental research, it also actively carries out numerical simulation research, using solvers including existing general commercial software and self-developed CFD solvers, and computational models include simple one-dimensional performance analysis models and two-dimensional and three-dimensional complex flow field analysis models. After years of development, a series of RBCC software has been developed, and its application scope includes conceptual design and pre-study, including RBCC engine performance analysis, engine mechanism type evaluation and selection, interstage conversion optimization, performance analysis of each modality, etc. The software can be organically combined to form a collaborative working environment, which can be analyzed in detail for a specific flight mission and the overall design of the RBCC engine that meets the mission requirements.

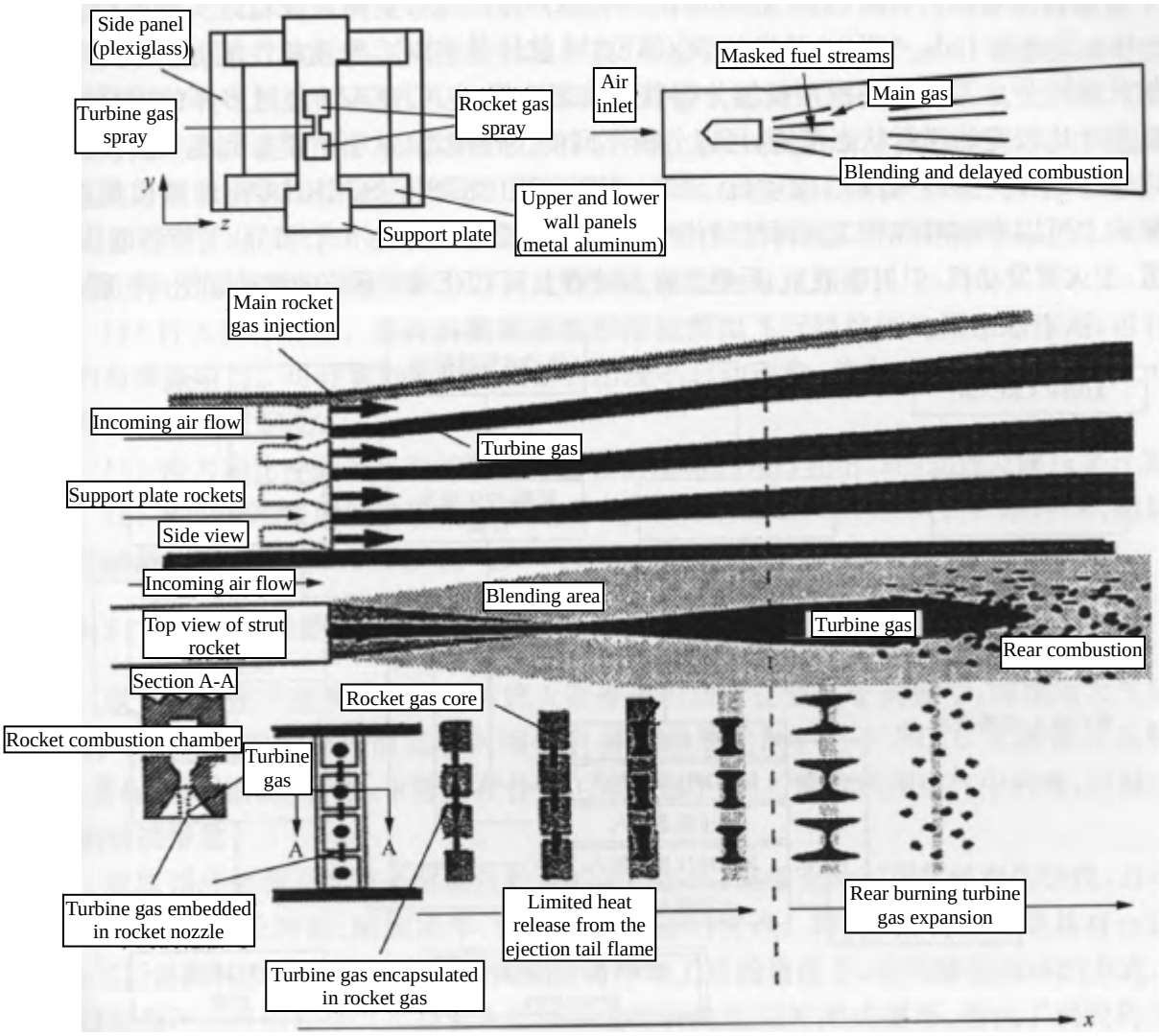

Figure 4-7: Improved combustion organization SPI

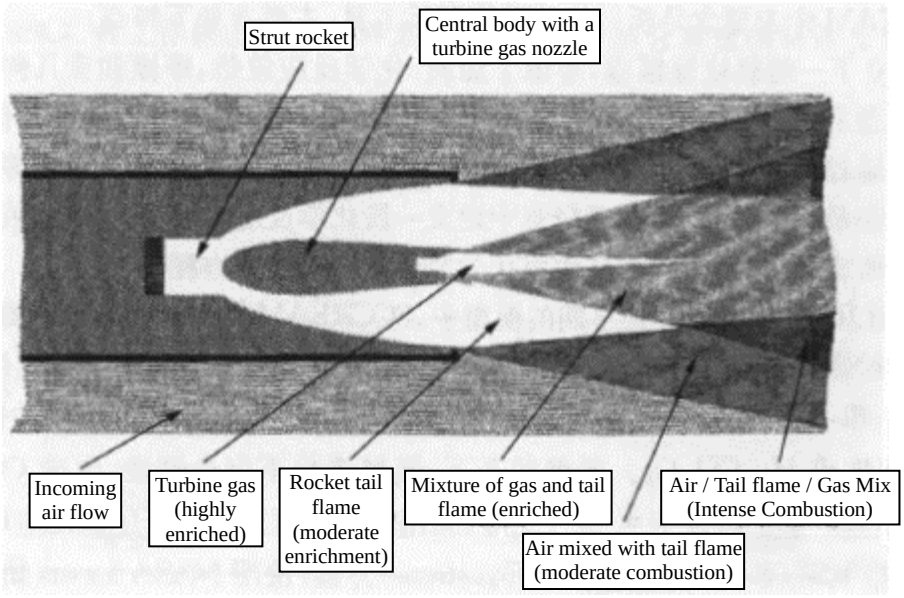

Figure 4-8: Jet interference of the SPI method

The SCCREAM software developed by the Space Systems Design Lab (SSDL) at the Georgia Institute of Technology in the United States is a typical representative of RBCC's engine performance analysis software [11,12]. The original model could only analyze the performance of the trigger mode, but after years of development, SCCREAM can be applied to a wide range of flight states, can analyze different working modes (from the trigger mode to the pure rocket mode), and can simulate four types of RBCC engines: SERJ, ERJ, ESJ, SESJ. The SCCREAM computational model can be axially symmetrical and binary in terms of geometry. According to the function, it can be divided into six parts: aircraft forebody, air intake, main rocket engine, ejection mixing chamber, rear combustion chamber and nozzle. Figure 4-9 shows the structure of the SCCREAM system.

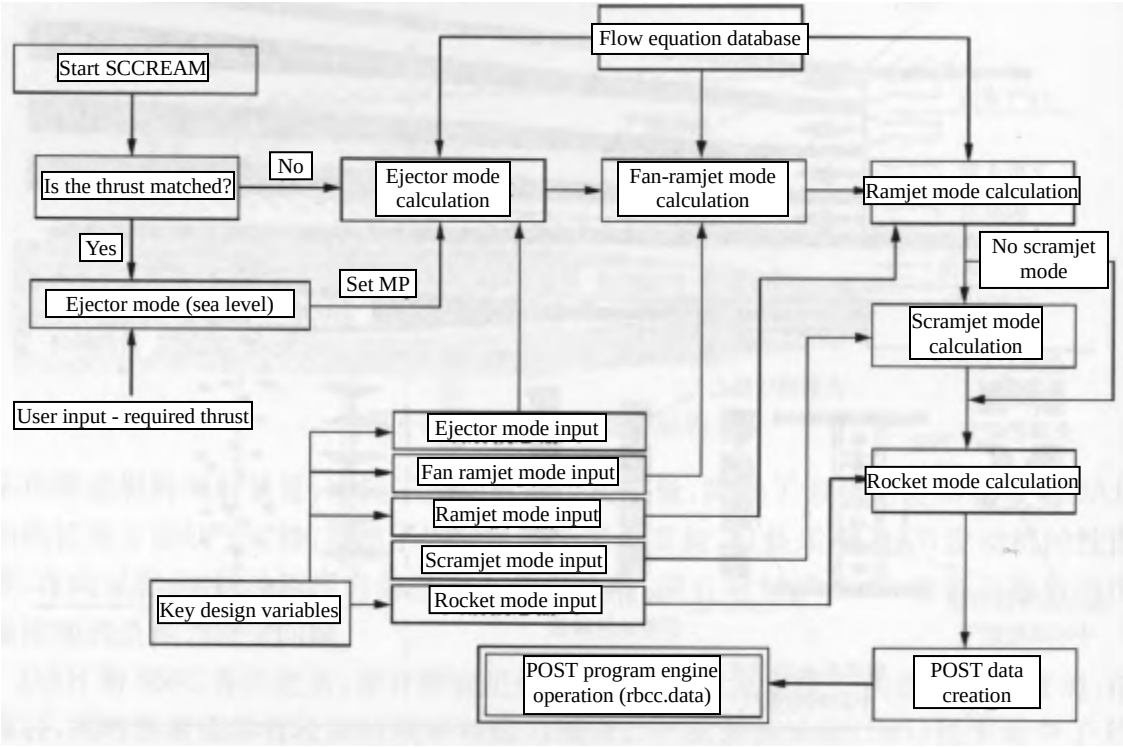

Figure 4-9: Structure of SCCREAM system

As a tool for conceptual analysis and rapid performance prediction, SCCREAM has the following characteristics:

(1) A one-dimensional combustion chamber model is established, which considers factors such as mass addition, exothermic chemical reaction, friction and variable geometric cross-sectional area. The combustion model is solved using the "influence coefficient method," i.e., the Mach number change is solved to solve for other flow variables. The heat of the chemical reaction is indexed into the flow equation by the change in total temperature, and the coupling method is as follows: first solve the total temperature at the end of the chemical reaction and the final composition of the fluid, and then define a exothermic interval of the chemical reaction in the combustion chamber, assuming that the total temperature and the composition of the fluid change linearly in this interval, so as to couple the chemical reaction into the flow equation.

(2) Simplified chemical reaction model: In the earlier model, SCCREAM adopted two different combustion models for oxygen enrichment and enrichment in the aftercombustion chamber. In the oxygen-rich state, a two-step calculation is used: first, it is assumed that the fuel is completely burned and only the final CO2 and H2O are generated; the user then defines an effective coefficient and some of the CO2 and H2O generated in the previous calculation will be decomposed into H2, CO, and O2. In the rich combustion state, the fuel is incompletely burned to generate CO2, CO, H2, and H2O, and the water-gas reaction occurs between these products, and the chemical reaction is calculated by the thermal calculation method.

(3) The Response Surface Equations (RSE) equation was used to calculate the gas composition and other parameters of the main rocket engine under various working conditions (changing the combustion chamber pressure and oxygen/fuel ratio) using the CEA (Chemical Equilibrium and Application Program) program developed by NASA Lewis Research Center.

Then, the coefficients of the RSE equation were calculated by statistical software. In this way, the parameters of the main rocket engine, such as total temperature, specific heat capacity, gas composition, etc., are expressed as a function of combustion chamber pressure and fuel/oxidizer ratio, and the required parameters can be quickly obtained by simply entering the combustion chamber pressure and fuel/oxidizer when calculating. This is useful for problems that require a large number of parameters to be determined and must be calculated for a long time before the results can be determined. The RSE equation is also used in the performance analysis of the rear body nozzle, which expresses the rear body wall pressure as a function of the rear body structure size, flight state and nozzle outlet state, and gives the analytical expression of the rear body pressure distribution through polynomial fitting, so that the pressure integral of the rear body wall can be quickly calculated and the rear body thrust and lift force can be obtained.

(4) Inclusion of forebody effects. By simulating the pre-compression of the aircraft forebody by means of oblique shock or cone shock wave, the lift force and frictional drag can be calculated. It can calculate and judge whether the inlet does not move, and automatically adjust the size of the relevant structure to smoothly realize the inlet start.

(5) Thrust and specific impulse are calculated by analyzing the momentum and static pressure of the engine inlet and outlet by using the control body method.

(6) The propellant that can be used in the main rocket is LH2/LO2, H2O2, CH4/O2, JP-5 (C10H19)/O2, and the fuel injected in the combustion chamber is CH4, JP-5 (C1OH19), JP-10 (C10H16).

4.1.5 RBCC system cycle scheme

The biggest advantage of air-breathing hypersonic propulsion over conventional rocket propulsion is the high specific impulse, that is, the use of oxygen in the atmosphere, rather than carrying its own oxidizer like traditional rocket engines. For the RBCC rocket circulation system, in order to maintain the characteristics of high specific impulse, it is also necessary to use the oxygen in the air as much as possible in each working mode to reduce the amount of oxidant carried.

The expansion cycle is a closed cycle that uses gaseous hydrogen to drive a turbine pump, which can make full use of the characteristics of hydrogen fuel, and does not require an oxidizer, and has the advantages of high specific impulse, simple structure and clean turbine working fluid. Therefore, when the aircraft has a constant speed, the aircraft structure and the engine structure require a large flow of cooling working fluid, the expansion cycle is adopted. The staged combustion cycle is a closed cycle in which the turbine exhaust is directly introduced into the combustion chamber for supplementary combustion, which avoids the shortcomings that the turbine exhaust and calorific value cannot be fully utilized and is also a way to ensure high specific impulse from the overall index of the propulsion system, so the staged combustion cycle should be adopted in the oxidant cycle.

The circulatory system schemes of each working mode of RBCC are summarized, and the following is analyzed with the system cycle diagram (Table 4-1).

Table 4-1: Circulatory system schemes for each operating mode of RBCC

RBCC operating mode	1 Launch rocket mode	2 Ramjet engine mode	3 Scramjet mode	4 Scramjet / rocket mode	5 Pure rocket mode
Mach number range	0~3	3~6	6~10	10~12	>12
Altitude range / km	0~12	12~24	24~30	30~40	40~ into orbit
Engine cycle •Hydrogen fuel •Oxidant	Gas generator cycle, staged combustion cycle	The expansion cycle is non-functional	The expansion cycle is non-functional	Expansion cycle, staged combustion cycle	Expansion cycle, staged combustion cycle

Mode 1: RBCC propulsion system, which accelerates from takeoff to *Ma* = 3 and works in a pipeline rocket projection, with a flight altitude range of 0~12km. The lower support plate rocket engine in this working mode is a propulsion work unit, and the fuel is hydrogen fuel and oxygen-rich gas, which produces combustion-rich gas mixed with air for further combustion. In order to avoid premature combustion of air and gas, which may cause thermal congestion of the engine, in the working process of the Aerojet's support engine, the secondary gas of the gas generator is injected between the primary rocket nozzles at the tail end of the RBCC central support plate, and the primary rocket plume is used to delay the mixing and combustion process of the secondary air flow and the secondary gas flow, so as to improve the combustion efficiency and achieve thrust gain. In order to realize the above working process, the design system circulation mode is shown in Figure 4-10(a), the turbine drive pump transports all the liquid hydrogen to the oxygen-rich pre-combustion chamber and burns with the hydrogen fuel to produce oxygen-rich gas, drives the turbine, and the turbine gas flows to the oxygen-rich gas nozzle of the support rocket. A part of the hydrogen flows into the fuel-rich gas generator, and the generated fuel-rich gas drives the turbine, and all the turbine gas flows to the fuel-rich gas nozzle of the support rocket; after the other part of the hydrogen cools the support plate and the support plate nozzle, it is injected into the hydrogen fuel nozzle of the support plate rocket. Since the support rocket produces rich gas, and the fuel from the turbine is also rich gas, it is necessary to carefully adjust the design of the oxygen-rich pre-combustion chamber, the fuel generator, and the mixing ratio of the support rocket to ensure that the support rocket can work stably.

Mode 2: Acceleration from *Ma* = 3 to *Ma* = 6 with an altitude range of 12~24km in the way a ramjet engine works.

Mode 3: Acceleration from *Ma* = 6 to *Ma* = 10 with an altitude range of 24~30km in the way a scramjet engine works.

As shown in Figure 4-10(b), in order to reduce the loss of specific impulse, hydrogen adopts an expansion cycle mode, liquid hydrogen flows through the turbine pump, flows through the fuselage parts and engine parts of the aircraft that need to be cooled, generates gas hydrogen through each heat exchanger to drive the turbine, and the gas hydrogen flowing out of the turbine is sprayed into the combustion chamber through the subsonic combustion/supergas hydrogen fuel nozzle according to the flight conditions and flight status.

Mode 4: At an altitude of 30~40 km, *Ma* > 10, the atmosphere is gradually thinning, and the supersonic combustion working mode is not enough to continue to provide power, so it is necessary to gradually switch to the rocket mode, and at the same time, the air inlet port is gradually closed with the increase of Mach number, and in this conversion process, the work works in a mixed mode of supersonic combustion and rocket. In this working mode, the oxygen circuit supply is restarted to provide oxygen-rich gas for the support rocket, and the hydrogen fuel supply is still carried out in the form of expansion cycle. All the liquid oxygen flows into the oxygen-rich pre-combustion chamber, and the oxygen-rich gas generated drives the turbine, and the oxygen-rich gas discharged from the turbine is then injected into the support plate rocket through the oxygen-rich gas nozzle; part of the liquid hydrogen enters the oxygen-rich pre-combustion chamber, and the other part flows through the parts that need to be cooled, and the gas hydrogen is generated through the heat exchanger to drive the work of the hydrogen turbine pump, and the part of the gas hydrogen discharged from the hydrogen turbine continues to supply the super-gas hydrogen nozzle, and the other part is injected into the support plate rocket engine through the gas hydrogen fuel nozzle. The supergas hydrogen flow rate gradually decreases, and the gas hydrogen flow rate of the support rocket gradually increases, gradually changing to the working mode of the complete rocket.

Mode 5: More than 40km, the atmosphere is thin, and the traditional rocket mode is used to accelerate the vehicle into orbit. The supergas hydrogen fuel is completely shut down, and its cycle and supply are the same as in mode 4, as shown in Figure 4-10(c).

According to the cycle scheme of the above-mentioned working mode system, under modes 1, 4 and 5, the working state of the support plate rocket is different, and the mixing ratio of the support plate rocket engine needs to be adjusted according to the different working modes from the generation of rich combustion gas to the pure rocket operation. Similarly, in modes 1, 4 and 5, the oxygen-rich pre-combustion chamber also needs to adjust the mixing ratio according to the different flight states to produce different proportions of oxygen-rich gas, so that the support plate rocket engine can work effectively.

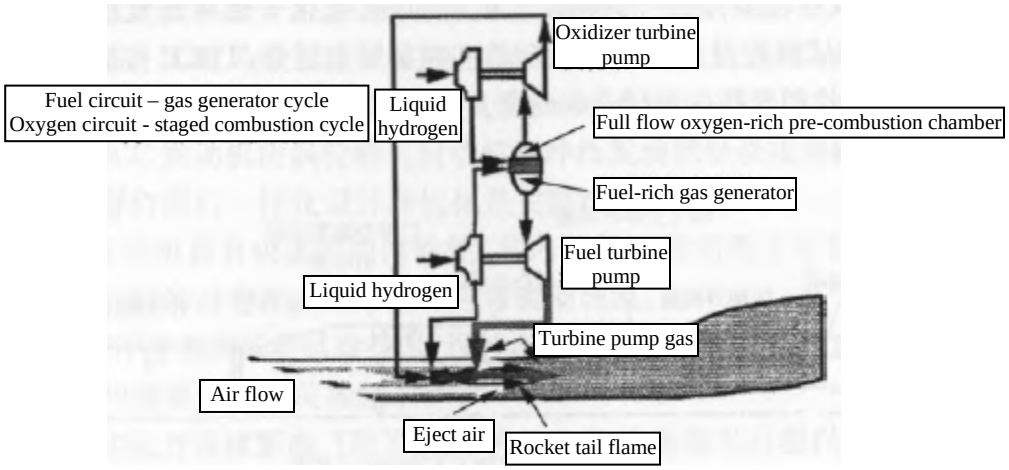

(a)

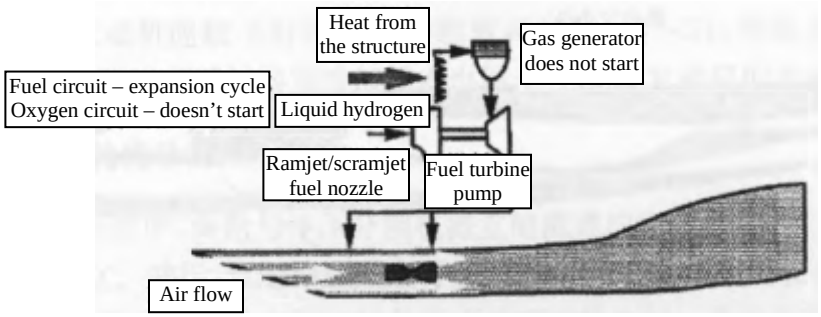

(b)

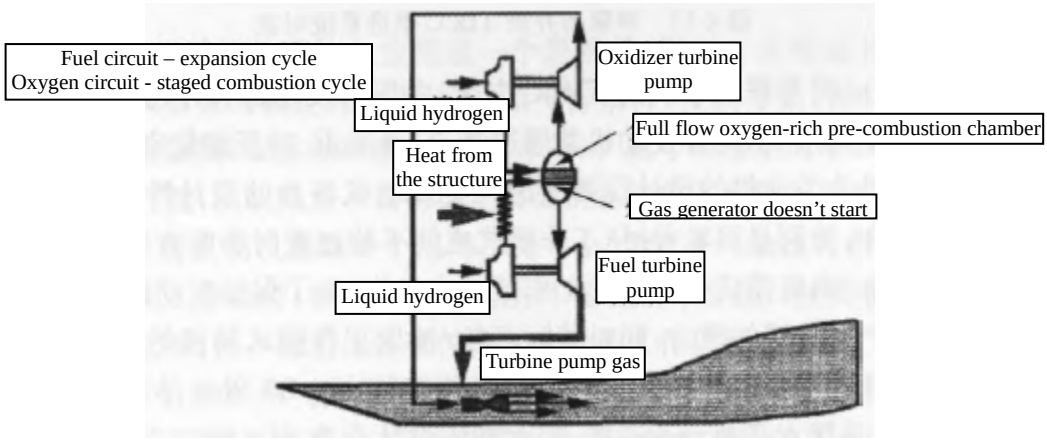

(c)

Figure 4-10: RBCC engine circulation system scheme

4.2: Turbine-based combined cycle engine propulsion system (TBCC)

4.2.1: TBCC System Scheme

Compared with RBCC, the aircraft with a maximum flight Mach number of less than 6 adopts the TBCC propulsion system, which has better economic performance. In the low-speed segment of the flight trajectory, the turbine engine is used to provide power, which is an order of magnitude greater than the specific impulse produced by the rocket boost.

TBCC is mainly a combination of gas turbine engine and ramjet (including subsonic combustion ramjet engine and scramjet engine). In terms of the layout of turbine engines and ramjet engines, TBCC propulsion systems can be roughly divided into two categories: coaxial and over/under. Figure 4-11 shows a comparison of series and parallel TBCC engines [13~16].

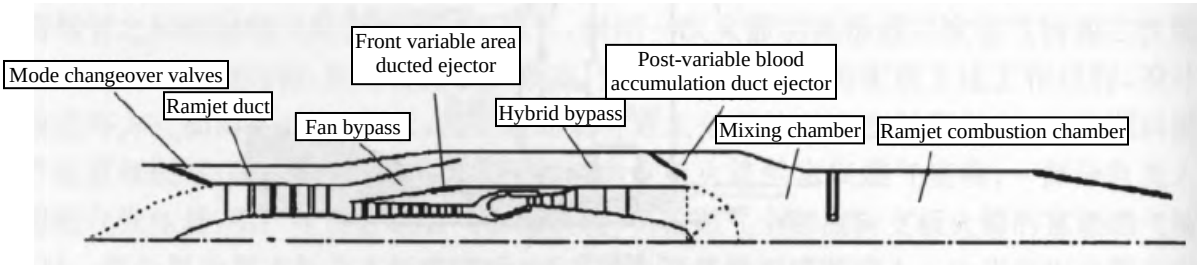

(a) Schematic diagram of the structure of the tandem layout TBCC scheme

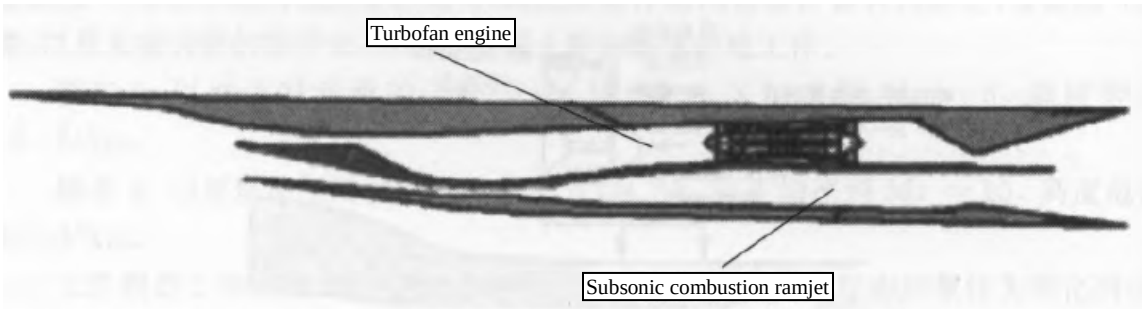

(b) Schematic diagram of the structure of the TBCC scheme with parallel layout

Figure 4-11: Comparison of tandem and parallel TBCC propulsion systems

Figure 4-11(a) shows a tandem TBCC scheme, which is composed of a turbofan engine and a ramjet engine, and adopts a coaxial front and rear placement structure, and the two engines share an air intake, an outer duct, a ramjet combustion chamber, and a nozzle. The characteristics of the tandem scheme determine that the design of this combined engine should not only consider the design characteristics of the two types of engines, but also take into account the system integration of the two types of engines, especially the key issue of the feasibility of the tandem scheme when the smooth transition between the turbine/ramjet working modes is carried out. In order to ensure that the engine can generate sufficient thrust at the most severe high-altitude Mach number under the most severe conditions, and at the same time take into account the stability of the turbine/ramjet working mode transition, the design point is selected in the Ma = 3, H = 20.9km climb state. The ramjet mode first climbs from H = 20.9 km, Ma = 3 to 28.3 km, Ma = 5, and then switches to hypersonic cruise, so the ram design point is H = 28.3 km, Ma = 5 climb state. In order to ensure that the above-mentioned working state can be reliable and stable and have good performance, the variable cycle engine scheme is adopted, and the engine is jointly controlled and optimized to work stably and reliably within the full envelope range through five variable geometric position adjustments, plus turbofan engine fuel regulation and ramjet engine fuel regulation. The 5 variable geometries of the tandem scheme include the low-pressure turbine variable pilot area, the 2D nozzle throat area, the front variable area duct injector, the rear variable area ducted injector, and the mode transfer valve.

Figure 4-11(b) shows a parallel layout of the TBCC scheme, in which the conditions for the conversion from turbofan mode to ram mode are Ma = 2.5 to 3.0. Before Ma = 2.5, the turbofan engine worked alone; when Ma = 2.5, the turbofan engine begins to turn into a throttling state, and the ramjet engine ignites; when Ma = 2.5 to 3, the turbofan and ramjet engine work together; after Ma = 3, the turbofan engine is switched off and the ramjet engine works separately. In order to ensure a smooth transition between turbofan engine and ramjet engine, the combined thrust provided by the two engines needs to be guaranteed to meet the demand thrust during the conversion process.

TBCC combined propulsion technology is a complex system engineering, and there are complex coupling relationships between the whole and the part, and between the part and the part. Whether it is to independently study a single component of the propulsion system or to study the overall performance of the engine, there are some technical difficulties. The key technologies of TBCC engine can be summarized as follows:

(1) Since the TBCC engine is composed of a turbojet engine and a ramjet engine in series or parallel, the integrated design and optimization of the two engines and their components is one of the key technologies.

(2) The internal airflow of TBCC engines is unsteady because of its fast acceleration performance, so it is important to consider the phenomenon of unsteady flow in the design of engine components.

(3) Based on CFD technology and wind tunnel test technology, the design of the air inlet with light weight, good adjustability, and wide adaptability is the key technology that needs to be solved in the study of the air intake.

(4) Since the rear body resistance directly affects the installation performance of the TBCC engine and the acceleration of the aircraft, the tail nozzle with low rear resistance is the key technology in the tail nozzle design.

(5) The high Mach number (Ma = 3 to 5) of the TBCC engine during cruising flight leads to a high inlet temperature of the engine, so the high-temperature resistant materials and cooling technology of the corresponding components are also one of the key technologies of the TBCC engine.

4.2.2: Mathematical model of the TBCC turbine engine

In the TBCC propulsion system, the turbine and the ramjet work in separate flow channels, so the working modes are relatively independent of the RBCC modes. The ramjet/scramjet mode can be calculated according to the previous chapter on scramjet engines, and the turbojet engine is the most complex and relatively independent subsystem of the thermal cycle, and its mathematical model can be divided into the following four types.

Type I model: The engine as a whole is treated as a black box, with the help of tables or fitting relationships to describe engine performance. The input parameters are the determined working state (such as flight conditions, control schemes, cycle parameters, etc.), and the output parameters are the characteristic data of the engine (such as engine thrust, fuel consumption rate, etc.). This model is the simplest and can obtain the steady-state performance of the engine very quickly, but the disadvantage is that it does not have the ability to describe the operation of the various components of the engine.

Type II model: each part of the engine is used as a "black box," the component characteristics of each component are given, and the aerothermal parameters of the import and export of each component are determined according to the common working conditions of the engine components. This type of model is often used to optimize the selection of engine design parameters but does not give detailed information about the operation inside the individual components.

Type III model: The flow of each stage of the vane ring is calculated according to the average middle diameter by directly using the main geometric dimensions of the airflow channel, and the relationship between the feature size, design parameters and aerodynamic characteristics of the component is given in detail. This type of model includes both the calculation of aerothermal parameters and the verification of the load strength of the stressed components.

Type IV model: The dimensions of several radii in several dimension vectors are counted as components to calculate the air flow field in the blade ring, including the full three-dimensional calculation of the flow field of the blade grid channel and the calculation of the stress field of the blade disc using the finite element method.

For these four models, the complexity and computation time of the adjacent levels increased exponentially. At present, with the rapid development of computer technology, except for the fourth type of model, which requires a long time of calculation, the first three types of models can realize the rapid completion of the calculation process. From the need to consider the overall modeling of the propulsion system, the second type of mathematical model can be used to complete the calculation of engine performance parameters, and the complexity of the model is greatly reduced compared with the third type of model. Therefore, it is more appropriate to choose the second type of mathematical model as the modeling method for the overall performance of turbojet engines. In addition, considering that in the same system, the mathematical models of different subsystems should have the same accuracy, so as to ensure the compatibility between the parts of the system. Therefore, the second type of mathematical model should also be used to describe the working characteristics of the ramjet engine circulation system.

The principle of modeling turbine engine components is to separate each part of the engine for aerothermal calculation, and then express the common work of the engine into a set of nonlinear aerothermal equations according to the aerothermodynamic laws that must be observed in the working process of the engine. According to the characteristic data of the engine object parts provided, the dynamic and static mathematical models that can describe the working process of the engine are established according to the aerothermodynamic method and the rotor dynamics equation. After establishing a model of mathematical logical relationships, simulating the "operation" of the engine is essentially a solution to a system of common work equations. The solution of the model boils down to solving a set of equilibrium equations that reflect the aerothermodynamics and rotor dynamics that must be met in order for the various components of the engine to work together. A common method for solving such nonlinear equations is the Newton-Raphson method, which is based on empirical knowledge to first give a set of initial values of the system of equations, then search in the direction of partial derivatives, and continuously correct the initial values through iteration to make them approximate the true solution of the system of equations.

The cost of establishing a model to meet the practical application requirements by using this method is relatively small, and it has a certain guiding role in the conceptual research of the new engine cycle and the selection and design of the new engine model, but it needs to be based on the mature theoretical knowledge of the physical process of the aero engine, and at least a complete set of working characteristic data of the engine components needs to be mastered.

4.2.3: TBCC intake and exhaust system

1. The working principle of the air intake system

Figure 4-12 shows the air intake system of the TBCC propulsion system in parallel. The air inlet is a single-inlet, dual-channel variable geometry. Among them, the compression surface CDEF is a movable mechanism, and the manifold MN can rotate around the *N* point, and the air inlet channel is diverted at the *M* point and enters the ramjet engine and the turbine engine, respectively. Under different engine working modes, the working situation of the intake tract can be briefly described as follows: in the design state, the compression wave system of the outer compression section is attached, and all the flow of the flow rate of the interception section Ac enters the inner flow channel by capturing the cross-section, the manifold MN is completely closed downward, and the ramjet engine works separately.

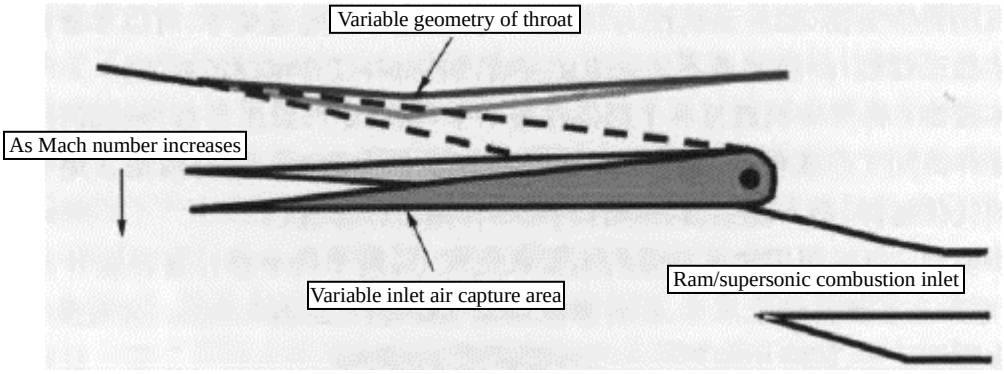

(a) Schematic diagram of the inlet structure

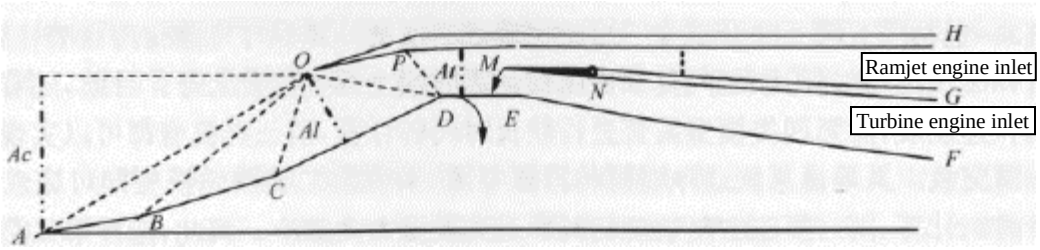

(b) Schematic diagram of the inlet structure

Figure 4-12: Schematic diagram of the parallel air inlet structure in the TBCC propulsion system

In the transitional working state, the manifold is opened to the position shown in Figure 4-12, and the internal compression surface DE moves downwards at the same time, increasing the area of the inlet throat, and the upper and lower two flow channels are opened at the same time, and the two engines work together; when the flight Mach number is low, the manifold MN is completely closed upward, and the DE continues to move downward, then the ramjet engine exits the working cycle, and the turbine engine works alone. Under different engine working modes, the inlet duct adjusts the critical cross-sectional area through the inner compression plate DE to control the Mach number of the throat, and controls the flow distribution ratio of the upper and lower flow channels by changing the position of the manifold MN.

2. The working principle of the exhaust system

The TBCC propulsion system with parallel upper and lower layout usually uses two flow paths to exhaust asymmetrical expansion nozzles, as shown in Figure 4-13. As with the intake tract design, the nozzles of the combined engine are often designed with variable geometry in order to operate over a wide range. When the engine condition changes, the cross-sectional area of the upper and lower channel outlets can be adjusted by changing the geometrically adjustable wall plate in the flow path, so as to realize the throttling control of the engine. When the engine working state changes, the throat area of the two flow channel outlets of the nozzle can be adjusted, which increases the degree of freedom of the nozzle working condition change. For this dual-channel nozzle, the two jets will inevitably mix with each other in the transitional operating state, resulting in a more complex outlet flow field.

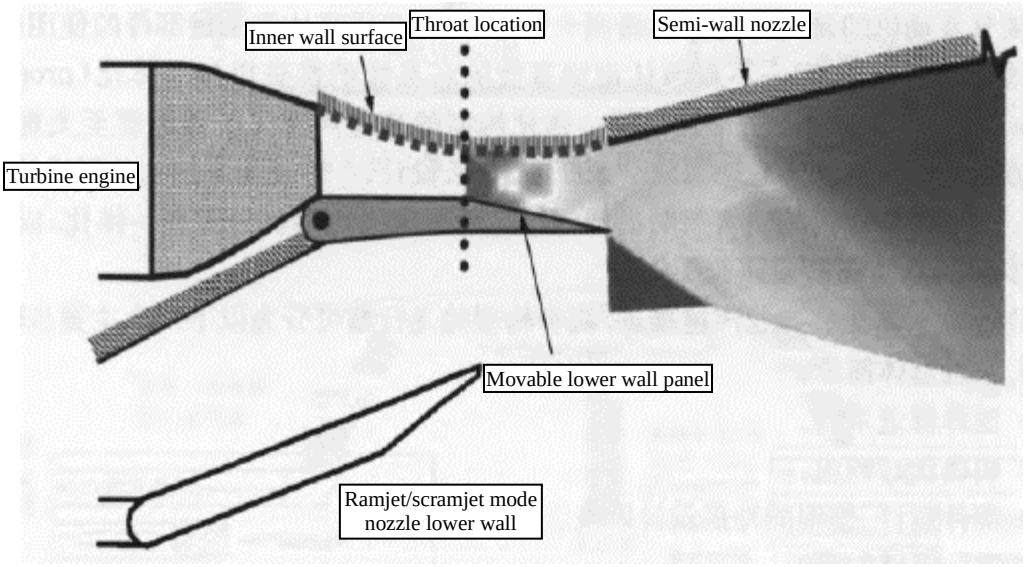

Figure 4-13: The asymmetrical nozzles are vented separately in dual flow paths

When establishing the calculation model of the nozzle in the transition working mode, it is necessary to consider the influence between the upper and lower channels. When the upper and lower engines work at the same time, a slip interface is generated between the two jets at the outlet. In the nozzle modeling, it is assumed that the slip plane is axially parallel to the engine and remains in the same direction, while the mixing of the air flow on both sides of the slip surface is not considered. The effective projection area of the turbine engine outlet is A9_up, and the effective projection area of the ramjet engine outlet becomes A9_down, so that the upper and lower outlet channels are calculated separately according to the changed nozzle outlet spray ratio, and Figure 4-14 gives a schematic diagram of the working state of the engine tail nozzle under the transitional working mode.

4.2.4: Integration of the TBCC propulsion system with the fuselage of a hypersonic vehicle

Due to the limitations of the temperature that the material can withstand, the limit of the turbojet engine that has been applied today is *Ma* = 2.5 to 3. Some research institutes, represented by the United States, are working to develop a new type of turbojet engine, which is also a key technology for future hypersonic vehicles.

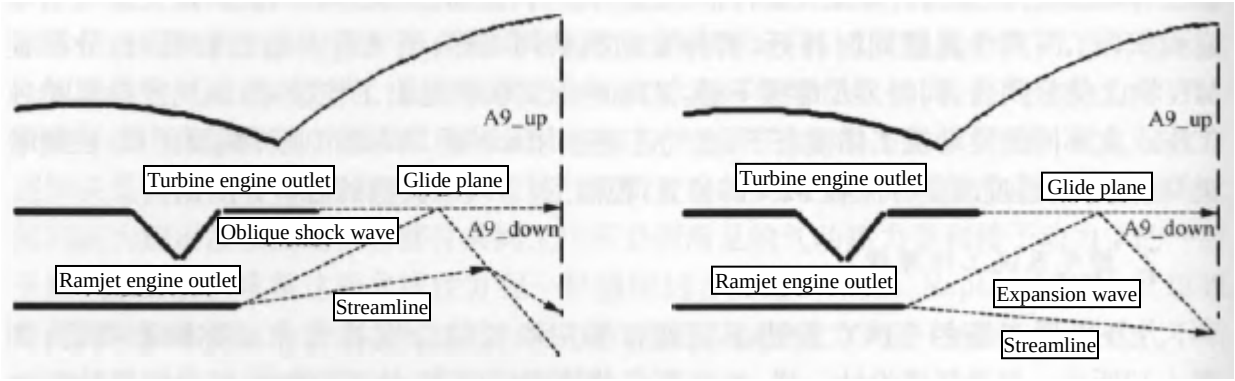

Figure 4-14: Schematic diagram of the working state of the nozzle under the transitional condition of the TBCC engine

Research activities include the New Turbo Accelerator (RTA) project at NASA's Galen Research Center in the United States, the Integrated High Performance Turbojet Engine (IHPTET) project at the U.S. Air Force Laboratory AFRL, and NASA's High Mach Number Turbojet (HIMATE) project, whose research goals are to increase the maximum Mach number of turbojet engines to more than 4 and improve the thrust-to-weight ratio and service life of key components. The development of these projects has gradually recognized the critical role of an effective and systematic propulsion/airframe integration (PAI) approach to the development of hypersonic vehicles in an integrated configuration. The approach must effectively combine the overall requirements with the system selection, design, integration, and detailed form factor design considerations. This section describes how turbojet engines can be integrated into hypersonic vehicle fuselages, and how research work can be carried out through a multi-step PAI approach.

Building a highly integrated hypersonic propulsion/airframe configuration for a vehicle can be broken down into the following six main steps.

(1) Clarify the overall needs.

(2) Select the propulsion system.

(3) Clarify design constraints.

(4) Component design, detailed shape design and the integration of the two.

(5) Aircraft performance analysis.

(6) Evaluate the design results and iterate.

Figure 4-15 shows the flow of this design step. The integration of TBCC propulsion system and hypersonic vehicle includes the selection, design and integration of high-speed and low-speed propulsion systems. For TBCC, the so-called high speed refers to $Ma \geq 4$, and the so-called low speed refers to $Ma < 4$, and $Ma = 4$ is usually the state of transition from low-speed to high-speed operation mode of the integrated propulsion system, that is, the state of transition from turbojet engine propulsion to ramjet/scramjet engine propulsion.

Based on the above-mentioned integrated design method, and in view of the requirements for the speed and acceleration of hypersonic vehicles, the first thing to solve for the TBCC propulsion system is the selection, design and integration of the high-speed propulsion system, because the high-speed propulsion system can affect the shape and flight performance of the aircraft to a greater extent.

Figure 4-16 shows different air-breathing propulsion systems that can be applied to hypersonic vehicles, including air intakes, engines, and tail nozzles, and these different propulsion systems and their components are represented as a function of Mach number. Typically, ramjet/scramjet engines are available at Mach numbers of 4 and above. Figure 4-16 also shows that a highly integrated mixed-pressure inlet and a highly integrated half-wall expansion nozzle are necessary to achieve high performance at high Mach numbers, requiring a length of surface and a large area ratio to provide an effective air flow capture rate, compressive performance, and large tail nozzle expansion thrust.

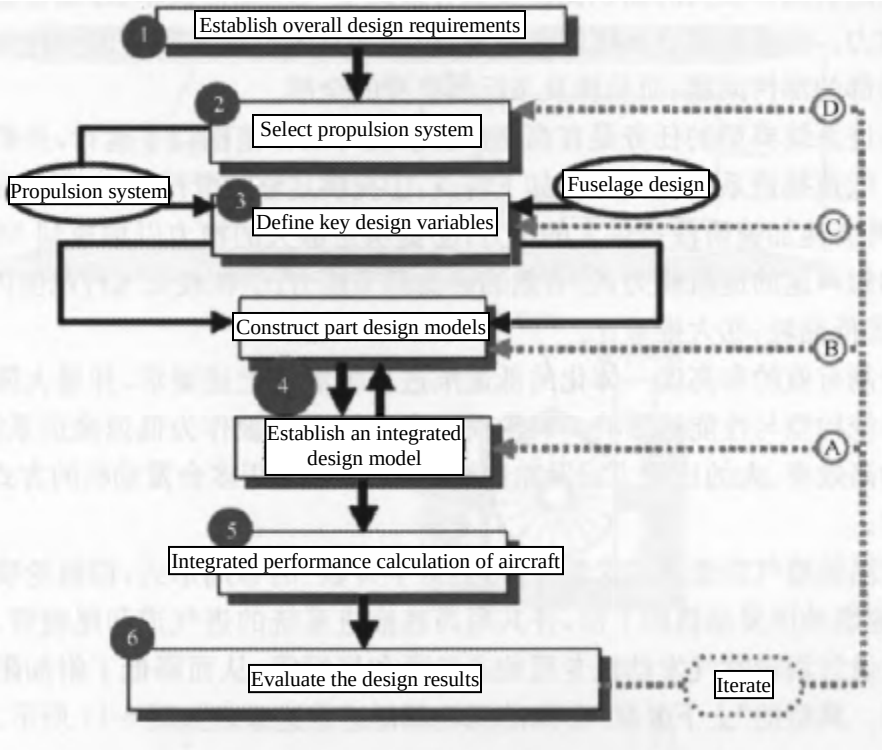

Figure 4-15: Propulsion and airframe integrated design flow

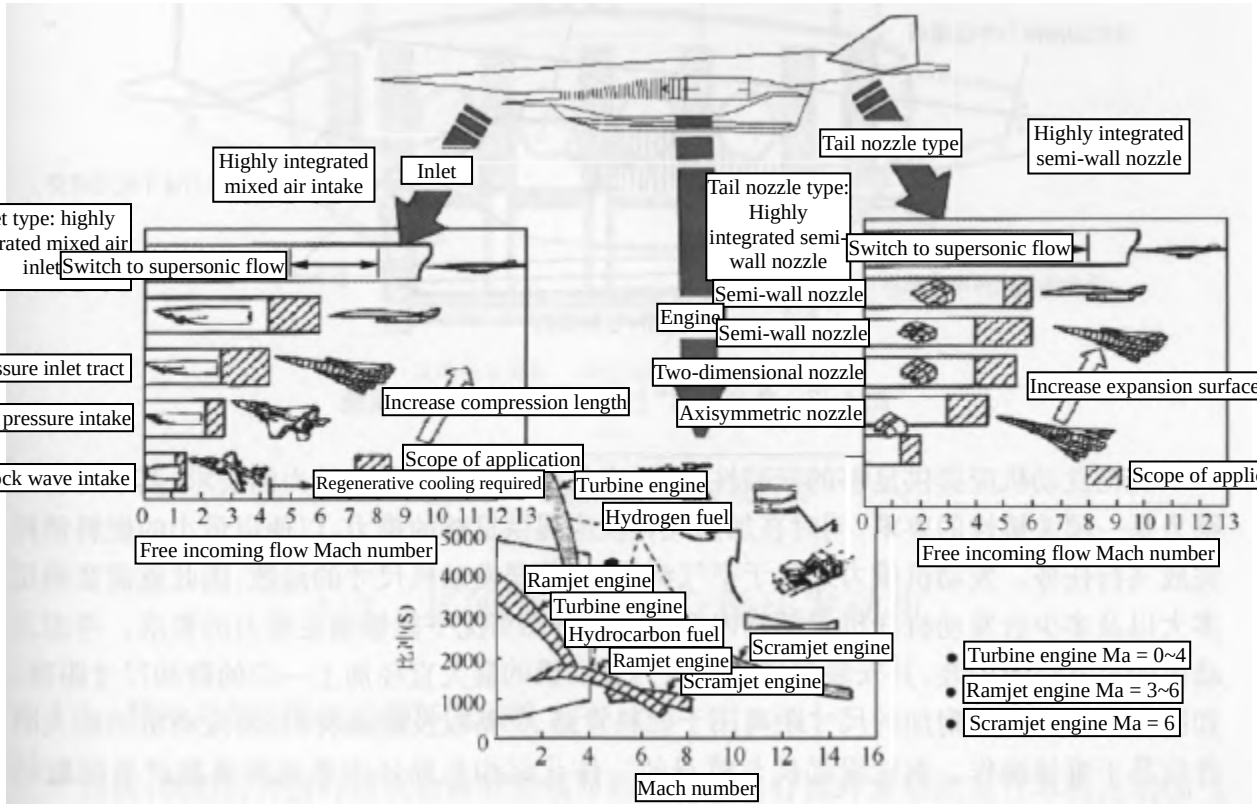

Figure 4-16: Propulsion system option selection

The design and integration of the air intake, scramjet engine and nozzle of the high-speed propulsion system is not just a local component problem but involves the whole fuselage of the aircraft. The typical task of a low-speed propulsion system is to operate below the operating range of a high-speed propulsion system and to extend the flight range of the aircraft. The low-speed propulsion system should have the following characteristics: (1) provide sufficient gliding thrust; (2) provide high thrust during take-off; (3) provide large thrust during the transonic acceleration phase, (4) provide sufficient thrust to accelerate to $Ma = 4$; (5) it has subsonic and supersonic cruising capabilities; (6) effective fuel regulation ability; (7) starting and restarting capabilities in a large flight range; (8) low fuel consumption; (9) large thrust-to-weight ratio.

It is necessary to develop an effective and highly integrated low-speed propulsion system to meet the above requirements and minimize the impact on the configuration and performance of the high-speed propulsion system. Turbojet engines are often used as low-speed propulsion systems, mainly due to their high efficiency, large specific thrust and specific impulse performance, and can be used with multiple engines to meet these requirements.

The typical installation scheme of a turbojet engine is a "top and bottom parallel" layout, that is, the turbojet engine is installed in the upper part of the ramjet/scramjet engine, and shares the intake tract and tail nozzle of the high-speed propulsion system, so that the common use does not need to design the special intake tract and tail nozzle of the turbojet engine, thus reducing the additional drag and the occupation of internal volume. Figure 4-17 shows a typical turbine-based low-speed propulsion system with a "top-down parallel" layout.

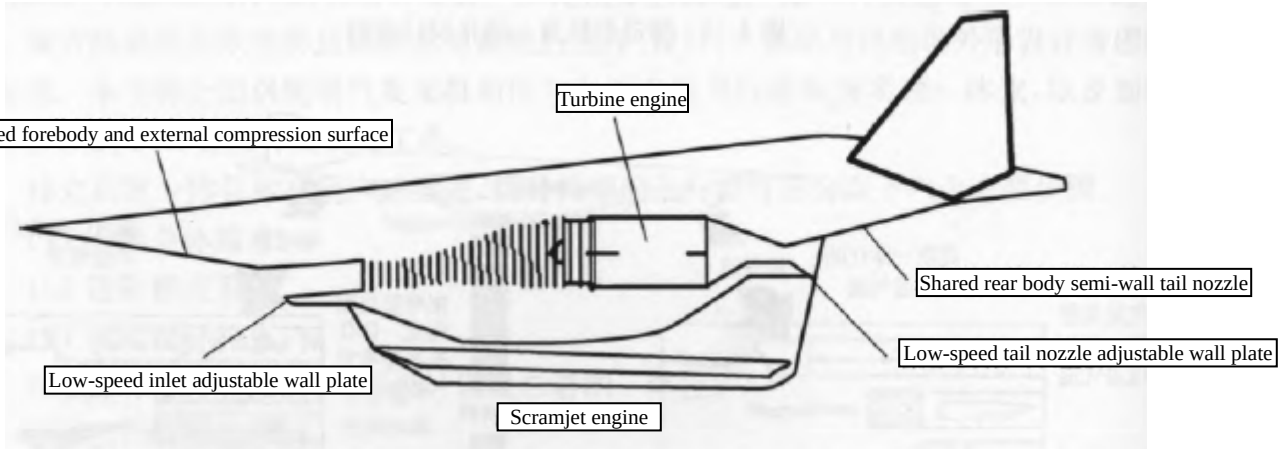

Figure 4-17: A typical low-speed "up and down" propulsion system

The turbine engine should provide sufficient mounting performance to meet the requirements for low-speed propulsion system power, where transonic thrust is a critical requirement, and sufficient thrust during the acceleration flight segment to complete the mission with minimal fuel consumption. Engine thrust is proportional to air flow, which is a function of engine size, so it is necessary to determine how large and how many engines can meet the thrust requirements if the internal layout of the fuselage structure allows. Considering the size of the engine and the installation, the installation envelope should be the maximum diameter of the engine plus a certain additional size distance. As shown in Figure 4-18(a), the additional size distance is used for fuel lines, circuits, and insulating materials, and the relevant accessories of the engine should be easy to maintain and operate. The integrated structure layout of the turbine engine and fuselage should also consider the structure of the high-speed propulsion system, as shown in Figure 4-18(b).

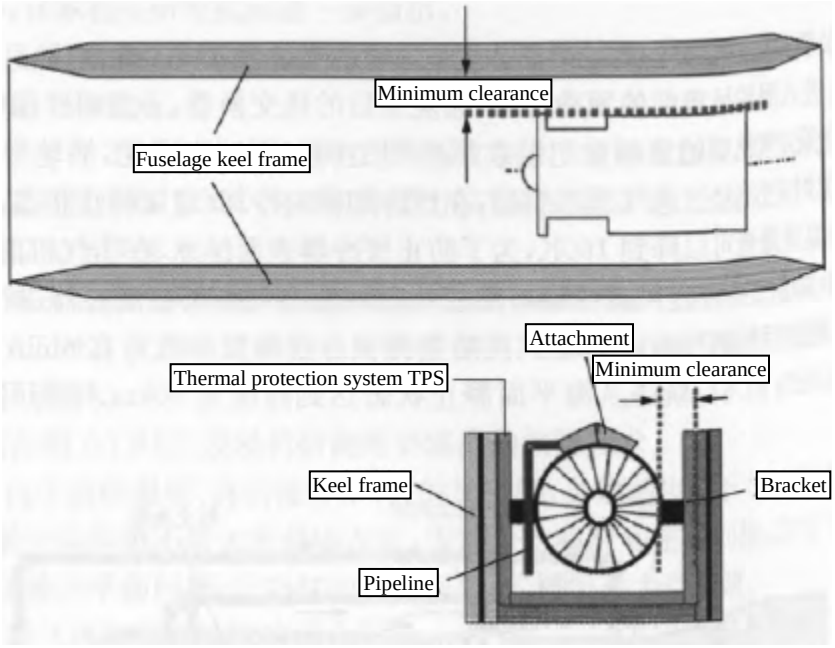

(a)

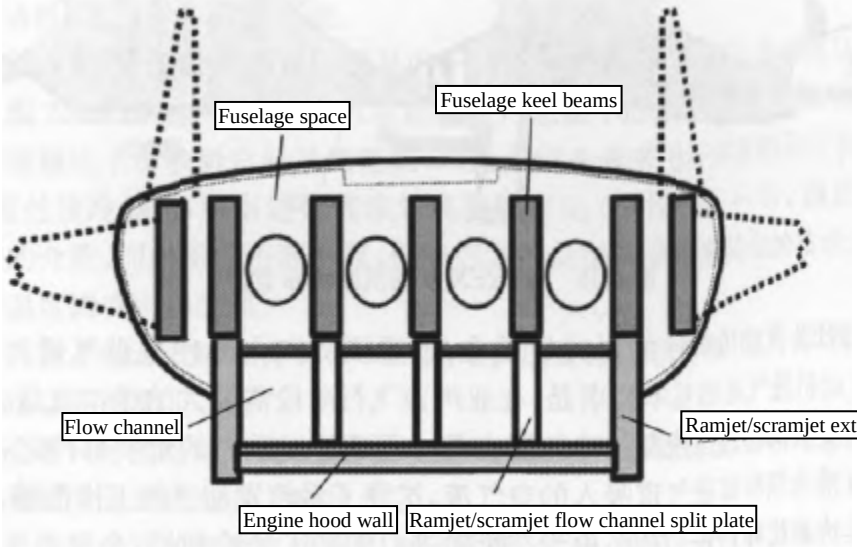

(b)

Figure 4-18: Installation scheme of a turbine engine

4.3: Other types of combined-cycle engines

4.3.1: Pre-cooled turbine-based combined-cycle engine

At present, a typical pre-cooled turbine-based combined-cycle engine with a pre-cooled turbine-based combined cycle engine stomach 0 turboramjet expansion cycle (ATREX) engine scheme has been conducted. Since 1986, the engine has been researched by the Japan Institute of Aerospace Science (ISAS), NAL, NASDA, and several major industrial groups, IHI, KHI, MHI, etc. The goal is to develop a repeatable system into a hypersonic vehicle or two-stage orbit entry (TSTO) [17-24].

The ATREX engine uses liquid hydrogen as the coolant, the gas and fuel to drive the turbine (Figure 4-19). The liquid hydrogen pressurized by the turbopump enters the pre-cooler in front of the turbofan and the heat exchanger behind the combustion chamber to cool the air on the one hand and vaporize the liquefied hydrogen on the other hand. When the engine is working, the air flow is compressed through the inlet tract and cooled in the pre-cooler (the ground is stationary, after the pre-cooler, the temperature of the gas can be reduced to 160K, in order to prevent the surface of the pre-cooler from freezing, a small amount of methanol can be sprayed in the front of the compressor), the cooled gas is compressed by the fan and the gaseous hydrogen flowing through the blade tip turbine is mixed in the mixer, and enters the combustion chamber for combustion, and the gas after combustion is discharged by the adjustable plug tail nozzle. This engine can make the aerospace aircraft follow the flight trajectory with a dynamic pressure of 50 kPa from the stationary state at sea level to the flight state with an altitude of 30 km and a flight Mach number of 6 within 6 minutes.

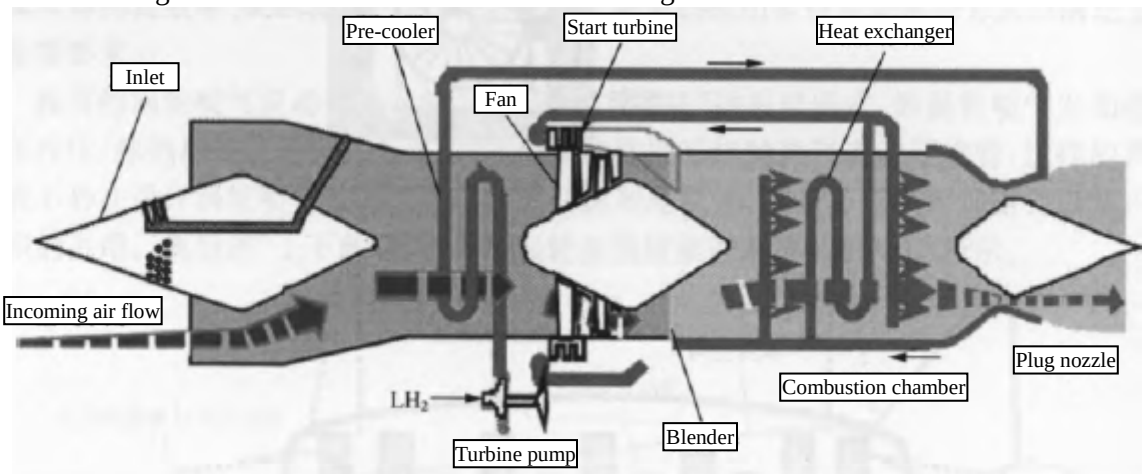

Figure 4-19: Schematic diagram of ATREX engine structure

During the research process of ATREX engine components, the two most important components were the air intake tract and the cooler. The basic requirements for the ATREX engine intake tract are: a large inlet flow during the subsonic flight phase and a high total pressure recovery during the hypersonic flight phase. The cooler is also one of the important components of the ATREX engine. On the one hand, the cooler cools the air flow drawn in the intake tract through liquid hydrogen, which expands the operating range of the turbine engine and increases the thrust and specific impulse of the turbine engine; on the other hand, due to the installation of pre-cooler at the fan inlet, the total pressure loss and flow field distortion of the airflow will be caused, the performance of the turbine engine will be reduced, and the available stability margin of the fan will be reduced. Therefore, it is necessary to develop a pre-cooler with compact structure, light weight, high heat exchange rate, small total pressure loss and no icing.

The common denominator of the pre-cooled TBCC engine represented by ATREX is that the engine inlet cools the incoming air to extend the engine operating range and increase the engine performance. The technical characteristics and technical advantages of this type of engine are similar, which are reflected in the following aspects:

(1) The aerodynamic heating of the turbomachinery and the channel under high-speed flight conditions is reduced, so the flight Mach number range can be extended, and the maximum flight Mach number can be extended from the conventional turbojet engine Ma = 3 to 3.5 to 5.5 to 6.0.

(2) The specific thrust (ratio of thrust to air flow rate) and specific impulse of the engine are improved.

(3) It can improve the thrust-to-weight ratio of the engine.

In addition, the relevant Japanese research institutions further pointed out:

(1) Hypersonic vehicles with pre-cooled TBCC engines as power units can achieve horizontal take-off and landing in the true sense.

(2) The pre-cooled TBCC engine is one of the engines capable of increasing thrust under high Mach number conditions.

(3) Hypersonic vehicles with pre-cooled TBCC engines as power units can safely return in the event of a general failure during takeoff.

(4) Based on the current turbine engine technology, the research on pre-cooled TBCC engines can be carried out.

(5) The successful ground test of the ATREX engine shows that this type of combined cycle engine has the possibility of practical application in the near future.

The following introduces the key technologies that need to be solved in the development of ATREX engines.

(1) Due to the high temperature, high temperature rise rate and large acceleration, the following problems must be solved: (i) find the best way to keep the gap between the fan and turbine blade tips not increasing; (ii) lubrication and sealing problems of bearings; (iii) sealing problems between air and hydrogen; (iv) thrust balance problems; (v) cooling of components; (vi) rotordynamics.

(2) Optimization of the structure of the inlet and nozzle.

(3) Control of the whole system of air intake-engine-nozzle.

(4) Engine/aircraft integration.

Among these technical problems, the main one is due to high temperatures. The ATREX engine accelerates from sea level (288 K inlet trum) to $Ma = 6$ (1680 K) in just 6 minutes, and the rapid temperature transients are beyond the scope of the test and many new design and testing techniques must be considered. In addition, since the maximum temperature of the fan inlet airflow can reach 660K ($Ma = 6$) after passing through the pre-cooler, it is necessary to use liquid hydrogen instead of using air as the cooling medium, but the low temperature of liquid hydrogen will bring other technical problems. There are also winds caused by rapid temperature transients.

Based on the analysis of the technical status of several different forms of pre-cooled TBCC engines, the key technologies of pre-cooled TBCC engines can be summarized as follows:

(1) Regardless of the form of pre-cooling, it is necessary to install a pre-cooling device in the intake tract, which will increase the weight of the engine, so the optimization of the engine weight is one of the key technologies.

(2) Due to the rapid acceleration performance of this type of engine, the flow of air flow in the inlet tract or other components belongs to unsteady flow, so this unsteady flow phenomenon must be considered in the component design process.

(3) Whether it is water spray cooling or heat exchanger cooling, anti-icing technology is a key technology that must be solved. This is because icing on the surface of the precooler can further increase total pressure loss and airflow distortion, and severe icing can also clog the airflow channels.

(4) The installation of the pre-cooler will cause serious total pressure loss and strong flow distortion of the inlet airflow, so under the premise of ensuring that the heat exchange rate is not reduced, how to design the pre-cooler with low total pressure loss and small airflow distortion is also a key technology that must be solved.

(5) Since this type of combined cycle engine is designed as an accelerator, the rapid temperature transient will cause the change of the blade tip gap of the fan and the turbine components, therefore, keeping the change of the fan blade tip gap small is the key technology that must be solved in the fan research process.

(6) The rear body resistance directly affects the installation performance of the engine and the acceleration of the aircraft, and how to study the tail nozzle with low rear body resistance with the help of CFD technology and wind tunnel blowing test technology is the key technology that must be solved in the tail nozzle research.

(7) In order to adapt to a wide working range, the air inlet of the pre-cooled TBCC engine should be adjustable, therefore, based on CFD technology and wind tunnel test technology, the design of light weight, good adjustability, wide range of adaptation of the air inlet is the key technology that needs to be solved in the study of air intake.

4.3.2: Cryogenic turbojet rocket combined cycle engine

The cryogenic turbojet rocket combined cycle engine is a propulsion system scheme that organically combines a deeply cooled turbojet engine and a liquid rocket engine, which is proposed by the Belgian expert Balepin and is called the KLIN cycle.

Figure 4-20 shows the cycle scheme of the KLIN cyclic propulsion system. The KLIN cycle engine consists of several rocket engines and several turbojet engines. Among them, the turbojet engine can be relatively stable within *Ma* = 0 to 6 (compressor inlet temperature 110 ~ 160K), which saves the oxygen carried by the liquid hydrogen combustion of the rocket engine in the low-speed stage; the rocket engine is partially turned on during takeoff, so that it can provide enough thrust during take-off, and the vertical take-off mode can be adopted, which solves the problem of insufficient thrust when other types of TBCC engines take off, and the structural weight gain caused by the large wingspan area and landing gear must be paid for horizontal take-off; after flying through the transonic region, the rocket engine throttles until the turbojet engine is switched off (*Ma* = 6), and the rocket engine is fully turned on. The turbojet engine can be separated from the aircraft and can be recycled, so the launch mode can be either a single-stage orbit entry (SSTO) or a two-stage orbit entry (TSTO).

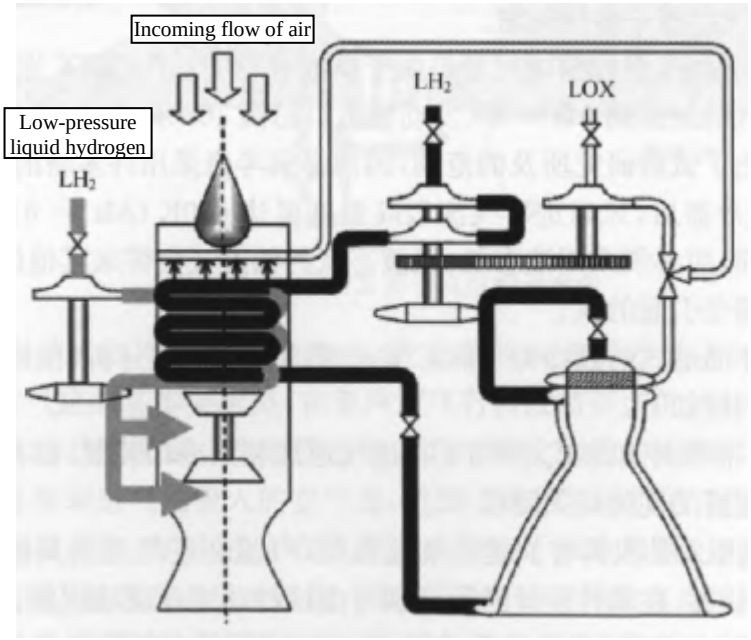

Figure 4-20: Cycle scheme of the KLIN cyclic propulsion system

The liquid hydrogen required for the combustion of rocket engines and turbojet engines is first used to cool the air entering the turbojet engine to 110 (sea level) to 160K (*Ma* = 6), greatly reducing the inlet temperature of the compressor, can reduce the compression work, and reduce the turbine load, and at the same time, if the converted speed remains unchanged, the physical speed will be reduced, these factors are conducive to reducing the engine structure and improving the thrust-to-weight ratio; liquid hydrogen, which is used as a coolant, absorbs energy in the pre-cooled heat exchanger, and then sends it to the rocket cooling system, and finally becomes gas hydrogen, which pushes the expansion turbine to do work. This additional heat absorption can increase the turbine output power, increase the pressure in the rocket combustion chamber, and thus increase the specific impulse of the rocket. The cryogenic turbojet engine always works in the design state, and the thrust adjustment can be achieved by shutting down the turbojet engine one after another, without adjusting the working state of the turbojet engine.

The key technology in the KLIN cycle is similar to that of the ATREX engine with a precooler. First, air cryogenic technology is required.

In order for the turbojet engine to work stably from *Ma* = 0 to *Ma* = 6, the temperature of the inlet air of the turbojet engine must be reduced to 110 K (*Ma* = 0) and 160~200 K (*Ma* = 6), which places high demands on pre-cooled heat exchangers, which can have a great impact on materials and lubrication, and can be difficult to implement. The other is anti-icing, anti-icing is a major problem of the pre-cooling cycle in the sea level state and low-altitude conditions, and the humidity of the air at high altitude is small, which naturally avoids the icing problem of the pre-cooling heat exchanger. Studies have shown that pre-cooled heat exchangers will not freeze at sea level and at low altitudes as long as one of the following conditions is met: first, the air temperature is lower than the dew point of water (273 K); second, the pressure of the steam part is lower than the pressure of the three-phase point. In the dry season or winter, if the above conditions are met, the pre-cooled heat exchanger will not freeze. In other cases, spraying coolant in front of the pre-cooled heat exchanger (liquid oxygen is the best coolant) will avoid icing of the pre-cooled heat exchanger. Studies of the KLIN cycle have shown that pre-cooled heat exchangers require only 4% to 6% liquid oxygen for the air flow to completely solve the anti-icing problem.

4.3.3: Air liquid combined-cycle engines

The air-liquefied engine is an advanced future engine, and its scheme has been studied a lot. The existing air liquefaction engine solutions are mainly divided into two categories: one is the basic air liquefaction engine (LACE); the other type is air liquefaction and enrichment system (ALES) [29~40].

The LACE scheme is a solution that uses cryogenic fuel to liquefy air and inject it into the combustion chamber. When the speed of the aircraft is very low, less air is inhaled, so the LACE alone cannot provide enough power. In order to solve this problem, it is necessary to combine the air liquefied engine with a normal engine, i.e. in the LACE solution, although air is used as an oxidizer, the liquid oxygen stored in the tank is still used. The basic air-liquefied engine system can operate in normal engine mode or in air-liquefied mode. All cooling tasks are carried out by liquid hydrogen, and the liquid air is pressurized and exchanged with the gaseous air to ensure the maximum liquefaction capacity of the system. The liquid air booster pump is powered by an oxygen turbine because the density of liquid air is close to that of liquid oxygen.

The ALES protocol liquefies and separates the inhaled air, with a portion of the liquid oxygen used to support combustion in the combustion chamber and the other part being stored. Therefore, this scheme only makes sense if the inhaled liquid oxygen is greater than the combustion requirement, otherwise there is no need for the inhaled air to be separated, and the LACE scheme should be used. Taking into account the gradual increase in the amount of air inhaled in real flight, the engine of the ALES scheme must be able to work in the LACE state.

The other existing programs are modifications of these two programs. For example, some options add a turbofan to the intake tract of the LACE solution to increase the suction capacity at low speeds. Different cooling methods in these two scenarios can also lead to different solutions.

Figure 4-21 shows the cycle diagram of the air liquid air-breathing rocket engine system. Very high efficiency can be achieved by using very low temperatures of liquid oxygen (LOX) and liquid hydrogen (LH2) close to the three-state point, as well as propellant recirculation between the condenser and the tank.

The features of the liquidated air circulation engine are as follows:

(1) Wide range of work. Liquid-air circulation engines offer a wide operating range because air-breathing engines use a combination of air, liquid oxygen, and liquid hydrogen propellants, while rocket engines use liquid hydrogen and liquid oxygen. The transition between the two ways of working is smooth. Cooling the intake tract and around the air condenser with cryogenic fuel allows the LEF recirculating engine to operate to a high Mach number close to 10.

(2) The combustion chamber pressure is high. Only a small amount of pump energy is required to compress the air to a liquid state. As a result, the combustion chamber pressure is limited only by the balance of circulating power.

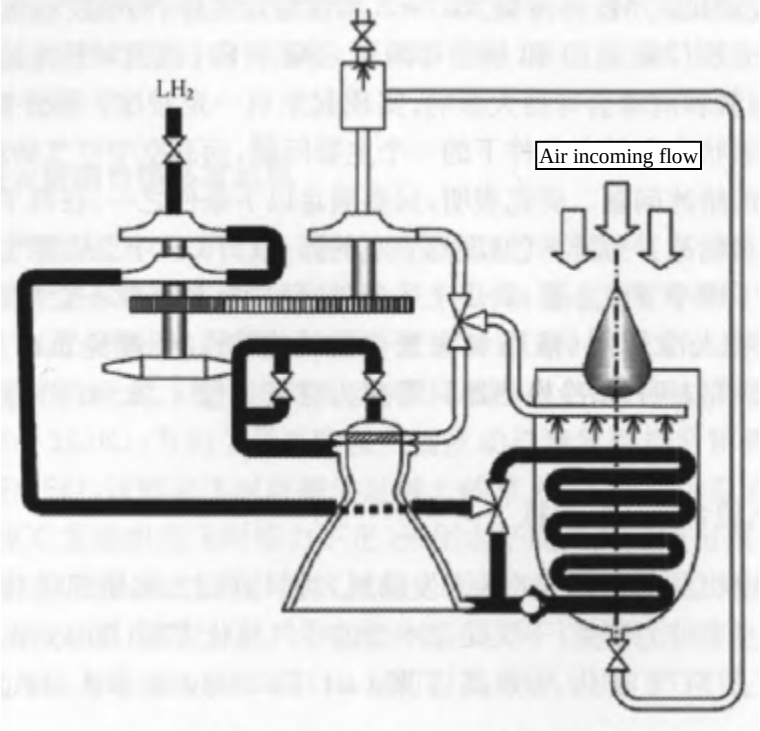

Figure 4-21: Cycle diagram of the air liquid air-breathing rocket engine system

By choosing the right system cycle, high combustion chamber pressures can be obtained, allowing small and lightweight engines to be designed at the same thrust level. During low-altitude flight, the high combustion chamber pressure prevents the separation of the air flow at the edge of the nozzle, which is also effective in improving the performance of the system. (3) low air consumption. Compared to other types of engines, the air flow per unit thrust consumed by a liquidated air circulation engine is lower. This is because the condensation rate of air varies with the heat capacity of the cryogenic fuel. Therefore, the specific impulse is also low, about 800s. However, it is precisely because of this characteristic that the size of the high enthalpy wind tunnel required to simulate high Mach number and high-altitude flight conditions can be reduced.

Cryogenic propellants cool the air during low Mach number flight and then return to the propellant tank. It provides a ram when flying at high Mach numbers, where no recirculation of propellant is required to obtain a sufficient air condensation rate.

Figure 4-22 is a typical layout of a liquidated air circulation engine. In order to facilitate the control of the flow rate of air in the intake tract, the head cone of the engine is variable. The air is liquefied in the condenser and pressurized by a pump before passing through the air condenser heat exchanger and delivered to the combustion chamber. Structurally, it differed from the usual engine by the addition of an air condenser.

The liquidified air circulation engine consists of two basic systems: one is a recirculation condenser connected to a storage tank; the other is a rocket engine system. During the low-speed flight phase, the recirculation system carries out effective air condensation with extremely low temperature propellants. When flying at high Mach numbers, the temperature of the recirculated propellant is enough to condense the air due to the action of the ramming in the air condenser. Turbo drive fluid, combustion type and combustion chamber coolant are the main characteristic parameters. They are all closely related to combustion chamber pressure cycle limits, engine performance and development risks.

According to this propellant recirculation system, there are three main types of circulation for liquid-air circulation engines.

(1) Cooling with oxidizer, oxidizer gas turbine cycle (OCOG). It is an oxidizer expansion cycle engine that utilizes an oxidizer, liquid oxygen, or liquid air as a combustion chamber coolant and turbine drive fluid.

The characteristics of this cycle system are: (1) The specific impulse is higher than that of other types of cycle engines. (2) The pressure in the combustion chamber is limited.

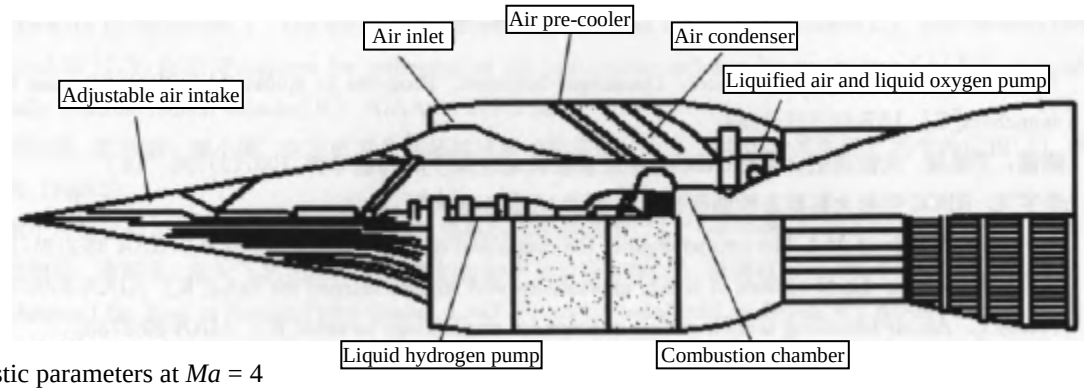

Characteristic parameters at *Ma* = 4	
Vacuum thrust	500t
Effective specific impulse	780s
Combustion chamber force	100kg/cm2
Liquid hydrogen : liquid oxygen : air ratio	1:4.5:12
Nozzle area ratio	40

Figure 4-22: Structural diagram of the Air liquid air-breathing rocket engine system

This is due to the fact that the expansion cycle and turbine gas temperature are also low at low flying speeds. (3) The temperature of the propellant in the nozzle varies greatly, which requires a special design of the nozzle element.

(2) Hydrogen cooling, hydrogen gas turbine cycle (HCHG). This is a fuel expansion cycle engine that uses hydrogen as a combustion chamber coolant and turbine drive fluid. It has a lower specific impulse compared to the OCOG cycle. This is because, in the fuel pump, the hydrogen enthalpy increases, but the performance of the air condenser decreases.

(3) Cooling with hydrogen, gas turbine cycle (HCCG). This cycle is a staged combustion cycle, which allows the performance of the engine not to change with the change of flight speed.

The characteristics of this system are: (1) maintaining high-power aspirated operation through the working mode of the rocket engine; (2) the pre-chamber will be designed to operate at a wide range of propellant inlet temperatures; (3) the oxidant can be used as a coolant in the combustion chamber. Since this scheme increases the bulk density of the liquid air, the specific impulse is higher.

The main key technologies for the development of liquidified air circulation engines are as follows:

(1) Obstructions in air liquefaction. It is almost impossible to separate oxygen from liquefied air. The first issue to be solved is the treatment of obstructions such as water and carbon dioxide in the process of liquid. This project includes two key technologies, namely, the design technology of the condenser to prevent the adsorption of obstacles in the condenser, and the technology to eliminate the harmful effects of these obstacles on the valves and turbopump gaskets.

(2) The efficiency of the air condenser. For lightweight engines, it is important to design high-efficiency air condensers. In this sense, the air condenser heat exchanger will have titanium and aluminum alloy pipes. This requires the technology to machine such alloy pipes for lightweight, large-format condensers.

(3) Very low net pressure head (net absorption pressure differential) pump. When the engine is started at atmospheric pressure at sea level, the liquefied air is almost saturated. Therefore, it is necessary to develop a very low net head pump that can operate in this state.

(4) The propulsion system of the liquid air circulation engine realizes adaptive control in different working conditions such as starting, low Mach number flight, high Mach number flight and rocket mode, so an adaptive closed-circuit control system is required.

The most important technologies for the development of a liquefied air circulation engine are design technology that avoids the formation of clogging substances in the air condenser, as well as starting program control and sea-level operation technology.

References

[1] Philippe Ramette, Michel Doublier, Dominique Scherrer. Progress in combined cycle propulsion for future launchers [C]. IAF-89-312, 1989.
[2] Chen Jian, Wang Zhenguo. Research progress of rocket-based combined cycle (RBCC) propulsion system [J]. Flight Missile, 2007(3):36-44.
[3] Li Yufei. Research on modal performance of RBCC launch rocket [D]. Xi'an: Northwestern Polytechnical University, 2004.
[4] Siebenbaar A, Bulman M J. The strutjet engine: the overlooked option for space launch [R]. AIAA 95-3124, 1995.
[5] Carl F Ehrlich Jr. Early studies of RBCC applications and lessons learned for today [R]. AIAA-2000-3105.
[6] Trefny C. An air-breathing launch vehicle concept for single-stage-to-orbit [R], AIAA-99-2730.
[7] Yungster S, Trefny C J. Analysis of a New Rocket-Based Combined-Cycle Engine Concept at Low Speed [R]. AIAA 99-2393, 1999.
[8] Liu Peijin. Study on modal performance and influencing factors of RBCC launch rocket [D]. Xi'an: Northwestern Polytechnical University, 2001.
[9] Huang Shenghong. Research on combustion flow of rocket-based combined power cycle (RBCC)[D]. Xi'an: Northwestern Polytechnical University, 2002.
[10] Lü Xiang. Research on performance analysis model of rocket-based combined cycle (RBCC) engine [D]. Xi'an: Northwestern Polytechnical University, 2005.
[11] Olds J, Bradford J. SCCREAM (Simulated Combined-Cycle Rocket Engine Analysis Module): a conceptual RBCC engine design tool [R]. AIAA 97-2760, 1997.
[12] Bradford J, Olds J. SCCREAM v. 5: a web-based airbreathing propulsion analysis tool [R]. AIAA 99-2104, 1999.
[13] Li Long. Modeling of overall performance and working characteristics of TBCC propulsion system [D]. Nanjing: Nanjing University of Aeronautics and Astronautics, 2008.
[14] CHEN Min, TANG Hailong, ZHU Daming. Hypersonic tandem combined power plant scheme[J]. Journal of Beijing University of Aeronautics and Astronautics, 2007, 33(3): 265-268.
[15] Zhu Daming, Chen Min, Tang Hailong, et al. Hypersonic turbine/ramjet combined engine scheme[J]. Journal of Beijing University of Aeronautics and Astronautics, 2006, 32(3): 263-266.
[16] Angel M Espinosa. Integration of turbine engines in hypersonic airbreathing vehicles [R]. AIAA 2003-4408, 2003.
[17] Balepin V V, Cipriano J, Berthus M Combined Propulsion for SSTO Rocket: From Conceptual Study to Demonstrator of Deep Cooled Turbojet [R]. AIAA-96-4497-CP, 1996.
[18] Shang Xusheng, Cai Yuanhu, Chen Yuchun. Research on the development of main components of pre-cooled ATREX engine [J]. Journal of Projectile, Arrow and Guidance, 2004, 24(3): 313-315.
[19] Wang Zhanxue, Qiao Weiyang. Development status and application prospect of pre-cooled turbine-based combined cycle engine [J]. Gas Turbine Test and Research, 2005, 18(1): 53-56.
[20] Shang Xusheng, Cai Yuanhu, Xiao Hong. Introduction to the development of pre-cooled air-breathing turbine ramjet expansion cycle engine [J]. Acta Armamentarii, 2006, 27(3):54-58.
[21] Nobuhiro Tanatusgu, Tetsuya Sato, and Yoshihiro Naruyo. Development Study One Atrex Engine [C]. IAF-96-S. 5.03, 1996.
[22] Tetsuya Sato, Nobuhiro Tanatsugu, Yoshihiro Naruyo. Development Study One Atrex Engine [C]. IAF-98-S. 5.01, 1998.
[23] Tetsuya Sato, Nobuhiro Tanatsugu, Hiroshi Hatta. Development study on the ATREX engine [C]. IAC-03-S. 5.02, 2003.
[24] Balepin V V. Maita M. KLIN Cycle: combined propulsion for vertical take off launcher [R]. AIAA Report, 1997.
[25] Vladimir Balepin, Hendrick P. Application of the KLIN cycle to a vertical takeoff lifting body launcher [R]. AIAA-98-1503, 1998.
[26] Vladimir Balepin, Patrick Hendrick. Lightweight low cost KLIN cycle derivative for a small reusable Launcher [R]. AIAA-99-4893, 1999.
[27] Vladimir Balepin, Czysz P A. Combined engine for a reusable launch vehicle (KLIN cycle) [R]. AIAA 2001- 1911, 2001.
[28] Xing Xiuqing, Zhao Xiaolu. Preliminary analysis of cryogenic turbojet-rocket combined cycle engine [J]. Propulsion Technology, 2000, 21(6):10-13.
[29] Huang Yiyong, Zhang Yulin. Parameter analysis of air liquefied engine [J]. Propulsion Technology, 2001, 22(1):22-25.

[30] Aoki T, Ogawara A. Study of LACE cycle for SSTO space plane [C]. IAF-88-252, 1988.
[31] Ogawara A, Nishiwaki T. The cycle evaluation of the advanced LACE performance [C]. IAF-89-313, 1989.
[32] Bond W H, Yi AC. Prospects for utilization of air liquefaction and enrichment system (ALES) propulsion in fully reusable launch vehicles [R]. AIAA-93-2025, 1993.
[33] Zheng Qingxiong, Chen Fuqun, Lian Xiaochun. Application of Liquidized Air Circulation in New Concept of Aerospace Aircraft Composite Cycle Propulsion Technology [J]. Propulsion Technology, 1992(2).
[34] Propulsion device with air liquefaction and concentration system for reusable launch vehicle [J]. Flying Missile, 1995, (10):29-33.
[35] Huang Xijun, Tang Hailong. Development and parameter analysis of LACE scheme for space shuttle [J]. Propulsion Technology, 1996, 1(1):64-70.
[36] Mamoru Oike, Kenjiro Kamijo, Daiho Tanaka. LACE for a fully-cycled R-cycle. AIAA-99-0091, 1999.
[37] Masataka MAITA, Yoshiaki OHKAMI, Tatsuo YAMANAKA. Conceptual study of space plane powered by hypersonic airbreathing propulsion system [R]. AIAA-90-5225, 1990.
[38] Miki Y, Togawa M, Tokunaga T. Advanced SCRAM-LACE system concept for single-stage-to-orbit space plane [C]. IAF-91-272, 1991.
[39] Dulepov N P, Lanshin A I, Tjurikov E V. The SSTO combined propulsion system on a basis of LACE and dm-SCRJ [R]. AIAA 2001-1842, 2001.
[40] Bond W H. Collection based combined cycle for earth to orbit propulsion [R]. AIAA 2006-217, 2006.

CHAPTER 5: INTEGRATED DESIGN TECHNOLOGY FOR HYPERSONIC VEHICLE FUSELAGE PROPULSION

5.1: Hypersonic aerodynamics

5.1.1: Hypersonic flow

The science of studying the laws of hypersonic air flow and the interaction between air and hypersonic vehicles, i.e., hypersonic aerodynamics is an emerging discipline. Over the past half century, the theoretical and experimental technology of hypersonic aerodynamics has developed rapidly, driven by the aerospace industry. As the name suggests, hypersonic flow is a flow with a speed much greater than the speed of sound, and the free-flow Mach number $Ma_\infty > 5$ is usually used as a sign of hypersonic flow, and the boundary of this Ma_∞ is not absolute, and whether the flow is a hypersonic flow is also related to the specific shape of the vehicle. For blunt bodies, $Ma_\infty > 3$ begins to show hypersonic flow characteristics, and for elongated bodies, Ma_∞ 10 does not begin to show hypersonic flow characteristics until it reaches 10[1-5].

1. The main characteristics of hypersonic flow

For hypersonic flow, certain physical phenomena become more and more important when the flight of the vehicle increases. These phenomena include highly nonlinear hydrodynamic characteristics due to high flow *Ma* and high-temperature physicochemical characteristics due to high flow energies (Fig. 5-1). Specifically, the following phenomena exist:

1) Small density ratio and thin shock layer

The region of flow between the shock wave and the object is called the shock layer, and the thin shock layer is a characteristic of hypersonic flow. This is because the larger the free-flow Mach number Ma_∞, the stronger the shock wave, the greater the compression of the gas after the shock wave, and the ratio of the density before and after the shock wave is small. For the complete gas with very high Mach numbers, the density ratio before and after the positive shock wave is about 1/6, while the density ratio of the real gas during the reentry flight of the Apollo spacecraft is about 1/20.

2) The viscous effect is strong and can dominate the entire flow field

The relationship between the laminar boundary layer thickness δ and the free-flow Mach number Ma_∞ and Reynolds number $Re_{\infty x}$ can be simplified under hypersonic conditions:

$$\frac{\delta}{x} \propto \frac{Ma_\infty^2}{\sqrt{Re_{\infty x}}} \tag{5.1}$$

where: the symbol ∞ — proportional relationship.

In high-altitude, hypersonic conditions, the δ becomes large, changing the effective shape of the object and affecting the calculation of the external viscous flow. In particular, due to the thin hypersonic shock layer, the thickness of the boundary layer cannot be omitted compared with the shock layer, and even the entire shock layer is sticky. The thickening of the boundary layer has an effect on the inviscous flow, which in turn affects the growth of the boundary layer, and the viscous interaction of hypersonic flow occurs. At this point, the classical Prandtl boundary layer theory fails.

3) There is a high-entropy layer

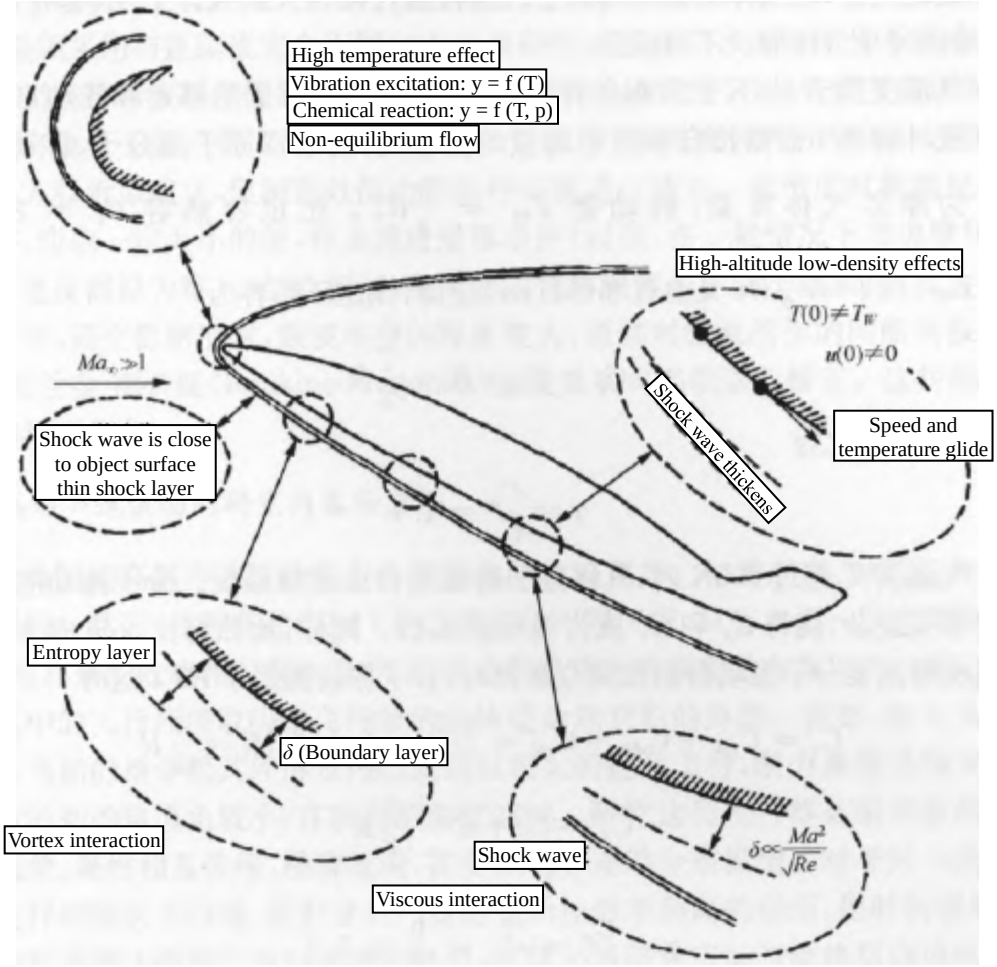

Figure 5-1: Schematic diagram of the physical characteristics of a hypersonic stream

Hypersonic vehicles with re-entry flight segments are made of blunt-tipped bodies, and even slender vehicles are made of micro-blunt-headed elongated bodies, because according to the self-similar solution of the hypersonic laminar boundary layer equations, the convective heat transfer at the head station point is inversely proportional to the square root of the radius of curvature of the head, and the thermal load can be reduced by passivating the head. So, in the hypersonic stream around the blunt-headed elongated body, the shock wave around the head is highly curved. The streamlines passing through different positions of the curve shock wave undergo different entropy increases, so that a layer of gas with a strong entropy gradient will cover the surface of the object to form an entropy layer and extend a considerable distance downstream of the head. The Crocco's theorem for the classical compressible flow is:

$$V \times (\nabla \times V) = -T \nabla S \qquad (5.2)$$

where: $\nabla \times V$ — curl of velocity field V;

∇S — Gradient of entropy S;

T — temperature;

∇ — differential operator;

X — vector product, in Equation (5-2), represents that an entropy layer with a strong entropy gradient is associated with a strong curl.

Due to the growth of the boundary layer along the object surface, the entropy value of the streamlines entering the outer edge of the boundary layer at different locations is different, and the characteristics of the outer edge of the boundary layer are affected by the entropy layer, and the vortex interaction occurs.

4) Hypersonic flow is high-energy flow with a high-temperature effect

When a hypersonic gas flow is decelerated by shock wave compression or viscous blockade, the kinetic energy of part of the directed motion is converted into the energy of the random motion of the molecules, i.e., the temperature of the gas increases.

This temperature rise can be so large that the gas exhibits a "non-complete gas" pattern, and the traditional assumption of a complete gas no longer holds.

At room temperature when the air temperature is lower than 800 K, only the movement of gas molecules and the excitation of rotational degrees of freedom need to be considered. According to the principle of equal division of energy according to the mean term of degrees of freedom in statistical physics, for a diatomic molecule, the moving energy $E_{shift} = \frac{3}{2}RT$, R is the molar gas constant, the rotational energy $E_{shift} = \frac{2}{2}RT$, the specific volume heat capacity $C_v = \partial E/\partial T = \partial(E_{shift+} E_{shift})/\partial T = \frac{5}{2}R$, and by Mayer's law, the specific pressure heat capacity is

$$C_p = C_v + R = \frac{7}{2}R \tag{5.3}$$

At this time, the specific heat capacity ratio is

$$\gamma = \frac{C_p}{C_v} = 1.4 \tag{5.4}$$

When the air temperature T exceeds 800K, the vibrational degrees of freedom of the gas molecules are excited. The relationship between the vibrational energy of the molecule and the temperature T is complex, so that Cp and C_v are a function of temperature. Similarly, the specific heat capacity ratio γ also becomes a function of temperature. When the temperature increases to the full excitation of the molecular vibrational degree of freedom, the molecular vibrational energy tends to RT, at this time:

$$C_v = C_{v移} + C_{v转} + C_{v振} = \left(\frac{3}{2} + \frac{2}{2} + \frac{2}{2}\right)R = \frac{7}{2}R \tag{5.5}$$

$$C_p = C_v + R = \frac{9}{2}R \tag{5.6}$$

$$\gamma = \frac{C_p}{C_v} = \frac{\frac{9}{2}}{\frac{7}{2}} = \frac{9}{7} \approx 1.3 \tag{5.7}$$

When the temperature of the gas increases further, a chemical reaction can occur. For the air at 1 atmosphere, the dissociation of the oxygen molecule O2 (O2→O+ O) begins at a temperature of about 2000K, at 4000K, the oxygen molecule is basically completely dissociated, at this temperature the dissociation of the nitrogen atom N2 (N2→N+ N) begins, and at 9000K the nitrogen molecule is basically completely dissociated. At temperatures above 9000 K, oxygen and nitrogen atoms begin to ionize ($N \rightarrow N^+ + e^-$, $O \rightarrow O^+ + e^-$) and the gas becomes a partially ionized plasma.

When the characteristic time of vibration relaxation and chemical reaction in the transition from non-equilibrium to equilibrium is very small compared with the time of the flow point flow through the flow field, the flow is called vibration and chemical equilibrium flow. For equilibrium chemically reactive gases, C_p and C_v are a function of pressure and temperature. If the vibration relaxation and chemical reaction characteristic time is much greater than the flow characteristic time, the flow is called vibration and chemical freezing flow. If the two feature times can be compared, it is called a non-equilibrium flow. For non-equilibrium flows, the analysis is much more difficult and requires coupling consideration of the fluid mechanics equations and the chemical kinetic equations. The specific heat capacity ratio γ a gas that depends only on temperature is a thermally complete gas, and a gas whose specific heat capacity ratio γ is constant is a calorimetric complete gas. For high-temperature gas flows, the specific heat capacity ratio γ is no longer constant, and this parameter is far less important in high-temperature gas dynamics than in general gas dynamics. The above phenomenon is known as the high temperature effect, also known as the true gas effect.

5) There is a low-density effect in high-altitude and hypersonic flows

When a hypersonic vehicle continues to fly at high altitudes with very low atmospheric density, the effect of the low density effect on aerodynamics is important. When the flight altitude is extremely high, the density will be so low that the mean free path of a molecule (the average distance a molecule travels between a collision with a neighbor) is of the same order of magnitude as the characteristic length of the aircraft.

The air medium no longer exhibits continuity, and this flow must be studied in a completely different way than the continuous flow. It is usually dealt with the technique of molecular kinematics. When the molecules reflected by the surface do not interact with the incident molecules after the surface of the aircraft collides, this flow is called free molecular flow. When the flight altitude drops to a certain altitude (e.g., 82 to 95 km), the boundary conditions at the object surface must be corrected, although the governing equations of the continuum are approximately true. At low density, the flow velocity at the object surface is not zero, and a certain value should be taken, which is called the velocity slip condition (in the past, the fluid velocity at the object surface was assumed to be zero after considering friction under normal circumstances). Similarly, the temperature of the gas at the wall is different from the wall temperature, which is called the temperature jump condition. In addition, at high altitudes and low densities, the thickness of the shock wave itself becomes larger, and the usual discontinuity assumptions for the shock wave are no longer valid, and the classic Rankine-Hugoniot shock wave relation must be corrected. These are all important physical phenomena at low density.

2. Research content and methods of hypersonic flow

A typical hypersonic flow encompasses many complex physical phenomena. At first glance, it seems impossible to analyze this flow. However, in different regions of the flow field of various hypersonic vehicles, only one or two of the above phenomena dominate, while the rest of the effects are relatively secondary, so it makes sense to deal with these phenomena separately. The environment in which a hypersonic vehicle flies in the atmosphere depends on the specific mission of the vehicle and its shape. For example, the orbiters of the space shuttle and the command modules of manned spacecraft are blunt or fly at a large angle of attack, and the drag coefficient is very large. They have a smaller initial orbital angle of re-entry flight, slowing down at higher altitudes. The study of such vehicles must account for high-altitude non-equilibrium thermochemical phenomena, viscous interactions, rarefaction effects, and even non-continuum models. For another type of slender aircraft such as long-range ballistic rockets, they are subjected to severe aerodynamic heating rates and high dynamic pressures, but for a short time, ablative thermal protection systems can be used to resist severe turbulent heating rates, which necessitates the study of the thermal interaction between the flow field and the ablation of the thermal protection layer. For example, a hypersonic vehicle equipped with an air-breathing propulsion system must work at a low altitude to meet the requirements of engine performance, and the huge aerodynamic load caused by high dynamic pressure and high Reynolds number, boundary layer transition, and severe surface heating have become important topics in the research of such aircraft. It should also be noted that for the same hypersonic vehicle, different flow characteristics in different regions of the flow field can be made, so different simplified approximations can be made for the problems to be solved.

In hypersonic aerodynamics, in addition to the complex flow field environment of the aircraft, there are many problems that need to be solved than classical aerodynamics. Hypersonic aerodynamics has three main topics, namely aerodynamics (lift, drag, torque, center of pressure, etc.), aerothermal (heat flux calculation, heat protection measures, etc.), and aerokinetics (optoelectronic characteristics of the flow field). Depending on the application requirements, the studies are carried out separately.

The aerodynamic and thermal environment of hypersonic vehicles is determined by three main means: theoretical analysis, experimental research and numerical calculation. These three instruments are mutually reinforcing. The experimental research includes two aspects: ground equipment simulation and flight test. Flight tests of full-scale aircraft can provide sufficient and reliable information, but flight tests of full-scale aircraft are expensive and can only be carried out after detailed design, research, and manufacturing. There are many parameters that need to be simulated for hypersonic ground equipment, including the free flow Mach number, Reynolds number, velocity, total enthalpy of flow, density ratio before and after shock wave, test gas, wall temperature to total temperature ratio, and thermochemical properties of the flow field. It is not possible to simulate all of these parameters simultaneously with a single device. For specific protocols, it is important to determine which parameters are critical. Hypersonic aerodynamic ground simulation is a partial simulation technique, and different ground equipment meets different requirements. Common hypersonic ground equipment are shock tubes, arc heaters, hypersonic wind tunnels, and free-flying ballistic targets.

For example, there are 493 aerodynamic tests, 139 aerothermal tests and 77 structural tests in the US Space Shuttle research program, and the total number of hours of equipment operation is 71 297 hours. With the development of computational fluid dynamics, ground simulation has added a new mission, which is to verify the computational program. Through the measurement of flow field density, velocity, surface pressure, heat flux, and aerochemical properties, and flow observation, the rationality of the calculation software is determined. Because of the importance and complexity of hypersonic ground simulation equipment and testing technology, the study of them has become an independent discipline.

5.1.2: Hypersonic aerodynamic engineering calculation methods

The aerodynamic characteristics of hypersonic vehicles are the prerequisites for determining their aerodynamic shape, flight trajectory and performance, and the surface pressure distribution and friction stress distribution, which are closely related to aerodynamic characteristics, are also important basis for determining the load conditions and thermal environment of hypersonic vehicles. Therefore, in the conceptual research and preliminary design stage of hypersonic vehicles, a large number of predictions in terms of aerodynamic characteristics are required, and a large number of numerical calculations and wind tunnel tests are not possible at this stage. Moreover, the current wind tunnel tests cannot fully simulate the real conditions of hypersonic flight, so it is necessary to develop simple and effective fast approximation calculations.

Since the mid-1950s, due to the rapid development of strategic missiles and re-entry vehicles, various engineering prediction theories have been developed and applied, such as Newton's theory, modified Newton's theory, wedge/cone cut, Newton's theory, shock wave expansion wave theory, and so on. These approximate prediction theories provide simple and fast calculation methods and are widely used in the aerodynamic calculations of waveriders, lifters, and wing-body combinations of hypersonic vehicles. However, they have certain limitations of application. The modified Newtonian theory is mainly used in the calculation of the pressure distribution of the head, which cannot give good results for the leeward side, and cannot reflect the influence of the ratio of *Ma* and the bluntness of the head on the pressure distribution of the rear part; the wedge/cone cutting method is based on the small perturbation theory and is not suitable for the case of large angle of attack; although the calculation of the blunt elongated body is good, the influence of *Ma* is still not considered, and the angle of attack is limited to the half cone angle. In order to solve the above problems, a variety of approximation methods can be used together, and different methods can be selected according to the different positions of the calculation objects, front/leeward conditions, angle of attack, and Mach number. A successful example is the supersonic and hypersonic anybody program (S/HABP) jointly developed by the U.S. Air Force and Douglas. In this program, 15 methods were selected for the windward side and 10 methods were selected for the leeward side. Table 5-1 illustrates the selection principles of the main calculation methods [6-8].

Table 5-1: Calculation methods for hypersonic aerodynamic engineering

Region		Low hypersonic speed		Hypersonic speed	
		Windward side	Leeward side	Windward side	Leeward side
Head	Round	Dahlem-Buck	Dahlem-Buck	Fix Newton	Prandtle-Meyer
	Flat	Cut the wedge	Dahlem-Buck	Fix Newton	Prandtle-Meyer
Body	Round	There are cones of attack	ACM	Fix Newton	Prandtle-Meyer
	Flat	Cut the wedge	ACM	Fix Newton	Prandtle-Meyer
Lift surface	Edged	Cut the wedge	Dahlem-Buck	Fix Newton	Prandtle-Meyer
	Ordinary	Cut the wedge	Dahlem-Buck	Fix Newton	Prandtle-Meyer

In order to deal with the situation when there is an angle of attack around the current, the equivalent body method was developed in the late 1960s and early 1970s. The idea is to equip the pressure distribution on the meridian surface of a blunt cone with an angle of attack around the flow to the pressure distribution of the blunt cone around a certain zero angle of attack, and then use the above method to calculate the pressure distribution of these equivalent zero angles of attack around the fluid, so as to obtain the aerodynamic results of the entire blunt cone around the flow with an angle of attack.

All of these methods are based on the theoretical analysis of hypersonic inviscid flow. Using these methods, it is possible to predict most of the aerodynamic characteristics of the aircraft, such as lift, viscous resistance, and pitching moment. However, it is not enough to calculate the viscous aerodynamic characteristics, as the hypersonic vehicle, as a complex system, also needs to fully consider the viscous drag, component aerodynamic interference, and even the additional aerodynamic characteristics of the engine.

5.1.3: Numerical simulation techniques for hypersonic flow

With the advent of computational fluid dynamics, numerical simulation has become the main research method of hypersonic aerodynamics, along with experimental research and theoretical analysis. The advent of supercomputers and massively parallel processors has greatly increased the computing speed and memory capacity, as well as the rapid development of computational fluid dynamics and graphics display technology, which has led to the rapid development of numerical simulation capabilities. Now it has become a reality to use numerical simulation to solve the full flow field of the whole aircraft. Numerical simulations can also partially replace the work of ground-based experimental equipment. It is worth pointing out that numerical simulation, experimental research, and theoretical analysis complement each other, and the physical and mathematical models used in numerical simulation often need to be obtained through theoretical analysis, while the correctness of numerical simulation software also needs to be verified or calibrated by experimental research [5].

The main steps of numerically solving the finite difference method for hypersonic inviscosity-free flow are as follows:

(1) Use the correct mathematical model to describe the physical or engineering problems to be solved and give appropriate boundary conditions.

(2) Establish a skin coordinate system and mesh division. The intimate coordinate transformation is used to transform the irregular physical domain into the regular computing domain, and the boundary of the physical domain is transformed into the grid line or grid surface of the computing domain, so that the processing of boundary conditions is simple and accurate.

(3) Select the appropriate difference method to discretize the governing equations. In the course of the development of computational fluid dynamics for decades, a series of explicit or implicit differential formats have been developed in order to improve the accuracy and efficiency of calculations. Among them, in order to capture the shock wave in the flow field, a series of formats to suppress the numerical oscillation near the shock wave and improve the shock resolution have also been developed. For specific physics problems, choosing the right format is crucial.

(4) Boundary processing. Step (3) only gives the processing of the points in the flow field, and in order for the calculation to proceed normally, the processing of the boundary points must also be given. The physical boundary conditions are embedded in the calculation program, and the numerical boundary conditions are determined according to the information transfer relationship between the flow field and the boundary.

(5) Analysis of numerical calculation results and application of explicit flow field technology. The process of numerical simulation of the flow field is actually a process of numerical experiments. After obtaining the calculation results by numerical methods, it is necessary to analyze the rationality and accuracy of the results from a physical point of view, check them against the experimental data, and find out the unreasonable factors, such as grid distribution, differential separation, boundary processing, and even mathematical model. In addition, the application of the explicit flow field technology enables people to quickly obtain the distribution curve of physical quantities and dynamically display the calculated flow field characteristics, which greatly improves the ability to analyze the numerical results, so that people do not have to do nothing in front of the vast data table.

5.2: Aerodynamic design of hypersonic vehicle "waverider"

5.2.1: Concept and aerodynamic characteristics of the aerodynamic shape of the "waverider"

For cruise aircraft, one of the main goals of the design is to give the aerodynamic shape with the minimum drag and the maximum lift-to-drag ratio, and the "waverider" aerodynamic shape is one of the most ideal among the aerodynamic shapes of many low-resistance aircraft [9-10].

A waverider is a supersonic or hypersonic vehicle with a streamlined shape and all of its leading edges have an attached shock wave. It is designed in contrast to the conventional method of determining the flow field by shape and then solving it but has a flow field and then derives the shape, and the flow field is determined by the exact solution of the known non-viscous flow equation. As shown in Figure 5-2, the flow field is determined by the oblique shock wave formula, and the leading edge plane of the shape coincides with the upper surface of the shock wave, as if riding on the wave surface of the shock wave, so it is called a "waverider." Because oblique and conic shocks can be precisely solved in supersonic flows, they form the basis for the inverse design of waveriders.

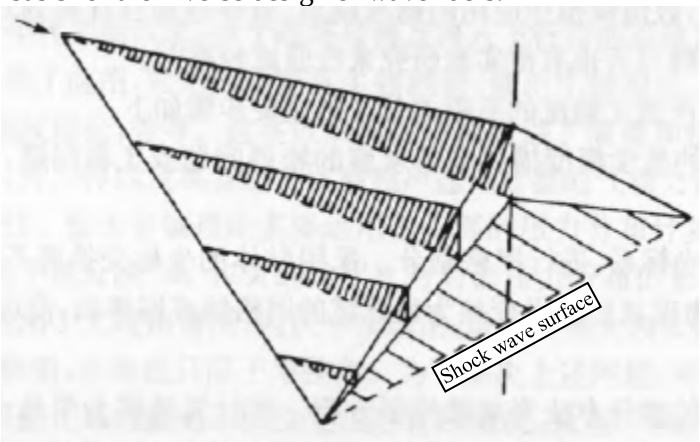

Figure 5-2: Λ-shaped profile and its cross-section in supersonic flow

The concept of a "waverider" was proposed by Nonweiler in 1959. Nonweiler first put forward the basic waverider concept of a ternary lifting body composed of a binary wedge flow, and then Venn, Flower and Nardo studied the called Λ-shaped waverider, which attracted the attention of aerodynamic experts from all over the world, and in 1990, the first academic conference on the shape of the waverider body was held at the University of Maryland in the United States, which pushed the research of the waverider to a new climax.

The waverider shape has three significant aerodynamic characteristics, namely low resistance, high lift, and large lift-to-drag ratio, especially for hypersonic vehicles.

The leading edge of the conventional shape in the supersonic flow is mostly a detached shock wave, and the pressure difference between the shock wave before and after the shock wave makes the wave resistance on the shape very large, and the leading edge and the upper surface of the waverider body are on the same surface as the shock wave, so a large differential pressure resistance is not formed, and the lower surface is subjected to a high pressure that is the same as the conventional shape under the design Mach number, and the high pressure of this flow will not leak around the leading edge to the upper surface, so that the pressure difference between the upper and lower surfaces will not communicate with each other like the conventional shape and reduce the pressure on the lower surface, so that the pressure is reduced. The waverider shape has a large lift force due to the absence of this loss, and the conventional shape must use a larger angle of attack to get the same amount of lift. At the same time, the lower surface of the waverider is often designed to be flatter, and the pressure difference between the upper and lower levels of the flat-bottom section is much larger than that of the conventional axisymmetric shape, so the lift force is also much larger.

The lift-to-drag ratio of the shape depends on its aerodynamic layout, for the conventional axisymmetric cylindrical shape, the upper surface of the head should be compressed by the air flow, so that the lift force decreases, the drag increases, and the side pressure of the head also affects the drag force but does not increase the lift, so if the head is cut off with a streamlined surface, the upper part of the fuselage of the streamlined surface is removed, and the streamlined airfoil surface is extended to the point of occurrence of the shock wave, forming the Λ shape in Figure 5-2, then the effect of the above-mentioned cylindrical fuselage reducing lift and increasing drag will disappear, and its lower surface will maintain a higher pressure. As shown in Figure 5-3, a comparison of the shape of the thin wing and the waverider below shows that the suction on its upper surface is negligible at hypersonic speed, so it has a large lift-to-drag ratio while maintaining a certain large volume. Figure 5-4 shows a comparison of the lift and lift-to-drag ratios of the waverider and the conventional shape. As can be seen from Figure 5-4, the lift-to-drag ratio of the waverider is much larger than that of the conventional shape at the same angle of attack.

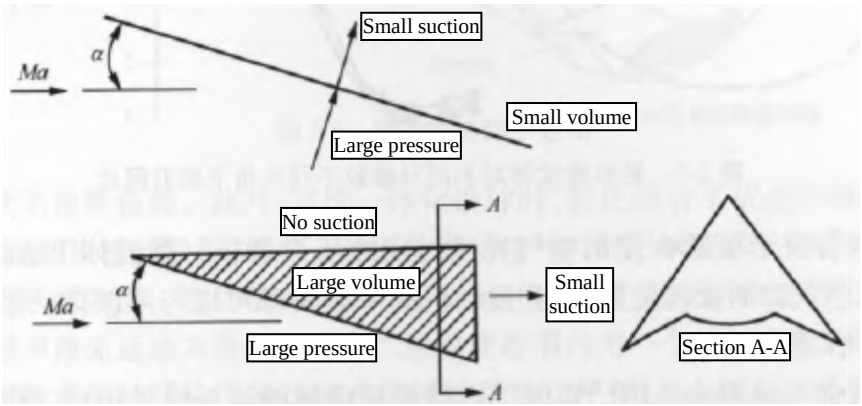

Figure 5-3: Comparison of thin wing and waverider profiles at hypersonic speeds

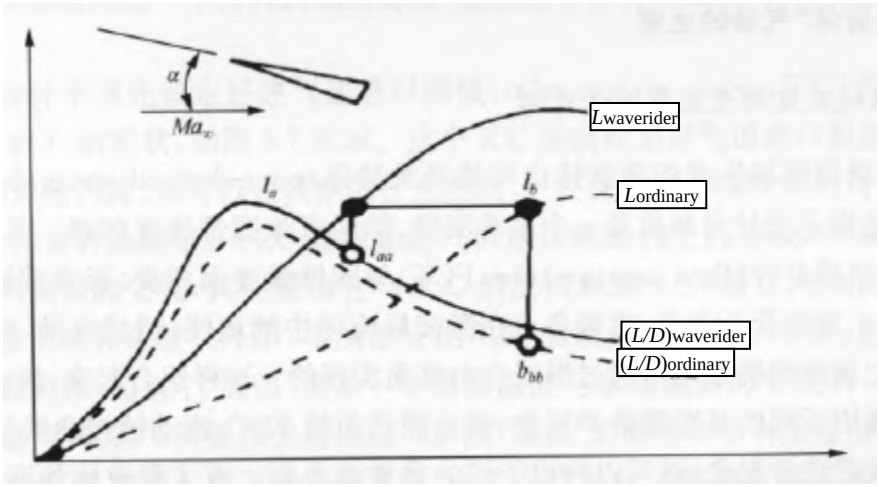

Figure 5-4: Comparison of lift L and lift-to-drag ratio L/D curves between waverider and conventional shapes

The advantages of the waverider shape are mainly reflected in the following four aspects.

(1) The biggest advantage of the shape of the waverider is low resistance, high lift, high lift-to-drag ratio, there is no flow field interference on its upper surface, no streamline deflection, and the shock wave is limited to the leading edge of the shape, so that the high pressure on the middle and lower surface of the compressible region is combined with the upward inclined shape to obtain the thrust component on the whole shape.

(2) The shape of the waverider body can still maintain favorable aerodynamic performance under the condition of deviating from the design. As shown in Figure 5-5. The upper part of Figure 5-5 is a cross-section of the wind tunnel test model in the shape of a waverider formed by an elliptical conic flow field, called an elliptical cone waverider (ECWR), and the L/D curve of the test is shown below Figure 5-5, the design conditions are $Ma = 4$, $\alpha = 0°$, when Ma and α change greatly, the change of L/D is relatively small, and when there is a sideslip angle (5° to 10°), the pressure distribution is not much different compared with the non-sideslip angle.

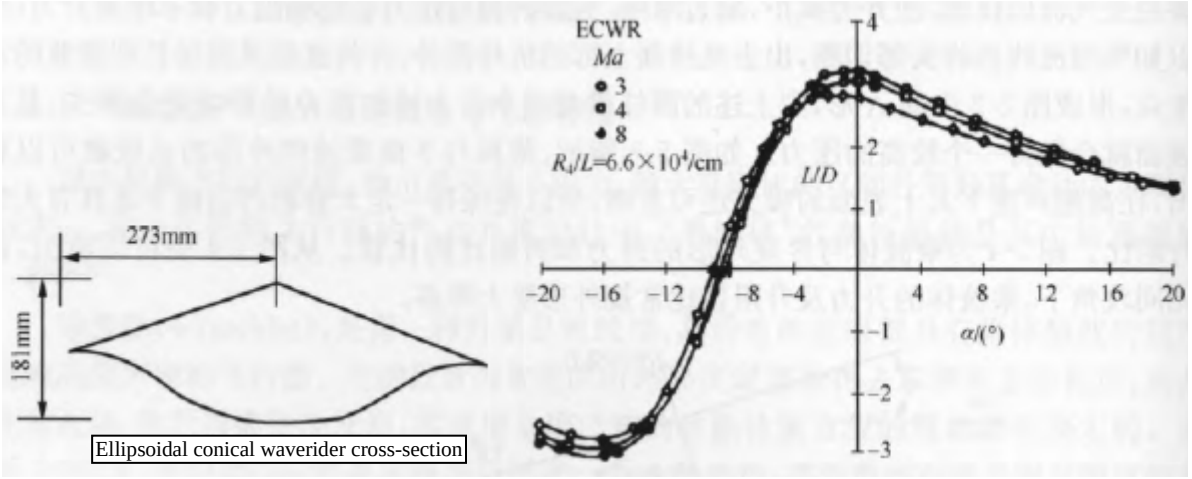

Figure 5-5: The lift-to-drag ratio of the conical waverider to different Mach numbers and different angles of attack

(3) The shape of the waverider is more suitable for the use of jet engines or ramjet engines. The lower surface of the waverider is a high-pressure area, which is an excellent location for the engine air intake, and the lower surface of the engine can be designed with the waverider so that it does not lose the resistance of the air intake.

(4) Because the shape of the waverider is designed with a known flow field that can be accurately solved, it is easier to optimize the design to find the optimal configuration. At present, great progress has been made in the study of the optimal waverider considering viscosity.

5.2.2: Formation of "waverider" aerodynamics

1. The flow field around the cone generates the shape of the waverider

The waverider generated by the flow field around the cone, also known as the cone-derived waverider, is shown in Figure 5-6. First, the design Mach number and a datum cone are selected, and then the solution of the flow around the cone is solved. Secondly, a cylindrical surface was selected as the flow capture tube (FCT) to intersect with the conic shock surface to form the leading edge of the waverider. Then, a number of points are selected on the leading edge curve to obtain the streamlines of each point in the flow field after the shock wave, and the flow surface is formed to form the lower surface of the wave-riding body, and the determination of the upper surface is realized by forming a free flow surface. In this way, the combination constitutes the forebody shape of the waverider, and different reference cone half-top angles, flow capture curves FCC, and the axial positions of the flow capture curve and the intersection line of the cone, or combined, can form different waverider shapes. With the upper and lower surfaces of the waverider shape and the corresponding flow field solution, the pressure coefficient of each point can be obtained, so as to calculate the lift-to-drag ratio L/D of the waverider. However, this waverider generated by the flow field around the conic also has its drawbacks. Due to the axisymmetric nature of the cone flow field, there are different degrees of gradients along the radial and longitudinal directions of the flow field on the inlet section of the inlet channel, which will adversely affect the operation of the engine.

2. The osculating cone theory generates the shape of the waverider

It can be seen from the waverider shape theory generated by the flow field around the conic that if the inlet of the engine is placed at its end section, the flow field has the properties of conical flow, and the uniformity is not good. In addition, when the forebody and engine are integrated into the design, the structure often requires the shape of the air intake at the end section to be flattened, which in turn requires that the shock shape is not a conical surface.

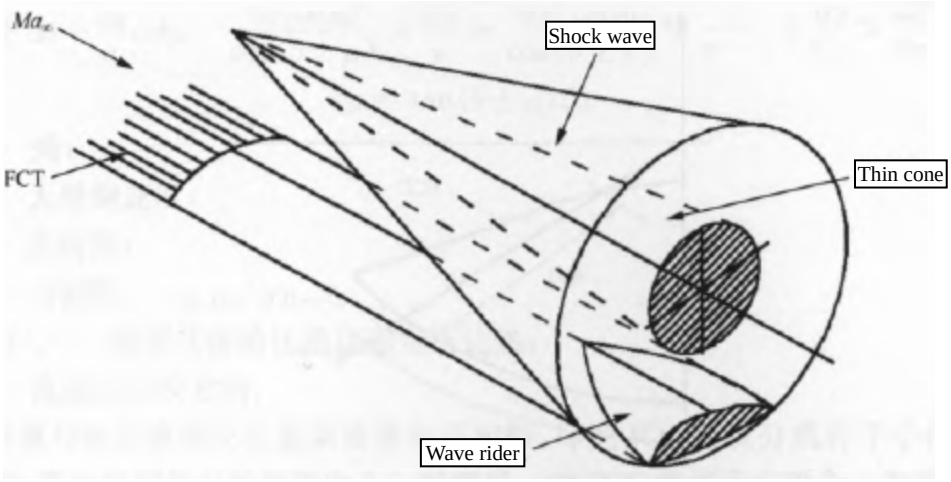

Figure 5-6: Schematic diagram of the conical waverider

In addition, when making an integrated design, optimization steps are often combined, and multiple iterations are required. Therefore, in the preliminary design stage, a method is needed that can not only meet the shape requirements of the air intake, but also quickly generate the shape of the shock wave and the shape of the waverider. The osculating cone (OC) theory proves that at any point in the flow field, the general equation of motion of three-dimensional supersonic flow can be approximated with an axisymmetric equation of motion within the range of secondary accuracy. The axis of this axisymmetric flow is within the osculating plane of the streamline passing through the point. As a result, the local three-dimensional flow can be described by a local two-dimensional flow (axisymmetric flow is also two-dimensional), which greatly saves computational time. The conical flow is a special axisymmetric flow with a simple and precise solution of the flow field, which is often used in practical designs.

In the shape of the inlet capture curve (ICC) and the bus FCC of the flow capture tube FCT, the shape of the inlet capture curve (ICC) and the flow capture tube FCT is preset, as shown in Figure 5-7. This ICC curve is the shock shape curve on the inlet section of the inlet duct, it can be an arc, or it can be other arbitrary curves, as long as the curve has no vertices, the center curve of curvature is continuous, and it is given by the designer. The FCC curve is the upper profile of the inlet section of the inlet channel, that is, the intersection of the lower surface of the waverider and the inlet section of the inlet channel, and its position is determined by its normal distance h(s) from the ICC, which is also given by the designer. In order to determine the shape of the shock wave and the shape of the waverider, the given ICC curve is divided into a number of small segments, and each curve is regarded as a small arc, which in turn is part of the intersection of a conic shock wave and the end section. This cone shock wave is called osculating cone, and the cone top position is determined by the center of curvature of this small "arc" and the given shock angle. The intersection of this osculating cone and the FCT cylinder is the leading edge point, from which a streamline can be obtained by tracing downstream. And so on, the osculating cone method described above is applied to each segment of the ICC curve, resulting in many small shock segments and many leading edge points and streamlines dragged downstream from these points. The envelope of these small segments of shock waves forms a new shock surface, also known as slope surface shock. The flow surface formed by those streamlines forms the lower surface of the waverider's shape. In the osculating cone method, the magnitude of the conic shock angle is constant, i.e., the shock intensity is constant. Of course, the position of the vertices of the cone is changing. Since only one cone flow field needs to be calculated, this method is very fast to calculate.

As can be seen from Figure 5-8, the conical flow properties of the inlet flow field of the inlet channel are significantly improved, and the flow field is more uniform. Since the cone angle of each osculating cone is the same, the intensity of the entire shock surface remains the same. In addition, in this method, the ICC curve is divided into many small segments, and the position of the cone apex angle of each small segment is different, so that the actual generated flow field becomes a non-axisymmetric three-dimensional flow field, and a more general waverider shape is obtained. In the actual design, different ICC curves and functions h(s) can be determined according to different needs.

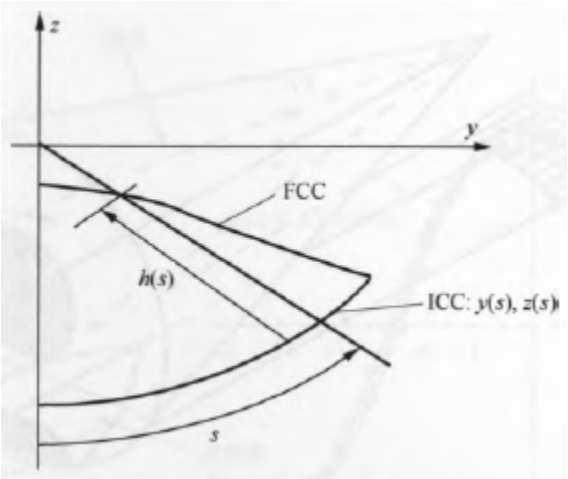

Figure 5-7: Relationship between ICC, FCC, and h(s).

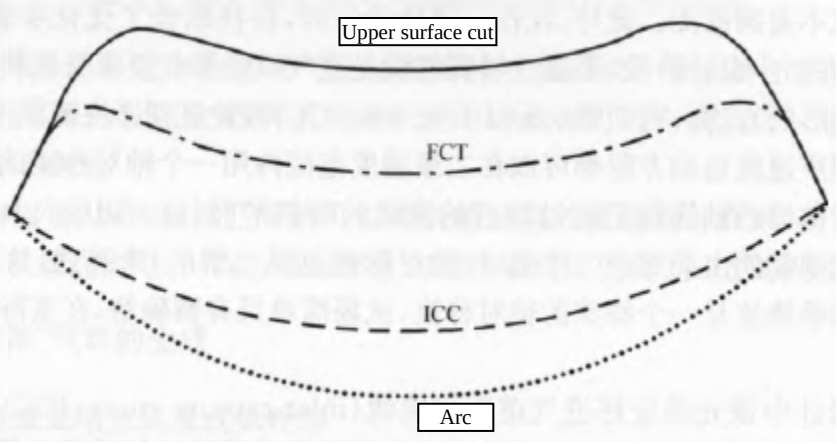

Figure 5-8: Cross-sectional curve of inlet

The function h(s) determines the distance of the shock wave from the lower surface of the waverider. The limit case of the ICC curve is a line segment, which evolves into a situation called the infinite radius of the osculating cone, i.e., the wedge flow field.

3. Kiss-cut axisymmetric flow generates the shape of the waverider

Using the osculating cone theory, it is a fast and effective method to define a single cone flow to calculate the three-dimensional flow field. By generalizing this method with some simple parameters, a more realistic waverider shape can be obtained. This is to use the osculating axisymmetry (OA) theory proposed by Sobieczky et al., which actually changes the straight shock wave in the osculating cone theory to a curved shock wave. Compared with the osculating cone theory, the parameters of the osculating axial symmetry theory are limited to the shock curve, or local shock angle. A single SGC (shock generatrix curve) curve guarantees equal post-wave pressure at each *x* constant section, so that the approximate accuracy can be obtained as the osculating cone theory calculation.

The specific calculations are carried out in combination with the inverse eigenline method of axisymmetric flow, such as the eigenline method with swirling flow [9]. In supersonic and hypersonic flows, given the geometry of a shock wave, it is equivalent to defining an initial line (non-characteristic line). According to the following compatibility conditions (5.8) and the eigenline Equation (5.9), the Cauchy problem can be solved in the dependency region after the shock wave and proceed in a direction perpendicular to the main stream.

$$\pm \mathrm{d}\theta + \frac{\mathrm{d}q}{q}\cot\mu - \frac{\sin\mu\sin\theta}{\cos(\theta\pm\mu)} \times \frac{\mathrm{d}x}{y} = \frac{\sin^3\mu\cos\mu}{\cos(\theta\pm\mu)} \times \frac{1}{\gamma-1} \times \frac{\mathrm{d}x}{C_p} \times \frac{\mathrm{d}S}{\mathrm{d}n} \tag{5.8}$$

$$\mathrm{d}y = \tan(\theta\pm\mu)\mathrm{d}x \tag{5.9}$$

where: S——entropy;

q——dimensionless velocity;

θ——flow angle;

μ——Mach number;

γ and C_p——specific heat ratio and constant pressure specific heat of ideal gas;

n——The normal direction of the streamline.

The specific calculation is similar to the shape of the waverider generated by the osculating cone theory, that is, the ICC curve is divided into several small segments, and each small segment is processed separately, and the center of curvature is found first. According to the single SGC curve and the principle that the intensity of the shock wave is constant in each χ: constant section, the vertex position of the axisymmetric shock wave is determined, and then the swirling characteristic line method is used to solve the post-wave flow field. Starting from the inlet section of the inlet duct, the streamlines of each point are found by interpolation method upstream, and all the streamlines are combined together to form a flow surface, which constitutes the lower surface of the waverider forebody.

Figure 5-9 is a comparison of the results of the intersection line on the inlet section of the inlet tract with the osculating cone method. The dotted line and dotted line in Figure 5-9 are the same as the ICC and FCT curves in Figure 5-8, respectively, the dashed line is the result of the osculating cone method, and the solid line is the result of the osculating axymmetric method, so you can clearly see the increase in the usable area.

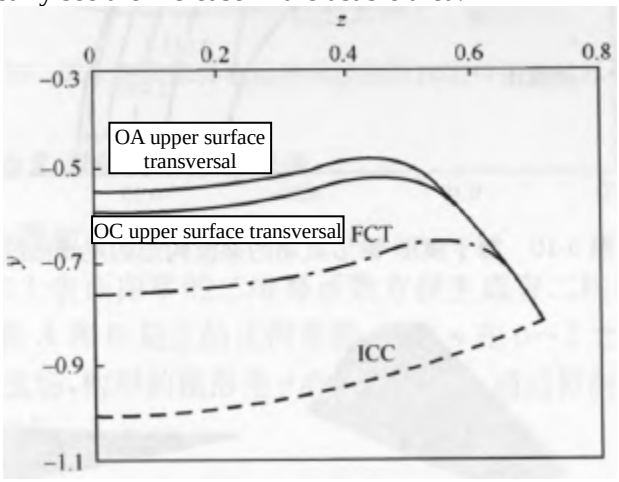

Figure 5-9: Comparison of inlet cross-section curves of the inlet tract

In the high Mach number range, the shock wave is very close to the surface of the object, and a small change in the shape of the shock wave means that the flow field that produces the shape of the shock wave may change greatly. The shock angle used in the calculation in Reference [9] did not change much. The results show that, compared with the osculating cone theory, the waverider shape obtained by the sniff-cut axial symmetry theory expands the usable volume and improves the volume efficiency when the wing area and projection area are reduced. In addition, although the axial symmetric flow field is calculated once for each segment, it is still a fast preliminary design method.

4. Wedge-cone hybrid flow generates a waverider profile

The wedge-cone hybrid flow was chosen in order to make the waverider configuration have both the characteristics of the planar wedge waverider configuration and the characteristics derived from the pyramidal flow waverider configuration, i.e., uniform flow from the lower surface of the wedge-shaped waverider configuration and high L/D and greater volume from the cone waverider configuration.

The specific steps for generation are [11]: First, the width-to-length ratio of the wedge-cone generator and the half-apex angle of the cone are selected. The solution then generates a flow field, which is solved by the three-dimensional Euler equation. Once the flow field is found, the waverider profile can be generated by any flow surface in the area between the object and the shock wave. For forebody design, the shape/surface profile of the trailing edge at the inlet can be determined by the needs of the intake tract and combustion chamber. Figure 5-10 shows the trailing edge curve traced upstream to form the lower surface of the waverider configuration. The center section of the trailing edge curve was chosen to be flat in order to provide uniform inlet characteristics and easy engine mounting. The remainder of the generation process is similar to other waverider configuration design programs, where the streamlines are traced upstream until they intersect the bow shock, the intersection between the flow surface and the shock wave is defined as the leading edge curve, and the upper surface is the flow surface in the same direction as the free flow. Figure 5-11 shows the wave-riding configuration generated by the wedge-cone geometry and trailing edge curve.

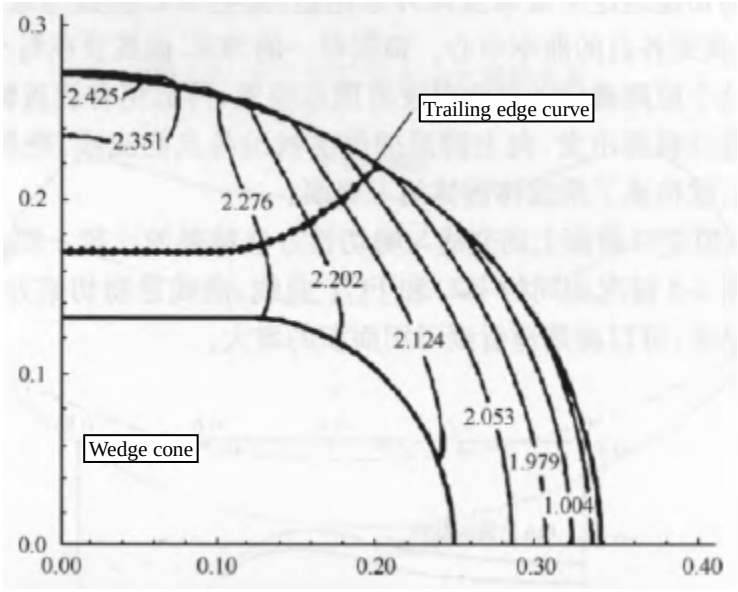

Figure 5-10: Trailing edge curve of wave-riding configuration originating from wedge-cone flow

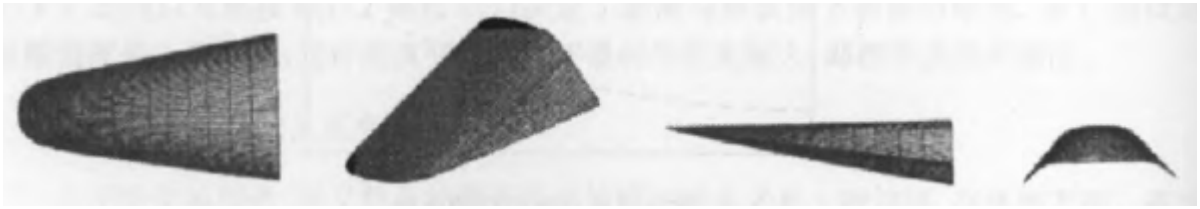

(a) Wing plane (b) oblique view (c) Side view (d) Bottom view

Figure 5-11: Wave-riding configuration originating from wedge-cone flow

5. The intersecting cone generates the shape of the waverider

This method was proposed by Sobieczky et al. [12] and has since been studied in depth by many researchers. In this method, the flow segment after the non-axisymmetric shock is treated as tapered in a plane defined by the intersecting cone. Within the exit surface, a series of planes are used along the shock surface to define the flow field. The shock angle is kept constant in each intersecting plane so that the heterogeneous spanwise direction remains a continuous surface. The conical flow vertices of each plane are determined by the shock angle and the local radius of curvature.

The specific generation steps are: first, given the free-flow Mach number, the shock wave, the shock wave in the exit plane, and the leading or trailing edge curve;

Second, the vertices and leading edge points of the intersecting cones are determined, and the lower surface of the waverider configuration can be constructed by tracing the streamlines along the known cone flow, similar to the generation of the waverider configuration originating from the cone flow. If the shock curve is flat, i.e., when its radius of curvature is infinite, the slope of the streamline will be constant, the slope is equal to the wedge angle, and its given free-flow Mach number produces the given shock angle. Figure 5-12 shows a schematic diagram of a typical wave-riding profile of an intersecting cone in the exit plane. The dashed lines in Figure 5-12 represent the intersection plane, and the circle symbols along the line define the points on the shock curve at the intersection plane, on the surface of the cone in the exit plane, and at the vertices of the intersecting cone.

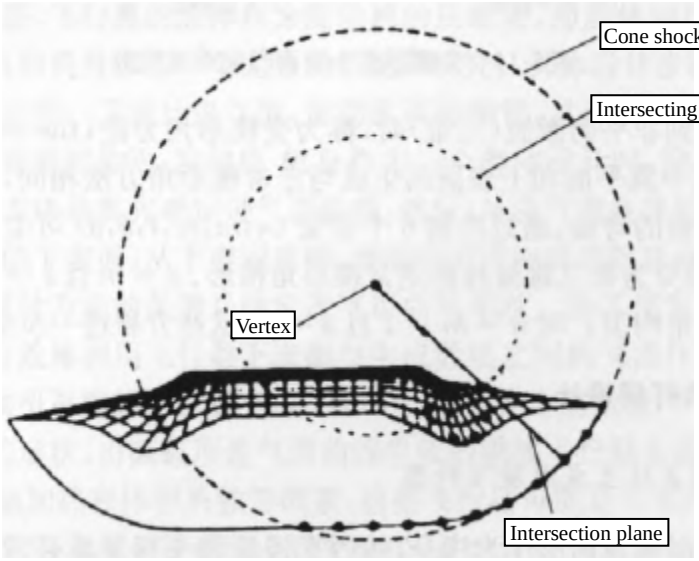

Figure 5-12: Schematic diagram of the wave-riding configuration originating from the flow of the intersecting cone in the exit plane

6. Constant and variable wedge angle methods for generating waverider configurations

The specific steps of this approach are as follows [13,14]:

A wave-multiplying configuration with a two-dimensional (plane) shock wave is generated using a two-dimensional power function equation that determines the curvature of the plane and the upper surface, as shown in Figure 5-13, where parameters *A* and *B* are positive proportionality constants, and the exponent *n* varies from *0* to 1. In order to ensure that it is a plane shock wave, i.e., originating from a wedge-shaped flow field, the wedge-shaped angle θ of the configuration must be constant. By controlling these five variables (A, B, n, L, θ), various wave-riding configurations can be generated.

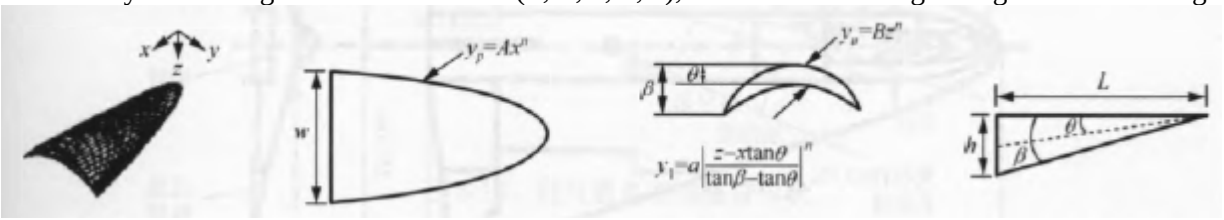

(a) Three-dimensional view (b) Wing plan (c) Bottom view (d) Side view

Figure 5-13: Constant wedge angular wave-multiplication configuration

When designing a waverider configuration assuming an attached leading edge shock, not all variables mixed with this geometry will result in a practical waverider configuration with an attached shock. The curvature of the lower surface with the attached shock wave must be less than the maximum shock wave attachment angle. Figure 5-14 shows the resulting waverider configuration. The requirement of attachment shock reduces the number of variables to 4, i.e., A, n, L, θ. As such, this method is called the constant wedge angle method (CWA).

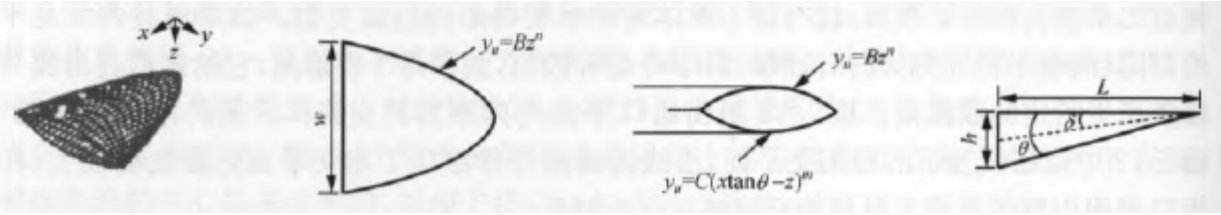

(a) Stereogram (b) Wing flat diagram (c) Bottom diagram (d) Side view

Figure 5-14: Wave-riding configuration with a small convex surface with variable wedge angle

When the above method is extended to non-planar shock waves (3D), it is called the variable wedge angle method (VWA), in which the generation of the wing plane and upper surface is the same as that of the constant wedge angle method, except that a third power function is added to determine the bending of the lower surface, and various wave-riding configurations can be generated by controlling 6 variables ($n, m, w, l, \theta, \delta$).

$n = m$, the model becomes a stationary wedge-shaped angular configuration with three-dimensional shock waves. When $n = m$ and $\delta = \beta$, the model changes to a stationary wedge-shaped angular configuration with planar shocks. For $n = m = 1$ and $\delta = \beta$, these equations are further changed to a λ-shaped multiplicative wave configuration.

5.2.3: "Waverider" aircraft design

1. The wave-riding aircraft is directly generated from the wave-riding configuration

This kind of aircraft uses the wave-riding configuration as the fuselage, and then directly assembles the necessary components of the aircraft, such as control surfaces, engines, cockpits, etc., to make it a hypersonic wave-riding aircraft with better performance and integrated engines and fuselage. This generation method is relatively simple, but it requires a lot of research work to explore the influence of various components on the aerodynamic performance of the aircraft.

Figure 5-15 is a $Ma = 4$ supersonic cruise vehicle directly generated by two wave-riding configurations [15], including a straight-wing model and a curved-wing model. This supersonic cruise vehicle, derived from the wave-riding configuration, includes a cockpit, propulsion system, and control surfaces.

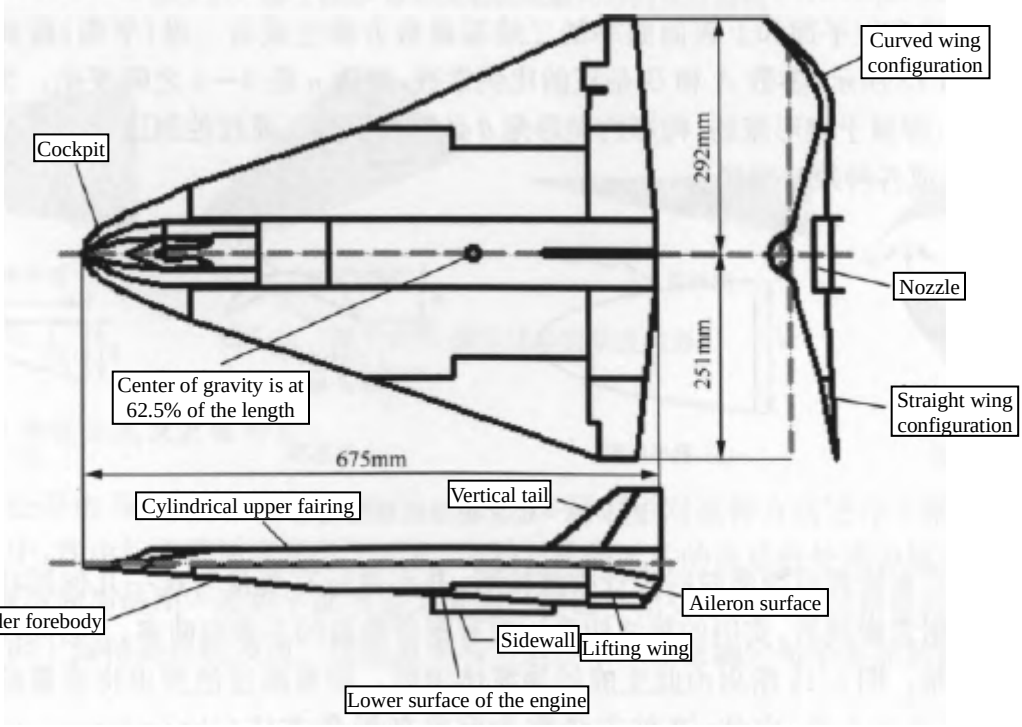

Figure 5-15: A $Ma = 4$ supersonic cruise vehicle derived from the waverider configuration

The propulsion system includes the intake tract compression ramp, the engine module and the nozzle/expansion surface, and the control surfaces include the lifting ailerons, ailerons and vertical tail. The study of this supersonic vehicle shows that compared with the pure wave-riding configuration, the lift-to-drag ratio of the supersonic waverider generated by the wave-riding configuration is reduced, but compared with the conventional aircraft, the aerodynamic performance of the supersonic aircraft is significantly improved after the optimization of the control surface and propulsion system [16~20].

2. Wave-riding aircraft with integrated design of wave-riding configuration-engine-fuselage

In this wave-riding aircraft, the front body of the aircraft is used as the compression surface of the engine, and the rear body is used as the nozzle of the aircraft, so the engine and fuselage need to be studied as a complete system. The specific design steps are as follows: (1) determine the length of the combustion chamber of the scramjet engine. (2) design the air intake, hood, and nozzle, see Figure 5-16. (3) generation of waverider forebodies. Reference [21] and [22] use an inverse design approach when designing the waverider configuration-engine-fuselage as a whole. In this method, the key to this design method is to determine the shape of the inlet curve by first determining the inlet curve, and then tracing the free streamline backward from the lower surface of the streamline/shock intersection to the upper surface of the wave-riding configuration. In order to maximize the mass flow captured by the engine, it is necessary to effectively use the airflow between the lower surface of the aircraft and the generated shock wave as the mass flow into the air intake, which requires that the bonnet lip should be rounded and as close as possible to the generated shock wave [23]. (4) optimize the design. First, the shape of the waverider forebodies was optimized, and the head of the waverider generated by the curve of the arc-shaped air inlet was pointed and the upper surface was concave [24], which may not be practical considering factors such as aerodynamic heating and volume coefficient. Therefore, the requirement for the uniformity of the orientation of the inlet tract height is somewhat relaxed and allows the inlet curve to be elliptical instead of a circular line. Secondly, the length of the forebody relative to the length of the aircraft is optimized, due to the nature of the conical flow, the position of the bonnet lip affects the pressure and angle of the lower surface of the aircraft, so the lift and drag of the aircraft are affected. At the same time, for a given inlet height, the position of the hood lip also determines the maximum radius of the hood lip in the cross-section [25~28].

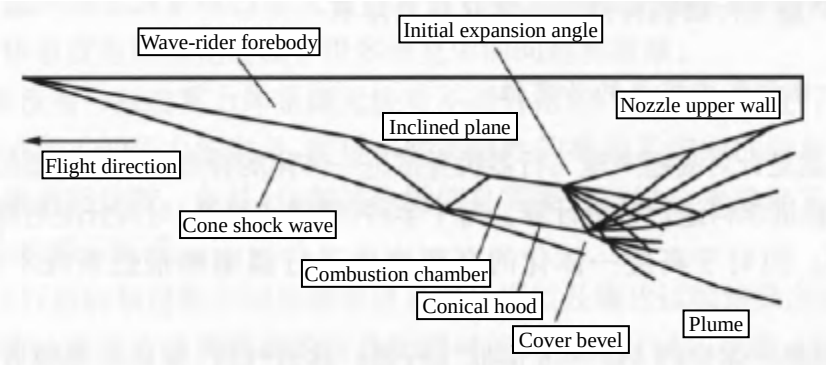

Figure 5-16: Inlet slope and nozzle shape

According to the above generation methods, different researchers use different wave-riding forebody generation methods to obtain wave-riding aircraft with different shapes. Figure 5-17 shows a hypersonic cruise vehicle (Ma = 10) with integrated wave-riding forebody-engine-fuselage generated in Reference [22]. Figure 5-18 shows a hypersonic acceleration vehicle (Ma = 10) with an integrated waverider-engine-fuselage generated in Reference [22], which is a waverider configuration derived from cone flow and optimized for the engine and nozzle. Figure 5-19 is a hypersonic cruise vehicle with Ma = 10 waverider configuration-engine-fuselage integration generated in Reference [11], the waverider forebody is derived from the waverider configuration of the intersecting cone, and the shape of the aircraft is obtained by optimizing the waverider shape for the maximum L/D and replacing the rear part of the center section of the forebody with the engine cross-section.

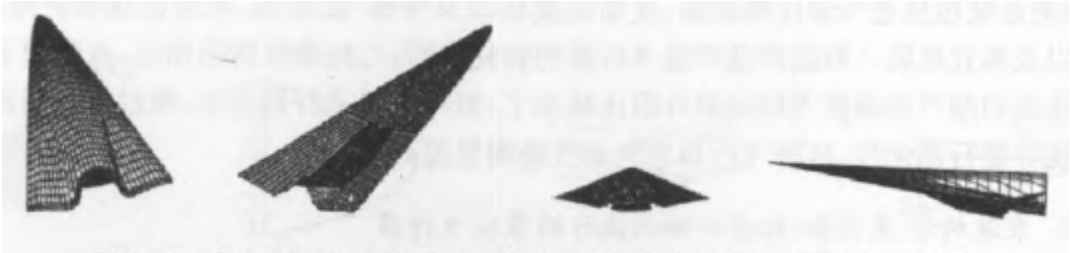

Figure 5-17: Hypersonic cruise vehicle with integrated wave-riding forebody-engine-fuselage (*Ma* = 10) [22]

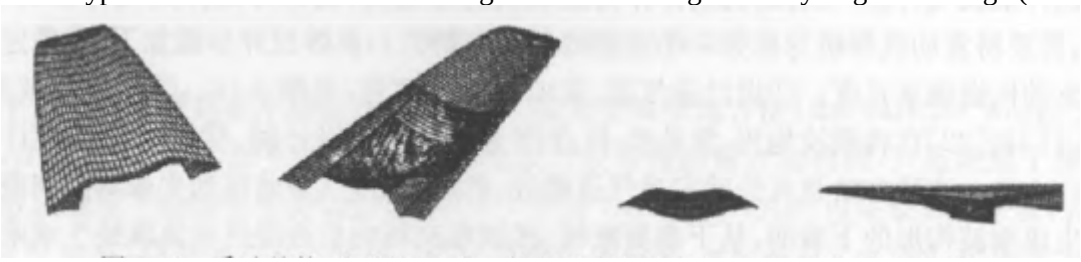

Figure 5-18: Hypersonic cruise vehicle with integrated wave-riding forebody-engine-fuselage (*Ma* = 10)[22]

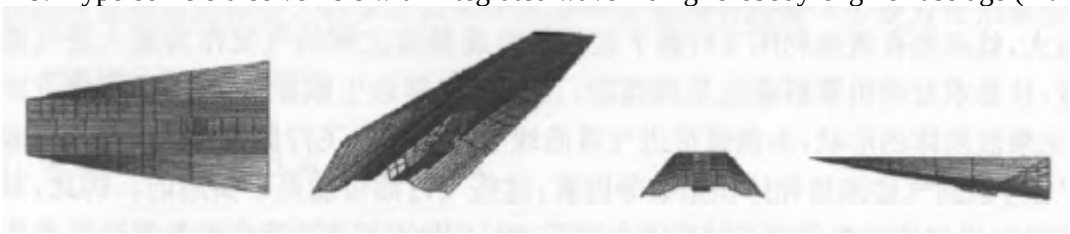

Figure 5-19: A hypersonic cruise vehicle with *Ma* = 10 waverider forebody-engine-fuselage integration [11]

5.3: Integrated design of hypersonic vehicle fuselage and propulsion

5.3.1: Integrated computing power system for hypersonic vehicle fuselage propulsion

1. Study the necessity of an integrated computing system

The computing power system is to determine how to divide each part of the aircraft into aerodynamic or propulsion disciplines for analysis and calculation according to the characteristics of hypersonic vehicle fuselage propulsion integration. Each discipline (pneumatic or propulsion) carries out the calculation of aerodynamic forces and moments for its assigned components. However, for highly integrated hypersonic vehicles, it is not a simple matter to define the propulsion system [29-31].

Figure 5-20 shows a non-integrated *Ma* = 6 cruise vehicle. Its air intake, engine, and nozzle are all contained in the pod of the propulsion system, completely separate from the fuselage. For this aircraft configuration, the aerodynamic and propulsion components have less interaction with each other, so the aerodynamic and propulsion analyses can be carried out relatively independently with relative ease.

On the contrary, as shown in Figure 5-21, for a hypersonic cruise vehicle with integrated fuselage propulsion, the different aircraft components are designed to be mutually reinforcing and contribute to their respective performance improvements. For example, the forebody of the aircraft generates a considerable degree of compression of the propulsion system tube flow, while its surface generates lift and pitch moments; the rear body expansion surface of the aircraft is designed to meet the requirements of optimal thrust, while also making a considerable contribution to the lift and pitch moments. Therefore, the expansion surface of the aircraft forebody and the rear body are the key parts in the aerodynamic calculation of the fuselage and the performance calculation of the propulsion system, and its proper and correct integrated design is the key to the entire aircraft design. At the same time, however, it should be noted that there is some degree of ambiguity in the definition of pneumatic and propulsion components.

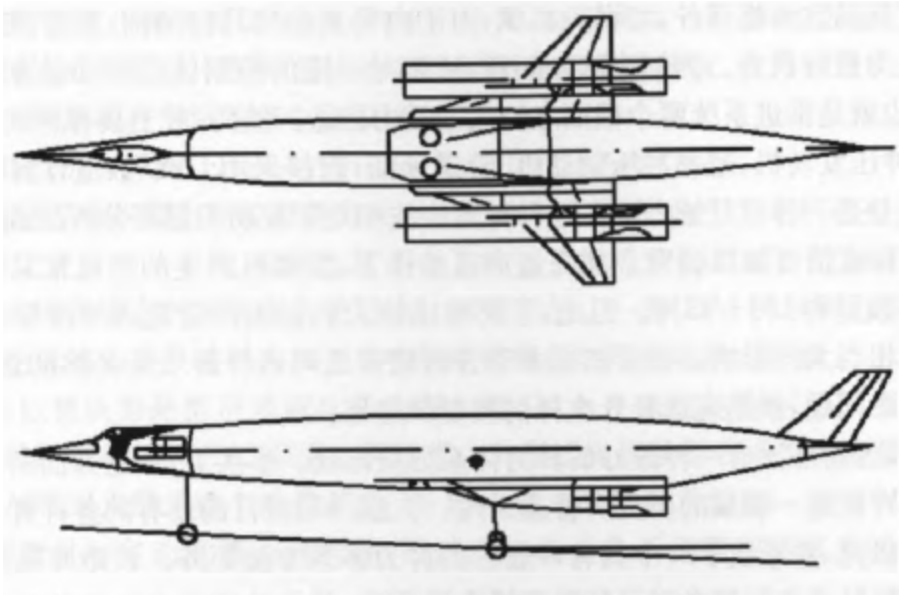

Figure 5-20: Non-integrated *Ma* = 6 cruise vehicle

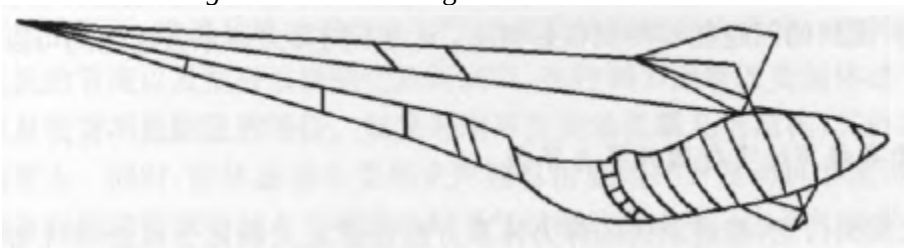

Figure 5-21: A hypersonic vehicle with integrated fuselage propulsion

This makes it inconvenient for the aerodynamics and propulsion disciplines to carry out their own independent research work.

The vague definition of hypersonic propulsion system has led to the existence of a variety of computing power methodologies in the field of hypersonic research. Due to the lack of standardization of the computing power system, there are many problems and difficulties in research.

First of all, without a consistent computing power system, it is impossible to evaluate and compare aircraft solutions of different shapes. The different definitions of thrust and propulsion-related drag make it impossible to directly compare some of the key propulsion system performance parameters, such as specific impulse and net thrust. In addition, detailed analysis information needs to be dimensionless according to conventionally defined performance parameters, which is difficult to achieve.

Secondly, there is a lack of continuity between the preliminary propulsion system analysis and the scale-down test results in the development of the aircraft. The type of information required for the chosen computing system method may not be available experimentally. Similarly, the amount measured by the experiment can provide some, but not all, of the forces determined in the preliminary analysis. For example, the resistance of the inlet tract comes from a variety of sources, including overflow resistance, additional resistance, etc., which is difficult to obtain with a force balance for wind tunnel testing. Usually, a force balance can only give the total resistance. This limits the accuracy of the preliminary analytical method to be validated by the test results.

Finally, it is difficult to study the influence of component design parameters on the overall performance of the aircraft. Each discipline is accustomed to the conventional method of calculating its most representative performance sensitivity. Different approaches to computing power systems only emphasize the impact of their specific performance. For example, the analysis of the propulsion system can determine the sensitivity of the forebody compression to its effects, while the effect of the rear body wall expansion on the thrust may not allow the aerodynamic discipline to optimize the lift-to-drag ratio.

For hypersonic air-breathing vehicles, additional complications include the analysis of the engine itself.

For engine components of non-hypersonic vehicles, such as turbomachinery, it is often difficult to directly integrate pressure and shear stresses due to the complex internal geometry. In order to solve this problem, the momentum equation is usually applied to a certain control body to derive the engine thrust, that is, the difference in the flow thrust between the two sections of the propulsion system. However, for engine concepts with open channels, such as ramjets, scramjets, and pipeline rockets, it is a feasible approach to integrate the quantities on the surface directly using CFD numerical calculations. The accuracy of this calculation method relative to the engine cycle analysis method or the empirical thrust standard data method needs to be studied. In hypersonic conditions, the force generated by the engine is typically only 1% to 10% of the amount of thrust flowing in the upstream and downstream sections. As a result, any error in the flow thrust will have a considerable impact on the derived engine thrust. The trade-off between cost and accuracy is a necessitating choice, which raises the question of what control body boundaries should be chosen.

Obviously, there is no one best way to do it. In fact, standardization efforts in this area have not been widely adopted by studies in this area. Reference [31] summarizes and studies the existing methods of various computing systems and forms a general matrix of computing system methods. This matrix is suitable for the study of the vast majority of hypersonic air-breathing vehicles in the wide Mach number range, and its methods are derived from existing application cases. Using this method, researchers engaged in the integration of airframe propulsion can flexibly choose the computing system method according to the specific situation. At the same time, the problems mentioned above can be well solved, because different computing system methods can be easily converted to each other.

2. About the computing power interface of hypersonic vehicles

As previously discussed, the computing power system approach to propulsion systems involves defining and differentiating between the surfaces on which propulsion and aerodynamic forces correspond to the surface of the aircraft. The method of the control body is also necessary to some extent to determine the forces generated by the engine, including the selection of the appropriate control body boundary. These two tasks lead to clear boundaries, which form the basis of a common matrix of methods for computing power systems. These interfaces are described below.

1) Aero-Propulsion Interface (API)

The interface between pneumatics and propulsion is called the pneumatic propulsion interface (API). It is the main dividing line between the analytical responsibilities of the pneumatics and propulsion disciplines. This does not mean that there is a division of labor between the airframe research team and the engine development team, as the engine is only considered as part of the propulsion system. An example of an API is shown in Figure 5-22, where the analysis of the propulsion system is responsible for determining the forces and moments acting on the ramjet surface, the inner surface of the engine, and the expansion surface of the rear body.

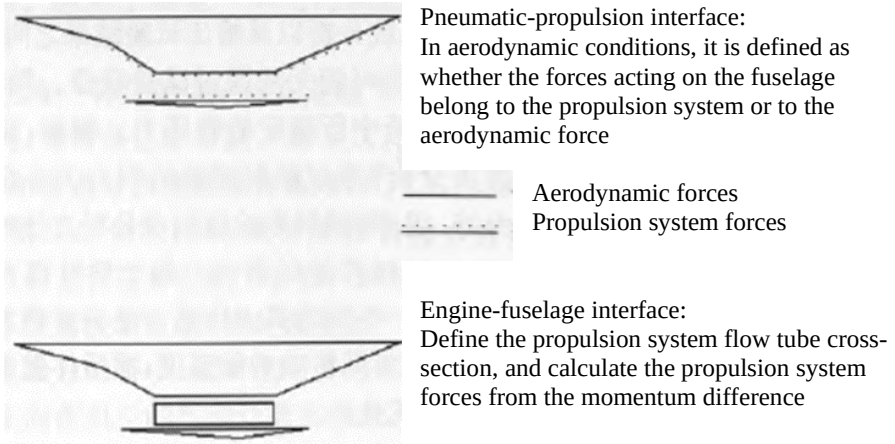

Figure 5-22: Definition of the pneumatic propulsion computing power interface

The 2D aircraft is only an extremely simplified representation, and the real aircraft configuration requires a more complex 3D API definition. In addition, interface boundaries may change depending on the Mach number, angle of attack, and engine airflow, which will be explained in more detail in subsequent chapters.

2) Engine-Airframe Interface (EAI)

The control body method used to derive the engine thrust leads to another interface, called the Engine Airframe Interface (EAI). The control body boundary defines this interface, and often the section of the propulsion system's flow tubes. For example, free flow, nozzle outlet, etc., the flow thrust on these cross-sections can be calculated. An example of EAI, as shown in Figure 5-22, shows that engine thrust is the difference in flow thrust between the inlet face of the engine and the section of the nozzle throat.

EAI can be considered as part of the forces acting on the propulsion system, which is provided by the development department of the engine. That is, the development department of the engine provides data sheets or thrust measurements in the form of net thrust between EAI sections. It should be noted that the API defines the entire propulsion system, while the EAI defines a part of the propulsion system that is only provided by the engine development department, and the analysis of the propulsion system of the airframe requires the calculation of the rest of the propulsion system.

3) Aero-Reference Conditions (ARC)

Under certain circumstances, the operation of the propulsion system has an effect on the flow field on the aerodynamic surface. This effect comes from the throttling of the engine air flow and the variable geometry of the propulsion system, which is able to change the intensity of the compression shock wave of the forebody intake tract and the characteristics of the nozzle plume expansion. With variable hood geometry, the pressure on the surface of the hood is more affected. At the same time, the forebody flow is also affected by the engine throttling regulation under subsonic free flow conditions. Other influences include the effect of nozzle gas on the trim aerodynamic surface of the horizontal tail. Since the analysis of aerodynamics is not responsible for determining the effects of the propulsion system, it is necessary to specify the aerodynamic reference conditions (ARCs) so that the aerodynamic forces can be completely independent of the influence of the propulsion system on the computing power.

ARC specifies the position of the engine flow and propulsion system geometry for each free flow condition. Since the propulsion system is operating in a non-ARC condition, the change of the force on the aerodynamic surface is changed to the correction of the non-reference force of the propulsion system. Therefore, the correction of the non-reference force under the reference condition is defined as 0. Figure 5-23 shows a typical ARC'S example and illustrates the force correction under non-reference conditions in the outer bonnet, in which all variable geometries have a reference position, the flow of the intake tract is initiated, and the nozzle pressure ratio is established. Corrections under non-reference conditions may be a function of Mach number, angle of attack, inlet flow, nozzle pressure ratio, and variable geometry settings.

It is important to clarify ARC for CFD numerical calculations and wind tunnel testing. Since the aerodynamic force and torque are eliminated as a function of the operating state of the propulsion system, numerical calculations and wind tunnel tests can save a lot of cost of calculations and tests by performing them under reference conditions, and the aerodynamic analysis does not need to simulate the working state of the propulsion system. The analysis of the propulsion system is responsible for providing aerodynamic reference conditions in the propulsion system analysis model to determine the modified datum under non-reference conditions. It is not necessary for the ARC to represent any real operating conditions of the propulsion system, as the objective is to define the conditions, which are easy and can be replicated with relative accuracy.

4) Synthesis of forces

Finally, the net thrust FNP (parallel to the direction of the aircraft velocity vector), the thrust lift force ΔL (perpendicular to the direction of the aircraft velocity vector), and the thrust pitch moment ΔM are the sum of the forces generated on the surface of the propulsion system defined by the API, plus the corrections due to the propulsion system operating under non-reference conditions. The other forces acting on the aircraft constitute the aerodynamic force. EAI's research team provides specific components of F_{NP}, ΔL, and ΔM.

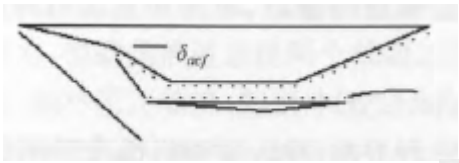

The surface on which the propulsion system dominates under aerodynamic reference conditions

- Critical inlet flow and inlet compression wedge at the reference position
- The ratio of the air flow pressure through the nozzle
- Variable nozzle outlet lower wall at the reference position

Typical pneumatic table
Typical propulsion surface

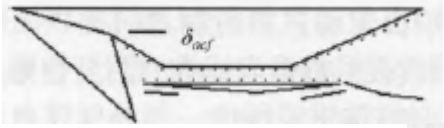

The surface dominated by the propulsion system under non-aerodynamic reference conditions

- Variable inlet tract wedge compression angle increases
- The nozzle pressure ratio increases

Typical propulsion table while
Since the propulsion system operates in a non-reference state, the aerodynamic surface has a component of force at an angle of δ

Figure 5-23: Typical aerodynamic reference conditions

5.3.2: Integrated design of air intake of hypersonic vehicle forebody

1. Design requirements for the integration of the air inlet of the forebody of hypersonic vehicles

Reference [32] and Reference [33] have studied the integrated design of scramjet engine and waverider aircraft. The results show that the overall performance of hypersonic cruise and acceleration vehicles is affected by the uniformity of the flow field during combustion, and uniform mass flow, pressure and temperature are very important for effective combustion. Therefore, the flow field provided to the engine by the aircraft forebody, whether in the spread direction or the height direction of the inlet tract, must be uniform in order to improve the working performance of the engine, for which the forebody is required to have a high pre-compression ratio and provide a uniform flow field at the inlet of the inlet (the gradient of pressure, velocity and density is as small as possible, and the direction angle of the air flow is as consistent as possible).

The objectives of forebody design optimization were identified in Reference [34]: higher static pressure at the inlet of the air intake; larger air quality flow rate to increase engine thrust while minimizing engine size and corresponding aircraft drag; smaller total pressure loss; small Mach number variation in the inlet section of the inlet tract; in the case of a certain change of attack angle and side slip angle, the fluctuation of the inlet flow field of the inlet tract is as small as possible to ensure the stable operation of the engine. At the same time, it is also pointed out in Reference [34] that the precompression performance of the forebody is affected by a large number of geometric parameters: the surface of the bottom of the forebody (elliptical, convex, flat, concave), the degree of lateral orientation (wide body, narrow body); the transition from the bottom surface of the forebody to the side (sharp transition, rounded transition), and the shape of the head of the aircraft (spire, arc, straight); the length of the forebody and the profile form of the longitudinal section; the aspect ratio of the forebody fuselage. It can be seen that there are a large number of possible geometries in the design of hypersonic vehicle forebodies. Figures 5-24 to 5-27 show the forebody design configurations used in foreign hypersonic test vehicles. In Reference [35], numerical simulations were used to comprehensively compare the configurations of various forms of hypersonic vehicle forebodies, including the convex, concave, and wave-riding forms at the bottom of the forebodies, the pointed and wide head forms, and the different leading edge arc radii. The results show that the forebody of waverider configuration can effectively reduce the transverse overflow, and has good precompression performance, uniform inlet flow field and aerodynamic characteristics of the inlet channel, but its disadvantage is that the effective volume inside the aircraft is small, which restricts the installation of fuel and internal instruments and equipment of the aircraft. The design of the lower surface of the forebody of other arches is not desirable, which will cause the uneven flow of the inlet section of the inlet channel; the blunt forebody head with a large arc radius at the leading edge will cause a large total pressure recovery loss and a thicker surface layer;

the "spatula" shaped wide forebody design will bring greater aerodynamic resistance. Therefore, the design of hypersonic vehicle forebodies needs to be compromised from many aspects, such as the impact on propulsion performance, the impact on aerodynamic performance, and other constraints on the overall design.

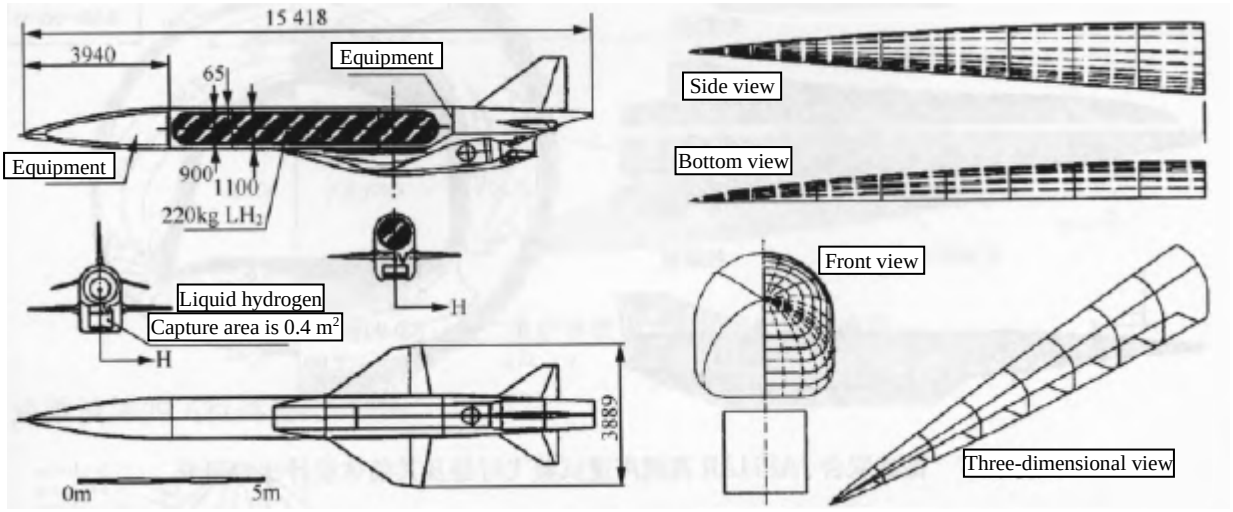

Figure 5-24: Improved design of the German HYTEX R-A3 hypersonic technology flight test vehicle and its forebody

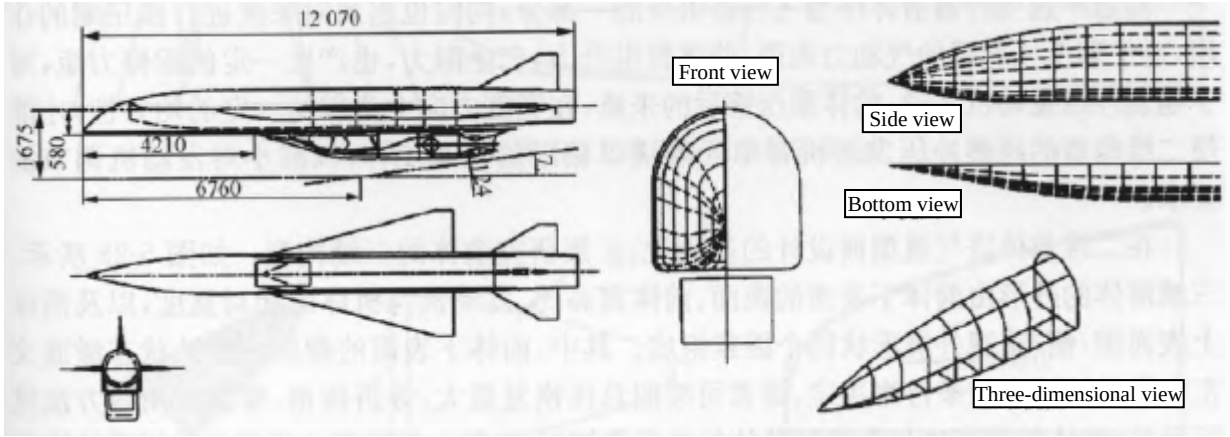

Figure 5-25: Improved design of the German hypersonic flight test platform D2 and its forebody

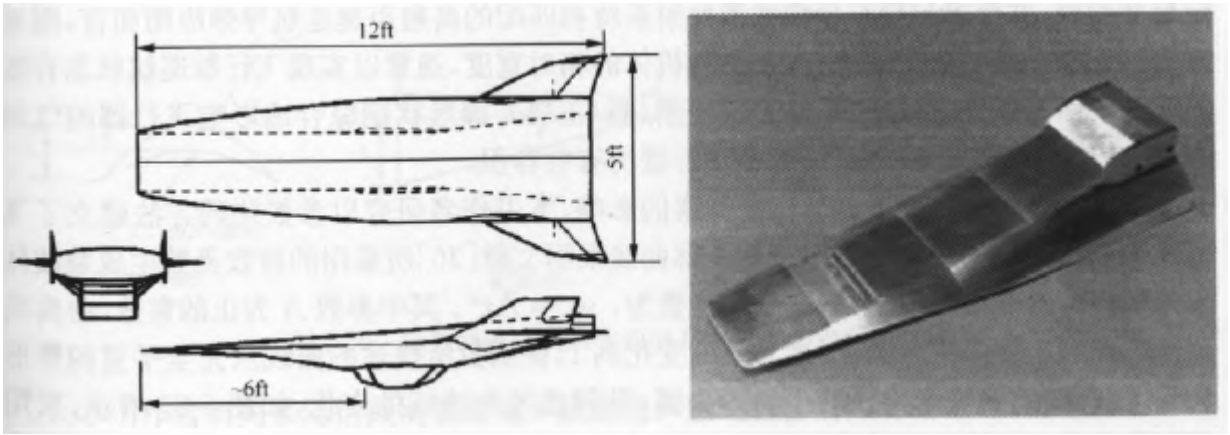

Figure 5-26: U.S. Hyper-X hypersonic test vehicle and its forebody components

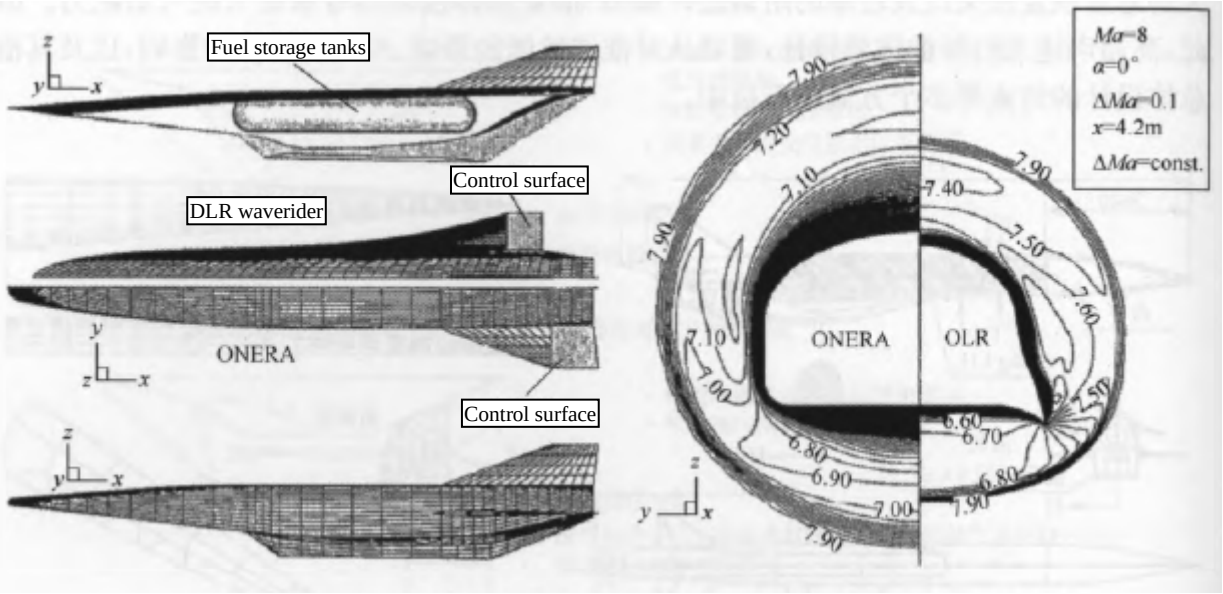

Figure 5-27: Comparative study of the design of the German-French joint JAPHAR hypersonic test vehicle and its forebody

2. Parametric modeling and performance index of the three-dimensional forebody of hypersonic aircraft

The hypersonic vehicle forebody is a part of the fuselage of the aircraft, and also plays the role of pre-compression of the incoming flow, for the aerodynamic force of the whole aircraft, the forebody provides lift, produces drag, and also produces a certain pitching moment, for the scramjet engine, the incoming flow after the pre-compression of the forebody should maintain a certain uniformity in the width direction, so as to make the unit modules of the two-dimensional configuration of the scramjet engine work in a similar state, so as to reduce the requirements for engine adjustment.

On the basis of the two-dimensional forebody inlet surface design, the three-dimensional configuration of the forebody was expanded. As shown in Figure 5-28, the shape of the three-dimensional forebody consists of four factors: the wedge surface of the lower surface of the forebody, the aspect ratio of the forebody, the relative width of the engine and the fuselage, and the shape of the upper surface of the forebody. Among them, the wedge surface of the lower surface of the forebody is determined by the condition that the shock waves of the design state meet at the lip of the engine, and can usually be designed according to the methods of maximum total pressure recovery, equal fold angle, equal shock angle, etc.; the aspect ratio of the forebody is closely related to the overall shape of the aircraft, and the larger aspect ratio can usually be designed with the shape of the waverider and applied to the hypersonic cruise aircraft, the first-stage carrier aircraft of the two-stage orbiting space launch vehicle, etc., while for the hypersonic cruise missile applications with certain size constraints and required to match the existing missile weapon launch system, a smaller forebody aspect ratio is usually selected; the relative width of the engine and the fuselage is usually determined by the conditions to achieve an effective thrust-drag balance in the cruising state of the aircraft; the profiled shape of the upper surface of the forebody comprehensively affects the aerodynamic force of the aircraft, the inlet conditions of the scramjet engine, and the effective volume of the aircraft.

In order to comprehensively reflect the influence of the above shape characteristic factors, the author of this book studies the three-dimensional forebody shape model of the aircraft by parametric method. The head curve of the aircraft is described according to the method of generating the configuration of the waverider aircraft using the exponential function adopted in Reference [36], and the basic curve function is: $\gamma_p = Ax^n$. When n changes from 0 to 1, the curve described by the function gradually changes from a completely straight rectangular head to a completely pointed triangular head, and the curve changes continuously, as shown in Figure 5-29. In addition, the aircraft configuration of the waverider can also be approximated through this function curve, which is used in Reference [36] to generate the aircraft configuration of the waverider, as shown in Figure 5-30.

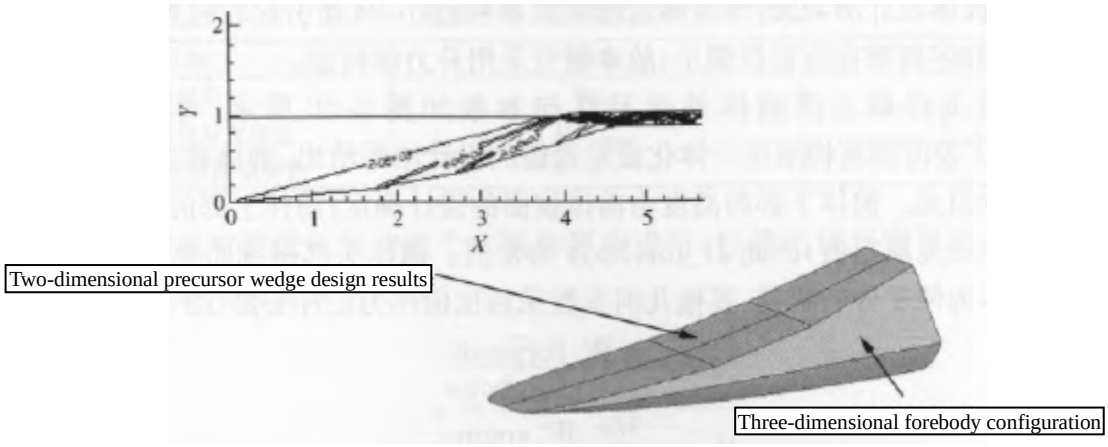

Figure 5-28: From a 2D forebody wedge design to a 3D forebody configuration

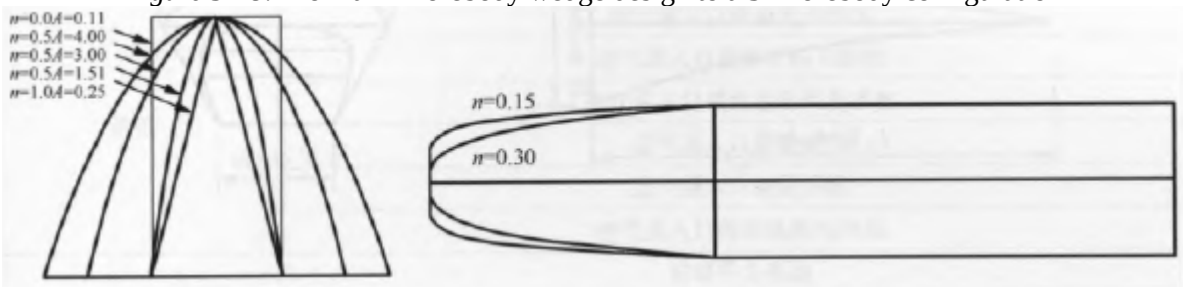

Figure 5-29: The exponential function curve controls the change of parameters

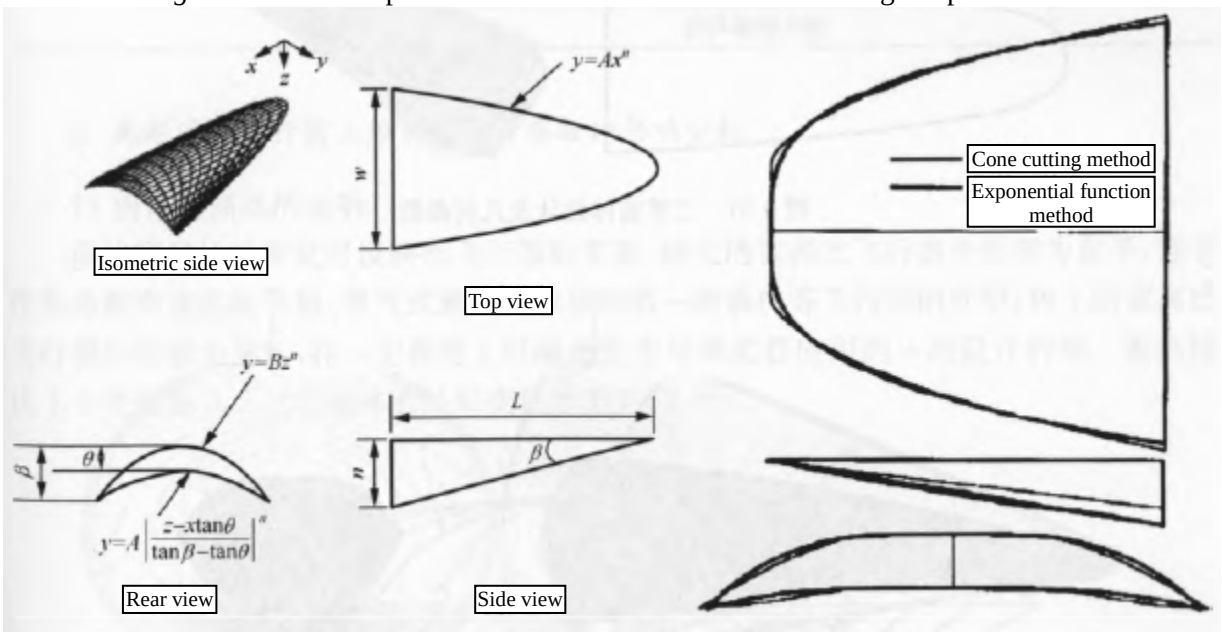

Figure 5-30: The wave-multiplication configuration generated by the exponential function and its comparison with the cone tangent configuration

The author of this book studies the use of exponential function curves to form the top-down, orthopedic and side-view curves of the forebody of hypersonic vehicles, and then forms a curved surface from the curves, and the lower surface of the forebody is designed with a transverse equal wedge angle, that is, a straight plane, mainly considering that the use of waverider design for small-scale aircraft will cause the arc radius of the edge of the forebody to be too small, thus causing strong aerodynamic heating.

At the same time, in view of the small effective volume of the waverider configuration, the lift body configuration is used in this study.

Figure 5-31 shows the shape and geometric parameters of the three-dimensional forebody of the hypersonic vehicle. The length of the forebody is L_forebody and the wedge surface of the lower surface is given by the design results of the integrated flow channel, and the height of the forebody is H_forebody composed of two parts: the upper and lower parts. The height of the lower part of the forebody is determined by the design of the forebody wedge; the height of the upper part of the forebody can be selected according to the design constraints, and a fixed value is taken in this study, so it is H_forebody constant. The shape of the top view of the head of the forebody is controlled by the parameter n of the exponential function, and the ratio is used as the design variable for other geometric parameters (Figure 5-32 and Table 5-2) for the convenience of analysis and research:

$$R_{WH} = \frac{W\_forebody}{H\_forebody} \tag{5.10}$$

$$R_{W\_engine} = \frac{W\_engine}{W\_forebody} \tag{5.11}$$

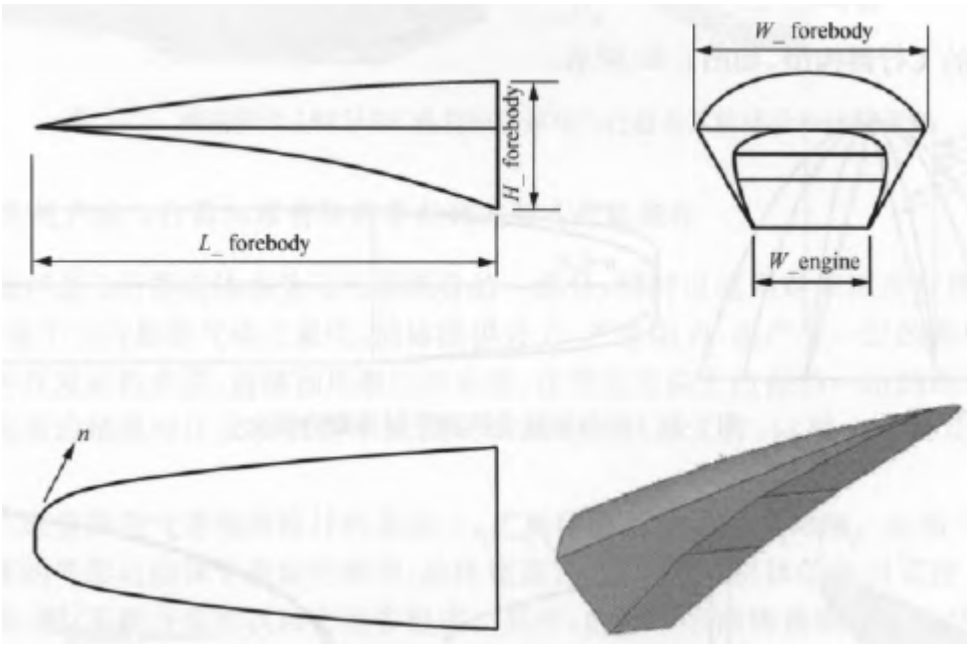

Figure 5-31: 3D forebody design and geometric parameters

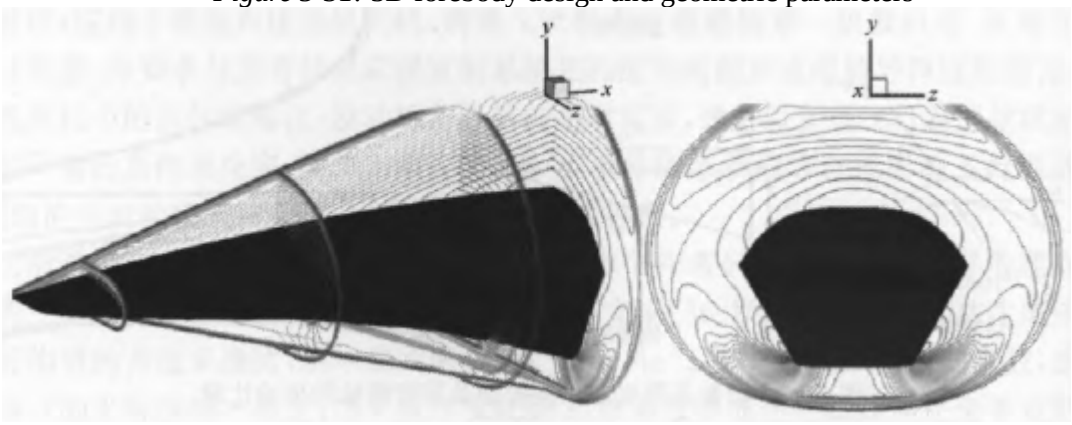

Figure 5-32: Three-dimensional forebody flow pressure contour plot

Table 5-2: Variables for the design of 3D forebodies for hypersonic vehicles

Name	Symbol	Range of variation
Forebody aspect ratio	RWH	1.5~3.5
Engine-to-fuselage width ratio	RW_engine	0.3~0.9
Forebody head width control parameter	n	0.1~0.6

The performance comparison is carried out from the influence on propulsion and aerodynamics, and the performance comparison parameters are shown in Table 5-3. The uniformity of the flow field in the inlet section of the inlet channel is defined as [37]:

$$\varepsilon = \frac{\sum_{j=1}^{n} \sqrt{(M_j - \overline{M})^2}}{n\overline{M}} \qquad (5.12)$$

That is, the average value of the relative deviation of the Mach number at each calculated grid point of the flow field of the inlet section of the inlet channel.

Table 5-3: Performance comparison parameters of 3D forebodies

Classify	Performance metrics
Push forward	Average static pressure at the inlet section of the inlet tract
	Average Mach number of inlet sections
	The total pressure recovery coefficient of the inlet section of the inlet tract
	Inlet mass flow rate
	Inlet flow coefficient of the inlet tract
	Flow field uniformity of the inlet section of the inlet duct
Pneumatic	Forebody lift coefficient
	Forebody drag coefficient
	Forebody lift-to-drag ratio
	Forebody pitching moment

3. Analysis of the influence of the design parameters of the three-dimensional forebody of the hypersonic vehicle

1) The effect of the aspect ratio of the forebody

The change of the aspect ratio of the forebody can reflect the width of the aircraft, and the larger aspect ratio aircraft is relatively flat, which is suitable for the shape of the aircraft such as hypersonic cruise aircraft and the first-stage carrier aircraft of air-breathing space launch vehicles. The smaller aspect ratio aircraft has a more slender profile, which can meet some of the design constraints of the missile weapon application to some extent. The aspect ratio is reduced from 1. The change from 5 to 3.5 The shape of the 3D forebody is shown in Figure 5-33.

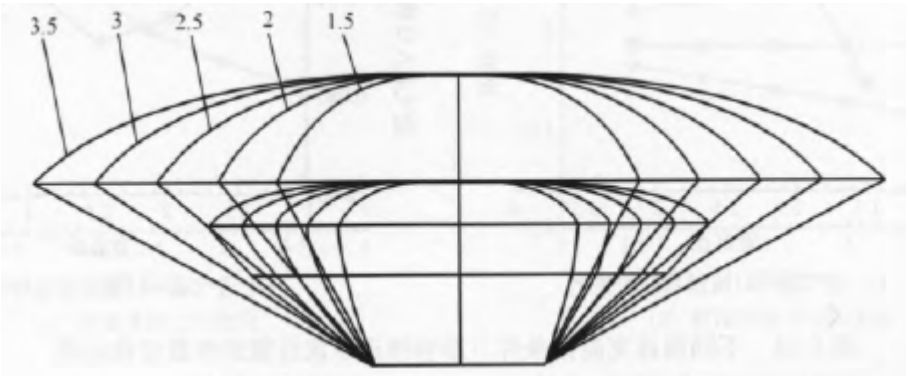

Figure 5-33: 3D forebody shapes with different aspect ratios

Figure 5-34 shows the parameter variation curve that affects the performance of the propulsion system, represented by the inlet section parameters of the inlet channel.

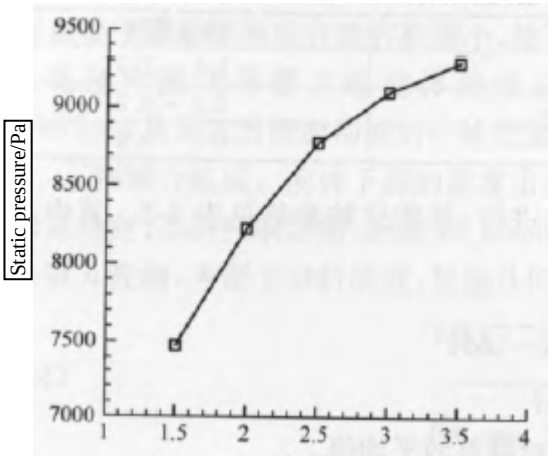

Aspect ratio

(a) Change in the average static pressure of the inlet section of the inlet tract

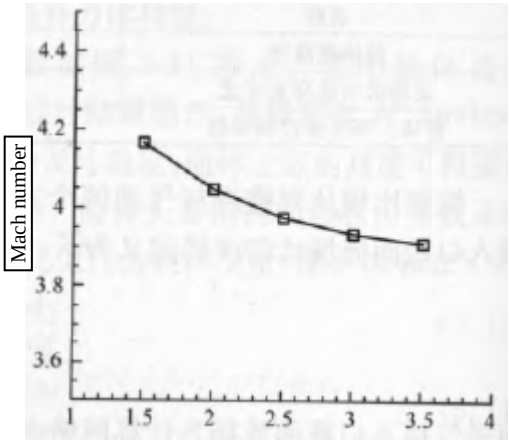

Aspect ratio

(b) Change in the average Mach number of the inlet section

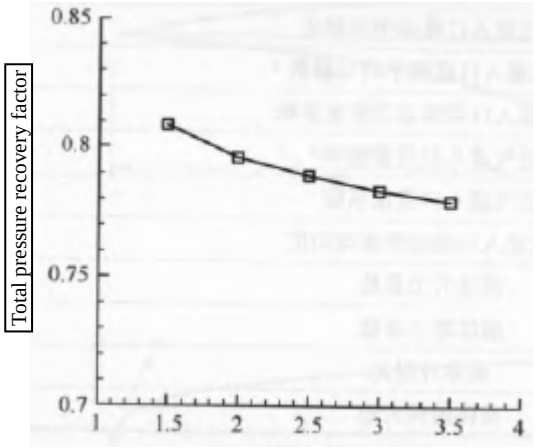

Aspect ratio

(c) Change in the total pressure recovery coefficient of the inlet section of the inlet tract

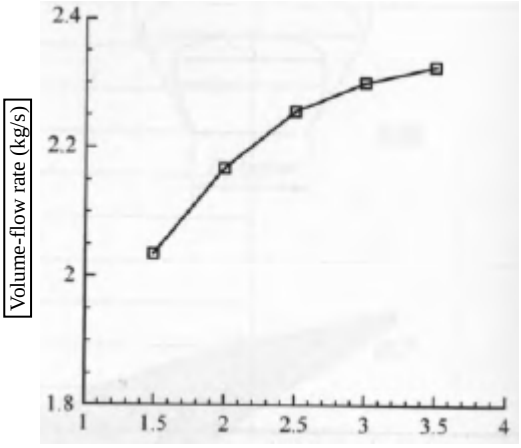

Aspect ratio

(d) Change in the mass flow rate at the inlet of the inlet tract

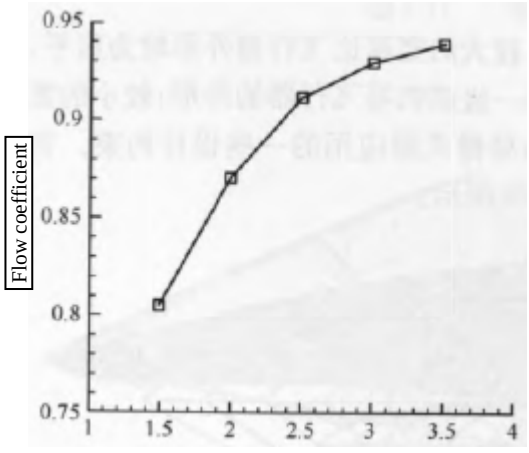

Aspect ratio

(e) Change in inlet flow coefficient of the inlet tract

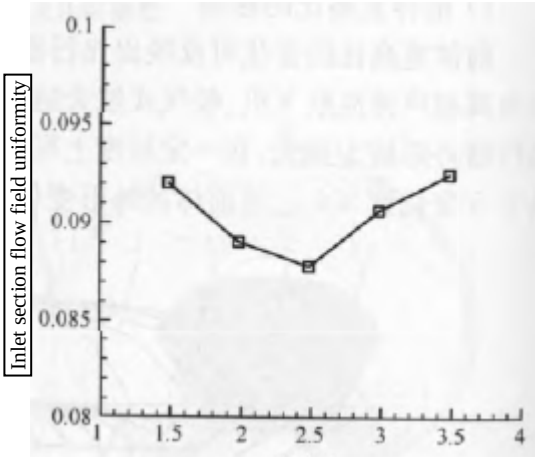

Aspect ratio

(f) Changes in the uniformity of the flow field at the inlet section of the inlet intake

Figure 5-34: Parameter variation curves affecting the performance of the propulsion system under different forebody aspect ratios

As can be seen from Figure 5-34, with the increase of the aspect ratio, the average static pressure of the inlet section of the inlet channel increases and the average Mach number decreases, indicating that the compressive performance of the forebody is enhanced. With the increase of the compression area of the forebody, the loss caused by friction increases, so that the total pressure recovery is reduced. The mass flow rate and inlet flow coefficient of the inlet section of the inlet passage increase with the increase of the aspect ratio, which indicates that the air trapping ability of the forebody has been enhanced, and the uniformity of the flow field does not show a consistent relationship with the change, but the change amplitude is not large.

Figure 5-35 shows the variation curve of the aerodynamic performance parameters of the forebody. As can be seen from Figure 5-35, with the increase of the aspect ratio, the lift coefficient and drag coefficient of the forebody increase, and the lower surface is the main source of lift, which also brings greater aerodynamic resistance, and the lift-drag ratio shows a downward trend, which is caused by the excessive drag brought by the side edge in the study of the change of aspect ratio. In terms of the pitching moment of the forebody, according to the definition of the coordinates of the aircraft body, the head-down moment is positive and the head-up moment is negative. As can be seen from Figure 5-35(d), with the increase of the aspect ratio, the head-down moment generated by the upper surface and the head-up moment generated by the lower surface both increase, but the total moment is negative, that is, the head-up moment, which increases slightly. This shows that the reasonable upper and lower surface design can eliminate the large negative head-up torque generated by the forebody, which is conducive to the trim design of the whole aircraft.

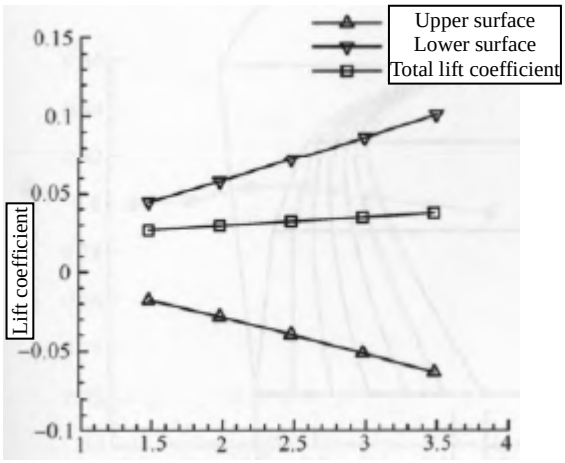

(a) Change in the lift coefficient of the forebody

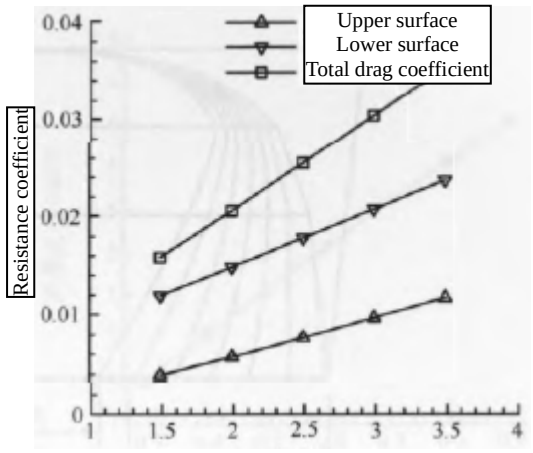

(b) Change in forebody drag coefficient

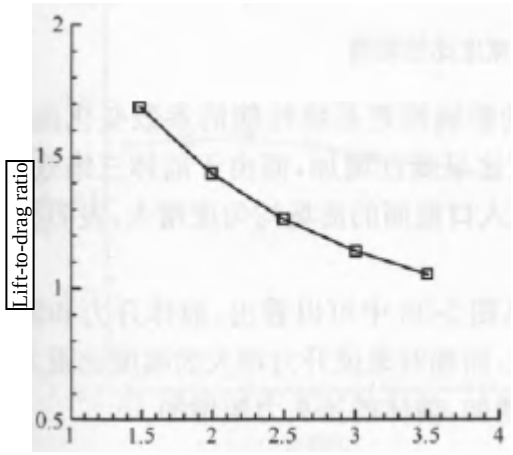

(c) Change in forebody lift-to-drag ratio

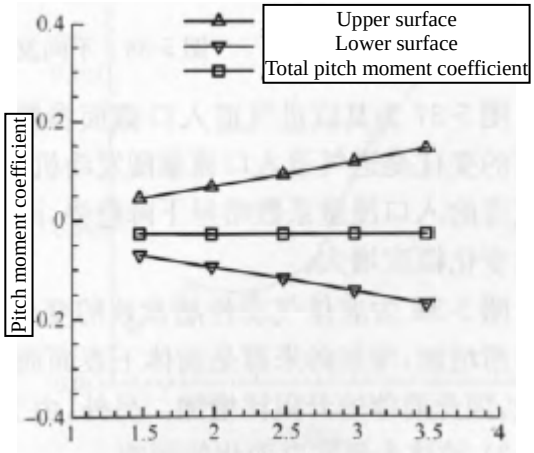

(d) Change in the pitching moment of forebody

Figure 5-35:
Variation curves of aerodynamic performance parameters of forebodies under different forebody aspect ratios

2) The effect of the engine-to-fuselage width ratio

The study of the width ratio of the engine to the fuselage is mainly to achieve the thrust and drag balance of the hypersonic vehicle in the cruising flight state in the design process. Due to the linkage characteristics of the forebody design, when the width ratio of the engine to the fuselage is changed, it is not only the increase of the engine width and the air capture area, but also the increase of the surface area under the forebody, which to a certain extent brings about the increase of the drag of the aircraft, as well as the change of lift and pitching torque. It should be pointed out that the change of the aspect ratio of the forebody, on the premise that the width of the engine remains unchanged, also reflects the change of the width ratio of the engine to the fuselage, but the aspect ratio of the forebody mainly reflects the narrow and flat form of the fuselage of the aircraft. The change in the engine-to-fuselage width ratio from 0.3 to 0.9 is shown in Figure 5-36.

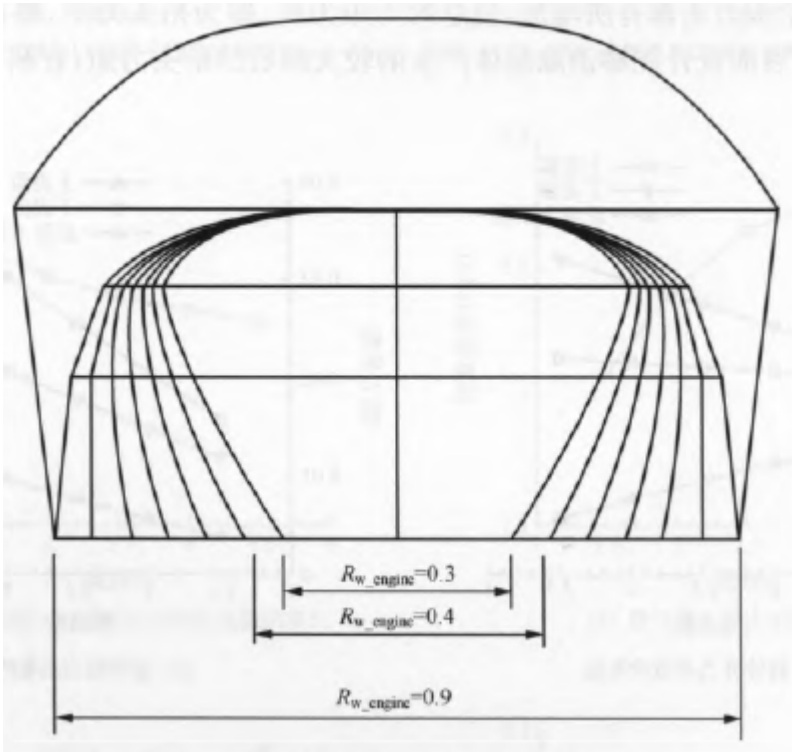

Figure 5-36: Configurations with different engine/fuselage width ratios

Figure 5-37 shows the parameter variation curve that affects the performance of the propulsion system, represented by the inlet section parameters of the inlet channel. The significant change is that the inlet flow rate of the inlet channel increases linearly with the engine/fuselage width ratio, while the inlet flow coefficient of the inlet channel decreases slightly due to the three-dimensional effect of the forebody, and the average flow field strength of the inlet section of the inlet channel increases, indicating that the change amplitude of the cross-section parameters increases.

Figure 5-38 shows the variation curve of the aerodynamic performance parameters of the forebody. As can be seen from Figure 5-38, both the lift and drag of the forebody have increased, and the source of the increase is the increase in the area of the lower surface of the forebody, and the increase in lift is relatively greater than the increase in drag, so the lift-to-drag ratio of the forebody increases. In addition, due to the increase in lift, the head-up moment of the forebody increases.

3) The effect of changes in the width of the head of the forebody

The top-down plane curve of the head of the hypersonic vehicle studied by the authors of this book is described by an exponential function curve, and with the change of the exponent, the forebody of the aircraft can transition from flat and continuous to the spire, which provides great convenience for studying the influence of the shape of the head of the forebody on the propulsion system.

Figure 5-39 shows the change of the exponential parameter of the exponential number function from 0.1 to 0.6 in the 3D forebody head.

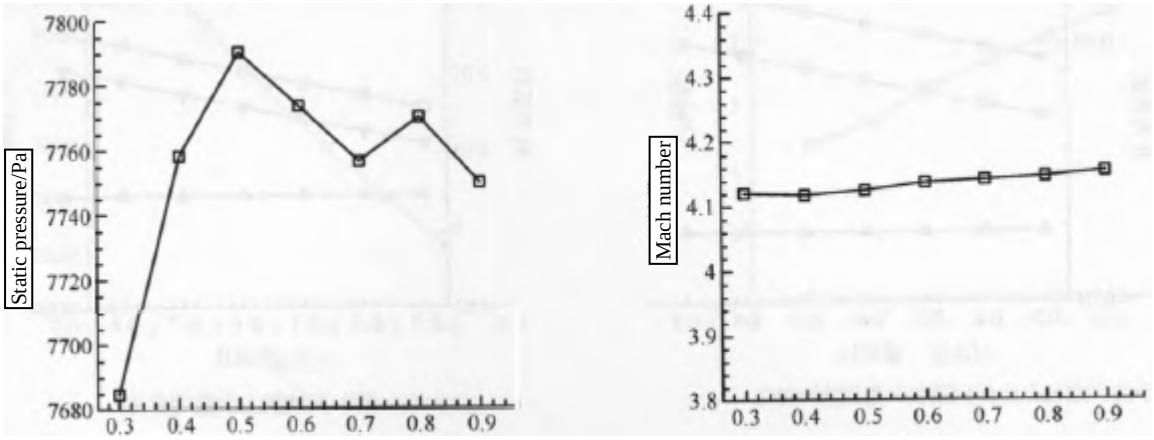

(a) Change in the average static pressure of the inlet section of the inlet tract

(b) Change in the average Mach number of the inlet section

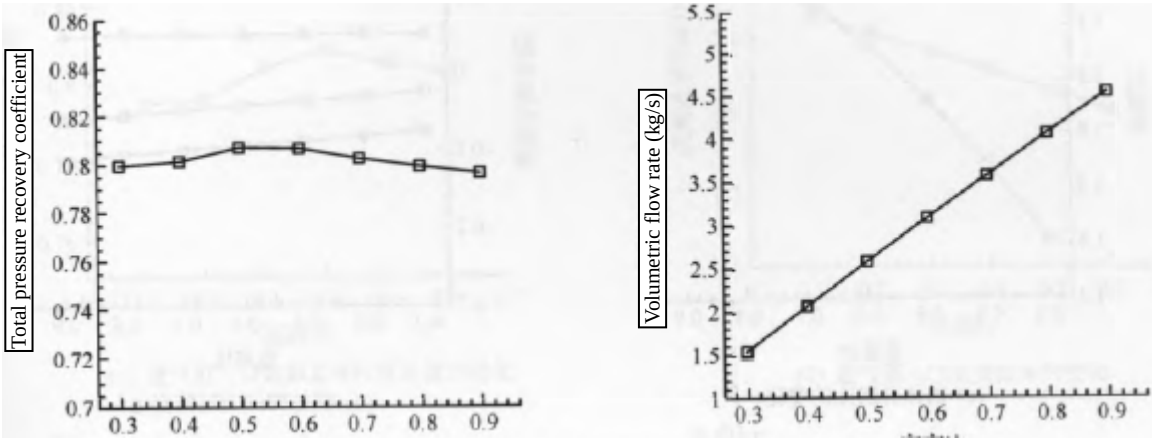

(c) Change in the total pressure recovery coefficient of the inlet section of the inlet tract

(d) Change in the mass flow rate at the inlet of the inlet tract

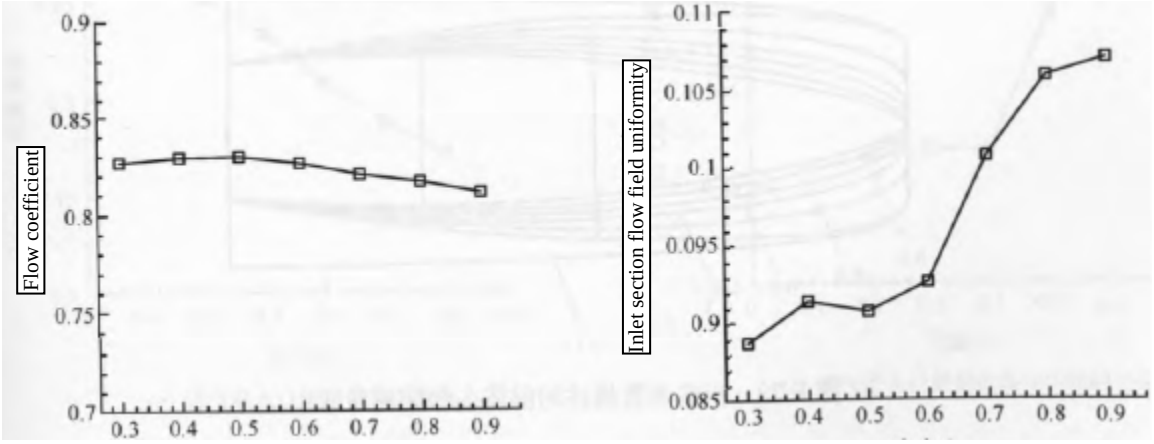

(e) Change in inlet flow coefficient of the inlet tract

(f) Changes in the uniformity of the flow field at the inlet section of the inlet intake

Figure 5-37: Parameter variation curves that affect the performance of the propulsion system under different engine width ratios

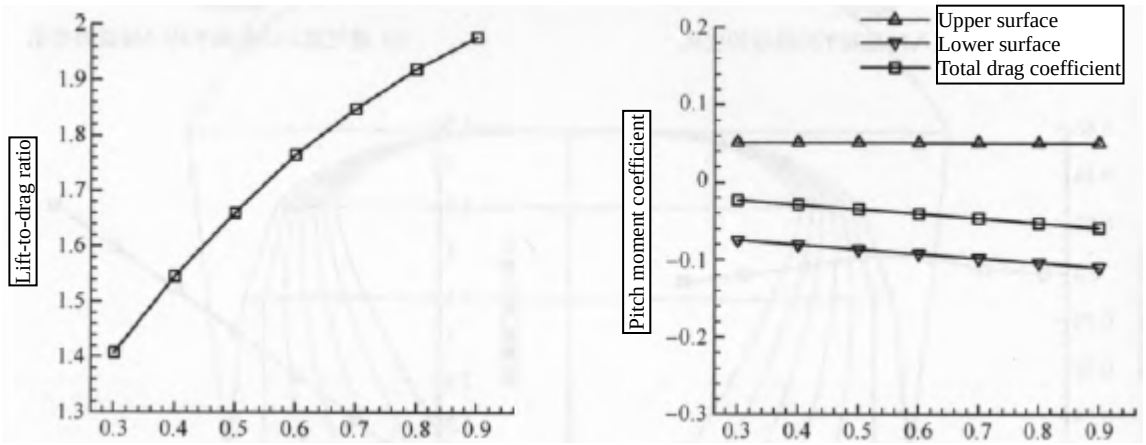

(c) Change in forebody lift-to-drag ratio (d) Change in the pitching moment of forebody

Figure 5-38: Variation curves of aerodynamic performance parameters affecting the forebody under different engine width ratios

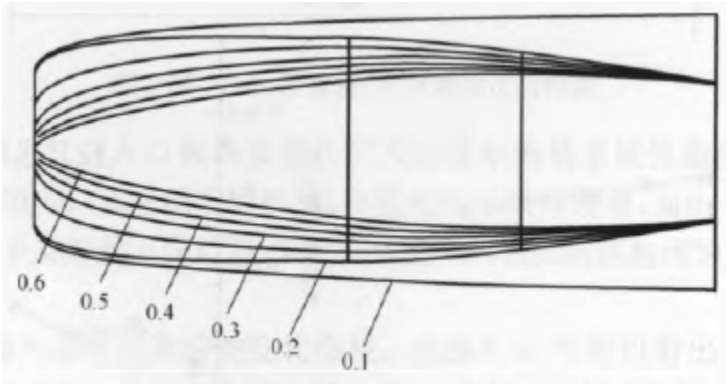

Figure 5-39: The top-down curve of the forebody head described by the exponential function

Figure 5-40 shows the parameter variation curve that affects the performance of the propulsion system, represented by the inlet section parameters of the inlet channel. As can be seen from Figure 5-40, the flatter head can compress the incoming flow more effectively and has a larger mass flow rate and flow coefficient, indicating that the forebody has strong air capture ability, less overflow, and relatively uniform flow field at the inlet section of the inlet channel.

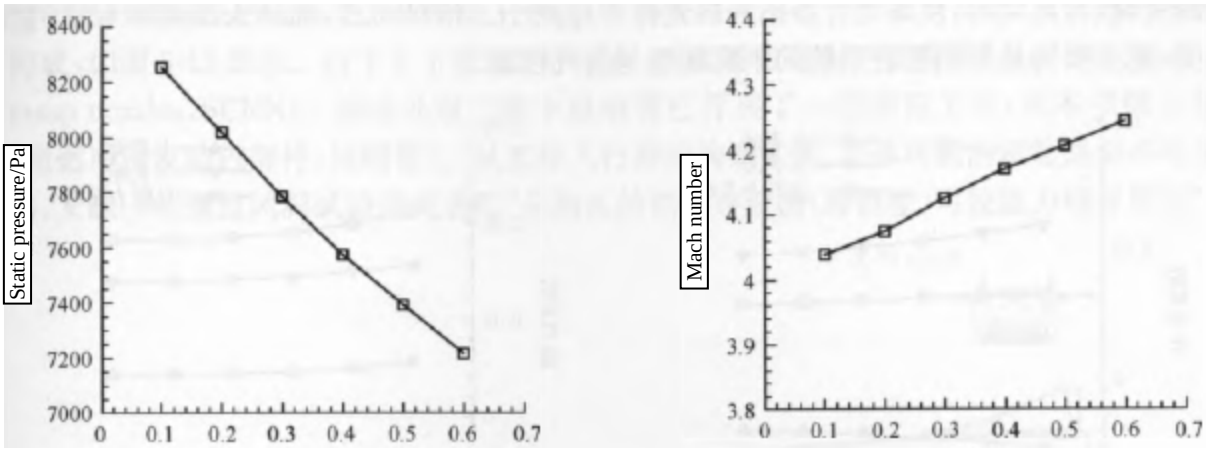

(a) Change in the average static pressure of the inlet section of the inlet tract

(b) Change in the average Mach number of the inlet section

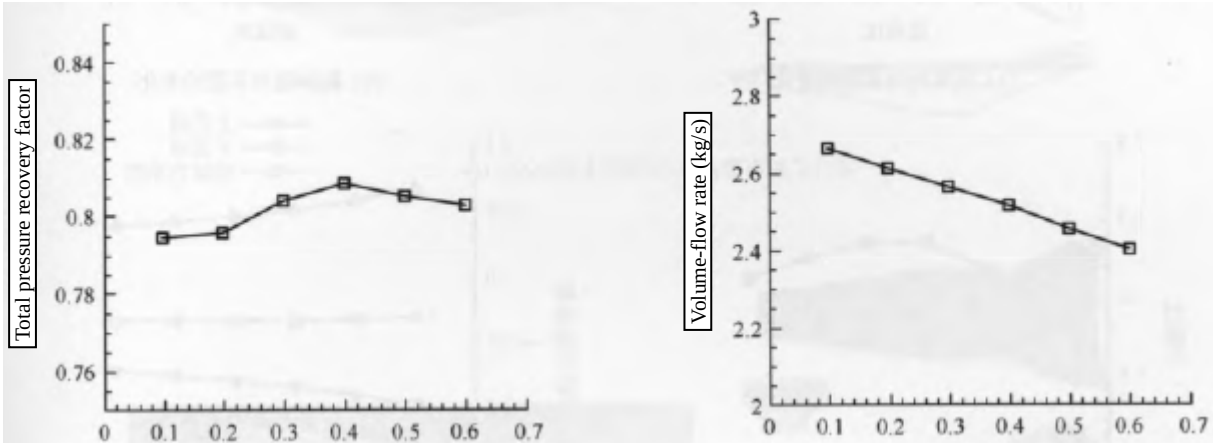

(c) Change in the total pressure recovery coefficient of the inlet section of the inlet tract

(d) Change in the mass flow rate at the inlet of the inlet tract

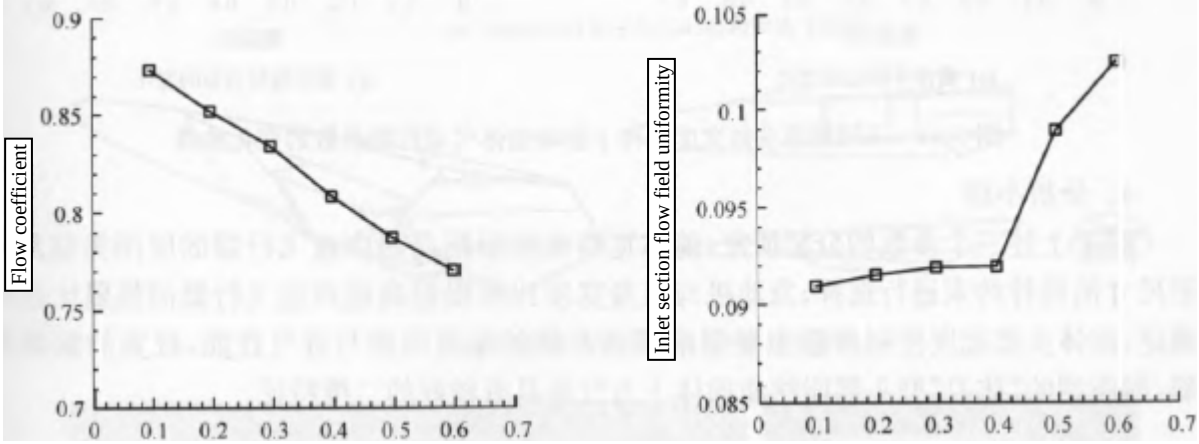

(e) Change in inlet flow coefficient of the inlet tract

(f) Changes in the uniformity of the flow field at the inlet section of the inlet intake

Figure 5-40: Parameter variation curves that affect the performance of the propulsion system under different forebody head widths

Figure 5-41 shows the change curve of aerodynamic force, with the increase of the shape index, the head of the forebody gradually becomes sharper, the lift force decreases slightly, and the drag also decreases slightly, but the amplitude of the change is not the same, so the lift-to-drag ratio of the forebody increases first and then decreases, and at the same time, the pitching moment of the aircraft raising its head decreases.

Comparatively speaking, the change of the flattening degree of the head of the forebody mainly affects the incoming flow compression and intake performance of the propulsion system.

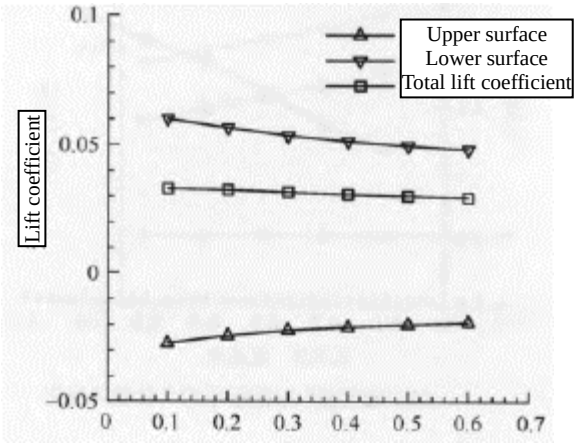

(a) Change in the lift coefficient of the forebody

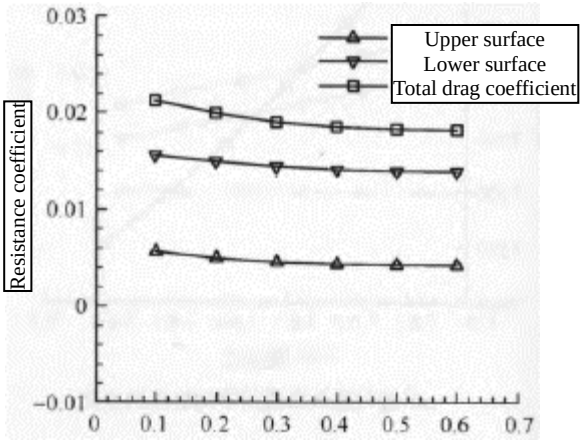

(b) Change in forebody drag coefficient

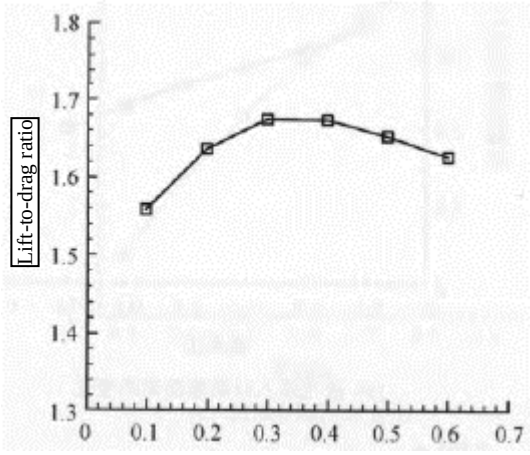

(c) Change in forebody lift-to-drag ratio

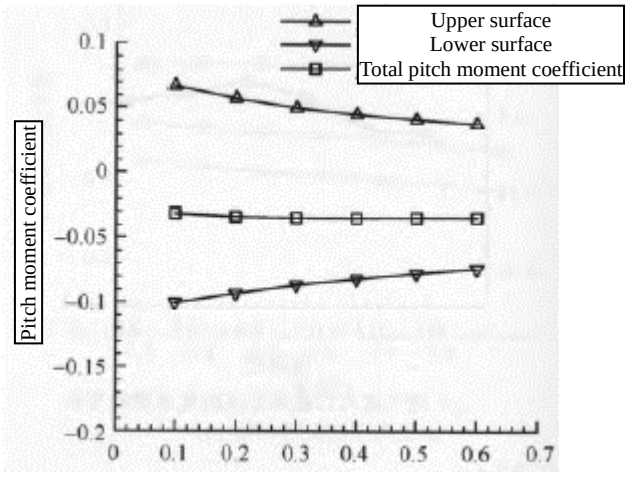

(d) Change in the pitching moment of forebody

Figure 5-41: Variation curves of parameters affecting the aerodynamic performance of the forebody under different forebody head widths

4) Analyze the summary

For the analysis of the above three parameters, the aspect ratio of the forebody should be selected according to the application type of the hypersonic vehicle and the design constraints of the external dimensions. The engine-to-fuselage width ratio should be determined according to the thrust-to-drag ratio of the hypersonic vehicle; the control parameters of the width of the forebody head mainly affect the incoming flow compression and intake performance of the propulsion system, and the wider forebody head, the so-called "spatula" head, can make the airflow below the forebody have better two-dimensional characteristics.

5.3.3: Integrated design of rear body nozzle of hypersonic vehicle

1. Three-dimensional configuration and design requirements for the integration of rear body nozzle of hypersonic vehicle

The scramjet nozzle and the rear body of the aircraft together form the exhaust system of the hypersonic vehicle. Figure 5-42(a) to (d) shows the shapes of several typical hypersonic vehicles in foreign countries. As can be seen from Figure 5-42, the rear body of the aircraft acts as an expansion surface for the gas to continue to expand, generating a thrust acting on the aircraft and a normal force perpendicular to the axis of the aircraft.

In terms of configuration, the nozzle and the rear body are composed of the upper and lower walls and the side walls on the left and right sides, as shown in Figure 5-43. Due to the asymmetry of the upper and lower walls, it is often referred to as a single expansion ramp nozzle (SERN). Some research work has been carried out on two-dimensional half-wall nozzles at home and abroad, see Chapter 2 of this book (scramjet engine components, tail nozzles). In terms of the configuration of the actual aircraft, the nozzles on both sides of the rear body are indispensable and the wind tunnel test in Reference [38] shows that "the use of long side deflectors (i.e., side walls) can slightly increase the thrust."

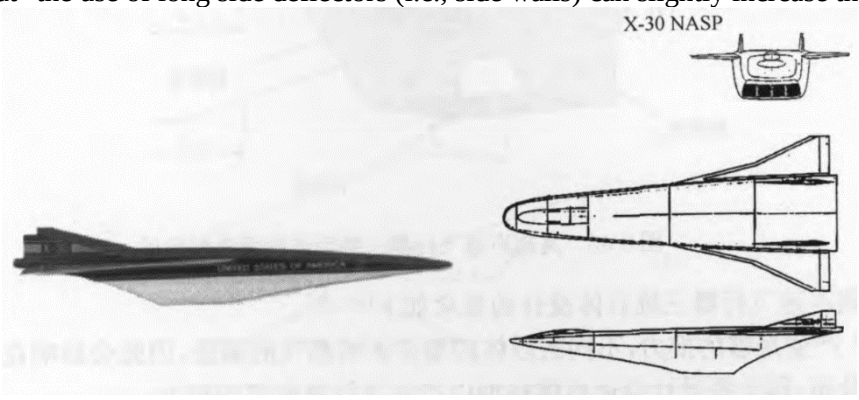

(a) The X-30 hypersonic vehicle in the NASP program

(b) The X-43 hypersonic vehicle in the Hyper-X program

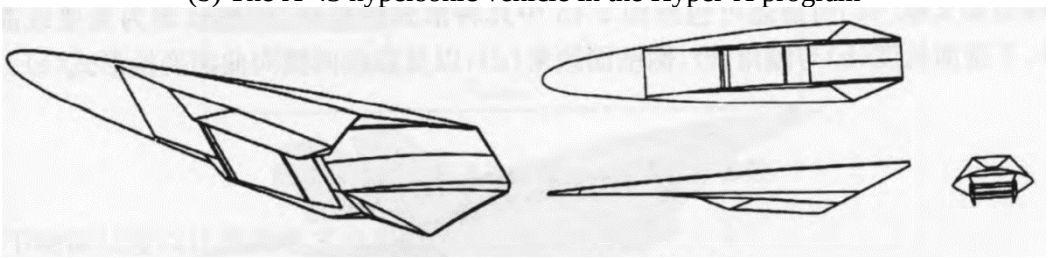

(c) French PROMETHEE hypersonic cruise missile

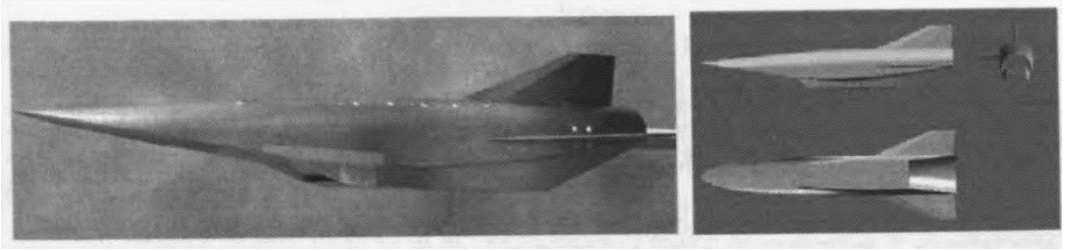

(d) The Franco-German joint JAPHAR supersonic vehicle

Figure 5-42: Exterior design of several foreign hypersonic vehicles

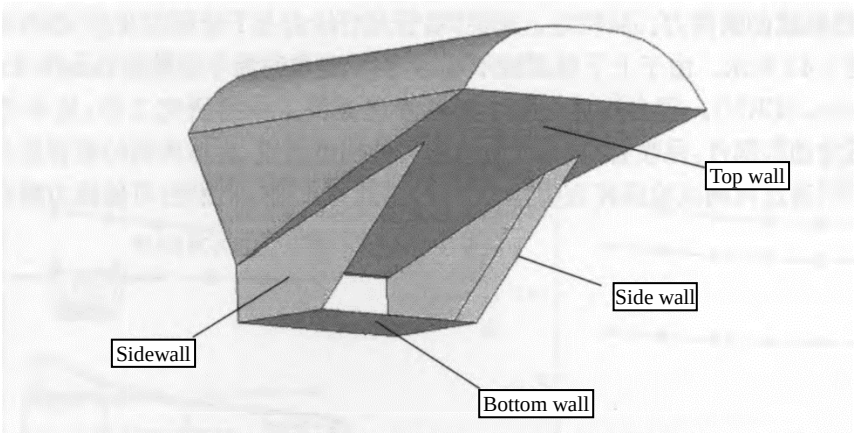

Figure 5-43: Typical configuration of a three-dimensional rear body nozzle for a hypersonic vehicle

The requirements for the design of the three-dimensional rear body of a hypersonic vehicle are as follows [39-43]:

(1) Generate enough thrust, different rear body configurations will affect the expansion of gas, so it will affect the pressure distribution on the rear body wall, so it is necessary to design a suitable rear body configuration to generate the thrust required by the aircraft.

(2) According to the overall needs of the aircraft, the normal force and the pitching moment are generated to meet the requirements, because the rear body is a half-wall type nozzle, there is a certain normal force, and affects the lift force and the pitching moment of the whole aircraft, different configurations will lead to different normal force components, and the design of the three-dimensional rear body configuration needs to be carried out according to the requirements of the overall performance index of the aircraft.

(3) It is necessary to avoid the influence of the rear gas tail flame on the horizontal tail fin.

(4) It is necessary to reduce the increase of structural mass caused by the lower wall surface and the side wall surface of the rear body as much as possible.

2. Analysis of the influence of design parameters

Figure 5-44 shows the general shape of a hypersonic vehicle, which is an integrated fuselage and propulsion. The three-dimensional configuration of the rear nozzle as described in Reference [44] can include several combinations of forms in Figure 5-45, namely, the expansion surface is a straight or curved wall (a), the length of the lower wall surface (b) and the inclination angle (c), the inclination angle of the side wall surface (d), and the transverse surface transformation form of the expansion surface (e).

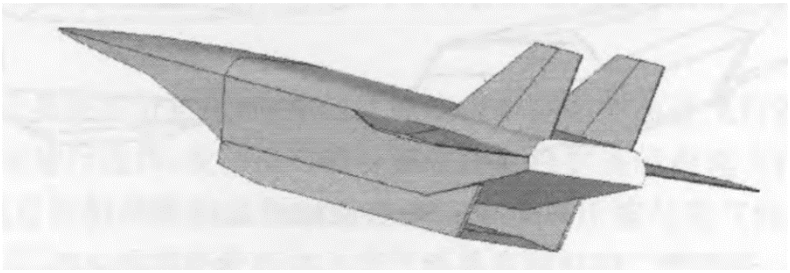

Figure 5-44: Typical aerodynamic shape of a hypersonic vehicle

Figure 5-43 shows the three-dimensional configuration of the rear nozzle of the hypersonic vehicle in this section, in which the length and width of the rear body are given by the overall design of the aircraft, and the geometric design parameters that can be changed include the length and inclination angle of the lower wall surface of the rear body nozzle, the inclination angle of the side wall, and the description parameters of the wall form of the upper wall surface (such as straight line, curved surface, curved surface, etc.).

In this study, the two-dimensional optimized surface obtained from Reference [45] is used for the upper wall surface, and the influencing parameters of the three-dimensional configuration are the length of the lower wall surface and the inclination angle of the side wall, as shown in Figure 5-46.

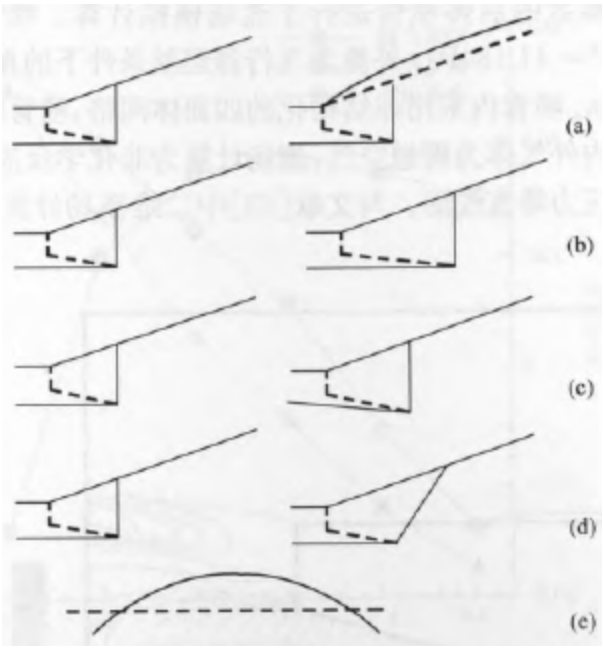

Figure 5-45: Configuration of the rear body nozzle of a hypersonic vehicle

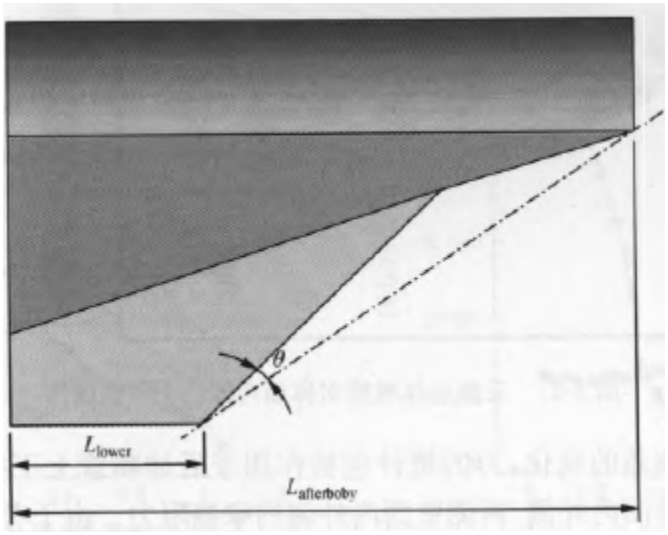

Figure 5-46: Design parameters of the rear body nozzle of a hypersonic vehicle

The length of the lower wall surface is given as a ratio

$$R_{\text{lower}} = \frac{L_{\text{lower}}}{L_{\text{afterbody}}} \tag{5.13}$$

where：L_{lower} - Length of the lower wall;

$L_{afterbody}$ - The length of the rear nozzle, that is, from the inlet of the inner nozzle to the tail end of the rear body of the aircraft.

Referring to the variation range in the analysis of the influence of lower wall length on the performance of two-dimensional half-wall nozzles in Reference [45], the R_{lower} value in this study varies from 0.1 to 0.6.

In Figure 5-46, the dashed line is the sealing position of the sidewall surface, and the sidewall inclination parameter θ is the angle between the outer edge of the sidewall surface and the dashed line, and the variation range is from 0° to the perpendicular line of the outer edge of the sidewall surface to the lower wall.

The flow field simulation calculation of the rear body nozzle with different configuration design parameters was carried out. Inlet parameters of the nozzle: *Ma* = 2.06, T = 1309.5K, P = 41 184Pa; the outflow is the free inflow parameter under the cruising condition of the aircraft: *Ma* = 6, T = 226K, P = 1197Pa. An unstructured tetrahedral mesh is used in the nozzle, and a structured hexahedral mesh is used in the extracorporeal flow field after the nozzle. The gas inside and outside the nozzle is ideal air, and the flow field is calculated as a non-chemical reaction flow. Figure 5-47 shows the pressure contour diagram in the symmetry plane of the rear body nozzle. Compared with the calculated results of the two-dimensional flow field in Reference [45], it can be seen that the flow field structure of the two is similar.

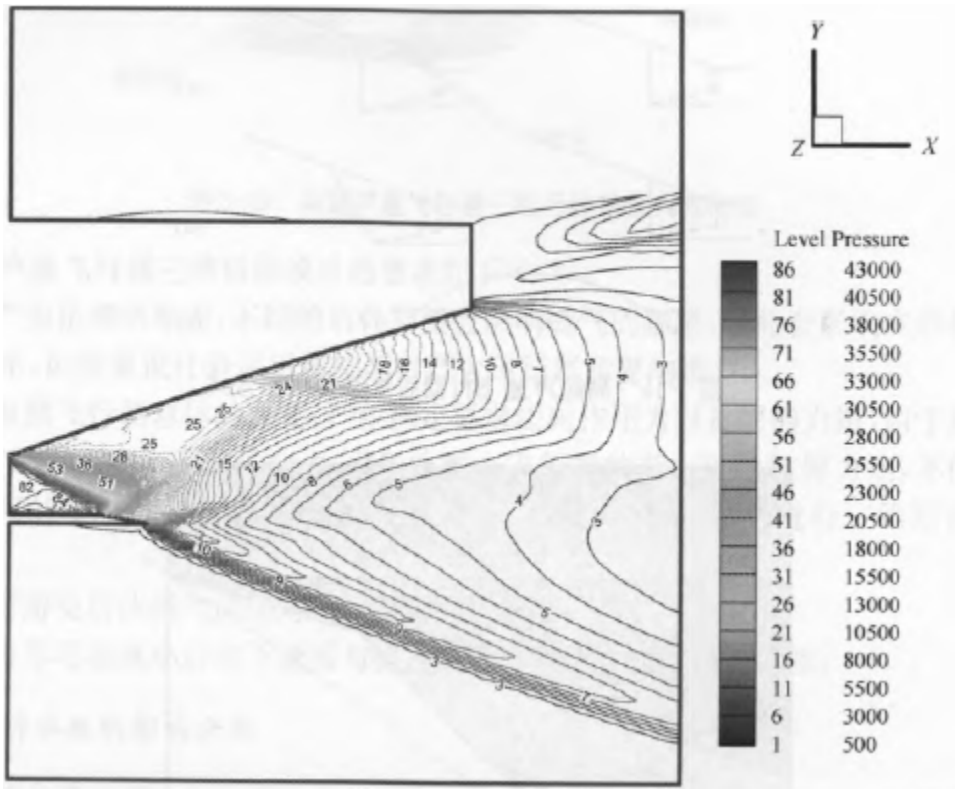

Figure 5-47: Pressure contour plot in the symmetry plane of the 3D rear body nozzle

Regardless of the change of the angle of attack of the aircraft, the force statistics include the pressure acting on the upper and lower walls of the rear body nozzle and the walls on both sides, as well as the frictional resistance of the upper wall, the inner and outer sides of the lower wall, and the inner and outer sides of the wall on both sides. Since the angle of attack a = 0 is considered, the axial force F_x = T, the normal force F_y = L, and the reference point of the moment are the center of gravity position of the aircraft, which is assumed to be 60% of the length of the aircraft, $0.5L_{afterbody}$ away from the front of the nozzle inlet.

1) The effect of the length of the lower wall

For the side wall sealing configuration, the length ratio of the lower wall surface is changed from 0.1 to 0.6, and the interval is 0.1, and the three-dimensional flow field is calculated, and the thrust coefficient, lift coefficient and pitching moment coefficient of each configuration are obtained, as shown in Figure 5-48, the thrust coefficient increases first with the increase of the length ratio of the lower wall, reaches the maximum when the length ratio of the lower wall is 0.4, and then decreases slightly; the lift coefficient decreases with the increase of the length ratio of the lower wall, and changes from positive lift to negative lift. The pitching moment also decreases with the increase of the ratio of the length of the lower wall, and changes from the head-down moment of the aircraft to the head-up moment.

Figure 5-49(a) shows the distribution of wall pressure on the rear nozzle when the wall length ratio changes under the side wall seal. As can be seen from Figure 5-49, when the lower wall length ratio changes from 0.1 to 0.4, the wall pressure on the rear body nozzle changes considerably, the length of the high-pressure area gradually increases, and the overall pressure distribution gradually increases, but the lower wall length ratio changes from 0.4 to 0.6, and the pressure distribution does not show a significant change.

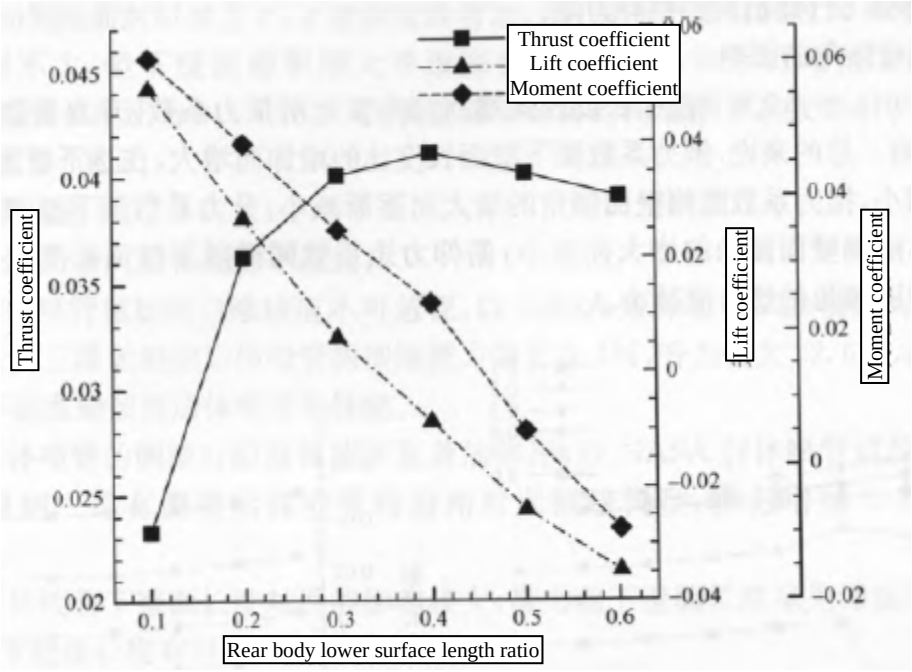

Figure 5-48: Effect of the length of the lower wall of the rear nozzle on the performance parameters

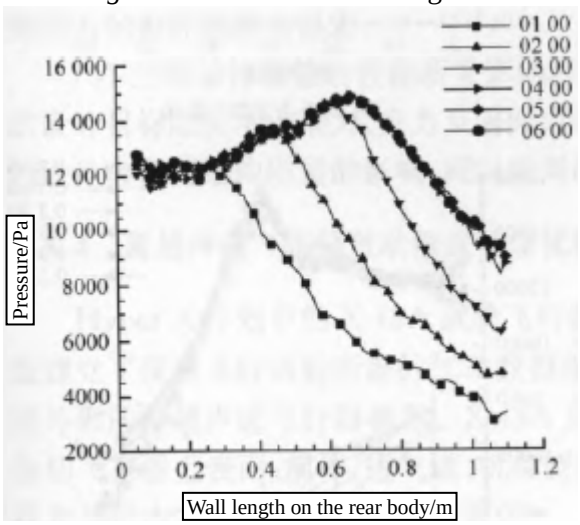

(a) Centerline pressure distribution on the upper surface of the posterior body

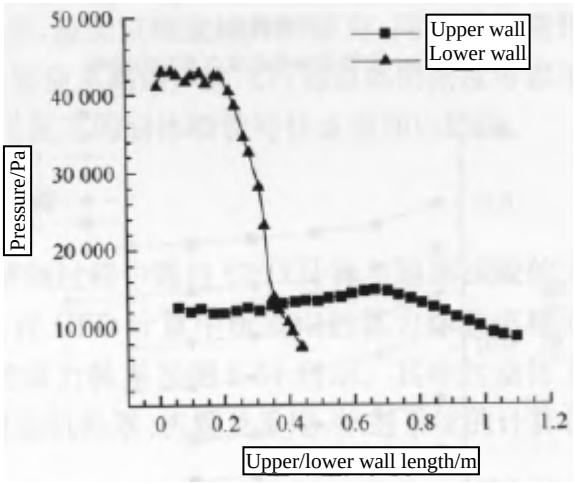

(b) Pressure distribution of the upper and lower wall centerlines of the "04 00" configuration

Figure 5-49: Effect of the length of the lower wall of the rear body nozzle on the pressure distribution of the centerline

This shows that the length of the lower wall surface effectively controls the expansion of the gas in the rear nozzle, and the too short lower wall surface makes the gas expand prematurely, and the pressure drops rapidly, so the thrust that can be generated is smaller, and the shorter length of the lower wall surface also makes the direction of the whole force more declinated, so the lift force generated by the normal component is also larger. With the increase of the length of the lower wall, the negative lift force generated by the pressure acting on the lower wall surface also increases, which gradually cancels the positive lift generated by the upper wall and makes the lift of the whole rear body nozzle turn from positive to negative. Figure 5-49(b) shows the pressure distribution of the upper and lower walls when the length ratio of the lower wall surface is 0.4 and the pressure distribution of the upper and lower walls in the sealed state of the side wall. It can be seen that the different rear body nozzle configurations will cause negative lift, as well as the pitching moment that makes the aircraft look up.

2) The influence of the pitching moment coefficient

Fig. 5-50 (a)~(c) shows the influence of the length of the lower wall and the inclination angle of the side wall on the thrust coefficient, lift coefficient and pitching moment coefficient. In general, the thrust coefficient increases with the increase of the length ratio of the lower wall, and gradually decreases after reaching the length ratio of the lower wall surface to 0.4, and the thrust coefficient gradually decreases with the increase of the inclination angle of the side wall, the lift coefficient decreases with the increase of the length ratio of the lower wall, and decreases with the increase of the inclination angle of the side wall, and the pitching moment coefficient also decreases with the increase of the length ratio of the lower wall and decreases with the increase of the inclination angle of the side wall.

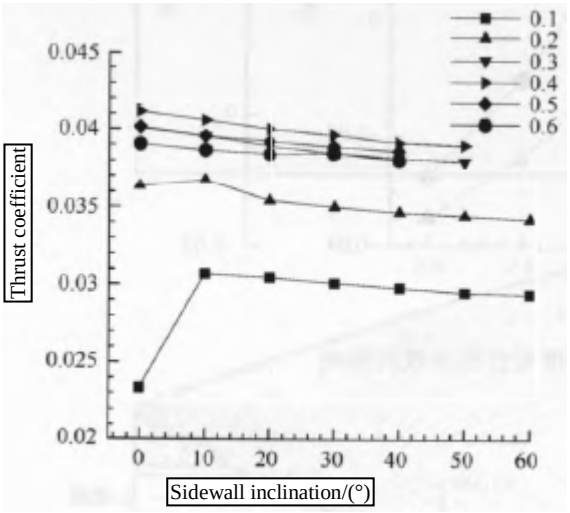

(a) The effect of the sidewall inclination angle on the thrust coefficient

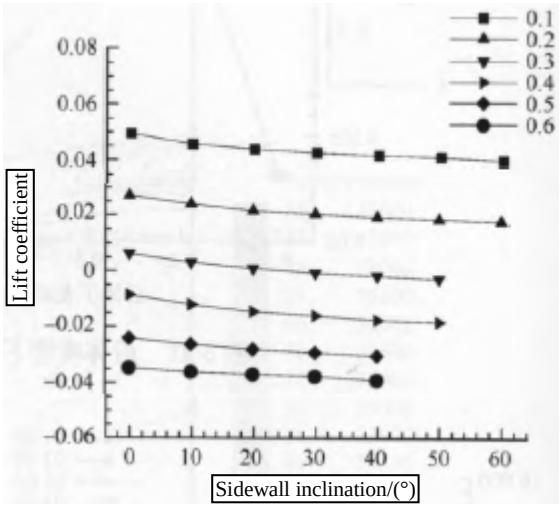

(b) Effect on lift coefficient

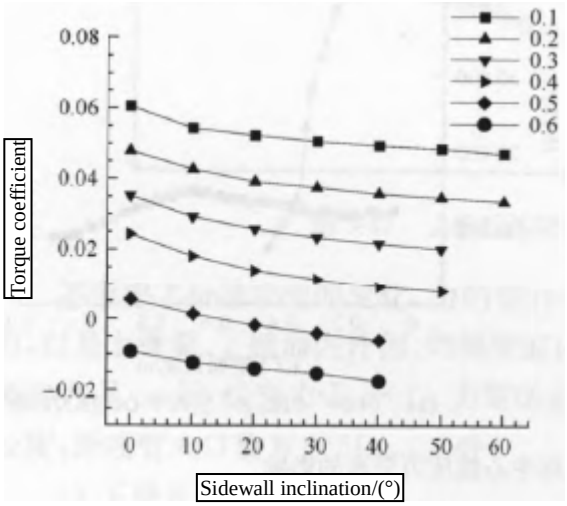

(c) Effect on pitching moment coefficients

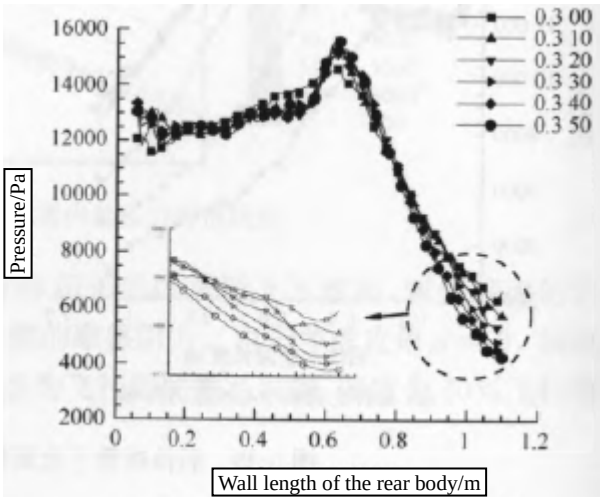

(d) Effect on the pressure distribution on the surface and center line of the posterior body

Figure 5-50: Effect of wall length and sidewall inclination of rear body nozzle on performance

Fig. 5-50(d) shows the influence of the change of the inclination angle of the side wall surface on the pressure distribution of the upper wall surface when the length ratio of the lower wall surface is 0.3, the pressure distribution in most areas is consistent, and the significant difference occurs in the tail section of the upper wall surface, the existence of the side wall surface makes the gas not expand excessively, so the pressure is higher, so with the increase of the inclination angle of the side wall surface, the force of the rear nozzle decreases, and the thrust, lift force and pitching moment decrease accordingly.

In addition, the accumulation of force in the calculation includes friction resistance in addition to the effect of pressure, and a larger wall area will lead to a larger friction resistance, so in the case of little difference in pressure action, the difference in friction resistance will be revealed, such as in the state of side wall sealing, the lower wall surface continues to increase, when the lower wall length ratio exceeds 0.4, the pressure distribution of the upper wall surface is not much different, but the increase of the lower wall surface area leads to the increase of friction resistance, so the thrust shows a slight downward trend, see Figure 5-48; when the length ratio of the lower wall surface is 0.1 and 0.2, the configuration thrust coefficient of the 0° inclination angle of the side wall surface is less than that of the configuration at the 10° inclination angle, as shown in Figure 5-50(a).

3) Analytical conclusions

From the above analysis, the following conclusions can be drawn:

(1) The three-dimensional effect of the flow field of the rear body nozzle cannot be ignored, taking the NASA rear body nozzle test model as an example, the thrust force is 3.2% larger and the lift force is 22.6% larger when the three-dimensional rear body nozzle configuration without side wall is calculated by the two-dimensional calculation model, so the performance of the two-dimensional calculation cannot accurately predict the performance of the rear body nozzle.

(2) The sidewall of the rear body nozzle has a significant effect on improving the performance, taking the NASA rear body nozzle test model as an example, the three-dimensional rear body nozzle configuration with side wall is numerically simulated and the thrust is increased by 5.4% and the lift is increased by 34.8%.

(3) The length of the lower wall of the rear body nozzle has a great influence on the performance, and the thrust increases first and then decreases with the length of the lower wall, and the length of the lower wall may produce negative lift.

(4) The change of the inclination angle of the side wall of the rear body nozzle mainly affects the thrust and lift force by changing the distribution of the pressure on the upper wall, but the larger side wall surface area will lead to greater frictional resistance, so the difference in frictional resistance is more significant when the pressure effect is not different.

(5) There are many factors affecting the performance of the three-dimensional rear body nozzle, which should be carefully analyzed and studied, and the design objectives of the rear body nozzle should not only consider the thrust, lift and pitch moment, but also consider the influence of different design parameters on the structural quality from the overall perspective of the hypersonic vehicle, and the characteristics of the rear body nozzle under the design condition should also be studied.

5.3.4: Numerical calculation of integrated aeropropulsion of hypersonic vehicles

During the development of the X-43A test vehicle in the Hyper-X program, the aerodynamic database required for predicting flight tests was established by means of CFD calculations and ground tests [46], and the computing power system used in CFD calculations is worthy of reference for hypersonic vehicles of this shape. Figure 5-51 shows the computing power system used by X-43A. The aerodynamic calculations include the upper surface of the aircraft, the forebody/air intake, the fuselage sidewalls, the engine cover, the wings and the vertical tail, and the propulsion system includes the flow channels in the engine and the rear nozzles.

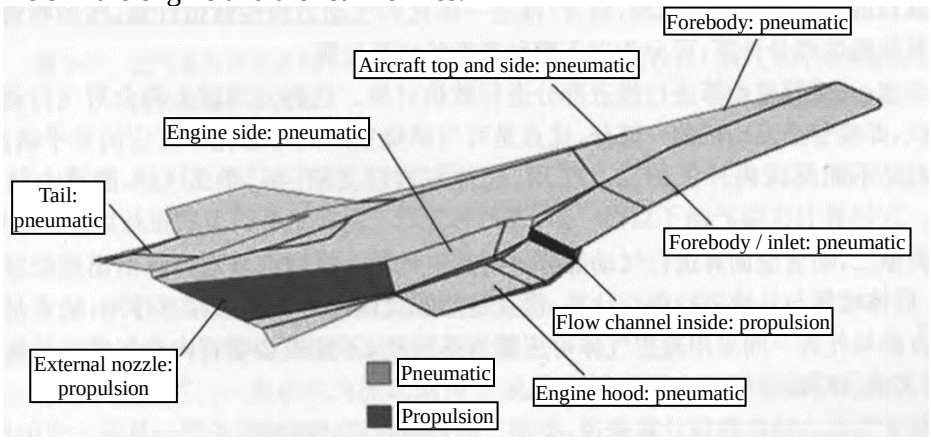

Figure 5-51: X-43A pneumatic and propulsion computing system

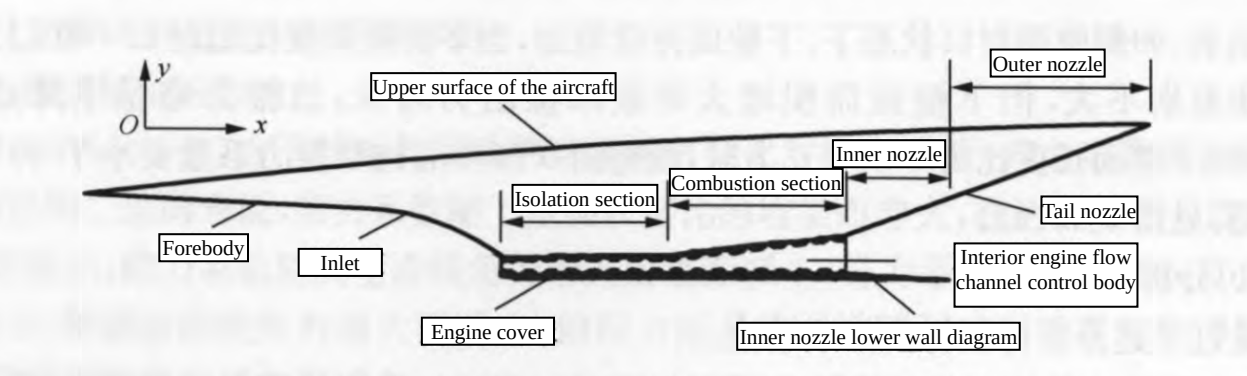

Figure 5-52: Names of components of the integrated form factor of a hypersonic vehicle [47]

Referring to Reference [47], the aerodynamic parameters of the hypersonic vehicle with integrated fuselage/propulsion are defined as follows:

(1) When the intake tract is closed

$$C_L = C_{Lv} + C_{Ln} \quad (5.14)$$

$$C_D = C_{Dv} + C_{Dn} \quad (5.15)$$

(2) When the engine is not working

$$C_L = C_{Lv} + C_{Le} + C_{Ln} \quad (5.16)$$

$$C_D = C_{Dv} + C_{De} + C_{Dn} \quad (5.17)$$

(3) When the engine is working

$$C_L = C_{Lv} + C_{Le} + C_{Ln} \quad (5.18)$$

$$C_D = C_{Dv} \quad (5.19)$$

$$C_T = C_{Te} + C_{Tn} \quad (5.20)$$

where: Subscript "v" - body system;

Subscript "e" - inner flow channel;

Subscript "n" - Tail nozzle.

In the configuration of the aircraft, it is assumed that when the inlet is closed, the combustion chamber outlet is also closed, that is, the internal flow channel is closed, so the calculation of aerodynamic force is only the force of the body and the nozzle. When the engine is working, the thrust of the engine is the net thrust in the inner flow channel and the tail nozzle, that is, the frictional resistance of the wall has been deducted, so the calculation of aerodynamic drag is only the part generated by the body.

According to the results of the current literature, the numerical calculation of the aerodynamic characteristics of the fuselage/propulsion integration can be divided into the following two types of calculation processes according to whether the nozzle wall is counted as the propulsion part.

Type 1: The nozzle wall is calculated for the propulsion part to be numerically calculated. This method is more in line with the general understanding of the aircraft, that is, the nozzle is a part of the engine, and the advantage is that the non-equilibrium flow can be considered together with the combustion chamber for chemical reactions, but the disadvantage is that it cannot reflect the interaction between internal and external flows, which is represented by the computing power system of X-43A in Reference [46].

Type 2, the nozzle wall is calculated for the pneumatic part for numerical calculation. The advantage is that the flow control equation and the outflow equation are used together with the compressible N-S equation of the ideal gas, which cannot simulate the non-equilibrium flow characteristics of the gas in the nozzle, which is used in Reference [47].

For the numerical calculation of aerodynamic characteristics, the numerical calculation process of type 2 has certain advantages over type 1.

Firstly, in the numerical calculation process of type I, both aerodynamic and propulsive calculations have to establish the calculation model of the rear body nozzle, which is a waste of certain computational resources because of the overlap of work; secondly, the inner flow channel in type II mainly reflects the working state of the combustion chamber of the engine, which can be calculated by different calculation models with various accuracies, and it can let the scientific research staff of propulsion part focus on the numerical simulation of chemical reaction flow in response to the supersonic The numerical simulation of the chemical reaction flow can be focused on the reaction of supersonic combustion characteristics. Finally, Type II is convenient for data transfer in the cross section where aerodynamic and propulsion calculations overlap, which can be one-dimensional uniform parameter transfer or two-dimensional planar parameter transfer, and at the same time, numerical simulation of the flow in the aft-body nozzle can well react to the interaction between the internal and external flow fields.

Reference [47] provides the process of integrated numerical simulation for the two states of engine non-working and engine working.

When the intake channel is opened, the engine does not work, and the air flow passes through the inlet channel, the isolation section, and the combustion chamber, and is discharged by the tail nozzle, so that no combustion and chemical reaction occur, and the inner flow channel plays the role of an air flow channel. The calculation is divided into two steps, as shown in Figure 5-53, the two-dimensional internal and external flow field integration is first simulated to obtain the flow parameters of the engine combustion chamber outlet as the inlet condition of the tail nozzle during the three-dimensional external flow calculation. With the improvement of computing power, it has become possible to carry out three-dimensional integrated calculation of internal and external flow fields, for example, in Reference [48], the numerical simulation of the integrated shape of the airframe/propulsion system of a hypersonic vehicle was carried out in Reference [48].

When the inlet tract is opened and the engine is working, the calculation is divided into three steps, as shown in Figure 5-54, the inlet parameters of the engine isolation section are estimated first, and then the one-dimensional calculation program of the engine inflow is used to obtain the flow parameters of the combustion chamber outlet, which is used as the inlet condition of the tail nozzle when the interaction between the tail nozzle and the outflow is calculated. Among them, the numerical calculation of engine inflow can be based on different calculation models, such as 2D or 3D, depending on the constraints of calculation accuracy, time, and cost.

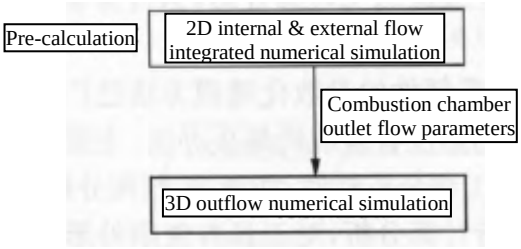

Figure 5-53: Integrated numerical simulation process of the engine with the air intake tract open and not working

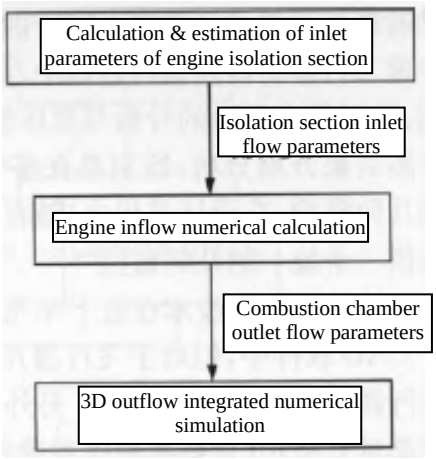

Figure 5-54: Numerical simulation process of engine operation with the air inlet tract open

To sum up, the numerical calculation process of aerodynamic characteristics of type 2 can be used to unify the three states of closed air intake, open air intake engine not working, and open air intake engine working into the following aerodynamic calculation form

$$X = X_{aero} + X_{engine} \tag{5.21}$$

where: X-pneumatic force, including lift, drag, pitching moment, etc.;

Subscript "aero" - flow field calculation completed by the aerodynamics discipline;

Subscript "engine" - calculation of the flow field completed by the flow channel in the engine (the inlet starts from the inlet of the isolation section and ends at the outlet of the combustion chamber).

When the air inlet is closed, $X_{engine} = 0$. In order to further analyze the effect and influence of the rear nozzle wall on the aerodynamic force, X aero can be split, i.e., X_{aero} = Xv+ Xn, where the subscript "v," "n" is defined as agreed in Section 5.3.4. Therefore, the calculation of the aerodynamic characteristics of the integrated hypersonic vehicle is calculated by the two disciplines of aerodynamics and propulsion, and the total aerodynamic characteristics of the aircraft can be obtained by superimposing the calculation results of the two.

In summary, the formula for calculating the aerodynamic coefficient is as follows:

$$\begin{cases} C_{\mathrm{L}} = C_{\mathrm{Lv}} + C_{\mathrm{Ln}} + C_{\mathrm{Le}} \\ C_{\mathrm{D}} = C_{\mathrm{Dv}} + C_{\mathrm{Dn}} + C_{\mathrm{De}} \\ C_{\mathrm{m}} = C_{\mathrm{mv}} + C_{\mathrm{mn}} + C_{\mathrm{me}} \end{cases} \tag{5.22}$$

The above aerodynamic coefficient parameters have the values of and three states respectively. Under the same flight conditions, but in the different fuel throttling states of the engine, the aerodynamic coefficient C_v of the outer surface of the fuselage can be regarded as unchanged, while the aerodynamic coefficients Cn and Ce change, in order to reduce the amount of repetition of the calculation, in this case, the numerical calculation process of type 1 can be adopted, and a calculation domain including the isolation section, the combustion chamber and the rear body nozzle can be established separately to calculate its force, and then with C_v calculates the total aerodynamic force superimposed, or takes a certain working state of the engine as a benchmark to give the correction results in other working states.

5.3.5: Parametric modeling methods for integrated geometry of hypersonic vehicles

1. About parametric shape modeling

The salient feature of the shape of the hypersonic vehicle is the integration of the fuselage and the propulsion system, and the design of the flow channel configuration of the fuselage and the propulsion system is inseparable. In the process of development and design of hypersonic vehicles, it is necessary to carry out the integrated design of fuselage and propulsion and carry out multidisciplinary analysis and overall design optimization such as aerodynamics, power, structure, and control. In particular, in the process of multidisciplinary design optimization (MDO), a parametric aircraft geometry model is required, and in the design optimization, new aircraft shapes are generated with the change of design parameters, providing a unified geometric model for the analysis of various disciplines [49,50].

With the rapid development of computer graphics technology in the past decade, the parametric modeling method for industrial parts has been widely used in CAD software, but there is still no systematic solution for the parametric geometry of the aircraft, mainly due to the complexity of the geometry of the aircraft. In addition, the existing commercial engineering analysis software, such as flow field and structural analysis software, needs to pre-process the model of CAD geometric modeling in order to carry out calculation and analysis, and it is difficult to automate the pre-processing process for the aircraft with complex shape, which brings considerable difficulties to the engineering implementation of the aircraft MDO. Therefore, the parametric modeling method of complex geometry of aircraft is still a problem that needs to be further studied in the future aircraft design, especially in multidisciplinary design optimization.

The parametric modeling of the aircraft shape should make the design parameters as few as possible and be suitable for the analysis of various sub-disciplines, such as the surface mesh required for engineering method calculation, the flow field mesh required for flow field calculation, and the finite element mesh required for structural analysis. In addition to meeting the above requirements, the parametric modeling of the hypersonic vehicle shape should also reflect the integrated geometric design of the fuselage shape and the flow channel surface of the propulsion system.

Reference [51] has made useful attempts in the parametric modeling of hypersonic vehicles, but there are some problems, such as too many design parameters and insufficient embodiment of the integrated characteristics of airframe propulsion. The authors of this book propose a parametric modeling method for the integrated shape of hypersonic vehicle fuselage and propulsion, which reduces the modeling parameters, simplifies the modeling process, is easy to program and implement, and can better reflect the overall and local characteristics of hypersonic vehicles.

2. The fuselage promotes an integrated shape modeling process

1) Modeling process

The integration of the fuselage and propulsion system of the hypersonic vehicle is its distinctive feature, and the lower surface of the fuselage of the entire aircraft constitutes a flow channel of the propulsion system. The flow channel starts from the head of the fuselage and extends to the tail of the fuselage, and the geometric surface on one side of the fuselage becomes the shape of the entire "keel" of the aircraft, which affects the design of the geometry of the lower surface of the aircraft and also determines the design of the main structural components on the aircraft. Therefore, the geometric design of the flow channel of the propulsion system is very important for the design and performance of hypersonic vehicles, and the design of the flow channel must be paid attention to in the process of integrated shape design. The fuselage propulsion integrated shape modeling method proposed in this book starts from the design of the two-dimensional flow channel of the propulsion system, and then builds the three-dimensional geometry of the aircraft, as shown in Figure 5-55. In the modeling process, the 3D fuselage of the aircraft is generated based on four modules: propulsion system flow channel design, fuselage top view profile design, fuselage side view contour design, and fuselage cross-section gradient form design. The wing is a diamond-shaped or hexagonal airfoil, which can be parameterized according to the usual way of defining the wing parameters, which will not be repeated here, but can be found in Reference [51], which focuses on the flow channel and fuselage generation method.

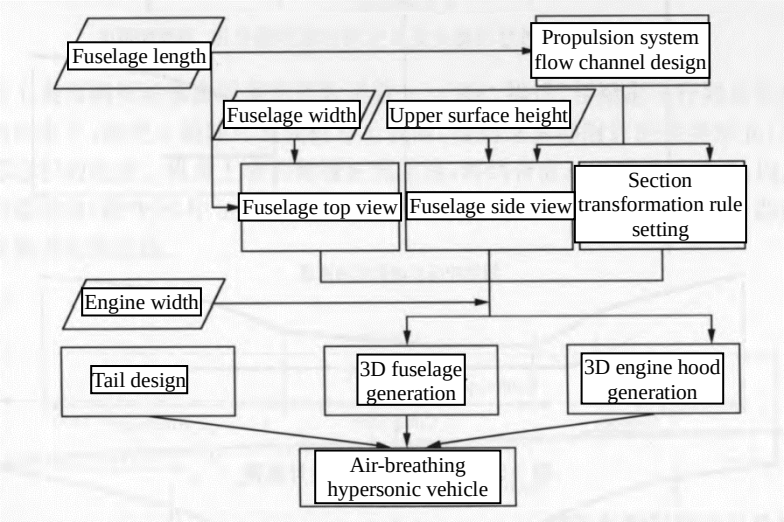

Figure 5-55: Integrated parametric modeling process of hypersonic vehicle fuselage propulsion

2) The profile design of the flow channel of the propulsion system

Under the constraints of the given total length of the aircraft, the design of the flow channel of the hypersonic vehicle propulsion system is carried out, including three parts: the forebody air intake, the combustion chamber (including the isolation section), and the rear nozzle. The forebody inlet consists of multiple compression wedges; the combustion chamber consists of an equal-section isolation section and an expansion section; the wall surface of the rear body nozzle is in the form of a curve.

Under the design conditions, the forebody air inlet requires the forebody shock waves to converge at the lip of the lower wall of the flow channel, and the angle of each compression wedge can be assigned according to the principle of equal shock angle and equal shock intensity [52], or the optimization algorithm can be used to optimize the design with the goal of maximizing the total pressure recovery [53,54]. Reference [55] identified five basic geometric control parameters that can be parameterized for the parametric design of the two-dimensional inlet through the analysis of the relationship between hypersonic two-dimensional inlet flow and geometric parameter constraints and parameter sensitivity analysis, which provides a practical way for the optimal design of two-dimensional inlet surface. The length of the medium-section isolation section of the combustion chamber and the length and expansion angle of the expansion section are usually determined by engineering experience [56]. The curve of the rear body nozzle can be described in the form of segmented arcs [57], cubic curves [58], or cubic spline functions [59,60]. Under the premise of the constraint of the total length of the aircraft, the length of each component is allocated, and the design of the three components is carried out to ensure that the dimensions of each other are matched with each other, that is, the design of the flow channel is formed, as shown in Figure 5-56. In Reference [61], the authors proposed a method of using BLISS hierarchical optimization for the design of the integrated flow channel of scramjet engine, decomposed the overall optimization and component optimization, and determined the design variables such as the length of the wedge surface and the angle of the wedge surface of the forebody inlet tract by its sub-design optimization module, so as to reduce the overall design parameters of the flow channel.

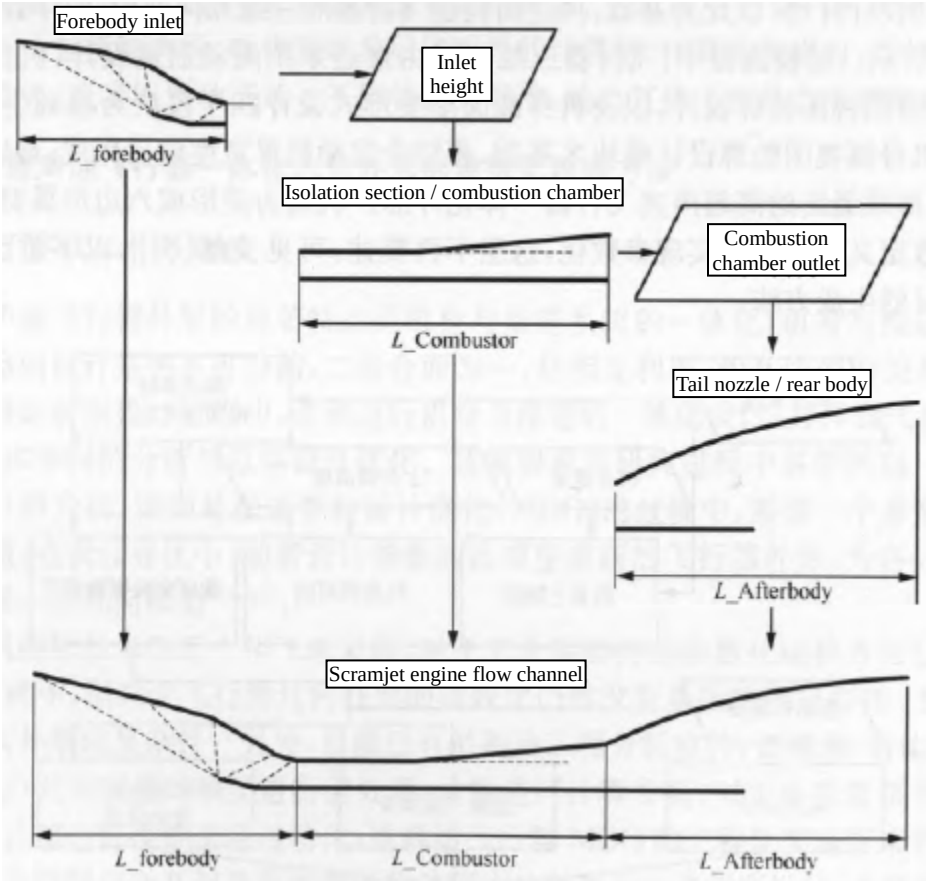

Figure 5-56: Flow channel surface design flow

3) Fuselage geometric feature description function

In order to achieve a uniform flow of scramjet engine modules, hypersonic vehicles usually use a flat spatula-shaped head. However, an excessively wide head can also cause problems such as resistance and increased structural mass, and the authors of this study analyzed the influence of the forebody width from two aspects: the inlet flow characteristics of the inlet and the aerodynamic characteristics of the forebody in Reference [62]. In order to describe the change of the width of the head of the aircraft with fewer design parameters, this study uses the power function $y = Ax^n$ to describe the top view curve of the fuselage, x and y are the coordinate value, n is the parameter that controls the change of the curvature of the contour curve, and A is the constant of the current function, which is determined by the length L, the width W, and the selected current n value, $A = W/(2L^n)$.

When the n value of this function is changed, the curve form can be changed, which is reflected in the change of the width of the head of the aircraft, as shown in Figure 5-57.

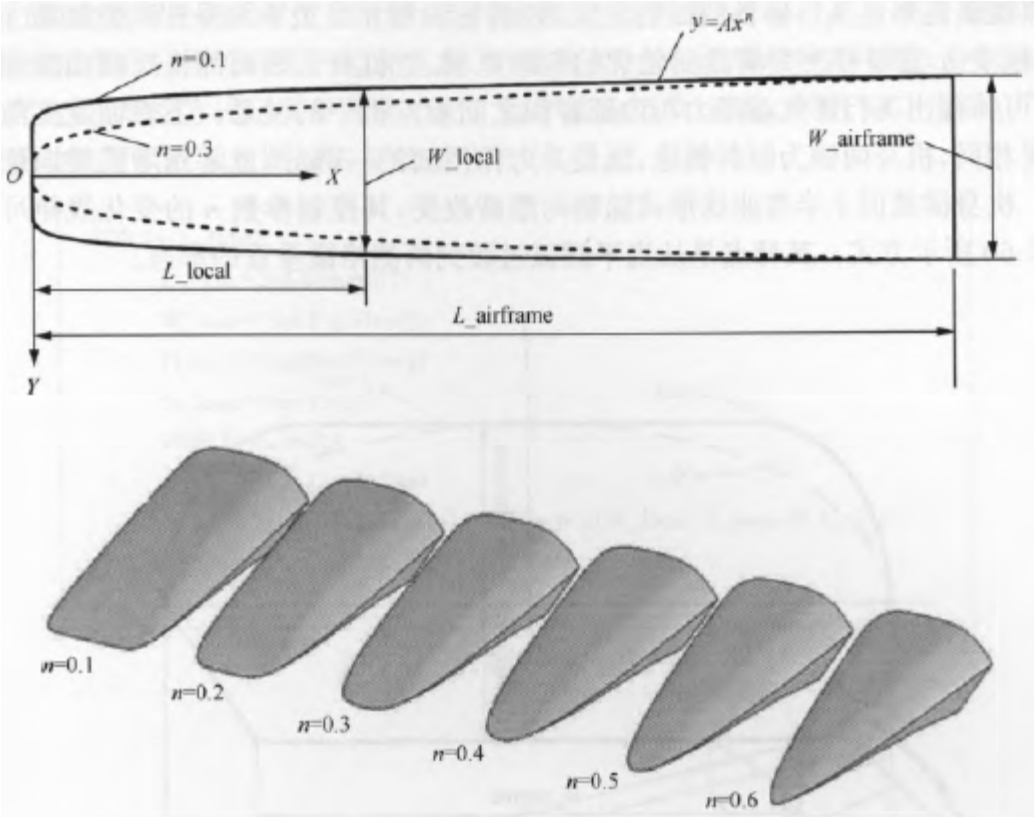

Figure 5-57: The influence of the top view profile definition and head shape control parameters of the fuselage

The side-view profile curve of the upper fuselage surface is described by the power function $z = Ax^n$. Under the constraints of a given total length and height of the upper surface of the vehicle, changing the value of *n* can change the form of the arches on the upper surface of the fuselage, especially near the head, reflecting the change of the internal volume of the vehicle. The side-view profile curves of the upper fuselage surface, combined with the results of the flow channel design and the definitions of the inlet channel sidewall leading edge inclination (a_1 in Figure 5-58) and the aft body nozzle sidewall inclination (a_2 in Figure 5-58), can be formed into the vehicle fuselage side-view profile curves.

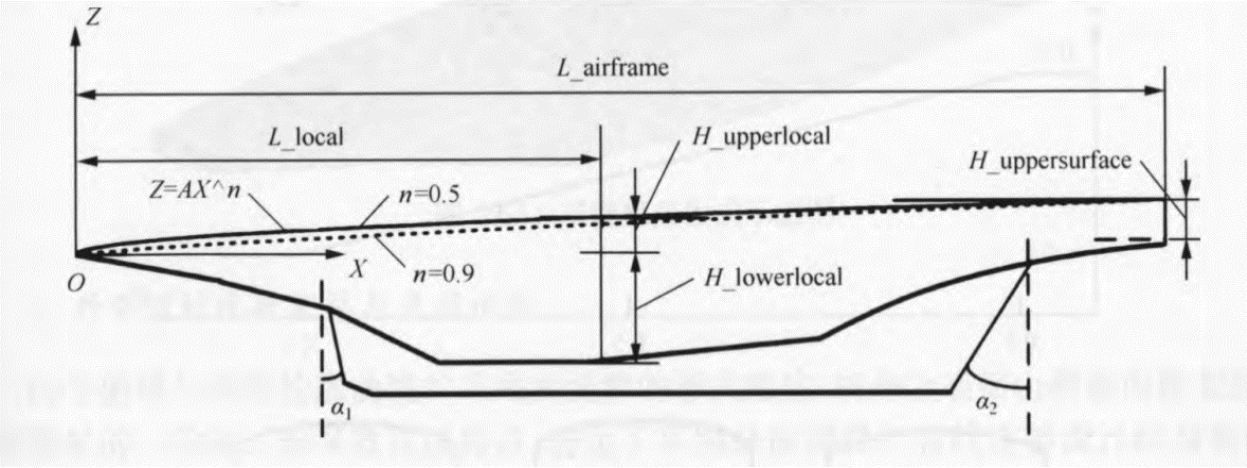

Figure 5-58: Fuselage side view profile definition

4) Fuselage cross-section gradient mode

The definition of a typical hypersonic vehicle cross-section is shown in Figure 5-59. The upper surface is described by the power function $y = Az^n$ and changing the value of n can change the envelope of the cross-section contour, which is compatible with the side-view contour curve of the upper surface of the fuselage and can reflect the relationship between the aerodynamic drag of the vehicle and the internal volume of the compromise. The width of the lower surface is the same as the width of the engine cowl, and the two sides of the fuselage are inclined side edges, which are part of the lifting surface and also play a role in enhancing the lateral stability. Fuselage cross-section of the upper part of the curve form with the axial gradual change, the change rule of its control parameter n can be designed as shown in Figure 5-60. It is characterized by the transition from a flat arc to a slightly vertical form on both sides.

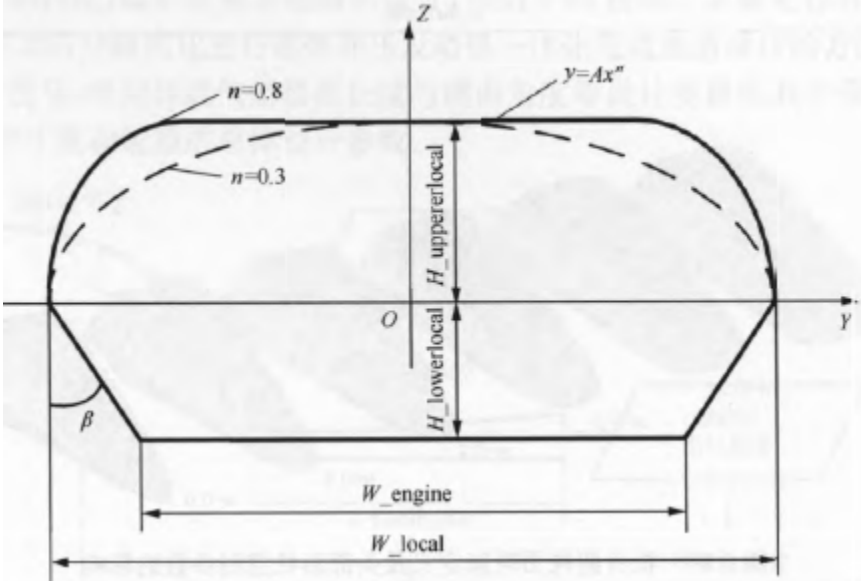

Figure 5-59: Definition of fuselage cross-sectional profile

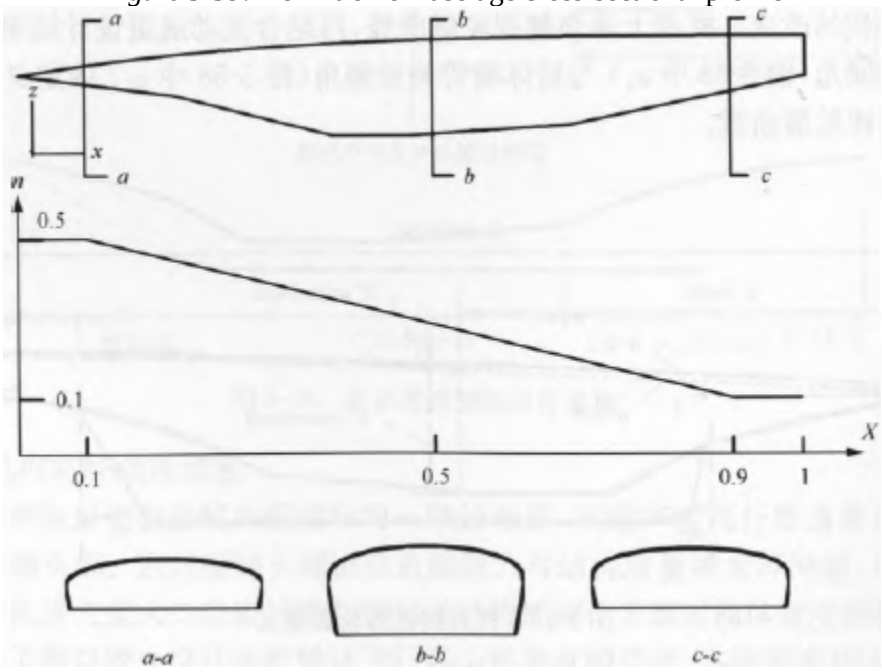

Figure 5-60: Definition of the gradient mode of the fuselage interface

5) Generation of three-dimensional fuselage and engine hood

The fuselage and hood of the aircraft are generated in the way of section by section along the axial direction, and the core is to generate the contour curves of each section, and the constraint parameters are the local contour width, contour height, and upper surface shape control parameters, which are respectively given by the subroutines defined by the top-down, side-view contour curves, and gradient modes. The program structure is simple and clear, as shown in Figure 5-61. Figure 5-62 and Figure 5-63 show the schematic diagram of the aircraft fuselage and engine hood.

```
FOR I=1: IMAX
    L_local=SubXlength(I)
    W_local=SubTopView(I)
    H_local=SubSideView(I)
    N_local=SubVn(I)
    FOR J=1:JMAX
        X(I,J,1)=L_local
        (Y(I,J,1),Z(I,J,1))=SubSection(W_local,H_local,N_local,J)
    END
END
```

Figure 5-61: The fuselage is upgraded to a code section by section

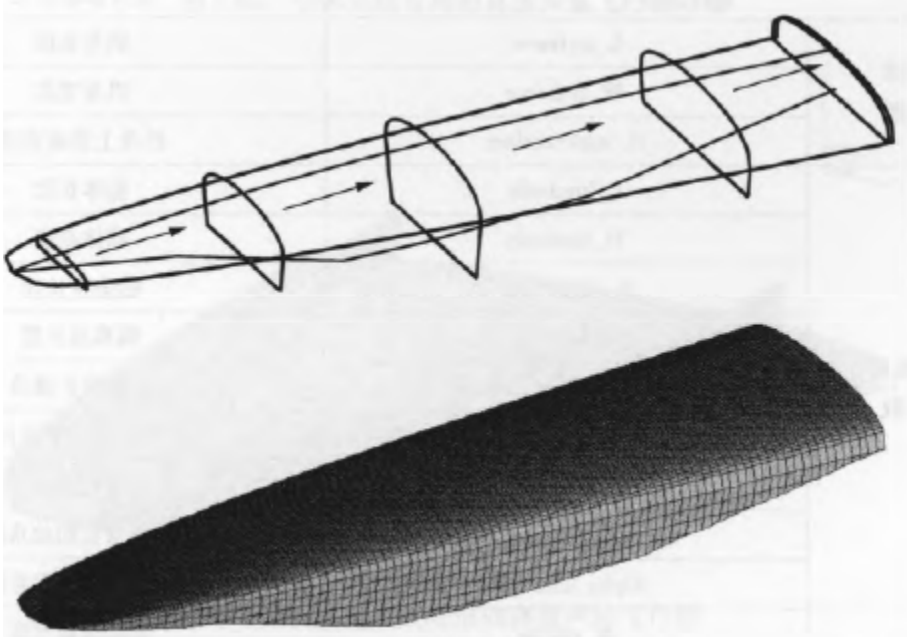

Figure 5-62: Schematic diagram of 3D fuselage generation

3. Summary of design parameters and application examples

As the top-view and side-view profile curves are described in the form of power function, the upper surface of the fuselage is formed by the gradient of the cross-section, which has good first-order and second-order derivative continuity characteristics and avoids the shortcomings of using the segmented arc and straight line connection to design the fuselage profile curves, which have a lot of parameters and may result in discontinuous derivative of the profile curves.

The fuselage profile design parameters are summarized in Table 5-4. In the design optimization, according to the actual situation, the design variables with large influence degree can be screened and considered, and some design parameters reflecting local details can also be added, such as the engine cowl leading edge angle, wall thickness and so on.

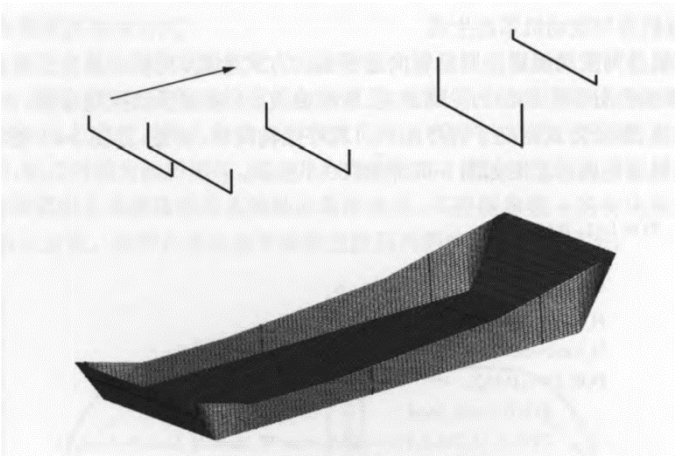

Figure 5-63: Schematic diagram of the hood being raised

Table 5-4: Summary of design parameters

Design parameters		Design parameter significance
Overall design parameters of the fuselage	L_airframe	Fuselage length
	W_airframe	Fuselage width
	H_uppersurface	Surface height of the fuselage
Engine flow channel design parameters	L_forebody	Premise length
	H_forebody	Premise height
	L_combustor	Combustion chamber length
	L_isolator	The length of the isolation segment
	Alpha_extcombustor	Combustion chamber expansion angle
	L_nozzleflap	The length of the wall under the rear nozzle
	H_afterbody	Rear body nozzle height
	Alpha_ininizzle	Rear body nozzle initial angle
	Alpha_endnozzle	Rear body nozzle outlet angle
Engine hood design parameters	W_engine	Hood width
	Alpha_intletedge	Engine hood leading edge inclination
	Alpha_nozzleedge	Engine hood trailing edge inclination
Shape control	N_nosetopview	The head of the fuselage looks down on the contour control parameters
	N_uppersideview	The upper surface of the fuselage is overlooked to control the contour parameters
	N_iniforeview	Initial parameters for the fuselage section profile gradient
	N_endforeview	Fuselage section profile gradient end parameter

Figures 5-64 and 5-65 are hypersonic vehicles with the same flow channel design parameters, resulting in a narrow-body conventional layout and a wide-body wave-riding profile, respectively.

The shape of the two species changes greatly, but the integrated geometric modeling method proposed in this section can be generated by the same program under the condition of changing the relevant parameters, which indicates that the method has strong multi-shape adaptability and large design space coverage.

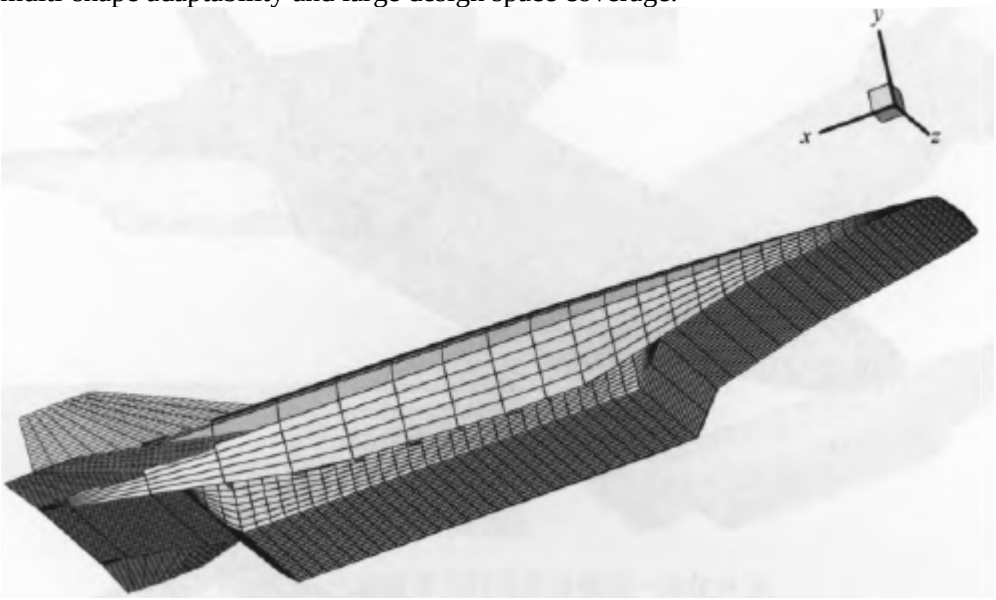

Figure 5-64: Shape of a hypersonic vehicle with a narrow-body conventional layout

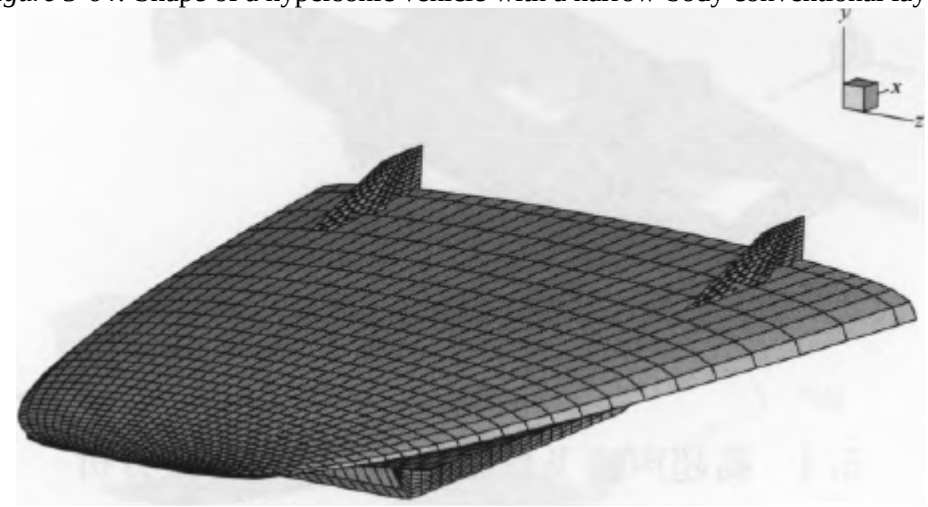

Figure 5-65: Wide-body wave-riding hypersonic vehicle

4. Application in the MDO process

The hypersonic vehicle shape obtained by this method has the characteristics of full value, and the surface is in the form of a surface grid (Fig. 5-66), and the engineering aerodynamic/thermal calculation method can be applied to calculate the aerodynamic force and aerothermal heat in the conceptual design stage, and the structural mass can be estimated according to the area integral of the surface element.

In further design analysis, if commercial engineering analysis software is required, this method can be easily exported as a data format file of PLOT3D, and most 3D geometric modeling software, CFD pre-processing software, and finite element analysis software can be read, which can realize seamless connection with commercial engineering analysis software. In addition, the cross-sectional data can also be output to form a preliminary design drawing of the aircraft fuselage structure, as shown in Figure 5-67.

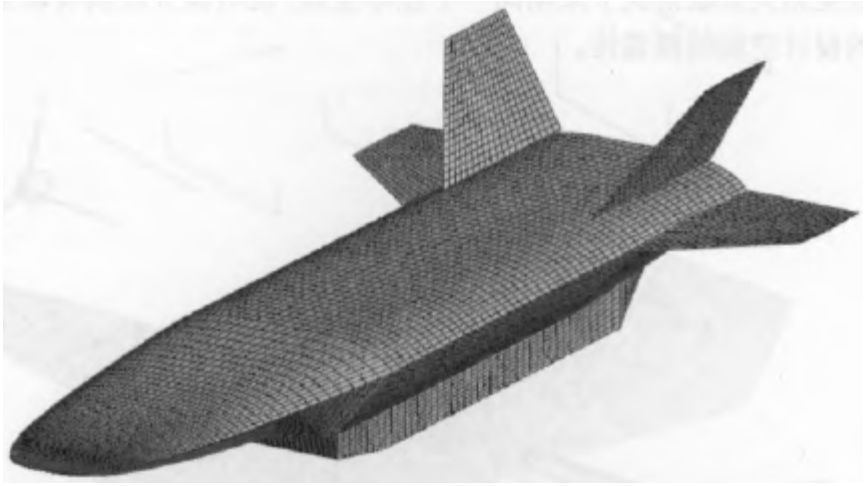

Figure 5-66: Aircraft surface mesh

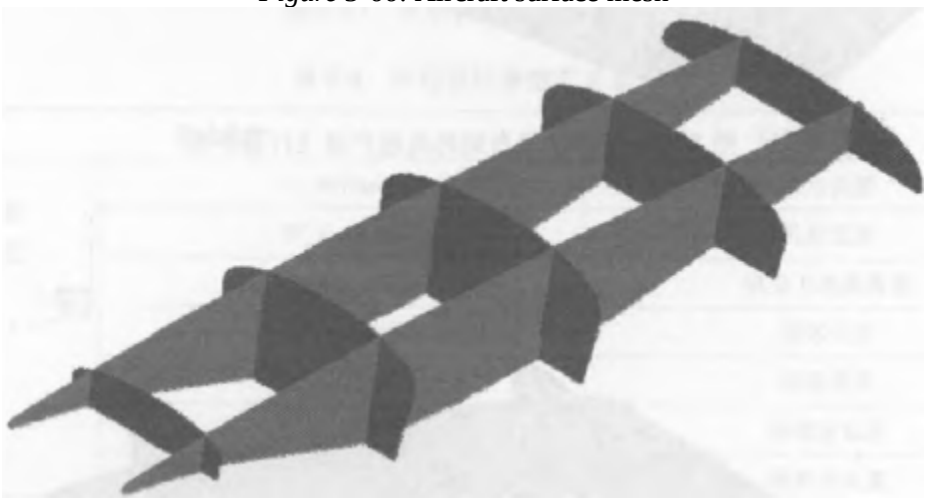

Figure 5-67: Schematic diagram of aircraft structure design

5.4: Analysis of integrated aerodynamic characteristics of hypersonic vehicles

5.4.1: Computational modeling of integrated aerodynamic characteristics

According to the integrated geometry modeling process described above, the 3D shape of the hypersonic vehicle is generated, and the 3D surface mesh data of the vehicle is generated, which is displayed as shown in Figure 5-68.

For hypersonic vehicles, the division of aerodynamic and propulsion computing power as shown in Figure 5-69 is adopted, the aerodynamic calculation of the entire outer surface of the aircraft (including the outer wall of the engine hood, except for the lower wall of the rear body nozzle), and the propulsion discipline is responsible for the calculation of the combustion chamber and rear body nozzle.

In order to estimate the aerodynamic characteristics of hypersonic inviscosity, based on the theory of hypersonic inviscosity, the aerodynamics discipline uses the component decomposition method to divide the aircraft into two large aerodynamic parts, the fuselage and the wing, and adopts different estimation methods according to the conditions of the front/leeward surface. Referring to Reference [63], the Dahlem-Buck method was used for the windward side of the fuselage, and the Prandtl-Meyer method was used for the leeward side.

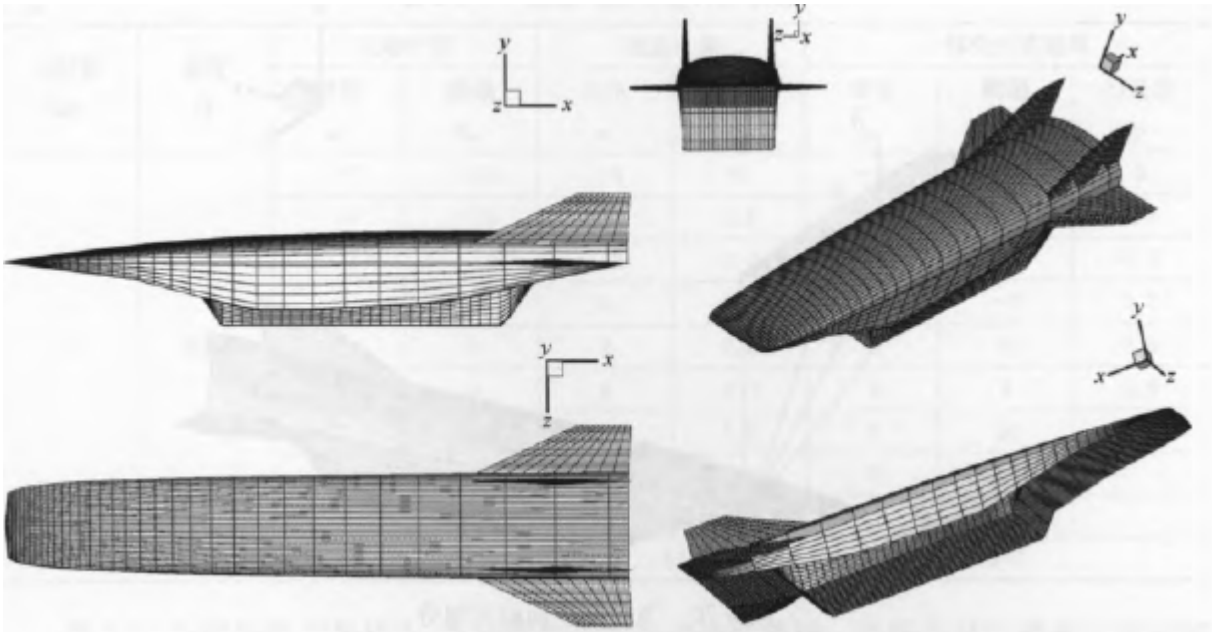

Figure 5-68: Integrated propulsion profile of the fuselage of a hypersonic vehicle

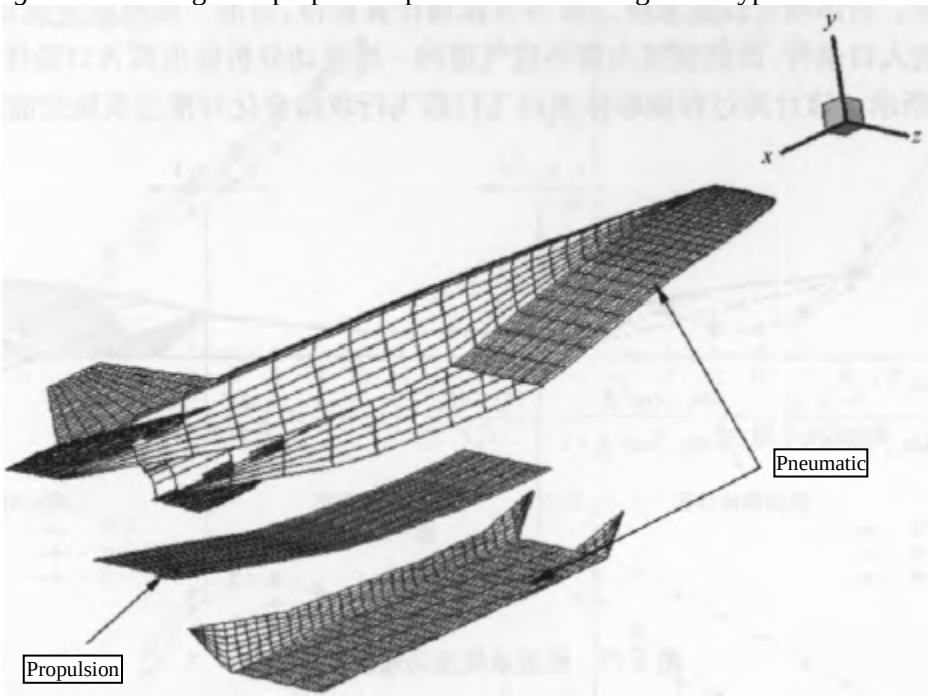

Figure 5-69: Computing power decomposition for pneumatic propulsion

The cone or Daheim-Barker method is used for the windward side of the wing, and the expansion wave method is used for the leeward side. In the aerodynamic engineering estimation of complex aircraft based on the above methods, the surface element method is widely used to divide the surface of the aircraft [63], that is, the surface of the aircraft is divided into several small surfaces, and then each small surface is replaced by a first-order plane surface element, and a series of plane surface elements are used to approximate the shape of the aircraft, and the aerodynamic force of each plane surface element is calculated, and then added to obtain the aerodynamic force of the whole aircraft. The generated hypersonic vehicle is embodied as a surface data grid, which can be easily used for the calculation of surface elements (Figure 5-70).

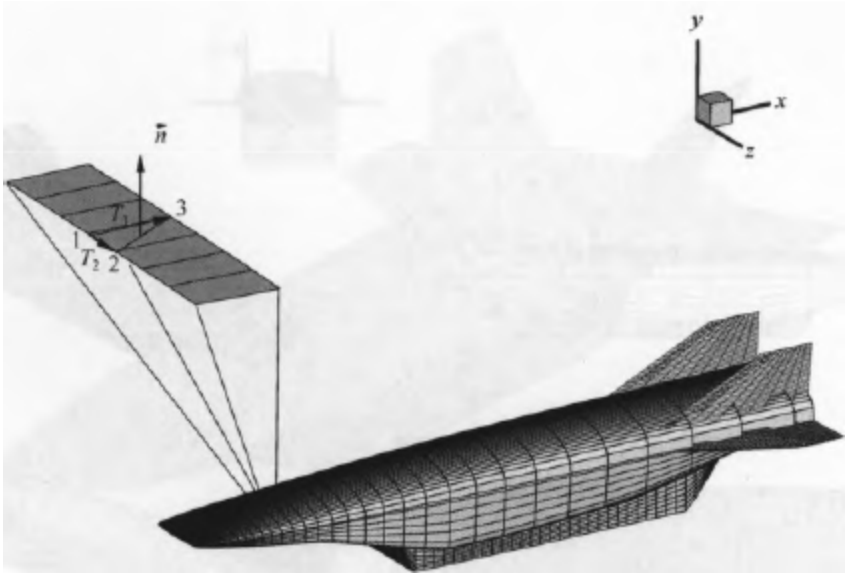

Figure 5-70: Surface element division of an aircraft

The purpose of the propulsion calculation is to obtain the thrust generated by the rear body nozzle, including axial thrust, normal thrust lift, and pitch moment. The performance of the rear body nozzle is calculated by the two-dimensional N-S flow field, the inlet conditions of the rear body nozzle are provided by the quasi-one-dimensional combustion chamber flow calculation, and the inlet conditions of the combustion chamber are given by the one-dimensional flow analysis of the front body air intake, as shown in Figure 5-71. The calculation process can reflect the influence of the change of the aircraft's flight angle of attack on the performance of the propulsion system.

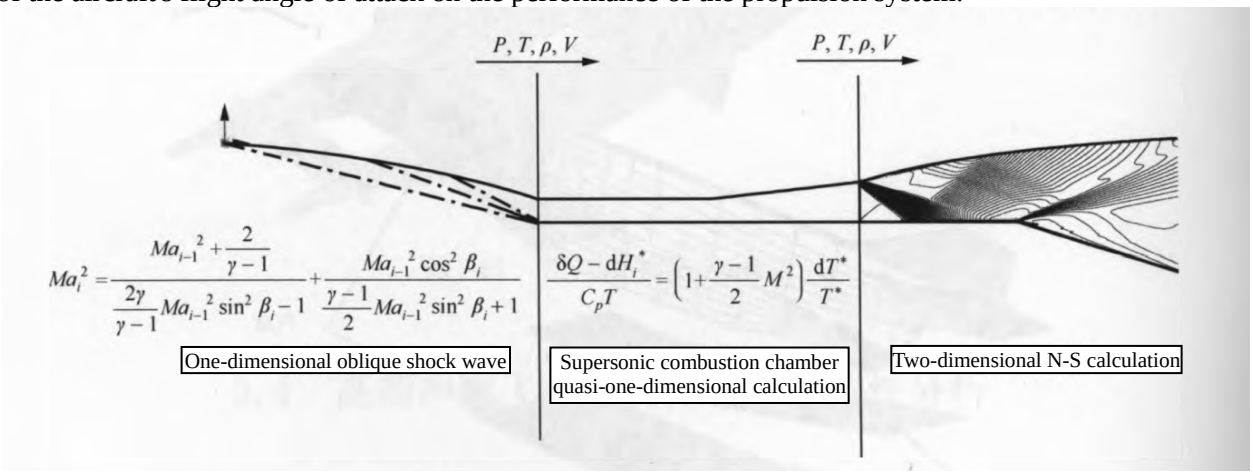

Figure 5-71: Flow channel calculation flow of the propulsion system

5.4.2: The influence of the working state of the engine on the aerodynamic characteristics of the integration

The performance calculation of the integration of aeropropulsion of the hypersonic vehicle in the cruising state of *Ma* = 6 and the altitude of 30 km is carried out, in which the aerodynamic calculation is for the angle of attack ranging from -6° to 10° and the pitch rudder deviation is -20°~20°, a total of 81 states were calculated for outflow aerodynamics; propulsion calculations were calculated for angles of attack ranging from -6° to 10°, engine ventilation not working, and engine operating with equivalent ratios from 0.5 to 1, a total of 63 states. Under the same angle of attack, the calculation results of the integrated performance are synthesized, and a total of 567 state data are formed (Table 5-5).

Table 5-5: Calculation status of integrated aerodynamic characteristics

Mach number Ma	Height H	Start the calculation		Advance computing		All-in-one calculation results		
		Angle of attack α	Rudder deviation δ_m	Angle of attack α	Equivalence ratio φ	Angle of attack α	Rudder deviation δ_m	Equivalence ratio φ
6	30km	-6	-20	-6	0	-6	-20	0
		-4	-15	-4	0.5	-4	-15	0.5
		-2	-10	-2	0.6	-2	-10	0.6
		0	-5	0	0.7	0	-5	0.7
		2	0	2	0.8	2	0	0.8
		4	5	4	0.9	4	5	0.9
		6	10	6	1.0	6	10	1.0
		8	15	8		8	15	
		10	20	10		10	20	
Total statuses		81		63		567		

Figure 5-72: The basic aerodynamic characteristic curve of the aircraft under the condition of 0° rudder declination.

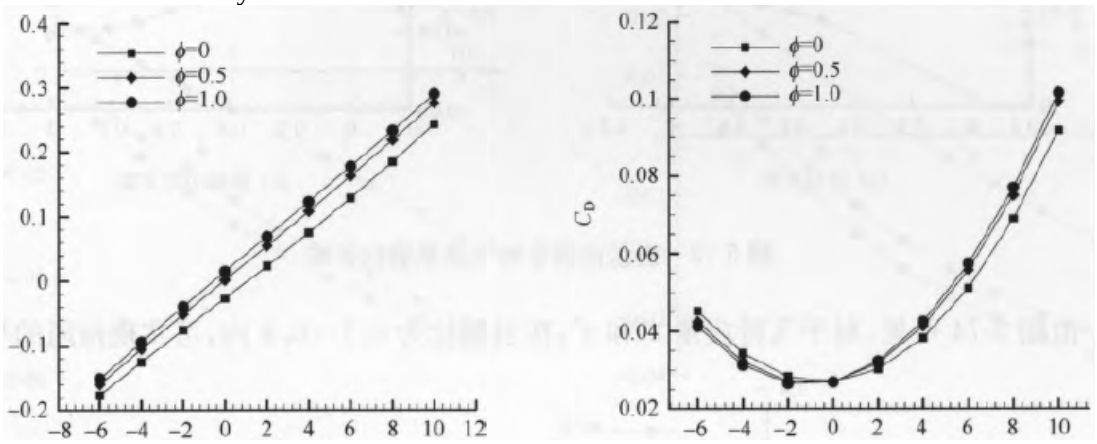

(a) Lift coefficient curve (b) Resistance coefficient curve

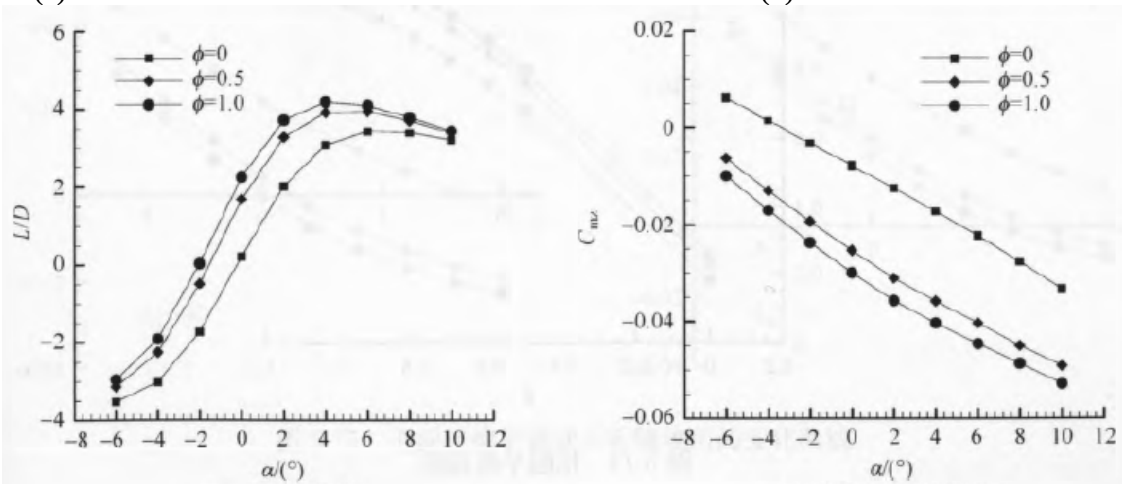

(c) Lift-to-drag ratio curve (d) Pitching moment coefficient curve

Figure 5-72: Integrated aerodynamic coefficient curve of a hypersonic vehicle

It can be seen from the figure that the lift coefficient and drag coefficient are increased under the condition of each angle of attack under the condition of each angle of attack, the increase of the lift coefficient is caused by the normal force component generated by the thrust of the rear body nozzle, and the increase of the drag coefficient is caused by the viscous resistance of the rear body nozzle when there is gas passing through the viscous resistance is greater than that of the non-gas ventilation state. At the same time, when the engine is in working condition, the additional lift generated by the thrust significantly increases the lift-to-drag ratio of the whole aircraft, but also increases the head-down torque of the aircraft, which requires a large rudder deviation for trim operation.

Figure 5-73 further shows the influence of engine equivalent ratio adjustment on the lift coefficient and pitching moment of the entire aircraft. From the engine ventilation not working to the engine ignition, the lift coefficient and pitching torque coefficient have increased significantly and continue to increase with the increase of the equivalent ratio.

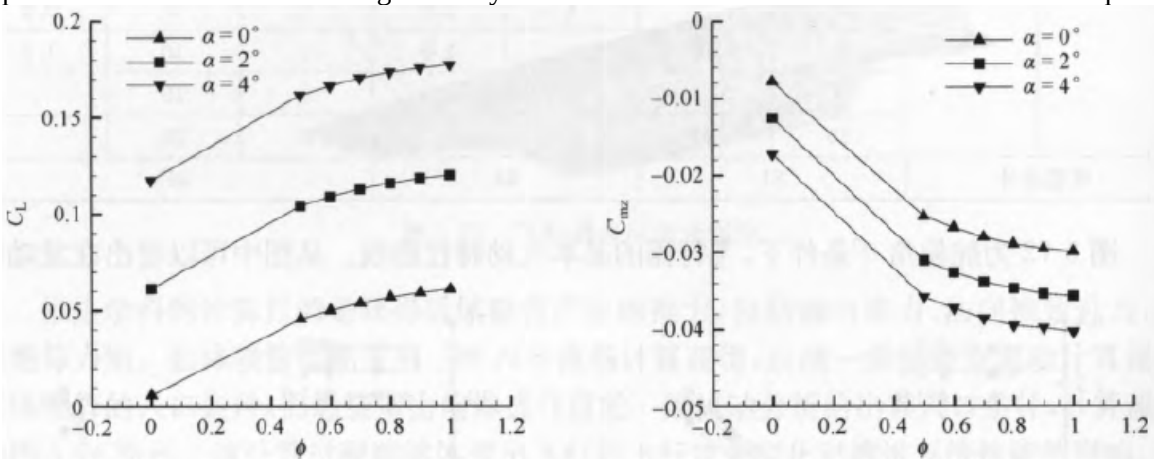

(a) Lift coefficient (b) Pitching moment coefficient

Figure 5-73: Effect of equivalence ratio adjustment on aerodynamic coefficient

As can be seen from Figure 5-74, for the flight angles of attack of 2° and 4°, the balance of thrust and drag can be achieved within the equivalent ratio of 0.7 to 0.8.

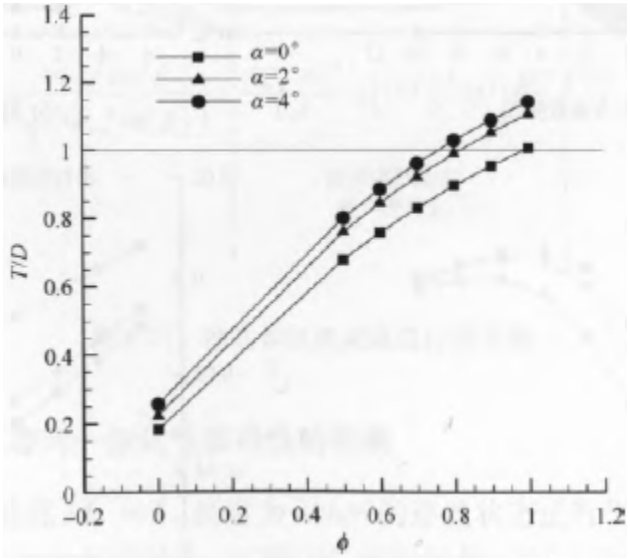

Figure 5-74: Push-drag equilibrium curve

5.4.3: The influence of engine working state on the stability and trim characteristics of the aircraft

As shown in Figure 5-75, under different deviation angles, the increase of the engine equivalent ratio will increase the pitching moment of the lower head, but it has static stability for the state of (^=0). Under the condition that the rudder deviation does not change, the steady state of each angle of attack is greatly affected by the engine equivalent ratio, so the rudder deflection needs to be adjusted. Figure 5-76 shows the influence of the engine working state on the rudder deflection required to maintain the stability of the aircraft under the conditions of 2° angle of attack and 4° angle of attack. When the angle of attack is 2°, the engine needs to jump from -5° to -10° to -12° from non-ignition to ignition. When the angle of attack is 4°, the engine needs to jump from -6° to -13° to -14° from non-ignition to ignition. However, taking the angle of attack of 2° as an example, when the rudder deflection changes, the drag coefficient of the aircraft will change, Figure 5-77 shows the increase of the drag coefficient caused by the increase of the engine equivalent ratio and the increase of the rudder deflection angle adjustment in the trim state. Figure 5-78 shows the effect of the increase of the engine equivalent ratio on the thrust resistance balance state of the aircraft in the trim state, the thrust increases after the engine equivalent ratio increases, but the rudder deflection needs to be adjusted for trimming, and after the trim state is reached, the trim drag generated increases the drag of the whole aircraft, so the thrust resistance balance is still not reached in the trim state.

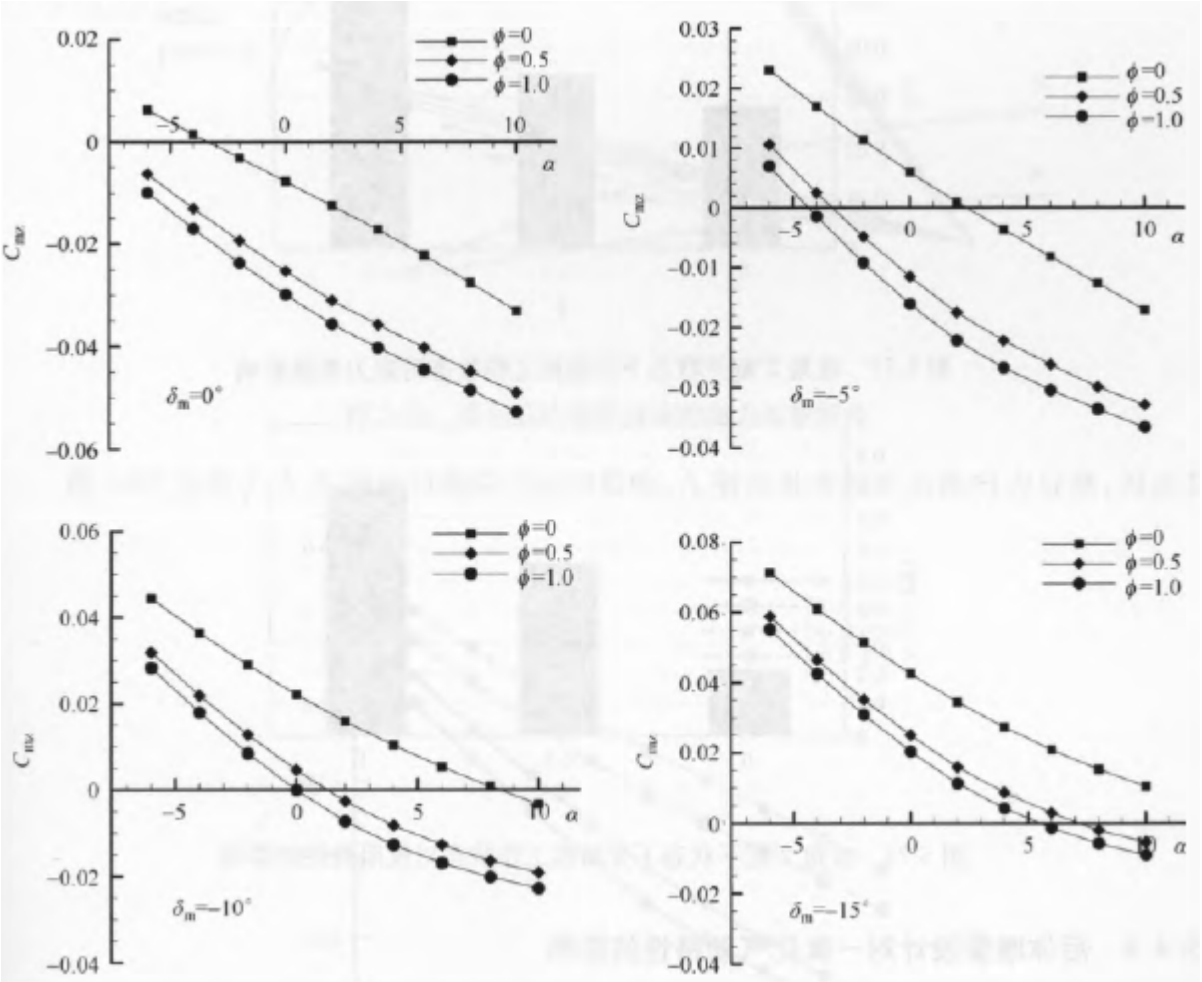

Figure 5-75: Pitch moment with different rudder deflection curves with angle of attack

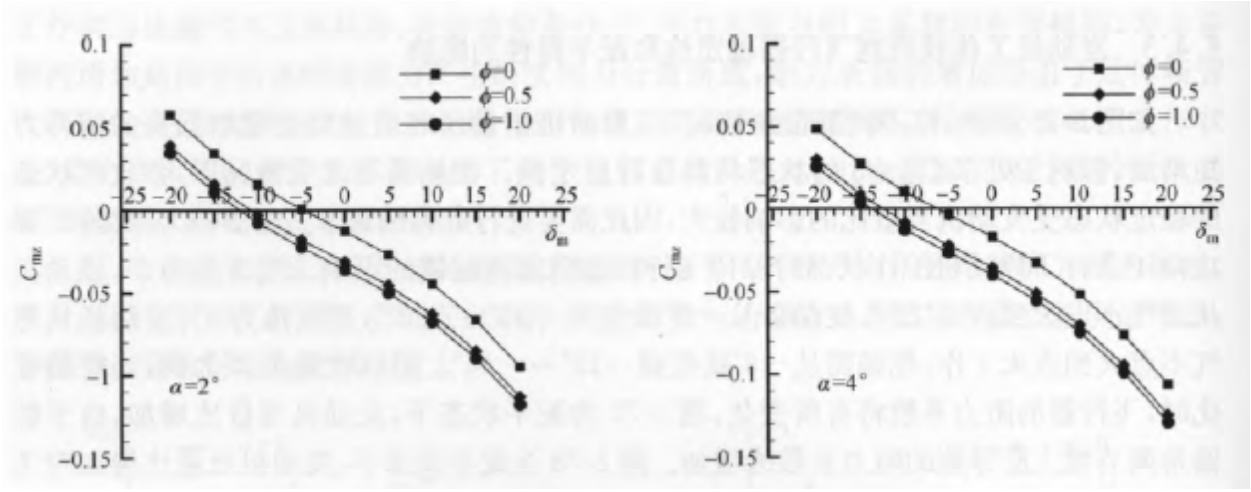

Figure 5-76: The influence of engine operating conditions on trim rudder declination angle at different angles of attack

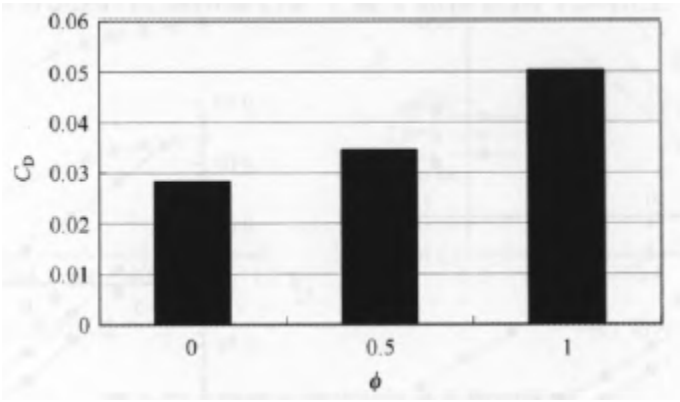

Figure 5-77: The influence of the engine working state on the drag coefficient at the 2° trim angle of attack

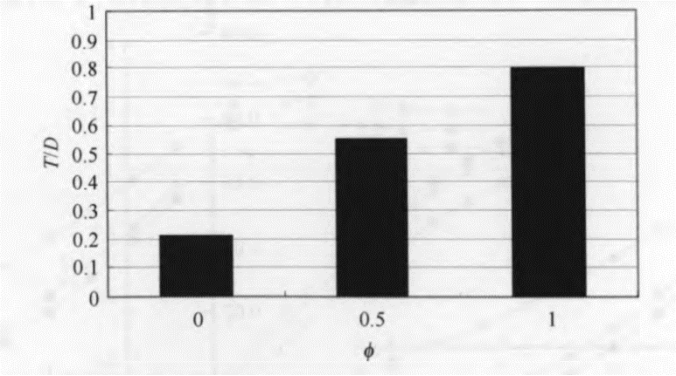

Figure 5-78: The influence of the engine operating state on the thrust resistance characteristics at the 2° trim angle of attack

5.4.4: Influence of rear body nozzle design on integrated aerodynamic characteristics

The different profile design of the rear body nozzle affects the expansion and discharge process of scramjet engine gas, and therefore the size and direction of thrust. As shown in Figure 5-79, the A and B surfaces have different outlet heights and upper surface curves. The performance calculation of the rear body nozzle of these two types shows that different profiles not only affect the magnitude and vector direction of thrust, but also affect the direction of the thrust vector line with the equivalent ratio.

In Figure 5-79, the A-shaped plane has a large normal force component, and the B-shaped plane has a large axial force component, so its effective thrust is also larger. For the A-shaped surface, the equivalent ratio increases, and the thrust vector line angle decreases gradually. For B-planes, an increase in the equivalent ratio increases the thrust vector line angle.

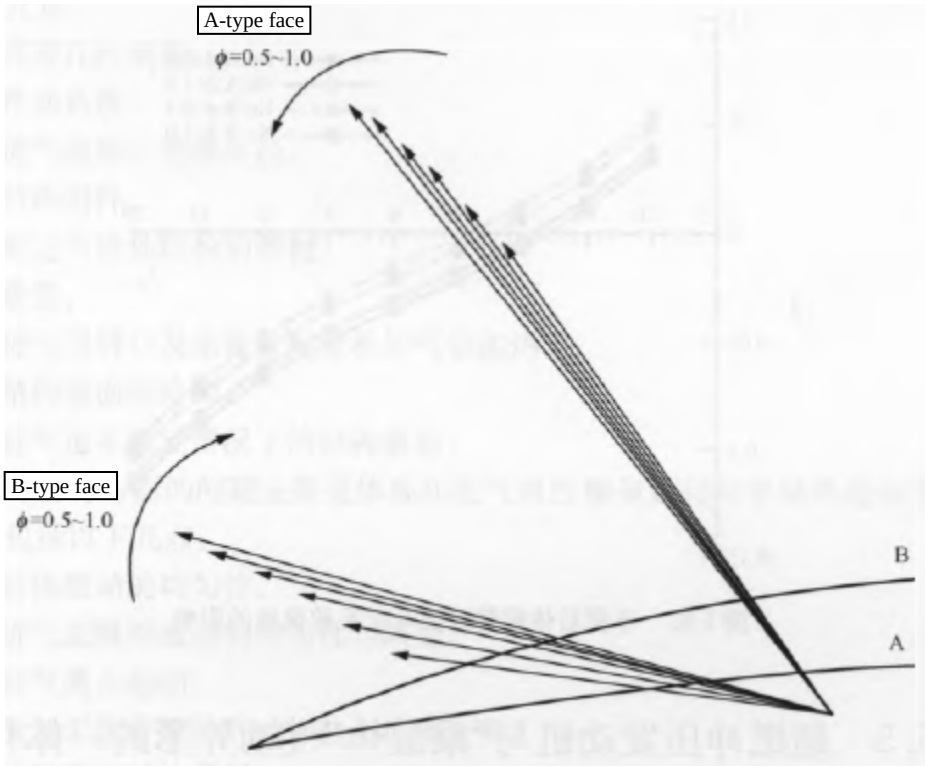

Figure 5-79: Thrust vectoring characteristics of different rear body nozzle profiles

Figure 5-80 analyzes the influence of the pitching moment of the A and B faces, and the A plane has a large normal force component, so the pitching moment generated by the A plane is also larger.

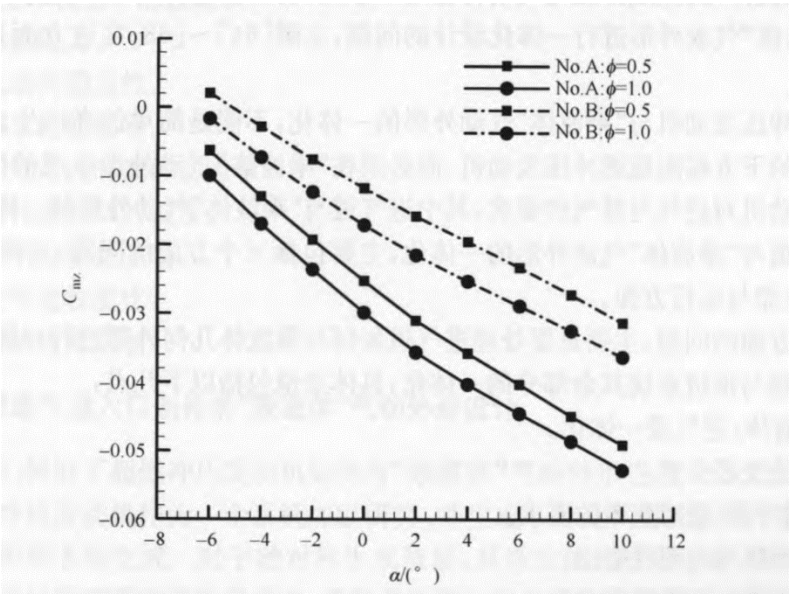

Figure 5-80: The influence of different rear body nozzle types on the pitching moment coefficient

As shown in Figure 5-81, the pitching moment generated by the B-shaped surface is smaller, so the trim rudder deflection angle can be reduced from 11° and 12° to 6° and 7° required for the A-shaped surface at an angle of attack of 2°.

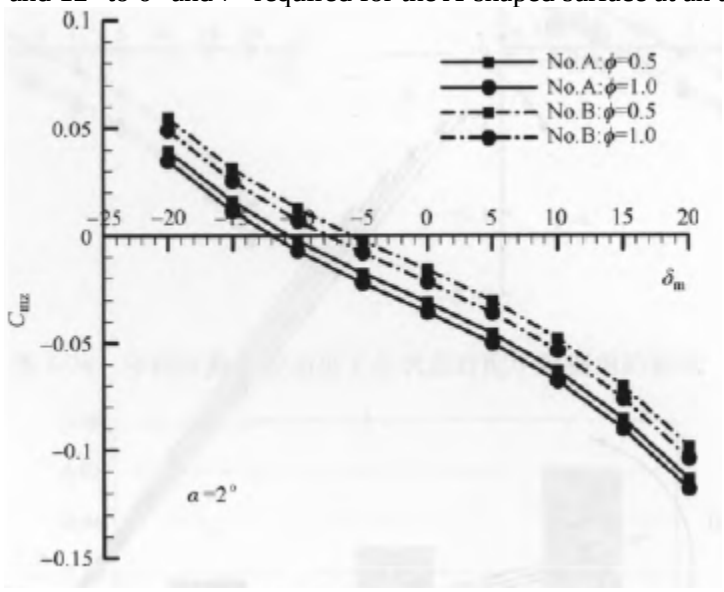

Figure 5-81: Effect of different rear body nozzle types on trim rudder declination

5.5: Integration of scramjet engine and "waverider" aerodynamic shape

5.5.1: Main Issues

The hypersonic vehicle in the shape of a "waverider" has a high lift-to-drag ratio, so it has attracted much attention and research. However, it is not enough to simply study the generation method and aerodynamic characteristics of the "waverider," and it is still necessary to consider and solve the problem of how to integrate the design of the scramjet engine with the aerodynamic shape of the "waverider," and relevant studies have been carried out in this regard in Reference [64]-[68].

The integration of scramjet engine and "waverider" aerodynamic shape cannot simply attach the scramjet engine below the generated "waverider" aerodynamic shape but must consider the requirements of scramjet engine for air intake and exhaust while generating the aerodynamic shape of "waverider," in which the integration of air intake duct and "waverider" aerodynamic shape is more important.

The integration of the air intake tract and the aerodynamic shape of the "waverider" mainly includes three aspects: the overall aspect, the structural aspect, and the performance and operation aspect.

The overall problem is to deal with how the intake tract is integrated with the waverider geometry and how the intake tract is integrated with the rest of the propulsion system, including the following:

(1) Forebody/inlet integration.
(2) Inlet position.
(3) Requirements for air flow capture rate.
(4) External to internal shrinkage ratio.
(5) Horizontal and three-dimensional compression.

(6) Integration with the combustion chamber tail nozzle.
(7) Integration with the cross-section of the shape of the waverider.

The structural aspects are mainly to deal with the design of the intake tract and the integration of the waverider structure, including the following:

(1) Variable geometry.
(2) Actuation system.
(3) Radius of the leading edge of the inlet lip.
(4) Structural attachments.
(5) Sealing of fixed and movable structures.
(6) Weight.
(7) Pneumatic heating of the inlet lip and the incoming flow distribution wallboard.
(8) Cooling of the structural wall.
(9) The structural load under the condition that the inlet tract does not move.

The performance and operation problems are mainly reflected in the impact of the inlet performance and operation on the overall engine performance, including the following:

(1) Uniformity of forebody flow.
(2) Uniformity and distortion of inlet laryngeal flow.
(3) The intake tract does not move.
(4) Separation of pneumatic heating and flow caused by shock wave interference.
(5) The boundary layer in the inlet tract.
(6) Starting characteristics.
(7) Mutual interference between air intakes.
(8) Boundary layer transition.
(9) Performance in non-design state.
(10) Overflow resistance.
(11) Stability of flow.
(12) Basic performance level.
(13) Fluid dynamics in the intake tract.
(14) The bluntness of the inlet lip.
(15) Horizontal and vertical compression.
(16) Inlet tract shrinkage ratio.
(17) Flow corner limit.

5.5.2: Aerodynamic design of the "waverider" considering the inlet conditions of the inlet channel

Reference [32] studied how to integrate the scramjet with the aerodynamic shape of the "waverider," and studied the waverider and the scramjet as a system to generate an integrated shape. The shape of the waverider forebody is generated by the requirements of the air intake. For axisymmetric flow fields, the bow shock wave of the waverider body is an arc-shaped curve.

In order to maximize the flow of captured air in the engine intake, the lip of the inlet should be as close as possible to the shock wave, so that the lip of the inlet tract becomes rounded. In order to use the same type of scramjet engine module transversely on the lower surface of the aircraft, the ideal shape of the lower surface of the aircraft at the cross-section of the inlet tract is an arc shape and has the same arc curve center as the shock wave, as shown in Figure 5-82. Thus, the lower surface of the forebody is formed by the forward tracing streamline to the shock wave starting from the known inlet tract curve. The upper surface is generated by tracing the streamlines backwards from the junction of the streamlines and the shock wave on the lower surface.

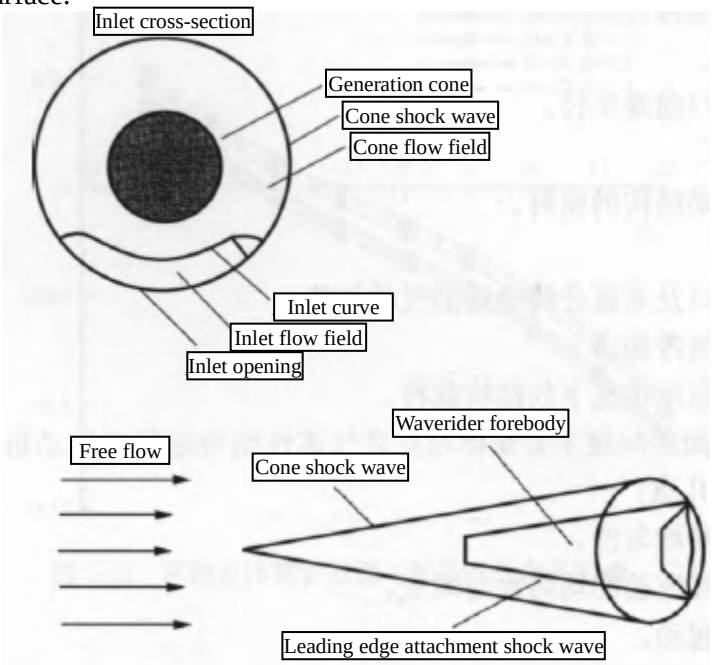

Figure 5-82: A waverider forebody generated from an arc-shaped inlet curve

Figure 5-83(a) shows the shape of the aircraft generated by the curve of the arc-shaped air intake. Although the height of the inlet duct is uniform, such a shape may not be feasible due to pneumatic heating and effective volume efficiency. However, if the restriction on the uniform height of the intake tract is relaxed and an elliptical inlet curve is adopted, the results of the two shapes shown in Figure 5-83 (b) and (c) can be formed. In Figure 5-83(b), the height of the inlet at the centerline is 2% higher than that of the outermost, and the height of the inlet at the centerline of the lower shape is 10% higher than that of the outermost. At the same time, the upper surface of the aircraft has changed a lot, from concave to convex. It can be seen that a small adjustment of the height of the inlet tract can make a considerable difference in the shape of the forebody.

In this study, the inlet curve is composed of an elliptical segment curve (with the same center as the shock arc) and a quadratic polynomial curve connecting the elliptic curve and the shock arc. Figure 5-84 shows the figure. Four parameters control the inlet curve: elliptical semi-minor axis, elliptical semi-major axis, the ratio of the inlet curve to the ellipse relative to the ellipse, and the span of the entire inlet curve.

The waverider is generated by a conical flow field, so the variation of the flow field characteristics in the span direction of the inlet section of the inlet tract is only affected by the change in the height of the engine module. The change in the vertical direction is only affected by the change in the flow between the cone and the shock wave. Figure 5-85 shows the distribution of the pressure and mass flow rate of the forebody shape in Figure 5-83(c) at the inlet cross-section, the change of pressure in the height direction is 8.5%, and the change of mass flow rate is 5%. It can be seen that after the appropriate adjustment of the inlet curve, the whole aerodynamic shape is improved, and the influence on the uniformity of the inlet parameters of the inlet is also small.

In order to facilitate the arrangement of a scramjet engine with a rectangular section on the lower surface of a hypersonic vehicle, a waverider design with a flat lower surface can be carried out with a small amount of sacrifice for the uniformity of the inlet [64], as shown in Figure 5-86.

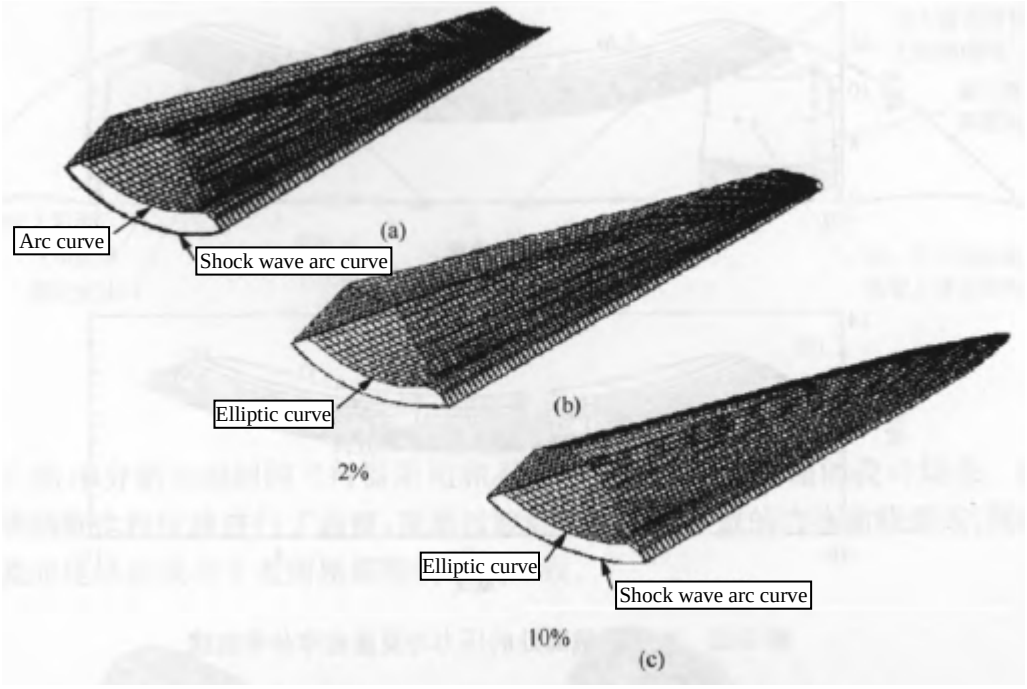

Figure 5-83: Waverider forebodies generated from arc-shaped and elliptical inlet curves

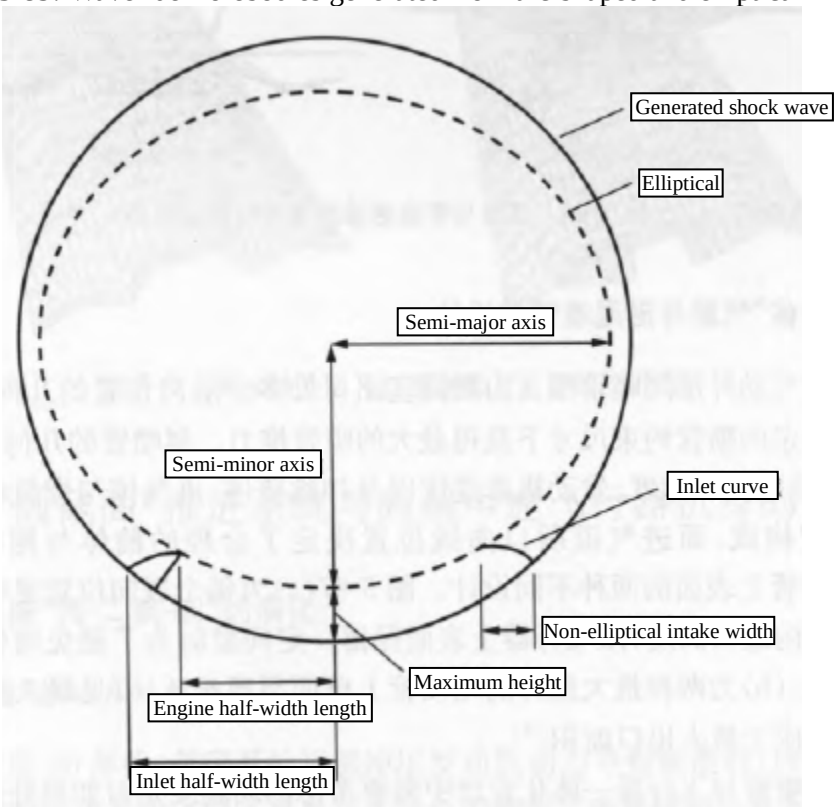

Figure 5-84: Design optimization parameters

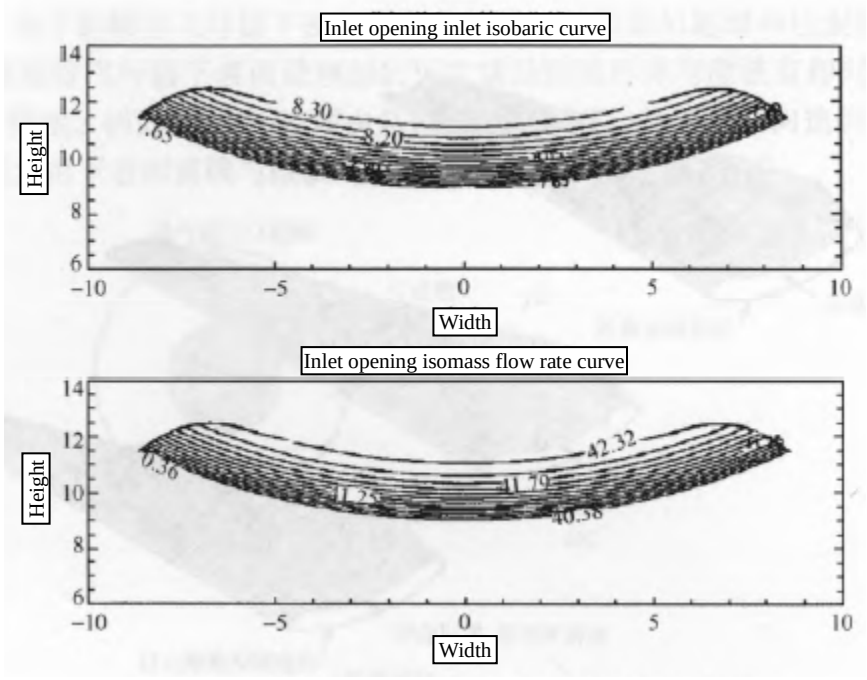

Figure 5-85: Pressure versus mass flow rate distribution curve at inlet cross-section

(a) Curved bottom (b) Flat bottom

Figure 5-86: Front view of an arc-shaped and flat-bottomed waverider aircraft

5.5.3: Design of "wave-riding" pneumatic shape tail nozzle

The aerodynamic shape of the "waverider" tail nozzle profile is determined by the geometrical parameters of multiple span positions at the outlet of the combustion chamber, and the profile design should obtain the maximum nozzle thrust at a given nozzle constraint size. The geometric constraints of the tail nozzle are composed of the position of the upper surface of the aircraft, the width of the combustion chamber outlet, the width of the engine cover, and the length of the tail nozzle after deducting the forebody, air intake and combustion chamber length, and the position of the inlet lip curve determines the reasonable ratio of the length of the forebody to the tail nozzle. Figure 5-87 shows two different designs on the upper surface of the tail nozzle. Figure 5-87(a) shows that the maximum height of the tail nozzle outlet at each radial position is the maximum height that can be used, and a certain gap is reserved with the upper surface of the aircraft to avoid interference between the nozzle gas and the air flow on the upper surface. (b) The design of the upper wall profile of the tail nozzle with two maximum thrust forces shows that the design of the maximum thrust tail nozzle profile does not correspond to the maximum outlet area [33].

Another issue that needs to be considered in the integrated design of the tail nozzle and the aircraft is how to deal with the bottom area of the aircraft. Compared with the accelerated aircraft, the waverider aircraft designed for cruise missions has a larger bottom area of the aircraft, because the width of the engine accounts for a small proportion of the aircraft, so the nozzle only occupies a small proportion of the bottom area of the aircraft. Reducing the bottom resistance is important when flying in the subsonic, transonic, and supersonic ranges. Therefore, for a cruise-type waverider hypersonic vehicle, its upper surface can be appropriately contracted downward to reduce the bottom area.

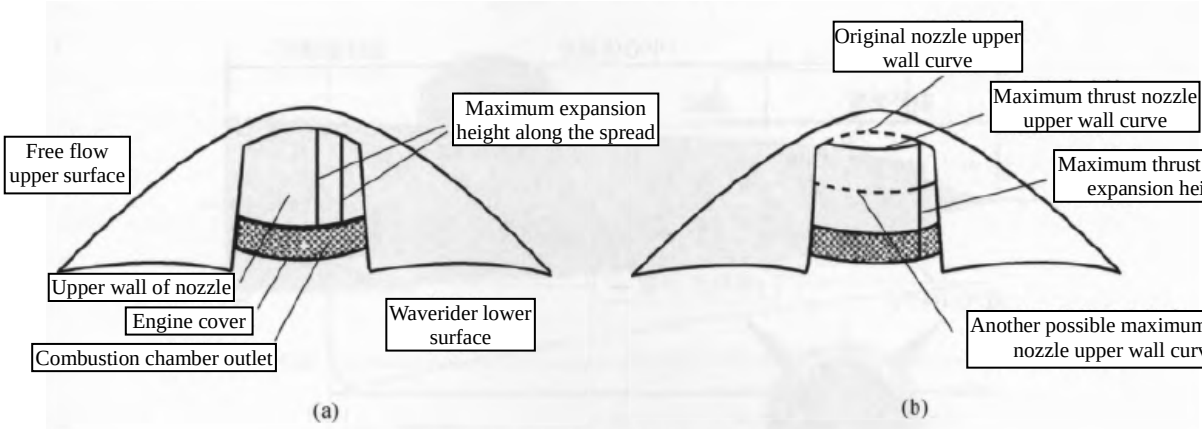

Figure 5-87: Design of the upper surface of the tail nozzle

Figure 5-88 shows the design results of the same aircraft with and without the downward shrinkage of the upper surface. The walls on both sides of the corresponding tail nozzle are also adjusted accordingly, and gradually transition to the form of edge curves consistent with the upper surface, and the tail curve of the upper surface of the aircraft is consistent with the tail curve of the lower surface.

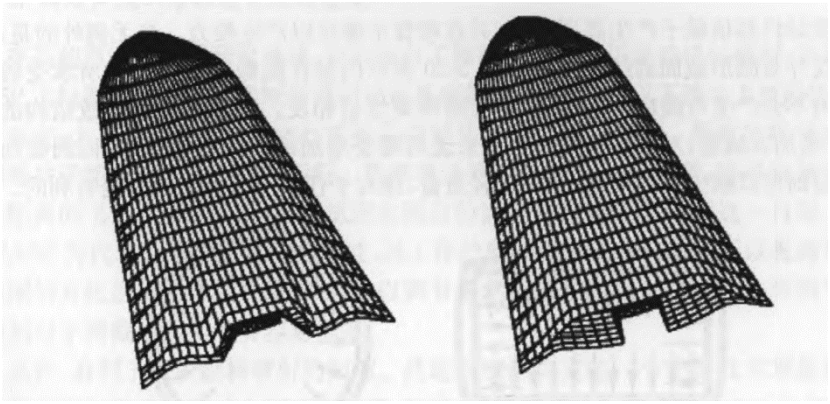

Figure 5-88: Improved design of the bottom and upper surfaces of the waverider shape aircraft

5.6: Integration of the "circular cross-section" propulsion system with the fuselage of a hypersonic vehicle

5.6.1: Evolution of the propulsion system "Circle-2D-Circle"

1. The origin of the "circular cross-section" propulsion system

As early as the 1960s, when the United States began to develop scramjet-powered missiles, it considered the configuration of "circular cross-section." A typical example is a missile demonstrator called SCRAM developed by the Applied Physics Laboratory of Johns Hopkins University in the United States, which has an internally turned air inlet and a circular cross-section combustion chamber, as shown in Figure 5-89. This configuration offers three benefits to hypersonic vehicles.

The first is the light weight of the structure. All jet propulsion systems that have been used, such as rockets, ramjets, and crash jet engines, rely on the generation of high-pressure gases that expand in the nozzle to generate thrust.

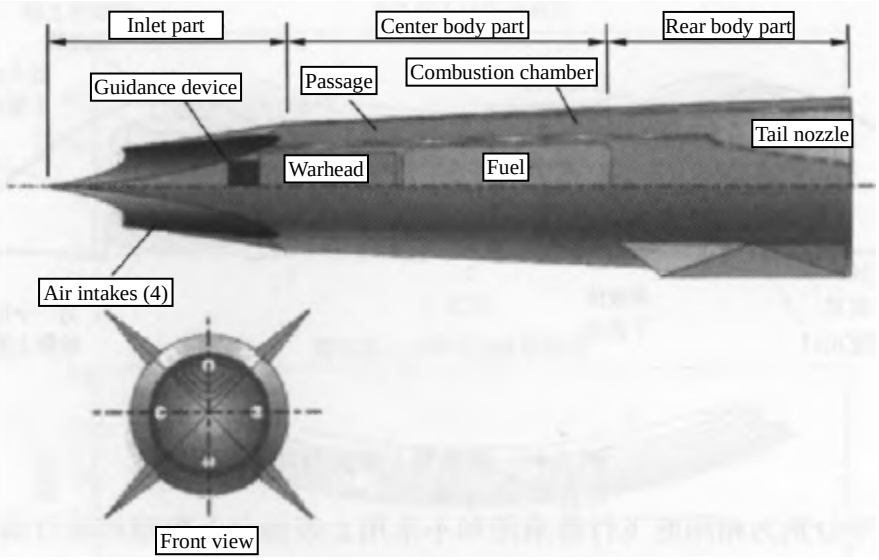

Figure 5-89: American SCRAM missile demonstrator

Without exception, these systems are designed as circular cross-sections. Figure 5-90 shows that the internal reaction pressure in a structure with a circular section does not produce bending stresses, while the opposite is true for a rectangular section structure. Bending stresses can lead to fatigue fracture of the structure and must be mitigated, and in the case of rectangular cross-section structures, it is necessary to increase the thickness of the back plate of the structure, while circular cross-section structures can reduce the amount of material used and thus reduce weight, which is advantageous for any aircraft.

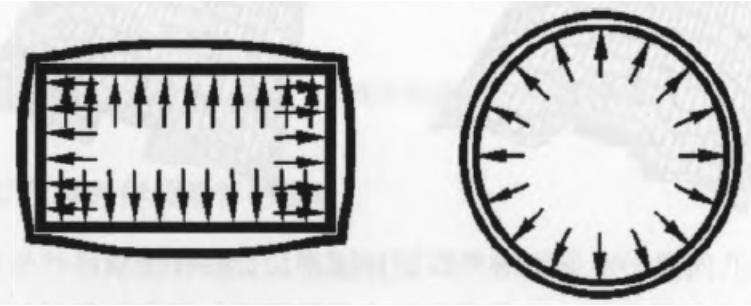

The rectangular structure needs to be reinforced at the back under pressure, and the density per unit area of the structure is 716m/ft^2.

The circular structure does not need to be reinforced on the back under pressure, and the unit area density of the structure is not 316m/ft^2.

Figure 5-90: Comparison of the internal pressure of a circular structure with that of a rectangular structure

The second is a reduction in cooling requirements as well as internal resistance. As shown in Figure 5-91, a pipe with a circular section provides the smallest circumferential area for a given flow cross-sectional area, which directly reduces the need for surface cooling and frictional resistance.

Finally, the length of the engine was reduced. The inward turn intake is ideal for combustion chambers where flow is converted into a circular cross-section and has also proven to be superior to equivalent two-dimensional rectangular air intakes. Three-dimensional compression of the intake tract is effective in reducing the length of the engine compared to two-dimensional inlet compression [69,70].

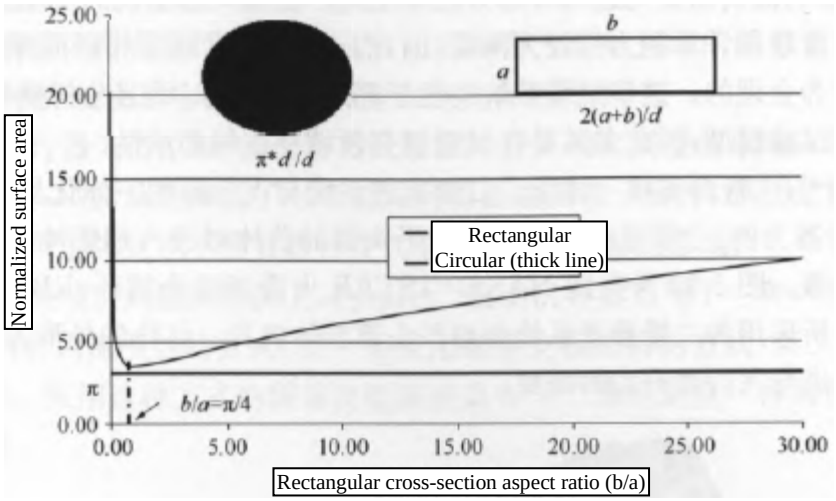

Figure 5-91: A circular section produces the smallest surface area

2. The development of hypersonic two-dimensional propulsion systems

In the field of hypersonic vehicle research, the development of a round-section scramjet engine has been temporarily abandoned, and the development of a two-dimensional rectangular section propulsion system represented by NASP aircraft has been tended to be developed for the following four reasons.

First of all, operation in the Mach range requires a variable-geometry inlet structure. All air-breathing propulsion systems benefit from the ability to operate over a wide range. When the booster reaches a higher speed at the point of separation, the cruiser can fly longer distances. In simple terms, the missile tries to achieve this under a fixed flow channel profile. For the single-stage orbit mission represented by NASP, the scope of its work is broader. The most feasible way to increase its operating range is to adopt a variable geometry structure that adjusts the cross-sectional area of the flow channel. And this adjustment of the two-dimensional configuration is much easier than that of the circular section.

Secondly, it is beneficial to reduce the gap of fuel injection. One of the main technical challenges in hypersonic combustion chambers is how to increase the degree to which the injected fuel penetrates into the high-velocity air stream so that it blends well with the supersonic stream, which is necessary to achieve high engine efficiency. The researchers found that a two-dimensional design with a large aspect ratio allows for a small injection distance between two opposing walls, resulting in effective fuel wall injection (Figure 5-92). This design scheme is also convenient for experimental studies and achieves better performance, but it brings a greater penalty for structural quality.

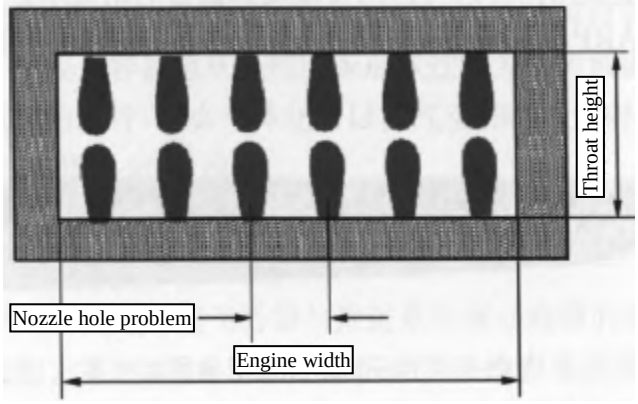

Figure 5-92: A 2D design with a large aspect ratio enables effective wall fuel injection

Thirdly, complex flow fields require advanced computational methods and tools. The flow field of hypersonic systems was quite complex, and the calculation methods and computing power were relatively weak at that time, so it was reasonable to focus on relatively simple two-dimensional systems at that time. These two-dimensional systems also facilitate the understanding of flow phenomena, and the ease of construction of analytical models for the manufacture of low-cost experimental models, hence the inevitability of experimental research in particular.

Finally, it is easy to integrate with the aircraft. The integration of the two-dimensional propulsion system with the aircraft is easy to understand and implement. In the case of NASP aircraft, for example, the 2D system usually uses a forebody with a flat head to pre-compress the air flow into the scramjet. Figure 5-93 shows the two-dimensional propulsion system and the flat-head forebody fuselage used in the NASA ISTAR rocket-based combined cycle (RBCC) engine demonstration and verification program. This solution meets the needs of both propulsion and aircraft lift.

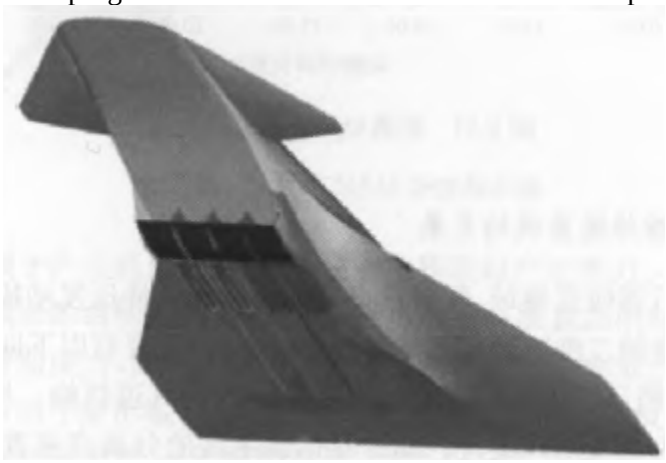

Figure 5-93: Integration of a two-dimensional propulsion system with a flat head forebody fuselage

3. The return of the "circular cross-section" propulsion system

In the past ten years, the development of scramjet engines has re-introduced the configuration of "circular cross-section," mainly to re-realize the advantages of this propulsion system. In 1997, Aerojet adopted the dual-combustion ramjet design method proposed by the Hopkins University Applied Physics Laboratory, that is, the scramjet engine combustion chamber with circular cross-section. In 2002, the American company Aerojet cooperated with Dr. Fred Billig, an authoritative expert in the field of hypersonic technology, to propose the concept of TBCC propulsion system applied to hypersonic cruise vehicles, which is an innovative and revolutionary program called Pyrojet™. As shown in Figure 5-94, the scheme adopts an inward-turning inlet configuration and a combustion chamber with a circular section. Another research program for a circular section combustion chamber is the HyCAUSE free-flight test project conducted by DARPA in the United States in cooperation with Australia.

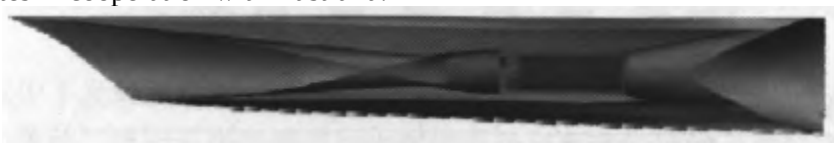

Figure 5-94: PyroJet™ RBCC propulsion system

There are six main reasons why the "circular cross-section" propulsion system has been re-raised.

First, there is a renewed awareness of the advantages of circular cross-section configurations, such as those listed at the beginning of this section in terms of structure, cooling, reduction of corner flow effects, and frictional resistance.

Second, in the flight range of the aircraft, the Mach number range of the cruise vehicle is smaller than that of the single-stage to orbit flight of the NASP type, which reduces the requirement for variable geometric surfaces. In addition, even for the PyroJet™ scheme, the variable geometry does not require forward movement of the leading edge of the air intake.

Thirdly, in solving the problem of fuel injection, the PyroJet™ engine scheme adopts an inflow injection method. As shown in Figure 5-95, there are two types of inflow injection mode, one is the method of using the cantilever support plate structure, and the other is the method of using the central ring stable flame support plate. A circular cross-section combustion chamber in this way has the same performance as a two-dimensional combustion chamber and has a lower structural weight.

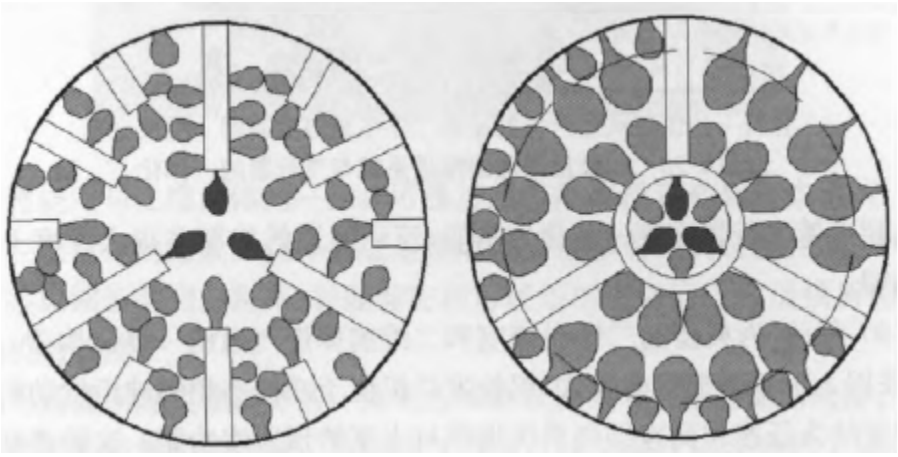

(a) Cantilever support plate method (b) The central ring stabilizes the flame support plate method

Figure 5-95: Injection mode of internal flow support plate

Fourth, in terms of computational tools, CFD technology has developed significantly since the NASP program, which allows scramjet engines to design three-dimensional flow channels according to requirements.

Fifth, the air intake tract has high performance. The TBCC system of the PyroJet™ solution uses an inward turning air intake to provide high-performance air intake conditions for long-range hypersonic cruise vehicles. The problem of priming the internally turned inlet can be solved by adjusting the internal contraction.

Sixth, in terms of integration with aircraft, scramjet engines with circular cross-section can be effectively integrated with aircraft. The inward turn intake can be easily transitioned from any leading edge shape to any circular section combustion chamber. When the same approach is applied to the design of the tail nozzle, the integration allows for both aerodynamic and propulsion improvements, rather than a compromise as in a 2D system, as shown in Figure 5-96.

5.6.2: Integration of the "circular cross-section" propulsion system with the fuselage of a hypersonic vehicle

In the past 20 years, the design and development of flow channels for hypersonic vehicles and propulsion systems have mainly focused on the two-dimensional rectangular cross-section scheme, and in recent years, it has gradually expanded to the design of three-dimensional schemes. The potential advantages are improved flow channel performance, structural efficiency, and greater flexibility in aircraft configuration design.

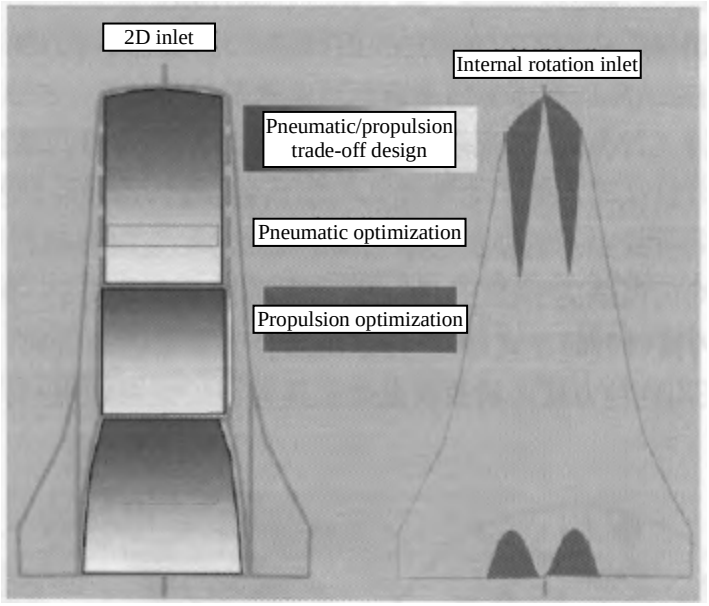

Figure 5-96: Integration of two-dimensional and circular-section propulsion systems with aircraft

Due to the highly integrated nature of the flow channel and the hypersonic vehicle, the configuration of the flow channel greatly affects the configuration of the entire vehicle.

As shown in Figure 5-97, it is a typical integrated configuration of the two-dimensional combustion chamber and the two-dimensional forebody air intake. For the TBCC propulsion system, the upper and lower parallel arrangements are adopted, and the turbine engine is located above the dual-modal scramjet engine. The forebody of the entire vehicle provide pre-compression of incoming streams for low- and high-speed propulsion systems. This type of integration can be analyzed using relatively simple engineering methods and 2D CFD methods. The application of 3D CFD methods is also mainly used to evaluate the overflow effect of forebody, as well as the effect of sidewalls and corners on inflow. The purpose of this aircraft configuration, which resembles a surfboard, is to maximize the pre-compressed surface of the aircraft's forebody.

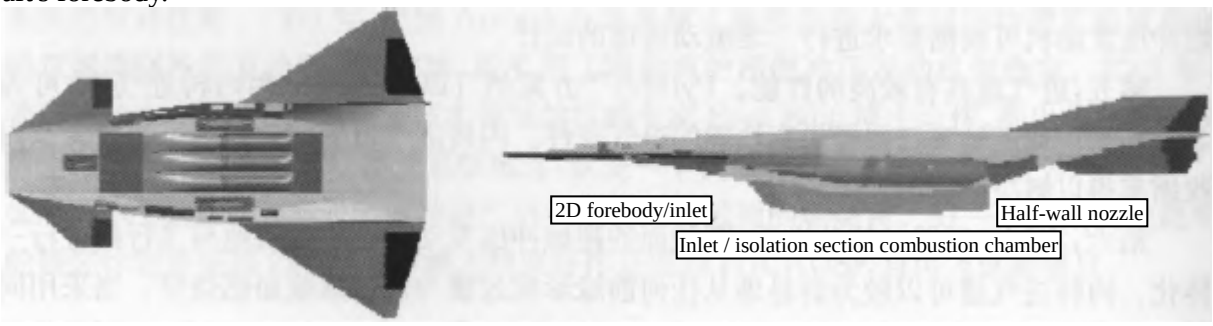

Figure 5-97: Integration of a typical 2D propulsion system with the airframe

Figure 5-98 shows the integrated configuration scheme of the circular cross-section combustion chamber and the two-dimensional forebody air intake. This scheme retains the relatively simple 2D forebody air intake, has the same air inlet characteristics as the fully 2D configuration aircraft, and also incorporates the advantageous circular section combustion chamber. In order to reduce the difficulty of comparative analysis, it is hoped that the outer dimensions of the full 2D configuration engine compartment can be kept unchanged, so that the shape of the aircraft is as close as possible, and the integrated design results of the flow channel of the low-speed turbine engine can still be retained.

However, it is not enough to scale the circular section isolation and combustion chamber from the full 3D flow channel, which will result in an increase in the inner flow channel and combustion chamber modules, thus eliminating the benefits of structural weight reduction and performance improvement due to the greatly reduced surface area. In addition, the change of combustion chamber from a two-dimensional forebody to a circular cross-section will be completed over a relatively short distance, and the variable geometry required for the flow channels of high-speed propulsion systems is difficult to achieve and to operate effectively in the large Mach number range.

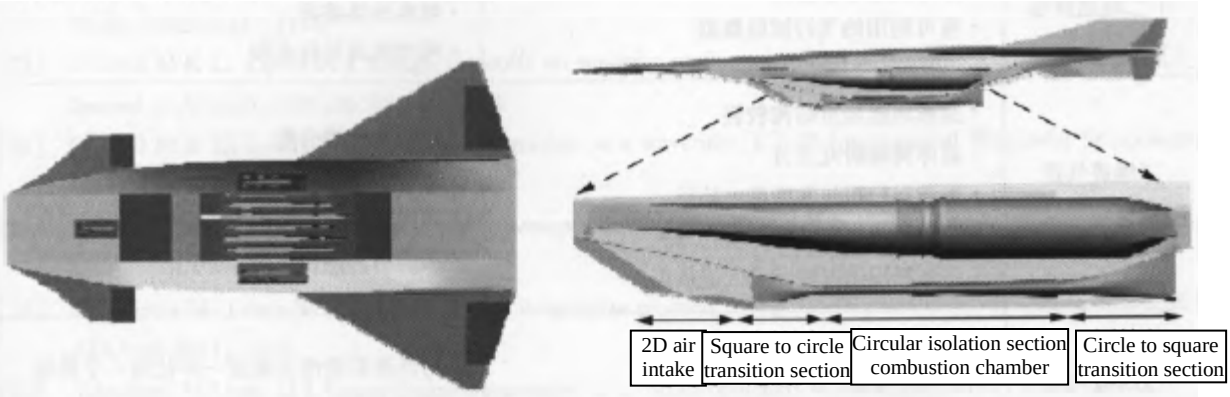

Figure 5-98: Integration of a round-section combustion chamber and a two-dimensional forebody inlet tail nozzle

The integration of the circular section combustion chamber with the 2D forebody can be achieved by improving the isolation section and the combustion chamber, not just by scaling the existing 3D design. This was done by gradually changing the ratio of the transition from a rectangle to a circle, and at the same time improving the scheme of fuel injection to shorten the distance between the combustion chambers and to provide the required flow capacity and shorten the length of the engine in a relatively short flow channel.

The best way to integrate the inlet tract with the circular section combustion chamber is to design a fully three-dimensional flow channel. This design is based on the study of streamlined tracing of the inward intake tract. The design of the inward intake is similar to that of the waverider shape, in that the flow field formed by a cone is formed by streamline tracing. Figure 5-99 shows the integrated design scheme of the flow channel of the full three-dimensional geometry and the aircraft, which can meet the integration requirements with the forebody, but it is difficult to adopt the variable geometric configuration.

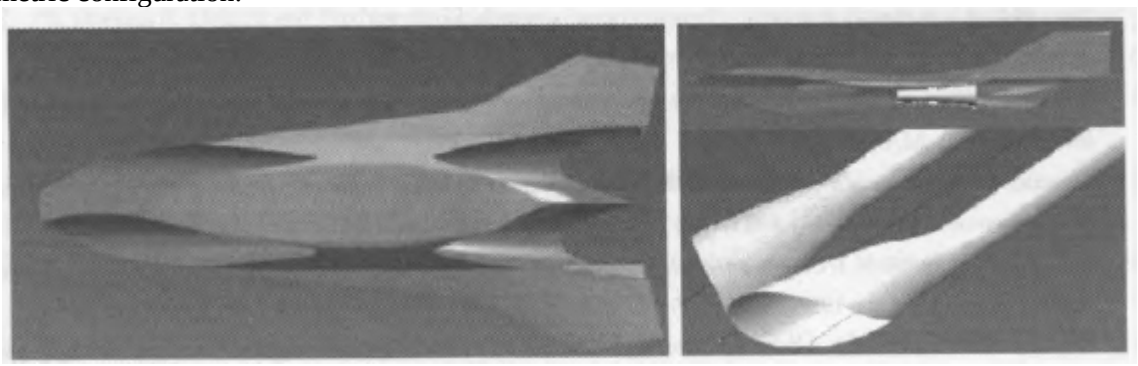

Figure 5-99: Integration of a circular section combustion chamber with an internal intake duct

Table 5-6 compares the above three propulsion airframe integration schemes, and points out the advantages and disadvantages of each.

Table 5-6: Comparison of propulsion fuselage integration schemes

All-in-one concept	Advantage	Shortcoming
Two-dimensional inlet duct twelve-dimensional combustion chamber	• Easier to analyze • There are databases available • Flight test data is available	• Large quality of construction • Two-dimensional compression shock wave is stronger • Higher thermal interception • Limited flexibility in configuration
Two-dimensional inlet duct ten-circle cross-section combustion chamber	• Lighter structure of the combustion chamber with circular section • The forebody flow field is well studied • Can be integrated with turbojet engines • A circular section combustion chamber database is under construction • There is a database of available square-to-round intakes	• Airways are difficult to analyze • Combination engines may require multiple flow channels • It is difficult to integrate the variable geometry of the inlet tract • Limited flexibility in configuration
Three-dimensional inlet duct ten-circle cross-section combustion chamber	• Good performance • Light weight of the structure • Easy to integrate with circular or circular cross-section isolation section combustion chamber • Integration with the aircraft form factor is more flexible	• Integration with low-speed turbine flow channels is a challenge • More difficult to analyze • The flow channel should be designed as a compromise with the integrated forebody

References

[1] John D Anderson Jr. Hypersonic and High Temperature Gas Dynamics [M]. McGraw-Hill Book Company, 1989.
[2] Huang Zhicheng. Aerodynamics of hypersonic vehicle [M]. Beijing: National Defense Industry Press, 1995.
[3] Che Jing. Research on optimal design of wave-riding layout of hypersonic vehicle [D]. Xi'an: Northwestern Polytechnical University, 2006.
[4] Xu Min, Yan Hengyuan. Calculation method of aircraft aerodynamic engineering [M]. Xi'an: Northwestern Polytechnical University Press, 1998.
[5] Qu Zhanghua, Zeng Ming, Liu Wei, et al. Hypersonic aerodynamics [M]. Changsha: National University of Defense Technology Press, 1999.
[6] Rejanette F R. A review of approximate methods used in aerodynamic heating analysis [R]. AIAA 85-0906.
[7] Jiang Guiqing, Liu Lianyuan. High-speed airflow heat transfer and ablation heat protection [M]. Beijing: National Defense Industry Press, 2003.
[8] Che Jing, Tang Shuo, He Kaifeng. Engineering calculation method for aerodynamic heating of waverider-like aircraft [J]. Journal of Ballistics, 2006, 18(4).
[9] Wang Zhuo, Qian Yiji. Shape design of wave riding aircraft [J]. Journal of Beijing University of Aeronautics and Astronautics, 1999, 25(2).
[10] Zhao Guilin, Hu Liang, Wen Jie. A review of the research on wave-riding configuration and wave-riding aircraft [J]. Progress in Mechanics, 2003, 33(3).
[11] Takashima N, Lewis M J. Waverider configurations based on non-axisymmetric flow fields for engine-airframe integration [R]. AIAA-94-0380, 1994.
[12] Soieczky H, Dougherty F C, Jones K. Hypersonic Waverider design from given shock waves [C]. 1st International Waverider Symposium, University of Maryland, Oct. 17-19, 1990.
[13] Starkley R P, Lewis M J. Simple analytical model for parametric studies of hypersonic waveriders [J]. Journal of Spacecraft and Rockets, 1999, 36(4). 516 523.
[14] Starkley R P, Lewis M J. Analytical off-design lift-to-drag-ratio analysis for hypersonic waveriders [J]. Journal of Spacecraft and Rockets, 2000, 37(5): 684 691.
[15] Pegg R J, Hahne D E, Cockrell C E Jr. Low-speed wind tunnel tests of two waverider configuration models [R]. AIAA-95-6093, 1995.
[16] Hahne D E. Evaluation of the low-speed stability and control characteristics of a Mach 5.5 waverider concept [R]. NASA-TM-4756, 1997.
[17] Pegg R J, Hunt J L, Petley D H. Design of a Hypersonic waverider-derived airplane [R]. AIAA-93-0401, 1993.
[18] Cockrell C E Jr. Interpretation of waverider performance data using computational fluid dynamics [R]. AIAA-93-2921, 1993.

[19] Cockrell C E Jr, Huebner L D, Finley D B. Aerodynamic performance and flow-field characteristics of two waverider-derived hypersonic cruise configurations [R]. AIAA-95-0736, 1995.
[20] Cockrell C E Jr, Huebner L D, Finley D B. Aerodynamic characteristics of two waverider-derived hypersonic cruise configurations [R]. NASA-TP-3559，1996.
[21] O'Neill M K L，Lewis M J. Optimized scramjet integration on a waverider [J]. Journal of Aircraft, Vol. 29，
No. 6, 1992:114, 1121.
[22] O'Neill M K L, Lewis M J. Design tradeoffs on scramjet engine integrated hypersonic waverider vehicles [J]. Journal of Aircraft, 1993,30(6): 943 952.
[23] O'Neill M K L, Lewis M J. Scramjet integration on a waverider [C]. 1st International Waverider Symposium, University of Maryland, 17~19, Oct. 1990.
[24] Lin S C, Luo Y S. Integrated design of hypersonic waveriders including inlets and tailfins [J]. Journal of Spacecraft and Rockets, 1995, 32(1) j48 54.
[25] Takashima N, Lewis M J. Engine-airframe integration on osculating cone waverider-based vehicle design [R]. AIAA-96-2551, 1995.
[26] Takashima N，Lewis M J. Navier-Stokes computation of a viscous optimized waverider [R]. AIAA-92~0305, 1992.
[27] Takashima N, Lewis M J. Optimization of waverider-based hypersonic cruise vehicles with off-design considerations [J]. Journal of Aircraft, 1999, 36(1): 235 245
[28] Takashima N, Lewis M J. Optimized mission-oriented waverider vehicle with base closure [R]. AIAA-96-0810, 1996.
[29] Gary A Sullins, Frederick S Billig. Force accounting for airframe integrated engines [R]. AIAA-87-1965.
[30] Lehrach R P C. Thrust/Drag Accounting for Aerospace Plane Vehicles [R]. AIAA-87-1966.
[31] Keith Numbers. Hypersonic Propulsion System Force Accounting [R]. AIAA 91-0228.
[32] O'Neill, Mary Kae，Mark J Lewis. Optimized scramjet integration on a waverider [J]. Journal of Aircraft 1992, V29(6):1114 1121.
[33] O'Neill, Mary Kae Lockwood, Mark J. Lewis. Design Tradeoffs on Scramjet Engine Integrated Hypersonic Waverider Vehicles [J]. Journal of Aircraft, 1993, V30(6): 943 952.
[34] bcrens M Thomas and Norbert C. Bissinger. Forebody Precompression Performance of Hypersonic Flight Test Vehicles [R]. AIAA-98-1574.
[35] Ph. Duveau, R. Hallard and Ph. Novelli Th. Eggers. Aerodynamic Performance Analysis of the Hypersonic Air-breathing Vehicle Japhar [C], 14th International Symposium on Air Breathing Engines, ISABE 99-7286.
[36] Ryan P Starkey, Mark J Lewis. A simple analytical model for parametric studies of hypersonic waveriders [R]. AIAA 98-1616, 1998.
[37] Liu Jia, Yao Wenxiu, Lei Maifang, et al. Study on the compression performance of hypersonic vehicle forebody [J]. 2004, 25(1):85 92.
[38] Shang Aidong. Scramjet nozzle test in hypersonic external flow field [J]. Flying Missile, 1994(3).
[39] Cubbage J M, Monta W J. Parametric Experimental investigation of a scramjet nozzle at Mach 6 with freon and argon or air used for exhaust simulation [R]. NASA TP-3048, 1991.
[40] Shigeya W. A scramjet nozzle experiment with hypersonic external flow [R]. AIAA-92-3289.
[41] Monta W J. Pitot survey of exhaust flow field of a 2-d scramjet nozzle at Mach 6 with air or freon and argon used for exhaust simulation [R]. NASA-TM-4361.1992.
[42] Chen Bing, Xu Xu, Cai Guobiao. Research on the optimal design of single-wall expansion nozzle based on genetic algorithm and space propulsion method [J]. Acta Aeronautics and Astronautics, 2007, 28(4): 827-832.
[43] Li Nian, Zhang Kunyuan, Xu Jinglei. Numerical simulation and verification of two-dimensional asymmetric nozzle [J]. Journal of Aerodynamics, 2004, 19(6): 802-805.
[44] Perrier P. Nozzle and afterbody design for hypersonic airbreathing vehicles [R]. AIAA 96-4548, 1996.
[45] Chen Bing, Xu Xu, Cai Guobiao. Optimization design of tail nozzle of two-dimensional scramjet engine [J]. Propulsion Technology, 2002, 23(5): 433 437-
[46] Walter C Engelund, Scott D Holland Jr, Charles E. Cockrell. Propulsion system airframe integration issues and

aerodynamic database development for the Hyper-X flight research vehicle [R]. ISOABE 99-7215. 1999.
[47] He Yuanyuan, Le Jialing, Ni Hongli. Numerical and Experimental Study of Air-breathing Hypersonic Body/Propulsion Integrated Vehicle. Experimental Fluid Mechanics, 2007, 21(2):29-34.
[48] Ye Youda, Wang Zhenya, Lu Sheng. Numerical simulation study on the integrated shape of hypersonic vehicle airframe/propulsion system [C]. Aerodynamics Frontier Research Papers.2003:35 40.
[49] Schmidt D K. Dynamics and control of hypersonic vehicles - the integration challenge for the 1990s [R]. AIAA 91-5057.1991.
[50] Wang Zhenguo, Chen Xiaoqian, Luo Wencai. Theory and application of multidisciplinary design optimization of aircraft [M]. Beijing: National Defense Industry Press, 2006.
[51] Che Jing. Research on optimal design of wave-riding layout of hypersonic vehicle [D]. Xi'an: Graduate School of Northwestern Polytechnical University, 2006.
[52] Liming, Song Wenyan, He Wei. Research on design method of hypersonic two-dimensional mixed-pressure forebody/air intake [J]. Journal of Aerodynamics, 2004, 19(4): 459-465.
[53] Song Daojun, Xu Jibin. Optimization design of hypersonic two-dimensional forebody air inlet integration [J]. Acta Aerodynamics Sinica, 2004, 22(3): 371-375.
[54] Chen Bing, Xu Xu, Cai Guobiao. Research on optimization design of hypersonic air inlet based on genetic algorithm and space propulsion method [J]. Journal of Astronautics, 2006, 27(5): 1010-1015.
[55] Fan Xiaoqiao, Li Hua, Li Xiaoyu, et al. Preliminary study on the parametric design method of hypersonic two-dimensional air intake [J]. Journal of Aerodynamics, 2007, 22(1): 66-72.
[56] Currom E T, et al. Scramjet Propulsion [M], AIAA, 2000.
[57] Xu Huasong, Gu Liangxian. Design of rear body nozzle of hypersonic vehicle [J]. Journal of Aerodynamics, 2007, 22(2):257-260.
[58] HE Xuzhao, Daniel Zhang, WANG Guangyuan, et al. Automatic optimization design of single-wall expansion nozzle for hypersonic vehicle [J]. Propulsion Technology, 2007, 28(2): 148-151.
[59] Chen Bing, Xu Xu, Cai Guobiao. Optimization design of tail nozzle of two-dimensional scramjet engine [J]. Propulsion Technology, 2002, 23(5):433-437.
[60] Che Jing, Tang Shuo. Integrated design of rear body/tail nozzle of hypersonic vehicle [J]. Flight Mechanics, 2006, 24(3):74-77.
[61] Xu X, Xu D J, Cai G R Optimization design for Scramjet and analysis of its operation performance [J]. ACTA Astronautica, 2005, (57): 390 403.
[62] Xu D J, Cai G B, Xu X, et al. Design studies for three-dimensional forebody of hypersonic vehicle-based on PNS optimization procedure [C]. 58th International Astronautical Congress, IAC-07-C4. 5.02, 2007.
[63] Huang Zhicheng. Hypersonic vehicle aerodynamics [M]. Beijing: National Defense Industry Press, 1995.
[64] Isaiah M Blankson, Paul Hagseth. Propulsion/airframe integration issues for waverider aircraft [R]. AIAA 93-0506, 1993.
[65] Mark J Lewis, Naruhisa Takashima. Engine/airframe integration for waverider cruise Vehicles [R]. AIAA 93-0507, 1993.
[66] Molvik G, Bowles J, Huynh L. A hypersonic waverider research vehicle with hydrocarbon scramjet propulsion: design and analysis [R]. AIAA-93-5097, 1993.
[67] Haney J W, Beaulieu W D. Waverider inlet integration issues [R]. AIAA 94-0383, 1994.
[68] Sheam-Chyun Lin, Yung-Wha Liu, Ming-Chiou Shen. Design of hypersonic waveriders with wing-body-tail- inlet-engine [R]. AIAA 96-2891, 1996.
[69] Melvin J. Bulman, Adam Siebenhaar. The rebirth of round hypersonic propulsion [R]. AIAA 2006-5035.
[70] Adam Siebenhaar, Thomas J. Bogar. The impact of round combustors on TBCC propulsion and hypersonic cruise vehicles [R]. AIAA 2006-7986, 2006.

Chapter 6: Thermal Protection Technologies for Hypersonic Vehicles

6.1: Hypersonic Vehicle Thermal Environment and Thermal Corridor

6.1.1: Hypersonic vehicle thermal environment

The two-stage space launch vehicle (TSTO) is a typical application of hypersonic vehicles. Figure 6-1 shows the relationship between the flight altitude of the TSTO and the Mach number. The TSTO first accelerates to the Mach number at the separation point, and within $6 \leq Ma \leq 13$, the first stage separates from the second stage. The first-stage air-breathing vehicle returns to the launch site, while the second-stage orbiter is propelled by a rocket engine to continue accelerating to orbit. The first stage of the air-breathing vehicle uses a turbine-based combined cycle engine (TBCC), which can work up to $Ma = 3.5$ for turbojet power and up to $Ma = 12$ for scramjet engines. The maximum Mach number that can be achieved by a turbojet engine, as well as the minimum and maximum Mach numbers of a scramjet engine, depend on the capabilities that can be verified by the test institute. Air-breathing powered aircraft are typically accelerated along an isodynamic trajectory by flight trajectory optimization. Dynamic pressure is the product of the density of the air and the square of the speed of flight, while aerodynamic heating is proportional to the cubic of the velocity and proportional to the square root of the density of the atmosphere, which decreases exponentially with increasing altitude. Figure 6-1 shows the three isodynamic lines of 100 PSF, 500 PSF, and 2,000 PSF, respectively.

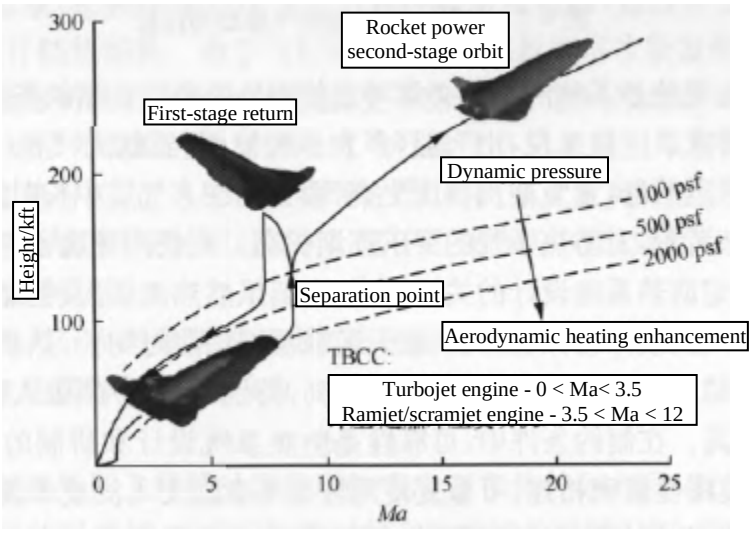

Figure 6-1: Relationship between the height of the TSTO and the Mach number

When the aircraft flies at a low altitude in the atmosphere at high speed, it will produce high dynamic pressure and strong aerodynamic heating. For air-breathing aircraft, a technical problem arises, that is, to balance the selection of the appropriate flight pressure, for the engine to improve its performance needs a high dynamic pressure, and the high dynamic pressure will produce greater aerodynamic heating on the leading edge of the wing and the fuselage.

Figure 6-2 shows a comparison of the aerodynamic heating of a reference sphere with a diameter of l ft flying along three trajectories, namely the spacecraft re-entry stage, the single-stage orbit vehicle (SSTO) ascent stage, and the space shuttle re-entry stage.

As can be seen from Figure 6-2(a), there is a large peak heat flux density in the reentry section of the spacecraft, but the duration is relatively short. The space shuttle has a relatively low peak heat flux density, but it continues to heat for a longer time; the single-stage orbiting vehicle has a long flight section and a high heat flux density. For air-breathing hypersonic vehicles, the radius of the leading edge of the wing is much smaller than l ft, and because the heat flux density is inversely proportional to the radius of the leading edge, the heat flux density experienced by the actual vehicle is much greater than that in Figure 6-2. Thermal load is another important aerodynamic heating parameter, which is the integral of the heat flux time and represents the total amount of heating to the system. Figure 6-2(b) shows a comparison of the thermal loads of the three flight trajectories. Therefore, in general, for the spacecraft, the aerodynamic heating environment is harsh, and the reentry heat flow is large, but the heating time is short, and the thermal load is relatively small; the aerodynamic heating environment of the space shuttle is also harsh, and the reentry heat flow is large, but the heating time is longer, the thermal load is relatively large, and the aerodynamic shape is required to be stable. The aerodynamic heating environment of the single-stage orbit vehicle (SSTO) is harsh and complex, especially when ascending, it accelerates to high Mach number in a large layer, which not only has a large heat flow, but also has a long heating time as a hypersonic flight, a large thermal load, and requires a stable aerodynamic shape.

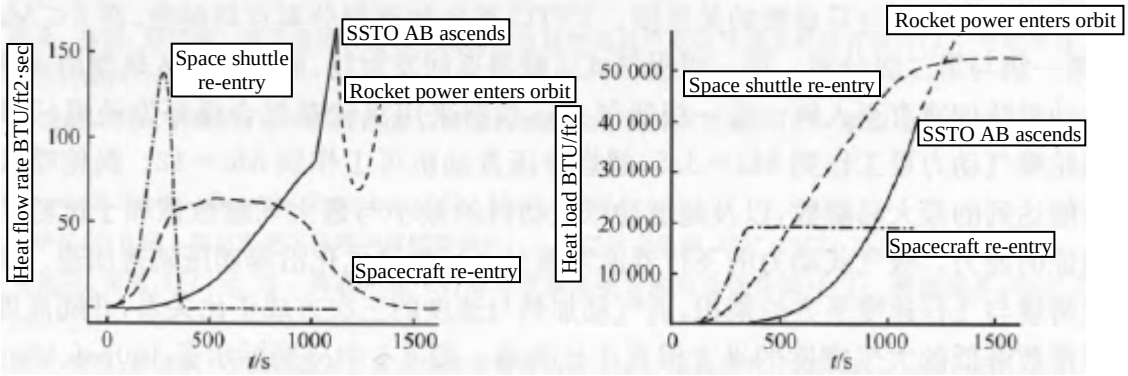

(a) Heat flux (b) Heat load

Figure 6-2: Comparison of aerodynamic heating of three flight trajectories

The design of thermal protection systems for hypersonic vehicles must take into account the environmental conditions and constraints of use and the corresponding technical and other assurance requirements. Generally speaking, from airships (mostly one-time use) to space shuttles (repeated use) to single-stage or two-stage-to-orbit space vehicles (higher degree of repeated use and long flight time in the atmosphere), the environment and constraints are becoming more and more complex and demanding, and the requirements for the heat protection system are gradually increasing. In the use of environmental conditions, the aerodynamic heating environment is particularly important, which is a key factor in determining the design of the heat protection system. Although the airship has a large heat flow, the heating time is short and it is mostly for one-time use, whereas the space shuttle or single-stage/two-stage-in-orbit spacecraft has a long heating time, a large heat load and has to be reused many times, which needs to maintain stable aerodynamic shape, and thus the requirements are relatively high, especially for the single-stage/two-stage-in-orbit spacecraft. In particular, single-stage/two-stage in-orbit spacecraft have higher requirements due to the harsh flight environment. Among the constraints, reliability is a necessary condition for the design and development of heat protection systems, and it is closely related to reusability, which is an important and indispensable factor when considering the design of heat protection systems for spaceplanes or single/two-stage-to-orbit space launch vehicles, and the development of heat protection structures and materials. Because of the large area of the heat protection system of a single-stage/two-stage-to-orbit space launch vehicle, which must be reused, it is of great importance to reduce its weight (mainly the weight of structures and materials) [1,2].

6.1.2: Hypersonic Vehicle Thermal Corridor

1. About the "Thermal Corridor"

The re-entry corridor of the aircraft refers to the area of the speed range where the heat-resistant material is limited by the temperature factor.

With the continuous development of aerospace technology, reusable space launch vehicles have become an important development direction in the world's aerospace field due to their advantages of high heat protection efficiency, light structural weight and low cost. The reusable thermal structure is fundamentally different from the previous one-time thermal structure, which requires repeated use in an aerodynamic and thermal environment, and does not allow the pyrolysis, ablation and detachment of structural materials. The re-entry performance indicators of reusable space launch vehicles can be formulated in different ways, such as the minimum total heating capacity, the lowest surface temperature, and the maximum lateral range [3].

The selection and analysis of the re-entry thermal corridor is a key and indispensable procedure in the heat-proof design of reusable space launch vehicles, the upper and lower boundaries of the re-entry thermal corridor of reusable space launch vehicles are mainly determined by the physical and chemical properties of structural materials and the use temperature limit, and the re-entry orbit is strictly limited by the thermal corridor, and must not pass through the thermal corridor, otherwise thermal damage may occur, resulting in devastating serious consequences. In the flight heat corridor, the aircraft can fly freely, and the heat-proof material will not be damaged due to excessive temperature. Therefore, the establishment of the physical model of the thermal corridor of reusable space launch vehicles and the study of the calculation method of the thermal corridor have important engineering application value for the design of thermal protection structure, the determination of flight trajectory and the optimization design of aerodynamic shape.

2. Physical modeling and calculation methods of thermal corridors

The determination of the reusable space launch vehicle re-entry thermal corridor is a mathematical multi-parameter optimization and boundary determination problem for a given aerodynamic shape and selected heat-resistant material. The upper and lower boundaries of the re-entry thermal corridor of reusable space launch vehicles are mainly determined by the physical and chemical properties of the structural materials and the service temperature limit. If the flight inclination angle is too large and the flight trajectory is too steep, a large aerodynamic heating rate will be generated, which will make the temperature of the outer surface too high and exceed the allowable use limit of the material, that is, beyond the boundary of the reentry heat corridor; if the flight inclination angle is too small, the flight trajectory is too gentle, and the flight time is too long, the total amount of aerodynamic heating will be increased, and the temperature of the internal structure will be too high under the action of heat conduction, exceeding its allowable temperature limit, and the heat-proof structure will also need to be redesigned. Because the thermal protection system of the aircraft needs to be reused many times, it is required that the outer surface of the heat-proof layer generally cannot have obvious physical and chemical changes, let alone serious ablation, which limits the selection of appropriate heat-proof materials, and determines that the temperature limit of the outer surface must be strongly limited to the flight speed. The temperature of the internal structure is not only related to the aerodynamic heating, but also related to the thermophysical properties and thickness of the material, but it can be solved by the heat-proof design of the internal structure, and the restriction on the flight trajectory is relatively weak. Based on the above analysis, a physical model of the reusable space launch vehicle re-entry thermal corridor can be established.

The aerodynamic heating experienced by the flight surface of a given aerodynamic shape is a complex function of the incoming flow state, which can be obtained by numerical solution of the N-S equation or by engineering methods, which can be expressed as

$$q_{eq} = f_1(T_w, H, V_\infty) \tag{6.1}$$

The thermal response of the heat-proof layer of a reusable aircraft with a complex shape follows the heat conduction equation, and the temperature field of the heat-proof layer can be obtained by solving the heat conduction equation numerically, and the temperature of the heat-proof layer is mainly determined by the outer boundary conditions given the heat-resistant material and the heat-proof structure, that is, the maximum surface temperature is strongly dependent on the aerodynamic heating rate

$$T_w = f_2(\varepsilon, q) \tag{6.2}$$

Substituting the heat flow Equation (6.1) into Equation (6.2) gives us

$$T_w = f_2[\varepsilon, f_1(T_w, H, V_\infty)] \tag{6.3}$$

Equation (6.3) can be written in the form of an equation

$$f(\varepsilon, T_w, H, V_\infty) = 0 \tag{6.4}$$

Given a set of flight altitudes, Equation (6.4) is iteratively solved, and finally the flight speed corresponding to the ultimate wall temperature of a given material can be calculated, which is the maximum speed at which the aircraft can fly safely at that altitude, and the envelope region of the entire altitude-velocity curve is the re-entry thermal corridor of the aircraft. In addition, the higher the temperature that the wall surface of the heat-proof layer can withstand, the greater the surface emissivity, the wider the corresponding thermal corridor, and the greater the choice of re-entry orbit. The boundaries of the thermal corridor corresponding to different locations and different flow regimes are also different, and delaying the occurrence of transition can increase the thermal corridor area, which is conducive to the heat protection design. When the pneumatic heating in some locations is very severe and the corresponding thermal corridor is too narrow to meet the requirements of the re-entry track, it is necessary to switch to a heat-resistant material with better performance.

The above reentry thermal corridor modeling and calculation methods proposed for re-entry orbit are also applicable to the concept of hypersonic vehicle thermal corridor that can fly for a long time in other atmospheres.

6.1.3: Engineering prediction methods for hypersonic aerothermal environments

1. Heat F exchange form

During the flight of the hypersonic vehicle, the speed is very high, due to the viscosity of the air, the airflow in the boundary layer of the object surface produces strong friction, as a result, the kinetic energy of the airflow irreversibly turns into heat energy, resulting in the increase of temperature near the wall, and the high-temperature air will continue to transfer heat to the low-temperature wall, causing strong aerodynamic heating. The larger the flight Mach number, the more serious the degree of heating of the high-temperature airflow to the surface of the aircraft, which may cause the surface of the aircraft to change its shape and change the structural strength and rigidity of the aircraft, which has a serious impact on ensuring the normal flight of the aircraft. Therefore, the phenomenon of aerodynamic heating is an important problem that cannot be avoided in hypersonic vehicles.

The phenomenon of aerodynamic heating is extremely complex, which is not only related to the flight speed, altitude and state of the attached surface layer of the aircraft, but also involves the interference of shock wave and attached surface layer, slipstream and stationary heat exchange. In thermal protection, it is also necessary to consider the constant and unsteady problems such as heat conduction, heat release of the forced movement of the fluid, and thermal radiation.

When the aircraft is flying at supersonic speed at high altitude, the surface of the aircraft is constantly exchanging heat with the external environment. Common forms of heat exchange include convective heating of high-temperature air flow, heat flux of direct solar radiation, radiative heat flux of the earth's surface, heat flux of atmospheric reflection of solar rays absorbed by the surface of the aircraft, heat flux of the surface of the aircraft radiating outward, heat conduction from the surface skin to the interior of the aircraft, and heat diffusion of multi-component gas mixtures in the boundary layer, etc. For a typical hypersonic vehicle, the main forms of heat exchange are convection heating (pneumatic heating) of the high-temperature air stream, heat flux radiating outward from the surface of the aircraft, and heat conduction inside the skin.

1) Pneumatic heating

Pneumatic heating here refers to the convective heat transfer due to the movement of the fluid in the boundary layer, which is often analyzed by Newton's formula in engineering

$$q_a = \alpha_T \Delta T = \alpha_T (T_{aw} - T_w) \tag{6.5}$$

where: α_T — heat exchange coefficient;

$T_{\alpha w}$ — adiabatic wall temperature;

T_w — wall-temperature.

In the surface layer, although the fluid velocity at the contact with the wall is zero, there is a temperature gradient in the surface layer, which causes heat conduction on the wall outward. Therefore, the temperature of the fluid at the adiabatic wall is less than the temperature at the station, which is called the recovery temperature in engineering, and is denoted as T_r, that is, $T_r = T_{\alpha w}$.

$$T_r = T_\infty \left(1 + \frac{\gamma - 1}{2} r M_\infty^2\right) \tag{6.6}$$

where: r—— recovery factor,

$$r = \frac{T_r - T_\infty}{T_0 - T_\infty} \qquad (6.7)$$

For laminar flow, $r = \sqrt{p_r} = 0.845$; $r = \sqrt[3]{p_r} = 0.88$. Therefore, the key to calculating the heat flux is the heat exchange factor α_T.

α_T is a dimensional, and according to the similarity theory, a dimensionless heat exchange coefficient is introduced: called the Stanton number *St*. It is defined as:

$$St = \frac{\alpha_T}{C_p \rho V} \qquad (6.8)$$

Where: C_p, p, V – the specific heat capacity, density, and velocity of the air flow at a constant pressure.

As we all know, St has the following Reynolds analogy relationship with the friction coefficient.

$$S_t = \frac{1}{2} C_f \frac{1}{S} = \frac{1}{2} p_r^{-2/3} C_f \qquad (6.9)$$

where: $S = p_r^{2/3}$ — Reynolds analogy factor.

Therefore the heat flux can be expressed as

$$q_w = \frac{1}{2} p_r^{-2/3} C_f C_p \rho V (T_r - T_w) \qquad (6.10)$$

C_f via Equation (6.11) to Equation (6.13) results in:

$$C_{f\text{level}} = \frac{0.664}{\sqrt{Re}} \qquad (6.11)$$

$$C_{f\text{turbulence}} = \frac{0.0592}{(Re)^{0.2}} \quad (Re \leqslant 10^7) \qquad (6.12)$$

$$C_{f\text{turbulence}} = 0.37 \times (\log Re)^{-2.584} \quad (10^7 \leqslant Re \leqslant 10^9) \qquad (6.13)$$

From the above formula, αT can be obtained, and then the heat flux can be obtained.

2) Surface thermal radiation

The heat flux q_r radiating outward from the surface of the aircraft is

$$q_r = \varepsilon \sigma T_w^4 \qquad (6.14)$$

Where: σ — Boltzmann constant: $\sigma = 57.6 \times 10^{-9} W / (m^2 \cdot K^4)$;

ε— The outward radiation coefficient of the skin, which is related to the surface material, the properties of the coating, and the temperature.

In order to achieve a lower surface equilibrium temperature, a layer with a higher emissivity coefficient is required. For most layers, the ε is between 0.7 and 0.9.

3) Heat conduction inside the skin

The heat conduction from the outer surface of the skin to the inside is

$$q_\lambda = -\lambda \left(\frac{\partial T}{\partial y} \right) \qquad (6.15)$$

where: λ – the thermal conductivity of the material.

Calculating this heat conduction will use the heat conduction equation within the skin. In general, the thickness of the skin is much smaller than the other two dimensions, so the heat conduction equation can be simplified to one dimension

$$\gamma \cdot c \frac{\partial T}{\partial t} = \frac{\partial}{\partial y} \left(\lambda \frac{\partial T}{\partial y} \right) \qquad (6.16)$$

Where: γ — material density;

c—specific heat of the material.

Let the δ be the thickness of the skin, and integrate Equation (6.16) in the direction of thickness (y), i.e.

$$\int_0^\delta \gamma \cdot c \frac{\partial T}{\partial t} \cdot dy = \int_0^\delta \frac{\partial}{\partial y}\left(\lambda \frac{\partial T}{\partial y}\right) \cdot dy = \left(\lambda \frac{\partial T}{\partial y}\right)\Big|_{y=0}^{y=\delta} \tag{6.17}$$

$$\gamma \cdot c \frac{\partial T}{\partial t}\delta = \left(\lambda \frac{\partial T}{\partial y}\right)\Big|_{y=\delta} - \left(\lambda \frac{\partial T}{\partial y}\right)\Big|_{y=0} = -\left(\lambda \frac{\partial T}{\partial y}\right)\Big|_{y=0} \tag{6.18}$$

$$q_\lambda = -\left(\lambda \frac{\partial T}{\partial y}\right)\Big|_{y=0} = \gamma \cdot c \cdot \delta \frac{\partial T}{\partial t} \tag{6.19}$$

Assuming that the thickness of the skin is very thin, when calculating the heat flux of an unsteady thermal process, Equation (6.19) can be performed with a forward difference, i.e.,

$$q_{\lambda \cdot i} = \gamma \cdot c \cdot \delta \frac{T_{w \cdot i} - T_{w \cdot i-1}}{\Delta t} \tag{6.20}$$

The initial condition is: $T_{w\cdot 0} = T_\infty$.

4) Heat flow equation

When the aircraft is cruising, the surface heat flow should reach a balance, and this process belongs to the constant heat process. When the aircraft accelerates to fly or climb, the flight altitude and speed change with time, so the wall temperature also changes with time, and this process belongs to the unsteady heat process. Regardless of the equation of motion, the heat flux equilibrium equation should be satisfied

$$q_a - q_r = q_\lambda \tag{6.21}$$

namely

$$\frac{1}{2} p_r^{-2/3} C_f C_p \rho V (T_r - T_w) - \varepsilon \cdot \sigma \cdot T_w^4 = \gamma \cdot c \cdot \delta \frac{dT_w}{dt} \tag{6.22}$$

When the aircraft is cruising, it can be considered that the skin surface has reached a certain equilibrium temperature. At this time, dTw/dt = 0, and therefore there is

$$\frac{1}{2} p_r^{-2/3} C_f C_p \rho V (T_r - T_w) = \varepsilon \cdot \sigma \cdot T_w^4 \tag{6.23}$$

2. Pneumatic heating calculation

The research on aerodynamic heating has been vigorously carried out along with the progress of the development of high-speed aircraft. The establishment of Prandtl's boundary layer theory provides a very effective analysis and calculation tool for the study of aerodynamic heating. With the improvement of the strategic and tactical performance of aircraft, the research content of aerodynamic heating has been continuously updated, expanded, and deepened. From the early two-dimensional simplified shape (such as flat plate, station, cone, cylinder) of aerodynamic heating calculations, such as the space shuttle complex shape of aerodynamic heating calculation; expanding from low-velocity boundary layer heat transfer calculations to include heat transfer calculations with mass ejection and chemical reactions; from the analysis of the pneumatic heating characteristics of the attached flow to the analysis of the pneumatic heating characteristics of the separation flow; from pneumatic heating of smooth walls to pneumatic heating of jaggery walls; from the boundary layer similarity solution method to the numerical simulation of the full N-S equation, it has undergone a dynamic development process.

At present, although there are CFD programs that are used to solve the N-S equation to predict the thermal environment of hypersonic vehicles, such as LAURA at NASA Langley Research Center, this method is time-consuming and not suitable for the conceptual research and optimization design of the aircraft, so it is very necessary to give the aerodynamic heating engineering calculation methods of hypersonic vehicles from the perspective of engineering applications, and these calculation methods are reliable when applied to the attached flow part of the aircraft, such as the Less of laminar flow method, reference temperature method for turbulence, etc.

However, there is no mature engineering estimation method for the separation zone, so it is necessary to carry out corresponding experimental and numerical studies.

Aerodynamic heating calculation, that is, by solving the heat flow balance equation, the temperature at any point on the surface of the aircraft can be obtained. Looking at the various heat fluxes in the equation, only the calculation of pneumatic heating is more complicated. Because the calculation of aerodynamic heating is mainly reflected in the calculation of the convection exchange coefficient, because the temperature in the boundary layer is varied, the parameters used in solving αT also change, which increases the difficulty of the calculation. In order to simplify the problem, the reference temperature (reference enthalpy) method is proposed.

1) Calculation of reference temperature method and heat flux density

(1) Reference temperature method. The reference temperature method introduces a definite reference temperature and replaces the varying air characteristic parameters in the boundary layer with parameters that do not change at the reference temperature (denoted by *). There are several reference temperatures, among which the Eckert reference temperature (T^*) is the most widely used:

$$T^* = T_e + 0.5\,(T_w - T_e) + 0.22(T_r - T_e) \tag{6.24}$$

where: the subscript e - the outer edge of the boundary layer.

After the reference temperature is obtained, the airflow parameters at the reference temperature can be obtained.

Viscosity coefficient at reference temperature

$$\mu^* = 1.498 \times 10^{-6} \frac{T^{*3/2}}{T^* + 122} \tag{6.25}$$

Density at reference temperature

$$\frac{\rho^*}{\rho_e} = \frac{T_e}{T^*} \tag{6.26}$$

Reynolds number at reference temperature

$$Re^* = \frac{\rho^* V_e x}{\mu^*} \tag{6.27}$$

P_r^* and C_p^* can be found from the graphs of the literature. The heat exchange coefficient is expressed as:

$$\alpha_{\text{level}} = 0.332(p_r^*)^{-2/3}(Re^*)^{-0.5} C_p^* \rho^* V_e \tag{6.28}$$

$$\alpha_{\text{turbulence}} = 0.0296(p_r^*)^{-2/3}(Re^*)^{-0.2} C_p^* \rho^* V_e \quad (Re_{tr} \leqslant Re \leqslant 10^7) \tag{6.29}$$

$$\alpha_{\text{turbulence}} = 0.185(p_r^*)^{-2/3}(\log Re^*)^{-2.584} C_p^* \rho^* V_e \quad (10^7 \leqslant Re \leqslant 10^9) \tag{6.30}$$

(2) Calculation of heat flux of the fuselage. When the angle of attack is zero, the expression is replaced by Equation (6.28) to Equation (6.30), and the heat flow on the surface of the fuselage can be expressed as

$$q_{\alpha\text{level}} = 0.332(p_r^*)^{-2/3}(Re^*)^{-0.5} C_p^* \rho^* V_e (T_r - T_w) \tag{6.31}$$

$$q_{\alpha\text{turbulence}} = 0.0296(p_r^*)^{-2/3}(Re^*)^{-0.2} C_p^* \rho^* V_e (T_r - T_w) \quad (Re_{tr} \leqslant Re \leqslant 10^7) \tag{6.32}$$

$$q_{\alpha\text{turbulence}} = 0.185(p_r^*)^{-2/3}(\log Re^*)^{-2.584} C_p^* \rho^* V_e (T_r - T_w) \quad (10^7 \leqslant Re \leqslant 10^9) \tag{6.33}$$

The Fay-Riddle formula can be used for standing heat flow

$$q_{ss} = 0.76 p_r^{-2/3} (\rho_s \mu_s)^{0.5} \sqrt{\left(\frac{du_e}{dx}\right)_s} (h_s - h_w) \tag{6.34}$$

where: subscript "s" — station;

$(du_e/dx)_s$ – the stationary velocity gradient, which can be obtained from the modified Newtonian formula.

$$\left(\frac{du_e}{dx}\right)_s = \frac{1}{R_0}\sqrt{\frac{2(P_s - P_\infty)}{\rho_s}} \tag{6.35}$$

The accuracy of the standing velocity gradient will be higher if it is calculated using the following formula, namely

$$\left(\frac{\mathrm{d}u_e}{\mathrm{d}x}\right)_s = \frac{V_\infty}{R_0}\sqrt{1.85\frac{\rho_\infty}{\rho_s}} \tag{6.36}$$

where: R_0—radius of curvature of station;

P_s—total pressure after positive shock wave;

ρ_s—the density of the standing airflow after the positive shock wave.

$$P_s = P_\infty(1.1667M_\infty^2 - 0.1667)(1+0.2M_2^2)^{3.5} \tag{6.37}$$

$$M_2^2 = \frac{M_\infty^2+5}{7M_\infty^2-1} \tag{6.38}$$

$$h_s = h_\infty + \frac{V_\infty^2}{2} = C_p(T_\infty)T_\infty + \frac{V_\infty^2}{2} \tag{6.39}$$

$$T_s = T_\infty(1+0.2M_\infty^2) \tag{6.40}$$

$$\rho_s = \frac{P_s}{RT_s} \tag{6.41}$$

In the presence of an angle of attack, severe aerodynamic heating will be generated on the windward surface, which is much more severe than at zero angle of attack, even if the flow regime is the same. In addition, the experimental results also show that on the windward side, the angle of attack pushes the transition point forward, which will further deteriorate the thermal environment on the windward side. The consideration of the angle of attack in engineering includes the equivalent cone method and the experimental data correlation method. The equivalence cone method is, on the center line, there is

$$\theta_k = \alpha + \theta \tag{6.42}$$

where: θ — the surface inclination of the surface to the axial coordinate axis x;

θ_k — Equivalent cone angle (local angle of attack).

In this way, finding the heat flow with an angle of attack becomes finding the heat flow of the equivalent cone with a zero angle of attack. According to the Mengele transform, the eigen-lengths in the Reynolds number also change accordingly on the cone

$$(Re_x)_{zhui} = \frac{\bar{x}\rho V}{\mu} \tag{6.43}$$

In laminar flow, $\bar{x}$ = x/3; in the case of streaming, $\bar{x}$ = x/2.

(3) Calculation of heat flux density of the standing point line of the leading edge of the wing. Without considering the influence of the fuselage on the wing, the aerodynamic heating of the leading edge of the wing can be calculated approximately according to the formula for calculating the heat flow at the leading edge of the swept cylinder

$$q_{ds} = \alpha_T(T_r - T_w) \tag{6.44}$$

$$\alpha_T = \theta'_w \cdot p_r^{-0.54}(\rho\mu)_w^{0.5}C_p\sqrt{\left(\frac{\mathrm{d}u}{\mathrm{d}x}\right)_{sl}} \tag{6.45}$$

The numerical calculation correlation of θ'_w is

$$\theta'_w = [1+1.5(\theta'_{wo})^{3.5}T_w/T_{\infty_0}]\cdot\theta'_{wo} \tag{6.46}$$

$$\theta'_{wo} = 0.0014\left(\frac{T_{\infty_0}}{T_{no}}\right)^{2.113} - 0.0109\left(\frac{T_{\infty_0}}{T_{no}}\right)^{1.113} + 0.516\left(\frac{T_{\infty_0}}{T_{no}}\right)^{0.113} \tag{6.47}$$

where: T_{∞_0}, T_{no} – the total temperature of the incoming flow and the conversion of kinetic energy perpendicular to the direction of the leading edge into heat.

$$T_{\infty_0} = T_\infty(1+0.2M_\infty^2) \tag{6.48}$$

$$T_{no} = T_\infty(1+0.2M_\infty^2\cos^2\Lambda) \tag{6.49}$$

where: Λ — wing leading edge sweep angle.

The expression for the stationary velocity gradient is:

$$\left(\frac{du}{dx}\right)_{sl} = \frac{1}{R_0}\sqrt{\frac{2(P_{wsl\Lambda} - P_\infty)}{\rho_{s0}}} \quad (\Lambda \leqslant 75^\circ) \tag{6.50}$$

$$P_{wsl\Lambda} = P_\infty (1.2M_{n\infty}^2)^{3.5}\left(\frac{2.4}{2.8M_{n\infty} - 0.4}\right)^{3.5} \tag{6.51}$$

where: $M_{n\infty}$—the normal component of the incoming Mach number at the leading edge of the wing;

$P_{wsl\Lambda}$—the total post-shock pressure corresponding to $M_{n\infty}$;

R_0—Radius of curvature of the leading edge of the wing.

The viscosity coefficient can be calculated according to the Sutherland formula, and the density of the gas is determined by the equation of state:

$$\mu_{w\Lambda} = 1.73 \times 10^{-6}\left(\frac{T_w}{261}\right)^{1.5}\left(\frac{375}{T_w + 114}\right) \tag{6.52}$$

$$\rho_{w\Lambda} = \frac{P_{wsl\Lambda}}{(287.06T_w)}, \quad \rho_{n0} = \frac{\rho_{wsl\Lambda}}{(287.06T_{n0})} \tag{6.53}$$

(4) Calculation of heat flux density along the chordal direction on the windward side of the wing. For the aerodynamic heating calculation on the windward side of the wing, Equation (6.51), Equation (6.52) and Equation (6.53) can still be used. However, the effect of the sweep angle on the angle of attack and the number of Mach numbers must be taken into account. When there is an angle of attack, the effective angle of attack α_e, the effective sweep angle; χ_e and the Mach number $M_{\alpha n}$ are changed to, respectively:

$$\alpha_e = \arctan\left(\frac{\tan\alpha}{\cos\chi_{w0}}\right) \tag{6.54}$$

$$\chi_e = \arcsin(\sin\chi_{w0} \cdot \cos\alpha) \tag{6.55}$$

$$M_{\alpha n} = M_{a\infty} \cdot \cos(\chi_{w0}) \tag{6.56}$$

2) Determination of airflow parameters at the outer edge of the boundary layer

The calculation of pneumatic heating is inseparable from the calculation of the airflow parameters (subscript e) at the outer edge of the boundary layer. In engineering, the empirical formula combining the improved quadratic shock wave expansion wave method with a certain accuracy and the modified Newton theory is often used.

$$C_{pe} = C_{p\max}\sin^2\theta_k \tag{6.57}$$

$$C_{p\max} = \frac{1}{0.7M_\infty^2}\left\{\left[\frac{5.76M_\infty^2}{5.6M_\infty^2 - 0.8}\right]^{3.5}\left[\frac{2.8M_\infty^2 - 0.4}{2.4}\right] - 1\right\} \tag{6.58}$$

$$P_e = P_\infty(1 + 0.7M_\infty^2 C_{pe}) \tag{6.59}$$

$$\sin\theta_c = [1.2\sin^2\theta_k + (M_\infty)^{-2}]^{0.5} \tag{6.60}$$

$$\frac{\rho_e}{\rho_\infty} = \frac{6M_\infty^2\sin^2\theta_c}{5 + M_\infty^2\sin^2\theta_c} \tag{6.61}$$

$$\frac{T_e}{T_\infty} = \frac{(7M_\infty^2\sin^2\theta_c - 1)(M_\infty^2\sin^2\theta_c + 5)}{36M_\infty^2\sin^2\theta_c} \tag{6.62}$$

$$M_e^2 = 5\left[\frac{T_\infty}{T_e}(1 + 0.2M_\infty^2) - 1\right] \tag{6.63}$$

$$V_e = 20.0467M_e\sqrt{T_e} \tag{6.64}$$

3) Boundary layer transition

The transition of the boundary layer from laminar flow to turbulence is carried out in an interval, so it is necessary to give the formula for calculating the heat flow in the transition zone. The interstitial factor is introduced Γ, and the heat flow in the transition zone is:

$$q_{\alpha tr} = (1-\Gamma)\cdot q_{\alpha 1} + \Gamma \cdot q_{\alpha 2} \quad (6.65)$$

$$\Gamma = \frac{1}{2}\left\{1+\tan\left[\frac{5(x-x_1)}{\Delta x_{tr}} - 2.5\right]\right\} \quad (6.66)$$

where: subscript 1 - the beginning of the transition zone;
subscript 2 – the end of the transition zone.
$\Delta x_{tr} = x_2 - x_1$ — length of the transfiring zone;
x_1, x_2 — coordinates of the start and end points of the transition zone;
$q_{\alpha 1}$, $q_{\alpha 2}$ – heat flux at x_1, x_2.

$$\frac{\Delta x_{tr}}{x_1} = [60 + 4.68 M_{e1}^{1.92}] Re_1^{-1/2} \quad (6.67)$$

Where: Re_1——Transition Reynolds number, in engineering, a variety of transition criteria have been established to calculate it, and the test formula is usually used [12]:

$$Re_1 = 10^{5.37-0.2326 M_{e1} - 0.004015 M_{e1}^2} \quad (6.68)$$

to calculate the initial position x_1 of the transition zone, where M_{e1} is the Mach number of the transition at x_1.

3. Calculation of wall temperature

The analysis of aircraft aerodynamic heating is mainly to obtain the distribution of surface temperature, so as to optimize the shape design and adopt appropriate materials and thermal protection measures.

1) Calculation of wall temperature in unsteady thermal process

The launch booster stage is an unsteady thermal process, the surface heat is very high, and the temperature is constantly changing, and obtaining the temperature-time history of the fuselage and wing station is helpful to understand the peak heat flow and temperature change. Differentiating Equation (6.22) gives the following differential formula as:

$$\alpha_{h\cdot i-1}(h_{s\cdot i-1} - C_{pw\cdot i-1} T_{w\cdot i-1}) - \varepsilon \cdot \sigma \cdot T_{w\cdot i-1}^4 = \gamma \cdot c \cdot \delta \frac{T_{w\cdot i} - T_{w\cdot i-1}}{\Delta t} \quad (6.69)$$

Among which, $\alpha_{h\cdot i-1}$ is calculated according to the airflow parameters of $T_{w\cdot i-1}$ and the outer edge of the instantaneous attached surface layer, and the initial temperature is the local ambient temperature. By solving the above difference equations, the time history of the temperature distribution can be obtained.

2) Calculation of wall temperature in the process of constant heat

The long-term cyclic flight section is a constant heat process, and the pneumatic heating has the characteristics of low heat flux and high enthalpy, and it can be considered that the temperature drop of the skin surface has reached a certain equilibrium. At this point, $dT_w/dt = 0$, so there is:

$$\frac{1}{2} p_r^{-2/3} C_f C_p \rho V (T_r - T_w) = \varepsilon \cdot \sigma \cdot T_w^4 \quad (6.70)$$

Equation (6.70) is an implicit form for the wall temperature T_w, and should be solved using an iterative method.

6.2: Fundamental research problems in hypersonic aerodynamics-thermal-elastic mechanics

6.2.1: Thermochemical reaction mechanism of high-temperature reactive gases

When the temperature of the air exceeds 800 K, the vibrations of the molecules are excited, and the air can no longer be regarded as a calorimetric complete gas; at temperatures above 2000 K, oxygen molecules begin to dissociate; at temperatures above 4000 K, nitrogen molecules begin to dissociate and nitrogen oxides begin to form.

At temperatures above 9000K, oxygen and nitrogen atoms begin to ionize. At high temperatures, air essentially becomes a reaction medium whose composition changes with changing temperature. Due to the rapid compression and high-velocity expansion of the strong shock wave, hypersonic flow may become an unsteady flow of a medium in a non-equilibrium thermodynamic state. The non-equilibrium thermodynamic state of a medium makes it difficult to describe its thermodynamic parameters by traditional physical property equations. The scale of the dissociation, ionization, thermal radiation, and non-equilibrium relaxation process of the dielectric microclusters breaks through the similarity criterion of aerodynamic experiments. The microscopic changes in the gaseous medium itself are strongly correlated with the macroscopic hypersonic flow through changes in the thermodynamic state of the medium. Therefore, the definition of the macroscopic thermodynamic properties of high-temperature air gases must be redefined. These include the transport coefficients of the medium (viscosity coefficient, thermal conductivity, conductivity coefficient, diffusion coefficient of each component), the correlation coefficient of the contact reaction between the medium and the wall, the chemical non-equilibrium relaxation process between the gas-phase reaction, the thermodynamic non-equilibrium relaxation process between various internal energy modes, the emission and absorption functions of the gas-phase medium and the wall radiation, and the coupling relationship between the radiation and ionization [8].

6.2.2: Hypersonic boundary layer transition

Supersonic boundary layer transition is a major problem in gas dynamics, and hypersonic boundary layer transition is more complex due to the influence of aerothermodynamics. With the development of hypersonic vehicles, the research on hypersonic boundary layer transition is more in-depth and urgent. In 2003, a U.S. technical committee to evaluate the development of hypersonic technology recommended supersonic boundary layer transition as a national research project. Supersonic boundary layer transition can lead to the intensification of heat conduction, the increase of thermal ablation rate, and the acceleration of the shape change of the head of the aircraft, resulting in the formation of macroscopic roughness downstream of the transition point, which aggravates the turbulent convective heat conduction.

According to the results obtained so far, the differences between the boundary layer transition results obtained by different prediction methods and experimental simulations are striking. The reason is that there are too many flow field parameters that affect the supersonic boundary layer transition to varying degrees, such as local flow Mach number, surface cooling, unit Reynolds number, aircraft head bluntness, high-entropy layer, lateral flow, object surface roughness, surface protrusion, mass jet, etc. In addition, if there is dissociation and ionization in hypersonic flow, then gas chemistry also affects the boundary layer transition. In order to predict boundary layer transition, a large number of supersonic and hypersonic flow experiments have been done considering the presence or absence of heat transfer, but no proper semi-empirical model has been obtained that can be used to accurately predict boundary layer transition. Recent studies have also shown that wind tunnel noise also affects boundary layer transitions, and that this effect is present in almost all hypersonic experimental results. Due to the lack of knowledge of the flight environment, a reasonable prediction of the Mach number in free flight is almost impossible. In summary, it is unthinkable to try to correlate all experimental data with a simple theoretical or empirical formula, and it is even more difficult because the position of the boundary layer transition is very sensitive to the measurement technique. In general, experimental studies, the measured significant increase in thermal conductivity indicates a transition of the boundary layer from laminar flow. In the study of flow displays, the schlieren technique is applied to reveal the transition through the vortex fragmentation of the boundary layer. According to the schlieren measurements of the flight experiments that have been obtained, the results of the boundary layer transition are as dispersed as indicated above, and sometimes the Mach number of the transition can vary by orders of magnitude. Some studies have shown that hypersonic flow boundary layer transitions can indeed occur on a considerable scale, which is closely related to incoming flow conditions and object surface shape. In general, all theoretical models of boundary layer transition and turbulence are semi-empirical in nature, which means that the results are at most equivalent to the experimental results on which the models are based. If, due to wind tunnel disturbances and other reasons, there is a question of confidence in the experimental results, then the calculations are the same. This conundrum suggests that in order to study supersonic boundary layer transitions, we need essentially more fundamental physical models that should not rely on empirical data from experiments, but only on governing equations and fluid physics, as in the case of large eddy simulations of turbulence theory. More recently, if we arrive at a transition model of hypersonic flow through painstaking efforts, then the model should take into account the thermochemical mechanism of the gas reaction, which further complicates the transition problem.

In addition, due to many factors, the wind tunnel and flight experiment data for hypersonic boundary layer transition are uncertain, so the greater difficulty we face is how to validate a good transition model. Therefore, the results of decades of research show that people have a certain understanding of hypersonic boundary layer transition, but the research on related boundary layer transition still has a long way to go.

6.2.3: Shock/Shock Interactions for Hypersonic Flow

Shock/shock interactions in hypersonic flow can have catastrophic consequences. Flight experiments on the X-15A-2 in October 1967 had already suggested this problem. At that time, the flight speed was Ma = 6.7, and the high-temperature air flow generated by the interaction between the head shock wave of the aircraft and the shock wave of the ramjet engine mount burned out the bracket like a torch and blew off the ramjet engine model. The supersonic jet generated by the shock wave interaction can lead to a sharp increase in thermal conductivity, which can vary by orders of magnitude in the shock wave impact region. Heat flow variations due to shock disturbances can also occur in the wing front and aircraft control surface areas. With the development of hypersonic vehicles with air-breathing engines, the oblique shock waves produced by the aircraft forebody, which is the pre-compression surface of the engine intake, act on the bow shock waves at the lower lip of the intake tract, which may produce viscous interactions. The oblique shock wave generated by the separation of the boundary layer of the aircraft forebody may also impact with the shock wave of the lower lip of the air intake, forming a viscous interaction of the three shock wave interactions, causing more serious heat transfer problems. Shock/shock interactions can cause serious problems for hypersonic vehicles, and aircraft designers often use conservative estimates to prevent aerothermodynamic problems that are not yet aware, which will make the aircraft's thermal protection system overweight and greatly reduce the aircraft's flight capability.

6.2.4: Aeroelasticity in a hypersonic thermal environment

The thermal environment formed by pneumatic heating and the aerodynamic force, inertial force and elastic force that constitute the aeroelastic problem form a coupling relationship with different degrees of strength, as shown in Figure 6-3.

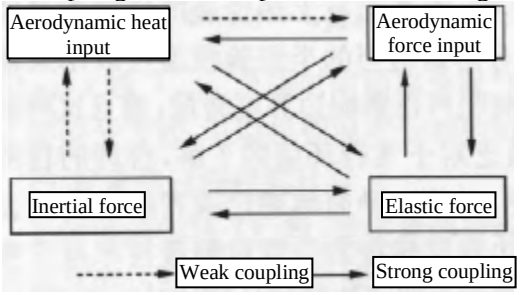

Figure 6-3: Coupling relationship of thermo-aeroelastic problems

In the process of analysis, it is generally considered that the weak coupling in the coupling relationship has little effect on the aeroelastic properties, so the influence of aerodynamic heating on the elastic force of the structure is emphasized. The influence of pneumatic heating on the elastic force of the structure is mainly in two aspects: first, the mechanical properties of the material change with the change of the ambient temperature of the material; second, pneumatic heating causes additional thermal stress in the structure, thereby changing the static and dynamic characteristics of the structure.

The aeroelastic problem is a multidisciplinary problem, and it is very complex to solve such a multidisciplinary coupling problem at one time, and it is difficult to realize it in engineering at present and for a long time. Based on the aforementioned assumption that only the influence of aerodynamic heating on the elastic force of the structure is considered in the analysis of thermo-aeroelastic problems, the analysis process is simplified, and the researchers propose a hierarchical solution method. The calculation process of the hierarchical solution is to decompose the coupling analysis of aerodynamics, aerothermal, and structural dynamics into two parts: stationary aerothermal-structural dynamics and unsteady aerodynamics-structural dynamics, and the analysis process of aeroelastic mechanical properties in thermal environment is shown in Figure 6-4. This method ignores the effects of structural deformation and vibration on the thermal environment [9].

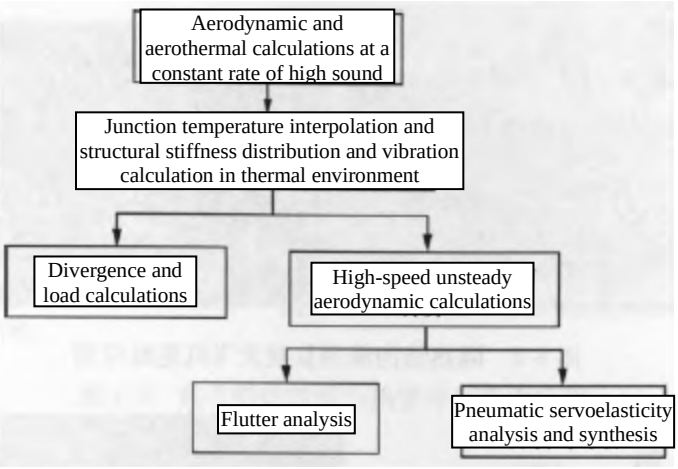

Figure 6-4: Analysis process of aeroelastic mechanical properties in a thermal environment

In the 1990s, the study of thermoaeroelasticity received extensive attention due to the advancement of the NASP program. At this stage, the analysis of thermoaeroelasticity not only focuses on the analysis and calculation of specific structures such as rudder surface and the whole machine, but also begins to consider and integrate the control system into the analysis of thermoaeroelastic mechanics, gradually forms the concept of aeroservo thermoelasticity, and establishes the corresponding analysis model. The coupling between aerodynamics, thermal, and structural problems can be solved using CFD, CSD, and computational thermodynamics (CTD) related methods and software, resulting in computational thermoaeroelastic mechanics (CATE). The coupling analysis method based on linear finite element, full potential flow and linear heat conduction is mature and widely used in engineering analysis. Coupled analysis methods based on nonlinear finite elements, Euler equations or N-S equations, and nonlinear heat conduction are one of the important research directions of thermoaeroelastic mechanics, which provides a theoretical method for finer simulation and deeper understanding of thermoaeroelastic coupling problems [10,11].

6.3: Aerospace thermal protection technology and typical thermal protection system scheme

6.3.1: Aerospace thermal protection technology

In the field of aerospace technology, a variety of technical approaches have been formed to deal with the harsh aerodynamic heating environment faced by hypersonic flight, which can be mainly divided into three technical approaches: passive heat protection, semi-passive heat protection, and active cooling [12,13].

1. Passive heat protection

The insulated structure is designed to withstand a moderate degree of heat flux density and a relatively short heating time. Figure 6-5 shows that the surface of the structure is subjected to pneumatic heating and a certain amount of heat is removed by radiation. The purpose of insulation is to minimize the heat transfer to the structure through the insulation layer and keep the structure within a certain temperature range. An example of a thermally insulating structure is the elevator surface structure of the space shuttle.

Figure 6-6 shows a heat sink structure, which is used to instantaneously withstand a moderate degree of heat flux density. When the surface of the structure is subjected to pneumatic heating, part of the heat is discharged by radiation, and the other part is absorbed by the structure. If the heat sink structure absorbs heat for a longer period of time, it will overheat the structure. NASA's X-15 test vehicle uses a heat sink structure on the leading edge of the wing.

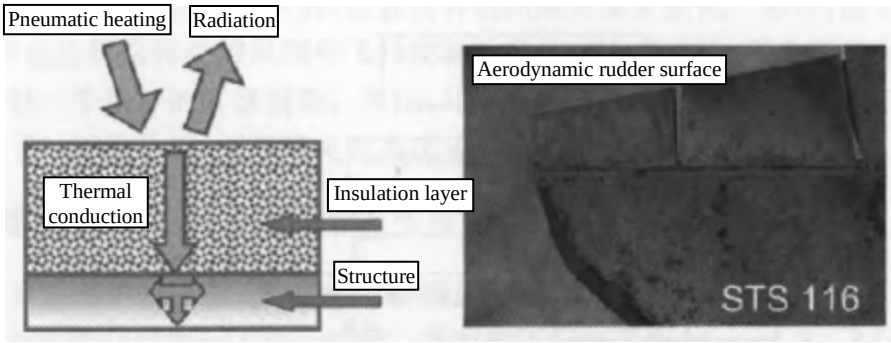

Figure 6-5: Schematic diagram of thermal insulation structure and application of space shuttle rudder surface

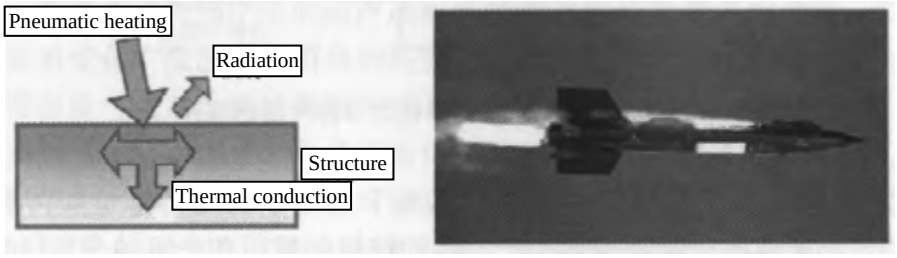

Figure 6-6: Heat sink structure and X-15 application

Figure 6-7 shows a thermal structure that is designed to withstand a moderate degree of heat flux density for a long period of time. Thermal structures are used for larger thermal loads and last for longer periods of time than heat sink structures, and the heat is radiated outwards and conducted inwards, allowing the structure to reach steady-state conditions and the entire structure to rise to a higher temperature.

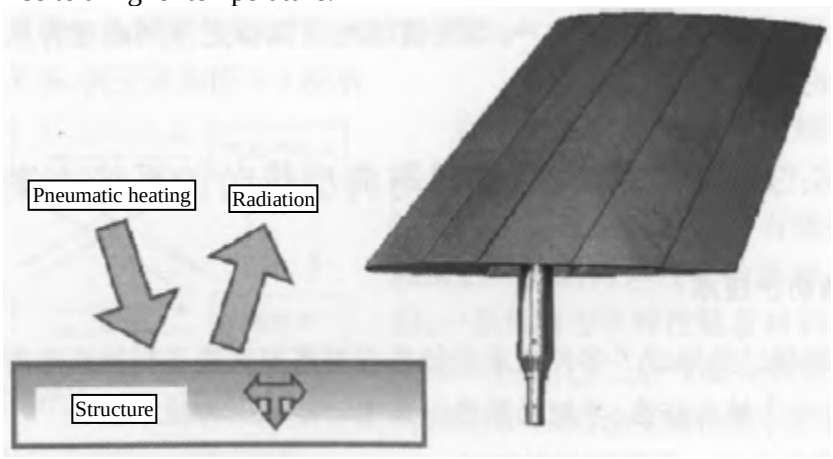

Figure 6-7: Schematic diagram of thermal structure and airfoil application

2. Semi-passive heat protection

Semi-passive heat protection is used for high heat flux densities and for long periods of time, such as heat pipes. The heat is transferred through the working fluid to other areas of the heat pipe and discharged by radiation. Figure 6-8 shows the leading edge structure of the heat pipe cooling wing.

Ablation is another semi-passive heat protection technique in which the purpose of ablation is to cool the structure. Ablation is used for very high heat flux densities, but lasts relatively short periods of time, as well as for one-time use. Figure 6-9 shows the application of ablation heat protection, that is, the heat protection shell at the bottom of the spacecraft, the heat is blocked by the consumption of the ablative material in the re-entry stage, and the heat is absorbed through the ablation process.

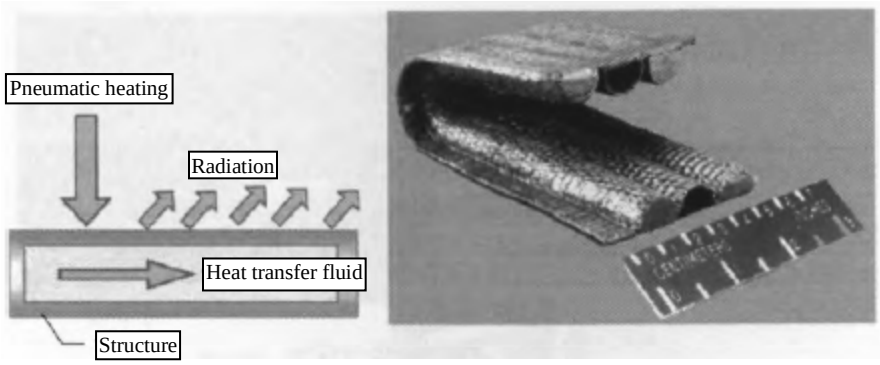

Figure 6-8: Schematic diagram of heat pipe heat protection and application of heat pipe cooling leading edge

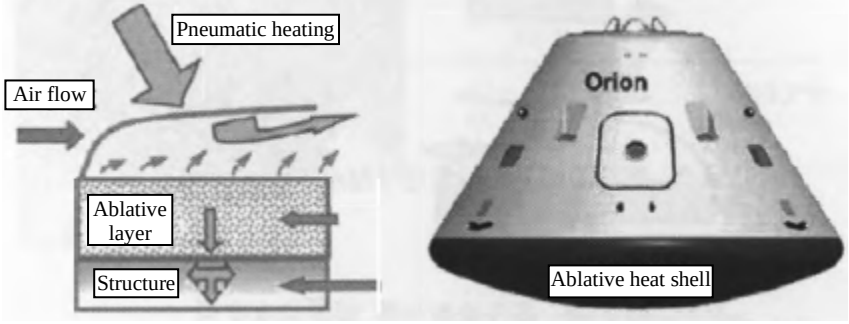

Figure 6-9: Schematic diagram of ablation and ablation shell application

3. Active cooling

Active cooling is used for higher heat flux density and long-term aerodynamic heating, and convection heat transfer cooling is a common form, such as the U.S. Space Shuttle SSME main engine used for the cooling of the propulsion system, where the coolant is heated and the heat is removed, and the structure remains hot and within a certain temperature range (Figure 6-10).

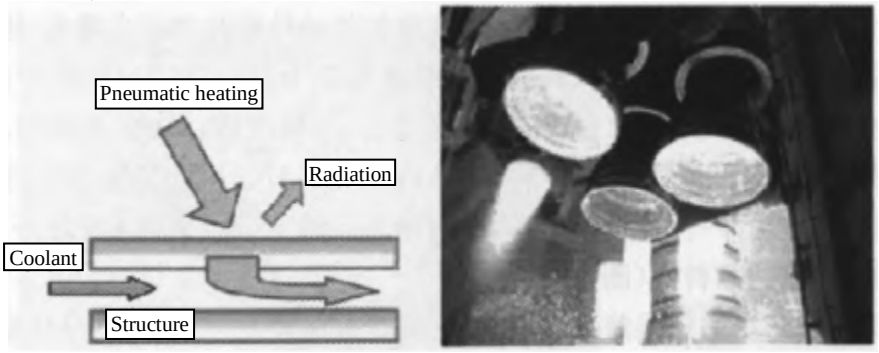

Figure 6-10: Active cooling structure and application

Thin-film cooling is another active cooling method used for propulsion systems (Figure 6-11). For thin film cooling, the coolant is sprayed into the flow at an upstream location, creating a thin, cooler-temperature insulation layer on the surface of the structure.

Another type of active cooling is evaporative cooling. Figure 6-12 shows a carbon/carbon combustion chamber test specimen, in which the coolant is continuously sprayed into the high-temperature hot gas stream through several discrete pores, and the heat flux density of the structure is also reduced.

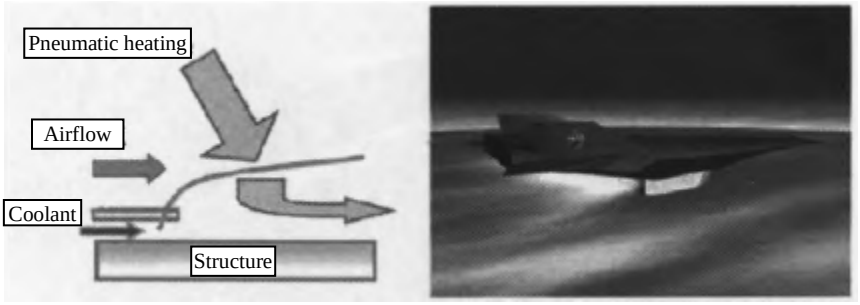

Figure 6-11: Thin film cooling and application

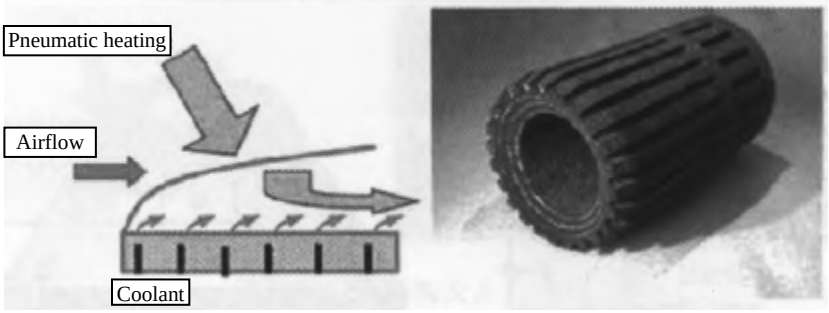

Figure 6-12: Evaporative cooling with carbon/carbon combustion chamber application

Different thermal protection technologies are applied to different aircraft according to the flight trajectory and flight mission. Figure 6-13 shows that different types of flights use different thermal protection technologies in the relationship between temperature and continuous heating time. Generally speaking, the aerodynamic heating of the spacecraft in the re-entry section is the most serious, its trajectory is steep, the heat flux density is very large, but the heating time is very short, the heat load is very small, and it is mostly used once, and it is not strictly required to maintain a stable aerodynamic shape and surface smoothness, so the ablation and heat protection design is mainly adopted; the X-15 test vehicle is subjected to aerodynamic heating period, so the heat sink structure is adopted; the SR-71 aircraft flies with a Mach number of 3, which is relatively low, and can adopt a thermal structure; the re-entry trajectory of the space shuttle is relatively stable, although the heat flow is not as large as that of the spacecraft, but the heating time is long, the heat load is large, and it is required to be reused, and the stable aerodynamic shape and surface smoothness must be maintained, so the surface heat insulation and radiation heat protection design are adopted; the single-stage/two-stage orbit space launch vehicle is most seriously heated in the ascent stage, and the aerodynamic heating is also more serious in the re-entry stage, and it must fly in the atmosphere for a long time and require hundreds of reuses, and at the same time it is necessary to solve the problems of cryogenic storage tanks, so the use of radiation heat protection (or + internal heat insulation) design, should consider the active cooling measures and structure-heat protection-storage tank (-inlet duct) integrated design. In short, different thermal protection schemes, structures, and materials are used according to different flight paths and flight missions (Figure 6-13).

The Space Shuttle uses a traditional truss skin aircraft structure, and the temperature of the structure is required to be kept below 350°F for reusable purposes. In terms of thermal protection measures, the space shuttle uses reusable surface insulation tiles on the windward side and reusable thermal blankets on the leeward side. For the leading edge and head cone, the temperature is greater than 2,300°F, so the reinforced carbon/carbon (RCC) material structure is used.

Figure 6-14 shows the maximum temperature of each part of the space shuttle surface.

The X-33 is a suborbital test vehicle conducted by NASA. The TPS used in the X-33 is similar to that of the Space Shuttle, but metal TPS is used on the windward side, as shown in Figure 6-15.

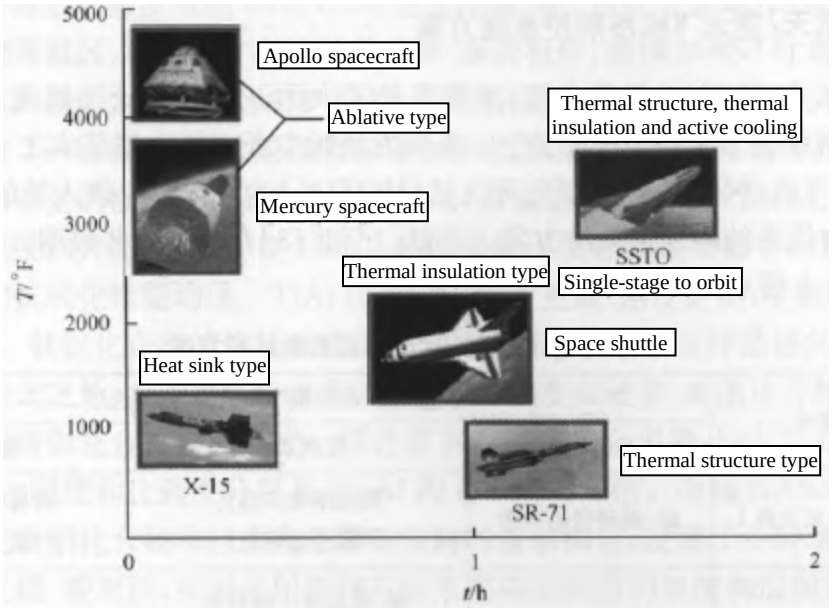

Figure 6-13: Thermal protection technology is used in different aircraft

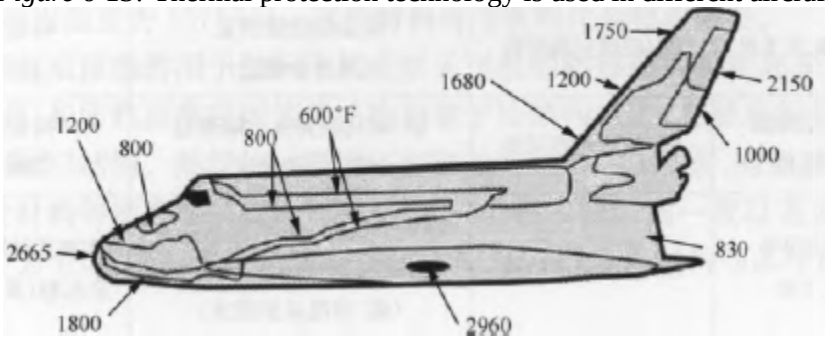

Figure 6-14: Maximum temperature of each part of the space shuttle's surface

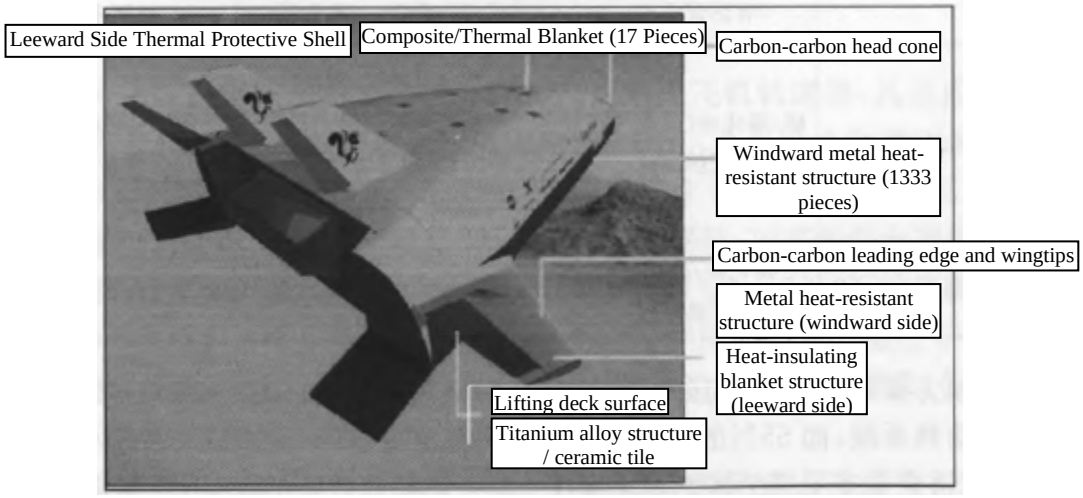

Figure 6-15: The thermal protection system used by the X-33

6.3.2: Typical aerospace/aerospace aircraft thermal protection system schemes

From the 1980s to the mid-1990s, the world's major aerospace powers carried out the development of space shuttles or aerospace aircraft, among which the thermal protection system program deserves special attention. The aerospace aircraft programs developed by various countries can basically be divided into two categories: one is the first-stage orbit program represented by the American Aerospace Aircraft (NASP) and the British Aerospace Aircraft (HOTOL); the second is the two-stage orbit scheme represented by the German Sänger. Documents [1] and [13] describe the thermal protection system profiles for these typical schemes, as shown in Table 6-1.

Table 6-1: Thermal protection schemes for typical space/aerospace aircraft

Type	Model	Layout and structure of thermal protection system, material selection		
		Maximum temperature	Higher temperatures	Lower temperatures
Space shuttle	U.S. Space Shuttle I	Carbon/carbon thin-shell thermal structure	Ceramic rigid heat-proof tile (aluminum alloy skin)	Ceramic flexible thermal insulation felt (titanium alloy skin)
	American Space Shuttle II	Carbon/carbon thin-shell thermal structure	Carbon / carbon panel + thermal insulation layer, superalloy panel + thermal insulation layer (aluminum alloy skin)	Titanium multi-layer wall (titanium skin)
	The former Soviet space shuttle	Carbon/carbon thin-shell thermal structure	Ceramic rigid heat-proof tile (aluminum alloy skin)	Ceramic flexible thermal insulation felt (aluminum alloy skin)
Aerospace aircraft	Space shuttle Helmes, France	Carbon/carbon thin-shell thermal structure	Carbon/Silicon Carbide Cover + Thermal Insulation (Carbon/Resin Skin)	Ceramic flexible thermal insulation felt (aluminum alloy skin)
	HOPE Space Shuttle, Japan	Carbon/carbon thin-shell thermal structure	Ceramic rigid heat-resistant tile or nickel-based alloy (or carbon/carbon) panel + thermal insulation (carbon/polyimide skin)	Ceramic flexible thermal insulation felt (carbon/resin skin)
	NASP in the United States	Carbon/carbon (and refractory metal) thin-walled thermal structures (with heat pipe structures)	Titanium-aluminum compounds or metal-matrix composites (or carbon/carbon) panels (+ insulation) based on them	Titanium alloy or metal matrix composite panel based on it (+ thermal insulation).
	American HOTOL	Carbon/silicon carbide (or carbon/carbon) thin-shell thermal structure	Front: Carbon/carbon (or carbon/ceramic) panel + insulation; Middle and rear: boron carbide/titanium panel + insulation	Titanium alloy or titanium matrix composite panel + thermal insulation
	Sänger, Germany	Silicon carbide/silicon carbide thin shell thermal structure	Nickel-based alloy multi-layer wall + thermal insulation layer	Titanium alloy multi-layer wall + thermal insulation layer

The carrier aircraft of the two-stage orbit scheme (Mach number of interstage separation is 6.8), the maximum temperature at the station is 1,336°C, 40% of the surface does not require a special heat protection system, while 55% of the surface (mainly the lower surface) is between 540 and 990°C, and for parts less than 500°C, a titanium alloy multi-layer wall structure will be used. For locations between 500 and 1,000°C, nickel-based alloy multilayer wall structures are used. In the highest temperature area, the silicon carbide/cinnamon carbide thin shell thermal structure was selected. For single-stage orbital aerospace aircraft, higher temperatures are required, such as the British HOTOL, which can be estimated to be as high as 1,723°C at the inlet lip, 1,477°C at the nose cone of the fuselage, and 1,423°C at the leading edge of the vertical tail.

NASP in the United States estimated that the local maximum temperature could reach 3,315°C and considered the selection of carbon/carbon (and refractory metal) thin-walled thermal structures and heat pipe technology. In the higher temperature region, in addition to considering carbon/carbon panels, the NASP program in the United States also developed titanium aluminum compounds or metal matrix composite panels based on them. Titanium-aluminum compound is an intermetallic compound, and there are two main types of research: Ti3Al and TiAl. Compared to titanium-based and nickel-based alloys, titanium-aluminum compounds have better high-temperature strength and lower density. The modulus of titanium alloys decreases with increasing temperature, while the properties of titanium-aluminum compounds increase with increasing temperature within the temperature range it can withstand, with a higher modulus at 1,000°C than that of titanium alloys at room temperature, and its creep resistance and oxidation resistance are good. Compared with Ti3Al, TiAl has lower density, harder stiffness, and higher temperature resistance, but it is less plastic and difficult to process. The excellent properties of titanium-aluminum compounds are due to their slow atomic motion and special dislocation motion between ordered lattices. In addition, in order to further improve the strength and hardness of Chin aluminum alloys, the United States has also carried out research on fiber-reinforced composite materials based on titanium-aluminum compounds. After the comparison of multiple schemes, it is shown that SiC/Ti3Al has excellent comprehensive properties, and its specific stiffness and specific strength are 2.5 times and 2 times that of Ti3Al, respectively. In order to simplify the effective combination of titanium-aluminum compounds and lightweight high-temperature honeycomb structures, the NASA Langley Research Center in the United States has developed an enhanced diffusion bonding process. For the aforementioned carbon/carbon panels, the United States adopts two methods to improve the interlaminar shear strength and interlaminar tensile strength, that is, one is to improve the strength of the matrix by optimizing the process, and the other is to use three-way reinforcement to improve the strength along the thickness direction. NASP in the United States also considers the selection of glass-ceramic matrix composites (service temperature of 815°C) and advanced ceramic matrix composites (service temperature of 1,371°C) in the sub-high temperature area. These materials are comparable to titanium-aluminum compounds.

The heat-proof structures developed or envisaged by various countries for space shuttles or aerospace aircraft can be divided into two categories: thermal structures with dual functions of structure (load-bearing) and heat protection, and independent external heat-proof (system) structures placed on top of cold structures and mainly responsible for heat protection. The thermal structure is generally based on radiation heat protection and can be made of high-temperature resistant structural materials such as carbon/carbon, ceramic matrix composites, metals, and metal matrix composites. The structure of the external heat protection system is generally based on surface insulation or internal heat insulation (surface radiation), which can be made of ceramics and ceramic matrix composites, carbon/carbon, metal materials and other materials.

6.4: Reusable Aerospace Vehicle Metal Thermal Protection System

6.4.1: Requirements for thermal protection systems for reusable space launch vehicles

The first generation of reusable space launch vehicles (RLVs) in the United States was the Space Shuttle orbiter, and 70% of its surface thermal protection system (TPS) used about 30,000 reusable ceramic heat protection tiles, which are 254 mm X 508 mm X 185 mm and 381 mm X 381 mm X 165 mm. The high-temperature heat-proof tiles underneath the orbiter fuselage are black, and the low-temperature heat-resistant tiles on the upper part of the orbiter fuselage are white, filled with Nomex strain isolation felt, and bonded to the aluminum alloy skin with room-temperature adhesive to resist the high temperature of the fuselage's upper surface at 399 to 649°C and the lower surface at 649°C to 1,260°C. During the orbiter's re-entry flight, 90% of the heat is radiated back to the atmosphere by the heat-proof tile, and the temperature of the aluminum alloy skin does not exceed 177°C. Since the Space Shuttle entered service, although the ceramic thermal protective tile has met the performance requirements of the Space Shuttle orbiter, there are still many problems:

(1) In the repetitive working environment, TPS withstands a high temperature of 649 to 1,627°C, which exceeds the temperature limit of repeated use, and its main parts produce brittleness, edge peeling, overheating, cracking, coating peeling and other phenomena, and there is much damage to secondary parts (gap filler, thermal insulation coating, etc.).

(2) The heat-proof tile absorbs moisture, increases the weight, affects the turnover period, increases the cost, and reduces the payload entering the orbit.

(3) When the orbiter ascends and lands, due to changes in airflow and pressure, the durability of TPS decreases and produces elastic deformation, which needs to be repaired and replaced. TPS is one of the key technologies for the development of reusable space launch vehicle RLV. The RLV is severely radiated by the thermal currents of the main engine when it lifts off; after entering orbit, as the atmospheric pressure drops, the thermal air flow expands, enveloping the tail of the launch vehicle, generating convective heating; when the main engine is turned off, it is pneumatically heated; on re-entry flight, it is again pneumatically heated. At the same time, the RLV travels back and forth between the space stations, and there are low-speed and high-speed micrometeoroids and space debris collisions. Therefore, the internal structure and cryogenic storage tank of the RLV must be protected from high-temperature heat flow erosion and burn-out during launch and re-entry. In order to invest in inexpensive commercial operations and meet the needs of commercial market competition, the requirements for the TPS of RLV are as follows:

(1) Reuse at least 100 times and can fly smoothly in adverse climatic conditions.

(2) Easy to manufacture, easy to operate, light weight and good working performance.

(3) Resistant to collisions of low-speed and high-speed particle clouds and space debris, and resistant to aerodynamic thermal, acoustic and thermal loads.

(4) Easy to inspect, maintain and quickly replace heat-proof materials and reduce costs.

It is not difficult to see that the TPS requirements of RLV are higher and more complex than those of the Space Shuttle orbiter, which not only solves the problems of strength and durability between heat-resistant and waterproof materials and coatings in large areas, but also reduces material and manufacturing costs while ensuring performance and quality [14].

6.4.2: Metal Thermal Protection System [14~20]

1.Development and characteristics of metal thermal protection systems

The development process of metal thermal protection system can be divided into the following four stages: one is the metal bracket structure (the first generation of metal thermal protection system); the second is the titanium alloy multi-layer wall structure (the second generation of metal thermal protection system), the three-dimensional super alloy honeycomb sandwich structure (the third generation of metal thermal protection system, and the fourth is the improved metal thermal protection structure (the fourth generation of metal thermal protection system).

The first generation of metal thermal protection structures were primitive metal bracket pleated structures with no thermal insulation inside and were originally used on the leeward side of aircraft such as Mercury, Gemini, Apollo, and X-15. The second generation of the metal thermal protection structure is a titanium alloy multi-layer wall structure that uses a high melting point aromatic polyamide thermal felt, but it is very mass and insulating is insulating. The third-generation metal thermal protection structure belongs to the superalloy honeycomb sandwich structure, the upper surface is Inconel617 honeycomb sandwich panel, the lower surface is titanium alloy honeycomb sandwich panel, the middle metal box is filled with lightweight thermal insulation felt, and the surrounding is Inconel617 flat side panel, in which the superalloy honeycomb sandwich panel is composed of superalloy metal foil and superalloy honeycomb sandwich, which is a pre-packaged honeycomb sandwich structure. The fourth-generation metal thermal protection structure is an improved metal thermal protection system, the sandwich panel mainly plays the role of bearing and anti-oxidation, the support bracket plays the role of transmitting load, heat insulation and adjusting the thermal deformation mismatch, and the thermal protection system is connected with the main structure using low-temperature mechanical bolts and bolt conduits.

The characteristics of TPS are as follows:

(1) In addition to TPS, the metal panel also plays the role of a supporting structure, reducing the weight by 15% to 20% compared with the traditional space shuttle ceramic heat-proof tile.

(2) Durable, no need for waterproof, no need for pneumatic shell, low cost.

(3) When re-entering the atmosphere to fly, it can be used as a thermal protective layer to withstand 982°C: high temperature and protect the carrier from the high temperature and aerodynamic stress of the atmosphere.

(4) The metal panel is laid on the outer surface of the aircraft skin to protect the equipment and fuel inside from the impact of micrometeoroids and space debris, even if the micrometeoroids penetrate a small hole in the panel, because there is a buffer layer composed of thermal insulation fibers between the panel and the storage tank, the hot gas cannot enter or approach the storage tank.

(5) Metal TPS is plastic, rain-proof, and the flight is not limited by rainy days, while the brittle heat-proof tile cannot fly in rainy days and is limited by climatic conditions.

(6) The metal TPS panel is directly and firmly fixed to the internal parts of the carrier with special bolts, while the usual TPS thermal insulation material is glued to the outside of the body and is not firm.

(7) The ceramic heat-resistant tile on the space shuttle takes a long time to maintain and overhaul, and the cost is very high, taking 60 to 70 days between flights; metal TPS only needs 50 people, 7 days of maintenance and overhaul time, which greatly saves time and shortens the flight interval cycle; for repairs, simply unscrew the panel corner screws and replace them with new panels [14].

2. Metal panel TPS

Figure 6-16 shows the shape of the heat-proof structure of a single metal honeycomb panel (304.8 mm X 304.8 mm). The upper surface is made of a 0.127 mm thick sheet and a regular hexagonal honeycomb core (Inconel 617 alloy) with a thickness of 0.038 mm, a grid edge length of 4.763 mm, and a height of 7.1 mm. The lower surface is made of a 0.152mm thick sheet brazed with a honeycomb core (Ti-6A1-4V alloy) of the same size. The sides are 0.076 mm thick corrugated sheet (Inconel 617 alloy) with corrugated edges, and the upper and lower flanges are brazed into a box.

The inside of the box is filled with 0.lg/cm^3 Cerra-chrome and 0.056 g/cm^3 Q blanket quartz fiber insulation to insulate and maintain the integrity of the thermal protection structure. The installation distance between the panel box and the panel box is 5mm to compensate for the thermal expansion of the panel surface. The corrugated side of the box creates a gap cover that prevents hot air from flowing at the panel junction, and the flanged down of the panel box also prevents hot air from reaching the bottom. There are 4 fixing holes at 4 corners on the upper surface of the panel box for screwing bolts, and the hole pipe is brazed together with the upper and lower surfaces. Before installing the panel box, a 25.4mm thick felt strip is laid out with 4.8mm thick Nomex felt, then coated with RTV (room temperature vulcanized adhesive), pasted on the outer skin, and the bolts are screwed into the Nomex felt, and the thickness of the felt is pressed to half of the original thickness, the compressed Nomex felt prevents hot air from entering it, reduces the vibration caused by sound load, and can also generate pretension at the fixing bolt to prevent the bolt from loosening. The bolts are then covered with threaded caps at the 4 fixing holes, and all gaps are filled with fiber insulation to reduce heat transfer and form metal TPS. This TPS can withstand high temperatures of 982 to 1,093°C, and the internal heat protection material organizes hot air flow into the skin structure and forms the TPS structure as a whole.

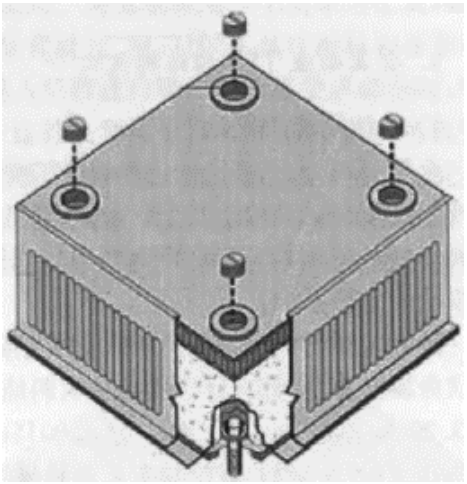

Figure 6-16: A pre-packaged ultra-heat-resistant alloy honeycomb TPS panel

3. TPS test of metal panels

In a simulated RLV flight environment, several properties of the TPS panel were tested. Experiments were carried out on the metal panels separately, and the arc heating jet test was carried out in a wind tunnel, where the arc provided a high-temperature airflow similar to that experienced by the vehicle during reentry.

Six different panel samples were placed in an arc-heated jet environment in a fuel chamber to verify the thermal and structural loads experienced by the panels during flight, and to verify the durability of the seals between the metal panels in a high-temperature flight environment. Aerothermal experiments were carried out in the wind tunnel of *Ma* = 8 in Hampton, Virginia, in which the high heat and wind shear of the panel were simulated during high-speed flight, and the panel structure was subjected to high temperature incoming flow of 1,093°C at *Ma* = 7. The design simulates the critical flight phase of the RLV to verify the durability and tightness of the panel when subjected to high-temperature supersonic flow. The maximum temperature of the outer surface of the TPS plate can reach 982 to 1037°C, while the maximum temperature of the inner structure is about 177°C, which also indicates that it has a good thermal protection effect.

Flight tests were conducted underneath the F-15 aircraft to verify the material's resistance to rain erosion above the speed of sound, with no signs of damage or wear at high speeds at *Ma* = 1.4 and an altitude of 10,973 m. The overall testing of the thermal protection system was also carried out in a special facility specially developed for the X-33 Advanced Technology Demonstrator in an environment capable of simulating supersonic speeds. Metal panel assemblies withstand the thermal, acoustic, compressive, and vibration loads experienced by the simulator. At Wright Pratt Air Force Base, the test facility simulates temperature, vibration and noise during take-off, ascent and rapid heating, and the X-33 Advanced Technology Demonstrator's panels are subjected to thermal, vibration and acoustic tests to verify the durability and longevity of the panels and seals.

4. Structural optimization of TPS for metal panels [21]

1) Optimization of the overall structure

Metal TPS opens up possibilities for many design optimizations. Superalloy metal foils of different thicknesses can be fabricated and attached to complex structural shapes. Metallic TPS can be integrated with many different kinds of substructures. For substructures with smooth surfaces, metal TPS panels can be assembled directly. For very rigid structures, a support structure for a thermal protection system is required.

Figure 6-16 shows the typical structure of a pre-packaged ultra-heat-resistant alloy honeycomb panel metal thermal protection system, which mainly includes a foil-like metal outer box. There is a fibrous insulation material structure inside; the outer surface of the metal outer box is a honeycomb sandwich panel with a skin thickness of 0.005in, a honeycomb core model of 0.0015in thickness, and a 3/16in honeycomb core. The side surface of the metal outer box is a 0.003in thick metal bubble to reduce thermal and mechanical pressure. The honeycomb sandwich skin is made from Inconel 617, a nickel-based ultra-heat-resistant alloy that allows TPS to be operate temperatures of 1,800 to 1,900°F[1] and even at temperatures as high as 2,000°F. On the adjacent edge of the panel, the outer skin extends about 0.3in of the flange to form a gap sealing cover, which is mainly used to block the gap of the adjacent, windward panel and prevent hot air from entering the gap between the plates. For the LFT2 panel, a gap of 0.2in is required to meet the thermal expansion of the outer skin of the panel. The size of the gap depends on the size of the deformation of the structure. The opposing lower flange acts as a base plate for the gap between the plates, accommodating the hot air flow in the gap. The super heat-resistant alloy TPS is mechanically connected to the spacecraft structure. The clamping access pipe provides a passage from the outer surface of the TPS panel to the inner surface of the panel, and the diameter of the hole on the inner surface is smaller than that of the clamping access tube. The clamping pressure is against the bottom of the tightening passage pipe to maintain the tight binding of the metal TPS to the structure. The tool can be clamped and loosened inside the tightening passage tube. There is a threaded end cap for the clamping access pipe that seals the clamping access pipe while the metal TPS is working. The clamped access tube is filled with fibrous insulation to reduce heat transfer.

[1] K = 5/9 (°F + 459.67), as below.

A 1-in-thick ribbon of high melting point aromatic polyamide is laid underneath the gap between the plates and is coated with RTV adhesive to prevent thermal short circuits. The mechanical clamping device clamps the compressed insulating felt to about half of its original thickness. Pre-clamping not only prevents heat flow under the panel, but also dampens vibrations from vibrations and acoustic loads, while at the same time providing a safeguard against loosening of fasteners. Preventing heat flow to the structural part is the main function of the insulation material inside. The metal box maintains the integrity of the TPS structure; poor durability, but effective insulation material is placed inside the metal box to form a pre-packaged ultra-heat-resistant alloy honeycomb panel metal thermal protection system.

After the end of the X-33 program, the NASA Langley Research Center continued to develop metal TPS, the next generation of which was to use ultra-heat-resistant honeycomb instead of the current Inconel sidewall, and use low-density insulation material inside, which had the advantage of sealing on its unheated plates and opening vents so that the external heating plates were not subjected to aerodynamic pressure. Many concepts of metal thermal protection systems have been improved. Figure 6-17 illustrates the next-generation super-heat-resistant alloy honeycomb TPS concept, which is a significant improvement over the existing metal TPS. At the same time, it is hoped that advanced heat protection materials can improve thermal insulation properties and reduce the quality of metal TPS. Improved brazing manufacturing techniques can make weight and cost significantly reduced. Improvements in several structures will further reduce quality and manufacturing costs, as well as increase operability. The lower flange can be omitted, making individual panels easy to remove without the need to disassemble adjacent panels. The lower surface can be further lightened and simplified by using a simple titanium frame, on which the metal foil is mounted, instead of using honeycomb panels with local cuts. However, the most innovative and effective modification is the use of quick disassembly and clamping devices. The clamping device uses a simple metal paper clip to fasten a pin-like structure to the structure. The clamping device is relaxed by gliding the "scissor-like" tool over the panel and the hold-down end. The gap cover has a narrow groove that the tool can insert for operation. As the panels expand when heated, the gap between the plates begins to shrink and the slider slides towards the adjacent panels. This clamping concept has no disassembly parts and can be operated quickly and easily, significantly reducing costs and the hassle of clamping tubes and clamping tube end caps. A proof of concept is possible, but the specifics are still being worked out. At the same time, increasing the size of the metal TPS panel (from 12 in^2 to 18 in^2) can also significantly reduce the total volume and save costs. The disadvantage is that the structure is too complex and there is a problem of matching the heat on the outside and inside, mainly because there must be a certain gap between the individual structures, from which radiant heat can enter the burned internal structure and the mass is also increased. NASA-Langley has further developed a super heat-resistant alloy honeycomb TPS panel, ARMOR (Adaptable Robust Metallic Operable Reusable), adaptive high-reliability metal reusable) TPS, to further improve and optimize this design. The side wall is arched, as shown in Figure 6-20, and is used to seal the gap between adjacent plates. The side walls are made of metal foil and do not assume the function of the structure, but only the function of sealing the internal insulation and the gaps between the plates. However, the corners of these "bow”-shaped sidewalls become new points of thermal pressure, which creates new problems.

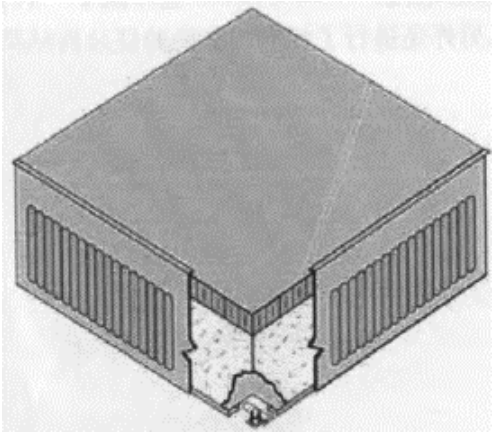

Figure 6-17: Next-generation prepackaged metal TPS board

2) Optimization of highly heat-resistant skin

In the design of Figure 6-16, the lower surface is a titanium honeycomb sandwich panel composed of a 0.006-inch thick skin and a 0.0015-in-thick 3/16-inch honeycomb core. In Figure 6-17, the inner surface of the 0.006-inch metal box is now made of Ti 6A1-4V titanium alloy foil. This reduces weight and simplifies the structure.

In the middle of the panel, the skin of the sandwich panel is chemically milled to a thickness of 0.003in. In the current concept, the chemically milled skin and honeycomb core below are simplified, and in order to reduce weight, a 0.003-inch foil is placed on the inner skin of the lower sandwich panel as a frame of compressed insulation. The lower honeycomb sandwich panel is used to stabilize the lower edge of the side. The lower surface of the panel has a through hole, which is covered with a mesh sieve to prevent liquid water from entering, discharging the pressure inside the panel from the surrounding environment, and limiting the pressure difference between the metal box and the metal box. Improved exterior honeycomb sandwich panel side panels can be made with PM 2000, a higher superalloy material. PM 2000 is an iron-based oxide discretely reinforced alloy that forms a layer of alumina oxide coating with good static oxide and impedance up to 2400°F. The test plan uses hot gas and arc heating environment to evaluate the material properties. If this alloy is suitable for the environment, it will significantly expand the range of applications for uncoated metal TPS.

3) Structural optimization of thermal insulation materials

Chromium at a density of 6 lb/ft3 and 3 Q felt fiber insulation with a density of 3.5 lb/ft3 were used in earlier TPS designs. In the current design, a lighter 3.01b/ft3 Saffil alumina fiber insulation is used. In order to further reduce the mass of the system, other insulation materials are also being studied. Insulation improvements include the coating of Saffil alumina fibers, better reflection of radiant heat and internal multi-screen insulation. Metal TPS considers several types of internal insulation. Figure 6-18 shows two different types of thermal insulation. Saffil alumina and IMI. Saffil alumina, manufactured by ICI Chemicals and Polymers Limited, is a fibrous insulating material with fine aluminum fibers (3 μm diameter) inside. Saffil alumina has many advantages as an internal TPS insulator, but there is no good characterization of the thermal properties of TPS applications. IMI, manufactured by MAN Technologies, has a multi-layer reflective screen separated by a fiber insulating base inside. The foil is a thin C/SiC composite layer structure coated with a reflective coating of gold or platinum. The reflective layer is separated by a thin layer of Saffil alumina or quartz fiber insulation. Preliminary steady-state thermal tests conducted at MDA have shown that the thermal conductivity of the special configuration IMI is half that of an equivalent mass of Saffil alumina. MAN Technologies uses its own thermal analysis program to design IMI stacking for special structures. NASA LaRC has also developed a thermal analysis program to predict the thermal properties of multi-layer insulation materials such as IMI and has also conducted experiments to verify the results.

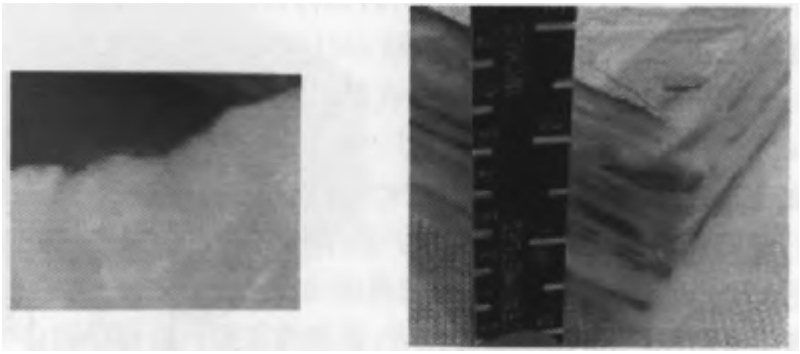

(a) Saffil alumina fiber (b) Internal multi-layer insulation

Figure 6-18: Thermal insulation structure inside a metal TPS

NASA Langley is also funding research into reflective coatings on Saffil alumina fibers that reduce thermal conductivity. Several coatings have been successfully applied to Saffil alumina using an inexpensive melt gel process, however, there is no good way to evaluate the effectiveness of the coating during the development of the coating. The Small Business Innovative Research (SBIR) program, funded by the NASA-Ames Research Center, has conducted research on another type of internal thermal insulation structure, primarily the development of a multi-layer thermal insulation structure.

Similarly, this thermal insulation structure also needs to be used to characterize the properties of TPS applied to metals.

4) Optimization of the assembly of a single metal thermal protection structure

The assembly of individual metal thermal protective structures optimizes TPS and liquid storage tanks for flight cycle testing, testing from cryogenic temperatures to extreme temperatures in excess of 1,400°F. A wide range of temperature and pressure variations can cause differences in the thermal expansion and contraction of the TPS and the tank, so the two must be matched to avoid damage to the TPS. The displacement of the bolt holes of the four bottom corners of the TPS connected to the outer rigid frame underneath is the same as that of the directly coupled tank. The bolt is fixed at one corner of the TPS, but the bolt on the other corners can be moved inside the expansion slot at the bottom of the TPS. The design of the expansion tank is mainly to constrain the translational and rotational degrees of freedom of the TPS plate, allowing the free expansion and contraction relative to the storage tank.

The corner bracket is a highly load-bearing structural component on the ARMOR TPS plate, as shown in Figure 6-19. Each component needed to meet relatively contradictory requirements: (1) provide adequate structural connections for the outer honeycomb sandwich panel and the inner titanium alloy frame; (2) prevent heat conduction between the outer surface of the high temperature and the internal structure of the low temperature; (3) adapt to the thermal expansion matching of the outer surface and the internal titanium alloy frame. The corner brackets are not designed to be straight, and the basic design method is to use a thin sheet of metal that is easy to bend in one direction and not easily deform in other directions. Sheet metal is placed on the corners of the plate, arranged on an arc tangent to the center of the panel. In this way, the outer honeycomb panel and the inner frame can be freely expanded by heat, and the constraint of the corner brackets connecting the two is minimal. However, the corner bracket is to bear the compressive force of the aerodynamic load, so the middle part of the bracket should be arranged as a rigid bead-like protrusion to prevent locking. The two ends of the corner bracket should be connected flexibly to accommodate the mismatch of thermal expansion. Corner brackets are machined to be very thin, mainly to reduce the thermal conductivity transferred from the outer surface to the interior, reducing bending stiffness and stress. According to the model of finite element analysis, the width, thickness, and convex geometry of the corner bracket are determined, and their optimal proportions are determined. The corner bracket is made of Inconel 718, mainly because of its high stress range values and its good creep resistance at elevated temperatures.

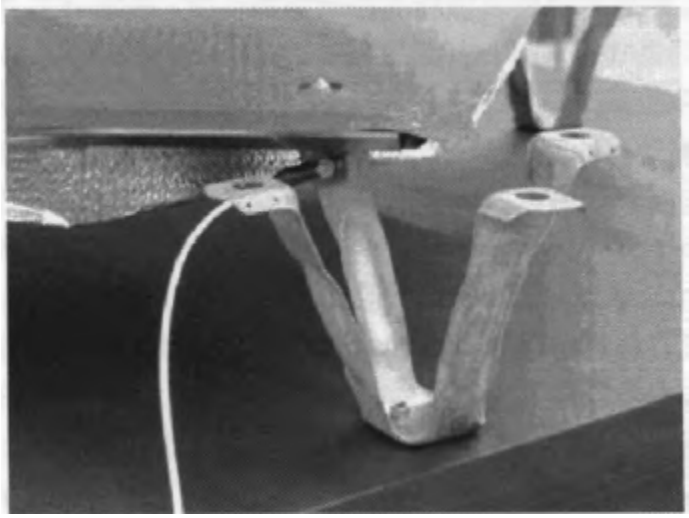

Figure 6-19: Bracket concept in a metal TPS board

5) Optimization of the assembly of multiple metal thermal protection structures

The materials and manufacturing techniques used for the X-33 Metal Thermal Protection System are broadly similar to those of the Ultra Heat-Resistant Honeycomb TPS, but the assembly parts vary greatly. The X-33's metal TPS forms a parachute that carries the aerodynamic pressure on the outer surface.

Each TPS panel consists of a super heat-resistant alloy sandwich screen with internal insulation and encapsulated by metal foil. Each plate is mechanically attached to the metal support frame at the corners. The extended metal foil overlaps to seal the gaps between the plates. Since the TPS is designed to carry the aerodynamic pressure of the external heating surface, the gap between the plates must also be able to carry the aerodynamic pressure to prevent the hot air from flowing through the metal and burning the internal structure. Experiments have shown that this lap seal is very effective, but it is only suitable for the relatively short heating history of the X-33, and if it is applied to the RLV, it needs to be significantly improved.

Another design problem was how to assemble the metal TPS with the underlying structure. For ARMOR metal TPS plates, cooled, mechanical clamping of the local surface is chosen. The mechanical fastener connects the corners of the titanium box inside to the substructure. The vertical, fold-box clamping access tube provides a mechanical clamping access for the exterior surface and internal structure. The Tightening Access Pipe uses a plug-in structure on the outer surface section to clamp the end cap of the access pipe to form a smooth and continuous outer surface. The clamping access tube is filled with fibrous Saffil alumina insulation. The holes in the frame structure inside the titanium are connected to the substructure by clamping fasteners and are slotted to accommodate the mismatch between the thermal expansion of the internal TPS plate and the substructure.

TPS is integrated with the outer surface of a rigid composite cryogenic tank. Development of a lightweight, thermally adaptable TPSSC (TPS support system) for thermal protection systems of titanium metal foils, connecting ARMOR TPS with cryogenic storage tank structure. Figure 6-20 shows the assembly of the ARMOR TPS plate and the cryogenic storage tank. TPSS or contact surface structure to realize the connection between TPS and the metal cover on the outer surface of the rigid storage tank. The design of TPSS needs to consider the following issues: (1) it must be able to transmit the mechanical load from the TPS to the storage tank structure; (2) provide a rigid grille structure to support the sealing around each TPS plate; (3) it can alleviate the thermal and mechanical thermal strain of the tank structure caused by the thermal pressure caused by the mismatch of the thermal expansion of the TPS plate(4) At the same time, the quality of the system cannot be increased.

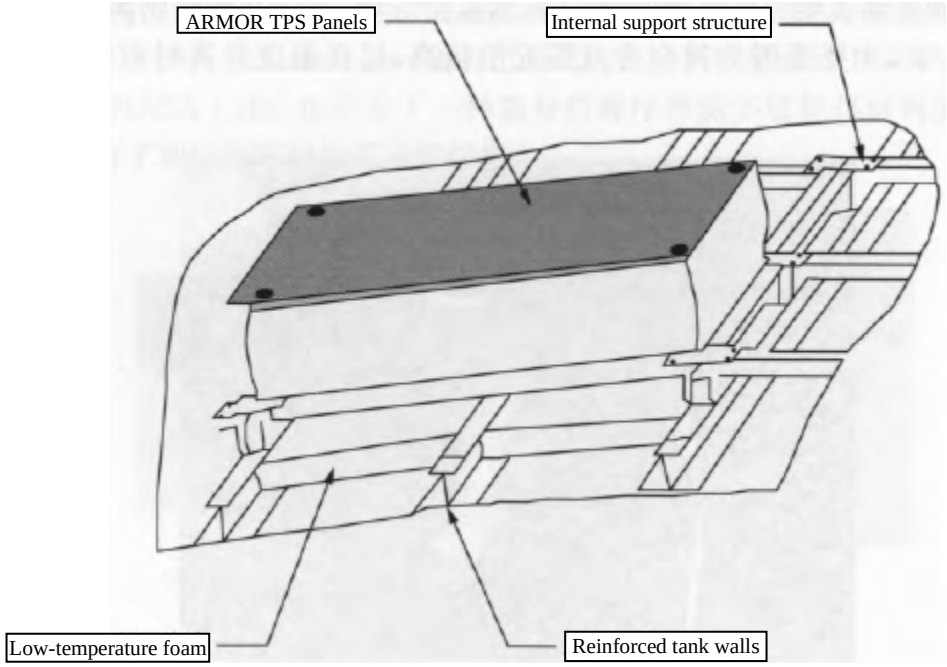

Figure 6-20: Assembling the ARMOR TPS with tank structure

TPSS is cold-formed from titanium foil and spot welded to the desired shape. The titanium sheet is mechanically connected to each corner of the assembly that is mechanically attached to the outer cover of the TPS panel. The two brackets of the frame are spot-welded together with each corner assembly. The other two plug-ins to be assembled, plugged into the bracket of the frame, provide a gliding connection that accommodates the mismatch of strain.

The brackets of each frame are titanium sheet box beams spot welded together. The bottom of each angular assembly is mechanically attached to the winding skin cover of the tank. TEEK8 low-temperature foam insulation is bonded between the outer surface of the tank and the rigid body [21].

6.4.3: Thermal insulation materials for metal thermal protection systems

The metal thermal protection system is composed of a three-layer structure of superalloy honeycomb cover on the surface, thermal insulation material and titanium alloy honeycomb panel on the inside. The surface is covered with a superalloy honeycomb cover to resist the impact of foreign objects during launch and flight. During the re-entry of the aircraft, the surface cover is heated by severe aerodynamic heating, reaching a maximum temperature of 1,100°C, while the fuselage is made of aluminum alloy, with a maximum design temperature of 176°C, and the function of the intermediate heat barrier material is to isolate the temperature difference above 900°C.

Due to the advantages of low thermal conductivity, large heat capacity and low cost, fiber insulation has always been the preferred material for spacecraft thermal protection system. The main function of fiber insulation is to limit the heat flux that enters the body. The Space Shuttle ceramic thermal insulation tile and thermal insulation felt are made of high-purity silica fiber. The X-33 was developed using Saffil thermal felt, a high-purity, polycrystalline ceramic fiber capable of operating temperatures up to 1,600°C. It is composed of 96% alumina and 4% cinnamon dioxide, and also contains components such as sodium, calcium, iron, nickel, magnesium and chloride, and the fibers have a melting point of up to 2,000°C and an average diameter of 3 μm. Although NASA discontinued the X-33 program in 2001, a metal thermal protection system was developed during this time, and thermal load tests were conducted at the Ames Research Center in an arc jet environment, and the panels were tested at 1,093°C in a wind tunnel at the Langley Research Center $Ma = 7$ to simulate high-speed flight. Tests have shown that the use of Saffil thermal insulation felt as an insulating material can fully meet the thermal insulation requirements of the design.

At present, the fiber insulation materials mainly include thermal insulation felts made of silica and aluminum oxide fibers. The finer the fiber diameter and the higher the purity of silica and aluminum oxide, the lower the thermal conductivity of the fiber insulation. However, the smaller the diameter of the fiber and the improvement of the purity, due to the limitation of the existing production process, it is difficult to reduce the thermal conductivity of the fiber insulation material by reducing the diameter of the fiber and improving the purity. In order to further reduce the thermal conductivity of fiber insulation, it is necessary to improve fiber insulation. Because thermal radiation is the dominant term for heat transfer at high temperatures, inhibiting thermal radiation in fiber insulation materials has become an effective way to reduce the thermal conductivity of fiber insulation materials.

On the basis of fiber insulation materials, multi-layer thermal insulation materials are also developed, mainly to reduce the thermal conductivity of thermal insulation materials by inhibiting the transmission of heat radiation. It is mainly composed of a heat shield and a fiber heat insulation felt in the middle of the heat shield. The substrate of the thermal insulation felt is made of carbon/silicon carbide composite sheet, which mainly takes into account the temperature at which the thermal insulation screen is used. A layer of gold or platinum is applied to both sides of the carbon/silicon carbide composite sheet using a vapor deposition process, due to the very low emissivity coefficients of gold and platinum at high temperatures. Experiments have proved that the thermal insulation effect of multi-layer thermal insulation material is indeed better than that of fiber insulation material in the process of aircraft reentry. Although the thermal insulation performance of multi-layer insulation materials is better than that of fiber insulation materials commonly used today, multi-layer insulation materials also have their disadvantages. Heat shields are too expensive to manufacture for large-scale use on reusable spacecraft. Therefore, in order to make the thermal insulation material used on the metal thermal protection system on a large scale, it is necessary to have both low cost and good thermal insulation performance, which requires the search for new solutions.

In addition, there are nanocomposite coatings to improve the fiber insulation material through the combination of stacking method and nanotechnology, that is, to improve the thermal insulation performance of the fiber thermal insulation felt by increasing the reflection of thermal radiation, which has the advantages of low production cost, small increase in quality, and obvious improvement in thermal insulation performance.

6.4.4: Thermal Analysis Methods for Metal Thermal Protection Systems [22-27]

The peculiarities of the structure of the metal thermal protection system determine the peculiarities of the thermal analysis. The metal thermal protection system itself has a complex structure and is composed of several parts, taking the superalloy honeycomb structure thermal protection system proposed by the United States during the development of the "X-33" space shuttle as an example, from the outside to the inside, it is a high-temperature coating, an upper honeycomb layer, a multi-layer thermal insulation, a lower honeycomb structure, a sealing felt, and then an internal cold structure. The four corners are connected to the internal structure with bolts, and there are small gaps between and under the plates.

Because the flight environment of the launch vehicle is harsh, the thermal analysis of the metal thermal protection system is much more complex than other projects, which is mainly manifested as: (1) The gap cannot be ignored, the heat transfer of the gap must be specially studied, and the insulation and honeycomb core also contain air. (2) The nonlinear behavior of the material is prominent. Because there is a large gradient of pressure and temperature variations, there are variations in the values of material properties. (3) The coupling of conduction, convection and radiation heat transfer modes makes it difficult to solve, with low solution efficiency and large error. (4) In thermal analysis, there are not only solid heat conduction, but also gas heat conduction and convection heat transfer. In solid thermal conductivity, there is both metal thermal conductivity with a large thermal conductivity coefficient and multi-layer thermal insulation with a small thermal conductivity coefficient to conduct heat. (5) There is a thermal short circuit phenomenon in the bolt, and sometimes the thermal short circuit will cause the failure of the whole protection system.

The main methods of thermal analysis of metal thermal protection system are:

1) One-dimensional finite element model

A simple one-dimensional finite element model can be used to model heat transfer in the direction of the thickness of the thermal shield. The elements and nodes are divided in the thickness direction, and the one-dimensional thermal conduction unit connects the nodes in the thickness direction of the thermal protection plate. The interpolation of the temperature values of each node is used to approximate the temperature field distribution in the thermal protection plate.

Complex models can also use 1D elements, but with multiple parallel heat transfer paths in the plate thickness direction. This allows nodes on different heat transfer paths to be parallel in the same plane to have different temperature values. At present, most of the thermal analysis of thermal protection systems in foreign countries uses the method of one-dimensional thermal model, and examples can be found in the literature [22].

However, the 1D model does not accurately simulate the heat transfer and temperature distribution of the entire shield, especially at the edges, connectors, and stiffeners. The biggest disadvantage of the 1D element model is that it ignores the thermal short circuit phenomenon of the plate edge and the gap between the plates, which are parallel to the plates. Two- and three-dimensional finite element models were proposed.

2) Two-dimensional finite element model

The 2D finite element thermal model is used not only for heat transfer analysis along the thickness direction, but also for heat transfer analysis in the same plane. Compared with the one-dimensional element model, the two-dimensional element model is a model with a complex structure and poor efficiency, but its accuracy is relatively high.

Max L. Blosser of NASA proposed a variable-thickness two-dimensional model, which is a thermal model with the same thickness substructure as the metal thermal protection system plate, which is a hybrid model between the two-dimensional and axisymmetric models. The element thickness can be changed so that the 2D model can simulate axisymmetric thermal conduction within the plate.

This method not only simulates the thermal short-circuit effect within the plate and at the edges of the internal structure, but also does a good job of simulating the two modes of heat transfer, radiative and conductive, away from the gaps in the corners of the plate. The units of the plate edges, support frames and mechanically connected fasteners are appropriately sized to simulate thermal shorts per unit area of the shield. Honeycomb structures, felt gaskets, thermal insulation, and air in crevices are also simulated with 2D heat conduction units. This 2D model can be used to simulate the deformation of a 3D thermal shield. According to the variable-thickness two-dimensional finite element thermal analysis model, a similar model of the superalloy honeycomb thermal protection plate is proposed.

3) 3D finite element model

The 3D finite element model can represent a heat transfer analysis in 3 directions in space.

This approach also requires more time to study and build the model than a simple model. For example, the thermal analysis model of two superalloy thermal shields for thermal testing at NASA's Johnson Space Research Center in the United States. For a quadripartite thermal shield, the 3D model can represent the entire plate with 1/8 of the plate, depending on the symmetry of the plate geometry and the symmetry of the structure and boundary conditions.

Of course, in the thermal analysis of the metal thermal protection system, because the thermal conductivity coefficient of the metal is large, the local thermal short circuit phenomenon is relatively small, so the error of the one-dimensional and two-dimensional models is relatively small. For structural materials with low thermal conductivity, such as C/C composites, especially at the connectors, it is necessary to use a 3D finite element model [24,25], otherwise there will be large errors and even serious error results.

4) A mixed model of three element types

Of course, when performing thermal analysis of metal thermal protection system plates, it is not necessary to use only one model, and the corresponding model should be established according to the need. For example, 3D elements are used for complex structures such as reinforcements, 2D elements are used for gaps between plates, and 1D elements are used for simple structures. The three-element type coupling algorithm can take full advantage of the advantages of the three elements to calculate the thermal protection system board temperature distribution. 3D finite element analysis is used for volume analysis and 2D finite element analysis is used for gaps.

The analysis method of metal thermal protection system needs to be further developed, and the existing problems and solutions are summarized as follows:

(1) The coupling effect of heat transfer mode. Heat transfer in metal thermal protection systems for reusable vehicle vehicles is particularly complex. Finite element models are computationally inefficient and often produce erroneous results. For example, the heat conduction equation is the temperature derivative equation, and the radiation equation is the 4th power of temperature, which is easy to cause the equation to be combined when solving in association. At present, the general treatment method is to use parallel models, that is, to use computational models in thermal analysis models, one is the calculation of heat conduction units, and the other is the calculation of radiation units. For example, a parallel model is used in a one-dimensional model to solve this problem. In order to study the decoupling algorithm of nonlinear equations, a unified equation of heat conductivity and radiation should be established to achieve the overall solution.

(2) Three-dimensional model research. In foreign countries, one-dimensional and two-dimensional models are mostly used in thermal analysis research, and three-dimensional models are used locally. With the rapid development of computer technology and the popularity of parallel computers, it is feasible to adopt 3D models.

(3) Application of spatiotemporal finite elements. In all current reports and literatures, the solution of the transient heat transfer equation is generally based on the assumption that time t is a fixed value, the unsteady state problem is transformed into a steady-state problem to solve the differential equation, and then the finite element method is used to discretize the calculation in space, and then the time is discretized by the difference method [27]. In the same differential equation, time and space are discretized in different ways, which is easy to cause the problem of slow convergence and oscillation of the result. The space-time finite element method is a method that has just been developed in recent years, which discretizes time and space at the same time, with fast convergence speed and stable results.

(4) Thermal conductivity of gradient coatings. In order to improve the crude sugar content of the surface, prevent catalysis and insulate the heat, the outermost layer of the metal thermal protection system is coated with a high-temperature coating. There are few reports on the research of this thin high-temperature coating at home and abroad. Because the distribution of the material inside the coating is inconsistent and the scale is small, it will cause a large error to describe it with the general heat transfer equation, so it can be studied by the microscale heat transfer theory. This is one of the current directions of thermal analysis research.

(5) Thermo-mechanical coupling problem. Under high temperature conditions, how to calculate the combination of heat and stress, how to coordinate the deformation of structures caused by thermal stress, the failure mechanism of thin layers, and the contact of connectors need to be studied in depth. In order to improve the overall effectiveness of the thermal protection system and reduce the weight, the best way is to carry out the thermal analysis and internal structure analysis and design of the thermal protection system at the same time. Further research is needed on the heat transfer of multi-layer insulation in metal thermal protection plates, the analysis and calculation of thermal stress, the establishment of fatigue failure criteria for thermal protection systems, and the realization of the integrated optimal design of aircraft structures in the real sense.

6.4.5: Health monitoring technology for thermal protection systems [28]

In order to reduce the loss of spacecraft and astronauts, the United States and other Western countries have been researching spacecraft fault diagnosis technology since the 1950s. In the 1970s, the concept of integrated health management (IVHM) for spacecraft was proposed. A spacecraft integrated health management (IVHM) system is a collection of tools and behavioral processes used to automate spacecraft health management behaviors. It is an integrated health management system that integrates system status monitoring, fault diagnosis and fault repair. It contains a ground health management (IGHM) system and an on-board health management (IVHM) system. But both are built on the basis of health monitoring in various subsystems. Among the many monitoring locations on spacecraft, thermal protection (TPS) is the most critical. Because if there is undetected damage in the thermal protection system, the consequences can be catastrophic. For example, in February 2003, the accident of the Columbia space shuttle in the United States left seven astronauts in space forever.

The development of thermal protection system has appeared in a variety of structural forms, including a variety of thermal insulation felt (tile) forms, sandwich structure forms, titanium multi-layer wall structures, metal heat-proof structures, and heat-proof structures of C-C panels, which are connected to the fuselage structure either directly on the surface or bolted to the fuselage. Metal thermal protection systems and C-C panels are considered to be the most promising forms of heat protection and are the key technologies for realizing the Reusable Aircraft (RLV) program.

In harsh flight environments, thermal protection systems can be damaged in many forms. For example, the loosening or even falling off of the connecting bolts, the cracking and burning of the skin, the temperature of the structure is too high, the coating is damaged, the panel is cracked, and so on. If any of the failure forms cannot be detected and dealt with in time before launch, it will lead to a series of negative reactions in the re-entry process, such as the destruction of the entire vehicle and the casualties of astronauts.

In addition to safety requirements, there are two other requirements that require the development of a new health monitoring system, namely cost savings and reduced grounding time. After a spacecraft has completed one flight, it must be inspected, repaired and replaced before the next flight. Current maintenance is largely manual, and with about 20,000 heat protection tiles on the shuttle, it now takes months and costs a lot to complete a single inspection. NASA's second-generation RLV aims to save costs by an order of magnitude in the medium term, and the long-term plan is to save costs by two orders of magnitude. At present, 25% to 30% of the average service cost of military or commercial aircraft is spent on inspection and repair. The goal was to be able to fly again in a few days. The key to achieving these two goals is to reduce the cost and time of ground operations and to develop more cost-effective and efficient structural health monitoring systems, which have led to the development of TPS health monitoring research.

For the health monitoring research of cover type heat-proof structure, there are two main aspects restricting its development: on the one hand, its application environment, and on the other hand, its complex structural form.

From the environmental point of view, due to the special application environment of the thermal protection system, it is very difficult to monitor its health, which can be summarized in the following six aspects:

(1) How to choose the right sensor so that it can detect all forms of damage.

(2) How to integrate the sensor into the existing system without changing the existing structural form.

(3) How to design the sensor so that it has the least impact on the structural performance, the least increase in quality, and the least increase in cost.

(4) How to distribute the position of the sensor, not only to ensure its sensitivity, but also to ensure its safety.

(5) How to develop an algorithm that can quickly realize damage detection.

(6) How to localize, quantify, and even estimate the life expectancy of the damage.

From the perspective of structural form, there are mainly two forms of cover-type heat-proof structure at present, the difference is only in the panel, that is, one panel is carbon/carbon composite material, or carbon/silicon carbide, and this form is used in high-temperature areas such as nose cone and wing front; another form of panel is metal honeycomb sandwich panels, which are used to protect the large area of the fuselage from heat, but the complex form of metal honeycomb sandwich panels makes health monitoring more difficult.

The panel-type TPS structure is mechanically connected, making it easier to maintain and inspect than TPS tiles connected by adhesive bonding. However, the panel structure also caused the problem of loose bolts, and the damage of the panel, which combines load-bearing and heat-resistant functions, is also a big problem. Damage to the thermal protection system can be divided into four levels: (1) loosening of the bottom of the bracket; (2) loosening of the panel; (3) impact; (4) severe plate damage. As shown in Figure 6-21, these four levels are the main part of monitoring.

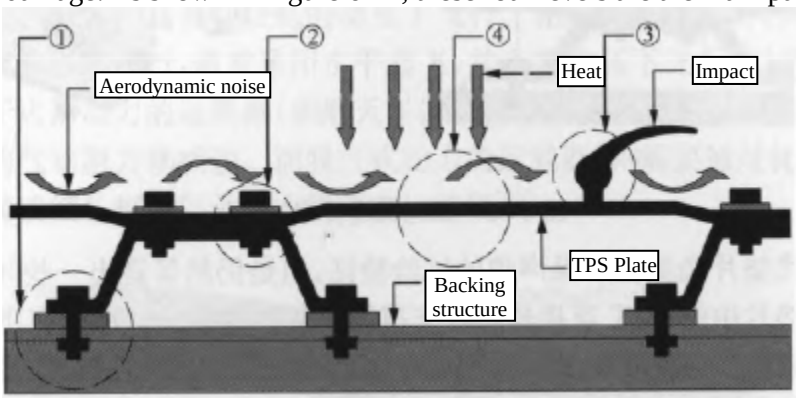

Figure 6-21: Schematic diagram of TPS health monitoring

As the basis of structural health monitoring, damage detection has been a very active research field for a long time, and there are many detection methods, but technically it can be divided into methods based on modal analysis and methods based on test signal processing. There are many methods for processing signals, but in general, they can be classified into two categories, that is, one is to analyze the response signal in the time domain; one is to find the non-time-domain characteristics of the signal, such as signal peaks and energy integration, and identify the damage to the structure by comparing these values. For the cover type heat shield with mechanical connection, the general detection idea is to use the pitch-catch method for detection, that is, the diagnostic wave is sent from the brake, and then the sensor receives a signal with damage information and analyzes the health state of the structure through the signal change caused by the damage.

The special application environment of the heat protection system requires sensors that can be integrated into the structure without changing the existing configuration of the structure, enabling the monitoring of critical damage. Researchers from Stanford University proposed a hierarchical monitoring idea for the cover-type thermal protection system, that is, without modifying the structural configuration, make full use of the characteristics of piezoelectric ceramics (PZT) that can be used as both a brake and a sensor to complete the damage detection. In order to detect the four damage types shown in Figure 6-21, the original sensor configuration is shown in Figure 6-22(a), and the two cylinders in the gasket are piezoelectric ceramic materials with a diameter and height of 6.35 mm. With a thin electrode layer at the bottom of the piezoelectric ceramic to connect the external wires, this gasket structure is easy to integrate into existing systems while meeting the sensitivity and durability of the product. For level 1 it can be done by two PZTs buried in one spacer, one as a brake and one as a sensor.

For Level 2, a pair of PZTs at one end of the bracket acts as a brake and a pair of PZTs at the other end act as sensors, and the diagnostic wave propagates along the bracket and is reflected in the response signal if there is a looseness in the panel connection. Unlike other levels, Level 3 relies on an external excitation source and uses a passive sensor network for detection, i.e., all PZTs are implemented as sensors. Level 4 is a severe destruction of the fingerboard, which can be achieved by a pitch-catch configuration between the brackets, with all 4 PZTs in one bracket acting as actuators and 4 PZTs in the other bracket acting as sensors. The addition of brakes will improve remote monitoring capabilities and will also improve the reliability of the system.

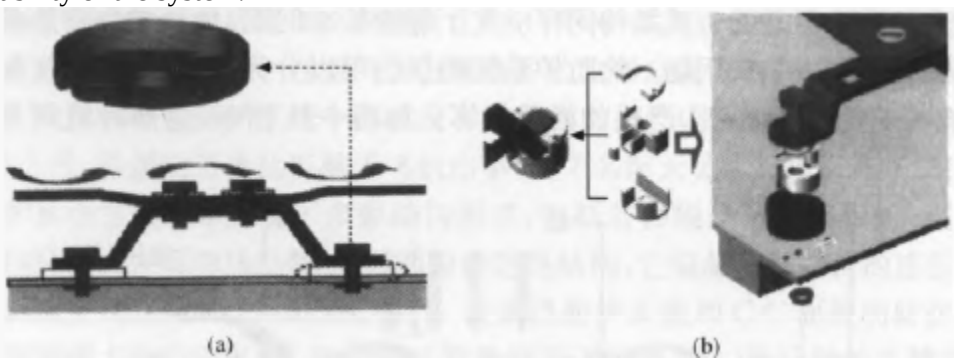

Figure 6-22: Piezoelectric ceramic sensor gasket

Although the first generation of gaskets has withstood the test and verification of noise furnaces, it still exposes some problems: (1) durability problems. The PZT in the first generation gasket is directly exposed to the contact surface of the support structure. In flight, there is a possibility that the sensor will fail under extreme mechanical loads. (2) due to the direct contact between PZT and the backing structure, the sensitivity of the sensor is affected. (3) the sensitivity of level 2 damage detection is low, and there is the interference of level 1 to level 2, and when the bottom of the bracket is loose at the same time as the panel, it is difficult to detect the looseness of the panel in this configuration. Therefore, in order to improve durability and sensitivity, the first generation prototype had to be modified.

Figure 6-22(b) shows a modified version of the first-generation configuration and the final second-generation gasket structure. Both modified and second-generation sensor gaskets are constructed of several parts, and the embedded PZT does not need to be in direct contact with the support structure. For this new configuration, the diagnostic wave coming out of the brake is mainly propagated along the bracket and does not dissipate into the backing structure as in the original configuration, so a high sensitivity can be obtained, while reducing the static pressure applied to the PZT and reducing the possibility of sensor failure. Another advantage of the second-generation design is that the number of PZT sensors is halved, the amount of data for signal analysis is reduced, and it is easy to wire.

In the future, damage detection should be developed to five levels: (1) identify whether there is damage in the structure; (2) determine the location of the injury; (3) identify the type of injury; (4) quantification of injury severity; (5) estimate the remaining life of the structure. Current research, particularly in the area of health monitoring of thermal protection systems, is limited to the first two levels. Therefore, the judgment of other types of injury, the quantification of the degree of injury, and the prediction of remaining life are the focus of future research.

The current research methods mainly rely on the processing of experimental signals, so the study of signal processing methods is one of the directions of research development. Of course, in order to realize the health monitoring of the structure in essence, it is necessary to deeply analyze the structure form and materials, understand the damage mechanism, grasp the impact of damage on the detection signal, and realize the interpretation of the damage signal from the theoretical analysis. At present, there are few studies in this area, and it will be the direction of future research efforts.

In addition, a sensor device that records temperature and other information with a microchip integrated into an RFID circuit and communicates with the outside world by wireless transmission. They are mainly realized in the monitoring of temperature, and future research will inevitably develop in the direction of wireless communication, miniaturization of sensors, and multi-functionality of sensors.

6.5: Thermal protection systems and structural components for air-breathing hypersonic vehicles

6.5.1: Technical difficulties in thermal structure

For air-breathing hypersonic vehicles, the aerodynamic/thermal, propulsion system and airframe are highly integrated, so the thermal protection system TPS and thermal structure are also highly integrated. Figure 6-23 shows a typical air-breathing hypersonic vehicle and its thermal environment, and the lower part of the entire vehicle is part of the propulsion system. This feature is very different from that of rocket-propelled vehicles, so it has a great impact on the structure of the respective fuselage, and also affects the way of thermal management and the selection and design of the thermal protection system scheme adopted. Rocket-powered launch vehicles, which do not have a cruising flight segment even within the atmosphere, are usually launched vertically, and quickly leave the atmosphere, and usually fly at lower dynamic pressures. Air-breathing vehicles, on the other hand, need to accelerate and cruise through the atmosphere, usually taking off horizontally and flying at high dynamic pressures so that the engines can better capture the air. For rocket-powered vehicles (such as the Space Shuttle), aerodynamic drag is not a problem in the ascending stage, while large aerodynamic drag is required in the descending stage to slow down. Air-breathing vehicles, on the other hand, need to be optimized to reduce drag, so thin or slender airframes and smaller wings are usually versus thicker wings [29].

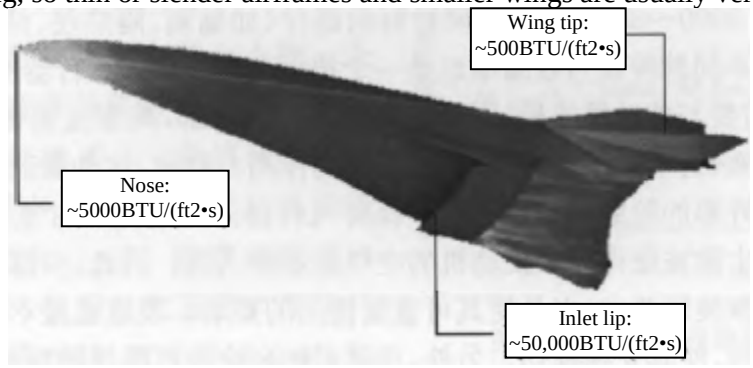

Figure 6-23: Typical air-breathing hypersonic vehicle and thermal environment

Mass and volume are another difference between a rocket and an air-breathing launch vehicle. Rocket-powered launch vehicles are very mass-sensitive, with a structural mass fraction of about 10% of the total take-off mass (GTOW). This means that for each increase in the structural mass of the LIB, the total take-off mass increases by 10lbs, while the air-breathing powered vehicle is more sensitive to volume, mainly affecting drag. The structural mass fraction accounts for about 30% of the total take-off mass. Mass is very important for air-breathing space vehicles, and volume is also an important aspect that affects drag.

The flight trajectory is also an important factor affecting the TPS of the thermal protection system. The rocket-powered launch vehicle is mainly subjected to large aerodynamic heating in the descent stage, and the ascent stage is shorter, so the thermal load is low. On the other hand, the air-breathing power vehicle is dominated by the ascent, descent and cruising stages, and flies at high dynamic pressure for a long time, so it is subjected to relatively large thermal loads.

Figure 6-24 shows the leading edge of the Space Shuttle and X-43. For rocket-powered launch vehicles, the leading edge is designed with a blunt shape in order to obtain large descent drag and low heat flux density. The leading edge of the air-aspirating power vehicle is sharper to achieve low drag and a small wing-to-thickness ratio, and the radius of the sharp leading edge and high dynamic pressure under this condition will result in a high heat flux density.

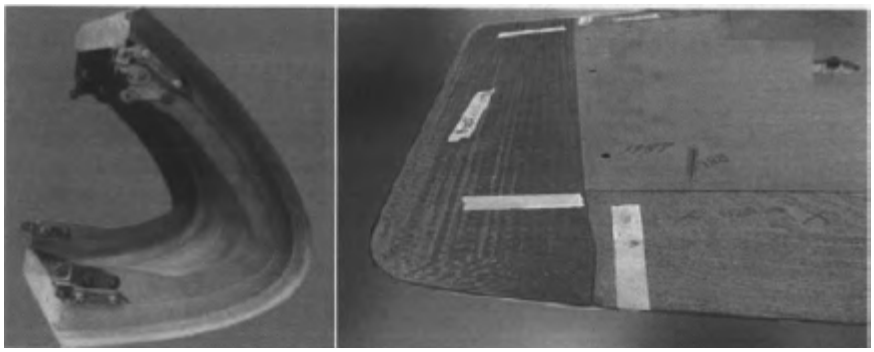

(a) Space Shuttle leading edge (b) X-43A leading edge

Figure 6-24: The obtuse leading edge of the Space Shuttle compared to the sharp leading edge of the X-43A

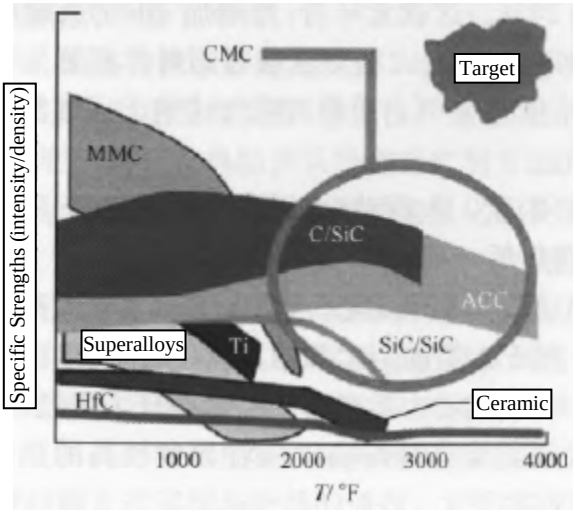

Figure 6-25: Relationship between specific strength and temperature of various materials

Thermal structure is an important technical difficulty for air-breathing hypersonic vehicles, one of which is that it has a large thermal gradient, that is, a temperature gradient. For example, cryogenic liquid hydrogen storage tanks have liquid hydrogen temperatures of -423°F and thermal shields on the outer surface that can reach temperatures of up to 2,000 to 2,000-3,000°F. The different stretch and shrinkage rates of components made of different materials (e.g. storage tanks, insulation, structures, TPS, etc.) over a wide temperature range are also a technical challenge. The control panel of an aircraft is usually thermally structured, and it needs to be connected to an actuator, which is placed inside the aircraft and has a much cooler temperature. Some structures are subjected to high force loads with thinner cross-sections (for low resistance), which are further exacerbated as the temperature increases. The stability of the profile is very important to maintain the performance of the aircraft. For example, the sharp leading edge of the head needs to create a shock wave to maximize the flow of air into the engine. Therefore, the leading edge of the head cannot be ablated, which is both a requirement to generate the desired shock wave and a requirement to make it reusable. Cracks are also not allowed, as cracks have the potential to allow heat flow into the structure, causing damage. In addition, there is a possibility that the windward side of the steps may cause localized high temperatures. The thermal expansion of the propulsion system causes other problems. For air-breathing hypersonic vehicles, the propulsion system typically includes the lower surface of the vehicle, the length of which increases by several inches when exposed to heat. Other issues to consider include manufacturing costs, lifetime costs, damage tolerances, low-speed impacts, high-speed impacts, weather, and reusability.

The above requirements have led to a new development of thermal protection, and it is no longer the thermal insulation fuselage of the space shuttle. New materials can make the aircraft have better heat resistance, such as the SR-71 high-altitude and high-speed reconnaissance aircraft using titanium alloy materials, the X-15 test vehicle using Inconel nickel-based materials, and the space shuttle orbiter using ceramic tiles and ceramic felt.

The material characteristics required for hypersonic vehicles are high temperature tolerance (2,000 to 4,000°F), high strength at high temperatures, high toughness, light weight, and good environmental adaptability. Figure 6-25 shows the specific strength (ratio of strength to density) and temperature of each material, and the desired material target in the upper right corner is the desired material target, i.e., high strength and low material density.

Metal-specific materials include metal matrix composites (MMC), superalloys, and titanium, all of which have high strength-to-weight but are used at temperatures below 2,000°F. Ceramic matrix composites (CMC), including C/SiC materials, advanced carbon/carbon materials and SiC/SiC materials, can still maintain high strength at high temperatures.

As discussed above, the outer surface of a hypersonic vehicle is subjected to harsh aerodynamically heated environments, so its fuselage must be thermally protected or designed to operate under harsh aerodynamically heated conditions. The leading edge, the fuselage and the pneumatic heat-shielding shell, as well as the thermal protection technology for the control surfaces, are discussed separately.

6.5.2: Leading edge

Figure 6-23 shows the typical heat flux density of the leading edge of the ascending stage of a single-stage orbiting vehicle (SSTO), in which the heat flux at the leading edge of the wing is about 500 Btu/(ft^2•s), the heat flux density at the leading edge of the head is about 5,000 Btu/(ft^2•s), and the heat flux density at the leading edge of the inlet lip can reach up to 50,000 Btu/(ft^2•s). Compared with the space shuttle's orbiter, the maximum heat flux density of the return capsule is about 700 Btu/(ft^2•s).

The leading edge radius is an important factor affecting the heat flux density. The heat flux density is proportional to the reciprocal of the square root of the radius of the leading edge. Figure 6-26 shows the heat flux as a function of radius, where the leading edge heat flux of the LIN radius is about 500 Btu/(ft^2•s). As the radius increases, the heat flux density decreases, but the air-breathing hypersonic vehicle requires a smaller leading edge radius, and when the radius decreases, the heat flux density increases rapidly.

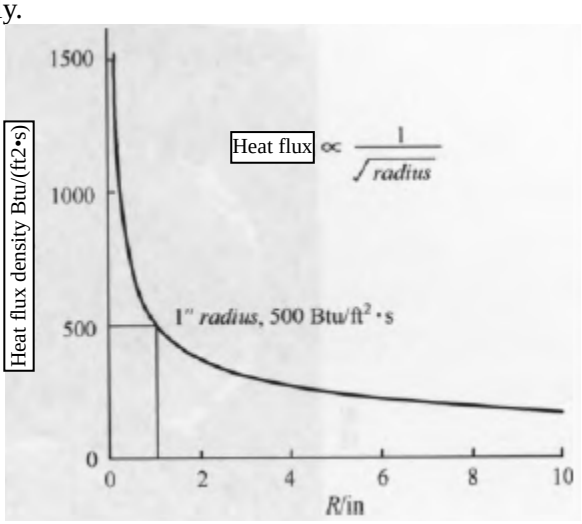

Figure 6-26: Effect of radius on heat flux

In addition to the maximum value of the image heat flux density, the radius of the sharp leading edge also affects the distribution of heat flux at the tangential position. As shown in Figure 6-27, the dark gray area is the heat flux distribution at the sharp leading edge of the hypersonic vehicle, and the middle line is the heat flux at the station. The light gray area is the heat flux distribution at the leading edge of the blunt head of the Space Shuttle orbiter. It can be seen that the distribution area of high heat flux at the leading edge is large, and the maximum heat flux value is located on the lower surface at large angles of attack. Therefore, the effect of pneumatic heating of the sharp leading edge is drastic and at the same time relatively local.

For sharp leading edges, passive, semi-passive, and active thermal protection schemes are available to cope with intense local pneumatic heating. The horizontal line in Figure 6-28 represents the dividing line between one-time use and multi-reusable, above a certain temperature, ablative materials are required, but only once. The priority of thermal protection solution selection is passive, heat pipe/semi-passive, and active cooling. Active cooling solutions will increase development costs, system complexity, and weight, but are a must for high heat flux densities.

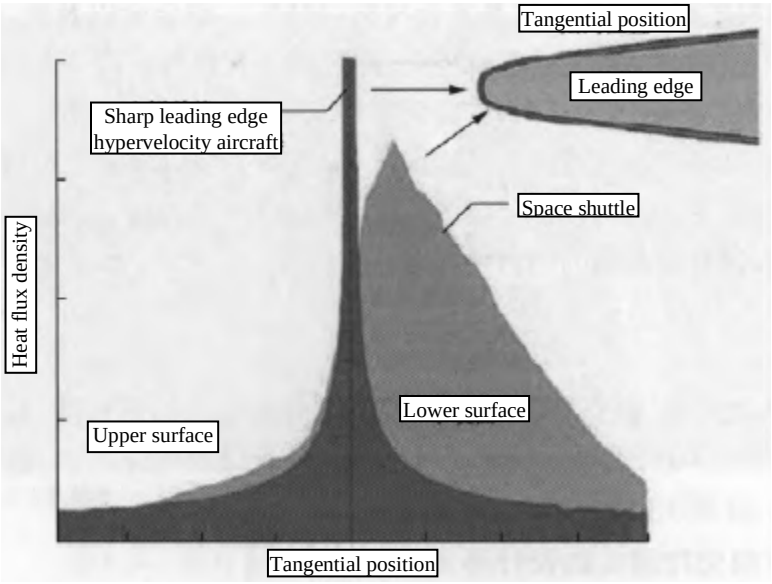

Figure 6-27: The distribution of heat flux in the tangential position of the sharp and blunt leading edges

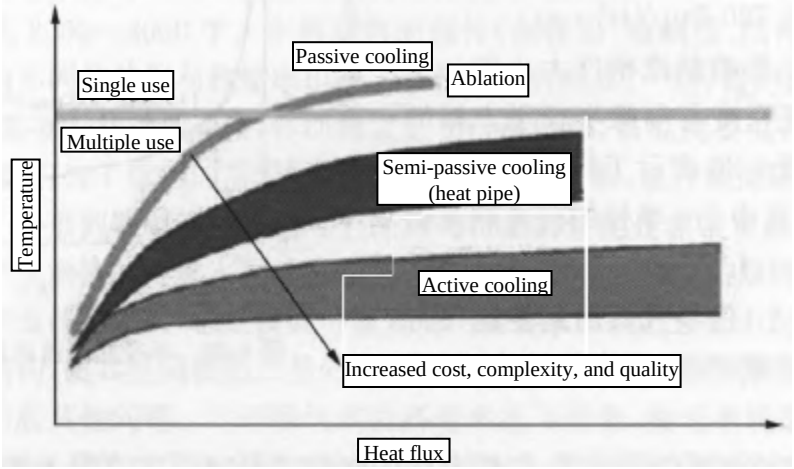

Figure 6-28: Thermal protection scheme for the leading edge1. Passive heat-proof leading edge

Figure 6-29 illustrates the energy transfer process of the passive heat protection front edge. In the stationary region, the net heat is transferred to the leading edge, and this heat is conducted in the posterior region and radiated out. The heat transferred from the post-station region is a function of the thermal conductivity of the leading edge material. There are two requirements for the materials applied to the leading edge: one is to use high-temperature materials to improve the heat resistance of the leading edge; the second is to keep the temperature as low as possible through proper design so that it can be reused.

1) High temperature coating

SiC coatings, such as those used in the space shuttle orbiter, can withstand temperatures up to 3,000°F. For air-breathing hypersonic vehicles, where temperature drops are higher than 3,000°F, this requires the use of other types of materials such as carbides, oxides, and diborides of hafnium and zirconium. These materials, such as hafnium and zirconium, can be used as components of composite substrates. Some materials, such as iridium, are more suitable as coating materials, as shown in Figure 6-30.

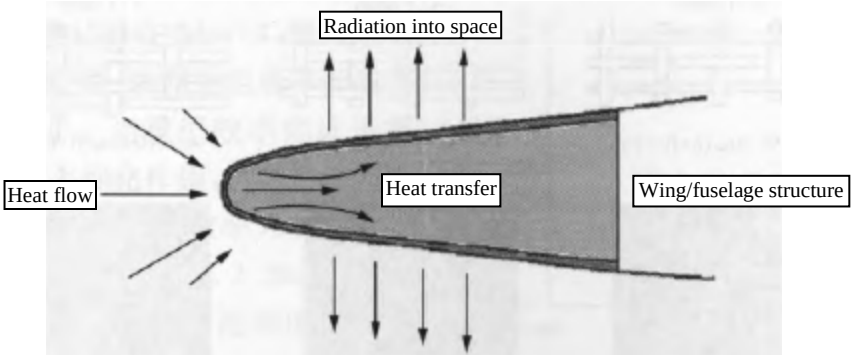

Figure 6-29: Heat transfer at the passive heat-proof leading edge

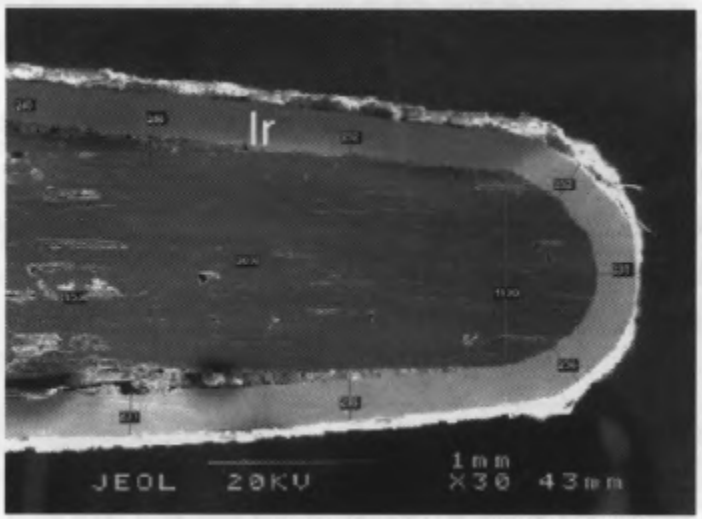

Figure 6-30: Cross-section of the C/C leading edge with iridium coating

2) Thermal conductivity

The thermal properties of the material also significantly affect the temperature of the structural surface. One such thermal property is the thermal conductivity of the fiber-woven structural material, which contains multiple grades of carbon-carbon fiber, each with different thermal conductivity. These carbon fibers can be woven in different ways, facilitating heat diffusion by taking advantage of their anisotropic heat conductivity, avoiding local concentration of heat and withstanding high heat flow environments. Figures 6-31 show three different fiber weaving methods, where 3:1 represents the ratio of the number of woven fibers in both directions of the plane. For a 3:1 weave, the thermal conductivity is 190 Btu/(h•ft•°F) in the direction of quantity "3" and 70 Btu/(h•ft•°F) in the direction of quantity "1." For the 3:1 weaving method, the thermal conductivity is increased in the direction of the primary quantity and decreased in the direction of the secondary quantity.

The leading edge specimens of the above braiding method were experimented in the arc heating wind tunnel, and the 5:1 braiding method could transfer more heat than the 3:1 braiding method, which verified the thermal performance and heat resistance of the anisotropic composites. However, it should be pointed out that although the thermal performance is improved in the direction of the principal quantity, the strength in the direction of the secondary quantity is weakened.

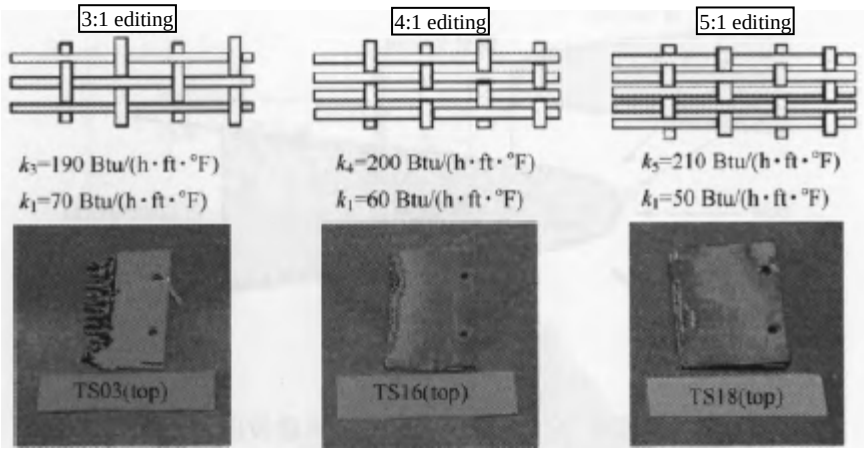

Figure 6-31: Thermal conductivity and leading edge arc test results for different braiding methods

3) Emissivity

Emissivity is another important parameter that affects surface temperature. As shown in Figure 6-32, the radiative equilibrium temperature is a function of surface heat flux and emissivity. Figure 6-32 illustrates the radiation equilibrium condition, in which the heat flux of convective heat transfer is discharged from the surface by radiation. For example, if the heat flux and radiant heat flux density for incoming convective heat transfer is 50 Btu/(h• ft•°F) and the emissivity is 0.8, the surface temperature is about 3,000°F, and if the emissivity is low, such as 0.3, the surface temperature rises to close to 4,000°F so that the same 50 Btu/(h•ft•°F) heat flow can be radiated.

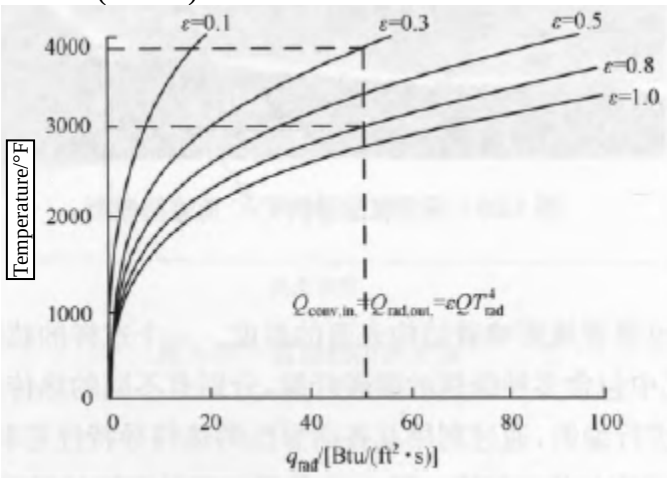

Figure 6-32: Effect of emissivity on radiation equilibrium temperature

4) Recombination (catalytic) effect

The recombination (catalytic) effect is another important parameter. In hypersonic streams, there is dissociated substance. For example, air will be ionized and recombined, and the surface of the aircraft acts as a catalyst to enhance the recombination effect. Whereas, recombination is a heat-proof process, which means that the recombination reaction will release heat, which will be supplied to the surface. In addition to the recombination of gases, the recombination of atoms on the surface of the aircraft can also lead to an increase in heat flux density. The silicon gas released from the leading edge surface coating reacts with an oxygen atom to form SiO, a typical example of this exothermic reaction that releases about 605 Btu/mol.

$$Si(g) + O \rightleftharpoons SiO$$

Figure 6-33 shows the relationship between recombination efficiency and heat flux. The data were obtained by arc heating test under the conditions of *Ma* = 4 and emissivity of 0.84, which showed that the recombination efficiency affected the surface heat flux density. When the recombination efficiency is close to zero, the surface is considered catalytic and the heat flux is about 10 Btu/(ft²•s). For a complete catalytic surface with a recombination efficiency of 1, the heat flux is about 28.3 Btu/(ft²•s), and the surface catalysis increases the surface heat flux by a factor of nearly 3.

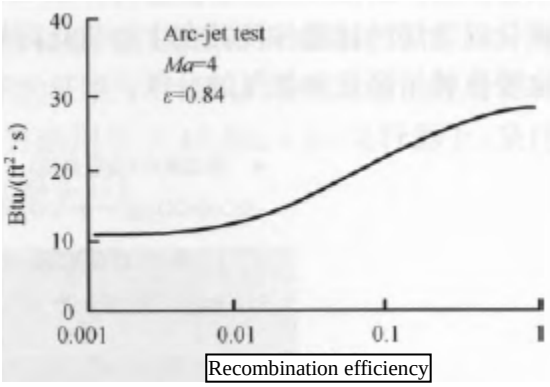

Figure 6-33: Relationship between recombination (catalysis) efficiency and heat flux density

5) Thermal expansion rate

Another important property is the rate of thermal expansion. As shown in Figure 6-34, when the rod with a uniform temperature T_0 is heated to the temperature, the length increases ΔL, one end is fixed, and the other end is unconstrained, then the ratio of ΔL to the original length of the rod L_0 should be changed, and the stress is zero. If the rod is fixed at both ends, the strain becomes zero and the stress is not zero. The stress is equal to the product of the modulus of elasticity E, the coefficient of thermal expansion α, and the temperature difference. The third bar in Figure 6-34 illustrates the main challenge of the thermal structure, which is due to the presence of a temperature gradient with non-zero stress and strain. Thermal stress is caused by the thermal expansion of the material, the temperature difference, and the structural and mechanical constraints, and it is difficult to express thermal stress in the same way as mechanical stress.

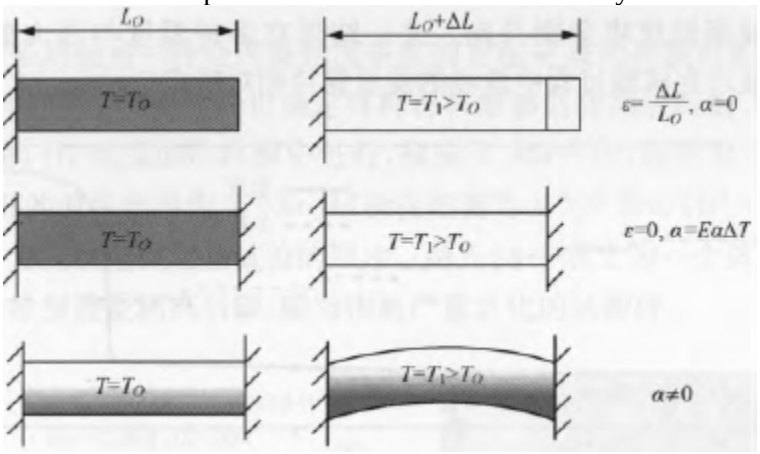

Figure 6-34: Effect of thermal expansion on stress and strain

6) Antioxidant properties

Oxidation resistance is an important factor in the long-term operation of high-temperature structures. In order to maximize the life of the structure, it should be allowed to work in the passive oxidation region. The first equation in Figure 6-35 is silicon carbide as a solid coating material covering the surface of a refractory composite structure. In the case of a hyperoxic stress environment, there is a large amount of oxygen around. Silicon carbide reacts with two oxygen molecules to form silica, which is a kind of protective barrier to the structure. Silicon is a protective layer that fixes and forms a structure. CO2 is released as a product of the reaction.

If it is a low-pressure working environment, it will produce an active oxidation reaction at high temperatures. In a low-pressure environment, there is not enough oxygen to utilize, and for every cinnamon atom, only 1.5 oxygen atoms can be utilized. The result of the reaction is the formation of SiO instead of SiO2, which acts as a protective layer. This result is an active oxidation process. Since SiO is an unstable gas, it does not form a protective layer.

The coating of silicon carbide is used by Bosera and detached from the surface of the structure in the form of SiO gas. Figure 6-35 shows the SiC coated specimen and its results under active oxidation. The conversion of passive and active oxidation processes is mainly dependent on temperature and partial pressure of oxygen.

• Passive oxidation (high temperature and high pressure)

-$SiC(s)+ 2O_2(g) \rightarrow SiO_2(s)+ CO_2(g)$

• Active oxidation (high temperature and low pressure)

-$SiC(s)+ 1.5O_2(g) \rightarrow SiO(g)+ CO_2(g)$

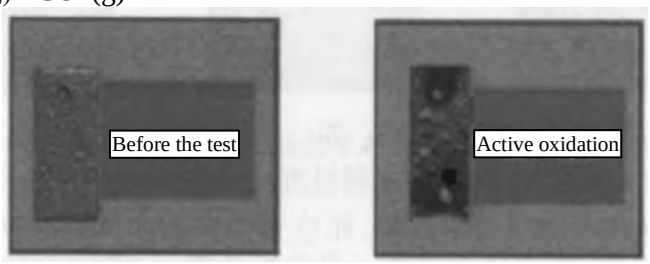

Figure 6-35: Before and after active oxidation test

The curve in Figure 6-36(a) shows the temperature-to-time and position-to-time curves of the specimen in the arc heated wind tunnel. As the test piece moves closer to the nozzle (decreasing in position X), the temperature gradually increases. Once the temperature and pressure transition to the active oxidation zone, the surface temperature of the test structure will increase dramatically. This result is present in a variety of temperature and pressure combinations. The Figure 6-36(b) curve shows that the energy of the flow field remained relatively constant during the test.

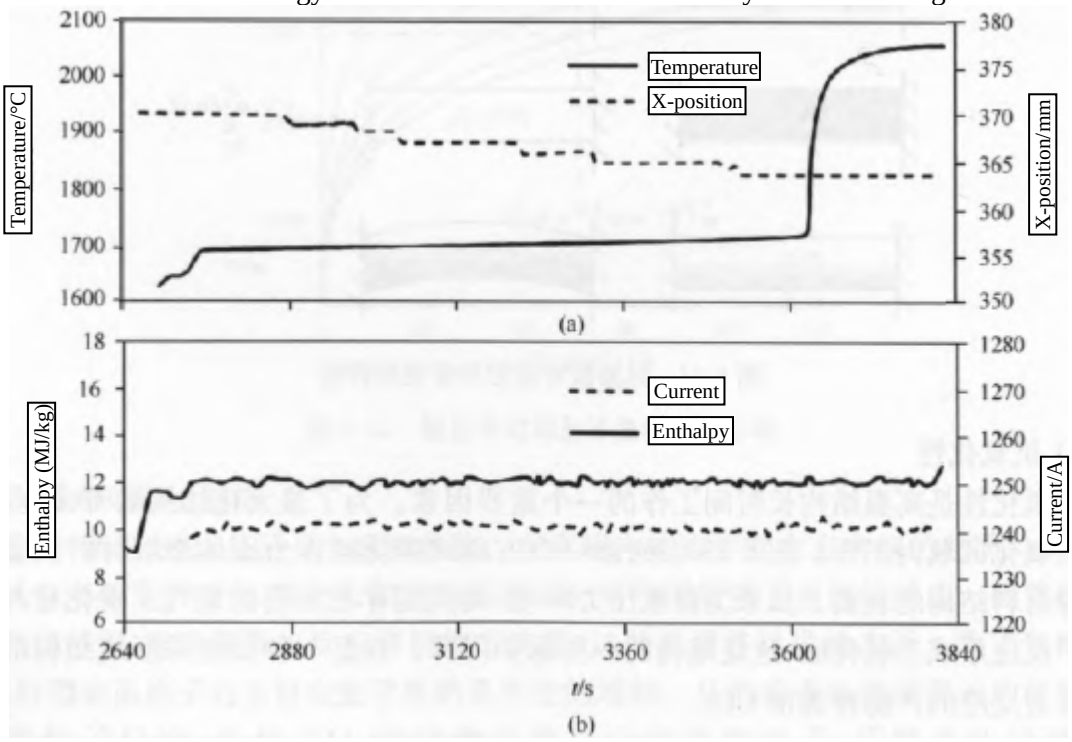

Figure 6-36: Temperature-to-time and flow-enthalpy-to-time curves

7) X-43 leading edge

Typical of the passive leading edge design, the X-43 *Ma* = 10 test vehicle head leading edge is designed to reach nearly 4,000 t after a 130s flight. As mentioned above, fibers with high thermal conductivity can be woven into anisotropic composites in order to transfer heat from the leading edge down to the maximum temperature. This method is used on X-43 *Ma* = 10 aircraft and is braided in a 3:1 (75/25) manner to obtain high thermal conductivity in the chord direction (Figure 6-37).

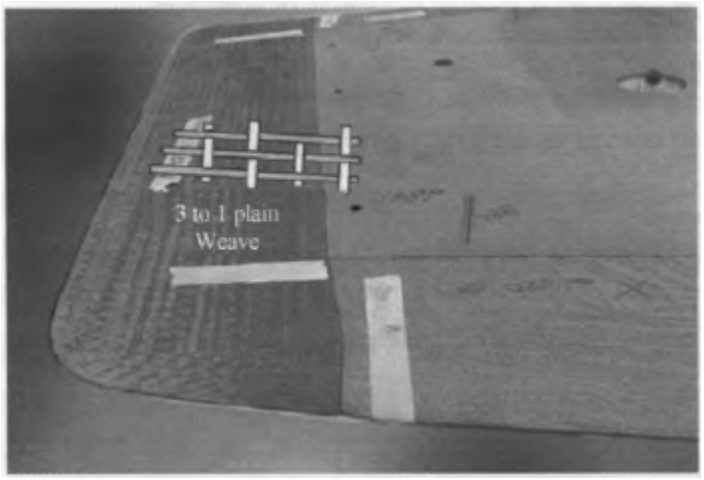

Figure 6-37: X-43 carbon/carbon leading edge with 3:1 braid

Another method used for the X-43 to deal with high heat flux was the use of a high-temperature material system, where a total of 13 different high-temperature materials were evaluated to determine which material would be suitable for the high-heat flow flight environment, and the tests were conducted in the H2 arc heated wind tunnel at the Arnold Research Center, simulating flight conditions at *Ma* = 10 at an altitude of 105,000 ft. The leading edge radius of the specimen head was 0.03 in, and the test lasted for 130 seconds with a heat flow of 1,300 Btu/(ft2 • s). Figure 6-38 shows the image of the leading edge arc heating test. In Figure 6-38, the upper right is a test piece that remains intact after testing, and the lower right is a test piece where the carbon/carbon structure is severely oxidized after the coating is peeled off.

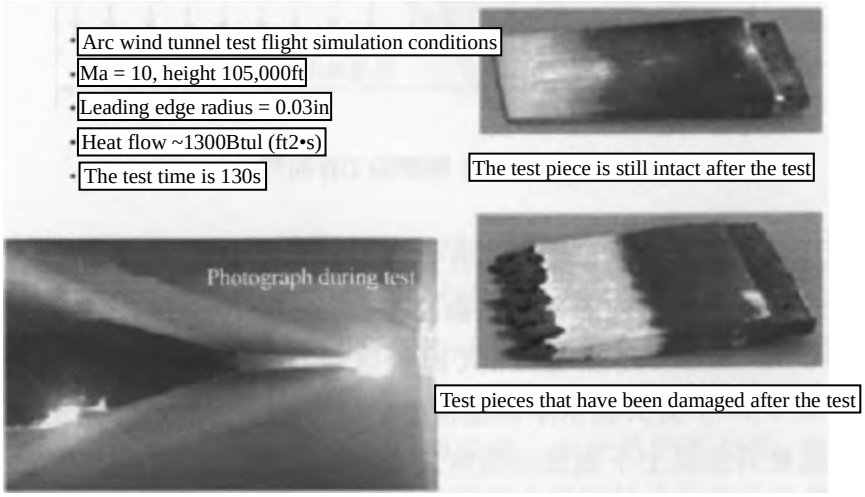

Figure 6-38: Arc heating test of X-43 leading edge coating

High thermal gradients result in large thermal stresses, also for the leading edge of the Hyper-X *Ma* = 10 test vehicle. After the leading edge of the head of the aircraft is heated by aerodynamics, the thermal expansion caused by high temperature causes the leading edge to be deformed. The simulation results of thermal structure modeling show that the compressive thermal stress caused by the constraint of thermal expansion may cause the leading edge structure to fail. The main problems caused by high thermal stress are whether the coated structural substrate will fail due to the high thermal stress; whether the coating will wrinkle and peel off; whether the peeling of the coating will cause oxidation of the substrate structure; whether slotting is required to stop the leading edge coating from wrinkling; how much slotting spacing can prevent the coating from peeling.

2. Heat pipe cooling leading edge

When the heat flux raises the temperature beyond the reusable temperature of the structure, other technical approaches need to be considered. The cooling leading edge of the semi-passive heat-protected heat pipe uses a heat pipe to reduce the temperature of the leading edge below the limit temperature of the material for reusability.

A heat pipe is a heat transfer device that carries a two-phase substance on its own, including a casing, a capillary path, and a flowing working fluid. Figure 6-39 shows the working diagram of the heat pipe. The heat is transferred to the part of the heat pipe, through the shell to the inner core, and through the evaporation of the flowing working fluid, the heat is absorbed. The evaporated material flows to the relatively low temperature section of the heat pipe, where it condenses, releasing the stored heat. The released heat is then transferred and discharged through the inner core and housing. The section where the heat is dissipated is called the condensation zone. Through the capillary action of the inner core, the liquid working fluid is returned to the heated area, i.e. the evaporator site. During normal operation, the heat pipe unit has a very high heat conduction efficiency and can maintain a relatively uniform temperature distribution along the entire length of the heat pipe.

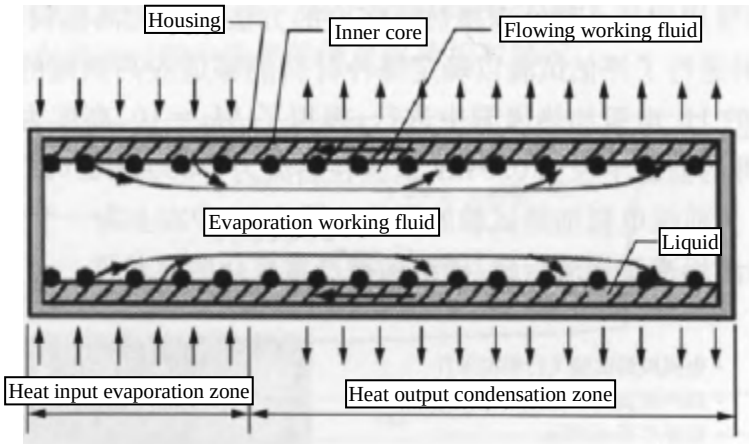

Figure 6-39: Schematic diagram of heat pipe

Heat pipes cool the station area by transferring heat almost isothermally to the area behind the station, so that the temperature after the station area is raised above the local radiation equilibrium temperature. When applied to leading edge cooling, heat pipe operation radiates heat at a low heat flow rate over a large area by absorbing high heat over a small area close to the station, as shown in Figure 6-40. The arrows in Figure 6-40 represent the net heat flux density. The use of heat pipes causes the leading edge surface to be isothermal, thus reducing the temperature of the stationary area and increasing the temperature of the upper and lower surfaces.

In the American NASP program, heat pipe cooling leading edge technology was studied. The leading edge adopts a carbon/carbon structure with Mo-Re heat pipes as the container, as shown in Figure 6-41, three Mo-Re heat pipes, each 30 inches long, are fabricated and embedded in the carbon/carbon structure. The heat pipes are D-shaped and use lithium as the flow fluid.

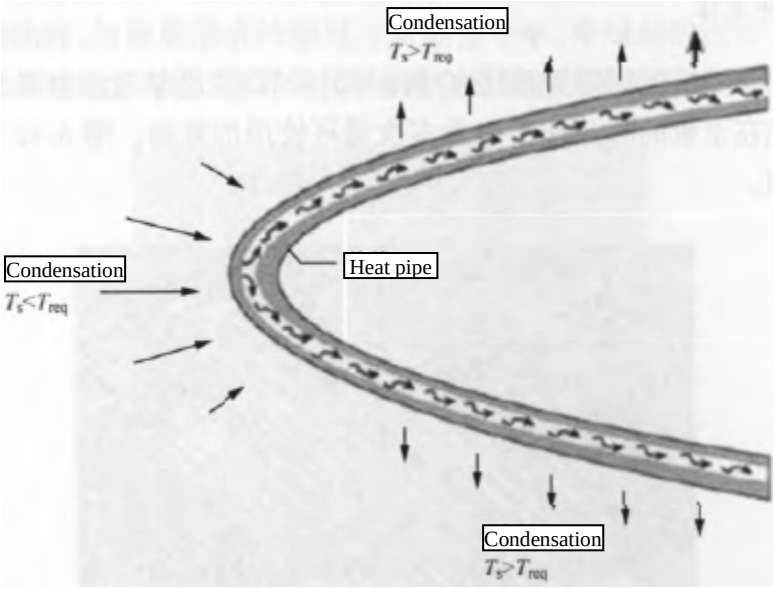

Figure 6-40: How the leading edge heat pipe works
T_s is the surface temperature; T_{req} is the radiation equilibrium temperature

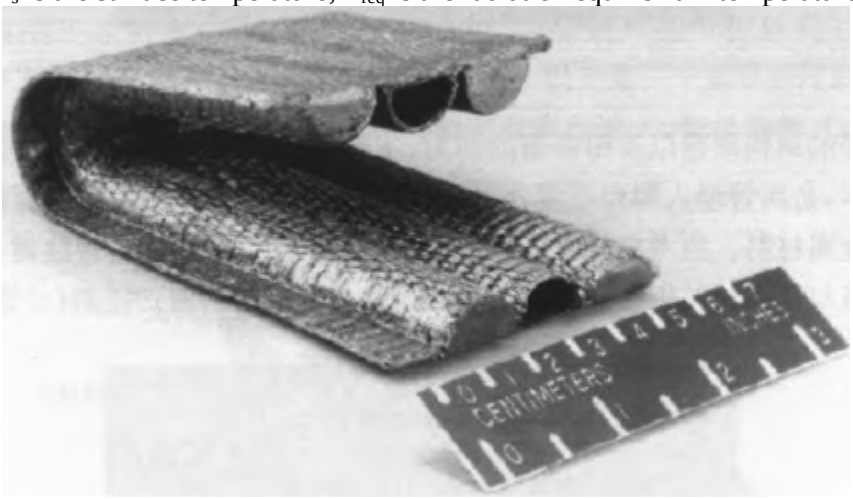

Figure 6-41: Leading edge of NASP heat pipe

For heat pipes embedded in carbon/carbon composites, material compatibility and thermal stress are two major challenges. Two materials, carbon and Mo-Re, are still problematic for long-term testing as housings. If Mo-Re comes into direct contact with carbon/carbon, a carbon-molybdenum compound will be formed, which is a function of time and temperature. Carbon can also seep into the heat pipes through the Mo-Re and damage the work of the heat pipes. This osmosis is a strong function of time and temperature. Thermal stress is another issue. Mo-Re has a greater coefficient of thermal expansion than C/C, so it is bound by C/C. Due to the hindrance of thermal expansion, there is a possibility that the straight section of the heat pipe will wrinkle during operation. The difficulty is that good thermal conductivity is required to transfer heat from the outer surface to the heat pipe, but at the same time, a certain loose fit is required to reduce thermal stress due to the mismatch of the coefficient of thermal expansion.

3. Active cooling of the leading edge

Active cooling measures are required for maximum heat flow situations, and metal active cooling fronts have been fabricated, where the main technical challenges are the interaction of hydrogen and the lifetime of multiple cycles. Figure 6-42 shows the internal structure of an active cooling leading edge.

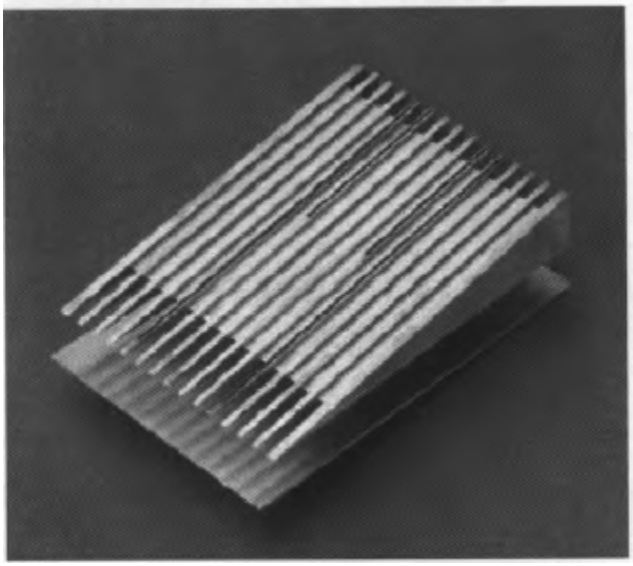

Figure 6-42: Internal structure of the active cooling leading edge

In order to achieve light construction weight and the ability to withstand high temperatures, active cooling can provide beneficial value. As a first step in development, the metal tube is embedded in a ceramic matrix composite. Materials used as coolant line vessels include super-heat-resistant alloys and poorly soluble metal materials. Figure 6-43 shows the structural scheme of the metal pipe, which includes three types: metal pipe inserted into the composite material (a), metal pipe and composite material interphase (b), and metal pipe in close contact with the composite material (c).

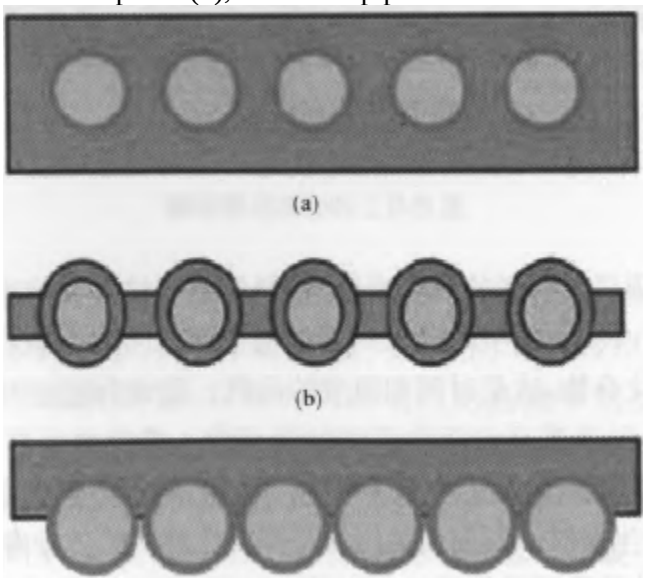

Figure 6-43: Active cooling leading edge structure type

The active cooling structure of the all-composite material will provide extremely low weight and high temperature resistance. However, there are still many technical challenges, including the optimal thermal conductivity in the direction of wall thickness, coolant sealing, manifold assembly, oxidation resistance, long life, and material compatibility. Figure 6-44 shows the active cooling test piece of the all-composite material.

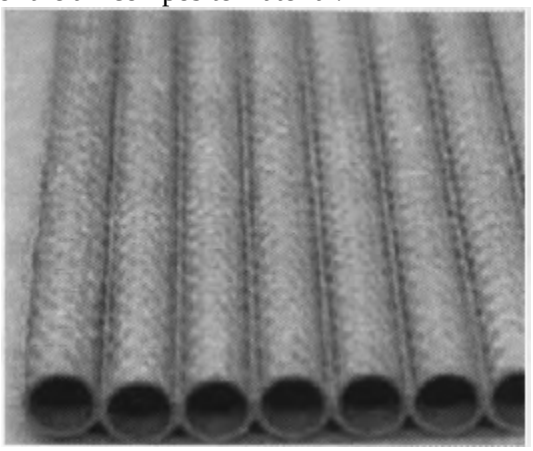

Figure 6-44: An all-composite actively cooled specimen

6.5.3: Control Panel

The control panel is used to control the flight of the aircraft. Figure 6-45 shows the two typical control surfaces of a hypersonic vehicle: elevator and rudder. For hypersonic vehicles, reducing drag is an important issue, so thinner control panels are mostly used. Control panels are designed and manufactured in a variety of forms, including insulated, thermal, and hybrid.

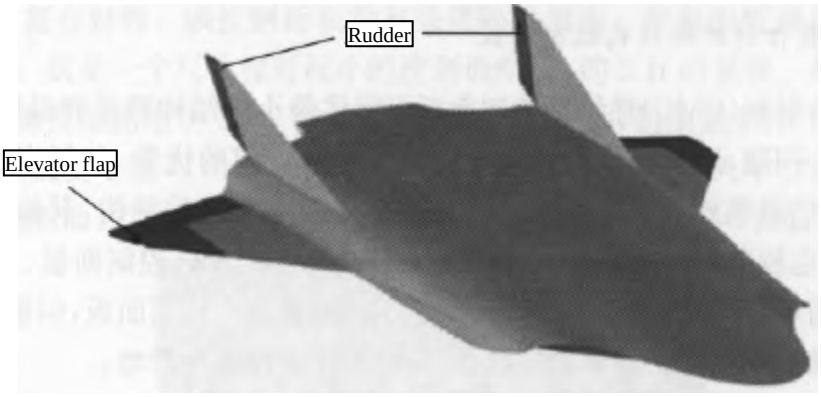

Figure 6-45: Control panel of a hypersonic vehicle

The requirements for the control panel vary depending on the design of the aircraft and the entire mission, including ground operation before take-off to post-landing cooling. For some insulated results, the maximum temperature is reached after landing. Requirements for reusability include the integrity of the anti-oxidation coating and the longevity of each component. It should be ensured that the life of each component exceeds the life of the entire control panel, or that the components are designed to be easily replaced. The geometry of the control panel is directly influenced by the flight controls (aerodynamics) and the connection to the aircraft. Mass, stiffness, and structural integrity indirectly influence the geometrical requirements. The mechanical requirements are usually generated by the pressure difference between the windward and leeward sides.

Thermal requirements include maximum temperature, thermal stress, oxidation resistance (active or passive), connection to cold structures (e.g. actuators), thermal radiation to control surfaces, etc. Functional requirements include the number and frequency of deflection. For example, the rudder surface of the X-38 re-entry vehicle has a deflection amplitude of ±20°, a frequency period of 0.1 to 0.7 Hz, and a design rotation of 874 r. The connection of the control surface to the aircraft also affects the design. For example, the control surface can be mounted at the rear of the aircraft, on the lower part, or at the trailing edge of the wing. Static and dynamic sealing around the hinges is also required to prevent heat flow into the aircraft. In the aircraft design process, some requirements need to be verified by analysis, some need to be checked and evaluated, and some must be verified by experiments.

1. Insulated control panel

Thermally insulated control panels have been successfully used on the Space Shuttle for many years. The advantages of insulated control panels include suitability for large structures, as well as minimal thermal expansion; the disadvantages include a large mass and a low thermal margin (due to the low temperature structure of the structure and its thick cross-section). Figure 6-46 shows a metal or polymeric matrix composite PMC control panel using ceramic tiles as thermal insulation materials.

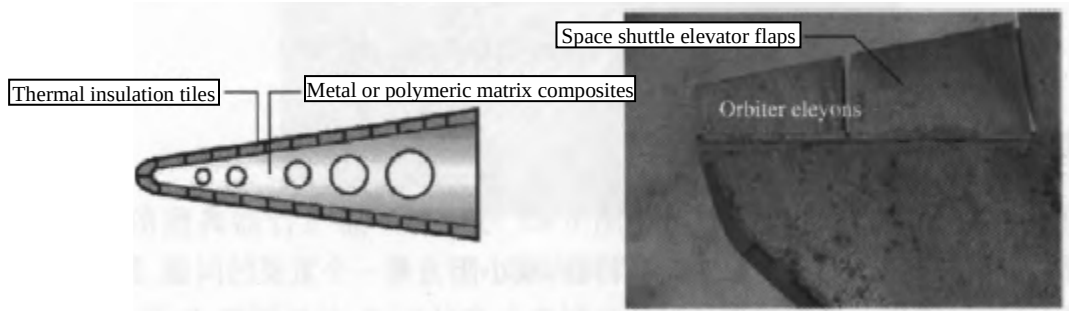

Figure 6-46: The thermal insulation control panel of the space shuttle

2. Ceramic matrix composite thermal structure control panel

Ceramic matrix composite (CMC) thermal structure control panels provide minimal structural mass and thinnest cross-sections, minimal thermal expansion fit issues, and good thermal margins. This method has certain advantages, including effective strength and stiffness, and no external thermal insulation requirements. This form of structure is not suitable for particularly large structures, its repair capacity is limited, and the risk of manufacturing is also high; it can be assembled with multiple small parts to form a CMC control panel. The advantage of this type of panel is that it is relatively easy to process, and the damaged parts can be replaced without having to scrap the entire control panel, but the disadvantage is that a large number of small parts can be assembled with tolerance gaps, and the number of parts can proliferate.

3. All-in-one manufacturing

Integrated manufacturing is another way of manufacturing. The advantages of this method are fewer connections and better mechanical properties. The disadvantages include difficult processing, correspondingly expensive manufacturing, and easy wear and tear during the manufacturing process. This manufacturing method has been prototyped by MT Aerospace in Germany, as shown in Figure 6-47. The component is manufactured using two-dimensional prepreg carbon fiber for hardening and pyrolysis, with further hardening through a chemical evaporation permeation process. The integrated manufacturing makes it possible for the component to be free of any fasteners that have the potential to increase the structural mass.

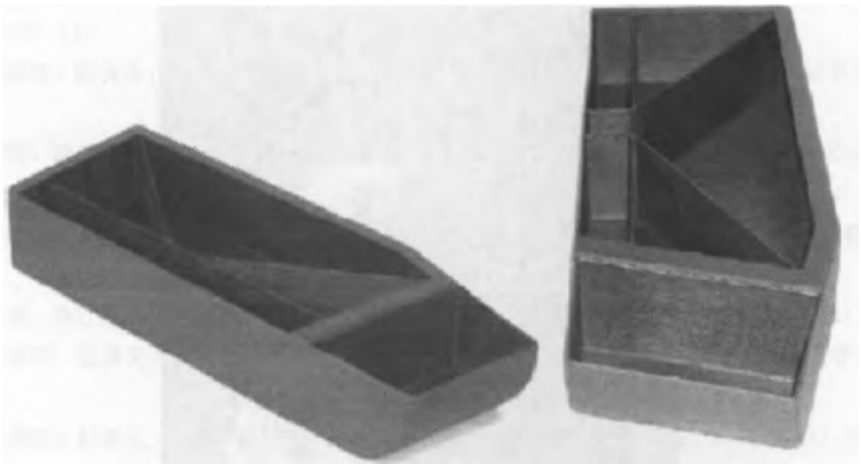

Figure 6-47: Integrally manufactured aileron components

4. Hybrid control panel

The hybrid control panel is a combination of CMC material and cryogenic material such as titanium or superalloy. The advantage of hybrid control panels is that they are suitable for larger structures. The upper surface of this structure does not need to be covered with TPS material, and the leading and trailing edges of the CMC can be replaced if damaged. The disadvantage is the matching problem caused by the different thermal expansion coefficients between the cold structure and the CMC material. Compared to the full CMC control panel, the weight of the hybrid control panel has increased by 30% to 40%. In addition, the thermal insulation of the box-shaped structure can lead to an increase in thickness, which will result in a reduction in the thickness of the structure and a reduction in the moment of inertia while thickening the cross-section.

The X-43 uses a hybrid control surface, as shown in Figure 6-48, and the structure is made of Haynes 230 superalloy, and the leading edge is made of C/C composite. The control panel is not thermally insulated. The control panel is connected to the actuator in the fuselage via a spindle. This is a relatively small control surface structure, on the order of about 2 ft. The Netherlands Space Center designed and manufactured a metal control rudder for the X-38 aircraft, as shown in Figure 6-49, with the initial rudder made of PM-1000 material and a maximum service temperature of 2,190°F. Due to the changing demand for rudders, DLN Space Center has designed and manufactured a hybrid titanium/ceramic rudder surface. For the crew return capsule (CRV), it is planned to use a metal/CMC hybrid rudder.

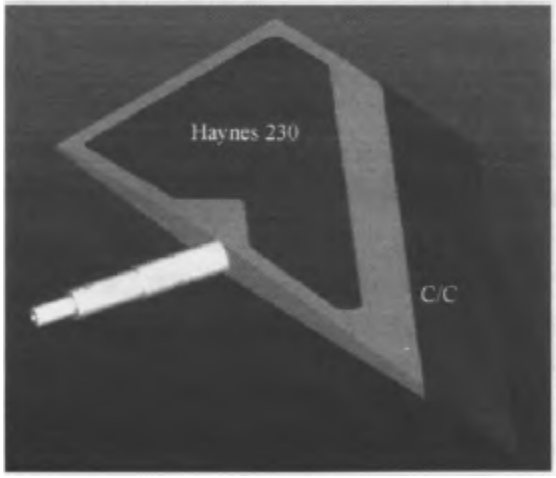

Figure 6-48: X-43 Hybrid Control Panel

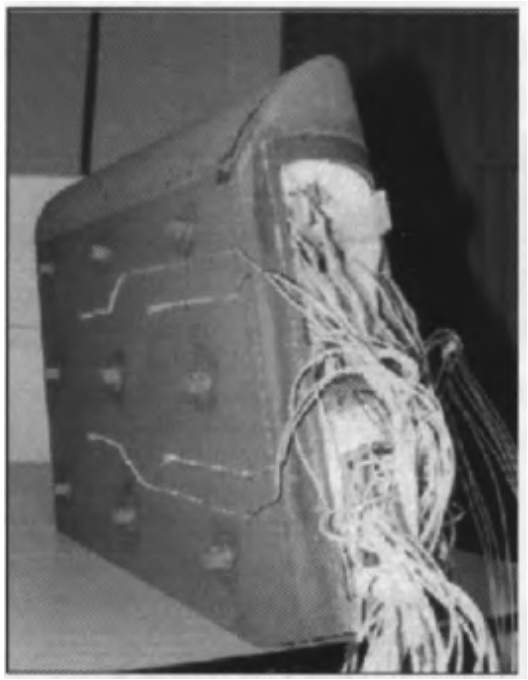

Figure 6-49: X-38 rudder surface

References

[1] HAN Hongshuo, SHI Dongmei, XU Daohua. Analysis and quantitative evaluation of structure and materials of space shuttle heat protection system [R]. Aerospace Information Research Report, HQ-B90052, 1990.

[2] David E Glass. Ceramic Matrix Composite (CMC) Thermal Protection Systems (TPS) and Hot Structures for Hypersonic Vehicles [R]. AIAA 2008-2682, 2008.

[3] WANG Anling, GUI Yewei, TANG Wei, et al. Physical modeling of thermal corridor of reusable aircraft [J]. Chinese Journal of Engineering Thermophysics, 2006, 27(5): 856-858.

[4] John D Anderson Jr. Hypersonic and High Temperature Gas Dynamics [M]. McGraw-Hill Book Company, 1989.

[5] Huang Zhicheng. Aerodynamics of hypersonic vehicle [M]. Beijing: National Defense Industry Press, 1995.

[6] Xu Min, Yan Hengyuan. Calculation method of aircraft aerodynamic engineering [M]. Xi'an: Northwestern Polytechnical University Press, 1998.

[7] Yang Zhi, Gao Xiaowei, Hypersonic Aerothermal Environment Engineering Algorithm [J]. Missile and Space Technology, 2010, (4): 19-23.

[8] Jiang Zonglin. Several basic research problems in hypersonic aerothermodynamics [C]. The 3rd Hypersonic Science and Technology Conference, October 2010, Wuxi, Jiangsu.

[9] Yang Chao, Xu Zan, Xie Changchuan. A review of the research on aeroelastic mechanics of hypersonic vehicles [J]. Acta Aeronautical Sinica, 2010, 31(1):1-11.)

[10] Qu Zhanghua, Zeng Ming, Liu Wei, et al. Hypersonic aerodynamics [M]. Changsha: National University of Defense Technology Press, 1999.

[11] Rejanette F R. A review of approximate methods used in aerodynamic heating analysis [R], AIAA 85-0906, 1985.

[12] Jiang Guiqing, Liu Lianyuan. High-speed airflow heat transfer and ablation heat protection [M]. Beijing: National Defense Industry Press, 2003.

[13] Huang Zhicheng. Heat protection system of aerospace aircraft [J]. Aerodynamic Experiment and Measurement Control, 1992, 6(2).

[14] Xia Deshun. Review of metal thermal protection system of repeater launch vehicle [J]. Missile and Space Launch Technology, 2002, (2):21-26.

[15] Cao Yi, Cheng Haifeng, Xiao Jiayu, et al. Research progress of metal thermal protection system in the United States [J]. Aerospace Materials and Technology, 2003, (3):9-12.

[16] Liu Luowei. Research progress of metal thermal protection system for RLV [J]. Flying Missile, 2004, (11):44-48.

[17] Yao Caogen, Lü Hongjun, Jia Xinchao. Research progress on materials and structures of metal thermal protection system [J]. Aerospace Materials and Technology, 2005, (2):9-13.

[18] Shi Liping, Li Yao, Hao Xiaodong. Research progress of metal thermal protection system [J]. Aerospace Materials Technology, 2005, (3):21-23.

[19] Ma Yu'e, Sun Qin, Lin Guomin. History and development dynamic analysis of metal thermal protection system for

reusable launch vehicle [J]. Mechanical Design and Manufacturing, 2005, (2):108-110.
[20] Yan Changhai, Meng Songhe, Chen Guiqing, et al. Development and status quo of thermal insulation materials for metal thermal protection system [J]. Missile and Space Launch Technology, 2006, (4): 48-52.
[21] Liu Shuang, Zhang Boming, Xie Weihua. Structural optimization progress of reusable aerospace technology thermal protection system [J]. Aerospace Manufacturing Technology, 2007, (3): 43-48.
[22] Ma Zhonghui, Sun Qin, Wang Xiaojun, et al. Heat transfer analysis and performance study of multilayer thermal insulation structure of thermal protection system [J]. Journal of Astronautics, 2003, 24(5): 543-546.
[23] Ma Yu'e, Sun Qin, Li Jianghai. Advances in thermal analysis methods for RLV metal thermal protection system [J]. Aeronautical Manufacturing Technology, 2006, (11):38-40.
[24] Xie Weihua, Zhang Boming, Du Shanyi. Finite element analysis and design of metal thermal protection system for reusable aircraft [J]. Acta Aeronautics and Astronautics, 2006, 27(4): 650-656.
[25] Xie Weihua, Zhang Boming, Du Shanyi. Finite element analysis of metal thermal protection system design [J]. Acta Aeronautics Sinica, 2006, 27(5):898-902.
[26] Zhao Ling, Lü Guozhi, Ren Keliang. Radiation-conduction composite heat transfer analysis of reusable aircraft thermal protection system [J]. Aircraft Design, 2007, 27(1): 32-35.
[27] Li Donghui, Xia Xinlin. Study on transient heat transfer method of metal thermal protection system [J]. Journal of Astronautics, 2009, 30(3):1195-1200.
[28] Du Shanyi, Xie Weihua, Zhang Boming. Research Progress on Health Monitoring of RLV Thermal Protection System [J]. Journal of Astronautics, 2007, 28(1):1-8.)
[29] David E Glass. Ceramic Matrix Composite (CMC) Thermal Protection System (TPS) and Hot Structures for Hypersonic Vehicles [R]. AIAA 2008-2682, 2008.

CHAPTER 7: HYPERSONIC VEHICLE NAVIGATION GUIDANCE AND CONTROL TECHNOLOGIES

7.1: Hypersonic Vehicle Navigation System Technology

7.1.1: The role and significance of navigation systems

In recent years, conventional cruise vehicles (weapons) have played an important role in high-tech warfare. For example, the U.S. Tomahawk cruise missile has attracted the attention of all countries because of its advantages of being mobile, flexible, difficult to defend, and destructive, and the cruise aircraft can be launched from a platform that has never considered carrying out the launch mission of a cruise aircraft. In addition to the above, it has many other advantages: good striking effect, strong penetration ability, high hit accuracy, and versatility. But there are also many shortcomings: the missile's flight speed is low, and it is easy to intercept once discovered; poor ability to replace attack targets; in the target area, cruise missiles do not have vertical maneuvering, and simple countermeasures can effectively confront them; the terrain assistance system (TERCOM) applies the geomorphological data information in the computer system of the aircraft with low accuracy, which is difficult to ensure the flight of the missile around obstacles, and is greatly affected by natural, seasonal and terrain changes. All these factors limit its application in modern warfare [1~3].

In view of the advantages and disadvantages of the above conventional cruise weapons, and then considering the strategic thinking of global intervention, rapid arrival, and in-depth strike, all military powers in the world have applied hypersonic technology to the field of cruise aircraft. Hypersonic vehicles (weapons) have many advantages: strong penetration capabilities and difficult interception; drilling deep into the ground has great damage power; fast flight speed, global reach; fleeting, difficult to detect, change direction to increase the ability to penetrate; win the first enemy and shorten the reaction time [4]; all these factors make hypersonic cruise vehicles (weapons) the main direction of development for both the attacking and defending sides.

In recent years, hypersonic cruise vehicles (weapons) have been rapidly developed in various countries [5]. For example, the U.S.'s Boeing "waverider", X series, and X-43 were test-launched; Russia's "Cold" and "rainbow" plans; Russia and India also test-fired the BrahMos supersonic cruise missile. The high speed and short flight duration of these new cruise missiles make it easier to detect, identify and attack active targets. The time required for a hypersonic missile to reach the target is only 1/10 of that of a subsonic missile, and the distance that the target moves after the missile launch is only 1/10 of that of a subsonic missile, so the area that the missile seeker must search is only 1/100. If the target starts moving after several minutes, the hypersonic missile can strike it as if it were a stationary target.

With the requirements of modern warfare and the development of aerospace technology, higher and higher requirements are put forward for the performance of various strategic and tactical hypersonic cruise vehicles. First of all, the high accuracy of the cruise aircraft is mainly guaranteed by the navigation system, so in a sense, the navigation system can be said to be the "eye" of the long-range cruise aircraft. Navigation technology is the key to making a cruise vehicle effectively exert its power [6]. In addition, the navigation system is the most basic link in the GNC system, which is related to the work of the guidance and control loop, and if the foundation is not accurate, the instructions formed by the guidance and control system will be wrong, resulting in off-target. For hypersonic cruise vehicles, because their speed is too fast, when the information provided by the navigation system is inaccurate, it will cause greater cumulative deviations, and it will not be able to fly according to the pre-selected flight path, and the purpose of precision strikes cannot be achieved. It can be seen that the design of navigation system is one of the key technologies of hypersonic cruise vehicles, but it is increasingly difficult for a single navigation system to meet the practical requirements [2,5,7].

Various forms of integrated navigation systems containing a variety of navigation sensors have become the main practical solutions of navigation systems at present, which can eliminate the shortcomings of a single navigation system, learn from each other's strengths, and achieve better accuracy. At present, the integrated navigation system applied to hypersonic vehicles is mainly based on inertial navigation, supplemented by satellite positioning and navigation systems, astronomical navigation systems, Doppler systems, terrain matching and other navigation systems. For example, the American Immortal Bird AI, the Fast Falcon high-speed cruise missile, the Patriot missile with a Mach number of 6, the Excalibur, the "Fast Hawk" missile, and the X-43 all use INS/GPS-based integrated navigation schemes; Russia's “Cold” and the "BrahMos" test-fired by India and Russia are also integrated navigation schemes based on inertial navigation and supplemented by satellite positioning and navigation systems. It can be seen that the integrated navigation technology plays an important role in the navigation system of hypersonic cruise vehicles.

7.1.2: Integrated Navigation Techniques

Navigation is a technology or method that guides a navigation body from the starting point to the destination, and can provide the aircraft's control system or control system with the aircraft's position, speed, heading and other real-time motion states, or a device that measures navigation parameters, called a navigation system, such as an inertial navigation system, a satellite positioning navigation system, an astronomical navigation system, etc.

Integrated navigation is a technology that uses two or more different navigation systems (or equipment) to measure the same navigation information source and uses the complementary characteristics of different navigation equipment to extract the errors of each system from the comparative value of these measured values and correct them, so as to improve the performance of the entire navigation system. A navigation system that uses integrated navigation technology is called an integrated navigation system. The integrated navigation system has higher navigation performance than either navigation system alone.

Modern aircraft can employ a variety of navigation sensors and devices. Among these navigation systems, inertial navigation systems (INS), especially strapdown inertial navigation technology (SINS), have become the main navigation systems used in missile weapon systems because of their high autonomy and anti-jamming capabilities, and their ability to provide complete, continuous and high data update rate navigation information. The navigation accuracy of the inertial navigation system has become one of the main factors determining the performance of the missile weapon system. However, the defect that the navigation accuracy of the system is constantly decreasing with the increase of working time restricts the application of inertial systems in medium and long-range missiles. Future combat requirements will inevitably promote the aircraft to have ultra-long combat distance and flight time, and improving the accuracy of inertial navigation system has become an important research topic. There are two ways to solve this problem: (1) improve the accuracy of inertial devices or develop new types of inertial devices. The inertial system is to measure the specific force and angular velocity of the carrier relative to the inertial space through inertial devices (accelerometers and gyroscopes), and obtain the three-dimensional position, velocity, and attitude information of the carrier. Therefore, the accuracy of the system mainly depends on the accuracy of the inertial device. Improving the accuracy of inertial devices is mainly by improving the machining accuracy of parts and components, and adopting new materials, new processes, and new technologies. This method is expensive and does not fundamentally change the nature of the measurement error of the inertial device accumulated over time, so the improvement of accuracy is limited; (2) on the basis of the existing navigation equipment, the inertial navigation system is comprehensively corrected and the drift of the inertial device is compensated by using the external reference information source that the navigation error does not accumulate with time. The essence of this method is to use a combined navigation system, mainly through software technology to improve navigation accuracy. Practice has proved that integrated navigation is an effective way to improve the accuracy of inertial navigation system.

Modern aircraft place increasing demands on the performance of navigation systems. In addition to inertial navigation systems, the navigation systems that can be used today for missile weapon systems include satellite positioning and navigation systems, astronomical navigation systems, terrain scene auxiliary navigation systems, Doppler radar velocity measurement systems, and other radio navigation systems. How to reasonably combine these navigation systems with inertial navigation systems to form a well-performing integrated navigation system is a research area worthy of attention. In several local wars in the 20th century and the beginning of the 21st century, integrated navigation technology, especially SINS/GPS/TANS integrated navigation, has been applied to weapon systems and has achieved remarkable results.

Facts have proved that the integrated navigation system composed of multiple sensors, especially the inertial multi-sensor integrated navigation and guidance system based on the inertial navigation system, is the main development trend of the navigation and guidance system of new advanced missile weapons [8~13].

1. Inertial (INS)/Satellite Integrated Navigation System

Satellite positioning and navigation is a satellite-based radio navigation system that uses the radio signals transmitted by satellites operating in orbit for timed ranging. With the characteristics of wide coverage, all-weather, all-day, high-precision, and near-continuous real-time, the user equipment has the advantages of small size, light weight, low power consumption, and easy operation, and is an ideal auxiliary navigation equipment for inertial navigation [14].

The combination of inertial/satellite positioning can not only overcome the shortcomings of each subsystem, but also realize the integration of navigation equipment, so that the volume, weight, and cost of the system can be reduced. Therefore, the inertial/satellite positioning combination is an ideal integrated navigation system. Over the years, the research of inertial/satellite positioning integrated navigation system has received widespread attention, and a large number of theoretical research results have been applied in practice.

At present, various models of precision-guided weapons in the United States have adopted the combined GPS/INS technology [15~19]. In the Gulf War in the 20th century, the "SLAM" (SLAM) AGM-84E air-to-ship missile, with GPS/INS combined guidance as the mid-course guidance, achieved remarkable results with its high hitting accuracy; in the recent Iraq war, the Tomahawk cruise-1 missile adopted a combination of GPS/INS/TANS technology, and showed its might in the war. It has been recognized by all countries. It can be seen that INS/satellite positioning integrated navigation is the most ideal and promising navigation method for missile weapon systems and occupies a special and important position in navigation applications. Because this combination combines the advantages of INS such as high reliability, good autonomy, continuous navigation, inherent high bandwidth, low noise and short-term high precision, and the advantages of satellite positioning and navigation error independent of time, long-term moderate accuracy, global or local sharing, etc., it overcomes the shortcomings of INS error accumulation over time, the need for external initialization, and the dependence of satellite positioning and navigation on external information, susceptibility to radio interference, positioning accuracy is related to the environment and carrier dynamics, and cannot directly provide the acceleration and attitude of the carrier. Due to the low data output rate, a navigation system with high autonomy, high precision, high reliability, and continuous real-time has been formed.

Currently, there are many satellite positioning and pit systems on a global scale and locally. Among these systems are the GPS of the United States and GLONASS of Russia, of which GPS is the most widely used and mature. The perfect combination of satellite positioning technology and other technologies (especially the original inertial navigation technology of missile weapon systems) has brought about a new breakthrough and revolution in missile weapon systems, especially medium- and long-range cruise missiles. Actual combat has proved that the application of satellite positioning technology has brought cruise missiles to a higher level, making it possible to attack from a distance, launch outside the defense zone, ignore after launching, rapid response, accurate hit, trajectory planning, and threat penetration. At present, most of the cruise missile navigation systems of advanced military countries use or are equipped with satellite positioning/INS integrated navigation systems. However, the GPS system and the GLONASS system are developed and controlled by their respective military departments, and mainly serve the military or allies of their respective countries. In order to break the control of the satellite navigation system by the military departments of one or two countries and meet the requirements of civilian use, many countries have gradually paid attention to the combined GPS/GLONASS system, developed a global navigation satellite system completely controlled by civilian people, and developed a geostationary satellite positioning and navigation system. China has also established the "Beidou" satellite positioning and navigation system. Now the more mature is the dual-satellite positioning and navigation system. Therefore, the combination of inertial navigation system and dual-satellite positioning and navigation system is the main navigation means used in various aircraft in China.

2. Inertial/Astronomical Navigation System (CNS) / Satellite Positioning and Navigation System

Astronavigation systems are full-fledged navigation systems with many advantages: autonomy and concealment.

The information provided does not drift over time, and the bearing from the Earth to the star remains essentially the same; it has the function of positioning and posture fixing and uses natural radiation sources such as stars and the sun as beacons, which basically reaches all-weather [23]. The INS/CNS navigation system has long been used on various strategic missiles.

At present, astronomical navigation systems have been widely used in various aircraft in space and low altitude. Reference [20] corrects the drift of platform systems in ballistic missiles using astronomical navigation with the aid of accurate position and course information that does not drift with time. For land-based missiles, INS/CNS guidance allows the missile to be launched as long as the initial alignment is completed, and the error can be corrected by starlight measurements, thereby shortening the launch time and correcting the platform drift. The performance of the INS/CNS/GPS triple system was analyzed. This system is an astronomical navigation to provide heading information assistance for inertial navigation, and GPS to provide position and speed information assistance. It can provide accurate position, velocity, and attitude information in long-distance ballistic missile flights. After analysis, the deviation at its landing point is increased by 20.26%, and the longitudinal deviation is increased by 18.45% compared with the inertial navigation system alone. Therefore, the satellite navigation and positioning system and astronomical navigation system are used to assist the inertial navigation system of ballistic missiles, which has ideal navigation accuracy and important practical value. Reference [21] and [22] also provide an integrated INS/GPS/CNS navigation scheme, which is basically the same as the modified scheme for inertial navigation in Reference [20], but it is somewhat different in terms of model construction. In addition, the astronomical navigation system is also an indispensable navigation system for the positioning and attitude determination of space vehicles.

7.1.3: Application of task equipment such as seeker in navigation systems

At present, most of the mission equipment used in aircraft is still imaging equipment, radar infrared and other guidance equipment. In the past, these devices were mainly used to estimate the state of motion using what they called "vision" technology. In many studies, most of them are used for ground navigation, image recognition, and estimation of information relative to the target, and the focus has been on the improvement of equipment, and there are not many studies that really combine it with other navigation equipment such as inertia.

The performance of the combined system of active radar seeker velocity information assisted strapdown inertial navigation was analyzed in Reference [23]. When the active radar seeker is turned on to the ground in flight, the Doppler effect can be used to obtain the velocity measurement value along the beam direction of the seeker to assist inertial navigation. The Kalman filter algorithm is used to establish the seeker velocity information-aided inertial navigation model, and the active radar/strapdown inertial navigation integrated navigation system is constructed. It is analyzed that the system can give meter-level velocity accuracy and suppress the shortcomings of the growth of inertial navigation position error with time. Importantly, this system not only improves the accuracy of the navigation system, but also saves the load on the aircraft.

In Reference [24], a close-knit scheme for using image information to assist inertial navigation systems is introduced, and a Kalman filter is established. This paper mainly uses the line-of-sight information formed by the optical imaging principle of the camera to transform the position information into position information to assist the inertial navigation system. The inertial navigation system with image assistance, the inertial navigation system without image assistance, and the combined system of image and GPS co-assisted inertial navigation are simulated and analyzed. The results show that the image information-assisted inertial navigation system can improve the position and velocity accuracy of the system and can achieve quite good accuracy in the image/GPS/inertial navigation combined system.

Reference [25] also studies the use of sight-of-sight information to assist guidance in the seeker of air-to-air bombs, as well as the estimation of the flight state of the target. The feasibility of seeker-assisted navigation has also been studied in Reference [26].

It can be seen that the line-of-sight information from the aircraft to the target formed by the seeker, imaging and other mission equipment is the key to assist the inertial navigation system.

7.2: Hypersonic Vehicle Dynamics Modeling Techniques

7.2.1: Modeling axisymmetric aircraft dynamics

In the field of hypersonic vehicle control technology, the Winged-Cone vehicle model of NASA's Langley Research Center is mostly used as the research object, because NASA provides detailed aerodynamic data and propulsion system data of the vehicle model [27,28].

As shown in Figure 7-1, the Winged-Cone aircraft has triangular wings, a single vertical tail, independent left and right lifting ailerons, and retractable horizontal canards. The main engine system is a variable-thrust combined engine system with thrust vector control, that is, an air-breathing engine with liquid hydrogen as fuel in the supersonic flight stage, and a rocket engine with liquid hydrogen and oxygen as propellant in the hypersonic stage. The four X-mounted oscillating engines can swing in the tangential direction respectively, and their numbers and swing angles δ_1, δ_2, δ_3, and δ_4 are shown in Figure 7-2. Therefore, the control of the aircraft includes aerodynamic rudder deflection, thrust magnitude control, and thrust vector control. It is assumed that the elevator, rudder, and engine oscillating rudder surfaces are modeled in the same way, i.e., the control commands are first limited by a limiter and then fed into a first-order actuator model. For a detailed introduction and aerodynamic data of the aircraft, see Reference [29], the disadvantage of this model is that it cannot reflect the influence of the propulsion system on the control system in the integration of airframe propulsion.

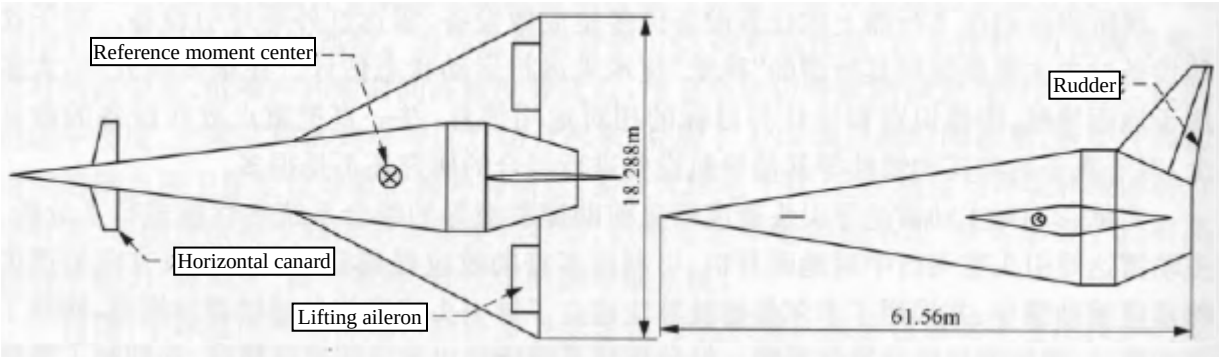

Figure 7-1: Top view and side view of the aerospace vehicle

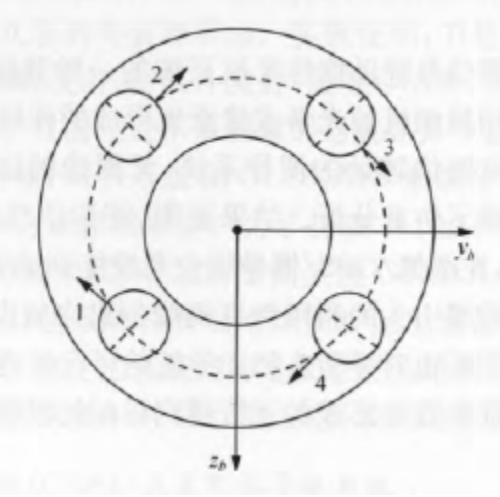

Figure 7-2: Swing engine layout

7.2.2: Integrated dynamics modeling of hypersonic vehicle fuselage propulsion

The dynamics of hypersonic vehicles are strongly influenced by changes in aerodynamic forces and propulsion systems, and it is difficult to separate these effects in practice [30~32]. Therefore, an integrated modeling approach is needed. Specifically, since the entire lower surface of the aircraft is part of the inlet and nozzle of the propulsion system, a significant propulsion lift is generated, and there is a propulsion moment acting on the aircraft, both of which vary with the propulsion force generated.

As shown in Figure 7-3, the two-dimensional Newtonian theory is used to represent the aerodynamic pressure distribution characteristics of the forebody, and the two-dimensional expansion wave theory is used to determine the pressure distribution of the rear body/nozzle. A 1D air/thermal/gas dynamics model was applied to characterize the airflow in a scramjet engine. From the above, an analytic expression for the stable derivative will be derived.

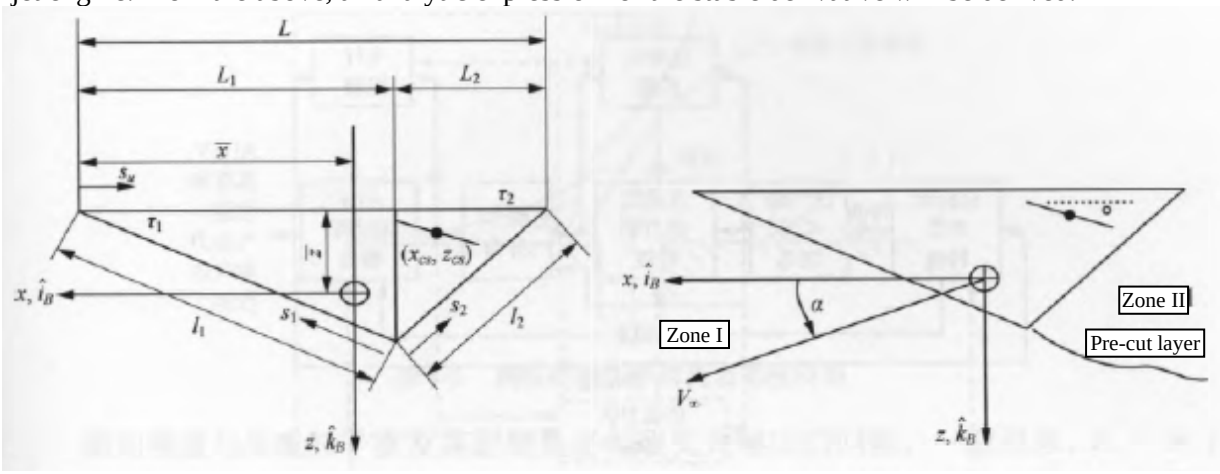

Figure 7-3: Modeling object of 2D hypersonic vehicle dynamics

7.2.3: Modeling of hypersonic vehicle control based on parametric profiles

In order to meet the three-dimensional shape and reflect the dynamics model of the airframe propulsion interaction, the authors of this book participated in a work on the control modeling of air-breathing hypersonic vehicles based on parametric shapes, as described in Reference [33]. Reference [33] describes a method for constructing parametric geometries for 6DOF flight simulations. The modeling process includes the parameterization of the aircraft geometry, the calculation of the aerodynamic force without viscosity, and the modeling of the scramjet engine. Among them, the parameterization of the geometry of the aircraft reflects the characteristics of the integration of hypersonic aircraft fuselage propulsion, the calculation of aerodynamic characteristics is based on engineering methods, the quasi-one-dimensional calculation model is used for the scramjet engine, the whole method system is simple and fast, and has good accuracy, and the trim calculation of the cruising state shows that the aerodynamic formula by multivariate fitting can be well applied to the aircraft control process.

7.2.4: Aeropropulsion/aerodynamic coupling of hypersonic vehicles

The new generation of hypersonic vehicles, represented by X-43A and X-51A, generally adopts air-breathing ramjet engines as the design scheme of high-speed flight propulsion system. Studies on this type of aircraft have shown that the aerodynamic shape of the aircraft is closely related to the performance of the propulsion system.

In the concept of integrated design of aircraft fuselage/propulsion system, the lower surface of the aircraft forebody is used as the pre-compression surface of the air intake, which determines the quality of the suction airflow of the propulsion system. As the outer expansion section of the engine, the lower surface of the rear body of the aircraft directly determines the angle between the static thrust direction and the flight direction of the scramjet engine. In addition, the front and rear bodies generate additional pitching moments due to aerodynamic forces and thrust, and in particular the rear bodies generate additional "thrust lift" due to the exhaust of the propulsion system. The inherent elastic properties of the aircraft body structure further complicate the above problems, and this kind of aeropropulsion/aeroelastic coupling problem has also received extensive attention, and Figure 7-4 shows the dynamics analysis framework of air-breathing hypersonic vehicles. Generally speaking, such problems are analyzed from the perspective of flight dynamics, and appropriate performance is obtained by designing appropriate flight control laws. The research on this kind of problem began with the NASP project in the United States, and the early research was generally to analyze the dynamic stability of the aircraft under the condition of airframe/propulsion/aeroelastic coupling, and the subsequent research mostly focused on the design of the flight control system considering the above coupling influences, and because it is usually difficult to obtain accurate information about the above nominal effects, it is necessary to study robust flight control system design methods considering the coupling uncertainty [34-39].

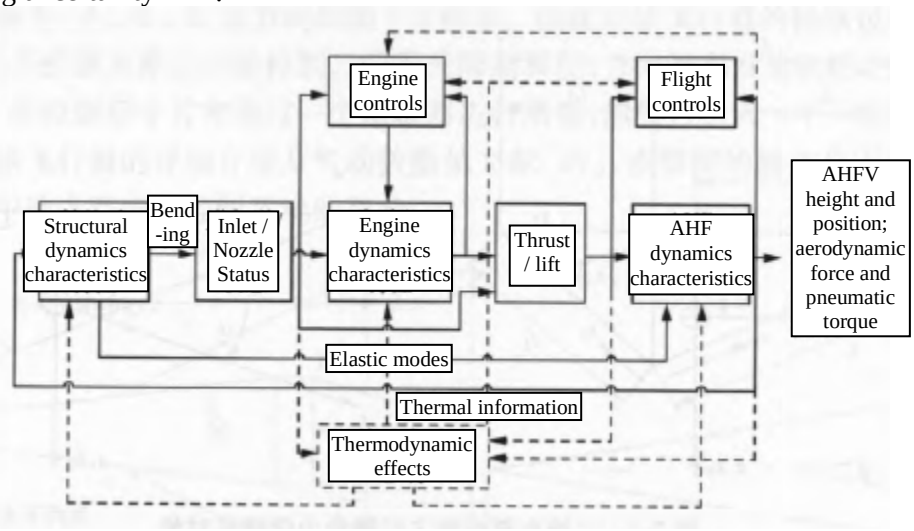

Figure 7-4: Framework for dynamic analysis of air-breathing hypersonic vehicles

7.3: Hypersonic Vehicle Manipulation and Attitude Measurement Technology

7.3.1: Manipulation techniques [27]

Due to the characteristics of high-speed flight and complex flight environment, hypersonic vehicles are also quite different from traditional aircraft in terms of dynamics, control, and guidance characteristics. Preliminary studies have shown that the dynamic characteristics and control characteristics of this aircraft are very different from those of traditional aircraft, and it is necessary to conduct in-depth and careful research from the physical mechanism and theoretical methods.

1. Pneumatic rudder control

Most conventional aircraft use pneumatic rudders, and the aircraft relies on it for pitch, yaw and roll control at medium and low altitudes, and can be controlled throughout the flight of the aircraft. The efficiency of the rudder surface in the air at low altitudes is very high. However, for hypersonic vehicles, due to their high flight altitude (usually more than 30km) and low air density, the air rudder is very efficient at low altitude (below 30km), which has obvious advantages, but the efficiency decreases quickly at high altitude (above 30km), which cannot meet the needs of aircraft maneuvering.

Due to the high speed of the aircraft and the large dynamic pressure, considering the structural strength and rotational torque of the rudder surface, the rudder surface cannot be as large as that of a subsonic aircraft, which objectively limits the dynamic characteristics and maneuverability of the aircraft. In addition, due to the high speed of the aircraft, the aerodynamic rudder alone cannot provide it with enough force to turn, and the turning radius may be very large, which cannot meet the requirements of its maneuverability, new ways must be sought, and new solutions must be studied.

2. Lateral jet control

Lateral jet control has been applied to anti-missile vehicles in recent years and was previously mainly used for attitude control of orbital vehicles, such as the American air-to-air missiles AIM9X and Patriot P3. Lateral jet control has many advantages, it can solve the problem of insufficient efficiency of the air rudder surface at high altitude, and its fast response at the guidance end greatly improves the guidance accuracy, but it also has many aerodynamic problems to be solved. A simple physical model of the flow is shown in Figure 7-5.

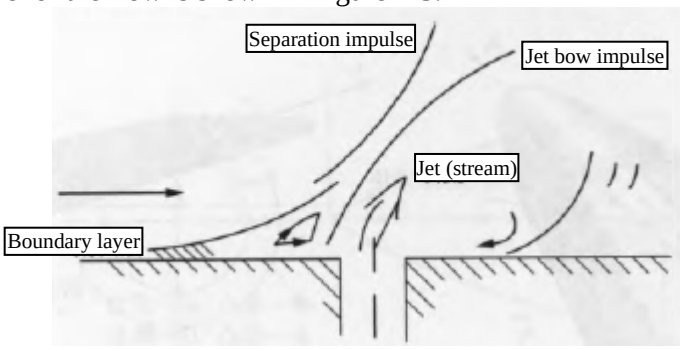

Figure 7-5: A simple flow physics model for side spray control

The interference between lateral jets and outflow and their effects is a problem that must be studied and solved. Generally speaking, $K = F + F_f$, where K is the jet interference coefficient, F is the side spray thrust, and F_f is the side spray interference force. The following 4 questions should be studied:

(1) The variation law and value of the interference coefficient K with the height h. In general, to 30km, K→1.

(2) the influence of flight *Ma* on the interference coefficient K.

(3) The influence of the location of the nozzle.

(4) The influence of the size of the nozzle, the parameters of the jet flow, the distribution of the peri-nozzle and the flight attitude of the aircraft are all contents that need to be studied.

3. Composite control

Compared with the traditional aerodynamic control mode, the composite control mode has many advantages, the most important of which is that it can greatly improve the response time of the interceptor missile, increase its ultimate usable overload and increase its maneuverability, thereby improving the guidance accuracy. For example, when aerodynamic control, the response time is 0.2 to 0.8s, and the maximum height available overload is not more than 15; when the direct lateral force is controlled, the response time is 0.025 to 0.ls, and the maximum height available overload is not less than 10. In order to fundamentally improve the guidance accuracy of the new-generation air defense aircraft, at the same time reduce the mass of the aircraft, and ensure that the aircraft has greater maneuverability, it is necessary to adopt new technology, and the composite control mode of aerodynamic force and direct lateral force is a relatively good technology. For interceptor missiles with composite control, it is crucial to design their flight control systems to meet the requirements of speed, stability, and accuracy [28].

(1) Pneumatic control rudder surface. The aircraft relies on it for pitch, yaw and roll control at medium and low altitudes, and the efficiency of the rudder surface in the air at low altitudes is very high.

(2) Rudder surface and side spray compound control. The use of rudder surface and side spray composite control system greatly improves the guidance accuracy of the aircraft, so that the aircraft has excellent performance of direct collision and low miss. Because of such a high guidance accuracy, the payload of the aircraft is very small, and the total weight and size of the aircraft are very small, which greatly improves the combat effectiveness of the weapon system. The composite control form of pneumatic control surface and side spray control is very creative, which has greatly developed from the previous single or pneumatic control surface as the main control mode, and greatly improved the combat performance of the aircraft. For example, the Patriot air defense aircraft of the United States uses this control scheme.

4. Metamorphic center control

Center of mass control is to move the warhead inside the fuselage to change the relative relationship between the center of mass and the center of mass of the aircraft, and then complete the attitude control response (Figure 7-6).

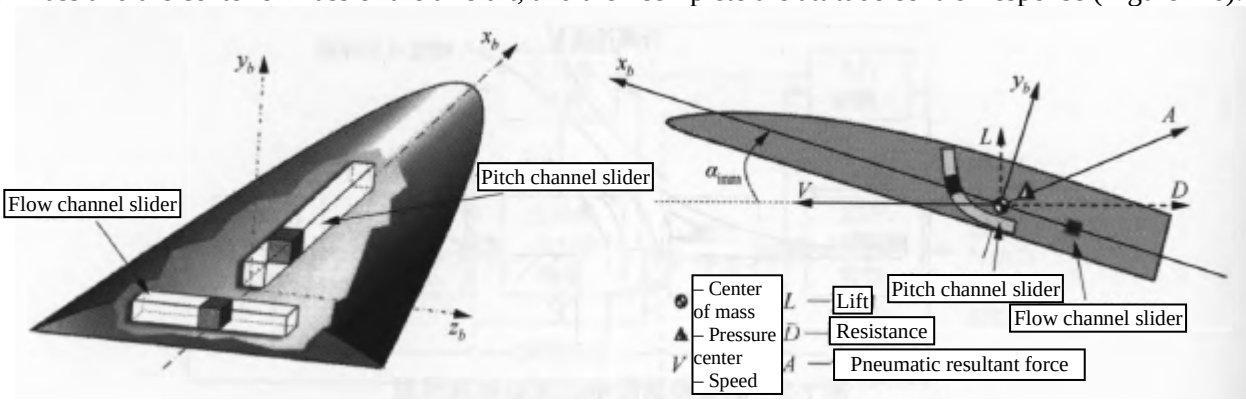

Figure 7-6: Center of mass attitude control

7.3.2 Embedded air data sensing systems

1. Role and demand

For the hypersonic vehicle powered by a ramjet engine, due to the high degree of integration between the engine and the body, the front and rear fuselages of the aircraft essentially become components of the ramjet engine, and the working conditions of the engine are highly sensitive to the aerodynamic attitude of the fuselage. For example, relevant foreign studies have shown that the control of the angle of attack should reach 0.5. The accuracy of the left and right. Under this requirement, the control of the flow field in the key area must be realized through the control of the aerodynamic attitude of the body, so as to meet the working requirements of the engine; at the same time, due to the highly integrated aerodynamic shape and aerodynamic heat and other factors, it will be difficult to apply the sensing methods such as pitot tubes commonly used in traditional conventional aircraft to hypersonic vehicles, which puts forward high requirements for the accurate acquisition of hypersonic atmospheric flight data, especially aerodynamic attitude data.

Atmospheric data such as total pressure, static pressure, angle of attack, and sideslip angle are the most basic parameters required by the main systems of the aircraft, such as flight control, fire control, navigation, and engines. Correct measurement of these parameters is very important for real-time control and post-flight data analysis, but due to the changes in the atmosphere and the constraints of sensor installation and performance, it is difficult to meet the accuracy requirements of the angle of attack obtained from the inertial navigation system alone. In order to improve the level of sensing and measurement technology and open up new ways of air data detection, many fruitful studies have been carried out abroad, among which the proposed and research of embedded air data sensing system (FADS) has opened up a new way to comprehensively improve the level of aircraft air data sensing and measurement technology.

The FADS technology measures the incoming pressure in real time by arranging a set of pressure measuring holes at a specific position of the fuselage, usually the head, and compares it with the mathematical model of pressure distribution at different Mach numbers and angles obtained by CFD calculation or wind tunnel test and uses a nonlinear recursive algorithm to reverse the parameter values such as attack angle and sideslip angle. Foreign studies have shown that the FADS system has been successfully applied to a variety of hypersonic vehicles and re-entry vehicles with blunt predecessors, and a feasibility study has been carried out on a hypersonic vehicle with a sharp-nosed shape.

2. Measurement principle of embedded air data system

The embedded air data system is a miniature barometric pressure sensor mounted on the surface of the head of the aircraft to measure and calculate atmospheric data such as total pressure, static pressure and angle of attack. Generally, four barometric pressure sensors are arranged on a certain cross-section of the head cone of the aircraft to measure the static pressure and angle of attack, and a barometric pressure sensor is placed at the apex of the cone to measure the total pressure, as shown in Figure 7-7.

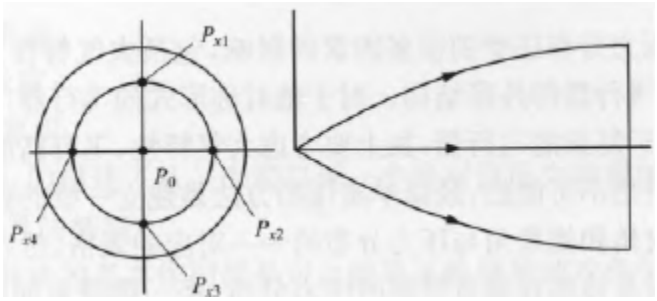

Figure 7-7: The basic layout of an embedded air data system sensor

In Figure 7-7, P_{x1}, P_{x2}, P_{x3}, and P_{x4} are the four measurement positions on the same cross-section, the first x of the subscript represents the serial number of the cross-section, which is called the "station," the second digit of the subscript represents the measurement position on the cross-section, and P0 is located at the vertex of the head. The total pressure Pt is measured with a barometric pressure sensor at P0, i.e.:

$$P_t = P_0 \quad (7.1)$$

Static pressure Ps is measured with barometric pressure sensors at P_{x1}, P_{x2}, P_{x3}, and P_{x4}, i.e.

$$P_s = 0.25\ (P_{x1}, P_{x2}, P_{x3}, P_{x4}) \quad (7\text{-}2)$$

Use the barometric pressure sensor at Px1, Px3 to measure the angle of attack barometric pressure Pa, i.e.

$$P_a = (P_{x1} - P_{x3}) \quad (7.3)$$

Among them, the angle of attack pressure Pa has a certain correspondence with the angle of attack.

In order to improve the measurement accuracy of the embedded air data measurement and sensing system of the aircraft, it is necessary to optimize the design of the measurement position of the barometric pressure sensor on the aircraft according to certain criteria and methods.

The results show that the optimal design should follow the following criteria: (1) select the position that maximizes the total pressure measurement, and (2) select the position that minimizes the static pressure measurement; (3) select the position where the measurement value of the angle of attack is maximized; (4) the same cross-section is selected for static pressure measurement and angle of attack air pressure measurement; (5) in addition to P_0, the distance between the optimal and sub-optimal stations is not less than 3 stations; (6) the distance between the optimal and sub-optimal stations of static pressure and angle of attack pressure is not less than 5 stations.

3. Key technologies and problems

1) Aerodynamic model of the pressure field of the aircraft forebody

The most basic idea of the FADS system is to estimate atmospheric parameters by measuring the surface pressure. In order to estimate atmospheric parameters, it is necessary to correlate the state of the atmosphere with the surface pressure, which is achieved through the establishment of an aerodynamic model that captures the characteristics of the flow field and can be adapted to the Mach number range. In order to be able to get atmospheric parameters in real time, the model had to be simple enough. At the same time, in order to describe the complex flow field problem by simplifying the model, the establishment of the FADS aerodynamic model can adopt the potential flow solution in the closed form at subsonic speed and the modified Newtonian flow theory at hypersonic speed, which is specifically related to the shape of the aircraft.

Since the surface pressure of the aircraft is related to the atmospheric parameters during the flight of the aircraft, it is possible to capture the atmospheric parameters by measuring the surface pressure of the aircraft, and indirectly obtain the angle of attack and sideslip of the aircraft. This is a reverse solution problem, the surface pressure of the aircraft is determined by the incoming flow conditions (Ma, p, ρ, α, β, etc.), and the incoming flow conditions need to be inverted according to the surface pressure, so it is necessary to establish a sensor function (derive atmospheric parameters from the data measured by the sensor).

The pressure distribution on the surface of the aircraft is also affected by many factors, including atmospheric characteristics, flight altitude, flight Mach number, etc., and most importantly, the shape and structure of the aircraft. For axisymmetric aircraft, the sensor function can be obtained analytically, but for complex aircraft, it is necessary to consider atmospheric characteristics, After the flight altitude and Mach number, it is almost impossible to get a simple analytical model, the most simple and practical method is to establish a one-dimensional data table, that is, according to different Mach numbers to establish a one-to-one corresponding table of attack angle and sideslip angle and pressure distribution, and then in the flight process, according to the Mach number obtained by inertial navigation and the pressure distribution measured by the sensor, the real-time angle of attack and sideslip angle can be obtained through the one-dimensional lookup table.

2) Arrangement of pressure measuring holes and pressure measuring pipelines

Pressure hole location selection: Since four atmospheric states and one scale parameter need to be estimated, at least five independent pressure measurements are used to obtain the entire atmospheric state. Estimating atmospheric parameters with five sensors is equivalent to a higher-order spline fit and leads to the sensitivity of the estimation algorithm to pressure measurement noise. Therefore, an additional sensor position is provided to reduce sensitivity to noise to increase the selection margin while achieving high performance. For example, the X-33 opted for a six-hole measuring scheme with five measuring positions at the head and a sixth at the edge of the C-C hood; the arrangement of the pressure holes of the atmospheric sensing system of the X-43A uses nine pressure holes to sensitive atmospheric parameters, four of which are used to calculate the angle of attack and sideslip angle, and the remaining five are used for flight data processing. The principle of choosing the location of the manometry is to be in an area where the pressure is relatively stable, that is, preferably before the laminar flow has not been converted; at the same time, it is best to measure the pressure to perceive the changes in the atmospheric parameters of the incoming flow to the greatest extent.

Manometry line arrangement: Each flight measurement subsystem is redundant and can produce usable results when the system hardware or software fails, i.e. this air data processing system must be redundant. Based on the above considerations, the design of the double pressure transmission pipeline can be carried out, and the details can be considered in the specific scheme.

The FADS system is based on the pressure line to measure the pressure signal, and the delay of the pressure must be considered. For the design of the real-time angle of attack estimation algorithm, the delay model of the manometry line is used to select the leg of the sensor to identify the FADS sensor that is out of the measurement range or is not available. Because each sensor has a different line length, each port (or pair of ports) corresponds to a pressure delay model.

At the same time, because the pressure value is transmitted to the sensor through the pressure measurement line for sensitivity, one is to use a high-precision absolute pressure sensor and a differential pressure sensor for measurement, and the other is a scheme in which each pressure measuring hole is transmitted through an absolute pressure sensor. The correlation studies show that the delay characteristics of the pressure measurement line in the absolute pressure measurement vary greatly over the entire pressure range. In contrast, the delay characteristics of a differential pressure sensor are essentially constant over the entire pressure range, in other words, the delay measured by the differential pressure with a pair of ports as input is only a function of the Mach number, independent of the input pressure, thus greatly simplifying the delay characteristic.

Because the length of the pressure line connected to each sensor is different, each pressure hole (or pair of pressure holes) corresponds to a pressure delay model. This pressure delay from the pressure orifice to the sensor is usually given in the form of a first-order filter:

$$\frac{P_{PPT}}{P_{port}} = \frac{k}{s+k} \tag{7.4}$$

Where: P_{PPT} — Measure the pressure value on the pressure measurement line;

k — a nonlinear function on the input pressure P_{port} and geometric measurements

$$k = \frac{1}{\tau} = \frac{P_{port}}{\mu}\left(\frac{g\pi D^4}{128LV_e}\right) \tag{7.5}$$

Where: D — nozzle diameter;

L — pipeline length;

V_e — effective volume.

Equation (7.4) and Equation (7.5) describe the delay characteristics from a port to an absolute pressure measurement.

3) Estimation algorithm and algorithm structure

The basic function of the real-time angle of attack estimation algorithm is to measure and estimate the angle of attack deviation obtained by the inertial navigation system based on the pressure measurement pipeline. The real-time FADS algorithm consists of two branches – FADS measurement and calculation and signal selection. All of these algorithms require Mach numbers to be provided by the inertial navigation system. At a relatively large speed, the Mach number provided by inertial navigation is more accurate if a representative atmospheric model is used.

The sensor layout given in the X-43A, although there are four pressure holes and four pressure sensors for real-time angle of attack estimation, only three angle of attack values can be obtained, i.e.:

$$\begin{aligned}
\alpha_1 &= \left[\frac{(P_{PPT2})}{\bar{q}}\right]C_{PPT2} \\
\alpha_2 &= \left[\frac{(P_{PPT4})}{\bar{q}}\right]C_{PPT4} \\
\alpha_3 &= \left[\frac{(P_{PPT3} - P_{PPT5})}{\bar{q}}\right]C_{PPT53}
\end{aligned} \tag{7.6}$$

where: α_1 — estimated forward angle of attack;

$\alpha 2$ — estimated backward angle of attack;

$\alpha 3$ — pseudo-differential angle of attack estimate;

C_{PPT} — the correction function of the manometer line with respect to the Mach number;

$\bar{q}$ — Dynamic pressure.

The sensor selection leg is to determine whether the FADS sensor has exceeded the measurement range or if the data is no longer available. There will be a certain deviation between the angle of attack value obtained by inertial navigation and the actual angle of attack, so the angle of attack value obtained by the inertial navigation system must pass through a first-order inertial link filter, which corresponds to the FADS angle of attack piezometer pipeline delay model obtained from the wind tunnel test data.

The filtered inertial navigation angle of attack is compared with two corresponding FADS angles of attack, and if the comparison value exceeds a certain limit value for a certain period of time, this FADS angle of attack value is considered unavailable. This limit is a function of the Mach number and is related to the delay that the system can tolerate.

The final FADS angle of attack value is the average of the values available in the previous three FADS angles of attack. The FADS final angle of attack is corrected by a first-order filter, and if all FADS sensors are not available, the deviation value is 0, that is, the FF will be used for flight control law calculation without any compensation.

4) Sensing components

For hypersonic vehicles, the measurement range is very wide, so the pressure sensors used in the FADS system need to have high measurement accuracy. In addition, atmospheric data estimates need to have high resolution over such a wide range. This can be considered to use two pressure sensors at the same pressure pore location with different entire measurement ranges, where one sensor has a very low range when the measurement pressure is relatively low and the other has a wide measurement range when the measurement pressure is high. This high-precision measurement over a wide measuring range can be achieved by structurally arranging it. However, it is difficult to place many sensors in the aircraft due to weight and space limitations. Therefore, it is best to use a pressure sensor with high accuracy with a wide range on each pressure hole.

5) Test conditions

The architecture and predictive model of the FADS need to be validated by static and dynamic pressure data from wind tunnel tests, so the required set of wind tunnel test conditions, processes, equipment, and conditions for testing must be considered. For example, it can provide continuous, closed-loop, variable-density supersonic wind tunnels and test areas for hypersonic airflow.

The internal layout of the test equipment of the American scramjet test aircraft object FADS contains 9 high-precision pressure sensors and a level, and the sensors are packed into the cooling jacket to prevent them from exceeding their operating limits during the test. The size of the model is 80% of the forebody of the original scramjet engine test vehicle, and the pressure measurement pipeline system used in the wind tunnel is the same as the hardware used in the test vehicle, and the Mach number range of the wind tunnel test is 3 to 8, the angle of attack is -6° to 12°, and the side slip angle range is -3°~3°. The analog and digital output signals are measured in the wind tunnel by high-precision pressure sensors, the digital signals are given by the high-precision pressure sensors at a sampling rate of 48.8 times/s, and the analog signals are given by a 16-bit A/D converter controlled by the wind tunnel computer.

FADS technology is an advanced air data sensing technology. The research and test experience of the United States, Japan, Russia and other countries in related fields shows that FADS technology is an insurmountable key technology for air-breathing hypersonic vehicles, and it is the core technology in the true sense.

7.4: Hypersonic vehicle guidance and control technology

7.4.1: Main Issues [40]

1) Real-time problems of the control system

Under hypersonic flight conditions, the response speed of the aircraft to the control is higher.

2) Control mode issues

In the process of hypersonic flight, the control efficiency of the control surface is greatly reduced compared with the subsonic/supersonic flight state. For example, under the flight condition of Mach number 5, the aircraft will descend by more than 1/3 at an altitude of 10,000m relative to 100m.

The higher the flight altitude, the more serious the problem, which may not provide enough control torque to meet the requirements of aircraft maneuvering; larger deflection of the control surface, in turn, will cause undesirable aerodynamic heating. Therefore, a combination of control surface and reaction control system is often used in the control of hypersonic vehicles [41,42].

3) Variable parameter problem

Due to the wide range of changes in operating conditions, the huge difference in aerodynamic characteristics of hypersonic vehicles at high and low altitudes, and the rapid changes in mass distribution, the dynamic characteristics and model parameters of the aircraft change very significantly in flight. When a hypersonic vehicle is flying in the atmosphere, the changes of local pressure and heat flux rate on the surface of the aircraft directly affect the aerodynamic characteristics of the aircraft due to the interference between shock waves and boundary layers in the local flow field caused by hypersonic airflow.

4) Uncertainty issues

Compared with subsonic/supersonic vehicles, hypersonic vehicles have many different flight characteristics, and some aspects cannot be fully mastered at present, which makes hypersonic dynamics present strong uncertainties. Hypersonic aerodynamics and propulsion characteristics are difficult to predict due to the lack of adequate flight tests and the inadequacy of ground test equipment. The integrated configuration of the engine and the fuselage makes the strong coupling between the elastic fuselage, the propulsion system and the structural dynamics lead to the flight dynamics of the air-breathing hypersonic vehicle to be very complex and uncertain. Under hypersonic conditions, the aerodynamic shape of the projectile is inevitably changed due to the ablation of the surface of the projectile, which affects the projectile model. The hypersonic vehicle uses lightweight materials, which are prone to aeroelastic vibration due to the disturbance of airflow and other factors during the flight. The various complex mechanical processes during the flight of an aircraft cannot be considered in complete detail in the aircraft control model used for control design. In addition, the flight is often subject to various disturbances that cannot be fully predicted in advance. The above factors directly lead to the distortion of the underlying structure and the uncertainty of the model and parameters of the hypersonic vehicle control system.

In addition, many random interference factors have a great influence on the flight state of the aircraft, for a typical hypersonic vehicle layout, the long-period mode is under-damped (or unstable), and the short-period mode is unstable, and its static stability boundary decreases with the increase of Mach number, and exhibits non-minimum phase characteristics [43]. The propulsion system of an air-breathing hypersonic vehicle is very sensitive to changes in the angle of attack [44]. All of the above features make the design of the controller for hypersonic vehicle control very challenging.

7.4.2: Flight Control Methods [45]

1. Gain preset control method

At present, most of the design of the control law of conventional aircraft flight control system at home and abroad adopts the traditional gain preset control method, which is an open-loop adaptive control, which changes the parameters of the controller by monitoring the operating conditions of the process and is an effective method in compensating for the change of parameters or the known nonlinearity of the object. For example, the X-43A flight test process is a gain preset control method.

When the aircraft is in a low dynamic pressure flight environment, and the system does not have particularly high requirements for the robust performance of the controller, the gain presetting method can be used, because this method has been widely used in engineering, the technology is relatively mature, and it is not limited by the speed of the computer. The design idea of the method is as follows: a plurality of linear controllers are used to approximate the required nonlinear controllers, many design points are selected in the flight envelope that needs to be designed with a preset gain controller, the principle of small perturbation is adopted, the nonlinear model is transformed into an approximate linear model at each design point, and then a linear controller is designed separately by using the traditional controller design method at each design point, so that the influence of nonlinearity can be overcome by switching between these linear controllers.

Finally, a complete nonlinear control law is obtained by interpolating between these linear controllers through a predetermined program.

The limitation of the gain preset control method is that the controller parameters are changed according to the open-loop mode, and there is no feedback from the performance of the closed-loop system, and when the dynamic characteristics and disturbance characteristics of the process are too significant, this method cannot obtain satisfactory control effect. In addition, the robustness of the gain preset controller is limited, and it is difficult to suppress the disturbance caused by uncertainty in complex environments. In addition, modeling errors can lead to abrupt changes in control law parameters when switching between different operating points, making it difficult to ensure the global stable performance of the system, especially when a system failure occurs, which requires an extremely large gain preset table. As a result, this approach may no longer be suitable when flight conditions become more complex.

2. Nonlinear control method

Nonlinear dynamic inverse is a new approach to designing flight control techniques that represents the nonlinear model of the aircraft as:

$$\begin{cases} \dot{\boldsymbol{x}} = f(\boldsymbol{x}) + g(\boldsymbol{x})u \\ \boldsymbol{y} = h(\boldsymbol{x}) \end{cases} \tag{7.7}$$

Where:

$$\boldsymbol{x} = [x_1, x_2, \cdots, x_n]^{\mathrm{T}}, \quad \boldsymbol{y} = [y_1, y_2, \cdots, y_n]^{\mathrm{T}}, \quad \boldsymbol{u} = [u_1, u_2, \cdots, u_n]^{\mathrm{T}}$$

The Lie differential is used to linearize the whole state feedback, i.e., y_i, differentiating γ_i times respectively until the control loser u_i appears in the differential formula, that is, in the final differential formula, at least one factor of u_i is not zero, when the sum of the differential degrees $\gamma = \gamma 1 + \gamma 2 + ... + \gamma m$ is equal to the order n of the system, the model can be fully linearized, and if $y < n$, the model can only be locally linearized. The biggest advantage of this approach over the gain preset method is that you don't have to think about how to interpolate the controller's "gain" during the design process. In addition, for systems with severe nonlinearity, the gain preset method may have a large error, but the feedback linearization method does not have this problem, because the linear model obtained by this method is an accurate linear model with no bias. Because the uncertainty of the model and other uncertain factors are not considered in the design process, the controller designed by the feedback linearization method cannot guarantee robustness, so it is usually used as a tool for model change in practical applications, and combined with other control methods with robust performance to design the control system of the aircraft.

After the feedback linearization, if the influence of uncertainty and the control action are in the same channel in the obtained aircraft linear model, the so-called control problem of matching uncertainty is obtained. In order to solve such problems, the dynamic inverse model obtained after linearization can be used as the inner loop, and the outer loop can be solved by the sliding mode control method with strong robust performance, so that the designed controller not only has the ability of nonlinear decoupling control, but also ensures the good robustness of the system.

If the effect of the aircraft uncertainty is not in the same channel as the control effect after the feedback is linearized, the so-called mismatch uncertainty control problem. This kind of control problem is rarely mentioned in the research, but it exists in a large number in practice, and there is no way to completely solve it at present, but for the uncertainty control problem of non-matching parameterizable aircraft, the backstepping method of parameter adjustment can be adopted. The backstepping method designs the sedation controller through the step-by-step correction algorithm to realize the global regulation or tracking of the system. At each step, the change of state coordinates, the adaptive adjustment function of uncertain parameters, and the calming function of a virtual control system with a known Lyapunov function are linked. It is suitable for uncertainty systems with state-linearized or strict parameter feedback and can be easily programmed with software.

3. Robust adaptive control method

Designing a flight controller with classical robust control (such as μ integrated design, quantitative feedback control, etc.) is actually to solve a very small optimization problem, and the best solution to the optimization problem is often obtained by considering the worst-case conditions, that is, a compromise between performance indicators and robustness, to a certain extent, at the expense of performance indicators. Adaptive control can adopt a variety of effective control design methods online and does not depend on the model of the object. The control law is directly adjusted according to the dynamic characteristics of the object. If the two are combined and applied to the control system of the aircraft, it can not only overcome the shortcomings of the classic robust control, which can only consider the worst conditions, but also ensure that the system has good robust performance.

The robust adaptive control method based on the online approximation model of neural network (or fuzzy system) is based on the ability of the Gaussian neural network (or fuzzy system) of a single hidden layer to approximate the arbitrary-dimensional continuous function online, and if it is used to approximate the uncertain part of the system model, and through the online parameter tuning, the strong robust performance of the controller can be guaranteed. The design idea of this method in the aircraft control system is as follows: firstly, the approximation method is used to approximate the unknown function of the uncertain influence in the aircraft model, that is, the approximation model function is used to replace the unknown function in the controller, and then the adaptive control law is constructed based on Lyapunov's stability theorem to ensure the stability and convergence of the whole control system. In addition, the online approximation method can be used to obtain the control model online, without considering that the model has a worst-case control problem. Generally speaking, the aircraft is subject to external disturbances and the mutation of its own model can also be regarded as a part of the uncertainty of the model, therefore, the maximum uncertainty is generally difficult to obtain, it will change with the change of the environment, and the requirements of classical robust control for the worst conditions limit its application in aircraft control. In addition, the adaptive inverse control method with neural network compensation also has a certain application prospect, the method adopts the output of the neural network to compensate the deviation between the inverse model and the actual model online, and this compensation process is carried out by adjusting the weight of the neural network online, and the adjustment rule of the weight is related to the uncertain model change, so as to ensure that the controller can effectively suppress the influence of uncertainty, and the whole control process is adaptive. In addition, the combined dynamic inverse control is a nonlinear control method, which can effectively decouple and coordinate the control of the nonlinear characteristics of the aircraft.

4. Other control methods

Fuzzy logic control uses expert knowledge and operator experience to form language rules directly into control strategies, its design does not depend on the accurate mathematical model of the controlled object, has good nonlinear control ability for nonlinear time-varying systems and systems that cannot establish mathematical models, and its control rules can also be optimized online by applying relevant methods, which is suitable for use in the controller design of highly nonlinear, time-changing, uncertain and strongly coupled complex aircraft models.

The total energy principle can also be used to study the control of the longitudinal mode of the aircraft, which was proposed by Boeing in 1979~1985 when it was working for NASA, after which NASA and Boeing conducted a large number of studies on total energy control systems, and in 1985 alone, five flight experiments were conducted on the B737. The design idea of applying the principle of total energy to the aircraft control system is to control the total energy of the aircraft by changing the engine thrust, and to coordinate the proportional distribution between kinetic energy and potential energy by adjusting the deflection of the elevator, so as to remove the coupling between the longitudinal flight trajectory and the speed of the aircraft, and realize the nonlinear decoupling control of its longitudinal mode. In addition, the controller is designed with little to no dependence on its own model, thus ensuring robust performance.

In recent years, with the development of control theory, many new control research directions have emerged, many of which are interdisciplinary disciplines between control theory and computer science or between control theory methods, which will contribute to the continuous improvement of the performance of flight control systems and provide new and feasible design methods for more complex aircraft control problems in the future.

7.5: Flight control techniques for reusable space launch vehicles [46,47]

7.5.1: Characteristics of the flight control system of reusable space launch vehicles

The reusable launch vehicle uses autonomous navigation and control technology. Its purpose is to establish and control the aircraft to fly according to the expected trajectory and use it as the outer loop control of the flight control system, send the desired attitude and propulsion instructions to the inner loop, and fuse with various signals of the stabilization control system to generate instructions to drive the change of the propulsion system and control surface. According to different flight purposes and accuracy requirements, the navigation control law needs to be divided according to different flight stages. Taking an airborne launch aircraft as an example, the flight phase can be divided into phases such as separation, dynamic climb, inertial climb, orbit cut-in, deorbiting, re-entry, terminal area flight, approach and landing, and abort flight.

The design features of the reusable launch vehicle flight control system have a lot in common with the Space Shuttle, but it emphasizes the following:

(1) Fully reusable, not partially reusable.

(2) Emphasize low cost, and when there is a contradiction between its cost and performance quality, first consider ensuring a lower cost.

(3) Fast reuse ability, short re-voyage time. It is easy to maintain and use, can take off again quickly.

(4) High reliability, easy maintenance and high performance, the ground system should be able to quickly detect potential problems of the aircraft.

7.5.2: Design requirements for reusable flight control systems

(1) It is necessary to ensure the accurate orbit control and attitude control of the aircraft during the entire flight phase.

(2) It is necessary to ensure the stability of maneuvering during the entire flight phase, including controlled flight from hypersonic to subsonic.

(3) It is necessary to ensure the safety and effectiveness of the flight control system during the whole flight stage, and to ensure that the mission modes of the flight control system can be easily and timely converted to each other, and to ensure that the transient change of conversion is small enough.

(4) Sufficient trim maneuvering ability should be ensured during the whole flight phase, and longitudinal and lateral maneuvering ability within sufficient distance should be ensured during the unpowered descent process.

(5) Precise energy control is guaranteed over the entire range of altitude and speed during the re-entry landing.

(6) In the whole flight process, it is necessary to ensure the effective coordination and appropriate conversion characteristics of the aerodynamic control surface, thrust vector control system and RCS (reaction thrust attitude control system) system.

(7) In the absence of the possibility of go-around, a successful approach and landing is guaranteed. This includes the high reliability and effectiveness of the automatic approach landing system, good flight quality characteristics, precise control of the landing site, and good ground taxiing stability.

(8) Ensure that the system has good maintainability and rapid reuse ability and realize the low cost of the system.

7.5.3: Key technologies for reusable flight control systems

1. Determination of design requirements

1) Determination of flight control system design requirements

(1) Determination of the scope and restrictions of the envelope and the weight index.

(2) System working environment conditions.

(3) System design specifications and system reliability requirements.

(4) Requirements for the use of aerodynamic control system, RCS (reaction thrust attitude control system) and thrust vectoring.

2) Research on flight control law design requirements

(1) Research and determination of flight profile and flight phase and determination of flight restrictions.

(2) Flight quality assessment criteria and design specifications.

(3) Analysis and study of the stability characteristics of basic layout manipulation.

(4) Top-level design requirements and modal settings of flight control law.

(5) The design requirements of the flight control law for the control mode and control power.

2. Key technologies for the design of operational stability and flight control laws

(1) Ensure good maneuverability and stability in the whole range of altitude and speed changes.

(2) Research on the design method of flight control law, design, coordination and conversion of flight control law and determination of parameters in each flight stage.

(3) Prevent the coupling of longitudinal and transverse motion caused by various reasons and lead to uncontrollable states such as deviation and divergence, including dynamic coupling, inertial coupling and aerodynamic coupling.

(4) RCS design parameter determination, aerodynamic control surface, RCS and thrust vector synthesis and coordination use.

(5) Integration of attitude control and orbit control.

(6) Ground flight quality simulation experiment verification and free flight experimental verification of control law design.

3. Key technologies for flight control system hardware design

(1) To ensure a high degree of reliability, redundancy management technology, light weight, advanced flight control system design technology.

(2) Comprehensive design of pneumatic control surface, RCS and thrust vector control.

(3) High-level automatic control system.

(4) Guarantee of manipulation of energy.

(5) Accurate and reliable flight parameters.

(6) Normal operation in a hot environment.

(7) Interface relationship with other systems.

(8) Low cost, good maintainability, and fast reuse ability.

(9) Sufficient experimental verification, such as full-scale system ground experiments.

References

[1] Luo Shijie, Hypersonic Cruise Vehicle Navigation System Scheme Research [D]. Xi'an: Northwestern Polytechnical University, 2006.

[2] Yang D. A review of navigational techniques employed in cruise missile and a proposed alternative solution [R]. N91-11744, 1991.
[3] Feng Yunsong. Characteristics and development trend of cruise missiles [J]. Aeronautical Science and Technology, 2004, (3):26-29.
[4] Zhou Yi, Wang Yongliang, Wang Ziyan. Characteristics and development status of hypersonic weapons [R]. Military Expo, 2004, (12).
[5] Roger F Blook, George F Gessler, William C Panter. The challenges of hypersonic-vehicle guidance, navigation and control [R]. AIAA-1990-3832, 1990.
[6] John D Schierman, David C Ward, Jason R Hull, et al. Adaptive guidance systems for hypersonic reusable launch vehicles [C]. IEEE-2001, 2001.
[7] Greenspan R L. Inertial Navigation Technology from 1970 [J]. Navigation. 1995, 42(1): 165 185.
[8] Qin Yongyuan, Zhang Hongqian, Wang Shuhua. Kalman filter and integrated navigation principle [M]. Xi'an: Northwestern Polytechnical University Press, 1998.
[9] Gan Guoqiang, Qiu Zhihe. Navigation and positioning [M]. Beijing: National Defense Industry Press, 2000.
[10] Yuan Xin, Yu Jixiang, Chen Zhe. Navigation system [M]. Beijing: Aviation Industry Press, 1993.
[11] Luo Jianjun, Yuan Jianping. Inertial navigation/dual-satellite positioning integrated navigation scheme and accuracy analysis [J]. Global Positioning System, 2005, (2):41-46.
[12] Ma Weihua. Design and interception probability calculation of inertial navigation/Beidou/pseudo-satellite integrated navigation [D]. Xi'an: Northwestern Polytechnical University, 2003.
[13] Dong Xurong, Zhang Shouxin, Hua Zhongchun. GPS/INS integrated navigation and positioning and its application [M]. Changsha: National University of Defense Technology Press, 1998.
[14] Wang Zhong, Ren Suping, Ouyang Shoucheng. Research on High Dynamic GPS/INS Integrated Navigation Algorithm [J]. Systems Engineering and Electronic Technology, 2001, 23(1):48-50
[15] Shen Gongxun, Sun Jianjun. Application of information fusion theory in inertial/astronomy/GPS integrated navigation system [M]. Beijing: National Defense Industry Press, 2001.
[16] Klotz H, Markus M, Grimm W. S. E. Strandmoe. Guidance and control for autonomous reentry and precision landing of a small capsule [C]. Proceeding of the 4th ESA International Conference, 2000.
[17] John W Hicks, Gary Trippensee. NASA hypersonic X-plane flight development of technologies and capabilities for the 21st century access to space [C]. NASA Dryden Flight Research Center AGARD Future Aerospace Technology in Service to the Alliance April 14-18, 1997.
[18] Douglas P Fuhry. Adaptive atmospheric reentry guidance for the Kistler K-l orbital vehicle [R]. AIAA- 1999-4211.
[19] Elmar M. Wallner Flaus H. Well, Klaus. Attitude control of a reentry vehicle with internal dynamics [R]. AIAA-2002-4647, 2002.
[20] Zhang Guoliang, Li Chengliang, Deng Fanglin, et al. Research on ballistic missile INS/GN SS/CNS integrated navigation system [J]. Missile and Space Launch Technology, 2004(2):11 15.
[21] Sun Jianfeng, Shen Gongxun. NS/GPS/CNC integrated navigation system [J]. Chinese Journal of Inertial Technology, 1994, 2(4):1 4.
[22] Li Yanhua, Fang Jiancheng, Jia Zhikai. Simulation research on INS/CNS/GPS integrated navigation system [J]. Chinese Journal of Inertial Technology, 2002, 10(6):6 11.
[23] Wang Anguo. History, current situation and development trend of astronomical navigation technology in the context of navigation warfare [R]. Astronomical Development, 2001, 19(2):326-330.
[24] Michael G Giebner. Tightly-Coupled Image-Aided Inertial Navigation System via a Kalman Filter [D]. Air University, 2003.
[25] Ge Zhiqiang, Huang Peikang. Covariance analysis of predetermined angle error of sight-of-sight pointing of ground-to-air missile [J]. Systems Engineering and Electronics, 2001, 23(1):1 4.
[26] Rotstein H, Refiner J, Ben-Ishai A. Kalman filter mechanization in INS/Seeker fusion and observability analysis [R]. AIAA-2001-4402, 2001.
[27] Xu Zhi, Hypersonic Aircraft Dynamics and Dynamic Characteristics Analysis [D]. Xi'an: Northwestern Polytechnical University, 2005.
[28] Wan Ziming, Li Yulin, et al. Flight mechanics and stabilization loop model of interceptor missile controlled by aerodynamic and direct lateral force composite control [J]. Modern Defense Technology, 2003, 31(2):18-22.
[29] Shaughnessy J D, Pinckney S Z, McMinn J D, et al. Hypersonic vehicle simulation model: winged-cone configuration [R], NASA TM-102610, 1990.
[30] McRuer D. Design and Modeling issues for integrated air-frame/propulsion control of hypersonic flight vehicles [C]. Proceedings of the American control conference, Boston, MA, June 1991: 729-735.
[31] Schmidt D K, Mamich H, Chavez F. Dynamics and control of hypersonic vehicles - the Integration challenge for the

1990’s [R]. AIAA Paper 91-5057, 1991.
[32] Schmidt D K. Dynamic and control of hypersonic aeropropulsive/aeroelastic vehicles [R]. AIAA Paper 92- 326, 1992.
[33] Li H F, Lin P, Xu D J. Control-oriented modeling for air-breathing hypersonic vehicle using parameterized configuration approach [J]. Chinese Journal of Aeronautics, 2011, 24(1): 81 89.
[34] Chavez F, Schmidt D K. An integrated analytical aeropropulsive/aero elastic model for the dynamic analysis of hypersonic Vehicles [R]. NASAARC92-2, 1992.
[35] Anderson J D. Modern Compressible Flow with Historic Perspective [M]. New York: McGraw-Hill，1982.
[36] League M, Farolhi S. Analysis of pressure distribution on hypersonic vehicles with power effects [R]. AIAA Paper 91-2491, 1991.
[37] Lees L. Hypersonic Flow [C]. The Fifth International Aeronautical Conference, Los Angeles, CA, 1995, 241-276.
[38] Calise A J, Buschek H. Research in robust control for hypersonic vehicles [R]. Progress Report No. 1 to NASA Langley Research Center, Contract No. NAG-1-1451, November 1992.
[39] Raney D L. Impact of aeroelasticity on propulsion and longitudinal flight dynamics of an air-breathing hypersonic vehicle [R]. AIAA-93-1367, 1993.
[40] Wu Hongxin, Meng Bin. Review of Hypersonic Vehicle Control [J]. Progress in Mechanics, 2009, 39(6):756-765.
[41] Zhang Jingnan, Sun Momeng, Zheng Zhiqiang. Discussion on the development of hypersonic weapon control technology [J]. Aviation Weapons, 2006, (4):11-13.
[42] Fidan B, Mirxnirani M, Ioannou P A. Flight dynamics and control of air-breathing hypersonic vehicles: review and new directions [R]. AIAA 2003-7081, 2003.
[43] Bolender M A, Doxnan D B. Flight path angle dynamics of air-breathing hypersonic vehicles [R]. AIAA 2006-6692, 2006.
[44] Walton J T. Performance sensitivity of hypersonic vehicles to change angle of attack and dynamic pressure [R]. AIAA Paper 89-2463, 1989.
[45] Liu Yanbin. Research on hypersonic vehicle modeling and its advanced flight control mechanism [D]. Nanjing: Nanjing University of Aeronautics and Astronautics, 2007.
[46] Zhang Ziyan. Flight control of reusable spacecraft [J]. Journal of Beijing University of Aeronautics and Astronautics.2003, 29(12):1105-1109.
[47] Sun Weimeng, Zhang Jingnan, Zheng Zhiqiang. Several growth points of hypersonic vehicle control technology [C]. Proceedings of the 12th Annual Conference on Control and Application of Chinese Society of Aeronautics and Astronautics, 2006:162-166.

Chapter 8: Wind Tunnel Testing Technology for Hypersonic Vehicles

Since its inception, aerodynamics has always been an indispensable and important link in the development of aircraft and is known as the "pioneer of aircraft development." As the demand for speed continues to increase, the problems faced by aerodynamics become more complex, and its role in the development of aircraft becomes more important. In hypersonic aerodynamics, in addition to the complex flow field environment around the aircraft, there are more problems to be solved than classical aerodynamics. Hypersonic aerodynamics has three main topics, namely aerodynamics (lift, drag, torque, center of pressure, etc.), aerothermal (heat flow calculation, heat protection measures, etc.), and aerokinetics (optoelectronic characteristics of the flow field, etc.). Because the aerodynamic, aerothermodynamic, and physicochemical phenomena of hypersonic flow are intertwined and affect each other, solving the problem of hypersonic aerodynamics is more difficult than ever before, and it also relies more on the close integration of multiple research methods.

In order to solve the aerodynamic problem of hypersonic vehicles, it is necessary to obtain data by three means: theoretical calculations, ground wind tunnel tests, and flight demonstration verification tests. These three instruments complement each other, supplement each other and validate each other. Finally, it is necessary to solve specific aerodynamic problems by comprehensively analyzing the results obtained by the three means.

Hypersonic aerodynamic ground wind tunnel testing requires simulating many parameters, including free-flow Mach number, Reynolds number, velocity, total enthalpy of flow, density ratio before and after shock wave, test gas, wall-to-temperature ratio, and thermochemical properties of the flow field. It is not possible to simulate all of the above parameters at the same time and must be simplified as needed. Therefore, hypersonic aerodynamic testing is a partial simulation technique with certain limitations. However, compared with flight tests, it costs less and is more flexible, easy to control, and easy to obtain data; compared with the numerical simulation of the calculation program, the test environment is more realistic, the test results are more reliable, and the discovery and research of some new aerodynamic phenomena often start with wind tunnel tests. Therefore, it has always played a key role in the development of hypersonic vehicles [1].

Judging from the history of aerospace development in various countries, huge human, material, and financial resources have been invested in hypersonic ground simulation tests in the development of hypersonic vehicles. For example, the U.S. Space Shuttle Research Program conducted a total of 709 ground simulation tests, with a total of 71,297 hours of testing [2].

In recent years, with the continuous heating up of the development of advanced hypersonic vehicles, there are more and more special hypersonic experimental research projects. This chapter will elaborate on some related issues of hypersonic vehicle wind tunnel testing, especially the scramjet engine wind tunnel free jet test and the hypersonic vehicle fuselage/propulsion integration test, which are closely related to hypersonic propulsion system technology.

8.1: Tasks and requirements for wind tunnel testing of hypersonic vehicles

8.1.1: Mission for wind tunnel testing of hypersonic vehicles

The aerodynamic wind tunnel test of hypersonic vehicles faces the following three major tasks.

1. Reveal the nature of air flow through experiments

Due to the complexity of air movements, aerodynamics, in particular, is inseparable from scientific experiments.

The development of aerodynamics depends to a considerable extent on the level of experimental research, and complex physical phenomena and problems in aerodynamics are first studied experimentally. For example, the existence and characteristics of the boundary layer, the interference of shock waves with the boundary layer, aerodynamic problems at high angles of attack, interstage separation, the flow of the bottom of the rocket engine, the influence of wind loads on the launch and flight process of spacecraft, the study of transonic jitter and control surface flutter, the mechanics of warhead aerodynamic heat protection and re-entry aerodynamics, communication interruption and particle cloud erosion, etc. Hypersonic aerodynamic experiments mainly focus on the study of dynamics in hypersonic flow.

2. Verify the results of theoretical analyses and calculations in aerodynamics

Aerodynamics, like any other natural science, requires experimental verification before it can be determined. In theoretical analysis and calculation, the necessary simplification of the studied phenomenon is generally carried out first, mathematical models and equations are established, and finally certain conclusions, formulas and data are obtained. Although theoretical analysis and calculation have the advantages of systematic, universal, time-saving, and labor-saving, there is always a certain difference between the simplification and assumption made and the real phenomenon, so the results obtained from theoretical analysis and calculation should be verified by experiments to verify the approximation degree and reliability of the period, and only in this way can it be applied to engineering design. Even the theoretical formulas that have been used in the aerodynamic design of various types of aircraft or their components have been modified by the empirical coefficients determined by experiments, and some formulas are obtained by fitting the experimental results.

3. Provide aerodynamic data for aircraft design

In the process of developing and modifying the aircraft, only by closely combining the theoretical calculation with the model aerodynamic test can we comprehensively solve the various complex aerodynamic problems we are facing. The general practice is to calculate according to the existing theoretical results and test results combined with specific requirements, put forward the direction for model development and selection, qualitatively determine various preliminary schemes, and then conduct tests through ground simulation equipment (wind tunnel or other test equipment) to obtain a large amount of data under various conditions for analysis, comparison, and finalization. Due to the complexity of the shape and flow phenomena of some aircraft, reliable aerodynamic data can only come from experiments, therefore, in the development process of modern aircraft, not only large-scale theoretical calculations, but also tens of millions of model aerodynamic tests.

In terms of specific research content, the main task of hypersonic wind tunnel test is to solve various hypersonic aerodynamic-related problems in the development process of hypersonic vehicles, mainly including:

(1) Hypersonic stationary aerodynamic load.
(2) Hypersonic unsteady aerodynamic load.
(3) Hypersonic aerodynamic layout.
(4) Superb boundary layer transition.
(5) Turbulence measurement and turbulence modeling.
(6) Hypersonic drag reduction.
(7) Hypersonic separation flow aerodynamics.
(8) Hypersonic inflow/propulsion.
(9) Hypersonic vortex motion and utilization of vortex lift.
(10) Hypersonic high angle of attack aerodynamic characteristics.
(11) Hinge moment of attitude control structure.
(12) Interstage/multi-body separation.
(13) Ablation/aerodynamic coupling.

(14) Rollover project.
(15) Static/dynamic stability of hypersonic vehicles.
(16) Kinetic problems of rarefied gases.

8.1.2: Requirements for wind tunnel testing of hypersonic vehicles

There are many types of aerodynamic tests for hypersonic vehicles. Test principles, test methods and wind tunnel conditions used are different, so different types of tests have their own specific requirements. According to the requirement of obtaining reliable test data at the minimum cost of aerodynamic testing, the general requirements for aerodynamic wind tunnel testing of hypersonic vehicles can be summarized as the following three points.

1. Similarity requirements

Hypersonic aerodynamic tests tend to use much smaller scale-down models than actual aircraft, so it is important to keep the wind tunnel tests aerodynamically similar to actual flight. Only by maintaining the similarity can the corresponding values of the simulated objects be obtained from the velocity field, pressure field, temperature field, aerodynamic force and torque obtained from the model test through dimensionless transformation. Aerodynamic similarity requires the following (necessary and sufficient) conditions for model testing:

(1) Geometrically similar, proportional to the corresponding size.

(2) The flow around the model and the flow around the prototype are flows of the same nature and can be described by the same basic equations of motion.

(3) The boundary conditions are similar, and the boundary conditions of the surface flow of the model are proportional to the corresponding prototypes.

(4) The initial conditions are similar, if it is an unsteady flow problem, the initial conditions of the model test should correspond to the prototype.

Due to the limitations of wind tunnel simulation, the test conditions often cannot meet all the similarity criteria, which requires the simulation of key parameters according to the physical nature of the problem, and the data correction, data correlation or direct ignorance of the relatively minor similarity conditions as the case may be.

2. Credibility requirements

The confidence of the test data includes two aspects: precision and accuracy. The accuracy of wind tunnel test data depends on the combination of a large number of interrelated factors. Figure 8-1 shows the flow chart of the wind tunnel data in the aerodynamic test. Errors in any one of the plots will result in errors in the final test data.

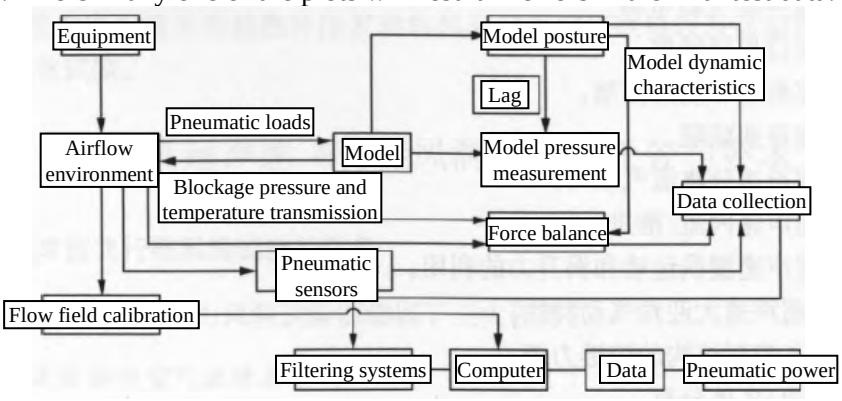

Figure 8-1: Wind tunnel data flow diagram for aerodynamic test [1]

As can be seen from Figure 8-1, the machining quality of the model and the flow field quality of the wind tunnel will directly affect the accuracy of the data. The inaccurate control and measurement of the attitude (angle of attack and sideslip angle) of the model relative to the direction of the airflow will inevitably increase the error of the data. The force and pressure acting on the model are the data directly required for the test, and the sensitivity of the balance, pressure sensor, temperature drift, pressure hysteresis, and the dynamic characteristics of the model and support system all affect its accuracy. All the measured parameters of the wind tunnel must be input to the computer for data processing through the data acquisition system, so the error of the data acquisition system and the error of data processing will also affect the accuracy of the final obtained aerodynamic coefficient. Therefore, to improve the accuracy of aerodynamic data, we should start from the above links and take corresponding methods to reduce the accumulation of errors.

According to the error theory, the accuracy of the wind tunnel test refers to the degree of agreement between the test value and the true value, and people usually regard the flight value of the aircraft as the true value. Since the shape and test environment of the wind tunnel model are not exactly the same as the geometry and flight environment of the real aircraft, the wind tunnel test data must go through a series of corrections (such as geometric non-simulation, bracket interference, air intake, jet, Reynolds number, elastic effect, etc.) before it can be compared with the flight data. However, the flight test itself has a series of errors, and its accuracy is much lower than that of the wind tunnel test, so the comparison of the wind tunnel test data with the real flight value still cannot determine the accuracy of the data. To solve the accuracy problem of wind tunnel test data at home and abroad, the accuracy is generally evaluated through the standard model (also known as calibration model) test. The so-called "standard model test" is to use the model whose aerodynamic characteristics have been well known to people, to carry out tests in different types and sizes of wind tunnels (some also carry out model free flight tests), comprehensively analyze and process the test data or compare with the theoretical calculation results to obtain the test data with the highest accuracy and the least interference as the "standard data," and use it to judge the accuracy of other wind tunnel test data.

It can be seen that the standard model test must be carried out before the new wind tunnel, new balance and new system or device related to the force measurement test are used to ensure the accuracy of the test. Currently, the widely used standard model of hypersonic aerodynamics is a set of HB models provided by the North Atlantic Treaty Advisory Group on Aeronautical Research and Development (AGARD), each of which represents a typical different type of spacecraft.

3. Economic requirements

Hypersonic flow is a flow of high energy. A comparison of the typical orbits and corresponding energy fluxes of various hypersonic vehicles shows that extremely high power is necessary to achieve a full simulation. In the $Ma \leq 10$ or speed range below 3,000 m/s, the power required for intercontinental missiles is 100 to 10,000 MW, the power required for hypersonic transport aircraft is 10 to 100 MW, and even the gliding lift vehicle with the lowest energy requirement is also on the order of 10 MW. The reality is that the acceleration of the fluid to a specified speed is accompanied by a large amount of energy loss, and the kinetic energy of the fluid is often not recovered efficiently, so the power required for the actual simulation will be one to two orders of magnitude greater than the ideal value described above. This places a heavy burden on the simulation of aerodynamic tests. On the one hand, in order to reproduce the flight state of the hypersonic real orbit, the high power value required by the continuous equipment is actually unattainable; on the other hand, even if the gap in state simulation is narrowed by the construction of high-power wind tunnel equipment, the cost of testing is staggering.

Therefore, when conducting hypersonic aerodynamic tests, it is necessary to consider the benefits of the experiment, desired goal and cost. First of all, it is necessary to make necessary trade-offs according to the analysis of the simulation criteria to minimize the simulation requirements. Secondly, it is necessary to select the appropriate equipment and test status according to the test items and accuracy requirements, reasonably arrange the tests, and effectively control the number of tests; thirdly, for special tests that cannot be simulated by conventional wind tunnel equipment, the test should be carried out by temporary impulse or pulse as much as possible, and the force measurement technology of transient measurement and processing should be vigorously developed.

8.2: Types of hypersonic wind tunnel equipment

8.2.1: Wind Tunnel Equipment Overview

Hypersonic aerodynamic ground simulation test equipment is the basic equipment for the development of various aerospace vehicles, basic aerodynamic research and productive tests. So far, most of the major aerodynamic research in the development of missile and space technology, as well as the research on new aerodynamic layouts in the development of various aerospace vehicles, have been mostly completed in wind tunnels. With the development of aerospace technology and various strategic and tactical missiles, hypersonic speed, supersonic speed and various high-speed and high-enthalpy test equipment have developed rapidly, hypersonic wind tunnels, ultra-high-speed test equipment, shock tubes and shock wave wind tunnels, cannon wind tunnels, heavy piston gun wind tunnels, low-density wind tunnels, arc heating wind tunnels, high-temperature thermal structure wind tunnels, thermal jet wind tunnels, long-shot wind tunnels, Ludwieg tube wind tunnels, arc jet wind tunnels (including plasma heating devices), expansion tubes and expansion wind tunnels, slow-piston compressor wind tunnels, ballistic targets, Countercurrent target impact test equipment has been developed to meet the rise of high-performance aerospace technology, and plays an important role in the research of aerodynamics, aerothermal, and aerophysiology.

Hypersonic wind tunnel equipment usually refers to ground simulation test equipment in the $Ma \geq 5$ speed range, and equipment operating in the state of high enthalpy becomes ultra-high-speed equipment. In a hypersonic wind tunnel, in order to avoid condensation of the air entering the test section, the air medium must be heated, and the lowest heating temperature is determined by the static pressure of the flow field in the test section equal to the saturated vapor pressure, i.e., using the Clausius-Clapeyron equation:

$$\tan p = B - A/T \tag{8.1}$$

where: p – unit of atmospheric pressure;

T – K unit.

For different gases**,** the constants B and A are slightly different, and B = 4.45 and A = 360 for air; B = 4.778, A = 359.09 for nitrogen. Using the isentropic flow relation with the specific heat ratio y as a constant, the minimum requirement for total temperature heating of air can be written:

$$\frac{360}{T_0}\left(1+\frac{2}{\gamma-1}Ma^2\right)=4.45+\frac{\gamma}{\gamma-1}\lg\left(1+\frac{2}{\gamma-1}Ma^2\right)-\lg P_0 \tag{8.2}$$

Knowing the Ma and the total pressure of the anterior chamber P_0, the T_0min value can be obtained. For Ma = 10, P_0 = 10Mpa, T_0 must be greater than 1000K, Ma = 20, P_0 = 100Mpa, T_0 must be greater than 3000K, so the hypersonic wind tunnel has higher temperature requirements than the supersonic wind tunnel airflow, sometimes in order to get as close as possible to the pressure and temperature environment near the aircraft during flight, the heating temperature of the required gas is far more than the temperature of gas condensation. At high temperatures, there is also a real gas effect, the specific heat ratio γ changes with temperature, and the oxygen and other components in the gas are successively dissociated, electrolyzed, and chemically equilibrated.

8.2.2: Types of hypersonic wind tunnel equipment

1. Conventional hypersonic wind tunnel

Conventional hypersonic wind tunnels are usually divided into two types: continuous and transient, and transient are divided into downblowing (high-pressure gas directly discharged to the atmosphere), blowing and suction (high-pressure-vacuum), and blowing (high-pressure-ejection). Wind tunnel test Ma = 5 to 12. Compared with supersonic wind tunnels, hypersonic wind tunnels have the following characteristics:

(1) The pressure of the high-pressure gas source is high, usually 22 to 40Mpa, and the operation time of the wind tunnel is related to the pressure and volume of the high-pressure gas source.

(2) It has a high-temperature and high-pressure fast valve, which is convenient for controlling the high-temperature and high-pressure medium from the heater outlet, and when the pressure and temperature meet the test requirements, the valve is required to be opened (or closed) quickly and conveniently under high-temperature and high-pressure conditions.

(3) In order to avoid liquefaction and condensation of the test medium, different forms of heaters are set in the wind tunnel.

There are usually two types of heaters: electric heating type and regenerative type, the electric heating structure is relatively simple but consumes more power, the regenerative structure is more complex, and the preheating time is longer. Electric heating type mainly includes resistance tube heater, resistance belt heater, the selection of high-temperature resistant alloys such as Kanthal alloy can be heated to 1450K (elements up to 1600K), with SiC can be heated to more than 2000K, under high temperature conditions, oxygen in the air will make the element oxidized seriously, by direct resistance heating and obtain high temperature, must be changed to nitrogen medium, then the real gas effect is also very small. Tungsten is used as a heating element, and nitrogen can be heated to 2200K. An arc jet pulse air heater is used, with Ma = 9, T_0 can reach 3200K, P_0 = 10.5Mpa, and t = 30s. The main type of heat storage heater is a cobblestone bed heater. The heating elements include Al2O3, SiC, ZrO2, ThO2, MgO, etc., but small particles of refractory materials and other impurities will pollute the airflow. Usually, in order to improve the quality of the gas and eliminate the impurities in the test gas, a 5-10μm filter is set at the outlet of the heater. There are also heat storage heaters that use resistance to heat the medium. In addition, there are gas heaters (which can be heated to 750K), orifice plate heaters (first use kerosene, etc. to heat the metal orifice plate, and then the air passes through the plate to heat the gas), graphite heaters (which can be heated to 3000K, requiring high purity of the medium nitrogen, T_0 > 3000K, there is a cyanation reaction), arc directly heats the medium nitrogen, argon, etc. (heated to 5500K), and combustion of hydrocarbon materials or hydrogen to heat the air, etc. There are also heaters that combine electric heating and regenerative heating.

(4) The nozzle should consider the problem of throat cooling and thermal deformation, and in order to reduce the thickness of the boundary layer at the outlet of the nozzle, the nozzle should have better cooling measures.

(5) The blowing wind tunnel should have an ejector, which was an annular nozzle ejector in the early days, and in order to improve the ejection efficiency, a new type of ejector has been introduced, such as multi-nozzle and multi-stage composite ejector. Most hypersonic wind tunnels in Europe and the United States use blow-suction type.

(6) Vacuum tank device, blowing and suction wind tunnel must have a vacuum ball or vacuum tank, and the operation time of the wind tunnel is related to the volume and vacuum degree of the vacuum tank.

2. Shock tube and shock wind tunnel

The shock tube is a tube with one section closed and the other end open or closed, the tube is divided into two sections with a diaphragm in the middle of the tube, and the two sides of the diaphragm are filled with gas of different pressures before the test. The section with lower pressure is called the low-pressure section or driven section, and the section with higher pressure is called the high-pressure section or driven section.

The shock wave wind tunnel uses the gas heated by shock wave compression as the gas source of the wind tunnel and is equipped with two diaphragms at the end of the low-pressure section, followed by a nozzle, a test section and a vacuum tank. When the incident shock wave reaches the end of the low-pressure section, it is reflected and propagates upstream, and the gas pressure and temperature after the shock wave compression rises, breaking through the second diaphragm, and the expansion and acceleration through the nozzle to obtain a hypersonic gas flow at the nozzle outlet.

Depending on the simulation requirements, seam run, sub-suture run, and over-stitch run (also known as balanced run) techniques can be used. Suture contact operation for maximum effective test time, sub-suture contact operation for the highest chamber pressure for high Reynolds number simulation, and through-suture contact operation for the highest chamber temperature.

The main features of the shock wave wind tunnel are as follows:

(1) The range of Mach number and Reynolds number is wide. The shock wave wind tunnel is a pulsed hypersonic wind tunnel, and the free flow Mach number range of its test section is very wide, generally up to 6 ~24. This requires a high detention temperature in the wind tunnel to prevent operation at high Mach numbers, the air flow in the wind tunnel test section condenses.

The free flow unit Reynolds number range of the shock wave wind tunnel test section is generally 3.8X103 to 5.0X108, and most of the high Mach number and high Reynolds number tests can only be completed in the shock wave wind tunnel.

(2) The operation of the shock wave wind tunnel requires a large pressure ratio. Like ordinary hypersonic wind tunnels, the pressure ratio of shock wave wind tunnels rises sharply as the Mach number increases. For example, when *Ma* = 10, the pressure ratio calculated by the positive shock loss in the test section is 42,439; when *Ma* = 15, the pressure ratio is 660,165. In order to form such a large pressure ratio, it is not enough to increase the stagnation pressure, it is also necessary to configure a vacuum system to maintain a high vacuum in the test section to meet the requirements of wind tunnel operation.

(3) The effective test time of the shock wave wind tunnel is short. The most significant feature of the shock wave wind tunnel is that the effective test time is short, generally only 2 to 20ms, so it is customary to call the shock wave wind tunnel pulsed wind tunnel.

3. Ludwieg Pipe Wind Tunnel

The Ludwieg tube is a long tube of equal diameter, one end is closed, and the other end is equipped with a diaphragm connected to the nozzle, test section, and acuum tank, which forms the Ludwieg pipe wind tunnel. The effective testing time of the Ludwieg Pipe Wind Tunnel depends on the length and inner diameter of the tube. The free-flow Mach number in the test section is generally 2 to 3, and in order to increase the Mach number in the test section, it is necessary to heat the gas in the tube to prevent condensation of the test gas when operating at high Mach numbers. German Ludwieg pipe wind tunnel with external heating, t = 0.3s, *Ma* = 5~6.9 and 9.3~11.7, P_{0max} = 4.2Mpa, 15.4Mpa, T_{0max} = 770K, 1270K, Re = lx107/m, 7x105/m, pipe diameter ϕ 0.508m, with a length of 80.5m.

4. Cannon Wind Tunnel

In the shock tube, the contact surface is replaced with a piston of limited mass, which is placed behind the diaphragm. When the diaphragm ruptures between the high-pressure section and the low-pressure section, the driving gas pushes the piston to accelerate the motion, and when the piston moves to a sound speed higher than the driven gas, a shock wave is generated in front of the piston, and the shock wave is reflected after reaching the end of the driven section, encountering the piston, and reflecting back and forth between the end of the driven section and the piston. After many reflections, the damping oscillation of the piston tends to be balanced, and at the same time, the driven gas is repeatedly compressed and heated to reach a high-pressure and high-temperature equilibrium state, and when it breaks through the diaphragm connected to the nozzle, it becomes the high-temperature and high-pressure gas source for the operation of the blast wind tunnel. This is similar to how a shock tube works. If you assume that the piston mass is zero, it is a shock wave wind tunnel. The advantage of the blast wind tunnel is that the piston separates the driven and driven gas, so that the expansion wave of the driven section does not affect the gas in the driven section, and the effective test time is longer (30 to 100 ms). The disadvantage of the cannon wind tunnel is that during the test, the air source parameters of the wind tunnel decay quickly, so that the effective time of the test is reduced, so it is necessary to properly match the initial conditions of the piston mass, the driving gas and the driven gas, so that the pressure of the gas source parameters is basically constant during the effective test time. Typical operating performance is 300 to 600 m/s, T_0 = 2000 K, P_0 = 35 Mpa, *Ma* = 8 to 12, and the drive gas can be air, hydrogen, or helium.

5. Long-shot wind tunnel

The piston of a long-shot wind tunnel is heavier than that of a gun wind tunnel, so it is also called a heavy piston gun wind tunnel. It can withstand high pressures, so it can operate at high Reynolds numbers. The heavy piston compresses the driven gas under the action of the high-pressure driving gas, and a shock wave is formed in front of the piston, and a very high pressure and temperature peak is formed in the front chamber of the wind tunnel with the forward movement of the shock wave, in order to maintain this peak, a one-way valve is set at the entrance of the front chamber, when the piston jumps back, under the action of reverse pressure difference, the one-way valve is closed, and the high-pressure and high-temperature gas is closed in the front chamber. When the diaphragm at the inlet of the nozzle ruptures, the high-pressure and high-temperature gas in the front chamber expands through the nozzle and flows into the test section, forming a hypersonic gas flow. Because the anterior chamber pressure is more than 5 to 10 times higher than the driving gas pressure, the Reynolds number is high.

The typical parameters of VKI long-shot wind tunnel are as follows: T_0 = 2000K, P_0 = 210Mpa, *Ma = 27*, *t* = 40ms; when *Ma* = 15, *Re* = 107/m, and when P_0 is higher, *Re* also increases.

6. Thermal jet wind tunnel

The thermal radiation wind tunnel consists of an arc chamber, a nozzle, a test section, and a vacuum box. A large amount of electrical energy is stored in the arc chamber, and the working gas is compressed and heated by discharge. When the pressure rises, the diaphragm at the entrance of the nozzle bursts, forming a hypersonic gas flow. The working time *t* = 20-100ms, the discharge power of the thermal radiation wind tunnel is large, and the required electrical energy is also large. The typical energy storage amount is 1.6-6.5MJ/m^2, and the largest thermal radiation wind tunnel (test section ϕ2.54m) has a 328MJ/m^2 energy storage device. The maximum energy storage capacity of the capacitor type can reach 33MJ/m2; the inductive energy storage can reach 16-328MJ/m^2; the direct power supply from the power grid can reach 33MJ/m2. Considering that the arc chamber material has serious pollution to the working gas at high temperatures (chemical, thermodynamic effects and mechanical effects), the working gas uses nitrogen, $T_0 \leq 4000$K, $P_0 \leq 140$Mpa, $v \leq$ 3km/s, providing *Ma* and scale Re aerodynamic simulation, its Re-Ma range is the same as the shock wave wind tunnel, but its effective test time is 1-2 orders of magnitude larger. If the pressure of the arc chamber increases, use a large arc chamber, increase the electrical energy, and the range of the thermal radiation wind tunnel can be expanded. In the test time of 100ms, it can be used for variable angle of attack test, dynamic stability test and ramjet engine test.

7. Hypersonic low-density wind tunnels

It is a rarefied gas dynamic test facility with a simulated altitude of 60~100 km. The low-density wind tunnel is composed of an air source, a dryer, a heater, a leakage valve, a front chamber, a nozzle, a test section, a stability box, a diffuser, a cooler and a vacuum system, etc., and the test time is greater than 100s, *Ma* = 10~25. The wind tunnel is tested under low-pressure, low-temperature, small-scale conditions.

8. Arc-heated wind tunnels

It is composed of arc heater, nozzle, test section, diffuser section, isolation valve, heat exchanger, ejector, etc. The power reaches the megawatt level and is used for aerodynamic and aerothermal experimental research. All kinds of arc heaters – vertical flow type, parallel flow type, stacked flow type, long segmented type, etc., do ablation performance test of thermal protection materials, sometimes need to measure the force while ablation, as well as measure the total enthalpy, heat flow, density, non-equilibrium temperature, etc.

9. High-temperature thermal structure wind tunnel

The wind tunnel is mainly used for the heat protection test and identification of large-size thermal structure components, the diameter of the wind tunnel is φ = 1~2 m, the test time is t = 120~180s, Ma, Re, and P simulate the flight environment, and the simulated altitude H = 25~40km. The high-temperature thermal structure wind tunnel is composed of a gas generator (methane + air, oxygen combustion), a nozzle, a test section, an over-expansion section and an ejector.

10. Ultra-high-speed free-flying ballistic target

It is composed of a model launcher and a ballistic range, the simulated launcher generally uses a two-stage hydrogen cannon, the emitter outlet has an expansion chamber, the pressure and temperature of the ballistic range are determined according to the requirements of the simulated environment, and the ballistic target can simultaneously simulate the application and secular flight altitude of the re-entry vehicle, and carry out re-entry aerodynamics, aerophysical studies – resistance, stability, photoelectric characteristics in the plasma sheath and wake, boundary layer transition, multi-wave interference, etc.

11. Counter-current wind tunnel

The countercurrent target consists of a supersonic/hypersonic wind tunnel, a shock wave wind tunnel, and a light air cannon. The high Mach number airflow flows from upstream to downstream in the wind tunnel, and the light air cannon fires the test model from downstream to upstream, which can obtain a higher relative velocity or Mach number of the model. The relative velocity is synthesized by the light air cannon and the wind tunnel, and the test technology is the same as that of the conventional ballistic target, which can measure the C_D for static/dynamic stability test. The countercurrent test time is short, the environmental conditions are not as good as the wind tunnel, but the test Mach number is high, which is suitable for radiation measurement of shock layer, material ablation, wake, heat exchange measurement, C_D of $Ma = 34$, stability and transition position measurement.

8.3: Hypersonic wind tunnel test format

Table 8-1 shows the hypersonic aerodynamic test items.

Table 8-1: Hypersonic aerodynamic test items and main characteristics

Serial number	Experimental project	Measured content	Main test equipment and the test device	Main application background
1	Full mode force test	Measurement of longitudinal and transverse aerodynamic characteristics of all modes	Six-component balances, pressure sensors, etc.	It provides a basis for the aerodynamic design of the aircraft
2	Pressure distribution test	Measurement of surface pressure distribution characteristics	Pressure sensors, electronic scanning valves, pressure measurement systems, etc.	Provide aerodynamic data for aircraft design
3	Hinge moment test	Measure the moment characteristics of the rudder hinge on the rudder surface	Hinged torque balances, pressure sensors, etc.	It provides a basis for aircraft servo design and control design
4	Dynamic stability test	Measure the dynamic stability characteristics of the model	Dynamic derivative measuring device, etc.	It provides a basis for the design of aircraft dynamic stability
5	Jet interference test	Measure the interference characteristics of jets with the force, moment, and pressure distribution of the model	Balances, pressure sensors, jet test devices, etc.	It provides a basis for the design of aircraft jet interference system
6	Interstage separation or multibody separation test	Measure the characteristics of force and moment and pressure distribution in interstage or multibody separations	Balances, pressure sensors, special support devices, jet flow test devices, etc.	It provides a basis for the design and control of aircraft separation scheme
7	Model free-fly test	Measure the motion characteristics of the model, and obtain static and dynamic aerodynamic characteristics	Model transmitters, high-speed cameras, data interpretation and processing systems, etc.	It provides a basis for the aerodynamic design of the aircraft
8	Small rolling torque test	Measure the roll torque characteristics of the model	Special balances, special support devices and other special devices, etc.	It provides a basis for the design of aircraft roll control
9	Airway test	Measurement of total pressure recovery, flow coefficient, internal surface pressure distribution characteristics, etc.	Flow meters, pressure sensors, electronic scanning valves, pressure measurement systems, temperature sensors	It provides a basis for the design of aircraft air intake
10	Thrust measuring device	Measure thrust characteristics	Balances, pressure sensors, thrust measurement benches, thrust generators, etc.	It provides a basis for the design of aircraft thrust device

8.3.1: Full mode force test

Aircraft full-mode force measurement test is the main form of hypersonic wind tunnel aerodynamic test, which is widely used in conventional hypersonic wind tunnel, shock wave wind tunnel, low-density wind tunnel and hypersonic propulsion wind tunnel testing.

The main objectives of the full-mode force measurement test of the aircraft are as follows:

(1) Measure the longitudinal and transverse aerodynamic characteristics of the aircraft under different Mach numbers and attitude angles, such as lift, drag, force, axial force, normal force, lateral force, pitch moment, yaw moment, roll moment and the characteristics of the center of pressure.

(2) Measure the elevator efficiency, rudder efficiency and aileron efficiency of the aircraft.

(3) Measure the aerodynamic contribution of each component of the aircraft, such as the wings and the fuselage, as well as the interference between the parts.

(4) Measure the longitudinal and transverse aerodynamic characteristics of the aircraft with Reynolds number.

In the hypersonic wind tunnel force measurement test, the Mach number and Reynolds number are usually fixed, and the model support mechanism is used to change the attitude angle of the model, such as the angle of attack, the sideslip angle, the roll angle, etc., and the balance is used to measure the force and moment of the air flow acting on the model.

8.3.2: Pressure distribution measurement test

The pressure distribution test is to measure the pressure distribution of various parts of the aircraft model, such as the ejection (aircraft) wing, the ejection (fuselage) body and other surfaces in the case of circling flow. The main objectives of the trial are:

(1) Provide the original data of aerodynamic load distribution for the structural strength calculation and ground static test of the aircraft.

(2) The aerodynamic characteristics of the aircraft can be obtained by integrating the surface pressure.

(3) Determine the position of the transition and separation of the boundary layer on the surface of the aircraft.

(4) Provide flow field parameters for the analysis of certain aerodynamic phenomena.

(5) Provide test data for verification of numerical calculation results.

The pressure distribution test of the aircraft is generally carried out by the full mode, and the local amplification model can also be selected as needed. There are multiple pressure measuring holes on the surface of the vertical model, and the arrangement of the pressure measuring points is generally determined according to the pressure distribution on the surface of the model. The pressure at the pressure hole in a conventional hypersonic wind tunnel is usually measured by a side-pressure catheter connected to a pressure sensor or electronic scanner pressure module outside the wind tunnel via a model strut and bracket. In the shock wave wind tunnel, the pressure sensor is placed directly at the pressure hole to measure the surface pressure value of the model.

8.3.3: Jet Interference Test

The jet reaction control characteristics (RCS) of the space shuttle, the aerodynamic characteristics of the escape vehicle of the manned spacecraft, the flight characteristics of the active stage of the rocket, the interstage separation characteristics of the rocket, the thrust vector control characteristics of the rocket, and the attitude control characteristics of the missile are all closely related to the jet jamming effect. The main objectives of the aircraft jet interference test are:

(1) Determine the interference of the engine jet (internal flow) to the external flow (outflow) around the aircraft, and reasonably arrange the relevant parts of the aircraft to reduce its drag and improve the flight stability and attitude control quality of the aircraft.

(2) Determine the interference of outflow to inflow, make full use of the influence of outflow, reasonably arrange the position, form and size of the engine and engine nozzle, and reasonably design the thermodynamic parameters of the engine nozzle outlet to obtain the maximum engine installation thrust.

8.3.4: Hypersonic airway test

The air inlet test is one of the important projects that should be carried out in the research on the integration of hypersonic vehicle body and engine. The performance of the air intake tract is closely related to the operating characteristics of the engine. The research content and purpose of the hypersonic vehicle air inlet test are as follows:

(1) Measure the static and dynamic characteristic parameters of the intake tract, including the flow coefficient of the inlet tract, the total pressure recovery coefficient and distortion index at the outlet, the drag characteristics, the load distribution of the inner and outer surfaces, etc., and study the matching characteristics of the inlet tract and the engine.

(2) To study the gas dynamics of the forebody to provide a better inlet flow field for the inlet of the inlet tract. The content involves the study of the mutual interference between the forebody boundary layer and the shock wave, the improvement of the inhomogeneity of the forebody flow field, and the influence of the thermodynamic and chemical disequilibrium of the actual gas.

(3) Study the internal flow characteristics of the inlet tract, determine the inner side wall and support plate surface with good performance, so that the inside of the inlet duct has reasonable compression characteristics, and the wall airflow is blocked in the throat of the support plate.

Figure 8-2 shows the test of the air inlet in the wind tunnel in the Hyper-X program.

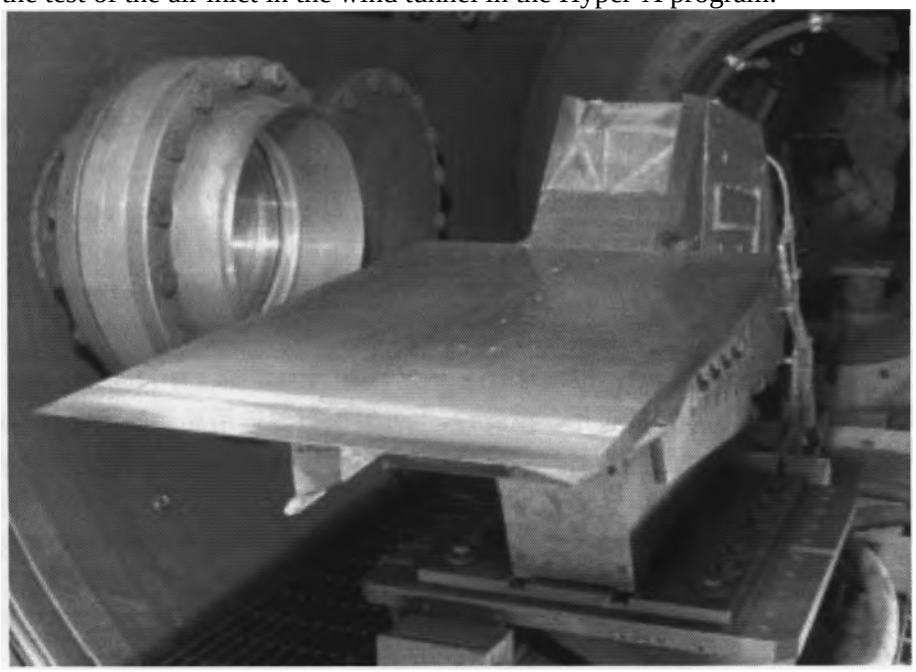

Figure 8-2: Wind tunnel test of the inlet tract in the Hyper-X program

8.3.5: Hinge moment test

The purpose of the hinge moment test of hypersonic vehicle is to measure the torque of the aerodynamic force of each rudder surface of the aircraft to the rudder rotating shaft, so as to give the control efficiency of the rudder surface and provide a basis for the design of appropriate control devices. At the same time, in the design of the rudder surface, the size of the hinge moment and the position of the center of the press are important bases for selecting the rudder surface form and the position of the rotating shaft.

8.3.6: Interstage separation and multi-body separation tests

There are many examples of inter-stage separation/multi-body separation of aircraft, such as the separation between the middle stage and the next stage of the launch vehicle, and the separation of the booster and the core stage; separation of the satellite from the rocket and throwing of the cap; re-enter the data compartment of the warhead and throw it out from the bottom of the warhead; the warhead is decelerated and drag in order to decelerate and increase drag during recovery, and the side-throwing mass resistance cone and drag cone measures are adopted; separation between orbiters and fuel tanks in the space shuttle;

and separation between the orbiter and the carrier aircraft in an aerospace aircraft (Figure 8-3).

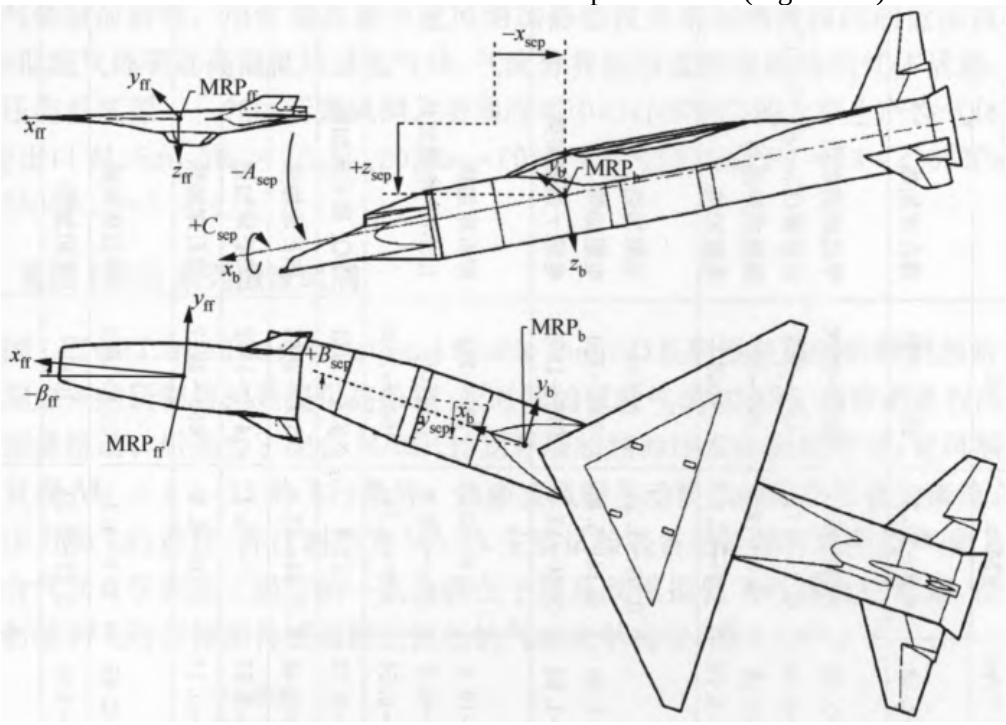

Figure 8-3: Schematic diagram of the separation of the X-43A from the booster rocket

The interstage separation/multi-body separation characteristics of the aircraft can be simulated and studied in the wind tunnel. The purpose of the test is as follows:

(1) During the separation period, it is studied whether each body can be correctly separated according to the predetermined requirements, and the parts after separation will not collide.

(2) Whether the amount of interference to the main body during separation is controlled within a certain range.

(3) Whether the main body can fly safely according to the predetermined orbit and attitude after separation.

8.4: Wind tunnels for hypersonic tests abroad

8.4.1: Overview of foreign hypersonic wind tunnels

In terms of conventional hypersonic wind tunnels, foreign countries have mainly carried out transformations in improving airflow quality, accurately measuring model attitude, accurate flow field calibration, improving test instruments and data acquisition and processing systems, etc., to meet the needs of model development, establish large-scale hypersonic high-Mach number wind tunnels, and continuously expand the scope of *Ma* and *Re* tests. “For example, the Y-306-3 wind tunnel in Russia has been put into use, and the NAL ϕ 1m in Japan, many wind tunnels have added 5-10μm airflow filters during the renovation to improve the quality of the test airflow, and the conical nozzle in the pulse wind tunnel has been changed to a surface nozzle” 1. The wind tunnel test is changed to full program control, which shortens the test time and increases the angle of attack range of the test. In short, the conventional hypersonic wind tunnel has been greatly improved in improving the reliability and repeatability of the test results, reducing the incoming flow disturbance and impurities, and the model delivery mechanism has been put into operation quickly, with an overload of less than 2g for the force measurement test and less than 6g for the heat measurement test, and the rebound phenomenon has been eliminated, and the delivery time is less than 0.5s (0.2s for heat measurement) (Table 8-2).

Table 8-2: Main foreign hypersonic test wind tunnels

Affiliation Device name	Mode/time/s	Test section size/m	Mach number	Reynold number / (x 10^{-7}1/m)	Total pressure/Mpa	Total temperature/K	Heating method
○ NASA ARC 3.5ft Hypersonic	Flush /240	ϕ 1.07	5,7,10	0.1~2.43	0.3~13.3	666~1922	Pebble bed heating
○ NASA LaRC							
8 ft HTT (Com *)	Flush /240	ϕ 1.07	5.8~7.3	0.1~0.72	10.2~16.3	1333~2000	Methane is burned for heating
20 in *Ma=6*	Flush type/180	0.51X0.52	6	0.16~3.44	0.2~3.74	450~565	Ejector use/17 min
CF4	Wash-down /20	ϕ 0.51	6	0.1~0.16	6.8~17	588~700	Regenerative heaters
Cont. Flow	Continuous	0.79X0.79	10	0.13~5.76	1.7~12.2	1005	Resistance heating
○ AEDC							
von Karman A	Continuous	1.0X1.0	1.5~6	0.1~1.54	0.09~1.38	~444	Resistance heating
von Karman B	Continuous	ϕ 1.27	6,8	0.1~1.54	0.14~5.8	388~750	Resistance heating
von Karman C	Continuous	ϕ 1.27	10		0.44~13.6	916~1250	Resistance + combustion heating
○ NSWC							
Hyper. #8	Ephemeral / (Com *).	ϕ 0.43~0.56	5~8	0.2~16.4	0.5~15	333~811	Pebble bed heating
Hyper. #8A (N2)	Flush /240	ϕ 0.61	18	0.07~0.2	20.4~59.8	2005	1.5 MW resistance heating
Hypervel. #9 (N2)	Wash-down /15	ϕ 1.52	10~14.5	0.02~6.56	0.0~0.34	1008~2033	
○ FluiDyne/20 in	Washdown	ϕ 0.51	11~14	0.23~0.72	13.6	833~2444	ZrO2 pebble bed heating
○ Grumman/36 in	Washdown	ϕ 0.91	8,10,14	0.06~1.48	0.34~13.6	555~1666	Pebble bed heating
○ McDonnel D/2 ft	Wash-down /60	ϕ 0.61	6,8,10	0.39~3.67	1.7~15.3	472~1372	Pebble bed heating
○ Northrop/30 in	Wash-down /30	ϕ 0.76	6,10,14	0.00~0.15	0.03~8.8	666~1777	Pebble bed heating
○ FRANCE ONERA /S4-MA	Wash-down /90	ϕ 0.67 (ϕ 1.0)	6 (10,12)	0.3~2.69	0.3~4.1	500~1843	Pebble bed heating
○ Germany/H2K	Flush type/40	ϕ 0.61	4.5~11.2	0.1~3.0	0.01~0.34	1000	Resistance heating
○ JAPAN							
NAL 50 cm HWT	Wash-down /120	ϕ 0.5	5,7,9,11	0.1~2.4	1~10	600~1300	Pebble bed heating
NAL 1.27m HWT	Washdown	ϕ 1.27	10	0.03~0.45	1~10	600~1200	Pebble bed heating

The pulsed hypersonic equipment is mainly to continue to improve the performance parameters of the wind tunnel, increase the enthalpy value, realize the velocity simulation, and conduct the study of real gas effects. The conventional hypersonic wind tunnel heater technology is used to heat the low-pressure driven gas in the shock wave wind tunnel, and the high-pressure low-temperature gas drives the high-temperature and low-pressure test gas, and the fast-moving gas piston is formed at the interface of the air flow, so that the front chamber obtains a high-pressure and high-temperature gas source – the gas piston wind tunnel. The large-scale production gas piston wind tunnel at the U.S. Naval Center (NSWC) has nozzle outlet ϕ1.5m, *Ma* = 10, 15, 20, *Re* = (0.4~3) X 10^7/m, P_0 = 43~310Mpa, T_0 = 1000~2800K, *t* = 1~4s.

8.4.2: American LENS series shock wave wind tunnel

The development of the LENS (Large Energy National Shock Tunnel) series of shock wave wind tunnels in the United States began in 1986. The wind tunnel was originally developed to provide high-quality, long-term test airflow for complex turbulent flows with high Reynolds numbers and high Mach books. Later, in order to cooperate with the NASP program to carry out research on scramjet engines, the wind tunnel was improved to reproduce *Ma* = 6~15 flight conditions. The active flow parameters of the shock wave wind tunnel are the total enthalpy of the incoming flow, the flight altitude pressure, and the flight speed, and it is planned to be used as the main test equipment of NASA to carry out aerothermal aero-optical research on hypersonic vehicles. The final improvement is to improve its performance at simulated low flight altitudes, making it possible to perform aero-optical distortion of the radiation field and the flow field near the aircraft detection sensor (Fig. 8-4) [3].

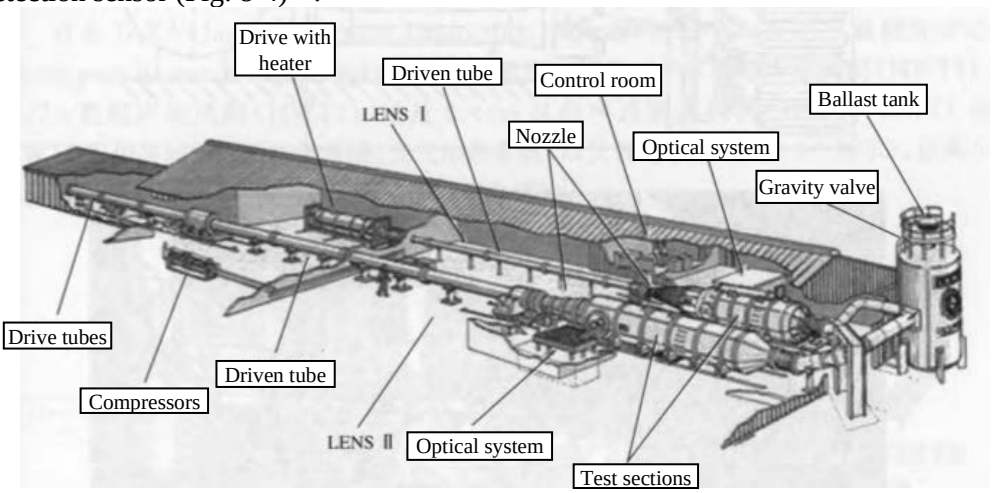

Figure 8-4: LENS I&II shock wave wind tunnel in the United States

Figure 8-4 shows the layout of the LENS I and II shock wave wind tunnels. The experimental simulation capability of the LENS I is *Ma* = 7~14; *Ma* = 3~7 for LENS II. In addition, LENS X is a non-reflective shock wave wind tunnel with the ability to simulate flight conditions with Mach 12 and above. The driven section of the LENS I is 18.5m long and has an inner diameter of 200mm; the electric heating driver is 7.71m long, 226mm inner diameter, and the maximum operating pressure of the wind tunnel is 200Mpa; the drive gases are nitrogen and hydrogen, and the gas flow speed can meet the operating conditions of the interface stitching up to 4.6 km/s. The driven section of LENS II is 30m long and has an inner diameter of 600mm; the driver is 18.5mm long and has an inner diameter of 600mm. The nitrogen/nitrogen mixture was used as the driving gas to match the operating conditions, and the test run time was as long as 30~80ms. LENS X is a large expansion wind tunnel designed to generate air with a low degree of dissociation, capable of generating hypersonic gas flow of 2.5~4.6 km/s, and also has the ability to simulate supersonic flow with a total pressure of 700 Mpa and a flow rate of 7 km/s. The LENS X is assembled using the main components of the LENS II, which is approximately 60m long, and uses a modified nozzle of the LENS II to connect the test section to the driven section.

The high-enthalpy wind tunnel of the LENS series uses double diaphragm technology to ensure good reproducibility of the wind tunnel test state.

8.4.3: Russian ITAM hypersonic wind tunnel AT-303

AT-303 is a hypersonic wind tunnel commissioned by the Institute of Theoretical and Applied Mechanics (ITAM) in Russia in 1999 (as shown in Figure 8-5). The test gas source in this wind tunnel is used as a complex and somewhat innovative part. The high-pressure gas source drives two pistons to adiabatic compress the test gas to a pressure of 3000bar and a high temperature of 2500K. After the gas is compressed, the fast-response vacuum valve downstream of the test section is opened, and the air flow through the nozzle forms a hypersonic flow, while the piston continues to move forward, and the piston stops when the test ends. Other parts of the tunnel include a conical nozzle with a 16° expansion angle, a test chamber, a diffuser section, a large vacuum valve, and an external vacuum tank [4,5].

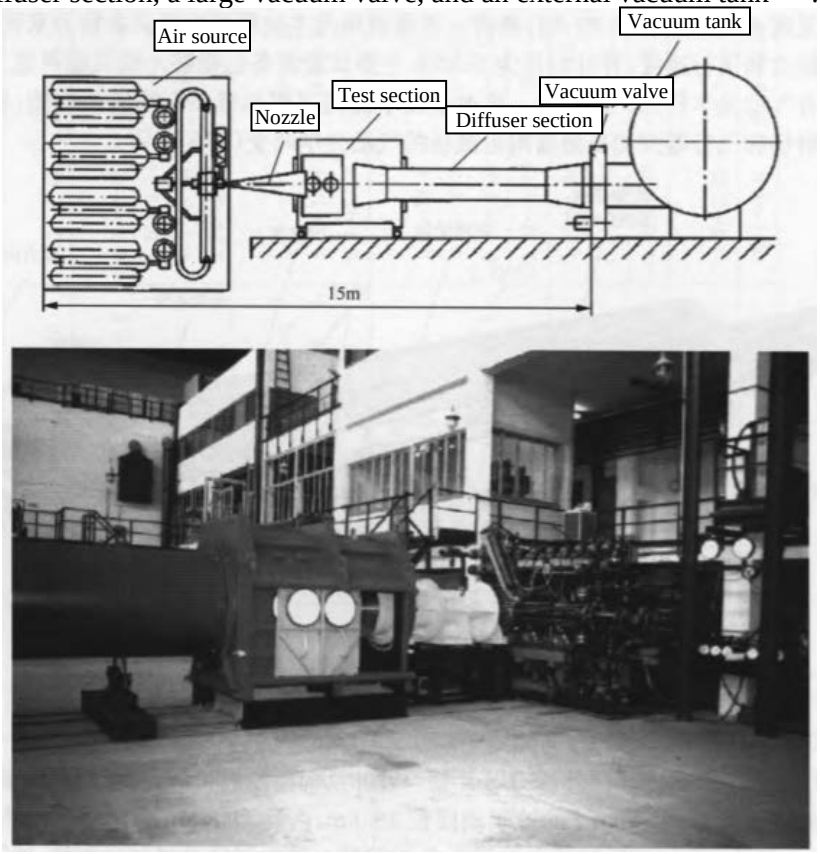

Figure 8-5: AT-303 hypersonic wind tunnel at ITAM, Russia

The AT-303 can perform wind tunnel experiments with high Reynolds numbers and *Ma* = 8~20, which can provide test data and design guidelines for scramjet engine design, fuselage propulsion integration, and aerodynamic characteristics. Wind tunnels can be used with 300mm and 600mm diameters, with the 300mm nozzle running *Ma* = 8 ~13 and the 600mm nozzle running *Ma* = 14~20 for 20~200 ms [3].

8.4.4: S4 hypersonic wind tunnel in France

The S4 hypersonic wind tunnel is part of the Modan Test Center of the French ONERA Large Test Equipment Division, located at the foot of the Alps, and was used to test the French HERMES space shuttle *Ma* = 6.4~10 in the 1980s. There are two axisymmetric nozzles in this wind tunnel: one is an outlet diameter of 0.68m and *Ma* = 6.4 nozzles; the other is an outlet diameter of 1m, *Ma* = 10 nozzle, which can be reached by changing the throat to *Ma* = 12. The wind tunnel uses an egg bed regenerative heater with a maximum temperature of 1850 K, and is a temporary, vacuum dome hypersonic wind tunnel with a vacuum ball volume of 4,000 m^3 and a test time of 25 seconds ~ l minute. In order to carry out the free jet test, the S4 wind tunnel has undergone the following adaptation modifications: (1) the fuel supply system is added, and the selected fuels are CH4 and H2; (2) develop a new nozzle, because the *Ma* number range of the test vehicle is 4~8, a new *Ma* = 6 nozzle design has been completed, and according to the conditions of the free jet test, a *Ma* = 4 and *Ma* = 7.5 nozzle will also be designed; (3) add an air suction system, the free jet test will produce a large number of combustion and incomplete combustion of various pollutants, in order to avoid the pollution of the vacuum ball, a suction system needs to be designed; (4) nozzle calibration device; and (5) the integration of the model and the nozzle [6].

8.4.5: JAXA hypersonic wind tunnel, Japan

Japan's JAXA (Japan Aerospace Exploration Agency) operates three hypersonic wind tunnels at the Aerospace Research Center in Tokyo: a 0.5m hypersonic wind tunnel (HWT1), a 1.27m hypersonic wind tunnel (HWT2), and a 0.44m hypersonic shock wave wind tunnel (HST). HWT1 and HWT2 use a common high-pressure air system, an air heating system, and a vacuum system (as shown in Figure 8-6), and the two wind tunnels can be tested as needed, up to four times a day [7].

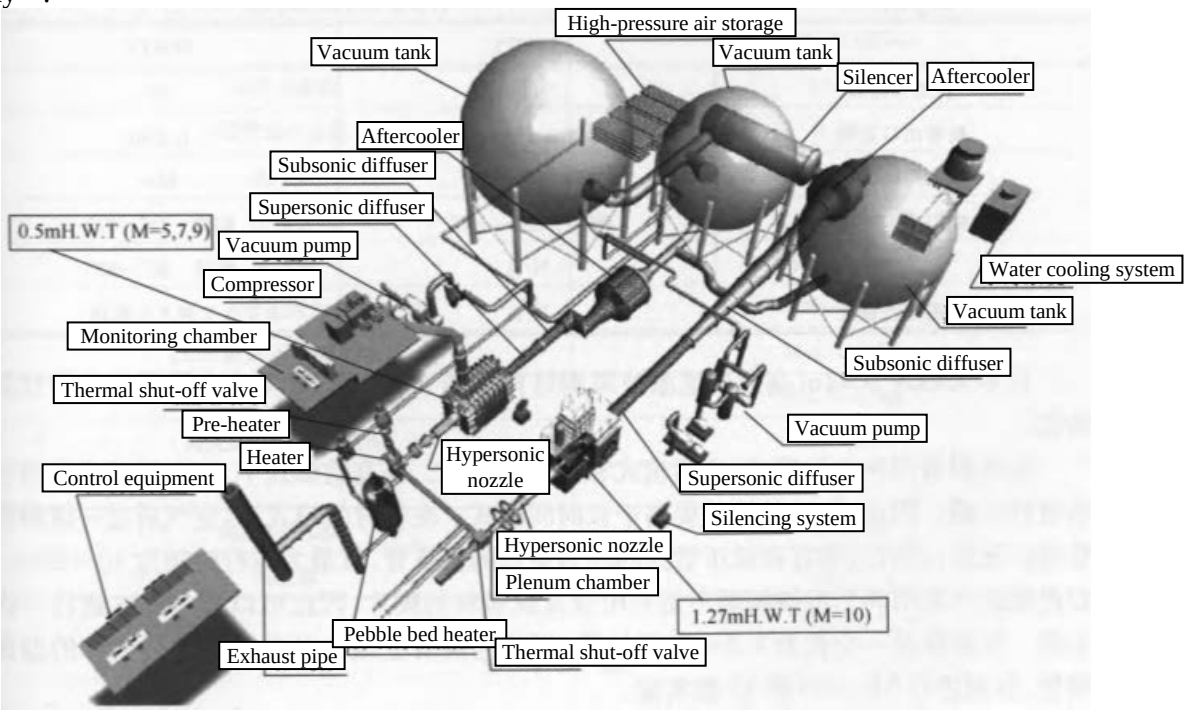

Figure 8-6: JAXA HWT1&2 hypersonic wind tunnel in Japan

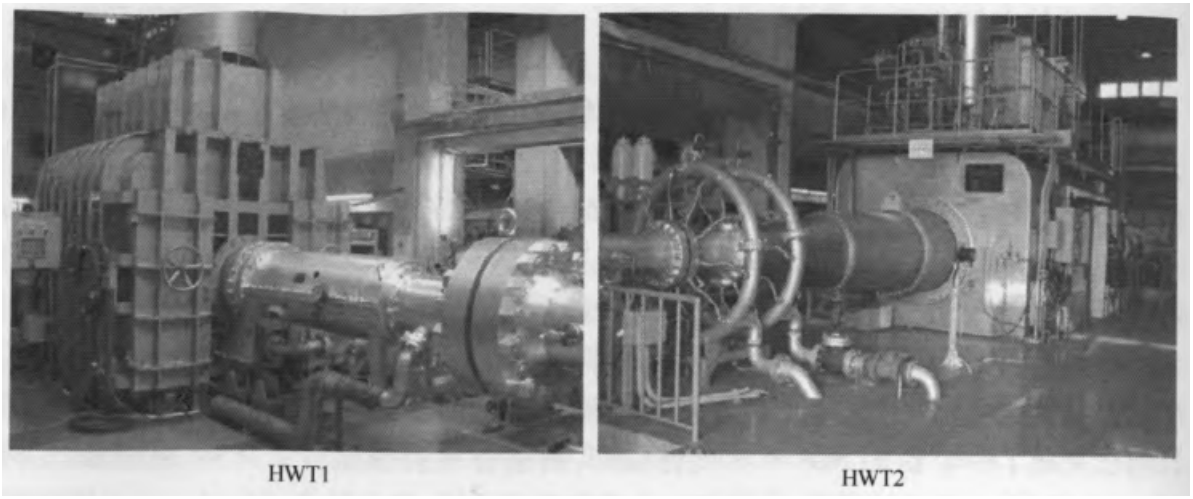

Figure 8-6: JAXA HWT1&2 hypersonic wind tunnel in Japan (continued)

Table 8-3 lists the main performance parameters of the wind tunnel.

Table 8-3: HWT1&2 hypersonic wind tunnel performance

Project	Performance	
Type	Downblow	
Stagnation pressure	1~9.9 Mpa	
Residence temperature	600~1200K	
High pressure air capacity	$36m^3$	
Vacuum tube volume	$1150m^3X2,2300m^3X1$	
	HWT1	HWT2
Nominal Mach number	5,7,9	10
Nozzle outlet diameter	0.44m	1.27m
Maximum duration	120s	60s
Model support system	Pitch—22°~+ 22°	Pitch—12°~47°
	N/A	Roll—90°~90°
Rapid pop-in device	N/A	0.2 enters the mainstream field

The structure of Japan's JAXA 0.44m hypersonic shock wave wind tunnel is shown in Figure 8-7. Table 8-4 shows the main performance parameters of the wind tunnel.

The wind tunnel has two modes of operation: high enthalpy mode and long time mode. In high enthalpy mode, the air is compressed through a two-stage shock tube. As a result, the enthalpy value of the airflow is higher than in the long-term mode. In long-term mode, the air is compressed through a primary shock tube, and the compression tube and the low-pressure tube together act as a longer low-pressure tube, with a maximum operating time of 30~50 ms. In this mode, two mechanical valves are used instead of metal or plastic diaphragms, so experiments can be performed every 15 minutes. The test section is a cylindrical section with a length of 1.5 m, which is connected to a vacuum tank downstream. Two axisymmetric profile nozzles can be used to perform experiments on Mach 10 and 12, respectively.

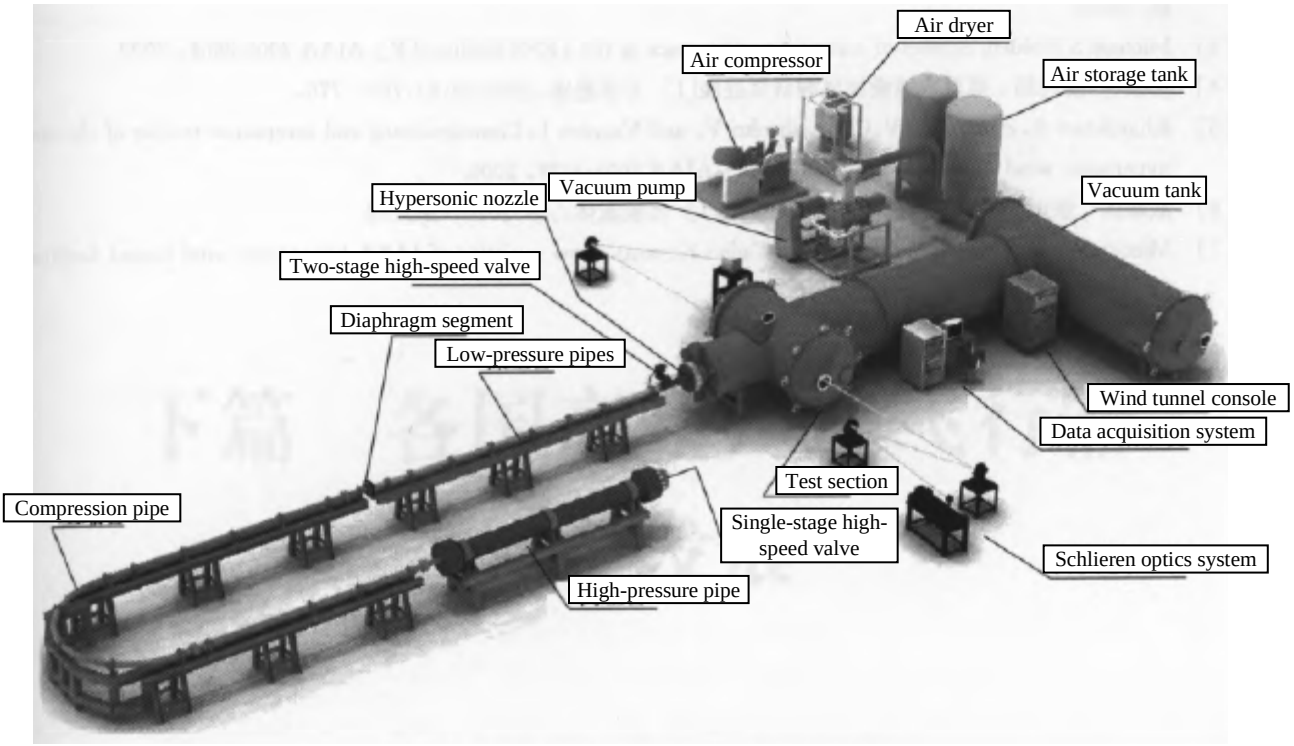

Figure 8-7: JAXA HST hypersonic shock wave wind tunnel, Japan

Table 8-4: HST hypersonic shock wave wind tunnel performance parameters

Project	Performance
Mode of operation	Long Time Mode (LDM)
	High enthalpy mode (HEM)
Nominal Mach number	10,12
Nozzle outlet diameter	0.44
High-pressure tubing	5m, 0.360m^3
Compression tubes	22m, 0.094m^3
Low-pressure pipes	6m, 0.026m^3
Stagnation pressure	0.5~4Mpa
Residence temperature in LDM mode	Max. 1400K
Enthalpy of lag in HEM mode	Max. 5MJ/kg
Maximum runtime LDM	30~50ms
HIM	1~5 ms
High-pressure air storage tanks	1.04m^3X2
Vacuum tank	18m^3

References

[1] Huang Zhicheng. Wind tunnel test of aerospace aircraft [J]. Aerodynamic Experiment and Measurement Control, 1991, 5(1).

[2] Chinese People's Liberation Army General Armament Department Military Training Textbook Editing Working Committee. Hypersonic aerodynamic test [M]. Beijing: National Defense Industry.

Press, 2004.
[3] Michael S Holden. Studies of scramjet performance in the LENS facilities [R]. AIAA 2000-3604, 2000.
[4] Jiang Zonglin, Yu Hongru. Research Progress of Hypersonic Shock Wave Wind Tunnel [J]. Progress in Mechanics, 2009, 39(6):766-776.
[5] Kharitonov A, Zvegintsev V, Chirkashenko V, and Vasenev L. Commissioning and acceptance testing of the new hypersonic wind Tunnel at ITAM RAS [R]. AIAA 2005-3328, 2005.
[6] Zhan Peiguo. Adaptive modification of the S4 hypersonic wind tunnel in France [J]. Experimental Fluid Mechanics, 2010, (24): 88.
[7] Minoru Watari, Noriaki Hirabayashi, Tadao Koyama. Flow qualities of JAXA hypersonic wind tunnel facilities [R]. AIAA 2006-8047, 2006.

PART II – THE DEVELOPMENT OF HYPERSONIC VEHICLE TECHNOLOGY IN VARIOUS COUNTRIES

[This page is intentionally left blank]

CHAPTER 9: U.S. HYPERSONIC VEHICLE TECHNOLOGY RESEARCH

9.1: The rise of scramjet engines (1950s)

The rise of scramjet cannot fail to mention the development of ramjet. Long before the outbreak of World War I, the French engineer René Lorin had already carried out theoretical research on ramjet engines. The ramjet engine is the simplest structure in the air-breathing engine family, and the whole engine is composed of three parts: the intake channel, combustion chamber, and tail nozzle. The conical diffuser of the inlet part generates a shock wave in supersonic flight conditions, which reduces the velocity of the incoming flow to subsonic speed, while increasing the temperature and pressure of the air flow, after entering the combustion chamber, it is mixed with the fuel ejected from the fuel nozzle for combustion, and the combustion process is kept stable by the flame stabilizer, and the high-temperature gas generated by the combustion chamber is discharged through the contraction-expansion nozzle, thereby generating thrust. Ramjet engines are simple engines with no turbine blades and no moving parts. Ramjet engines have been widely used in target aircraft, surface-to-air missiles, anti-ship missiles, air-to-surface missiles, etc., and the working Mach number range is usually in the range of Ma = 1~3.

The working performance of ramjet engines at higher Mach numbers is an important research direction in this research area. The X-7 reusable test vehicle was used in the United States to verify the working performance of the ramjet engine in the range of Ma = 3~4, but as the flight Mach number is further increased, the compression process of decelerating the incoming air to subsonic speed will cause the temperature of the air flow to rise sharply, exceeding the limits that the engine construction materials can bear. Therefore, studies have shown that Ma = 6 is the highest limit of ramjet engine operation.

In the 1950s, there were already some experiments to try to achieve combustion under supersonic air flows, and researchers from the former National Advisory Committee for Aeronautics (NACA) were at the Lewis Flight Propulsion Laboratory In order to verify the feasibility of supersonic combustion, the experiment of boron hydride combustion was carried out in a supersonic wind tunnel, and the stable combustion of about 2s was achieved under the conditions of Ma = 1.5, 2, and 3. Richard J. Weber and John B. MacKay, researchers at the Lewis Research Center, who participated in the study, then considered whether stable supersonic combustion could be achieved in the internal flow channel, and if this idea could be realized, the problem of the ramjet engine's internal flow temperature surge at high Mach numbers would be solved, and the performance of the ramjet engine would be greatly improved. Through theoretical research, Weber and MacKay concluded that there are certain requirements for the realization of a scramjet engine in the following aspects, namely, the total pressure recovery of the inlet tract, the temperature effect of the combustion chamber, the airflow velocity to expansion ratio of the nozzle and the pressure loss, the area of the combustion chamber, and the friction with the wall. At the same time, it is believed that the use of hydrogen fuel has certain advantages. These studies have shown that scramjet engines are more efficient than conventional ramjet engines above Ma = 5.

In September 1958, Weber and MacKay published their findings. In the research report submitted to NASA, the performance of scramjet and ramjet engines in the range of Ma = 4~7 was analyzed and compared, and it was noted that scramjet engines still have considerable potential above Ma = 7. At the same time, some technical difficulties in the development of scramjet engines are also described, including fuel injection and blending, aerodynamic characteristics of the combustion chamber, wall cooling, wall friction loss, and nozzle performance.

It was also proposed to use an expanded combustion chamber configuration to avoid the thermal congestion that would occur with an equal-section combustion chamber. These fundamental technical problems are still difficult to solve in the field of hypersonic technology to this day.

Also in September 1958, the first International Conference on Aeronautical Sciences was held, at which Ferri from Berkeley Institute of Technology in the United States introduced the research work and progress of achieving stable combustion in a $Ma = 3.0$ supersonic gas stream. In the decades that followed, Ferri became a major leader in the development of hypersonic technology in the United States. In the same year, scramjet research was also carried out at McGill University in Montreal, with early research focusing on the air intake, fuel injection and combustion, and tail nozzle of scramjet engines in the range of $Ma = 10\sim25$.

In 1961, Dueger of the Johns Hopkins University Laboratory of Applied Physics published the results of a study comparing the performance of kerosene-fueled ramjets with scramjets. The conclusions of the study are similar to those of Weber and MacKay of the Lewis Research Center, that is, scramjet engines perform better than conventional ramjets in the range of $Ma = 6$ to 8, and still have considerable advantages at higher Mach numbers [1].

9.2: Early days of research on scramjet engines (1960s)

The performance advantages of hydrogen-fueled scramjet engines at high Mach numbers and the potential to reach orbit entry speeds have led scramjets to be considered for hypersonic cruise flights and single-stage orbit missions as soon as they appeared. In the 1960s, the United States increased its investment in the aerospace field, and in this context, the research on the scramjet engine with the application goal of single-stage orbit mission also received greater funding. At the same time, the U.S. Air Force sees great potential for military applications of hypersonic technology, so it also supports research on technologies related to scramjet engines for aerospace aircraft.

In the early years of research and development of the hydrogen-fueled scramjet engine in the United States, the main leader was undoubtedly Ferri. His technical guidance, as well as his leadership at the Berkeley Institute of Technology's Aerodynamics Laboratory (PIBAL) and General Applied Science Laboratory (GASL), laid the foundation for the development of scramjets. In his early research, Ferri proposed the use of an expanded combustion chamber, described the chemistry of the hydrogen-air system, analyzed the turbulent mixing problem, and identified the key problem of controlling the heat release law corresponding to the shape of the combustion chamber to avoid strong shock waves. Along with these fundamental studies, Ferri further investigated how to maximize the performance of a fixed-geometry scramjet, in particular, the development of a scramjet with high performance at a wide Mach number. Ferri believed that a high-performance scramjet engine could be achieved, i.e. by coupling the wave compression effect caused by combustion, which is known as thermal compression. Billig's research validated this hypothesis, and he theoretically analyzed that large performance gains could be achieved at lower and higher Mach numbers, and he also pointed out that it was difficult to adjust the injection process to achieve the desired thermal compression process [2].

GASL had two research programs on scramjet engines in the 1960s, one of which was the Scramjet Incremental Flight Test Vehicle (IFTV) program funded by the U.S. Air Force, which began in April 1965.

Four hydrogen-fueled scramjet engines are located around the vehicle, and the planned test flight scenario accelerates the test vehicle to 5,400 ft/s and an altitude of 56,000 ft, with the demonstrator accelerating to at least 6,000 ft/s. And in the ground-based test program for the development of scramjet engine modules, the problem of mutual interference between the intake tract and the combustion chamber was encountered, which delayed the progress of the program. In January 1967, an unpowered flight test launch of a model scramjet engine was carried out, but the entire program was cancelled in August 1967, and the three-dimensional scramjet engine based on the thermal compression method was not able to be verified by flight tests.

Research on another engine was also funded by the U.S. Air Force in 1964-1968. The engine is known as a low-speed fixed-geometry scramjet engine with an engine design operating range from *Ma* = 3~12 with a variable aerodynamic shrinkage ratio. The fixed-geometry engine is based on Ferri's design for the integration of the intake duct and combustion chamber. Different models of air intakes and engines were tested in the program.

In the study of these engines, it is not difficult to see that Ferri's desire is to meet the needs of engine engineering applications by adjusting the pneumatics and heat during fuel injection, mixing and combustion. However, due to the limitations of the computational means available at the time and the technical difficulty of controlling heat release and avoiding inflow separation, it was actually very difficult to realize Ferri's wishes, but Ferri's work greatly contributed to the development of hypersonic technology research in the United States and internationally.

In addition to GASL, scramjet research and ground trials were carried out by other research institutes funded by the U.S. Air Force during the same period, including the variable geometry engine from the Joint Aeronautical Research Laboratory, the integrated engine model from General Electric, and the dual-mode engine from Marquette.

9.3: SCRAM Missile Program (1961 to 1977)

Early research in supersonic combustion in the Applied Physics Laboratory at Hopkins University began with combustion studies in external supersonic gas streams. The wedge-shaped wings are observed to inject fast-reacting fuel and produce violent combustion. In the *Ma* = 5 test, considerable lift and thrust are generated, and the results of experimental and computational analysis also show that the amount of net thrust obtained is very small and lacks practical application value. However, these experimental studies verified that stable combustion can be formed in the supersonic gas stream, which prompted the researchers to start a study on the feasibility of supersonic combustion in the inner channel, that is, to form a scramjet, and further studies showed that scramjet can produce net thrust and have higher efficiency than traditional subsonic ramjet engines operating in the range of *Ma* = 6~8.

Based on the results obtained, in 1961 the Laboratory of Applied Physics began research on the preliminary conceptual design of a scramjet-powered missile. The initial design is the same hybrid internal and external compression method as the traditional axisymmetric air intake, but it requires a complex variable geometry system to ensure the activation of the air intake, but for a single-use lightweight missile, a fixed geometry of the air intake is more advantageous. Therefore, a new inlet profile is proposed, that is, the design method of streamline tracing, and the improved inlet duct has the characteristics of self-starting. From 1961 to 1977, the Johns Hopkins University Applied Physics Laboratory carried out a research program called SCRAM (Super Sonic Combustion Ramjet Missile) for shipborne defense missiles [3].

The SCRAM weapon system proposes two form factor designs, as shown in Figure 9-1, and the main mission of the missile is to act as a ship-to-air missile to defend against bomber threats. Both missile designs were compatible with the launchers of U.S. Navy ships at that time. The missile is separated after being accelerated by a solid booster rocket to the speed at which the scramjet engine works, at a rate of *Ma* = 3.5~4. In the Type 1 scheme, the engine and the missile are a whole, that is, the other parts of the missile are concentrated in and around the four modules, the engine with the head intake, and the engine exhaust device constitutes the basic shape of the missile, because this configuration has a large air intake capture area and the weight ratio of the missile, so its acceleration ability is very strong, but the small aspect ratio makes the configuration have the aerodynamic characteristics that need to be controlled by the large tailed snake. In the Type 2 scheme, four external engines are used, and other missile components are assembled inside a pointed cylinder. In the bomb-loaded equipment, the engine is partially buried in the body of the projectile. After the missile is put into a ready state, the engine ejects from the missile to the flight position shown in Figure 9-1.

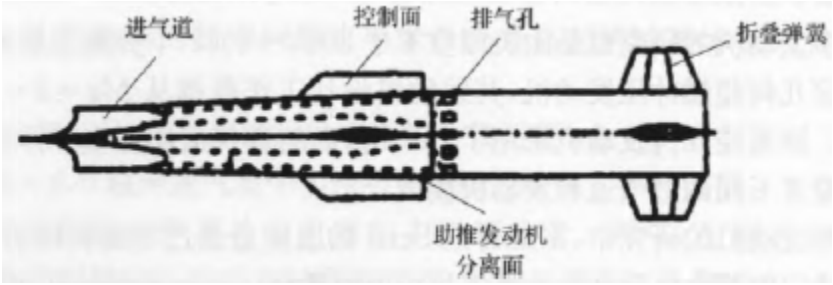

(a) Type 1 SCRAM missile

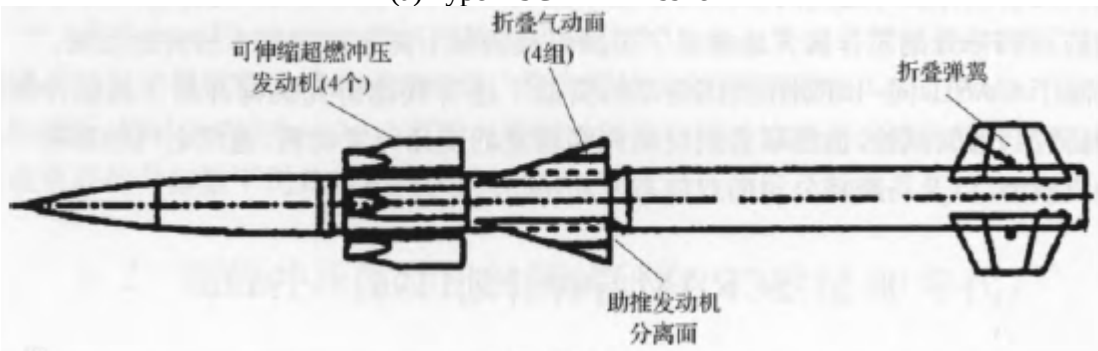

(b) Type 2 SCRAM missile

Figure 9-1: SCRAM missile outline scheme

In the 1970s, a variety of SCRAM configurations were tested according to the goal of simplifying the structural design and improving the performance of the aircraft. Because the material properties do not meet the requirements, the maximum speed of the test is low. With the introduction of the vertical launch box into new naval vessels, the design of the SCRAM was required to be compatible, but its performance still exceeded the performance of the full-course rocket engine propelled missile.

The SCRAM program proposes the concept of a modular intake-combustion chamber-nozzle configuration; developed development design and analysis techniques; tests on individual components validate the method used. The components were successfully assembled in a viable engine, and the feasibility of a liquid-fuel ramjet engine was clearly demonstrated by the engine free-jet test in the state of Ma = 5~7.2. Key research results include:

The concept of a dual-modal engine was demonstrated, that is, the engine works under subsonic combustion and supersonic combustion, and the modal change proceeds smoothly;

Combustion efficiency was measured over the entire fuel equivalent ratio variation range ($0 \leq ER \leq 1$);

Developed an intake-combustion chamber isolation tube design process that prevents excessive compression and minimizes shear and heat loss;

It is verified that under the conditions of Ma = 5 and sea level altitude, the acceleration ability of the missile can reach 11 g.

The development of test setups, measurement methods, and the modeling of the cycle process can fully describe the flow phenomena in scramjet engines.

Although the SCRAM program successfully demonstrated the technology required for flight tests, there were still three major drawbacks: first, the fuel used was flammable and toxic, which caused great trouble in the logistics of weapons and equipment when used as a missile; second, there is not enough space for the installation of active radar equipment; third, there is still no breakthrough in the structural materials required for passive cooling of the entire aircraft.

Thus, the SCRAM program ended in 1977, but in the same year, J.L. Keirsey, of the Applied Physics Laboratory at The Johns Hopkins University, proposed a new follow-up concept, a conceptual scheme of missiles powered by a dual-combustion chamber ramjet engine (DCR). The scheme can be based on conventional hydrocarbon fuels and has enough space for the installation of an active radio-frequency radar (or other type of seeker), which is capable of meeting the combat mission of long-range wide-area defense. Unlike SCRAM missiles, DCR-powered missiles are limited to a maximum flight speed of *Ma* = 6, mainly due to the limitations of the heat resistance of passively cooled materials.

In 1983, a more detailed concept of DCR powered missiles was formed, called the Wide-Area Defense Missile (WADM) or Hypersonic WADM, as shown in Figure 9-2. The missile is 21 inches in diameter and fits into a vertical launch box, 256 inches long, with a launch mass of 3,750 lbs. and a solid boost to *Ma* = 3.2. It is capable of cruising at sea level at *Ma* = 3.5, at an altitude of 80,000~100,000 ft, and can be *Ma* = 4 to6 makes long-range flights, loading a warhead of about 200lbs. Through the surface-launched missile technology plan, the engine-related technologies of the program have been studied, including air intake, isolation section, fuel injector, fuel supply and control, combustion chamber, materials, structure, guidance, flight control, aerodynamic characteristics, boosters, ramjet engine power performance, and other subsystems. Unfortunately, Congress ended the program in 1986.

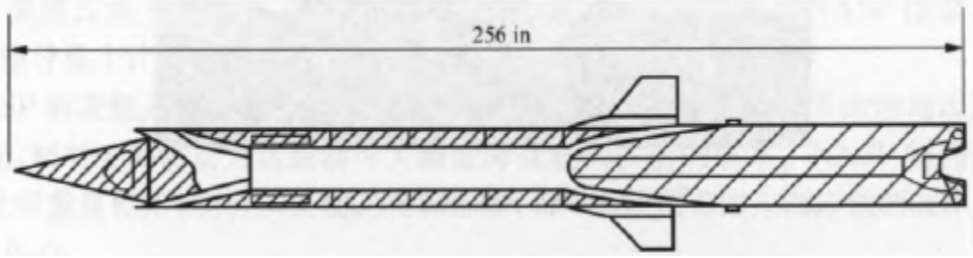

Figure 9-2: Schematic diagram of the DCR ramjet-powered missile

9.4: Hypersonic Research Engine Program (1964 to 1974)

In addition to scramjet research funded by the U.S. Air Force, NASA and the Navy have also carried out a number of scramjet research projects, the most important of which is NASA's Hypersonic Research Engine (HRE) program. The HRE program began in 1964 with the goal of conducting flight tests of scramjet engines with full flight quality on the X-15A-2 demonstrator, but the X-15 demonstrator program was cancelled in 1968 and this flight test program was not carried out.

Due to the cancellation of the flight test program, the focus of the study shifted to ground wind tunnel testing of two full-scale HRE model engines, one of which was called the Structures Assembly Model (SAM), which was tested in an 8ft high-temperature wind tunnel at NASA's Langley Research Center under *Ma* = 7 conditions to demonstrate the engine's performance. Another test engine, called the Aerothemodynamic Integration Model (AIM), was tested in the hypersonic test wind tunnel at NASA's Galen Research Center at Mach numbers 5, 6 and 7. The pilot engine model was designed and manufactured by AiResearch Manufacturing. The SAM engine, which uses a structure cooled by hydrogen fuel to meet the requirements of flight quality, was tested on the ground in 1971 and 1972, through which the design and manufacture of cooling channels were mastered. The AIM test engine was designed with a water-cooled structure, which was thoroughly inspected in September 1972 and had a fuel combustion test performed in October 1973.

The HRE program ended in April 1974 with a total of 52 tests running for a total of two hours. Comprehensive data on the performance of the intake tract and combustion chamber were obtained in the range of *Ma* = 5~7. It is worth mentioning that a two-dimensional combustion chamber model was built and tested in the program for the development of an annular HRE combustion chamber. This combustion chamber test setup verifies the performance of the expanded combustion chamber configuration and investigates the chemical kinetics as well as the loss of performance due to fuel blending (Fig. 9-3).

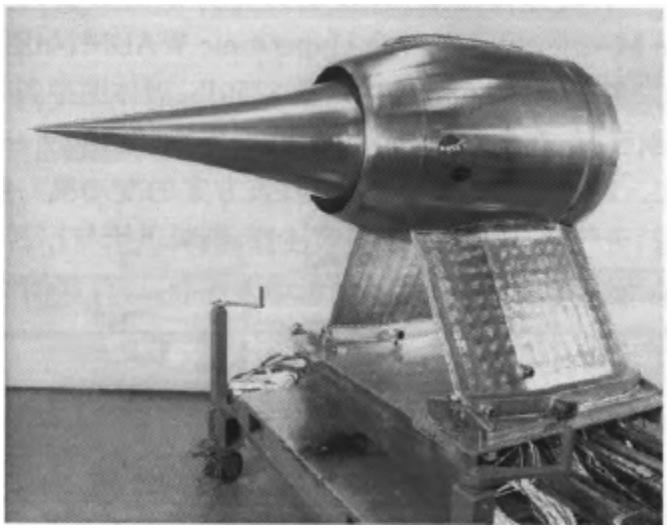

Figure 9-3: HRE hypersonic research engine

9.5: National Aerospace Aircraft Program (1986-1995)

9.5.1: Proposal of the NASP program

As early as the 1960s, the U.S. Air Force began a research program on aerospace aircraft, including the conceptual design of single-stage and two-stage orbital aerospace aircraft, which ended in 1970, during which ground tests of scramjet engines and artillery flight tests were carried out.

In 1975, NASA began studying the possibility of replacing the space shuttle. A research team at NASA's Langley Research Center conducted research and analysis on a rocket-powered single-stage orbital space launch vehicle program. Another research group has been working on a two-stage orbital space launch vehicle scheme, in which the first stage of the launch vehicle uses an air-breathing engine and the considered separation Mach numbers range from *Ma* = 0.8 to 10. In the scheme of *Ma* = 10 separation, the first stage is propelled by a scramjet engine in the range of *Ma* = 6 to 10.

In 1978, Boeing submitted a fully reusable single-stage orbital space vehicle (RASV) scheme to the Air Force Space Department for skid-assisted takeoff. At the same time, the U.S. Air Force was also studying the role of military personnel in space. These two efforts were subsequently merged into the Advance Military Spaceflight Capability (AMSC) program. Soon after, the U.S. Air Force's Aeronautical Systems Division began working on the Trans-Atmospheric Vehicle (TAV) concept. The United States Air Force's Department of Aerospace Aircraft is gradually moving from the Space Department to the Department of Aeronautical Systems, and this shift in responsibility is mainly due to the need to make space launch vehicles operate like airplanes if the cost of space transportation is to be greatly reduced. Boeing's RASV concept met exactly this requirement and was therefore adopted.

The space launch vehicle proposed by Boeing does not have to be launched from the east or west coast of the United States, like a launch vehicle or space shuttle, but can take off and land at any air base in the United States.

At a time when Boeing was working with the U.S. Air Force Space Department on a fully reusable single-stage orbit space launch vehicle, DARPA could begin research on an advanced space launch vehicle and had adopted a single-stage orbital space aircraft scheme with a breathing combined cycle engine with a combined cycle propulsion system using ramjet and scramjet engines, where the scramjet engine worked until the orbit speed. Compared with rocket-powered launch vehicles, this scheme has more operational flexibility, and reduces the total weight and launch cost of the aircraft by a larger scale.

In 1986, U.S. President Ronald Reagan proposed the idea of the "Orient Express" in his State of the Union address. The "Orient Express" is a *Ma* = 5 hypersonic aircraft concept, commercially operated on the transpacific route. At the time, this idea was somewhat confused with DARPA's single-stage orbit entry plan for the "Copper Canyon." DARPA launched the Copper Canyon program in 1984, and two years later, the Reagan administration announced that DARPA would lead the National Aerospace Plane (NASP) program jointly conducted by the U.S. Department of Defense and NASA. The NASP Joint Program Office was established in the U.S. Air Force Aeronautical Systems Division, and two years after the program began, its responsibilities were transferred to the U.S. Air Force, and DARPA withdrew from the program. In 1988, the Pentagon established the NASP Office of Cooperation, and in 1990, the NASP Office of National Planning, which was responsible for leading the development of the entire program.

NASP's vision is to develop a single-stage orbital space launch vehicle that can revolutionize the state of space transportation and significantly reduce the cost of space launch compared to rocket-powered launch vehicles. The NASP will be fully reusable like a regular aircraft, capable of taking off and landing from airfields without having to use rocket launch pads on the East or West Coast of the United States (Figure 9-4).

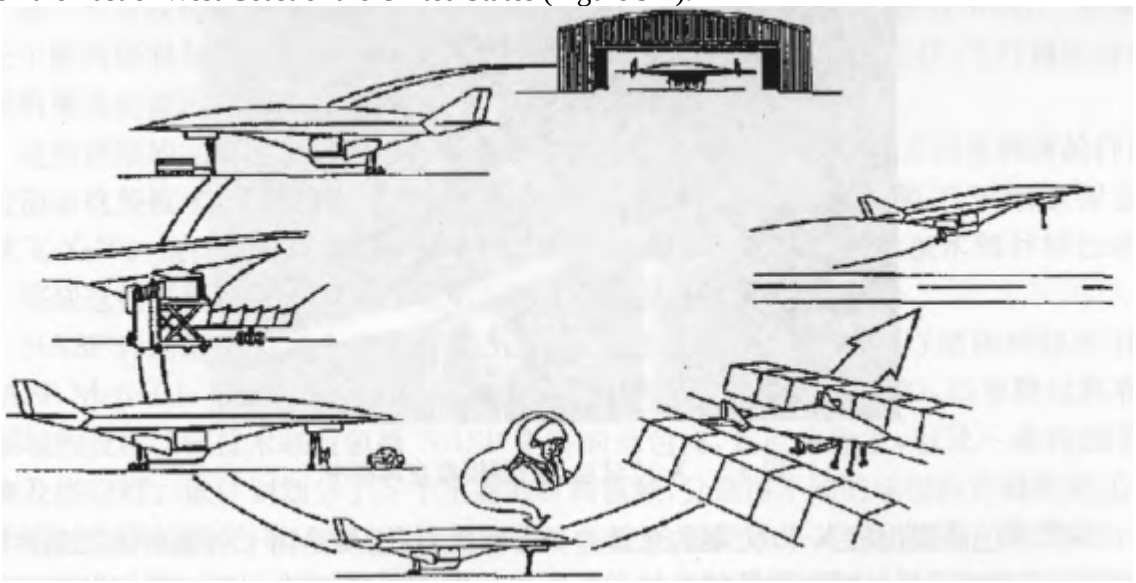

Figure 9-4: Schematic diagram of NASP maintenance, take-off, and landing operations

The specific goal of the NASP program is to develop the technology needed for putting an air-breathing, single-stage spacecraft into orbit and to demonstrate a test vehicle, the X-30. In 1984, DARPA had established a baseline scheme for a single-stage orbital space launch vehicle with a polar orbit carrying capacity of 25,000 lbs , and the total weight of the concept in the "Copper Canyon" program was 50,000 lbs, the development time was 5 years, and the cost was about $5 billion, so the program was later called the "5-5-50" program.

From 1984 to 1986, DARPA carried out the conceptual design of the X-30 test vehicle, developed the required technologies, and increased technical readiness in an effort to reduce the risks of the tests. During this time, DARPA persuaded Congress and the government, and in 1986, with the support of the President of the United States, approved the National Aerospace Aircraft (NASP) program, which was co-led by the U.S. Department of Defense and NASA, and the NASP program began.

9.5.2: Conceptual design of the NASP X-30 test vehicle

After the establishment of the NASP Joint Program Office in 1986, the benchmarking proposed in DARPA1984 was demonstrated, resulting in an improved so-called "official benchmark" scheme. The improved X-30 benchmark scheme (Figure 9-5) has a total weight twice as much as the original Copper Canyon program. The official NASP X-30 benchmark scheme, improved in 1986, was provided to the contractor as a reference point for their conceptual definition studies. From 1986 to 1988, a total of eight contractors, five of which were engaged in the development of aircraft airframes and three of which were involved in the development of propulsion systems, were involved in the definition and validation phase of the conceptual scheme. Each propulsion system development contractor is to support all aircraft airframe development contractors, and each aircraft airframe development contractor independently works on the conceptual design of a single-stage to orbit aerospace aircraft with a polar orbital carrying capacity of 10,000 pounds. All contractors are also involved in joint technology research and development projects with the government. At the end of the concept definition and validation phase, the contractor will be screened. The contractor who determines the most promising option through screening will move on to the next stage of competition to determine who will eventually proceed with the development of the X-30.

Figure 9-5: Model of the X-30 test vehicle in a wind tunnel

The total weight of the X-30 proposed by different contractors varies greatly, mainly due to the large differences in engine performance estimates, aerodynamic data calculations and material selection. In particular, the sensitivity of the gross aircraft weight to the uncertainty of the performance of the scramjet engine will be carried out throughout the planning process.

As a result of the screening, three aircraft airframe development contractors, such as General Dynamics, McDonnell Douglas, and Rockwell, were selected to continue the conceptual design work. Two propulsion system development contractors, Pratt, Whitney and Rocketdyne, were selected to continue their research work. At the end of the concept definition and validation phase, two form plans and two engine concepts were formed. Over the next two years, these options were further studied and the final option was determined.

In 1990, the development contractor completed their design, thus ending the competitive phase of work. The uncertainty of the total weight of the aircraft and the performance of the engines has been reduced, but the design of the two fuselages and two engines will still be maintained, and it is hoped that the government will choose one from each of them. However, the government's decision was not to choose from the options, but to have a joint national team of five aircraft fuselage development contractors work together on the X-30, so in the summer of 1990, the NASP National Program Office (NPO) was formed, and after several iterations, the NASP NPO defined the baseline NASP X-30 test vehicle program in 1992, and proposed a timeline and budget for development.

The X-30 is a manned research test vehicle capable of taking off and landing from an ordinary airport runway, capable of reaching orbital velocity (Ma = 25), a length between 150 and 200 ft, and a gross take-off weight of 250,000 to 300,000lbs. The X-30 is a specific test vehicle that understands hypersonic flight, not one with a clear application, and is a member of the American family of X-Series test vehicles designed to go beyond existing technologies, explore uncharted areas of science, and provide the necessary design approach to build the next generation of space carriers. The development budget of the X-30 reached $15 billion, which posed a very serious funding problem for both the US Air Force and NASA.

9.5.3: Research on key technologies in the NASP program

The NASP program has three phases of development, the first of which is the conceptual research phase under the responsibility of DARPA, which dates back to 1982; the second stage is the key technology development and demonstration stage; the third stage is to decide whether to proceed with the detailed design, construction and flight testing of the X-30 test vehicle after reviewing the results of the second phase.

The end of the second phase is marked by the completion of the necessary top-level key technology demonstrations to improve the maturity of the technology in order to reduce the risk of the third phase of development and flight testing. These hallmarks that must be completed include: the design of the aircraft, the demonstration of the engine concept; demonstration of materials and structures; properties of cryogenic propellants.

These top-level milestones are closely linked to a set of technical goals and serve as technical milestones that demonstrate to a point where the technology matures to the third stage of the program, which is the construction and flight of the X-30. These milestones are marked by major technical trials, and the goal of step-by-step demonstration of the technology has been achieved. The completion of these milestones is the main task of the second phase of the NASP program.

The NASP program has formed a technology consortium to develop technologies in the field of materials and structures through a program called the NASP Materials and Structures Augmentation Program (NMASAP). The technology alliance includes NASP's main contractor, government labs, and a range of subcontractors and suppliers. The program is divided into five main material areas, each with different contractors carrying out research work.

Through collaborative research, the NMASAP program has achieved certain research results, including the development of new titanium alloys, intermetallic compounds, and composite fibers, obtaining data on the strength, thermal conductivity, and fatigue properties of these new materials, as well as the development of new material preparation processes and coating materials that prevent oxidation and hydrogen embrittlement of materials. As a result of these results, NASP turned to these new materials for structural components, as well as conducting large-scale trials of these components to validate their capabilities for X-30 structures.

The main structural component was the torsion-resistant wing box made of titanium composite, which was successfully welded in the manufacture of this titanium composite sub-component, and the cutting and drilling were also carried out by special equipment. The completion of the fabrication of this structural component demonstrates that titanium composites can produce components of acceptable quality.

A combined thermal and force load test was carried out on the torsionally stabilized wing box, i.e., heating by radiation on the upper and lower surfaces while applying a bending moment representative of the wing load.

Another structural component is the wing, which contains a carbon-silicon-carbon composite material that is part of the NASP thermal protection system to protect the surface of the aircraft under severe thermal loads. The third structural component is a titanium fuselage section containing a cryogenic fuel tank, which has been tested to withstand high temperatures while keeping the fuel tank cold, with a maximum test temperature of 1,300°F. Other achievements in material construction technology include the development and testing of active cooling components for the aircraft head, wing leading edge, nozzle, engine, and air intake.

In the area of scramjet propulsion, NASP plans to retrofit some of the major hypersonic test rigs to increase their ability to conduct scramjet components and integrated testing. The improved test device can be used to test the scale model of the X-30 engine with $Ma = 8$. Some arc-heated propulsion test units have also been modified to expand the scope of their tests. In addition, a new shock wave wind tunnel was built to test the components of the propulsion system in the $Ma = 8$ to 24 range. In the NASP program, these test units were used to study a variety of scramjet systems and their subsystems.

The aerodynamic achievements of the NASP program include: aircraft shape design and performance calculation; computational fluid dynamics (CFD) was validated and applied as the main design tool. Collect test data for CFD validation and calibration; the data of low-speed performance and drag were obtained, and a database of aerodynamic, stable, and dynamic influence control of the X-30 configuration was established through CFD and wind tunnel tests.

Another key technology is the preparation, transfer, and storage of slurry hydrogen fuel. In total, more than 40,000 gallons of slurry hydrogen fuel were manufactured in the second phase of NASP, of which 53% to 62% were solids, and an average of 60% of the technical requirements have been met. Pressure push-off transfer experiments were also carried out on slurry hydrogen fuel, which transferred the fuel from the manufacturing chamber to the cryogenic storage tank.

9.5.4: Adjustments to the NASP program

In the autumn and winter of 1992, the U.S. Defense Science Council conducted a review of the X-30 and, in view of the exorbitant development budget, decided that adjustments to the NASP program were necessary. The Defense Science Council believes that the NASP program is not yet enough for the development of the X-30, the goals of the previous stage have not been well accomplished, and a number of key technical issues have not been resolved. The Defense Science Council proposed to use flight tests to solve the problems of uncertainty in the performance of scramjet engines, prediction of boundary layer transitions, and stability control. In addition, additional time is needed to increase the maturity of the engine materials and coating technology.

Taking into account the opinion of the Defense Science Council, the NASP NPO proposed a series of flight tests and proposed the Hypersonic Flight Experiments (HYFLITE) program. HYFLITE plans to conduct three flight tests. HYFLITE I is a boundary layer transition test, HYFLITE II is a scramjet engine performance and operation test, and HYFLITE III is a demonstration test of stability and control technology for a scaled X-30 shape test vehicle. The NASP HYFLITE program has a budget of less than $2 billion and is expected to be completed in six years. At the same time, research on materials, structures and subsystem technologies continues.

NASP NPO believes that spending $2 billion on the HYFLITE program will reduce the development of the X-30 by at least $2 billion and shorten the development cycle by 2 years, and believes that the development of the X-30 can be actively promoted. This initiative is believed to reduce the cost of development, and the delayed flight test can also reduce the risk of the entire program, but the first X-30 flight test into orbit is still considered to be possible at the beginning of the 21st century.

In the summer of 1993, the U.S. Air Force organized an independent review team to demonstrate the proposed HYFLITE program, with the participation of members of the former Defense Science Council. However, the review team felt that the $2 billion required for HYFLITE could not be realized, so the objectives and requirements of flight testing needed to be redefined to minimize the cost of flight testing. The NASP review committee quickly developed a consensus that the uncertainty of scramjet performance at high Mach numbers was the biggest problem facing the NASP program. Based on the comments and requirements of the review committee, the NASP NPO proposed the Hypersonic Test Program (HySTP). The cost of the HySTP program is $40 million, with a five-year period of flight tests of scramjets to determine the performance of scramjets under *Ma* = 15 conditions.

9.5.5: End of NASP program

Funding applications for the HySTP program were submitted to Congress in the hope of approval for the 1995 fiscal year. NASA pledged to Congress to support the HySTP program in its original budget, but the U.S. Air Force only pledged funding for fiscal year 1995, not for the planned years. As a result, Congress does not approve the budget for the HySTP program unless the U.S. Air Force supports it in its original budget. Since the U.S. Air Force was unable to secure the HySTP budget in January 1995, the NASP program was terminated.

After the end of the NASP program, NASA continued its research on hypersonic technology, while the US Air Force continued its research work in its proposed HyTech program.

9.6: Hypersonic Technology Program (1995-2003)

9.6.1: Overview of the HyTech Program

In 1995, after the end of the NASP program, the United States carried out a series of research programs on key technologies in order to maintain its development in the field of hypersonic technology, and the Hypersonic Technology (HyTech) program of the United States Air Force was one of them [4,5].

The objective of the HyTech program is to develop and demonstrate the operational capabilities, performance and structural feasibility of the propulsion system of a hydrocarbon-fueled scramjet engine in the *Ma* = 4 to 8 range. HyTech is a technology development program focused on the development of engines and single-use missiles, which is only the first step in the application of scramjet engines, and the results of this program can be extended to higher Mach numbers and the application of reusable scramjet engines.

The main part of the HyTech program is the SFSFC (Storable Fuel Scramjet Flowpath Concepts) program, which incorporates a research base from the industrial sector. The SFSFC plans to start with the demonstration of component performance and gradually develop to the demonstration of integrated regenerative cooling ground engine, and the application prospect of technology development is a fully hydrocarbon fuel hypersonic vehicle. The SFSFC program is divided into three phases. The goal of SFSFC Phase 1, which is also Phase 1 of the HyTech program, is to develop the conceptual design of two viable hydrocarbon-fueled scramjet engines, as well as the key component technologies associated with the engines. By the end of this stage, the air inlet test, the heat sink combustion chamber test, the design and research of hypersonic missile, the design of thermal management system and the demonstration of fuel cooling structure were carried out on the two engine design schemes, namely the support plate configuration and the two-dimensional flow channel configuration.

The goal of Phase 2 is to integrate key technologies into a complete system performance demonstrator. Phase 3 of the research will revolve around the demonstration of an all-in-flight engine with a flight weight structure and a demonstration of its performance and durability in a free-jet test facility. At the beginning of Phase 2, the scramjet engine with a two-dimensional flow channel configuration was selected for further research, and the SFSFC program was renamed the Hypersonic Scramjet Engine Technology (HySET) program, and the second and third phases of the original HyTech program became the first and second phases of the HySET program, respectively. For each phase, the performance metrics of components, subsystems, and engines are quantified to determine the performance achieved. The operational and performance data obtained from the test is further analyzed and used to further improve the design of the engine and subsystems for better performance. These performance indicators were improved at each stage, and the final performance indicators necessary for the engine and missile as a whole met the objectives of the system technology and mission.

9.6.2: Technical Challenges

From an operational point of view, hydrocarbon fuels are easy to use and have better safety than hydrogen fuels; secondly, the existing ground test device has good applicability in the range of Mach number. In addition, theoretically analyzing the upper limit of hydrocarbon fuel work is $Ma = 8$. Therefore, HyTech plans to focus on engine development in the $Ma = 4$ to 8 range and use hydrocarbon fuels, which have a higher density than hydrogen fuels for aircraft applications. In this Mach number range, a flow channel with a fixed profile can be used instead of the variable geometry technique, thus avoiding the mechanical complexity associated with the variable geometry flow channel. From an application perspective, missile applications that focus on single-use missiles have much lower reliability requirements than reusable and manned aerial vehicles.

Figure 9-6 shows the technical challenges faced in the development of scramjet engines. In terms of components, including intake tracts, isolation sections, nozzles, fuels, and fuel systems, as well as structures and materials, another technical challenge that is not explicitly represented in the diagram is the integration of these components and the ability of the engine to operate as a whole.

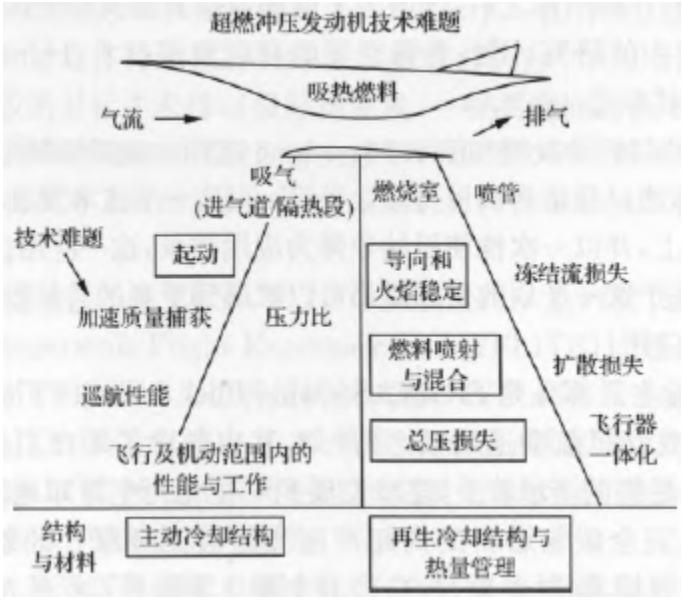

Figure 9-6: Technical challenges of a scramjet

1) Inlet Tract/Isolation Section

The challenges of compression system components include both performance and runnability, the latter being more critical to the success of the design. Specifically, these technical challenges include inlet tract pneumatics, air quality capture, compression ratios, thermal cycling efficiency, and pressure ratios. The so-called "activation" of the inlet means that the inlet is operated at supersonic speed, that is, supersonic flow is established in the compressed part of the intake. When the inlet is not pneumatic, a strong shock wave is located in front of the inlet lip, which will cause the airflow to overflow at the inlet opening, resulting in high drag and structural loads. The amount of overflow affects the thrust generated by a scramjet engine, as the engine thrust is directly proportional to the air quality flow rate. Inlet tract activation also affects the contraction ratio, which is very tightly defined. Therefore, for fixed geometrical flow channels, the maximum shrinkage ratio is a major challenge. Inlet tract activation, air quality capture, and shrinkage ratios often determine engine design, so thermal cycling efficiency is relatively a by-product of the design rather than a design goal. The pressure ratio of the inlet/isolation section combination is also an important operational challenge for the design of a scramjet engine with a two-modal fixed geometry. Several factors affect the pressure ratio, including the cross-section aspect ratio, sidewall configuration, inlet shock intersection location, combustion chamber fuel nozzles, and boundary layer characteristics of the isolation section wall.

2) Combustion chamber

The technical challenges in the combustion chamber are mainly focused on fuel-related issues, i.e. stable combustion through ignition, flame stabilization, and adequate mixing of air and fuel. The geometry of the ignition has an important influence on the delay of fuel ignition. In most cases, the ignition delay time of the fuel is much greater than the time it takes for air to flow through the channels in the engine, usually on the order of LMS, or even less. To solve this problem, a return zone is usually set up in the ignition, or near the fuel nozzle, so that the fuel can be stored long enough for the fuel to ignite and burn. Igniters, also known as flame stabilizers, allow fuel to mix with air and create a backflow, thereby extending residence time, ignition and stable combustion. However, when designing these flame stabilizers, there is a trade-off between geometry and total pressure loss.

The stabilization of combustion is also embodied in the process of stable cycling, which is another fuel characteristic about flame stabilization. The stable cycling process shows that the equivalent ratio is an important stability parameter in the combustion chamber. Stability parameters are speed, geometry of the flame stabilizer, and temperature and pressure. The stability cycle gradually expands for different fuels, from methane (CH4), ethane (C2H6), ethylene (C2H4) to hydrogen. The stable cycle performance of liquid hydrocarbon fuel is similar to that of ethane, and the research also hopes to further expand the stable cycle performance by cracking hydrocarbon fuel (but in any case, it is lower than that of hydrogen fuel). In addition, the speed of stable ignition can be increased by adding silane (SiH4).

3) Nozzle

Unlike the inlet tract and combustion chamber, the challenge for a nozzle is primarily performance and efficiency, not operability. The thrust coefficient of the nozzle is the most sensitive parameter that determines the cycle efficiency of the entire scramjet engine, but since the design of the flow channel is usually determined by the consideration of the runnability of the intake tract, isolation section and combustion chamber, the performance of the nozzle has received relatively little attention. The challenge of nozzle performance is to characterize various losses such as underexpansion, separation, chemical kinetics, and friction through the gas discharge channel, where the losses due to underexpansion and separation are the largest for nozzles in fixed profile flow channels, and the losses in chemical kinetics and friction are relatively small. In addition, the nozzle challenge is not only related to the performance of the scramjet, but also affects the performance of the aircraft, as well as the thrust vector of the nozzle and the pitching moment induced. If the thrust vector of the nozzle is too large, it will cause the aircraft control surface to be overtrimmed, which will cause additional drag. The thrust vectoring angle can be controlled during the design process by changing the engine inclination angle as well as the wall angle of the nozzle. This is an iterative design process, which is a challenge for aircraft integration.

4) Material/Structure

Due to the extremely harsh environment experienced by hypersonic flight, hypersonic vehicles also face great challenges in terms of structure and materials. The same problem is faced by the application of the engine, and the combustion in the flow channel can also cause a very extreme operating environment, under a high temperature, high pressure load, and at the same time accompanied by hot oxygen and fuel decomposition products mixed with corrosion. Without cooling, the material will be exposed to temperatures that exceed the melting point of most metallic structural materials, so active cooling is required, especially for long-life, reusable, high-Mach number operation, and the design of manned aircraft and their engines.

The materials used for the flow channels need to be molded into lightweight siding and complex-shaped components such as fuel ignitors and fuel nozzles through advanced processing methods. The fabrication of structures, especially actively cooled structures, requires the development of advanced manufacturing processes, in particular to be able to meet the needs of long flights, as well as sealing technology between panels in a thermal flow channel environment. At the same time, the design methods for thermal structures need to be further developed and validated.

5) Fuel

Challenges in the fuel sector are primarily related to their use, including endothermic cooling performance, as well as increasing ignition delay and combustion speed. The high velocity of incoming air during hypersonic flight exposes the aircraft structure, especially the combustion chamber, to very severe aerothermal loads. The temperature of the combustion chamber structure without cooling will exceed 3000K, which is more than the current existing structural materials can withstand. Regenerative cooling of the engine structure is necessary with fuel, which is based on the heat sink capacity of the fuel. However, high temperatures of hydrocarbon fuels will lead to coking blockage, which will clog the cooling channels and cause catastrophic structural damage.

In terms of ignition delay, hydrogen has the shortest ignition delay, while methane has the longest ignition delay, with liquid hydrocarbon fuel in between. Liquid hydrocarbon fuel can be cracked and reused as an endothermic cycle fuel, and the ignition delay time will be shortened due to the change in the composition of the injection fuel, so as to improve the stability of combustion, and the ignition delay time can also be changed by adding additives to the fuel.

6) Integration and operational capabilities

The operation of a breathed bimodal scramjet engine is completely different in the case of subsonic combustion and supersonic combustion. Different modes of operation require different fuel injection positions to regulate the heat release law of the combustion chamber so that the engine can run efficiently. The variable geometry of the engine regulates the air flow in the engine as well as the heat release pattern. Different fuel injection methods, i.e. varying the amount of fuel entering the combustion chamber for different conditions at different Mach numbers, will result in differences in density, velocity, and other physical properties within the engine. In the flight Mach number range, the density can be changed by one order of magnitude, and the viscous force can be changed by two orders, so how to make the hypersonic vehicle and its engine achieve reliable and stable flight and operation within the flight envelope is a huge challenge.

9.6.3: Main research outputs

1) Inlet Tract/Isolation Section

Through a series of inlet scale model tests, the starting characteristics, performance and running ability of the inlet were tested. In the first phase of the HyTech program, the scaled-down inlet model verified the performance and operational capability of the flight engine inlet through a total of 121 tests, with the simulated inlet operating range from $Ma = 4$ to 8. The angle of contraction of the inlet larynx, the speed of initiating the gate, the overflow of the guidance area, and the expansion angle of the isolation section were studied. Another inlet model was mainly used to study the length of the isolation section, the expansion angle of the isolation section, the possible self-starting configuration, and the sidewall configuration, and in this experimental study, a self-starting inlet configuration with a swept sidewall was developed.

As a result of these tests, the static pressure ratio of the inlet tract and the isolation section was significantly increased. The test results are further applied to the configuration design of the benchmark HySET engine, as shown in Figure 9-7.

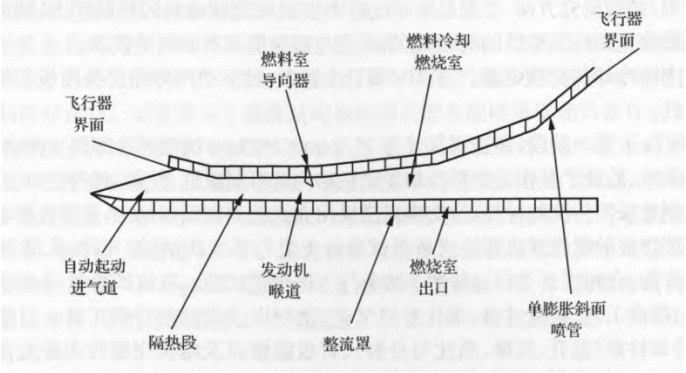

Figure 9-7: Preliminary design of a HyTech 2D flow channel scramjet engine

The application of scramjet engines in aircraft is also continuing, and the flow channel with two-dimensional design can be increased or decreased according to the requirements of different thrust of the aircraft. At the same time, the researchers realized that the aspect ratio of the flow channel could affect the performance of the inlet and isolation sections, so in the first phase of the HySET program, a new inlet model was constructed to study this possible effect, and the test results were closer to the target of the final component. The performance of the inlet tract, such as the aerodynamic shrinkage ratio, kinetic energy efficiency, and mass flow rate, meets or exceeds the predetermined technical targets, but the operational performance of the inlet tract, such as the compression ratio, is slightly smaller than the predetermined targets.

2) Combustion chamber

In the first phase of the HyTech program, a combustion chamber model with a heat sink structure was tested, followed by a verification test of the performance and operational capability of the flight quality engine combustion chamber in the first phase of the HySET program. 172 and 115 tests of the direct-coupled combustion chamber were carried out to simulate the operation capacity of the fixed geometry combustion chamber in the range of Ma = 4 to 8 using JP-7 fuel.

The combustion chamber inlet pressure, the fuel-air equivalent ratio, the fuel temperature, the fuel decomposition, the fuel injection position, the fuel injection scheme, and the geometry of the flame guide were studied in the HyTech and HySET programs. In the first phase of the HyTech program, two other flame guide design schemes were studied on the basis of the baseline flame guide design technology. The swept wedge and swept bracket were fabricated, and experimental studies were carried out on a direct-connected combustion chamber test bench to compare the test results of the combustion chamber performance and operating capacity with that of the reference flame guide.

In the first phase of the HySET program, a performance optimization study was carried out using a new direct-coupled supersonic combustion test bench, and the results of the combustion chamber test were completely close to the expected combustion chamber design goals. In the second phase of the HySET program, the performance of the combustion chamber, including combustion efficiency and maximum pressure rise, was further tested through a semi-free jet test.

The free-jet tests carried out included 60 Ma = 6.5 trials and 35 Ma = 4.5 trials. The test data show that under the condition of an equivalent ratio close to 1, the combustion chamber performance represented by the combustion efficiency meets or even exceeds the expected indicators. The test data also showed significant heat loss in the test model built with copper. The loss of heat causes the fuel and wall temperatures to be lower than expected from a real engine. In order to be able to completely heat the engine wall before injecting hydrocarbon fuel, it is necessary to extend the time for combustion in silicon yards.

3) Material/Structure

In terms of materials/structures, the focus is on the thermal protection of the entire engine flow path, and the structural integrity of the engine combustion chamber is also studied, including research and improvement of low-cost manufacturing technologies.

(1) Active cooling of the heat exchange panel. In the HySET program, a great deal of research work has been done on actively cooled heat exchange panels.

In the first phase of HyTech, a 15.2 cm X38.lcm fuel cooling heat exchange panel was fabricated, and a pilot study was carried out to verify its manufacturability, performance, runnability, and durability as a fuel cooling engine structure. The panel is manufactured using conventional materials, the heat exchange channel is machined on the panel with a vertical milling cutter, and finally a backplate is welded. The combustion chamber with this panel was tested eight times on a direct-connected supersonic combustion test bench. The panels were actively cooled with JP-7 fuel, and tests were carried out under conditions equivalent to the number of Mach 7 in flight. In this trial, the panel's materials, manufacturing processes, assembly processes, catalytic coating processes, sealing, and design and analysis tools are comprehensively studied. The performance, running capacity, and durability indicators of the panels were characterized by the total thermal load, JP-7 cooling performance (temperature rise, pressure drop, enthusiasm, and decomposition), backplate temperature, and structural integrity.

In the first phase of the HySET program, research on cooling panels continues, focusing on low-cost manufacturing techniques, scaling issues, and panel durability testing. In order to develop a low-cost manufacturing technology, the flow channels on the panels are processed using a water mill process, which is very effective for machining complex channel shapes, such as those in the fuel injection area.

Another low-cost manufacturing technology developed in the first phase of the HySET program is laser welding, which uses a panel with a fuel channel to weld to a backplate, as opposed to the previous brazing method. The test results show that the heat exchange panel welded by this technology has satisfactory results in terms of structural strength and deformation controllability.

At the beginning of 2000, two laser-welded 15.2 cm X 76.2 cm panels were tested. One of them was tested on a scramjet engine test bench, in which the panel was mounted on the test model as the lower wall panel of the combustion chamber, and was tested with ethylene fuel under the conditions of Ma = 6.5 and dynamic pressure of 750 psf. Further experiments using JP-7 fuel successfully verified the feasibility of the panel design, thermal structure model, and collected the corresponding data.

Another laser-welded panel was tested for durability in an arc-heated wind tunnel. In this test, the panels are mounted in a test chamber filled with nitrogen, and the real combustion chamber conditions are simulated by arc radiation heating, and the test is carried out for up to 5 to 10 minutes. JP-7 fuel is used as a coolant at a small flow rate. These tests demonstrated not only survivability under conventional flight conditions, but also considerable margin to operate in more harsh flight environments.

In addition to the 15.2 cm x 76.2 cm panels, in the first phase of the HySET program, a full-size combustion chamber sidewall panel was developed, which was manufactured using a water grinding process as well as a laser welding process. The design of the sidewall heat exchanger panel remains unchanged at the width of the fuel flow channel, and the distance between the two channels is gradually increased as the rear of the panel widens, and the maximum allowable spacing is limited by the thermal conductivity and cooling efficiency. Therefore, the cooling channel of the side wall is divided into multiple sections, each of which is formed by the cross channel of the transverse channel with the original channel. The transverse flow channel acts as a redistribution to ensure uniform flow through the flow channel.

Prior to the formal manufacture of the sidewall panels, a water flow test was carried out to verify the distribution of the coolant flow. Subsequently, the fabricated sidewall panels were also subjected to thermal radiation tests in an arc-heated wind tunnel, and several sets of quartz lamps were used to simulate the thermal load strength and distribution of the combustion chamber.

(2) Leading edge structure. Another consideration in the field of thermal protection of scramjet engines is the leading edge of the hood, which has a small arc radius and is subject to considerable heat flow, so it is more difficult to protect against heat. The research work mainly focuses on the selection of structural materials for the leading edge of the engine hood and the design of the structure.

A series of tests on leading edge structure specimens were carried out in the arc heating wind tunnel. These specimens are manufactured from different ceramic matrix composites. In addition, some optical fiber braiding materials have been tested to try to reduce the damage of the ceramic leading edge and provide an efficient heat conduction pathway. The test demonstrated that the best performance of the leading edge structure is that it can withstand heating conditions for up to 10 min. The test successfully solved the problem of connecting the ceramic leading edge with the metal main engine. In addition, the width of the leading edge was enlarged to the width required for the full engine, and the small leading edge segments were connected to each other to create a wide engine leading edge member.

(3) Combustion chamber box aeroacoustics and pressure measurement. The dynamic pressure, i.e. acoustic load, is very intense in the combustion chamber of a scramjet engine, with the entire sound pressure exceeding 180 dB. Therefore, it is necessary to check the performance of the main engine structure under acoustic and hydrostatic loads. Design and manufacture of a HySET scramjet engine combustion chamber test piece, its box structure includes an integrated cooling channel panel, flame guide and flame stabilizer, and combustion chamber expansion section, the whole test piece is a two-end open combustion chamber box structure.

The purpose of the test was to demonstrate the structural performance of the combustion chamber design, in particular the area at the corners of the sidewall and engine undercover panels and the body panels. The test was carried out at room temperature, the sound pressure load reached 178 dB, and the combustion chamber box test piece was structurally intact.

(4) Other achievements. Other research has been carried out in the area of structural materials, including the design of fuel cycle flame guides and the testing of their thermostructural properties. There are considerable challenges in the design and manufacture of this more complex component, and some low-cost methods for manufacturing complex components have been developed in the research work, and one of the better methods is to use three-dimensional modeling to manufacture molds and then carry out the casting of parts, through which some specimens have been manufactured, and very good results have been obtained.

In addition, the influencing factors of shock wave interference are studied. In the case of shock disturbances, the heat load is amplified, and the heating capacity is extremely high in the local area, and the inaccurate estimation of this phenomenon can lead to very serious consequences. In this regard, the shock wave amplification effect is estimated by CFD calculations and verified by some thermal structure tests.

4) Integration and operational capabilities

In the first phase of the HyTech program, a model of a semi-free jet engine made of heat sink material was designed, built and tested. The engine has a flow channel profile of a real flight engine design as well as a flame guide. The tests were carried out under the cruising condition of $Ma = 8$ and demonstrated the performance of the combustion chamber as well as the performance of the positive thrust. Both of these goals were achieved, i.e., the pressure rise of the combustion chamber and the positive net thrust were obtained, and both were in good agreement with the forecasts. These results also validate the tools for flow channel design and analysis. The pressure rise data was also compared with the results of previous tests with the direct combustion chamber, and the results were in good agreement. The same comparisons were also carried out in the second phase of the HySET program and the results were also consistent with the calculated predictions.

9.7: ARRMD Program (1998-2001)

9.7.1: Battlefield demand for rapid response missiles

The development of long-range high-speed missiles using hypersonic technologies will be able to respond to threats over a fairly large range, which will greatly increase the capabilities of combat aircraft.

Hypersonic cruise missiles (flying Mach numbers greater than 5 times the speed of sound) combine many advantages such as high speed, high destruction ability, high survivability, and long-range strike, which will unprecedentedly improve the capabilities of combat aircraft and can quickly respond to long-range threats, including time-critical targets, reinforced targets, deep-buried targets and highly defended targets. Developers of long-range precision strike weapons hypersonic cruise missiles must consider the following factors in order to accomplish their combat missions: the missile's flight performance, the compatibility of the launch platform, and the corresponding C4ISR (Command, Control, Communications, Computers, Intelligence, Surveillance and Reconnaissance) capability; homing ability; precise guidance and navigation capability; survivability; the destructive ability of the warhead.

Hypersonic cruise missiles typically fly at altitudes of more than 90,000 ft and cruise speeds greater than 6,000 ft/s, are capable of full powered flight, can maneuver to change their flight trajectory and hit targets at considerable speeds. Such maneuverability and impact speed allow hypersonic cruise missiles to strike time-critical, highly defensive, and solid or deeply buried targets. The altitude and speed during cruising flight make it a fairly high battlefield survivability, which greatly reduces the time required for flight compared to subsonic cruise missiles. Moreover, such a high battlefield survivability is only a simple trajectory of "climb-cruise" performed by the missile, so the time required for mission planning can be greatly reduced. The enormous kinetic energy generated during high-speed impact is capable of destroying solid or deeply buried targets. For targets that are protected from angles that are likely to be attacked, hypersonic cruise missiles can attack from any angle, thus increasing their damage capability compared to ballistic missiles.

9.7.2: Design Requirements and Conceptual Solutions

The Defense Advanced Research Project Agency's (DARPA) Affordable Rapid Response Missile Demonstrator (ARRMD) program began in 1998. Its goal is to conduct flight tests of a long-range hypersonic cruise missile to demonstrate its performance. The design cost of the ARRMD program was required to be 3,000 missiles with an average combat unit price of $200,000 in fiscal 1998. This puts forward a cost requirement for the design of the missile, that is, under the constraint of a unit price of 200,000 US dollars, a missile that can meet the requirements of combat missions and maximize the effectiveness of the weapon system. In order to meet this cost requirement, the contractors of the program have access to commercially proven technologies to a certain extent and to use existing experience in missile development. The proposed baseline cost of $200,000 is for air-launched and includes missiles, associated subsystems and a basic warhead. For the ship-launched model, the cost is slightly higher due to the need for a relatively larger booster [6].

The demonstration missile concept in the ARRMD program must meet the performance requirements set by the program to the greatest extent possible within the required cost constraints. The most critical of the planned objectives are the requirements for range and speed, and the missiles must use fuel that is readily available in combat logistics. The performance objectives of the ARRMD program are as follows:

- The range of powered flight is 400 to 600 n mile.[1]
- range 400 nautical miles flight time less than 7 min;
- accuracy error of striking at the target is less than 35ft;
- impact speed on the target is 4,000 ft / s;
- Ability to resist the threat of surface-to-air missiles from 2005 and beyond;
- compatibility with combat aircraft of the Air Force and Navy, strategic bombers capable of the Air Force, as well as carrier-based vertical launchers of the Navy;

[1] 1 n mile = 1,852m, as below.

• flexibility of combat missions in a battlefield environment;

• minimum warhead load is 250lbs, which can be modularly loaded with smart cluster bombs, integral bombs and kinetic immersion bombs

• use of conventional liquid hydrocarbon fuels;

• able to be stored maintenance-free for at least 10 years.

The ARRMD program is carried out in two phases, the first phase is 18 months, and the main task is to reduce the risk of flight tests through the development of key technologies and clarify the concept design scheme; the second phase focused on flight test demonstrations. The purpose of the first phase is to conduct a cost and feasibility study of the two candidate missile conceptual designs in order to reduce the risk of development. A series of component demonstration tests showed that the use of key low-cost manufacturing techniques could enable candidate missile concepts to meet the cost requirement of $200,000 per unit, and in the process developed a cost estimation model to improve the accuracy of cost estimation related to the manufacture of missile components and integrated missile systems. The design and development of the missile included a preliminary design review and a series of wind tunnel tests on performance and operational capability to determine the operational characteristics of key engine components, integrated engines, high-temperature materials, and active cooling structures.

The data obtained from the first phase provided cost, performance, and operational information for the second phase of flight test demonstrations. At the same time, the data from the first phase supported the analysis and comparison of the feasibility and cost of the two proposed conceptual options, so that DARPA could decide whether to proceed to the second phase of work.

As originally planned, the second phase will begin with a 30-month flight demonstration of the most promising missile concept design, which will include detailed design of the selected option, flight demonstration of the missile's aeropropulsion performance and capabilities, and further refinement of the manufacturing process for large-format components. Eventually, a cost assessment will be carried out to confirm that the cost requirements are met, and the missile's operational capability will be assessed.

DARPA's Tactical Technology Office is responsible for the implementation of the ARRMD program as the management department of the program. The U.S. Air Force Laboratory (ARFL) is the contract agent for DARPA, contracting with Boeing to carry out two phases of the ARRMD program. Boeing was asked to conduct the same research on both missile concepts, while its subcontractors Aerojet and Pratt & Whitney (P&W) were working on the propulsion system. The Hopkins Applied Physics Laboratory served as DARPA's lead technical advisor to the missile in design, cost evaluation, and analysis of combat effectiveness, with AFRL and Air Force Aeronautical Systems Command providing the necessary technical support.

Phase 1 research work will develop two conceptual designs for missiles proposed by Boeing. The first conceptual design is based on the "waverider" configuration developed by P&W in the U.S. Air Force's HyTech program (as shown in Figure 9-8). The engine section of the propulsion system is rectangular, integrated into the lower surface of the aircraft, and the lower surface of the aircraft is used to provide compression of the incoming flow to the air intake. The compressed air flow through the forebody inlet enters the combustion chamber, where the hydrocarbon fuel burns efficiently in a predominantly supersonic combustion mode thanks to the innovative fuel initiator (PILOT).

The engine combustion chamber is actively cooled with liquid heat sink fuel. The nozzle of the engine is integrated with the lower surface of the rear of the aircraft. The cruise vehicle is boosted by a solid booster to the number of Mach numbers that can be relayed by scramjet engines. When the aircraft is used as the launch platform, the booster is connected with the cruise vehicle by being installed on both sides; when the naval ship is used as the launch platform, the solid booster tail is connected in series to meet the requirements of vertical launch system compatibility.

Another missile concept, proposed by Boeing and Aerojet, is based on the application of surface-to-air missiles originally developed in the Navy's ship-launched missile technology program and uses twin-chamber ramjet engine technology.

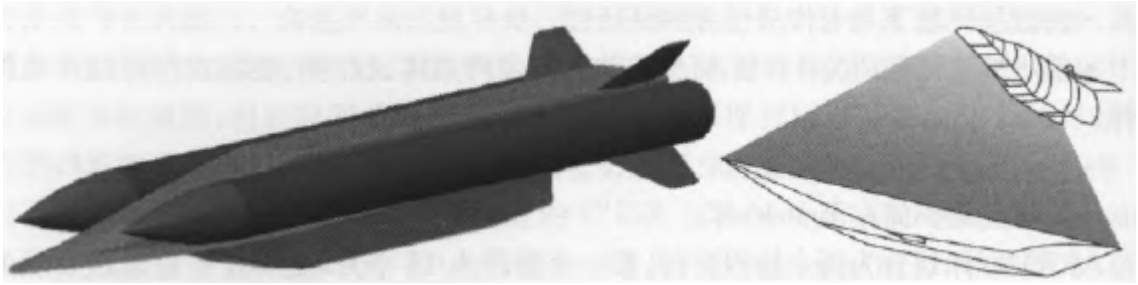

Figure 9-8: ARRMD missile demonstrator based on waverider configuration

The scheme is axisymmetrical, with a tapered head for multiple inlet modules (as shown in Figure 9-9). These inlet modules distribute the incoming flow, part of which goes into the subsonic combustion chamber and the other part into the supersonic combustion chamber in the rear. The fuel is added to the subsonic combustion chamber, which heats and partially cracks the fuel. The combustible gas is further fully mixed and burned with air in a supersonic combustion chamber. The design relies on high-temperature material technology and thermal insulation of the engine and airframe structure. The interpolated booster is used in the air-launched configuration to accelerate the missile to the Mach number of the relay point, while the tandem booster is used in the scheme of ship-launched missiles.

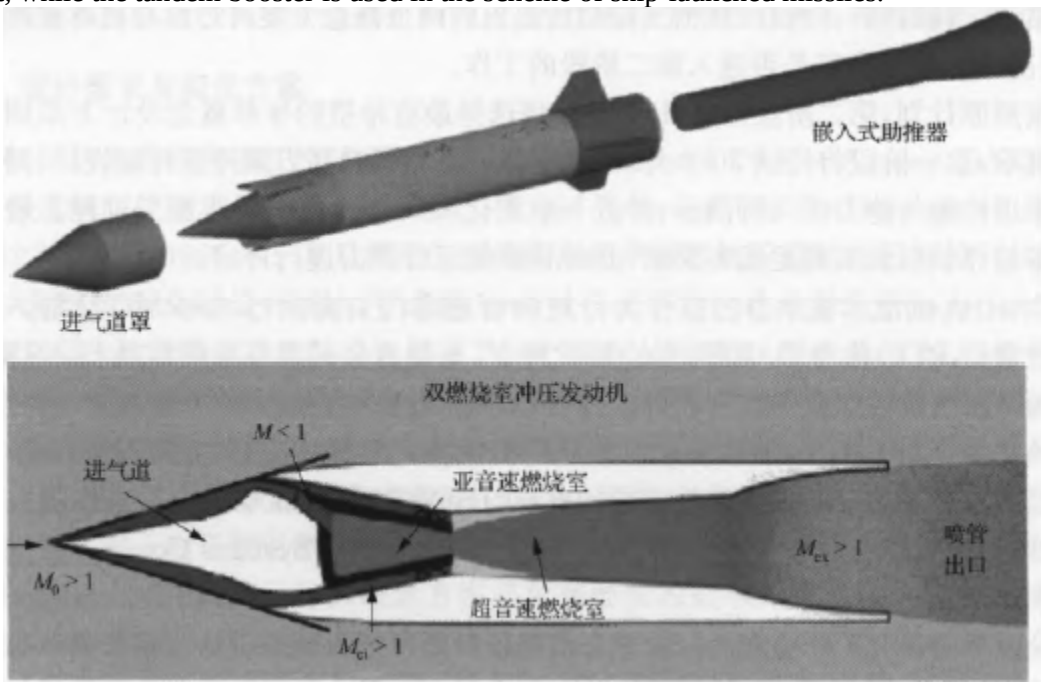

Figure 9-9: Demonstrator of a dual-combustion ramjet engine-powered ARRMD missile

The ARRMD program is not a program for the development of technology, but a program for demonstrating technologies with the latest level of development, developed by the US Navy and Air Force. The U.S. Bureau of Naval Research (HWT) has launched a program called Hypersonic Weapon Technology (HWT) to develop and conduct test demonstrations of technologies for key components, particularly for long-range strike missile applications. The program is a joint effort between the Naval Aviation Weapons Development Center, the Johns Hopkins University Applied Physics Laboratory, and the Naval Surface Weapons Development Center. The Center for the Development of Weapons of Naval Aviation is responsible for the management of the program, the guidance control of missiles, as well as airframe technology. The Laboratory of Applied Physics is responsible for the technology of the propulsion system, and the Center for the Development of Surface Weapons of the Navy is responsible for the warhead technology. In the HWT propulsion system program, research efforts have focused on DCR engine technology, which is applied in the ARRMD program. In addition, research on HWT warheads has led to the development of multifunctional warheads that can be applied to the weapon concept scheme of the ARRMD program.

The U.S. Air Force has partnered with P&W to develop hydrocarbon-fueled scramjet engines under the HyTech program for applications in the *Ma* = 4 to 8 range, including long-range strike missiles, global arrival aircraft, and orbital vehicles. The wide range of applications in the HyTech program is due to the use of heat-sink hydrocarbon fuels as well as active cooling structures. In the ARRMD program, Boeing and P&W's wave-riding missile solution uses and relies on the technology developed by HyTech.

To facilitate coordinated communication, a memorandum of understanding was established between the hypersonic technology program of the US Navy and Air Force and the DARPA flight demonstration program. Initially, the

memorandum of understanding established and signed between DARPA and the Bureau of Naval Research stated that "their plans are in some form a whole, providing the greatest convenience to each other in achieving the overall goal of achieving a hypersonic cruise missile." The memorandum also states that "DARPA expects the ONR's HWT program to provide the necessary technical foundation for the ARRMD program and continue to develop the technology to eventually complete the development of hypersonic weapon systems." At the same time, it noted that "the key goals of the DARPA program are the manufacturability and affordability of weapons systems and provide near-term opportunities for flight demonstrations of hypersonic missile technology." Subsequently, the memorandum of understanding was also extended to the U.S. Air Force's HyTech program, "DARPA, ONR, and AFRL will coordinate their programs and establish a common technology development roadmap to support the development of hypersonic weapons." The ARRMD, HWT and HyTech programs will support each other and integrate as one."

The technologies demonstrated in the ARRMD program will contribute to the development of affordable rapid-response missiles. The ARRM missile is capable of compatibility with a wide range of launch platforms and is capable of using battlefield target information from both national and tactical sources. With modular or multi-functional warheads, ARRM missiles will have the ability to strike time-critical, solid, deeply buried and highly defended targets. For this basic battlefield operation mode, the target detection and positioning adopts a variety of available reconnaissance means, including early warning aircraft, ground radar, and reconnaissance satellites, etc., the target positioning adopts the global positioning system (GPS), the information is transmitted to the combat command through the satellite communication chain, the target position information of GPS is transmitted to the missile, and the missile is launched after receiving the order, and in the process of flight, the updated target information is continuously transmitted to the missile, and when it reaches the air above the target area, the terminal maneuvering flight is carried out until the target is destroyed. For fixed or deeply buried targets, ARRM missiles are loaded with kinetic energy to immerse the warhead and hit the target vertically at high speed; for soft targets, high-explosive or cluster warheads will be loaded to strike targets at the same high speed; against moving targets, it is possible to carry multiple warheads, slightly reduce the speed of the missile, and detonate the multiple warheads in the appropriate area.

9.7.3: Technical Challenges

1) The overall scheme of missiles and thermal protection technology

The flight demonstration of a hypersonic cruise missile presents a considerable number of key technical challenges. At a top-level level, some of the challenges are common to any conceptual design solution, but the path to solving these challenges is often to address the technical problems of a particular conceptual solution. Affordability is a must-meet missile design requirement for the ARRMD program. Therefore, ARRMD focuses on demonstrating affordable vehicles to validate the possibilities of long-range supersonic weapon systems.

Perhaps the biggest challenge for sustained hypersonic flight is how to deal with the external thermal environment. Flight speeds greater than Mach 6 will result in temperatures of more than 1,000°F on the surface of the missile, and over 4,000°F in the combustion chamber and tail nozzle without active cooling. The solution to survive in this thermal environment depends on specific missile concepts and their components. For a large area of the outer surface of the missile, it is enough to use high-temperature materials with or without coating.

Missile components that are directly exposed to the air flow, such as control surfaces and air intakes, require special measures, since the leading edge causes the interaction of shock waves. Inside the missile, critical subsystems, including warhead loads, electronics, and fuel systems, must be protected from the effects of external heat.

The biggest thermal stress challenge is the combustion chamber. Overcoming the thermal environment in the combustion chamber is directly related to another key technical challenge: making liquid hydrocarbon fuels burn efficiently in supersonic streams, and the two ARRMD missile concepts have completely different approaches to solving this problem.

The propulsion system solution for the concept of hypersonic missiles in wave-riding configurations was originally proposed by the US Navy, NASA Langley Research Center and Joint Technology Research Center. The Joint Technical Research Center developed a rectangular combustion chamber configuration and embedded a small subsonic aspirated igniter in the walls of the combustion chamber. The igniter captures a small portion of the air flow and burns a small amount of fuel. Its gas stabilizes supersonic combustion in the main combustion chamber where the fuel is mainly combusted. This engine type requires liquid hydrocarbon fuel to be atomized through a nozzle. The combustion chamber uses endothermic fuel, and a heat exchanger on the side wall provides the ability to atomize the fuel, producing a partially pyrolytic product into the combustion chamber. In this method, a heat exchanger is used to cool the combustion chamber wall.

The actively-cooled combustion chamber is able to control the temperature of the walls and provides the potential for flight in conditions of $Ma = 8$, but the actively-cooled structure and the corresponding fuel system must be cost-effective. The performance of the combustion chamber has been demonstrated under the condition of $Ma = 4$ to 8 in the HyTech program and satisfactory combustion chamber performance has been obtained.

The main technical challenges for missiles in the waverider configuration include:

• Integration of subsystems within an affordable range, so that the engine can be cooled, the intake tract starts smoothly, and the heated fuel can be controlled;

• Integration with affordable boosters;

• Controllability of the aircraft over the entire flight envelope.

The ARRMD program benefits from the ongoing research work on engine technology by the HyTech program. Under the ARRMD program, the designed test vehicle will gradually mature and conduct tests of force and torque in the wind tunnel. Key low-cost manufacturing technologies will also be demonstrated.

The DCR-powered hypersonic missile concept combines the characteristics of a ramjet engine with a scramjet engine by embedding a subsonic combustion chamber as a trigger in front of the incoming stream of the supersonic combustion chamber. This igniter prepares hydrocarbon fuel for supersonic combustion. Approximately 25% of the air flow is captured by the two inlet ducts and enters the embedded subsonic combustion chamber, where it is mixed with all the fuel. After combustion, the combustion-rich gas is followed by a supersonic combustion chamber with air captured by the four internal turning intakes. These inlet ducts compress and pool the air flow into a ring of flow, the inlet of which is the outlet of the subsonic combustion chamber. The combustion process begins in a subsonic combustion chamber and ends in a cylindrical supersonic combustion chamber with the gas discharged through an extended nozzle.

The design of this combustion chamber allows the hypersonic missile to run on conventional hydrocarbon fuel and with a liquid nozzle. Since the combustion process does not require any additional energy to be added to the liquid fuel, the entire combustion chamber can be passively cooled when flying at a Mach number of about 6.5.

The main technical challenges for DCR-powered missiles include:

• The development and application of affordable materials of construction that allow subsonic and supersonic combustion chambers, intake ducts and tail nozzles to withstand extremely high temperatures;

• Affordable and complex intake duct and subsonic combustion chamber fabrication and assembly processes;

• Engine operating performance from *Ma* = 3 to 6.5;

• The dimensions and volume of the missile are designed so that it can accommodate sufficient fuel as well as an effective warhead.

The development and component testing of the DCR was supported by the U.S. Navy from 1977 to 1986 and continued under the HWT program. The first phase of the ARRMD program demonstrates key low-cost manufacturing technologies and the performance of an integrated propulsion system.

2) Homing, C4ISR and the final stage

Homing and destructive performance are essential elements of a weapon system. The ARRMD program is focused on the demonstration of a viable hypersonic strike missile, the main result of which is a flight test demonstration of the missile, flying at least 400 n miles with an accuracy of striking against point targets in the range of 35 ft. The final long-range strike weapon required the ability to accurately locate and identify the target to be hit, process the target information in real time, and finally destroy the target with precision. Accurate target localization and destructiveness require the accuracy of the terminal sensor and guidance system, the ability to communicate real-time target information updates during flight, and the time when the weapon warhead detonates. These requirements are especially important for mobile and redeployment targets. For time-critical targets such as tactical missile launchers, the capabilities are determined by two crucial factors:

• the ability to detect and identify targets with sufficient accuracy for an effective strike;

• the ability to relay information to missile launchers within the required time.

The ability to target targeting defines the requirements of many other major weapons systems and determines the probability of success of the mission as a whole.

For different combat environments, a variety of ways and means of target positioning can be selected, including satellites, manned reconnaissance aircraft, unmanned reconnaissance aircraft, ground radar, etc., these means and technologies are also constantly developing, and some are applied to tactical ballistic missile launchers and other real-time identification of time-critical targets. For long-range strikes, hypersonic cruise missiles use these means to play the role of a maximum leverage efficiency. The time to hit the target was reduced by 5-6 times, which greatly increased the effectiveness of the entire weapon system.

A number of space-based reconnaissance tools can be used to identify tactical missile launchers and locate the launch area quickly and accurately. This precision strike capability made it possible to reduce the requirements for the warhead. However, if this means cannot provide sufficiently accurate positioning information, terminal guidance must be used. In this case, it is necessary to provide sufficiently accurate target positioning information by means such as unmanned reconnaissance aircraft for terminal guidance. Alternatively, the missile is designed to be active end-homing, or to be equipped with a warhead with end-guidance capabilities (e.g., a dexterous bomb).

To combat targets that exist for a short time and are redeployed, the ARRMD program is designed to carry dexterous warheads, such as BAT or LOCAAS. In this case, the key technology is how to thermally protect the sub-warhead, especially when throwing, the speed of the missile is as high as *Ma* = 3. For deep-buried reinforced targets, the ARRM missile can carry a kinetic energy immersion blast projectile of 2501b to hit at a terminal velocity of 4,000 ft/s. For surface targets with relatively low defensiveness, a large area of the warhead can be used.

3) Compatibility of the launch platform

In the design of missile weapons, the compatibility of the launch platform puts forward some binding requirements for the design. The goal of the ARRMD program is to be compatible with most launch platforms. The mass of the missile is limited to the maximum weight that the F/A-18 fighter can carry. The length should be able to meet the requirements of the B-52 and B-1 strategic bomber rotary throwing frames. The geometrical cross-section dimensions were required to be able to meet the constraints of the Navy's vertical launch device.

9.7.4: Subsequent Development of the ARRMD Program

The ARRMD program ended in 2001 and flight demonstration tests could not be carried out as planned. But the conceptual design of its two missiles was continued. The DCR powered missile program continues in the US Navy's HyFly program; the waverider configuration missile scheme continued as the overall reference scheme for engine development in the HyTech program, and eventually evolved into the test vehicle scheme used in the X-51A program.

9.8: Hyper-X program and X-43A flight tests

9.8.1: Hyper-X Program Overview

One of the harshest criticisms of the project at the end of the National Space Aircraft (NASP) program was that only the most critical component, the scramjet engine, was simulated in the wind tunnel, without actual flights. Therefore, NASA's Langley and Dryden Research Center jointly launched the Hyper-X project to develop a vehicle capable of flight tests at a speed of $Ma = 10$, and the X-43A is a significant achievement of the project [7~11].

The X-43A test vehicle runs on hydrogen fuel and has been tested in flight tests to verify the performance of an actual scramjet. Off-the-shelf boosters were used to carry NASA B-52 aircraft for air launch. The X-43A's lift body shape is derived from McDonnell Douglas' $Ma = 10$ cruise vehicle research for NASA's Langley Research Center. Phase III of the contract calls for the conceptual design of a research vehicle powered by a hydrogen-fueled scramjet engine to provide flight test data on the operation and performance of the scramjet engine at speeds of $Ma = 7$ and $Ma = 10$. The data from the $Ma = 7$ test will be directly comparable to the results of the ground test with the same engine and combined flow path, and the results of the $Ma = 10$ test will be able to provide flight test data for 5 to 10 seconds at the Mach number of the flight. The widest range of available calculation tools are used for the design of aircraft and engines, and flight data can verify the accuracy of these design methods.

After the conceptual design was completed, NASA began looking for a team of contractors to complete the design and manufacture of the vehicle and support the flight test program. Two teams competed for this phase of the project, one consisting of McDonnell Douglas and Pratt & Whitney, and the other including MicroCraft, North American Aerospace Industries, and GASL, with NASA choosing the latter team. As the Hyper-X project progressed, the industry changed, with MicroCraft and GASL being incorporated into ATK GASL, while North American Aerospace Industries and McDonnell Douglas were both acquired by Boeing. As a result, the team that designed and built the X-43A and connectors to connect and separate the vehicle from the modified Pegasus booster rocket was formed by ATK GASL and Boeing.

The design and manufacturing phase of the Hyper-X project began in March 1997. A critical design review of the aircraft took place in February 1998, with the first aircraft and connectors delivered to NASA's Dryden Research Center on October 11, 1999 and March 31, 2000, respectively. The second $Ma = 7$ aircraft and connector were delivered on January 29, 2001 and February 5, 2001, respectively. The first flight test, which took place on 2 June 2001, was unsuccessful due to overloading of the booster control surface in an untested environment and led to a sustenance of the flight test program for several years in order to identify the cause of the failure and to make appropriate improvements to the launch vehicle and flight test track. During this period, the $Ma = 10$ aircraft, which differed from the $Ma = 7$ aircraft in terms of engine design and thermal protection systems, was completed on May 2, 2002 and delivered to NASA's Dryden Research Center on June 17, 2002.

A flight test of *Ma* = 7 was successfully conducted on March 27, 2004 and a flight test with Mach number 10 was successfully completed on 16 November 2004 following a re-validation of the preparatory work prior to the flight test. Both tests set a record for the speed of an air-breathing engine aircraft in the atmosphere.

The responsibilities of the ATK GASL/Boeing team are as follows: ATK GASL is responsible for the overall management of the contractor team, the structural design of engines and connectors, the structural design of aircraft structures, the design and manufacture of fuel and ignition systems, aircraft, Boeing is responsible for aircraft aerodynamics and structural design, aircraft thermal management, aircraft subsystem design and technical specifications, flight control and engine control laws, aircraft control system software, aircraft management system, and aircraft thermal protection pads. Major subcontractors include Honeywell, Inc., which is responsible for aircraft management systems; and Moog, which is responsible for the electromechanical drive mechanism and control unit. SAIC designed and Goodrich manufactured the carbon-carbon leading edge of the *Ma* = 7 aircraft, while the leading edge of the *Ma* = 10 aircraft was manufactured by MER Ltd. The battery, which is the main power source, is supplied by Eagle-Picher. The high-pressure solenoid valves and regulators are made from VALCOR. Jansen Aircraft Systems Controls, Inc. (JASC) offers fluid control valves for hydrogen and silanes. The modular measuring system was completed by L23 (formerly Aydin Vector).

9.8.2: Overall design of the X-43A test vehicle

Taking into account its flight envelope, the X-43A has a very traditional design. From an aerodynamic point of view, it can be described as a lift-body structure with control surfaces at the rear of the fuselage, including a full-moving horizontal tail and dual vertical tails with rudders (Figs. 9-10). The design is based on the concept of a vehicle with a global trajectory of *Ma* = 10 hypersonic cruise. Due to the need for high-speed cruising, the leading edge is designed to be sharp in order to reduce drag, and the control surface is correspondingly thin. The lower part of the front fuselage is designed to provide an external compression slope for the scramjet intake tract, while the lower part of the rear fuselage is designed to provide a single expansion nozzle face. The upper surface of the fuselage has a gentle curvature, and the front section of the fuselage contains a large ballast segment, so that the center of gravity of the aircraft is high enough to provide near-neutral longitudinal stability.

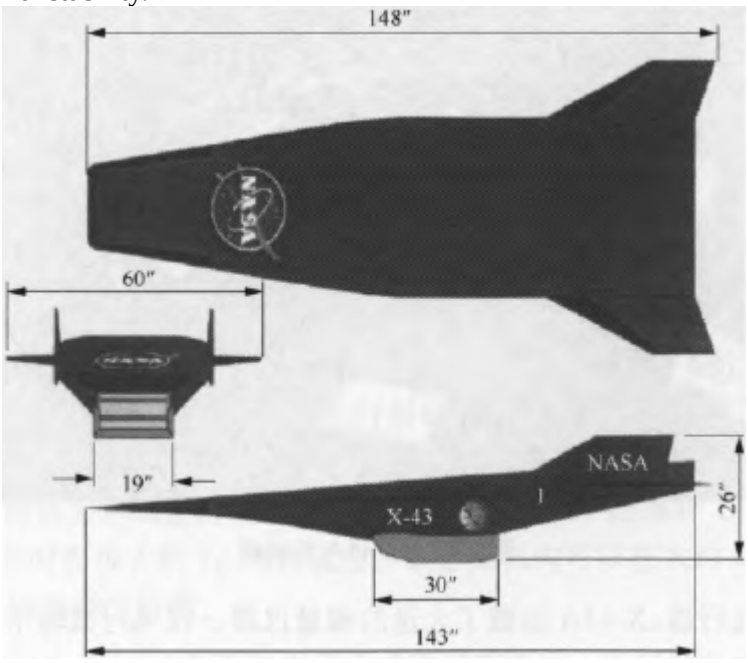

Figure 9-10: X-43A test vehicle

The fuselage truss and partitions of the aircraft are made of steel, titanium, aluminum and other materials, and are covered with steel and aluminum skin. These materials are determined by the hardness requirements of the aircraft, while titanium is chosen for the tail compartment due to the need for thermal protection. For the sake of aircraft balancing, a solid tungsten wedge weighing about 392 kg was used in the front compartment. The X-43A body is thermally protected by a carbon-carbon leading edge (wrapped around a tungsten wedge to form a fuselage strip), and the upper and lower surfaces are covered with reinforced alumina heat-resistant (AETB) porcelain tiles. The metal skin is designed in a number of relatively simple, low-cost faceted shapes, allowing the OML to be machined into the TPS heat-resistant porcelain tile. The design feature of the heat-resistant porcelain tile is that the machining of the outer surface is carried out after the porcelain tile is installed on the fuselage. As a result, the surface coating is carried out after the machining is completed, thus avoiding hot baking. Both the horizontal and vertical tail wings are thermal structures (Hinatuan nickel-steel alloy) and are thermally protected only along its leading edge. For the *Ma* = 7 aircraft, the horizontal surface is only protected from heat by carbon-carbon lining; in the case of *Ma* = 10 aircraft, both horizontal and vertical surfaces are protected with carbon-carbon. The engine uses a cool-dissipating Cooper alloy (Glidcop) with an active water cooling system on its fairing and leading edges of the sidewalls.

The engine of the aircraft is manufactured as a separate unit (Figure 9-11). The engine adopts a rectangular flow path and fuselage integration design, and its front and rear fuselages act as epitaxy of the engine's internal compression and expansion surfaces, providing external compression and expansion surfaces. The aircraft uses gaseous hydrogen fuel and silane ignition agent, and in order to ensure sufficient operation time, hydrogen and hydrogen/silane mixed ignition agent are $5.9x10^7$, respectively Pa and 3.1X107 Pa pressure storage. The Glidcop engine compartment is mounted on an unlured steel stiffening seat, which is connected to the fuselage. A key feature of the engine is the movable inlet cover, which closes the booster section to protect the internal flow path, opening while the engine is working and closing again during the descent of the aircraft from the test site. The fairing and vertical leading edge of the engine are sharp, and the booster section and the engine working section are thermally protected by water cooling. Oxidized coatings are applied to the front of the engine fairing and at critical locations throughout the engine to provide additional thermal protection. The aircraft subsystem also integrates a nitrogen blowing system, which can cool the corresponding aircraft subsystem during the flight test phase.

Figure 9-11: X-43A engine

As a research vehicle, the X-43A is equipped with a large number of measuring instruments. During flight tests, more than 500 individual instruments are monitored and recorded.

Since the aircraft is not recovered after the flight, these measurement parameters are transmitted to the ground and the flight receiver via the transmitter, and most of the critical data (related to engine performance) is relayed throughout the flight. Measurements include surface temperature and pressure, internal temperature and pressure, structural stresses, and flight trajectory parameters from the onboard inertial navigation system and global positioning system receiver (INS/GPS). For the purpose of trajectory tracking and temperature measurement, multiple S2-band transmitters and a C2-band transponder are installed on the aircraft. In addition to the engine performance and flow path data obtained during the engine test phase of the flight test, aerodynamic data can also be obtained through pre-programmed maneuvers during the deceleration from the flight test site to Mach 1.

The aircraft management and control system consist of a flight management unit (FMU), an electromechanical transmission mechanism, and its controller (a transmission mechanism that controls the four serpentine servos and engine fairings), and a measurement system. The FMU provides fully automated control of these systems, initiating events based on pre-programmed timelines, aircraft measurement system data, and on-board INS/GPS data. The system also includes engine control software, as well as innovative software to detect and avoid engine intake tract immobility. All on-board equipment is powered by electricity, which requires ample battery capacity. Since the FMU, transmission mechanism and controller, measurement system, and battery are all finished parts, the internal void of the aircraft is minimized (Figure 9-12).

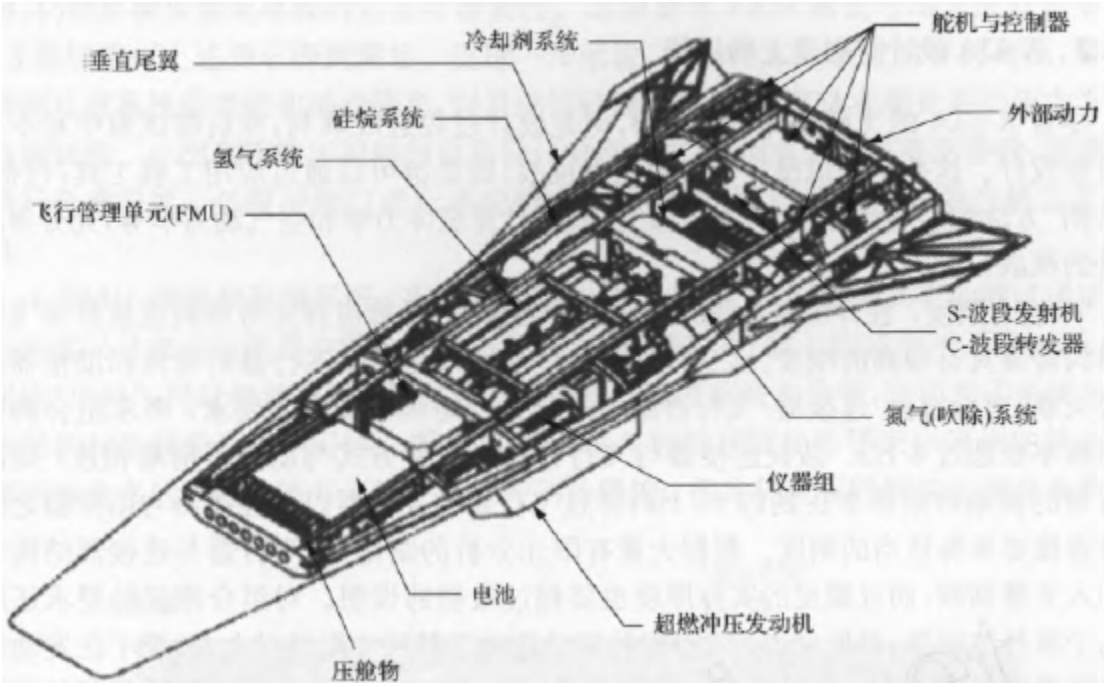

Figure 9-12: X-43A test vehicle system layout

The research vehicle is connected to the modified Pegasus booster via a specially designed connector (Figure 9-13). More than just a connection structure, the connector also integrates a separation system and water cooling and nitrogen blowing (as well as cooling) in the booster section of the flight track. Like the aircraft fuselage, the connector structure is mainly made of steel and aluminum and is covered with a layer of cork insulation on the outside. The separation system is based on a set of cruise missile launchers designed for the B-1B project, but never used. When these systems are installed, the piston has an effect on the aircraft's titanium rear bulkhead, providing approximately 9g of acceleration at start. The separation mechanism can complete the separation of the X-43A from the connector 2 booster in about 0.35 s.

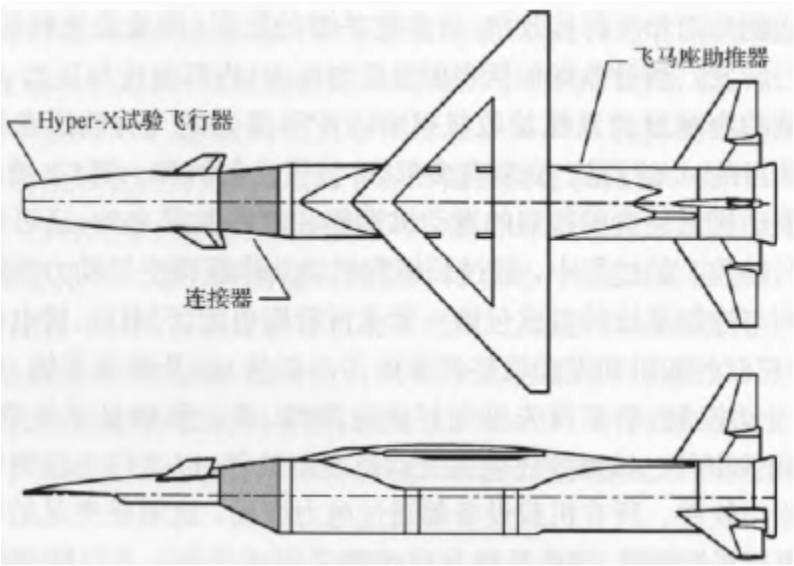

Figure 9-13: The carrier and connector of the X-43A test vehicle

9.8.3: X-43A Design and Manufacturing Challenges

Despite the unique flight conditions of the X-43A, the design process went well and there was little need for redesign in subsequent tests. This is not to say that there are no challenges in the design, but rather that the challenges can be adequately addressed by applying engineering tools, including "rule of thumb" methods and cutting-edge computational tools such as finite element modeling, computational fluid dynamics, and aerodynamics.

• Combined stiffness: At the beginning of the detailed structural design process, it is clear that the structural needs of the connector and the aircraft need to have a high degree of stiffness. The reason for this requirement is that the bending of the aircraft is related to the booster control system, which requires the initial bending moment frequency of the booster/connector/aircraft combination, which is required to exceed 8 Hz. Assuming that the connector is connected to the front end of the booster by cantilever with the aircraft, the initial bending moment frequency of the aircraft needs to reach about 65 Hz, and the bolted connection between the aircraft and the connector and the connector and the booster needs to have appropriate stiffness. According to the conclusion of a large number of finite element analyses, a large amount of steel needs to be added to the structure of the aircraft and connectors, and the actual thickness of the skin is greater than originally envisaged. The requirements for combined stiffness also create several additional problems: for example, the mass of the vehicle is too large relative to its size, so that a ballistic trajectory is required to maintain a suitable angle of attack during the engine test phase; on the other hand, it may be possible to reduce the deflection of the skin, eliminating the need for gaps between AETB ceramic tiles.

• Thermal protection: Where possible, the thermal protection system of the aircraft should be designed with passive thermal protection as much as possible. Due to the shape of the aircraft, a large part of the front section of the aircraft fuselage is made of solid tungsten material, which simplifies the thermal protection design of this area. Carbon-to-carbon leading edge and fuselage strips are used for thermal protection at the edges where tungsten wedges are heated, while a relatively short flight time prevents most of the tungsten wedge head surface from being heated. In general, the large area thermal protection (AETB protective tile) is designed according to the amount of heating at a speed of $Ma = 10$ and has a thickness of approximately 1.3 cm (except in the case where it needs to be thickened to obtain the desired aerodynamic shape). It is difficult to cover such a thin tile on a flexible surface, but as mentioned above, the stiffness requirement minimizes the deflection of the vehicle's surface, so that the traditional (as used by the space shuttle) attachment method can be used in its entirety. It is more difficult to design thermal protection for horizontal and vertical control surfaces, because the control surfaces are thermal structures and it is better to use a solid or near-solid design, but due to the consideration of the center of gravity, this design cannot be adopted.

Therefore, these control surfaces adopt a combined welded structure, which has the problem of difficult processing. Nevertheless, the fabrication of the control surface has been completed according to the design. Due to its relatively small radius and the need to cover the carbide cinnamon coating, the carbon-carbon leading edge and fuselage strip are also difficult to manufacture. In addition, different approaches are used at the junction of aircraft with Mach numbers of 7 and 10 to take full advantage of the heat dissipation of the metal structure at higher Mach numbers. However, taking this series of measures has led to a change in the mechanical properties of carbon-carbon materials, which must be taken into account during the design process. In addition to the challenges of the external hypersonic environment, the internal heat generated due to the long refueling and flight preparation times also needs to be considered in the design of the bracket contact surfaces and heat sinks, so that the blow-off system can be cooled after the final manufacturing is completed.

• Propulsion and Fuel System: Although the X-43A's engine is largely designed to dissipate heat, the leading edge of the engine and its deflector must be water-cooled to resist the high amount of heating faced during the booster and engine testing phases. Since a certain amount of water is lost with each cycle, careful consideration must be given to the amount of water on board. Integral cooling requires carrying water not only on the X-43A, but also on the connector for the cooling water of the booster stage. Of course, this must have corresponding connectors, which will occupy a certain space in the rear compartment of the aircraft. Although it is possible to deform due to constant changes in the amount of heating, it is still important to ensure that the fairing is fully mobile. A thorough analysis of the FEM heat and pressure is required to ensure that these requirements are met. Furthermore, the high pressures inherent in fuel and ignition require special attention to system integrity and vibration isolation, as well as ignition performance testing of silane/hydrogen mixtures at such high pressures. Small high-pressure hydraulic control valves are also one of the design difficulties, and due to their high-pressure characteristics, they need to be properly placed. Valves must be tested and redesigned multiple times to achieve the required qualified workmanship and reliability.

• FMU, measurement and telemetry systems: The X-43A (and its booster rockets and connectors) have the number of test channels that may be unprecedented for its size. Because the measurement subsystem, like other subsystems on the aircraft, requires the procurement of "finished parts," and the connection between the measurement device and the recording device also requires wiring and conduits, so the packaging of the subsystem inside the aircraft becomes a difficult problem. Figure 9-14 illustrates the challenges encountered in assembling wires and conduit bundles. Although it is not necessary to take special measures to provide so many measurement channels, special attention is still paid to the wiring of the measuring system (and this can only be done during assembly).

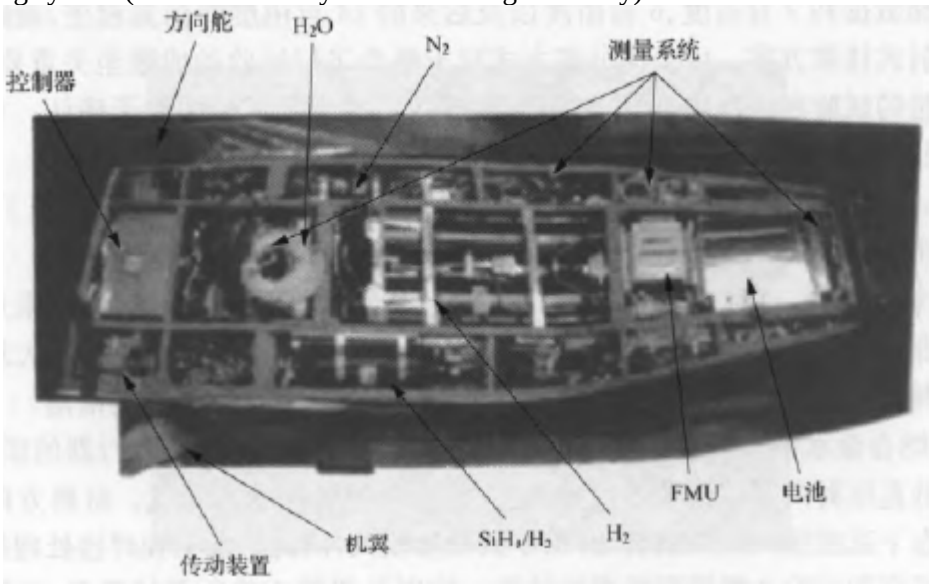

Figure 9-14: System installation

Early tests of the measurement system, as well as the telemetry system, also showed that the heat generated by the aircraft's internal electrical equipment was not fully considered. Telemetry emitters, in particular, produce an amount of heating that is almost equivalent to that of a small light bulb. During the design process, it was assumed that the aircraft structure would be designed to cool the electrical equipment with sufficient heat dissipation, but this proved to be the case, in part because the FMU was required to remain active throughout the pre-launch preparation phase. Therefore, the nitrogen blowing system, which was originally used only as an interior of the aircraft, had to function as a cooling system at the same time. This requires additional capacity and blow-out connections inside the connector to deliver blow-out gas from the B-52 carrier aircraft and from the connector in the booster section to the aircraft prior to release.

Power & Transmission: Another area that has a significant impact on the design and manufacture of the small X-43A is the design and installation of the power supply and transmission. Both subsystems are based on the existing installations, with some changes to the battery box and transmission mechanism. In order to save space, all the servo controllers were housed in the same box, and in the original design, there was significant crosstalk interference between neighboring controllers. This required the drivetrain's subcontractor to make several iterations to overcome the challenge. In addition, all power and drivetrain components (like most of the electrical components on an aircraft) are connected via standard aircraft connectors, which are oversized for the small X-43A aircraft. Wiring needs to be well designed and installed to minimize the potential for electromagnetic interference (EMI).

• Connectors: Due to stiffness considerations, special design of explosive bolt joints is required to minimize shear forces. Initial sample testing found that the expansion of the bolts in the connector could lead to failure. This problem has been solved with minor design modifications before the design is finalized. The key issue encountered in the connector design process is the design of the separation system. The system must be able to smoothly and quickly separate the booster/connector from the aircraft under the conditions of dynamic pressure of 4.78X105Pa, Mach number 7 and 10. It has been documented that this technology has not been implemented before. The most important requirement was to provide a very rapid separation (so that the booster would not come into contact with the aircraft due to the lifting of the aircraft due to the separation of the aircraft) and that the separation could be done with the controllable residual force of the aircraft. At the same time, the booster/connector/aircraft must maintain an overall stiffness of more than 8 Hz before the connector is separated from the aircraft. In the design phase, the proposal from the project planning phase was adopted, i.e., an asymmetrical connection between the aircraft and the connector along the lower part of the rear fuselage of the aircraft. The transmission mechanism of this scheme adopts the B-1B ejection pylon-type transmission device, and its reliability and performance have been fully tested. Based on these performance data and simulation programs of 3 degrees of freedom, 6 degrees of freedom, and later 14 degrees of freedom, the ejection pylon scheme was finally selected in the design. Since this separation method is critical to the success or failure of the entire flight test, a large number of tests and computational simulations were carried out, which were not confirmed until the first successful flight test. In the flight test, the separation was done exactly as expected.

During the Hyper-X project, there were a number of manufacturing challenges, but all of them were overcome, as confirmed by the success of flight tests. Here are some of the most challenging challenges.

• Tungsten Ballast Section: The X-43A has probably the largest tungsten object ever installed in the nose compartment, and the tungsten alloy used in it is called Densalloy 180. The ballast section is made by melting several large pieces of tungsten raw material together in a large furnace. The process must be used to avoid the slippage of individual parts during the melting process.

• Haina alloy horizontal and vertical tail: As mentioned earlier, in order to reduce the mass and maintain the center of mass of the aircraft, the internal structure of the horizontal and vertical tail of the aircraft is machined, and the surface is welded. In terms of material, the nickel steel alloy with high strength at high temperature is selected, and because of its high hardness, machining and welding treatment need to go through many repeated studies and tests to obtain satisfactory results. In particular, the high temperature required for the welding process will cause the deformation of the skin surface to be greater than the surface wave degree specified in the aircraft technical specifications. A team of experts from ATK GASL and Boeing developed a successful welding method after repeated design and welding trials.

• Leading edge: To minimize aerodynamic drag, the leading edge of the X-43A is designed with a very small radius of curvature (0.08cm). Later, the radius requirement for Mach 10 aircraft was relaxed to 0.13cm. This increases the difficulty of the fabrication of carbon-carbon materials and the coating of carbonized cinnamon. As in the case of horizontal and vertical tail structures, the development of appropriate manufacturing processes and processes requires many iterations of design and trial. Experts from various contractors, including subcontractors SAIC and NASA, formed a team of experts to assist in the development of the process to achieve satisfactory performance for these thin leading edges.

• Profile: As mentioned above, the X-43A's heat shield tile installation is unique, and the final profile is created after the heat shield tile is installed on the aircraft body. This process is carried out on a large three-axis machine, and the processing equipment can be reduced to a minimum by clamping the body compartment on the machine in a single form. After the CNC machine has completed the surface profile forming, the OML is measured for final confirmation and a protective layer is applied to the surface of the heat-resistant tile at room temperature, resulting in the black characteristics shown on the X-43A picture. This method of processing the profile line greatly simplifies the manufacture of the X-43A thermal protection system and results in the OML of the aircraft with excellent performance.

• Assembly and Inspection: Although the small size of the X-43A allows the OML machining process mentioned above to be carried out in situ, it also significantly increases the assembly difficulty of the aircraft subsystem. Most of the difficulties encountered during the final assembly of the aircraft are due to the use of space-standard connectors and accessories to ensure that the aircraft reliably obtains the necessary flight test data as required. Due to the operation at low pressure conditions (non-vacuum), all equipment used on the vehicle must be able to be used at altitudes of 30,000m and higher, which in some respects are more stringent than space flight. This is especially true for both electrical and electronic subsystems, which necessitate the use of large connectors and accessories, which take up valuable assembly space. The equipment layout and custom brackets were designed iteratively, some connectors were modified, and some non-standard, high-density German-made connectors were used, resulting in a complete success of the assembly.

The small size of the aircraft caused a lot of inconvenience to the inspection, although the entire upper surface of the aircraft has been designed to be detachable in order to provide the required access to maneuver. Extensive flight-tested components are used wherever possible, and special attention is paid to their installation and removal. In fact, in order to reduce the difficulty of system testing, the upper surface was not mounted to the aircraft until before the flight (Fig. 9-15), the upper surface skin fastener holes on the porcelain tile were sealed with ceramic plugs, and the surface polishing was carried out after the aircraft was mounted on the B-52.

Figure 9-15: Pre-flight preparations

• Safety: Fuel and ignition systems require special operating safety procedures. The ignition agent uses a mixture of hydrogen and silane (SiH4) that can be self-ignited, which burns as soon as it comes into contact with air. This feature is very useful for leak detection (even a small amount of leakage can lead to silica precipitation). This also means that special safety precautions must be taken when delivering fuel to the aircraft. To do this, several ventilation and blowing cycles must be established in the fuel system to remove combustibles from the test personnel area through special ventilation ducts on the aircraft. The associated safety regulations also make ground support and auxiliary equipment more complex than originally envisaged.

• Separation system: The main challenge encountered during the final assembly and testing phase of the project is the testing of the separation system. Although the ejection pylon, which is the basis of the separation system, has been fully tested, the changes made in the X-43A have not been tested, and both the explosive bolt separation system and the ejection pylon, which are the aircraft and connectors, need to be tested to be confirmed. In this test, the shock load encountered at this stage was measured using a partially installed X243A structural component, and the results were compared with the load specified in the subsystem qualification specification (Figure 9-16). The test results show that the separation method selected in the design can make the aircraft detach from the connection section reliably and quickly, and the shock load fully meets the requirements. However, these tests could not give data on the aerodynamic loads encountered in flight. The successful separation of the vehicles of *Ma* = 7 and *Ma* = 10 proved that the design adopted was correct, even smoother than previously expected.

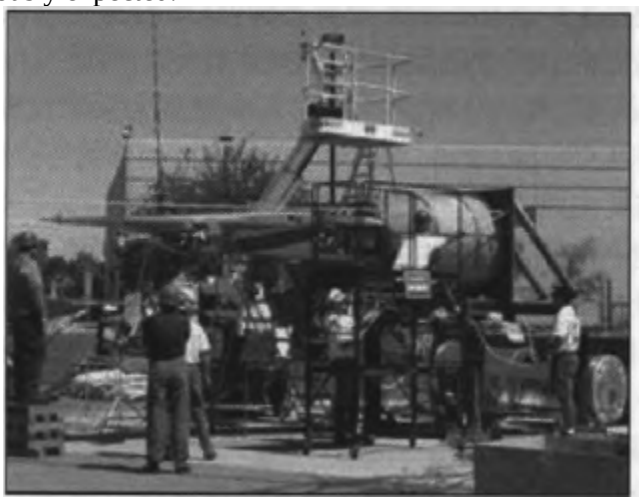

Figure 9-16: Full-scale separation test

There are several other issues to be aware of. Handle change control, configuration control, and documentation with care. Design and manufacture of several specialized tools, support equipment, emergency interrupt boxes, measurement data integration methods, and disassembly fixtures to support assembly and flight operations. Members of the government and contractor teams perform detailed stage inspections at various stages of the manufacturing completion process. The X-43A's miniaturization and highly dense loading design pose challenges for inspection and testing procedures, and the need for specialized tools far exceeds most designs.

9.8.4: X-43A flight test

NASA's X-43A conducted its first flight test on June 12, 2001, but failed due to a malfunction in the booster rocket control system.

On March 27, 2004, the X-43A underwent a second flight test with the aim of achieving thrust greater than drag with the integrated airframe/engine. The flight test was conducted at NASA's Dryden Flight Research Center.

At an altitude of 12,190m, the B-52B dropped a booster rocket with a total mass of 17,010kg and an X-43A vehicle. After 5s, the Pegasus booster rocket ignites. The location of the drop was about 92.6 km west of the coast of Southern California, entering the waters of the Naval Air Warfare Center range. A few seconds later, the X-43A rose rapidly, reaching a maximum dynamic pressure of 78,988 Pa when it climbed to an altitude of 14,330 m at a speed of *Ma* = 3.5. After reaching an altitude of 19,810m, it begins to fly level to form a negative angle of attack to suppress the rate of climb and thus gain greater speed. The booster rocket stalled after 82s of separation from the B-84B. At 95s, at an altitude of 28,950 m and *Ma* = 6.83, a dynamic pressure of 50,744 Pa (288 m/s equivalent airspeed), and a pair of pistons pushed the X-43A out of the booster rocket, and the X-43A separated from the booster rocket.

After a short period of stabilization, the X-43A's intake valves opened to allow air to enter the engine, which were hinged to the bottom of the intake and opened forward as a lower intake lip. After that, the X-43A stabilized again, because the airflow into the engine was sorted out and became even. There are a number of pressure sensors inside the engine, and the sensors measure the pressure data curve in the 5 seconds without fuel supply.

Subsequently, in order to ignite the hydrogen fuel, a silane chemical that burns in the air is injected into the combustion chamber for 3 seconds with the aim of igniting the hydrogen fuel. When the injection of silane decreases, the injection of hydrogen fuel increases, and this process lasts for 8s. To measure performance at different mixing ratios, when the concentration of hydrogen fuel rises and exceeds the chemically calculated ideal fuel composition ratio, the hydrogen fuel injection is reduced to a sustainable combustion amount until the fuel injection is stopped.

Two P-3 maritime patrol planes of the Navy followed the direction of the aircraft, collected telemetry data, and filmed the entire flight test. According to the information, it is estimated that approximately 1.36kg of hydrogen fuel was consumed during the flight. If these fuels allow the aircraft to fly 7km horizontally at a speed of *Ma* = 8s for 17s, then the flight range that a unit of hydrogen fuel can support should be 12.5km. Hydrogen fuel produces about 3 times as much propulsion as kerosene, so the flight range that a unit of kerosene can support should be 4km.

The X-43A hypersonic vehicle still has many practical problems to consider, such as its very narrow nose cone made of high-density tungsten plate with a mass of 362.88kg, which is designed to move the center of mass of the vehicle forward, which accounts for 29% of the total mass of the vehicle. The problem created by this layout is how to keep the aircraft balanced in combat. The engine of the X-43A uses copper heat absorbers, which cool the air intakes in a water-cooled manner. The above method is feasible for short flights of 10 seconds, but it is a big problem for long flights. Hydrogen fuels are flammable and fast, but the actual hydrocarbon fuels do not have these advantages.

The flight test on 16 November 2004 was postponed several times, the last of which was on 15 November, when a failure required two reboots of the X-43A's computer, each of which took 40 minutes, which made the flight postponement beyond the effective time and could not meet the daytime requirements for the NASA Dryden Flight Research Center B-52B carrier aircraft. The flight test conducted by the Dryden Flight Research Center was also the last research test flight of the historic "008" B-52B aircraft (which began in 1959).

The X-43A is mounted on the front end of the first stage of the Pegasus booster rocket, manufactured by Orbital Sciences, a modified one. The combination has a total mass of 19,505kg and is carried under the right wing of the B-52B carrier aircraft. At 2:43 p.m. PST, B-52B aircraft dropped a Pegasus booster rocket carrying X-43A westward over the Pacific Ocean 92.6km off the coast of Southern California. The solid rocket engine brought the X-33,528A to the permissible conditions for a flight of *Ma* = 10 at an altitude of 43m.

7 to 8 seconds after the rocket engine ignited, a pair of pistons pushed the X-43A forward from the booster rocket at *Ma* = 9.8. Unlike the significant desoldering of the X-43A and the booster rocket during the *Ma* = 6.83 flight on March 27, there was very little desoldering. Engineers learned from the last flight test and made the right adjustments for this higher speed flight.

The intake valve of a scramjet engine is closed throughout the booster section. But after the X-43A separated from the booster rocket for 2.5s, the intake valve opened down as a lower intake lip. After 3 seconds of separation, the scramjet engine ignited at an altitude of 33,528 m, *Ma* = 9.65, and a dynamic pressure of 50,241 Pa (287 m/s equivalent airspeed). At this time, the X-43A still had a slight climb of 2.1° on the original trajectory of the booster rocket.

The in-flight gaseous hydrogen fuel worked for 10 to 12s. The fuel contains combustible chemical silanes to ensure successful ignition, and for the first 4 seconds of fuel combustion, the hydrogen fuel works at two flow rates to test different fuel mixing ratios. The flow rate is changed repeatedly for comparison, and when the hydrogen supply pressure becomes smaller, the flow rate gradually decreases. The engine worked in pure air for 8 to 9 seconds to test its characteristics without fuel. After 21s of separation, the intake valve closes for the rest of the flight.

The aircraft decreases in altitude under approximately continuous dynamic pressure and maneuvers at a gradually decreasing Mach number to compare with the predicted aerodynamic characteristics. A Navy P-3 aircraft, after separation, received telemetry data for at least 14min in the direction of transmission. It is likely that at this point the craft crashed into the Pacific Ocean after flying approximately 1,368 km and was no longer recovered.

The angle of attack (AOA) of the X-43A was controlled at 1° to meet the designed operating conditions of the engine, but the angle of attack to meet the mass was 5°. The greater angle will increase drag, while also increasing the compression of the shock wave and engine efficiency. Good characteristics are a balance of factors like this.

Scramjet engines use shock waves to decelerate and pressurize the airflow so that the airflow remains supersonic when it enters the combustion chamber. The isolation section is to prevent the transient combustion pressure from damaging the upstream shock system. To ensure that the head shock wave was not absorbed by the lower intake valves, flight tests of *Ma* = 9.8 were carried out at a small angle of attack of 1°. While a large angle of attack is more efficient, it is also more risky. In the flight test of *Ma* = 6.83, the shock wave was basically consumed in the combustion chamber, but in the flight test of *Ma* = 9.8, the shock wave easily passed through the entire engine.

Officials from the Hyper-X program said preliminary data analysis from the flight test showed that thrust and drag were about the same, as NASA had predicted. They mention that the X-43A is derived from McDonnell Douglas' *Ma* = 10 cruise aircraft, suggesting that this cruise thrust range is exactly what was planned. However, if the intake tract is operating at an angle of attack that does not support the mass of the aircraft, it is difficult to convert "thrust equals drag" into anything meaningful.

The flight consumed a total of 1.72kg of hydrogen fuel, burned a total of 10 to 12 seconds, and the fuel-air ratio was 20% to 30% higher than the chemically calculated value. There are a lot of uncertainties in the gas stream, so make more fuel than air in the fuel-air mixture to avoid lean oil combustion.

Compared to the flight on 27 March 2004, the higher velocity of this flight resulted in an airflow stagnation temperature of approximately 3,038°C, a surface temperature of 1,982°C on the surface of the aircraft's nose cone, and a heating rate twice as high. The flight on March 27 produced a maximum temperature of 1,427°C on the leading edge of the wing. The thermally strengthened structure consists of a change from the hollow structure of the vertical tail to the leading edge of the solid reinforced carbon-carbon composite wing. The surface of the leading edge of the wing is covered with a hafnium carbide coating, and the nose cone is made blunt to better generate the shock wave of the leading edge of the body to reduce the heating rate. The engine has a thicker thermal shield and the water-cooled tunnel at the front edge of the bonnet has been changed. The engine and fuselage are also equipped with new control software.

The free flight of the X-43A *Ma* = 9.8 on November 16, 2004 was very important because it was very difficult to do ground tests at such high speeds. According to Robert Bakos, vice president of ATK GASL, initial analysis of the data shows that a series of reflected wave channels with a duration of 0.005s are working very well.

The integrated airframe/engine produces effective thrust and is operating in a state close to the results of pre-analysis and wind tunnel testing. These two results will advance other hypersonic programs that have not yet been tested by increasing confidence in the effectiveness of the design. Anthony Castrogiovanni, president of ATK GASL, said after the November 16 test: "The flight test was able to be successfully carried out 2 times in a row, which will be of interest to the US Department of Defense." "The Hyper-X program cost a total of $230 million for three flight tests.

9.9: NASA's Advanced Aerospace Transportation Hypersonic Program

9.9.1: ASTP Program

NASA's Office of Aerospace Technology (OAT) is dedicated to encouraging the development of aerospace transportation technology. NASA's Marshall Space Flight Center (MSFC) has developed the Advanced Space Transportation Program (ASTP), which focuses on the development of future aerospace transportation technologies. The main goal of the ASTP program is to develop a third-generation space transportation system that will reduce the cost of carrying by 100 orders of magnitude and improve safety by 10,000 orders of magnitude compared to existing conditions. One of the three investment areas of the ASRP program, the Hypersonic Investment Area (HIA), is focused on the development of second-generation reusable space launch vehicles. The plan is to improve the design and operation margin by achieving a number of challenging objectives to improve the robustness and service life of the real system, reduce maintenance costs, and improve reliability.

The development of hypersonic air-breathing systems, as well as other technologies for the vehicle, will make it possible to achieve this goal. Air-breathing vehicles increase the efficiency of the propulsion system, significantly reduce the amount of propellant carried, and enable horizontal takeoff. Horizontal take-off also reduces the required thrust, which further reduces the mass of the entire engine. Compared with rocket-powered vehicles, air-breathing propulsion vehicles have a 2 to 4 times improvement in structural mass fraction and design robustness. The improvement of the structural mass score expands the margin between design and operation. Air-breathing propulsion vehicles are superior in many respects to existing vertical take-off rockets.

The air-breathing vehicle has a larger launch window. In atmospheric flight, the aerodynamic force generated by the aircraft can be effectively converted into kinetic energy into orbit, or the flight trajectory can be flexibly changed according to the flight conditions. The launch window of an air-breathing vehicle can reach several hours depending on the angle of inclination of the orbit, while a rocket-powered vehicle has only a few minutes. The expanded launch window increases mission flexibility. Other advantages include a small orbital inclination, changing orbit or canceling the launch mission during launch, having higher safety, etc.

NASA's HIA conducts research in propulsion technology, airframe technology, systems analysis, and flight testing. The following is an overview of the planned technology advancement and the research work that has been carried out in the four areas.

9.9.2: Technical Pathways

Figure 9-17 is the technical roadmap of the program, which aims to complete the development of key technologies by 2017 and carry out the development of a new third-generation air-breathing transport system with initial launch capability by 2025. The program has three main technical pathways: systems research for the Vision Vehicle; ground & Flight Demonstrations; one of the key components of the research on the development of key technologies is the "Large Size Reusable Demonstration Verification Vehicle," which is scheduled to begin in 2010. This will allow the development timeline of the main technology to focus on the demonstration validation vehicle.

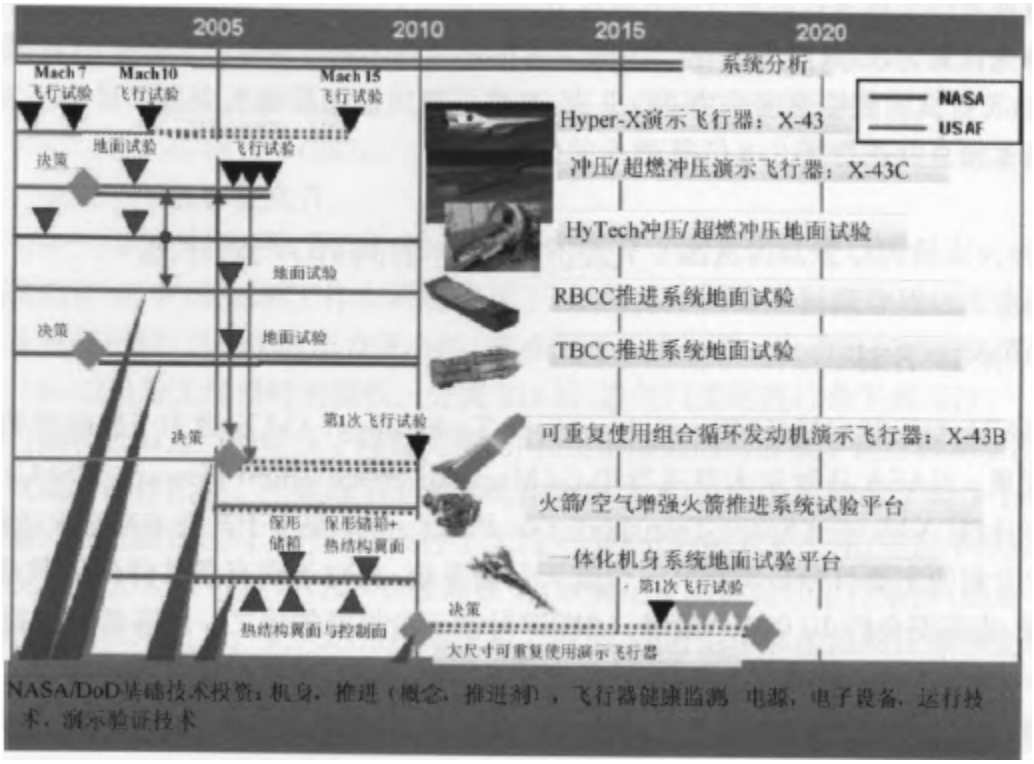

Figure 9-17: ASTP-HIA Program Technical Roadmap

Some NASA-funded research teams have given technologies that need to be prioritized for the development of third-generation transportation systems, and the top 8 are:

- Scramjet propulsion technology;
- High Mach number turbo propulsion technology;
- rocket-based combined cycle propulsion technology;
- Turbine-based combined cycle propulsion technology;
- Long life, lightweight body technology;
- Long-life, lightweight propulsion system component technology;
- Smart system technology;
- Highly operable systems technology.

These aspects represent the core direction of the ASTP-HIA program. The ASTP-HIA consists of the following four sub-projects:

- Systems analysis projects;
- Propulsion projects:
  - RBCC (ISTAR) project
  - TBCC (RTA) project
  - PR&T project
- Airframe projects:
  - Flight Demonstration Items:

- X-43A project (includes *Ma* = 10 flight tests only, funded by ASTAP)
- Project X-43B
- X-43C project
- X-43D project
- Large size flight demonstrator

9.9.3: System Analysis Project

The responsibility of the Systems Analysis Project is to screen the Vision Aircraft Scheme for the Third Generation Aerospace Transportation System, i.e., to carry out an overall scenario study. A variety of two-stage and single-stage SSTO schemes have been evaluated. These systematic studies have expanded the evaluation of the program from dry weight or gross take-off weight to safety, reusability, operational capability, and lifetime cost.

Different schemes are used to evaluate the advantages of each technology from the level of the system, and give the degree to which the technology of the target scheme is realized, so as to give the shortcomings of the technology, and the research results will give a complete quantitative form of the required technology system.

9.9.4: Advancing technical projects

The development of propulsion technology is mainly focused on two aspects: rocket-based combined cycle engines (RBCC) and turbine-based combined cycle engines (TBCC). This technical area is further divided into three main projects:

- Integrated System Test of an Air-breathing Rocket (ISTAR);
- Revolutionary Turbine Accelerator (RTA);
- Propulsion Research and Technology (PR&T).

1. ISTAR Project

The goal of the ISTAR project is to develop a rocket-based combined cycle engine (RBCC) system and a demonstration of its own powered acceleration flight from subsonic speed separated from the carrier aircraft to the working relay point of the scramjet engine with the X-43B. RBCC is a combined propulsion method of rocket engine and air-breathing dual-mode scramjet engine integrated with a flow channel. The rocket engine is powered until the scramjet engine can obtain enough compressed air to flow to produce effective thrust, usually around $Ma = 3$. Dual-modal scramjet operates in subsonic combustion ramjet mode at $Ma = 3$ to 6 and supersonic combustion in the $Ma = 6$ to 7 range. At $Ma \geq 12$, the rocket engine ignited again and finally launched the vehicle into low-Earth orbit.

The study of scramjet engines originated in the 1950s, and then the NASP program and the ART program gave impetus to the development of combined cycle propulsion systems, including great advances in aerodynamic and supersonic combustion. The goal of the ISTAR project is to achieve an engine with flight mass, while its key technologies include regenerative cooling structures, hot gas valves, etc.

The ISTAR project conducts ground engine testing in two phases. Phase 1 completes the design of the engine concept and the overall planning of the project. In the second phase, engine development and ground testing will be carried out. The ISTAR project worked with Boeing Rocketdyne, Pratt & Whitney Liquid Space Propulsion, and Gencorp Aerojet units to design, manufacture, and ground test the RBCC engine system, but the technical aspects of the entire project remain overseen by NASA.

Figure 9-18 shows the ISTAR engine system of the X-43B test vehicle.

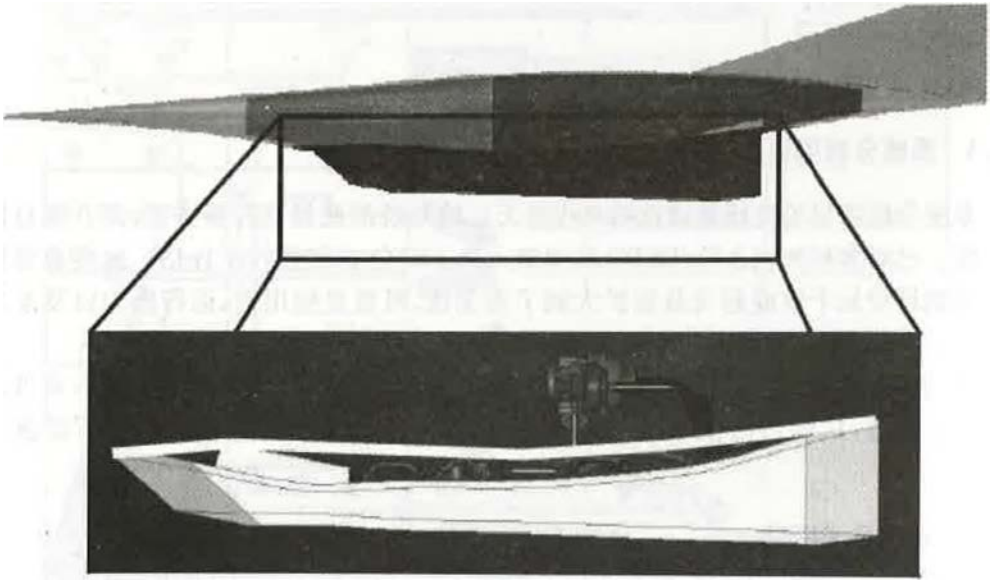

Figure 9-18: ISTAR engine system of the X-43B test vehicle

2. RTA Project

As part of the ASTP program, NASA's Galen Research Center is responsible for researching the use of turbine-based combined cycle propulsion systems as a power modality for the low-speed phase of in-orbit flight. The use of a turbine-based combined propulsion system can make the space into orbit flight run like an ordinary aircraft, which can greatly reduce the cost of reuse and improve the safety of the system. In addition, if it can be achieved to operate like a normal aircraft, it will be possible to use existing airport and ground equipment, which will change the way people fly in orbit.

The goal of the RTA project is to develop a turbine-based combined cycle propulsion system in stages. Turbine propulsion systems are available to propel aircraft or missiles to speeds of $Ma = 3$. By 2010, the RTA project aims to increase the maximum Mach number by 25 percent, increase the thrust-to-weight ratio by 250 percent, and increase the service life of components by two times. By 2015, the maximum Mach number will be increased by 35%, the thrust-to-weight ratio will be increased by 375%, and the service life of components will be increased by 4 times.

The first step of the RTA project is to develop a turbine-powered accelerator that can achieve a minimum of $Ma = 4$ and to use advanced technology to greatly improve maintenance and operational capabilities. To achieve this, PTA has developed a mesoscale ground-level system-level engine demonstrator to improve the Technology Readiness Level (TRL) for the development of turbodynamic accelerator propulsion systems. The TRA program also works with other NASA research centers, the U.S. Department of Defense DoD, and academic institutions to determine the readiness of current technologies, and coordinates with other technology development programs to maximize available funding, including Ultra Efficient Engine Technology (UEET), an integrated high-performance turbine engine technology (Integrated High Performance Turbine Engine Technology, IHPTET), and the General Versatile Affordable Advanced Turbine Engine (VAATE) research program. GE Aircraft Engine was awarded a contract to develop a 1/2 scale ground test engine.

The RTA program also includes a parallel research program to develop a high-efficiency dual-mode scramjet engine, which will provide an integrated scramjet engine for the RTA turbine engine. The scramjet engine under study has a slight increase in size compared to the engine in the X-43C test vehicle program (HyTech), and the lower limit of effective operation can be reduced to Mach 3.5 to 4.2.

In addition, the RTA project provides the overall conceptual design of the small-scale TBCC propulsion system for the X-43B test vehicle, with the aim of drawing out the research problems arising from the application of the integration of the new turbo-accelerated power system on the high-flying Mach number aircraft. The flight test demonstrated that the relay point of the combination of the turbo acceleration power system and the scramjet engine was $Ma = 4$. For the X-43B test vehicle, the turbo acceleration power system and the flow channels of the scramjet engine are independent of each other. The flight demonstration will be used to investigate the conversion of low- to high-speed propulsion systems, as well as critical propulsion and airframe integration issues, particularly inlet and nozzle performance at high Mach numbers.

3. PR&T projects

The goal of the PR&T project is to develop propulsion system technology that will enable low-cost third-generation hypersonic space carriers and make space launches as safe as civil aviation transportation is today. Specific objectives include the development of material technology for propulsion systems as well as design techniques for components to achieve the high thrust-to-weight ratio propulsion systems required for the launch vehicle. At the same time, these propulsion systems require high reliability and low maintenance, so it is necessary to develop health monitoring systems for propulsion systems. The development of propulsion system technology includes two aspects: basic technology and component development.

The basic technology field includes the development of technologies at the basic level that enable or improve propulsion systems, such as advanced materials and structural technologies, the development of design tools, measurement system technologies, and auxiliary technologies related to propulsion systems. In this area, the following sub-projects are divided:

- Materials and structures for long-life lightweight propulsion systems;
- Safe, long-life design;
- Basic technology for air-aspirated engine components (involving components such as intake tracts, compressors, turbines, combustion chambers, nozzles, and thermal management);
- Numerical system simulation;
- Test measurements:
- Advanced propellants;
- Propulsion System Assistive Technology.

Component development is the application of basic technology to the design of propulsion system components. When the development and testing of components is completed, these components will be integrated and carried out flight tests on the system integrated test vehicle or flight test platform.

9.9.5: Airframe Technology Items

The purpose of the Airframe Technology project is to develop and demonstrate airframe-related technologies for third-generation space carriers, with three main objectives:

- Improve the margin of structural weight design;
- Improve the margin of multiple loads, including thermal, structural, aerodynamic, and aerothermal;
- Increase the margin of operation of the launch vehicle.

The technical challenges to achieve its goals and objectives include the aircraft's low-drag design, weight minimization, flight Mach numbers ranging from 0-25-0 (i.e., takeoff, climb, orbit and landing), small aerodynamic control margins, high volumetric efficiency, and high dynamic pressure flight.

The approach to solving the technical challenges of the airframe focuses on three aspects: structure, materials, and aerodynamics/thermal, as shown in Figure 9-19. Structural material technology includes integrated airframe design, integrated thermal structure and materials, and thermal protection systems. The aerodynamic/thermal aspects include aerodynamic and aerothermal numerical calculations, as well as wind tunnel tests at NASA's Langley Research Center and Arms Research Center. Ways to address technical challenges and improve performance margins and repeatability include:

- Integrated fuel storage tank;
- Thin control surfaces;
- Thermal structure;
- High Mach number separation;
- Boundary layer transition;
- Sharp leading edge;
- Thermal protection system for thin parts;
- High-precision design and analysis tools;
- Sealing of moving parts;
- Airframe health monitoring.

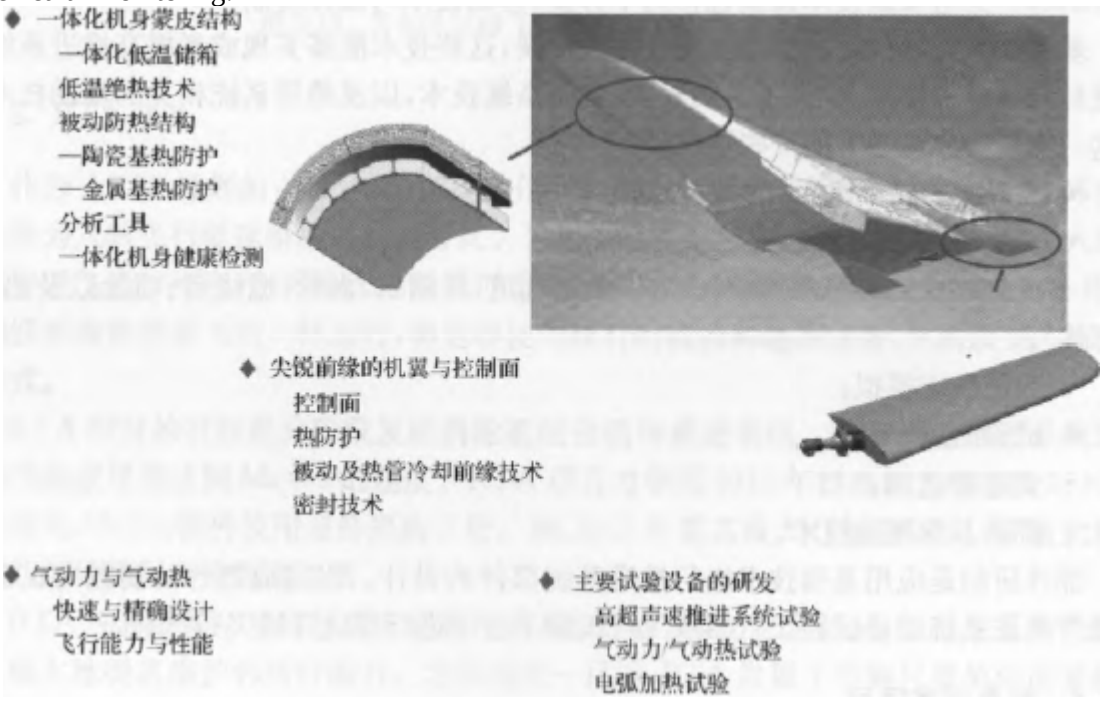

Figure 9-19: Research focus of airframe technology

As shown in Figure 9-20, the airframe research project also focuses on solving the problems related to the flight of air-breathing vehicles, which involves the whole process from take-off, orbit entry, and return to landing, including drag reduction, boundary layer transition, aerodynamic heating at large angles of attack, and reaction control system (RCS).

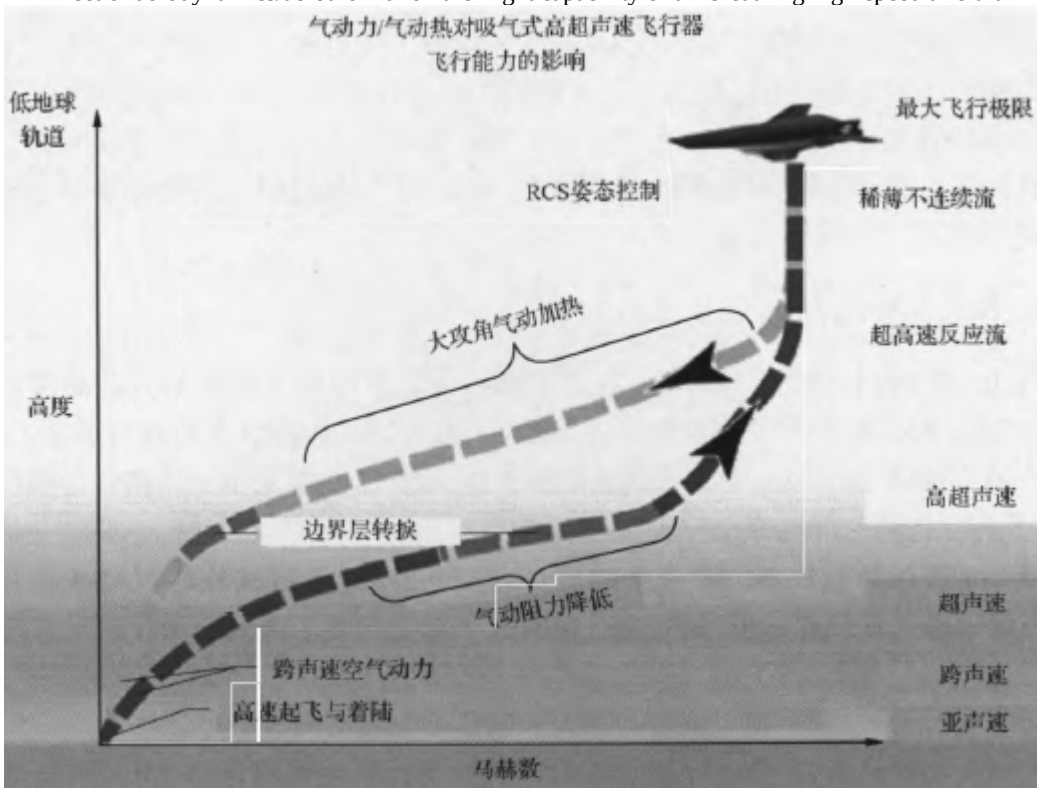

Figure 9-20: Flight problems related to air-breathing powered aircraft

9.9.6: Flight Demonstration Project

The ASTP program has planned a number of hypersonic flight demonstration verification programs with the aim of increasing propulsion and airframe technology to the level of technical readiness 6 through flight tests. Again, these flight tests are primarily about validating propulsion technology, rather than on specific conceptual solutions. The technologies to be validated include computational tools and methods for ground testing, which will be used in the development of future hypersonic vehicles with practical applications. Flight tests are mainly focused on the propulsion system, so the construction of test vehicles is still mainly based on existing aircraft technology to maximize cost efficiency. In addition, other flight test platforms will be developed for non-propulsion technologies. These propulsion-related flight demonstration projects, known as the X-43 series of flight tests, include the following studies:

- Flying weight, actively cooled structure;
- Reusable and long-run trials;
- Wide Mach number operation of scramjet engine and conversion of subsonic combustion and scramjet modes;
- Combined cycle test;
- The performance of powered aircraft flying in large flight envelope ranges;
- Hypersonic flight characteristics ($Ma > 15$);
- Integrated flight health monitoring technology;
- Enhance the understanding of the working performance of the engine;
- Validation analysis tools;

• Develop cost estimation models.

The hypersonic flight demonstration project is based on the Hyper-X experimental research vehicle and the U.S. Air Force's HyTech scramjet technology program. The project will also extend flight testing beyond the Hyper-X program to include low and high Mach numbers, while also demonstrating a more complex flyweight-active cooling engine system. These flight demonstrations will increase knowledge and awareness of long-running and maneuverable missions and gradually transition the subject to a real-world flight environment.

1. Project X-43A

The Hyper-X program began in 1996 with the development of the first scramjet-powered hypersonic vehicle, the X-43A. The X-43A demonstrates powered vs. unpowered flight using gaseous hydrogen fuel at $Ma = 7$ and $Ma = 10$. The flight test of the powered X-43A test vehicle was limited to 10 seconds, mainly due to the limitation of the amount of fuel carried, as well as the limited heat sink uncooled engine structure heat resistance.

The Hyper-X program is not an ASTAP-funded project, but the Hyper-X flight test is an important step in NASA's development of hypersonic technology, while reducing the risk of flight testing for subsequent X-43C flight demonstrations.

2. Project X-43C

After the X-43A flight test, the planned subsequent flight test demonstration was the X-43C project, as shown in Figure 9-21. The X-43C demonstrator vehicle features a scramjet engine system actively cooled by hydrocarbon fuel, a joint effort between NASA and the U.S. Air Force, leveraging technology developed in NASA's Hyper-X program and the U.S. Air Force's HyTech program. The X-43C test vehicle will run on hydrocarbon fuel and fuel with a flight weight to cool scramjet engines and have an overall length of 16 ft (12 ft for the Hyper-X test vehicle). The use of hydrocarbon fuel on small-scale test vehicles has a longer powered operating time compared to hydrogen fuel. The X-43C project is planned to carry out three flight tests, the test vehicle flight is not recovered, each test vehicle has three scramjet engine modules, that is, three flow channels integrated into one engine, each module is a single-module scramjet developed by the HyTech program. Each test vehicle was boosted to Mach 5, the X-43C's engine started work in the same way as in the Hyper-X program, and the test vehicle was accelerated to Mach 7. The powered flight time will last 5min. Each flight test will demonstrate the performance of the propulsion system, the operational capability of the scramjet, and the flight maneuverability to extend the flight envelope. The X-43C has increased in length compared to the X-43A test vehicle due to the fact that hydrocarbon fuel combustion requires a longer engine length, while the engine thickness and effective volume have increased, allowing it to carry more fuel. The larger engine width increases the amount of air captured, which also correspondingly increases the thrust required to accelerate flight. With the exception of the fuel supply system, the subsystems of the X-43C test vehicle are similar to those of the X-43A.

The design of the X-43C engine is based on the technologies developed by the US Air Force HyTech program. The first ground-based demonstrator engine for HyTech's flight weight fuel cooling, tested in 2002, was conducted in a single-module (single-flow channel) fixed-geometry configuration to provide structural validation, measurement of engine performance, and de-risk overall X-43C engine development. Another GDE-2 test engine was also developed for the geometry of the X-43C test vehicle using a single flow channel, with the goal of demonstrating the propulsion system performance, thermal management characteristics, and variable geometry performance of closed-loop control. The test results of GDE-2 validated the design of the final flight test engine flow channel. The X-43C flight test engine will use three modular scramjet engines developed by HyTech to form a complete engine type, as shown in Figure 9-22.

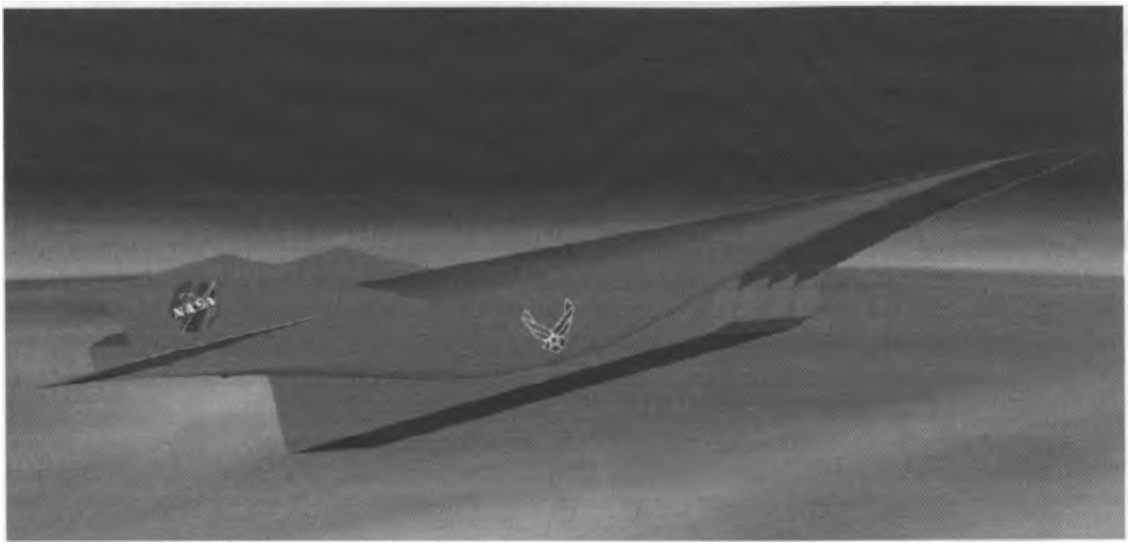

Figure 9-21: X-43C test vehicle

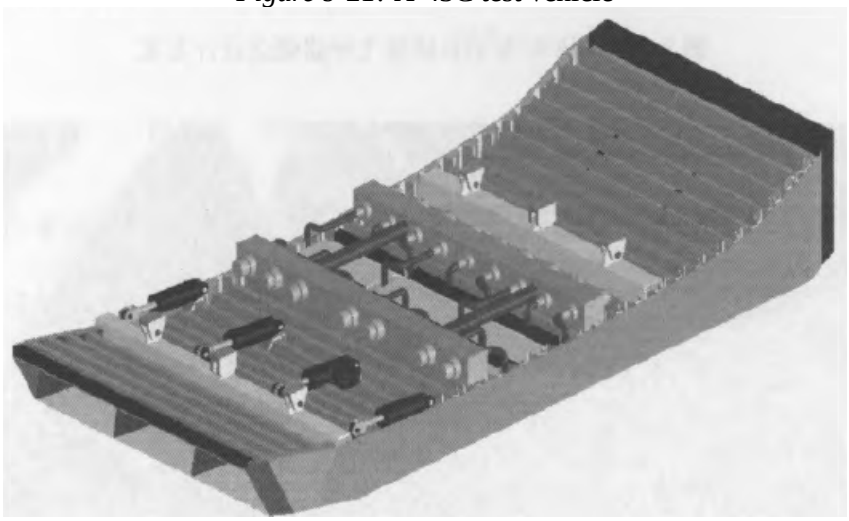

Figure 9-22: X-43C flight test engine type

3. Project X-43B

The combined cycle propulsion system can better meet the needs of future hypersonic vehicle applications. The ISTAR and TRA sub-projects of the ASRP program have carried out the development of a combined cycle propulsion system for RBCC and TBCC, respectively, and are planned to conduct flight tests on a 35 to 45 ft long flight demonstrator, called the X-43B. In order to make the test vehicle as small as possible, the design scheme is to use air launch, and use hydrocarbon fuel, the test vehicle is driven by the power of the combined propulsion system, from Ma = 0.7 to Ma = 7, and the demonstration verifies the working state of the subsonic to hypersonic and complete scramjet engine. It will be the first fully reusable hypersonic technology demonstrator vehicle that can conduct multiple flight tests and gradually expand the flight envelope, as well as the duration of the flight. The X-43B test vehicle will act as a lever for previous ground and flight test programs.

Figure 9-23 shows the conceptual design of the RBCC-powered X-43B test vehicle with a total length of 33 ft. Due to the small design size and the liquid hydrogen fuel carried, the density of the aircraft is large, so on the basis of the lift body configuration, the aerodynamic layout of large horizontal wing surface and canard wing is adopted. During the conceptual design phase, flight tests of the powered X-43B test vehicle in NASA's Langley 16 ft transonic wind tunnel were carried out taking into account the transonic pitch moment (Figs. 9-24). The test was completed in February 2002, and in order to use the existing test model, the model in the test did not have a horizontal tail and canard, but the data obtained still had the role and significance of verifying the design and calculation methods.

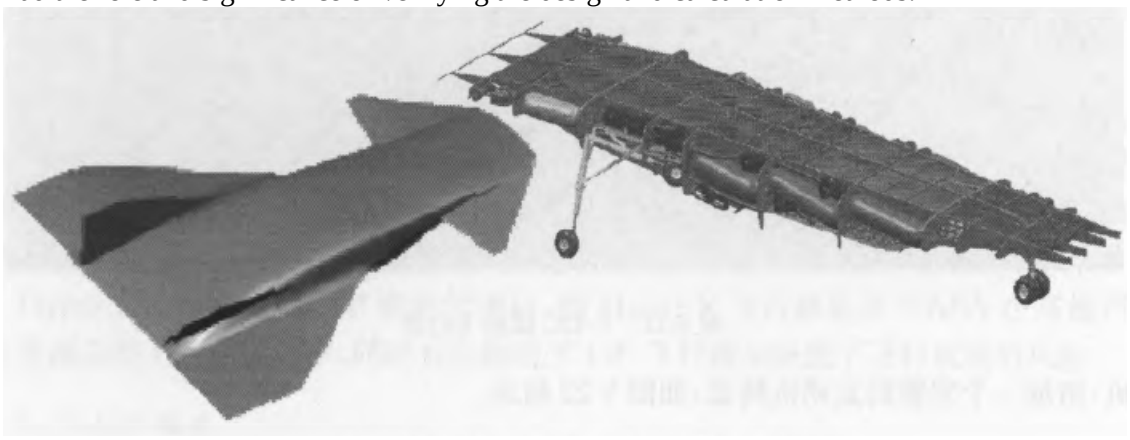

Figure 9-23: Conceptual design of the RBCC X-43B test vehicle

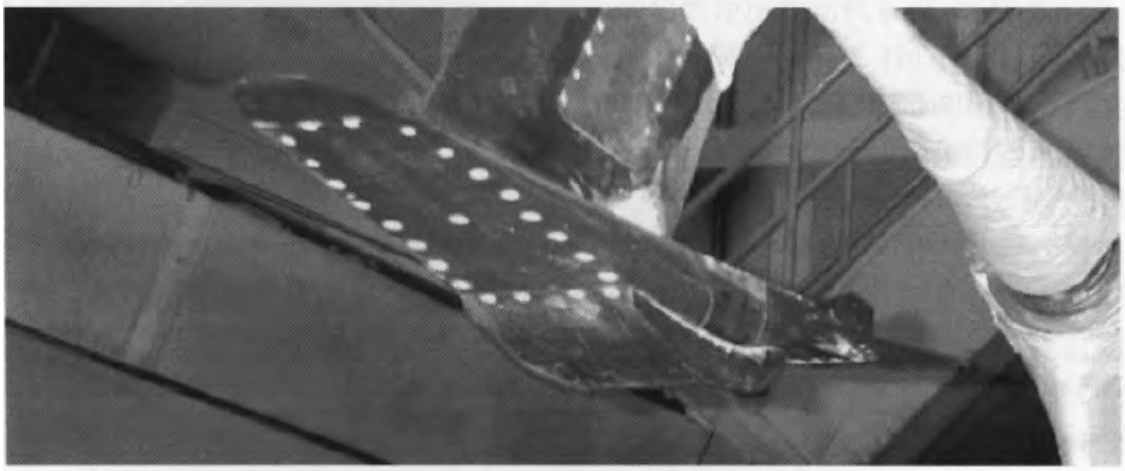

Figure 9-24: X-43B wind tunnel test of RBCC power

The TBCC-powered X-43B test vehicle, shown in Figure 9-25, has a total length of 40 ft and uses a small turbojet engine developed under the RTA program, as well as a variable-geometry scramjet engine. The shape of the test vehicle is different from the RBCC scheme but adopts the X-43C form factor. There is enough space inside the aircraft to install four RTA turbojet engines with a diameter of 19 inches and a length of 67 inches, and its air intake, diffuser and tail nozzle occupy a considerable amount of space, but the fuel storage space can meet the fuel needs to be carried during the flight, and there is a certain margin. On the other hand, the installation of the turbojet engine is able to match the HyTech hydrocarbon-fueled dual-modal scramjet engine, which has a variable geometry design.

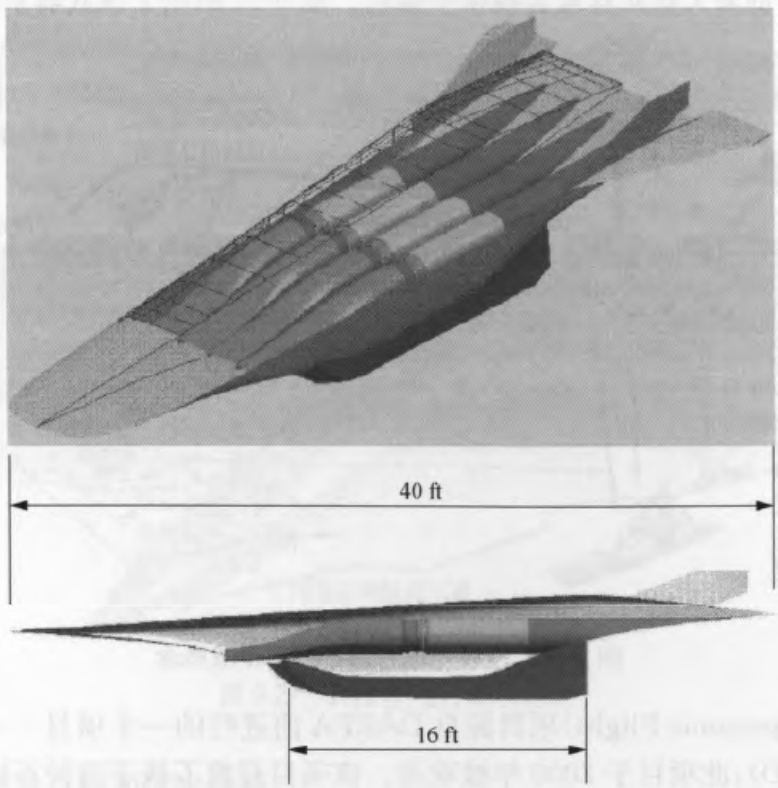

Figure 9-25: Conceptual design of the TBCC X-43B test vehicle

4. Project X-43D

With the X-43A test vehicle successfully testing the flight of a hydrogen-fueled scramjet engine in *the conditions of Ma = 7* and *Ma = 10*, NASA wanted to demonstrate engine performance at higher Mach numbers (greater than 15), hence the name X-43D test flight program. In order to reduce the size of the test vehicle and the cost of the project, the test vehicle is planned to conduct a short test period (about 30 seconds), according to which the encapsulated liquid hydrogen fuel will eventually make the entire vehicle 24 ft long, and its booster rocket will use a solid rocket with two-stage "Peace Guardian" missiles.

5. Large Size Reusable Demonstration Aircraft (LSRD)

The ASTP plan also proposes to eventually develop a large-scale reusable vehicle, which will be used as a comprehensive demonstration of the technology of an operational aerospace vehicle by 2025.

9.10: HyFly Program

Due to the U.S. Department of Defense's focus on striking time-sensitive targets, the Defense Advanced Research Projects Agency (DARPA) and the U.S. Navy jointly proposed a project to adopt a hypersonic air-breathing missile technology with twin-chamber ramjet engine propulsion technology, the HyFly project [12, 13]. It is a project in the hypersonic technology development roadmap initiated by the National Aeronautics and Space Administration (NAI). The initial motivation for the project was to serve an intelligence surveillance and reconnaissance system capable of identifying and locating moving targets, requiring an aircraft vehicle that could quickly reach the vicinity of the target and strike the target before it escaped. In such combat missions, the fight against such targets may require the deployment of large quantities of weapons or the carrying of submunitions. Figure 9-26 illustrates the operational concept of this weapon system.

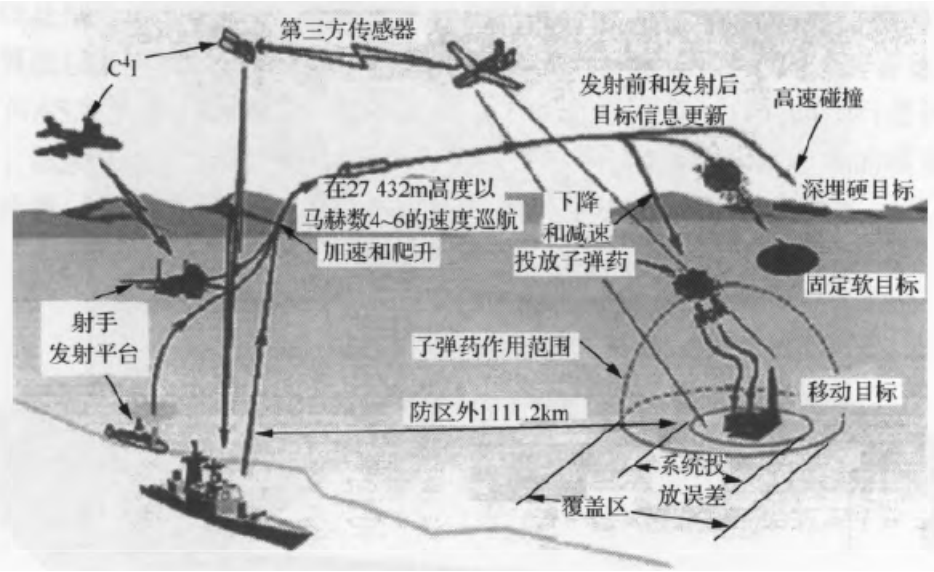

Figure 9-26: Operational concept of a hypersonic strike missile

The HyFly (Hypersonic Flight) project originated from a pre-DARPA project — the Rapid Response Missile Verifier (ARRMD), which was cancelled in 2000. The project developed missiles based on two different propulsion concepts, a hydrocarbon dual-combustion chamber ramjet engine (DCR) and a hydrocarbon scramjet. After the cancellation of the ARRMD project, the Navy did not stop relevant research, but continued to work on DCR technology. Therefore, when DARRA proposed the HyFly project, it already had the relevant propulsion technology to directly serve the HyFly project. The HyFly project aims to bring the scramjet technology of hypersonic long-range missiles to maturity, as well as conduct technical demonstrations and flight tests. The project will eventually lead to a hypersonic vehicle with an air-breathing propulsion system.

The main objectives and success markers of the project include verifying that the vehicle is capable of sustaining cruise flights at a speed of $Ma = 6$ and verifying that the aircraft is capable of obtaining a range of 740.8 km; the demonstrator was able to successfully dispense submunitions.

9.10.1: Concept/Structure of the Aircraft

Figure 9-27 shows a schematic diagram of the HyFly aircraft. The aircraft adopts the structure of a conical head and a cylindrical missile body, with an air intake channel installed on the shoulder, a control wing installed on the tail of the missile body, and a protruding cable pipe on both sides of the half of the center line. The air intake of the DCR is mounted at the transition between the conical head and the cylindrical body (i.e., the shoulder). During the launch and acceleration to the test conditions, the air intake tract was always covered. During free flight, the stability and control of the aircraft are maintained by the movable wings mounted on the tail of the aircraft. The test vehicle has a submunition bay, and submunition dispersal tests will be carried out in flight tests later in the project.

The test vehicle was propelled to the speed required for the ramjet engine to begin working using a solid rocket booster that was previously used in the Supersonic Low-Altitude Target (SLAT) program, which was equipped with stabilizers for increased stability.

The twin-chamber ramjet engine used in the tests is also known as a scramjet guided by a subsonic combustion ramjet. The test vehicle has two intakes that slow down the incoming flow and create a subsonic airflow for liquid hydrocarbon fuel gas generators. The oil-rich gas supplied by the gas generator is injected into the supersonic gas stream obtained by the other four inlet channels. Combustion takes place in this supersonic gas stream, and the combustion products are accelerated through a fixed nozzle.

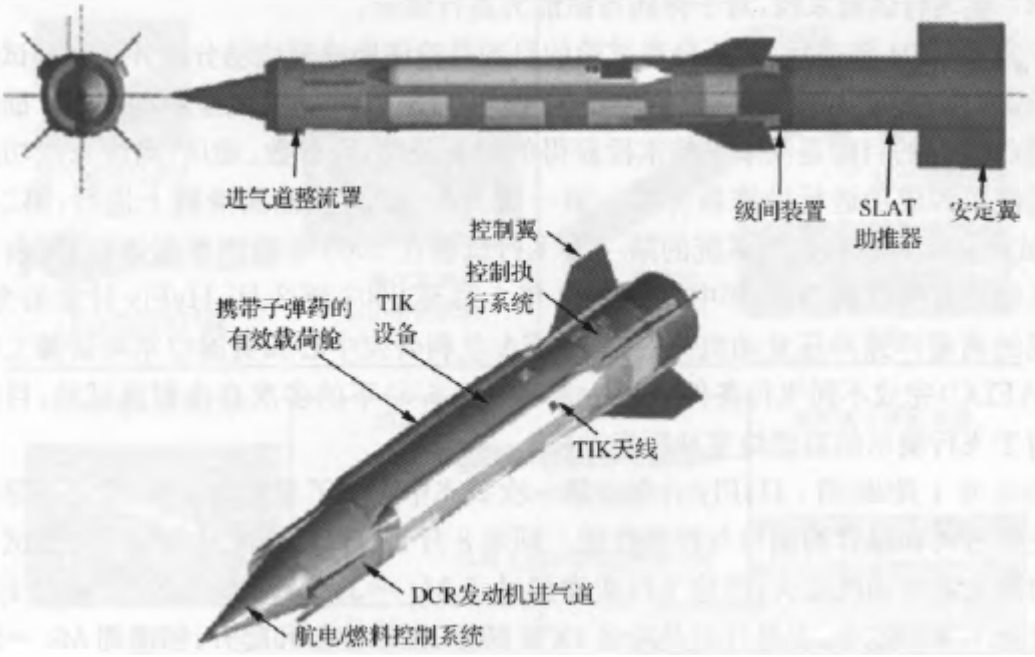

Figure 9-27: Schematic diagram of the HyFly aircraft

9.10.2: Flight Test Process and Test Objectives

Figure 9-28 shows the operation of the HyFly test vehicle in flight tests. A typical flight test consists of the following processes.

Figure 9-28: Working process of the HyFly test vehicle

(1) The test vehicle is launched from the carrier aircraft, and the solid rocket booster boosts the test vehicle to the starting speed of the OCR.

(2) intake hood was discarded, the DCR propulsion system began to work, and the test vehicle separated from the booster and began to fly autonomously.

(3) At the end of the free-flight test, the propulsion system stopped working, and the aircraft slowed down and descended until it splashed down.

(4) At the end of the flight test, the ability to dispense submunitions was demonstrated.

The purpose of the STV separation test, planned for 2004, is to verify the successful separation and conversion of the booster to the stable aerodynamic control of the test vehicle. The STV is equipped with a Guidance/Navigation/Control (GNC) system with full pneumatic control. The purpose of the Booster Test Vehicle (BTV) is to demonstrate the test conditions (Mach number, dynamic pressure, altitude) obtained at the end of the booster, the successful ejection of the inlet fairing and the successful separation of the booster. The first BTV test was carried out on a ground skid, and the second and third BTV tests were flight tests. The first system-wide flight test was conducted in the fourth quarter of 2005, and the remaining system-wide flight tests continued until mid-2006. From May 2002 to February 2003, the full-scale, fully integrated hypersonic ramjet engine of the HyFly program completed multiple free-jet tests under different flight conditions (*Ma* = 3.5, 4.1, 6.5) at the NASA Langley Research Center and the Arnold Engineering Development Center (AEDC) of the United States Air Force.

On January 26, 2005, the HyFly program completed a non-powered launch in the first test flight, verifying the safe separation of the missile from the carrier aircraft and the guidance and control performance of the missile. On August 26 of the same year, the HyFly program achieved the ignition of a solid rocket engine in the second test flight, and the booster flight speed exceeded that of *Ma* = 3. On September 25, 2007, the HyFly Verification Bomb conducted flight tests, the main purpose of which was to verify the DCR transfer, fuel control and climb, acceleration to *Ma* = 5, which was the first flight test of the DCR. However, in the launch test, after the booster was separated, due to the failure of the fuel control system of the verification bomb, the velocity only reached *Ma* = 3.5, and the expected target of *Ma* = 5 was not achieved, and the test was only partially successful. On January 16, 2008, HyFly plans to conduct another launch test with a target of *Ma = 6*. The purpose of the test is to verify the relay performance and acceleration performance of the dual-chamber ramjet engine again (the missile accelerates from *Ma* = 3.5 to *Ma* = 6), evaluate the advanced ceramic matrix composite structure of the twin chamber ramjet engine, obtain flight performance data and measure the accuracy of the final section. A Boeing F-15E fighter jet launched a HyFly verification bomb over the US Navy's maritime range at Cape Mugu, and after accelerating by the rocket engine to *Ma = 3*, the scramjet engine did not work according to the predetermined program, and the verification bomb crashed into the Pacific Ocean after flying for about 58s. According to the Defense Advanced Research Projects Agency, the main reason for the failure of the tests was that the scramjet engine did not operate according to the intended requirements.

9.10.3: Technical Challenges

The HyFly project faces technical challenges from both a hypersonic DCR missile and an integrated missile/booster system. The main technical problems faced include: DCR scramjet flow channel performance, aircraft aerodynamics, aerodynamic heating and stability/control problems; high-temperature materials and structural problems in the projectile body, combustion chamber and inlet fairing; figure 9-29 shows the technical challenges faced by the HyFly project and some measures to solve these technical problems.

There are other issues involved in an integrated missile/booster system, such as the conversion of pneumatic control at the end of the booster, the abandonment of the inlet hood and the separation of the booster, and the starting of the aspirated engine.

The HyFly project aims to validate the key technology of a hypersonic air-breathing missile using twin-combustion ramjet engine propulsion technology. It is believed that a dual-chamber ramjet engine is a low-risk solution because of the low starting Mach number of a dual-chamber ramjet compared to a pure scramjet, and the HyFly project is derived from a project previously undertaken by DARPA, the Decision-Response Missile Demonstrator (ARRMD) There is a certain technical basis, so the risk of the project should be relatively low, but according to the progress of the project and the reported test situation, the project still encountered a lot of problems, the progress was much delayed than the original plan, and the flight test was not smooth.

Figure 9-29: Key technologies and risk mitigation measures for the HyFly project

9.11: X-51A flight test program (2005~)

9.11.1: Strategic Context

In August 2001, the United States Government promulgated guidelines for national defense planning, which instructed the United States Department of Defense to maintain absolute superiority over hostile countries in areas such as space. To meet this requirement, Air Force Space Command defines an Operationally Responsive Space (ORS): "ORS ensures that the U.S. Air Force has the ability to quickly put personnel and materials into orbit, to maneuver to any location in Earth-centric space, and to support and return to Earth personnel in orbit." At present, the US Air Force's launch system is completely disposable, requiring a preparation cycle of up to several years, and requires certain modifications or even customization of the carrier vehicle for specific payloads. In addition, the current cost of transportation is $10,000 per pound, which severely limits the ability to transport large numbers of people and materials into orbit. The current development of the new generation of Evolved Expandable Launch Vehicles (EELVs) due to their cost and design intent, cannot meet the U.S. Air Force's requirements for rapid response space, but reusable launch vehicles (RLVs) and hypersonic propulsion systems will have the potential to surpass single-use launch vehicles. Hypersonic reusable space launch vehicles will allow the United States to maintain a technological advantage over its adversaries in order to meet the president's requirements.

NASA and DOD have been conducting research on the application of hypersonic technology since the 1960s, hoping to develop an economically affordable, cyclically usable, and reliable fast orbit launch system, but so far no program has been able to achieve the usable capabilities, mainly due to the technical difficulty, political considerations and the cost of large-scale programs. But the two agencies still saw the potential for hypersonic air-breathing propulsion to provide a rapid response and low-cost entry into orbit and meet the requirements of U.S. space transportation in 2020 and beyond, so they updated their research programs in the late 1990s. Hypersonic reusable launch vehicles can take off from existing airport runways like ordinary aircraft, so they are more flexible and capable.

Reusability will reduce operating costs, transition costs, and lifetime costs due significantly to single-use vehicles. Reusable space launch vehicles can be designed to be maintainable to the level of a standard aircraft or include an integrated health screening system. At the same time, NASA has realized the benefits of hypersonic and reusable, reducing the focus of hypersonic research on the manned space vehicle program.

Access to space is the primary responsibility of the U.S. Air Force, and this responsibility has increased as the U.S. Air Force has gradually transformed into a force in the sky and space. EELVs meet current non-rapid response requirements, but future requirements must be considered today. The U.S. Air Force Scientific Advisory Committee believes that "RLVs offer great potential to meet all the requirements of future U.S. space forces," and specifically noted that hypersonic propulsion needs to be prioritized as a key area of technology. The Air Force Laboratory Propulsion Technology Council is working on a step-by-step development path to achieve this goal, as shown in Figure 9-30.

Figure 9-30: U.S. Air Force hypersonic technology development route

This step-by-step development route will gradually develop and mature the technology, from small-sized missiles to large-size reusable space launch vehicles, rather than a single ultimate development goal like NASP. The Advanced Tactical Air-Launched Missile (ASALM) is an early hypersonic missile that was tested in 1979 and uses a high-speed ramjet engine to achieve a hypersonic speed of $Ma = 5.5$. Although it reaches hypersonic speeds, ramjet engines become very inefficient due to subsonic combustion. Later, the development of the scramjet engine of small size overcame the efficiency problem of the ramjet engine by supersonic combustion. U.S. Air Force laboratories have already tested scramjet engines on the ground, but the first flight test will be the X-51A Scramjet Engine Demonstrator (SED), as shown in Figure 9-31. The X-51A SED is primarily a technology demonstration vehicle but can be directly converted into hypersonic cruise missile applications. After the scramjet technology matured through the X-51A program, the next step in the development route was to complete the U.S. Air Force's Robust Scramjet program and Combined-Cycle Engine Component Development program. Every step of the development along the technological route has a direct military application.

The technology reached by the X-51A flight can be converted into a fast-response cruise missile, which is the most immediate and current application of hypersonic speed. Applications for medium-sized scramjet engines include large-sized missiles, hypersonic reconnaissance and strike aircraft, or small space launch vehicles. The ultimate development goal is to achieve a large-scale hypersonic reusable space launch vehicle that meets the requirements of the Air Force and the Department of Defense for rapid response and operational unmanned space access.

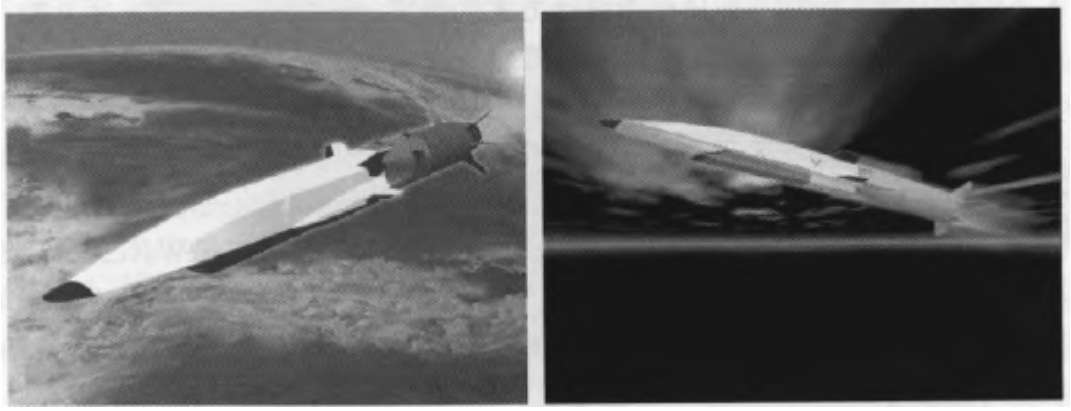

Figure 9-31: X-51A flight plan

9.11.2: Origin of the Plan

In the mid-1990s, after the end of the NASP program, the U.S. Air Force continued to carry out research in the hypersonic field with the Hypersonic Technology (HyTech) program, but research goals were greatly reduced. Under the HyTech program, its sub-program, the Storable Fuels Scramjet Flowpath Concepts (SFSFC) program, began in 1995 with the aim of developing technology for hydrocarbon-fuel-cooled scramjet engines and demonstrating their presence in Mach 4 to 48. The running capacity, working performance, and the bearing capacity of the structure in the range. In addition to new technologies in materials, structures, and fuel cooling, many technical challenges involving the design of intake tracts, isolation sections, combustion chambers and nozzles have been studied and solved. The SFSFC program was named the Hydrocarbon Scramjet Engine Technology (HySET) program in 1999. At the same time, NASA launched the Hyper-X program in 1995 to continue the research work on the hydrogen-fueled scramjet engine carried out in the NASP program. The Hyper-X program eventually carried out flight test research under the code name X-43 test vehicle. Aware of the country's future need for high-speed strike weapons, DARPA stepped in in 1997. In the Affordable Rapid Response Missile Demonstrator (ARRMD) program, research is carried out on two hydrocarbon fuel concept missiles: a wave-riding airframe missile with a 2D HyTech program engine, and a dual-combustion axisymmetric ramjet (DCR) powered missile proposed by the Hopkins University Applied Physics Laboratory. In 1999, DARPA selected engines developed by the HyTech program, but research on both engines continued. Due to budget constraints, the scope of the HySET program was reduced to ground trials of fly-weight engines at Ma = 4.5 to 6.5. Due to the increase in development costs, DARPA abolished the ARRMD 10 in 2000, but two of the conceptual solutions, with the support of the Department of Defense, were developed as separate development programs. The axisymmetric DCR scheme was adopted by the U.S. Navy as a future high-speed strike weapon, so in 2002 the U.S. Navy and DARPA cooperated to support the continued development of this scheme by starting the Hypersonic Flight Demonstration (HyFly) program.

The U.S. Air Force maintains its leadership with the HyTech program and has reached an agreement with NASA to use the engines developed in the HyTech program on the X-43C Hyper-X test vehicle and test the flow channels of three HyTech engines. But NASA canceled the X-43C program in 2003. The U.S. Air Force continued its research with the support of its own budget and launched the Single Engine Demonstrator (SED) program, which carried out flight tests of the HyTech scramjet engine, which revived the study of the waverider fuselage design in the ARRMD program. DARPA began working with the Air Force in 2005 to fund the development of the program, which is called the Scramjet Engine Demonstrator (SED) program, which is interestingly still abbreviated as SED. The SED is not a weapons development program like the HyFly program, but more a research test vehicle program like the X-43 Hyper-X program. Considering that the program represents the interests of the entire country, the Air Force awarded the program in July 2005 to the X-test vehicle, the X-51A, Scramjet Engine Demonstrator-WaveRider (SED). The letter A in the X-51A indicates that this is the first design scheme of the X-51 family of test vehicles, and other different schemes may be tested in the future, and these schemes will use roughly the same fuselage, but the propulsion system or supersonic combustion propulsion system of the aircraft may be different, and will be given the X-51B, X-51C, etc.

The main purpose of the X-51A program is to conduct flight tests of a scramjet engine developed in the US Air Force's HyTech program, using endothermic hydrocarbon fuel, boosted by a solid booster, and the vehicle self-accelerating from Ma = 4.5 to 6.5. In addition, the plan includes a number of other test objectives: first, to obtain ground and flight test data for actively cooled, self-controlled, and operational scramjet engines. These data will be used to develop and calibrate design guidelines and tools, or to further understand physical phenomena, as well as to develop computational design tools for scramjet engine design. The second goal was to demonstrate the adaptability of a scramjet engine on endothermic fuel in flight. The third goal is to generate a positive thrust force that allows the scramjet to propel the vehicle to flight [14].

9.11.3: Research Team

The X-51A program is carried out by a national team of several government research institutes and industrial enterprises, the composition of which is shown in Figure 9-32. The core of the team includes the U.S. Air Force Laboratory Program Office at Wright-Patterson Air Force Base in Ohio, and the SED-WR collaborative team consisting of Boeing and Pratt & Whitney Rocketdyne Space Propulsion. The project office is staffed by the Aeronautical Systems Center (ASC) at Wright-Patterson Air Force Base, and the ASC will conduct an independent project review of the program until flight testing begins. The Defense Advanced Research Projects Agency (DARPA)'s Tactical Technology Office (TTO) provides management and technical support, as well as a portion of the program's development. The X-51A Flight Test Organization (RTO) is the 412th Hypersonic Flight Test Team (HFTT) at the Flight Test Center at Edwards Air Force Base and is responsible for the test site area and its support in cooperation with the Naval Air Systems Command. The 419th Flight Test Squadron at Edwards Air Force Base will provide test carrier aircraft and conduct flight tests over Pacific waters. Ground testing of the engine was conducted in an 8 ft high-temperature wind tunnel (8 ft HTT) at NASA's Langley Research Center (NASA-LaRC), with personnel from NASA's hypersonic propulsion division providing technical support and analysis of ground test data. In addition, multiple divisions of the U.S. Air Force Laboratory, including the Aircraft Division, the Quartermaster Division, the Sensors Division, and the Materials and Manufacturing Division, provide additional technical support. These agencies are working to achieve the goals and objectives of the technology. From 2003 to 2010, research and development funding totaled $246,500 ($246.5M), which was provided jointly by DARPA and the Air Force.

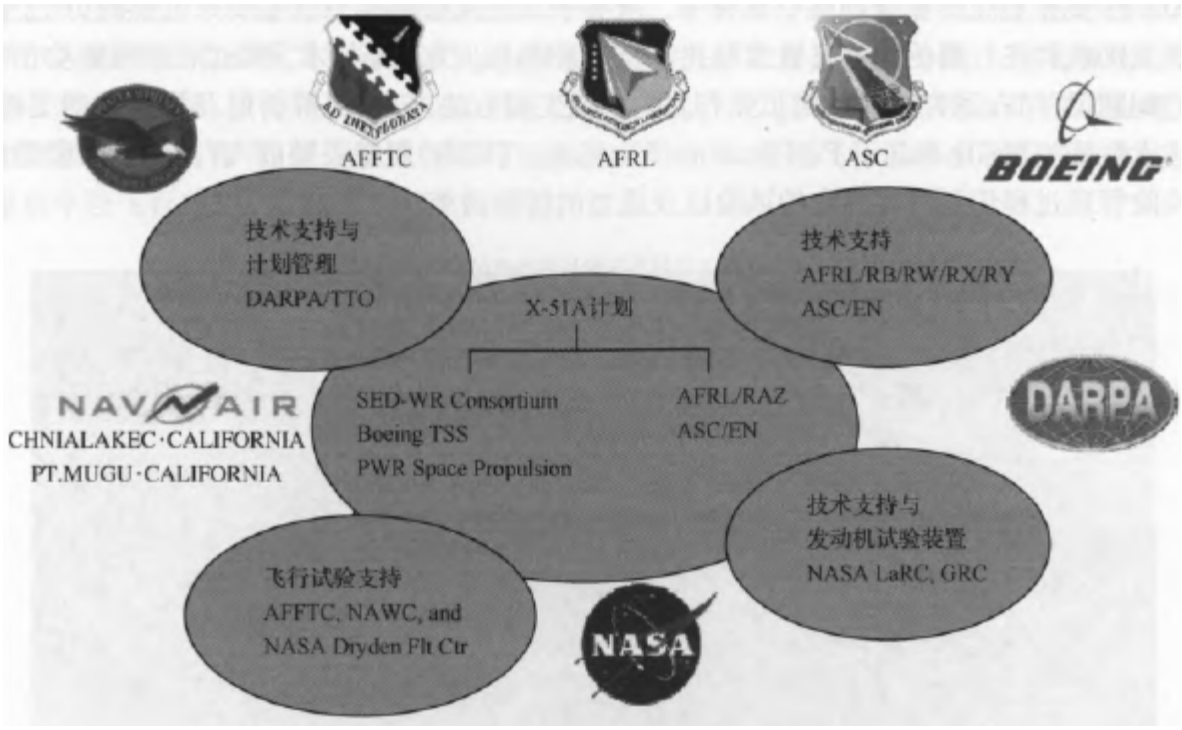

Figure 9-32: X-51 National Research Team

9.11.4: Planned Paths

Despite the significant improvement in computing methods, it is still necessary to carry out flight tests. It is very difficult to perform high-speed flight simulation on the ground. In the United States, only a small number of free-jet units have the capacity to conduct long-term ground tests, and only for small-sized scramjet engines. Two of these are owned by the U.S. government, the Aerodynamic Propulsion Test Unit (APTU) at the Arnold Engineering Development Center (AEDC), and the 8ft high-temperature wind tunnel at NASA LaRC. The third installation is the Leg VI wind tunnel at the Alliant Techsystems General Applied Science Laboratory (ATK/GASL). Even these world-class wind tunnels are limited in their capabilities, limiting the size of the model, the time it can take, and the purity of the air to be flowed through. In addition, the test can only be carried out under fixed flight conditions, such as Mach number and dynamic pressure, so the dynamic installation performance of the aircraft is difficult to obtain from the data obtained. On the contrary, flight tests are almost unlimited enough to provide quasi-steady-state operating state data of scramjet engines for up to 240 seconds. Installing active cooling in a ground test will make the test more complex and challenging. Therefore, the only effective and low-cost way to validate the design guidelines and design tools for future large-scale hypersonic air-breathing vehicles is to conduct flight tests of a small-scale scramjet engine, known as the X-51A.

Although primarily tests of the propulsion system, the X-51A program essentially goes beyond flight tests of the HyTech scramjet. There are two parallel routes for the integration of the engine into the aircraft, as shown in Figure 9-33, and these two routes need to be developed in a balanced manner. The data obtained from the ground test during the hypersonic flight test should not only ensure the success of the flight test, but also correct the flight test and ground data to improve the accuracy of the predictive analysis program, so that it can be better applied to the design of the aircraft in the future. Another process, which is also quite important, is the process of aircraft development, including all the routine tasks of aircraft development. The engine must be seamlessly integrated with the aircraft fuselage, which is critical for hypersonic vehicles. In addition, the B-52H and the AT-ACMS booster that provides propulsion to the correct flight conditions will be integrated into the overall system.

All subsystems and on-board electronics are validated, and the software used to control the engines and aircraft is written and integrated into the system. To avoid problems that may arise during the development of the technology, the X-51A research team used a robust systems engineering approach, including specification trees and interface control documentation. Technical Performance Measures (TPMs) track key aircraft characteristics, and the robustness risk management process identifies possible risks and appropriate mitigation measures.

The X-51A program is not just an engine experiment.
Flight experiments with scramjet engines require the simultaneous development of other related technologies

Figure 9-33: X-51A Program Development Path

9.11.5: Test vehicle system composition

The X-51A test vehicle is shown in Figure 9-34, consisting of a cruise vehicle, connectors, and boosters, and is called an Air Vehicle Demonstrator (AVD). The vehicle used for the HyTech engine test is derived from a truncated waverider fuselage developed in the ARRMD program. The engine flow channel includes a self-starting air intake with a design state of *Ma* = 7, and a two-dimensional fuselage integrated nozzle. The fuselage was built by Boeing's "Ghost" team, and the engines built by PWR will be fitted to the fuselage.

Figure 9-34: Composition of the X-51A experimental vehicle

A modified Lockheed Martin tactical missile was adopted as a booster, and the test vehicle was accelerated to the working speed of a scramjet engine and separated. The connectors are characterized by airflow that allows scramjet engines to start during the booster phase, and pneumatic heating preheats the fuel before the engine is ignited. The AVD is separated from the connector between the cruise vehicle and the cruise vehicle will be propelled by a scramjet engine to fly alone (Figures 9-35 and 9-36).

Figure 9-35: The X-51A model in the Purdue University Pilot Wind Tunnel

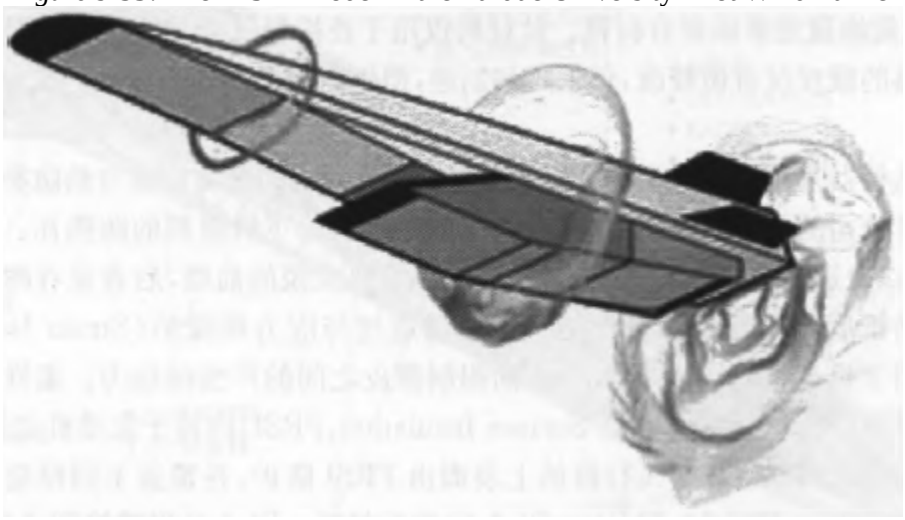

Figure 9-36: Schematic diagram of the X-51 flow field

The materials used to manufacture the aircraft are mainly traditional metal materials, which are used to make basic structures and are covered with lightweight TPS foam materials and TPS heat-resistant tile materials, as shown in Figure 9-37. The internal fuselage and cabin section are made of machined aluminum. The head of the aircraft is made of tungsten material and covered with silica thermal protection material, which is used to protect the high thermal load of the head of the aircraft and serves as a counterweight for longitudinal stability. It is connected to the fuselage via an Inconel head adapter to block heat conduction to the rear fuselage.

Figure 9-37: X-51A Structure and Thermal Protection Materials

The skin of the cruise vehicle with the connector, as well as the four full-motion tails of the booster, are made of aluminum. Two horizontal aluminum tails were added to the booster to improve flight stability during the booster phase. The scramjet engine is manufactured from thin-walled Inconel panels, which are fuel-cooled. The cruiser's four full-motion tails are also Inconel, with a carbon-carbon composite covering the leading edge. Titanium is only used in the airwash structure of the connector and the tail cone of the booster. The skin of the booster has not been modified and is still made of steel, but the steel booster nozzle has been extended to increase the expansion ratio and improve performance.

The cruise aircraft uses two types of TPS materials for thermal protection, namely thermal protective tile and thermal protective foam. Thermal shields are Boeing's reusable insulation tiles, similar to those used in the belly of the space shuttle. Heat-proof tiles are used on the keel part and on the compression surface of the air inlet. The former is due to the local need for a sharp leading edge, and the latter is due to the swallowing of ablated and separated materials that will affect engine performance after entering the engine. Heat-resistant tiles are used on the fuselage by bonding with Strain Isolation Pad (SIP) to absorb the stresses generated between the heat-resistant tiles and the aluminum skin underneath. Flexible Reusable Surface Insulation (FRSI) is lined with engine mounting slots to isolate heat transfer between the fuselage and the engine. The upper surface of the aircraft is protected by FRSI and covered with Boeing Light-Weight Ablator (BLA-S) foam of different thicknesses. The BLA-S can be sprayed onto the surface of the aircraft quickly, easily and cost-effectively, and can be sanded or cut to the exact desired aircraft contour. In addition, any analyses or notches can be filled and flattened immediately before the flight. Its honeycomb enhanced, BLA-HD, is used in the inner layer of the aircraft's nozzle to withstand the thermal combustion products from scramjet engines. The thermal management of the entire aircraft is passive, which is achieved by selecting different materials and material thicknesses based on the thermal load on different parts, while the engine uses active fuel cooling.

Like most aircraft, the X-51A has strict internal volume constraints, so the aircraft's subsystems are tightly wrapped under an aluminum skin, as shown in Figure 9-38. In order to maximize the space available for fuel, the X-51A uses an integrated fuel tank structure, that is, the fuel is not a separate fuel tank, but a wall of the fuel tank consisting of skin and partitions. The battery is located at the head of the aircraft, behind the tungsten cap. Rechargeable lithium-ion batteries provide 28V, 150V, and 270V DC power for on-board electronics, flight test equipment, tail actuators, and fuel pumps. The blasting thermobattery separator is used in the Flight Termination System (FTS). The subsystem in the rear of the battery compartment includes on-board electronics. The aircraft navigation system is a combined inertial and GPS system. Guidance and Control Units (GCUs) are also used to determine the direction and speed of an aircraft during flight. The Full Authority Digital Engine Control (FADEC), developed for the F-22 Raptor fighter PWR F119 engine, is used to control the fuel supply of scramjet engines. GCU and FADEC communicate via the MIL-STD-1553B serial bus. A small FTI contains a data acquisition unit and several other sensors that transmit the collected data wirelessly through three S-band antennas. The subsystem compartment is followed by the JP-7 monolithic fuel tank, which occupies the middle part of the vehicle. A number of engine subsystems are also located in this section, including fuel pumps and vinyl bottles for ignition of scramjet engines. A small nitrogen tank is used to maintain the pressure in the integrated fuel storage tank. The fuel storage tank stored approximately 265lbs of usable JP-7 liquid fuel. The rear of the aircraft is mainly a nozzle, as well as an actuator to control the tail and a flight termination system (FTS). The engine is integrated into the aircraft, as shown in Figure 9-39. The forebody, air inlet compression wedge, and nozzle are both part of the aircraft and part of the engine flow path, thus forcing close cooperation and integrated design between the aircraft fuselage and the engine manufacturer.

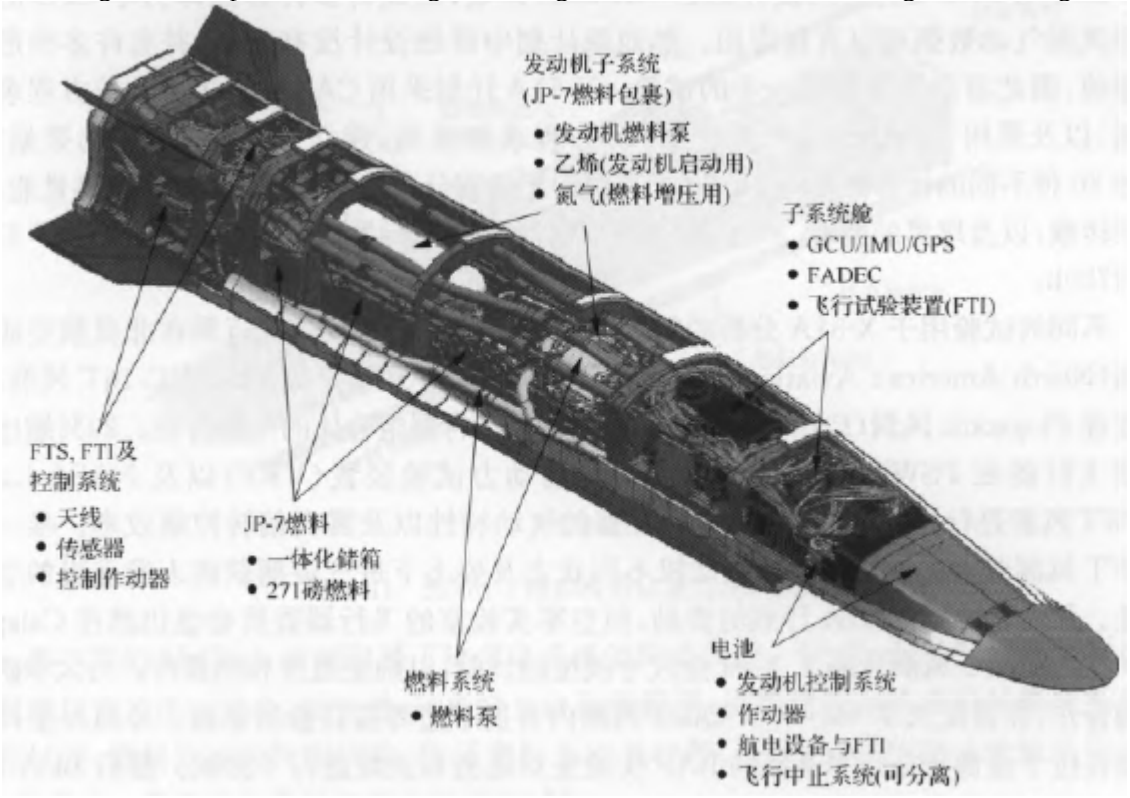

Figure 9-38: X-51A subsystem composition

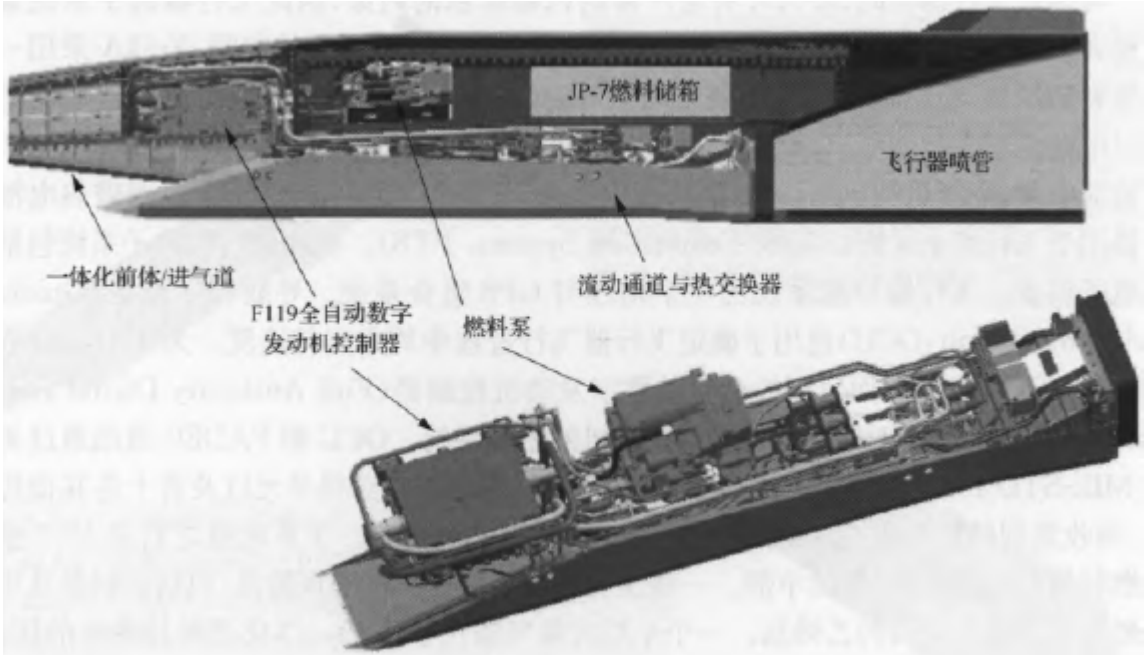

Figure 9-39: X-51A engine system composition

The design of the X-51A is different from the development of traditional aircraft, and most of the design work is not through scaled models and wind tunnel tests, but mainly through numerical calculation tools, and then verified by the data obtained from wind tunnel tests. Since the design of the X-51A vehicle is derived from the ARRMD program, much of the computational fluid dynamics (CFD) work and wind tunnel aerodynamic data can be applied directly. However, the detailed design was not completed in the original plan and there were many cosmetic modifications, so further testing was necessary. X-51A plans to use Cart3D to solve the flow field with Euler's equation and OVERFLOW to solve the flow field with the full NS equation and establish a complete aerodynamic database. More than 80 different computational grids and nearly 2,000 examples are used to study separation safety, aerothermal, aircraft performance, boundary layer transition, and tail deflection. A total of 3,200 wind tunnel tests were carried out for 1,700 hours on test and cruise vehicles.

Different tests are used for specific aspects of X-51A analysis. The 14% scaled-down test vehicle was conducted in the North American Aviation Research Tunnel (NAART), the NASA-LaRC 16T wind tunnel, and the Boeing Ploysonic Wind Tunnel (PSWT) to determine the aerodynamic characteristics of the test vehicle assembly. The 20% scaled cruise vehicle was tested at PSWT, AEDC's von Kármán Aerodynamic Test Facility (VKF) and the NASA-LaRC UPWT wind tunnel to determine the aerodynamic characteristics of the cruise vehicle and the efficiency of wing surface deflection control. The only test carried out in the PSWT wind tunnel was to test the air flow captured into the engine in the intake tract in different states and attitudes of the engine. Although not funded by the X-51A program, the Air Force Laboratory's Aircraft Committee conducted trials of a full-scale model of the X-51 in Calspan's LENS~2 wind tunnel to determine temperature and thermal loads. In collaboration with university research institutes, boundary layer transition experiments were carried out in the *Ma* = -6 Quiet Wind Tunnel at Purdue University. A full-scale model of the X-51A was tested with telemetry and antennas at the BAF laboratory at Edwards Air Force Base. Finally, the thermal protection test of BLA-HD for nozzles will be carried out at ATK/GASL in the summer of 2009.

9.11.6: Engine development and testing

Figures 9-40 and 9-41 show the composition of the HyTech scramjet engine system, including the fuel supply system. Liquid JP-7 fuel enters from the front of the scramjet and is distributed to the walls of the heat exchanger (HEX). As the fuel flows through the heat exchanger, it absorbs the heat from the combustion of the scramjet, keeping the temperature of the thin-walled surface below the melting point of the Inconel 625 metal. By adjusting the supply pressure via the JP-7 fuel pump, FADEC keeps the pressure in the heat exchanger above a certain threshold to boil the fuel on the wall and reaches a supercritical thermal state when the fuel leaves the heat exchanger. The hot fuel then passes through the valve in a gaseous form through the fuel distribution valve, which is injected into the combustion chamber by nozzles at various points in the flow channel. Since scramjet engines require hot pyrolysis of JP-7 fuel to maintain combustion, but also need heat to heat the fuel, a separate fuel ethylene is required on board to ignite the engine and heat the JP-7 fuel to a temperature that can be sustained by combustion.

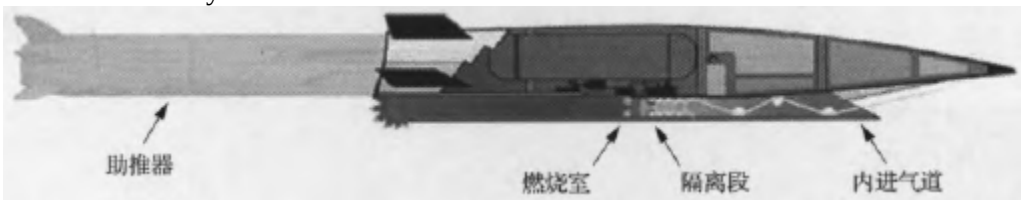

Figure 9-40: Schematic diagram of the X-51A engine composition

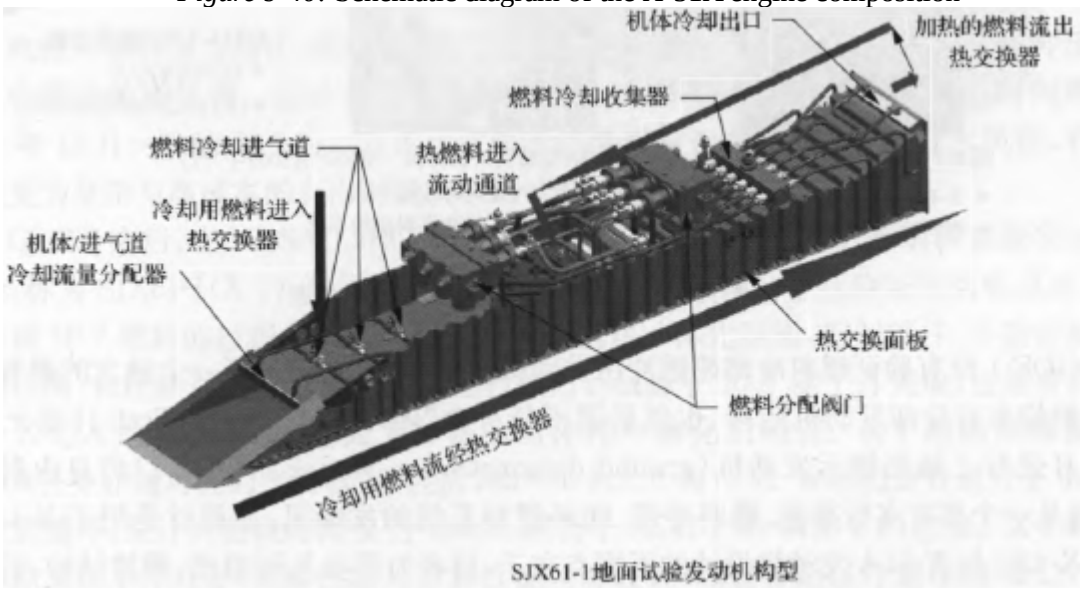

Figure 9-41: SJX61-1 fuel cooling test engine composition

The U.S. Air Force's HyTech program has developed many of the building blocks of this system. HyTech's component and development tests include a direct combustion chamber test bench, an intake/isolation section free jet model, a heat exchanger sub-component test to simulate the thermal load of the combustion chamber, a fuel distribution valve performance test, a closed-loop fuel system and software. After the demonstration of the performance of these components, a series of tests were carried out on larger and more complex free jets.

Figure 9-42 shows the development process of HyTech engine technology. In January 2001, a Performance Test Engine (PTE) made of heat sink material was tested in ATK/GASL's Leg VI free-jet wind tunnel.

PTE is a HyTech performance and runnability test engine model, which provides valuable data for subsequent engine development. The HyTech program took a major step forward in June 2003 with the completion of the world's first flyweight-ready free-jet test of a hydrogen-fueled scramjet engine, known as Ground Demonstration Engine 1 (GDE-1). GDE-1 verified the process of creating a flight mass engine and showed the ability of the X-51A to withstand thermal and pressure loads during flight. GDE-1 was designed as a flight cycle, with a total of 50 ground tests simulating flight conditions of *Ma* = 4.5 and 6.5 in the ATK/GASL Leg VI free-jet wind tunnel.

Figure 9-42: Development of the HyTech scramjet engine

The GDE-1 did not verify the feasibility of fuel-cooled scramjet engines, and it used a separate fuel system to supply the combustion chamber and cool the engine structure, which means that it was not a "closed loop." As a result, HyTech planned to conduct a ground show in March 2006; free-jet testing of the ground demonstration engine 2 (GDE-2), an engine with flight weight, fuel cooling, closed-loop fuel system, originally designed for X-43C program. The difference between the X-43C and X-51A engine design is that the former is a variable geometry and riveted structure, while the latter is a fixed inlet flow channel geometry and a welded structure, but the entire engine is generally similar, and the components of the fuel system are exactly the same. GDE-2 simulated flight conditions at *Ma* = 5.0 in an 8ft wind tunnel at NASA-LaRC, with a total of 300 seconds of combustion time (Figs. 9-43). The integrated closed-loop fuel supply system, software, and combustion chamber worked well and provided valuable experience for the development program of the X-51A engine.

Extensive testing of X-51A combustion chamber components was carried out on the Cell V direct-link test rig at the United Technologies Research Center (UTRC). The direct-attached test bench simulates the ability of the isolation section and the combustion chamber to work together, and the fuel distribution can be adjusted via the fuel distribution valve. In the UTRC, a flight simulation of the independent flight state in 30 was carried out, and the ignition of the engine ethylene, the conversion to JP-7 fuel, and the sensitivity of the independent performance of the JP-7 to the combustion chamber equivalent ratio, fuel distribution, flight pressure, and the conversion of the working mode of the scramjet engine at high Mach numbers were studied.

Figure 9-43: GDE-2 engine in a NASA-LaRC 8 ft wind tunnel

A total of three direct-coupled models were tested in the X-51A program, spanning from December 2004 to August 2006. The results of the direct-connect test help to reduce the technical risk of the engine and contribute to the test efficiency of more complex and costly free-jet demonstrations.

GDE-2 was followed by testing of the first X-51A ground test engine, known as the SJX61-1 (X-1), in a NASA-LaRC 8 ft high-temperature wind tunnel, as shown in Figure 9-44. The purpose of the X-1 test includes verifying engine ignition performance, conversion to JP-7 fuel, closed-loop fuel system, engine thermal integration, control hardware, and verifying the performance of the flow channel, and the operational capability required for the X-51A mission. The test was completed in July 2007 and was the first demonstration of the entire X-51A's flow path, including the vehicle's forebody and integrated nozzle. The X-1 ground test simulated the flight state corresponding to the X-51A mission plan, including Ma = 4.6, 5.0 and 6.5. In total, the engine underwent 40 ground test cycles, with a total burn time of up to 1,000s, equivalent to the GDE-1 and GDE-2 combined. The X-1 closed-loop fuel supply system worked well, and the test performance matched the computing performance well, meeting and exceeding the level required for the planned X-51A mission.

Additional testing of the HyTech engine is the SJX61-2 (X-2) engine, which will be flight approved in the spring of 2008. The engine's JP-1 fuel supply system will be identical to the flight configuration, and ethylene ignition will be carried out to simulate the flight process. Tests of the X-2 were planned to be carried out at Mach numbers 4.6 and 5.0, and the dynamic pressure was consistent with the trajectory of the X-51A, and the dynamic pressure in abnormal conditions was also tested to increase confidence in the success of the X-51A's flight. After the completion of the X-2 tests, the HyTech engine technology is expected to reach a medium risk level and can be used for subsequent flight tests of the X-51A.

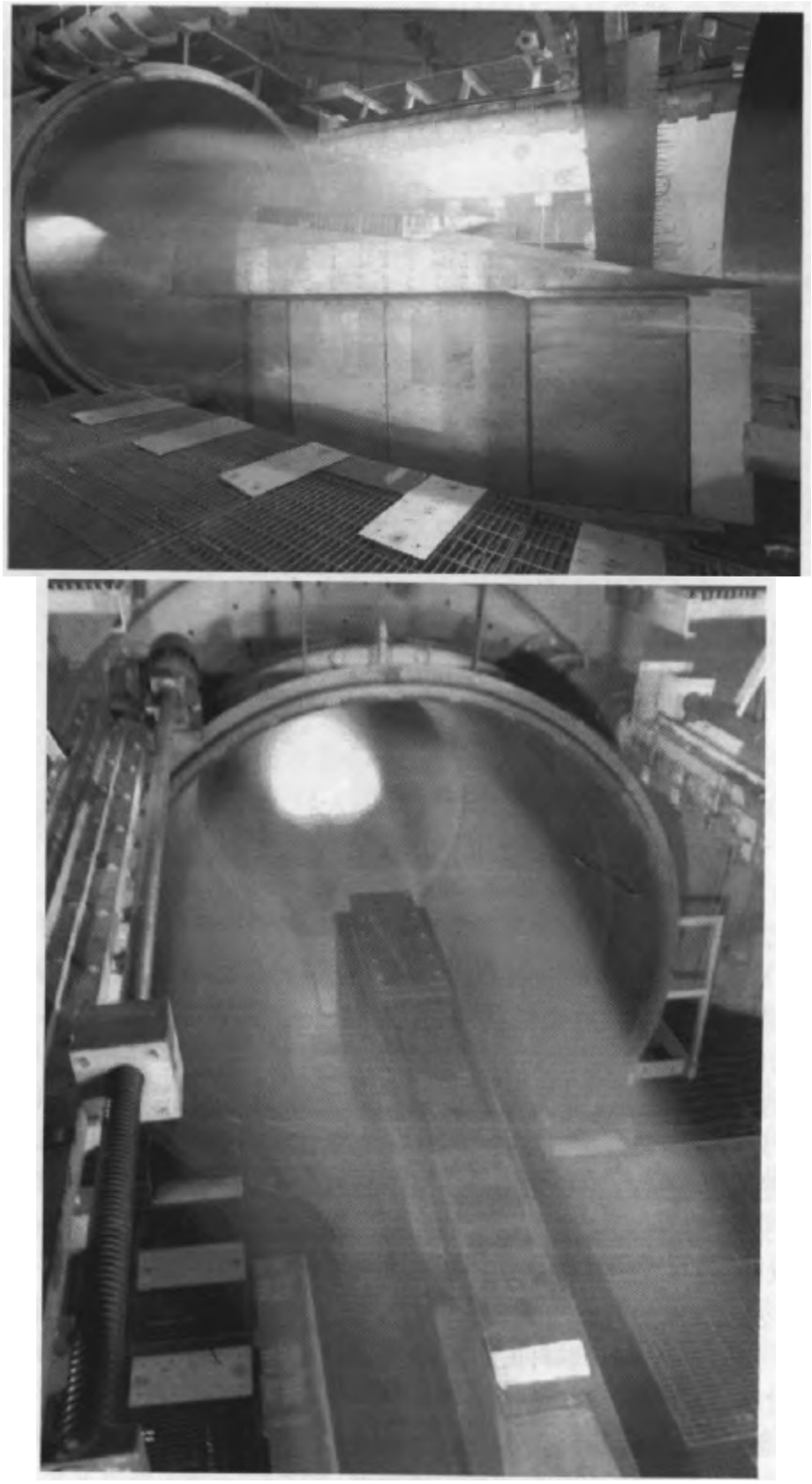

Figure 9-44: SJX61-1 engine in a NASA-LaRC 8 ft wind tunnel

9.11.7: Flight Test Program Arrangement

The X-51A is scheduled for four flight tests in August 2009 at the NAS Pt. Mugu NAWC test site in California. Like the X-43A Hyper-X flight test, a hypersonic vehicle equipped with a scramjet engine is mounted by a subsonic carrier aircraft and propelled by a solid rocket to the appropriate altitude and Mach number to obtain a flight condition in which the scramjet engine is starting to work. Unlike the X-43A, the X-51A will fly accelerated by a scramjet engine, from *Ma* = 4.5 to 6 (+). The test vehicle with booster was mounted on the left flank of the B-52H Stratofortress bomber. The X-51A is mounted on the 4,000-lb heavy-duty adapter, as shown in Figure 9-45. When mounted on the wing, the test vehicle communicates with the B-52 via a monitoring device and sends commands through the standard JDAM MIL-STI-1760 interface to receive power from the carrier aircraft via cable before switching to the test vehicle's lithium-ion battery power. The X-51A release process uses standard JDAM procedures.

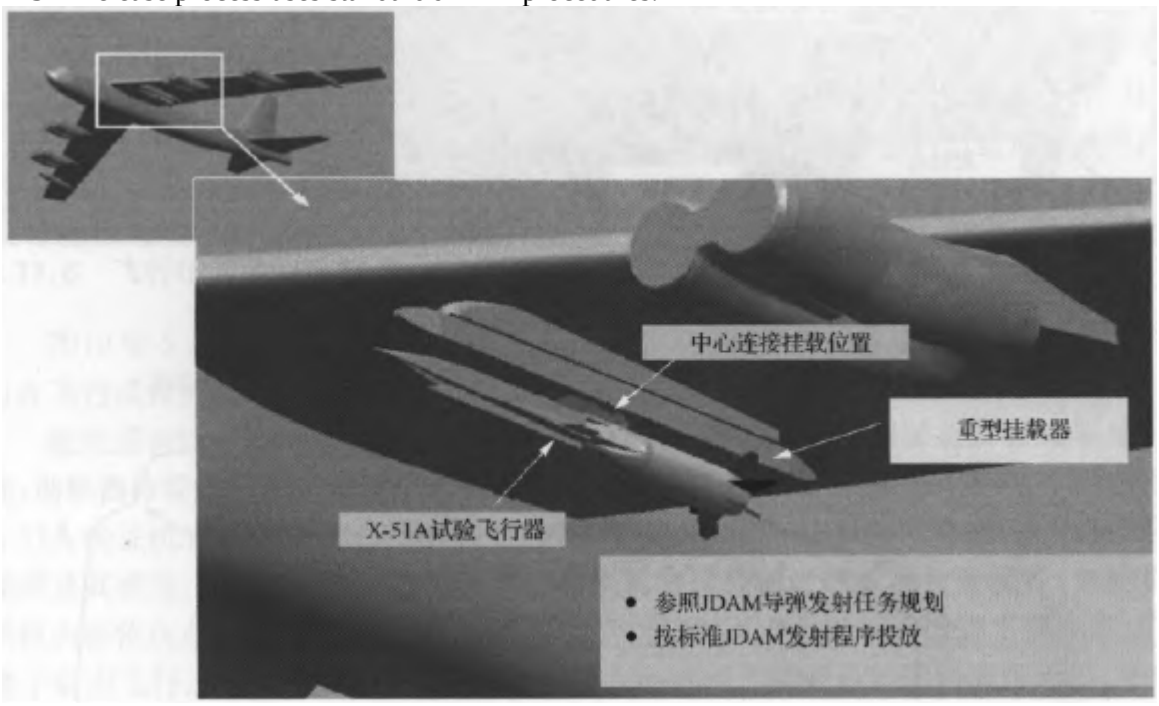

Figure 9-45: The X-51A test vehicle is mounted on the B-52

After taking off from Edwards Air Force Base, the B-52H carrier flew in a southwesterly direction. On the westward straight segment, the B-52H will maintain a flight Mach number of 0.8 and an altitude of 49,500 ft and conduct an aircraft inspection. The first is the experimental test, in which the aircraft conducts a self-test antenna to receive signals for verification. During the second check, if the B-52H has reached the launch point located in the Pacific Ocean, and all the launch conditions are met, the X-51A test vehicle will be released, and the booster will be ignited after the free fall of 4s. The ATACMS solid rocket booster has an operating time of about 35s and accelerates the test vehicle to a flight Mach number of 4.5 and an altitude of 60,000 ft. During the booster phase, the scramjet intake will be activated, and as the high-velocity airflow passes through the inlet tract and connectors, the pneumatic heating will begin to raise the wall temperature of the flow channel, and a small amount of JP-7 will flow into and fill the wall lines of the heat exchanger (Fig. 9-46).

Immediately before the booster is turned off, the test cruise vehicle is separated from the booster and connector. After a short coasting phase, the ethylene is injected and ignited in the flow channel, completing the heating of the engine walls as well as the internal JP-7 fuel.

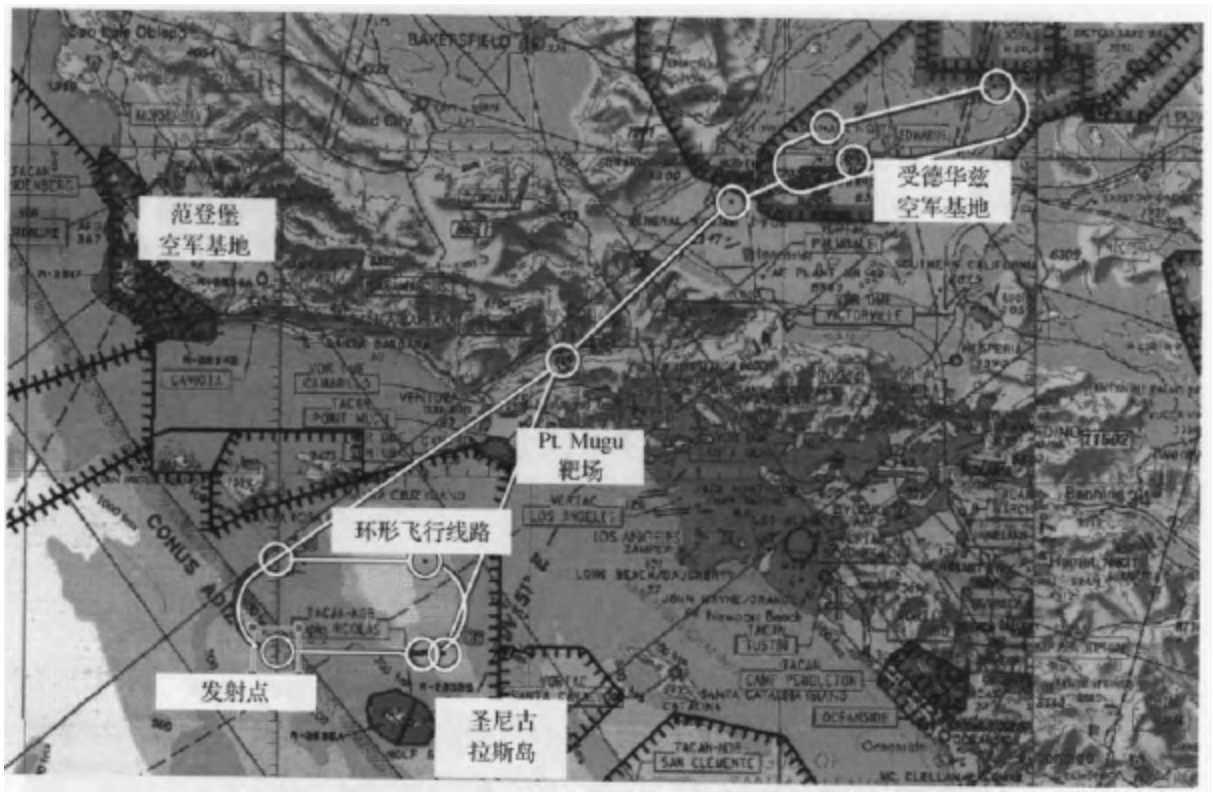

Figure 9-46: Flight test path

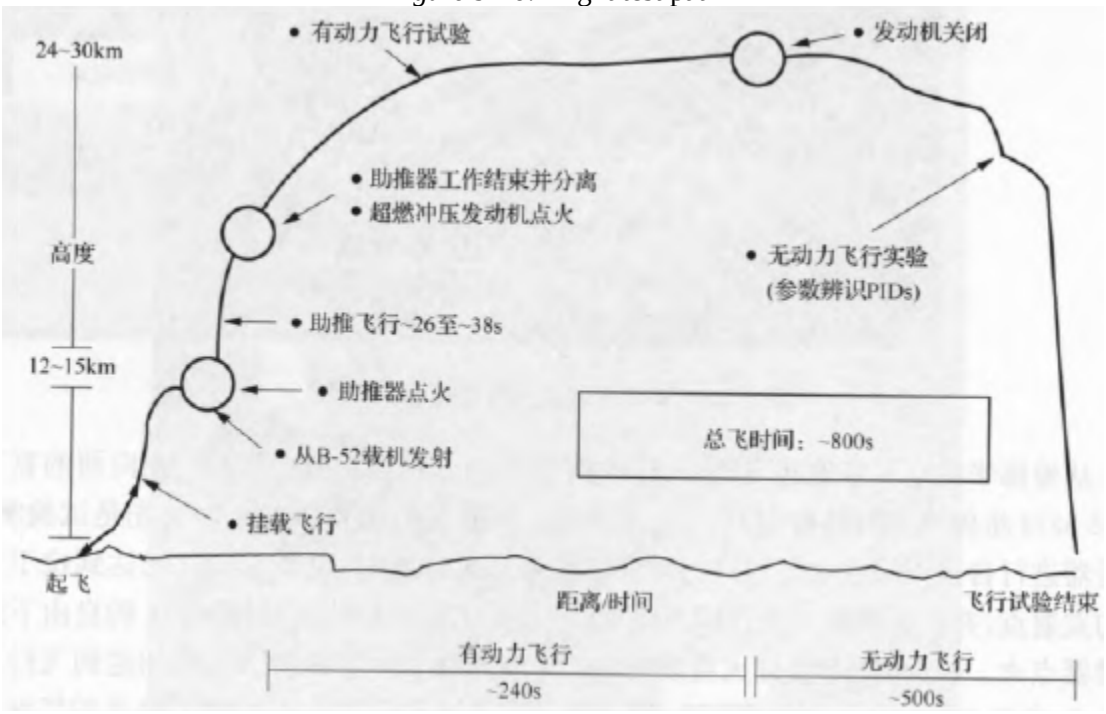

Figure 9-47: Flight test section

When the fuel has been heated to the minimum ignition temperature, the scramjet engine begins to inject heated hydrocarbon JP-7 fuel into the flow channel. The conversion process lasts for several seconds until the ethylene is completely depleted and the engine will run on only JP-7 fuel.

FADEC controls a set of fuel distribution valves, which control the equivalent ratio of the entire combustion, the equivalent ratio of cooling, the position of the injection, within the range of Mach numbers in which the engine operates. The engine will continue to work until the fuel it is carrying runs out. The flight test process is shown in Figure 9-47.

The JP-7 carried on board has 256lbs of fuel, which can provide about 240s of scramjet burn time. All four flights will use the same flight trajectory, which can be optimized to achieve a maximum Mach number of around 6. During the test, the aircraft will wirelessly transmit the temperature, pressure, stress and acceleration data of the aircraft and engine to the Navy's P-3D Orion patrol aircraft. Mugu test site, as well as the Vandenberg AFB test site. When the scramjet engine is turned off, the aircraft will taxi unpowered and perform a series of parameter-identifying maneuvers. Valuable data on the flight characteristics of the vehicle in the hypersonic range will be provided, which can be compared with the wind tunnel test database. The aircraft will continue to descend and decelerate until it splashes in an area of about 400 nautical miles from the release point. The aircraft is not recovered after the test flight.

The full flight test program is expected to commence in early 2009, with ground tests continuing in April-May 2009, followed by an initial flight readiness assessment in May. The X-51A's first flight test will be conducted in June 2009 to verify wireless data transmission and control room display capabilities. Pre-launch flight tests were conducted in July 2009. The first free-flight test will take place in August 2009, followed by a second flight test eight weeks later. The third and fourth trials will be conducted in October and November, six weeks apart. After the completion of the flight data analysis, the final research report will be summarized in fiscal year 2010.

9.11.8: Conduct of flight tests

On May 26, 2010, a U.S. military base on the Pacific coast of southern California successfully flew the X-51A flight test aircraft.

As originally planned, the B-52 aircraft dropped the entire X-51A test system at an altitude of approximately 15,000m. First, the booster burns continuously for 30s, accelerating the entire system to Ma = 4.6 to 4.8. During the boosting process, air enters the scramjet engine of the X-51A demonstrator and exits through the interstage stage to activate the intake tract and begin to gradually heat the engine and its fuel. After the booster is separated, the X-51A demonstrator will continue to glide for several seconds with the help of inertia, and then ignite ethylene and fuel in turn inside the engine to reach thermal equilibrium, and then accelerate continuously using only the combustion of JP-7 fuel. The whole powered flight process is about 300s, and the expected flight speed is Ma = 6.5. As all fuel is depleted, the X-51A demonstrator will begin to slow down, followed by 500s of unpowered flight, gradually descent and finally crash into the Pacific Ocean.

However, the first test flight did not go smoothly as envisaged, and despite the success, some unexpected circumstances arose. The B-52H carrier aircraft took off from Edwards Air Force Base, climbed to a predetermined altitude, and released the X-51A test system consisting of a booster and a demonstrator at a flight speed of Ma = 0.8. After about 4s, the booster ignited according to a predetermined procedure, boosting the X-51A demonstrator to Ma = 4.8. Subsequently, the X-51A demonstrator separated from the booster and the interstage section, and successfully completed a gentle 180-degree roll maneuver according to the predetermined procedure. In the process, the X-51A demonstrator changed the air intake from an upper position to an abdominal position, and the flight speed was slightly reduced to Ma = 4.73.

Subsequently, the SJY61 scramjet engine first ignited ethylene, and then transitioned to the ignition and combustion of JP-7 hydrocarbon fuel. The X-51A demonstrator then began to accelerate gradually, but telemetry data showed that the acceleration was slightly below the design value, and the temperature at the rear of the engine bay was significantly higher than the design value. Range safety officials found that the X-51A demonstrator had begun to slow down and that the telemetry had been lost, so they ordered the test flight to be terminated and the aircraft initiated a self-destruct program.

As a result, the SJY61 scramjet engine only worked for 140s, which did not reach the expected 300s time, and the flight speed of the aircraft reached Mach 5 and did not accelerate to Mach 6 or more. PWR said that the relevant data initially showed that the SJY61 engine worked exactly according to the design requirements and achieved some of the most critical things in the first test flight: igniting ethylene, transitioning to mixed combustion of ethylene and JP-7 fuel, reaching the conditions of JP-7 fuel combustion, continuing to burn with only JP-7 fuel, and continuing to work for 140s. Before the X-51A self-destructed, there was still some fuel left in the aircraft.

As a result, PWR has mastered a number of key technologies that will allow it to quickly produce scramjet engines with longer combustion times. The designed flight time of 5 minutes is not a limitation of the propulsion system but is limited to the capacity of the fuel tank with fuel. If the design of a fuel tank of a larger capacity is improved, the X-51A modification can further increase the flight time.

Despite the fact that the flight duration did not reach the expected goals, the test group was still satisfied with the results. An AFRL spokesperson said that the first flight scored a B, and the next time it will get an A. Brink, AFRL's manager in charge of the X-51 program, said that the test flight was a 95 percent success, the flight control software was flawless, and it was not clear what the specific cause of the slowdown in acceleration and short flight time was, and the initial speculation was that it could be a sealing problem or actuator failure, but also believed that the X-51A demonstrator's drag when flying at low Mach numbers may have been incorrectly estimated. The news media in the United States fully affirmed the first flight. The Christian Science Monitor described the X-51A's flight speed as faster than "Superman" and likened its scramjet engine to the technical difficulty of lighting a match in a hurricane and keeping the flame from extinguishing. The Los Angeles Times described the first test flight of the X-51A demonstrator: an aircraft that looks like a surfboard detached from under the wing of a B-52H carrier aircraft, and then disembarked at more than 5,600x103/ H flew over the Pacific Ocean, dishonoring past flight records and rekindling enthusiasm for the development of hypersonic vehicles. Perhaps, Brink's comments are more incisive and evocative. He stated that the technological leap of the scramjet was equivalent to the huge leap from piston to jet engines in late World War II (Figure 9-48).

Figure 9-48: Flying B-52 carrying X-51 aircraft

After the Boeing B-52 aircraft carried the X-51 to the launch point "perfectly," the rocket thrusters successfully advanced the X-51 to *Ma* = 5, and the scramjet engine built by Pratt & Whitney Rockdyne successfully ignited with ethylene as the initial fuel. During the subsequent switch to JP-7 conventional fuel, the air intake failed to activate. Efforts to restart and restore optimal conditions to the staff then failed. According to NASA, the reason why the intake tract does not activate is that the shock wave is too fast, passing over the front end of the air intake, causing the air pressure of the engine airflow to drop sharply. The scramjet engine relies on extremely precise shock wave movements and engine airflow. There is no wind tunnel that allows air to move at hypersonic speeds, making hypersonic testing extremely difficult.

Charlie Brink, Air Force Program Manager, said: "Obviously, we were disappointed and we were expecting a better outcome. However, we are still satisfied with the data collected from this flight. We will continue to examine this data to learn more about this new technology. Every time this exciting new technology is tested, it is one step closer to success."

During the second flight test of the X-51 Waverider hypersonic vehicle on June 13, 2011, the second flight of the X-51 was prematurely terminated because the air intake tract of the scramjet engine was not activated. Under the control of the operator, the aircraft splashed down the coast of California.

9.12: Falcon Project

9.12.1: Program Background

The U.S. Air Force and Defense Research Projects Agency (DARPA) launched the Falcon project in 2003 to develop hypersonic technologies that can be developed and demonstrated to achieve global reach. Vehicles to achieve this mission include the reusable Hypersonic Cruise Vehicle (HCV). The Falcon project then intended to develop and demonstrate the technologies required for HCVs, including high-lift-to-drag ratio aerodynamic shapes, high-speed turbine-based combined cycle propulsion systems, high-temperature materials, thermal protection systems, and advanced navigation guidance and control technologies. The Falcon project prepared to develop a series of hypersonic technology vehicles (HTVs) to conduct flight tests to demonstrate the required technology step by step, as shown in Figure 9-49. [15]

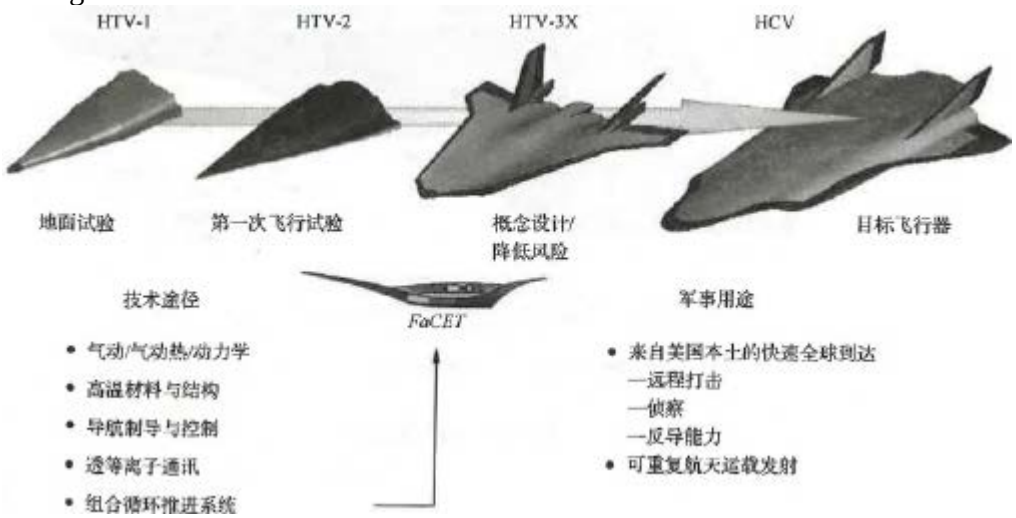

Figure 9-49: Overview of the Falcon project

Hypersonic Technology Vehicle 1 (HTV-1) is an unpowered, maneuvering, hypersonic re-entry vehicle that uses the latest technology to cope with the technical difficulties in materials and manufacturing. A series of HTV-1 ground trials were conducted to develop and validate the aircraft's aerodynamics, aerodynamic heating, thermostructural properties, and advanced carbon-to-carbon composite manufacturing methods.

Compared with HTV-1, HTV-2 has a more advanced aerodynamic design, thermal protection system and improved navigation guidance and control system. The detailed design of the HTV-2 has been completed and trial production of the prototype has begun. The HTV-2 flight tests will be launched from the Minotaur IV Lite launch vehicle at Vandenberg Air Base in 2009.

The Falcon project was originally intended to develop the HTV-3 to validate reusable thermal protection materials, but at the beginning of the second phase of the Falcon project, DARPA chose to turn to the propulsion technology needed to develop a reusable hypersonic test platform. The mission, called FaCET (Falcon Combined-cycle Engine Technology), aims to develop a reusable hydrocarbon fuel-based turbine-based combined cycle propulsion system that can take off from an ordinary runway and accelerate to *Ma* = 6. Propulsion system research in collaboration with the High Speed Turbine Engine Demonstration (HiSTED) program has led to the development of the HTV-3 as a flight test platform, which can take off from a normal runway, cruise at *Ma* = 6, and land on the runway. The new design, called the HTV-3X, is a highly integrated flight test platform that demonstrates a variety of key hypersonic technologies, including aerodynamic form factors with high lift-to-drag ratios, lightweight, reusable, high-temperature materials, thermal management for active cooling, automatic flight control, and turbine-based combined cyclic propulsion, all of which are illustrated in Figure 9-50.

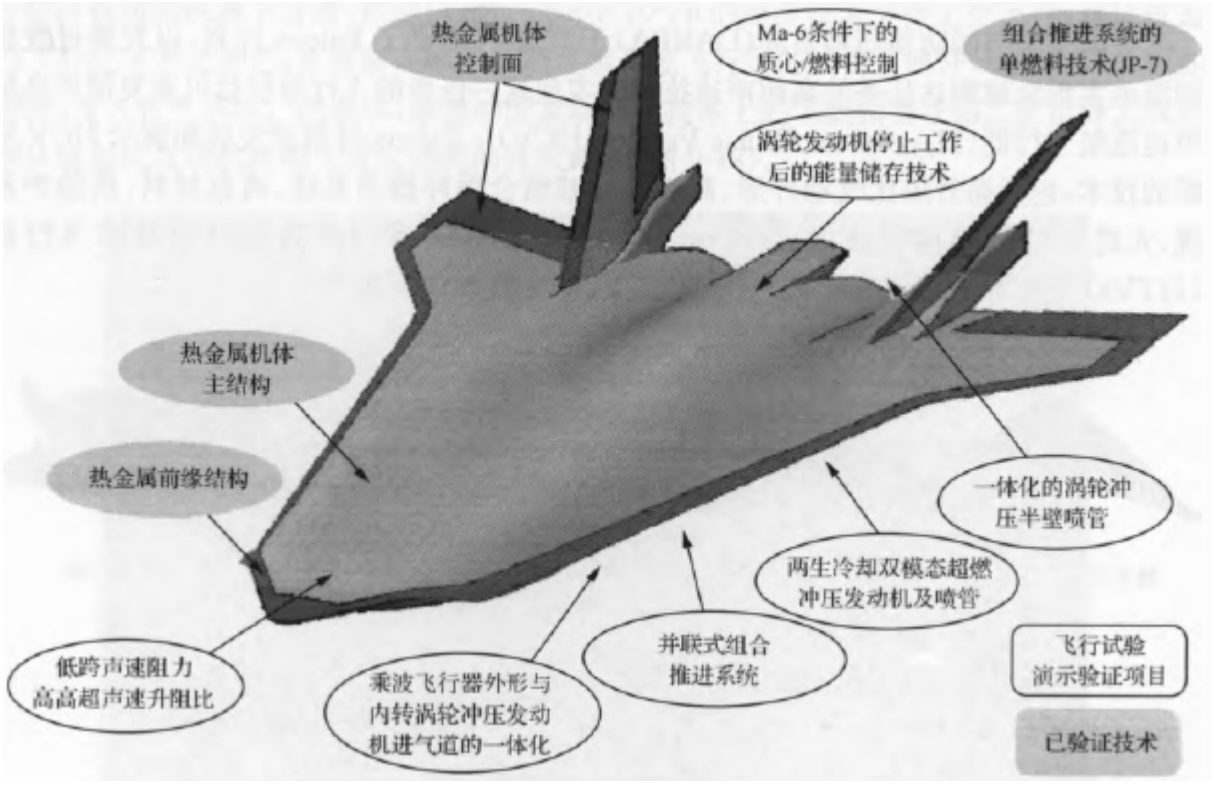

Figure 9-50: Key technologies of the HTV-3X

9.12.2: Turbine-based combined cycle propulsion system

The propulsion system of a reusable hypersonic vehicle must be able to operate in a very wide flight environment, i.e., a wide range of free-flowing pressures and Mach numbers. There is no single type of engine that can meet the requirements of all operating ranges. Therefore, the choice of propulsion system must be combined-cycle, i.e. including turbojet and scramjet (bimodal/scramjet). The turbine-based combined cycle TBCC propulsion system consists of three working stages, as shown in Figure 9-51. The take-off, landing, and supersonic phases of the aircraft are propelled by turbojet engines. In the higher supersonic to low hypersonic flight phase, the ramjet mode is used, that is, the engine is inside the subsonic combustion process. When the aircraft accelerates to cruising flight conditions, the combustion process is converted to supersonic combustion.

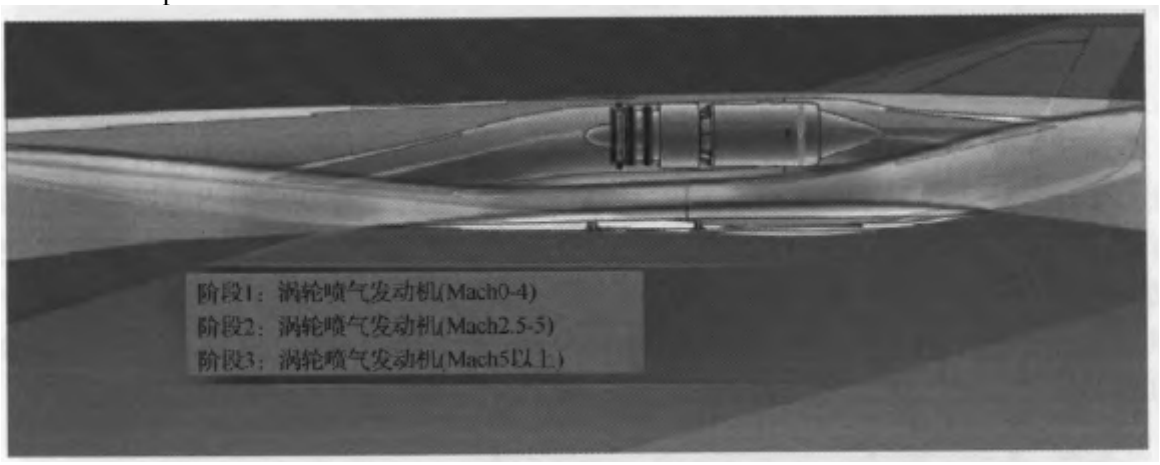

Figure 9-51: Concept of a turbine-based combined cycle propulsion system

The TBCC propulsion system consists of two flow channels, the upper one for the low-speed flow channel and the lower one for the high-speed flow channel. In the design of the HTV-3X, the two TBCC propulsion systems share the intake and exhaust components. Integrating these flow channels into a complete propulsion system presented a significant technical challenge for the HTV-3X design. Figure 9-52 shows the HTV-3X TBCC propulsion system and the complexity of its integration.

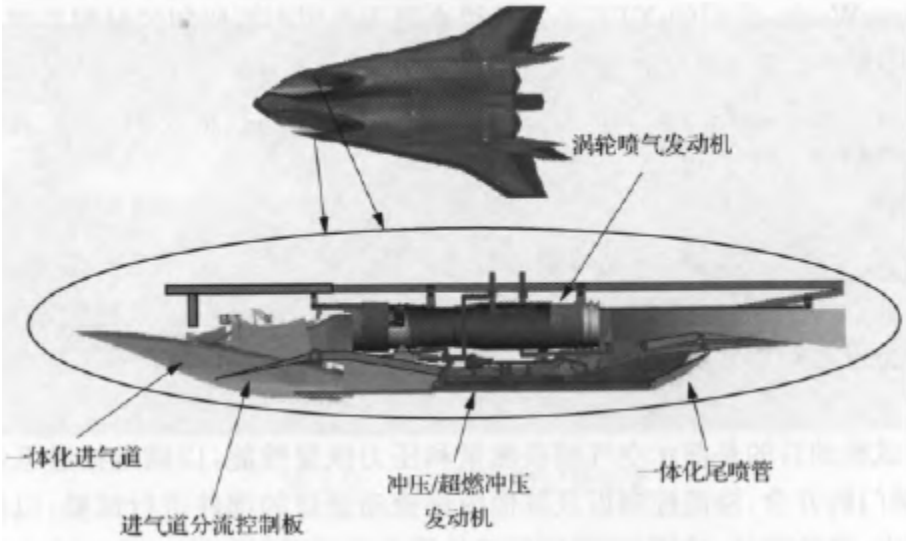

Figure 9-52: HTV-3X turbine-based combined cycle propulsion system

Perhaps the most important aspect of TBCC design and development is the simultaneous presence of air flow and combustion in both flow channels during operation. The flight corridor of the HTV-3X must be carefully designed to ensure that the propulsion system is within the operating range, so that the aircraft can achieve cruising conditions in the most economical and fuel-efficient way. The intake and exhaust air are controlled by variable geometry to separate the air flow in the upper and lower flow channels. The HTV-3X features an inward-turning intake design that effectively provides air flow through each engine cycle. Fuel control is carried out according to each flow channel and the respective fuel allocation, and through fine adjustment, the modal conversion and thrust provided by the high-speed propulsion flow channel are realized.

In general, TBCC engines require a high degree of integration in order to effectively accelerate from zero Mach number takeoff to a cruising altitude of $Ma = 6$. Improper integration will complicate the system and increase the weight of the engine. The aircraft requires multiple actuators for mechanical control of the inlet tract, gas outlet door, boundary layer overflow, etc. Alternatively, one possible way to advance the layout is to do it side-by-side.

9.12.3: Development of TBCC-related technologies

The development of TBCC engine technology requires demonstration tests of individual engine technologies as the first step to verify the performance and feasibility of the entire engine. HiSTED plans to conduct ground tests of turbojet engines in the flight conditions of the HTV-3X. The FaCET plans to conduct ground tests on the intake, combustion chamber and tail nozzles, respectively, as well as free-jet engine tests integrated with turbojet engines. Ground testing of an integrated TBCC system is necessary to develop and demonstrate the capabilities of the required propulsion system, but the limitations of current test equipment are also a challenging factor.

1) HiSTED

The HiSTED program is derived from the Reusable Combined Cycle Program (RCCP) and is jointly funded by the U.S. Air Force and DARPA to develop and demonstrate turbine-based combined cycle propulsion systems. The goal of HiSTED is to carry out ground tests of turbojet engines $Ma = 4$.

The two HiSTED participants are Williams International and LibertyWorks. Williams International will test the XTE88 engine on AEDC's test facility in November 2008, and LibertyWorks will test the XTE18 engine on their own test facility. LibertyWorks' XTE18 engine is derived from the $Ma = 3$ turbojet-powered engine used in the U.S. Navy's time-critical long-range strike missile.

These tests will demonstrate the performance of the turbine engine, support the technological development of the HTV-3X, and expand its use in large-format reusable aircraft.

2) FaCET

FaCET conducts ground tests on the components of the flow channel of the TBCC engine, i.e., the air intake, combustion chamber, and nozzle, to verify the performance of each component. Each component will be tested in the Mach range in which the TBCC engine operates, with a particular focus on the Mach range for combined engine conversions. Subsequently, the ground tests of the free-jet engine were carried out in an integrated manner.

The purpose of the inlet test is to demonstrate the air capture flow and pressure recovery performance to meet the performance requirements of the propulsion system, and to test the opening and closing of mechanical doors, overflow control, and other components of the internal flow channel to ensure smooth start-up in turbojet and ramjet/scramjet working modes over a wide range of Mach numbers. Figure 9-53 is a scaled-down model test conducted in Lockheed Martin's 4'X4' wind tunnel, which will verify the transition from turbojet to ramjet/scramjet mode to hypersonic vehicle state and cruising speed, and the results will also be used to validate the analysis and prediction tool (Figures 9-54 to 9-56).

Figure 9-53: FaCET inlet test model

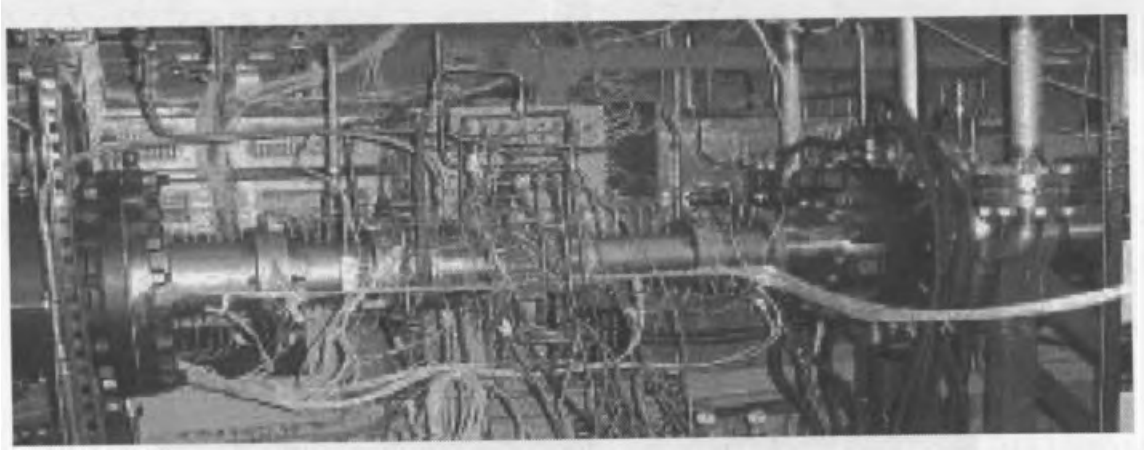

Figure 9-54: FaCET direct-coupled combustion chamber test bench

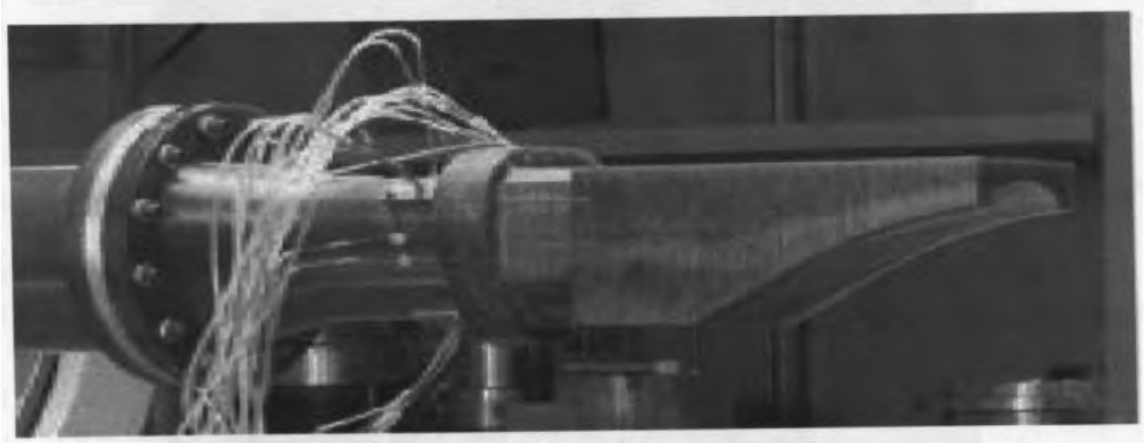

Figure 9-55: FaCET nozzle test setup

Figure 9-56: FaCET free-jet engine model with support bench

9.12.4: HTV-2 flight test

The HTV-2 program began in 2003 when the U.S. military wanted to build an aircraft that could reach anywhere in the world in an hour. The aircraft has been tested in computer models and wind tunnels, but researchers can only simulate a top speed of 15 times the speed of sound, so practical testing is the only way to determine whether the aircraft can maintain high speeds.

In 2008, DARPA proposed a program to develop a fighter-like HTV-3. The aircraft, which is designed to have "unmatched performance" with other supersonic aircraft and can reach six times the speed of sound, will enter service in 2012. However, due to budget cuts in the U.S. Congress in 2009, the project was put on hold, and DARPA switched to the development of the HTV-2 (Figure 9-57).

Figure 9-57: Rendering of HTV-2

In April 2010, the Falcon made its first launch, but it was not perfect. Technical data show that the take-off and separation of the "Falcon" from the rocket went smoothly, but 9 minutes after entering the flight test, the telemetry station lost contact with the "Falcon." The U.S. Department of Defense said that at that time, the system detected an abnormality in the flight pattern, so the forced guidance aircraft crashed into the sea.

Since its test failure in April 2010, the Falcon HTV-2's design and flight modes have been improved. On the morning of August 11, 2011, local time, the Minotaur IV rocket was successfully launched with the Falcon HTV-2 aircraft from Vandenberg Air Force Base in California, USA, but after separating from the rocket at the edge of space, the Falcon lost contact when flying alone and returning to Earth (Figure 9-58).

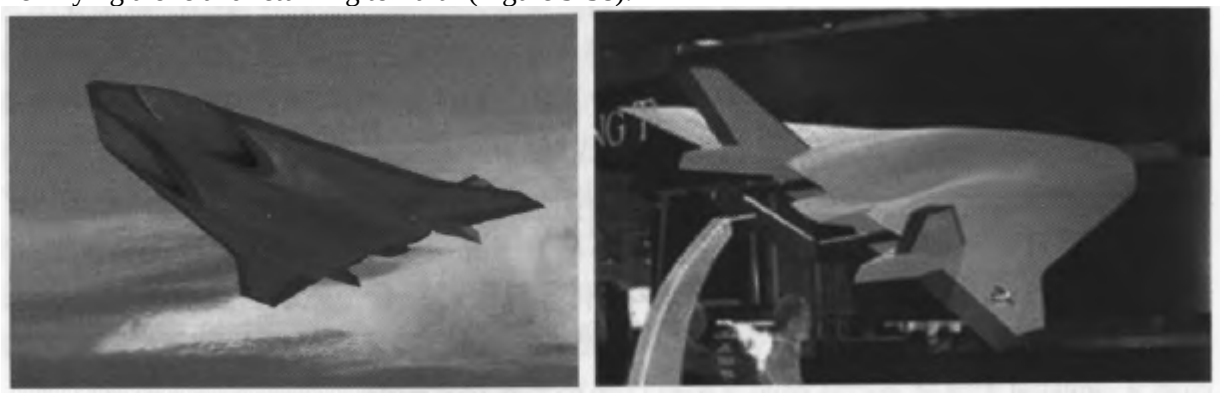

Figure 9-58: Conceptual design of HCV

References

[1] Hopkins University Applied Physics Laboratory. Ramjet Engine Technology [M]. Li Cunjie, et al., trans., Beijing: National Defense Industry Press, 1980.

[2] Edward T Curran. Scramjet engines: The first forty years [J]. J. of Propulsion and Power, 2001, 17(6):1138-1148.

[3] Shang Dong-ae. SCRAM missile with scramjet engine as power unit [J]. Flying Missile, 1994, (6).

[4] Mercier R A, Ronald T M F. Hypersonic Technology (HyTech) Program Overview [R]. AIAA-1998-1566, 1998.

[5] Zhan Yun. Hypersonic Technology (HyTech) Program [J]. Flying Missile, 2003, (3).

[6] Michael E White, Walter R Price. Affordable hypersonic missiles for long-range precision strike [J]. Johns Hopkins APL Technical Digest, 1999, 20(3).

[7] Hunt J, Eiswirth E. NASA's dual-fuel airbreathing hypersonic Vehicle Study. NIAA 96-4591, 1996.

[8] Liu Tonglin. Development and prospect of hypersonic technology in the United States [J]. Aerospace Control, 2004, 22(4).

[9] Phillip J Joyce, John B Pomroy. The Hyper-X launch vehicle： Challenges and design considerations for hypersonic flight testing [R]. AIAA 2005-3333.

[10] Phillip T Harsha, Lowell C Keel. X-43A vehicle design and manufacture [R]. AIAA 2005-3334, 2005.

[11] Laurie A Marshall, Catherine Bahm, Griffin P Corpening. Overview with results and lessons learned of the X- 43A Mach 10 flight [R]. AIAA 2005-3336, 2005.

[12] Wen Jie. U.S. Navy's HyFly Program [J]. Flying Missile, 2008, (2):10-13.

[13] Zhu Aiping, Ma Ling. HyFly Project Introduction [J]. Flight Missile, 2010, (5): 39-42.

[14] Joseph M Hank, James S Murphy, Richard C Mutzman. The X-51A scramjet engine flight demonstration program [R]. AIAA, 2008-2540, 2008.

[15] Steven H. Walker, Col Jeffrey Sherk, Dale Shell. The DARPA/AF Falcon program: The hypersonic technology vehicle#2 (HTV-2) flight demonstration phase [R]. AIAA 2008-2539, 2008.

Chapter 10: Russian Hypersonic Vehicle Technology Research

As the successor of the Soviet Union's scientific and technological and military strength, Russia occupies an important position in the field of hypersonic vehicle technology. The Central Research Institute of Aerofluid Power of the Soviet Union, the Baranov Central Aero Engine Research Institute, the Tulayev Union Design Bureau, the Moscow Aviation Institute and other units have long been committed to the basic theoretical research of hypersonic technology and have made major breakthroughs in subsonic/scramjet engines, hydrocarbon fuels, high-temperature resistant materials, CFD technology and integrated design technology.

Russia achieved supersonic combustion for the first time in 1991 in high-altitude flight tests, marking that Russia has entered the stage of flight tests of hypersonic technology. In the 1990s, there were four important flight test programs of hypersonic technology in Russia: the “Cold” program and the "Eagle" program jointly conducted by the Central Research Institute of Aerofluid Power and the Baranov Central Aero Engine Research Institute; the Rainbow-D2 program is a joint project of the Rainbow Design Bureau and the Central Research Institute of Aerohydrodynamics, and the Eagle-31 flight test program is a joint project of the Tulayev Union Design Bureau, the Torch Design Bureau, the MiG and the Moscow Aircraft Production Complex. The development of these plans is of great significance for exploring the mechanism of supersonic combustion and hypersonic aerodynamics, and also has important reference value for the design of flight test schemes.

Further reports on the development of Russian hypersonic vehicle technology were rare after 2000, but in mid-February 2004 Russia conducted a test launch of a strategic missile, which Russian President Vladimir Putin commented on as capable of breaking through the US ballistic missile defense system. Western analysts believe that the test is to further verify the scramjet technology and demonstrate the scheme. Prior to this test, Russia had conducted at least one pre-launch test of a hypersonic missile. In July 2001, an ICBM launched a hypersonic test vehicle, both of which were reportedly tested using Topol-M (SS-25) missiles.

It is possible that Russia is pinning its hopes on hypersonic vehicle technology to counter the growing U.S. ICBM defense capability. Due to the lack of sufficient strategic weapons systems, Russia urgently needs to guarantee its ability to break through enemy defense systems, and the reduction of Russia's nuclear weapon delivery system and its nuclear warhead stockpile may also be the reason for promoting the research of hypersonic vehicle technology [1~7].

10.1: "Cold" program

Among the flight tests of hypersonic technology in Russia, the first to be carried out was the “Cold” program (Kholod), which was carried out by the Baranov Central Aero-Engine Research Institute of Russia in cooperation with the Zhukovsky Central Research Institute of Aerohydrodynamics and other units.

10.1.1: Test model of symmetrical subsonic/scramjet engine

The test model of the sub(sonic)/combustion ramjet engine of the Central Aero Engine Research Institute is axisymmetric. Russia is a world leader in the design technology of axisymmetric ramjet engines and has successfully applied it in several models of anti-ship missiles.

The axisymmetric subsonic/scramjet engine model is an autonomous system that includes a subsonic/scramjet engine carrying hydrogen fuel, a fuel monitoring/measurement system, a telemetry system, and more.

The program control system controls the combustion state of the engine, and the ground telemetry station receives the data from the telemetry system for processing. The total mass of the test model is 595kg, the length is 4.3m, the maximum diameter is 750mm, and it can carry 17kg (300L[3]) of liquid hydrogen fuel. The test engine had an air intake tract diameter of 230mm and a length of 1.28m.

Many parts of the engine and its mounts are made of common materials, with the air intake tract and center cone, combustion chamber and liquid hydrogen fuel tank made of stainless steel, and the aluminum-iron-chromium powder metallurgy at the tip and leading edge of the fairing, which can withstand temperatures of more than 1,200°C.

There is a flame stabilizer in the test combustion chamber, three rows of nozzles in the intake tract of the engine model, two rows of nozzles I and II in the ramjet engine for subsonic combustion, and I to m nozzles in ultrasonic combustion to achieve a two-mode combustion transition (Fig. 10-1).

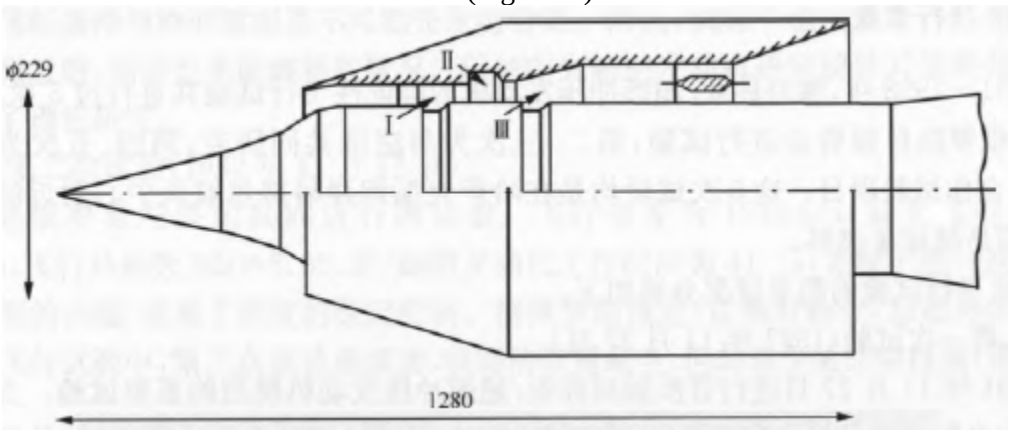

II + III subsonic combustion I + II + III supersonic combustion

Figure 10-1: Air flow path diagram of the test engine model

10.1.2: Test Flyer

The symmetrical subsonic/scramjet engine test vehicle uses the 5B28 missile from the long-range, medium- and high-altitude surface-to-air missile system SA-5 "Gammon" (Russian name "Vega," system code C-200), which has begun to be decommissioned. The missile is an important component of the C-200 system, which was developed by the Torch Design Bureau in the early 1960s and equipped in the early 70s. It is a family of systems, including SA-5, SA-5A, SA-5B, SA-5C, SA-5D, SA-5E, and the corresponding Russian code names are C-200, C-200B, etc., which are developed to intercept high-altitude reconnaissance aircraft, long-range air-to-surface missile carriers, high-altitude long-range support jammers and command aircraft (the maximum speed of the target is 1,200 m/s).

The missile has a combat range of 17 to 320 km and an interception altitude of 0.3 to 35 km. The length of the projectile is 10.8 m, the diameter (level II) is 860 mm, the launch mass is about 7,000 kg, the maximum flight speed is *Ma* = 5, and the maneuverability is 20 g. It adopts a fixed position to launch, with a fixed high and low angle, and the azimuth can be followed.

The 5B28 missile is a two-stage parallel system. Four solid rocket boosters were bundled around the body of the Class II projectile. After the booster is finished, it is separated to all sides by the pneumatic asymmetrical force of the head. Each booster has a thrust of 20t. The second stage has an "X" shape in a normal aerodynamic layout, with 4 large swept wings and a fully moving tail rudder. The main engine is a liquid rocket engine with liquid fuel N204, which can be safely stored for a long time, and has a thrust of 31.36 to 96 kN.

The 5B28 missile was modified for use as a test carrier for axisymmetric subsonic/scramjet engines, with the warhead and irrelevant systems disassembled and disassembled, measurement equipment added, and the engine model mounted on the head of the 5B28 missile (Figure 10-2).

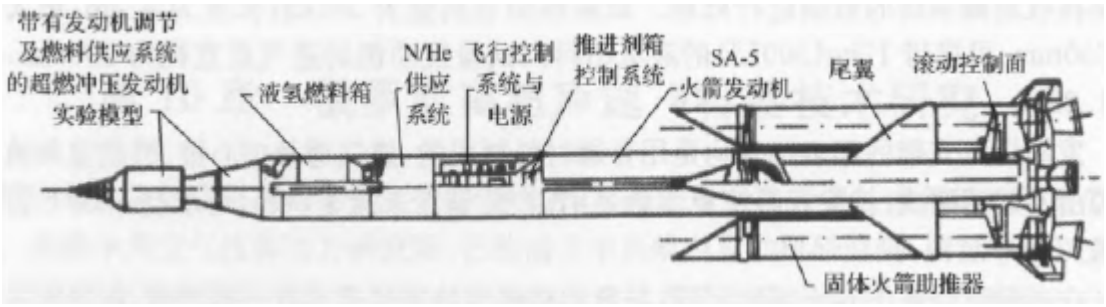

Figure 10-2: Layout and structure of the test vehicle

10.1.3: Flight Tests

From 1991 to 1998, five confirmatory flight tests of axisymmetric subsonic/scramjet engines were conducted: the first was self-financed by Russia, the second and third were joint research with France, and the fourth and fifth were joint test projects with NASA of the United States. The five tests were conducted at a range near the Baikonur Space Center in Kazakhstan and were fueled by hydrogen.

A brief summary of the five flight tests is provided below.

1) First test (November 27, 1991)

On November 27, 1991, the first tethered test of an axisymmetric subsonic/scramjet engine model was conducted. For this test, the Central Aero Engine Research Institute conducted two launch tests in 1989 and 1990 to verify the ballistics of the test vehicle, and the test engine did not work. At the end of the flight, the test vehicle was recovered. In the five subsequent tests, the test vehicle was not designed to be recyclable.

The trial was largely successful. The missile flies 180km, the flight duration is about 130s, the maximum flight altitude reaches 35km, and the trajectory is very flat. The maximum flight speed reaches 1,653 m/s, and the maximum flight Mach number $Ma = 5.6$.

During the flight time, the test vehicle completed two independent pre-programmed firing of the subsonic/scramjet engine through a programmed control system.

The first lasted nearly 20s. Starting at 18 km altitude, $Ma = 3.5$, and ending at 28 km altitude, $Ma = 6$;

The second time lasted almost 10s. It starts at 22 km at an altitude of $Ma = 4.5$ and ends at an altitude of 18 km with $Ma = 3.5$.

The purpose of the test was to verify the ignition system of the engine. In the final 5s of the first time, supersonic combustion was achieved.

This is the first time in the world that the conversion of a ramjet engine from the subsonic combustion mode to the supersonic combustion mode has been realized in flight tests. This event is of great significance in the field of the development of modern engine technology, it marks the stage of scramjet engine from the theoretical research of ground tests to the stage of application development, and further establishes Russia's leading position in this field of expertise. After the success of the test, Russia informed the Western countries of the results of the test. At the beginning of 1992, an American scientific and technical publication reported that while we were still conducting theoretical research, the Russians were already conducting flight tests. In the mid-1990s, the United States accelerated the development of hypersonic technology, which had a lot to do with this event.

When the test engine achieved supersonic combustion, the gas velocity of the combustion chamber reached $Ma = 3$. During the test flight, more than 200 parameters were tested, including measurements of the combustion chamber wall temperature and pressure. No direct measurement of thrust was carried out in the test.

In flight tests, liquid hydrogen flows out and flows around the engine's combustion chamber to cool the combustion chamber. When liquid hydrogen cools the combustion chamber, it absorbs heat and becomes gaseous hydrogen. Gaseous hydrogen passes through a regulator and is injected into the combustion chamber by a row of nozzles. Depending on the flight conditions, it was decided to use a gaseous hydrogen injection to change the combustion mode.

Although this test is the world's first flight test to achieve a mode conversion from subsonic-combustion to supersonic combustion, the Russian Central Aero-Engine Research Institute believes that the test has not achieved 100 percent success, but only 80 percent success. This result is not caused by the engine, but by the control system. At that time, it was considered that the SA-5 missile was designed to intercept air targets and required a highly accurate control system; as a result, the original accurate height control system was replaced by a newly designed low-precision height control system. As a result, there was a deviation of 1.5 km in altitude and the flight speed was not stable enough. The situation was improved during later flight tests. This flight test verified the results of ground tests and theoretical research. However, it is not possible for the flight conditions at high altitude to coincide perfectly with the ground simulation. As a result, there were also situations in the tests that were not studied in the ground tests and could not be explained at the time. Later, the Central Aero Engine Research Institute conducted in-depth theoretical research on these problems.

2) Second test (November 17, 1992)

This is a joint Russian-French test. The flight speed is 1,535 m/s, the maximum flight altitude is 22.4 km, the flight Mach number Ma = 5.35, and the subsonic/scramjet engine working time is 41.5s. According to Russian reports, the second of the five flight tests of axisymmetric subsonic/scramjet engines was the most successful and the most complete data obtained, but it was rarely reported in detail (Fig. 10-3).

Figure 10-3: The test vehicle is ready for launch

3) Third test (March 1, 1995)

This experiment with France was a failure. Due to a failure of the power supply system, the missile did not reach the predetermined point. Its flight speed is 1712 m/s, its maximum altitude is 30 km, and its maximum flight Mach number is Ma = 5.8. Due to a problem with the power supply, the valve controlling the hydrogen fuel did not open, the hydrogen fuel did not enter the combustion chamber, and the test engine did not ignite to work.

However, the experiment did not cause a disaster.

4) The fourth test (August 1, 1997)

The fourth and fifth tests were carried out by the Central Aero-Engine Research Institute of Russia in cooperation with NASA of the United States, with a contract amount of $1.8 million. At that time, NASA proposed that the Mach number of flights was 6.5 > and strive for *Ma* = 7. However, Russia believes that such tests cannot be done, and even if the engine can reach *Ma* = 8, the test vehicle cannot fly in such conditions. The final test requirement is *Ma* = 6 to 6.5.

This contract called for improvements to the SA-5 test vehicle. Therefore, the purpose of the fourth flight was not to test the experimental engine, but to evaluate the improved SA-5 test vehicle. In the SA-5 missile, the wing is designed to increase lift and maneuverability, while in the test vehicle, it provides lift and also plays the role of a stabilization system.

Back in late 1990, before the first flight experiments conducted by the Central Aero Engine Research Institute, Russian aerospace officials visited several NASA research centers, including the Dreiden Research Center. During the visit, the outline of the “Cold” program was introduced, and the intention of cooperative development was proposed. Finally, in November 1996, an agreement was reached for joint development.

NASA continuously pursued the test of a *Ma* = 6.5 scramjet engine. The purpose of the joint U.S.-Russian pilot study is to:

• Verify the results of basic theoretical research;
• Verify the established mathematical models, software and correction systems;
• Achieve supersonic combustion;
• Calculation of thrust;
• Increased awareness of the complexities of flight tests;
• Compare the test equipment with the level of testing technology in the two countries.

In addition, the United States believes that the same program of the United States is much more costly, and that the joint testing method of the agreement is a low-cost and effective way to obtain valuable flight data, while Russia aims to use its equipment and site advantages to obtain funds for sustainable development.

5) The Fifth Experiment (February 12, 1998)

(1) Test the engine model. NASA's contract called for the redesign and manufacture of four identical test engines to improve the SA-5 launch vehicle. The U.S. side conducted structural tests and tests on two of the test engines at the Central Aero Engine Research Institute, and then transported them back to the NASA Langley Research Center for a new round of planned ground tests in a 2.438m high-temperature wind tunnel. The third is a test engine and the fourth is a backup engine.

(2) Design improvements. In order to obtain the expected full scramjet engine operating mode of *Ma* = 6.5 and better heat load requirements, the combustion chamber and active cooling system of the scramjet engine were redesigned, and the insulation material in front of the air intake tract was also required. The original *Ma* = 6 inlet center cone and geometry remain unchanged, because the two conditional geometries have little impact on the performance of the inlet tract.

The uncooled front inlet insulating material was replaced with a material with a higher heat capacity (called Fehral in Russia). The hot wall lining of the flow path is replaced by nickel alloy to copper. The good thermal conductivity of copper and the improved cooling channel design greatly improve the engine cooling performance, so that the engine can withstand longer test times in harsh flight conditions. The internal geometry of the combustion chamber has been improved to improve combustion efficiency and stability.

The design of *Ma* = 6.5 retains three combustion injection positions along the axial direction of the combustion chamber, each with 40 fuel injectors, distributed in a circular pattern along the engine.

The diameter of the fuel injector is about 2 mm, which corresponds to the angle of the longitudinal combustion chamber pipe shaft, and the first and second positions are determined to be 30°, and the third position is 45°. Between the first and second positions, the combustion chamber is lengthened to 45 mm. The second-position high-resistance flame stabilizer chamber is simplified to a simple backward stepped geometry. The liquid hydrogen fuel is circulated through the engine cooling liner to cool the combustion chamber and internal nozzles before being injected into the engine in gaseous form.

The SA-5 test booster was improved, which reduced the mass to 124kg and reduced the drag by 6%.

(3) Flight preparation. Preparations for the launch began on February 10, 1998. Despite the fact that the local ambient temperature began to drop, reaching -20° C at night and -10° C during the day, the refueling of the test vehicle engines with propellant and oxidizer began on February 11. The SA-5 test vehicle was carefully refueled in a safe area 6 km from the actual launch site. Then, it is slowly transported to the launch system detection position for detection.

On the morning of February 12, the weather was clear. Began refueling the test scramjet engine. In the first step, nitrogen is used to blow air from the entire engine's propulsion system. The blowing process is monitored until the air content in the exhaust is less than 0.002%. These steps are taken to prevent moisture in the air from forming in the system, which is also an important safety measure to ensure that all oxygen is removed from the system before hydrogen fuel is injected. The final step in the preparation process was to inject 18kg of liquid hydrogen fuel into the test engine over a period of about 2 hours, and when the fuel was fully filled, the ventilation ducts removed the remaining hydrogen.

(4) Test flights. At 2 p.m. on February 12, 1998, the ambient temperature was -10°C, the wind was level 2, and the wind was northerly. The SA-5 test vehicle carried out a successful launch at an angle of 52°, and the SA-5 flew 170km to the west with a flight duration of about 116s. Initially, it was boosted by a strap-on solid rocket booster for 5 seconds, and at 4 seconds of flight the scramjet engine began to simplify the flow pre-cooling with its liquid hydrogen fuel. At 18s, the rocket autopilot begins to give a dive command of 2.3°/s until 33s of flight, and then continues to fly to 57.5s with a constant pitch/altitude descending trajectory. After that, the autopilot pitch control system was disconnected, but the test vehicle completed the inertial flight trajectory until the command terminated the flight at 116s.

As can be seen from the recovery of the scramjet engine from the range 170 km from the launch site, the external mechanism of the engine is somewhat flattened. On-site testing found that there were no obvious burn marks in the inlet tract or combustion chamber section. After the engine was recovered from the test range, it underwent a relatively thorough flight inspection of the inner flow channel in Moscow. The results showed no signs of thermal damage to the inner engine.

According to the analysis of preliminary flight data, the entire engine underwent supersonic combustion with a near-optimal combustion/air ratio, and the engine also gained positive thrust. According to the Central Aero Engine Research Institute, this is the longest continuous work they have conducted in the flight test of a scramjet engine.

(5) Test evaluation. This joint Russian/American program gave impetus to the development of hypersonic air-breathing ramjet engines in the aerospace sector, bringing them to a new level of Ma = 6.5. Successfully completed the program of ground and flight tests of scramjet engines with 4 engines.

The program obtained valuable flight data for a range of flight conditions with a maximum of Ma = 3.5 to 6.45 and a fairly high dynamic pressure flight condition. Ground and flight test data have been analyzed and can be used to justify existing and future plans, and have become a valuable resource for information in the design of programs, including the U.S. Hyper-X.

Significant improvements to the “Cold” hypersonic flight test vehicle, scramjet test model and SA-5 launch system make the flight research system a valuable experimental equipment for hypersonic technology. Russia has developed a complete set of launch systems and permanent flight test bases, while studying ways to reduce the cost of testing scramjet engines, obtaining valuable data on flight and ground tests of full-scale test engines, and improving design methods. In addition, NASA and CIAM [ЦИАМ] work together on design, testing, engineering analysis and other research results.

In view of the many insurmountable difficulties encountered in practical application with axisymmetric subsonic/scramjet engines, Russia announced the completion of the “Cold” program after the completion of the five flight tests mentioned above (Table 10-1).

Table 10-1: Results of five flight tests of the "Cold" program

Date of the trial	1991.11.27	1992.11.17	1995.3.1	1997.8.1	1998.2.12
Maximum flight speed/(m/s)	1653	1535	1712	1832	1830
Maximum flight altitude / km	35	22.4	30	33	27.1
Maximum flight Mach number (Ma)	5.6	5.35	5.8	6.2	6.5
Scramjet engine working time/s	27.5	41.5	—	—	77

10.2: "Eagle" program

In consideration of the future application prospect and application background, the Central Aero Engine Research Institute has jointly developed the "Eagle" hypersonic technology development program (also known as the IGLA program) with the Central Aerofluid Power Research Institute in parallel with the "Cold" program (Figure 10-4).

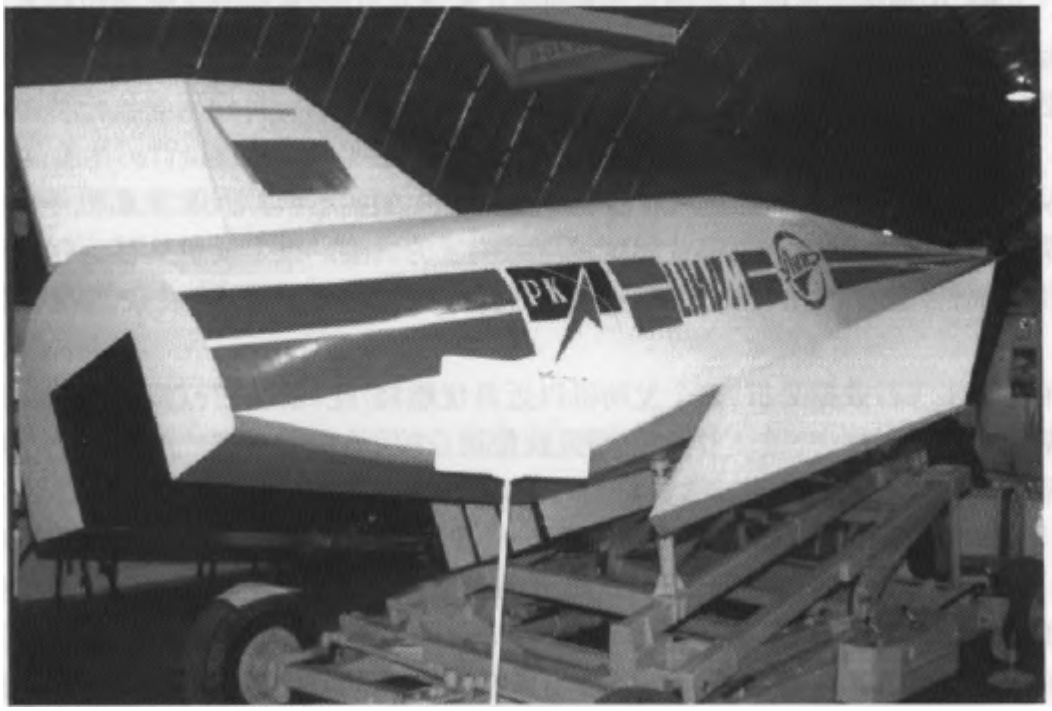

Figure 10-4: IGLA test vehicle

10.2.1: "Eagle" test vehicle

"Eagle" is a winged hypersonic test vehicle, the technical specifications of the vehicle are as follows:
Length: 7.9m;
Wingspan: 3.6m;

Mass: 2,200kg;
Mass of liquid hydrogen fuel carried: 18kg;
Test speed range: *Ma* = 6 to 14;
Flight altitude: 0 to 80 km.

The test vehicle adopts a lift body configuration, which is similar to the shape of the Buran space shuttle, with a head radius of 40 mm. According to the Central Aero Engine Research Institute, not many of the structural materials used in the test flights are new materials, which can be mass-produced in Russia (Fig. 10-5 to Fig. 10-7).

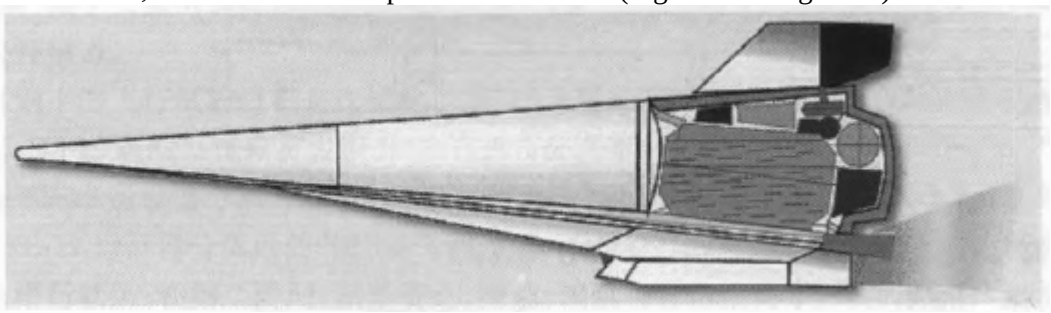

Figure 10-5: Eagle test vehicle

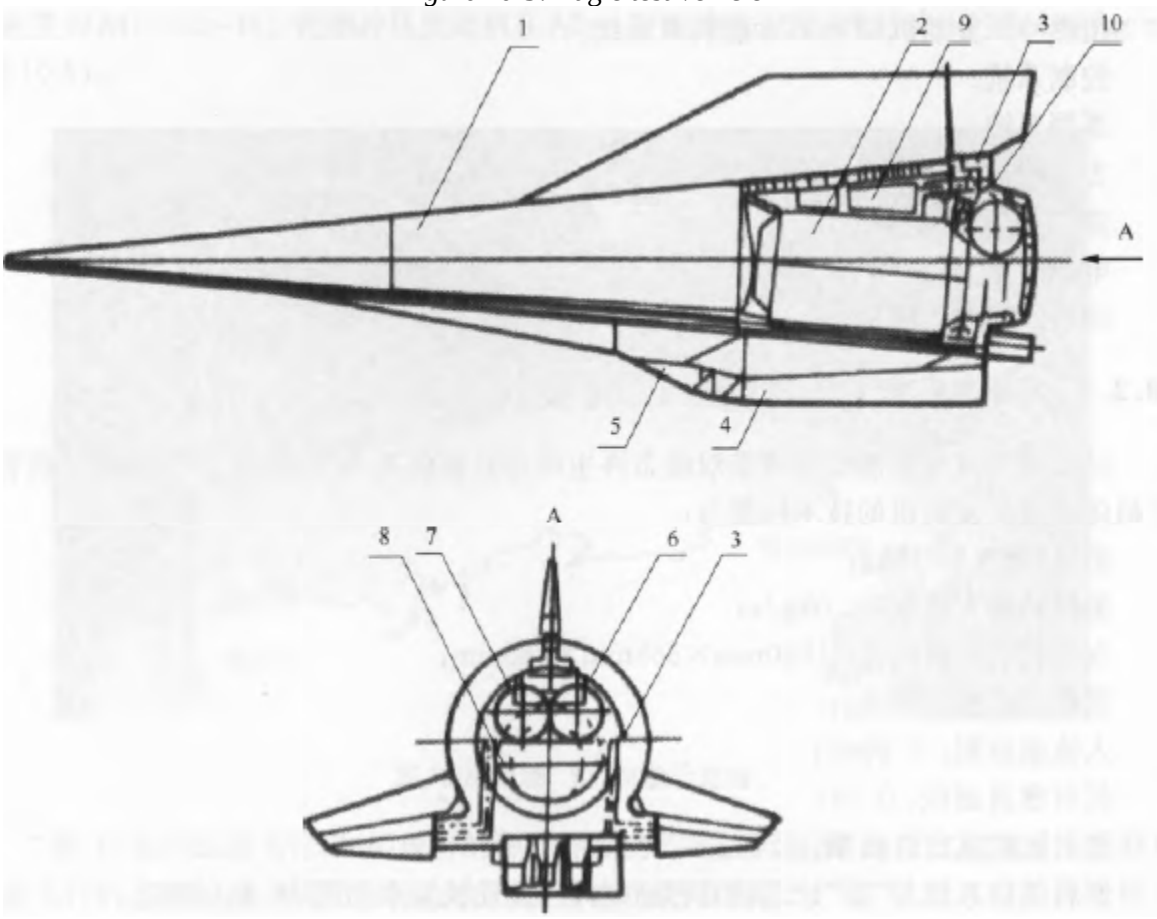

Figure 10-6: Schematic diagram of the structure of the Eagle test vehicle

1. Hypersonic test vehicle, 2. Liquid hydrogen fuel tank, 3. Rudder assembly, 4. Scramjet engine, 5. Tail,
6. Spherical nitrogen cylinder, 7. Spherical helium cylinder, 8. Recovery umbrella bag, 9. Telemetry system equipment, 10. Pressurized feedback system

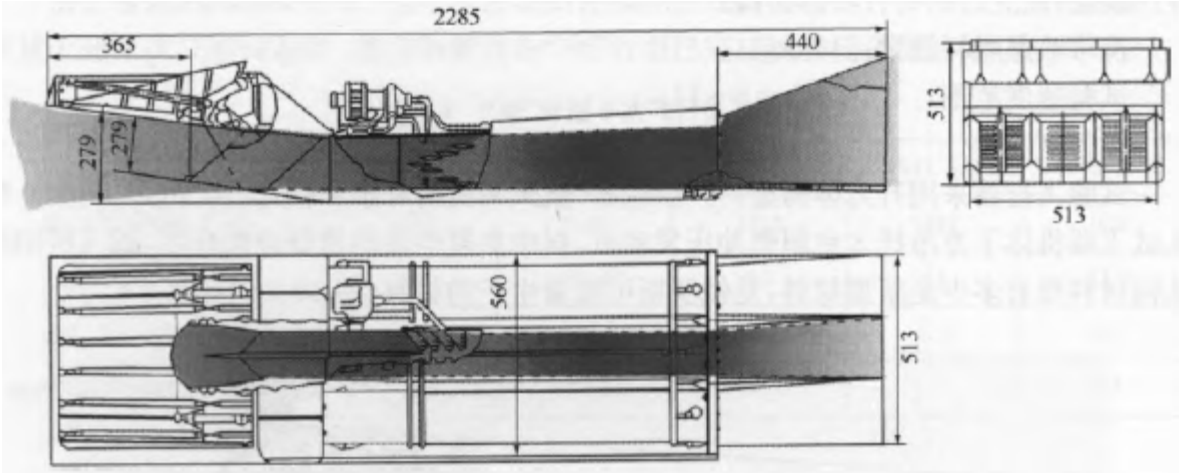

Figure 10-7: Diagram of the internal structure of the test engine

The "Eagle" superb winged test vehicle consists of the following components:

Airframe:

Triangular wing with rudder vertical tail

scramjet engines (3 units) (including fuel pump system);

control systems;

telemetry systems;

rudder-actuated electro-hydraulic system;

thermal control system;

power supply systems;

recycling parachute systems.

10.2.2: Scramjet test model

The test ramjet engine model is a two-dimensional dual-modal regenerative cooled scramjet engine, with the air intake tract and tail nozzle located under the fuselage. The technical performance of the engine is:

Fuel (liquid hydrogen): 18kg;

Maximum flow rate of hydrogen fuel: 1.0kg/s;

Engine geometry: 1,900mm X 565mm X 385mm;

Engine mass: 200kg;

Inflow cross-sectional area: 0.26m2;

Relative laryngeal area: 0.09;

Relative combustion chamber outlet area: 1.45.

The fuel supply system is essentially the same as the axisymmetric scramjet engine of the “Cold” program, with little change.

10.2.3: "Eagle" test launch vehicle

The launch vehicle of the "Eagle" hypersonic test vehicle uses the decommissioned SS-19 Stiletto intercontinental surface-to-surface strategic ballistic missile.

The missile, which has three variants, was deployed in the early 1970s and was developed by the Chelomeyi Design Bureau (now the Salyut Scientific Research and Production Complex) and manufactured by the Khrunichev Machine Plant. It has a range of 10,000km, a projectile length of 27.0m, a projectile diameter of 2.5m, and a launch mass of about 100t. The missiles were propelled by liquid rocket engines, launched from underground silos, and hundreds of SS-19 missiles were converted into "Rumble" commercial launch vehicles in batches. The modified SS-19 missile was used as a carrier of the "Eagle" test vehicle.

10.2.4: "Eagle" test

The "Eagle" has conducted a large number of ground tests and wind tunnel blowing tests, and has achieved important results, but there have been no public reports of flight tests.

The planned flight test process was as follows: the "Eagle" test vehicle was installed at the position of the warhead of the SS-19 missile; after being ready for launch, the SS-19 launch system was launched vertically; at an altitude of 80 km, it reaches a speed of 5,900 m/s. The "Eagle" test vehicle was separated from the SS-19 launch vehicle. Subsequently, the hypersonic test vehicle flew in the following four stages: in the first stage, the "Eagle" test vehicle separated from the SS-19 operator first reduced its altitude at a certain dive angle and turned into a taxiing state at a high altitude with high atmospheric density; in the second stage, adjust the attitude, roll, yaw and azimuth are zero, and maintain the cruising level flight state; in the third stage, the scramjet model test is carried out according to the given flight conditions; in the fourth stage, the scramjet engine is recovered and landed after combustion, and the test is completed. The entire test range is 6,000 to 8,000 km, and the flight speed is Ma = 12 to 14 when entering the third stage. The scramjet engine was tested in an ignition test at Ma = 10, at which time the dynamic pressure was about 5,000 kg/m^2 (Fig. 10-8).

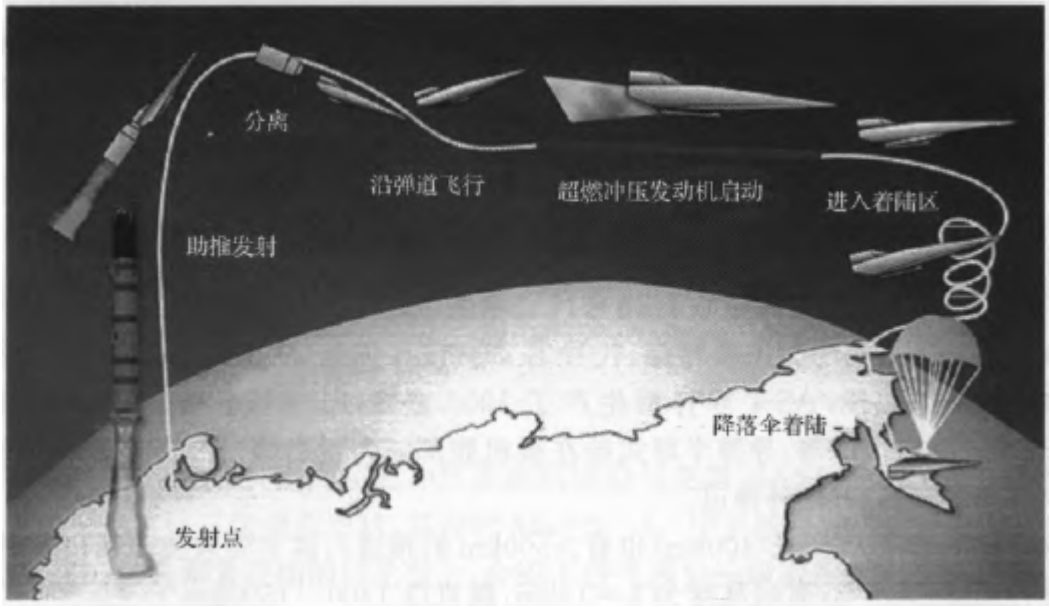

Figure 10-8: Schematic diagram of the flight test of the Eagle

The test flight of the "Eagle" program uses the existing ballistic missile tracking and control station to conduct telemetry, and it is also possible to use the satellite system to obtain various information about the test flight. Russia's vast territory and abundant range resources have provided extremely favorable conditions for the "Eagle" test flight.

10.3: Rainbow-D2 Project

The Rainbow Design Bureau and the Central Aero Engine Research Institute jointly developed a hypersonic technology development program, with the Central Aero Engine Research Institute responsible for the development of the scramjet engine and the Rainbow Design Bureau responsible for the development of the flight test vehicle. Subsequently, the German Aerospace Corporation, the German Aerospace Research Institute, and the Munich Turbine Engine Association also took part in the research of the program and successfully carried out tests in Germany. Although the Rainbow-D2 test vehicle was publicly exhibited at the 1997 air show, details of its subsequent performance are scarce (Figure 10-9).

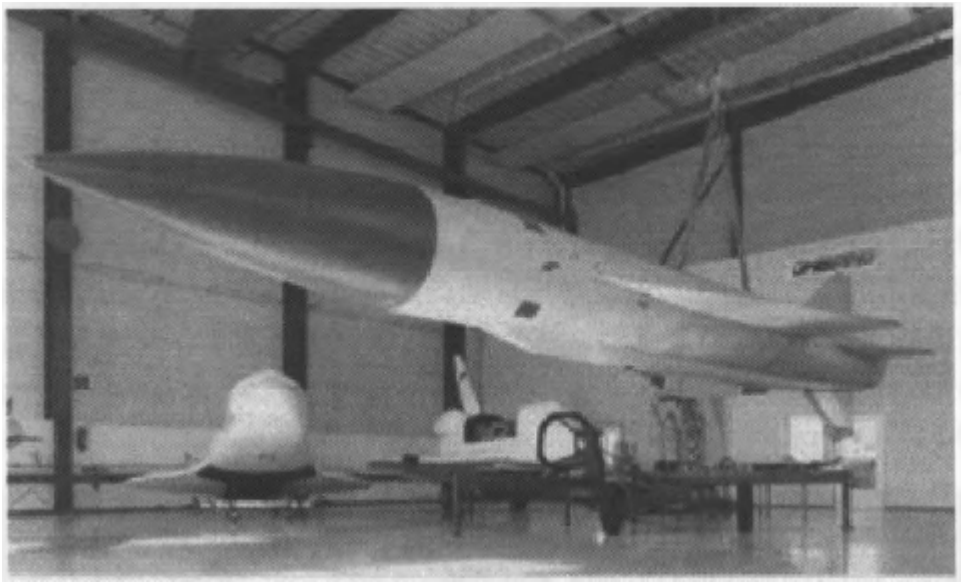

Figure 10-9: Rainbow-D2 test vehicle

10.3.1: Rainbow-D2 test vehicle

The Rainbow-D2 test vehicle uses the AS-4 (Kitchen) long-range strategic air-to-surface missile (Tug. 10-10) developed by the Rainbow Design Bureau itself, which is known as the Storm missile in Russia and codenamed X-22. The missile was developed at the end of the 1950s, and was equipped and put into service in 1964, and more than 1,000 AS~4 missiles were produced, and the technology is mature. Its carrier aircraft are Tu-95K, Tu-22K, Tu-22M2/M3, etc., and the missile is half-buried and hung on the belly of the carrier aircraft. In the belly of the fuselage is equipped with a special plate type to hang the missile. The missile has two types of ballistics: high and low.

The missile has a range of 300 to 400 km (> 500 km have also been reported), which depends mainly on the launch altitude of the carrier aircraft. The missile flies at a speed of Ma = 3, the cruising altitude is h = 15km, and the carrier aircraft launches the missile in flight conditions of 1,300 to 1,500 km/h (Tu-22M). The AS~4 missile is 11.3m long, 900mm in diameter, 3.0m in wingspan, and has a launch mass of 4,900kg. The missile is equipped with a 350kt TNT-equivalent nuclear warhead or a 1,000kg conventional warhead with a large payload. Thus, the modified missile is sufficient to carry a test engine and test equipment with a payload of > 800kg.

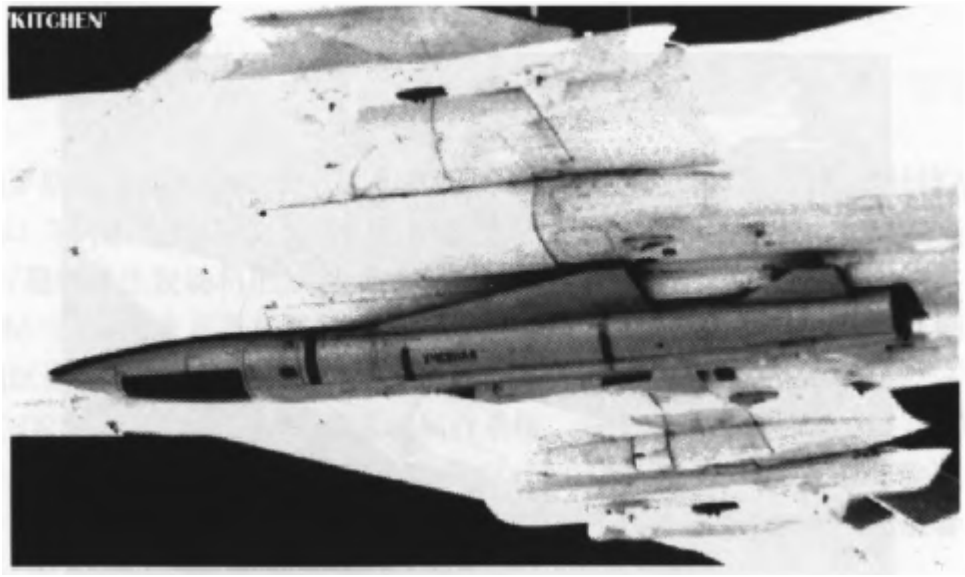

Figure 10-10: Schematic diagram of the AS4 missile

Modified test vehicle performance:
Range: 570km;
Flight speed: *Ma* = 2.5 to 6.5;
Flight altitude: 15 to 30 km
Maximum speed duration: 70s.
Testing & Test Equipment:
Mass: 700kg;
Volume: 1.5m3;
Geometric size: 0.65mX0.7mX6.0m.

The test and test equipment are installed in the fairing in the middle and lower parts of the missile body and under the projectile body. Test data were detected by aerial helicopters and ground telemetry stations.

10.3.2: Experimental scramjet model

The scramjet model of the Central Aero Engine Research Institute is different from the engine model of NASA in that its intake tract is in the shape of a three-stage wedge, and its design is *Ma* = 5~7. At a discussion meeting with the Japanese hypersonic vehicle technology research group, the Central Aero Engine Research Institute introduced the issue of whether there is a separation of surface layers in the three-stage or four-stage inclined plane configuration of the air intake and reported the results of the test. It shows that because there is no separation of the surface layer, the design structure of the three-level inclined plane is simple. However, the specific situation of the combustion chamber is not introduced. The test engine was subjected to direct-coupled and free-jet tests on the T-131Б and T-131B supersonic combustion test benches of the Central Research Institute of Aerofluid Dynamics. The presence of pillar-like protrusions and wing-shaped ejectors from the front of the engine suggests that they were used in the tests, but it is unclear whether they were used in ground or flight tests (Figs. 10-11 and Fig. 10-12).

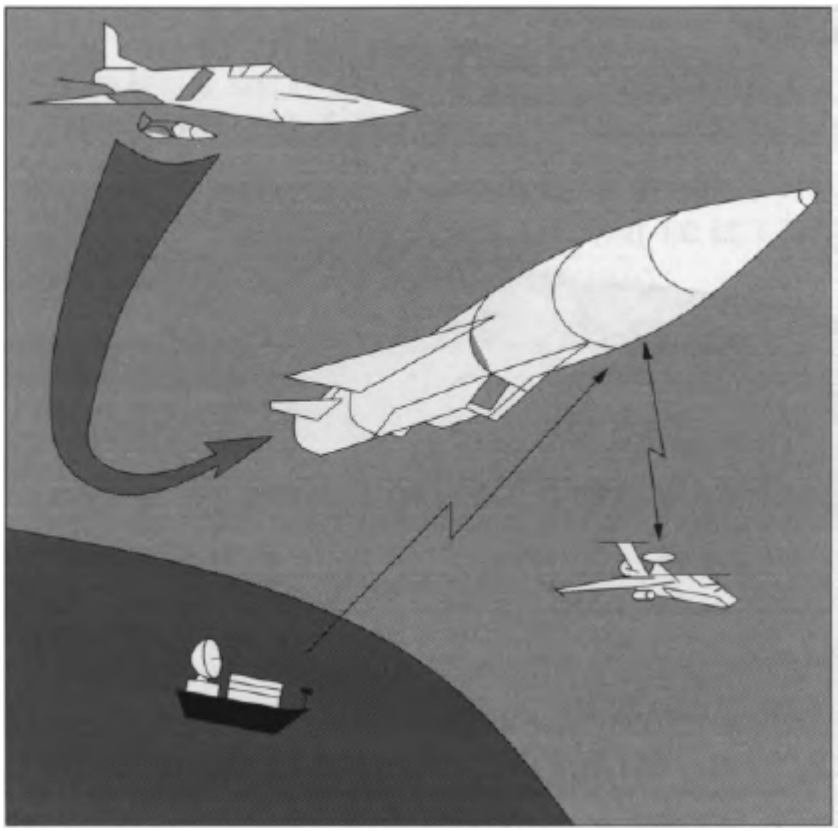

Figure 10-11: Flight test system diagram

Figure 10-12: A model of a test scramjet engine

10.3.3: Flight Tests

Although the Rainbow Design Bureau conducted a large number of ground tests with TsAGI [ЦАГИ], there are no detailed reports of flight tests of the Rainbow-D2 to date.

Judging by the Russian materials, flight tests of the Rainbow-D2 do not have anything unique about it. After making technical preparations, it was lifted off by the Tu-22M3 aircraft carrier to launch the Rainbow-D2 test vehicle under predetermined flight conditions; the aircraft completes the test of the subsonic/scramjet engine under program control; recovery is then carried out with a parachute at the intended landing site. During the flight, the Tu-22M aircraft and Mi-8 helicopters control the aircraft, and the ground station receives telemetry information; the Mi-8 helicopter returned the test engine and test equipment for evaluation.

The Rainbow D2 test vehicle has a complex recovery system. It uses a three-stage parachute recovery with a deceleration of the first two stages, and its area is 10m2, 24m2, respectively. At an altitude of 1.4 km, the 750 m2 recovery main parachute was opened, and the test vehicle was reversed 180 degrees up and down, that is, the belly where the test engine and test equipment were located were facing upward, to prevent damage to the test equipment when landing at a speed of 9 m/s (Figure 10-13).

Full bomb recovery is adopted, and the test vehicle and the test engine are not separated. The test vehicle was scrapped after use, and the test engine was evaluated and qualified. According to the Rainbow Bureau, the head hit the ground first during the recovery, and the head was damaged, and the test engine and test equipment were safe.

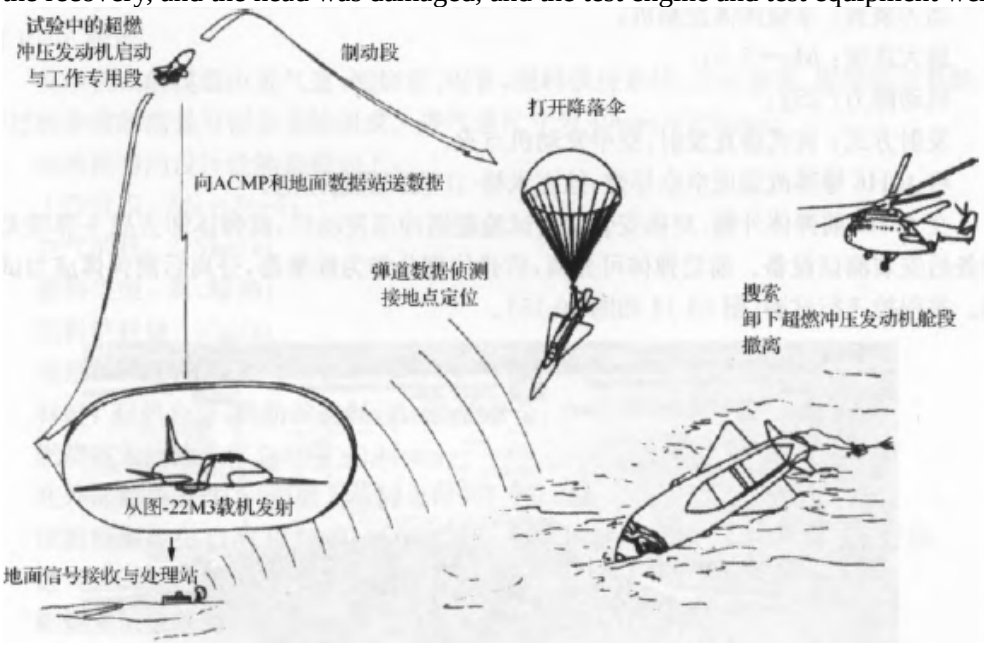

Figure 10-13: Schematic diagram of the recovery of the Rainbow-D2 test vehicle

10.4: Project “Eagle-31”

The program was carried out jointly by the Tulayev Union Design Bureau, the Torch Design Bureau, and the MiG Design Bureau. The Soyuz Design Bureau was responsible for the development of the test engine, the Torch Design Bureau was responsible for the development of the test engine, and the MiG Design Bureau supplied the MiG-31 experimental carrier aircraft.

10.4.1: Test Pilots

The test vehicle of the "Eagle-31" supersonic test program is the 40H6 missile in the C-300A (C-300B is the Gladiator SA-12 system) surface-to-air missile system.

The C-300 system is Russia's advanced long-range, medium-altitude defense system, named Grumble in the West, codenamed SA-10. The system is developed by the diamond research and production consortium, which is divided into type A C-300II, type B C-300IIMy, and type C C-300IIMY-1. Type A uses 5B55K missiles, Type B uses 5B55P missiles. Type C is the latest with anti-missile capabilities and uses 40H6 missiles. All types of missiles were developed by the Torch Design Bureau. Technical performance of the missile:

Range: 150km (max);
Shot height: 27km(max);
Length: 7.5m;
Bore: 515mm;
Wingspan: 1.14m;
Launch mass: 1,800kg;
Power plant: single-stage solid engine;
Maximum speed: *Ma* = 5.5;
Maneuverability: 25g;
Launch mode: vertical launch of cartridge type, ignition of air engine.

The 40H6 missile was converted into an air-to-air missile, hung on a MiG-31 belly launcher.

On the outside of the 40H6 front bomb, two test scramjet engines are symmetrically installed, and test equipment is installed after the warhead and other unrelated equipment are removed from the front bomb. The front and rear projectiles can be separated, the rear projectile body part is used as a booster, and the front projectile body becomes a test vehicle after separation. Programmable flight test (Figures 10-14 and 10-15).

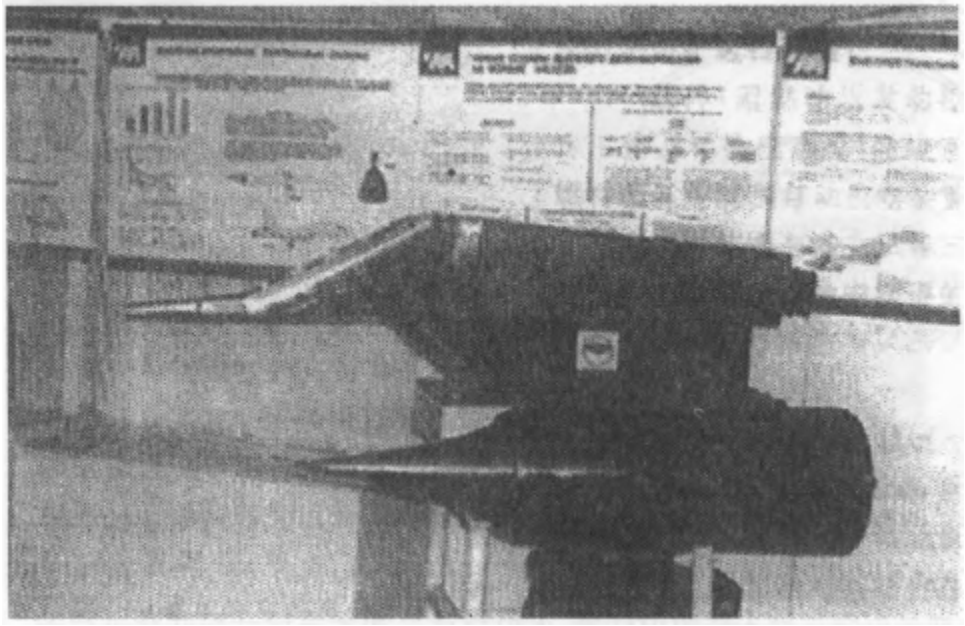

Figure 10-14: Scramjet engine of TMKB-Soyuz [ТМКБ-Союз] design

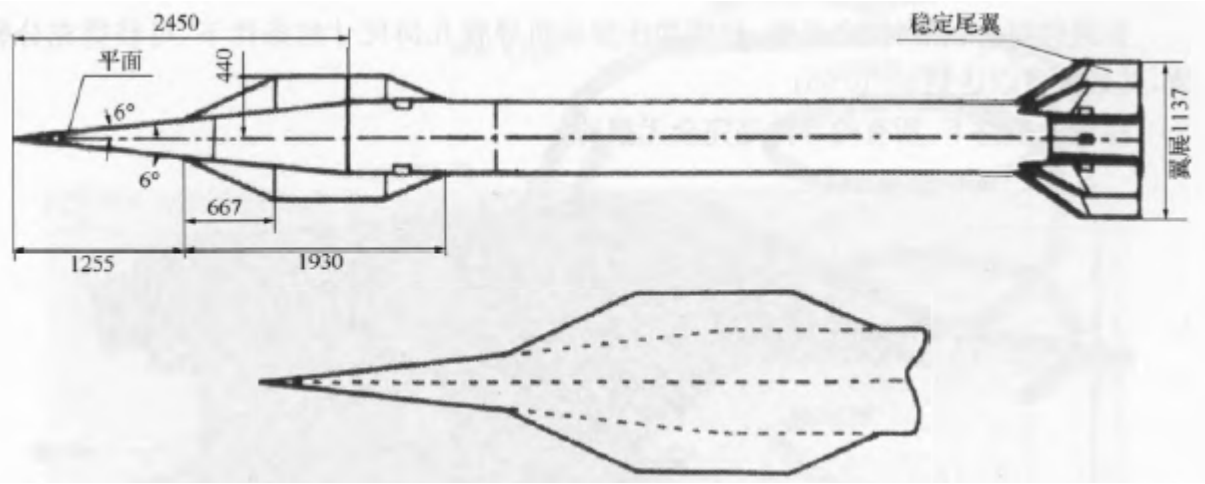

Figure 10-15: 40H6 missile with test vehicle

10.4.2: Test model of subsonic/scramjet engines

The test model of the subsonic/scramjet engine designed by TMKB-Soyuz [ТМКБ-Союз] is a two-dimensional two-modal engine, as shown in Figure 10-16.

The engine test model consists of an air intake, combustion chamber, nozzle, fuel supply system, ignition device, combustion stabilization system, and a measurement and recording system for working process parameters. The size of the intake tract is 40mmX100mm.

The design performance parameters of the experimental model are as follows:

Working range: *Ma* = 5 to 6;

Air consumption: 2.5kg/s;

Fuel Type: Hydrogen, Kerosene;

Fuel consumption: 60g/s;

Mass: 60kg;

Material: heat-resistant alloy, thermal protection material, iron-stroke-recruitment alloy;

Total trouble-free working time of combustion chamber: 180min;

Under external heat dissipation conditions, the total trouble-free time of the model: 60 minutes.

The test model has been tested on the ground in TsAGI [ЦАГИ] and CIAM [ЦИАМ], and the test content and conditions are:

Inlet test range: *Ma* = 3 to 6, *Re* = 1,000,000;

Combustion chamber test range: *Ma* = 2 to 2.5, T = 1100 to 1930K;

Combined test range of inlet tract and combustion chamber: *Ma* = 5 to 6.2, T0 = 800 to 1970K;

fuel supply and fuel gasification systems;

Scramjet engine start-up procedure.

The main results of the ground test study are:

Through the test, it is proved that in the range of *Ma*, *Re*, T_0 and other parameters (*Ma* = 1.1 to 1.2), supersonic stable combustion can be achieved in the combustion chamber

With the selected fuel supply and mixing system, stable ignition and combustion of the air-fuel mixture can be achieved (starting from T_0) = 1260 K, *Ma* = 5, *a* = 2.2 to 6);

Under the conditions of optimal combination, fuel mixing system, and scramjet duct geometry, full combustion can be obtained, and its efficiency can reach η= 0.95;

Under the test conditions, all components were completely non-destructive.

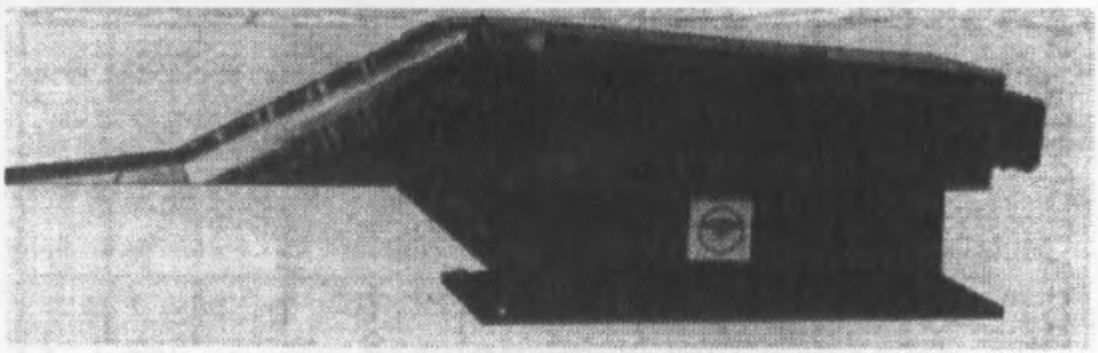

Figure 10-16: Model of subsonic and supersonic ramjet engine with TMKB-Soyuz [ТМКБ-Союз]

10.4.3: Flight Tests

Many problems were solved in the TsAGI [ЦАГИ] and CIAM [ЦИАМ] ground tests and wind tunnel tests (*Ma* = 4 to 7). However, the ground laboratory can only carry out engine combustion under normal flight conditions, and the material cooling system test cannot fully give the real dynamic pressure and flight conditions at high altitude. To do this, it was also necessary to conduct flight tests of a hypersonic test vehicle, with a scramjet engine as part of the test vehicle to study the real flight conditions at *Ma* > 6, H = 15 to 40km.

The objectives of the planned flight tests are as follows:

At *Ma* = 4 to 12, the supply process of the fuel combustion process;

Study of the start-up process of a large scramjet engine (repeated start at any predetermined ballistic point or scramjet engine when the scramjet engine is turned off);

Evaluate the range of fuel combustion stability in the combustion chamber;

Select the normal operating range of the intake, combustion chamber and nozzle and evaluate their performance;

Determine the fuel consumption and thrust values during the flight;

Evaluation of thermal protection against high-temperature conditions and large scramjet engines;

Selection of fuel injection systems and automatic controls for the combustion chamber (when scramjet engines work stably and when changing modes);

Comparing test data of ground and high-altitude tests, and comparing and analyzing the characteristics of the air inlet and combustion chamber obtained from the flight test with the characteristics of the wind tunnel test.

When designing a model of a scramjet engine for ground tests, the TMKB-Soyuz [ТМКБ-Союз] took into account the integration with the test vehicle and combined it with it to the maximum extent possible in order to finally test the maturity of its design.

The flight test process of the "Eagle-31" is arranged as follows (as shown in Figure 10-17): the modified test vehicle is hung on the belly of the carrier aircraft MiG-31, and the horizontal acceleration at an altitude of 15 to 17 km after the carrier aircraft reaches the test area is 50 to 60 seconds, and the flight speed of the carrier aircraft can reach *Ma* = 2.5 to 2.6 at this time; then climb with a maneuvering capacity of 2.5 to 3.0g; after 20 to 30 seconds of climbing, the large hypersonic test vehicle separates from the carrier aircraft at a flight trajectory angle of 20° to 30°; after reaching the safe distance of the carrier aircraft (3 to 5 seconds after separation), the booster (40H6 missile) is ignited;

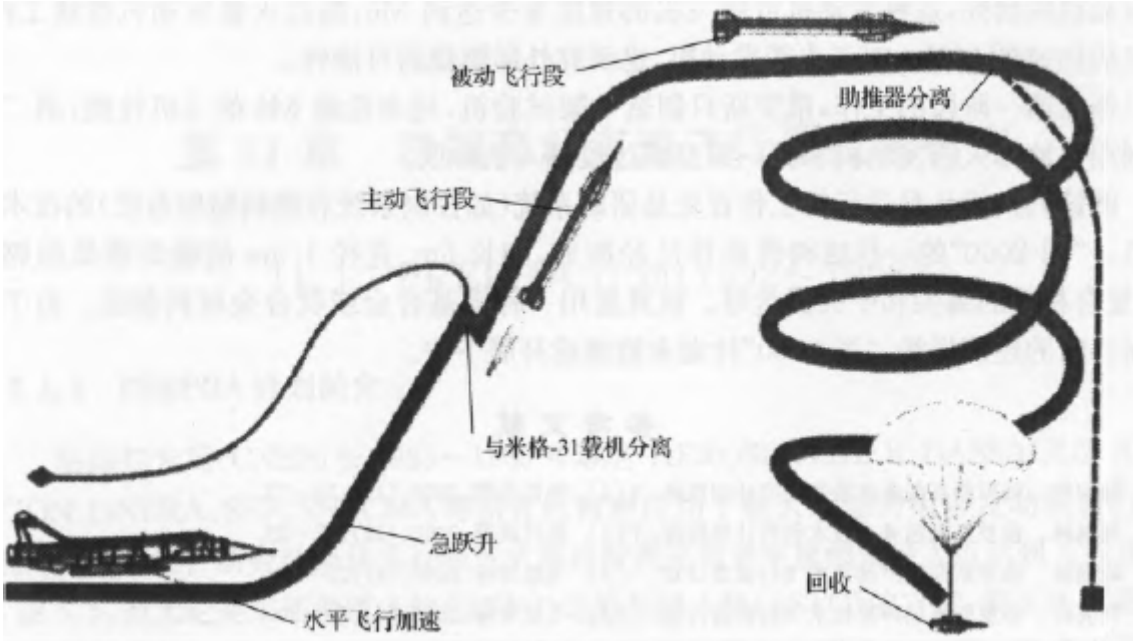

Figure 10-17: Schematic diagram of the trajectory of the test flight

After 25s, the flight Mach number of the hypersonic test vehicle reaches *Ma* = 10; after two flight stages, the large hypersonic test vehicle was transferred to a horizontal, zero-angle of attack stable flight (the test scramjet engine was ignited and in an active working state); after the test mission, the test vehicle was separated from the booster (the middle and rear missile bodies of the 40H6 missile) and recovered by parachute for analysis and evaluation. Flight conditions are pre-set before the test; the flight speed is *Ma* = l.8 to 9.8, the flight altitude H = 15 to 40km, and the dynamic pressure is 10 to 200kPa. The test scramjet engine had a test working time of 40 seconds at the maximum Mach number.

TMKB-Soyuz [ТМКБ-Союз] is confident in this scheme and considers it a feasible and low-cost solution. This is because they have adopted their own developed aircraft and equipped with missiles with mature technology, which can be tested with minor modifications. In addition, the carrier aircraft is launched at a high altitude at a speed of *Ma* > 2.5, which greatly reduces the requirements for the booster, is technically easy to implement, reduces the quality of the booster system, and saves money.

10.5: Study of the hypersonic aircraft "Tu-2000"

The Russian Tupolev Design Bureau began designing the Tu-2000 hypersonic aircraft from 1986 on. The main purpose is to compete with the American Aerospace Aircraft Program (NASP). At the Moscow Air Show in August 1992, Russia presented a mock-up of the Tu-2000 aircraft, which resembles the American X-30 aircraft in appearance. More than a dozen Russian design bureaus were involved in the research work on the Tu-2000.

The Tu-2000 aircraft is considered to be equipped with three types of propulsion units: a military-type turbojet engine, a scramjet engine and a rocket engine for orbit. The Tu-2000 runs only on hydrogen fuel. Tests of the liquid hydrogen-fueled engine on the Tu-154 aircraft have shown that the technical staff is well equipped to solve the various technical problems of this cryogenic propulsion system, especially all the technical problems related to gas expansion and control in the supply system. The Tu-2000 is designed with eight scramjet engines, mounted underneath the rear body.

The Central Aero-Engine Research Institute of Russia and the Tulayev Union Design Bureau carried out research on a scramjet engine that allowed the aircraft to reach speeds of at least M6, after which the rocket engine continued to work, accelerating the aircraft to M25. For rocket engines, the possibility of external combustion is also studied.

As the first phase of work, Russia built only one test aircraft to test the performance of the M6 aircraft; the second stage transitions to orbit with a liquid rocket engine and another prototype.

The work carried out by the Tupolev Design Bureau began first of all with the development of a technical demonstrator for systems such as control systems and fuel injection systems. Some structural components of the Tu-2000 have been fabricated, such as a 5m long and 1.5m diameter carbon fiber cryogenic fuel tank, composite wingtips and central wing boxes, etc. The wing box is manufactured with a nickel-based alloy or titanium alloy material. Due to the economic situation in Russia at that time, the Tu-2000 program could not be continued.

References

[1] Liu Tonglin. Russian Hypersonic Technology Research Program. Part 1 [J]. Modern Weapons, 2000, (11):35-37.
[2] Liu Tonglin. Russian Hypersonic Technology Research Program. Part 2 [J]. Modern Weapons, 2000, (12):27-29.
[3] Liu Tonglin. Russian Hypersonic Technology Flight Test Program. I [J]. Flight Missile, 2000, (4):23-30.
[4] Liu Tonglin. Russian Hypersonic Technology Flight Test Program. II [J]. Flight Missile, 2000, (5):28-30.
[5] Liu Tonglin. Russian Hypersonic Technology Flight Test Program. III [J]. Flight Missile, 2000, (6):17-23.
[6] Liu Tonglin. Russian Hypersonic Technology Flight Test Program. IV [J]. Flight Missile, 2000, (7):18-23.
[7] Cong Min. Russia continues to develop hypersonic propulsion system [J]. Flying Missile, 2010, (2):9-10.

CHAPTER 11: FRENCH HYPERSONIC VEHICLE TECHNOLOGY RESEARCH

11.1: PREPHA program (1992~1998)

11.1.1: PREPHA program introduction

From 1985 to 1989, the French space agency (CNES) cooperated with AEROSPATIALE, DASSAULT AVIATION, ONERA, SEP, SNECMA, and other research institutes to conduct a systematic evaluation study of combined engines used in space transportation. the results of the study suggest that subsonic combustion can reach a maximum flight Mach number of 6 or 6.5 in the air-breathing propulsion stage, but it is impossible to achieve fully reusable space transportation by using two-stage orbit entry (TSTO) or single-stage orbit entry (SSTO). Therefore, it is recommended to further explore the possibility of using supersonic combustion to achieve reusable space delivery.

In 1992, France launched the French National Research and Technology Development Program for Advanced Hypersonic Propulsion, referred to as the PREPHA program, which was supported by the French Ministry of Defense, the Ministry of Research and Technology, and the French National Space Agency. Given France's research base in ramjet technology, PREPHA plans to focus on hydrogen-fueled scramjet engines as well as ground trials. Five research institutes in France, AEROSPATIALE, DASSAULT AVIATION, SEP, SNECMA, and ONERA jointly formed a research team called G5 to carry out the program [1~5].

The research and application prospects considered by the PREPHA program are large-scale scramjet engines for space launch vehicles, as shown in Figure 11-1. However, due to the complexity of the construction of the test system and the cost constraints, it was not possible to carry out full-scale scramjet test research on the ground, so the PREPHA project decided to carry out the research based on the close combination of numerical and experimental methods, and set the goal of developing a method of numerical and experimental research to meet the needs of the research on a general-purpose single-stage orbiting vehicle. On the other hand, the PREPHA program is positioned to obtain a first-hand technical approach to the design of scramjet engine components.

The PREPHA program focuses its research efforts on the following five themes:
design and ground testing of scramjet engine components for testing;
development of relevant ground test equipment;
study of physical models and numerical calculation methods;
materials;
systems research.

11.1.2: Establishment of the test setup

A significant portion of the PREPHA project effort has been devoted to the construction of new test installations, which have further expanded the understanding of the mechanisms of physical phenomena of high-velocity air flow and blended air flows, and have carried out experimental studies on scramjet combustion chambers and experimental studies to evaluate the properties of high-temperature materials in typical environments.

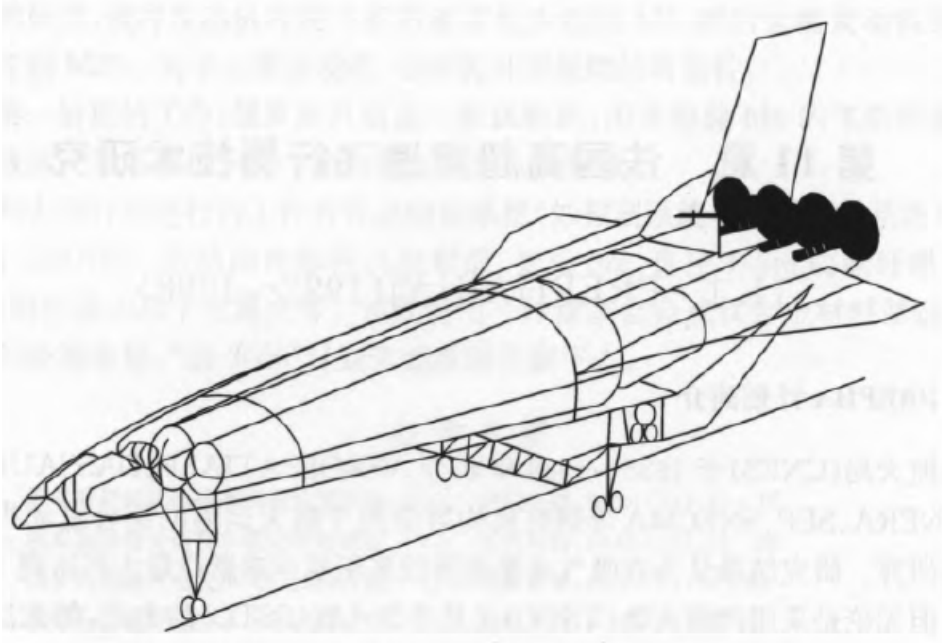

Figure 11-1: Conceptual design of a single-stage orbital aerospace aircraft in the PREPHA program

1. ONERA's supersonic combustion test device

1) ATD 5

France has a strong research strength in ramjet engine research, and has a number of test benches that can be used for the research of solid fuel ramjet engines and liquid fuel ramjet engines, with a maximum test capacity of simulated flight conditions of $Ma = 4.5$.

With the support of the PREPHA program, ONERA built a new test unit called ATD 5, which was used to carry out experimental studies of a direct-coupled scramjet engine that burns hydrogen and a heat exchanger to heat the air to obtain the required air temperature with a maximum simulated flight of $Ma = 7.5$. The main performance indicators of the test bench are:

Air flow: 4kg/s;

Total incoming pressure: 4MPa;

Total incoming temperature: 2400K;

Hydrogen fuel flow: 300g/s;

Total hydrogen fuel pressure: 8MPa;

Total hydrogen fuel temperature: 300K;

Cross-section of test section: 100mmX100mm.

In addition to the test chamber of scramjet engines, the test bench is also used for basic research on fuel injection, experimental studies of injector configurations, and evaluation of the heat resistance of materials.

2) LAERTE

LAERTE is used to carry out detailed studies of supersonic combustion, including the use of optical measurement methods such as CARS, LIF, Rayleigh Scattering, etc. The experimental study of helium/air blending and hydrogen/air blending and combustion processes has been carried out in this pilot plant, and a large number of valuable test data have been obtained. The performance indicators of the test bench are as follows:

Total incoming temperature: 1800K;

Total incoming pressure: 8 bar;
Total nitrogen temperature: 650K;
Total nitrogen pressure: 8.5 bar;
Total hydrogen temperature: 500K;
Total hydrogen pressure: 8 bar;
Test section cross-section: 45mmX45mm.

3) S4MA Wind Tunnel

S4MA is a hypersonic wind tunnel for aerodynamic testing of re-entry aircraft, which can provide heating without water vapor pollution for 30kg/s of incoming air through alumina pebble heating bed, with a maximum simulation capacity of flight Ma = 6.5, a total temperature of 1800K, and a total pressure of 150 bar.

In the PREPHA program, the wind tunnel was considered to improve its performance in order to carry out free-jet tests on larger scramjet engines with a test capacity of Ma = 7.5, a total incoming temperature of 2400 K, and force tests on scramjet engines with partial air intakes and nozzles. However, due to research funding constraints, the improvement plan was not implemented, but the wind tunnel still has the potential to test scramjet engines.

2. AEROSPATIALE's scramjet test device

With the support of the PREPHA program, a new ramjet test unit was built in France to carry out experimental studies on the combustion chamber of large-scale scramjet engines, the main performance indicators of which are as follows:

Air flow: 100kg/s;
Total incoming pressure: 8MPa;
Total incoming temperature: 1800K;
Hydrogen fuel flow: 1.5kg/s;
Total hydrogen fuel pressure: 6MPa;
Total hydrogen fuel temperature: 300K.

The test bench can be used for the test of the combustion chamber of a large-size hydrogen or hydrocarbon fuel scramjet engine with a cross-sectional size of 200mmX200mm and can also be used to verify the thermodynamic properties of the structural thermodynamic properties of the inlet tract or nozzle of different geometric configurations, the fuel injector structure and the fuel injection structure of the support plate.

3. Material testing device

The ONERA ATD 5 test bench and the AEROSPATILE hypersonic wind tunnel described above can also be used to study material properties. Tests of active cooling systems made of thermally structural composites have been carried out on the ATD 5 test bench.

In order to carry out more detailed experimental studies to evaluate the thermal properties of materials, a new test bench called BLOx4 was built in the PREPHA project, which can simulate typical and specific flight environments, and to conduct experimental analysis of the oxidation process of materials used to make engine and aircraft structures.

4. Development of measurement technology

The PREPHA program also supports the development of high-temperature airflow measurement technologies, including pressure sensors, thin-film thermal sensors, surface friction measurement technologies, spectral temperature measurement technologies, and equipment and technologies such as actively cooled pitot rakes.

11.1.3: CFD Numerical Calculations

In the PREPHA project, ONERA improved and developed a number of numerical calculation procedures for the characteristics of thermochemical reactions in hypersonic flow and carried out corresponding experimental studies to improve and verify the physical models used and evaluate the accuracy of the calculation procedures.

For the aerodynamics of external flow, a computational program called FLU3M was developed, which combines multiple methods for solving equations (Euler, PNS, NS), speculative flow models, gas effect models, and multi-zone solutions. Experiments to investigate the flow mechanism to validate and improve the physical model used in the procedure were carried out, including:

boundary layer transition and the development of the forebody boundary layer;

shock-shock interference and shock-boundary layer interference in the intake tract;

development of boundary layers of half-wall nozzles;

mutual interference of internal and external flows at the outlet of the nozzle.

For thermochemical reactive flows, ONERA has developed a program called MSD, which solves the unsteady 3D N-S equations using a finite volume method for multi-zone structured meshes, with the option of different turbulence models as well as combustion models. MSD also has the ability to solve parabolic N-S, and can quickly and cost-effectively perform numerical calculations of three-dimensional full-propulsion flow channels by coupling the full N-S equation and the PNS equation.

The understanding and modeling of fuel mixing and combustion processes in combustion chambers is the result of a number of mechanistic experimental studies carried out by laboratories affiliated to the National Center for Scientific Research (CNRS) and ONERA, which provide detailed analyses of the air/hydrogen mixture and combustion processes through the use of optical diagnostic techniques (LIF, CARS, etc.).

The simultaneous implementation of experiments and numerical calculations, as well as the comparison of results, helped to improve the CFD numerical calculation procedures, which already had the ability to design scramjet engine components.

11.1.4: Scramjet engine component research

For each of the scramjet components, a conceptual design study was carried out in the PREPHA program to define a feasible component design. Based on the preliminary design of the component, combined with the ability to consider the test equipment, a scaled-out model was designed for experimental studies with the aim of estimating its performance and examining the impact of the main parameters.

1. Forebody

For the forebody of the hypersonic vehicle, the design parameters were studied by numerical calculation, including the bluntness of the head, the curved form of the windward side, and the influence of the width of the head. In addition, a forebody design configuration was experimentally studied in ONERA's S4MA wind tunnel, and the wall pressure, heat flux density, infrared thermal imagery, and the total/static pressure of the inlet section were measured. The results obtained are used to improve the numerical calculation procedure, which helps to better predict the flow at the inlet of the inlet and the thermal load on the surface of the forebody.

2. Intake tract

Due to the technical difficulties, only a fixed geometry of the combustion chamber was considered in the PREPHA program, but under different flight conditions, the capture area of the air inlet could be changed to produce the corresponding geometric shrinkage ratio at different Mach numbers. This variable geometry of the inlet channel ONERA has been studied for many years, and this concept has been applied to the design of SSTO aircraft to meet their needs and constraints.

After the numerical design study, the inlet model was experimentally studied in ONERA's R2Ch wind tunnel with *Ma* = 5 and 7, and a special device was used to assist in the activation of the air intake, so that the geometric shrinkage ratio could reach 4, and the large declination angle would not cause much length.

After the initial experimental study, the research further focused on the intake tract of the scramjet engine modal operation, and a new test model was designed and constructed, and tests were carried out in the ONERA S3MA wind tunnel from *Ma* = 2 to 5.5, with the aim of studying the maximum shrinkage ratio, the effect of the thickness of the forebody boundary layer, the maximum declination angle of the compression surface, etc.

The test results are in good agreement with the predictions of numerical calculations, but due to the constraints of planning funds, the design optimization cannot be further completed. However, the results of experimental studies have confirmed that there is no reason to assume that the inlet tract has high performance in such a wide range as *Ma* = l.5 to 12, especially for single-stage orbital space launch vehicles, which have strict mass flow limits.

3. Nozzle with rear body

The research focuses on the single-wall expanded nozzle (SERN), and the influence of different design parameters is studied by numerical simulation, including the lower wall surface and its length of movable or fixed nozzle, and the curved surface form of the expansion surface. From the perspective of the global optimization of the aircraft, a short fixed downward slope lower wall surface and a limited expansion surface height were finally selected.

DASSAULT AVIATION and ONARE designed a rear-body nozzle test model with an internal hydrogen heater, which was tested in the s4ma wind tunnel with a *Ma* = 4. The test results are helpful to evaluate the adaptability and accuracy of the numerical calculation program FLU3M to the calculation of the flow field of the rear body nozzle, and the influence of different design parameters on the interaction between the gas and the outer surface boundary layer of the aircraft can be further studied through the verification and verification procedures.

The test model from the above tests can also be used in ONERA's S3MA wind tunnel to investigate the overexpansion of the nozzle at low Mach numbers. However, due to program funding constraints, the trial was not able to be carried out under the PREPHA program. However, it should be pointed out that the change of thrust vector at low Mach numbers seriously affects the overall performance of SSTO aircraft.

4. Combustion chamber

The main part of the PREPHA program focused on the study of scramjet combustion chambers, and two experimental combustion chambers, the CHAMOIS combustion chamber and the MONOMIT combustion chamber, were prototyped.

The CHAMOIS combustion chamber was designed by AEROSPATIALE on the basis of numerical calculations. The design of the test model overcomes the constraints of the size of the test setup (inlet cross-section 212 mm X 212 mm) and reflects to the greatest extent possible the characteristics of a large combustion chamber:

support plate fuel injection structure;

the interaction of the wall with the fuel injection of the support plate;

the interaction between the support plate and the fuel injection of the support plate;

inhomogeneity of the incoming stream (including the boundary layer and shock waves caused by the incoming wedge, etc.).

The first step of the pilot study was carried out on the ONERA ATD 5 test bench and data on fuel injection permeation, air/hydrogen ignition, fuel/air blending and combustion stabilization were obtained. At the same time, the numerical calculation was carried out by AEROSPATIALE, SEP and ONERA, and the structures of different fuel injection plates were compared, and finally the two structural schemes were selected and tested separately on the ATD test bench. The structure of the CHAMOIS combustion chamber fuel injection support plate was determined by the test.

In addition, AEROSPATIALE, ONERA, SEP and SNECMA have carried out numerical studies to determine the geometry of the combustion chamber. Subsequently, three series of combustion chamber tests were carried out on the test device of AEROSPATIALE under simulated flight conditions of Ma = 6, taking into account various conditions such as uniform and non-uniform incoming flow.

In 1997 CHAMOIS carried out the final trial, improving the fuel injection system and applying all available measurement systems. The results of all these experiments contribute to a better understanding of the process of thermal congestion as the equivalent ratio increases, and to investigate the optimal location and distribution of fuel injection plates.

The CHAMOIS combustion chamber has a structure with partial air intake ducts and tail nozzles, and there is no water vapor pollution at Ma = 6.5 and slight water vapor pollution at Ma = 7.5. In order to obtain the test data under the flight condition of Ma = 7.5 and observe the effect of water vapor pollution, a new small combustion chamber test model called MONOMIMAT was built, which has an inlet section of 100 mm X 100 mm and only one fuel support structure, and the test model was designed and manufactured by ONERA, and the test of Ma = 7.5 with polluted incoming air was carried out on the ATD 5 test device. The MONOMIAT combustion chamber can also be used to analyze transonic combustion chamber modes in order to determine the feasibility of a two-mode scramjet engine work transition with a hot throat plugging.

The thrust of the CHAMOIS combustion chamber was initially measured directly by the force measurement system of the S4MA wind tunnel, and the accuracy of the two force measurement methods was compared in a subsequent study:

force balances in wind tunnels;

Surface pressure measurement takes into account both heat and surface friction losses.

Since the fuel injection support plate is not convenient for installing a protruding measuring device, the second method requires an additional calculation of the force applied by the support plate. The second method is less accurate than the first, but it is relatively economical and allows for the necessary data to be compared with the results of the experiments, so ONERA has developed a new force measuring system for fuel support plates, which is planned to be tested in the MONOMIAT combustion chamber.

In addition, AEROSPATIALE has developed a simple method for calculating the thrust at the outlet of the combustion chamber and used it in the CHAMOIS combustion chamber test to quickly compare the effect of different combustion chamber configurations or fuel injection plate configurations on performance.

5. Integration of propulsion systems

In order to predict the thrust-drag balance characteristics, DASSAULT AVIATION and the Russian academy of sciences conducted joint research on a free-jet wind tunnel with a scramjet type of scramjet engine type with Ma = 8, using hydrogen fuel, measuring the axial force of the engine, and also carrying out numerical calculations.

11.1.5: Materials and cooling structure studies

The study of materials is carried out at two levels.

Firstly, the goal is to use existing composite materials (such as carbon-cinnamon carbon fiber, carbon silicon, carbon, ceramic glass, etc.) to study the adaptability of these materials in hypersonic air-breathing propulsion systems using hydrogen fuel. Numerical calculations were developed to predict the oxidation process, and thermal protection tests were carried out on the new BLOx4 test bench. In addition, the ATD 5 test bench has carried out a series of tests to verify the feasibility of the composite components and the hydrogen fuel cooling method.

Another level of objective is to study new types of materials, including metal compounds, metal-based or metal-based composites. Evaluative tests were carried out on metal compound materials, and metal matrix composites were also studied from a manufacturing perspective.

11.1.6: Research on the overall system of hypersonic vehicles

1. Flight test

Due to the cost and size constraints of the ground test setup, as well as the high sensitivity of the aeropropulsion balance, the development of scramjet technology necessarily requires large-scale flight tests. The direct construction of a full-featured vehicle is costly and carries a very high technical risk, so it is necessary to start with the development of a small-scale test vehicle.

France has participated in flight tests of an axisymmetric hydrogen-fueled engine conducted by CIAM in Russia, which is close to the design of the ESOPE combustion chamber (ONERA conducted ground tests in the 1970s), but the height of the combustion chamber of this engine is not representative of a large-scale operational scramjet engine. In addition to this tentative exploration, the PREPHA program analyzed the needs of flight testing in detail and evaluated the capabilities of a series of typical test vehicles that met the requirements. The study concluded that there was an urgent need for an aircraft capable of assessing the balance between aerodynamic drag and thrust in the propulsion system. Depending on the results obtained in question, ONERA and AEROSPATILE drew sketches of a number of autonomously powered test vehicles.

2. Design of single-stage to orbit (SSTO) aircraft

In the PREPHA program, a design scheme and propulsion system of a universal single-stage orbit SSTO vehicle were proposed. The development of this design guided the design of the scramjet components and the evaluation of the potential to further expand the capabilities of the high-speed air-breathing propulsion system. The missions under consideration include a 500 km circular orbit with an inclination angle of 28.5° from the French Guiana cosmodrome.

The propulsion system takes into account four combined cycle propulsion systems using hydrogen slurry fuel: a two-aisle turborocket scramjet-rocket combination and a turbojet-dual-modal scramjet-rocket combination, and a single-aisle rocket-dual-mode scramjet-rocket combination and a launch dual-mode scramjet-rocket combination. The above four propulsion systems are applied to the simulation of the flight trajectory of the SSTO aircraft, and the results show that the concept of choosing a rocket-bimodal scramjet-rocket combination has advantages, and the subsequent work is to gradually carry out the detailed design of the fuselage and propulsion system for this concept. The final results show that under the given hypothetical conditions, the aircraft can meet the mission requirements, with a total take-off mass of 487 tons under no load and a total take-off mass of 540t under 5t load conditions.

The above study was carried out for horizontal take-off vehicles. Given the difficulties of building auxiliary booster vehicles and the cost constraints, vertical take-off is an alternative option.

Performance studies have shown that the vertical take-off VTO vehicle has a total take-off mass of 503t with the help of a 700t thrust rocket, which is comparable to the previous 487t horizontal take-off HTO vehicle.

On the other hand, the feasibility and advantages of in-flight oxygen collection were also studied. The results show that the *Ma* = 5 high-speed cruise flight aircraft can greatly reduce the initial oxygen carrying capacity during takeoff, and can more easily design the aircraft with large payload without affecting the large increase in take-off mass.

Systematic studies have shown considerable advantages of a combined cycle propulsion system using a dual-modal scramjet engine to improve the performance of reusable space launch vehicles, even in the following cases:

If rocket propulsion is adopted, the technical level cannot achieve a fully reusable space launch vehicle, and the combined cycle propulsion system still has hope to break through the technical barrier;

If rocket propulsion is used, reusable space launch vehicles can be designed, and combined propulsion can still improve design margins, as well as safety, reliability and economy.

11.2: JAPHAR PROGRAM (1997-2002)

11.2.1: Introduction to the JAPHAR Program

In the 1990s, France carried out research on the PREPHA program, and Germany carried out research on the conceptual design of a two-stage orbiting space launch vehicle called the Sänger program. After the completion of these two programs, researchers from the two countries have come to the same conclusion, that is, it is difficult for hypersonic vehicles to be applied in the near future, and key technologies such as scramjet engines need to be further studied, and further research needs to be carried forward step by step. Based on this understanding, ONERA in France and DLR in Germany decided to join forces in 1997 to carry out research together, and the JAPHAR (Joint Airbreathing Propulsion for Hypersonic Application Research) program was born. The JAPHAR program was funded by two research institutes, DLR and ONERA, and jointly leveraged the research resources of both (Fig. 11-2) [6].

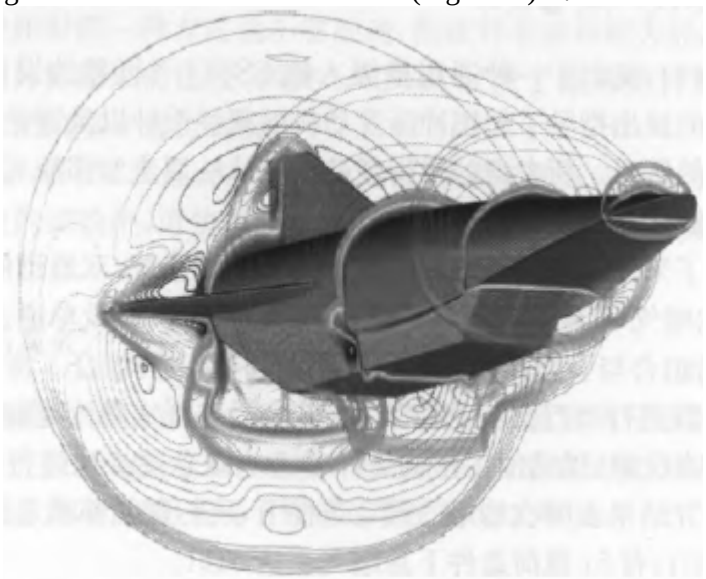

Figure 11-2: Flow field calculation of the test vehicle in the JAPHAR program

The development of scramjet engines is a long-term task, and research institutions need to carry out continuous research to obtain the most comprehensive understanding and gradually promote the maturity of the technology and realize the application of the technology. At the same time, the application of scramjet engine should not be based on its own basic research but should consider the prospects of its application from the perspective of the overall concept. Therefore, the JAPHAR program has two main development goals.

The first goal of the program is to further develop the technology of the bimodal scramjet engine, to study the working mechanism in depth, and to improve the calculation accuracy of numerical simulations. The bimodal scramjet engine, which can transition from subsonic combustion to supersonic combustion, is the most promising engine for wide Mach number flights, with a range of Ma = 2 to 12. While previous studies focused on single-mode scramjet engine experiments, a new dual-mode scramjet engine was built in the JAPHAR program to conduct experimental studies on ONERA's scramjet test facility, which can simulate flight conditions up to Ma = 7.5.

The second goal of the program is to study the problem of the balance of thrust and drag in the case of airframe/engine integration. Thrust-drag balancing is a great challenge for air-breathing hypersonic vehicles, and it is important to establish such a balance both in terms of component performance and in terms of the overall performance of scramjet engines. Therefore, the project hopes to develop a method that can be applied to the test vehicle, which can be used as a reference vehicle to guide the research work in various fields of the research plan, and the test vehicle is also necessary to evaluate the performance of the scramjet, which is also an important aspect of the research direction, and can also carry out further international cooperation on the flight demonstration of the performance of the scramjet engine on a larger scale.

11.2.2: Research Pathways of the JAPHAR Program

The JAPHAR project is based on a blueprint for the test vehicle and defines the design of the various components of the propulsion system from a holistic perspective. This also reflects the basic characteristics of this type of air-breathing propulsion, that is, the high degree of integration of the aircraft and the propulsion system, and the need for a mutually coupled design. This is critical, not only to establish a balance of thrust and drag, but also to obtain a realistic estimate of component performance versus the overall performance of the aircraft, and to optimize the design of the component for the entire mission.

The research plan defines the overall scheme and mission of the test vehicle and outlines the framework of the research.

The central objective of the research is to demonstrate the thrust-drag balance of a dual-modal scramjet engine, which is a flight test powered by a dual-mode scramjet engine between Ma = 4 and 8, and covers the working methods of various engines. In the case of Ma = 4, the engine operates in the subsonic combustion mode, in Ma = 6 it contains two modes of subsonic combustion and supersonic combustion, and in Ma = 8 it operates in the full supersonic combustion mode.

Another question concerns the dimensions of the test engine. Previous research in Germany and France has been considering propulsion systems for future space transportation. Under this goal, it is necessary to consider the large size engine of the large size of the aircraft. In the case of scramjet engines, this means that fuel injection and blending with air require the use of fuel injection plates in order to inject fuel throughout the engine cross-section. However, for small combustion chambers, there is no such constraint and fuel can be injected directly from the wall. Fuel blending is a fundamental problem in the scramjet engine process, and this problem is even more critical for large combustion chambers. The height design of the test engine therefore needed to be determined on the basis of the large scramjet engine it represented, the fuel of which needed to be injected from the support plates. The same issue concerns the design of the size of the test vehicle and the cost of the final demonstration flight test.

Through a multifaceted trade-off, the JAPHAR plan chose a 10 m length test vehicle with a mass of about 2 t.

From the cost point of view, the test vehicle should be able to carry out multi-point flight tests. In order to be able to test the ability to cover the range of *Ma* = 4 to 8, it can be carried out during deceleration flight, and it is not required to have the ability to accelerate from *Ma* = 4 to 8. The flight test program required an analysis of the initial size, mass, and capabilities of the booster.

Another key issue is the choice of fuel. PREPHA and Sänger had previously planned to use hydrogen fuel, as well as in the scramjet tests. Although the use of gaseous hydrogen fuel has the problem of large storage volume, the complexity and high cost of using cryogenic fuel technology can be avoided. At the same time, the technology of active engine cooling is not considered. These fuel-related technology choices are also consistent with the fact that the combustion chamber work in flight tests lasted only a very short time.

The first principle for the selection of different technical solutions for aircraft applications is to be as simple and low-cost as possible, thus excluding the use of variable geometries and limiting the use of composite structures. The goal of the program is limited to the development of scramjet technology.

Focusing on the size parameters of the aircraft and the planning of the flight mission, the JAPHAR program defines several main tasks: the core work is to study the DMR combustion chamber and its fuel injection system, and to carry out experimental studies; carry out aerodynamic numerical calculation research at the same time as the DMR design to define the entire propulsion system and its integrated configuration with the aircraft; the study of aerodynamics is directly linked to the study of the system, both as a task for the design of the aircraft and for the integration of the various parts of the overall project through the estimation of the thrust-drag balance. Another way is to define the components from the aircraft as a whole, study each component through numerical simulation and design a test model for ground testing. At the beginning of the study, the components were analyzed independently, but as the research work progressed, the goal was to integrate the various parts of the study so that they could be considered in a real working environment and to study how they interact with each other, which is essential for hypersonic air-breathing propulsion systems.

At the same time, the JAPHAR program also believes that basic research should be carried out on an ongoing basis in order to raise awareness of scramjet control and to develop research tools and tools for future projects. As a result, previous tests on supersonic combustion will continue. In France, the experimental research carried out by ONERA's LAERTE laboratory under the PREPHA program will continue and new diagnostic technologies will be developed and applied. In Germany, the DLR laboratory has also carried out basic experimental studies on the Mil test bench. These experiments enrich the test data of supersonic combustion research and directly support the modeling work in this research plan. The PREPHA project's study of the blending and combustion of fuels in supersonic gas streams was useful for the evaluation and improvement of the model. The results of the basic experimental studies were also used in the numerical calculations of the combustion chamber of scramjet engines, in particular the MSD aerothermochemical reaction program developed by ONERA in the PREPHA program.

Another aspect of the research work was the development of measurement techniques for the development of scramjets. The refinement of the ground test apparatus was also combined with the needs of flight tests, which were also carried out as part of the design of the test vehicle.

11.2.3: Research on dual-modal scramjet engines

The concept of the DMR engine was developed under the PREPHA program, but in the JAPHAR program it has gone beyond the previous trials of the first-generation scramjet engine, and the new engine is required to be able to provide propulsion power for the aircraft in a wide range of Mach numbers.

The main aspect of DMR research is to define a supersonic combustion chamber to be able to combust at subsonic and supersonic speeds sequentially, and from a large number of theoretical studies, supersonic combustion is more advantageous at Mach 6.5.

The optimal combustion chamber geometry is different for each mode of operation and relies on the Mach number. At high Mach numbers, the combustion chamber channels of equal cross-section have the best combustion efficiency. At *Ma* = 8, it is not possible to work at a high equivalent ratio, and the geometry of the combustion chamber should have a certain expansion angle. When the flight Mach number decreases, the cross-section of the combustion chamber should be increased, unless the capture area of the air intake tract is reduced.

One possible way to meet the requirements without a variable geometry is to design two combustion chambers with different fuel nozzle positions so that the combustion process takes place in different positions depending on the number of Mach flies. Figure 11-3 illustrates this design idea.

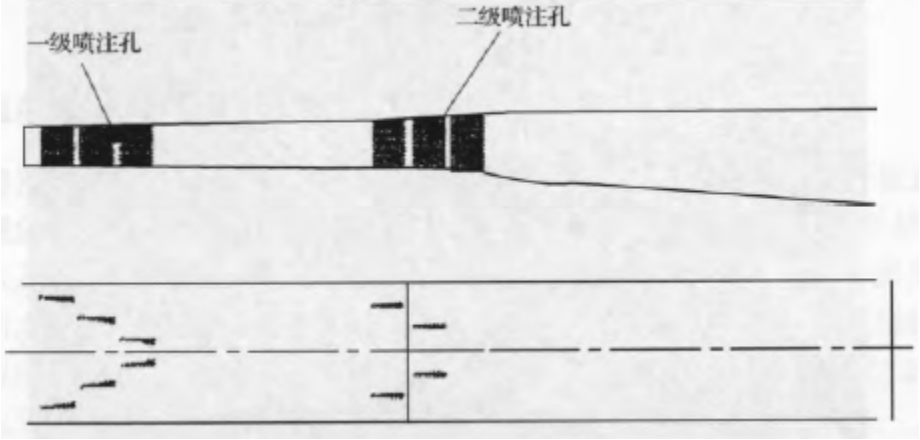

Figure 11-3: DMR two-stage combustion chamber concept

The first stage of the engine has a slightly expanded cross-section and is arranged with a first-stage fuel nozzle plate, which is used for supersonic combustion in high Mach number flight conditions, through which all fuel is injected. Subsequently, the cross-sectional expansion angle of the second-stage combustion chamber is increased, and the fuel nozzle support plate of the second-stage is arranged for subsonic combustion, and the fuel is injected from here, and the combustion occurs in the larger part of the engine here, and the front part serves as a diffuser for the intake tract. In order to avoid the problem of the need to use a throat in the tail of subsonic combustion and the suppression of supersonic combustion, a solution of thermal throat is adopted.

In order to eliminate the occurrence of strong shock wave system during subsonic combustion, the conversion from subsonic to supersonic combustion can be realized by reducing the equivalent ratio. To optimize the combustion process, a portion of the fuel is ejected from the fuel injection plate of the first stage to reduce the flow at the end of the first part of the combustion chamber with a slightly greater than Mach number 1. As the Mach number increases, more amounts of hydrogen fuel are injected from this stage of fuel nozzles, and eventually at *Ma* = 8 all hydrogen fuel is injected from here, i.e., at the entrance to the combustion chamber.

The design of this DMR, as well as its dimensions, took into account the possibility of a test vehicle. The selection of the engine height should not only be in line with the characteristics of the large-size engine represented, but also from the perspective of the aircraft as a whole. Another decision was made on the size of the test setup that could be used for DMR testing. In fact, one of the main tasks of the program is to design, manufacture and test the DMR concept under consideration within the framework of cooperation.

As part of the PREPHA program, a high-enthalpy test bench, ATD 5 (Fig. 11-4), was specially built at ONERA's research center in Palaiseau for supersonic combustion and scramjet engine combustion chamber tests, which can simulate a maximum flight of *Ma* = 7.5, thanks to a high-pressure air circulation system with two hydrogen combustion chambers that can reach a maximum station temperature of 2400 K. Part of the air can also be heated by a heat exchanger, which can change the pollution ratio of water vapor in the air. This test set-up, which was used for scramjet testing under the PREPHA program, successfully simulated the flight environment of *Ma* = 7.5 in October 1998, reaching the maximum test conditions expected by the program.

The test plant is the only one in Europe that can meet these test conditions, with a maximum flow rate of 4 kg/s at high Mach numbers. This also limits the maximum size of the test combustion chamber to 100mmX100mm. The selection of the 100 mm height of the DMR test model in the JAPHAR program matched the capabilities of the test rig and was able to reflect the important influencing parameters of the support plate fuel injection.

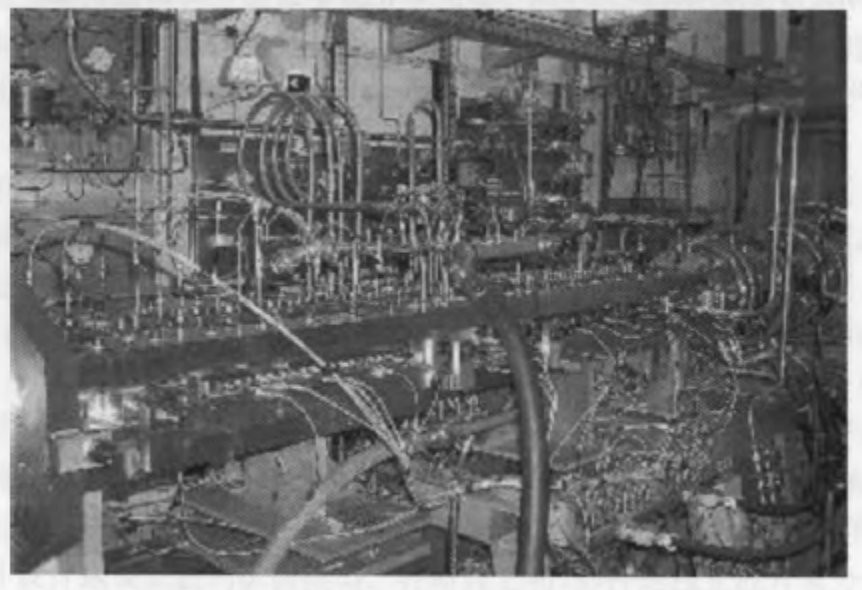

Figure 11-4: ATD5 scramjet engine test bench

Considering the application of the test vehicle, the reference size of the engine inlet section was selected as 100mmX400mm, and for the ground test, the scaled engine was designed, and in each section of the combustion chamber, the fuel injection support plate was nearly included.

The engine was tested at a small scale and could not achieve real performance, but the same design process and the same design tools were used to design a small combustion chamber for ground testing, which is based on the same working principle. The goal is to validate the entire design and check that it achieves the desired results, rather than replicating the entire vehicle's engine on the ground for testing.

The study of the engine is carried out within the framework of the overall study of the entire aircraft propulsion system and through numerical simulation from the perspective of thrust and drag balance evaluation. At the same time, the research on the reduced engine is also studied by numerical simulation, and the calculation program is calibrated by comparing it with the test data.

The above analysis illustrates the selection of the reference engine height and applies it to the reduced engine for testing. The width of the engine is also limited to 100mm, which makes the first stage combustion chamber can only be arranged with one fuel support plate, and the insufficient part is supplemented by wall injection, while the second stage combustion chamber is arranged with two fuel support plates.

In parallel with the development of the DMR, research was also carried out on its fuel injection system, which is a key component of the DMR, and the specific research was carried out at the DLR laboratory in Lampoldshausen, with the goal of comparing and characterizing the characteristics of the different fuel injection plates and applying them to the test combustion chamber. Figure 11-5 shows two types of fuel injection plates, designed to improve the blending of hydrogen fuel in air, tested on the M11 test bench, and applied a variety of optical diagnostic techniques to study the characteristics of the blending process, and a new probe was used to sample the gas.

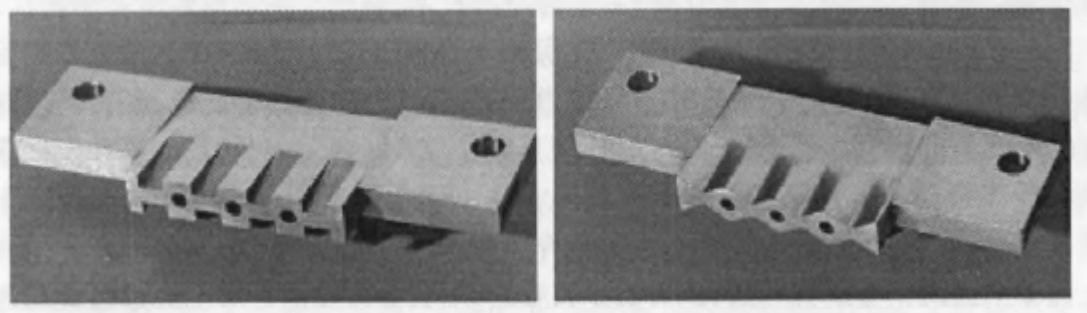

Figure 11-5: Structure of a fuel injection support plate studied by the DLR laboratory in Germany

11.2.4: Basic research on supersonic combustion

In order to support the development of the engine, basic research on supersonic combustion related problems was carried out to better understand the physical phenomena of the combustion process and to improve the fuel injection system, a key component of the DMR engine. Numerical simulation methods are widely used for the initial design, engine optimization and analysis of ground tests, so it is necessary to improve the level of numerical simulation calculation tools, which are necessary for the development of DMR technology, and also to obtain the test model of supersonic combustion for the verification of the calculation program and further refinement of the physical model. Research in this area has been initiated in previous research programs, both ONERA and DLR, and further in the JAPHAR program.

For this purpose, two test units with optical diagnostic capabilities are available at ONERA and DLR, one of which is the LAERTE unit, located in Palaiseau, ONERA, which uses optical diagnostic methods to study combustion problems in detail. The two optical laboratories are permanently located in the vicinity of the experimental setup, and the instruments are housed with special consideration in order to be well insulated from the thermal environment of the combustion setup. It is equipped with a variety of optical diagnostic equipment such as CARS, PLIF, Rayleigh Scattering and Laser Velocimeter.

11.3: PROMETHEE program (1999~2002)

11.3.1: PROMETHEE program introduction

In the PREPHA program, the French company MBDA Missile Systems (formerly the Aerospatiale Matra Missile Division) and ONERA have made significant contributions to the development of hypersonic technology. In the program, first-hand knowledge of scramjet engines was obtained, the design of components of the bimodal scramjet engine was carried out, including the air intake tract, combustion chamber, fuel injection support plate and tail nozzle, and the study of hypersonic air-breathing vehicle systems was carried out, including the design and evaluation of space launch vehicles, hypersonic missiles and test vehicles.

The PREPHA program ended in 1999, and in order to preserve personnel in the field, as well as research equipment, and to improve the mastery of hypersonic air-breathing propulsion, MBDA and ONERA carried out a number of research activities, including:

With the support of the French Ministry of Defense, MBDA-France, in cooperation with the Moscow Institute of Aviation Research (MAI), developed a bimodal scramjet engine with a wide Mach number (Ma = 2 to 12) with variable geometries and ground tests on kerosene and hydrogen fuel. MBDA also conducts cooperative research on supersonic combustion with other Russian research departments and cooperates with the European EADS space launch vehicle program to develop fuel cooling structures.

In addition, with the support of DGA and USAF, ONERA is working with Pratt & Whitney and Snecma in the A3CP program to develop composite technologies for cooling structures in heat sink fuels.

At the same time, ONERA also leads the cooperation program JAPHAR with the DLR laboratory in Germany, the goal of which is to continue the basic research in the PREPHA program and to improve and validate the numerical calculation procedures for aerothermochemical reactions, and to study the bimodal scramjet engine of hydrocarbon fuel to operate at *Ma* = 4~8 range, and develop a verification test method for the aircraft using this engine to achieve thrust-drag balance. The collaboration ended in 2002, but ONERA continues to lead some of the subsequent numerical and experimental research work. Based on these research initiatives, ONERA and MBDA have jointly conducted research on hypersonic air-breathing engines for aerospace transport applications. These research efforts resulted in a program, launched in 1999 and supported by the French Ministry of Defence, to study key technologies related to hydrocarbon-fueled bimodal scramjet engines and to gradually realize the possibilities of their application. The program is named PROMETHEE, and its research content includes [7~10]:

The overall scheme and propulsion system of a typical hypersonic missile are proposed, and systematic research is carried out (Fig. 11-6).

Design and optimize the experimental combustion chamber model;

endothermic hydrocarbon fuel technology;

Implement the technology needed for ground trials and flight demonstrations.

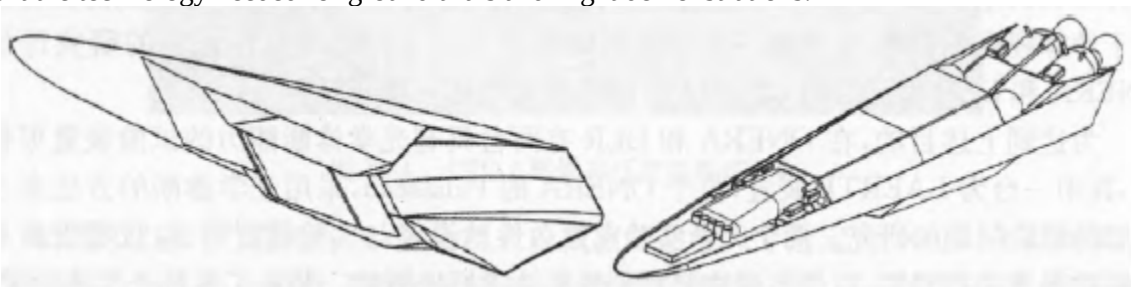

Figure 11-6: Conceptual design of the missile in the PROMETHEE program

11.3.2: Main objectives of the PROMETHEE program

The ramjet-powered French ASMP and ASMP-A missiles have realized the strategic value of this type of air-to-surface missile, further increasing the speed of the missile to more than *Ma* = 6, extending its range and the penetration capability of the warhead, which can further enhance the capability of the ramjet-powered missile. Flying at high altitude at high speed greatly reduces the relative speed and maneuverability of the interceptor aircraft.

The advantages of using ramjet power for high-speed long-range flight for reconnaissance missions have also been studied, and it has been found that it can improve the ability to cruise and respond to the mission.

The ability to cruise at high speeds can also be applied to tactical missiles, especially when lethality is not a major factor and speed is critical (e.g., buried deep underground targets or time-critical targets, e.g., ground-based mobile defense systems).

In this range, a compromise can be made by comprehensively considering range, load capacity, average/maximum/terminal velocity, penetration capacity, load efficiency, etc.

All of these aspects have important implications for the design of the propulsion system, such as keeping the Separating Mach number as low as possible to increase the range, but a higher Detached Mach number helps to reduce flight time and engine complexity, as well as the cost of tactical missiles.

The goal of the PROMETHEE program is to master the design methods of propulsion systems that can be applied to hypersonic cruise missiles, taking into account some constraints when applying them in practice.

The main technical step is to design a bimodal scramjet engine with a wide Mach number hydrocarbon fuel and master the method of adjusting its performance.

For the application of missiles, the technical problems such as low Mach number starting, wide Mach number operation and small size are solved in a limited way. Under this research content, most of the technical problems and subsystems related to the design of operational integrated aeropropulsion configurations can be broadly presented in a typical way, and most of the possible problems to be studied include:

Short engine lengths for use in small aircraft that are limited by the capacity of the carrier;

At low Mach numbers $Ma = 2$ can be started so that the high specific impulse characteristics of the air-breathing engine can be used to increase the total range, and cruise flight at high Mach numbers ($Ma = 8$) to enhance the penetration capability of the missile;

Propulsion systems are designed with the smallest possible variable geometry components to operate in a wide Mach number flight area, and composite structures with active hydrocarbon fuel cooling, i.e., endothermic hydrocarbon fuels can be broken down and regulated by the fuel supply system, and then cooled through the cooling channel of the engine combustion chamber before entering the combustion chamber.

Much of the work on the design of dual-modal scramjet engines for hydrogen fuels has been carried out in PREPHA, JAPHAR and other research projects, in particular the development of numerical simulation programs that take into account fuel blending and combustion processes, but there is a need to work on supersonic combustion of hydrocarbon fuels to achieve the same level of predictability as hydrogen fuels.

11.3.3: Technical Pathways of the PROMETHEE Program

The goal of the PROMETHEE program is to explore the technical difficulties in designing a hydrocarbon-fueled dual-modal scramjet, taking into account the specific constraints applied to long-range air-to-ground ballistics.

At the beginning of the program, the conceptual design of a typical missile was carried out, which defined the requirements for the propulsion system. The concepts of the various propulsion systems proposed were compared by means of flight simulations. The numerical simulation results provide a series of flight points that can be used to select appropriate test conditions and scale-down for the direct-coupled combustion chamber model (Figs. 11-7).

The model engine has been designed, fabricated, and installed on ONERA's ATD8 test rig. At the same time, MBDA-France and ITAM cooperated to build a model of a scaled forebody and air intake tract to study the adaptability of different configurations to the test vehicle in a wide range of Mach numbers. The model was tested in various configurations at the ITAM test bench in 2001 and 2002.

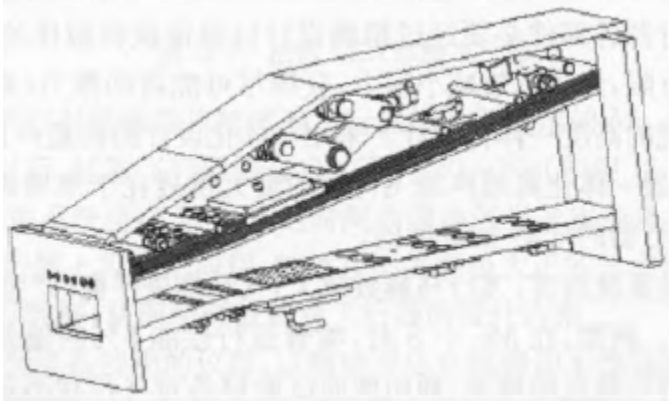

Figure 11-7: Combustion chamber test model

At the same time, system research is refining the overall design and mass margin of the aircraft and engines. The aerodynamic force of different aircraft shapes is numerically calculated, and finally the performance of the missile will be improved.

In addition, consideration is given to how to improve the prediction capabilities of existing test installations and their ground tests to meet the development needs of future practical application aircraft. Therefore, it is necessary to improve ONERA's S4 hypersonic test device to enable it to perform integrated full-scale semi-free jet testing of small-sized vehicles, which will be used for testing on LEA test vehicles (Figures 11-8).

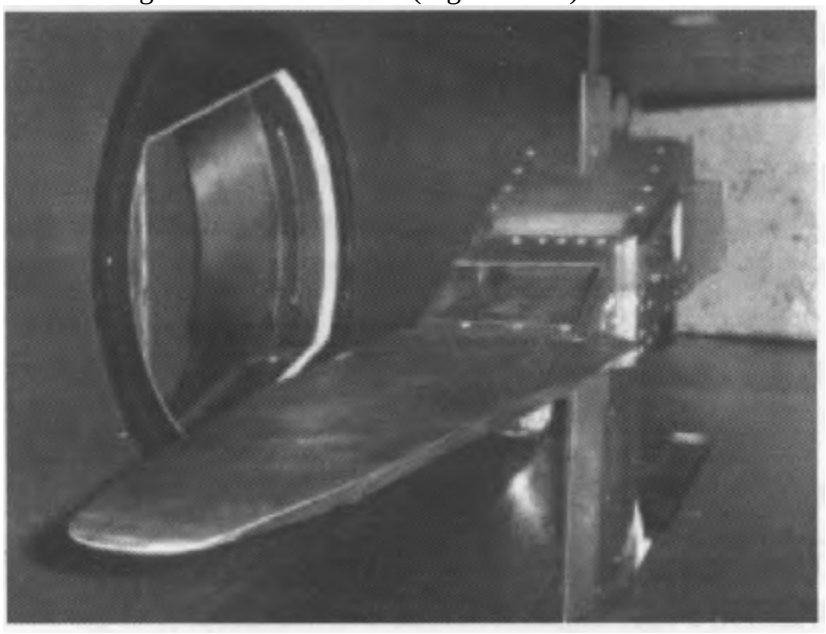

Figure 11-8: Typical forebody air intake at ITAM in Russia

11.4: LEA flight test program (2003~)

11.4.1: Background to the LEA Flight Test Program

At the heart of air-breathing hypersonic technology are scramjet technology and integrated airframe/propulsion vehicle technology. The components of an air-breathing hypersonic vehicle must be precisely designed to ensure optimal aero-propulsion performance. Due to the limited thrust of this type of aircraft, in order to effectively reduce drag and obtain the highest possible thrust (effective specific impulse), it is necessary to adopt a highly integrated design of the airframe system and the propulsion system. The components of the hypersonic vehicle with integrated design are closely related and affect each other. The biggest challenge in the development of integrated hypersonic vehicles is to accurately evaluate the interaction between the airframe and the propulsion system and determine the aero-propulsion performance of the aircraft.

For air-breathing propulsion systems, the greater the flight Mach number, the more sensitive the aeropropulsion balance (the thrust produced minus drag, i.e., the net thrust). For example, a 5% deviation in the running performance of a nozzle can cause a 35% decrease in net thrust at $Ma = 8$; moreover, as the number of Mach numbers in flight increases, it becomes increasingly difficult to simulate the flight state using ground test equipment. In general, in a ground test facility, the air is heated to the appropriate temperature and then accelerated through a nozzle to the appropriate Mach number before entering the test area. Regardless of the heating process, there will always be some free radicals, often accompanied by some contaminants. When these substances enter the conveyed air, they alter the combustion process.

The sensitivity of aeropropulsion balance and the limited ability of ground tests to perform in real-world flight conditions necessitate the development of a ground R&D method that closely combines test and digital methods. However, this approach to development is challenging, and it must be verified to accurately determine flight performance before it can be applied in the real world, so as to ensure design margins and identify the right direction to optimize system design. Flight tests, which allow the validation of this R&D method, became a necessity, and for this reason, MBDA and ONERA launched the LEA flight test program with the support of the French government [11-17].

The LEA flight test program mainly covers the following aspects: (1) to determine a method for the development of hypersonic vehicles using ground tests and digital simulations; (2) the development of the tools (experimental or digital) required to achieve the above objectives, (3) the application of the method to the development of simplified scientific test vehicles, and (4) the validation of the method through a series of flight tests.

The LEA flight test program was launched in 2003 in four phases. After several years of implementation, the LEA program has undergone some adjustments in terms of schedule and number of flight tests. In early 2006, the preliminary design of the LEA testing machine was completed, its propulsion system was determined, and it passed the preliminary design phase evaluation and is currently in the critical design phase. Due to delays, the final completion of the LEA program was postponed to 2013, and the number of flight tests was reduced from six to four due to financial constraints.

11.4.2: Test Principles of the LEA Flight Test Program

In order to control costs, the LEA flight test program will use a small, non-recyclable vehicle and apply existing technology wherever possible. Figure 11-9 shows the CAD model of the LEA aircraft.

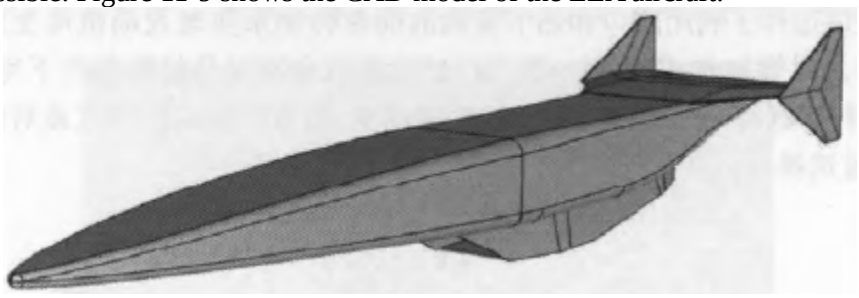

Figure 11-9: French LEA test vehicle

The principle of the test is to use an air-launched booster to accelerate the vehicle to be tested to a given Ma = 4 to 8. Then, after being separated from the booster and stabilized, the test vehicle will fly autonomously for 20 to 30 seconds (as shown in Figure 11-10). During autonomous flight, the air-breathing propulsion system will ignite over a period of 5 to 10 seconds with the change in the oil-gas equivalent ratio. This method has been applied to the X-43A aircraft in the United States, and it is possible to obtain flight data at the appropriate Mach number without the need for a large positive aerodynamic propulsion balance, thus slightly relaxing the design constraints on the aircraft.

LEA aircraft will be equipped with special instruments to accurately assess the aeropropulsion balance with and without combustion and to determine the contribution of the various components of the propulsion system to this balance. All measured parameters will be transmitted back to the ground via telemetry and recorded using an on-board data logger that will be recovered after the aircraft crashes (Figures 11-10).

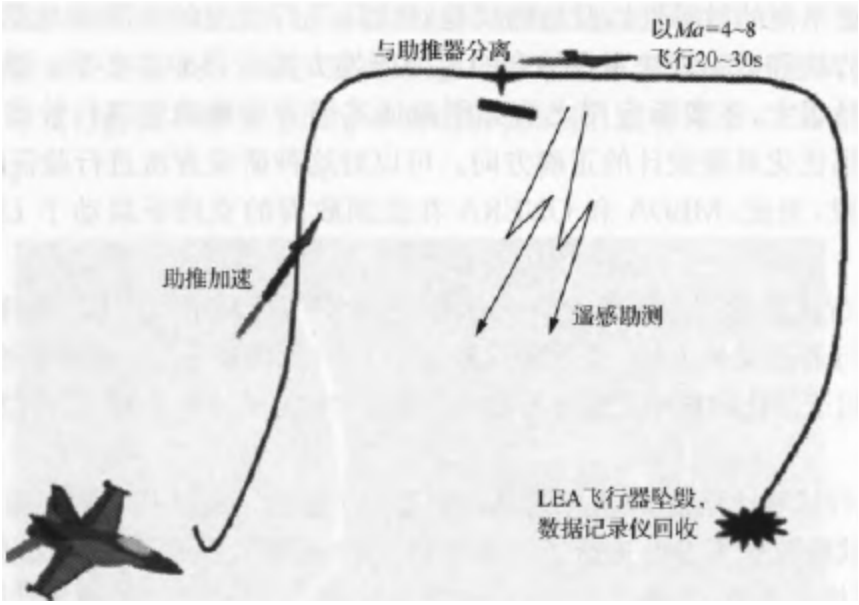

Figure 11-10: LEA flight test process in France

11.4.3: The status of LEA aircraft research and development

1. Propulsion system concept for LEA aircraft

In the selection of the concept of the air-breathing propulsion system, the LEA test vehicle referred to all the research and development achievements in the field of engines in recent years, and finally chose the scheme of using the simple rotation of the lip and thermal throttle valve to achieve the variable geometry of the engine (Fig. 11-11). Nonetheless, because each flight test will be conducted under constant Mach number conditions, each LEA test vehicle will use a fixed engine geometry that represents the variable geometry chosen for the Mach number of the test flight.

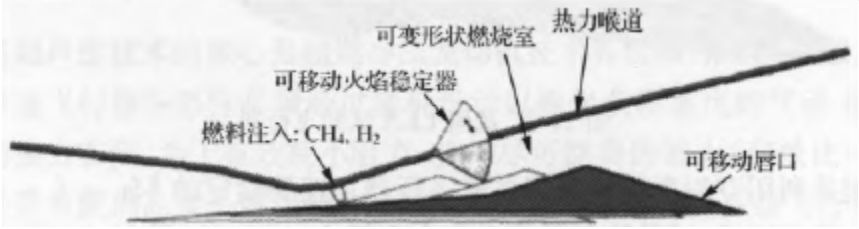

Figure 11-11: Geometrically variable structure scheme in LEA

In order to control the complexity and cost of the system, the combustion chamber will be equipped with a metal heat sink structure coated with a high-temperature and low thermal conductivity coating.

The vast majority of supersonic combustion tests in France have been carried out on hydrogen fuel. Due to the low density of hydrogen fuel, the consideration of fuel tank size restrictions should be avoided as much as possible, and once gaseous hydrogen fuel is used, it will inevitably cause a series of difficulties such as excessive aircraft size and difficult to match the acceleration system. Liquid hydrocarbon fuels are also being considered, but the current experience with their application is limited, and it is difficult to ensure stable ignition and efficient combustion without pretreatment in the regenerative cooling system. The final selected fuel was a gaseous mixture of CH4 and H2.

With this blending, the fuel density can be increased, which can be used to limit the size of the fuel tank. At the same time, it is also possible to change the H2/CH4 ratio during the flight to ensure stable ignition and control the heat dissipation of the combustion chamber.

In order to apply this particular fuel, work has been carried out to rewrite existing computational codes. The rewritten code has been validated in basic tests carried out on ONER-ALAERTE's state-of-the-art test equipment. In addition, the ONERA ATD 5 test facility has been upgraded to accommodate future LEA engine CH4/H2 tests. Moreover, in order to obtain first-hand experience with the fuel, preliminary tests have been carried out in the existing JAPHAR combustion chamber.

2. Research and development of pneumatic-propulsion structure

The combustion chamber design is still a work in progress and combines digital simulation and ground testing. Two sets of equipment, the Moscow Aviation Institute (MAI) and ONERA, each applied different technologies to complete the design of the full-scale connecting tubes for the combustion chamber structure. After MAI developed the preheater, a full-scale water-cooled model (2/3 scaled) was tested with *Ma* = 2 to 7+, initially using a mixture of H2 and K as fuel, and later a mixture of CH4 and H2. A full-scale model is being prepared.

A copper alloy heat sink model will be tested on the ONERA ATD 5 test bench with a *Ma* = 4 to 7.5 level. A full-scale model known as CLEA is being manufactured and will soon be ready for application. Mixtures of CH4 and H2 may be tested in the future.

A number of parametric studies were carried out on the aircraft forebody to determine a series of design parameters to achieve good pre-compression while satisfying the technical constraints. After that, the inlet design was optimized, and a series of preliminary tests were carried out in the range of *Ma* = 2 to 8, as shown in Figure 11-12. In the summer of 2008, researchers conducted a series of tests on a 1/3 size model of the forebody and the inlet subsystem to examine the forebody boundary layer transition and its effect on the performance of the inlet tract.

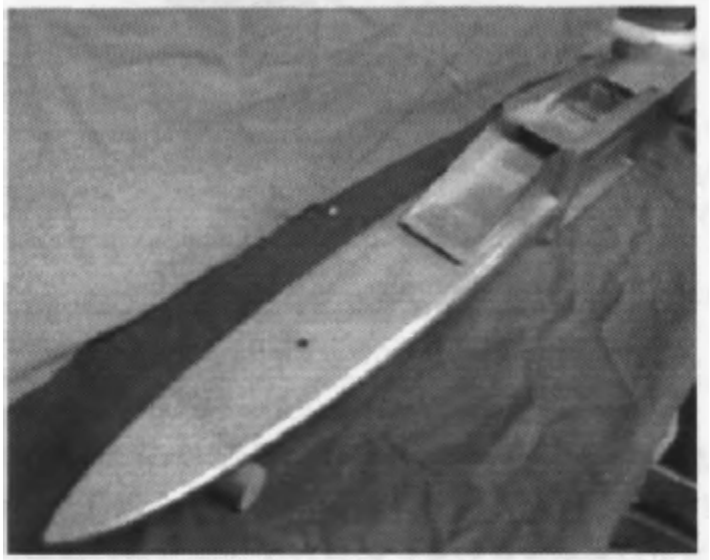

Figure 11-12: Aircraft forebody and air intake tract for testing under *Ma* = 2 to 4 conditions

Due to the special structure of the rear body and nozzle of the aircraft, the current research work is still focused on optimizing the propulsion performance and better understanding the interaction between the propulsion jet and the external airflow, so as to accurately determine the influence of the propulsion jet on the external aerodynamics.

In the preliminary design stage, the aerodynamic performance of the LEA aircraft and the aircraft-booster combination was estimated by calculation. In May 2008, a series of aerodynamic tests were carried out at the ONERA Modane test center using a 1/4 size model. The separation phase of the LEA aircraft from the booster is risky and must be carefully studied. In order to identify all the elements in the separation process in detail, some preliminary computational simulations were carried out to determine the aerodynamic interactions. In order to optimize the sequence and timing of the separation of the aircraft from the booster and the opening of the air intake, the structure of the closure and opening of the air intake cover was considered in the study. A lot of work has been done to study the full-body calculation tools, and the results include two calculation methods: block NtT calculation and overall NtT calculation. These two methods have been widely used in the estimation and optimization of the aerodynamic balance of aircraft. These calculations can be used to improve R&D methods, as well as to understand phenomena such as thermal deformation that affect the balance of aeropropulsion, and to evaluate correlations that should be considered in aircraft performance models.

3. Aircraft design

A lot of work has also been done on the selection of the underlying technologies for the LEA aircraft and its propulsion system. The preliminary design of the aircraft was completed in early 2006 and passed the preliminary design evaluation, as shown in Figure 11-13. In this phase, the main focus is on integrated integration, quality optimization and detailed definition of the internal layout, instruments and equipment.

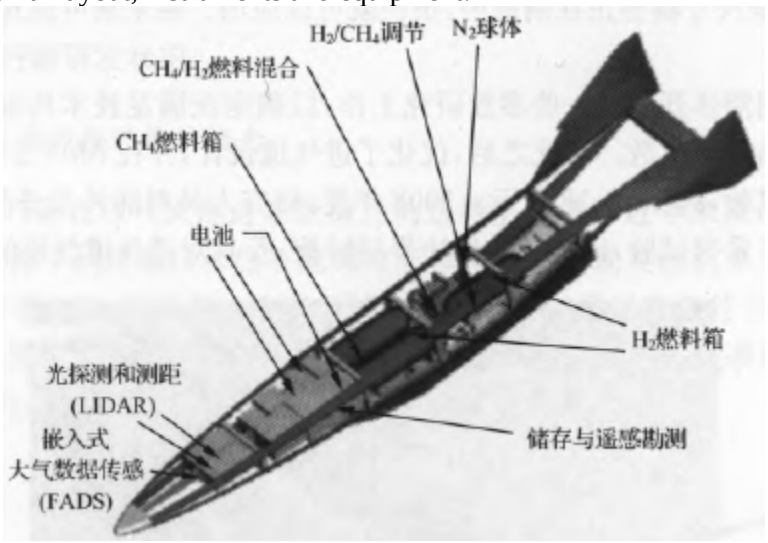

Figure 11-13: Preliminary design of the LEA aircraft

4. Ground test

The ground test plan of the LEA program is shown in Figure 11-14. To conduct the free-jet trial, the LEA program evaluated two alternatives. One of the options was to upgrade the S4Ma wind tunnel at the ONERA Modane test center in the French Alps. The scheme can be tested with an existing alumina pebble bed heater that can be used to test with a gas not affected by water vapor at Mach numbers up to 6.5 (1800 K). It is also possible to easily perform tests at $Ma = 7.5$ by adding a pre-burner or upgrading the pebble bed heater. Option two is to upgrade the METHYLE pilot facility, which can leverage the existing fuel system and the robust capabilities associated with mass stream and extraction. In order to verify the feasibility of upgrading the S4Ma wind tunnel and METHYLE equipment, and to accurately assess the corresponding costs, LEA planned to carry out a detailed study activity.

Figure 11-14: LEA ground test program

The LEA flight test plan is divided into four stages: preliminary design, key design, pre-test preparation and flight test. The preliminary design phase was completed in 2006 and is currently in the critical design phase, with four flight tests with Mach numbers of 4 to 8 to be completed between 2011 and 2013. The program is significant for improving the design, development, and testing capabilities of air-breathing hypersonic vehicles in France and may lead to innovations in research and development methods.

References

[1] Christophe Rothmund, Dominique Scherrer, Marc Bouchez. Propulsion system for airbreathing launcher in the French PREPHA program [R]. AIAA 96-4498, 1996.
[2] Marc Bouchez, Yan Kergaravat, Didier Saucereau. Scramjet combustor design in French PREPHA Program-final status in 1998 [R]. AIAA-98-1534, 1998.
[3] Falempin F, Scherrer D, Rostand Ph. French hypersonic propulsion program PREPHA: Results, Lessons and Perspectives [R]. AIAA-98-1565, 1998.
[4] Serre L. Towards a low risk airbreathing SSTO program: a continuous robust PREPHA based TSTO [R]. AIAA-99-4946, 1999.
[5] Philippe Reijasse, Reynald BUR, Bruno Chanetz. The French program Prepha: experimental analysis of aerodynamical interactions occurring on a hypersonic spacecraft [R]. AIAA 99-0610, 1999.
[6] Novelli Ph, Koschei W. JAPHAR: A joint ONERA-DLR research project on high speed airbreathing propulsion [R] ISABE, 99-7091, 1999.
[7] Francois Falempin. The French Promethee program main goals and status in 1999 [R]. AIAA 99-4814, 1999.
[8] Francois Falempin. The French Promethee program status in 2000 [R]. AIAA 2000-3341, 2000.
[9] Laurent Serre, Francois Falempin. The French Promethee program on hydrocarbon fueled dual mode ramjet status in 2001 [R]. AIAA 2001-1871, 2001.
[10] Laurent Serre, Francois Falempin. Promethee: The French Military Hypersonic Propulsion Program Status in 2002 [R]. AIAA 2002-5426, 2002.
[11] Francois Falempin, Laurent Serre. LEA flight test program: A first step towards an Operational Application of High-Speed Airbreathing Propulsion. AIAA 2002-5249, 2002.

[12] Francois Falempin, Laurent Serre. LEA flight test program-Status in 2004. 55th International Astronautical Congress, 2004.
[13] Liu Xiangjing, Ye Lei. France's LEA flight test program [J]. Flight Missile, 2008, (12):5-9.
[14] Francois Falempin, Laurent Serre. LEA flight test program status in 2006 [R]. AIAA 2006-7925, 2006.
[15] Francois Falempin, Laurent Serre. The French LEA flight test program-status in 2008 [R]. AIAA 2008-2541, 2008.
[16] Francois Falempin, Laurent Serre. The French LEA flight test program-status in 2009 [R]. AIAA 2009-7227, 2009.
[17] Francois Falempin, Laurent Serre. The French LEA flight test program-status in 2011 [R]. AIAA 2011-2200, 2011.

CHAPTER 12: GERMAN HYPERSONIC VEHICLE TECHNOLOGY RESEARCH

12.1: Sänger Program (1988~1995)

In 1988, the German Federal Ministry of Research and Technology launched the Hypersonic Technology Programme to develop advanced space transport systems. The plan is based on the concept of the aerospace transportation system named Singer, as shown in Figure 12-1, which is used as a common research object for all key technologies, facilitating coordination and leading the development of key technologies. Sänger is a reusable two-stage orbital air-space transport system named after the famous German aerospace pioneer Eugan Sänger (1905-1964). In this German hypersonic technology project, Sänger is not an aerospace aircraft development project, but only a reference concept vehicle in the program, and the developed technology can be widely applied to other possible aerospace transportation systems in the future [1-4].

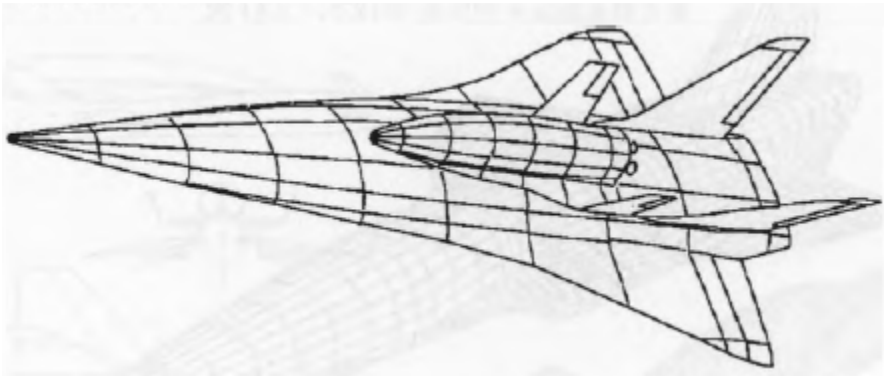

Figure 12-1: Sänger Aerospace Aircraft

Sänger is a two-stage orbital spaceplane program developed by Germany in the 1980s, and it is named after German rocket expert Eugen Sanger. In 1984, MBB (later part of the German Aerospace Corporation) began a concept study and in 1985 a preliminary concept was provided.

The Sänger scheme divides the entire system into two stages, the first stage is the carrier aircraft, and the second stage is the orbiter, and the orbiter is composed of the carrier aircraft on the back. The first stage uses a turboramjet combination engine with a service life of 100 cycles. There are two types of second stage: manned second stage and cargo second stage. The manned second stage is used to transport people and small quantities of cargo, with a service life of 50 times; Sänger takes off horizontally at conventional airports with a runway length of 2,500 m. The aircraft flew to an altitude of 31km and flew at a speed of *Ma* = 7, after which the orbiter separated from the carrier aircraft. The carrier aircraft returns and lands horizontally at a conventional airfield. The orbiter uses its own liquid rocket engine to enter Earth orbit. Manned vehicles can carry 2 to 12 people and 2 to 4 tons of cargo into Earth orbit. The orbital altitude of the manned mission of the space station is 500 km and the orbital inclination is 28.5°C, and the orbital altitude of the manned mission is 300 km and the orbital inclination is 104°. When performing reconnaissance missions, it is possible to enter any low Earth orbit. The cargo vehicle can carry 2.3 to 15.0 tons of payload, depending on the Earth orbit reached. The payload sent to geosynchronous orbit is 23,00kg, the maximum altitude of the orbit is 36,000km, the orbital inclination angle is 0°, and the payload sent to the low earth orbit is up to 15t;

when transporting the payload of the solar system mission, the orbital altitude is 200km, and the orbital inclination is 23°; the orbital altitude of the polar orbital mission is 80/600km, and the orbital inclination is 104°; payloads can also be transported into specific orbits. After re-entering the atmosphere, the manned vehicle glides back to a horizontal landing like the American space shuttle.

By the end of 1987, the Sänger aerospace aircraft had carried out 150,000 hours of program research work. According to the original plan, the Sänger was put into use in 2004. The German side believes that the "HOTOL" horizontal take-off and landing plan proposed by Britain to the European Space Agency is extremely difficult to develop as the next generation of the French "Hales" space shuttle. Therefore, Germany has also proposed "Sanger" as the second generation of the "Helmes" space shuttle jointly developed by the European Space Agency, as a replacement plan for "HOTOL" when it cannot be realized due to technical difficulties in power. The research cost of "Sanger" is between $8 billion and $10 billion.

In order to develop the key technologies required for aerospace aircraft, Germany also launched the hypersonic technology program, the HYTEX (hypersonics technology program) program, from 1990 to 1995, which aims to carry out flight tests of scramjet engines on test vehicles, as shown in Figure 12-2. The program also collaborated with Russia to conduct flight tests based on Russia's RADUGA Rainbow D2 test vehicle.

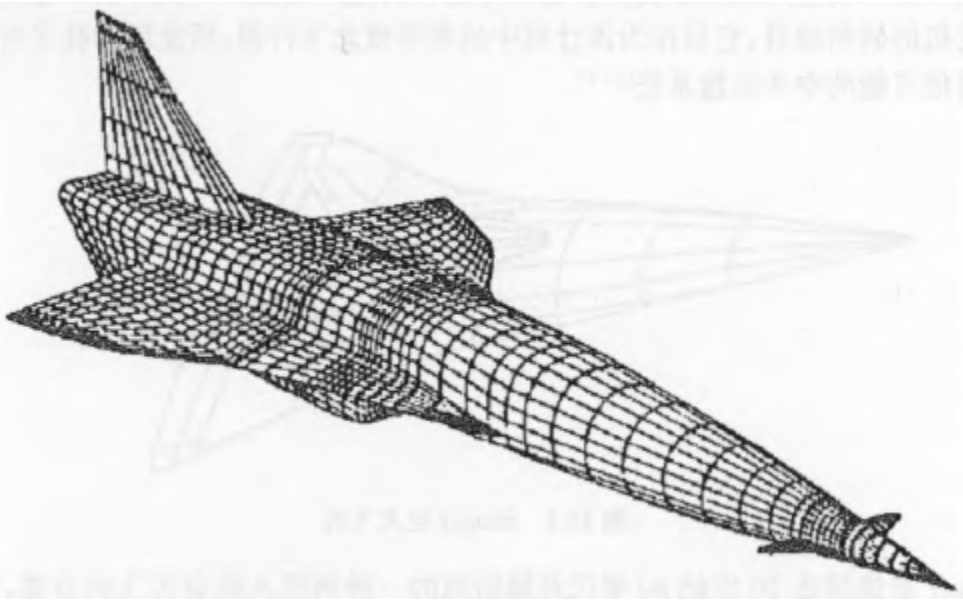

Figure 12-2: HYTEX, the test aircraft in the Sänger aerospace plane program

12.2: FESTIP TSTO program research (1994~1998)

From 1994 to 1998, ESA launched a research program called the Future European Space Transportation Investigation Programme (FESTIP). The program, which was attended by several major ESA member states, proposed as many as 16 options for the air-space transport system (Figure 12-3), and through an evaluation of the options, taking into account the risks of the technology and the near-term achievability, FSSC-15 and FSSC-16 were selected as options for further detailed studies and flight tests of related technologies [5-9].

In the FESTIP program, the German side proposed a new two-stage orbital air-space transport system based on the Sänger aerospace aircraft, codenamed FSSC-12, and carried out some new research and design work on the program, although it was not selected by ESA for further development, but the technical results achieved in it are still worth summarizing and learning (Figure 12-4).

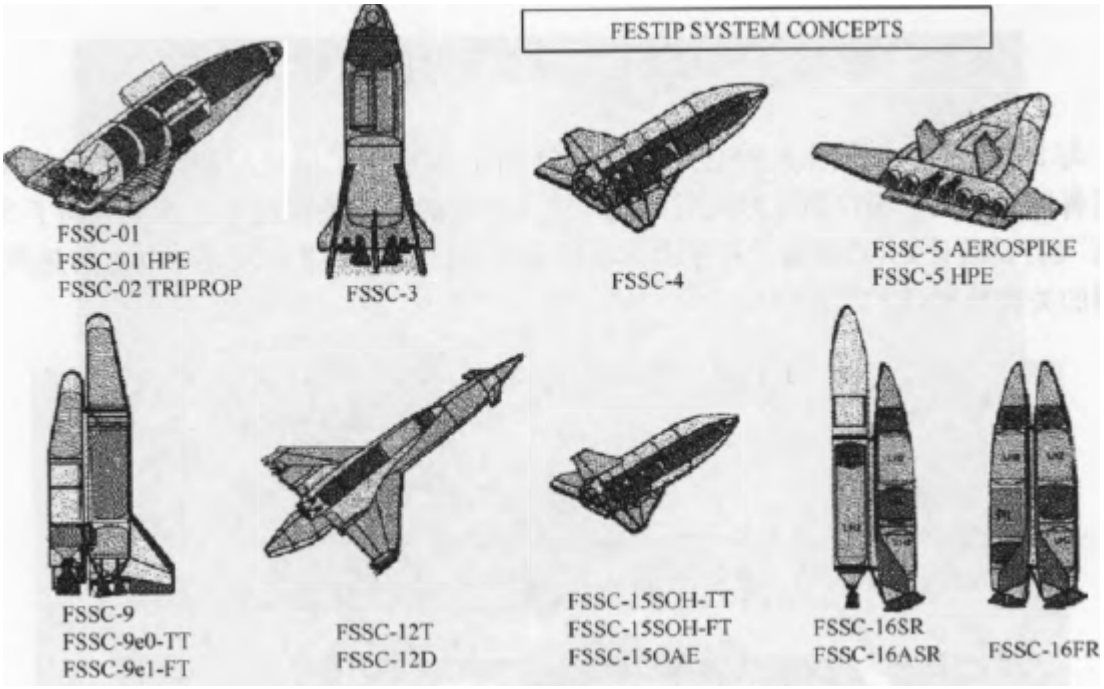

Figure 12-3: FESTIP series air and space transportation system scheme

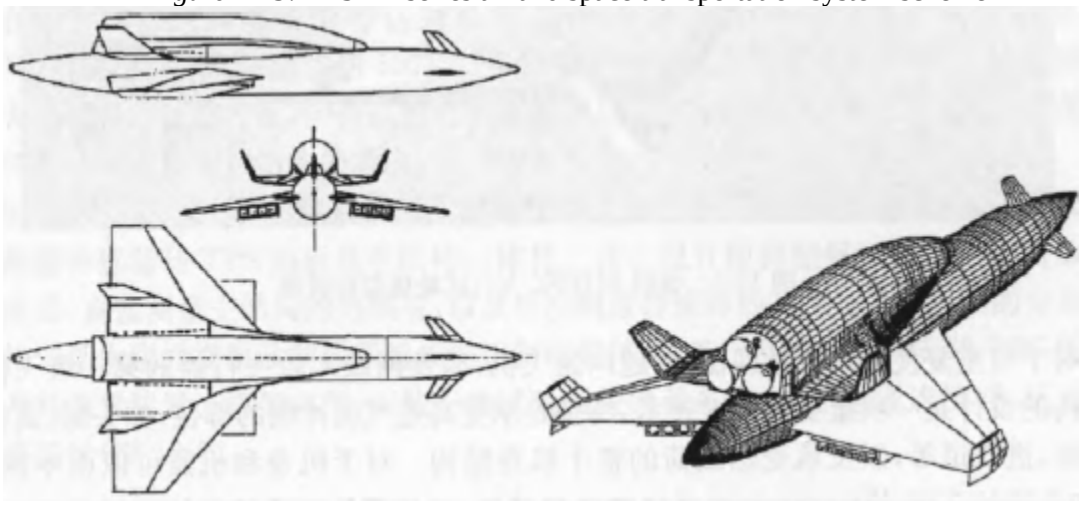

(a) Plan T

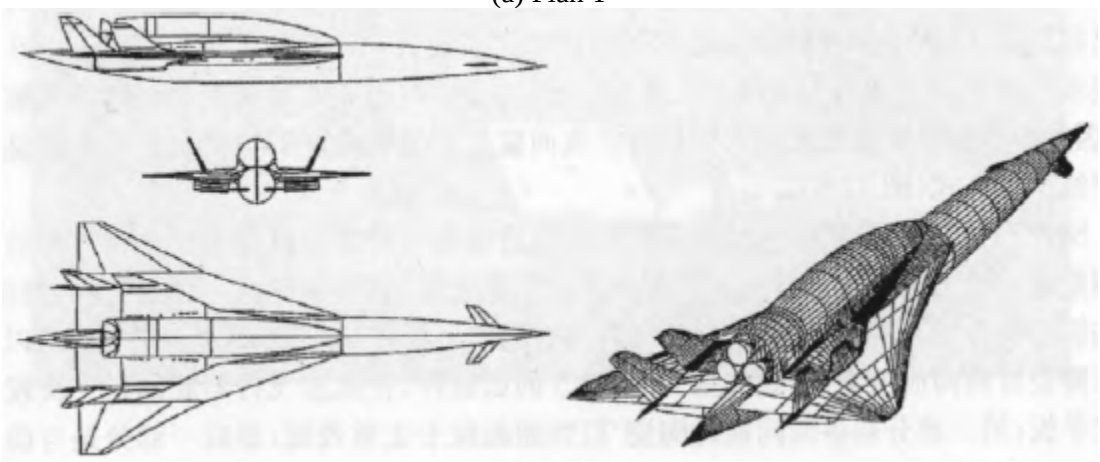

(b) Plan D

Figure 12-4: FESTIP TSTO Scheme

12.3: SHEFEX I flight testing (2005)

Different from the huge aerospace aircraft program in the 1990s, after learning the lessons of history, after 2000, countries are more inclined to gradually develop various key technologies of hypersonic vehicles. Germany has launched the SHEFEX flight test program, hoping to gradually develop and mature the key technologies of hypersonic vehicles through several flight tests of individual technologies (Figure 12-5) [10].

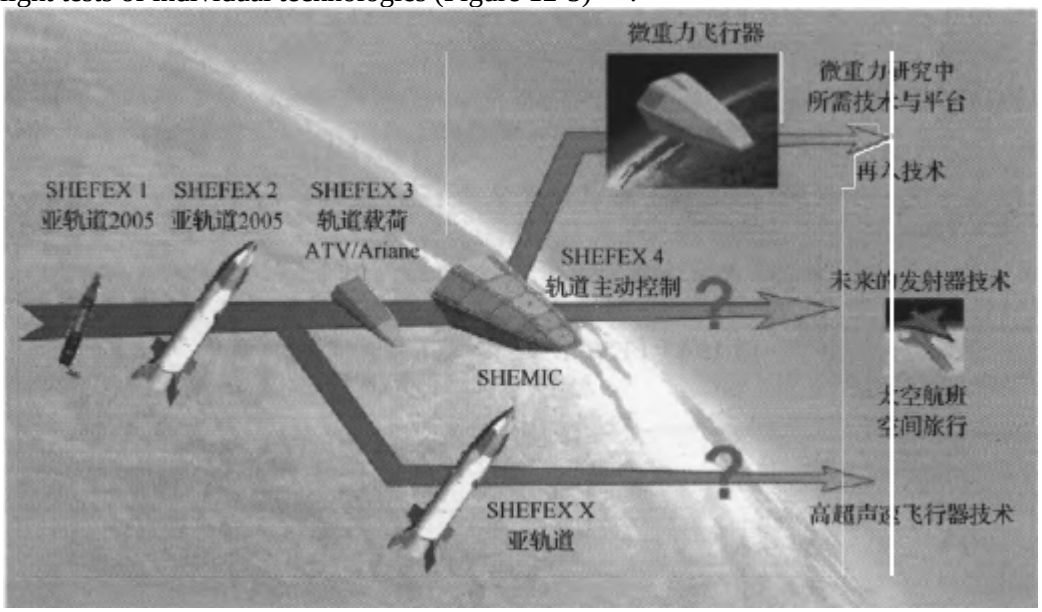

Figure 12-5: SHEFEX flight test planning roadmap in Germany

For reusable space launch vehicles, hypersonic aircraft, and first-stage vehicles with two stages into orbit, the design of thermal structures is an important key technology, especially for the parts that are subjected to high-speed air currents, such as the head, wing leading edge, control surfaces, air intakes, etc., as well as the entire fuselage structure that bears thermal loads. The fuselage and wings can be designed differently, such as different TPS thermal protection structures or thermal skin structures, which affect the performance of the system and the development cost of the aircraft. The economic aspect is an important aspect of evaluating reusable delivery systems, and the current reusable TPS technology has been developed, but the complexity of design and manufacturing due to the different components makes the application of TPS very expensive. From a structural point of view, the flat plate form is the simplest and most economical solution of all, so it would be very economical to consider TPS thermal protection in the form of a flat plate for the surface of a reusable space launch vehicle (Fig. 12-6).

The purpose of the SHEFEX I flight test was to study the aerothermal phenomena of sharp leading edges and faceted surfaces and their interaction with each other. The design of the test vehicle selected several typical locations that may be present on a reusable space launch vehicle, such as sharp leading edges, convex and concave surfaces. The test vehicle is divided into four sections: the front is a sharp leading edge and a head cone made of flat ceramic material; followed by 6 TPS test pieces, at the bottom of the test vehicle is a large ceramic plate; the third part is an isotropic ceramic TPS panel located on the upper and lower surfaces; the last part is the over-the-top adapter that connects with the booster.

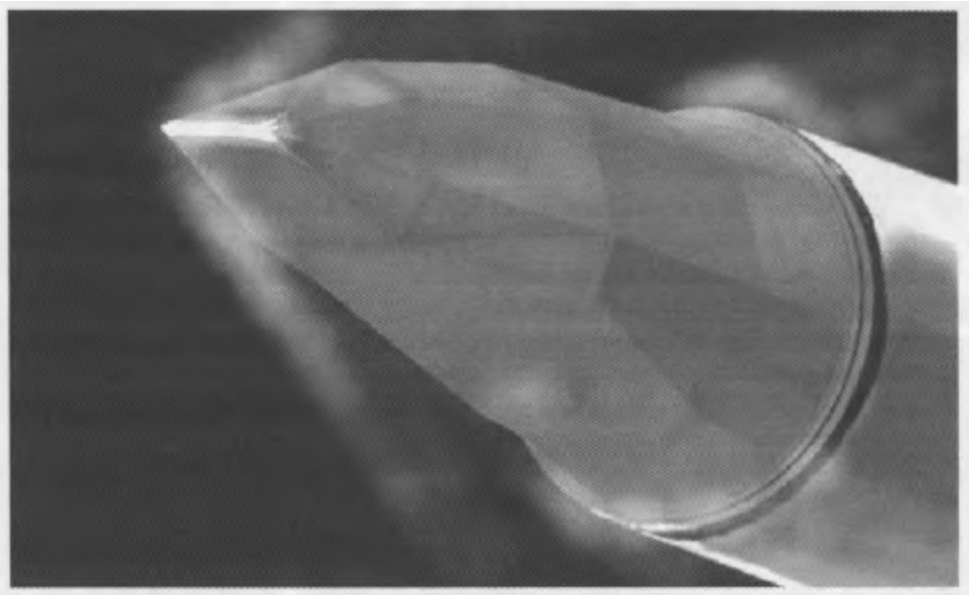

Figure 12-6: Renderings of the SHEFEX I flight tester

Reaching a maximum of *Ma* = 7 and maintaining it for 30 seconds under the booster of a sounding rocket will bring the temperature of the leading edge to 1,600°C, while the tail panel will reach 500°C. Although the entire thermal load does not reflect the entire process of re-entry of a reusable vehicle, this experiment has been used to study the bearing capacity of surface ceramic TPS, the effect of flow under hypersonic conditions, and the response of the structure.

The SHEFEX test vehicle consists of an aluminum main frame structure and thermal protection panels. All measurement sensors required during the flight are integrated with the TPS panel and the main structure. This design makes it possible to experiment with different panels and surface coatings, to directly measure the thermal response of the main structure, and to replace the type of measurement sensor with different distributions. The basic structure consists of an aluminum frame structure consisting of rigid beams and stiffeners, and a TPS test panel and its measuring device can be installed based on the frame structure. Inside the frame, some test-related equipment, including thermocouple connectors, pressure sensors, and pyrometers are installed (Fig. 12-7).

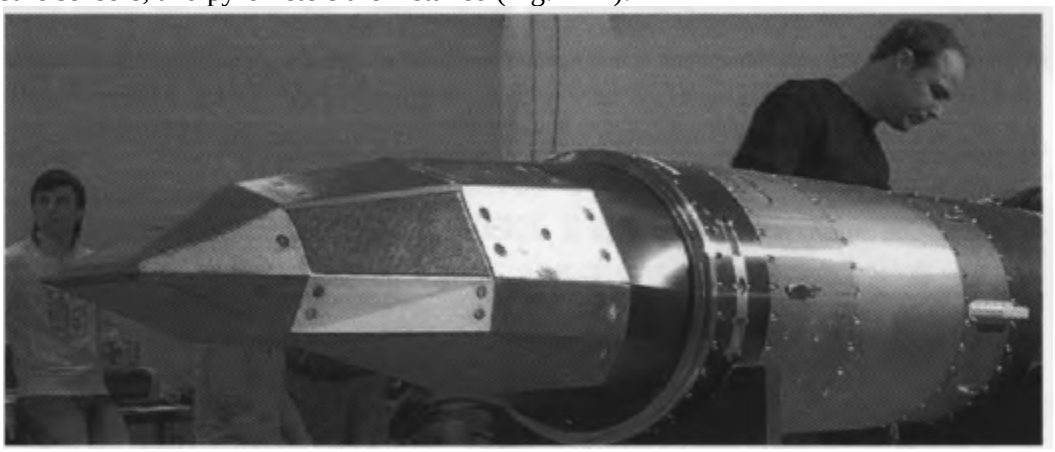

Figure 12-7: SHEFEX I flight tester

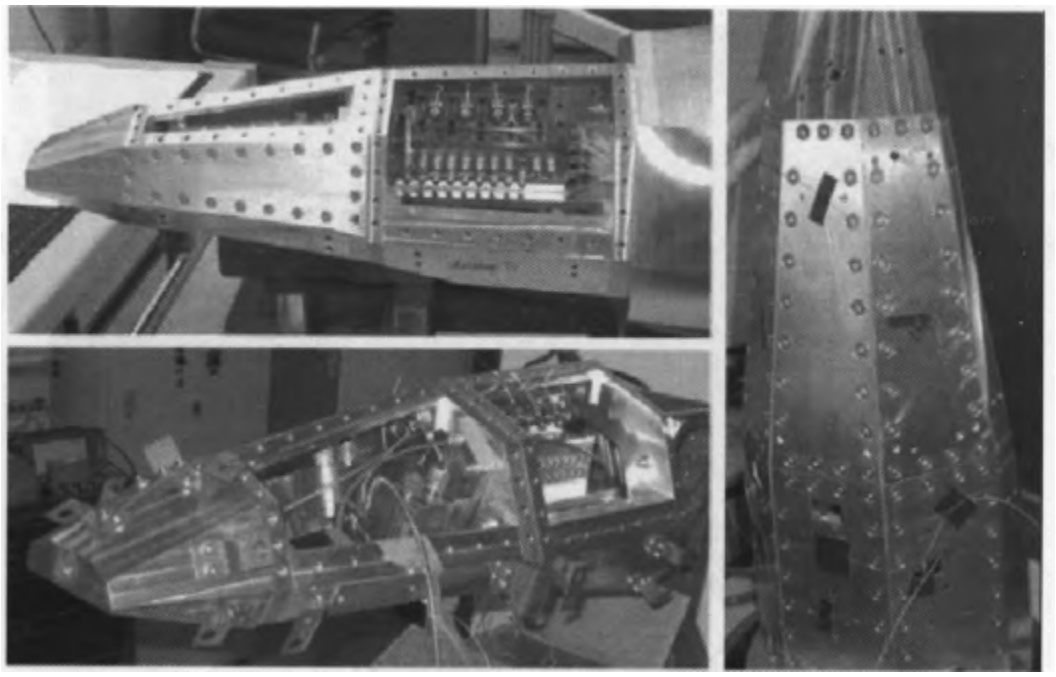

Figure 12-7: SHEFFEX I flight tester (continued)

The thermal protection system is designed by CMC panels using a segmented concept and manufactured by DLR using liquid silicon, a technology developed with the support of ESA's program, and its main components are fiber-ceramic covered plates that are fixed in the center and the four corners are flexibly connected so that thermal expansion is not hindered when heated (Figures 12-8 and 12-9).

Figure 12-8: Thermal protection and thermal insulation panel

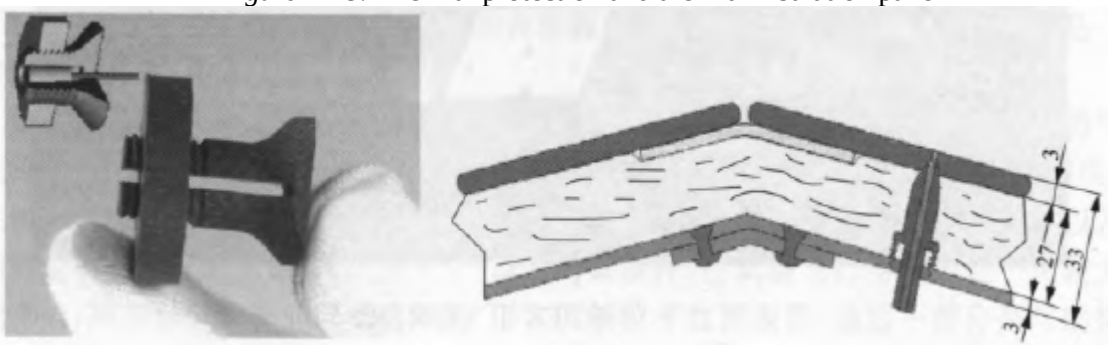

Figure 12-9: The fastening screws of the SHEFFEX flight test TPS panel and the gasket between the panels

12.4: SHEFEX II flight testing (2008)

12.4.1: Development Background

The SHEFEX II test vehicle is the second step in the roadmap of the SHEFEX series development project in Germany, and the preparation of the SHEFEX II test vehicle has begun following the success of the SHEFEX I flight test. SHEFEX II continues to use a two-stage sounding rocket engine system and continues to undergo technical testing and demonstration verification. Based on the experience gained during the SHEFEX I test and the flight data collected, the vehicle for this test was redesigned and equipped with an active control system for active aerodynamic control during the re-entry stage. The tester will integrate mechanical actuators, automatic electrical control units, pneumatic control units made of ceramic materials such as rudder and wings, with a focus on improved guidance and navigation control (GNC) units. In addition, the SHEFEX II is equipped with a number of test loads such as active cooling thermal protection modules, advanced sensor instruments, high-temperature antenna inserts, etc.

12.4.2: Introduction to Test Pilots

During the SHEFEX flight tests, the German Aerospace Center focuses on the research and development of re-entry and hypersonic technologies. With a modified sounding rocket engine system (previously used for low-gravity research tests), it is possible to conduct high-efficiency flight tests in a short period of time. In addition to testing materials and structures, the effectiveness of simulation tools and ground test results can be adjusted and verified by comparing actual flight data with digital simulation and ground test results.

Following the success of the first spiral shape test vehicle, SHEFEX I, on October 27, 2005, preparations for follow-up tests began. The SHEFEX I performed a 20s flight of $Ma = 6$ and obtained complete high-value aerodynamic data. The use of flight tests and all the experience gained so far will be used to solve new scientific problems and support the expansion of its flight envelope in the SHEFEX II test, doubling the Mach number and reentry time.

Using a two-stage sounding rocket engine from Brazil as the propulsion system, the SHEFEX II continues to undergo technical testing and demonstration validation. Based on the experience gained during the SHEFEX I test and the flight data collected, the vehicle for this test was modified and equipped with an active control system that can perform active aerodynamic control in the re-entry stage. In addition to the multi-faceted ceramic thermal protection system, key technical tests will be carried out on ceramic aerodynamic control components, front cabin winglets, mechanical transmissions, and automatic flight control units. In addition, the GNC system of SHEFEX II includes different inertial navigation platforms and star-sensitive sensors, which can provide precise information about the position and orientation of the aircraft.

A number of other test instruments, including active cooling thermal protection modules, advanced sensor instruments that measure temperature, heat flow, and pressure, and high-temperature antenna inserts, will also be tested with the SHEFEX II. A number of companies and universities in Germany and other countries are also planning to carry out test vehicles to conduct research and demonstration demonstrations of thermal protection units based on advanced metal and ceramic materials, new fiber optic sensors and sensor systems (developed for the European Space Agency's EXPERT mission).

A hypersonic scour flow data system using a series of specially arranged forward pressure sensors is mounted on the head of the load as a passive test rig. With them, systems and advanced algorithms for active control can be evaluated on future hypersonic missions.

The launch system of the SHEFEX II is based on the Brazilian V S40 monolithic system (consisting of two parts the console and the spacecraft), with a total length of 12.6m and a mass of 67t.

The S40 is the 1st stage propulsion unit of a solid rocket engine. Within 60s after ignition, a propulsion system with a mass of 4 pushed the SHEFEX II to an altitude of 54km. In the 1st ballistic stage after the separation of the 1st stage, the 2nd stage solid rocket engine (S44) will be reset to a horizontal attitude before firing. The mass of the 2nd stage propellant is 800kg, which propels the SHEFEX payload to apogee (about 270km). After the spin-free maneuvering separation of the rocket engine, the attitude control system adjusts the reentry angle of the load to about 35°. The re-entry stage, the beginning of the experiment, will begin at 100 km, at which altitude the effects of the atmosphere begin to be felt. In the current flight envelope, the aircraft will fly for 45 seconds at a maximum Mach number of *Ma* = 11 (about 3 km/s) in the re-entry stage. High Mach numbers will result in extremely high heat flow at the head of the load, the winglets in the front compartment, and the tip edge of the stabilizing wing. At these exposure points the temperature will reach more than 1800°C. At the end of the entire re-entry stage, at about 20 km, the dynamic pressure will increase to $4x10^5$ Pa (Fig. 12-10).

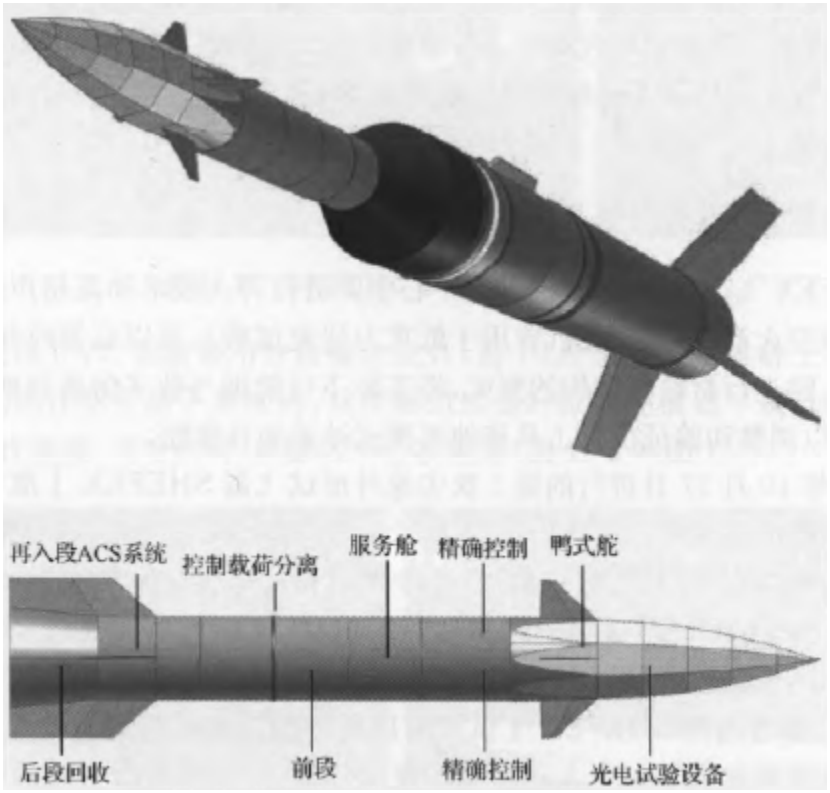

Figure 12-10: SHEFEX II test vehicle

12.4.3: Introduction to Subsystems

1. Rocket Motor System (RMS)

After weighing various configurations and reviewing various possible performance metrics and associated ballistics, the researchers finally selected the Stage 2 configuration with Brazil's S40 solid rocket booster. The RMS was originally developed and designed by the Brazilian Aerospace Center (CTA) to collect space flight data from the S44 engine as the 4th stage of the CVA's satellite vertical launch system. The S44 engine's casing and interstage connections are lightweight construction, with Kevlar composite materials and a burn time of 60 seconds.

The VS40 was first launched in April 1993 at an elevation angle of 81.8°, rising to a climactic point of 950 km, flying a range of 2,680 km and a load mass of 197 kg.

Two flights have been carried out so far, both of which have been successful [5]. The main focus here is on the test section of the SHEFEX II test vehicle, which corrected the parabolic trajectory of a conventional unguided sounding rocket, lowered the commanding altitude and extended the re-entry stage and flight in the atmosphere. Ballistic correction requires a steering maneuver outside the atmosphere in a state of spin after the first stage is burned out and separated, using the ACS air-conditioned propulsion system. Before the S44 engine is ignited, the detached vehicle will be re-steered and the rolling shaft will be aligned at a low angle (e.g. 0° to 10°). After the S44 burns out, it is released from rotation by the cable retraction device. The ACS system will set the height at the time of re-entry, and due to the limited thrust of the air-conditioning system, the system also has a certain inertia, and the steering process takes about 100 seconds.

1) Mechanical flight system

When carrying an unusual load pattern on a new aircraft, the navigation system, ballistic characteristics and the need for recovery operations using aerodynamics for braking at low altitudes all pose a number of technical challenges in the mechanical design, the main of which are the following: the aerodynamic stability of the aircraft as a whole during the ascent phase (despite the load with a tail and canard rudder), the active separation of the two stages of the engines after the extended glide section, the combination of the two cold gas propulsion systems at the optimal point, and the separation of the load at hypersonic speeds for braking before recovery.

2) Fairing and engine wings

To solve the problem of load wings and canard rudders, a fairing can be covered over the entire load, but this increases the mass and may reduce the performance of the first stage; the performance impact on Stage 2 is even greater unless it is ejected during the spin phase prior to ignition. In the end, a compromise was adopted, with a small fairing attached to the loaded wings and ejected after the S44 burned out and the spin was released. The fairing is made of composite material and contains two or four parts about 1.4m long, separated by a pyrotechnic thruster on the load and connecting modules. After reaching the commanding heights, the canard rudders were held in place by retractable wings, which required larger and lighter wings on the S40 due to their exposure. The S40 has a wingspan of more than 1m, and the extended root chord over the engine housing improves stability during the launch phase. The design and manufacture of the wings was carried out by the Stuttgart branch of the German Institute of Aerospace Technology, which is responsible for materials research.

3) Load connection module

The interface between the S44 engine and the load serves several functions, and the cable retraction and release spin system can release the 2Hz spin to stabilize the system and prepare for the ignition of the S44. The front end of the attachment module is used to lock the fairing of the rear wing of the load. Once the fairing is disengaged, the structure that connects the module to the small-diameter end of the rear section of the load is released, while the three disengaging pistons accelerate to push the load away from the engine.

4) Load the wings

The wingspan of the load is small, it is a fixed stabilizing surface, the length of the chord is 1200 mm, the wingspan is 230 mm, and it is composed of high-temperature resistant composite materials to withstand the aerodynamic and thermal loads of the re-entry section. In order to control the roll rate of the S44 engine with a large inertia, the roll thruster must be embedded in the wings to maximize the instantaneous torque. In addition, since these wings will be aimed at the initial load axis, the side control thrusters need to be embedded in the front end of the wing. That is, a notch-mounted roll thruster must be included in the wing, which is activated before the fairing is separated.

5) Recycling

At an altitude of about 15 km in the descent section, the load will be separated into two parts at high speed by means of a release locking device, which brings instability and will produce a tumbling motion, accompanied by rapid deceleration, and the speed has dropped to 250 m/s when the load is reduced to an altitude of 4.5 km, at which point the recovery parachute can be disengaged from thermal protection. The experience gained from the SHEFEX I load shows that the application of aerodynamic braking is justified if the problem of the rammed air shock absorber needle can be solved and the center of gravity of the load is correctly placed.

Like the SHEFEX I, the high-speed recovery system of the SHEFEX II is installed at the rear of the load.

2. Airborne data communication and telemetry

The service system consists of a redundant S-band transmission system with two 10 W RF transmitters and two antenna systems. In this way, the ground station can receive both polarization and frequency diversity signals via the downlink datalink. An antenna system uses four MORABA high-temperature antennas, which were validated in the SHEFEX I flight test; the other antenna system consists of two relay antennas, which are housed under the RFWhipox thermal protection radome. In addition, all Pulse Code Modulation (PCM) data is recorded by the on-board SSD and can be retrieved after load recovery. The remote control system for the loads is the same as in the SHEFEX I project. The on-board system integrates two L-band remote command receivers with two high-temperature antennas placed at 180°.

During the ascent phase of the aircraft, the real-time image data taken by the camera downwards is transmitted to the ground station using an S-band 10 W image transmitter. The RF output of this transmitter shares the same data fusion network and antenna sequence as the transmission of the loaded TX 1 PCM, except that the left-handed circular polarization method is used here to further decouple the transmitter. After the S44 and the load fairing are separated, the forward camera mounted on the load antenna is activated, occupying this link. When the two load compartments are separated, the RF transmitter video input switches to the 3rd camera to monitor the recovery process before the recovery system is activated.

The color image signal is in PAL-G format using the CCIR 405 standard. The PCM data of the load and all image information are recorded on the solid hard disk of the load. The payload is equipped with a 400 W transponder and a corresponding antenna system, which uses circular polarization to receive and transmit information. In addition, the ORION CPS receiver from the German Institute of Aerospace Technology is used to receive speed and position information.

3. Launch mission and implementation

At the Andenes range, 3m and 6m single-pulse trajectory tracking stations are used to receive PCM data and image information for the load, and all receive links are configured for polarization and frequency diversity reception. In this way, high-quality data transmission is possible within the range of the range's monitorable ballistics. The positioning and operation of the ARR mobile radio station is the same as that of SHEFEX I. In flight, the location of the control station is very important, with the support of this control station, the aircraft can receive load data during the descent phase and when the flight altitude is less than 100km.

THE MORABA mobile tracking and control station will be deployed on the plateau of the city of Longyearbyen. At this position, the aircraft can receive a load signal when it appears at ground level, i.e. about 70 km from the ascent stage of the flight. From this point on, the load data can be received, and the demodulated PCM signal will be sent back to the Andenes range using an underground high-speed fiber optic line. Since the theoretical landing point of the load is 300 km from the ground, the RF data link can be lowered to a height of about 4 km. Since the recovery process starts after the load separation at an altitude of 15 km, most of the recovery activities can be detected. Once the downlink is built, the 2nd load radio remote station will transmit the commands here, which are transmitted by the load engineer via fiber optics.

Using a 10 W payload transmitter to transmit PCM data, the initial connection strength is expected to be ideal at 6 dB (excluding diversity enhancement in the pre-detection section) for the time period during which the main tracking station at the Andenes range will be able to monitor. The minimum image signal quality of the TV link is about 30dB. At all times, whether for high-energy shocks or for load command transmission, sufficient bandwidth and an appropriate signal-to-noise ratio are guaranteed.

Since the VS40 aircraft is realigned by the active control system prior to ignition, a fully redundant terminal flight system is required.

In the event of an accident, the system will perform the self-destruct operation of the S44 engine. In the combustion stage of the 1st stage, the system behaves like a conventional unguided rocket. The ignition of the second stage is determined by a series of conditions: (1) the precession is complete; (2) the ignition time window is opened; (3) the TC flame retardant system is not activated.

The on-board inertial navigation platform transmits signals to the ignition system, which allows for 2nd stage pointing and correction. With telemetry, load engineers and safety personnel can verify this information on the ground and correlate it with additional information such as GPS loads and radar. If the attitude control system fails, the remote control system for the load cancels the ignition signal from being transmitted to the ignition system of the second stage. If all requirements are met, stage 2 will be ignited at the scheduled time (Figures 12-11).

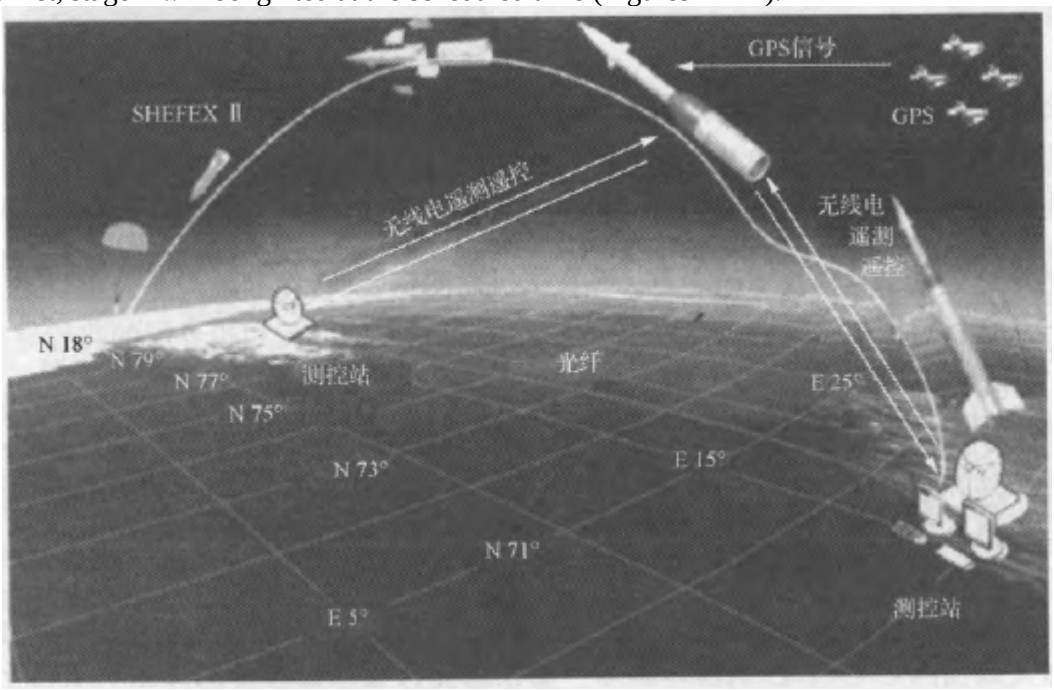

Figure 12-11: Schematic diagram of the flight test process of SHEFEX II

4. Load head structure

The main structure of the load head is the same as that of the SHEFEX I, which is an aluminum alloy structure consisting of a combination of a rigid frame and spare parts. The space is enclosed by flat aluminum panels that form the inner mould line (ML), which are also used to install the flat thermal protection system (TPS) surfaces and test setups. Measurement equipment was installed in the rack, including thermocouple connection and compensation box, pressure sensor, pyrometer, data processing system, and a system with test equipment. The load head is divided into 8 independent surfaces with circular symmetry, and the control surface from the endpoint to the brake module is divided into 5 sections. In this way, 40 planes are installed on the load head, 32 of which can be equipped with different test equipment (Fig. 12-12).

5. Thermal protection system

The basic active refrigeration TPS system is based on a segmented design developed in the ESA project. The main unit in this design is a fiber-ceramic cover supported by a movable frame at the central column and face corners, so that thermal expansion is not suppressed. Lightweight fiber-ceramic insulating pads were installed under the cover plates, and research on active refrigeration systems was carried out simultaneously. Based on the experience gained during the development of the combustion chamber of a fluid-cooled ceramic rocket engine, the technology can be used to design TPS components with large loads at the sharp edge or exposed to heat flow that exceeds the temperature limit of the material. First, the screening of different porous ceramic materials and refrigeration gases demonstrates the potential of this technology.

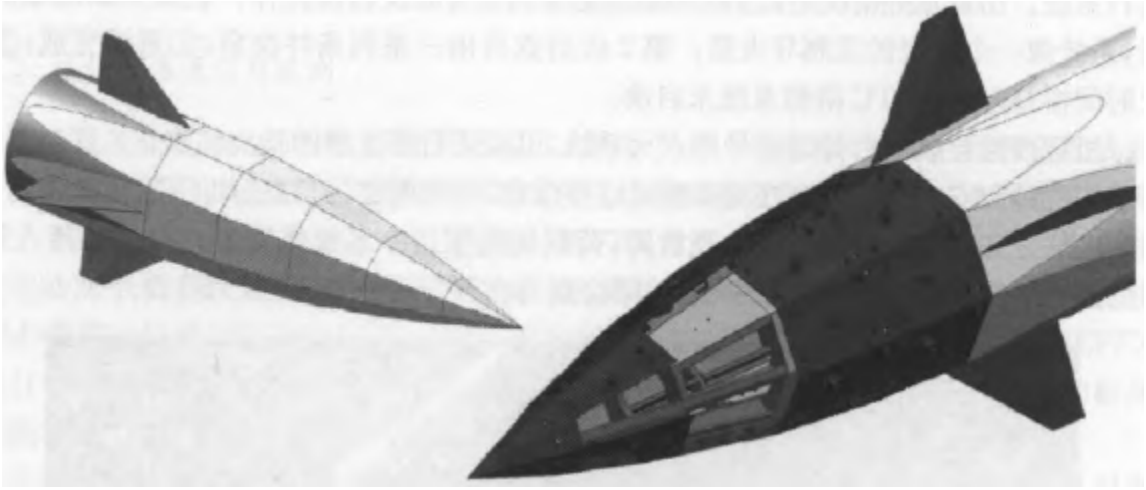

Figure 12-12: SHEFEX II test load head

Plasma wind tunnel tests have shown that a small amount of gas can be consumed in a hypersonic airflow to produce a powerful cooling effect. However, considering the heat conduction and interaction of the surrounding airflow and the boundary layer, efforts need to be made to study the parameters related to the cooling effect.

Active refrigeration systems may be used in situations where the thermal environment is harsh and the passive refrigeration system is not up to the task. The evaporative cooling test uses a porous ceramic material on the outer surface, through which the coolant flows into the boundary layer. In this way, evaporative cooling is facilitated by two physical phenomena, as the porous structure is convection-cooled by the coolant and the cooling layer of the external hot surface, reducing the heat transfer from the high-temperature environment to the surface of the aircraft.

In the center of the planar thermal protection system panel, a porous detector will be embedded. The coolant passes through the porous detector and is pressed through a pressure ring into the surrounding C/C-Si/C TPS material. The accumulator is connected to the C/C-SiC ceramic by riveted ceramic fasteners, and the accumulator itself is made of stainless steel.

At this point, the numerical finite element analysis of a large number of test devices has been completed, and a similar configuration has been perfected in the plasma wind tunnel test. In addition, the head-air impact characteristics of the load resulting from the impact between the boundary layer and the refrigerant gas will be simulated by CFD computational fluid dynamics and tested in the wind tunnel.

12.4.4: Aerodynamic Problems

The main challenge in the hypersonic aerodynamic environment is related to the ability to simulate the hypersonic gas field using the currently limited ground test equipment. Reproducing the hypersonic airflow that will be subjected to re-entry in a wind tunnel is not yet possible, and it is unlikely to be possible in the near future. In addition, the database of hypersonic aerothermodynamics collected during flight tests is very limited and even less documented in the publicly available literature. The aerodynamic design of hypersonic vehicles relies heavily on computational fluid dynamics (CFD), which cannot be validated in ground test equipment. As a result, engineers designing hypersonic vehicles must adopt a combination of CFD, wind tunnel testing, and flight testing. In addition to these design challenges, flight tests will also validate the performance of thermal protection systems and their materials, as well as gain experience with other systems. In fact, the abundance of scientific data from the SHEFEX I flight tests shows that the relevant direct tests are a fundamental source for gaining the essential knowledge of hypersonic flight and developing more complex vehicles.

The experience gained from SHEFEX I has led the German Institute of Aerospace Technology to implement a plan for a gradual transition to a fully automated re-entry vehicle, which may be implemented with aerodynamic control in future aircraft.

The disadvantage of ballistic reentry is that it is limited in maneuverability and it is difficult to break through the limitations of the flight trajectory, such as heat flow or total load. These difficulties can only be overcome by actively controlling the aerodynamics of the reentry stage, so the flight tests carried out to verify the control and guidance algorithms of the reentry stage are very important for the development of future aircraft.

In addition, from a hydrodynamic point of view, flight tests of actively aerodynamically controlled vehicles can provide a platform to gain experience with wing performance and wing heating phenomena resulting from shock wave boundary layer interactions and shock interactions. Therefore, the goal of the SHEFEX II test is to validate the re-entry of a fully aerodynamically controlled hypersonic vehicle for the first time in Europe. If a multi-faceted axisymmetric aircraft structure is adopted, the re-entry trajectory is designed to be at an altitude of between 100 and 20 km, and it will re-enter the atmosphere at a speed of $9 < Ma < 11$.

In addition to addressing the above-mentioned system-level challenges, the Centre for Aerodynamics and Fluid Technology Research is also working on a number of other future-oriented projects, namely virtually designed space vehicles. Due to significant advances in computer technology and CFD technology, interdisciplinary disciplines consisting of the combination of fluid mechanics and structural mechanics, or the combination of aerodynamics and flight mechanics have developed. In the design process of hypersonic vehicles, the interdisciplinary discipline of fluid mechanics and flight mechanics can be used to directly analyze the aircraft. This is especially important for hypersonic vehicles, where the design requires complex aerodynamic data, i.e., Mach numbers, angles of attack and yaw, and declination of control surfaces. In addition, the full ballistic process from hypersonic cruise/re-entry to subsonic landing needs to be covered.

In the current situation, it is still too long to calculate the free motion of the aircraft in the full trajectory using the intersection of CFD and flight mechanics, so it is necessary to first evaluate the models generated by the control surface tilt algorithm SOSE developed by the German Aerospace Research Institute and the ballistic optimization algorithm REENT developed by the University of Stuttgart in the SHEFEX II flight test. The cross-flow model allows the design to take into account both dynamic and unpowered phases (e.g., inertia variables over time are also taken into account due to fuel consumption), and the dynamical system will perform a predetermined operation in a 6DOF simulation state.

The current code is appropriate for the experimental definition of a multistage sounding rocket, and in further applications, more complex hydrodynamic methods can be introduced, such as the Euler and Navier Stokes codes of the German Aerospace Research Institute TAU. This multidisciplinary design, including CFD and flight mechanics simulations, will enable a full-power analysis of a controlled free-flying vehicle. In the MPULSE project of the German Aerospace Research Institute, the code TAU uses a 6-degree-of-freedom motion model, which can be combined with digital aerodynamics to directly simulate the motion state of a rigid body. The prerequisite is that the aircraft control surfaces are taken into account in the simulated maneuvering flight.

The integration of control planes presents challenges for digital research, especially meshes that must be synchronized with control planes. In order to avoid the deflection of the control surfaces and generate new meshes, overlaid grids and chimera-techniques are used to integrate the control surfaces. This new multidisciplinary design approach will be validated by the SHEFEX II flight test, which will contribute to the design of future hypersonic vehicles and control systems. This method will provide more accurate dynamic analysis that can accurately predict the dynamic characteristics of hypersonic vehicles, which is important for wingless structures such as wingless vehicles and re-entry capsule structures.

SHEFEX II is an important step in the German Aerospace Institute's roadmap for the development of hypersonic and reentry technologies, which is expected to be used for the first time in recovery tests. The system will provide a high-quality microgravity free-flying platform with return capability from sounding rocket tests, active aerodynamic control of the re-entry stage, and special cavity technology to improve the vehicle's cost-effectiveness ratio. The SHEFEX II mission is no longer a stand-alone project, nor is it just a repetition of the first test but is part of a long-term flight test program for re-entry technology and related R&D projects.

References

[1] Hogenauer E, Koelle D. SANGER, the German aerospace vehicle program [R]. AIAA-1989-5007, 1989.
[2] Dietrich E Koelle. Advanced two-stage launch vehicle concepts (SANGER) [R]. AIAA-90-1933, 1993.
[3] Lederer R, Schwab R. Hypersonic airbreathing propulsion activities for SANGER [R]. AIAA-1991-5040, 1991.
[4] Hirschel E. Aerothermodynamics and propulsion integration in the SANGER technology programme [R]. AIAA 1991-5041, 1991.
[5] Heribert Kuczera, Paul Krammer, Peter Sacher. The German hypersonics programme-status report 1991 [R]. AIAA-91-5001, 1991.
[6] Kuczera H, Hauck H. The German hypersonics technology programme-status report 1992 [R]. AIAA-1992-5002.1992.
[7] Kuczera H, Hauck H, Sacher P. The German hypersonics technology programme status 1993 and perspectives [R]. AIAA-1993-5159, 1993.
[8] Weingartner S. SANGER-The reference concept of the German hypersonics technology program [R]. AIAA-1993-5161.1993.
[9] Hirschel E H. The hypersonics technology development and verification strategy of the German hypersonics technology programme [R]. AIAA-1993-5072, 1993.
[10] Jiang Qi, Ma Ling. Germany's SHEFEX II hypersonic test vehicle [J]. Flying Missile, 2009, (6):21-28.

CHAPTER 13: JAPANESE HYPERSONIC VEHICLE TECHNOLOGY RESEARCH

13.1: Scramjet research in Japan

The research of the Japanese scramjet engine began in the 1980s. In 1991, the first generation of scramjet engine model was designed, which is a module based on the integrated engine of fuselage propulsion, and the main parameters of the model are shown in Table 13-1. The model engine was tested on the ramjet engine test facility (RJTF). The model consists of six main components, namely the leading edge of the inlet channel, inlet flow channel, isolation section, fuel nozzle, combustion chamber expansion section, and nozzle. These components are combined in multiple modules and can be parameterized for experimental studies. The entire model engine is 2,100 mm in length and has the same inlet and outlet cross-sections, both 200 mm wide and 250 mm high. The projected area of the engine inlet and including the engine wall thickness is less than 20% and 25% of the nozzle outlet area of the test bench, respectively, which is conducive to the operation of the wind tunnel [1].

Table 13-1: Main size parameters of the first generation scramjet model in Japan

Intake tract	Length/mm Cross-Section/(mmXmm)					610 200x200				
Quarantine segments	Length/mm			Short 100				Long 200		
Combustion chamber	Length/mm Equal cross-sectional length/mm			160		800		60		
Fuel nozzles	Diameter/mm				Position/mm (distance from steps)			quantity		
		Sidewalls	Top	Support plates	Sidewalls	Top	Support plates	Sidewalls	Top	Support plates
	Main vertical nozzle	1.5	—	1.5	30	—	30	12x2	—	12x2
	Main vertical nozzle	1.5	—	1.5	16	—	16	12x2		12x2
	Main parallel nozzle	3.0	—	3.0	0	—	150	12x2		12
	Ignition nozzle	0.5	0.5	—	-50	-70/-50		94	7/6	

The scramjet model tests were carried out, including the heat sink model, the water cooling model, and the liquid hydrogen cooling model, all of which had the same inner channel geometry but with different support plates and wedge surfaces for comparative study. Engine cooling is also a key technology in the development of scramjet engines, so the liquid hydrogen cooling model was tested to test the effect of liquid hydrogen cooling and the impact on engine performance.

In most of the tests, different support plates and wedges were added to the model engine to increase the pressure of the combustion chamber section in order to achieve better combustion performance. The injection section of the fuel, with swept steps on the side and upper walls, is used to stabilize the flame. The front part of this section is an isolator of equal cross-section to prevent the fluctuation caused by combustion from being transmitted to the inlet tract and affecting the performance of the inlet tract. The 100 mm and 200 mm length isolation section models were tested to compare their performance. In terms of fuel nozzles, multiple rows of vertical injection and parallel injection nozzles are set up respectively.

After a series of experimental studies on the first-generation scramjet model, the design and manufacture of the second-generation engine model was carried out in 2000 based on the original model, and experimental research began in March of the same year. The second-generation engine model focuses on the principle verification and testing of the rocket-based combined cycle engine (RBCC), which can be applied to single-stage orbital aerospace aircraft, as shown in Figure 13-1.

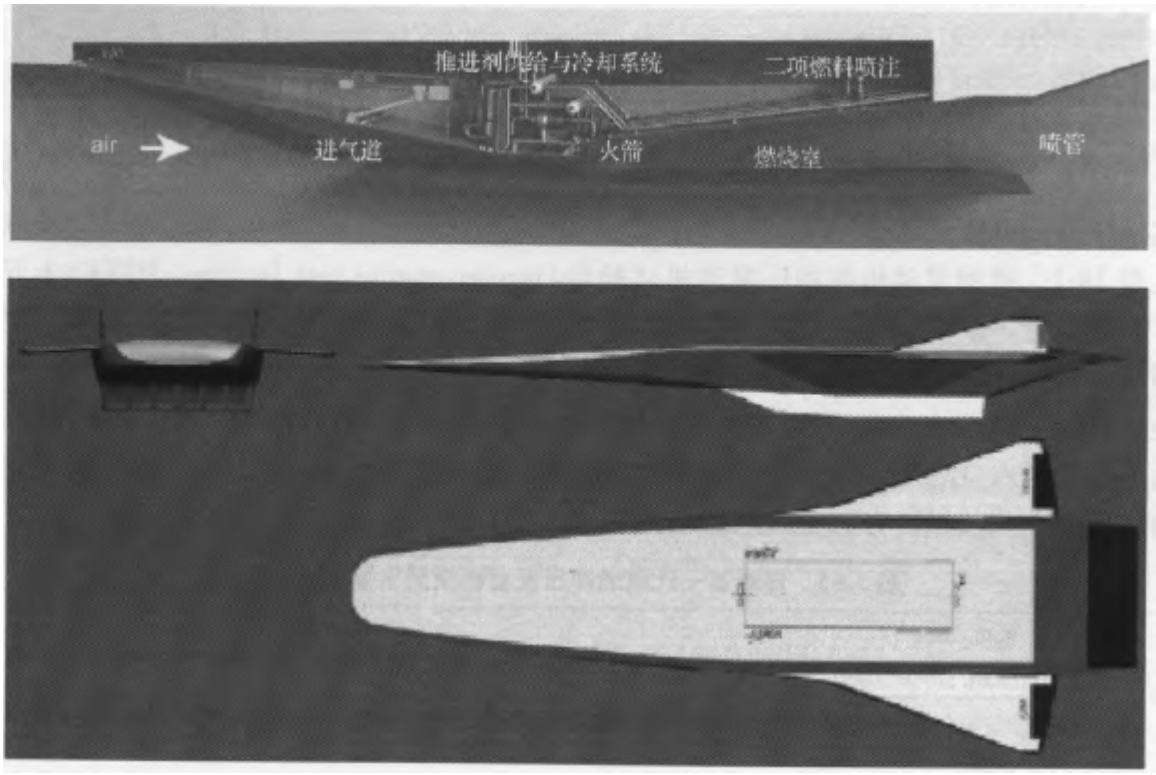

Figure 13-1: Japanese RBCC engine and its application aircraft

13.2: Aerospace Aircraft Program Study

Japan has long been aware of the need to improve the reliability of launch vehicles while reducing the cost of space transportation. To this end, in April 1999, the Japan Science and Technology Agency established the Space Activities Committee to manage the development of space transportation systems. The committee has an RLV research and development team, which is responsible for the development of RLV. In May 2000, the Committee on Space Activities presented a plan for the development of RLVs from existing single-use launch vehicles (ELVs). Among them, the two-stage orbit launch vehicle (TSTO) is the target system, with an air-breathing engine in the first stage and a reusable rocket engine in the second stage (Figure 13-2) [2].

The development plan for the Japanese RLV was originally intended to be divided into three phases, and the research results of each stage were reviewed and revised.

Phase 1 research focused on engine systems, including air-breathing engines and reusable rocket engines. The HOPE experimental vehicle will undertake the flight test mission of the second stage of the launch vehicle. In the first five years of the first phase, the focus was on the development of the ATREX engine with a turbofan diameter of 30 cm. The ATREX engine allows the HOPE to fly with a Mach number of 6. In addition to basic technology research, the first phase will also develop a 10-ton class reusable engine. The results of these basic technical studies will be subjected to ground and air tests. In the supersonic and re-entry flight areas, the system performance of the launch vehicle will be evaluated and verified by subsequent flight tests of HOPE.

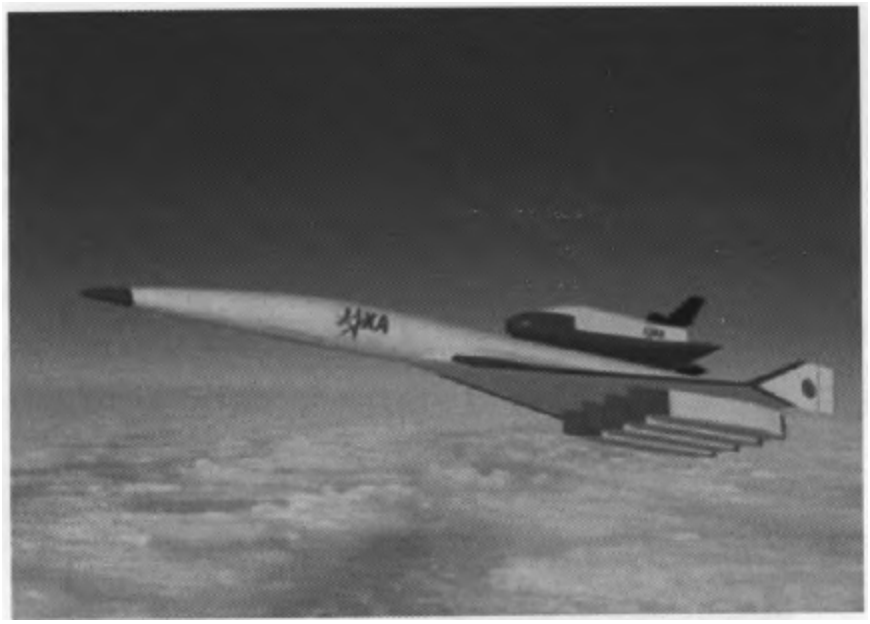

Figure 13-2: Japan's two-stage orbit launch vehicle scheme

HOPE has the ability to be reused to some extent, and the high-speed flight experience of the HOPE program has contributed to the development of the second stage of the TSTO, as well as to the development of experimental vehicles with air-breathing engines.

The second stage will be the development of a large-scale experimental vehicle for the TSTO stage. Each vehicle will be separately tested for flight, in which the second-stage experimental vehicle will be launched by the existing ELV. This stage will also include the development of an ATREX engine with a turbofan diameter of 60 cm and a reusable LE-7A rocket engine. Two ATREX engines with a turbofan diameter of 60 cm will be installed on the experimental vehicle of the first stage, with a take-off mass of 20 tons and a flight Mach number of 6 at an altitude of 30 km, which will return to the take-off runway after the flight tests. The first stage of the experimental vehicle will carry 1 simulated second stage of the experimental vehicle for individual tests at the highest altitude. The second-stage experimental vehicle weighs 120 tons and uses reusable engines in the 100-ton thrust stage, which is launched by the ELV and enters the LEO orbit, and flies back to the runway and lands horizontally after the orbital re-entry test. If possible, the results of the development of the second stage of the experimental vehicle can be applied to the development of RLVs (including TSTO and SSTO) at any time.

Phase 3 will involve the creation of a full-scale experimental vehicle. It can transport a payload of 8 tons to low earth orbit. The first stage of the experimental vehicle is equipped with six ATREX engines with a turbofan diameter of 120 cm, and the second stage is still using the second stage design. The vehicle will verify the reliability and operational capability of the two-stage orbit entry RLV system.

After the completion of the three research phases, an operational TSTO launch vehicle will be developed in 2015 as a future RLV for Japan. In parallel with the development and work of the RLV, Japan will also improve the ELV to provide a better space transportation system to meet the needs of various geosynchronous orbit transportation, deep space exploration, and other planetary exploration missions. The planning of the Committee on Space Activities also states that the successful development of the TSTO reusable launch vehicle would give Japan the capability to develop a manned space transportation system.

Japan has been carrying out the research and development of reusable launch vehicles in accordance with the above plan for many years, but since 2002, the H-2 launch vehicle has failed one after another, and Japan has stopped the HOPE program and decided to rebuild the framework for the technological development of the space transportation system.

13.3: HOPE Flight Test Research Program

In order to verify the re-entry technology of the space transportation system, Japan decided to implement the HOPE program in 1992. The program's reusable vehicle, called the H-II Orbiting Plane Experiment Vehicle, or HOPE-X for short, is an unmanned reusable space vehicle that is launched by a conventional rocket, operates in low-Earth orbit, transports cargo, or performs scientific experiments, re-enters the atmosphere, and lands horizontally on a runway. The function of HOPE-X is to use the reuse transfer vehicle to and from the International Space Station (ISS) to verify the system integration technology of the re-entry vehicle and the basic key technologies of the re-entry vehicle in terms of aerodynamics, thermal management, heat protection, guidance and control, and automatic landing (Figure 13-3).

Figure 13-3: HOPE-X reusable space launch vehicle

Prior to the first flight of HOPE-X, the HOPE program consisted of a series of preliminary flight tests (Figs. 13-4), which were [3]:

OREX (the Orbital Re-entry Experiment);
HYFLEX (the Hypersonic Flight Experiment);
ALFLEX (the Automatic Landing Experiment);
HSFD (High-Speed Flight Demonstrations).

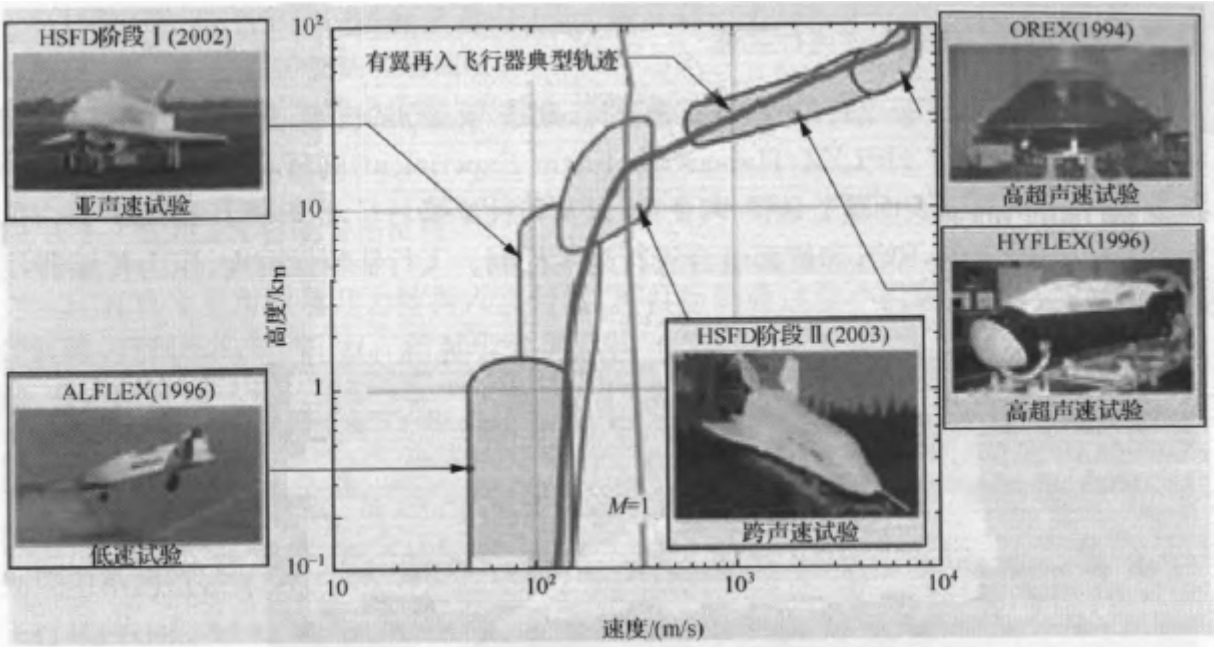

Figure 13-4: HOPE series flight test flight envelope

13.3.1: OREX Orbital Reentry Test

The OREX (Orbital Reentry Experiment) flight test is part of the H-II Orbiting Plane (HOPE) program, which aims to gain experience in designing and manufacturing reentry vehicles and obtain reentry flight data that is difficult to obtain from ground tests. The OREX vehicle was launched into orbit by an H-II rocket in February 1994, and the test obtained data for the re-entry phase: (1) aerodynamic and aerothermal data for the re-entry stage; (2) data on the structure of heat-resistant materials in the re-entry stage; (3) data on communication blockage in the re-entry phase; (4) GPS navigation data in the re-entry and orbit phases.

The OREX has a blunt cone shape, and the front of the aircraft is heated by aerodynamic re-entry and is made of carbon-carbon composite materials and ceramic heat-resistant tiles. These heat-resistant materials, as well as thermal protection materials, are planned to be used in HOPE. Temperature sensors and pressure sensors are installed on the aircraft. The head of the OREX has a radius of 1.35 m, a diameter of 3.40 m, a height of 1.46 m, a launch mass of about 865 kg, and a reentry mass of about 761 kg (Figure 13-5).

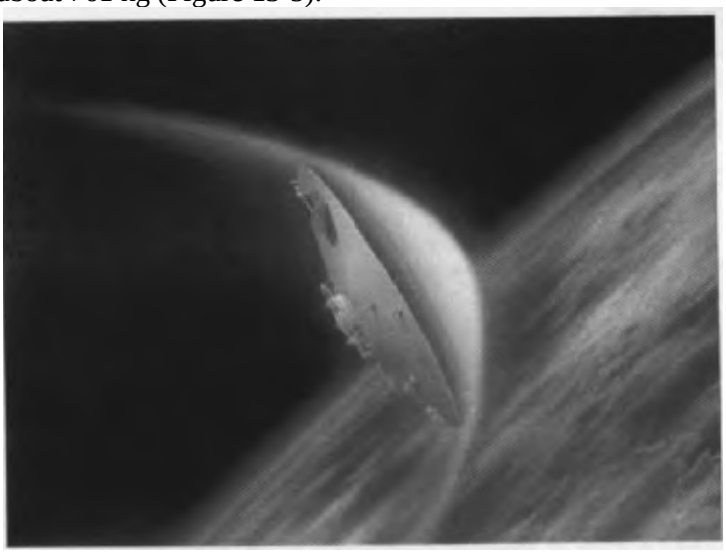

Figure 13-5: OREX re-entry flight tester

13.3.2: HFLEX hypersonic flight test

The HFLEX (Hypersonic Flight Experiment) hypersonic flight test was carried out in order to accumulate the technology of design, manufacturing, and operation under hypersonic flight conditions, and to obtain data that is difficult to obtain from ground tests (Figs. 13-6 and Fig. 13-7). The surface of the aircraft is covered with carbon-carbon-ceramic tiles, as well as flexible insulation, which are planned for HOPE. IMU is used for navigation, RCS, and rudder surface combination for altitude control. Aircraft devices have temperature and pressure sensors, as well as refractometers.

Figure 13-6: HFLEX hypersonic flight tester

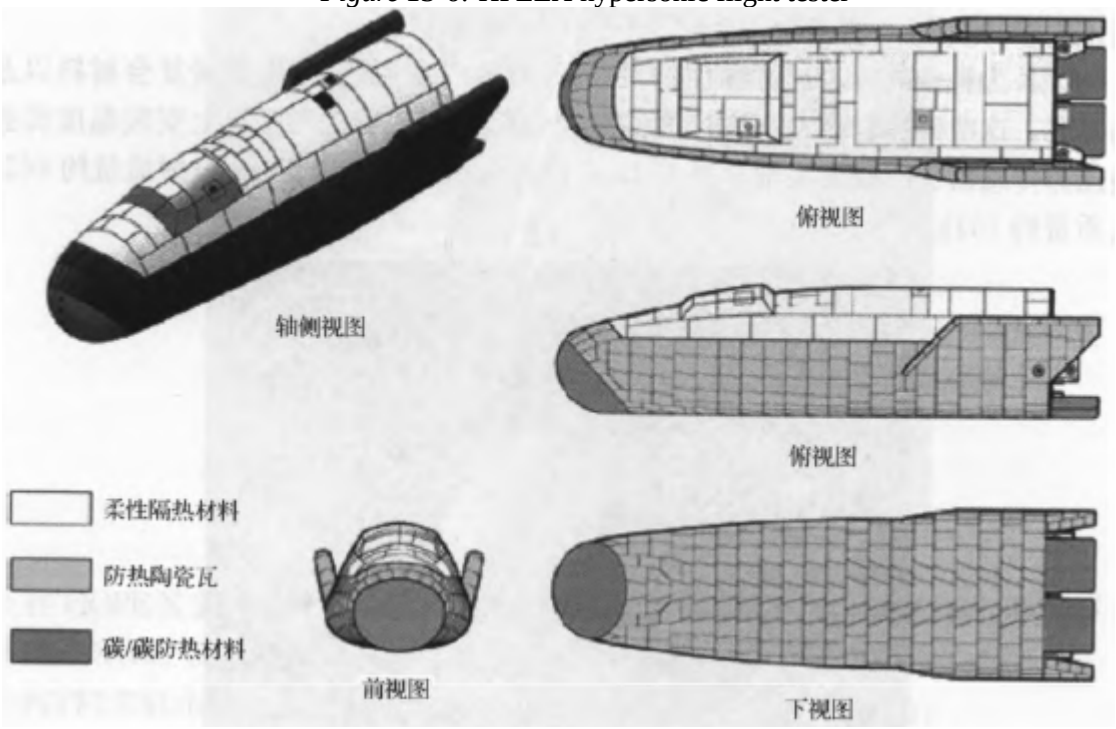

Figure 13-7: HFLEX thermal protection system

The HFLEX vehicle was launched on a J-I rocket in February 1996. Some useful data was collected during the flight, which ended up splashing on the surface of the sea and not being able to successfully recover it.

The main parameters of the aircraft are mass 1,054kg, projection area 4.27m2, length 4.40m, width 1.36m, height 1.04m, head radius 0.40m.

13.3.3: ALFLEX automatic landing test

The HOPE-X uses a lift-body re-entry vehicle, the goal of which is to reduce the mass by reducing the wings while generating lift through the shape of the airframe. Compared with the winged body configuration, the lift-body reentry vehicle is a wingless blunt body shape, which has slightly worse flight performance in the atmosphere, but has the advantage of smaller aerodynamic heating and large payload capacity in the reentry stage. The difficulty of landing necessitated research on autonomous landing technology, and it was planned to use a small, low-cost flight test vehicle for landing flight tests (Figure 13-8).

Figure 13-8: ALFLEX Autonomous Landing Test Vehicle

ALFLEX (Automatic Landing Flight Experiment) is a research project carried out in Japan on the aerodynamic design technology and guidance and control technology of winged reentry vehicles. The test vehicle is in the configuration of winged bodies. The winged configuration provides flexibility for the aircraft to operate and land on the runway like a normal aircraft. The test vehicle is released by a helicopter from a certain altitude, captures the set path, and automatically lands. Between July and August 1996, 13 trials were conducted in Australia, all of which were successful.

The main parameters of the aircraft are length 6.10m, width 3.78m, height 1.35m, mass 760kg.

13.3.4: HSFD high-speed flight demonstration test

The objectives of the first phase of the HSFD (High Speed Flight Demonstration) are: (1) to verify the landing system of the future space transportation system; (2) verify the performance of the guidance system from the final terminal area energy management stage to the approach to the landing section and the landing section; (3) verification of command/telemetry systems in arrow-borne and ground facilities; (4) accumulate experience in autonomous flight technology; (5) development of design technologies for fully autonomous flight, including automatic landing.

The first phase of the trial is mainly used to reduce the risk of HOPE-X development and increase the probability of success. In addition, Phase 1 will generate additional by-products that can be used in the development of future space transportation systems (STS), such as the development of a fully automated, unmanned test vehicle platform, fully automated flight control design technology, and verification of the flight performance of hybrid differential GPS/inertial navigation systems.

On October 18, 2002, NASDA and NAL successfully completed the first flight test of the HSFD Phase 1 test vehicle. The test vehicle has a length of 3.8 m, a wingspan of 3.0 m, a height of 1.4 m, a wing area of 4.4 m^2, a total mass of 735 kg, and a thrust of 4410 N. It is powered by a jet engine and flies autonomously with a landing device. During the test, the vehicle flew to an altitude of about 5 km, with a maximum flight Mach number of 0.6, and finally landed on a 1,800 m long runway with a total flight time of 9.5 minutes. The main task of this test is to verify the autonomous flight performance of the experimental vehicle and the process of fully automatic landing under the control of the flight control computer, in addition to the performance of the navigation system. On November 5, 2002, Japan conducted the second flight test of the HSFD Phase 1 experimental vehicle, which rose to an altitude of 2,500 m and then rapidly descended at an angle of attack of 13°.

As a result, the flight test was a success. On November 16, 2002, Japan successfully conducted its third flight test at an altitude of 5 km. Since then, the HSFD program has entered Phase 2 (Figures 13-9).

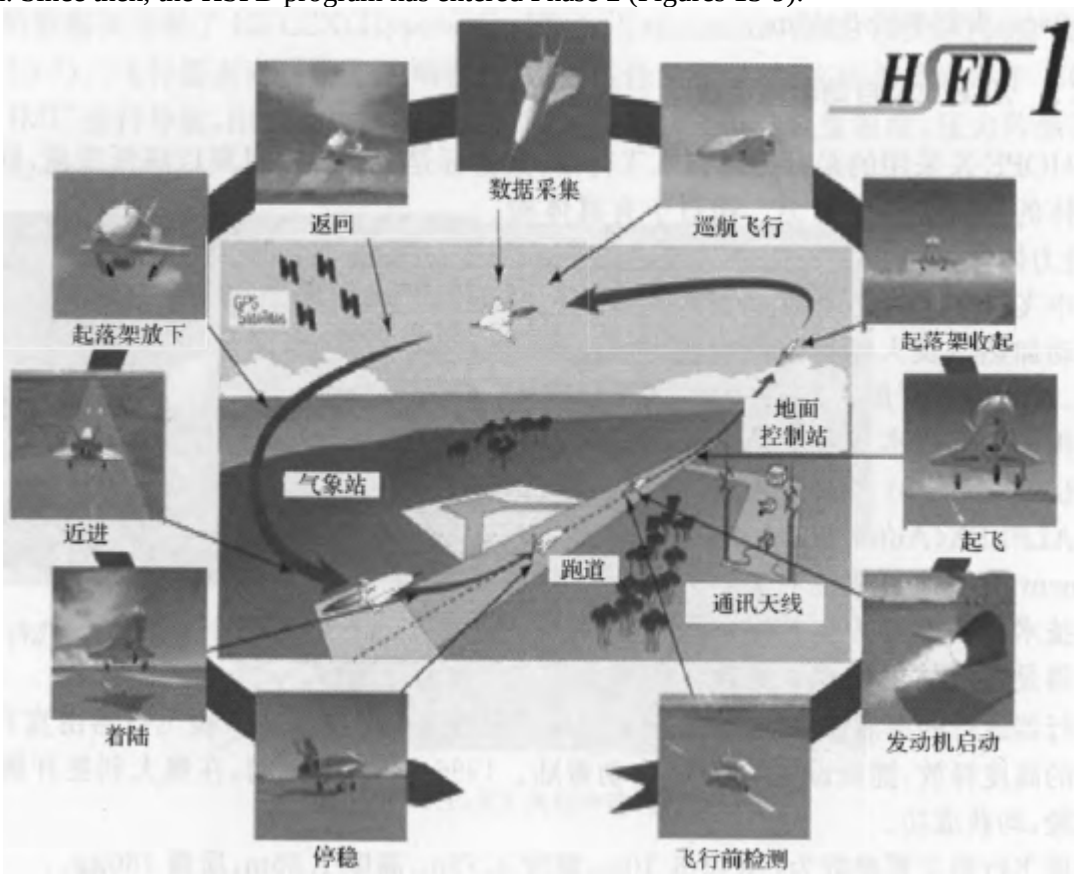

Figure 13-9: HSFD flight test procedure

The second phase of the HSFD test, with the objective of evaluating the transonic aerodynamic characteristics of the HOPE-X, was carried out in July 2003. The approach to testing at this stage is very unique. The test vehicle is carried by a stratospheric balloon to a specific altitude and then released, and then accelerates to free fall. During the data acquisition phase, the aircraft flies at a constant Mach number while constantly changing the quasi-stationary angle of attack. This makes it possible to use flight data to estimate the aerodynamic characteristics of the aircraft in a wide range of angles of attack. After the data is collected, the aircraft is recovered using a parachute and airbag system. The recovered aircraft will be refurbished for use on the next flight. The flight of the aircraft is carried out autonomously under the control of the navigation, guidance, and control computer system of the arrow. The aerodynamic data collected during the flight test will be used to reduce the uncertainty of the HOPE-X aerodynamic data (Figs. 13-10).

The flight booking test for the second phase of the HSFD was carried out in collaboration with the French Space Agency (Centre National d'Etuds Spatials, CNES). CNES is responsible for the development, operation, and recovery of the balloon after landing, as well as the weather observation of the test. The analysis of flight test data was carried out jointly by NAL, NASDA and CNES.

The on-board equipment of the Phase 2 experimental vehicle consists of 7 subsystems:

(1) Structural subsystem.

(2) Actuation subsystem, which includes lifting aileron and rudder control surface.

(3) Navigation, guidance, and control subsystem, which is used to control the attitude of the aircraft and ensure that the aircraft flies according to the trajectory to obtain the required data.

(4) Communication and measurement subsystem, which uses on-board sensors to obtain data and send it to the ground through telemetry devices.

(5) Power/signal supply subsystem, which distributes signals and provides power to arrow-borne instruments.
(6) Recovery subsystem, which consists of a recovery parachute system and an airbag system.
(7) Emergency subsystem, which is used to land the aircraft in the designated area in an emergency.

In order to reduce development costs, the design of the components is as common as possible to Phase 1, especially the navigation system, flight control computer, control plane actuation system and telemetry/command system with the experimental vehicle of Phase 1. Composite differential GPS/inertial guidance systems use GPS carrier phase to improve accuracy. A new algorithm proposed by the NAL Guidance Research Group will be applied to the guidance system. In the event of an emergency, the automated flight control system is used to maintain the established transonic Mach number during the data acquisition phase and to send remote control commands from the ground to automatically guide the aircraft to land at the designated location. The well-designed measuring system achieves sufficient accuracy to evaluate the aerodynamic characteristics. It uses an air data system to estimate the atmospheric velocity vector by means of a 5-port pressure measuring detector mounted on a nose probe rod. The recovery parachute and emergency drag parachute are tucked away in the tail of the fuselage, and the airbags are mounted in the landing gear compartment, which will replace the landing gear of the Phase 1 experimental vehicle. The test vehicle has a length of 3.81m, a wingspan of 2.42m, a height of 1.20m, a total mass of 500kg, and a wing area of 3.41m2.

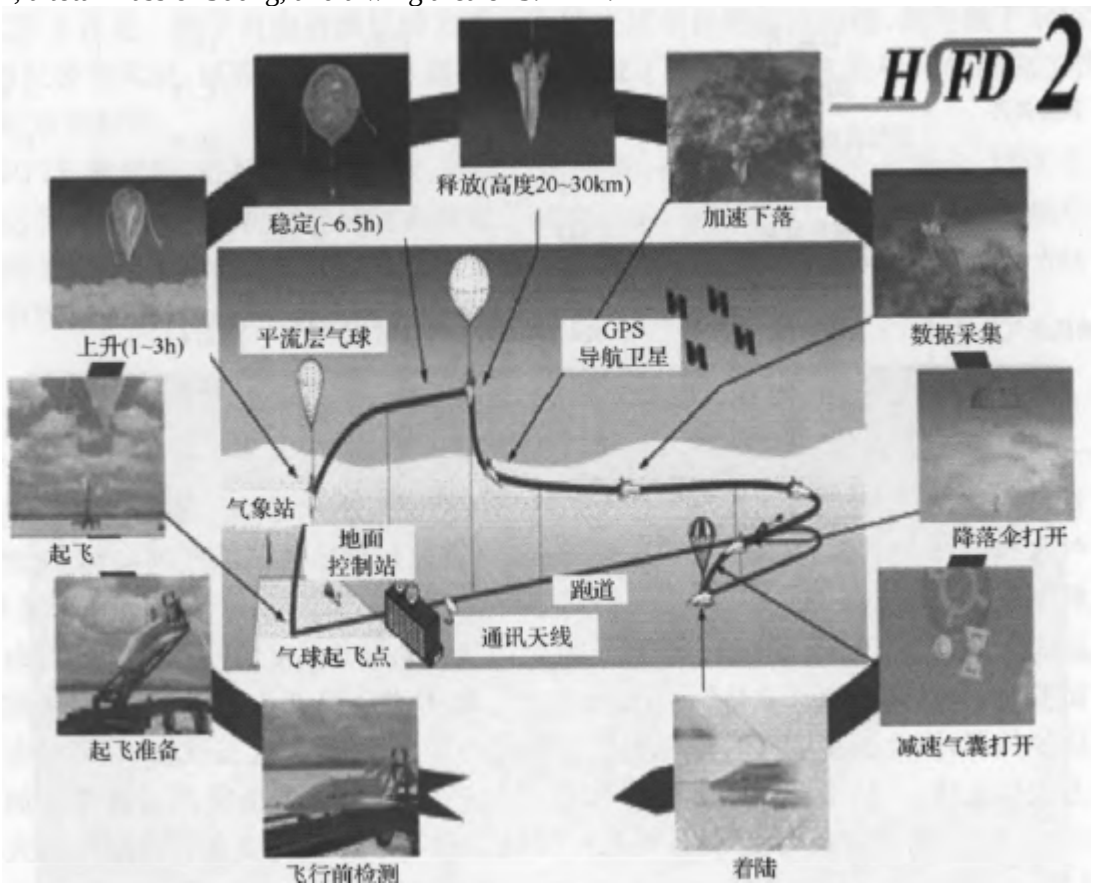

Figure 13-10: HSFD flight test procedure

13.4: Hypersonic test equipment and research institutes

13.4.1: Free Jet Test Bench for Ramjet Engines

The ramjet free jet test bench (RJTF) is one of the largest hypersonic test facilities in Japan.

In 1987, the Japan Science and Technology Agency's Research and Development Bureau established a development policy for the development of winged spacecraft and commissioned the Japan Aerospace Industries Association to conduct a survey of supersonic ramjet engine test equipment, and in 1988, the RJTF entered the design stage, which lasted five years and was completed in 1993 [4].

RJTF began construction in 1989 and gradually completed the construction of heat storage heater and high temperature air supply system, completed the construction of direct combustion heater and fuel H2 supply system and cooling water system, construction of measurement and control system, construction of nozzle and thrust measurement system.

The size of the main nozzle outlet of the RJTF test bench is 510mmX510mm, the design simulation is *Ma* = 4, 6, 8, the corresponding height H = 20km, 25km, 35km, the diameter of the test section cabin is 3.0m, the length is 5.1m, and the main performance indicators are shown in Table 13-2.

Table 13-2: Key features of RJTF

Flight conditions	*Ma*	8	6			4
	Height	35	25			20
Device conditions	Heater	S+ M8V	M6V		M6S	M4
	Total temperature/K	2600	1580		1655	872
	Total pressure/MPa	10.0	5.25		4.78	0.86
	Air Flow/(kg·s^{-1})	6.16	29.8		30.9	45.9
	Oxygen flow	2.16		5.44		
	Hydrogen flow	0.181		0.446		
Engine intake conditions	But	6.73	5.30		3.41	
	Static temperature/K	324	275		274	
	Static pressure/kPa	1.6	5.3		12.3	
Maximum blowing time/s		30	60		60	60

The test bench is designed with two-stage heating, the maximum simulated total temperature of the two-stage combination is 2600K, the first stage is a non-polluting regenerative air heater (SAH), and the second stage is a direct-fired hydrogen fuel air heater (VAH) with a certain amount of pollution (referring to the effect on the test air being heated). The heating part of the regenerator can raise the air temperature to 1700 K, and T_0 = 2600 K when the *Ma* = 8 state test is performed, the lifting temperature of the second-stage direct combustion heater is 900K. In the *Ma* = 4 state test, only the first stage of the regenerator heater (872K) can be used to meet the simulated total temperature requirements, and there is no need to start the direct combustion heater, so the cleanliness of the test air is very high. In the *Ma* = 6 state test, there are two heating options: a regenerative heater alone (1655K) and a direct combustion heater (1580K) alone. In the use of direct combustion heaters, it is necessary to supplement the part lost due to the direct participation of oxygen in the test air to combustion, and the proportion of oxygen to the test air quality is 23.2%, and both heating methods can be selected, and various conditions should be compared to determine which heating method to use. In the case of the *Ma* = 8 test, two heating methods must be worked in tandem, and the amount of nourishment is much smaller because the amount of direct combustion heating in the second stage is smaller.

The advantage of the two-stage heating method is that the pollution of the test air is reduced, and the work of the test engine is carried out under conditions close to the real air intake. This is very favorable to the scramjet engine at hypersonic speeds. Under the conditions of high-altitude flight, the air flow into the ramjet engine is not large, and the absolute value of the net thrust produced is small, so if the number of free radicals, atomic groups, and impurities H, O, NO_x, OH, and H2O in the combustion products produced by the direct combustion and heating is large, it will inevitably have an effect on the engine's startup and combustion performance, so that the range of deviations between the net thrust and the air flow corresponding to the net thrust is enlarged, and the true value of the net thrust is not easily obtained.

Two-stage heating can not only meet the requirements of air purity, but also be conducive to the realization of simulated high temperature (direct combustion heating mode, high and fast heating), RJTF uses two-stage heating mode to achieve total temperature simulation, which increases the credibility of the study of the combustion performance of engine test pieces.

Considering the characteristics of the integration of scramjet engine and fuselage, the Mach number of the aerodynamic section of the engine inlet is taken as the design Mach number of the nozzle, which is different from the Mach number of the aircraft in the flight state, which is the Mach number after the precompression of the fuselage forebody, so the Mach number of the nozzle design is lower than the Mach number in the flight state. In the selection of the cross-sectional shape of the nozzle, after weighing the pros and cons, it is determined to be square and rectangular, mainly considering the matching of the airflow line with the inlet of the engine test piece, and the square and rectangular outlet streamlines are significantly better than the circular outlet streamlines. The simulation of the inlet airflow also has the problem of a surface layer, and the square or rectangular section is conducive to the pre-formation of the surface layer in the nozzle, as an integrated design, the simulation of the inlet state of the air inlet is more realistic. In view of the characteristics of scramjet engine, the RJTF free jet engine test bench simulation adopts the integral simulation method, which is similar to the aerodynamic wind tunnel test method, the head of the test piece is placed in the equal Mach number area, but not in the equal Mach number test section in the wind tunnel, but in the equal Mach number diamond cone, and the tail is in the overflow diffuser with high Mach number flow, in fact, this is a semi-free jet test method. In order to solve the starting problem of the test bench, the 1/5 scale model wind tunnel of RJTF was first made, the starting characteristics under various conditions were tested, the data were obtained, and the starting problem was successfully solved through a large number of preliminary research work.

After the completion of the RJTF, a large number of tests were carried out, and from the statistical point of view, only until April 2001, the test bench has been tested more than 200 times, and the engine test has also verified the test equipment, and the test technology has made progress. In March 2002, the Institute of Aeronautics and Astronautics achieved the first effective thrust in a scramjet test, and soon after, it achieved the highest effective thrust in the world at that time in the $Ma = 8$ test (Figs. 13-11).

Figure 13-11: A scramjet model on an RJTF test bench

13.4.2: Free piston shock wave wind tunnel

In 1997, Japan built a large-scale free-piston shock wave wind tunnel (HIEST), which can generate a high temperature of 10,000°C, a total enthalpy of 25MJ/kg at the station, and an airflow velocity of 7km/s. It is driven by high-pressure air piston compressed air, driving pressure ratio 50, forming a high pressure of 50 to 150MPa, simulating the dissociation state under air stagnation pressure, continuous effective working time of 2ms, test model 500mmX500mm, wind tunnel diameter and ϕ0.35m, With a total length of 80 meters, it is the world's first-class large-scale shock wave wind tunnel, and it is a wind tunnel with mechanical design characteristics, which is used to simulate the reentry characteristics of the scramjet engine of the reentry aircraft. A large number of tests were carried out in the wind tunnel, which was also built at the Aerospace Research Institute (Figure 13-12).

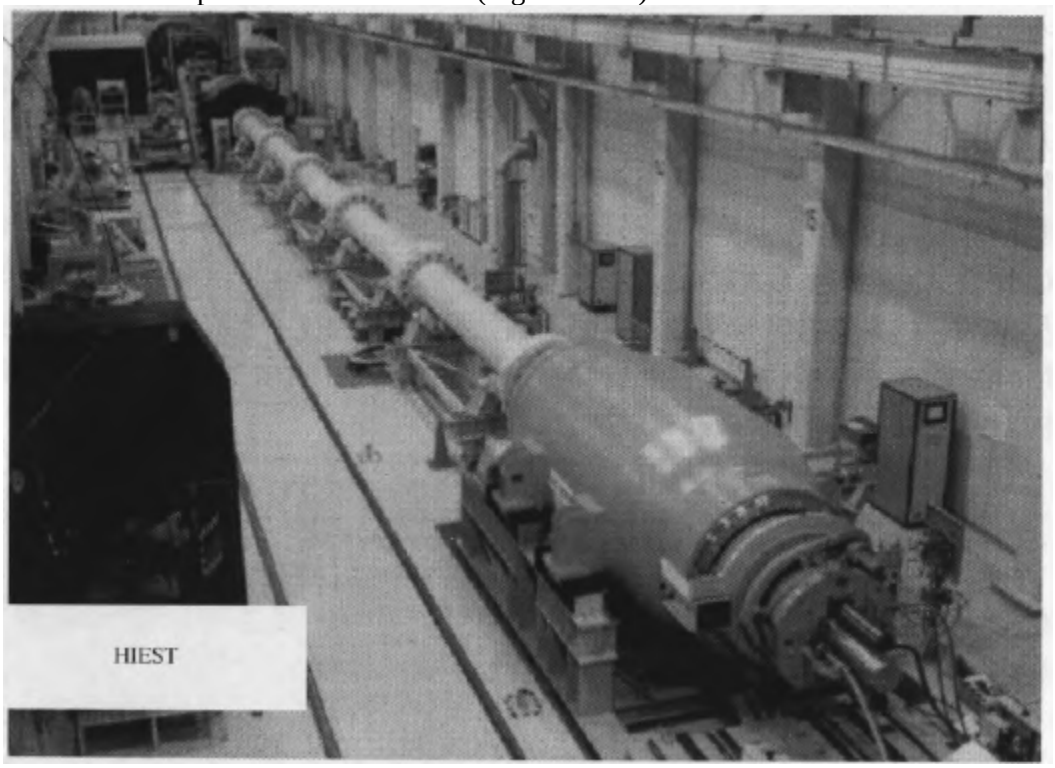

Figure 13-12: HIEST free-piston shock wave wind tunnel in Japan

13.4.3: Relevant research institutions

At present, JAXA is the main institution conducting hypersonic technology research in Japan, and other research institutes involved in hypersonic technology research are: Muroran Institute of Technology and Tokyo Institute of Technology; institutions of higher learning are mainly Tohoku University and the Department of Aeronautics and Astronautics of the University of Tokyo. Judging from the available literature, the vast majority of the work was carried out by JAXA, and a small amount of work was carried out by other research institutes and universities, and there is no relevant literature from the industry at present. On October 1, 2003, JAXA was established as a result of the merger of ISAS, NAL, and NASDA (Table 13-3).

Table 13-3: JAXA was formed by merging three units

Abbreviation of the organization	The full name of the organization in English	The Chinese name of the institution	Main research directions
MALE	Institute of Space and Astronautical Science	Institute of Space and Space Sciences	Engaged in space and planetary research
NAL	National Aerospace Laboratory of Japan	National Aerospace Laboratory, Japan	Focus on the research and development of next-generation aviation technology
NASDA	National Space Development Agency of Japan	National Space Development Agency, Japan	Responsible for the development of large launch vehicles, such as H-IIA, as well as research work on satellites and the International Space Station
JAXA	Japan Aerospace Exploration Agency	Japan Aerospace Search Agency	

The history of the Institute of Aerospace Sciences (ISAS) dates back to 1955, when the Pencil rocket launch test was conducted at the University of Tokyo. ISAS was founded at the University of Tokyo in 1964, and in February 1970, it successfully launched Japan's first artificial satellite, OSUMI, into orbit with an L-4S solid-propellant rocket, making Japan the fourth country in the world to launch a satellite into space. In 1981, ISAS spun off from the University of Tokyo to become a joint research institute. Superb work: Studied the fully reusable two-stage orbit entry (TSTO) vehicle scheme, conducted a methodology study for conceptual design, and optimized the design of the engine, fuselage and trajectory. The first stage of the aircraft adopts a turbine combined cycle engine, and the turbine combined cycle engine is experimentally studied.

Established in 1955 as an aeronautical laboratory, the National Aerospace Laboratory (NAL) was renamed the National Aerospace Laboratory in 1963 when the Aerospace Division was added. Superb work: Mainly researched related technologies for space vehicle propulsion. Since 1987, the concept of the space shuttle has been studied, and the related scramjet technology has been carried out, the shape and trajectory of the space shuttle have been optimized, and various schemes that can be used for single-stage orbital space vehicles have been studied, including the combination of various rocket engines and ramjet engines. Structural and thermal protection of scramjet engines for space vehicles has been studied and tests have been carried out.

The National Space Development Agency (NASDA) of Japan was established on October 1, 1969 to promote the peaceful use of space as the core force of space development. Advanced work: The Vertical Take-Off Vertical Landing (VTVA) two-stage orbit vehicle was studied, and the re-entry and terminal guidance of the first stage vehicle were simulated.

On October 1, 2003, ISAS, NAL, and NASDA merged into a single administrative agency: the Japan Aerospace Exploration Agency (JAXA). The merger of these three institutions will enable Japan to achieve better results in space exploration, both in basic research and in the development of systems for practical applications. At the same time, it also means that Japan has brought together the most advanced modern aerospace technology to create new energy for Japan's space challenge. Of course, the new institutions also face the challenge of administrative restructuring, but the restructured institutions will be more efficient.

JAXA's current sub-institutions include:

Center for Aerospace Research (ARC); airport Division of the Center for Aerospace Research; Tsumuba Space Center (TK-SC);

Sagamihara Campus, Tanegashma Space Center (TNSC); Uchinoura Space Center (USC); Earth Observation Centre (EOC); Earth Observation Research and Applications Center (EORC); Kakuda Space Center (KSPC); Noshiro Test Center (NTC); Sanriku Balloon Center (SBC); Katsuura tracks the communication station; Usuda Centre for Outer Space; Masuda tracking communication station; Okinawa tracking communication station; Ogagawara transmitting station.

After the merger of the three units to form JAXA, active and fruitful work in the field of hypersonic technology continues. JAXA is actively developing technologies for future reusable aircraft, and has studied both single-stage and two-stage orbit entry schemes. A partially reusable two-stage orbiting vehicle is currently being studied, using a smaller vehicle to reduce costs; the first pole is a winged reusable aircraft with 6 engines; the second level is non-reusable. FESTIP, an optimized design tool for the conceptual study of future space-entry flight systems, was developed, and numerical and experimental studies were carried out on various components of scramjet engines.

JAXA has been actively engaged in the hypersonic flight demonstration program. In 2003, the HSFD (Hypersonic Flight Demonstrator) flight test was carried out in Sweden, and the test vehicle was carried out by balloons in the 20sThe purpose of the 30km altitude launch is to measure the aerodynamic parameters of the aircraft in the transonic range. Flight tests of a new scramjet engine were carried out in March 2006 using Hyshot from the University of Queensland, Australia, and flight tests of a pre-cooled turbojet engine was planned for 2007. JAXA also plans to begin a single-stage RAFLEX (Reliable Ascent Flight Experiment) flight test program in 2008, which is jointly conducted by JAXA and Mitsubishi Heavy Industries, with the aim of demonstrating the technology of a reusable space transportation system under flight conditions and demonstrating its navigation and control technology. In the future, the vehicle will be used for flight tests of air-breathing engines. At present, the flight demonstrator uses a rocket engine, a winged body, vertical take-off, and horizontal landing, and uses four ISAS small engines, fueled by liquid hydrogen and liquid oxygen.

References

[1] Nobuo Chinzei. Progress in Scramjet Engine Tests at NAL-KRC [R]. AIAA-2001-1883, 2001.
[2] Cao Zhijie. Japan reusable launch vehicle program [J]. Space International, 2003, (4):10-14.
[3] Su Xinxin. Inventory of Japan's hypersonic program [J]. Flying Missile, 2008, (5):26-31.
[4] Chen Yanhui. Japan's hypersonic air-aspirated engine test equipment and test technology [J]. Flying Missile, 2006, (2):41-48.

Chapter 14: Australian Hypersonic Vehicle Technology Research

With its unique geographical conditions, advanced test technology and resources, Australia has not only attracted Germany, Britain, Japan, Italy and other countries to cooperate with it, but also made the United States an important ally in the field of hypersonic technology. At present, Australia is actively promoting a number of international cooperation projects on hypersonic technology. The leader of hypersonic research and development in Australia is Dr. Raymond Stalker of the United Kingdom. In the 1960s, Stalker led the Australians to build a shock wave wind tunnel and began to study hypersonic flow. It was not until 1987, when the T4 shock wave wind tunnel at the University of Queensland was put into operation, that the testing of scramjet engines made great progress.

Since the 1990s, the University of Queensland Hypersonic Center has established cooperative relations with more than 20 universities and research organizations in Australia and abroad. Domestic ones include Australia's Defence Science and Technology Organisation (DS-TO), the Australian National University and the Defence College of the University of New South Wales, and internationally the National Aeronautics and Space Administration (NASA), Astrotech, the U.S. Air Force Research Laboratory (AFRL), the German Aerospace Center (DLR), the UK's QinetiQ (formerly the government's defense research institute), Japan's JAXA, and South Korea's Seoul National University.

Since 1997, Australia has reached cooperation agreements with the United Kingdom, Japan, and other countries, and the Hyshot project has been gradually launched. In April 2004, Australia's DSTO and the United States' DARPA signed the "Australia/United States Joint Hypersonic Test" (HyCAUSE). At present, the project has been successfully implemented. In November 2006, AFRL of the United States and DSTO of Australia signed a HIFiRE agreement, ready to invest 70 million U.S. dollars to conduct up to 10 hypersonic flight tests in the next eight years. With the help of these bridges of cooperation, and with Australia's unique resource advantages, Australia has overcome one obstacle after another on the road to the development of hypersonic technology and has become one of the world's leading hypersonic fields [1].

14.1: HyShot Program

The HyShot program is an international cooperation program developed in the 1990s and is a successful example of international hypersonic technology cooperation. In this project, a variety of hypersonic vehicle components (especially propulsion systems) developed by many countries have been successfully tested by sounding rockets, and a large number of valuable test data have been obtained, which has played an important role in promoting the research of hypersonic technology in participating countries.

The countries participating in the project are Australia, the United Kingdom, the United States, France, Germany, South Korea and Japan. The project is led by the University of Queensland, Australia, with the participation and funding of the Australian DSTO, the Australian Department of Defence, the Australian Space Technology Command, the Australian Department of Industry, Scientific Resources, the Australian Space Research Institute, the Australian Research and Development Unit, the British Quintic, the British Defense Assessment and Research Agency, the United States, the United States, the United States Air Force Scientific Research Office (AFOSR), the German Aerospace Center (DLR), National University of Korea and National Aerospace Laboratory (NAL) of Japan.

The program conducted a large number of ground tests, including sensor response time, structural integrity of individual components, vibration testing, shock testing, vacuum testing, and source code evaluation.

The most important ground tests were the wind tunnel tests of the engines, which were carried out in the T4 shock wave wind tunnel at the Hypersonic Centre of the University of Queensland, Australia (which was upgraded in 2004 to simulate a *Ma* = 10 flight at an altitude of 30 km). In order to ensure the success of the test (especially to ensure stability during re-entry), extensive aerodynamic tests were also carried out on the ground.

On October 30, 2001, the first launch test was conducted at the Bumera Range in Australia, as shown in Figure 14-1, with a two-dimensional combustion chamber engine designed by the University of Queensland, called HyShot1 (Figure 14-2), which ended in failure. On July 30, 2002, a second launch test was conducted at the Woomera range, using the HyShot2 two-dimensional combustion chamber engine, and during the landing, the scramjet engine experienced a brief ignition combustion at a speed of *Ma* = 7.6. The trial was a success. Two more launch tests were conducted at the Woomera range on 25 and 30 March 2006, both of which were successful. On March 25, 2006, the HyShot3 three-dimensional combustion chamber engine (Fig. 14-3) designed by the British company QinetiQ was launched, and on the 30th, the HyShot4 engine (Fig. 14-4) developed by Japan was launched, with a mass of 100 kg and an advanced fuel injector.

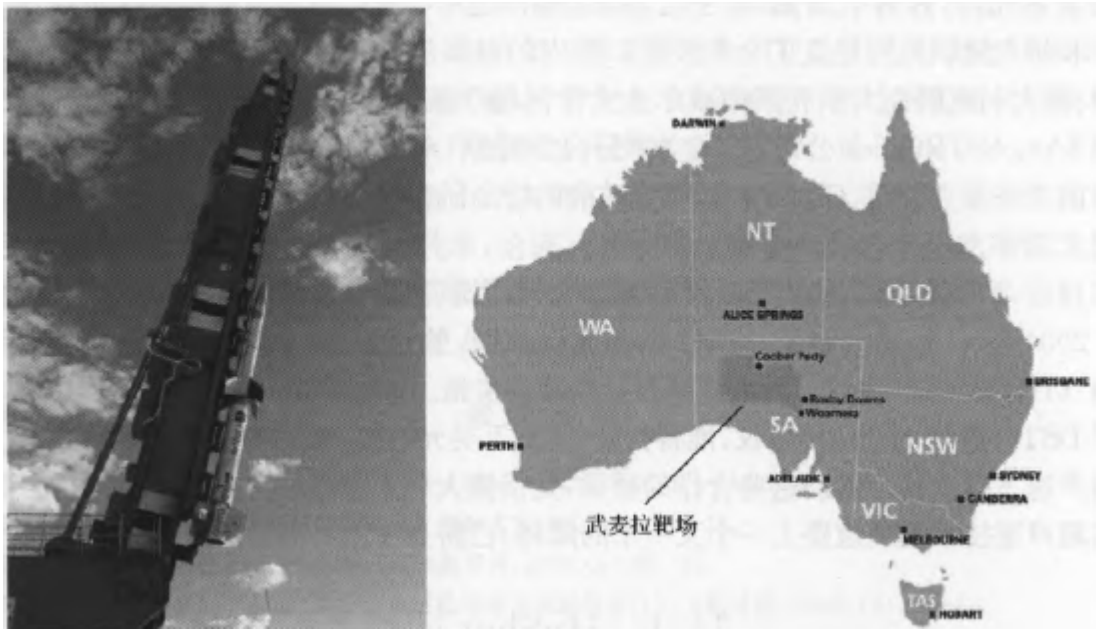

Figure 14-1: HyShot Program Test Vehicle and Test Flight Launch Site

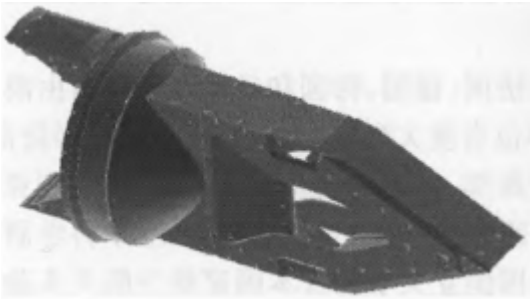

Figure 14-2: HyShot 1/2 flight tester

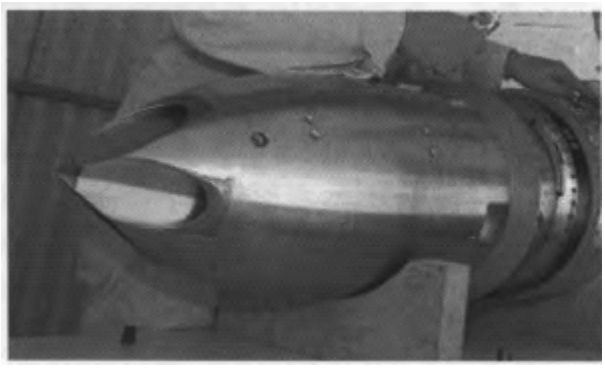

Figure 14-3: HyShot3 flight tester

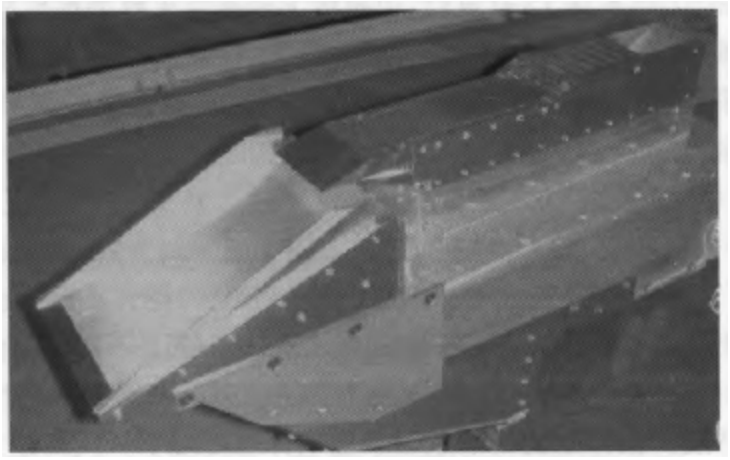

Figure 14-4: HyShot 4 flight tester

Through the series of tests of HyShot, the technology of sounding rockets applied to hypersonic flight tests is becoming more and more mature. At the same time, with the advancement of the project, the relevant facilities of the shooting range have been improved, and the level of data tracking, transmission and processing has been greatly improved.

14.2: HyCAUSE flight test

The Hypersonic Collaborative Australia/United States Experiment (HyCAUSE) is a scramjet flight test project, funded by the U.S. DARPA, conducted by researchers in the United States and Australia that began in April 2004 [2].

The plan develops a hypersonic vehicle scheme using an inward-turning scramjet engine, that is, the inward-turning inlet can be better integrated with the configuration of the wave-riding vehicle, as shown in Figure 14-5. The scramjet model was tested in the T4 wind tunnel of the University of Queensland in Australia and the LE 1 wind tunnel in CUBRC in the United States to study the performance and operation ability of this type of hydrogen engine under Mach10 conditions, covering a wide range of dynamic pressure to fuel equivalent ratios.

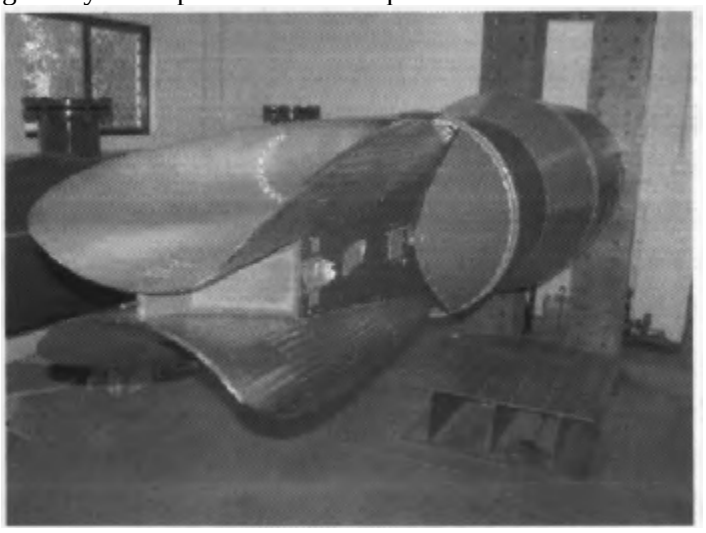

Figure 14-5: HyCAUSE flight test engine model

The flight test was carried out on June 15, 2007, and was propelled by a two-stage uncontrolled sounding rocket to fly according to a ballistic trajectory, and it was planned to test the re-entry Mach 10 with a dynamic pressure of 500 to 1600 psf. However, due to the failure of the booster, the test did not achieve the expected results, and the data analysis after the test showed that the test engine went through the process of starting the intake tract, not starting and restarting, but the hydrogen fuel was not able to burn under the conditions of the inlet tract starting.

14.3: HIFiRE Flight Test Program

HIFiRE stands for Hypersonic International Flight Research and Experimentation (HIFiRE) and is a collaboration between U.S. Air Force Laboratories and the Australian Defence Science and Technology Organization. The aim of the program is to carry out basic research and verification of the key technologies needed to realize the next generation of hypersonic aerospace vehicle systems at a low cost, and the program will accelerate the development and maturity of component technologies through the testing of basic problems. Specific trial objectives include [3]:

(1) Develop and validate computational models for hypersonic flow.
(2) Carry out ground test research on the typical flight environment of hypersonic speed.
(3) Development of flight test equipment and measurement technology.
(4) Develop the design technology of hypersonic flight test and integrated load.
(5) Carry out flight tests of key technologies in a real hypersonic environment.
(6) Develop methods for correcting numerical models, ground test and flight test data.
(7) Evaluation of hypersonic technology and test methods.

The scope of the HIFiRE program includes 10 specific areas of research and flight testing, which will be conducted at the Woomera Proving Ground in Australia. These 10 aspects are: pneumatic propulsion integration technology; aerodynamics; pneumatic heating; high-temperature materials and structures; thermal management technology; navigation technology; guidance technology; control technology; sensor technology; weapon system component technology. The research work on these projects includes modeling, simulation, and ground testing, but the main is the study of mechanistic phenomena and component technologies through flight tests. Flight conditions range from Ma = 5 to 12, and the flight trajectory includes a ballistic trajectory as well as a long-term atmospheric flight trajectory.

In terms of high-temperature materials and structures, the research involved includes thermal protection systems, leading edge structures and materials, airframe main structures, and coating technologies. In terms of aerodynamics, he focuses on the study of hypersonic flow mechanisms, including boundary layer transition and shock-dominated flow. In aerothermics, he focuses on non-equilibrium and rarefied gas flow fields, aerodynamic heating, and plasma gas dynamics. In terms of aircraft form design, chemical reaction flow is studied by developing effective numerical calculation methods and constructing coupled models of aerodynamic, thermal, and chemical reactions through unstructured meshes.

There are nine flight test projects, the first of which was launched in 2008, with the main purpose of studying the basic aerodynamic phenomena of axisymmetric conical configurations under Ma = 7.5 flight conditions, and to develop flight measurements and devices, as well as paving the way for the subsequent HIFiRE program. The flight test program will lead to the development of a collaborative design environment and validate the effectiveness of engineering processes and tools.

The technical objectives of the first HIFiRE flight test include: studying the interaction between boundary layer transition and shock wave boundary layer in the context of hypersonic vehicles; numerical simulation methods for the interaction between boundary layer transition and shock wave boundary layer under hypersonic conditions are developed. Experiments on the interaction between boundary layer transition and shock wave boundary layer were carried out in the ground test environment. development of correction methods between numerical simulation, ground test and flight test data; development and evaluation of new measuring devices and technologies;

development of high-speed measuring devices;

The flight test consists of a number of test items, launched by a two-stage sounding rocket, and the flight test will evaluate the following three aspects: the main test is to study the boundary layer transition under hypersonic conditions at a cone angle of 7 degrees; the second test was to study the interaction of the shock wave boundary layer and test a new measurement device. Incidentally, tests were carried out on inertial measurement devices.

The first flight of HIFiRE was successfully completed on May 7, 2009 at the Woomera range. A second successful flight test was conducted in March 2010, this time led by the United States, and subsequent tests will be led by the United States. The HIFiRE collaboration has been successful at several key points such as the design and assembly of hypersonic vehicles, the design of complex electronic devices, and the flight system. HIFiRE is a high-profile international collaboration that undoubtedly plays a very important role in the research and validation of future hypersonic technologies in the United States and Australia.

References

[1] Li Wenjie, Gu Yutian, He Ye. The development of Australia's hypersonic technology from the perspective of international cooperation projects [J]. Flying Missile, 2010, (9):42-44.
[2] Steven Walker, Frederick Rodgers, Alan Pauli. HyCAUSE flight test program [R]. AIAA 2008-2580, 2008.
[3] Douglas J Dolvin. Hypersonic international flight research and experimentation [R]. AIAA 2008-2581, 2008.

Chapter 15: Research on Hypersonic Vehicle Technology in Other Countries

15.1: Overview of UK Hypersonic Vehicle Technology Research

15.1.1: The HOTOL Program

"HOTOL" is a non-manned single-stage orbital aerospace aircraft proposed by the United Kingdom in 1982, and its launch is accelerated by a pulley, aspirated propulsion to Mach 5, and then transformed into rocket engine propulsion. In 1989, the United Kingdom and the Soviet Union jointly modified the "HOTOL" program to the "An-225/HOTOL" program, using the Soviet Union's An-225 transport aircraft to launch from the air. With the end of the "Cold War," the world pattern changed, and the program was also put on hold [1].

"HOTOL" is a kind of horizontal take-off and landing, single-stage orbital aerospace aircraft developed by British Aerospace Corporation, Rolls-Royce, and other companies, mainly used to put satellites into orbit, and can also perform the construction and maintenance of space military platforms, the recovery of satellites from orbit, military reconnaissance and surveillance, various defense and attack tasks, among which defense and attack tasks include anti-satellite and intercontinental investment of strategic weapons. The program originated as an initiative of the Space & Communications division of British Aerospace. According to the division's forecasts, at the beginning of the 21st century there will be a need for a new space launch vehicle to complement and eventually replace the American shuttle with the French "Ariane" rocket. This is because forecasts for the commercial satellite launch market indicate an annual growth rate of 5 to 7 payload tonnage in orbit, i.e. doubling every 10 to 15 years, which means that the demand for launches in the 21st century will exceed the combined carrying capacity of the Space Shuttle fleet and the French "Ariane" rockets. Space shuttles and Ariane rockets are expensive to launch, $3 million per ton for low-Earth orbit; at $30 million per ton for geostationary orbit, the goal of the "HOTOL" program is to reduce the cost of launching payloads by at least 80 per cent by:

Achieve horizontal take-off and landing from a general runway with a minimum of auxiliary personnel (estimated to be 200 to 250 people);

Fully reusable, with no scrapped hardware;

When launching and recovering satellites as the main task, unmanned operation is adopted, which saves the quality and cost of life support system, and reduces the cost of launch preparation and testing.

In April 1983, British Aerospace and Rolls-Royce set up a working group to explore the "HOTOL" proposal. In September 1984, a model of the "HOTOL" program was exhibited at the Farnborough Air Fair, and in January 1985, at the European Space Agency (ESA) long-term planning meeting held in Rome, the British Minister of Defence recommended the "HOTOL" program as a successor to the "Helmes" aerospace aircraft for the European Space Agency to make decisions. In November of the same year, the British Ministry of Defence, the Department of Foreign Trade and Industry, the Aerospace Corporation, and Rolls-Royce reached an agreement to conduct a conceptual study of the "HOTOL."

The shape of the "HOTOL" is similar to that of the "Concorde," with triangular wings, mounted at the rear of the aircraft, and the "HOTOL" has no horizontal tail and vertical tail, and relies on a full-motion vertical front wing for course maneuvering and course stability. In order to achieve a single-stage orbit, the "HOTOL" has a hybrid air-aspirated propulsion system without a horizontal tail and a vertical power unit, which has a dual-function rocket combustion chamber that uses the inhaled air as an oxidizer at low altitudes, and this working state is maintained until an altitude of 26 km, when the aircraft reaches a speed of $Ma = 5$, and then uses liquid oxygen as an oxidizer (Figure 15-1).

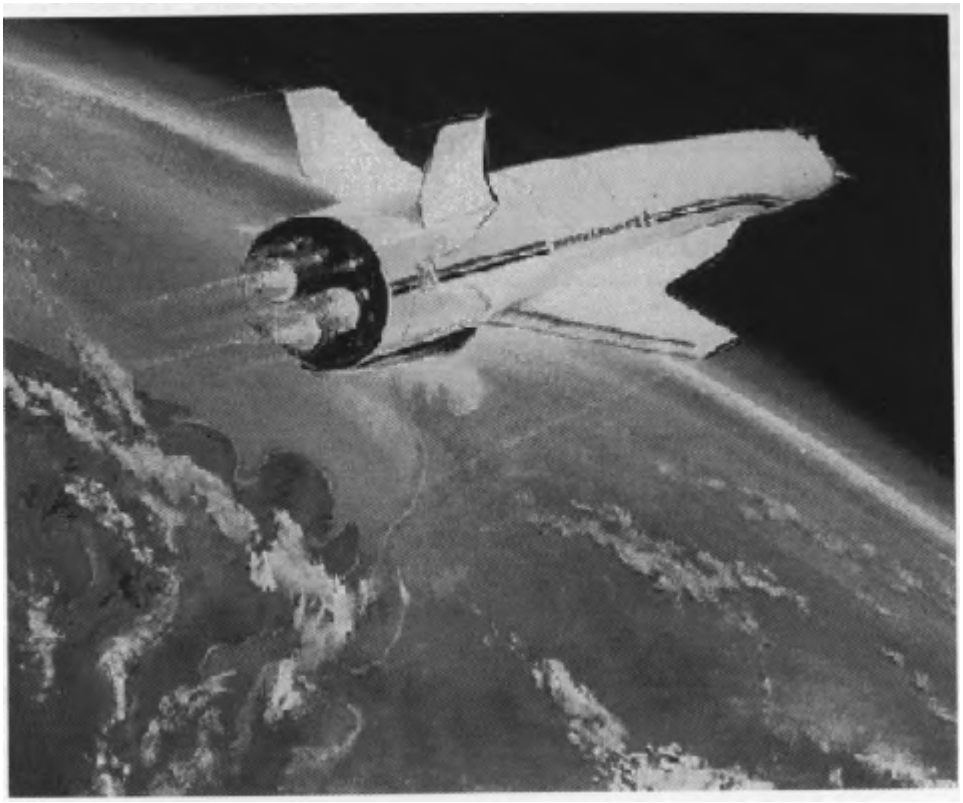

Figure 15-1: Flight renderings of the HOTOL aircraft

15.1.2: SHyFE Flight Test Program

SHyFE (the sustained hypersonic flight experiment) is a flight test program carried out by QinetiQ with the support of the British Ministry of Defence, the purpose of which is to demonstrate the maximum operating Mach number of a ramjet engine through a new design and the use of advanced high-temperature materials, that is, to demonstrate the flight performance of a low-cost ramjet powered aircraft at $Ma = 6$. QinetiQ is a major arms manufacturer in the UK, and the program is supported and cooperated by universities such as the University of Oxford, the Royal College in London, and a number of commercial companies [2,3].

The SHyFE test vehicle has a mass of less than 30 kg, is boosted by a solid rocket engine to $Ma = 4$ at an altitude of 15 km, and then accelerated by a ramjet engine to $Ma = 6$ at an altitude of 32 km and cruising for about 200 km. The SHyFE test vehicle is axisymmetric (Fig. 15-2), which makes full use of the UK's existing aerodynamic data and successful experience in the ram(jet)-propelled surface-to-air missile "Sea Javelin." The first phase of three-year work began in 2002 with the overall design of the test vehicle, as well as the study of the main components, including aerodynamic shape, air intake, combustion chamber, flight control system and structural design. The inlet duct test was carried out in the HDT (high density tunnel) wind tunnel of QinetiQ and the combustion chamber test on the combustion test bench, and the C/SiC structural material used was verified.

In June 2005, SHyFE began the second phase of research work, with the first flight test planned for August 2009 and the second flight test in 2010. The first flight test uses C/SiC material for a small number of components, and it is planned to fly only for a short time, and the second flight test uses all C/SiC material to fly the full flight trajectory. But the plan has so far been delayed.

The use of advanced thermal protection materials is key to the SHyFE program and to achieving high Mach number ramjet engine flight. During the cruise flight of the test vehicle, the temperature of the combustion chamber will reach 2400K, and the thickness of the insulation layer between the combustion chamber and the internal system is only 15mm, so as to prevent the fuel from exceeding the maximum temperature limit of 423K.

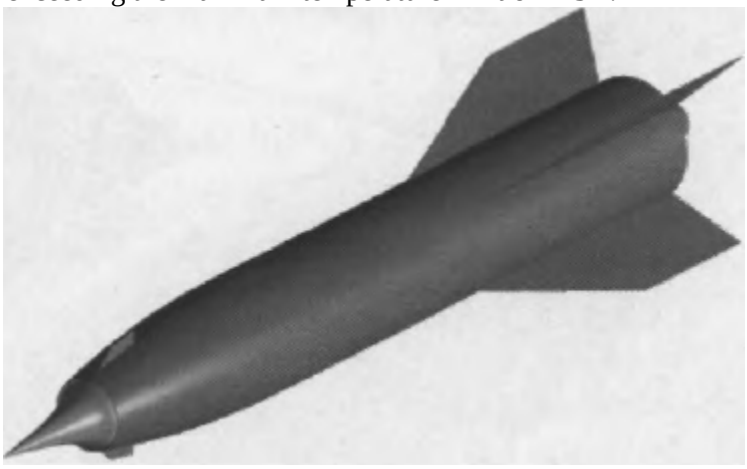

Figure 15-2: SHyFE test vehicle

15.1.3: SKYRON Reusable Launch Vehicle

The SKYLON reusable launch vehicle is designed primarily to reduce the cost of entering space. SKYLON is derived from the HOTOL project in the UK, but has undergone significant changes in the general layout, as shown in Figure 15-3. As can be seen from the figure, the engine is installed on the delta wing wingtip in the middle of the fuselage and is symmetrically distributed in the engine compartment to solve the balance problem of the aircraft. The engine was changed from HOTOL's RB545 to a synergistic air-breathing rocket engine (SABRE) to provide higher performance. The slender fuselage is equipped with propellant tanks and payload compartments. SKYLON uses its landing gear for horizontal take-off and landing, with the front wing surface responsible for pitch control, ailerons for roll control, and vertical tail for yaw control when SKYLON is flying in the atmosphere [4,5].

The features of the SKYLON reusable launch vehicle are as follows: (1) reusable; (2) single-stage orbit entry; (3) Unmanned driving; (4) have the ability to abort the flight; (5) it has good user operability; (6) large-range re-entry lateral maneuvering capability; (7) the environmental harm is small.

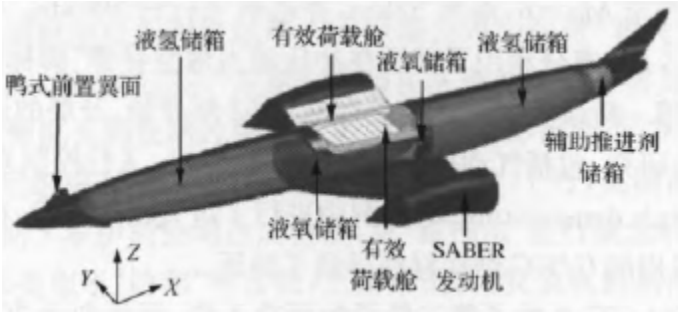

Figure 15-3: SKELLON layout

The development of the SKYLON reusable launch vehicle is scheduled to be completed in nine and a half years, at a cost of 9.518 billion euros (U.S. $12.95 billion, 2004 currency, the same below), and will eventually develop a launch vehicle with a service life of 200 times, with a probability of failure of 1% and a probability of damage of 0.005%, and it is expected that 30 will be produced in batches, each at a cost of 565 million euros ($768 million). In service, the SKYLON launch vehicle costs €6.9 million ($9.39 million) per relaunch launch.

One of the key in the development is the SABRE engine, which has the ability to work in two modes, and in the working mode of the rocket engine, the SABRE engine is a closed-cycle liquid oxygen/liquid hydrogen high specific impulse rocket engine; in the working mode of the aspirated engine, the atmosphere replaces liquid oxygen, and the specific impulse is increased by 3 to 6 times. The airflow enters the engine through a two-shock axisymmetric intake and is cryogenically cooled before compression. Before entering the main combustion chamber, the liquid hydrogen fuel stream cools the closed-cycle nitrogen circuit. In aspiration mode, the engine works like a turbo-cycle engine and is capable of generating static thrust, so the development of the engine can be carried out outdoors at a test facility. After the engine was converted from aspirated to rocket-like mode of operation, SKYLON sharply climbed high and rushed out of the atmosphere, reducing drag to a minimum. Using the same set of rocket combustion chambers, nozzles and pumps in both modes reduces the mass gain caused by the addition of a separate air-breathing engine, while also eliminating the drag caused by the "dead weight" of the launch vehicle during the aspirated ascent flight phase. The SABRE engine operates during the suction mode, and in order to produce a reasonable level of thrust while retaining a high nozzle area ratio, the airflow must pass through the pump to a typical rocket combustion chamber pressure, 10 to 20 MPa. Therefore, the goal of the thermodynamic cycle is to utilize the minimum fuel flow and to take advantage of the properties of liquid hydrogen to provide a high-pressure gas stream. Especially in the case of high Mach numbers, the airflow must be cooled in order to reduce the cycle power requirements and achieve a reasonable air compressor outlet temperature (Fig. 15-4).

Figure 15-4: Internal structure of SABRE engine

15.1.4: Hypersonic airliner

Since the supersonic passenger aircraft "Concorde," Britain has always had the dream of developing hypersonic passenger aircraft, and in recent years has put forward a number of hypersonic passenger aircraft programs, among which the A2 development program has attracted more attention.

On February 5, 2008, British engineers unveiled plans to develop a hypersonic aircraft that could fly from Europe to Australia in five hours. The hypersonic aircraft, currently codenamed A2, was designed by the British engineering company Reaction Engines and is expected to carry 300 passengers and reach a top speed of 6,400 km/h. The company's director, Alan Bond, said the plan was supported by the European Space Agency and that the hypersonic aircraft was expected to be ready for service within 25 years.

"The A2 aircraft was designed to take off from Brussels International Airport and smoothly fly out of the European continent at a subsonic speed of Mach 0.9 over the North Atlantic," Bond said. The plane will then accelerate to five times the speed of sound, fly over the North Pole, fly over the Pacific Ocean and eventually reach Australia. He said the flight took only four hours and 40 minutes.

According to the design, the A2 aircraft will be 143m long, compared to the 73m of the Airbus A380 jumbo airliner. The A2 can fly continuously for 20,000 km with a full tank of fuel. The fuel it uses is liquid hydrogen, which releases water and nitrogen oxides after combustion and does not cause carbon dioxide pollution. The disadvantage of hypersonic aircraft is that they do not have windows, as flying at hyperspeeds generates a lot of heat. To this end, the designers planned to install flat-screen TVs in the windows to simulate the feeling of looking out of the windows (Figure 15-5).

Figure 15-5: Conceptual drawing of the British A2 hypersonic airliner

15.2: Overview of Hypersonic Vehicle Technology Research in Italy

Italy's strengths in hypersonic vehicle technology are aerothermal testing and thermal protection structural material technology. Italy's National Aerospace Research Center (CIRA) has a 70MW continuous-flow hypersonic plasma wind tunnel, SCIROCCO, which simulates the thermal protection structure of the aircraft during its re-entry into the Earth's atmosphere. The wind tunnel can reach a diameter of about 2 m, a temperature of 9,727°C, and a speed of $Ma = 16$, which can be used for testing scramjet engines and re-entry vehicles. Researchers at CIRA are developing thermal structures based on ultra-high temperature ceramics that can be used for thermal protection of elongated aircraft with sharp head cones and wing leading edges, and the performance of these structures can be verified in wind tunnel tests [6].

In addition, CIRA is conducting a flight project of an unmanned space vehicle (USV) to develop technology and flight test beds for aerospace vehicles. The vehicle is capable of taking off from any airfield like a normal aircraft, arriving at a space base in low Earth orbit, and returning at a speed of $Ma = 25$. The first flight tests were completed in early 2007. CIRA is also a key participant in the European Space Agency's EXPERT re-entry flight test (Fig. 15-6).

Figure 15-6: Unmanned space vehicle at CIRA, Italy

15.3: Overview of Hypersonic Vehicle Technology Research in India

In recent years, the potential of hypersonic technology for the application of space and missiles has aroused great interest in India. In addition to its focus on the design and construction of launch vehicles and satellites, India has several hypersonic flight programs, including the Capsule Recovery Test (SRE), the Reusable Vehicle (RLV), the scramjet engine development, and the Hypersonic Technology Demonstrator (HSTDV). Among them, the HSTDV project has attracted much attention. The aim of the project is to verify the performance of an aircraft propelled by a scramjet engine in autonomous mode. In addition to verifying the design and performance of scramjet engines, the HST-DV project will also validate aerodynamic performance, aerothermal design, materials, and thermal protection techniques during high Mach number flight [7,8].

15.3.1: HSTOV aircraft structure and composition

The HSTDV project includes the launch of an air-breathing hypersonic vehicle, called a cruise vehicle (CV).

The vehicle is launched to an altitude of 30 to 35 km using a rocket booster, and then transferred to a single-modal scramjet engine fueled by kerosene, reaching a speed of *Ma* = 6.5, and continuously flying for 20s. Figure 15-7 shows the shape of the HSTDV.

Figure 15-7: Outline of the HSTDV aircraft

The 5.6 m long and 1,000 kg mass of the 5.6 m High Speed Technology Demonstrator currently being built has a cross-sectional flat octagonal shape with a pair of short wings in the middle of the fuselage and a sloping vertical tail at the rear of the fuselage. The length of the air intake is 3.7 m, and it is cross-cut and rectangular in shape. The scramjet engine is located in the lower middle part of the fuselage (its development is also underway), and the tail part of the fuselage serves as part of the exhaust nozzle. There were two parallel shutters in the front of the fuselage for increased thrust. The flaps on the trailing edge of the wing are used for aircraft roll control. The deflectable nozzle is located at the rear end of the combustion chamber and has a deflection angle of up to 25° to ensure satisfactory performance during the engine opening and closing phases. The lower surfaces, wings and tail of the fuselage are made of titanium, while the upper surface of the fuselage is made of aluminum alloy composites.

The inner surface of the double-wall engine is made of niobium alloy material, and the outer surface is made of chromium titanium alloy material.

Israel and the UK's Cranfield University have provided partial assistance to India's Hypersonic Technology Demonstrator program, which includes wind tunnel testing. There may be other countries that are also providing technical assistance to India. For a long time, the collaborators of the Indian defense industry were mainly Russian, which conducted a lot of research on hypersonic propulsion systems.

The HSTDV is planned to feature a scramjet engine on hydrocarbon fuel, which is injected into the combustion chamber through a series of staggered injection rods. The DRDL-designed full-scale scramjet combustion chamber measured the aerodynamic characteristics with/without injection rods in the HST4 shock wave wind tunnel. The designed scramjet combustion chamber is 1.8 m long, rectangular, and truncated, with one end close to the inlet channel being 100 mm X 230 mm and the outlet end being 250 mm X 230 mm, as shown in Figure 15-8.

The tests carried out consisted of measuring the static pressure and heat flux density distribution along the walls of the combustion chamber and the model total drag of the injection rod with/without fuel. The aerodynamic resistance of the scramjet combustion chamber is measured using an accelerometer balancing system. The model is mounted on a linear gear, which in turn is mounted on a support disk, so that it can move freely in the air flow. Four accelerometers are mounted on the exterior of the freely movable model, and the accelerometer signals emitted are used to calculate the aerodynamic drag of the supersonic air flow through the model. The static pressure distribution along the combustion chamber is measured using a Kulite pressure sensor, while the heat flux density distribution is measured by a surface-mounted platinum film meter.

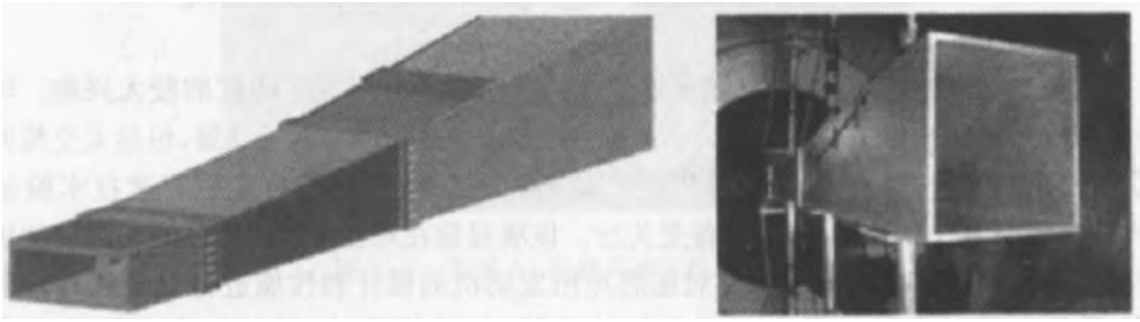

Figure 15-8: Design of scramjet combustion (left) and installation in the HST4 wind tunnel test section (right)

DRDL conducted an experimental study of the inlet tract (uncontrolled) of the HSTDV scaled model in the HST 4 shock wave wind tunnel. The inlet test consists of measuring the static pressure in the combustion chamber of a scramjet engine with compression skews and scramjet engines at different angles of attack. The pressure measurement uses a Kulite pressure sensor.

15.3.2: Indian Hypersonic Test Facility

The key to the success of the hypersonic program is the ability to simulate a hypersonic flight environment in the laboratory and the ability to use a rocket as a launch platform for flight tests. As a result, India has also begun to build large-scale experimental equipment, including hypersonic wind tunnels and shock wave wind tunnels. Currently, existing medium-size, high-speed experimental equipment is being used to acquire basic design data and validate CFD code. The High Roast Aerodynamics Group at the Indian Institute of Science (IISc) has been instrumental in ground testing of many aircraft profiles.

The IISc Centre for Aerospace Engineering is one of India's leading research institutes. The center has a range of conventional hypersonic wind tunnel equipment, including the HST1 shock wind tunnel (50mm diameter A1 shock tube and 300mmX300mm test section), HST2 shock wind tunnel (50mm SS shock tube and 300mmX300mm test section), HST4 shock wind tunnel (165mm SS shock tube and 100mm diameter test section), and free-piston hypersonic shock wind tunnel HST3 (165mm compression tube, 39mm/50mm shock tube, 20kg piston and 300mm free jet section).

Figure 15-9 shows the high-speed device of IISc. The HST4 Shock Wave Wind Tunnel is currently being retrofitted in India by adding a compression tube with a diameter of 600mm and a length of 42m to make it a free-piston shock wave wind tunnel.

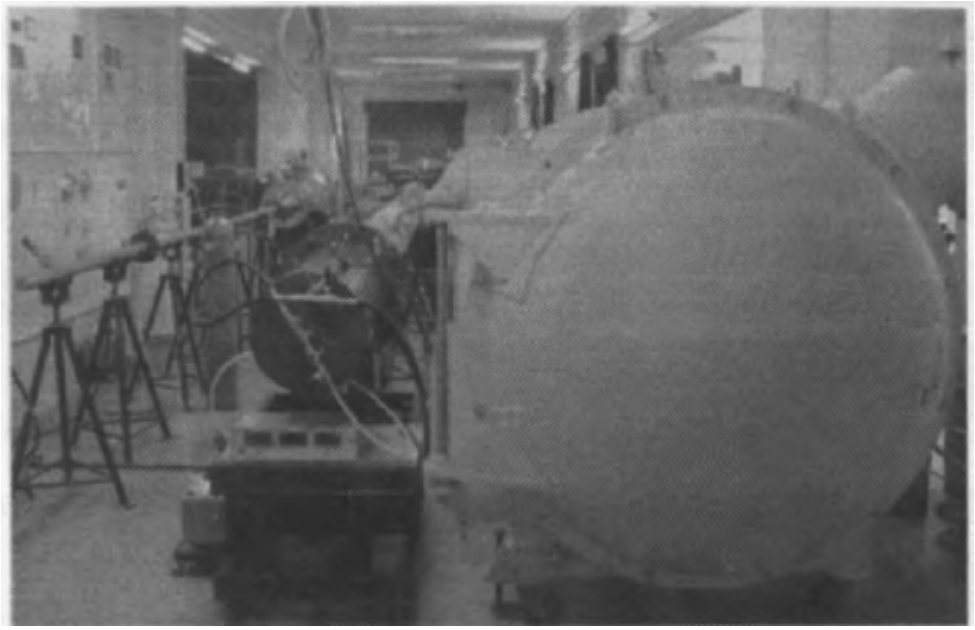

Figure 15-9: IISc hypersonic test equipment

As India's national power grew, so did its desire to become a military and political power. Therefore, driven by the ongoing research boom of hypersonic technology around the world, India has also carried out a lot of research on hypersonic technology. HSTDV is one of the outstanding representatives, through the research of this project. India has completed the design of hypersonic test vehicles and the design of scramjet engines and ground tests, and this has led to the construction of hypersonic related test facilities, which has played an important role in promoting the research of hypersonic technology.

References

[1] Yang Guangbo. HOTOL engine revealed [J]. China Aerospace, 1994, (1):37-41.

[2] Graham J Dadd, Rachel E Owen, John Hodges. Sustained hypersonic flight experiment (SHyFE) [R]. AIAA 2006-7926, 2006.

[3] Jenny S Goodman, Peter T Ireland. Thermal modelling for the sustained hypersonic flight experiment [R]. AIAA 2006-8071, 2006.

[4] Kang Kaihua, Ding Wenhua. British future SKYLON reusable launch vehicle [J]. Missile and Space Launch Technology, 2010, (6):53-56.

[5] Roger Longstaff, Alan Bond. The SKYLON project [R]. AIAA 2011-2244, 2011.

[6] Chen Xiangling, Zhu Aiping. Italy and Australia cooperate in the research of hypersonic technology [J]. Flying Missile, 2009. (10):4.

[7] Wei Guofu. India vigorously develops hypersonic technology [J]. Flying Missile, 2008, (6):1, 2.

[8] Wen Suli, He Xuhong, Ye Lei. Indian Hypersonic Technology Verifier HSTDV [J]. Flying Missile, 2010, (5):75, 76.

CHAPTER 16: SUMMARY AND PROSPECTS

16.1: Summary of research on hypersonic vehicle technology

Through the decomposition of the key technologies of hypersonic vehicles and the analysis of the research content of the main key technologies, as well as the combing of the development process of foreign hypersonic vehicle technology, the author of this book summarizes the characteristics of hypersonic vehicle technology and development as follows.

1. Power first, overall traction

The core key technology of hypersonic vehicles is scramjet engine technology, and hypersonic flight is based on the concept of scramjet engines application. At the same time, because the propulsion system of hypersonic vehicles is closely related to the overall design of the aircraft, all countries have proposed an overall plan for the application of hypersonic vehicles while carrying out research on scramjet engines, so as to promote the research of scramjet engines, as well as the setting of research content and research directions of other related technologies.

2. Integrated design of fuselage and propulsion system

Hypersonic vehicles are completely different from other general types of aircraft, the fuselage and propulsion system are closely related, the two use each other, but also affect each other, so the propulsion system of hypersonic aircraft

cannot be separated from the overall design of the aircraft, especially the aerodynamic shape of the aircraft fuselage and independent, the integrated design of the aircraft fuselage and propulsion system must be carried out, in a sense, there is no engineering sense of hypersonic aircraft propulsion system engine development, there is no independent product form. The design of the propulsion system needs to be carried out in parallel with the overall design of the hypersonic vehicle.

3. Multidisciplinary coupling

Hypersonic vehicles involve aerodynamics, structural mechanics, aeroelastic mechanics, flight control and other disciplines, the coupling relationship between disciplines is very close, only one or two disciplines as the starting point for design, it is inevitable to meet the requirements of each discipline, and it is impossible to realize the feasibility of the design scheme, in the case of multidisciplinary coupling, it is necessary to carry out multidisciplinary integrated design and optimization.

4. National research plan

The development of hypersonic vehicles involves all disciplines and professional categories of aerospace, and no one research structure can carry out all the research and development work.

5. Pay attention to basic research

Although the scramjet engine has been developed for 50 years, there are still many problems that are difficult to explain in its complex working mechanism, and how to realize the engineering application is a very difficult task, and in addition, all disciplines of the aircraft under hypersonic flight conditions are also facing unprecedented problems. Therefore, we cannot blindly think that hypersonic vehicles can be realized based on the existing research foundation and understanding, but still need to pay attention to basic research, solve problems from the source, and propose innovative solutions.

6. Aircraft solutions are diverse

In the research of various countries, the aerodynamic shape of the hypersonic vehicle presents a diversified characteristic, which fully reflects the bold assumptions of scientists and engineers in various countries for the future aircraft, from the current research it is difficult to say which aerodynamic shape and overall scheme is optimal, or even feasible, so we should open our minds and propose and explore more new forms of aircraft solutions.

16.2: Trends in hypersonic vehicle technology

1. Hypersonic cruise missiles became the first application form of hypersonic vehicle technology

The American X-51A hypersonic test vehicle can be said to be a technical verification machine for future hypersonic cruise missiles, so hypersonic cruise missiles will become the first application form of hypersonic vehicle technology.

2. The overall aerodynamic shape of hypersonic vehicles is diverse

From the research point of view, the overall aerodynamic shape of the hypersonic vehicle is not limited to a specific form, as long as it can achieve effective flight, any form is allowed, in the existing research, there are based on the shape of the lifting body, the shape of the waverider, the axisymmetric shape, in recent years, the rise of the research on the inward intake and the circular section propulsion system, resulting in more peculiar and novel aircraft shape design schemes.

3. Flight control is the key to the viability of hypersonic vehicles

The flight process of hypersonic aircraft involves complex inflow and outflow, not only to realize the control of the aircraft attitude based on aerodynamics, but also to realize the effective organization and control of the inflow of the propulsion system, and to solve and coordinate the relationship between the two, in order to achieve feasible flight, there are still a large number of uncertainties in the flight process to affect the flight control, a slight deviation will lead to the irretrievable failure of the aircraft, it can be seen that flight control may be the bottleneck difficulty of the hypersonic vehicle to the feasible road, but the solution does not only depend on the control technology itself, but also needs to rely on the overall coordinated design of the aircraft and the multidisciplinary design.

4. Multidisciplinary integrated design and optimization is the only way for the development of hypersonic vehicles

The intrinsic high coupling characteristics of hypersonic vehicles inevitably determine that multidisciplinary integrated design and optimization is the only way for the development of hypersonic vehicles, and the form of scientific research organization should also be constructed in accordance with the close coordination of multiple disciplines and disciplines.

5. Compared with the turbine-based propulsion system with rotating parts, the two-stage orbit entry powered by the rocket-based combined cycle engine is the first choice for reusable space vehicles. The rocket-based combined cycle engine is less technically difficult than the turbine-based propulsion system with rotating parts, and it is the power mode that can be realized as the first step of the reusable space launch vehicle, and the two-stage orbit entry reduces the difficulty of system design, and should also be studied as the preferred scheme.

6. The key technologies of hypersonic vehicles need to carry out a large number of flight demonstration and verification tests

Because the flight environment experienced by the hypersonic vehicle is difficult to fully simulate in a ground wind tunnel, the final technical verification still needs to be tested in flight, and before the practical application is realized, the key technologies of the hypersonic vehicle still need to carry out a large number of flight demonstration and verification tests, gradually improve the maturity of the technology, and on this basis, carry out the flight test of system integration, improve the technical maturity of system integration, and effectively reduce the risk of development.